Elements of Propulsion

Gas Turbines and Rockets

Jack D. Mattingly

Foreword by
Hans von Ohain
German Inventor of the Jet Engine

American Institute of Aeronautics and Astronautics

AIAA Education Series
Joseph A. Schetz
Editor-In-Chief

Elements of Propulsion: Gas Turbines and Rockets

Jack D. Mattingly
Professor Emeritus
Department of Mechanical Engineering
Seattle University, Seattle, Washington

Foreword by
Hans von Ohain
German Inventor of the Jet Engine

EDUCATION SERIES
Joseph A. Schetz
Series Editor-in-Chief
Virginia Polytechnic Institute and State University
Blacksburg, Virginia

Published by the
American Institute of Aeronautics and Astronautics, Inc.
1801 Alexander Bell Drive, Reston, Virginia 20191-4344

American Institute of Aeronautics and Astronautics, Inc., Reston, Virginia

1 2 3 4 5 6 7 8 9 10

Library of Congress Cataloging-in-Publication Data

Mattingly, Jack D.
Elements of propulsion: gas turbines and rockets/Jack D. Mattingly; foreword by Hans von Ohain.
p. cm.—(Education series)
Includes bibliographical references and index.
ISBN 1-56347-779-3 (alk. paper)
1. Aircraft gas-turbines. 2. Airplanes—Jet propulsion. 3. Jet engines.
4. Rocket engines. I. Title. II. Series: AIAA education series.

TL709.M388 2006
629.134'353–dc22 2006017363

I have been blessed to share my life with Sheila, my best friend and wife. She has been my inspiration and helper, and the one who sacrificed the most to make this work possible. I dedicate this book and the accompanying software to Sheila.

I would like to share with all the following passage I received from a very close friend about 30 years ago. This passage provides guidance and focus to my life. I hope it can be as much help to you.

FABRIC OF LIFE

I want to say something to all of you
Who have become a part
Of the fabric of my life
The color and texture
Which you have brought into
My being
Have become a song
And I want to sing it forever.
There is an energy in us
Which makes things happen
When the paths of other persons
Touch ours
And we have to be there
And let it happen.
When the time of our particular sunset comes
Our thing, our accomplishment
Won't really matter
A great deal.
But the clarity and care
With which we have loved others
Will speak with vitality
Of the great gift of life
We have been for each other.

Gregory Norbert, O.S.B.

Page is intentionally blank

Page is intentionally blank

Page is intentionally blank

Page is intentionally blank

Foreword to the Second Edition

We are very pleased to present the Second Edition of *Elements of Propulsion: Gas Turbines and Rockets* by Jack D. Mattingly. The original edition was a well-received, comprehensive, and in-depth treatment of these important topics. This new edition has updated the material and expanded the coverage, and we anticipate that it will be equally well received. An interesting feature of the first edition was a very extensive foreword by the jet engine pioneer, Hans Von Ohain. Indeed, it is so extensive and comprehensive that it is more a historical overview and introduction than a foreword. We deem it so useful that it is included in this edition as well. This Second Edition has ten chapters, seven appendices and more than 850 pages.

Jack Mattingly is extremely well qualified to write this book because of his broad expertise in the area. His command of the material is excellent, and he is able to organize and present it in a very clear manner. He is such a proficient author that he is the co-winner of the Martin Summerfield Book Award for another volume in this series.

The AIAA Education Series aims to cover a very broad range of topics in the general aerospace field, including basic theory, applications, and design. A complete list of titles can be found at http://www.aiaa.org. The philosophy of the series is to develop textbooks that can be used in a university setting, instructional materials for continuing education and professional development courses, and also books that can serve as the basis for independent study. Suggestions for new topics or authors are always welcome.

Joseph A. Schetz
Editor-in-Chief
AIAA Education Series

Page is intentionally blank

Table of Contents

Foreword to the First Edition

Background

The first flight of the Wright brothers in December 1903 marked the beginning of the magnificent evolution of *human-controlled, powered flight.* The driving forces of this evolution are the ever-growing demands for improvements in

1) Flight performance (i.e., greater flight speed, altitude, and range and better maneuverability);
2) Cost (i.e., better fuel economy, lower cost of production and maintenance, increased lifetime);
3) Adverse environmental effects (i.e., noise and harmful exhaust gas effects);
4) Safety, reliability, and endurance; and
5) Controls and navigation.

These strong demands continuously furthered the efforts of advancing the aircraft system.

The tight interdependency between the performance characteristics of aerovehicle and aeropropulsion systems plays a very important role in this evolution. Therefore, to gain better insight into the evolution of the aeropropulsion system, one has to be aware of the challenges and advancements of aerovehicle technology.

The Aerovehicle

A brief review of the evolution of the aerovehicle will be given first. One can observe a continuous trend toward stronger and lighter airframe designs, structures, and materials—from wood and fabric to all-metal structures; to lighter, stronger, and more heat-resistant materials; and finally to a growing use of strong and light composite materials. At the same time, the aerodynamic quality of the aerovehicle is being continuously improved. To see this development in proper historical perspective, let us keep in mind the following information.

In the early years of the 20th century, the science of aerodynamics was in its infancy. Specifically, the aerodynamic lift was not scientifically well understood. Joukowski and Kutta's model of lift by circulation around the wing and Prandtl's boundary-layer and turbulence theories were in their incipient stages. Therefore, the early pioneers could not benefit from existent

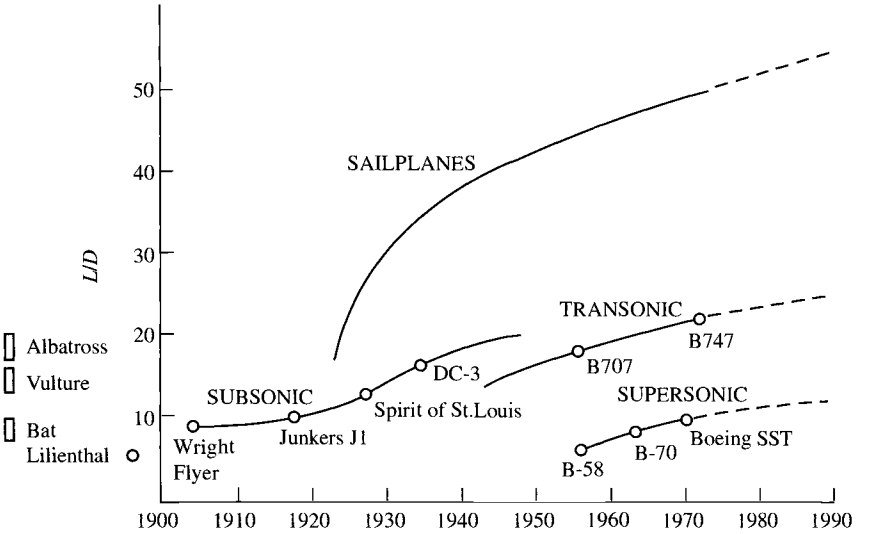

Fig. 1 Progress in lift/drag ratio L/D.

scientific knowledge in aerodynamics and had to conduct their own fundamental investigations.

The most desirable major aerodynamic characteristics of the aerovehicle are a low *drag coefficient* as well as a high *lift/drag ratio* L/D for cruise conditions, and a high *maximum lift coefficient* for landing. In Fig. 1, one can see that the world's first successful glider vehicle by Lilienthal, in the early 1890s, had an L/D of about 5. In comparison, birds have an L/D ranging from about 5 to 20. The Wright brothers' first human-controlled, powered aircraft had an L/D of about 7.5. As the L/D values increased over the years, sailplanes advanced most rapidly and now are attaining the enormously high values of about 50 and greater. This was achieved by employing ultrahigh wing aspect ratios and aerodynamic profiles especially tailored for the low operational Reynolds and Mach numbers. In the late 1940s, subsonic transport aircraft advanced to L/D values of about 20 by continuously improving the aerodynamic shapes, employing advanced profiles, achieving extremely smooth and accurate surfaces, and incorporating inventions such as the engine cowl and the retractable landing gear.

The continuous increase in flight speed required a corresponding reduction of the *landing speed/cruise speed* ratio. This was accomplished by innovative wing structures incorporating wing slots and wing flaps that, during the landing process, enlarged the wing area and increased significantly the lift coefficient. Today, the arrowhead-shaped wing contributes to a high lift for landing (vortex lift). Also, in the 1940s, work began to extend the high L/D value from the subsonic to the transonic flight speed regime by employing the swept-back wing and later, in 1952, the area rule of Whitcomb to reduce *transonic drag rise*. Dr. Theodore von Kármán describes in his memoirs, *The Wind and*

Beyond,* how the *swept-back wing* or simply *swept wing* for transonic and supersonic flight came into existence:

> The fifth Volta Congress in Rome, 1935, was the first serious international scientific congress devoted to the possibilities of supersonic flight. I was one of those who had received a formal invitation to give a paper at the conference from Italy's great Gugliemo Marconi, inventor of the wireless telegraph. All of the world's leading aerodynamicists were invited.
>
> This meeting was historic because it marked the beginning of the supersonic age. It was the beginning in the sense that the conference opened the door to supersonics as a meaningful study in connection with supersonic flight, and, secondly, because most developments in supersonics occurred rapidly from then on, culminating in 1946—a mere 11 years later—in Captain Charles Yeager's piercing the sound barrier with the X-1 plane in level flight. In terms of future aircraft development, the most significant paper at the conference proved to be one given by a young man, Dr. Adolf Busemann of Germany, by first publicly suggesting the swept-back wing and showing how its properties might solve many aerodynamic problems at speeds just below and above the speed of sound.

Through these investigations, the myth that sonic speed is the fundamental limit of aircraft flight velocity, the *sound barrier* was overcome.

In the late 1960s, the Boeing 747 with swept-back wings had, in transonic cruise speed, an L/D value of nearly 20. In the supersonic flight speed regime, L/D values improved from 5 in the mid-1950s (such as L/D values of the B-58 Hustler and later of the Concorde) to a possible L/D value of 10 and greater in the 1990s. This great improvement possibility in the aerodynamics of supersonic aircraft can be attributed to applications of artificial stability, to the area rule, and to advanced wing profile shapes that extend laminar flow over a larger wing portion.

The hypersonic speed regime is not fully explored. First, emphasis was placed on winged reentry vehicles and lifting bodies where a high L/D value was not of greatest importance. Later investigations have shown that the L/D values can be greatly improved. For example, the maximum L/D for a "wave rider" is about 6.† Such investigations are of importance for hypersonic programs.

The Aeropropulsion System

At the beginning of this century, steam and internal combustion engines were in existence but were far too heavy for flight application. The Wright brothers recognized the great future potential of the internal combustion engine and developed both a relatively lightweight engine suitable for flight application and an efficient propeller. Figure 2 shows the progress of the propulsion systems over the years. The Wright brothers' first aeropropulsion system had a shaft power of 12 hp, and its power/weight ratio (ratio of power output to total propulsion system weight, including propeller and transmission) was about 0.05 hp/lb.

---

*Von Kármán, T., *The Wind and Beyond*, Little, Brown, Boston, 1967.

†Heiser, W. H., and Pratt, D.J., *Hypersonic Airbreathing Propulsion*, AIAA Education Series, AIAA, Washington, DC, 1994.

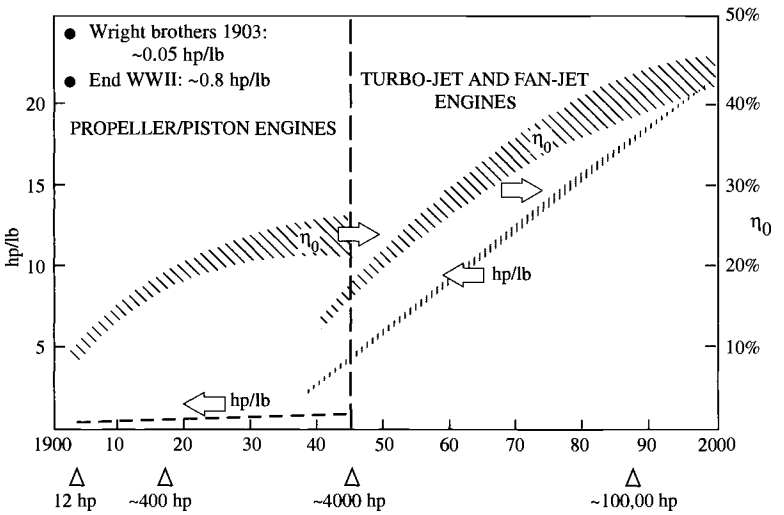

Fig. 2 Trends of power per weight (hp/lb) and overall efficiency (η_O) of aeropropulsion systems from 1900 to 2000.

Through the subsequent four decades of evolution, the overall efficiency and the power/weight ratio improved substantially, the latter by more than one order magnitude to about 0.8 hp/lb. This great improvement was achieved by engine design structures and materials, advanced fuel injection, advanced aerodynamic shapes of the propeller blades, variable-pitch propellers, and engine superchargers. The overall efficiency (engine and propeller) reached about 28%. The power output of the largest engine amounted to about 5000 hp.

In the late 1930s and early 1940s, the turbojet engine came into existence. This new propulsion system was immediately superior to the reciprocating engine with respect to the power/weight ratio (by about a factor of 3); however, its overall efficiency was initially much lower than that of the reciprocating engine. As can be seen from Fig. 2, progress was rapid. In less than four decades, the power/weight ratio increased more than 10-fold, and the overall efficiency exceeded that of a diesel propulsion system. The power output of today's largest gas turbine engines reaches nearly 100,000 equivalent hp.

Impact on the Total Aircraft Performance

The previously described truly gigantic advancements of stronger and lighter structures and greater aerodynamic quality in aerovehicles and greatly advanced overall efficiency and enormously increased power output/weight ratios in aeropropulsion systems had a tremendous impact on flight performance, such as on flight range, economy, maneuverability, flight speed, and altitude. The increase in flight speed over the years is shown in Fig. 3. The Wright brothers began with the first human-controlled, powered flight in 1903; they continued to

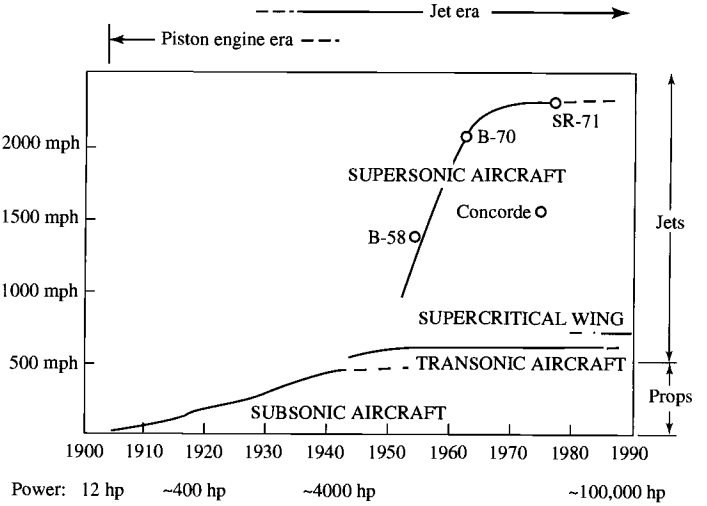

Fig. 3 Aircraft speed trends.

improve their aircraft system and, in 1906, conducted longer flights with safe takeoff, landing, and curved flight maneuvers. While the flight speed was only about 35 mph, the consequences of these first flights were enormous:

1) Worldwide interest in powered flight was stimulated.
2) The science of aerodynamics received a strong motivation.
3) The U.S. government became interested in power flight for potential defense applications, specifically reconnaissance missions.

In 1909, the Wright brothers built the first military aircraft under government contract. During World War I, aircraft technology progressed rapidly. The flight speed reached about 150 mph, and the engine power attained 400 hp. After World War I, military interest in aircraft systems dropped, but aircraft technology had reached such a degree of maturity that two nonmilitary application fields could emerge, namely:

1) Commercial aviation, mail and passenger transport (first all-metal monoplane for passenger and mail transport, the Junkers F13, in 1919, sold worldwide);
2) Stunt flying leading to general aviation (sport and private transportation).

In the period from 1920 to 1940, the speed increased from about 150 to 350 mph through evolutionary improvements in vehicle aerodynamics and engine technology, as discussed previously. At the end of World War II, the flight speed of propeller aircraft reached about 400–450 mph, and the power output of the largest reciprocating engines was about 5000 hp. This constituted almost the performance limit of the *propeller/reciprocating engine propulsion system.* Today, the propeller/reciprocating engine survives only in smaller, lower-speed aircraft used in general aviation.

In the late 1930s, jet propulsion emerged that promised far greater flight speeds than attainable with the propeller or piston engine. The first jet-propelled experimental aircraft flew in the summer of 1939 (the He-178), and in early 1941, the first prototype jet fighter began flight tests (He-280). In 1944, mass-produced jet fighters reached a speed of about 550 mph (Me-262).

In the early 1950s, jet aircraft transgressed the sonic speed. In the mid-1950s, the first supersonic jet bomber (B-58 Hustler) appeared, and later the XB-70 reached about Mach 3. Also during the 1950s, after more than 15 years of military development, gas turbine technology had reached such a maturity that the following commercial applications became attractive: 1) commercial aircraft, e.g., Comet, Caravelle, and Boeing 707; 2) surface transportation (land, sea); and 3) stationary gas turbines.

In the 1960s, the high-bypass-ratio engine appeared, which revolutionized military transportation (the C5A transport aircraft). At the end of the 1960s, based on the military experience with high-bypass-ratio engines, the second generation of commercial jet aircraft came into existence, the *widebody* aircraft. An example is the Boeing 747 with a large passenger capacity of nearly 400. Somewhat later came the Lockheed L-1011 and Douglas DC10. By that time, the entire commercial airline fleet used turbine engines exclusively. Advantages for the airlines were as follows:

1) Very high overall efficiency and, consequently, a long flight range with economical operation.
2) Overhaul at about 5 million miles.
3) Short turnaround time.
4) Passenger enjoyment of the very quiet and vibration-free flight, short travel time, and comfort of smooth stratospheric flight.
5) Community enjoyment of quiet, pollution-free aircraft.

By the end of the 1960s, the entire business of passenger transportation was essentially diverted from ships and railroads to aircraft. In the 1970s, the supersonic Concorde with a flight speed of 1500 mph (the third generation of commercial transport) appeared with an equivalent output of about 100,000 hp.

Summary

In hindsight, the evolution of aerovehicle and aeropropulsion systems looks like the result of a master plan. The evolution began with the piston engine and propeller, which constituted the best propulsion system for the initially low flight speeds, and had an outstanding growth potential up to about 450 mph. In the early 1940s, when flight technology reached the ability to enter into the transonic flight speed regime, the jet engine had just demonstrated its suitability for this speed regime. A vigorous jet engine development program was launched. Soon the jet engine proved to be not only an excellent transonic but also a supersonic propulsion system. This resulted in the truly exploding growth in flight speed, as shown in Fig. 3.

It is interesting to note that military development preceded commercial applications by 15–20 years for both the propeller engine and the gas turbine engine. The reason was that costly, high-risk, long-term developments conducted

by the military sector were necessary before a useful commercial application could be envisioned. After about 75 years of powered flight, the aircraft has outranked all other modes of passenger transportation and has become a very important export article of the United States.

The evolutions of both aerovehicle and aeropropulsion systems have in no way reached a technological level that is close to the ultimate potential! The evolution will go on for many decades toward capabilities far beyond current feasibility and, perhaps, imagination.

How Jet Propulsion Came into Existence

The idea of airbreathing jet propulsion originated at the beginning of the 20th century. Several patents regarding airbreathing jet engines had been applied for by various inventors of different nationalities who worked independently of each other.

From a technical standpoint, *airbreathing jet propulsion* can be defined as a special type of internal combustion engine that produces its net output power as the rate of change in the kinetic energy of the engine's working fluid. The working fluid enters as environmental air that is ducted through an inlet diffuser into the engine; the engine exhaust gas consists partly of combustion gas and partly of air. The exhaust gas is expanded through a thrust nozzle or nozzles to ambient pressure. A few examples of early airbreathing jet propulsion patents are as follows:

1) In 1908, Lorin patented a jet engine that was based on piston machinery (Fig. 4a).

2) In 1913, Lorin patented a jet engine based on ram compression in supersonic flight (Fig. 4b), the *ramjet.*

3) In 1921, M. Guillaume patented a jet engine based on turbomachinery; the intake air was compressed by an axial-flow compressor followed by a combustor and an axial-flow turbine driving the compressor (Fig. 4c).

These patents clearly described the airbreathing jet principle but were not executed in practice. The reason lies mainly in the previously mentioned strong interdependency between aerovehicle and aeropropulsion systems. The jet engine has, in comparison with the propeller engine, a high exhaust speed (for example, 600 mph and more). In the early 1920s, the aerovehicle had a flight speed capability that could not exceed about 200 mph. Hence, at that time, the so-called propulsive efficiency of the jet engine was very low (about 30–40%) in comparison to the propeller, which could reach more than 80%. Thus, in the early 1920s, the jet engine was not compatible with the too-slow aerovehicle. Also, in the early 1920s, an excellent theoretical study about the possibilities of enjoying jet propulsion had been conducted by Buckingham of the Bureau of Standards under contract with NACA. The result of this study was clear—the jet engine could not be efficiently employed if the aerovehicle could not greatly exceed the flight speed of 200 mph; a flight speed beyond 400 mph seemed to be necessary. The consequences of the results of this study were that the aircraft engine industry and the scientific and engineering community had no interest in the various jet engine inventions. Thus the early jet engine

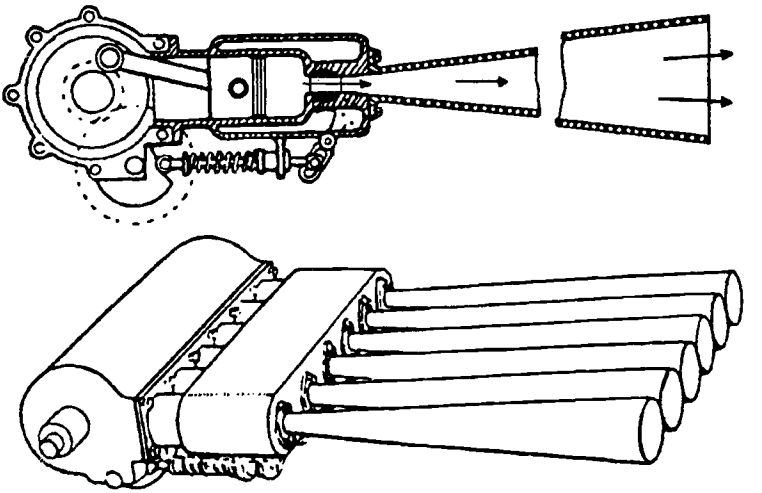

Fig. 4a Lorin's 1908 patent.

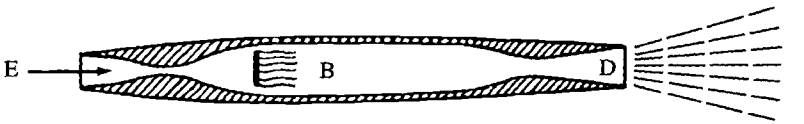

Fig. 4b Lorin's 1913 patent.

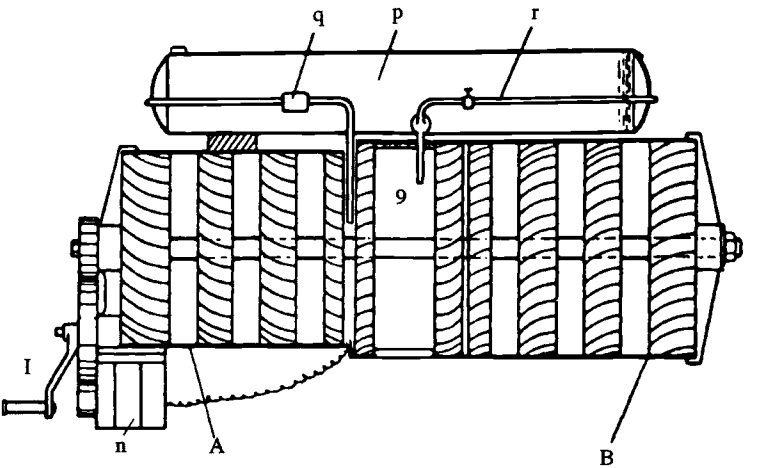

Fig. 4c 1921 Guillaume patent.

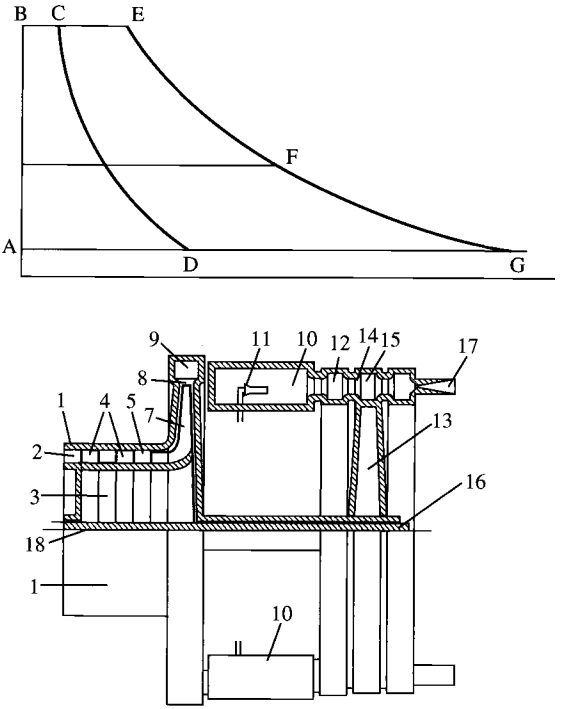

Fig. 5 Whittle's turbojet patent drawing. (National Air and Space Museum.)

concepts were forgotten for a long time. They were unknown to Sir Frank Whittle, to me, and to the British and German patent offices. In 1939, however, the retired patent examiner Gohlke found out about the early jet patents and published them in a synoptic review.

The first patent of a turbojet engine, which was later developed and produced, was that of Frank Whittle, now Sir Frank (see Fig. 5). His patent was applied for in January 1930. This patent shows a multistage, axial-flow compressor followed by a radial compressor stage, a combustor, an axial-flow turbine driving the compressor, and an exhaust nozzle. Such configurations are still used today for small- and medium-power output engines, specifically for remote-controlled vehicles.

Turbojet Development of Sir Frank Whittle

Frank Whittle[‡] was a cadet of the Royal Air Force. In 1928, when he was 21 years old, he became interested in the possibilities of rocket propulsion and

[‡]Boyne, W. J., and Lopez, D. S., *The Jet Age, Forty Years of Jet Aviation*, Smithsonian Inst. Press, Washington, DC, 1979.

propeller gas turbines for aircraft, and he treated these subjects in his thesis. He graduated and became a pilot officer, continuously thinking about airbreathing jet propulsion. In 1929, he investigated the possibilities of a ducted fan driven by a reciprocating engine and employing a kind of afterburner prior to expansion of the fan gas. He finally rejected this idea on the basis of his performance investigations. The same idea was conceived later in Italy and built by Caproni Campini. The vehicle flew on August 28, 1940, but had a low performance, as predicted by Sir Frank in 1929.

Suddenly, in December 1929, Frank Whittle was struck by the idea of increasing the fan pressure ratio and substituting a turbine for the reciprocating engine. This clearly constituted a compact, lightweight turbojet engine. He applied for a patent for the turbojet (Fig. 5) in January 1930.

Frank Whittle discussed this idea with fellow officers and his superior officer. They were very impressed, and a meeting was arranged between him and officials of the British Air Ministry, Department of Engine Development. This department, in turn, sought advice from Dr. A. A. Griffith, who was interested in the development of a propeller gas turbine. Dr. Griffith expressed doubts about the feasibility of Whittle's turbojet concept from a standpoint of too-high fuel consumption. Actually, *in high-speed flight*, the turbojet has great advantages over a propeller gas turbine due to the fact that the turbojet is much lighter than the propeller gas turbine and can fly faster because of the absence of the propeller. Whittle rightfully considered the turbojet as a fortunate synthesis or hybrid of the "propeller gas turbine" and "rocket" principles. As Sir Frank recalls, the department wrote a letter that, in essence, stated that any form of a gas turbine would be impractical in view of the long history of failure and the lack of turbine materials capable of withstanding the high stresses at high temperatures. Whittle's outstanding and very important views were that the flying gas turbine had great advantages over a stationary gas turbine power plant due to the efficient ram pressure recovery, low environmental temperature in high altitude, and high efficiency of the jet nozzle. Unfortunately, these views were ignored by the department.

Frank Whittle (Fig. 6) tried to interest the turbine industry in his concept of jet propulsion, but he did not succeed. Lacking financial support, Whittle allowed his patent to lapse. A long, dormant period was ahead for Frank Whittle's jet propulsion ideas.

After five years, in mid-1935, two former Royal Air Force (RAF) officers tried to revive Whittle's turbojet concept. Whittle was enthused and wrote, "the jet engine had, like the Phoenix, risen from its ashes."[§] At that time, Whittle was under enormous pressure. He was preparing for the examination in mechanical sciences (Tripos); his goal was to graduate with "First-Class Honors." Now, in addition, he had to design his first experimental jet engine in late 1935. In March 1936, a small company, Power Jets Ltd., was formed to build and test Whittle's engine, the W. U. (Whittle Unit). In spite of all the additional work, Whittle passed his exam in June 1936 with First-Class Honors.

[§]Boyne, W. J., and Lopez, D. S., *The Jet Age, Forty Years of Jet Aviation*, Smithsonian Inst. Press, Washington, DC, 1979.

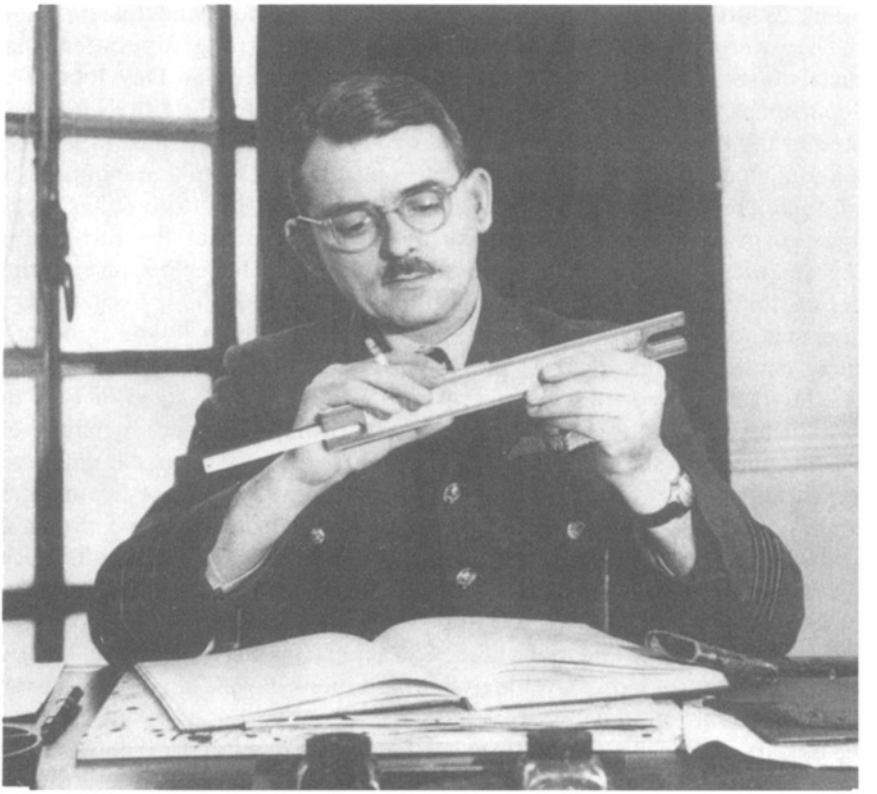

Fig. 6 Frank Whittle using slide rule to perform calculations. (Bettman.)

In April 1937, Whittle had his bench-test jet engine ready for the first test run. It ran excellently; however, it ran out of control because liquid fuel had collected inside the engine and started to vaporize as the engine became hot, thereby adding uncontrolled fuel quantities to the combustion process. The problem was easily overcome. This first test run was the world's first run of a bench-test jet engine operating with liquid fuel (Fig. 7). In June 1939, the testing and development had progressed to a point that the Air Ministry's Director of Scientific Research (D.S.R.) promised Frank Whittle a contract for building a flight engine and an experimental aircraft, the Gloster E28/29 (Gloster/Whittle). On May 15, 1941, the first flight of the Gloster/Whittle took place (Fig. 8).

Senior ministry officials initially showed little interest, and a request for filming was ignored; however, during further flight demonstrations, interest in jet propulsion increased. Of particular interest was a performance demonstration given to Sir Winston Churchill. At that occasion, the Gloster/Whittle accelerated away from the three escorting fighters, one Tempest and two Spitfires.

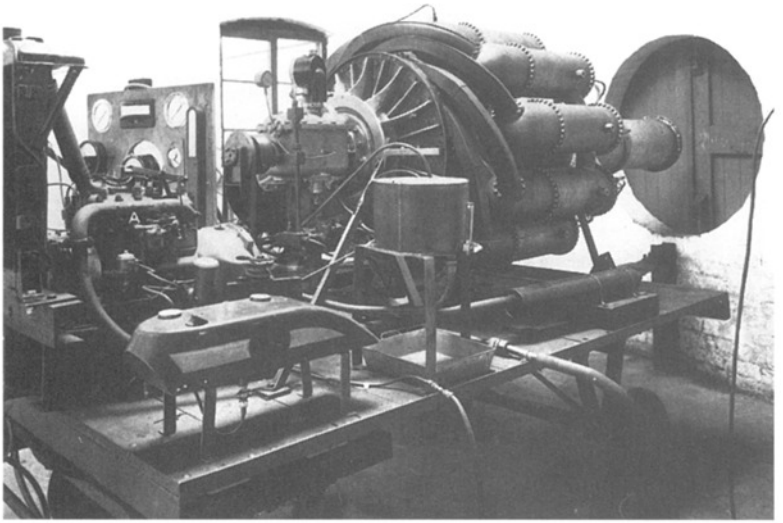

Fig. 7 Whittle's first experimental engine after second reconstruction in 1938. (National Air and Space Museum.)

Several British aircraft engine corporations adapted the work of Frank Whittle. Specifically, Rolls-Royce, due to the efforts of Sir Stanley G. Hooker,[¶] developed the first operational and the first production engine for the two-engine Gloster Meteor, Britain's first jet fighter. In March 1943, the Gloster Meteor prototype made its first flight, powered by two de Haviland (H-1) radial jet engines. In July 1944, the Meteor I, powered with two Rolls-Royce Welland engines, became operational. Its only combat action (in World War II) was in August 1944 in a successful attack against the German V1 flying bomb; it was the only fighter with sufficient level speed for the purpose. Mass production began with the Meteor III powered by two Rolls-Royce Dervents in 1945. The Meteor remained the RAF's first-line jet fighter until 1955.

From the beginning of his jet propulsion activities, Frank Whittle had been seeking means for improving the propulsive efficiency of turbojet engines.[¶] He conceived novel ideas for which he filed a patent application in 1936, which can be called a *bypass engine* or *turbofan.* To avoid a complete new design, Whittle sought an interim solution that could be merely "tacked on" to a jet engine. This configuration was later known as the *aft fan.* Whittle's work on *fan jets* or *bypass engines* and *aft fans* was way ahead of his time. It was of greatest importance for the future or turbopropulsion.

[¶]Schlaifer, R., and Heron, S. D., *Development of Aircraft Engines, and Fuels*, Pergamon Press, New York, 1970; reprint of 1950 ed.

Fig. 8 Gloster E28/29. (National Air and Space Museum.)

Whittle's Impact on U.S. Jet Development

In the summer of 1941, U.S. Army Air Corp General Henry H. Arnold was invited to observe flight demonstrations of the Gloster/Whittle. He was very impressed and decided this technology should be brought over to the United States. In September 1941, an agreement was signed between U.S. Secretary of War Stimson and Sir Henry Self of the British Air Commission. The United States could have the engine W1X and a set of drawings of the Whittle W2B jet engine, provided that close secrecy was maintained and the number of people involved were held to a minimum. Under these conditions, open bids for the jet engine development were not possible. General Arnold chose General Electric for jet engine development because of the great experience this company had in the development of aircraft engine turbosuperchargers. The W2B engine was built and tested on March 18, 1942, under the name *GE 1-A*. This engine had a static thrust of 1250 lb and weighed 1000 lb.[3] In the meantime, the Bell Aircomet (XP-59A) was being designed and built. On October 3, 1942, the Aircomet with two GE 1-A engines flew up to 10,000 ft. This aircraft, while in the first tests seemed to have good performance characteristics, had an incurable "snaking" instability and so provided a poor gun platform for a fighter pilot. Also, another serious shortcoming was that the top speed was not sufficiently above that of an advanced propeller fighter. For these reasons, the Bell XP-59A with two GE 1-A engines (W2B) did not become a production fighter. From these experiences, it appeared that an engine of more than 4000-lb thrust was required for a single-engine fighter that would be capable of more than 500 mph operational speed. Lockheed was chosen to design a new jet fighter because when the project was discussed with the engineering staff, Lockheed's Kelly Johnson assured them a single-engine jet fighter in the "500 plus" mph class could be built on the basis of a 4000-lb thrust engine.

General Electric developed the 4000-lb thrust engine, the 140 (an advanced version of Whittle's W2B engine), and Lockheed built the P80A Shooting Star, which flew on June 11, 1944. Although it did not enter combat during World War II, the Shooting Star became the United States' front-line fighter and outranked the Gloster Meteor with an international speed record (above 620 mph near the ground).

By about 1945, Frank Whittle had successfully completed, with greatest tenacity under the most adverse conditions, the enormous task of leading Great Britain and the United States into the jet age.

Other Early Turbojet Developments in the United States

Independent of European influence, several turbojet and propeller gas turbine projects had been initiated in the United States in 1939 and 1940. Although these projects had been terminated or prematurely canceled, they had contributed significantly to the know-how and technology of aircraft gas turbines, specifically their combustor and turbomachinery components.

One of these projects was the 2500-hp Northrop propeller gas turbine (Turbodyne) and a high-pressure-ratio turbojet under the excellent project leadership of Vladimir Pavelecka. Although the development goal of the large aircraft gas turbine engine was essentially met in late 1940, the project was canceled because the Air Force had lost interest in propeller gas turbines in view of the enormous advancement of the competitive jet engines.

Westinghouse had developed outstanding axial turbojet engines. The first very successful test runs of the Westinghouse X19A took place in March 1943. In the beginning of the 1950s, the Navy canceled the development contract, and top management of Westinghouse decided to discontinue work on turbojet engines.

The Lockheed Corporation began to work on a very advanced turbojet conceived by an outstanding engineer, Nathan C. Price. This engine was so far ahead of its time that it would have needed a far longer development time than that provided by the contract. The development contract was canceled in 1941.

Pratt & Whitney had started to work on its own jet propulsion ideas in the early 1940s but could not pursue these concepts because of the too-stringent obligations during wartime for the development and production of advanced aircraft piston engines. After World War II, Pratt & Whitney decided to go completely into turbojet development using axial-flow turbo-machinery. The company began with the construction of a gigantic test and research facility. The government gave Pratt & Whitney a contract to build a large number of 5000-lb thrust Rolls-Royce Nene engines with a radial compressor of the basic Whittle design. Subsequently, Pratt & Whitney developed its own large axial-flow, dual-rotor turbojet and later a fan-jet with a small bypass ratio for the advanced B52.

Turbojet Development of Hans von Ohain in Germany

My interest in aircraft propulsion began in the fall of 1933 while I was a student at the Georgia Augusta University of Gottingen in physics under

Prof. R. Pohl with a minor in applied mechanics under Prof. Ludwig Prandtl. I was 21 years old and beginning my Ph.D. thesis in physics, which was not related to jet propulsion.

The strong vibrations and noise of the propeller piston engine triggered my interest in aircraft propulsion. I felt the natural smoothness and elegance of flying was greatly spoiled by the reciprocating engine with propellers. It appeared to me that a steady, thermodynamic flow process was needed. Such a process would not produce vibrations. Also, an engine based on such a process could probably be lighter and more powerful than a reciprocating engine with a propeller because the steady flow conditions would allow a much greater mass flow of working medium per cross section. These characteristics appeared to me to be most important for achieving higher flight speeds. I made performance estimates for several steady flow engine types and finally chose a special gas turbine configuration that appeared to me as a lightweight, simple propulsion system with low development risks. The rotor consisted of a straight-vane radial outflow compressor back-to-back with a straight vane radial inflow turbine. Both compressor and turbine rotors had nearly equal outer diameters, which corresponds to a good match between them.

In early 1935, I worked out a patent for the various features of a gas turbine consisting of radial outflow compressor rotor, combustor, radial inflow turbine, and a central exhaust thrust nozzle. With the help of my patent attorney, Dr. E. Wiegand, a thorough patent search was made. A number of interesting aeropropulsion systems without a propeller were found, but we did not come across the earlier patents of Lorin, Guillaume, and Frank Whittle. (I learned for the first time about one of Frank Whittle's patents in early 1937 when the German Patent Office held one of his patents and one patent of the Swedish corporation Milo, against some of my patent claims.)

My main problem was finding support for my turbojet ideas. A good approach, it seemed to me, was to first build a model. This model should be able to demonstrate the aerodynamic functions at very low-performance runs. The tip speed of this model was a little over 500 ft/s. Of course, I never considered high-power demonstration runs for two reasons. The cost for building such an apparatus could easily be a factor of 10 or 20 times greater than that for building a low-speed model. Also, a test facility would be required for high-performance test or demonstration runs. I knew a head machinist in an automobile repair shop, Max Hahn, to whom I showed the sketches of my model. He made many changes to simplify the construction, which greatly reduced the cost. The model was built at my expense by Hahn in 1935 (Fig. 9).

In mid-1935, I had completed my doctoral thesis and oral examination and had received my diploma in November 1935. I continued working in Prof. Pohl's institute and discussed with him my project "aircraft propulsion." He was interested in my theoretical write-up. Although my project did not fit Pohl's institute, he was extremely helpful to me. He let me test the model engine in the backyard of his institute and gave me instrumentation and an electric starting motor. Because the combustors did not work, the model did not run without power from the starting motor. Long, yellow flames leaked out of the turbine. It looked more like a flame thrower than an aircraft gas turbine.

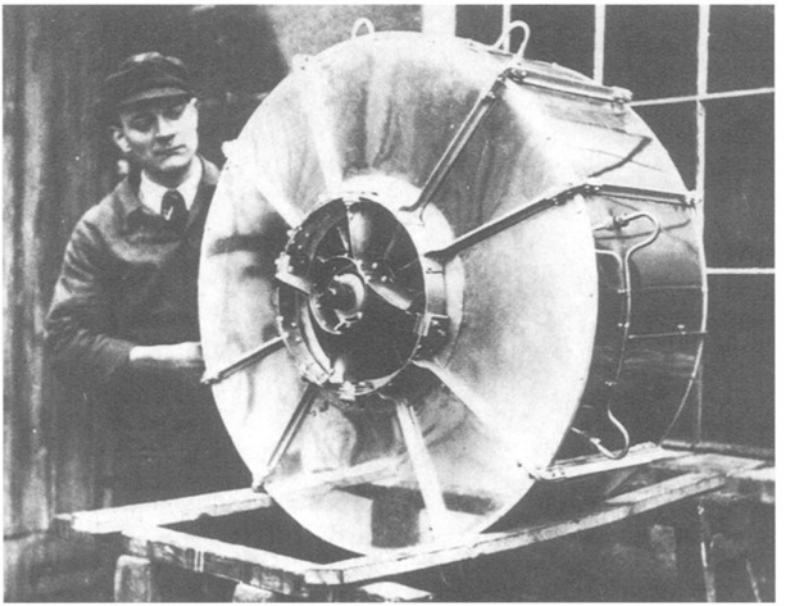

Fig. 9 Max Hahn with model engine. (National Air and Space Museum.)

I asked Prof. Pohl to write me a letter of introduction to Ernst Heinkel, the famous pioneer of high-speed aircraft and sole owner of his company. Professor Pohl actually wrote a very nice letter of recommendation. I had chosen Heinkel because he had the reputation of being an unconventional thinker obsessed with the idea of high-speed aircraft. Intuitively, I also felt that an aircraft engine company would not accept my turbine project. I learned later that my intuition was absolutely right. Today, I am convinced no one except Heinkel (see Fig. 10) would have supported my jet ideas at that time. Heinkel invited me to his home on the evening of March 17, 1936, to explain the jet principle to him. He, in turn, gave me a view of his plan. He wanted the jet development to be apart from the airplane factory. For this purpose, he intended to construct a small, temporary building near the Warnow River. I was very enthusiastic about this idea since it gave me a feeling of freedom and independence from the other part of the company and an assurance of Heinkel's confidence in me. Also, he strongly emphasized that he himself wanted to finance the entire jet development without involvement of the German Air Ministry. Finally, he explained to me that he had arranged a meeting between me and his top engineers for the next morning.

On March 18, 1936, I met with a group of 8 to 10 Heinkel engineers and explained my jet propulsion thoughts. Although they saw many problems, specifically with the combustion, they were not completely negative. Heinkel called me to a conference at the end of March. He pointed out that several uncertainties, specifically the combustion problems, should be solved before the gas

Fig. 10 Ernst Heinkel (left) and Hans von Ohain (right). (National Air and Space Museum.)

turbine development could be started. He wanted me to work on this problem and to report to him all the difficulties I might encounter. He offered me a kind of consulting contract that stated that the preliminary work (combustor development) could probably be completed in about two months. If successful, the turbojet development would then be started, and I would receive a regular employment contract. I signed this contract on April 3, 1936, and would start working in the Heinkel Company on April 15.

The first experiments with the model in early 1936 had convinced me that the volume of the combustion chambers was far too small for achieving a stable combustion. This was later substantiated in a discussion with combustion engineers at an industrial exhibit. I found a simple way to correct this condition. Cycle analysis of my model clearly showed that for high turbine inlet temperatures, such as 700°C and higher, a centrifugal compressor with a radial inflow turbine was most suitable as a basis for combustor development. My greatest problem was how to develop a functioning combustor in a few months. In my judgment, such a development would need at least six months, more likely one year, while Heinkel's estimate was two months. I had grave doubts whether Heinkel would endure such a long development time without seeing any visible progress, such as an experimental jet engine in operation. However, to avoid any combustor difficulties, I was considering a hydrogen combustor system with a nearly uniform turbine inlet temperature distribution. This hydrogen combustor system should be designed so that it could be built without any risk or need for preliminary testing.

My idea was to separate the compressor and turbine on the rotor by a shaft and to employ an annular connecting duct from the exit of the compressor diffuser to

the inlet of the turbine. Within this annular duct, I wanted to place a row of hollow vanes (about 60). These hollow vanes would have blunt trailing edges with many small holes through which hydrogen gas jets would be discharged into the air wakes behind the blunt trailing edges. In this way, the hydrogen combustion would be anchored at the blunt trailing edges of the hollow vanes. I was absolutely certain this combustor system would successfully function without any development or preliminary testing. I was also certain that no pretesting or development was necessary for the simple radial-flow turbomachinery. Testing of the hydrogen demonstrator engine (Fig. 11) showed that my judgment was correct on both points.

By mid-May 1936 I had nearly completed the layout of the hydrogen demonstrator engine. To build this engine was, for me, most important, not only for quick achievement of an impressive demonstration of the jet principle, but also for very significant technical reasons:

1) One reason was to obtain a solid basis for the design of the flight engine and the development of the liquid-fuel combustor, which should be started as a parallel development as soon as possible.

2) To achieve this solid basis, the hydrogen engine was the surest and quickest way when one does not have compressor and turbine test stands.

3) The anticipated step-by-step development approach: First testing the compressor-turbine unit with the "no-risk" hydrogen combustor and then

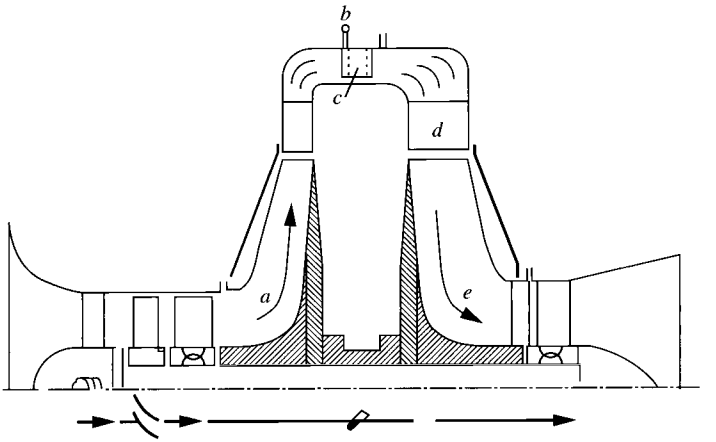

RADIAL TURBOJET (He S-1)
WITH HYDROGEN
(Built in 1936; tested in April 1937)

Radius of rotor-1 ft
Thrust-250 lb
10,000 rpm

Fig. 11 Von Ohain's hydrogen demonstrator engine.

using the tested turbomachine for exploring its interaction with the liquid-fuel combustor system seemed to be good protection against time-consuming setbacks.

Now came the greatest difficulty for me: How could I convince Heinkel that first building a turbojet with hydrogen gas as fuel would be a far better approach than trying to develop a liquid-fuel combustor under an enormous time pressure? According to my contract, of course, I should have worked on the liquid-fuel combustor with the (impossible) goal of having this development completed by June 1936. I briefly explained to Heinkel my reasons for the hydrogen engine and emphasized this engine would be a full success in a short time. I was well prepared to prove my point in case Heinkel wanted me to discuss this matter in a conference with his engineers. Surprisingly, Heinkel asked only when the hydrogen demonstrator could run. My shortest time estimate was half a year. Heinkel was not satisfied and wanted a shorter time. I told him that I had just heard that Wilhelm Gundermann and Max Hahn would work with me, and I would like to discuss the engine and its time schedule with them. So, Heinkel had agreed with my reasons to build the hydrogen jet demonstrator first.

About a week after my discussion with Heinkel, I joined Gundermann and Hahn in their large office. I showed them the layout of the hydrogen engine. Gundermann told me he had attended my presentation to the group of Heinkel's leading engineers in March 1936. He was surprised that I departed from the liquid-fueled turbojet program. I explained my reasons and also told about Heinkel's strong desire to have the hydrogen engine built in less than half a year. After studying my layout, both men came to the conclusion that it would not be possible to build this engine in less than six months, perhaps even longer. Gundermann, Hahn, and I began to work as an excellent team.

The engine was completed at the end of February 1937, and the start of our demonstration program was in the first half of March, according to Gundermann's and my recollections. The first run is clearly engraved in my memory: Hahn had just attached the last connections between engine and test stand; it was after midnight, and we asked ourselves if we should make a short run. We decided to do it! The engine had a 2-hp electric starting motor. Hahn wanted to throw off the belt-connecting starter motor and hydrogen engine if self-supporting operation was indicated. Gundermann observed the exhaust side to detect possible hot spots—none were visible. I was in the test room. The motor brought the engine to somewhat above 2000 rpm. The ignition was on, and I opened the hydrogen valve carefully. The ignition of the engine sounded very similar to the ignition of a home gas heating system. I gave more gas, Hahn waved, the belt was off, and the engine now ran self-supporting and accelerated very well. The reason for the good acceleration probably was twofold: the relatively low moment of inertia of the rotor and the enormously wide operational range of the hydrogen combustion system. We all experienced a great joy that is difficult to describe. Hahn called Heinkel, and he came to our test stand about 20 minutes later, shortly before 1:00 a.m. We made a second demonstration run. Heinkel was enthused—he congratulated us and emphasized that we should now begin to build the liquid-fuel engine for flying.

The next day and until the end of March, Heinkel began to show further demonstration runs to some of his leading engineers and important friends. The next day following our "night show," Heinkel visited us with Walter and Siegfried Guenther (his two top aerodynamic designers) for a demonstration run. They were very impressed and asked me about the equivalent horsepower per square meter. I replied, "A little less than 1000," but hastened to add that the flight engine would have more than 2500 hp/m^2 because of the much greater tip speed and greater relative flow cross sections. During April, we conducted a systematic testing program.

After the first run of the hydrogen engine, Heinkel ordered his patent office to apply for patents of the hydrogen engine. Because of earlier patents, the only patentable item was my hydrogen combustion system.

I became employed as division chief, reporting directly to Heinkel, and received an independent royalty contract, as I had desired. An enormous amount of pressure was now exerted by Heinkel to build the flight engine.

During the last months of 1937, Walter and Siegfried Guenther began with predesign studies of the first jet-propelled aircraft (He-178) and specified a static thrust of 1100 lb for the flight engine (He.S3). The aircraft was essentially an experimental aircraft with some provisions for armament.

In late 1937, while I was working on different layouts of the flight engine, Max Hahn showed me his idea of arranging the combustor in the large unused space in front of the radial-flow compressor. He pointed out that this would greatly reduce the rotor length and total weight. Hahn's suggestion was incorporated into the layout of the flight engine (see Fig. 12). In early 1938, we had a well-functioning annular combustor for gasoline. The design of the flight engine was frozen in the summer of 1938 to complete construction and testing by early 1939.

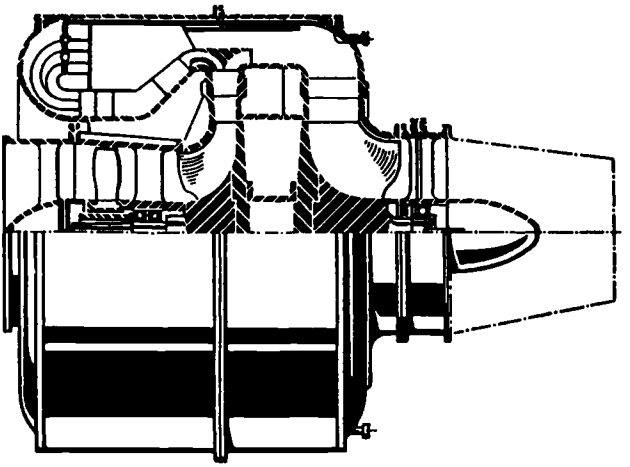

Fig. 12 1937 design of the He.S3 turbojet engine.

In spring 1939, aircraft and engine were completed, but the engine performance was too low: about 800-lb thrust, while a thrust of 1000–1100 lb was desirable to start the aircraft from Heinkel's relatively short company airfield. We made several improvements, mostly optimizing the easily exchangeable radial cascades of the compressor-diffuser and turbine stator. In early August, we had reached 1000 lb of thrust. We made only several one-hour test runs with the flight engine. However, upon suggestion of the Air Ministry, we completed a continuous 10-hour test run with a rotor that was not used for flight tests.

On August 27, 1939, the first flight of the He-178 with jet engine He.S3B was made with Erich Warsitz as pilot (Fig. 13). This was the first flight of a turbojet aircraft in the world. It demonstrated not only the feasibility of jet propulsion, but also several characteristics that had been doubted by many opponents of turbojet propulsion:

1) The flying engine had a very favorable ratio of net power output to engine weight—about 2 to 3 times better than the best propeller/piston engines of equal thrust power.

2) The combustion chambers could be made small enough to fit in the engine envelope and could have a wide operational range from start to high altitude and from low to high flight speed.

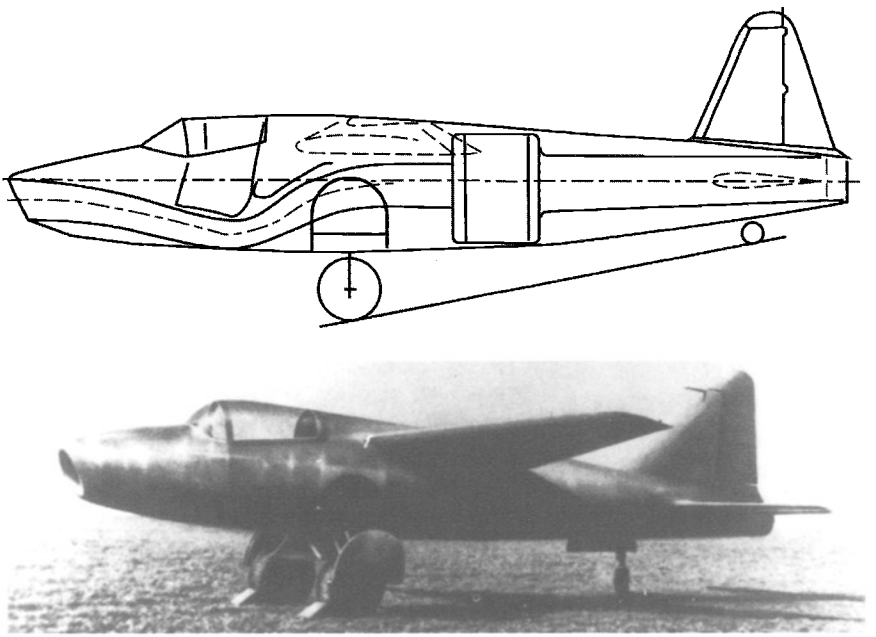

Fig. 13 The world's first jet-powered aircraft, the Heinkel He-178, was powered by the von Ohain–designed He.S3B turbojet engine. (National Air and Space Museum.)

The advantages of developing a flight demonstration turbojet in Heinkel's aircraft company were unique. Among the advantages were complete technical freedom, lack of importance attached to financial aspects, no government requirements, and no time delays; the aircraft was, so to speak, waiting for the engine. These great advantages were true only for the initial phases of jet engine development up to the first flight demonstrator. For making a production engine, however, enormous disadvantages included complete lack of experts in fabrication (turbomachinery, etc.), materials, research (turbines), accessory drives, control systems, no machine tools or component test stands, etc. Heinkel was very aware of this situation. His plan was to hire engineers from the aircraft engine field and to purchase an aircraft engine company.

Other Early Turbojet Developments in Germany

The following events developed at the same time, which was of great importance for the early phases of the turbojet evolution:

1) Professor Herbert Wagner privately started an aircraft gas turbine development project.
2) The Air Ministry became aware of Heinkel's turbojet project in 1938 and exerted a strong influence on the engine industry to start turbo development projects.
3) Heinkel purchased an aircraft engine corporation and received a contract for development and production of a high-performance turbojet engine.

In 1934, Wagner conceived the idea of an axial-flow propeller gas turbine while he was a professor of aeronautics in Berlin and formed a corporation to pursue these ideas. (I heard about Wagner's project for the first time in spring of 1939.) By introducing a design parameter that was the ratio of propeller power input to total net power output, he had conceived a gas turbine engine that was a cross between a turbojet and a propeller gas turbine.

Wagner first explored what would happen if the propeller power input was 50% of the total power output. This condition was favorable for long-range transport. Then in 1936, he investigated the "limiting case" of zero propeller power input, which constituted a turbojet. This engine was of great interest for high-speed aircraft because of its light weight.

The unique feature of Wagner's design was the utilization of 50% reaction turbomachinery (or *symmetric blading*). A compressor with 50% reaction blading has the greatest pressure ratio and efficiency for a given blade approach Mach number; but the design is difficult because of the inherently strong three-dimensional flow phenomena. This problem was solved by one of Wagner's coworkers, Rudolf Friedrich.

At the time Wagner was working on the turbojet engine, in about 1936, he became technical director of the Junkers Airframe Corporation in Dessau. The jet engine work was conducted in the Junkers machine factory, which was located in Magdeburg. The head of his turbojet development was Max A. Mueller, his former "first assistant."

In late fall, 1938, Wagner had decided to leave the Junkers Corporation, but he wanted to obtain funds from the Air Ministry for the continuation of his turbojet development work. The Air Ministry agreed to Wagner's request under the

condition that the jet development be continued at the Junkers Aircraft Engine Company in Dessau. This seemed to be acceptable to Herbert Wagner. However, his team of about 12 very outstanding scientists and engineers (among them the team leader, Max A. Mueller, and the highly regarded Dr. R. Friedrich) refused to join the Junkers Aircraft Engine Company under the proposed working conditions. Heinkel made them very attractive work offers that convinced Wagner's former team to join the Heinkel Company. Heinkel added Wagner's axial turbojet to his development efforts (designated as the He.S30). Thus, in early 1939, Heinkel had achieved one goal—to attract excellent engineers for his turbojet development.

In early 1938, the Air Ministry had become aware of Heinkel's private jet propulsion development. The Engine Development Division of the Air Ministry had a small section for special propulsion systems that did not use propellers and piston engines, but rather used special rockets for short-time performance boost or takeoff assistance. Head of this section was Hans Mauch. He asked Heinkel to see his turbojet development in early summer 1938, more than one year before the first flight of the He-178. After he saw Heinkel's hydrogen turbojet demonstrator in operation and the plans for the flight engine, he was very impressed. He thanked Heinkel for the demonstration and pointed out that turbojet propulsion was, for him, a completely *unknown* and new concept. He soon became convinced that the turbojet was the key to high-speed flight. He came, however, to the conclusion that Heinkel, as an airframe company, would never be capable of developing a production engine because the company lacked engine test and manufacturing facilities and, most of all, it lacked engineers experienced in engine development and testing techniques. He wanted the Heinkel team to join an aircraft engine company (Daimler-Benz) and serve as a nucleus for turbojet propulsion development. Furthermore, he stated that Ernst Heinkel should receive full reimbursement and recognition for his great pioneering achievements. Heinkel refused.

In the summer of 1938, Mauch met with Helmut Schelp, who was in charge of jet propulsion in the Research Division of the Air Ministry. Mauch invited Schelp to join him in the Engine Development Division. Schelp accepted the transfer because he saw far greater opportunities for action than in his Research Division. In contrast to Mauch, Schelp was very well aware of turbojet propulsion and was convinced about its feasibility. He was well versed in axial and radial turbomachinery and with the aerothermodynamic performance calculation methods of turbojet, ramjet, and pulse jet. Like Mauch, he was convinced of the necessity that the aircraft engine companies should work on the development of turbojet engines. However, Schelp did not see a necessity for Heinkel to discontinue his jet engine development. He saw in Heinkel's progress a most helpful contribution for convincing the engine industry to also engage in the development of turbojets, and for proving to the higher echelons of the Air Ministry the necessity of launching a turbojet development program throughout the aircraft engine companies.

Schelp worked out the plans and programs for jet propulsion systems, decided on their most suitable missions, and selected associated aircraft types. Schelp's goal was to establish a complete jet propulsion program for the German aircraft engine industry. He also talked with Hans Antz of the Airframe Development Division of the Air Ministry to launch a turbojet fighter aircraft development as

soon as possible. This became the Me-262. To implement the program, Mauch and Schelp decided to visit aircraft engine manufacturers—Junkers Motoren (Jumo), Daimler-Benz, BMW Flugmotorenbau, and Bradenburgische Motorenweke (Bramo). Mauch and Schelp offered each company a research contract to determine the best type of jet engine and its most suitable mission. After each study was completed and evaluated, a major engine development contract might be awarded.

The industry's response to these proposals has been summed up by Schlaifer in *Development of Aircraft Engines, and Fuels*: "The reaction of the engine companies to Mauch's proposals was far from enthusiastic, but it was not completely hostile."**

Anselm Franz and Hermann Oestrich were clearly in favor of developing a gas turbine engine. Otto Mader, head of engine development at Jumo, made two counter arguments against taking on turbojet propulsion developments. He said, first, that the highest priority of Jumo was to upgrade the performance of its current and future piston engines, and that this effort was already underpowered; and, second, Jumo did not have workers with the necessary expertise in turbomachine engine development! After several meetings between Mader and Schelp, however, Mader accepted the jet engine development contract and put Franz in charge of the turbojet project. At that time, Dr. Anselm Franz was head of the supercharger group. Daimler-Benz completely rejected any work on gas turbine engines at that time. Meanwhile, BMW and Bramo began a merger, and after it was finalized, Hermann Oestrich became the head of the gas turbine project for BMW.

These developments show that the aircraft engine industries in Germany did not begin to develop jet engines on their own initiative, but rather on the initiative and leadership of Mauch, and specifically of Helmut Schelp of the technical section of the German Air Ministry. Without their actions, the engine companies in Germany would not have begun development work on turbojet propulsion. The net result of Schelp's planning efforts was that two important turbojet engine developments were undertaken by the German aircraft engine industry, the Junkers Engine Division and BMW.

The Jumo 004 (shown in Fig. 14), developed under the leadership of Anselm Franz, was perhaps one of the truly unique achievements in the history of early jet propulsion development leading to mass production, for the following reasons:

1) It employed axial-flow turbomachinery and straight throughflow combustors.

2) It overcame the nonavailability of nickel by air-cooled hollow turbine blades made out of sheet metal.

3) The manufacturing cost of the engine amounted to about one-fifth that of a propeller/piston engine having the equivalent power output.

4) The total time from the start of development to the beginning of large-scale production was a little over four years (see Table 1).

5) It incorporated a variable-area nozzle governed by the control system of the engine, and model 004E incorporated afterburning.

**Schlaifer, R., and Heron, S. D., *Development of Aircraft Engines, and Fuels*, Pergamon Press, New York, 1970; reprint of 1950 ed.

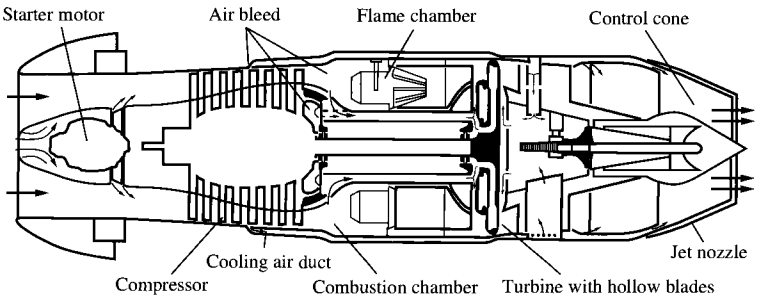

Fig. 14 Drawing of Jumo 004B turbojet engine showing air cooling system [thrust = 2000 lb, airflow = 46.6 lb/s, pressure ratio = 3.14, turbine inlet temperature = 1427°F, fuel consumption = 1.4 (lb/h)/h, engine weight = 1650 lb, diameter = 30 in., length = 152 in., efficiencies: 78% compressor, 95% combustor, 79.5% turbine].

The preceding points reflect the design philosophy of Dr. A. Franz for the Jumo 004, which was lowest possible development risk, shortest development time, dealing with a complete lack of heat-resistant materials, and minimizing manufacturing cost. From this design philosophy, it is understandable that the Jumo 004 engine, while fully meeting the requirements, did not have the highest overall performance compared to some contemporary experimental axial-flow engines, such as the He.S30 and others. If it had been possible for the Jumo 004 to employ heat resistant materials, then the engine thrust, the thrust/weight ratio, and the efficiency would have been increased substantially. Also the engine life could have been drastically increased from about 25 h to well over 100 h. However, because the combat life of a German fighter was well below 25 h, the economical optimum could tolerate a short engine life and the avoidance of nickel. Furthermore, to avoid any development risk or time delay, the compressor type chosen for the Jumo 004 was one where essentially all the static pressure increase occurs in the rotor and none in the stator (a free-vortex type of compressor having constant axial velocity over the blade span). Although such a compressor type does not have the best performance, at that time it was best understood. The previously described points show that the Jumo 004 represented an outstanding compromise between engine performance, the existent design constraints due to materials shortage, the need for short development time, and earliest possible production.

Table 1 Jumo 004 development and production schedule

Start of development	Fall 1939
First test run	Oct. 11, 1940
First flight in Me-262	July 18, 1942
Preproduction	1943
Beginning of production	Early 1944
Introduction of hollow blades	Late 1944
About 6000 engines delivered	May 1945

The BMW 003 turbojet engine, which was developed under the leadership of Hermann Oestrich, was also a resounding success. Because its thrust was smaller than that of the Jumo 004, it was ideally suited for the He-162. After World War II, Oestrich and a group of prominent scientists and engineers from Germany went to France and helped lay the foundation for France's turbojet industry.

Now I would like to go back to the end of 1939, when Heinkel began to make plans for buying an engine company. After the first flight of the He-178 on August 27, 1939, Heinkel invited high officials of the Air Ministry to see a flight demonstration of the He-178. This demonstration took place on November 1, 1939. At that occasion, Heinkel offered the development of a jet fighter, the He-280, which had two outboard engines under the wing. Heinkel received a contract for this aircraft in early 1940. In addition, I believe Udet and Heinkel had made an agreement that Heinkel would get official permission to buy the Hirth Engine Company, if the first flight of the He-280 could be demonstrated by April 1941.

The He-280 had severe restrictions with respect to distance of the engine nacelle from the ground. It actually was designed for the axial engine He.S30 (the Wagner turbojet engine). It appeared, however, unlikely that the He.S30 would be ready in time. On the other hand, it was impossible to use an engine of the He.S3B type, which had powered the He-178, because the diameter of this engine type would have been far too large. Under these conditions, I could see only one possible solution for succeeding in time, and this solution had extreme high risk. I employed a radial rotor similar to that of the He.S3B and combined it with an axial (adjustable) vane diffuser and a straight throughflow annular combustor.

The company designation of this engine was He.S8A. We had only about 14 months for this development, but we were lucky—it worked surprisingly well, and Heinkel could demonstrate the first flight of the He-280 on April 2, 1941. The government pilot was Engineer Bade. Earlier flights in late March were done by Heinkel's test pilot, Fritz Schaefer.

A few days after this demonstration, Heinkel obtained permission to buy the Hirth Motoren Company in Stuttgart, which was known for its excellent small aircraft engines. This company had outstanding engineers, scientists, machinists, precision machine tools, and test stands. Heinkel relocated the development of the He.S30 to his new Heinkel-Hirth engine company to make use of the excellent test and manufacturing facilities. In the summer of 1942, the He.S30 was ready for testing. It performed outstandingly well. The continuous thrust was about 1650 lb. From a technical standpoint, this engine had by far the best ratio of thrust to weight in comparison to all other contemporary engines. The superiority of the He.S30 was, in large part, the result of its advanced 50% reaction degree axial-flow compressor, designed by Dr. R. Friedrich. However, the success of the He.S30 came too late. The He-280 had been thoroughly tested. While it was clearly superior to the best contemporary propeller/piston fighter aircraft, the He-280 had considerably lower flight performance than the Me-262 with respect to speed, altitude, and range. Also, the armament of the He-280 was not as strong as that of the Me-262. For these reasons, the He.S8 and the He.S30 were canceled in the fall of 1942; the He-280 was officially

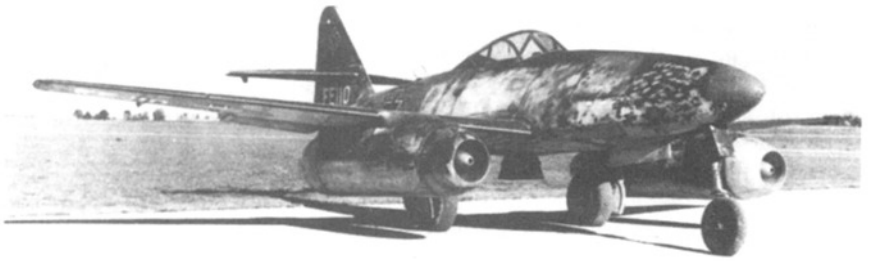

Fig. 15 Messerschmitt Me-262 jet fighter. (National Air and Space Museum.)

canceled in early 1943. The Me-262 (Fig. 15) went on to become the first operational jet fighter powered by two Jumo 004B turbojet engines. The Air Ministry did give full recognition to the excellence of the 50% reaction degree compressor type as most suitable for future turbojet developments.

Thus, in the fall of 1942, Heinkel had lost his initial leadership in jet aircraft and turbojet engines. Ironically, this happened when he had just reached his goal of owning an aircraft engine company with an outstanding team of scientists and engineers. It was the combined team of the original Hirth team, the Heinkel team, and Wagner's team. These conditions made Heinkel fully competitive with the existent aircraft engine industry. The Air Ministry had recognized the excellence of Heinkel's new team and facilities. Helmut Schelp, who in the meantime had become the successor of Hans Mauch, was in favor of the Heinkel-Hirth Company's receiving a new turbojet engine development contract. He clearly foresaw the need for a strong engine for the advanced Me-262, the Arado-234, the Junkers-287, and others. This new engine was supposed to have a thrust of nearly 3000 lb with a growth potential to 4000 lb as well as a high pressure ratio for improving the fuel economy. We began working on the He.S011 engine in the fall of 1942. The He.S011 was an axial-flow design with 50% reaction degree compressor blading, similar to that designed by Dr. Friedrich, and a two-stage, axial-flow, air-cooled turbine. Note that Helmut Schelp not only had established the performance specifications, but also had contributed to the overall design with excellent technical input and suggestions pertaining to the advanced diagonal inducer stage, the two-stage air-cooled turbine, and the variable exhaust nozzle system.

I was in charge of the He.S011 development, while the local director of the Heinkel-Hirth plant, Curt Schif, was in charge of He.S011 production. The top engineer of the Hirth Corporation was Dr. Max Bentele. He was well known for his outstanding knowledge in dealing with blade vibration problems. Upon special request of the Air Ministry, he had solved the serious turbine blade vibration problems of the Jumo 004 in the summer of 1943.

Dr. Bentele was responsible for the component development of the He.S011. After considerable initial difficulties, he achieved excellent performance

characteristics of compressor and turbine that made it possible, by the end of 1944, for the performance requirements of the 011 to be met or surpassed. He also contributed to the preparation for production of the 011, which was planned to start in June 1945. The end of World War II, of course, terminated the production plan before it had started. Only a few He.S011 engines are in existence today, and they are exhibited in several museums in the United States and Great Britain.

In other countries, such as Russia and Japan, interesting developments in the field of propeller gas turbines and turbojets had also been undertaken. It is, however, not sufficiently known to what extent these developments were interrelated with, or influenced by, the previously described jet developments and what their development schedules had been.

In summary, at the end of the 1930s and in the first half of the 1940s, turbojet propulsion had come into existence in Europe and the United States. It had been demonstrated that the turbojet is, for high-speed flight, uniquely superior to the propeller/piston engines because of the following two major characteristics:

1) The ratio of power output to weight of the early turbojets was at least 2 or 3 times greater than that of the best propeller/piston engines. This is one necessary condition of propulsion systems for high-speed flight and good maneuverability.

2) Because, in the turbojet, the propeller is replaced by ducted turbomachinery, the turbojet is inherently capable as a propulsion system of high subsonic and supersonic flight speeds.

In the following, it will be discussed how the turbojet engine progressed to the performance capabilities of today.

Evolution of Airbreathing Turbopropulsion Systems to the Technology Level of Today

The early turbojets were used as propulsion systems for high-speed fighter and reconnaissance aircraft. For these applications, the early turbojets (because of their superior power/weight ratios) were far more suitable propulsion systems than the traditional propeller/piston engines. However, the early turbojets were not suitable for those application areas where greatest fuel economy, highest reliability, and a very long endurance and service life were required. For making airbreathing turbojet propulsion systems applicable for all types of aircraft, ranging from helicopters to high-speed, long-range transports, the following development goals were, and still are, being pursued:

1) Higher overall efficiency (i.e., the product of thermodynamic and propulsion efficiencies),
2) Larger-power-output engines,
3) Larger ratios of power output to engine weight, volume, and frontal area,
4) Greater service life, endurance, and reliability,
5) Strong reduction of adverse environmental exhaust gases,
6) Reduced noise.

To achieve these goals, parallel research and development efforts were undertaken in areas such as

1) Fundamental research in combustion processes, development, and technology efforts for increasing specific mass flow through combustors and reducing the total pressure drop; and for achieving nearly 100% combustion efficiency with a more uniform temperature profile at combustor exit.
2) Minimizing the excitation of vibrations (including aeroelastic effects) and associated fatigue phenomena.
3) Continuous improvement of the structural design and structural materials, such as composite materials, heat- and oxidation-resistant alloys and ceramics.
4) Increasing the turbine temperature capability by improving air cooling effectiveness. Also increasing the polytropic turbine efficiency.
5) Improvement of the compressor with respect to greater specific mass flow, greater stage pressure ratio, greater overall pressure ratio, and greater polytropic efficiency.
6) Advanced controllable-thrust nozzles and their interactions with the aircraft.
7) Advanced control systems to improve operation of existing and new engines.

All of these research and development areas were, and still are, of great importance for the progress in turbopropulsion systems; however, the compressor can perhaps be singled out as the key component because its advancement was a major determining factor of the rate of progress in turbo engine development. This will become apparent from the following brief description of the evolution of the turbopropulsion systems.

Development of High-Pressure-Ratio Turbojets

The first step to improve the early turbojets was to increase their overall efficiency. To do this, it was necessary to increase the thermodynamic cycle efficiency by increasing the compressor pressure ratio. The trend of compressor pressure ratio over the calendar years is shown in Table 2.

In the early 1940s, it was well understood that a high-pressure-ratio (above 6:1), single-spool, fixed-geometry compressor can operate with good efficiency only at the design point, or very close to it. The reason is that at the design

Table 2 Trend in compressor pressure ratios

Calendar years	Compressor pressure ratio
Late 1930 to mid-1940	3:1 to about 5:1
Second half of 1940s	5:1 and 6:1
Early 1950	About 10:1
Middle to late 1960s	20:1 to about 25:1
End of century (2000)	30:1 to about 40:1

point, all compressor stages are matched on the basis of the compressibility effects. Consequently, under off-design conditions where the compressibility effects are changed, the stages of a high-pressure-ratio compressor are severely mismatched, resulting in a very low off-design efficiency. For example, at an operational compressor rpm (which would be substantially below the design rpm), the compressibility effects are small. Under such off-design conditions, the front stages tend to operate under *stalled* conditions, while the last stages tend to work under *turbining* conditions. Such compressor characteristics are unacceptable for the following reasons:

1) There are enormous difficulties in starting such an engine.
2) Very poor overall efficiency (or poor fuel economy) exists under part-load operation.
3) Very low overall efficiency exists at high supersonic flight speed (because the corrected rpm is very low as a result of the high stagnation temperature of the air at the compressor inlet).

By the end of the 1940s and early 1950s, excellent approaches emerged for the elimination of these shortcomings of simple high-pressure-ratio compressors. Pratt & Whitney, under the leadership of Perry Pratt, designed a high-pressure-ratio jet engine (the J57) with a *dual-rotor* configuration. (In later years, triple-rotor configurations were also employed.) The ratio of rpm values of the low- and high-pressure spools varies with the overall pressure ratio and, in this way, alleviates the mismatching effects caused by the changes in compressibility. At approximately the same time, Gerhard Neumann of General Electric conceived a high-pressure-ratio, single-spool compressor having automatically controlled *variable stator blades.* This compressor configuration was also capable of producing very high pressure ratios because it alleviated the mismatching phenomena under off-design operation by stator blade adjustment. In addition, the controlled variable-stator-compressor offers the possibility of a quick reaction against compressor stall. The variable-stator concept became the basis for a new, highly successful turbojet engine, the J79, which was selected as the powerplant for many important supersonic Air Force and Navy aircraft. A third possibility to minimize mismatching phenomena was *variable front-stage bleeding*, which was employed in several engines.

Before I continue with the evolution of the turbo engines toward higher overall efficiencies, a brief discussion about the research and development efforts on compressor bladings and individual stages is in order. Such efforts existed to a small degree even before the advent of the turbojet (in Switzerland, Germany, England, and other countries). However, in the mid-1940s, those research efforts began to greatly intensify after the turbojet appeared. It was recognized that basic research and technology efforts were needed to continuously increase 1) stage pressure ratio and efficiency and 2) mass throughflow capability.

Very significant contributions had been made by universities, research institutes, and government laboratories (NACA, later NASA; Aero Propulsion Laboratory, and others), and industry laboratories. Many outstanding research results were obtained from universities in areas of rotating stall, three-dimensional and nonsteady flow phenomena and transonic flow effects, novel flow visualization techniques for diagnostics (which identified flow regions having improvement possibilities), understanding of noise origination, and many others.

Two examples where government laboratories had achieved very crucial advancements that were later adapted by industry were the following: In the early 1950s, the NACA Lewis Research Center, under the leadership of Abe Silverstein, advanced compressor aerodynamics to transonic and supersonic flow, critical contributions for increasing the compressor-stage pressure ratio. He initiated a large transonic and supersonic compressor research program. Many in-depth studies furnished information for utilizing this new compressor concept. Later, the Air Force Propulsion Laboratory, under the leadership of Arthur Wennerstrom, conducted advanced compressor research and introduced a very important supersonic compressor concept, which was particularly applicable for front stages because it solved the most difficult combined requirements of high mass flow ratio, high pressure ratio, high efficiency, and broad characteristics.

The continuous flow of research and technological contributions extended over the last four decades and is still going on. The total cost may have been several hundred million dollars. Some of the results can be summarized as follows: The polytropic compressor efficiency, which was slightly below 80% in 1943, is now about 92%; the average stage pressure ratio, which was about 1.15:1 in 1943, is now about 1.4:1 and greater; the corrected mass flow rate per unit area capability grew over the same time period by more than 50%.

The improvement in compressor efficiency had an enormous impact on engine performance, specifically on the overall engine efficiency. The substantially increased stage pressure ratio and the increased corrected mass flow rate per unit area capability resulted in a substantial reduction of engine length, frontal area, and weight-per-power output.

Let us now return to the 1950s. As previously stated, the new turbojets employing a dual-rotor configuration or controlled variable-stator blades were capable of substantially higher pressure ratios than the fixed-geometry, single-spool engines of the 1940s. Engine cycle analysis showed that the high power-per-unit mass flow rate needed for the advanced engines required higher turbine inlet temperatures. This requirement led to continuous major research efforts to achieve high-efficiency combustion with low pollution, to increase the effectiveness of turbine blade-cooling methods, and to improve the temperature capabilities of materials. Thus the turbojets of the 1950s had made substantial progress in thermodynamic efficiency and propulsive thrust per pound of inlet air per second. The latter characteristic means that the velocity of the exhaust gas jet had increased.

Development of High-Bypass-Ratio Turbofans

For supersonic flight speeds, the overall efficiency of these turbojets was outstanding. However, for high subsonic and transonic flight speeds (around 500–600 mph), the velocity of the exhaust gas jet was too high to obtain a good propulsive efficiency. Under these conditions, the *bypass engine* (also called *turbofan* or *fan-jet*) became a very attractive approach for improving the propulsive efficiency. The first fan-jets had a relatively small bypass ratio of about 2:1. (*Bypass ratio* is the ratio of mass flow bypassing the turbine to mass flow passing through the turbine.) In the early 1960s, the U.S. Air Force had established requirements for military transports capable of an extremely long

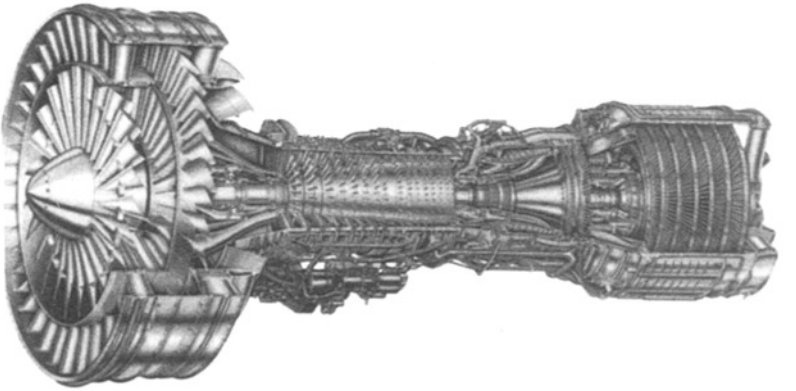

Fig. 16 The TF39 high-bypass-ratio turbofan engine used on the Lockheed C5 transport. (Courtesy of General Electric Aircraft Engines.)

range at high subsonic cruise speeds. Such requirements could be met only by employing propulsion systems of highest possible thermodynamic and propulsive efficiencies, which led to the following engine characteristics:

1) Very high compressor pressure ratios between 20:1 and 30:1, which could be achieved by combining the concepts of variable stator and dual rotor,
2) Very high turbine inlet temperatures,
3) Very high bypass ratios, around 8:1.

The first engine of this type was the TF39 (Fig. 16), a military transport engine developed by General Electric under the leadership of Gerhard Neumann. Four of the TF39 turbofan engines powered the Lockheed C5A.

The Air Force Propulsion Laboratory, under the leadership of Cliff Simpson, had played a key role in the establishment of these requirements. Simpson also succeeded in convincing the highest Air Force and Department of Defense echelons of the significance of this new type of airbreathing propulsion system, which he considered a technological breakthrough. (At that time, it was difficult to generate interest in advanced airbreathing propulsion system concepts, since the nation's attention was focused on rocket propulsion for space exploration.)

The advantages of the high-bypass-ratio turbofan engines can be summarized as follows:

1) High overall efficiency, resulting in a long flight range,
2) Strong increase in propulsive thrust at low flight speeds, which is important for takeoff, climbing, and efficient part-load operation,
3) Lower jet velocity, which leads to great noise reduction, and
4) Low fuel consumption, which reduces chemical emissions.

These characteristics had been demonstrated in the late 1960s and early 1970s. They also became of great interest for commercial aircraft and led to the development of the *widebody* passenger aircraft.

During the 1980s, the continuous flow of advanced technology of turbo engine components had brought a high degree of maturity to the various aircraft gas turbine engine types, such as the following: 1) the previously discussed high-bypass-ratio engines, 2) the low-bypass-ratio engines with afterburning for supersonic flight, and 3) the pure turbojet for high supersonic flight Mach numbers of approximately 3.

The small and medium aircraft shaft-power gas turbines also benefited enormously from the continuous improvement of turbomachinery technology. These small gas turbines are used in helicopters and subsonic propeller aircraft. The high power/weight ratio and the high thermodynamic efficiency of the advanced shaft-power gas turbine engines played a key role in the advancement of helicopters.

Future Potential of Airbreathing Jet Propulsion Systems

In the future, major advancement of airbreathing jet propulsion systems can be expected from

1) Evolutionary improvements of the established large-bypass-ratio turbofan engines for transonic flight speeds and the low-bypass-ratio turbofan, or pure turbojet engines, for supersonic flight speeds,
2) Improvements and new approaches to engine-airplane integration, and
3) New approaches to airbreathing propulsion systems for high supersonic and hypersonic flight speeds.

The evolutionary improvements of established engine types will result in greater fuel economy and better performance characteristics. By the end of the century, one can expect polytropic efficiencies of turbine and compressor of nearly 95%. Furthermore, one will see considerably increased single-stage pressure ratios; significantly higher turbine inlet temperatures resulting from better heat- and oxidation-resistant materials, and more effective blade-cooling methods; and much lighter structural designs and materials (composite materials). This technological progress may result in an overall engine efficiency increase of about 20% and in a weight reduction for given horsepower output by probably a factor of 2 and higher.

For the evolution of high-bypass-ratio engines at cruise speeds between 500 and 600 mph, the following trend is important; the greater the turbine inlet temperature and the higher the polytropic efficiencies of the compressor and the turbine, the higher the optimum pressure ratio of the gas turbine engine and the bypass ratio of the fan. In the future, this trend will lead to larger bypass ratios; hence, the fan shroud will become relatively large in diameter and will contribute substantially to the weight and external drag of the propulsion system. Several solutions are conceivable to alleviate this problem, but at this time it is not possible to predict the most promising approach.

One way is to eliminate the fan shroud by using an unshrouded fan (having a multiplicity of swept-back fan blades, see Fig. 17), also called a *prop-fan.* This configuration is currently in an experimental state and may become very important in the future for improving fuel economy. Another possibility

Fig. 17 PW-Allison 578DX propulsion system. (Courtesy of Allison Gas Turbine Division.)

may lie in the development of a transonic airframe configuration in which the large fan shrouds have a dual function: They contribute, in part, to the stability of the aircraft (horizontal and vertical stabilizer surfaces) while serving at the same time as a shroud for the fan. Finally, it may be conceivable that, in the future, a practical airframe and wing configuration can be developed that will be capable of extending a high lift/drag ratio to a flight speed regime that is very close to the speed of sound (a kind of well-known "supercritical" airframe configuration proposed by Whitcomb of NASA). If such an airframe configuration could be developed, the bypass ratio at these relatively high flight speeds would be substantially lower than that for flight speeds around 500 mph and, therefore, a shrouded fan would be most applicable.

Perhaps a most interesting question is: Can one expect a future supersonic passenger transport that is economically feasible in view of the progress of future transonic passenger transports? The general trend of the airplane lift/drag ratio is decreasing with increasing flight Mach number, while the overall efficiency of aeropropulsion systems increases with increasing flight Mach number. Currently, the lift/drag ratio of the Boeing 747 compared to that of the supersonic Concorde is about 3:1. In the future, the corresponding ratio may decrease to about 2:1, and the structural weight of the supersonic aircraft will greatly be improved. Such improvements may be the result of advancements in the aerodynamic shape, the structure, the structural airframe materials, and the best use of artificial stability. The overall efficiency of the supersonic flight engine can also be improved, including its capability of cruising subsonically with only one

engine. This is important in case one of the two engines fails. Under this condition, the mission must be completed at subsonic speed without requiring an additional fuel reserve. It appears that advanced supersonic-cruise aircraft systems have the potential to achieve these conditions and, thus, become economically acceptable in the future.

New Approaches to Engine–Airplane Integration

In general, the investigations of engine–airplane integration have the goal to avoid or minimize losses due to adverse interface phenomena between the engine inlet stream or exhaust jet and the air vehicle. However, many favorable effects can be achieved by properly integrating functions of the propulsion system with functions of the airplane. Historically, Prof. Ackeret (University of Zurich, Switzerland) had first suggested, in 1921, reaccelerating the boundary-layer air near the trailing edge of the wing. He showed that this method of producing the propulsive thrust can result in substantial gains in overall efficiency of the propulsion system. In the 1970s, various investigations had shown that similar results can be obtained by using momentum exchange of the high-pressure bypass air with the boundary-layer air.

Other uses of bypass air are to energize the boundary layer at proper locations of the wing to prevent boundary-layer separation and to increase the circulation around the wing (often called *supercirculation*). This method may become important for advanced short-takeoff-and-landing (STOL) applications. For future V/STOL applications, new methods of thrust vectoring and thrust augmentation may have very attractive possibilities. Also, bypass air may be used for boundary-layer suction and ejection in advanced laminar systems.

Airbreathing Propulsion Systems for High Supersonic and Hypersonic Speeds

In airbreathing propulsion systems, the combined compression by ram and turbo compressor is of great benefit to the thermodynamic propulsion process up to flight Mach numbers approaching 3. When the flight Mach number increases further, the benefits of the turbo compressor begin to decrease and the engine begins to operate essentially as a ramjet. When the flight Mach number exceeds about 3.5, any additional compression by a turbo compressor would be a disadvantage. Thus, if the engine operates best as a pure subsonic combustion ramjet, it fits in a flight Mach number regime from about 3.5 to 5. Beyond flight Mach numbers of about 6, the pressure and temperature ratios would be unfavorably high if the engine continued to operate as a subsonic combustion ramjet. The reasons are as follows:

1) High degree of dissociation of the combustor exhaust flow, reducing the energy available for exhaust velocity,

2) Pressures far too high for Brayton cycle operations or for the structure to withstand.

For these reasons, the cycle will be changed from a subsonic to a supersonic combustion ramjet, and hydrogen will be used as fuel because hydrogen has the greatest 1) combustion heat and fuel-air concentration range, 2) diffusion speed and reaction speed, and 3) heat-sink capabilities.

This supersonic combustion ramjet cycle is characterized by a reduction of the undisturbed hypersonic flight Mach number to a somewhat lower hypersonic Mach number with an increase in entropy, which should be as low as possible. The deceleration process must be chosen in such a manner that the increases in static pressure and entropy correspond to a high-performance Brayton cycle. The internal thrust generated by the exhaust gas must be larger than the external drag forces acting on the vehicle.

To minimize the parasitic drag of the ramjet vehicle systems, various external ramjet vehicle configurations have been suggested. However, theoretical and experimental investigations will be necessary to explore their associated aero-thermochemical problems.

For the experimental research, one may consider investigations using free-flight models or hypersonic wind tunnels with true temperature simulation. Historically, it may be of interest that many suggestions and investigations had been made as to how to achieve clean hypersonic airflows with true stagnation temperatures. I remember much work and many discussions with Dr. R. Mills, E. Johnson, Dr. Frank Wattendorf, and Dr. Toni Ferri about "air accelerator" concepts, which aimed to avoid flow stagnation and the generation of ultrahigh static temperatures and chemical dissociation.

Since the Wright brothers, enormous achievements have been made in both low-speed and high-speed airbreathing propulsion systems. The coming of the jet age opened up the new frontiers of transonic and supersonic flight (see Fig. 3). While substantial accomplishments have been made during the past several decades in the field of high supersonic and hypersonic flight (see Ref. 2), it appears that even greater challenges lie ahead.

For me, being a part of the growth in airbreathing propulsion over the past 60 years has been both an exciting adventure and a privilege. This foreword has given you a view of its history and future challenges. The following book presents an excellent foundation in airbreathing propulsion and can prepare you for these challenges. My wish is that you will have as much fun in propulsion as I have.

Hans von Ohain
German Inventor of the Jet Engine
December 14, 1911–March 13, 1998

Preface

This undergraduate text provides an introduction to the fundamentals of gas turbine engines and jet propulsion. These basic elements determine the behavior, design, and operation of the jet engines and chemical rocket motors used for propulsion. The text contains sufficient material for two sequential courses in propulsion: an introductory course in jet propulsion and a gas turbine engine components course. It is based on one- and two-course sequences taught at four universities over the past 25 years. The author has also used this text for a course on turbomachinery.

The outstanding historical foreword by Hans von Ohain (the German inventor of the jet engine) gives a unique perspective on the first 50 years of jet propulsion. His account of past development work is highlighted by his early experiences. He concludes with predictions of future developments.

The text gives examples of existing designs and typical values of design parameters. Many example problems are included in this text to help the student see the application of a concept after it is introduced. Problems are included at the end of each chapter that emphasize those particular principles. Two extensive design problems for the preliminary selection and design of a gas turbine engine cycle are included. Several turbomachinery design problems are also included.

The text material is divided into five parts:

1) Introduction to aircraft and rocket propulsion (Chapter 1),
2) Review of fundamentals (Chapter 2),
3) Rocket propulsion (Chapter 3),
4) Analysis and performance of airbreathing propulsion systems (Chapters 4–8),
5) Analysis and design of gas turbine engine components (Chapters 9 and 10).

Chapter 1 introduces the types of airbreathing and rocket propulsion systems and their basic performance parameters. Also included is an introduction to aircraft and rocket systems that reveals the influence that propulsion system performance has on the overall system. This material facilitates incorporation of a basic propulsion design problem into a course, such as new engines for an existing aircraft.

The fundamental laws of mass conservation, momentum, and thermodynamics for a control volume (open system), the properties of perfect gases, and compressible flow properties are reviewed in Chapter 2. New material on

analysis of one-dimensional gas dynamics [enthalpy-kinetic energy (H-K) diagram] is presented in Chapter 2 to help student understanding of engine cycles from scramjets to afterburning turbofans. Fundamentals of thermochemistry are presented for later use in analysis of chemical rockets in Chapter 3.

Chapter 3 presents the fundamentals of rocket propulsion. Emphasis in this chapter is on chemical propulsion (liquid and solid) with coverage of rocket motor performance. The chapter also covers requirements and capabilities of rocket propulsion.

The analysis of gas turbine engines begins in Chapter 4 with the definitions of installed thrust, uninstalled thrust, and installation losses. This chapter also reviews the ideal Brayton cycle, which limits gas turbine engine performance.

Two types of analysis are developed and applied to gas turbine engines in Chapters 5–8: parametric cycle analysis (thermodynamic design point) and performance analysis. The text uses the cycle analysis methods introduced by Frank E. Marble of the California Institute of Technology and further developed by Gordon C. Oates (deceased) of the University of Washington and Jack L. Kerrebrock of the Massachusetts Institute of Technology. The steps of parametric cycle analysis are identified in Chapter 5 and then used to model engine cycles from the simple ramjet to the complex, mixed-flow, afterburning turbofan engine. Families of engine designs are analyzed in the *parametric analysis* of Chapters 5 and 7 for ideal engines and engines with losses, respectively. Chapter 6 develops the overall relationships for engine components with losses. The *performance analysis* of Chapter 8 models the actual behavior of an engine and shows why its performance changes with flight conditions and throttle settings. The results of the engine performance analysis can be used to establish component performance requirements. To keep the size of the new edition down, the analysis of some engine cycles has been moved to the electronic Supporting Materials available with this book.

Chapter 9 covers both axial-flow and centrifugal-flow turbomachinery. Included are basic theory and mean-line design of axial-flow compressors and turbines, quick design tools (e.g., repeating-row, repeating-stage design of axial-flow compressors), example multistage compressor designs, flow path and blade shapes, turbomachinery stresses, and turbine cooling. Example output from the COMPR and TURBN programs is included in several example problems.

Inlets, exhaust nozzles, and combustion systems are modeled and analyzed in Chapter 10. The special operation and performance characteristics of supersonic inlets are examined and an example of an external compression inlet is designed. The principles of physics that control the operation and design of main burners and afterburners are also covered.

The appendices contain tables with properties of standard atmosphere and properties of combustion products for air and $(CH_2)_n$. There is also material on turbomachinery stresses as well as useful data on existing gas turbine engines and liquid-propellant rocket engines.

Eight computer programs are provided for use with this textbook:

1) AFPROP, properties of combustion products for air and $(CH_2)_n$
2) ATMOS, properties of the atmosphere
3) COMPR, axial-flow compressor mean-line design analysis
4) EQL, chemical equilibrium analysis for reactive mixtures of perfect gases

5) GASTAB, gas dynamic tables
6) PARA, parametric engine cycle analysis of gas turbine engines
7) PERF, engine performance analysis of gas turbine engines
8) TURBN, axial-flow turbine mean-line design analysis

The AFPROP program can be used to help solve problems of perfect gases with variable specific heats. The ATMOS program calculates the properties of the atmosphere for standard, hot, cold, and tropical days. The EQL program calculates equilibrium properties and process end states for reactive mixtures of perfect gases, for different problems involving hydrocarbon fuels. GASTAB is equivalent to traditional compressible flow appendices for the simple flows of calorically perfect gases. It includes isentropic flow; adiabatic, constant area frictional flow (Fanno flow); frictionless, constant area heating and cooling (Rayleigh flow); normal shock waves; oblique shock waves; multiple oblique shock waves; and Prandtl-Meyer flow. The PARA and PERF programs support the material in Chapters 5–8. PARA is very useful in determining variations in engine performance with design parameters and in limiting the useful range of design values. PERF can predict the variation of an engine's performance with flight condition and throttle (Chapter 8). Both are very useful in evaluating alternative engine designs and can be used in design problems that require selection of an engine for an existing airframe and specified mission. The COMPR and TURBN programs permit preliminary design of axial-flow turbomachinery based on mean-line design.

As already suggested, the author has found the following two courses and material coverage very useful for planning.

Introductory Course

Chapter 1, all
Chapter 2, as needed
Chapter 3, all
Chapter 4, all
Chapter 5, Sections 5.1–5-9
Chapter 6, Sections 6.1–6.9
Chapter 7, Sections 7.1–7.4
Chapter 8, Sections 8.1–8.5

Gas Turbine Engine Components Course

Chapter 2, as needed
Chapter 8, Sections 8.1–8.3
Chapter 9 and Appendix E, all
Chapter 10, all

The material in Chapters 2 and 9 along with Appendix E of this text have also been used to teach the major portion of an undergraduate turbomachinery course.

Jack D. Mattingly
April 2006

Page is intentionally blank

Acknowledgments

I am deeply indebted to Professor Gordon C. Oates (deceased) and Dr. William H. Heiser. Professor Oates taught me the basics of engine cycle analysis during my doctoral studies at the University of Washington and later until his untimely death in 1986. While Dr. Heiser was a Distinguished Visiting Professor at the U.S. Air Force Academy from 1983 to 1985, we developed an outstanding engine design course and wrote the first edition of the textbook *Aircraft Engine Design*. We have continued to work and teach together over the past 23 years, and he has been my friend and mentor.

Special thanks to Brigadier General Daniel H. Daley (USAF, retired, and former Head, Department of Aeronautics, U.S. Air Force Academy), who sponsored my studies under Professor Oates and guided me during the compilation of the teaching notes "Elements of Propulsion." These notes were used for over a decade in the Academy's propulsion courses before the publication of *Elements of Gas Turbine Propulsion* in 1996 and are the basis for this textbook. Most recently General Daley helped me develop Chapters 2 and 3 and the general content of this new textbook—I couldn't have done this book without his help.

I also thank all of the students who have been in my propulsion courses and my coworkers at the Department of Aeronautics, U.S. Air Force Academy, Colorado; the Air Force Institute of Technology (AFIT), Wright-Patterson Air Force Base, Ohio; the Air Force Aero Propulsion and Power Laboratory, Wright-Patterson Air Force Base, Ohio; Seattle University; and University of Washington. Many of these students and coworkers provided insight and guidance in developing this material.

I acknowledge the hard work and determination of Scott Henderson, who worked all of the problems and design problems and checked my solutions. He made significant improvements to the quality and clarity of these problems.

I would like to thank the following reviewers and users for their many helpful comments and suggestions: John Anderson, University of Maryland; Saeed Farokhi, University of Kansas; Afshin Ghajar, Oklahoma State University; Frank Redd, Utah State University; Lt. Col. Brenda Haven, Wright-Patterson AFB, Ohio; Aaron Byerley, U.S. Air Force Academy, Colorado; and David T. Pratt, University of Washington.

Page is intentionally blank

Nomenclature

A = area; constant
a = speed of sound; constant
b = constant
C = effective exhaust velocity [Eq. (1.53), Eq. (3.4)]; circumference; work output coefficient
C_A = angularity coefficient
C_C = work output coefficient of core
C_D = coefficient of drag; discharge coefficient
C_F = thrust coefficient
C_{fg} = gross thrust coefficient
C_L = coefficient of lift
C_p = pressure coefficient
C_{prop} = work output coefficient of propeller
C_{tot} = total work output coefficient
C_V = velocity coefficient
C^* = characteristic velocity [Eq. (3.38)]
c = chord
c_p = specific heat at constant pressure
c_v = specific heat at constant volume
c_x = axial chord
D = drag
d = diameter
E = energy; modulus of elasticity
e = internal energy per unit mass; polytropic efficiency; exponential, 2.7183
F = force; uninstalled thrust; thrust
F_g = gross thrust
f = fuel/air ratio; function; friction coefficient
g = acceleration of gravity
g_c = Newton's constant
g_0 = acceleration of gravity at sea level
H = enthalpy; dimensionless enthalpy [Eq. (2.86)]
h = enthalpy per unit mass; height
h_{PR} = low heating value of fuel
$\overline{h_f^o}$ = enthalpy of formation
I = impulse; impulse function, $PA(1 + \gamma M^2)$

I_{sp} = specific impulse [Eq. (1.55), Eq. (3.6)]
K = constant; dimensionless kinetic energy [Eq. (2.86)]
K_P = equilibrium constant [Eq. (2.119)]
L = length
M = Mach number; momentum
$\dot{M}$ = momentum flux, $\dot{m}V$
m = mass
$\dot{m}$ = mass flow rate
$\mathscr{M}$ = molecular weight
N = number of moles; revolutions per minute
n = load factor; burning rate exponent
n_b = number of blades
P = pressure
P_c = electrical output power
P_f = profile factor
P_s = weight specific excess power
P_t = total pressure
Q = heat interaction
$\dot{Q}$ = rate of heat interaction
q = heat interaction per unit mass; dynamic pressure, $\rho V^2/(2\,g_c)$ electric charge
$\tilde{q}$ = dimensionless heat release [Eq. (5.70)]
R = gas constant; extensive property; radius; additional drag
$\mathscr{R}$ = universal gas constant
r = radius; burning rate
$^\circ R$ = degree of reaction
S = uninstalled thrust specific fuel consumption; entropy
$\dot{S}$ = time rate of change of entropy
S_w = wing planform area
s = entropy per unit mass; blade spacing
Sa = stream thrust function [Eq. (2.94)]
T = temperature; installed thrust
T_t = total temperature
t = time; airfoil thickness
U = blade tangential or rotor velocity
u = velocity
V = absolute velocity; volume
v = volume per unit mass; velocity
W = weight; width
$\dot{W}$ = power
w = work interaction per unit mass; velocity
$\dot{w}$ = weight flow rate
x, y, z = coordinate system
z_e = energy height [Eq. (1.25)]
Z = Zweifel tangential force coefficient [Eq. (9.97)]
α = bypass ratio; angle; coefficient of linear thermal expansion

α_c = specific mass [Eq. (3.33)]
β = angle
Γ = $\sqrt{\gamma\left(\frac{2}{\gamma+1}\right)^{(\gamma+1)/(\gamma-1)}}$; constant
γ = ratio of specific heats; angle
Δ = change
δ = change; dimensionless pressure, P/P_{ref}; dead weight mass ratio; deviation
∂ = partial differential
ε = nozzle area ratio; rotor turning angle; slip factor
ϕ = installation loss coefficient; fuel equivalence ratio; function; total pressure loss coefficient
Φ = function; cooling effectiveness; flow coefficient; dimensionless stream thrust [Eq. (2.95)]
η = efficiency
λ = payload mass ratio
ν = stoichiometric coefficient
θ = angle; dimensionless temperature, T/T_{ref}
Π = product
π = pressure ratio defined by Eq. (5.3)
ρ = density, $1/v$
Σ = sum
σ = control volume boundary; dimensionless density, ρ/ρ_{ref}; tensile stress
τ = temperature ratio defined by Eq. (5.4); shear stress; torque
$\tau\lambda$ = enthalpy ratio defined by Eq. (5.7)
ω = angular speed
ψ = thermal compression ratio, T_3/T_0

Subscripts

A = air mass
a = air; atmosphere
AB = afterburner
add = additive
b = burner or combustor; boattail or afterbody; blade; burning
bo = burnout
C = core stream
c = compressor; corrected; centrifugal; chamber
DB = duct burner
d = diffuser or inlet; disk
dr = disk/rim interface
dry = afterburner not operating
e = exit; exhaust; Earth
ext = external
F = fan stream
f = fan; fuel; final

fn = fan nozzle
g = gearing; gas
H = high-pressure
HP = horsepower
h = hub
i = initial; inside; ideal
int = internal
j = jet
L = low-pressure
M = mixer
m = mechanical; mean; middle
max = corresponding to maximum
N = new
n = nozzle
nac = nacelle
O = overall; output
o = overall; outer
opt = optimum
P = propulsive; products
p = propellant
pl = payload
prop = propeller
R = reference; relative; reactants
r = ram; reduced; rim; rotor
ref = reference condition
s = stage; separation; solid; stator
SL = sea-level
SLS = sea-level static
T = thermal
t = total; turbine; throat; tip; thermal
vac = vacuum
w = forebody; wing
wet = afterburner operating
x, y, z = directional component
σ = control volume
$0, 1, 2, \ldots, 19$ = different locations in space

Superscripts

* = state corresponding to $M = 1$; corresponding to optimum state
$^-$ = average

Page is intentionally blank

1
Introduction

1.1 Propulsion

The *Random House College Dictionary* defines *propulsion* as "the act of propelling, the state of being propelled, a propelling force or impulse" and defines the verb *propel* as "to drive, or cause to move, forward or onward."[1] From these definitions, we can conclude that the study of propulsion includes the study of the propelling force, the motion caused, and the bodies involved. Propulsion involves an object to be propelled plus one or more additional bodies, called *propellant.*

The study of propulsion is concerned with vehicles such as automobiles, trains, ships, aircraft, and spacecraft. The focus of this textbook is on the propulsion of aircraft and spacecraft. Methods devised to produce a thrust force for the propulsion of a vehicle in flight are based on the principle of jet propulsion (the momentum change of a fluid by the propulsion system). The fluid may be the gas used by the engine itself (e.g., turbojet), it may be a fluid available in the surrounding environment (e.g., air used by a propeller), or it may be stored in the vehicle and carried by it during the flight (e.g., rocket).

Jet propulsion systems can be subdivided into two broad categories: airbreathing and non-airbreathing. Airbreathing propulsion systems include the reciprocating, turbojet, turbofan, ramjet, turboprop, and turboshaft engines. Non-airbreathing engines include rocket motors, nuclear propulsion systems, and electric propulsion systems. We focus on gas turbine propulsion systems (turbojet, turbofan, turboprop, and turboshaft engines) in this textbook.

The material in this textbook is divided into three parts:

1) Basic concepts and one-dimensional gas dynamics,
2) Analysis and performance of airbreathing propulsion systems, and
3) Analysis of gas turbine engine components.

This chapter introduces the types of airbreathing and rocket propulsion systems and the basic propulsion performance parameters. Also included is an introduction to aircraft and rocket performance. The material on aircraft performance shows the influence of the gas turbine engine on the performance of the aircraft system. This material also permits incorporation of a gas turbine engine design problem such as new engines for an existing aircraft.

Numerous examples are included throughout this book to help students see the application of a concept after it is introduced. For some students, the material on basic concepts and gas dynamics will be a review of material covered in other

courses they have already taken. For other students, this may be their first exposure to this material, and it may require more effort to understand.

1.2 Units and Dimensions

Since the engineering world uses both the metric SI and English unit system, both will be used in this textbook. One singular distinction exists between the English system and SI—the unit of force is defined in the former but derived in the latter. Newton's second law of motion relates force to mass, length, and time. It states that the sum of the forces is proportional to the rate of change of the momentum ($\boldsymbol{M} = m\boldsymbol{V}$). The constant of proportionality is $1/g_c$:

$$\sum \boldsymbol{F} = \frac{1}{g_c}\frac{\mathrm{d}(m\boldsymbol{V})}{\mathrm{d}t} = \frac{1}{g_c}\frac{\mathrm{d}\boldsymbol{M}}{\mathrm{d}t} \tag{1.1}$$

The units for each term in the preceding equation are listed in Table 1.1 for both SI and English units. In any unit system, only four of the five items in the table can be specified, and the latter is derived from Eq. (1.1).

As a result of selecting $g_c = 1$ and defining the units of mass, length, and time in SI units, the unit of force is derived from Eq. (1.1) as kilogram-meters per square second ($\mathrm{kg \cdot m/s^2}$), which is called the *newton* (N). In English units, the value of g_c is derived from Eq. (1.1) as

$$g_c = 32.174\,\mathrm{ft \cdot lbm/(lbf \cdot s^2)}$$

Rather than adopt the convention used in many recent textbooks of developing material or use with *only* SI metric units ($g_c = 1$), we will maintain g_c in all our equations. Thus g_c will also show up in the equations for *potential energy* (PE) and *kinetic energy* (KE):

$$\mathrm{PE} = \frac{mgz}{g_c}$$

$$\mathrm{KE} = \frac{mV^2}{2g_c}$$

The total energy per unit mass e is the sum of the specific internal energy u, specific kinetic energy ke, and specific potential energy pe:

$$e \equiv u + \mathrm{ke} + \mathrm{pe} = u + \frac{V^2}{2g_c} + \frac{gz}{g_c}$$

There are a multitude of engineering units for the quantities of interest in propulsion. For example, energy can be expressed in the SI unit of *joule*

Table 1.1 Units and dimensions

Unit system	Force	g_c	Mass	Length	Time
SI	Derived	1	Kilogram, kg	Meter, m	Second, s
English	Pound-force, lbf	Derived	Pound-mass, lbm	Foot, ft	Second, s

(1 J = 1 N · m), in British thermal units (Btu), or in foot-pound force (ft · lbf). One must be able to use the available data in the units provided and convert the units when required. Table 1.2 is a unit conversion table provided to help you in your endeavors.

Table 1.2 Unit conversion table

Unit	Conversion
Length	1 m = 3.2808 ft = 39.37 in.
	1 km = 0.621 mile
	1 mile = 5280 ft = 1.609 km
	1 nm = 6080 ft = 1.853 km
Area	1 m^2 = 10.764 ft^2
	1 cm^2 = 0.155 $in.^2$
Volume	1 gal = 0.13368 ft^3 = 3.785 liter
	1 liter = 10^{-3} m^3 = 61.02 $in.^3$
Time	1 h = 3600 s = 60 min
Mass	1 kg = 1000 g = 2.2046 lbm = 6.8521 × 10^{-2} slug
	1 slug = 1 lbf · s^2/ft = 32.174 lbm
Density	1 slug/ft^3 = 512.38 kg/m^3
Force	1 N = 1 kg · m/s^2
	1 lbf = 4.448 N
Energy	1 J = 1 N · m = 1kg · m^2/s^2
	1 Btu = 778.16 ft · lbf = 252 cal = 1055 J
	1 cal = 4.186 J
	1 kJ = 0.947813 Btu = 0.23884 kcal
Power	1 W = 1 J/s = 1 kg · m^2/s^3
	1 hp = 550 ft · lbf/s = 2545 Btu/h = 745.7 W
	1 kW = 3412 Btu/h = 1.341 hp
Pressure (stress)	1 atm = 14.696 $lb/in.^2$ or psi = 760 torr = 101,325 Pa
	1 atm = 30.0 inHg = 407.2 inH_2O
	1 ksi = 1000 psi
	1 mmHg = 0.01934 psi = 1 torr
	1 Pa = 1 N/m^2
	1 inHg = 3376.8 Pa
Energy per unit mass	1 kJ/kg = 0.4299 Btu/lbm
Specific heat	1 kJ/(kg · °C) = 0.23884 Btu/(lbm · °F)
Temperature	1 K = 1.8°R
	K = 273.15 + °C
	°R = 459.69 + °F
Temperature change	1°C = 1.8°F
Specific thrust	1 lbf/(lbm/s) = 9.8067 N/(kg/s)
Specific power	1 hp/(lbm/s) = 1.644 kW/(kg/s)
Thrust specific fuel consumption (TSFC)	1 lbm/(lbf · h) = 28.325 mg/(N · s)
Power specific fuel consumption	1 lbm/(hp · h) = 168.97 mg/(kW · s)
Strength/weight ratio (σ/ρ)	1 ksi/(slug/ft^3) = 144 ft^2/s^2 = 13.38 m^2/s^2

1.3 Operational Envelopes and Standard Atmosphere

Each engine type will operate only within a certain range of altitudes and Mach numbers (velocities). Similar limitations in velocity and altitude exist for airframes. It is necessary, therefore, to match airframe and propulsion system capabilities. Figure 1.1 shows the approximate velocity and altitude limits, or *corridor of flight*, within which airlift vehicles can operate. The corridor is bounded by a *lift limit*, a *temperature limit*, and an *aerodynamic force limit.* The lift limit is determined by the maximum level-flight altitude at a given velocity. The temperature limit is set by the structural thermal limits of the material used in construction of the aircraft. At any given altitude, the maximum velocity attained is temperature-limited by aerodynamic heating effects. At lower altitudes, velocity is limited by aerodynamic force loads rather than by temperature.

The operating regions of all aircraft lie within the flight corridor. The operating region of a particular aircraft within the corridor is determined by aircraft design, but it is a very small portion of the overall corridor. Superimposed on the flight corridor in Fig. 1.1 are the operational envelopes of various powered aircraft. The operational limits of each propulsion system are determined by limitations of the components of the propulsion system and are shown in Fig. 1.2.

The analyses presented in this text use the properties of the atmosphere to determine both engine and airframe performance. Since these properties vary with location, season, time of day, etc., we will use the U.S. standard atmosphere[2] to give a known foundation for our analyses. Appendix A gives the properties of the U.S. standard atmosphere, 1976, in both English and SI units. Values of the pressure P, temperature T, density ρ, and speed of sound a are given in dimensionless ratios of the property at altitude to its value at sea level (SL), the reference value. The dimensionless ratios of pressure, temperature, and density

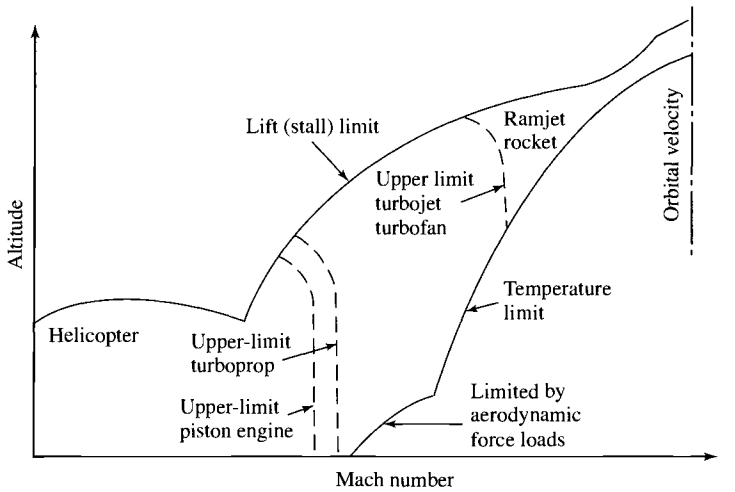

Fig. 1.1 Flight limits.

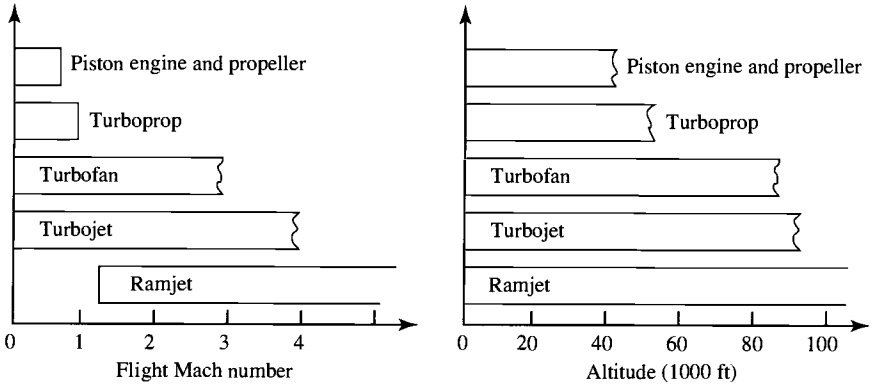

Fig. 1.2 Engine operational limits.

are given the symbols δ, θ, and σ, respectively. These ratios are defined as follows:

$$\delta \equiv \frac{P}{P_{\text{ref}}} \tag{1.2}$$

$$\theta \equiv \frac{T}{T_{\text{ref}}} \tag{1.3}$$

$$\sigma \equiv \frac{\rho}{\rho_{\text{ref}}} \tag{1.4}$$

The reference values of pressure, temperature, and density are given for each unit system at the end of its property table.

For nonstandard conditions such as a hot day, the normal procedure is to use the standard pressure and correct the density, using the perfect gas relationship $\sigma = \delta/\theta$. As an example, we consider a 100°F day at 4-kft altitude. From Appendix A, we have $\delta = 0.8637$ for the 4-kft altitude. We calculate θ, using the 100°F temperature; $\theta = T/T_{\text{ref}} = (100 + 459.7)/518.7 = 1.079$. Note that absolute temperatures must be used in calculating θ. Then the density ratio is calculated using $\sigma = \delta/\theta = 0.8637/1.079 = 0.8005$.

1.4 Airbreathing Engines

The turbojet, turbofan, turboprop, turboshaft, and ramjet engine systems are discussed in this part of Chapter 1. The discussion of these engines is in the context of providing thrust for aircraft. The listed engines are not all the engine types (reciprocating, rockets, combination types, etc.) that are used in providing propulsive thrust to aircraft, nor are they used exclusively on aircraft. The thrust of the turbojet and ramjet results from the action of a fluid jet leaving the engine; hence, the name *jet engine* is often applied to these engines. The

turbofan, turboprop, and turboshaft engines are adaptations of the turbojet to supply thrust or power through the use of fans, propellers, and shafts.

1.4.1 Gas Generator

The "heart" of a gas turbine type of engine is the gas generator. A schematic diagram of a gas generator is shown in Fig. 1.3. The compressor, combustor, and turbine are the major components of the gas generator which is common to the turbojet, turbofan, turboprop, and turboshaft engines. The purpose of a gas generator is to supply high-temperature and high-pressure gas.

1.4.2 Turbojet

By adding an inlet and a nozzle to the gas generator, a turbojet engine can be constructed. A schematic diagram of a simple turbojet is shown in Fig. 1.4a, and a turbojet with afterburner is shown in Fig. 1.4b. In the analysis of a turbojet engine, the major components are treated as sections. Also shown in Figs. 1.4a and 1.4b are the station numbers for each section.

The turbojet was first used as a means of aircraft propulsion by von Ohain (first flight August 27, 1939) and Whittle (first flight May 15, 1941). As development proceeded, the turbojet engine became more efficient and replaced some of the piston engines. A photograph of the J79 turbojet with afterburner used in the F-4 Phantom II and B-58 Hustler is shown in Fig. 1.5.

The adaptations of the turbojet in the form of turbofan, turboprop, and turboshaft engines came with the need for more thrust at relatively low speeds. Some characteristics of different turbojet, turbofan, turboprop, and turboshaft engines are included in Appendix B.

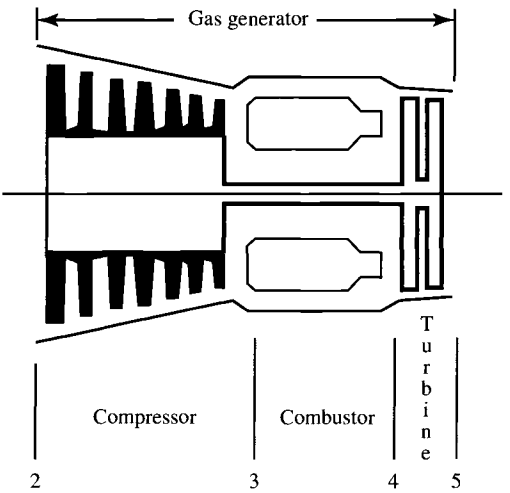

Fig. 1.3 Schematic diagram of gas generator.

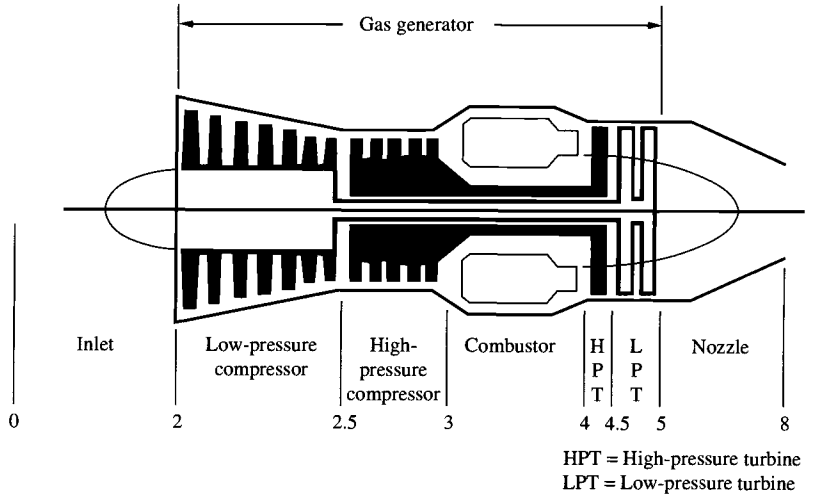

Fig. 1.4a Schematic diagram of a turbojet (dual axial compressor and turbine).

The thrust of a turbojet is developed by compressing air in the inlet and compressor, mixing the air with fuel and burning in the combustor, and expanding the gas stream through the turbine and nozzle. The expansion of gas through the turbine supplies the power to turn the compressor. The net thrust delivered by the engine is the result of converting internal energy to kinetic energy.

The pressure, temperature, and velocity variations through a J79 engine are shown in Fig. 1.6. In the compressor section, the pressure and temperature increase as a result of work being done on the air. The temperature of the gas

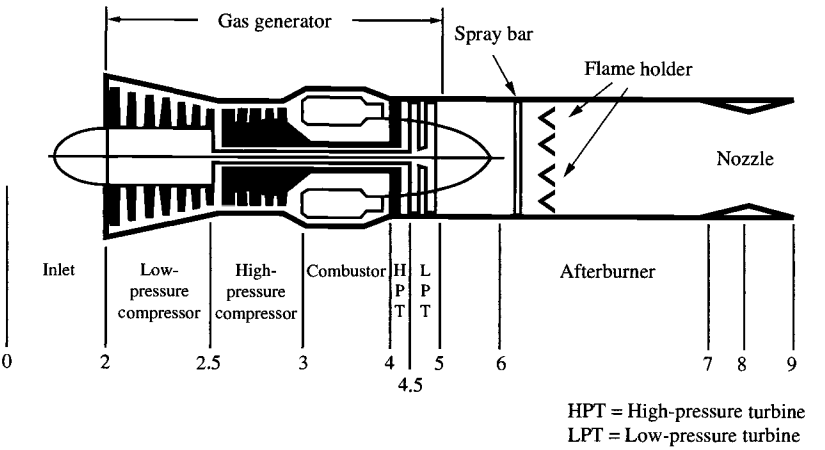

Fig. 1.4b Schematic diagram of a turbojet with afterburner.

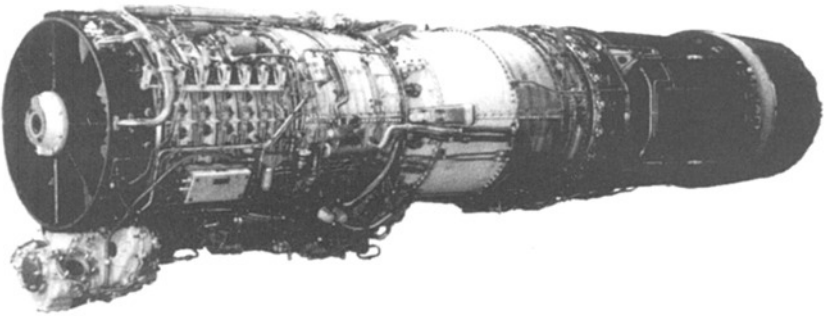

Fig. 1.5 General Electric J79 turbojet with afterburner. (Courtesy of General Electric Aircraft Engines.)

is further increased by burning fuel in the combustor. In the turbine section, energy is being removed from the gas stream and converted to shaft power to turn the compressor. The energy is removed by an expansion process that results in a decrease of temperature and pressure. In the nozzle, the gas stream is further expanded to produce a high exit kinetic energy. All the sections of the engine must operate in such a way as to efficiently produce the greatest amount of thrust for a minimum of weight.

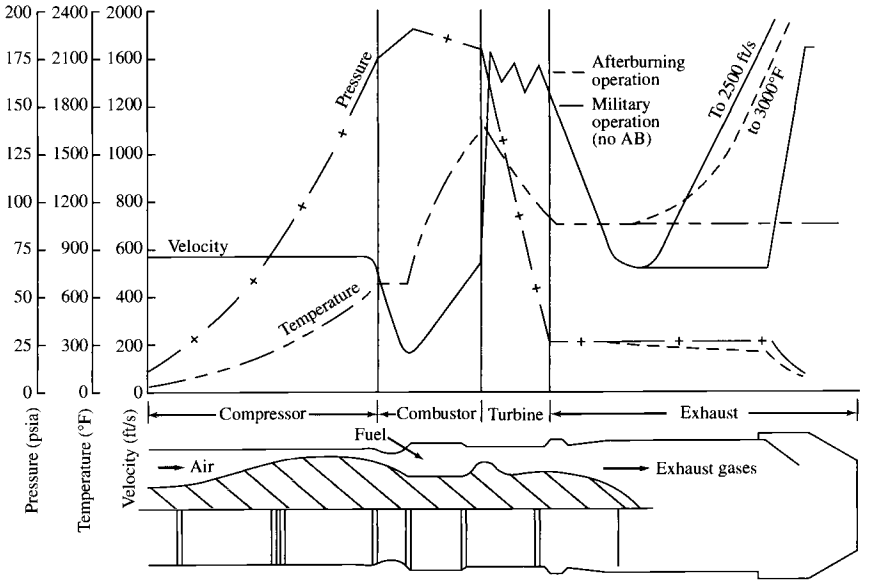

Fig. 1.6 Property variation through the General Electric J79 afterburning turbojet engine. (Courtesy of General Electric Aircraft Engines.)

1.4.3 Turbofan

The turbofan engine consists of an inlet, fan, gas generator, and nozzle. A schematic diagram of a turbofan is shown in Fig. 1.7. In the turbofan, a portion of the turbine work is used to supply power to the fan. Generally the turbofan engine is more economical and efficient than the turbojet engine in

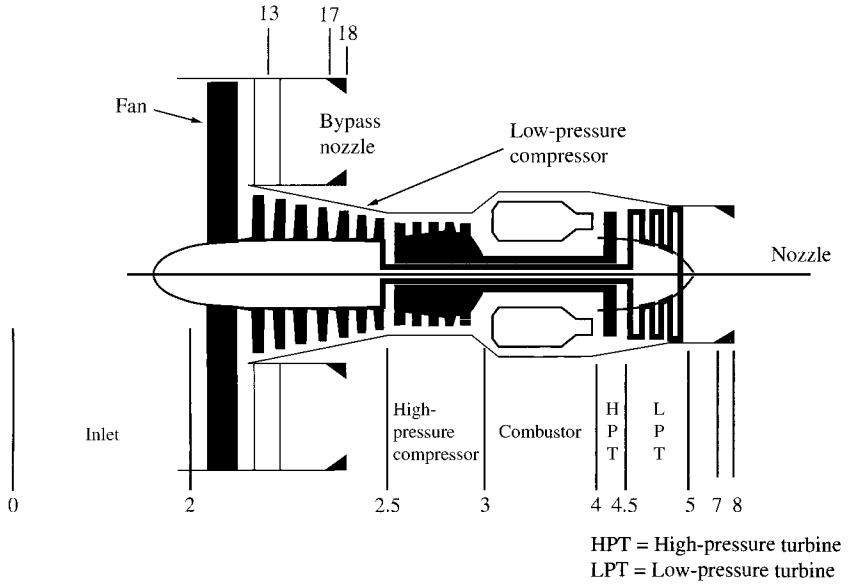

Fig. 1.7 Schematic diagram of a high-bypass-ratio turbofan.

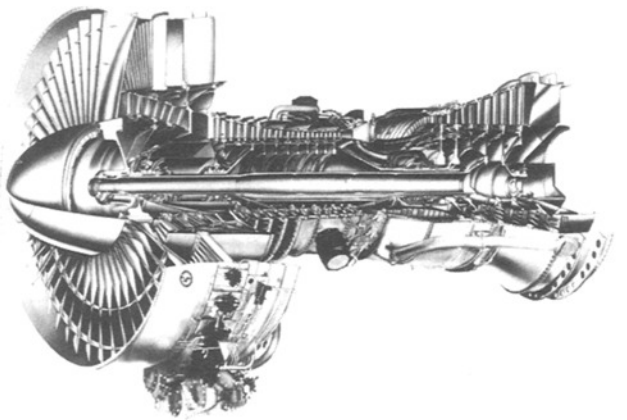

Fig. 1.8a Pratt & Whitney JT9D turbofan. (Courtesy of Pratt & Whitney.)

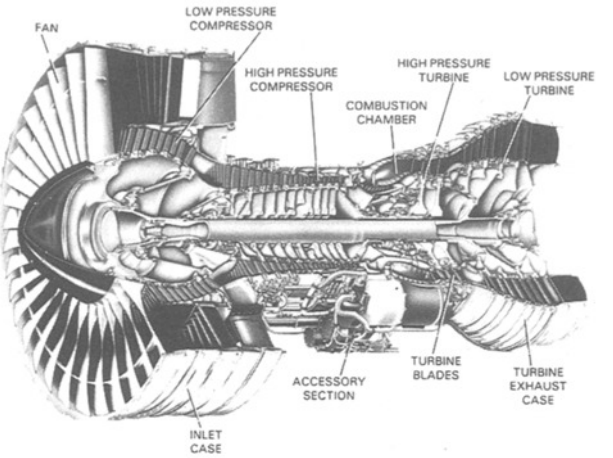

Fig. 1.8b Pratt & Whitney PW4000 turbofan. (Courtesy of Pratt & Whitney.)

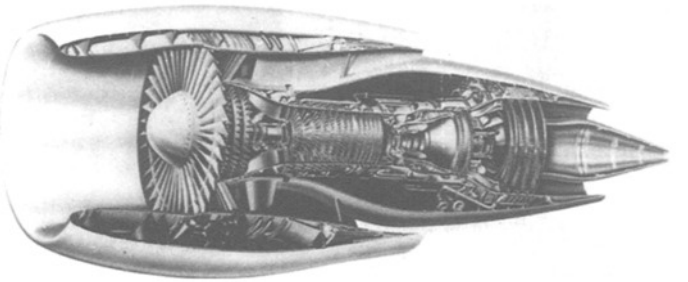

Fig. 1.8c General Electric CF6 Turbofan. (Courtesy of General Electric Aircraft Engines.)

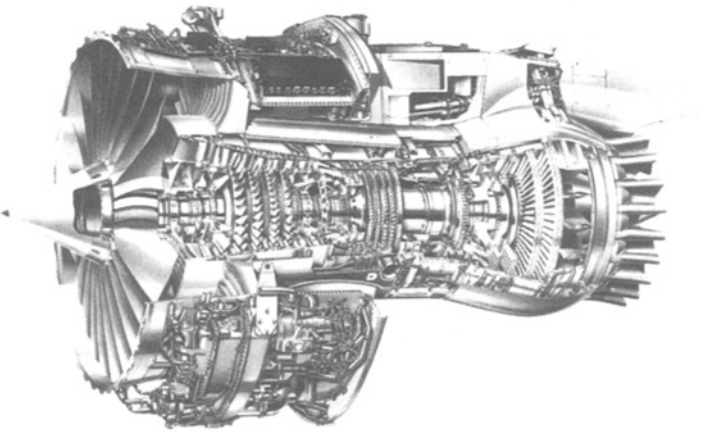

Fig. 1.8d Rolls-Royce RB-211-524G/H turbofan. (Courtesy of Rolls-Royce.)

subsonic flight. The *thrust specific fuel consumption* (TSFC, or fuel mass flow rate per unit thrust) is lower for turbofans and indicates a more economical operation. The turbofan also accelerates a larger mass of air to a lower velocity than a turbojet for a higher propulsive efficiency. The frontal area of a turbofan is quite large compared to that of a turbojet, and for this reason more drag and more weight result. The fan diameter is also limited aerodynamically when compressibility effects occur. Several of the current high-bypass-ratio turbofan engines used in subsonic aircraft are shown in Figs. 1.8a–1.8f.

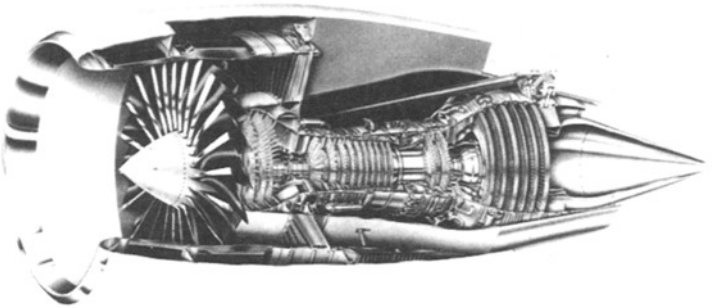

Fig. 1.8e General Electric GE90 turbofan. (Courtesy of General Electric Aircraft Engines.)

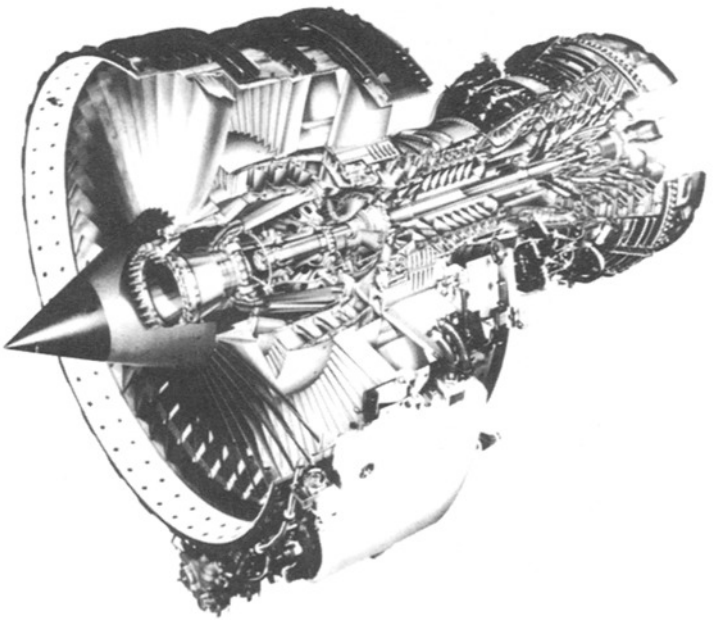

Fig. 1.8f SNECMA CFM56 turbofan. (Courtesy of SNECMA.)

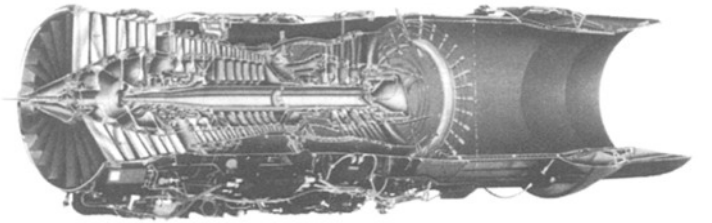

Fig. 1.9a Pratt & Whitney F100-PW-229 afterburning turbofan. (Courtesy of Pratt & Whitney.)

Figures 1.9a and 1.9b show the Pratt & Whitney F100 turbofan and the General Electric F110 turbofan, respectively. These afterburning turbofan engines are used in the F15 Eagle and F16 Falcon supersonic fighter aircraft. In this turbofan, the bypass stream is mixed with the core stream before passing through a common afterburner and exhaust nozzle.

1.4.4 Turboprop and Turboshaft

A gas generator that drives a propeller is a turboprop engine. The expansion of gas through the turbine supplies the energy required to turn the propeller. A schematic diagram of the turboprop is shown in Fig. 1.10a. The turboshaft engine is similar to the turboprop except that power is supplied to a shaft rather than a propeller. The turboshaft engine is used quite extensively for supplying power for helicopters. The turboprop engine may find application in vertical takeoff and landing (VTOL) transporters. The limitations and advantages of the turboprop are those of the propeller. For low-speed flight and short-field takeoff, the propeller has a performance advantage. At speeds approaching the speed of sound, compressibility effects set in and the propeller loses its aerodynamic efficiency. Because of the rotation of the propeller, the propeller tip will approach the speed of sound before the vehicle approaches the speed of sound. This compressibility effect when one approaches the speed of sound limits the design of helicopter rotors and propellers. At high subsonic speeds,

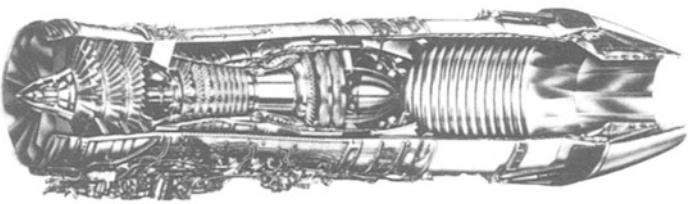

Fig. 1.9b General Electric F110-GE-129 afterburning turbofan. (Courtesy of General Electric Aircraft Engines.)

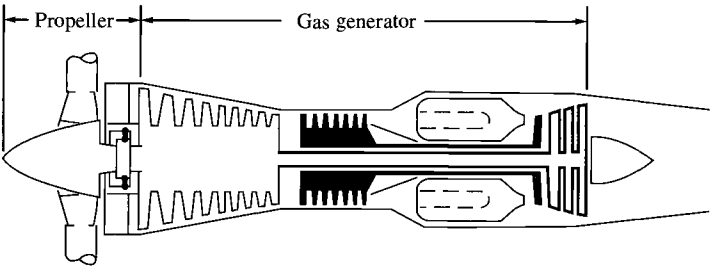

Fig. 1.10a Schematic diagram of a turboprop.

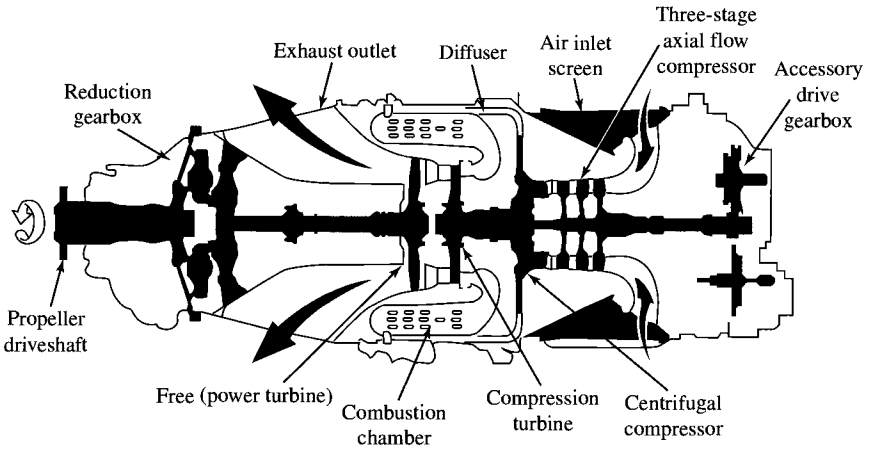

Fig. 1.10b Canadian Pratt & Whitney PT6 turboshaft. (Courtesy of Pratt & Whitney of Canada.)

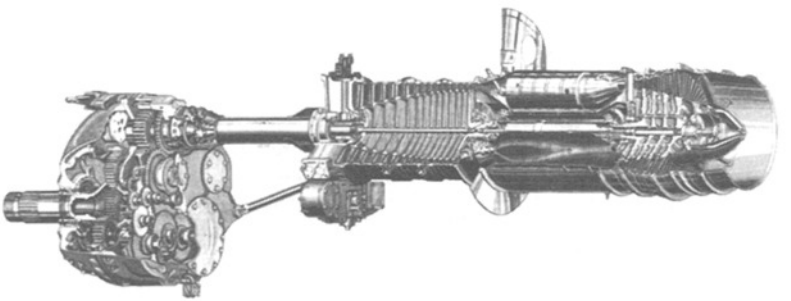

Fig. 1.10c Allison T56 turboshaft. (Courtesy of Allison Gas Turbine Division.)

the turbofan engine will have a better aerodynamic performance than the turboprop since the turbofan is essentially a *ducted turboprop.* Putting a duct or shroud around a propeller increases its aerodynamic performance. Examples of a turboshaft engine are the Canadian Pratt & Whitney PT6 (Fig. 1.10b), used in many small commuter aircraft, and the Allison T56 (Fig. 1.10c), used to power the C-130 Hercules and the P-3 Orion.

1.4.5 Ramjet

The ramjet engine consists of an inlet, a combustion zone, and a nozzle. A schematic diagram of a ramjet is shown in Fig. 1.11. The ramjet does not have the compressor and turbine as the turbojet does. Air enters the inlet where it is compressed and then enters the combustion zone where it is mixed with the fuel and burned. The hot gases are then expelled through the nozzle, developing thrust. The operation of the ramjet depends on the inlet to decelerate the incoming air to raise the pressure in the combustion zone. The pressure rise makes it possible for the ramjet to operate. The higher the velocity of the incoming air, the greater the pressure rise. It is for this reason that the ramjet operates best at high supersonic velocities. At subsonic velocities, the ramjet is inefficient, and to start the ramjet, air at a relatively higher velocity must enter the inlet.

The combustion process in an ordinary ramjet takes place at low subsonic velocities. At high supersonic flight velocities, a very large pressure rise is developed that is more than sufficient to support operation of the ramjet. Also, if the inlet has to decelerate a supersonic high-velocity airstream to a subsonic velocity, large pressure losses can result. The deceleration process also produces a temperature rise, and at some limiting flight speed, the temperature will approach the limit set by the wall materials and cooling methods. Thus when the temperature increase due to deceleration reaches the limit, it may not be possible to burn fuel in the airstream.

In the past few years, research and development have been done on a ramjet that has the combustion process taking place at supersonic velocities. By using a supersonic combustion process, the temperature rise and pressure loss due to deceleration in the inlet can be reduced. This ramjet with supersonic combustion is known as the *scramjet* (supersonic combustion ramjet). Figure 1.12a shows the schematic of a scramjet engine similar to that proposed for the National

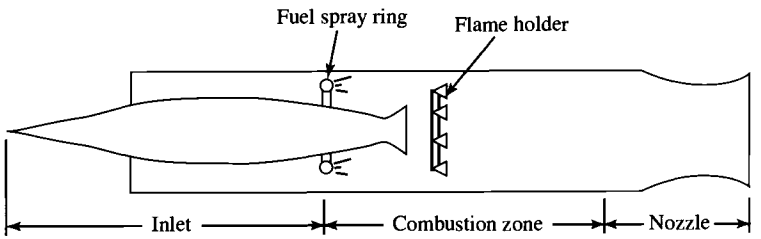

Fig. 1.11 Schematic diagram of a ramjet.

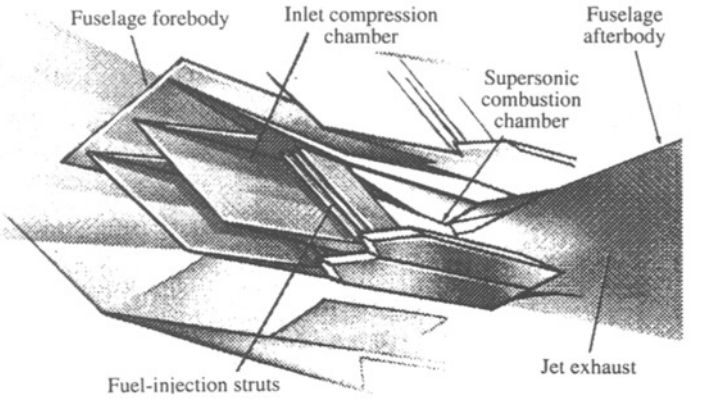

Fig. 1.12a Schematic diagram of a scramjet.

AeroSpace Plane (NASP) research vehicle, the X-30 shown in Fig. 1.12b. Further development of the scramjet for other applications (e.g., the Orient Express) will continue if research and development produces a scramjet engine with sufficient performance gains. Remember that since it takes a relative velocity to start the ramjet or scramjet, another engine system is required to accelerate aircraft like the X-30 to ramjet velocities.

1.4.6 Turbojet/Ramjet Combined-Cycle Engine

Two of the Pratt & Whitney J58 turbojet engines (see Fig. 1.13a) are used to power the Lockheed SR71 Blackbird (see Fig. 1.13b). This was the fastest aircraft

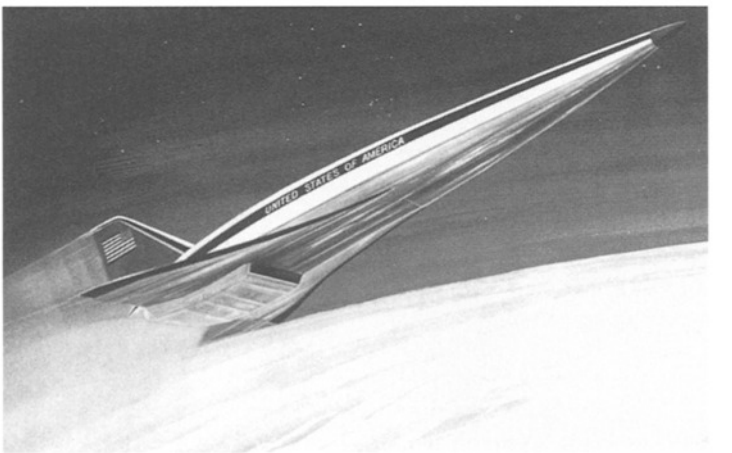

Fig. 1.12b Conceptual drawing of the X-30. (Courtesy of Pratt & Whitney.)

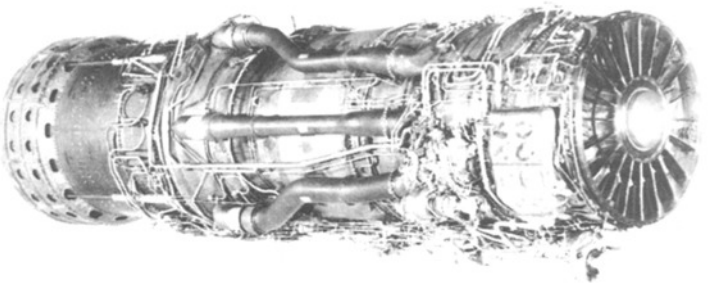

Fig. 1.13a Pratt & Whitney J58 turbojet. (Courtesy of Pratt & Whitney.)

(Mach 3+) when it was retired in 1989. The J58 operates as an afterburning turbojet engine until it reaches high Mach level, at which point the six large tubes (Fig. 1.13a) bypass flow to the afterburner. When these tubes are in use, the compressor, burner, and turbine of the turbojet are essentially bypassed, and the engine operates as a ramjet with the afterburner acting as the ramjet's burner.

1.4.7 Aircraft Engine Performance Parameters

This section presents several of the airbreathing engine performance parameters that are useful in aircraft propulsion. The first performance parameter is the thrust of the engine that is available for sustained flight (thrust = drag), accelerated flight (thrust > drag), or deceleration (thrust < drag).

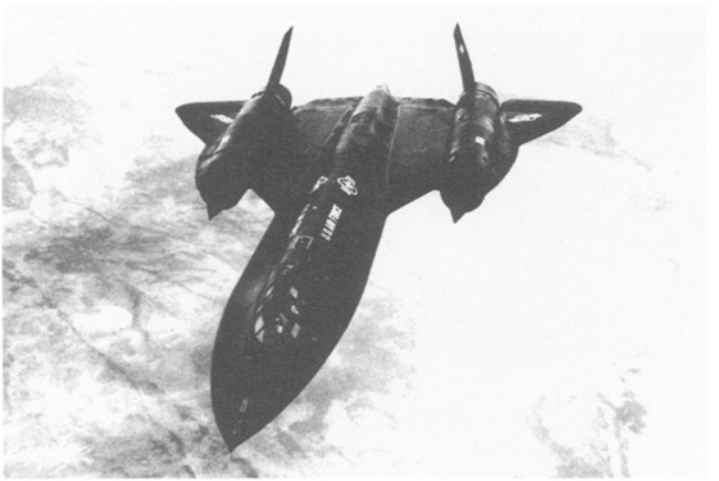

Fig. 1.13b Lockheed SR71 Blackbird. (Courtesy of Lockheed.)

As derived in Chapter 4, the uninstalled thrust F of a jet engine (single inlet and single exhaust) is given by

$$F = \frac{(\dot{m}_0 + \dot{m}_f)V_e - \dot{m}_0 V_0}{g_c} + (P_e - P_0)A_e \tag{1.5}$$

where

$\dot{m}_0$, $\dot{m}_f$ = mass flow rates of air and fuel, respectively
V_0, V_e = velocities at inlet and exit, respectively
P_0, P_e = pressures at inlet and exit, respectively

It is most desirable to expand the exhaust gas to the ambient pressure, which gives $P_e = P_0$. In this case, the uninstalled thrust equation becomes

$$F = \frac{(\dot{m}_0 + \dot{m}_f)V_e - \dot{m}_0 V_0}{g_c} \qquad \text{for } P_e = P_0 \tag{1.6}$$

The installed thrust T is equal to the uninstalled thrust F minus the inlet drag D_{inlet} and minus the nozzle drag D_{noz}, or

$$T = F - D_{\text{inlet}} - D_{\text{noz}} \tag{1.7}$$

Dividing the inlet drag D_{inlet} and nozzle drag D_{noz} by the uninstalled thrust F yields the dimensionless inlet loss coefficient ϕ_{inlet} and nozzle loss coefficient ϕ_{noz}, or

$$\begin{aligned} \phi_{\text{inlet}} &= \frac{D_{\text{inlet}}}{F} \\ \phi_{\text{noz}} &= \frac{D_{\text{noz}}}{F} \end{aligned} \tag{1.8}$$

Thus the relationship between the installed thrust T and uninstalled thrust F is simply

$$T = F(1 - \phi_{\text{inlet}} - \phi_{\text{noz}}) \tag{1.9}$$

The second performance parameter is the thrust specific fuel consumption (S and TSFC). This is the rate of fuel use by the propulsion system per unit of thrust produced. The uninstalled fuel consumption S and installed fuel consumption TSFC are written in equation form as

$$S = \frac{\dot{m}_f}{F} \tag{1.10}$$

$$\text{TSFC} = \frac{\dot{m}_f}{T} \tag{1.11}$$

where

F = uninstalled thrust
S = uninstalled thrust specific fuel consumption

T = installed engine thrust
TSFC = installed thrust specific fuel consumption
$\dot{m}_f$ = mass flow rate of fuel

The relation between S and TSFC in equation form is given by

$$S = \text{TSFC}(1 - \phi_{\text{inlet}} - \phi_{\text{noz}}) \tag{1.12}$$

Values of thrust F and fuel consumption S for various jet engines at sea-level static conditions are listed in Appendix B. The predicted variations of uninstalled engine thrust F and uninstalled thrust specific fuel consumption S with Mach number and altitude for an advanced fighter engine[3] are plotted in Figs. 1.14a–1.14d. Note that the thrust F decreases with altitude and the fuel consumption S also decreases with altitude until 36 kft (the start of the isothermal layer of the atmosphere). Also note that the fuel consumption increases with Mach number and that the thrust varies considerably with the Mach number. The predicted partial-throttle performance of the advanced fighter engine is shown at three flight conditions in Fig. 1.14e.

The takeoff thrust of the JT9D high-bypass-ratio turbofan engine is given in Fig. 1.15a vs Mach number and ambient air temperature for two versions. Note the rapid falloff of thrust with rising Mach number that is characteristic of this engine cycle and the constant thrust at a Mach number for temperatures of 86°F and below (this is often referred to as a *flat rating*). The partial-throttle performance of both engine versions is given in Fig. 1.15b for two combinations of altitude and Mach number.

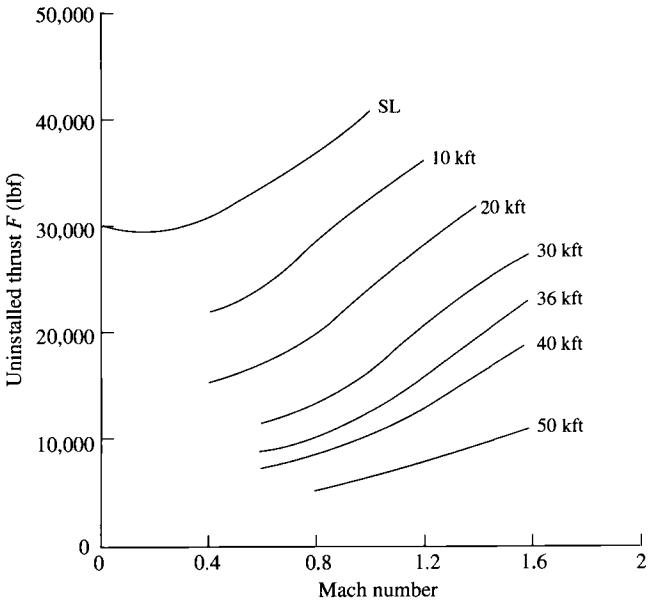

Fig. 1.14a Uninstalled thrust F of an advanced afterburning fighter engine at maximum power setting, afterburner on. (Extracted from Ref. 3.)

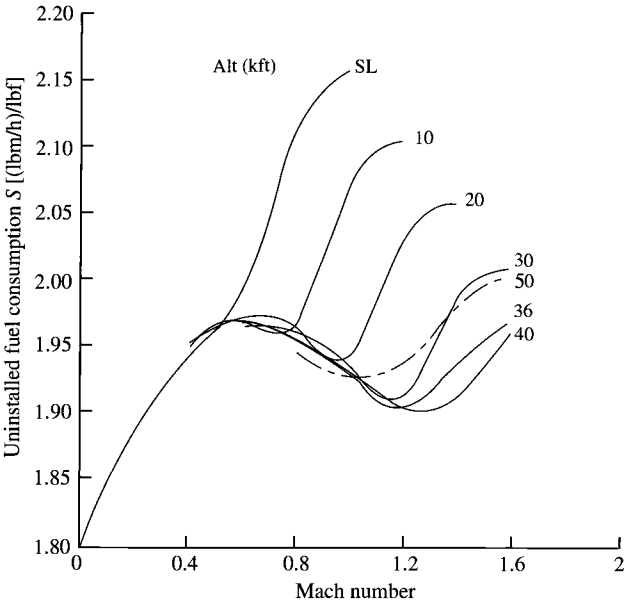

Fig. 1.14b Uninstalled fuel consumption S of an advanced afterburning fighter engine at maximum power setting, afterburner on. (Extracted from Ref. 3.)

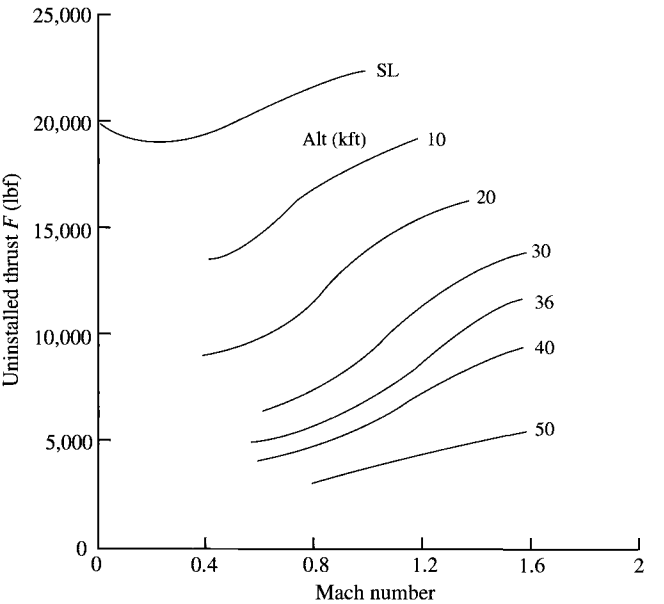

Fig. 1.14c Uninstalled thrust F of an advanced afterburning fighter engine at military power setting, afterburner off. (Extracted from Ref. 3.)

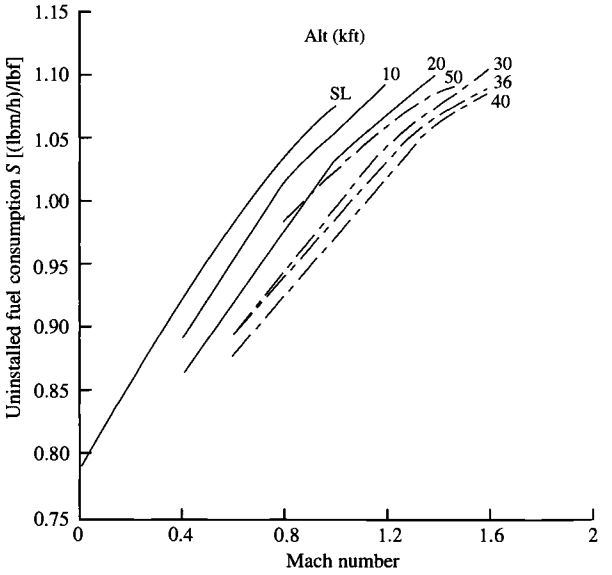

Fig. 1.14d Uninstalled fuel consumption S of an advanced afterburning fighter engine at military power setting, afterburner off. (Extracted from Ref. 3.)

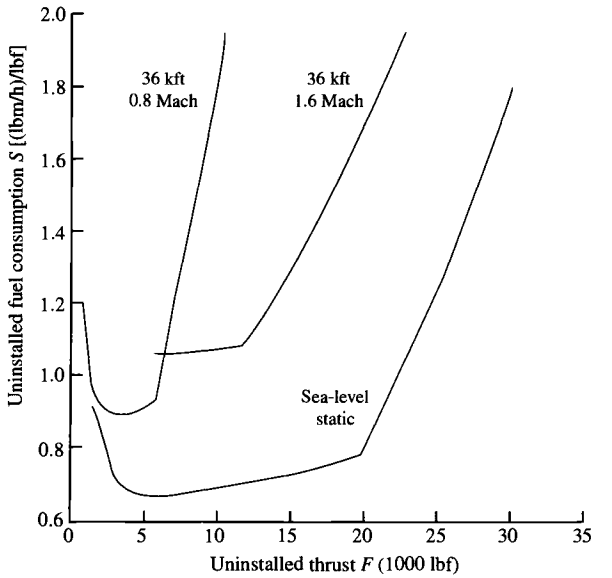

Fig. 1.14e Partial-throttle performance of an advanced fighter engine. (Extracted from Ref. 3.)

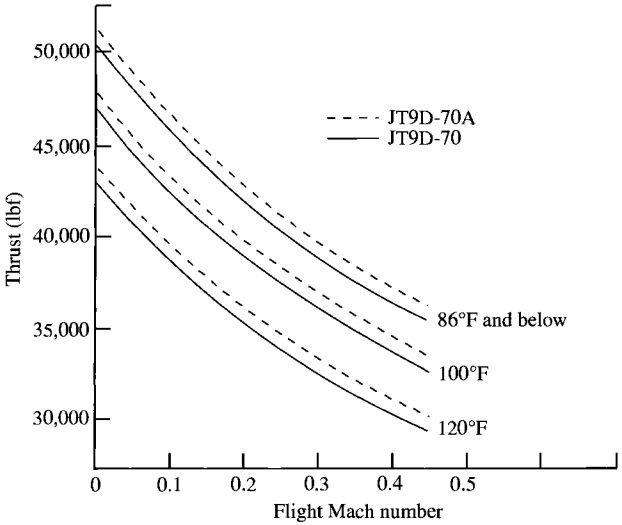

Fig. 1.15a JT9D-70/-70A turbofan takeoff thrust. (Courtesy of Pratt & Whitney.)

Although the aircraft gas turbine engine is a very complex machine, the basic tools for modeling its performance are developed in the following chapters. These tools are based on the work of Gordon Oates.[4] They permit performance calculations for existing and proposed engines and generate performance curves similar to Figs. 1.14a–1.14e and Figs. 1.15a and 1.15b.

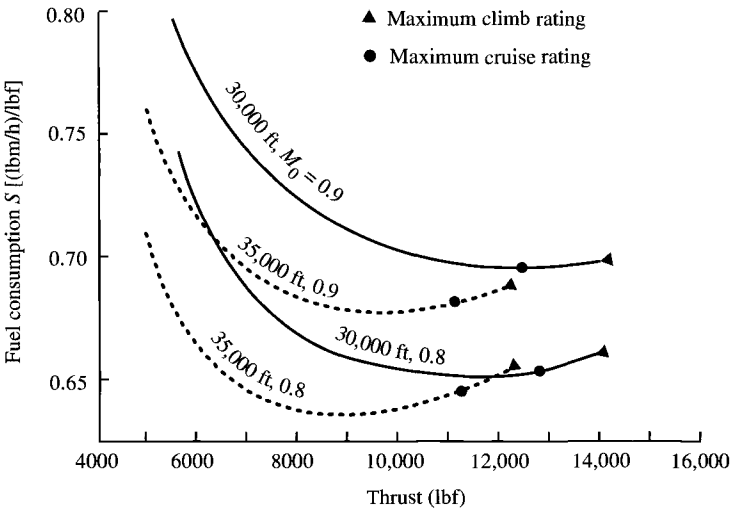

Fig. 1.15b JT9D-70/-70A turbofan cruise-specific fuel consumption. (Courtesy of Pratt & Whitney.)

Table 1.3 Typical aircraft engine thrust installation losses

Flight condition:	$M < 1$		$M > 1$	
Aircraft type	ϕ_{inlet}	ϕ_{noz}	ϕ_{inlet}	ϕ_{noz}
Fighter	0.05	0.01	0.05	0.03
Passenger/cargo	0.02	0.01	—	—
Bomber	0.03	0.01	0.04	0.02

The value of the installation loss coefficient depends on the characteristics of the particular engine/airframe combination, the Mach number, and the engine throttle setting. Typical values are given in Table 1.3 for guidance.

The thermal efficiency η_T of an engine is another very useful engine performance parameter. *Thermal efficiency* is defined as the net rate of organized energy (shaft power or kinetic energy) out of the engine divided by the rate of thermal energy available from the fuel in the engine. The fuel's available thermal energy is equal to the mass flow rate of the fuel $\dot{m}_f$ times the fuel lower-heating value h_{PR}. Thermal efficiency can be written in equation form as

$$\eta_T = \frac{\dot{W}_{\text{out}}}{\dot{Q}_{\text{in}}} \tag{1.13}$$

where

η_T = thermal efficiency of engine
$\dot{W}_{\text{out}}$ = net power out of engine
$\dot{Q}_{\text{in}}$ = rate of thermal energy released ($\dot{m}_f h_{PR}$)

Note that for engines with shaft power output, $\dot{W}_{\text{out}}$ is equal to this shaft power. For engines with no shaft power output (e.g., turbojet engine), $\dot{W}_{\text{out}}$ is equal to the net rate of change of the kinetic energy of the fluid through the engine. The power out of a jet engine with a single inlet and single exhaust (e.g., turbojet engine) is given by

$$\dot{W}_{\text{out}} = \frac{1}{2g_c}[(\dot{m}_0 + \dot{m}_f)V_e^2 - \dot{m}_0 V_0^2]$$

The propulsive efficiency η_P of a propulsion system is a measure of how effectively the engine power $\dot{W}_{\text{out}}$ is used to power the aircraft. *Propulsive efficiency* is the ratio of the aircraft power (thrust times velocity) to the power out of the engine $\dot{W}_{\text{out}}$. In equation form, this is written as

$$\eta_P = \frac{TV_0}{\dot{W}_{\text{out}}} \tag{1.14}$$

where

η_P = propulsive efficiency of engine
T = thrust of propulsion system

V_0 = velocity of aircraft
$\dot{W}_{out}$ = net power out of engine

For a jet engine with a single inlet and single exhaust and an exit pressure equal to the ambient pressure, the propulsive efficiency is given by

$$\eta_P = \frac{2(1 - \phi_{inlet} - \phi_{noz})[(\dot{m}_0 + \dot{m}_f)V_e - \dot{m}_0 V_0]V_0}{(\dot{m}_0 + \dot{m}_f)V_e^2 - \dot{m}_0 V_0^2} \tag{1.15}$$

For the case when the mass flow rate of the fuel is much less than that of air and the installation losses are very small, Eq. (1.15) simplifies to the following equation for the propulsive efficiency:

$$\eta_P = \frac{2}{V_e/V_0 + 1} \tag{1.16}$$

Equation (1.16) is plotted vs the velocity ratio V_e/V_0 in Fig. 1.16 and shows that high propulsive efficiency requires the exit velocity to be approximately equal to the inlet velocity. Turbojet engines have high values of the velocity ratio V_e/V_0 with corresponding low propulsive efficiency, whereas turbofan engines have low values of the velocity ratio V_e/V_0 with corresponding high propulsive efficiency.

The thermal and propulsive efficiencies can be combined to give the *overall efficiency* η_O of a propulsion system. Multiplying propulsive efficiency by

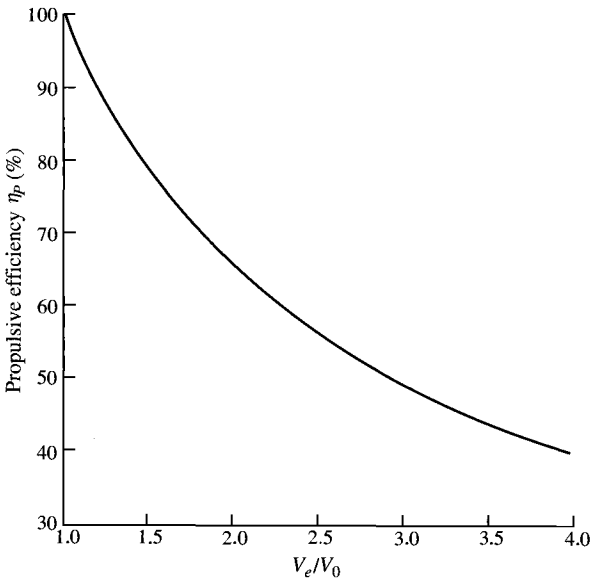

Fig. 1.16 Propulsive efficiency vs velocity ratio (V_e/V_0).

thermal efficiency, we get the ratio of the aircraft power to the rate of thermal energy released in the engine (the overall efficiency of the propulsion system):

$$\eta_O = \eta_P \eta_T \tag{1.17}$$

$$\eta_O = \frac{TV_0}{\dot{Q}_{\text{in}}} \tag{1.18}$$

Several of the preceding performance parameters are plotted for general types of gas turbine engines in Figs. 1.17a, 1.17b, and 1.17c. These plots can be used to obtain the general trends of these performance parameters with flight velocity for each propulsion system.

Since $\dot{Q}_{\text{in}} = \dot{m}_f h_{PR}$, Eq. (1.18) can be rewritten as

$$\eta_O = \frac{TV_0}{\dot{m}_f h_{PR}}$$

With the help of Eq. (1.11), this equation can be written in terms of the thrust specific fuel consumption as

$$\eta_O = \frac{V_0}{\text{TSFC} \cdot h_{PR}} \tag{1.19}$$

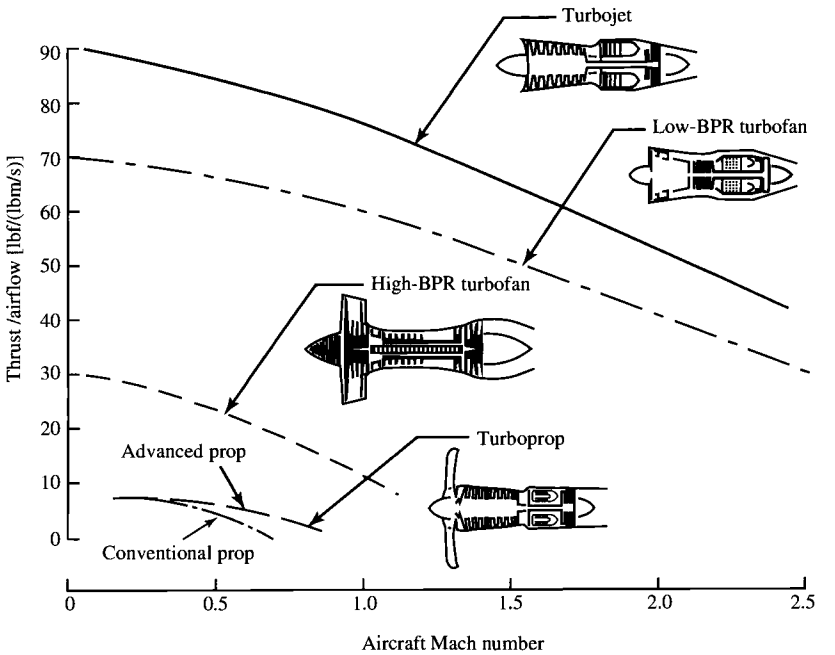

Fig. 1.17a Specific thrust characteristics of typical aircraft engines. (Courtesy of Pratt & Whitney.)

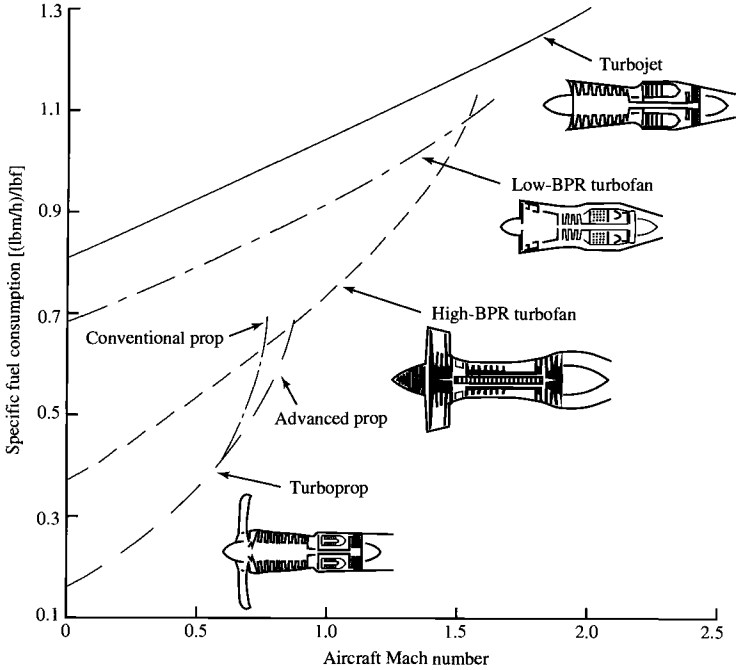

Fig. 1.17b Thrust-specific fuel consumption characteristics of typical aircraft engines. (Courtesy of Pratt & Whitney.)

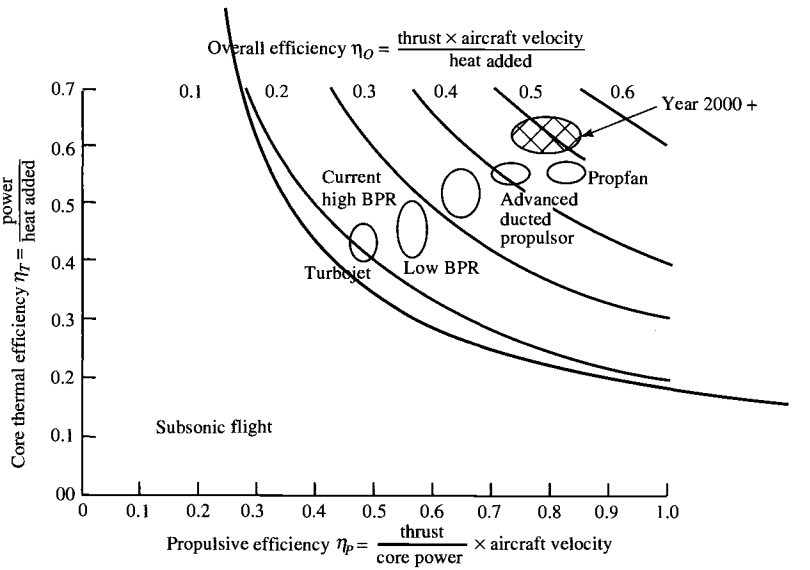

Fig. 1.17c Efficiency characteristics of typical aircraft engines. (Courtesy of Pratt & Whitney.)

Using Eqs. (1.17) and (1.19), we can write the following for TSFC:

$$\text{TSFC} = \frac{V_0}{\eta_P \eta_T h_{PR}} \tag{1.20}$$

Example 1.1

An advanced fighter engine operating at Mach 0.8 and 10-km altitude has the following uninstalled performance data and uses a fuel with $h_{PR} = 42{,}800$ kJ/kg:

$$F = 50 \text{ kN} \quad \dot{m}_0 = 45 \text{ kg/s} \quad \text{and} \quad \dot{m}_f = 2.65 \text{ kg/s}$$

Determine the specific thrust, thrust specific fuel consumption, exit velocity, thermal efficiency, propulsive efficiency, and overall efficiency (assume exit pressure equal to ambient pressure).

Solution:

$$\frac{F}{\dot{m}_0} = \frac{50\,\text{kN}}{45\,\text{kg/s}} = 1.1111 \text{ kN/(kg/s)} = 1111.1 \text{ m/s}$$

$$S = \frac{\dot{m}_f}{F} = \frac{2.65\,\text{kg/s}}{50\,\text{kN}} = 0.053\,\text{(kg/s)/kN} = 53\,\text{mg/N} \cdot \text{s}$$

$$V_0 = M_0 a_0 = M_0 \left(\frac{a_0}{a_{\text{ref}}}\right) a_{\text{ref}} = 0.8(0.8802)340.3 = 239.6 \text{ m/s}$$

From Eq. (1.6) we have

$$V_e = \frac{F g_c + \dot{m}_0 V_0}{\dot{m}_0 + \dot{m}_f} = \frac{50{,}000 \times 1 + 45 \times 239.6}{45 + 2.65} = 1275.6 \text{ m/s}$$

$$\eta_T = \frac{\dot{W}_{\text{out}}}{\dot{Q}_{\text{in}}} = \frac{(\dot{m}_0 + \dot{m}_f)V_e^2 - \dot{m}_0 V_0^2}{2 g_c \dot{m}_f h_{PR}}$$

$$\dot{W}_{\text{out}} = \frac{(\dot{m}_0 + \dot{m}_f)V_e^2 - \dot{m}_0 V_0^2}{2 g_c}$$

$$= \frac{47.65 \times 1275.6^2 - 45 \times 239.6^2}{2 \times 1} = 37.475 \times 10^6 \text{ W}$$

$$\dot{Q}_{\text{in}} = \dot{m}_f h_{PR} = 2.65 \times 42{,}800 = 113.42 \times 10^6 \text{ W}$$

$$\eta_T = \frac{\dot{W}_{\text{out}}}{\dot{Q}_{\text{in}}} = \frac{37.475 \times 10^6}{113.42 \times 10^6} = 33.04\%$$

$$\eta_P = \frac{F V_0}{\dot{W}_{\text{out}}} = \frac{50{,}000 \times 239.6}{37.475 \times 10^6} = 31.97\%$$

$$\eta_O = \frac{F V_0}{\dot{Q}_{\text{in}}} = \frac{50{,}000 \times 239.6}{113.42 \times 10^6} = 10.56\%$$

1.4.8 Specific Thrust vs Fuel Consumption

For a jet engine with a single inlet and single exhaust and exit pressure equal to ambient pressure, when the mass flow rate of the fuel is much less than that of air and the installation losses are very small, the specific thrust $F/\dot{m}_0$ can be written as

$$\frac{F}{\dot{m}_0} = \frac{V_e - V_0}{g_c} \tag{1.21}$$

Then the propulsive efficiency of Eq. (1.16) can be rewritten as

$$\eta_P = \frac{2}{Fg_c/(\dot{m}_0 V_0) + 2} \tag{1.22}$$

Substituting Eq. (1.22) into Eq. (1.20) and noting that TSFC = S, we obtain the following very enlightening expression:

$$S = \frac{Fg_c/\dot{m}_0 + 2V_0}{2\eta_T h_{PR}} \tag{1.23}$$

Aircraft manufacturers desire engines having low thrust specific fuel consumption S and high specific thrust $F/\dot{m}_0$. Low engine fuel consumption can be directly translated into longer range, increased payload, and/or reduced aircraft size. High specific thrust reduces the cross-sectional area of the engine and has a direct influence on engine weight and installation losses. This desired trend is plotted in Fig. 1.18. Equation (1.23) is also plotted in Fig. 1.18 and shows that fuel consumption and specific thrust are directly proportional. Thus the aircraft manufacturers have to make a tradeoff. The line of Eq. (1.23) shifts in the desired direction when there is an increase in the level of technology (increased thermal efficiency) or an increase in the fuel heating value.

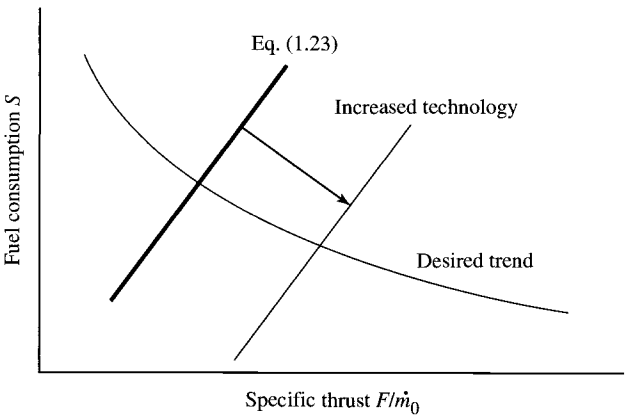

Fig. 1.18 Relationship between specific thrust and fuel consumption.

Another very useful measure of merit for the aircraft gas turbine engine is the thrust/weight ratio F/W. For a given engine thrust F, increasing the thrust/weight ratio reduces the weight of the engine. Aircraft manufacturers can use this reduction in engine weight to increase the capabilites of an aircraft (increased payload, increased fuel, or both) or decrease the size (weight) and cost of a new aircraft under development.

Engine companies expend considerable research and development effort on increasing the thrust/weight ratio of aircraft gas turbine engines. This ratio is equal to the specific thrust $F/\dot{m}_0$ divided by the engine weight per unit of mass flow $W/\dot{m}_0$. For a given engine type, the engine weight per unit mass flow is related to the efficiency of the engine structure, and the specific thrust is related to the engine thermodynamics. The weights per unit mass flow of some existing gas turbine engines are plotted vs specific thrust in Fig. 1.19. Also plotted are lines of constant engine thrust/weight ratio F/W.

The engine companies, in conjunction with the U.S. Department of Defense and NASA, are involved in a large research and development effort to increase the engine thrust/weight ratio F/W and decrease the fuel consumption while maintaining engine durability, maintainability, etc. An earlier program was called the *integrated high-performance turbine engine technology* (IHPTET) *initiative* (see Refs. 5 and 6).

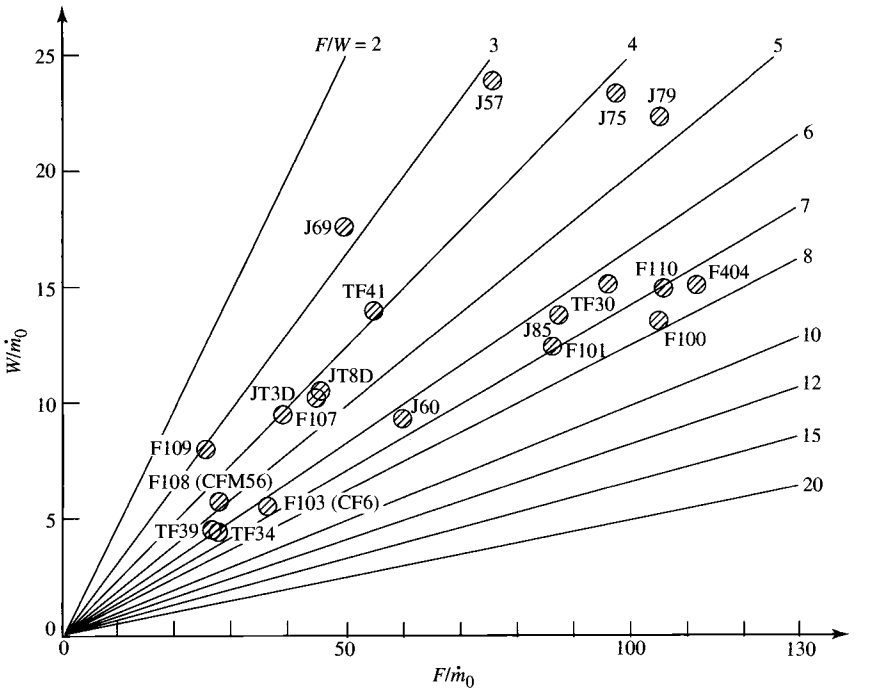

Fig. 1.19 Engine thrust/weight ratio F/W.

1.5 Aircraft Performance

This section on aircraft performance is included so that the reader may get a better understanding of the propulsion requirements of the aircraft.[7] The coverage is limited to a few significant concepts that directly relate to aircraft engines. It is not intended as a substitute for the many excellent references on this subject (see Refs. 8–11).

1.5.1 Performance Equation

Relationships for the performance of an aircraft can be obtained from energy considerations (see Ref. 12). By treating the aircraft (Fig. 1.20) as a moving mass and assuming that the installed propulsive thrust T, aerodynamic drag D, and other resistive forces R act in the same direction as the velocity V, it follows that

$$\underset{\substack{\text{rate of}\\ \text{mechanical}\\ \text{energy}\\ \text{input}}}{[T-(D+R)]V} = \underset{\substack{\text{storage}\\ \text{rate of}\\ \text{potential}\\ \text{energy}}}{W\frac{dh}{dt}} + \underset{\substack{\text{storage}\\ \text{rate of}\\ \text{kinetic}\\ \text{energy}}}{\frac{W}{g}\frac{d}{dt}\left(\frac{V^2}{2}\right)} \tag{1.24}$$

Note that the total resistive force $D+R$ is the sum of the drag of the clean aircraft D and any additional drags R associated with such proturberances as landing gear, external stores, or drag chutes.

By defining the energy height z_e as the sum of the potential and kinetic energy terms

$$z_e \equiv h + \frac{V^2}{2g} \tag{1.25}$$

Eq. (1.24) can now be written simply as

$$[T-(D+R)]V = W\frac{dz_e}{dt} \tag{1.26}$$

By defining the *weight specific excess power* P_s as

$$P_s \equiv \frac{dz_e}{dt} \tag{1.27}$$

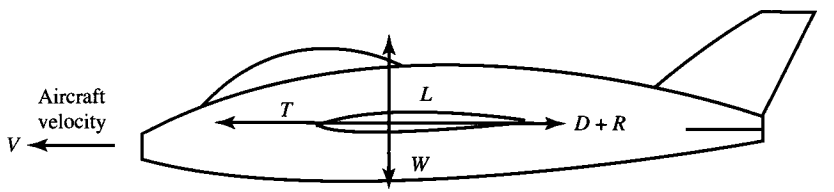

Fig. 1.20 Forces on aircraft.

Eq. (1.26) can now be written in its dimensionless form as

$$\frac{T-(D+R)}{W}=\frac{P_s}{V}=\frac{1}{V}\frac{\mathrm{d}}{\mathrm{d}t}\left(h+\frac{V^2}{2g}\right) \tag{1.28}$$

This is a very powerful equation that gives insight into the dynamics of flight, including both the rate of climb $\mathrm{d}h/\mathrm{d}t$ and acceleration $\mathrm{d}V/\mathrm{d}t$.

1.5.2 Lift and Drag

We use the classical aircraft lift relationship

$$L=nW=C_L q S_w \tag{1.29}$$

where n is the load factor or number of g perpendicular to V ($n=1$ for straight and level flight), C_L is the coefficient of lift, S_w is the wing planform area, and q is the dynamic pressure. The dynamic pressure can be expressed in terms of the density ρ and velocity V or the pressure P and Mach number M as

$$q=\frac{1}{2}\rho\frac{V^2}{g_c}=\frac{1}{2}\sigma\rho_{\mathrm{ref}}\frac{V^2}{g_c} \tag{1.30a}$$

or

$$q=\frac{\gamma}{2}PM_0^2=\frac{\gamma}{2}\delta P_{\mathrm{ref}}M_0^2 \tag{1.30b}$$

where δ and σ are the dimensionless pressure and density ratios defined by Eqs. (1.2) and (1.4), respectively, and γ is the ratio of specific heats ($\gamma=1.4$ for air). The reference density ρ_{ref} and reference pressure P_{ref} of air are their sea-level values on a standard day and are listed in Appendix A.

We also use the classical aircraft drag relationship

$$D=C_D q S_w \tag{1.31}$$

Figure 1.21 is a plot of lift coefficient C_L vs drag coefficient C_D, commonly called the *lift-drag polar*, for a typical subsonic passenger aircraft. The drag coefficient curve can be approximated by a second-order equation in C_L written as

$$C_D=K_1C_L^2+K_2C_L+C_{D0} \tag{1.32}$$

where the coefficients K_1, K_2, and C_{D0} are typically functions of flight Mach number and wing configuration (flap position, etc.).

The C_{D0} term in Eq. (1.32) is the zero lift drag coefficient that accounts for both frictional and pressure drag in subsonic flight and wave drag in supersonic flight. The K_1 and K_2 terms account for the drag due to lift. Normally K_2 is very small and approximately equal to zero for most fighter aircraft.

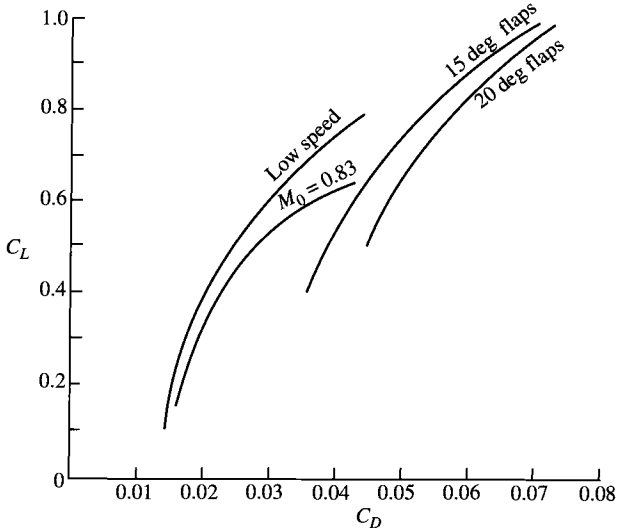

Fig. 1.21 Typical lift-drag polar.

Example 1.2

For all the examples given in this section on aircraft performance, two types of aircraft will be considered.

a) Fighter aircraft (HF-1). An advanced fighter aircraft is approximately modeled after the F-22 Advanced Tactical Fighter shown in Fig. 1.22. For convenience, we will designate our hypothetical fighter aircraft as the HF-1, having the following characteristics:

Maximum gross takeoff weight $W_{TO} = 40{,}000$ lbf (177,920 N)
Empty weight = 24,000 lbf (106,752 N)
Maximum fuel plus payload weight = 16,000 lbf (71,168 N)
Permanent payload = 1600 lbf (7117 N, crew plus return armament)
Expended payload = 2000 lbf (8896 N, missiles plus ammunition)
Maximum fuel capacity = 12,400 lbf (55,155 N)
Wing area $S_w = 720$ ft^2 (66.9 m^2)
Engine: low-bypass-ratio, mixed-flow turbofan with afterburner
Maximum lift coefficient $C_{L\max} = 1.8$
Drag coefficients given in Table 1.4

b) Passenger aircraft (HP-1). An advanced 253-passenger commercial aircraft approximately modeled after the Boeing 787 is shown in Fig. 1.23. For convenience, we will designate our hypothetical passenger aircraft as the HP-1, having the following characteristics:

Maximum gross takeoff weight W_{TO} = 1,645,760 N (370,000 lbf)
Empty weight = 822,880 N (185,500 lbf)

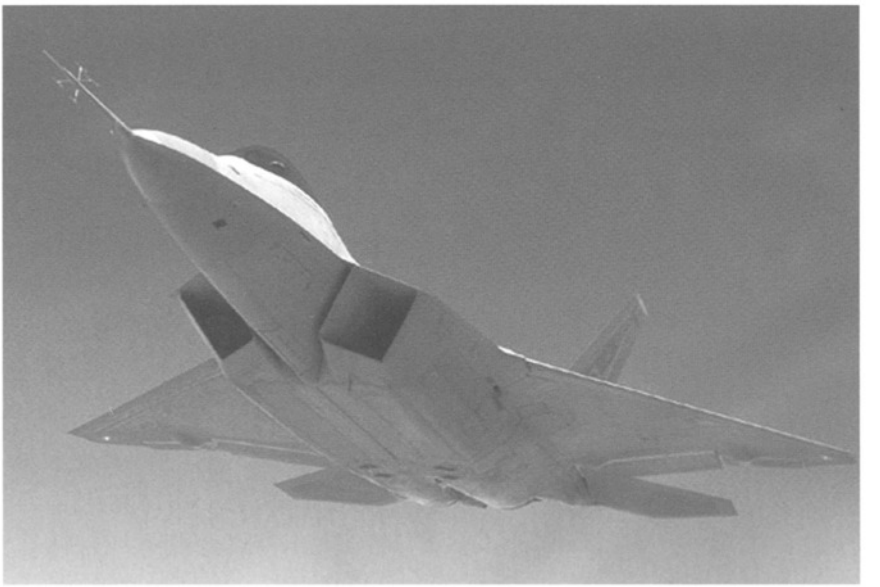

Fig. 1.22 F-22, Advanced Tactical Fighter. (Photo courtesy of Boeing Defense & Space Group, Military Airplanes Division.)

Maximum landing weight = 1,356,640 N (305,000 lbf)
Maximum payload = 420,780 N (94,600 lbf, 253 passengers plus 196,000 N of cargo)
Maximum fuel capacity = 716,706 N (161,130 lbf)
Wing area $S_w = 282.5\ \text{m}^2$ (3040 ft^2)
Engine: high-bypass-ratio turbofan
Maximum lift coefficient $C_{L\max} = 2.0$
Drag coefficients given in Table 1.5.

Table 1.4 Drag coefficients for hypothetical fighter aircraft (HF-1)

M_0	K_1	K_2	C_{D0}
0.0	0.20	0.0	0.0120
0.8	0.20	0.0	0.0120
1.2	0.20	0.0	0.02267
1.4	0.25	0.0	0.0280
2.0	0.40	0.0	0.0270

Fig. 1.23 Boeing 787. (Photo courtesy of Boeing.)

Table 1.5 Drag coefficients for hypothetical passenger aircraft (HP-1)

M_0	K_1	K_2	C_{D0}
0.00	0.056	−0.004	0.0140
0.40	0.056	−0.004	0.0140
0.75	0.056	−0.008	0.0140
0.83	0.056	−0.008	0.0150

Example 1.3

Determine the drag polar and drag variation for the HF-1 aircraft at 90% of maximum gross takeoff weight and the HP-1 aircraft at 95% of maximum gross takeoff weight.

a) Fighter aircraft (HF-1). The variation in C_{D0} and K_1 with Mach number for the HF-1 are plotted in Fig. 1.24 from the data of Table 1.4. Figure 1.25 shows the drag polar at different Mach numbers for the HF-1 aircraft. Using these drag data and the preceding equations gives the variation in aircraft drag with subsonic Mach number and altitude for level flight ($n = 1$), as shown in Fig. 1.26a. Note that the minimum drag is constant for Mach numbers 0 to 0.8 and then increases. This is the same variation as C_{D0}. The variation of drag with load factor n is shown in Fig. 1.26b at two altitudes. The drag increases with increasing

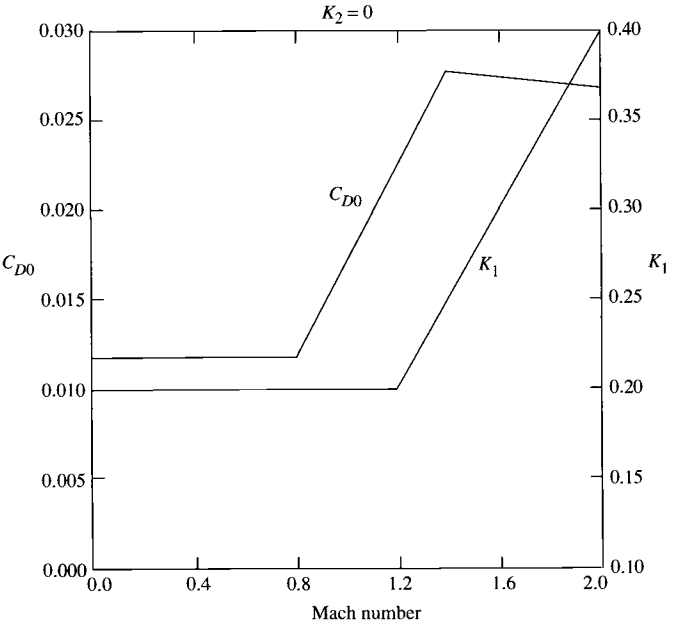

Fig. 1.24 Values of K_1 and C_{D0} for HF-1 aircraft.

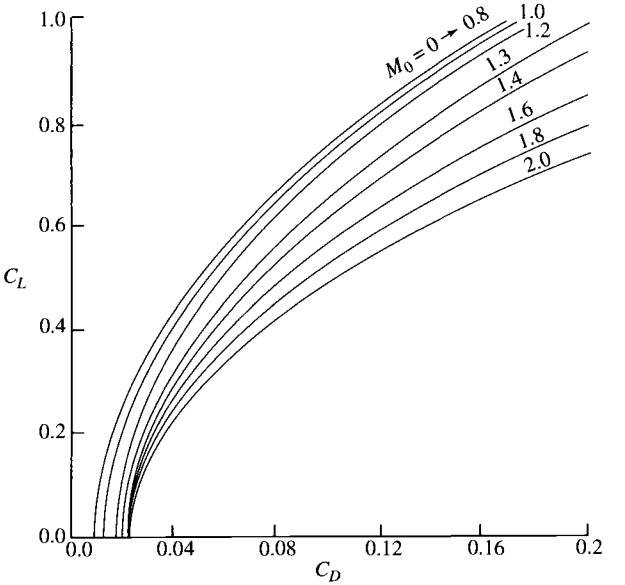

Fig. 1.25 Lift-drag polar for HF-1 aircraft.

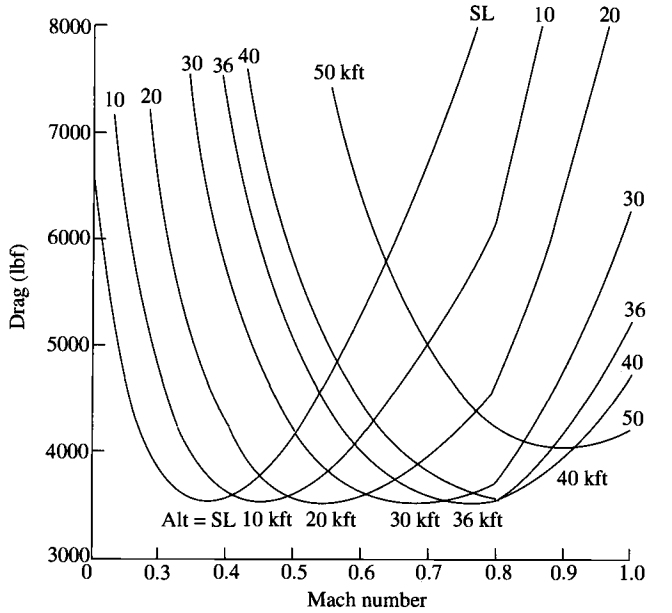

Fig. 1.26a Drag for level flight ($n = 1$) for HF-1 aircraft.

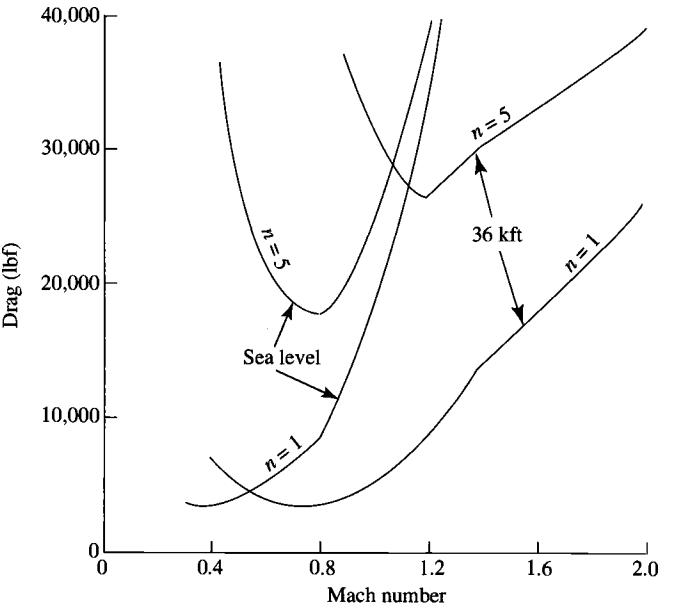

Fig. 1.26b Drag of HF-1 aircraft at sea level and 36 kft for $n = 1$ and $n = 5$.

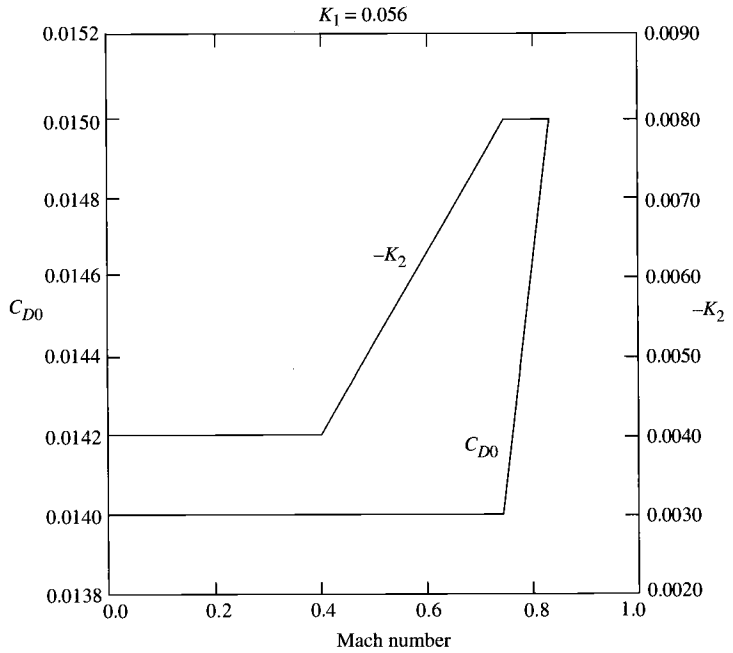

Fig. 1.27 Values of K_2 and C_{D0} for HP-1 aircraft.

load factor, and there is a flight Mach number that gives minimum drag for a given altitude and load factor.

b) Passenger aircraft (HP-1). The variation in C_{D0} and K_2 with Mach number for the HP-1 is plotted in Fig. 1.27 from the data of Table 1.5. Figure 1.28 shows the drag polar at different Mach numbers for the HP-1 aircraft. Using these drag data and the preceding equations gives the variation in aircraft drag with subsonic Mach number and altitude for level flight ($n = 1$), as shown in Fig. 1.29. Note that the minimum drag is constant for Mach numbers 0 to 0.75 and then increases. This is the same variation as C_{D0}.

Example 1.4

Calculate the drag at Mach 0.8 and 40-kft altitude of the HF-1 aircraft at 90% of maximum gross takeoff weight with load factors of 1 and 4.

Solution: We begin by calculating the dynamic pressure q:

$$q = \frac{\gamma}{2}\delta P_{\text{ref}} M_0^2 = 0.7 \times 0.1858 \times 2116 \times 0.8^2 = 176.1 \text{ lbf/ft}^2$$

From Fig. 1.24 at $M = 0.8$, $C_{D0} = 0.012$, $K_1 = 0.20$, and $K_2 = 0$.

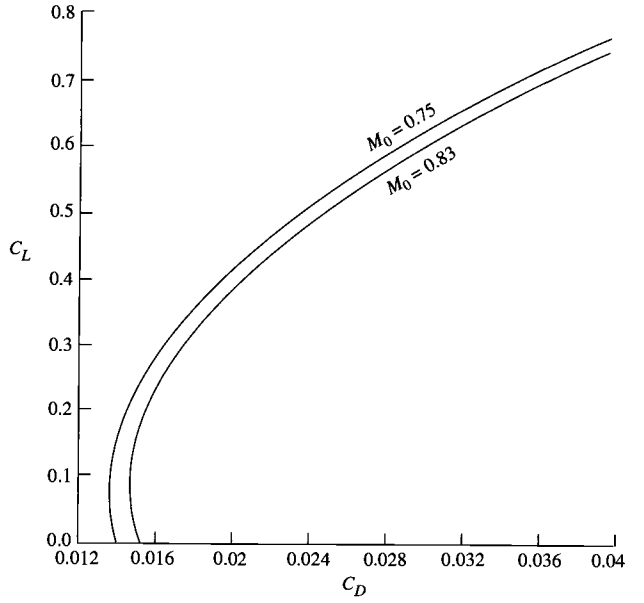

Fig. 1.28 Lift-drag polar for HP-1 aircraft.

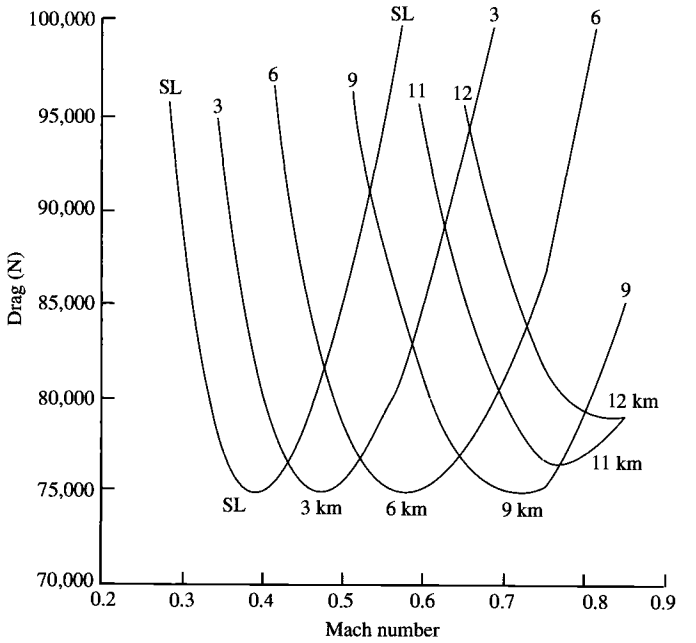

Fig. 1.29 Drag for level flight (n = 1) for HP-1 aircraft.

Case 1: $n = 1$

$$C_L = \frac{nW}{qS_w} = \frac{1 \times 0.9 \times 40{,}000}{176.1 \times 720} = 0.2839$$

$$C_D = K_1 C_L^2 + K_2 C_L + C_{D0} = 0.2(0.2839^2) + 0.012 = 0.0281$$

$$D = C_D q S_w = 0.0281 \times 176.1 \times 720 = 3563 \text{ lbf}$$

Case 2: $n = 4$

$$C_L = \frac{nW}{qS_w} = \frac{4 \times 0.9 \times 40{,}000}{176.1 \times 720} = 1.136$$

$$C_D = K_1 C_L^2 + K_2 C_L + C_{D0} = 0.2(1.136^2) + 0.012 = 0.2701$$

$$D = C_D q S_w = 0.2701 \times 176.1 \times 720 = 34{,}247 \text{ lbf}$$

Note that the drag at $n = 4$ is about 10 times that at $n = 1$.

1.5.3 Stall, Takeoff, and Landing Speeds

Stall is the flight condition when an aircraft's wing loses lift. It is an undesirable condition since vehicle control is lost for a time. During level flight (lift = weight), stall will occur when one tries to obtain a lift coefficient greater than the wing's maximum $C_{L\max}$. The *stall speed* is defined as the level flight speed that corresponds to the wing's maximum lift coefficient, or

$$V_{\text{stall}} = \sqrt{\frac{2g_c}{\rho C_{L\max}} \frac{W}{S_w}} \tag{1.33}$$

To keep away from stall, aircraft are flown at velocities greater than V_{stall}.

Takeoff and landing are two flight conditions in which the aircraft velocity is close to the stall velocity. For safety, the takeoff speed V_{TO} of an aircraft is typically 20% greater than the stall speed, and the landing speed at touchdown V_{TD} is 15% greater:

$$\begin{aligned} V_{\text{TO}} &= 1.20 V_{\text{stall}} \\ V_{\text{TD}} &= 1.15 V_{\text{stall}} \end{aligned} \tag{1.34}$$

Example 1.5

Determine the takeoff speed of the HP-1 at sea level with maximum gross takeoff weight and the landing speed with maximum landing weight.

From Appendix A we have $\rho = 1.255\ \text{kg/m}^3$ for sea level. From Example 1.2b we have $C_{L\max} = 2.0$, $W = 1{,}645{,}760$ N, $S_w = 282.5\ \text{m}^2$, and

$$V_{\text{stall}} = \sqrt{\frac{2 \times 1}{1.225 \times 2.0} \frac{1{,}645{,}760}{282.5}} = 69.0\ \text{m/s}$$

Thus

$$V_{\text{TO}} = 1.20 V_{\text{stall}} = 82.8\ \text{m/s}\ (\approx 185\ \text{mph})$$

For landing, $W = 1{,}356{,}640$ N, and

$$V_{\text{stall}} = \sqrt{\frac{2 \times 1}{1.225 \times 2.0} \frac{1{,}356{,}640}{282.5}} = 62.6\ \text{m/s}$$

Thus

$$V_{\text{TD}} = 1.15 V_{\text{stall}} = 72.0\ \text{m/s}\ (\approx 161\ \text{mph})$$

1.5.4 Fuel Consumption

The rate of change of the aircraft weight dW/dt is due to the fuel consumed by the engines. The mass rate of fuel consumed is equal to the product of the installed thrust T and the installed thrust specific fuel consumption. For constant acceleration of gravity g_0, we can write

$$\frac{dW}{dt} = -\dot{w}_f = -\dot{m}_f \frac{g_0}{g_c} = -T(\text{TSFC})\left(\frac{g_0}{g_c}\right)$$

This equation can be rewritten in dimensionless form as

$$\frac{dW}{W} = -\frac{T}{W}(\text{TSFC})\left(\frac{g_0}{g_c}\right)dt \tag{1.35}$$

1.5.4.1 Estimate of TSFC. Equation (1.35) requires estimates of installed engine thrust T and installed TSFC to calculate the change in aircraft weight. For many flight conditions, the installed engine thrust T equals the aircraft drag D. The value of TSFC depends on the engine cycle, altitude, and Mach number. For preliminary analysis, the following equations (from Ref. 12) can be used to estimate TSFC in units of (lbm/h)/lbf, and θ is the dimensionless temperature ratio T/T_{ref}:

1) High-bypass-ratio turbofan

$$\text{TSFC} = (0.4 + 0.45 M_0)\sqrt{\theta} \tag{1.36a}$$

2) Low-bypass-ratio, mixed-flow turbofan
Military and lower power settings:

$$\text{TSFC} = (1.0 + 0.35M_0)\sqrt{\theta} \tag{1.36b}$$

Maximum power setting:

$$\text{TSFC} = (1.8 + 0.30M_0)\sqrt{\theta} \tag{1.36c}$$

3) Turbojet
Military and lower power settings:

$$\text{TSFC} = (1.3 + 0.35M_0)\sqrt{\theta} \tag{1.36d}$$

Maximum power setting:

$$\text{TSFC} = (1.7 + 0.26M_0)\sqrt{\theta} \tag{1.36e}$$

4) Turboprop

$$\text{TSFC} = (0.2 + 0.9M_0)\sqrt{\theta} \tag{1.36f}$$

1.5.4.2 Endurance. For level unaccelerated flight, thrust equals drag ($T = D$) and lift equals weight ($L = W$). Thus Eq. (1.35) is simply

$$\frac{dW}{W} = -\frac{C_D}{C_L}(\text{TSFC})\left(\frac{g_0}{g_c}\right)dt \tag{1.37}$$

We define the endurance factor (EF) as

$$\text{EF} \equiv \frac{C_L}{C_D(\text{TSFC})}\frac{g_c}{g_0} \tag{1.38}$$

Then Eq. (1.37) becomes

$$\frac{dW}{W} = -\frac{dt}{\text{EF}} \tag{1.39}$$

Note that the minimum fuel consumption for a time t occurs at the flight condition where the endurance factor is maximum.

For the case when the endurance factor is constant or nearly constant, Eq. (1.39) can be integrated from the initial to final conditions and the following expression obtained for the aircraft weight fraction:

$$\frac{W_f}{W_i} = \exp\left(-\frac{t}{\text{EF}}\right) \tag{1.40a}$$

or

$$\frac{W_f}{W_i} = \exp\left[-\frac{C_D}{C_L}(\text{TSFC})t\frac{g_0}{g_c}\right] \tag{1.40b}$$

1.5.4.3 Range. For portions of aircraft flight where distance is important, the differential time dt is related to the differential distance ds by

$$\mathrm{d}s = V\,\mathrm{d}t \tag{1.41}$$

Substituting into Eq. (1.37) gives

$$\frac{\mathrm{d}W}{W} = -\frac{C_D}{C_L}\frac{\text{TSFC}}{V}\frac{g_0}{g_c}\mathrm{d}s \tag{1.42}$$

We define the range factor (RF) as

$$\text{RF} \equiv \frac{C_L}{C_D}\frac{V}{\text{TSFC}}\frac{g_c}{g_0} \tag{1.43}$$

Then Eq. (1.42) can be simply written as

$$\frac{\mathrm{d}W}{W} = -\frac{\mathrm{d}s}{\text{RF}} \tag{1.44}$$

Note that the minimum fuel consumption for a distance s occurs at the flight condition where the range factor is maximum.

For the flight conditions where the RF is constant or nearly constant, Eq. (1.42) can be integrated from the initial to final conditions and the following expression obtained for the aircraft weight fraction:

$$\frac{W_f}{W_i} = \exp\left(-\frac{s}{\text{RF}}\right) \tag{1.45a}$$

or

$$\frac{W_f}{W_i} = \exp\left(-\frac{C_D}{C_L}\frac{\text{TSFC} \times s\, g_0}{V\quad g_c}\right) \tag{1.45b}$$

This is called the *Breguet range equation.* For the range factor to remain constant, C_L/C_D and V/TSFC need to be constant. Above 36-kft altitude, the ambient temperature is constant, and a constant velocity V will correspond to constant Mach and constant TSFC for a fixed throttle setting. If C_L is constant, C_L/C_D will remain constant. Since the aircraft weight W decreases during the flight, the altitude must increase to reduce the density of the ambient air and produce the required lift ($L = W$) while maintaining C_L and velocity constant. This flight profile is called a *cruise climb.*

Example 1.6

Calculate the endurance factor and range factor at Mach 0.8 and 40-kft altitude of hypothetical fighter aircraft HF-1 at 90% of maximum gross takeoff weight and a load factor of 1.

Solution:

$$q = \frac{\gamma}{2}\delta P_{\text{ref}} M_0^2 = 0.7 \times 0.1858 \times 2116 \times 0.8^2 = 176.1 \text{ lbf/ft}^2$$

From Fig. 1.24 at $M = 0.8$, $C_{D0} = 0.012$, $K_1 = 0.20$, and $K_2 = 0$:

$$C_L = \frac{nW}{qS_w} = \frac{1 \times 0.9 \times 40{,}000}{176.1 \times 720} = 0.2839$$

$$C_D = K_1 C_L^2 + K_2 C_L + C_{D0} = 0.2(0.2839^2) + 0.012 = 0.0281$$

Using Eq. (1.36b), we have

$$\text{TSFC} = (1.0 + 0.35M_0)\sqrt{\theta} = (1.0 + 0.35 \times 0.8)\sqrt{0.7519} = 1.110\,(\text{lbm/h})/\text{lbf}$$

Thus

$$\text{EF} = \frac{C_L}{C_D(\text{TSFC})}\frac{g_c}{g_0} = \frac{0.2839}{0.0281 \times 1.110}\frac{32.174}{32.174} = 9.102 \text{ h}$$

$$\text{RF} = \frac{C_L}{C_D}\frac{V}{\text{TSFC}}\frac{g_c}{g_0}$$

$$= \frac{0.2839}{0.0281}\frac{0.8 \times 0.8671 \times 1116\,\text{ft/s}}{1.110\,(\text{lbm/h})/\text{lbf}}\frac{3600\,\text{s/h}}{6080\,\text{ft/nm}}\frac{32.174}{32.174}$$

$$= 4170 \text{ nm}$$

Example 1.7

Determine the variation in endurance factor and range factor for the two hypothetical aircraft HF-1 and HP-1.

a) Fighter aircraft (HF-1). The endurance factor is plotted vs Mach number and altitude in Fig. 1.30 for our hypothetical fighter aircraft HF-1 at 90% of maximum gross takeoff weight. Note that the best endurance Mach number (minimum fuel consumption) increases with altitude, and the best fuel consumption occurs at altitudes of 30 and 36 kft. The range factor is plotted vs Mach number and altitude in Fig. 1.31 for the HF-1 at 90% of maximum gross takeoff weight. Note that the best cruise Mach number (minimum fuel consumption) increases with altitude, and the best fuel consumption occurs at an altitude of 36 kft and Mach number of 0.8.

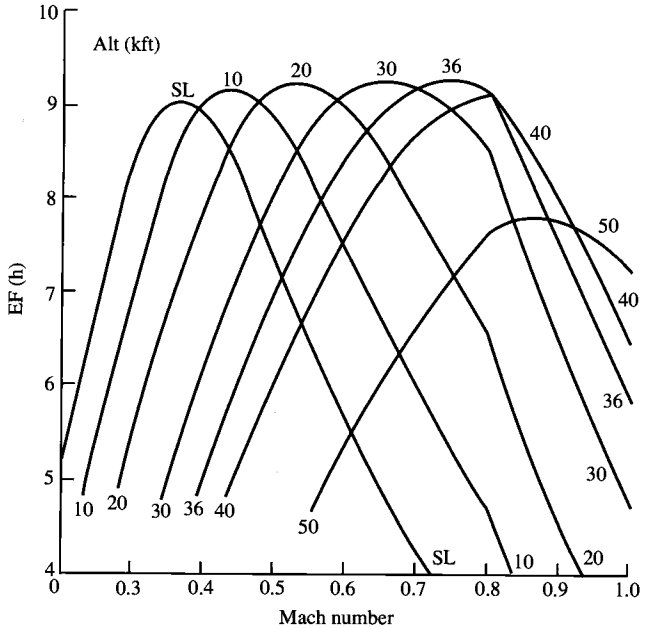

Fig. 1.30 Endurance factor for HF-1 aircraft.

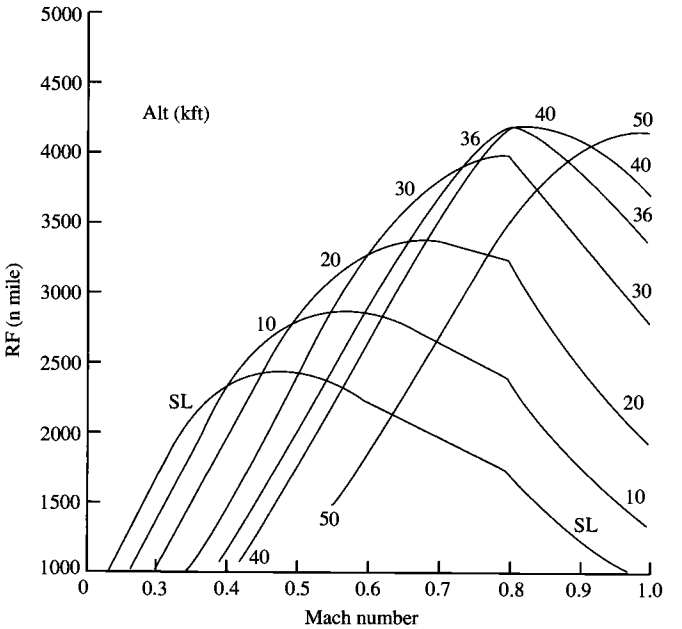

Fig. 1.31 Range factor for HF-1 aircraft.

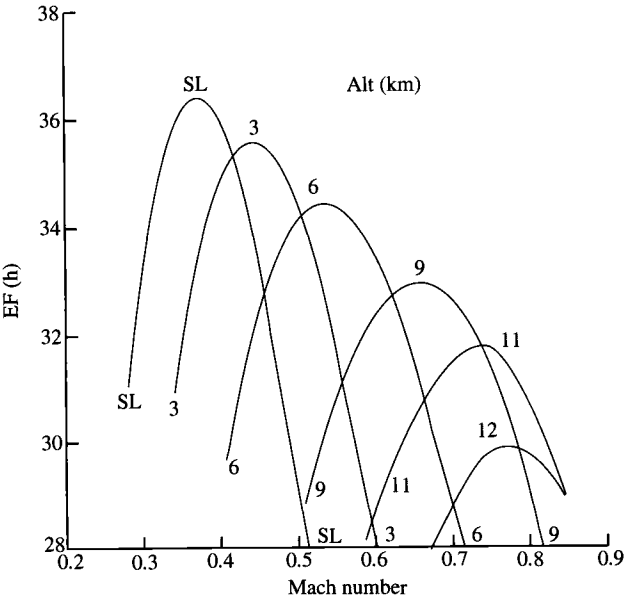

Fig. 1.32 Endurance factor for HP-1 aircraft.

b) Passenger aircraft (HP-1). The endurance factor is plotted vs Mach number and altitude in Fig. 1.32 for our hypothetical passenger aircraft HP-1 at 95% of maximum gross takeoff weight. Note that the best endurance Mach number (minimum fuel consumption) increases with altitude, and the best fuel consumption occurs at sea level. The range factor is plotted vs Mach number and altitude in Fig. 1.33 for the HP-1 at 95% of maximum gross takeoff weight. Note that the best cruise Mach number (minimum fuel consumption) increases with altitude, and the best fuel consumption occurs at an altitude of 11 km and Mach number of about 0.83.

Since the weight of an aircraft like the HP-1 can vary considerably over a flight, the variation in range factor with cruise Mach number was determined for 95 and 70% of maximum gross takeoff weight (MGTOW) at altitudes of 11 and 12 km and is plotted in Fig. 1.34. If the HP-1 flew at 0.83 Mach and 12-km altitude, the range factors at 95% MGTOW and at 70% MGTOW are about the same. However, if the HP-1 flew at 0.83 Mach and 11-km altitude, the range factor would decrease with aircraft weight, and the aircraft's range would be less than that of the HP-1 flown at 0.83 Mach and 12-km altitude. One can see from this discussion that the proper cruise altitude can dramatically affect an aircraft's range.

1.5.4.4 Maximum C_L/C_D. For flight conditions requiring minimum fuel consumption, the optimum flight condition can be approximated by that

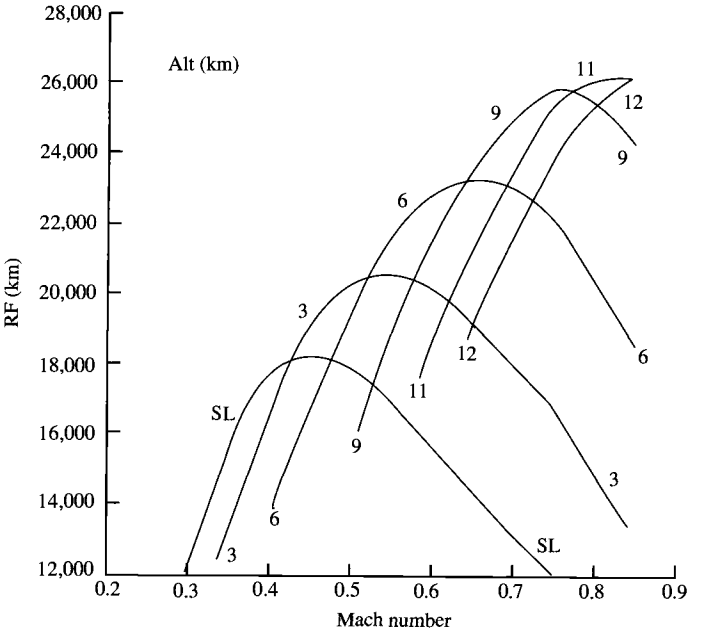

Fig. 1.33 Range factor for HP-1 aircraft for various altitudes.

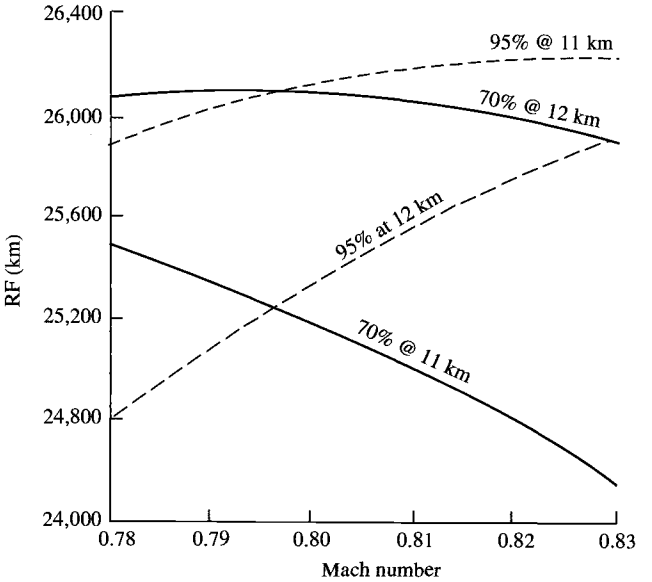

Fig. 1.34 Range factor for HP-1 aircraft at 70 and 95% MGTOW.

corresponding to maximum C_L/C_D. From Eq. (1.32), the maximum C_L/C_D (minimum C_D/C_L) can be found by taking the derivative of the following expression, setting it equal to zero, and solving for the C_L that gives minimum C_D/C_L:

$$\frac{C_D}{C_L} = K_1 C_L + K_2 + \frac{C_{D0}}{C_L} \tag{1.46}$$

The lift coefficient that gives maximum C_L/C_D (minimum C_D/C_L) is

$$C_L^* = \sqrt{\frac{C_{D0}}{K_1}} \tag{1.47}$$

and maximum C_L/C_D is given by

$$\left(\frac{C_L}{C_D}\right)^* = \frac{1}{2\sqrt{C_{D0}K_1} + K_2} \tag{1.48}$$

The drag D, range factor, endurance factor, and C_L/C_D vs Mach number at an altitude are plotted in Fig. 1.35 for the HF-1 aircraft and in Fig. 1.36 for the HP-1. Note that the maximum C_L/C_D occurs at Mach 0.8 for the HF-1 and at Mach 0.75 for the HP-1, the same Mach numbers where drags are minimum. The endurance factor is a maximum at a substantially lower Mach number than that corresponding to $(C_L/C_D)^*$ for the HF-1 due to the high TSFC and its increase with Mach number [see Eq. (1.36b)]. The endurance factor for

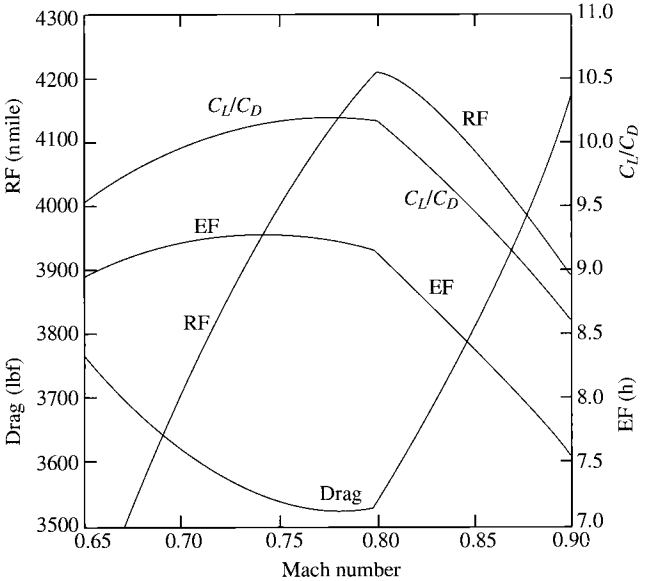

Fig. 1.35 Comparison of drag C_L/C_D, endurance factor, and range factor for the HF-1 at 36-kft altitude.

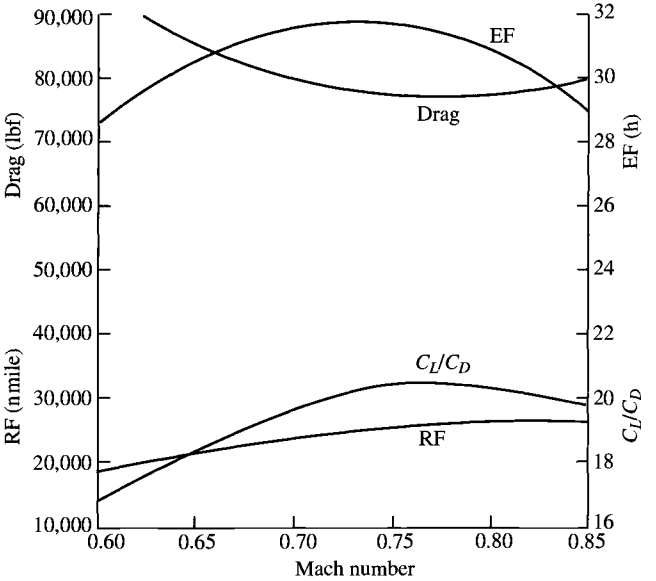

Fig. 1.36 Comparison of drag C_L/C_D, endurance factor, and range factor for the HP-1 at 11-km altitude.

the HP-1 is a maximum at the same Mach number that C_L/C_D is maximum due to the lower TSFC of the high-bypass-ratio turbofan engine [see Eq. (1.36a)].

The Mach number for an altitude giving a maximum range factor is called the *best cruise Mach* (BCM). The best cruise Mach normally occurs at a little higher Mach than that corresponding to $(C_L/C_D)^*$. This is because the velocity term in the range factor normally dominates over the increase in TSFC with Mach number. As a first approximation, many use the Mach number corresponding to $(C_L/C_D)^*$ for the best cruise Mach.

Example 1.8

Calculate the Mach giving maximum C_L/C_D at 20-kft altitude for the HF-1 aircraft at 90% of maximum gross takeoff weight and a load factor of 1.

Solution: From Fig. 1.24 at $M_0 < 0.8$, $C_{D0} = 0.012$, $K_1 = 0.20$, and $K_2 = 0$:

$$C_L^* = \sqrt{\frac{C_{D0}}{K_1}} = \sqrt{\frac{0.012}{0.2}} = 0.2449$$

$$q = \frac{W}{C_L S_w} = \frac{0.9 \times 40{,}000}{0.2449 \times 720} = 204.16\,\text{lbf/ft}^2$$

$$M_0 = \sqrt{\frac{q}{(\gamma/2)\delta P_{\text{ref}}}} = \sqrt{\frac{204.16}{0.7 \times 0.4599 \times 2116}} = 0.547$$

1.5.4.5 Accelerated flight. For flight conditions when thrust T is greater than drag D, an expression for the fuel consumption can be obtained by first noting from Eq. (1.28) that

$$\frac{T}{W} = \frac{P_s}{V[1 - (D + R)/T]}$$

We define the ratio of drag $D + R$ to thrust T as

$$u \equiv \frac{D + R}{T} \tag{1.49}$$

The preceding equation for thrust to weight becomes

$$\frac{T}{W} = \frac{P_s}{V(1 - u)} \tag{1.50}$$

Now Eq. (1.35) can be rewritten as

$$\frac{dW}{W} = -\frac{\text{TSFC}}{V(1 - u)} \frac{g_0}{g_c} P_s \, dt$$

Since $P_s \, dt = dz_e$, the preceding equation can be expressed in its most useful forms as

$$\frac{dW}{W} \frac{\text{TSFC}}{V(1 - u)} \frac{g_0}{g_c} dz_e = -\frac{\text{TSFC}}{V(1 - u)} \frac{g_0}{g_c} d\left(h + \frac{V^2}{2g}\right) \tag{1.51}$$

The term $1 - u$ represents the fraction of engine power that goes to increasing the aircraft energy z_e, and u represents that fraction that is lost to aircraft drag $D + R$. Note that this equation applies for cases when u is not unity. When u is unity, either Eq. (1.39) or Eq. (1.44) is used.

To obtain the fuel consumption during an acceleration flight condition, Eq. (1.51) can be easily integrated for known flight paths (values of V and z_e) and known variation of $\text{TSFC}/[V(1 - u)]$ with z_e.

1.5.5 Aerospace Vehicle Design—A Team Effort

Aeronautical and mechanical engineers in the aerospace field do many things, but for the most part their efforts all lead to the design of some type of aerospace vehicle. The design team for a new aircraft may be divided into four principal groups: aerodynamics, propulsion, structures, and flight mechanics. The design of a vehicle calls on the extraordinary talents of engineers in each group. Thus the design is a team effort. A typical design team is shown in Fig. 1.37. The chief engineer serves as the referee and integrates the efforts of everyone into the vehicle design. Figure 1.38 shows the kind of aircraft design that might result if any one group were able to dominate the others.

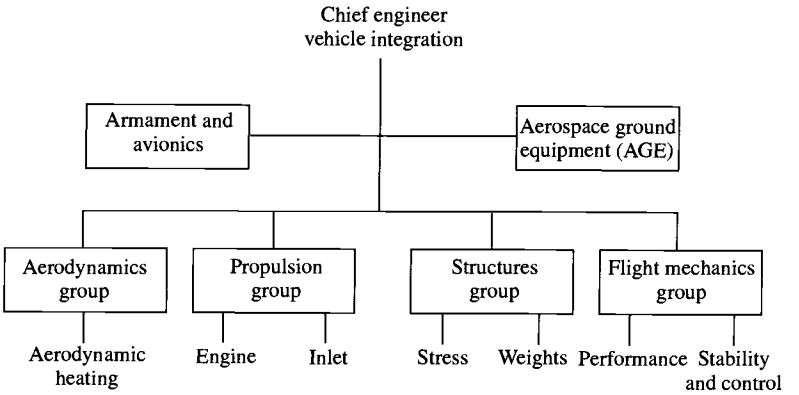

Fig. 1.37 Organization of a typical vehicle design team.

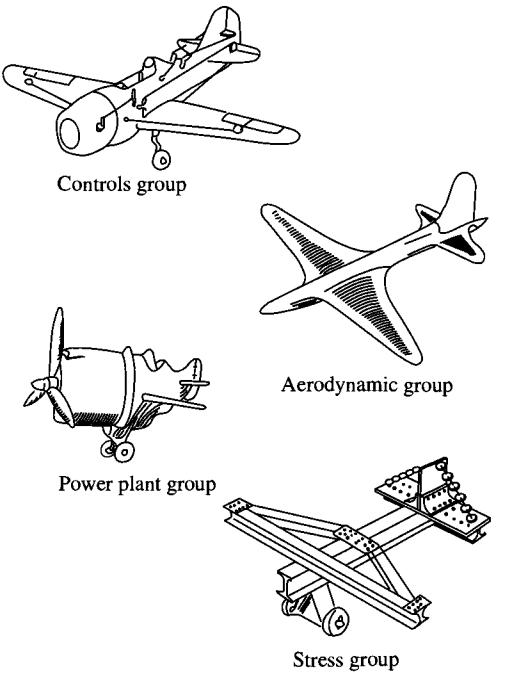

Fig. 1.38 Aircraft designs.

1.6 Rocket Engines

Non-airbreathing propulsion systems are characterized by the fact that they carry both fuel and the oxidizer within the aerospace vehicle. Such systems thus may be used anywhere in space as well as in the atmosphere. Figure 1.39

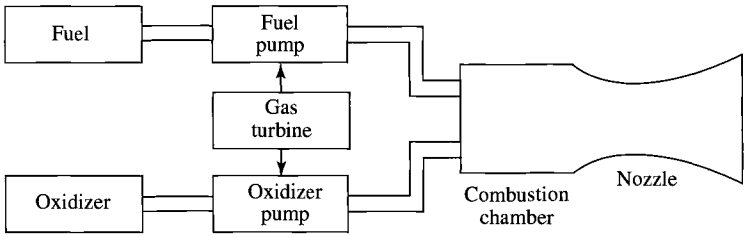

Fig. 1.39 Liquid-propellant rocket motor.

shows the essential features of a liquid-propellant rocket system. Two propellants (an oxidizer and a fuel) are pumped into the combustion chamber where they ignite. The nozzle accelerates the products of combustion to high velocities and exhausts them to the atmosphere or space.

A solid-propellant rocket motor is the simplest of all propulsion systems. Figure 1.40 shows the essential features of this type of system. In this system, the fuel and oxidizer are mixed together and cast into a solid mass called the *grain*. The grain, usually formed with a hole down the middle called the *perforation*, is firmly cemented to the inside of the combustion chamber. After ignition, the grain burns radially outward, and the hot combustion gases pass down the perforation and are exhausted through the nozzle.

The absence of a propellant feed system in the solid-propellant rocket is one of its major advantages. Liquid rockets, on the other hand, may be stopped and later restarted, and their thrust may be varied somewhat by changing the speed of the fuel and oxidizer pumps.

1.6.1 Rocket Engine Thrust

A natural starting point in understanding the performance of a rocket is the examination of the static thrust. Application of the momentum equation developed in Chapter 2 will show that the static thrust is a function of the propellant flow rate $\dot{m}_p$, the exhaust velocity V_e and pressure P_e, the exhaust area A_e, and the ambient pressure P_a. Figure 1.41 shows a schematic of a stationary rocket

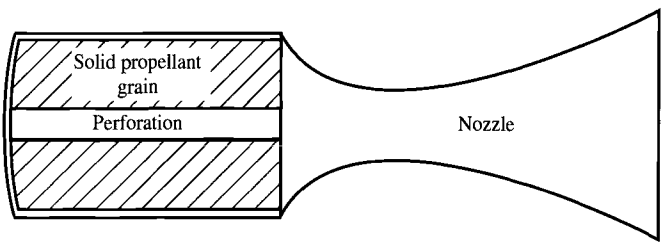

Fig. 1.40 Solid-propellant rocket motor.

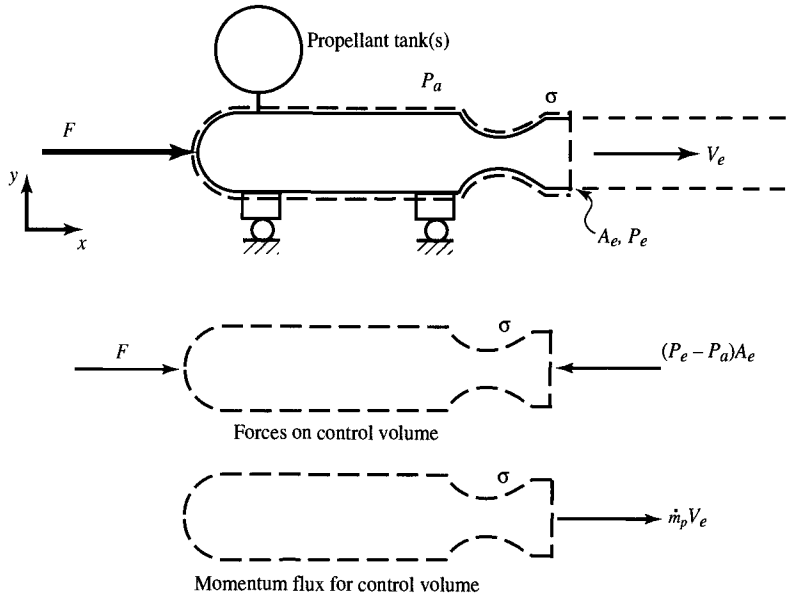

Fig. 1.41 Schematic diagram of static rocket engine.

to be considered for analysis. We assume the flow to be one-dimensional, with a steady exit velocity V_e and propellant flow rate $\dot{m}_p$. About this rocket we place a control volume σ whose control surface intersects the exhaust jet perpendicularly through the exit plane of the nozzle. Thrust acts in the direction opposite to the direction of V_e. The reaction to the thrust F necessary to hold the rocket and control volume stationary is shown in Fig. 1.41.

The momentum equation applied to this system gives the following:

1) Sum of forces acting on the outside surface of the control volume:

$$\sum F_x = F - (P_e - P_a)A_e$$

2) The net rate of change of momentum for the control volume:

$$\Delta(\text{momentum}) = \dot{M}_{\text{out}} = \frac{\dot{m}_p V_e}{g_c}$$

Since the sum of the forces acting on the outside of the control volume is equal to the net rate of change of the momentum for the control volume, we have

$$F - (P_e - P_a)A_e = \frac{\dot{m}_p V_e}{g_c} \tag{1.52}$$

If the pressure in the exhaust plane P_e is the same as the ambient pressure P_a, the thrust is given by $F = \dot{m}_p V_e / g_c$. The condition $P_e = P_a$ is called *on-design* or *optimum expansion* because it corresponds to maximum thrust for the given chamber conditions. It is convenient to define an *effective exhaust velocity* C such that

$$C \equiv V_e + \frac{(P_e - P_a)A_e g_c}{\dot{m}_p} \tag{1.53}$$

Thus the static thrust of a rocket can be written as

$$F = \frac{\dot{m}_p C}{g_c} \tag{1.54}$$

1.6.2 Specific Impulse

The *specific impulse* I_{sp} for a rocket is defined as the thrust per unit of propellant weight flow:

$$I_{sp} \equiv \frac{F}{\dot{w}_p} = \frac{F}{\dot{m}_p} \frac{g_c}{g_0} \tag{1.55}$$

where g_0 is the acceleration due to gravity at sea level. The unit of I_{sp} is the second. From Eqs. (1.54) and (1.55), the specific impulse can also be written as

$$I_{sp} = \frac{C}{g_0} \tag{1.56}$$

Example 1.9

Find the specific impulse of the space shuttle main engine (SSME) shown in Fig. 1.42a that produces 470,000 lbf in a vacuum with a propellant weight flow of 1030 lbf/s. By using Eq. (1.55), we find that the SSME has a specific impulse I_{sp} of 456 s (= 470,000/1030) in vacuum.

An estimate of the variation in thrust with altitude for the space shuttle main engine is shown in Fig. 1.42b. The typical specific impulses for some rocket engines are listed in Table 1.6. Other performance data for rocket engines are contained in Appendix C.

1.6.3 Rocket Vehicle Acceleration

The mass of a rocket vehicle varies a great deal during flight due to the consumption of the propellant. The velocity that a rocket vehicle attains during powered flight can be determined by considering the vehicle in Fig. 1.43.

The figure shows an accelerating rocket vehicle in a gravity field. At some time, the mass of the rocket is m and its velocity is V. In an infinitesimal time dt, the rocket exhausts an incremental mass dm_p with an exhaust velocity V_e

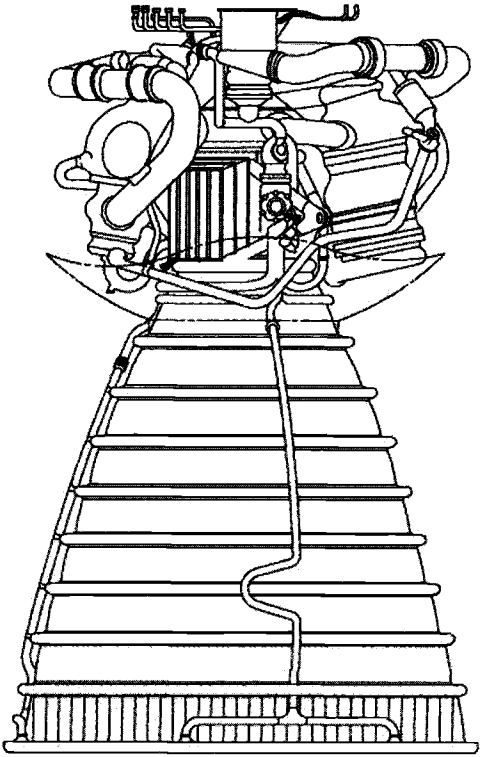

Fig. 1.42a Space shuttle main engine (SSME).

relative to the rocket as the rocket velocity changes to $V + \mathrm{d}V$. The net change in momentum of the control volume σ is composed of the momentum out of the rocket at the exhaust plus the change of the momentum of the rocket. The momentum out of the rocket in the V direction is $-V_e\,\mathrm{d}m_p$, and the change in the momentum of the rocket in the V direction is $m\,\mathrm{d}V$. The forces acting on the control volume σ are composed of the net pressure force, the drag D, and the gravitational force. The sum of these forces in the V direction is

$$\sum F_V = (P_e - P_a)A_e - D - \frac{mg}{g_c}\cos\theta$$

The resultant impulse on the rocket $\left(\sum F_V\right)\mathrm{d}t$ must equal the momentum change of the system $\Delta(\text{momentum}) = (-V_e\,\mathrm{d}m_p + m\,\mathrm{d}V)/g_c$. Thus

$$\left[(P_e - P_a)A_e - D - \frac{mg}{g_c}\cos\theta\right]\mathrm{d}t = \frac{-V_e\,\mathrm{d}m_p + m\,\mathrm{d}V}{g_c}$$

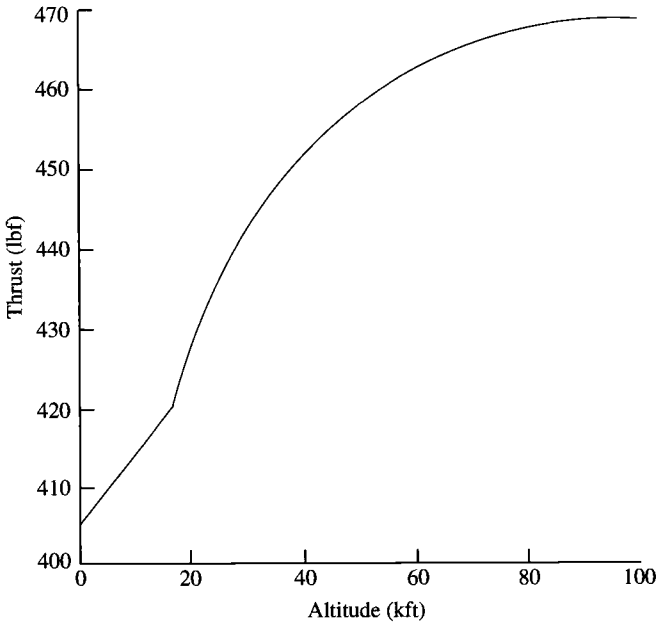

Fig. 1.42b Rocket thrust variation with altitude.

From the preceding relationship, the momentum change of the rocket ($m\ dV$) is

$$\frac{m\ dV}{g_c} = \left[(P_e - P_a)A_e - D - \frac{mg}{g_c}\cos\theta\right]dt + \frac{V_e\ dm_p}{g_c} \tag{1.57}$$

Since $dm_p = \dot{m}_p\ dt = -(dm/dt)dt$, then Eq. (1.57) can be written as

$$\frac{m\ dV}{g_c} = \left[(P_e - P_a)A_e + \frac{\dot{m}_p V_e}{g_c} - D - \frac{mg}{g_c}\cos\theta\right]dt$$

Table 1.6 Ranges of specific impulse I_{sp} for typical rocket engines

Fuel/oxidizer	I_{sp}, s
Solid propellant	250
Liquid O_2: kerosene (RP)	310
Liquid O_2: H_2	410
Nuclear fuel: H_2 propellant	840

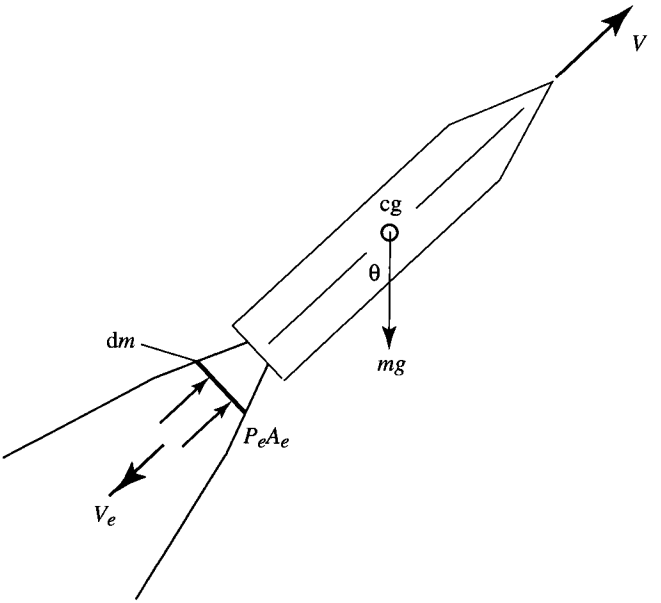

Fig. 1.43 Rocket vehicle in flight.

By using Eq. (1.53), this relationship becomes

$$\frac{m\,\mathrm{d}V}{g_c} = \left(\frac{\dot{m}_p}{g_c}C - D - \frac{mg}{g_c}\cos\theta\right)\mathrm{d}t$$

or

$$\mathrm{d}V = -C\frac{\mathrm{d}m}{m} - \frac{Dg_c}{m}\mathrm{d}t - g\cos\theta\,\mathrm{d}t \tag{1.58}$$

The velocity of a rocket along its trajectory can be determined from the preceding equation if C, D, g, and θ are known.

In the absence of drag and gravity, integration of Eq. (1.58) gives the following, assuming constant effective exhaust velocity C:

$$\Delta V = C\,\ell n\frac{m_i}{m_f} \tag{1.59}$$

where ΔV is the change in velocity, m_i is the initial mass of the rocket system, and m_f is the final mass. Equation (1.59) can be solved for the mass ratio as

$$\frac{m_i}{m_f} = \exp\frac{\Delta V}{C} \tag{1.60}$$

Example 1.10

We want to estimate the mass ratio (final to initial) of an H_2-O_2 ($C = 4000$ m/s) rocket for an Earth orbit ($\Delta V = 8000$ m/s), neglecting drag and gravity. Using Eq. (1.59), we obtain $m_f/m_t = e^{-2} = 0.132$, or a single-stage rocket would be about 13% payload and structure and 87% propellant.

Problems

1.1 Calculate the uninstalled thrust for Example 1.1, using Eq. (1.6).

1.2 Develop the following analytical expressions for a turbojet engine:

(a) When the fuel flow rate is very small in comparison with the air mass flow rate, the exit pressure is equal to ambient pressure, and the installation loss coefficients are zero, then the installed thrust T is given by

$$T = \frac{\dot{m}_0}{g_c}(V_e - V_0)$$

(b) For the preceding conditions, the thrust specific fuel consumption is given by

$$\text{TSFC} = \frac{Tg_c/\dot{m}_0 + 2V_0}{2\eta_T h_{PR}}$$

(c) For $V_0 = 0$ and 500 ft/s, plot the preceding equation for TSFC [in (lbm/h)/lbf] vs specific thrust $T/\dot{m}_0$ [in lbf/(lbm/s)] for values of specific thrust from 0 to 120. Use $\eta_T = 0.4$ and $h_{PR} = 18{,}400$ Btu/lbm.

(d) Explain the trends.

1.3 Repeat 1.2c, using SI units. For $V_0 = 0$ and 150 m/s, plot TSFC [in (mg/s)/N] vs specific thrust $T/\dot{m}_0$ [in N/(kg/s)] for values of specific thrust from 0 to 1200. Use $\eta_T = 0.4$ and $h_{PR} = 42{,}800$ kJ/kg.

1.4 A J57 turbojet engine is tested at sea-level, static, standard-day conditions ($P_0 = 14.696$ psia, $T_0 = 518.7°$R, and $V_0 = 0$). At one test point, the thrust is 10,200 lbf while the airflow is 164 lbm/s and the fuel flow is 8520 lbm/h. Using these data, estimate the exit velocity V_e for the case of exit pressure equal to ambient pressure ($P_0 = P_e$).

1.5 The thrust for a turbofan engine with separate exhaust streams is equal to the sum of the thrust from the engine core F_C and the thrust from the bypass stream F_B. The bypass ratio of the engine α is the ratio of the mass flow through the bypass stream to the core mass flow, or $\alpha \equiv \dot{m}_B/\dot{m}_C$. When the exit pressures are equal to the ambient pressure,

the thrusts of the core and bypass stream are given by

$$F_C = \frac{1}{g_c}[(\dot{m}_C + \dot{m}_f)V_{Ce} - \dot{m}_C V_0]$$

$$F_B = \frac{\dot{m}_B}{g_c}(V_{Be} - V_0)$$

where V_{Ce} and V_{Be} are the exit velocities from the core and bypass, respectively, V_0 is the inlet velocity, and $\dot{m}_f$ is the mass flow rate of fuel burned in the core of the engine.

Show that the specific thrust and thrust specific fuel consumption can be expressed as

$$\frac{F}{\dot{m}_0} = \frac{1}{g_c}\left(\frac{1 + \dot{m}_f/\dot{m}_C}{1+\alpha}V_{Ce} + \frac{\alpha}{1+\alpha}V_{Be} - V_0\right)$$

$$S = \frac{\dot{m}_f}{F} = \frac{\dot{m}_f/\dot{m}_C}{(F/\dot{m}_0)(1+\alpha)}$$

where $\dot{m}_0 = \dot{m}_C + \dot{m}_B$.

1.6 The CF6 turbofan engine has a rated thrust of 40,000 lbf at a fuel flow rate of 13,920 lbm/h at sea-level static conditions. If the core airflow rate is 225 lbm/s and the bypass ratio is 6.0, what are the specific thrust [lbf/(lbm/s)] and thrust specific fuel consumption [(lbm/h)/lbf]?

1.7 The JT9D high-bypass-ratio turbofan engine at maximum static thrust ($V_0 = 0$) on a sea-level, standard day ($P_0 = 14.696$ psia, $T_0 = 518.7°$R) has the following data: the air mass flow rate through the core is 247 lbm/s, the air mass flow rate through the fan bypass duct is 1248 lbm/s, the exit velocity from the core is 1190 ft/s, the exit velocity from the bypass duct is 885 ft/s, and the fuel flow rate into the combustor is 15,750 lbm/h. Estimate the following for the case of exit pressures equal to ambient pressure ($P_0 = P_e$):

(a) The thrust of the engine
(b) The thermal efficiency of the engine (heating value of jet fuel is about 18,400 Btu/lbm)
(c) The propulsive efficiency and thrust specific fuel consumption of the engine

1.8 Repeat Problem 1.7, using SI units.

1.9 One advanced afterburning fighter engine, whose performance is depicted in Figs. 1.14a–1.14e, is installed in the HF-1 fighter aircraft. Using the aircraft drag data of Fig. 1.26b, determine and plot the variation of weight specific excess power (P_s in feet per second) vs flight Mach number for

level flight ($n = 1$) at 36-kft altitude. Assume the installation losses are constant with values of $\phi_{\text{inlet}} = 0.05$ and $\phi_{\text{noz}} = 0.02$.

1.10 Determine the takeoff speed of the HF-1 aircraft.

1.11 Determine the takeoff speed of the HP-1 aircraft at 90% of maximum gross takeoff weight.

1.12 Derive Eqs. (1.47) and (1.48) for maximum C_L/C_D. Start by taking the derivative of Eq. (1.46) with respect to C_L and finding the expression for the lift coefficient that gives maximum C_L/C_D.

1.13 Show that for maximum C_L/C_D, the corresponding drag coefficient C_D is given by

$$C_D = 2C_{D0} + K_2\sqrt{\frac{C_{D0}}{K_1}}$$

1.14 An aircraft with a wing area of 800 ft^2 is in level flight ($n = 1$) at maximum C_L/C_D. Given that the drag coefficients for the aircraft are $C_{D0} = 0.02$, $K_2 = 0$, and $K_1 = 0.2$, find

(a) The maximum C_L/C_D and the corresponding values of C_L and C_D
(b) The flight altitude [use Eqs. (1.29) and (1.30b)] and aircraft drag for an aircraft weight of 45,000 lbf at Mach 0.8
(c) The flight altitude and aircraft drag for an aircraft weight of 35,000 lbf at Mach 0.8
(d) The range for an installed engine thrust specific fuel consumption rate of 0.8 (lbm/h)/lbf, if the 10,000-lbf difference in aircraft weight between parts b and c is due only to fuel consumption

1.15 An aircraft weighing 110,000 N with a wing area of 42 m^2 is in level flight ($n = 1$) at the maximum value of C_L/C_D. Given that the drag coefficients for the aircraft are $C_{D0} = 0.03$, $K_2 = 0$, and $K_1 = 0.25$, find the following:

(a) The maximum C_L/C_D and the corresponding values of C_L and C_D
(b) The flight altitude [use Eqs. (1.29) and (1.30b)] and aircraft drag at Mach 0.5
(c) The flight altitude and aircraft drag at Mach 0.75

1.16 The Breguet range equation [Eq. (1.45b)] applies for a cruise climb flight profile with constant RF. Another range equation can be developed for a level cruise flight profile with varying RF. Consider the case where we keep C_L, C_D, and TSFC constant and vary the flight velocity with aircraft

weight by the expression

$$V = \sqrt{\frac{2g_c W}{\rho C_L S_w}}$$

Using the subscripts i and f for the initial and final flight conditions, respectively, show the following:

(a) Substitution of this expression for flight velocity into Eq. (1.42) gives

$$\frac{dW}{\sqrt{W}} = -\frac{\sqrt{W_i}}{RF_i} ds$$

(b) Integration of the preceding between the initial i and final f conditions gives

$$\frac{W_f}{W_i} = \left[1 - \frac{s}{2(RF_i)}\right]^2$$

(c) For a given weight fraction W_f/W_i, the maximum range s for this level cruise flight corresponds to starting the flight at the maximum altitude (minimum density) and maximum value of $\sqrt{C_L}/C_D$.

(d) For the drag coefficient equation of Eq. (1.32), maximum $\sqrt{C_L}/C_D$ corresponds to $C_L = (1/6K_1)(\sqrt{12K_1C_{D0} + K_2^2} - K_2)$.

1.17 An aircraft begins a cruise at a wing loading W/S_w of 100 lbf/ft^2 and Mach 0.8. The drag coefficients are $K_1 = 0.056$, $K_2 = -0.008$, and $C_{D0} = 0.014$, and the fuel consumption TSFC is constant at 0.8 (lbm/h)/lbf. For a weight fraction W_f/W_i of 0.9, determine the range and other parameters for two different types of cruise.

(a) For a cruise climb (maximum C_L/C_D) flight path, determine C_L, C_D, initial and final altitudes, and range.

(b) For a level cruise (maximum $\sqrt{C_L}/C_D$) flight path, determine C_L, C_D, altitude, initial and final velocities, and range.

1.18 An aircraft weighing 70,000 lbf with a wing area of 1000 ft^2 is in level flight ($n = 1$) at 30-kft altitude. Using the drag coefficients of Fig. 1.24 and the TSFC model of Eq. (1.36b), find the following:

(a) The maximum C_L/C_D and the corresponding values of C_L, C_D, and Mach number (Note: Since the drag coefficients are a function of Mach number and it is an unknown, you must first guess a value for the Mach number to obtain the drag coefficients. Try a Mach number of 0.8 for your first guess.)

(b) The C_L, C_D, C_L/C_D, range factor, endurance factor, and drag for flight Mach numbers of 0.74, 0.76, 0.78, 0.80, 0.81, and 0.82

(c) The best cruise Mach (maximum RF)
(d) The best loiter Mach (maximum EF)

1.19 An aircraft weighing 200,000 N with a wing area of 60 m^2 is in level flight ($n = 1$) at 9-km altitude. Using the drag coefficients of Fig. 1.24 and TSFC model of Eq. (1.36b), find the following:
(a) The maximum C_L/C_D and the corresponding values of C_L, C_D, and Mach number (Note: Since the drag coefficients are a function of the Mach number and it is an unknown, you must first guess a value for the Mach number to obtain the drag coefficients. Try a Mach number of 0.8 for your first guess.)
(b) The C_L, C_D, C_L/C_D, range factor, endurance factor, and drag for flight Mach numbers of 0.74, 0.76, 0.78, 0.80, 0.81, and 0.82
(c) The best cruise Mach (maximum RF)
(d) The best loiter Mach (maximum EF)

1.20 What is the specific impulse in seconds of the JT9D turbofan engine in Problem 1.7?

1.21 A rocket motor is fired in place on a static test stand. The rocket exhausts 100 lbm/s at an exit velocity of 2000 ft/s and pressure of 50 psia. The exit area of the rocket is 0.2 ft^2. For an ambient pressure of 14.7 psia, determine the effective exhaust velocity, the thrust transmitted to the test stand, and the specific impulse.

1.22 A rocket motor under static testing exhausts 50 kg/s at an exit velocity of 800 m/s and pressure of 350 kPa. The exit area of the rocket is 0.02 m^2. For an ambient pressure of 100 kPa, determine the effective exhaust velocity, the thrust transmitted to the test stand, and the specific impulse.

1.23 The propellant weight of an orbiting space system amounts to 90% of the system gross weight. Given that the system rocket engine has a specific impulse of 300 s, determine:
(a) The maximum attainable velocity if all the propellant is burned and the system's initial velocity is 7930 m/s
(b) The propellant mass flow rate, given that the rocket engine thrust is 1,670,000 N

1.24 A chemical rocket motor with a specific impulse of 400 s is used in the final stage of a multistage launch vehicle for deep-space exploration. This final stage has a mass ratio (initial to final) of 6, and its single rocket motor is first fired while it orbits the Earth at a velocity of 26,000 ft/s. The final stage must reach a velocity of 36,700 ft/s to escape the Earth's gravitational field. Determine the percentage of fuel that must be used to perform this maneuver (neglect gravity and drag).

Gas Turbine Design Problems

1.D1 *Background (HP-1 aircraft).* You are to determine the thrust and fuel consumption requirements of the two engines for the hypothetical passenger aircraft, the HP-1. The twin-engine aircraft will cruise at 0.83 Mach and be capable of the following requirements:

1) Takeoff at maximum gross takeoff weight W_{TO} from an airport at 1.6-km pressure altitude on a hot day (38°C) uses a 3650-m (12-kft) runway. The craft is able to maintain a 2.4% single-engine climb gradient in the event of engine failure at liftoff.
2) It transports 253 passengers and luggage (90 kg each) over a still-air distance of 11,120 km (6000 n mile). It has 30 min of fuel in reserve at end (loiter).
3) It attains an initial altitude of 11 km at beginning of cruise ($P_s = 1.5$ m/s).
4) The single-engine craft cruises at 5-km altitude at 0.45 Mach ($P_s = 1.5$ m/s).

All of the data for the HP-1 contained in Example 1.2 apply. Preliminary mission analysis of the HP-1 using the methods of Ref. 12 for the 11,120-km flight with 253 passengers and luggage (22,770-kg payload) gives the preliminary fuel use shown in Table P1.D1.

Analysis of takeoff indicates that each engine must produce an installed thrust of 214 kN on a hot day (38°C) at 0.1 Mach and 1.6-km pressure altitude. To provide for reasonable-length landing gear, the maximum diameter of the engine inlet is limited to 2.2 m. Based on standard design practice (see Chapter 10), the maximum mass flow rate per unit area is given by

$$\frac{\dot{m}}{A} = 231.8\frac{\delta_0}{\sqrt{\theta_0}} \quad (\text{kg/s})/\text{m}^2$$

Table P1.D1

Description	Distance, km	Fuel used, kg
Taxi		200[a]
Takeoff		840[a]
Climb and acceleration	330	5,880[a]
Cruise	10,650	50,240
Descent	140	1,090[a]
Loiter (30 min at 9-km altitude)		2,350
Land and taxi		600[a]
	11,120	61,200

[a]These fuel consumptions can be considered to be constant.

Thus on a hot day (38°C) at 0.1 Mach and 1.6-km pressure altitude, $\theta = (38 + 273.1)/288.2 = 1.079$, $\theta_0 = 1.079 \times 1.002 = 1.081$, $\delta = 0.8256$, $\delta_0 = 0.8256 \times 1.007 = 0.8314$, and the maximum mass flow through the 2.2-m-diam inlet is 704.6 kg/s.

Calculations (HP-1 Aircraft).

1) If the HP-1 starts out the cruise at 11 km with a weight of 1,577,940 N, find the allowable TSFC for the distance of 10,650 km for the following cases:
   (a) Assume the aircraft performs a cruise climb (flies at a constant C_D/C_L). What is its altitude at the end of the cruise climb?
   (b) Assume the aircraft cruises at a constant altitude of 11 km. Determine C_D/C_L at the start and end of cruise. Using the average of these two values, calculate the allowable TSFC.
2) Determine the loiter (endurance) Mach numbers for altitudes of 10, 9, 8, 7, and 6 km when the HP-1 aircraft is at 64% of W_{TO}.
3) Determine the aircraft drag at the following points in the HP-1 aircraft's 11,120-km flight based on the fuel consumptions just listed:
   (a) Takeoff, $M = 0.23$, sea level
   (b) Start of cruise, $M = 0.83$, 11 km
   (c) End of cruise climb, $M = 0.83$, altitude = ? ft
   (d) End of 11-km cruise, $M = 0.83$, 11 km
   (e) Engine out (88% of W_{TO}), $M = 0.45$, 5 km

1.D2 *Background (HF-1 Aircraft).* You are to determine the thrust and fuel consumption requirements of the two engines for the hypothetical fighter aircraft HF-1. This twin-engine fighter will supercruise at 1.6 Mach and will be capable of the following requirements:

1) Takeoff at maximum gross takeoff weight W_{TO} from a 1200-ft (366-m) runway at sea level on a standard day.
2) Supercruise at 1.6 Mach and 40-kft altitude for 250 nm (463 km) at 92% of W_{TO}.
3) Perform 5-g turns at 1.6 Mach and 30-kft altitude at 88% of W_{TO}.
4) Perform 5-g turns at 0.9 Mach and 30-kft altitude at 88% of W_{TO}.
5) Perform the maximum mission listed in the following.

All of the data for the HF-1 contained in Example 1.2 apply. Preliminary mission analysis of the HF-1 using the methods of Ref. 12 for the maximum mission gives the preliminary fuel use shown in Table P1.D2:

Analysis of takeoff indicates that each engine must produce an installed thrust of 23,500 lbf on a standard day at 0.1 Mach and sea-level altitude. To provide for optimum integration into the airframe, the maximum area of the engine inlet is limited to 5 ft^2. Based on standard design practice (see Chapter 10), the maximum mass flow rate per unit

Table P1.D2

Description	Distance, nm	Fuel used, lbm
Warmup, taxi, takeoff		700[a]
Climb and acceleration to 0.9 Mach and 40 kft	35	1,800[a]
Accelerate from 0.9 to 1.6 Mach	12	700[a]
Supercruise at 1.6 Mach and 40 kft	203	4,400
Deliver payload of 2000 lbf	0	0[a]
Perform one 5-g turn at 1.6 Mach and 30 kft	0	1,000[a]
Perform two 5-g turns at 0.9 Mach and 30 kft	0	700[a]
Climb to best cruise altitude and 0.9 Mach	23	400[a]
Cruise climb at 0.9 Mach	227	1,600
Loiter (20 min at 30-kft altitude)		1,100
Land		0[a]
	500	12,400

[a]These fuel consumptions can be considered to be constant.

area for subsonic flight conditions is given by

$$\frac{\dot{m}}{A} = 47.5 \frac{\delta_0}{\sqrt{\theta_0}} \quad (\text{lbm/s})/\text{ft}^2$$

Thus at 0.1 Mach and sea-level standard day, $\theta = 1.0$, $\theta_0 = 1.002$, $\delta = 1.0$, $\delta_0 = 1.007$, and the maximum mass flow through the 5-ft^2 inlet is 238.9 lbm/s. For supersonic flight conditions, the maximum mass flow rate per unit area is simply the density of the air ρ times its velocity V.

Calculations (HF-1 Aircraft).

1) If the HF-1 starts the supercruise at 40 kft with a weight of 36,800 lbf, find the allowable TSFC for the distance of 203 nm for the following cases:
   (a) Assume the aircraft performs a cruise climb (flies at a constant C_D/C_L). What is its altitude at the end of the cruise climb?
   (b) Assume the aircraft cruises at a constant altitude of 40 kft. Determine C_D/C_L at the start and end of cruise. Using the average of these two values, calculate the allowable TSFC.
2) Find the best cruise altitude for the subsonic return cruise at 0.9 Mach and 70.75% of W_{TO}.
3) Determine the loiter (endurance) Mach numbers for altitudes of 32, 30, 28, 26, and 24 kft when the HF-1 aircraft is at 67% of W_{TO}.

4) Determine the aircraft drag at the following points in the HF-1 aircraft's maximum mission based on the fuel consumptions just listed:
   (a) Takeoff, $M = 0.172$, sea level
   (b) Start of supercruise, $M = 1.6$, 40 kft
   (c) End of supercruise climb, $M = 1.6$, altitude = ? ft
   (d) End of 40-kft supercruise, $M = 1.6$, 40 kft
   (e) Start of subsonic cruise, $M = 0.9$, altitude = best cruise altitude
   (f) Start of loiter, altitude = 30 kft

2
Review of Fundamentals

2.1 Introduction

The operation of gas turbine engines and of rocket motors is governed by the laws of mechanics and thermodynamics. The field of mechanics includes the mechanics of both fluids and solids. However, since the process occurring in most propulsion devices involves a flowing fluid, our emphasis will be on fluid mechanics or, more specifically, gas dynamics.

Understanding and predicting the basic performance of gas turbine engines and rocket motors requires a closed set of governing equations (e.g., conservation of mass, energy, momentum, and entropy). For transparency, understanding, and capturing the basic physical phenomena, we model the gas as a *perfect gas* and the flow as *one-dimensional flow*, in which the fluid properties are constant across the flow and vary only in the direction of flow (axial direction).

This chapter is intended as a review of thermodynamics and one-dimensional gas dynamics that are the foundation of this textbook. We include new material from *Hypersonic Airbreathing Propulsion* by Heiser and Pratt[13] on the graphical solution and description of one-dimensional gas dynamics in Section 2.8 to improve the reader's comprehension of this fundamental material.

This chapter concludes with a short section on chemical reactions to provide the fundamentals needed to understand reacting flows (e.g., combustion). With this material, we will predict the equilibrium state of reacting flows and the performance of liquid-fuel rocket motors. For further study, the student is directed to references such as Ref. 14.

2.2 Equations of State and Conservation of Mass

The state of a system is described by specifying the values of the properties of the system. Pressure P, temperature T, specific internal energy e, and density ρ or specific volume $v = 1/\rho$ are some basic thermodynamic properties. The specification of any two independent intensive properties will fix the thermodynamic state of a simple (meaning in absence of motion and force fields) system and, therefore, the values of all other thermodynamic properties of the system. The values of the other properties may be found through equations of state. The most common working fluid addressed in this book is a gas that is modeled using the perfect gas equations of state.

A function relating one dependent and two independent thermodynamic properties of a simple system of unit mass is called an *equation of state.* When the three properties are P, v, and T as in

$$f(P, v, T) = 0 \tag{2.1}$$

the equation is called the *thermal equation of state.* In general, we cannot write the functional relationship equation (2.1) in the form of an equation in which specified values of the two properties will allow us to determine the value of the third. Although humans may not know what the functional relation equation (2.1) is for a given system, one does exist and nature always knows what it is. When the solution set of Eq. (2.1) cannot be determined from relatively simple equations, tables that list the values of P, v, and T (elements of the solution set) satisfying the function may be prepared. This has been done for water (in all of its phases), air, and most common gases.

The functional relation between the internal energy e of a simple system of unit mass and any two independent properties for the set P, v $(=1/\rho)$, T is called the *energy equation of state.* This equation can be written functionally as

$$e = e(T, v) \qquad \text{or} \qquad e = e(P, v) \qquad \text{or} \qquad e = e(P, T) \tag{2.2}$$

As with the thermal equation of state, we may not be able to write an analytical expression for any of the functional relations of Eq. (2.2). The important thing is that energy is a property; hence, the functional relations exist.

If the solution sets of the thermal and energy equations of state of a simple system of unit mass are known, all thermodynamic properties of the system can be found when any two of the three properties P, v, T are specified. From the solution set, we can form a tabulation of v and e against specified values of P and T for all states of the system. From these known values of P, T, v, and e, we can determine any other property of the simple system. For example, the value of the property *enthalpy* h is found for any state of the system by combining the tabulated values of P, v, and e for that state by

$$h \equiv e + Pv \tag{2.3}$$

Four other definitions are listed here for use in the later sections of this chapter: specific heat at constant volume c_v, specific heat at constant pressure c_P, ratio of specific heats γ, the speed of sound a, and the Mach number M:

$$c_v \equiv \left(\frac{\partial e}{\partial T}\right)_v \tag{2.4}$$

$$c_P \equiv \left(\frac{\partial h}{\partial T}\right)_P \tag{2.5}$$

$$\gamma \equiv c_p/c_v \tag{2.6}$$

$$a^2 \equiv g_c\left(\frac{\partial P}{\partial \rho}\right)_s = \gamma g_c\left(\frac{\partial P}{\partial \rho}\right)_T \tag{2.7}$$

$$M = V/a \tag{2.8}$$

2.2.1 Definition of Steady Flow

Consider the flow of fluid through the control volume σ shown in Fig. 2.1. If the properties of the fluid at any point i in the control volume do not vary with time, the flow is called *steady flow*. For such flows we may conclude that for any property R within σ

$$\frac{dR_\sigma}{dt} = 0 \qquad \text{in steady flow} \tag{2.9}$$

2.2.2 Definition of One-Dimensional Flow

If the intensive stream properties at a permeable control surface section normal to the flow directions are uniform, the flow is called *one-dimensional*. Many flows in engineering may be treated as steady one-dimensional flows. The term *one-dimensional* is synonymous in this use with *uniform* and applies only at a control surface section. Thus the overall flow through a control volume may be in more than one dimension and still be uniform (one-dimensional flow) at permeable sections of the control surface normal to the flow direction. The flow in Fig. 2.2 is called one-dimensional flow because the intensive properties, such as velocity, density, and temperature, are uniform at sections 1 and 2.

2.2.3 Conservation of Mass Equation

The law of mass conservation for any control volume system σ is simply

$$\frac{dm_\sigma}{dt} = \dot{m}_{\text{in}} - \dot{m}_{\text{out}} \tag{2.10a}$$

where

$$\dot{m} = \int_A \rho V_\perp \, dA \tag{2.10b}$$

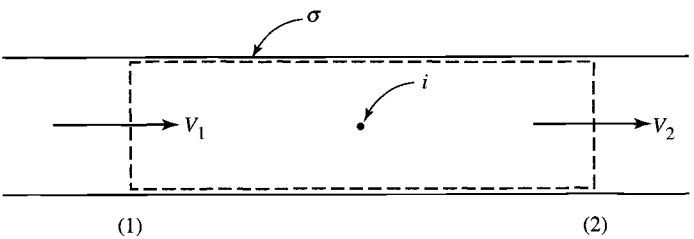

Fig. 2.1 Control volume for steady flow.

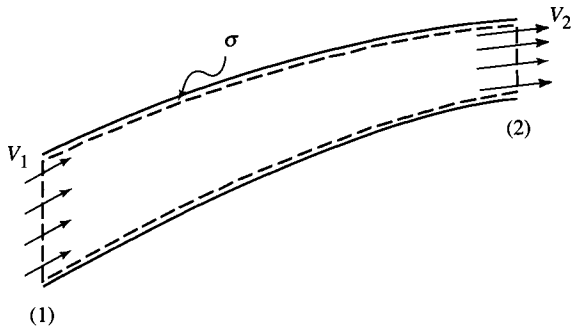

Fig. 2.2 One-dimensional flow through a convergent duct. The flow is uniform at sections 1 and 2, hence one-dimensional, even though the flow direction may vary elsewhere in the flow.

and $V_\perp$ is the velocity component normal to area A. This equation is known as the *conservation of mass equation.* For steady flows through any control volume, Eq. (2.10a) simplifies to

$$\dot{m}_{\text{out}} = \dot{m}_{\text{in}} \tag{2.11}$$

If the flow is steady and one-dimensional through a control volume with a single inlet and exit such as shown in Fig. 2.2, then by Eq. (2.10b)

$$\dot{m} = \rho A V_\perp \tag{2.12a}$$

which is called the *one-dimensional mass flow equation*, and

$$\rho_1 A_1 V_{\perp_1} = \rho_2 A_2 V_{\perp_2} \tag{2.12b}$$

2.3 Steady Flow Energy Equation

We consider steady one-dimensional flow of a fluid through a control volume and surface σ (Fig. 2.3). Fluid crosses σ at the in and out stations only. A shaft-work interaction $\dot{W}_x$ and heat interaction $\dot{Q}$ occur at the boundary of σ. If the energy within the control volume does not change with time (steady flow), the first law of thermodynamics can be written as

$$\dot{Q} - \dot{W}_x = \dot{m}\left(h + \frac{V^2}{2g_c} + \frac{gz}{g_c}\right)_{\text{out}} - \dot{m}\left(h + \frac{V^2}{2g_c} + \frac{gz}{g_c}\right)_{\text{in}} \tag{2.13}$$

where the dimensions of $\dot{Q}, \dot{W}_x$, etc., are those of power or energy per unit time. Dividing by $\dot{m}$ gives

$$q - w_x = \left(h + \frac{V^2}{2g_c} + \frac{gz}{g_c}\right)_{\text{out}} - \left(h + \frac{V^2}{2g_c} + \frac{gz}{g_c}\right)_{\text{in}} \tag{2.14}$$

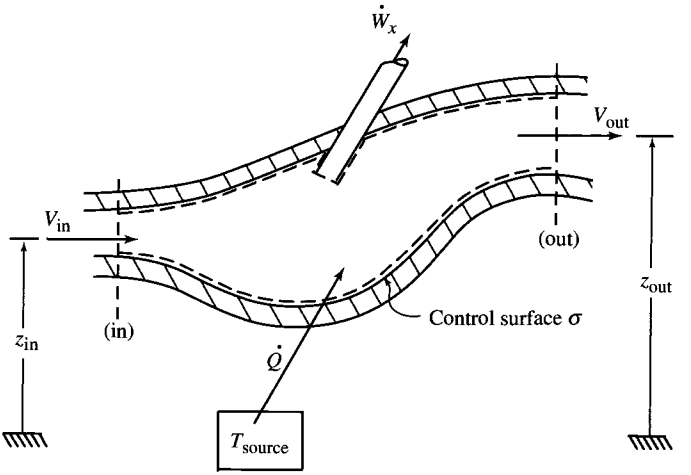

Fig. 2.3 Steady flow through control volume σ.

where q and w_x are the heat and shaft-work interactions per unit mass flow through σ. All of the terms in this equation have units of energy per unit mass.

Example 2.1

The first step in the application of the steady flow energy equation is a clear definition of a control surface σ. This is so because each term in the equation refers to a quantity at the boundary of a control volume. Thus, to use the equation, one needs only to examine the control surface and identify the applicable terms of the equation.

In the application of Eq. (2.14) to specific flow situations, many of the terms are zero or may be neglected. The following example will illustrate this point. The perfect gas equation (presented in detail later in this chapter) is used to model the relationship between change in enthalpy and temperature of the gas.

Consider a turbojet aircraft engine as shown in Fig. 2.4a. We divide the engine into the control volume regions:

σ_1: inlet	σ_4: turbine
σ_2: compressor	σ_5: nozzle
σ_3: combustion chamber	

Let us apply the steady flow energy equation to each of these control volumes. In all cases, the potential energy change $(gz/g_c)_{out} - (gz/g_c)_{in}$ is zero and will be ignored.

It is advisable in using the steady flow energy equation to make two sketches of the applicable control surface σ, showing the heat and shaft work interactions (q, w_x) in one sketch and the fluxes of energy $[h, V^2/(2g_c)]$ in the second sketch. The term $[h + V^2/(2g_c)]_{out}$ is a flux per unit mass flow of internal energy

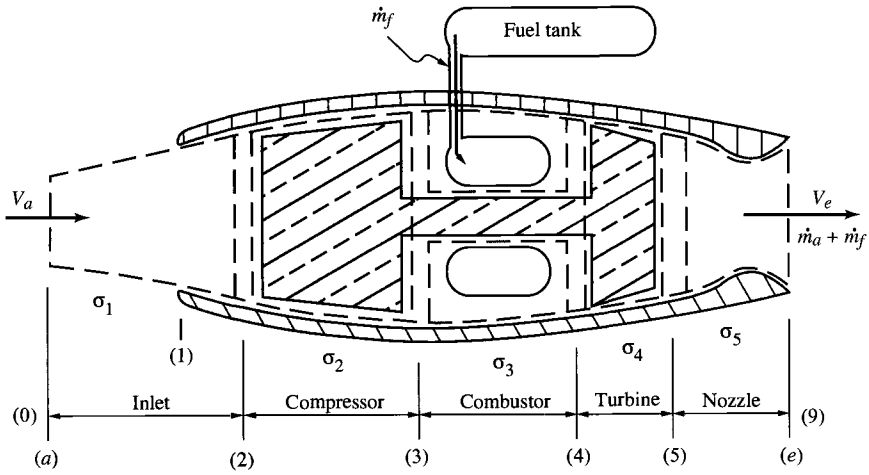

Fig. 2.4a Control volume for analyzing each component of a turbojet engine.

e, kinetic energy $V^2/(2g_c)$, and flow work Pv. We will use the expression *flux of energy* to include the flow work flux also.

a) Inlet and nozzle: σ_1 and σ_5. There are no shaft work interactions at control surfaces σ_1 and σ_5. Heat interactions are negligible and may be taken as zero. Therefore, the steady flow energy equation, as depicted in Fig. 2.4b, for the inlet or nozzle control surfaces gives the result

$$0 = \left(h + \frac{V^2}{2g_c}\right)_{\text{out}} - \left(h + \frac{V^2}{2g_c}\right)_{\text{in}}$$

Nozzle: numerical example Let the gases flowing through the nozzle control volume σ_5 be perfect with $c_p g_c = 6000\ \text{ft}/(\text{s}^2\text{-}^\circ\text{R})$. Determine V_9 for $T_5 = 1800^\circ\text{R}$, $V_5 = 400\ \text{ft/s}$, and $T_9 = 1200^\circ\text{R}$.

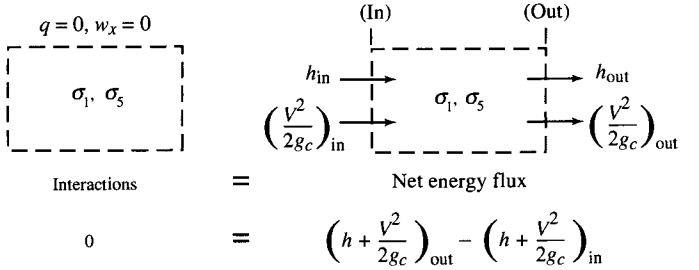

Fig. 2.4b Energy equation applied to control volumes σ_1 and σ_5.

Solution: From the steady flow energy equation with 5 and 9 as the in and out stations, respectively, we have

$$h_9 + \frac{V_9^2}{2g_c} = h_5 + \frac{V_5^2}{2g_c}$$

and

$$V_9 = \sqrt{2g_c(h_5 - h_9) + V_5^2} = \sqrt{2c_p g_c(T_5 - T_9) + V_5^2}$$

or

$$= \sqrt{2(6000)(1800 - 1200) + 400^2}$$

so

$$= 2700 \text{ ft/s}$$

b) Compressor and turbine: σ_2 and σ_4. The heat interactions at control surfaces σ_2 and σ_4 are negligibly small. Shaft work interactions are present because each control surface cuts a rotating shaft. The steady flow energy equation for the compressor or for the turbine is depicted in Fig. 2.4c and gives

$$-w_x = \left(h + \frac{V^2}{2g_c}\right)_{\text{out}} - \left(h + \frac{V^2}{2g_c}\right)_{\text{in}}$$

Compressor and turbine: numerical example For an equal mass flow through the compressor and turbine of 185 lb/s, determine the compressor power and the turbine exit temperature T_5 for the following conditions:

$c_p g_c = 6000 \text{ ft}^2/(\text{s}^2\text{-}^\circ\text{R})$

Compressor	Turbine
$T_2 = 740^\circ\text{R}$, $T_3 = 1230^\circ\text{R}$	$T_4 = 2170^\circ\text{R}$, $T_5 = ?$
$V_2 = V_3$	$V_4 = V_5$

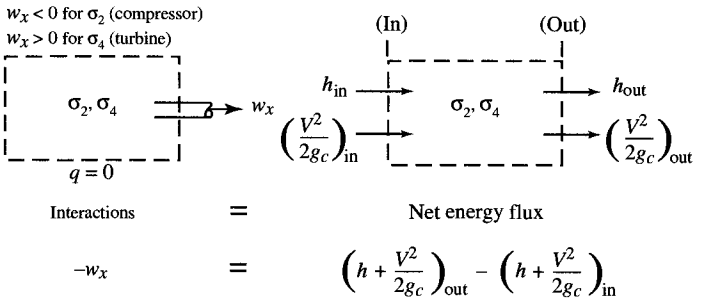

Fig. 2.4c Energy equation applied to control volumes σ_2 and σ_4.

Solution: The compressor power $\dot{W}_c = (\dot{m}w_x)_{\sigma_2}$ is, with $V_2 = V_3$,

$$\begin{aligned}\dot{W}_c &= -\dot{m}(h_3 - h_2) = -\dot{m}c_p(T_3 - T_2)\\ &= -(185\ \text{lbm/s})\frac{6000\,(\text{ft/s})^2}{32.174\,\text{ft-lbf/(lbm-s}^2)}(1230 - 740)\\ &= -16.9 \times 10^6\ \text{ft-lbf/s} \times \frac{1\ \text{hp}}{550\ \text{ft-lbf/s}}\\ &= -30,700\ \text{hp}\end{aligned}$$

The minus sign means the compressor shaft is delivering energy to the air in σ_2.

The turbine drives the compressor so that the turbine power $\dot{W}_t = (\dot{m}w_x)_{\sigma_4}$ is equal in magnitude to the compressor power. Thus $\dot{W}_t = -\dot{W}_c$, where, from the energy equation,

$$\dot{W}_t = \dot{m}(h_5 - h_4) \quad \text{and} \quad \dot{W}_c = -\dot{m}(h_3 - h_2)$$

Thus

$$\dot{m}c_p(T_5 - T_4) = -\dot{m}c_p(T_3 - T_2)$$

and

$$\begin{aligned}T_5 &= T_4 - (T_3 - T_2)\\ &= 2170°\text{R} - (1230°\text{R} - 740°\text{R}) = 1680°\text{R} = 1220°\text{F}\end{aligned}$$

c) Combustion chamber: σ_3. Let us assume that the fuel and air entering the combustion chamber mix physically in a mixing zone (Fig. 2.4d) to form what we will call *reactants* (denoted by subscript R). The reactants then enter a combustion zone where combustion occurs, forming *products* of combustion (subscript P) that leave the combustion chamber. We apply the steady flow energy equation to combustion zone σ_3. Because the temperature in the combustion zone is higher than that of the immediate surroundings, there is a heat interaction between σ_3 and the surroundings that, per unit mass flow of reactants, is negligibly small ($q < 0$ but $q = 0$). Also the velocities of the products leaving and of the reactants entering the combustion zone are approximately equal. There is no shaft work interaction for σ_3. Hence the steady flow energy equation, as depicted in Fig. 2.4d, reduces to

$$h_{R_3} = h_{P_4} \tag{2.15}$$

We must caution the reader about two points concerning this last equation. First, we cannot use the relation $c_p\Delta T$ for computing the enthalpy difference between

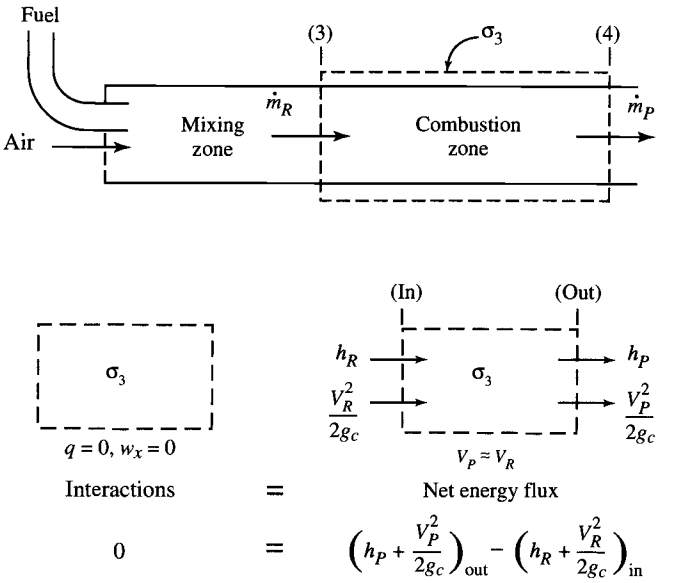

Fig. 2.4d Energy equation applied to control volumes σ_3.

two states of a system when the chemical aggregation of the two states differs. Second, we must measure the enthalpy of each term in the equation relative to the same datum state. To place emphasis on the first point, we have introduced the additional subscripts R and P to indicate that the chemical aggregations of states 3 and 4 are different.

To emphasize the second point, we select as our common enthalpy datum a state d having the chemical aggregation of the products at a datum temperature T_d. Then, introducing the datum state enthalpy $(h_P)_d$ into the last equation, we have

$$h_{R_3} - h_{P_d} = h_{P_4} - h_{P_d} \tag{2.16}$$

Equation (2.16) can be used to determine the temperature of the products of combustion leaving an adiabatic combustor for given inlet conditions. If the combustor is not adiabatic, Eq. (2.16), adjusted to include the heat interaction term q on the left-hand side, is applicable. Let us treat the reactants and products as perfect gases and illustrate the use of Eq. (2.16) in determining the temperature of the gases at the exit of a turbojet combustion chamber via an example problem.

Combustion chamber: numerical example For the turbojet engine combustion chamber, 45 lbm of air enters with each 1 lbm of JP-8 (kerosene) fuel. Let us assume these reactants enter an adiabatic combustor at 1200°R. The heating value h_{PR} of JP-8 is 18,400 Btu/lbm of fuel at 298 K. [This is also called the

lower heating value (LHV) of the fuel.] Thus the heat released $(\Delta H)_{298K}$ by the fuel per 1 lbm of the products is 400 Btu/lbm (18,400/46) at 298 K. The following data are known:

$$c_{pP} = 0.267 \text{ Btu/(lbm°R)} \qquad \text{and} \qquad c_{pR} = 0.240 \text{ Btu/(lbm°R)}$$

Determine the temperature of the products leaving the combustor.

Solution: A plot of the enthalpy equations of state for the reactants and the products is given in Fig. 2.5. In the plot, the vertical distance $h_R - h_P$ between the curves of h_R and h_P at a given temperature represents the enthalpy of combustion ΔH of the reactants at that temperature (this is sometimes called the *heat of combustion*). In our analysis, we know the enthalpy of combustion at $T_d = 298$ K (536.4°R).

States 3 and 4, depicted in Fig. 2.5, represent the states of the reactants entering and the products leaving the combustion chamber, respectively. The datum state d is arbitrarily selected to be products at temperature T_d. State d' is the reactants' state at the datum temperature T_d.

In terms of Fig. 2.5, the left-hand side of Eq. (2.16) is the vertical distance between states 3 and d, or

$$h_{R_3} - h_{P_d} = h_{R_3} - h_{R_{d'}} + h_{R_{d'}} - h_{P_d}$$

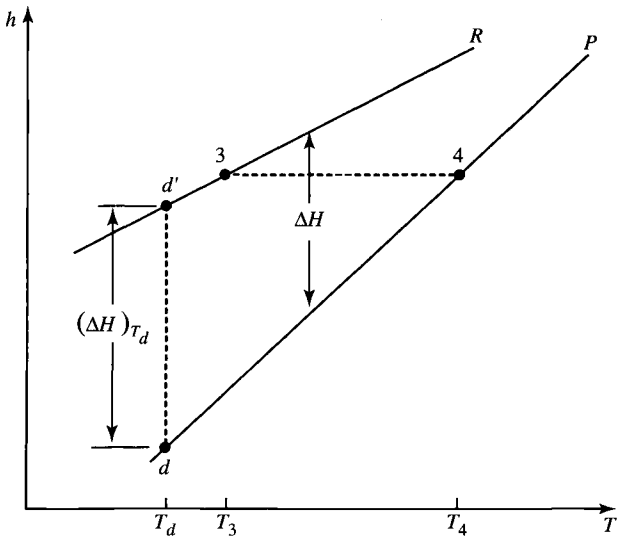

Fig. 2.5 Enthalpy vs temperature for reactants and products treated as perfect gases.

and since

$$\Delta h_R = c_{pR}\Delta T \qquad \text{and} \qquad h_{R_{d'}} - h_{P_d} = (\Delta H)_{T_d}$$

then

$$h_{R_3} - h_{P_d} = c_{pR}(T_3 - T_d) + (\Delta H)_{T_d} \tag{i}$$

Similarly, the right-hand side of Eq. (2.16) is

$$h_{P_4} - h_{P_d} = c_{pP}(T_4 - T_d) \tag{ii}$$

Substituting Eqs. (i) and (ii) in Eq. (2.16), we get

$$c_{pR}(T_3 - T_d) + (\Delta H)_{T_d} = c_{pP}(T_4 - T_d) \tag{2.17}$$

We can solve this equation for T_4, which is the temperature of the product gases leaving the combustion chamber. Solving Eq. (2.17) for T_4, we get

$$\begin{aligned} T_4 &= \frac{c_{pR}(T_3 - T_d) + (\Delta H)_{T_d}}{c_{pP}} + T_d \\ &= \frac{0.240(1200 - 536.4) + 400}{0.267} + 536.4 \\ &= 2631°\text{R} \ (2171°\text{F}) \end{aligned}$$

This is the so-called adiabatic flame temperature of the reactants for a 45 : 1 mixture ratio of air to fuel weight. For the analysis in portions of this book, we choose to sidestep the complex thermochemistry of the combustion process and model it as a simple heating process. The theory and application of thermochemistry to combustion in jet engines are covered in many textbooks, such as the classic text by Penner (see Ref. 14).

2.4 Steady Flow Entropy Equation

From the second law of thermodynamics, we have for steady state

$$\dot{S}_{\text{out}} - \dot{S}_{\text{in}} \geq \frac{\dot{Q}}{T_{\text{source}}} \tag{2.18}$$

where $\dot{S} = \dot{m}s$, $\dot{Q}$ is the rate of heat interaction into the control volume σ, and T_{source} is the heat source temperature as shown in Fig. 2.3. For steady state and adiabatic flow through a control volume, this reduces to the statement that the entropy flux out is greater than or equal to the entropy flux in

$$\dot{S}_{\text{out}} \geq \dot{S}_{\text{in}}$$

For one outlet section (2) and one inlet section (1), this and the continuity condition [Eq. (2.11)] yield

$$s_2 \geq s_1 \tag{2.19}$$

2.5 Steady Flow Momentum Equation

Newton's second law of motion for a control volume σ is

$$\sum \boldsymbol{F}_\sigma = \frac{1}{g_c}\left(\frac{\mathrm{d}\boldsymbol{M}_\sigma}{\mathrm{d}t} + \dot{\boldsymbol{M}}_{\text{out}} - \dot{\boldsymbol{M}}_{\text{in}}\right) \tag{2.20}$$

where $\boldsymbol{M}_\sigma = \int_\sigma \boldsymbol{V}\,\mathrm{d}m$ is the momentum of the mass within the control volume σ and $\dot{\boldsymbol{M}}_{\text{out}} = \int_{\text{out}} \boldsymbol{V}\mathrm{d}\dot{m}$ is the momentum flux leaving the control volume. In words, Eq. (2.20) says that the net force acting on a fixed control volume σ is equal to the time rate of increase of momentum within σ plus the net flux of momentum from σ. This very important momentum equation is in fact a *vector* equation, which implies that it must be applied in a specified direction to solve for an unknown quantity.

Applying control volume equations to a steady flow problem gives useful results with only a knowledge of conditions at the control surface. Nothing needs to be known about the state of the fluid interior to the control volume. The following examples illustrate the use of the steady one-dimensional flow condition and the momentum equation. We suggest that the procedure of sketching a control surface (and showing the applicable fluxes through the surface and the applicable forces acting on the surface) be followed whenever a control volume equation is used. This situation is similar to the use of free body diagrams for the analysis of forces on solid bodies. We illustrate this procedure in the solutions that follow.

Example 2.2

Water ($\rho = 1000$ kg/m^3) is flowing at a steady rate through a convergent duct as illustrated in Fig. 2.6a. For the data given in the figure, find the force of the fluid $F_{\sigma D}$ acting on the convergent duct D between stations 1 and 2.

Solution: We first select the control volume σ such that the force of interest is acting at the control surface. Because we want the force interaction between D and the flowing water, we choose a control surface coincident with the inner wall surface of D bounded by the permeable surfaces 1 and 2, as illustrated in Fig. 2.6a. By applying the steady one-dimensional continuity equation [Eq. (2.11)], as depicted in Fig. 2.6b, we find V_1 as follows:

$$\rho_1 A_1 V_1 = \rho_2 A_2 V_2$$

$$V_1 = \frac{A_2}{A_1} V_2 \qquad (\rho_1 = \rho_2)$$

$$= 3 \text{ m/s}$$

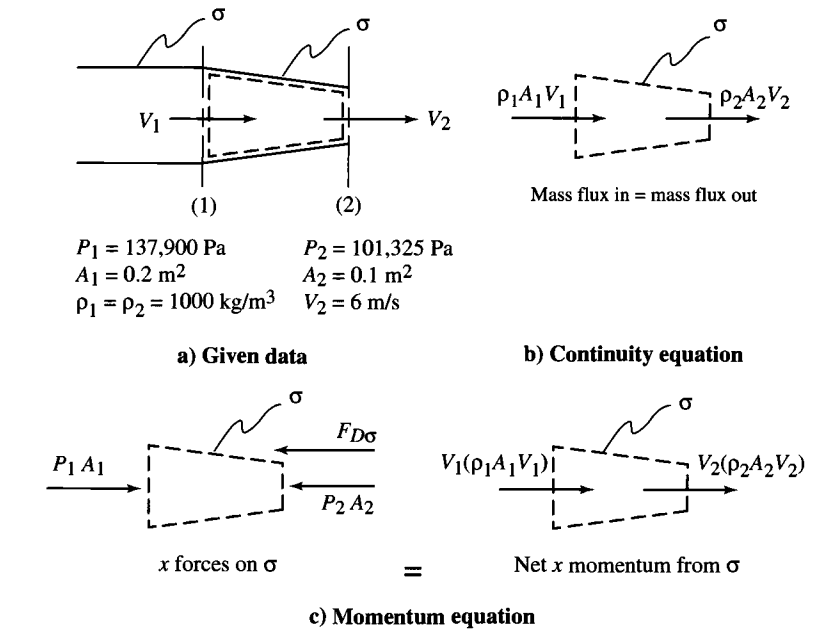

Fig. 2.6 Flow through a convergent duct.

With V_1 determined, we can apply the momentum Eq. (2.20) to σ and find the force of the duct walls on σ, denoted by $F_{D\sigma}$ ($F_{\sigma D} = -F_{D\sigma}$). By symmetry, $F_{D\sigma}$ is a horizontal force, and so the horizontal x components of forces and momentum fluxes will be considered. The x forces acting on σ are depicted in Fig. 2.6c along with the x momentum fluxes through σ.

From Fig. 2.6c, we have momentum:

$$P_1 A_1 - F_{D\sigma} - P_2 A_2 = \frac{1}{g_c}\left[(\rho_2 A_2 V_2)V_2 - (\rho_1 A_1 V_1)V_1\right]$$

And by Fig. 2.6b, continuity:

$$\rho_1 A_1 V_1 = \rho_2 A_2 V_2 = \dot{m}$$

Combining the continuity and momentum equations, we obtain

$$P_1 A_1 - F_{D\sigma} - P_2 A_2 = \frac{\dot{m}}{g_c}(V_2 - V_1)$$

or

$$F_{D\sigma} = P_1A_1 - P_2A_2 - \frac{\dot{m}}{g_c}(V_2 - V_1)$$

With $\dot{m} = \rho_1 A_1 V_1 = 1000\ \text{kg/m}^3 \times 0.2\ \text{m}^2 \times 3\ \text{m/s} = 600\ \text{kg/s}$, we have

$$F_{D\sigma} = 137,000\ \text{N/m}^2 \times 0.2\ \text{m}^2 - 101,325\ \text{N/m}^2 \times 0.1\ \text{m}^2 - 600\ \text{kg/s} \times (6 - 3)\ \text{m/s}$$

or

$$F_{D\sigma} = 27,580\ \text{N} - 10,132\ \text{N} - 1800\ \text{N}$$

and

$$= 15,648\ \text{N} \qquad \text{acts to left in assumed position}$$

Finally, the force of the water on the duct is

$$F_{\sigma D} = -F_{D\sigma} = -15{,}648\ \text{N} \qquad \text{acts to right}$$

Example 2.3

Figure 2.7 shows the steady flow conditions at sections 1 and 2 about an airfoil mounted in a wind tunnel where the frictional effects at the wall are negligible. Determine the section drag coefficient C_d of this airfoil.

Solution: Since the fluid is incompressible and the flow is steady, the continuity equation may be used to find the unknown velocity V_B as follows:

$$(\rho AV)_1 = (\rho AV)_2 \qquad \text{that is, } \dot{m}_1 = \dot{m}_2$$

or

$$\rho_1 A_1 V_A = \rho_2 \left(\frac{2}{3}V_B + \frac{1}{3}V_C\right) A_2$$

but

$$\rho_1 = \rho_2 \qquad \text{and} \qquad A_1 = A_2$$

$$V_A = \frac{2}{3}V_B + \frac{1}{3}V_C$$

thus

$$V_B = \frac{3}{2}V_A - \frac{1}{2}V_C = 31.5\ \text{m/s}$$

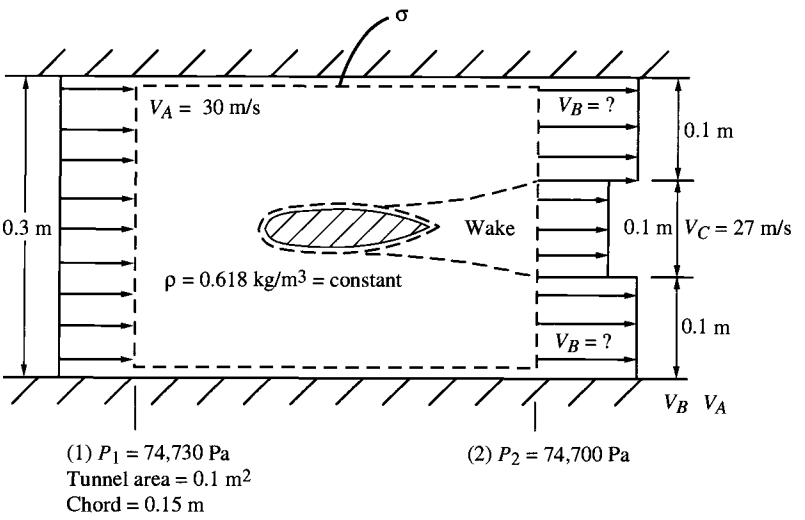

Fig. 2.7 Wind tunnel drag determination for an airfoil section.

The momentum equation may now be used to find the drag on the airfoil. This drag force will include both the skin friction and pressure drag. We sketch the control volume σ with the terms of the momentum equation as shown in Fig. 2.8.

Taking forces to right as positive, we have from the sketch

$$\sum F_\sigma = P_1A_1 - P_2A_2 + F_{D\sigma}$$

$$\dot{M}_1 = (\rho_1 A_1 V_A)V_A = \rho_1 A_1 V_A^2$$

$$\dot{M}_2 = \rho_2\left(\frac{2}{3}A_2\right)V_B^2 + \rho_2\left(\frac{1}{3}A_2\right)V_C^2$$

$$= \rho_2 A_2\left(\frac{2}{3}V_B^2 + \frac{1}{3}V_C^2\right)$$

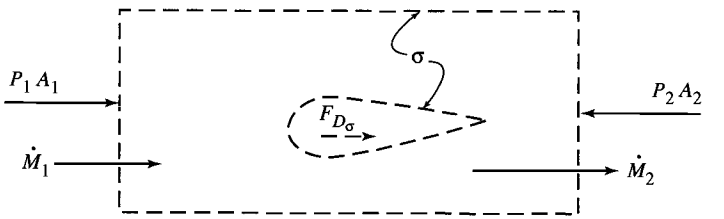

Fig. 2.8 Sketch for momentum equation for airfoil section.

For $\rho = \rho_1 = \rho_2$ and $A = A_1 = A_2$,

$$-F_{D\sigma} = (P_1 - P_2)A + \frac{\rho A}{g_c}\left(V_A^2 - \frac{2}{3}V_B^2 - \frac{1}{3}V_C^2\right)$$

or

$$= (74{,}730 - 74{,}700)\ 0.1 + 0.618 \times 0.1\left[30^2 - \frac{2}{3}(31.5^2) - \frac{1}{3}(27^2)\right]$$

$$= 3.0\ \text{N} - 0.278\ \text{N}$$

$$-F_{D\sigma} = 2.722\ \text{N} \qquad \therefore F_{D\sigma} \quad \text{acts to left}$$

$F_{\sigma D}$ = drag force for section

$= -F_{D\sigma}$ and $F_{\sigma D}$ acts to left

$$F'_D = \frac{F_{\sigma D}}{b} = \frac{2.722\,\text{N}}{0.333\,\text{m}} = 8.174\ \text{N/m}$$

$$C_d = \frac{F'_D}{qc} \quad \text{and} \quad q = \frac{\rho V_\infty^2}{2g_c} \quad \text{where} \quad V_\infty = V_A$$

$$C_d = \frac{F'_D}{[(\rho V_\infty^2)/(2g_c)]c} = \frac{8.174}{(0.618 \times 30^2/2)0.15} = 0.196$$

Example 2.4

Figure 2.9 shows a test stand for determining the thrust of a liquid-fuel rocket. The propellants enter at section 1 at a mass flow rate of 15 kg/s, a velocity of 30 m/s, and a pressure of 0.7 MPa. The inlet pipe for the propellants is very flexible, and the force it exerts on the rocket is negligible. At the nozzle exit, section 2, the area is 0.064 m^2, and the pressure is 110 kPa. The force read by the scales is 2700 N, atmospheric pressure is 82.7 kPa, and the flow is steady.

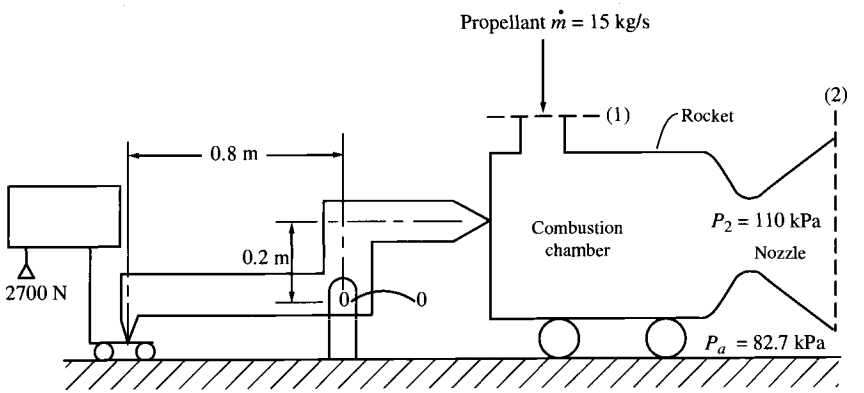

Fig. 2.9 Liquid-fuel rocket test setup.

Determine the exhaust velocity at section 2, assuming one-dimensional flow exists. Mechanical frictional effects may be neglected.

Solution: First, determine the force on the lever by the rocket to develop a 2700 N scale reading. This may be done by summing moments about the fulcrum point 0 (see Fig. 2.10a). Sum the horizontal forces on the rocket engine as shown in Fig. 2.10b. We note that the unbalanced pressure force on the exterior of the rocket engine is P_aA_2, and the interior forces (pressure and friction) are contained within the force $F_{C\sigma}$. Next, draw an internal volume σ around

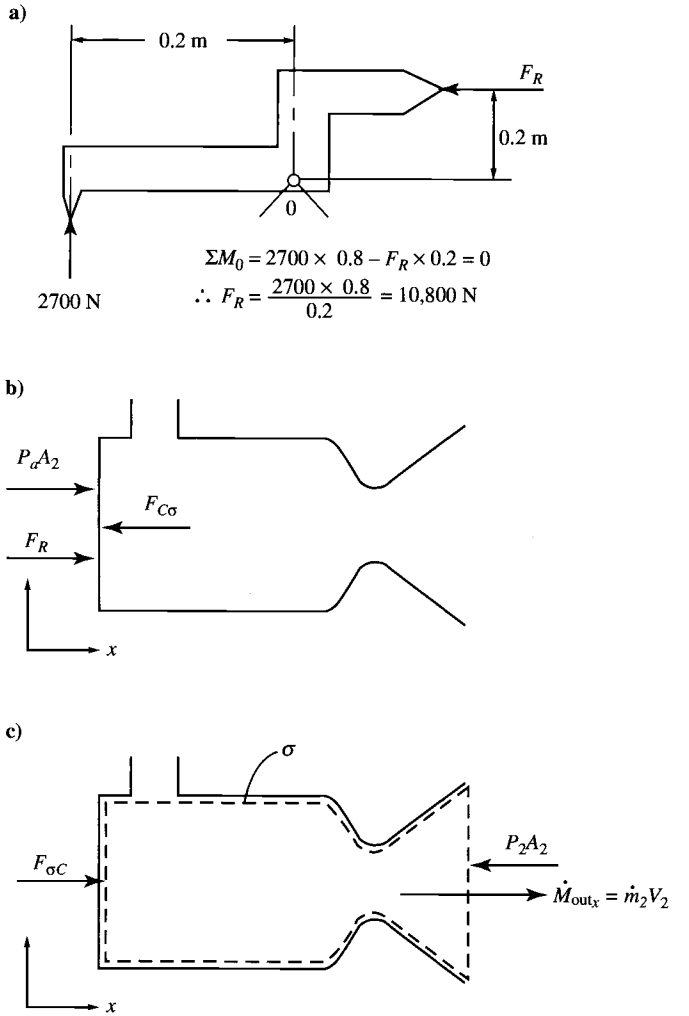

Fig. 2.10 Momentum equation sketch $\Sigma F_\sigma = (\dot{M}_2 - \dot{M}_1)/g_c$.

the fluid within the rocket engine as shown, and indicate the horizontal forces and momentum flux (see Fig. 2.10c).

Summing the forces on the rocket engine as shown in Fig. 2.10b, we obtain

$$F_R + P_a A_2 = F_{C\sigma}$$

Applying the momentum equation to the control volume σ shown in Fig. 2.10c, we obtain

$$F_{\sigma C} - P_2 A_2 = \frac{\dot{m}_2 V_2}{g_c}$$

Combining these two equations to remove $F_{\sigma C}$ gives

$$F_R - (P_2 - P_a)A_2 = \frac{\dot{m}_2 V_2}{g_c}$$

which is the same as Eq. (1.52). Because the flow is steady, the continuity equation yields $\dot{m}_1 = \dot{m}_2 = 15$ kg/s. Therefore,

$$\begin{aligned} V_2 &= \frac{F_R - (P_2 - P_a)A_2}{\dot{m}_2/g_c} \\ &= \frac{10{,}800 - [(110 - 82.7) \times 10^3\ \text{N/m}^2](0.064\ \text{m}^2)}{15\ \text{kg/s}} \\ &= 603.5\ \text{m/s} \end{aligned}$$

2.6 Perfect Gas

2.6.1 General Characteristics

The thermodynamic equations of state for a perfect gas are

$$P = \rho RT \tag{2.21}$$

$$e = e(T) \tag{2.22}$$

where P is the thermodynamic pressure, ρ is the density, R is the gas constant, T is the thermodynamic temperature, and e is the internal energy per unit mass and a function of temperature only. The gas constant R is related to the universal gas constant $\mathcal{R}$ and the molecular weight of the gas $\mathcal{M}$ by

$$R = \frac{\mathcal{R}}{\mathcal{M}} \tag{2.23}$$

Values of the gas constant and molecular weight for typical gases are presented in Table 2.1 in several unit systems; $\mathcal{R} = 8.31434$ kJ/(kmol-K) $= 1.98718$ Btu/(mol-°R).

Table 2.1 Properties of ideal gases at 298.15 K (536.67°R)

Gas	Molecular weight	c_p, kJ/(kg · K)	c_p, Btu/(lbm · °R)	R, kJ/(kg · K)	R, (ft · lbm)/(lbm · °R)	γ
Air	28.97	1.004	0.240	0.286	53.34	1.40
Argon	39.94	0.523	0.125	0.208	38.69	1.67
Carbon dioxide	44.01	0.845	0.202	0.189	35.1	1.29
Carbon monoxide	28.01	1.042	0.249	0.297	55.17	1.40
Hydrogen	2.016	14.32	3.42	4.124	766.5	1.40
Nitrogen	28.02	1.038	0.248	0.296	55.15	1.40
Oxygen	32.00	0.917	0.217	0.260	48.29	1.39
Sulfur dioxide	64.07	0.644	0.154	0.130	24.1	1.25
Water vapor	18.016	1.867	0.446	0.461	85.78	1.33

From the definition of enthalpy per unit mass h of a substance [Eq. (2.3)], this simplifies for a perfect gas to

$$h = e + RT \tag{2.24}$$

Equations (2.24) and (2.3) combined show that the enthalpy per unit mass is also only a function of temperature $h = h(T)$. Differentiating Eq. (2.24) gives

$$\mathrm{d}h = \mathrm{d}e + R\,\mathrm{d}T \tag{2.25}$$

The differentials $\mathrm{d}h$ and $\mathrm{d}e$ in Eq. (2.25) are related to the specific heat at constant pressure and specific heat at constant volume [see definitions in Eqs. (2.4) and (2.5)], respectively, as follows:

$$\mathrm{d}h = c_p\,\mathrm{d}T$$
$$\mathrm{d}e = c_v\,\mathrm{d}T$$

Note that both specific heats can be functions of temperature. These equations can be integrated from state 1 to state 2 to give

$$e_2 - e_1 = \int_{T_1}^{T_2} c_v\,\mathrm{d}T \tag{2.26}$$

$$h_2 - h_1 = \int_{T_1}^{T_2} c_p\,\mathrm{d}T \tag{2.27}$$

Substitution of the equations for $\mathrm{d}h$ and $\mathrm{d}e$ into Eq. (2.25) gives the relationship between specific heats for a perfect gas

$$c_p = c_v + R \tag{2.28}$$

and γ is the ratio of the specific heat at constant pressure to the specific heat at constant volume, or, as in Eq. (2.6),

$$\gamma \equiv c_p/c_v$$

The following relationships result from using Eqs. (2.28) and (2.6):

$$\frac{R}{c_v} = \gamma - 1 \tag{2.29}$$

$$\frac{R}{c_p} = \frac{\gamma - 1}{\gamma} \tag{2.30}$$

The Gibbs equation relates the entropy per unit mass s to the other thermodynamic properties of a substance. It can be written as

$$\mathrm{d}s = \frac{\mathrm{d}e + P\ \mathrm{d}(1/\rho)}{T} = \frac{\mathrm{d}h - (1/\rho)\ \mathrm{d}P}{T} \tag{2.31}$$

For a perfect gas, the Gibbs equation can be written simply as

$$\mathrm{d}s = c_v \frac{\mathrm{d}T}{T} + R\frac{\mathrm{d}(1/\rho)}{1/\rho} \tag{2.32}$$

$$\mathrm{d}s = c_p \frac{\mathrm{d}T}{T} - R\frac{\mathrm{d}P}{P} \tag{2.33}$$

These equations can be integrated between states 1 and 2 to yield the following expressions for the change in entropy $s_2 - s_1$:

$$s_2 - s_1 = \int_{T_1}^{T_2} c_v \frac{\mathrm{d}T}{T} + R\,\ell n\frac{\rho_1}{\rho_2} \tag{2.34}$$

$$s_2 - s_1 = \int_{T_1}^{T_2} c_p \frac{\mathrm{d}T}{T} - R\ \ell n\frac{P_2}{P_1} \tag{2.35}$$

If the specific heats are known functions of temperature for a perfect gas, then Eqs. (2.26), (2.27), (2.34), and (2.35) can be integrated from a reference state and tabulated for further use in what are called *gas tables.*

The equation for the speed of sound in a perfect gas is easily obtained by use of Eqs. (2.7) and (2.21) to give

$$a = \sqrt{\gamma R g_c T} \tag{2.36}$$

2.6.2 Calorically Perfect Gas

A *calorically perfect gas* is a perfect gas with constant specific heats (c_p and c_v). In this case, the expressions for changes in internal energy e, enthalpy h, and

entropy s simplify to the following:

$$e_2 - e_1 = c_v(T_2 - T_1) \tag{2.37}$$

$$h_2 - h_1 = c_p(T_2 - T_1) \tag{2.38}$$

$$s_2 - s_1 = c_v \ln\frac{T_2}{T_1} - R \ln\frac{\rho_2}{\rho_1} \tag{2.39}$$

$$s_2 - s_1 = c_p \ln\frac{T_2}{T_1} - R \ln\frac{P_2}{P_1} \tag{2.40}$$

Equations (2.39) and (2.40) can be rearranged to give the following equations for the temperature ratio T_2/T_1:

$$\frac{T_2}{T_1} = \left(\frac{\rho_2}{\rho_1}\right)^{R/c_v} \exp\frac{s_2 - s_1}{c_v}$$

$$\frac{T_2}{T_1} = \left(\frac{P_2}{P_1}\right)^{R/c_p} \exp\frac{s_2 - s_1}{c_p}$$

From Eqs. (2.29) and (2.30), these expressions become

$$\frac{T_2}{T_1} = \left(\frac{\rho_2}{\rho_1}\right)^{\gamma-1} \exp\frac{s_2 - s_1}{c_v} \tag{2.41}$$

$$\frac{T_2}{T_1} = \left(\frac{P_2}{P_1}\right)^{(\gamma-1)/\gamma} \exp\frac{s_2 - s_1}{c_p} \tag{2.42}$$

2.6.3 Isentropic Process

For an isentropic process ($s_2 = s_1$), Eqs. (2.41), (2.42), and (2.21) yield the following equations:

$$\frac{T_2}{T_1} = \left(\frac{P_2}{P_1}\right)^{(\gamma-1)/\gamma} \tag{2.43}$$

$$\frac{T_2}{T_1} = \left(\frac{\rho_2}{\rho_2}\right)^{\gamma-1} \tag{2.44}$$

$$\frac{P_2}{P_1} = \left(\frac{\rho_2}{\rho_2}\right)^{\gamma} \tag{2.45}$$

Note that Eqs. (2.43), (2.44), and (2.45) apply only to a calorically perfect gas undergoing an isentropic process.

Example 2.5

Air initially at 20°C and 1 atm is compressed reversibly and adiabatically to a final pressure of 15 atm. Find the final temperature.

Solution: Because the process is isentropic from initial to final state, Eq. (2.43) can be used to solve for the final temperature. The ratio of specific heats for air is 1.4:

$$T_2 = T_1\left(\frac{P_2}{P_1}\right)^{(\gamma-1)/\gamma} = (20 + 273.15)\left(\frac{15}{1}\right)^{0.4/1.4}$$

$$= 293.15 \times 2.1678 = 635.49 \text{ K } (362.34°\text{C})$$

Example 2.6

Air is expanded isentropically through a nozzle from $T_1 = 3000°\text{R}$, $V_1 = 0$, and $P_1 = 10$ atm to $V_2 = 3000$ ft/s. Find the exit temperature and pressure.

Solution: Application of the first law of thermodynamics to the nozzle gives the following for a calorically perfect gas:

$$c_pT_1 + \frac{V_1^2}{2g_c} = c_pT_2 + \frac{V_2^2}{2g_c}$$

This equation can be rearranged to give T_2:

$$T_2 = T_1 - \frac{V_2^2 - V_1^2}{2g_cc_p} = 3000 - \frac{3000^2}{2 \times 32.174 \times 0.240 \times 778.16}$$

$$= 3000 - 748.9 = 2251.1°\text{R}$$

Solving Eq. (2.43) for P_2 gives

$$P_2 = P_1\left(\frac{T_2}{T_1}\right)^{\gamma/(\gamma-1)} = 10\left(\frac{2251.1}{3000}\right)^{3.5} = 3.66 \text{ atm}$$

2.6.4 *Mollier Diagram for a Perfect Gas*

The Mollier diagram is a thermodynamic state diagram with the coordinates of enthalpy and entropy s. Because the enthalpy of a perfect gas depends on temperature alone,

$$dh = c_p\, dT$$

temperature can replace enthalpy has the coordinate of a Mollier diagram for a perfect gas. When temperature T and entropy s are the coordinates of a Mollier diagram, we call it a *T-s diagram.* We can construct lines of constant pressure and density in the T-s diagram by using Eqs. (2.34) and (2.35). For a calorically

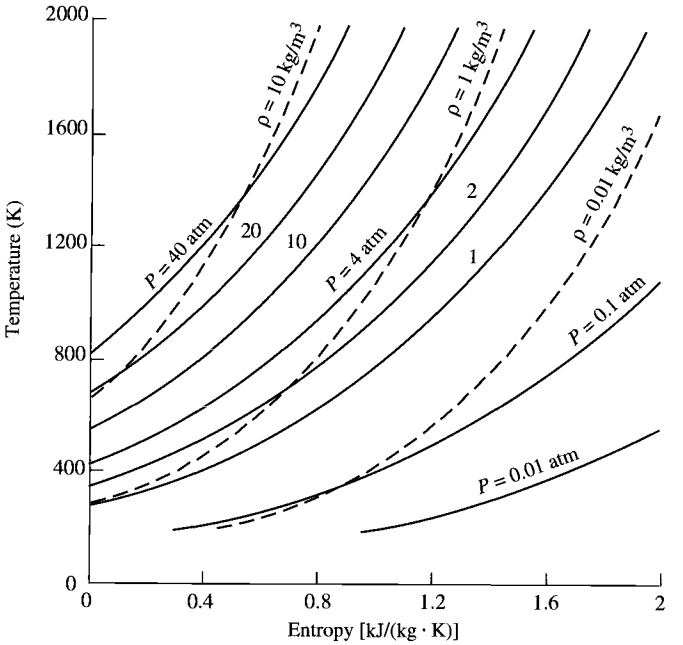

Fig. 2.11 A *T-s* diagram for air as a calorically perfect gas.

perfect gas, Eqs. (2.39) and (2.40) can be written between any state and the entropy reference state ($s = 0$) as

$$s = c_v \ell n \frac{T}{T_{\text{ref}}} - R \ell n \frac{\rho}{\rho_{\text{ref}}}$$

$$s = c_p \ell n \frac{T}{T_{\text{ref}}} - R \ell n \frac{P}{P_{\text{ref}}}$$

where T_{ref}, P_{ref}, and ρ_{ref} are the values of temperature, pressure, and density, respectively, when $s = 0$. Because the most common working fluid in gas turbine engines is air, Fig. 2.11 has been constructed for air by using the preceding equations with these data:

$$c_p = 1.004 \text{ kJ/(kg·K)}, \qquad T_{\text{ref}} = 288.2 \text{ K} \qquad \rho_{\text{ref}} = 1.225 \text{ kg/m}^3$$
$$R = 0.286 \text{ kJ/(kg·K)}, \qquad P_{\text{ref}} = 1 \text{ atm} = 101,325 \text{ Pa}$$

2.6.5 Mixtures of Perfect Gases

We consider a mixture of perfect gases, each obeying the perfect gas equation:

$$PV = N\mathcal{R}T$$

where N is the number of moles and $\mathcal{R}$ is the universal gas constant. The mixture is idealized as independent perfect gases, each having the temperature T and occupying the volume V. The partial pressure of gas i is

$$P_i = N_i \mathcal{R} \frac{T}{V}$$

According to the Gibbs–Dalton law, the pressure of the gas mixture of n constituents is the sum of the partial pressures of each constituent:

$$P = \sum_{i=1}^{n} P_i \tag{2.46}$$

The total number of moles N of the gas is

$$N = \sum_{i=1}^{n} N_i \tag{2.47}$$

The ratio of the number of moles of constituent i to the total number of moles in the mixture is called the *mole fraction* χ_i. By using the preceding equations, the mole fraction of constituent i can be shown to equal the ratio of the partial pressure of constituent i to the pressure of the mixture:

$$\chi_i = \frac{N_i}{N} = \frac{P_i}{P} \tag{2.48}$$

The Gibbs–Dalton law also states that the internal energy, enthalpy, and entropy of a mixture are equal, respectively, to the sum of the internal energies, the enthalpies, and the entropies of the constituents when each alone occupies the volume of the mixture at the mixture temperature. Thus we can write the following for a mixture of n constituents.

Energy:

$$E = \sum_{i=1}^{n} E_i = \sum_{i=1}^{n} m_i e_i \tag{2.49}$$

Enthalpy:

$$H = \sum_{i=1}^{n} H_i = \sum_{i=1}^{n} m_i h_i \tag{2.50}$$

Entropy:

$$S = \sum_{i=1}^{n} S_i = \sum_{i=1}^{n} m_i s_i \tag{2.51}$$

where m_i is the mass of constituent i.

The specific heats of the mixture follow directly from the definitions of c_p and c_v and the preceding equations. For a mixture of n constituents, the specific heats are

$$c_p = \frac{\sum_{i=1}^{n} m_i c_{pi}}{m} \qquad \text{and} \qquad c_v = \frac{\sum_{i=1}^{n} m_i c_{vi}}{m} \tag{2.52}$$

where m is the total mass of the mixture.

2.6.6 Gas Tables

In the case of a perfect gas with variable specific heats, the specific heat at constant pressure c_p is normally modeled by several terms of a power series in temperature T. This expression is used in conjunction with the general equations presented and the new equations that are developed next to generate a gas table for a particular gas (see Ref. 15).

For convenience, we define

$$h \equiv \int_{T_{\text{ref}}}^{T} c_p \, \mathrm{d}T \tag{2.53}$$

$$\phi \equiv \int_{T_{\text{ref}}}^{T} c_p \frac{\mathrm{d}T}{T} \tag{2.54}$$

$$P_r \equiv \exp\frac{\phi - \phi_{\text{ref}}}{R} \tag{2.55}$$

$$v_r \equiv \exp\left(-\frac{1}{R}\int_{T_{\text{ref}}}^{T} c_v \frac{\mathrm{d}T}{T}\right) \tag{2.56}$$

where P_r and v_r are called the *reduced pressure* and *reduced volume*, respectively. Using the definition of ϕ from Eq. (2.54) in Eq. (2.35) gives

$$s_2 - s_1 = \phi_2 - \phi_1 - R\,\ell n \frac{P_2}{P_1} \tag{2.57}$$

For an isentropic process between states 1 and 2, Eq. (2.57) reduces to

$$\phi_2 - \phi_1 = R\,\ell n \frac{P_2}{P_1}$$

which can be rewritten as

$$\left(\frac{P_2}{P_1}\right)_{s=\text{const}} = \exp\frac{\phi_2 - \phi_1}{R} = \frac{\exp(\phi_2/R)}{\exp(\phi_1/R)}$$

Using Eq. (2.55), we can express this pressure ratio in terms of the reduced pressure P_r as

$$\left(\frac{P_2}{P_1}\right)_{s=\text{const}} = \frac{P_{r2}}{P_{r1}} \tag{2.58}$$

Likewise, it can be shown that

$$\left(\frac{v_2}{v_1}\right)_{s=\text{const}} = \frac{v_{r2}}{v_{r1}} \tag{2.59}$$

For a perfect gas, the properties h, P_r, e, v_r, and ϕ are functions of T, and these can be calculated by starting with a polynomial for c_p. Say we have the seventh-order polynomial

$$c_p = A_0 + A_1 T + A_2 T^2 + A_3 T^3 + A_4 T^4 + A_5 T^5 + A_6 T^6 + A_7 T^7 \tag{2.60}$$

The equations for h and ϕ as functions of temperature follow directly from using Eqs. (2.53) and (2.54):

$$h = h_{\text{ref}} + A_0 T + \frac{A_1}{2} T^2 + \frac{A_2}{3} T^3 + \frac{A_3}{4} T^4 + \frac{A_4}{5} T^5 + \frac{A_5}{6} T^6 + \frac{A_6}{7} T^7 + \frac{A_7}{8} T^8 \tag{2.61}$$

$$\phi = \phi_{\text{ref}} + A_0 \ell n T + A_1 T + \frac{A_2}{2} T^2 + \frac{A_3}{3} T^3 + \frac{A_4}{4} T^4 + \frac{A_5}{5} T^5 + \frac{A_6}{6} T^6 + \frac{A_7}{7} T^7 \tag{2.62}$$

After we define reference values, the variations of P_r and v_r follow from Eqs. (2.55) and (2.56), and the preceding equations.

2.6.7 Comment for Appendix D

Typically, air flows through the inlet and compressor of the gas turbine engine whereas products of combustion flow through the engine components downstream of a combustion process. Most gas turbine engines use hydrocarbon fuels of composition $(CH_2)_n$. We can use the preceding equations to estimate the properties of these gases, given the ratio of the mass of fuel burned to the mass of air. For convenience, we use the fuel/air ratio f, defined as

$$f = \frac{\text{mass of fuel}}{\text{mass of air}} \tag{2.63}$$

The maximum value of f is 0.0676 for the hydrocarbon fuels of composition $(CH_2)_n$.

Given the values of c_p, h, and ϕ for air and the values of combustion products, the values of c_p, h, and ϕ for the mixture follow directly from the mixture

Table 2.2 Constants for air and combustion products used in Appendix D and program AFPROP (from Ref. 16)

Air alone		Combustion products of air and $(CH_2)_n$ fuels	
A_0	2.5020051×10^{-1}	A_0	7.3816638×10^{-2}
A_1	$-5.1536879 \times 10^{-5}$	A_1	1.2258630×10^{-3}
A_2	6.5519486×10^{-8}	A_2	$-1.3771901 \times 10^{-6}$
A_3	$-6.7178376 \times 10^{-12}$	A_3	$9.9686793 \times 10^{-10}$
A_4	$-1.5128259 \times 10^{-14}$	A_4	$-4.2051104 \times 10^{-13}$
A_5	$7.6215767 \times 10^{-18}$	A_5	$1.0212913 \times 10^{-16}$
A_6	$-1.4526770 \times 10^{-21}$	A_6	$-1.3335668 \times 10^{-20}$
A_7	$1.0115540 \times 10^{-25}$	A_7	$7.2678710 \times 10^{-25}$
h_{ref}	−1.7558886 Btu/lbm	h_{ref}	30.58153 Btu/lbm
ϕ_{ref}	0.0454323 Btu/(lbm · °R)	ϕ_{ref}	0.6483398 Btu/(lbm · °R)

equations [Eqs. (2.49)–(2.52)] and are given by

$$R = \frac{1.9857117\ \text{Btu/(lbm} \cdot {}^\circ\text{R)}}{28.97 - f \times 0.946186} \tag{2.64a}$$

$$c_p = \frac{c_{p\ \text{air}} + f c_{p\ \text{prod}}}{1 + f} \tag{2.64b}$$

$$h = \frac{h_{\text{air}} + f\ h_{\text{prod}}}{1 + f} \tag{2.64c}$$

$$\phi = \frac{\phi_{\text{air}} + f \phi_{\text{prod}}}{1 + f} \tag{2.64d}$$

Appendix D is a table of the properties h and P_r as functions of the temperature and fuel/air ratio f for air and combustion products [air with hydrocarbon fuels of composition $(CH_2)_n$] at low pressure (perfect gas). These data are based on the preceding equations and the constants given in Table 2.2, which are valid over the temperature range of 300–4000°R. These constants come from the gas turbine engine modeling work of Capt. John S. McKinney (U.S. Air Force) while assigned to the Air Force's Aero Propulsion Laboratory,[16] and they continue to be widely used in the industry. Appendix D uses a reference value of 2 for P_r at 600°R and $f = 0$.

2.6.8 Comment for Computer Program AFPROP

The computer program AFPROP was written by using the preceding constants for air and products of combustion from air with $(CH_2)_n$. The program can calculate the four primary thermodynamic properties at a state (P, T, h, and s) given the fuel/air ratio f and two independent thermodynamic properties (say, P and h).

To show the use of the gas tables, we will resolve Examples 2.5 and 2.6, using the gas tables of Appendix D. These problems could also be solved by using the computer program AFPROP.

Example 2.7

Air initially at 20°C and 1 atm is compressed reversibly and adiabatically to a final pressure of 15 atm. Find the final temperature.

Solution: Since the process is isentropic from initial to final state, Eq. (2.58) can be used to solve for the final reduced pressure. From Appendix D at 20°C (293.15 K) and $f = 0$, $P_r = 1.2768$ and

$$\frac{P_{r2}}{P_{r1}} = \frac{P_2}{P_1} = 15$$

$$P_{r2} = 15 \times 1.2768 = 19.152$$

From Appendix D for $P_{r2} = 19.152$, the final temperature is 354.42°C (627.57 K). This is 7.9 K lower than the result obtained in Example 2.5 for air as a calorically perfect gas.

Example 2.8

Air is expanded isentropically through a nozzle from $T_1 = 3000°\text{R}$, $V_1 = 0$, and $P_1 = 10$ atm to $V_2 = 3000$ ft/s. Find the exit temperature and pressure.

Solution: Application of the first law of thermodynamics to the nozzle gives the following for a calorically perfect gas:

$$h_1 + \frac{V_1^2}{2g_c} = h_2 + \frac{V_2^2}{2g_c}$$

From Appendix D at $f = 0$ and $T_1 = 3000°\text{R}$, $h_1 = 790.46$ Btu/lbm and $P_{r1} = 938.6$. Solving the preceding equation for h_2 gives

$$h_2 = h_1 - \frac{V_2^2 - V_1^2}{2g_c} = 790.46 - \frac{3000^2}{2 \times 32.174 \times 778.16}$$

$$= 790.46 - 179.74 = 610.72\,\text{Btu/lbm}$$

For $h = 610.72$ Btu/lbm and $f = 0$, Appendix D gives $T_2 = 2377.7°\text{R}$ and $P_{r2} = 352.6$. Using Eq. (2.58), we solve for the exit pressure

$$P_2 = P_1 \frac{P_{r2}}{P_{r1}} = 10\left(\frac{352.6}{938.6}\right) = 3.757\,\text{atm}$$

These results for temperature and pressure at station 2 are higher by 126.6°R and 0.097 atm, respectively, than those obtained in Example 2.6 for air as a calorically perfect gas.

2.7 Compressible Flow Properties

For a simple compressible system, we learned that the state of a unit mass of gas is fixed by two independent intensive properties such as pressure and temperature. To fully describe the condition and thus fix the state of this same gas when it is in motion requires the specification of an additional property that will fix the speed of the gas. Thus three independent intensive properties are required to fully specify the state of a gas in motion.

At any given point in a compressible fluid flowfield, the thermodynamic state of the gas is fixed by specifying the velocity of the gas and any two independent thermodynamic properties such as pressure and temperature. However, we find that to specify the velocity directly is not always the most useful or the most convenient way to describe one-dimensional flow. There are other properties of the gas in motion that are dependent on the speed of the gas and that may be used in place of the speed to describe the state of the flowing gas. Some of these properties are the Mach number, total pressure, and total temperature. In this section we define these properties and describe briefly some of the characteristics of compressible flow.

2.7.1 Total Enthalpy and Total Temperature

The steady flow energy equation in the absence of gravity effects is

$$q - w_x = \left(h + \frac{V^2}{2g_c}\right)_{\text{out}} - \left(h + \frac{V^2}{2g_c}\right)_{\text{in}}$$

For a calorically perfect gas this becomes

$$q - w_x = c_p\left(T + \frac{V^2}{2g_c c_p}\right)_{\text{out}} - c_p\left(T + \frac{V^2}{2g_c c_p}\right)_{\text{in}}$$

The quantities $h + V^2/(2g_c)$ and $T + V^2/(2g_c c_p)$ in these equations are called the *stagnation* or *total enthalpy* h_t and the *stagnation* or *total temperature* T_t, respectively.

Total enthalpy:

$$h_t \equiv h + \frac{V_2}{2g_c} \tag{2.65}$$

Total temperature:

$$T_t \equiv T + \frac{V_2}{2g_c c_p} \tag{2.66}$$

The temperature T is sometimes called the *static temperature* to distinguish it from the total temperature T_t. When $V = 0$, the static and total temperatures are identical. From these definitions, it follows that, for a calorically perfect gas,

$$\Delta h_t = c_p \Delta T_t$$

Using these new definitions, we see that the steady flow energy equation in the absence of gravity effects becomes

$$q - w_x = h_{t\,\text{out}} - h_{t\,\text{in}} \tag{2.67}$$

or, for a calorically perfect gas,

$$q - w_x = c_p(T_{t\,\text{out}} - T_{t\,\text{in}}) \tag{2.68}$$

If $q - w_x = 0$, we see from Eqs. (2.67) and (2.68) that $h_{t\,\text{out}} = h_{t\,\text{in}}$ and that, for a calorically perfect gas, $T_{t\,\text{out}} = T_{t\,\text{in}}$.

Consider an airplane in flight at a velocity V_a. To an observer riding with the airplane, the airflow about the wing of the plane appears as in Fig. 2.12. We mark out a control volume σ as shown in the figure between a station far upstream from the wing and a station just adjacent to the wing's leading edge stagnation point, where the velocity of the airstream is reduced to a negligibly small magnitude.

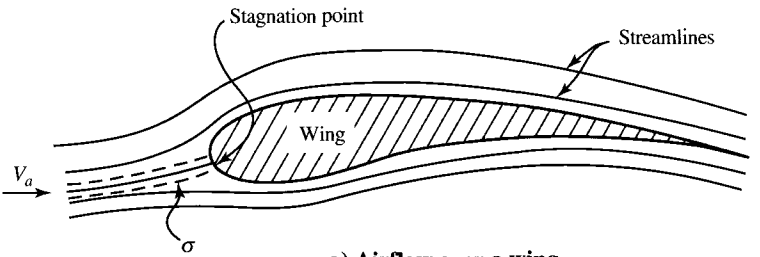

a) Airflow over a wing

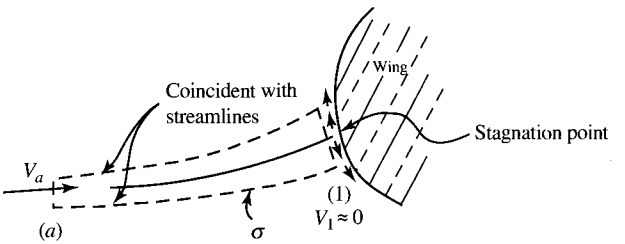

b) Enlarged view of flow in the neighborhood of the stagnation point

Fig. 2.12 Control volume σ with freestream inlet and stagnation exit conditions (reference system at rest relative to wing).

Applying the steady flow energy equation to the flow through σ of Fig. 2.12, we have

$$q - w_x = \left(h + \cancel{\frac{V^2}{2g_c}}^{0}\right)_1 - \left(h + \frac{V^2}{2g_c}\right)_a$$

or

$$0 = c_p T_1 - c_p \left(T + \frac{V^2}{2g_c c_p}\right)_a$$

From this equation, we find that the temperature of the air at the stagnation point of the wing is

$$T_1 = T_a + \frac{V_a^2}{2g_c c_p} = T_{ta}$$

Thus we see that the temperature, which the leading edge of the wing "feels," is the total temperature T_{ta}.

At high flight speeds, the freestream total temperature T_{ta} is significantly different from the freestream ambient temperature T_a. This is illustrated in Fig. 2.13, where $T_{ta} - T_a$ is plotted against V_a by using the relation

$$(T_t - T)_a = \frac{V_a^2}{2g_c c_p} = \frac{V_a^2}{12,000} \approx \left(\frac{V_a}{110}\right)^2 {}^\circ\text{R}$$

with V_a expressed in ft/s. Because the speed of sound at 25,000 ft is 1000 ft/s, a Mach number scale for 25,000 ft is easily obtained by dividing the scale for V_a in Fig. 2.13 by 1000. (Mach number M equals V_a divided by the local speed of sound a.) Therefore, Mach number scales are also given on the graphs.

Referring to Fig. 2.13, we find that at a flight speed of 800 ft/s corresponding to a Mach number of 0.8 at 25,000-ft altitude, the stagnation points on an airplane experience a temperature that is about 50°R higher than ambient temperature. At 3300 ft/s ($M = 3.3$ at 25,000 ft), the total temperature is 900°R higher than ambient! It should be evident from these numbers that vehicles such as the X-15 airplane and reentry bodies experience high temperatures at their high flight speeds.

These high temperatures are produced as the kinetic energy of the air impinging on the surfaces of a vehicle is reduced and the enthalpy (hence, temperature) of the air is increased a like amount. This follows directly from the steady flow energy equation, which gives, with $q = w_x = 0$,

$$\left(h + \frac{V^2}{2g_c}\right)_{\text{in}} = \left(h + \frac{V^2}{2g_c}\right)_{\text{out}}$$

or

$$\Delta h = c_p \Delta T = -\Delta\left(\frac{V^2}{2g_c}\right)$$

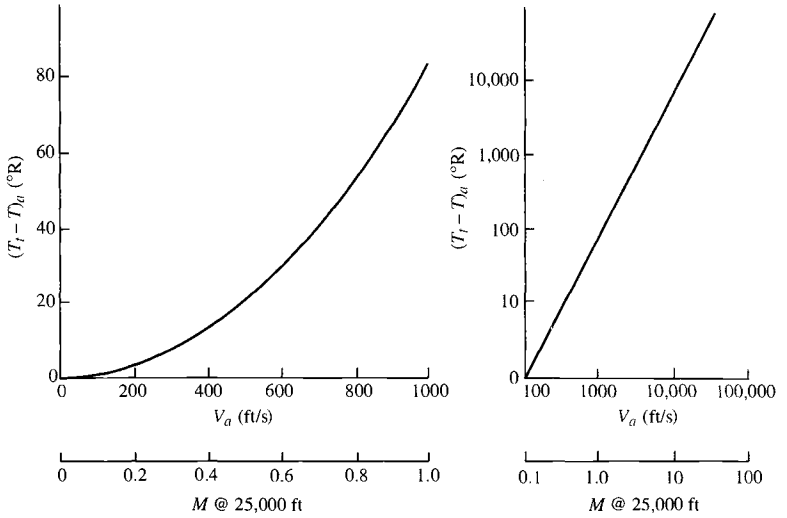

Fig. 2.13 Total temperature minus ambient temperature vs flight speed and vs flight Mach number at 25,000 ft [$g_c c_p$ is assumed constant at 6000 ft^2/(s^2-°R); therefore, these are approximate curves].

and

$$\Delta T = -\frac{\Delta V^2}{2g_c c_p}$$

Thus a decrease in the kinetic energy of air produces a rise in the air temperature and a consequent heat interaction between the air and the surfaces of an air vehicle. This heat interaction effect is referred to as *aerodynamic heating.*

Example 2.9

The gas in a rocket combustion chamber is at 120 psia and 1600°R (Fig. 2.14). The gas expands through an adiabatic frictionless (isentropic) nozzle to 15 psia. What are the temperature and velocity of the gas leaving the nozzle? Treat the gas as the calorically perfect gas air with $\gamma = 1.4$ and $g_c c_p = 6000$ ft^2/(s$^2 \cdot$ °R).

Solution: Locate the state of the combustion chamber gas entering control volume σ on a T-s diagram like Fig. 2.11 in the manner depicted in Fig. 2.15. Then, from the diagram, find s_1. Because the process is isentropic, $s_2 = s_1$. The entropy at 2, along with the known value of P_2, fixes the static state of 2. With 2 located in the T-s diagram, we can read T_2 from the temperature scale as 885°R, and we can verify this graphical solution for T_2 by using the isentropic relation (2.43) with $\gamma = 1.4$. Thus $T_2 = (1600°\text{R})(15/120)^{0.286} = 885°\text{R}$ (checks).

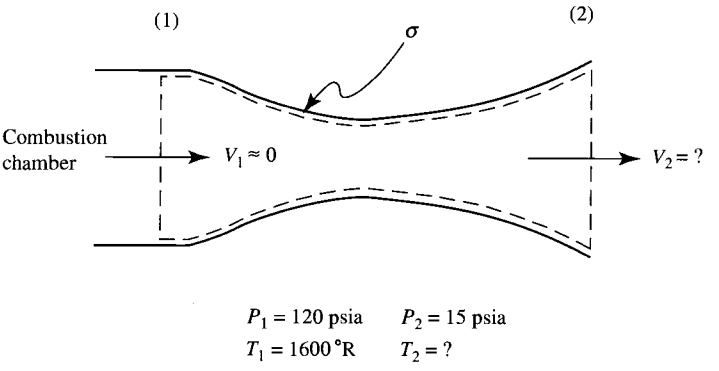

Fig. 2.14 Rocket exhaust nozzle.

If, in addition to P_2 and T_2, the total temperature T_{t2} of the flowing gas at 2 is known, then the state of the gas at 2 is completely fixed. For with P_2 and T_2 specified, the values of all thermodynamic properties independent of speed (the *static* properties) are fixed, and the speed of the gas is determined by T_2 and T_{t2}.

From the steady flow energy equation (Fig. 2.15), we find that $T_{t2} = T_{t1} = T_1$ and, hence, V_2 from the relation

$$\frac{V_2^2}{2\,g_c c_p} = T_{t2} - T_2$$

We see from this equation that the vertical distance $T_{t2} - T_2$ in the T-s diagram is indicative of the speed of the gas at 2, which is $V_2^2 = 2(6000)(1600 - 885)\text{ft}^2/\text{s}^2$. Thus $V_2 = 2930$ ft/s.

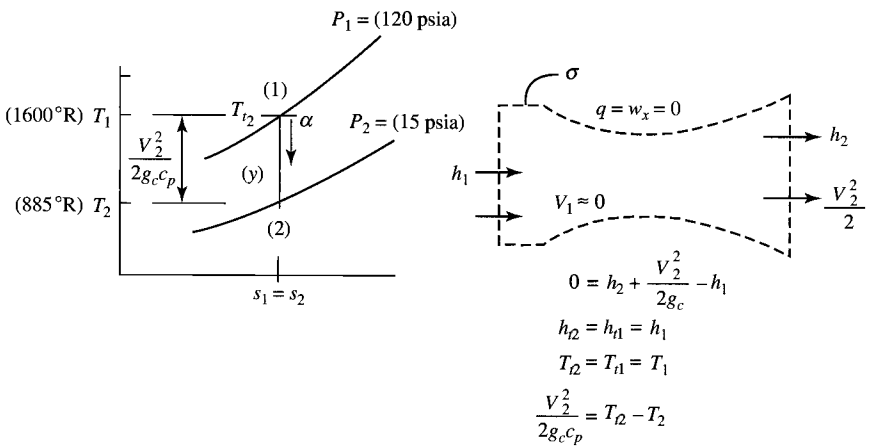

Fig. 2.15 Process plot for example rocket nozzle.

The series of states through which the gas progresses in the nozzle as it flows from the combustion chamber (nozzle inlet) to the nozzle exit is represented by path line α in the T-s diagram. The speed of the gas at any intermediate state y in the nozzle is represented by the vertical distance on the path line from 1 to the state in question. This follows from the relations

$$T_{ty} = T_1 \qquad \text{and} \qquad \frac{V_y^2}{2g_c c_p} = T_{ty} - T_y = T_1 - T_y$$

2.7.2 Stagnation or Total Pressure

In the adiabatic, no-shaft-work slowing of a flowing perfect gas to zero speed, the gas attains the same final stagnation temperature whether it is brought to rest through frictional effects (irreversible) or without them (reversible). This follows from the energy control volume equation applied to σ of Fig. 2.16 for a calorically perfect gas. Thus, from

$$q - w_x = c_p(T_y - T_1) + \frac{V_y^2 - V_1^2}{2g_c}$$

with $q = w_x = 0$ and $V_y = 0$, T_y becomes

$$T_y = T_0 = T_1 + \frac{V_1^2}{2g_c c_p}$$

Because the energy control volume equation is valid for frictional or frictionless flow, $T_y = T_0$ is constant and independent of the degree of friction between 1 and y as long as $q = w_x = V_y = 0$.

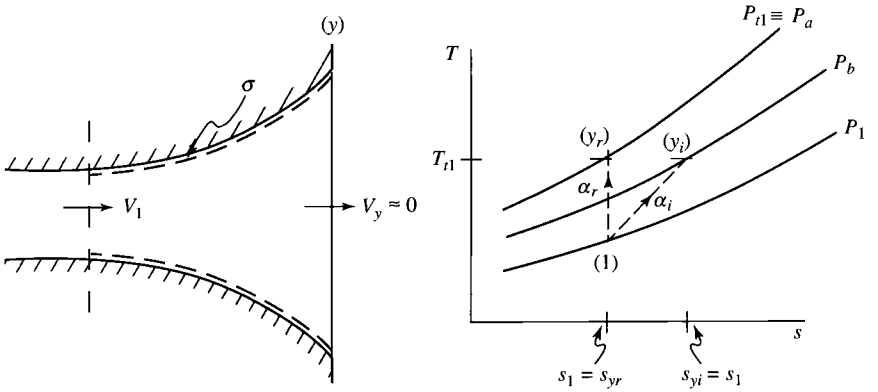

Fig. 2.16 Definition of total pressure.

Although the gas attains the same final temperature T_0 in reversible or irreversible processes, its final pressure will vary with the degree of irreversibility associated with the slowing down process. The entropy state and control volume equations for the flow through σ are

$$c_p \ell n \frac{T_y}{T_1} - R \ell n \frac{P_y}{P_1} = s_y - s_1 \geq 0 \tag{2.69}$$

Since $T_y = T_0 = \text{const}$ from Eq. (3.5), the final value of P_y depends on the entropy increase $s_y - s_1$, which in turn is a measure of the degree of irreversibility between 1 and y.

When the slowing down process between 1 and y is reversible, with $s_y - s_1 = 0$, the final pressure is defined as the total pressure P_t. The final state is called the *total state* t_1 of the static state 1. Using this definition of total pressure, we have, from Eq. (2.43),

$$P_t \equiv P\left(\frac{T_t}{T}\right)^{\gamma/(\gamma-1)} \tag{2.70}$$

These ideas are illustrated in the T-s diagram of Fig. 2.16. Let us imagine the flowing gas at station 1 to be brought to rest adiabatically with no shaft work by means of a duct diverging to an extremely large area at station y, where the flow velocity is zero. If the diverging duct is frictionless, then the slowing down process from 1 to y is isentropic with the path line α_r in the T-s diagram of the figure. If the diverging duct is frictional, then the slowing down process from 1 to y is irreversible and adiabatic ($s_{yi} > s_1$) to satisfy the entropy control volume equation for adiabatic flow and is shown as the path line α_i, in the T-s diagram.

The total pressure of a flowing gas is defined as the pressure obtained when the gas is brought to rest isentropically. Thus the pressure corresponding to state y_r of the T-s diagram is the total pressure of the gas in state 1. The state point y_r is called the *total* or *stagnation state* t_1 of the static point 1.

The concepts of total pressure and total temperature are very useful, for these two properties along with the third property (static pressure) of a flowing gas are readily measured, and they fix the state of the flowing gas. We measure these three properties in flight with pitot-static and total temperature probes on modern high-speed airplanes, and these properties are used to determine speed and Mach number and to provide other data for many aircraft subsystems.

Consider a gas flowing in a duct in which P and T may change due to heat interaction and friction effects. The flow total state points t_1 and t_2 and the static state points 1 and 2, each of which corresponds to flow stations 1 and 2, are located in the T-s diagram of Fig. 2.17. By definition, the entropy of the total state at any given point in a gas flow has the same value as the entropy of the static state properties at that point. Therefore, $s_{t1} = s_1$ and $s_{t2} = s_2$.

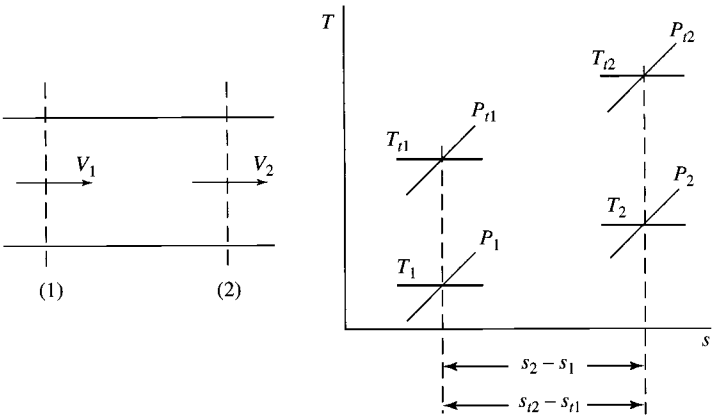

Fig. 2.17 Entropy change in terms of the stagnation properties T_t and P_t.

From the entropy equation of state of a perfect gas, the entropy change between 1 and 2 is

$$s_2 - s_1 = c_p \ell n \frac{T_2}{T_1} - R \ell n \frac{P_2}{P_1}$$

The entropy change between total state points t_1 and t_2 is

$$s_{t2} - s_{t1} = c_p \ell n \frac{T_{t2}}{T_{t1}} - R \ell n \frac{P_{t2}}{P_{t1}} \tag{2.71a}$$

Since $s_{t1} = s_1$ and $s_{t2} = s_2$, we have

$$s_{t2} - s_{t1} = s_2 - s_1$$

Therefore, the change of entropy between two states of a flowing gas can be determined by using total properties in place of static properties.

Equation (2.71a) indicates that in an adiabatic and no-shaft-work constant-T_t flow (such as exists in an airplane engine inlet and nozzle, or flow through a shock wave), we have

$$s_2 - s_1 = -R \ell n \frac{P_{t2}}{P_{t1}} \tag{2.71b}$$

By virtue of this equation and the entropy control volume equation for adiabatic flow, $s_2 - s_1 \geq 0$. Thus, in a constant-T_t flow,

$$\frac{P_{t2}}{P_{t1}} \leq 1$$

Hence the total pressure of air passing through an engine inlet and nozzle or a shock wave cannot increase and must, in fact, decrease because of the irreversible effects of friction.

2.7.3 T/T_t and P/P_t as Functions of Mach Number

The speed of sound a in a perfect gas is given by

$$a = \sqrt{\gamma g_c RT}$$

Using this relation for the speed of sound and Eq. (2.8), we can write the Mach number as

$$M^2 = \frac{V^2}{\gamma g_c RT}$$

With the help of this expression for the Mach number, we can obtain many useful relations that give gas flow property ratios in terms of the flow Mach number alone. Two such relations for T/T_t and P/P_t are

$$\frac{T}{T_t} = \left(1 + \frac{\gamma - 1}{2} M^2\right)^{-1} \tag{2.72}$$

$$\frac{P}{P_t} = \left(1 + \frac{\gamma - 1}{2} M^2\right)^{-\gamma/(\gamma-1)} \tag{2.73}$$

Equations (2.71) and (2.72) appear graphically in Fig. 2.18 and are given in the isentropic flow functions of the GASTAB program for user input γ value. These equations show that for each freestream Mach number (hence, for each flight Mach number of an airplane), the ratios P/P_t and T/T_t have unique values.

Both Fig. 2.18 and the corresponding equations provide Mach numbers and ambient temperatures for known values of P, P_t, and T_t. For example, we are given the following in-flight measurements:

$$P = 35.4\,\text{kPa} \qquad T_t = 300\,\text{K} \qquad P_t = 60.0\,\text{kPa}$$

From these data, $P/P_t = 0.59$. If we enter Fig. 2.18 with this value of P/P_t, we find $M = 0.9$ and $T/T_t = 0.86$. Then we obtain the ambient temperature by using $T = (T/T_t)\, T_t = 0.86(300) = 258$ K.

Figure 2.18 shows that in a sonic ($M = 1.0$) stream of gas with $\gamma = 1.4$,

$$\frac{P}{P_t} = 0.528$$

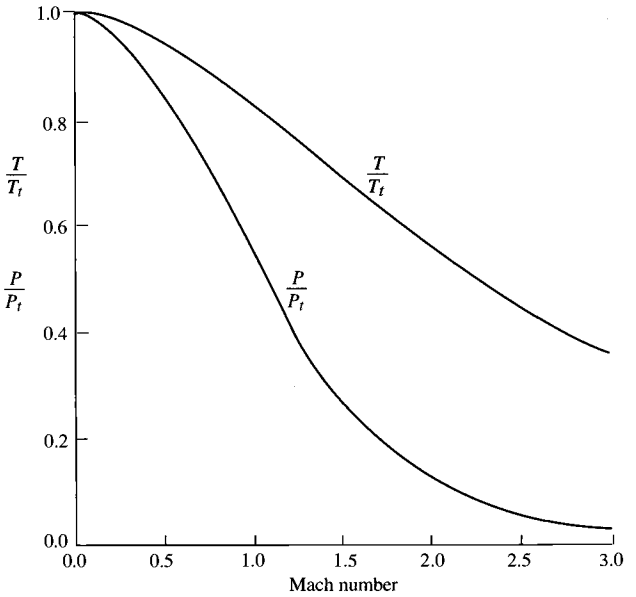

Fig. 2.18 P/P_t **and** T/T_t **vs Mach number** ($\gamma = 1.4$).

and

$$\frac{T}{T_t} = 0.833$$

and for supersonic flow,

$$\frac{P}{P_t} < 0.528$$

and

$$\frac{T}{T_t} < 0.833$$

Consider the one-dimensional steady flow of a gas in a duct with T_t and P_t constant at all stations along the duct. This means a total temperature probe will measure the same value of T_t at each duct station, and an isentropic total pressure probe will measure the same value of P_t at each station. The path line of α of the flow is a vertical line in the T-s diagram. The state points on the path line can be categorized as follows.

Subsonic:

$$T > 0.883\,T_t \qquad P > 0.528\,P_t$$

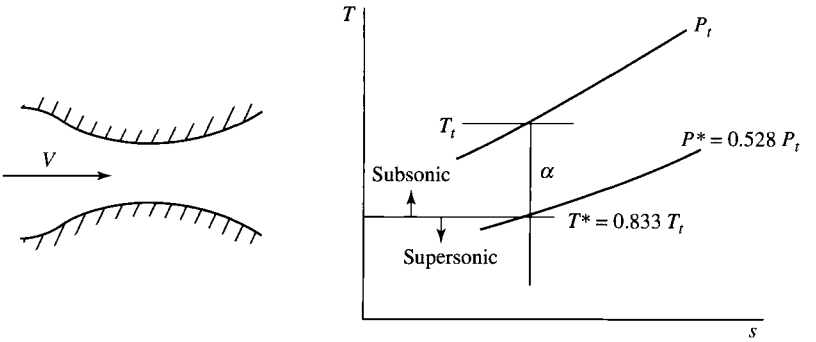

Fig. 2.19 Subsonic and supersonic state points in an isentropic flow.

Sonic:

$$T = 0.883\,T_t \qquad P = 0.528\,P_t$$

Supersonic:

$$T < 0.883\,T_t \qquad P < 0.528\,P_t$$

Figure 2.19 delineates the subsonic, sonic, and supersonic portions of path line α.

The thermodynamic properties at the state point where $M = 1$ on α are denoted by P^*, T^*, V^*, etc. (read as P star, etc.) and the state is called the "star state." In addition, the cross-sectional flow area at the $M = 1$ point is indicated by A^*. The magnitude of A^* is determined by the relation

$$A^* = \frac{\dot{m}}{\rho^* V^*} \tag{2.74}$$

2.7.4 Mass Flow Parameter

The stream properties at any general station of a calorically perfect gas are related by Eqs. (2.21), (2.36), (2.66), (2.70), (2.72), (2.73), and the one-dimensional mass flow equation

$$\dot{m} = \rho A V$$

The mass flow per unit area at duct area A in the flow of a calorically perfect gas is given by the expression

$$\frac{\dot{m}}{A} = \rho V = \frac{PV}{RT} = \frac{V}{\sqrt{\gamma g_c RT}} \frac{P\sqrt{\gamma g_c}}{\sqrt{RT}} = M\sqrt{\frac{\gamma g_c}{R}} \frac{P}{P_t} \sqrt{\frac{T_t}{T}} \frac{P_t}{\sqrt{T_t}}$$

where the one-dimensional flow equation [Eq. (2.12a)], the perfect gas equation of state [Eq. (2.21)], the perfect gas speed of sound equation [Eq. (2.36)], and the

definition of Mach number have been used. Replacing the static/total property ratios with Eqs. (2.72) and (2.73) and rearranging, we obtain the grouping defined as the *mass flow parameter* (MFP):

$$\text{MFP} \equiv \frac{\dot{m}}{A}\frac{\sqrt{T_t}}{P_t} \tag{2.75}$$

$$\text{MFP}(M) = \frac{\dot{m}}{A}\frac{\sqrt{T_t}}{P_t} = \sqrt{\frac{\gamma g_c}{R}} M\left(1 + \frac{\gamma - 1}{2}M^2\right)^{\frac{\gamma+1}{2(\gamma-1)}} \tag{2.76}$$

Thus the MFP is a unique function of the Mach number in a calorically perfect gas. Values of the mass flow parameter are plotted in Fig. 2.20 for $\gamma = 1.4$ and $\gamma = 1.3$, and calculated in the GASTAB program for user input values of γ and mean molecular weight $\mathcal{M}$. From Fig. 2.20 and the GASTAB program, one sees that the maximum value of the mass flow parameter occurs when the Mach number is unity. Thus, for a given total temperature and pressure T_t and P_t, the maximum mass flow rate per area corresponds to a flow Mach number of 1.

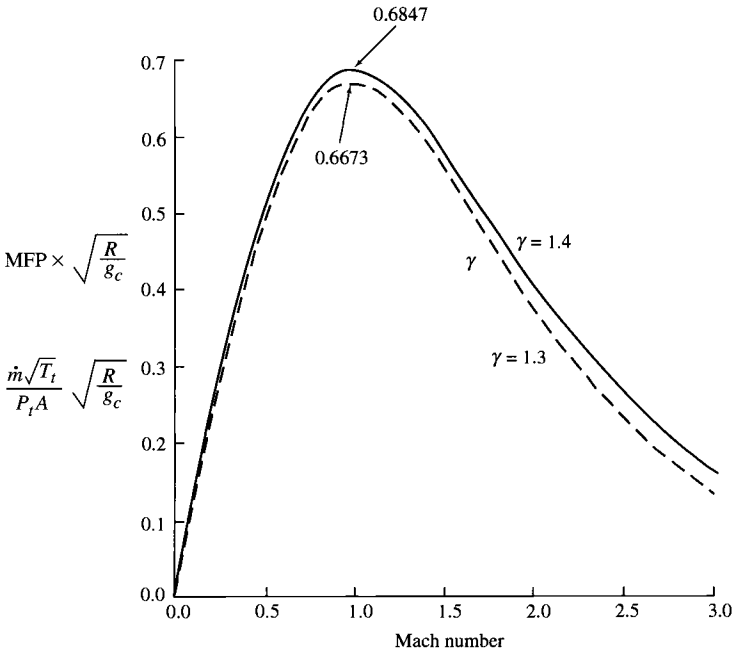

Fig. 2.20 Mass flow parameter vs Mach number ($\gamma = 1.4$ and $\gamma = 1.3$).

2.7.5 Isentropic Area Ratio A/A^*

The ratio of the one-dimensional flow area A at any flow station to the one-dimensional area for that same flow rate at sonic velocity A^* is a unique function of the Mach number M at the flow station and the ratio of specific heats γ. Consider the isentropic flow of a calorically perfect gas in an isentropic duct from ρ, M, P, T, and A to the sonic state where the properties are ρ^*, $M^* = 1$, P^*, T^*, and A^*. Because both states have the same mass flow, we write

$$\dot{m} = \rho A V = \rho^* A^* V^*$$

Rewriting gives

$$\frac{A}{A^*} = \frac{\rho^* V^*}{\rho V} = \frac{P^*}{T^*}\frac{T}{P}\frac{1}{M}\frac{a^*}{a} = \frac{1}{M}\frac{P^*/P}{T^*/T}\sqrt{T^*/T} = \frac{1}{M}\frac{P^*/P}{\sqrt{T^*/T}} \tag{i}$$

However,

$$\frac{T}{T^*} = \frac{T/T_t}{T^*/T_t} = \left[\frac{2}{\gamma+1}\left(1+\frac{\gamma-1}{2}M^2\right)\right]^{-1} \tag{ii}$$

and

$$\frac{P}{P^*} = \frac{P/P_t}{P^*/P_t} = \left[\frac{2}{\gamma+1}\left(1+\frac{\gamma-1}{2}M^2\right)\right]^{-\gamma/(\gamma-1)} \tag{iii}$$

Substitution of Eqs. (ii) and (iii) into (i) gives

$$\frac{A}{A^*} = \frac{1}{M} = \left[\frac{2}{\gamma+1}\left(1+\frac{\gamma-1}{2}M^2\right)\right]^{(\gamma+1)/[2(\gamma-1)]} \tag{2.77}$$

and A/A^*, P/P_t, and T/T_t are plotted vs Mach number in Fig. 2.21 for $\gamma = 1.4$ and calculated in GASTAB for user input γ value.

Example 2.10

Air at a total temperature of 300 K and total pressure of 1 atm flows through a 2-m^2 duct at a Mach number of 0.5.

1) What must the area of the duct be for the flow to isentropically accelerate to Mach 1?

2) What is the mass flow rate of air through the duct?

Solution: From GASTAB for $M = 0.5$ and $\gamma = 1.4$, $A/A^* = 1.3398$ and MFP = 0.0301563.

1) The area of the duct at $M = 1$ is then

$$A^* = \frac{A}{A/A^*} = \frac{2}{1.3398} = 1.4928\,\text{m}^2$$

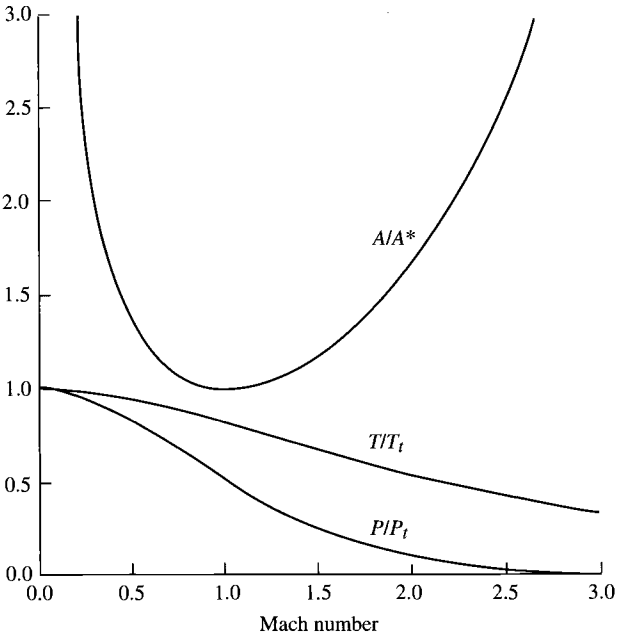

Fig. 2.21 A/A^*, P/P_t, **and** T/T_t **vs Mach number** ($\gamma = 1.4$).

2) The mass flow rate can be calculated by using the MFP as follows:

$$\dot{m} = \frac{P_t A}{\sqrt{T_t}}\text{MFP} = \frac{101,325 \times 2\text{N}}{\sqrt{300\,\text{K}}}0.0301563\,\text{kg} \cdot \sqrt{\text{K}}/(\text{N} \cdot \text{s}) = 352.83\,\text{kg/s}$$

2.7.6 Impulse Function *I*

The impulse function I is defined by

$$I \equiv PA + \dot{m}V/g_c \tag{2.78}$$

Using one-dimensional mass flow equation ($\dot{m} = \rho AV$) and equations for a calorically perfect gas, Eq. (2.78) can be rewritten as

$$I = PA(1 + \gamma M^2) \tag{2.79}$$

From Eq. (2.20) for steady state, the streamwise axial force exerted on the fluid flowing through a control volume is $I_{\text{exit}} - I_{\text{entry}}$, while the reaction force exerted by the fluid on the control volume is $I_{\text{entry}} - I_{\text{exit}}$.

The impulse function makes possible almost unimaginable simplification of the evaluation of forces on aircraft engines, rocket engines, and their components. For example, although one could determine the net axial force exerted on the fluid flowing through any device by integrating the axial components of pressure and viscous forces over every infinitesimal element of internal wetted surface area, it is certain that no one ever has. Instead, the integrated result of the forces is obtained with ease and certainty by merely evaluating the change in impulse function across the device.

Compressible flow functions tabulate the impulse function as a ratio to that at the star state ($M = 1$) or I/I^*. We note that

$$\frac{I}{I^*} = \frac{P}{P^*}\frac{A}{A^*}\frac{1+\gamma M^2}{1+\gamma} \tag{2.80}$$

2.8 One-Dimensional Gas Dynamics—Finite Control Volume Analysis and the *H-K* Diagram

Much of the material in this section, through page 121, is reprinted from *Hypersonic Airbreathing Propulsion*, by Heiser and Pratt, Section 2.6,[13] with permission of the publisher.* Minor adaptations have been made to the original text.

The six example cases that follow are based on the steady, one-dimensional flow of a calorically perfect gas as shown in Fig. 2.22. They are meant to show the breadth and power of one-dimensional analysis, while demonstrating several key features of hypersonic flows that play prominent roles in ramjets and scramjets and familiarizing the reader with applying the set of governing equations.

The reader should be aware that the example cases are also found in the subroutines of the GASTAB program (Gas Tables) included with this textbook.

Example Case 2.1: Constant Energy Flows

Consider a one-dimensional flow without energy interactions with the surroundings, i.e.,

$$w_x = q = 0$$

Under these conditions, the energy equation, Eq. (2.14), reduces to

$$h_i + \frac{V_i^2}{2g_c} = h_e + \frac{V_e^2}{2g_c} = h_t \tag{2.81}$$

which means that the *total enthalpy* h_t is a fixed property of constant energy flows, even if the gas is *not* calorically perfect. The total enthalpy is also equal

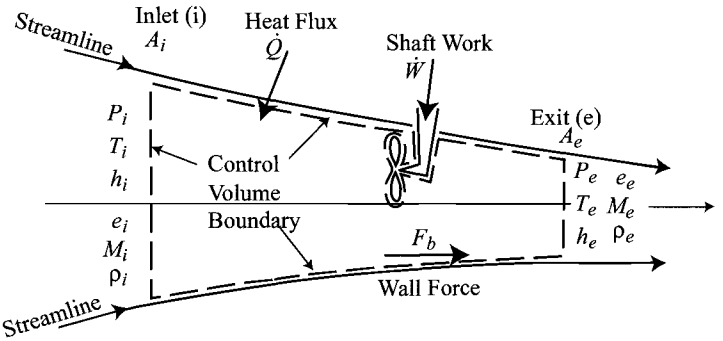

Fig. 2.22 Finite control volume for one-dimensional gas dynamics.

to the enthalpy that would exist locally if the flow were brought completely to rest without energy interactions, and is therefore also known as the *stagnation enthalpy.*

For a calorically perfect gas, Eqs. (2.38) and (2.81) can be combined to yield

$$c_p T_i + \frac{V_i^2}{2\,g_c} = c_p T_e + \frac{V_e^2}{2\,g_c} = c_p T_t \tag{2.82}$$

where T_t is the *total temperature.* This expression may be rearranged with the help of Eqs. (2.8) and (2.36) to show that

$$T_t = T_i\left(1 + \frac{\gamma - 1}{2} M_i^2\right) = T_e\left(1 + \frac{\gamma - 1}{2} M_e^2\right) \tag{2.83}$$

It is interesting and productive to portray Eq. (2.82) in terms of the *dimensionless static enthalpy* c_pT/c_pT_{ti} and the *dimensionless kinetic energy* $V^2/(2g_c c_p T_{ti})$, or

$$\frac{c_p T}{c_p T_{ti}} + \frac{V^2}{2\,g_c c_p T_{ti}} = 1 \tag{2.84}$$

which can be written simply as

$$H + K = 1 \tag{2.85}$$

where

$$H \equiv \frac{c_p T}{c_p T_{ti}} \qquad \text{and} \qquad K \equiv \frac{V^2}{2\,g_c c_p T_{ti}} \tag{2.86}$$

as shown in Fig. 2.23. The state of the flow *must* be somewhere on this straight line. This line will be referred to as a *constant total enthalpy line.*

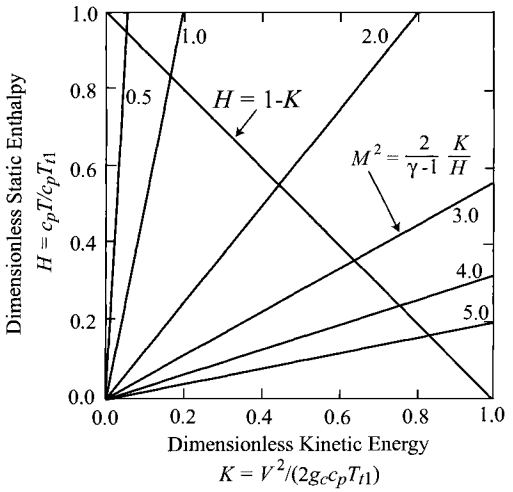

Fig. 2.23 Dimensionless energy diagram for the constant energy flow of a calorically perfect gas, showing the relationship between dimensionless static enthalpy H and the dimensionless kinetic energy K, Eq. (2.85). The straight lines emanating from the origin are lines of constant Mach number, Eq. (2.87), increasing from left to right.

From the definition of the Mach number, isolines of constant Mach number M are given by the straight line

$$\frac{\gamma - 1}{2} M^2 H - K = 0 \tag{2.87}$$

which is a ray passing through the coordinate origin (Ref. 17). Lines of constant Mach number are shown on Fig. 2.23 along with a line of constant enthalpy, Eq. (2.85).

Equation (2.71b) may now be combined and manipulated to show that

$$\frac{s_e - s_i}{R} = -\ell n\left(\frac{P_{ti}}{P_{te}}\right) \tag{2.88}$$

where the *total pressure* [Eq. (2.73)]

$$P_t = P\left(1 + \frac{\gamma - 1}{2} M^2\right)^{\frac{\gamma}{\gamma - 1}}$$

is a fixed property of constant energy *isentropic* flows of calorically perfect gases. Because the entropy can only increase for this type of flow, Eq. (2.88) shows that the total pressure can only decrease as the flow proceeds. Because γ for air is 1.40 or less, the exponent of this expression is at least 3.50, which means

that the dependence of the total pressure on flight Mach number is *remarkably* strong for a natural process.

Note should also be taken of the fact that, according to Eq. (2.88),

$$\pi = \frac{P_{te}}{P_{ti}} = e^{-(s_e - s_i)/R} \leq 1 \tag{2.89}$$

which means that the *total pressure ratio* π depends exponentially on the entropy increase. In other words, the total pressure ratio should be expected to decrease very rapidly as entropy, the natural indicator of the effects of dissipation or *flow losses*, increases.

Example Case 2.2: Impulse Function and Stream Thrust Function

Consider a one-dimensional flow for which all properties at the inlet and exit planes are known. In this situation Eq. (2.12) becomes

$$\dot{m} = \rho_i V_i A_i = \rho_e V_e A_e \tag{2.90}$$

and Eq. (2.20) becomes

$$F_b = (P_e A_e + \dot{m} V_e / g_c) - (P_i A_i + \dot{m} V_i / g_c) \tag{2.91}$$

so that the total force acting on the flow within the control volume can be directly determined.

In the regime where the fluid behaves as a calorically perfect gas, the axial momentum equation may be rearranged into several useful forms. For example, with the help of Eqs. (2.78) and (2.79), Eq. (2.91) becomes

$$F_b = P_e A_e (1 + \gamma M_e^2) - P_i A_i (1 + \gamma M_i^2) = I_e - I_i \tag{2.92}$$

where [Eq. (2.79)]

$$I = PA(1 + \gamma M^2)$$

Next, multiplying Eq. (2.91) by g_c and dividing through by Eq. (2.90), and using Eq. (2.21), we find that

$$\frac{F_b g_c}{\dot{m}} = V_e (1 + g_c R T_e / V_e^2) - V_i (1 + g_c R T_i / V_i^2) = Sa_e - Sa_i \tag{2.93}$$

where

$$Sa = \frac{I g_c}{\dot{m}} = V(1 + g_c R T / V^2) \tag{2.94}$$

The latter expression is known in compressible fluid mechanics as the *stream thrust function* (*Sa* originally standing for mass flow rate specific thrust of air). The stream thrust function is the parameter that most easily leads to the

determination of mass flow rate specific thrust, a quantity often used in performance evaluations to eliminate dependence on absolute size.

Finally, dividing Eq. (2.94) by $\sqrt{g_c c_p T_t}$ and rearranging, we find that the *dimensionless stream thrust function* for *axial flow* as

$$\Phi = \frac{Sa}{\sqrt{g_c c_p T_{ti}}} = \sqrt{\frac{1}{2}\left(\frac{2\,g_c c_p T_{ti}}{V^2}\right)}\left\{2\left(\frac{V^2}{2\,g_c c_p T_{ti}}\right) + \frac{\gamma - 1}{\gamma}\left(\frac{c_p T}{c_p T_{ti}}\right)\right\} \tag{2.95}$$

or

$$\Phi = \frac{Sa}{\sqrt{g_c c_p T_{ti}}} = \sqrt{\frac{1}{2K}}\left\{2K + \frac{\gamma - 1}{\gamma} H\right\} \tag{2.96}$$

Note that Φ depends upon the same dimensionless quantities that are found in Eq. (2.84). Equation (2.95) is portrayed in Fig. 2.24 for typical values of Φ and γ, where it can be seen that the curve resembles an ellipse passing through the origin. For a given Φ, the state of the flow *must* be somewhere on this curved line. For the *special* case of constant area flow with heat interaction but without friction, this line is known in the classical literature as a *Rayleigh line.* However, the same relation applies to the *much* more *general* situations to be encountered here, and so the line will *not* be referred to by that name. The breaks at the right end of the line are meant to remind us that it may not be possible to find *mean* values of the gas constants valid over the entire range, although one may judiciously select the range for which they are suitably accurate.

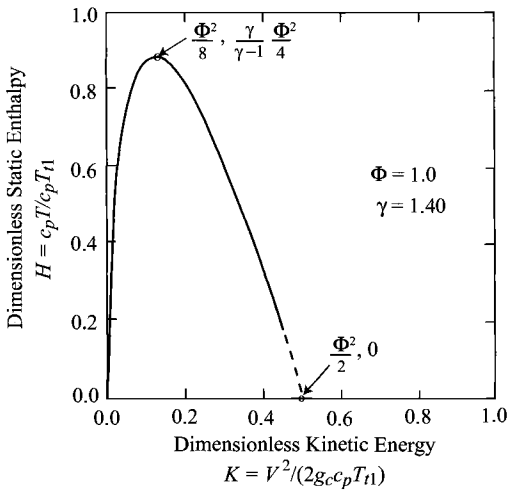

Fig. 2.24 Dimensionless energy diagram for the constant stream thrust flow of a calorically perfect gas, showing the relationship between dimensionless static enthalpy H and the dimensionless kinetic energy K, Eq. (2.95).

Example Case 2.3: Normal Shock Waves

Normal shock waves are discontinuities in one-dimensional, constant through-flow area, axial flows that are subject to the three constraints of constant mass flow, constant energy, and constant stream thrust. The upstream and downstream or *jump* conditions for normal shock waves can therefore be obtained for calorically perfect gases by the simultaneous solution of Eqs. (2.84) and (2.95) for constant values of c_pT_{ti} and Φ. A typical *graphical* solution is portrayed in Fig. 2.25, which combines Figs. 2.23 and 2.24.

Straightforward mathematical manipulations of Eqs. (2.84) and (2.95) yield the more familiar closed-form, *algebraic* solutions for the jump conditions of normal shock waves. For example, the two dimensionless kinetic energy solutions are

$$K = \frac{V^2}{2g_c c_p T_{ti}} = \left\{ \frac{\gamma\Phi}{(\gamma+1)\sqrt{2}} \pm \sqrt{\frac{1}{2}\left(\frac{\gamma\Phi}{\gamma+1}\right) - \left(\frac{\gamma-1}{\gamma+1}\right)} \right\}^2 \tag{2.97}$$

and the respective dimensionless static enthalpy solutions are [Eq. (2.85)]

$$\frac{c_pT}{c_pT_{ti}} = 1 - \frac{V^2}{2g_c c_p T_{ti}} \qquad \text{or} \qquad H = 1 - K$$

To prove that these two solutions correspond to supersonic and subsonic flow, it is first necessary to observe that straight lines emanating from the origin of Fig. 2.25 are lines of constant Mach number, larger slopes belonging to lower Mach numbers. Next, it can be seen from the geometry of this diagram that there is only one value of Φ for which the constant stream thrust function line is tangent to the constant energy line *at point c* and for which there is one solution (rather than two or zero). This condition arises when the discriminant of Eq. (2.97) is zero, and consequently

$$\Phi_c = \sqrt{2\left(1 - \frac{1}{\gamma^2}\right)} \tag{2.98}$$

($\Phi_c = 0.990$ for $\gamma = 1.40$), and

$$K_c = \frac{V_c^2}{2\,g_c c_p T_{ti}} = \frac{\gamma-1}{\gamma+1} \tag{2.99}$$

$\{K_c = V^2/(2\,g_c c_p T_{ti}) = 0.167 \text{ for } \gamma = 1.40\}$. Using Eqs. (2.83) and (2.99) reveals that at point c

$$M_c = 1 \tag{2.100}$$

Finally, returning to the geometry of Fig. 2.25, it follows that all values of Φ that have two solutions must have one that is subsonic and one that is supersonic. The

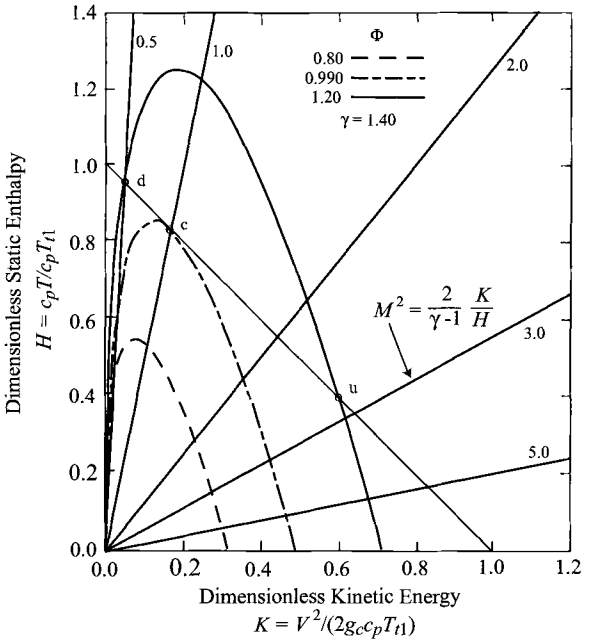

Fig. 2.25 Graphical solution for the jump condition of normal shock waves based on Eqs. (2.84) and (2.95). The straight lines emanating from the origin are lines of constant Mach number, increasing from left to right as indicated by their labels.

normal shock therefore takes the flow from the upstream, supersonic condition (point *u*) to the downstream, subsonic condition (point *d*).

Before moving on, it is worth noting in anticipation of coming topics that the graphical presentation of Fig. 2.25 has the special virtue that constant values of such primal physical quantities as static enthalpy, static temperature, kinetic energy, velocity, Mach number, and functions of Mach number only all appear as straight lines.

The GASTAB software is included to help solve problems. As an example, consider air ($\gamma = 1.4$) flowing at Mach 2.0 enters a normal shock. From normal shock tab of GASTAB, the downstream Mach number is 0.5774, the static pressure ratio across the normal shock is 4.5, and the total pressure ratio across the normal shock is 0.7209. Other example problems are included within the Supporting Material.

Example Case 2.4: Constant Area Heating and Thermal Choking

Consider a frictionless, one-dimensional flow of constant area for which there is only a total heat interaction q with the surroundings, i.e.,

$$F_{bx} = w_x = 0 \qquad A_i = A_e \qquad \dot{m}_i = \dot{m}_e = \dot{m}$$

Under these circumstances, which correspond to classical Rayleigh flow, Eq. (2.12) becomes

$$\rho_i V_i = \rho_e V_e \tag{2.101}$$

and Eq. (2.91) becomes

$$P_i + \rho_i V_i^2/g_c = P_e + \rho_e V_e^2/g_c \tag{2.102}$$

which means that the stream thrust function Sa is constant. Taking the working fluid to be calorically perfect, we must therefore reach the conclusion that

$$\Phi = \frac{Sa}{\sqrt{g_c c_p T_{ti}}} = \Phi_i = \text{const} \tag{2.103}$$

where Φ_i (the *inlet* dimensionless stream thrust function) as given by Eq. (2.95) and $c_p T_{ti}$ (the *inlet* total enthalpy) may be evaluated from the known inlet conditions.

Equation (2.14) becomes

$$c_p T_i + \frac{V_i^2}{2\,g_c} + q = c_p T_{ti}\left(1 + \frac{q}{c_p T_{ti}}\right) = c_p T_e + \frac{V_e^2}{2\,g_c} = c_p T_{te} \tag{2.104}$$

or

$$\frac{T_{ti}}{T_{te}} = \frac{c_p T_e}{c_p T_{ti}} + \frac{V_e^2}{2\,g_c c_p T_{ti}} = 1 + \frac{q}{c_p T_{ti}} \equiv \tau_e \geq 1 \tag{2.105a}$$

or

$$\frac{T_{ti}}{T_{te}} = H + K = 1 + \frac{q}{c_p T_{ti}} \equiv \tau_e \geq 1 \tag{2.105b}$$

where τ_e is the *total temperature ratio* and the primary indicator of *dimensionless heating*. Equations (2.103) and (2.105b) may be combined to find the *algebraic* solution for the two possible exit conditions, namely

$$K_e = \frac{V_e^2}{2 g_c c_p T_{ti}} = \left\{ \frac{\gamma \Phi_i}{(\gamma+1)\sqrt{2}} \pm \sqrt{\frac{1}{2}\left(\frac{\gamma \Phi_i}{\gamma+1}\right) - \tau_e\left(\frac{\gamma-1}{\gamma+1}\right)} \right\}^2 \tag{2.106}$$

and

$$\frac{c_p T_e}{c_p T_{ti}} = \tau_e - \frac{V_e^2}{2\,g_c c_p T_{ti}} \tag{2.107a}$$

or

$$H_e = \tau_e - K_e \tag{2.107b}$$

Equations (2.103) and (2.105b) can also be solved *graphically*, as shown in Fig. 2.26, where the positive root of Eq. (2.106) belongs to supersonic inlet conditions and the negative root to subsonic inlet conditions. Because τ_e may be treated as an independent variable, Fig. 2.26 reveals that heating the flow drives it toward an exit Mach number of 1 regardless of whether it was initially subsonic or supersonic. Thus, in the typical example of Fig. 2.25, a τ_e of 1.20 reduces the supersonic branch Mach number from an inlet value of 2.74 to an exit value of 1.89, and increases the subsonic branch Mach number from 0.493 to 0.598.

The remarks about the tangent point solution made in the previous example case also apply here, in particular that point c is the sonic condition, at which the discriminant of Eq. (2.106) must be zero, or

$$\tau_c = \frac{T_{t^*}}{T_{ti}} = \Phi_i^2 / \left\{2\left(1 - 1/\gamma^2\right)\right\} \tag{2.108}$$

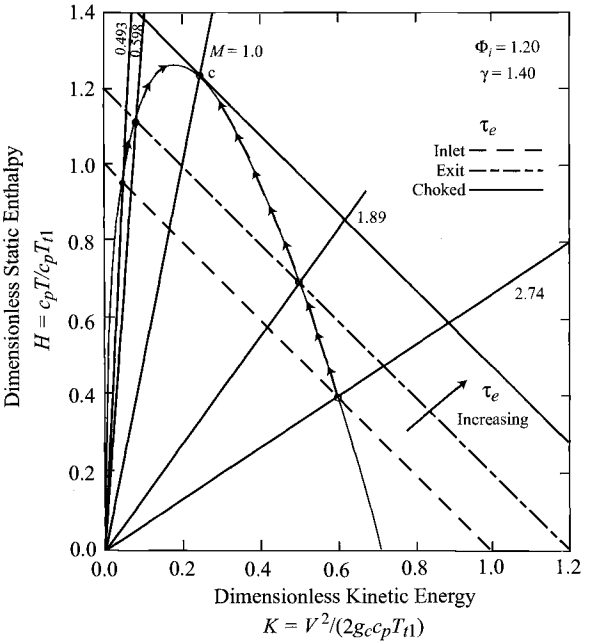

Fig. 2.26 Graphical solution for the frictionless, constant area heating based on Eqs. (2.103) and (2.104). The straight lines emanating from the origin are lines of constant Mach number, increasing from left to right as indicated by their labels.

($\tau_c = 1.47$ for $\Phi_i = 1.20$ and $\gamma = 1.40$), and

$$K_c = \frac{V_c^2}{2\,g_c c_p T_{ti}} = \frac{1}{2}\left(\frac{\gamma \Phi_i}{\gamma + 1}\right)^2 \tag{2.109}$$

$\{K_c = V_c^2/(2g_c c_p T_{ti})i = 0.245$ for $\Phi_i = 1.20$ and $\gamma = 1.40\}$.

Most importantly, Fig. 2.26 clearly demonstrates that for any inlet condition there is a maximum amount of energy that can be added before the exit Mach number reaches 1. There are *no* solutions to the governing equations for $\tau_e > \tau_c$. Once that point has been reached, it is physically impossible to add any more energy without forcing the upstream conditions to change, and the flow is said to be *thermally choked.* The conditions necessary for thermal choking can and do occur in practice, especially when the inlet Mach number is not far from 1, and should not be considered merely as an intellectual curiosity.

Finally, it is also possible to show that the entropy always increases as the flow is heated. This is best done by substituting the preceding results into the Gibbs equation and rearranging to show that

$$\frac{s_e - s_i}{c_p} = \ell n\left\{\left(\frac{M_e}{M_i}\right)^2 \left(\frac{1 + \gamma M_i^2}{1 + \gamma M_e^2}\right)^{\frac{\gamma+1}{\gamma}}\right\} \tag{2.110}$$

Since the grouping

$$\frac{M^2}{(1 + \gamma M^2)^{\frac{\gamma+1}{\gamma}}}$$

has a maximum when M is 1, and since heating always drives M toward 1, it follows that heating is always accompanied by increased entropy.

The GASTAB software is included to help solve problems. As an example, consider air ($\gamma = 1.4$) flowing at Mach 0.5 in a constant area duct heated from 300 to 400 K. From Rayleigh flow tab of GASTAB, the maximum total temperature of the flow ($T_{t^*} = T_t \tau_c$) is 433.9 K (=300/0.6914). For the exit temperature of 400 K ($T_t/T_{t^*} = 400/433.9 = 0.9219$), the exit Mach number is 0.7197 and the total pressure ratio is $0.9314[P_{t2}/P_{t1} = (P_{t2}/P_{t^*})/(P_{t1}/P_{t^*}) = 1.0377/1.1141]$. Other example problems are included within the Supporting Material.

Example Case 2.5: Constant Area Friction and Frictional Choking

Consider a one-dimensional flow of constant area without energy interactions and frictional force F_f with the surroundings, i.e.,

$$q = w_x = 0 \qquad A_i = A_e$$

Under these circumstances, which correspond to classical Fanno line flow, Eq. (2.12b) becomes [Eq. (2.101)]

$$\rho_i V_i = \rho_e V_e$$

the energy equation, Eq. (2.14), reduces to [Eq. (2.81)]

$$h_i + \frac{V_i^2}{2g_c} = h_e + \frac{V_e^2}{2g_c} = h_t$$

and Eq. (2.20) becomes

$$-F_f = A\left(P_i + \rho_i V_i^2/g_c\right) - A\left(P_e + \rho_e V_e^2/g_c\right) = I_i - I_e \tag{2.111}$$

Taking the working fluid to be calorically perfect, Eq. (2.81) becomes [Eq. (2.82)]

$$c_p T_i + \frac{V_i^2}{2g_c} = c_p T_e + \frac{V_e^2}{2g_c} = c_p T_t$$

which can be written simply as [Eq. (2.85)]

$$H + K = 1$$

where [Eq. (2.86)]

$$H \equiv \frac{c_p T}{c_p T_{ti}} \qquad \text{and} \qquad K \equiv \frac{V^2}{2g_c c_p T_{ti}}$$

and Eq. (2.111) becomes

$$\frac{F_f g_c}{\dot{m}} = V_i(1 + g_c RT_i/V_i^2) - V_e(1 + g_c RT_e/V_e^2) = Sa_i - Sa_e \tag{2.112}$$

where [Eq. (2.94)]

$$Sa = \frac{Ig_c}{\dot{m}} = V(1 + g_c RT/V^2)$$

Using the dimensionless stream thrust function Φ [Eq. (2.96)], Eq. (2.112) becomes

$$\frac{F_f g_c/\dot{m}}{\sqrt{g_c c_p T_{ti}}} = \Phi_i - \Phi_e \tag{2.113}$$

which means that the change in stream thrust function is directly proportional to the frictional force F_f.

Graphical solution of Eqs. (2.85) and (2.103) is presented in Fig. 2.27. Consider flow entering at $M_i = 0.5$ and $\Phi_i = 1.20$ (point d in Fig. 2.27). If the frictional force decreases the dimensionless stream thrust function to $\Phi_e = 0.99$, then the exit flow chokes with $M_e = 1$ (point c in Fig. 2.27). There is no solution

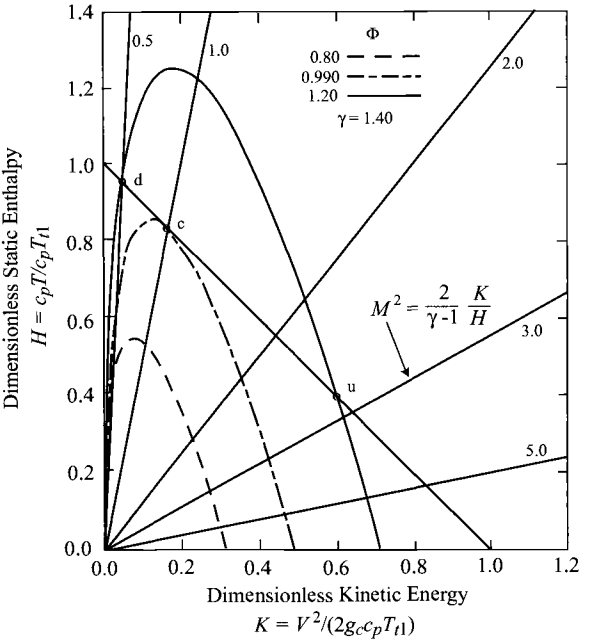

Fig. 2.27 Graphical solution for the frictionless, constant area frictional flow based on Eqs. (2.85) and (2.113). The straight lines emanating from the origin are lines of constant Mach number, increasing from left to right as indicated by their labels.

for further decreases of Φ with the same inlet conditions. Similarly, flow entering at $M_i = 2.74$ and $\Phi_i = 1.20$ (point u in Fig. 2.27) will choke when Φ is decreased to 0.99.

H-K diagram. The great utility of graphically displaying flow processes in terms of dimensionless static enthalpy vs dimensionless kinetic energy has been amply demonstrated by the elementary example cases already considered. This method of presentation will prove even more valuable in explaining and illustrating the more complex internal flow behavior of airbreathing engines. To ease communications, this diagram will hereinafter simply be called the *H-K diagram* (H for dimensionless static enthalpy and K for dimensionless kinetic energy).

Please note that the *H-K* diagram, for all its other virtues, is *not a state diagram* because only one axis is an intensive thermodynamic property. In other words, there is no necessary relationship between a point on the *H-K* diagram and the other intensive thermodynamic properties of the fluid, such as static pressure or static entropy. Nevertheless, the *H-K* diagram will provide more than enough information to reveal the things we really need to know about the flow. Also, under some frequently encountered conditions, such as one-dimensional flow with known $\dot{m}$, A, and T_{ti}, the *H-K* diagram *is* a state diagram.

An especially useful generalization for moving about the *H-K* diagram, based on the assemblage of preceding example cases, is that heating, friction, and area decrease *all* act separately and together to drive the Mach number toward 1. They may therefore in an intuitive sense be said to *block*, *constrict*, *obstruct*, *restrict*, or *occlude* the flow. Similarly, cooling, reverse friction (i.e., any streamwise force), and area increase could be said to *unblock*, *enlarge*, *relieve*, *open*, or *free* the flow. You will find these mental images helpful in what follows.

Figure 2.28 shows the *H-K* diagram with representative constant-property isolines. The *H-K* diagram will be used in this text to improve understanding of the flow through airbreathing engines.

The *H-K* diagram often provides a convenient means for visualizing, comprehending, and even analyzing the operation of propulsion devices, as illustrated in the following for the scramjet engine.[17] It is important to note that the dimensionless stream thrust function at a given Mach number is not some arbitrary value but is specified by Eq. (2.114) as rearranged into the Mach number form:

$$\Phi = \sqrt{\frac{\tau_e(\gamma-1)M^2}{1+\dfrac{\gamma-1}{2}M^2}}\left(1+\frac{1}{\gamma M^2}\right) \tag{2.114}$$

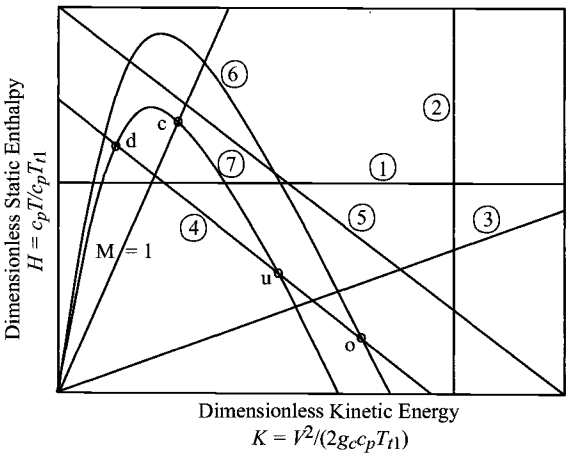

Fig. 2.28 The *H-K* diagram, depicting representative constant-property isolines. Key: 0 = freestream reference state. Point *c* = choked condition at constant impulse. Points *u* and *d* denote end states of normal shock. Circled numbers denote isolines of constant property as follows: 1) static enthalpy, static temperature; 2) kinetic energy, velocity, pressure (for frictionless heating or cooling only); 3) Mach number; 4) total enthalpy, total temperature (adiabat), $\tau \equiv T_t/T_{t0} = 1$; 5) post-heat release adiabat, $t > 1$; 6) impulse function/stream thrust, area (for frictionless flow with heating or cooling only), case $I = I_0$; 7) impulse function, case $\Phi > \Phi_0$.

Example Case 2.6: Scramjet

The basic concept of the scramjet is that the flow must remain supersonic throughout to avoid the high static temperatures that reduce performance by causing chemical dissociation of the combustion products, as well as the high static pressures that cause structural problems. Consequently, in practical terms, when the freestream Mach number exceeds 5–6, the flow is designed to enter the combustor at supersonic speeds, and the device is known as the supersonic combustion ramjet, or scramjet.

Figure 2.29 shows the *H-K* diagram for air with $\gamma = 1.40$ being processed by a scramjet that is powering a vehicle at a freestream Mach number of 10.0, where Eq. (2.114) has been used to show that $\Phi_0 = 1.390$. The air is first decelerated and compressed from the freestream condition (point 0) to the burner entry condition (point 1) by means of a combination of isentropic compression and oblique shock waves. The purposes of this compression are to provide a large enough static temperature ratio T_1/T_0 for satisfactory thermodynamic cycle efficiency (usually in the range of 6–8, and 6.50 for this example) and to produce high enough values of P_1 and T_1 to support complete and stable combustion in the burner. Even when these criteria have been met, the burner entry $M_1 = 3.340$ remains supersonic, as Fig. 2.29 clearly reveals.

The air is then heated in a combustion process that releases the chemical energy of the fuel. The heating is represented in this type of analysis by an increasing total temperature, in this example case by a factor of 1.40. The precise path of this process depends on the philosophy of the burner design, and two of many possible different types are depicted in Fig. 2.29. The first,

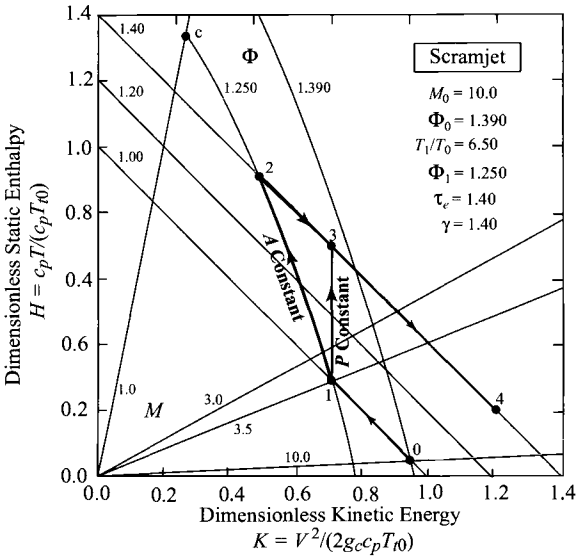

Fig. 2.29 The *H-K* diagram for an example scramjet.

joining point 1 to point 2, is frictionless, constant area heating, which is a Rayleigh line having $\Phi_1 = 1.250$. The second, joining point 1 to point 3, is frictionless, constant pressure heating, which is found in Problem 2.49d also to be a line of constant velocity. There is clearly no danger of reaching point c and thermal choking for either combustor in this scenario.

The heated air is then accelerated and expanded from a burner exit condition such as point 2 or 3 to the freestream static pressure at point 4. Because there are total pressure losses in the scramjet, the Mach number at point 4 can never be quite as large as the freestream Mach number, but it can be large enough that the kinetic energy and velocity at point 4 exceed that of point 0, which means that the scramjet produces net thrust. As a corollary, the total pressure losses and therefore the precise location of point 4 also depend on the type of burner design. Nevertheless, the *H-K* diagram makes it clear that the potential thermodynamic performance is greater for constant area heating than for constant velocity heating because each increment of heat is added at a higher temperature in the former case.

The readers are encouraged to expand their familiarity and facility with the *H-K* diagram by either explaining the impact of other heating processes (e.g., constant temperature or constant Mach number) on the potential thermodynamic performance of the scramjet, or by constructing the *H-K* diagram for the ramjet, for which the combustor Mach number is very subsonic.

2.9 Nozzle Design and Nozzle Operating Characteristics

Figure 2.30 shows flow through a nozzle from a subsonic flow (state 1) through the sonic conditions (state $*$) to supersonic flow (state 2). The flow is isentropic, and both the total temperature and total pressure are constant. For analysis, we consider accelerating a gas through a nozzle with mass flow rate $\dot{m}_c$. Let the flow originate in a large storage chamber (Fig. 2.31) at chamber pressure

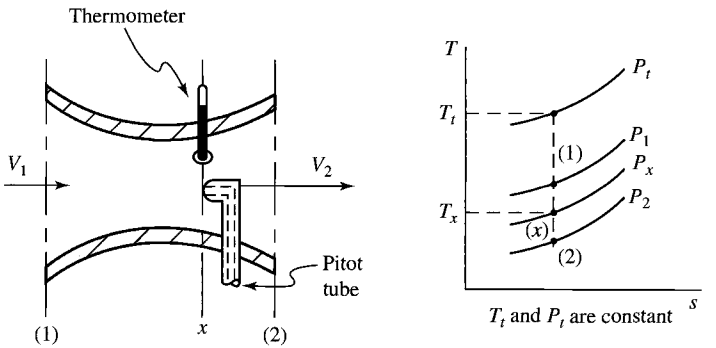

Fig. 2.30 Simple nozzle flow.

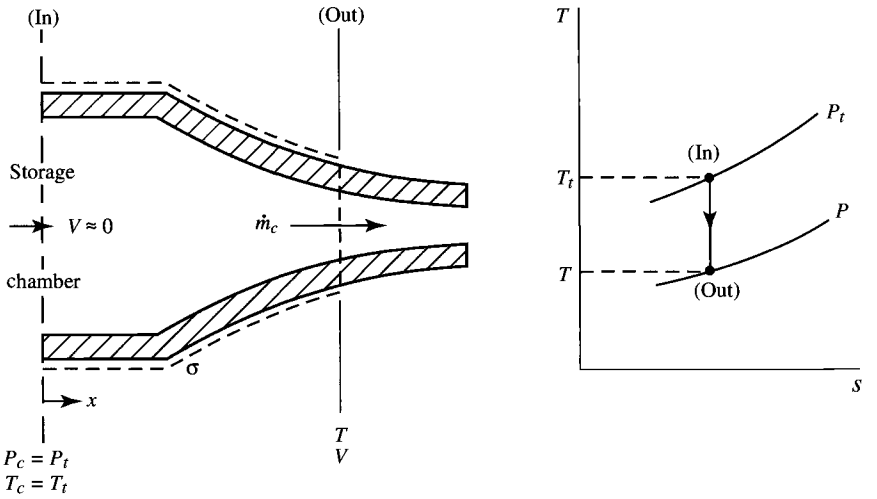

Fig. 2.31 Control volume for simple nozzle flow.

$P_c = P_t$, and chamber temperature $T_c = T_t$. The stream properties at any station in the flow are related by the following equations:

$$P_c = P_t = P(T_t/T)^{\gamma/(\gamma-1)} \tag{i}$$

$$T_c = T_t = T + V^2/(2\,g_c c_p) \tag{ii}$$

$$\dot{m}_c = \rho AV = PAV/(RT) \tag{iii}$$

For given chamber gas conditions P_c, T_c, R, γ, and known $\dot{m}_c$, there are four variables P, T, V, A in these three equations. We may select one variable as independent and find each of the remaining three in terms of this one. Practical problems generally fall into two categories:

1) Nozzle design. We wish to pass a given mass flow with minimum frictional losses between two regions of different pressure (storage chamber at P_c and exhaust region at P_a) with, say, some assumed variation in pressure between the two regions.

2) Nozzle operating characteristics. Given a nozzle, what mass rates of flow and pressure distribution will prevail through the nozzle for various nozzle pressure ratios ($P_n = P_c/P_a$)?

In case 1, our independent, or known, variable is pressure P, which is a function of position x. In case 2, our independent, or known, variable is area A, which is a function of position x. We will consider each case in turn.

2.9.1 Nozzle Design

We shall illustrate the design of a nozzle by example.

Example 2.11

Assume we wish to expand gases at 28 lbm/s from a high-altitude second-stage rocket combustion chamber to an ambient pressure of 0.618 psia (≈70 kft altitude). Pertinent data simulating the Agena rocket engine are as follows:

$$P_c = 206 \text{ psia}, \qquad c_p g_c = 6000 \text{ ft}^2/(\text{s}^2\text{-}^\circ\text{R}), \qquad T_c = 5000^\circ\text{R}$$

$$\text{Nozzle length} = 30 \text{ in.}, \qquad \dot{m}_c = 28 \text{ lbm/s}$$

$$Rg_c = 1715 \text{ ft}^2/(\text{s}^2\text{-}^\circ\text{R}), \qquad \text{Exit pressure} = 0.618 \text{ psia}$$

To solve the problem, we must determine the flow area, gas temperature, velocity, and Mach number (A, T, V, and M) at each nozzle station. Assume all sections of the nozzle are circular, and assume simple area flow. Figure 2.32 provides the length of, and pressure in, the nozzle to be designed.

Solution: For the given conditions, the constants of Eqs. (i) through (iii) are known. Thus

$$P_t = P_c = 206 \text{ psia}, \qquad T_t = T_c = 5000^\circ\text{R}, \qquad \dot{m}_c = 28 \text{ lbm/s}$$

$$Rg_c = 1715 \text{ ft}^2/(\text{s}^2\text{-}^\circ\text{R}), \qquad c_p g_c = 6000 \text{ ft}^2/(\text{s}^2\text{-}^\circ\text{R}), \qquad \gamma = 1.4$$

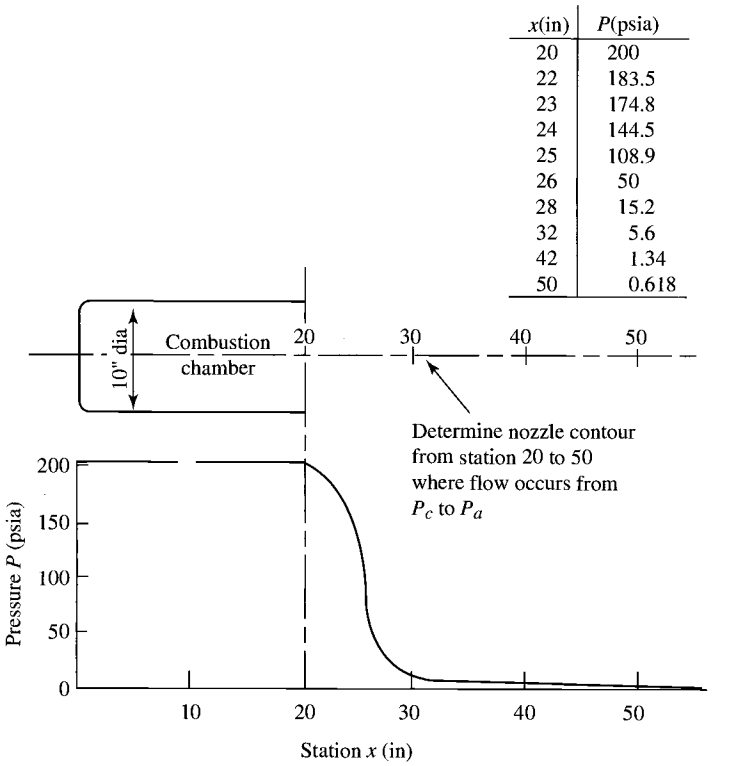

Fig. 2.32 Nozzle pressure distribution.

Rewrite Eqs. (i) through (iii) as

$$T = T_t(P/P_t)^{(\gamma-1)/\gamma} \tag{iv}$$

$$V = \sqrt{2g_c c_p(T_t - T)} \tag{v}$$

$$A = \dot{m}RT/(PV) \tag{vi}$$

With P known (Fig. 2.32), use Eq. (iv) to find T at any given station. Equation (v) will then give V. With T and V determined, and $\dot{m}$, R, and P known, Eq. (vi) gives the nozzle area A at the selected station. In this manner, the nozzle area and gas properties can be found at all stations. The Mach number follows from

$$M = V/\sqrt{\gamma R g_c T} \tag{vii}$$

The results of the computation outlined are plotted in Fig. 2.33. The curves and nozzle contour in this figure illustrate that in order to *decrease* P and *increase* V in a simple area flow:

A *converging* nozzle contour is required in *subsonic* flow.
A *diverging* nozzle contour is required in a *supersonic* flow.

Thus we find that the typical shape of a nozzle that is accelerating a gas from rest to supersonic speeds is convergent-divergent (C-D). At the design operating point of a *supersonic* C-D nozzle, the flow is subsonic up to the throat, sonic at the throat, and supersonic after the throat. The exit plane pressure P_e equals the exhaust region pressure P_a. We shall denote the nozzle pressure ratio for the

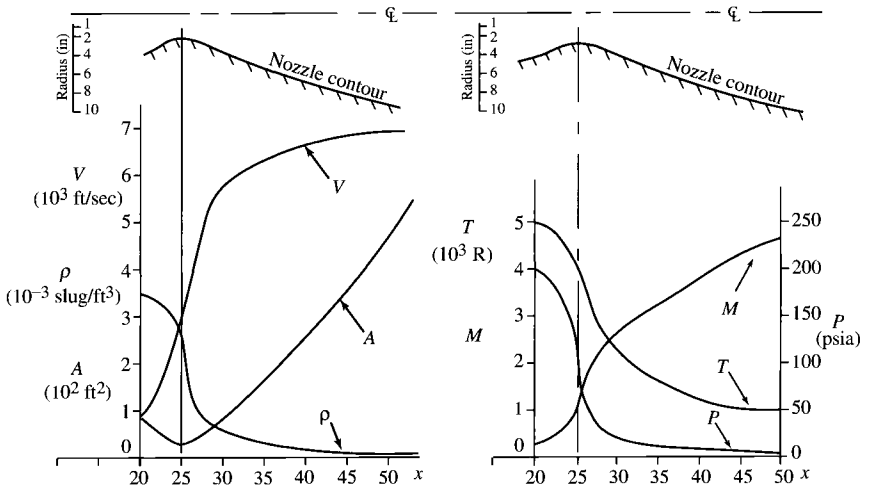

Fig. 2.33 Nozzle flow properties vs station for air.

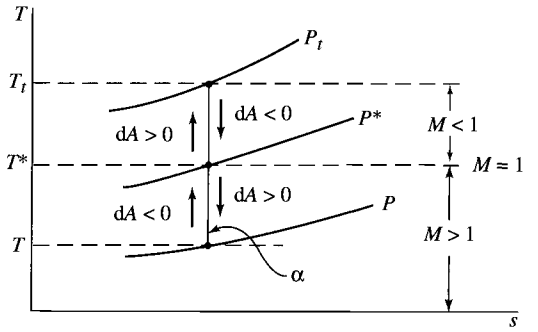

Fig. 2.34 Isentrope line ∝.

design point as $P_{\bar{n}}$, where

$$P_{\bar{n}} = (P_n)_{\text{design}} = \left(\frac{P_c}{P_a}\right)_{\text{design}}$$

The path line of an isentropic flow is called an *isentrope.* The area variation required to progress along an isentrope in a given direction is shown in the *T-s* diagram of Fig. 2.34. To progress *downward* along the isentrope requires a converging area ($dA < 0$) in subsonic flow and diverging area ($dA > 0$) in a supersonic stream. To progress *upward* along the isentrope requires a converging area ($dA < 0$) in supersonic flow and diverging area ($dA > 0$) in subsonic flow. This is why the engine intakes on the Concorde and various other supersonic aircraft converge from the inlet entrance to a throat and then diverge to the compressor face. This design reduces the speed of the air entering the compressor. Since P, T, ρ, and $V^2/(2g_c c_p)$ can be displayed in the *T-s* diagram, the isentrope line ∝ properly interpreted summarizes most of the characteristics of isentropic flow.

The stream area/velocity variations discussed can be explained on the basis of the continuity equation by examining how the gas density varies with velocity in an isentropic flow. Area, velocity, and density are related as follows by the one-dimensional steady flow continuity equation:

$$A = \frac{\dot{m}}{\rho V} \quad (\dot{m} = \text{const})$$

By reference to a *T-s* diagram, with lines of constant density thereon, we know that in an isentropic flow, ρ decreases as V increases. In subsonic flow, V increases faster than ρ decreases so that, according to the preceding equation, A must decrease. In supersonic flow, ρ decreases more rapidly than V increases, and therefore A must increase to satisfy the continuity equation.

Last, we have the important result that $M = 1$ in the throat of a nozzle accelerating a gas. When $M = 1$ at the throat, the nozzle reaches maximum possible mass flow for the given chamber pressure and temperature, and the nozzle is

said to be *choked*, and M will equal 1 only at the nozzle throat. In a decelerating diffuser flow, on the other hand, the throat Mach number may be less than, equal to, or greater than 1.

2.9.2 Nozzle Operating Characteristics for Isentropic Flow

Having designed a nozzle for a specific operating condition, we now examine its off-design operating characteristics. We wish to answer the following question: Given a nozzle, what are the possible isentropic pressure distributions and mass flow rates through the nozzle?

A simple way to investigate this question is to deal with a single equation that contains all the restrictions placed on the flow by the perfect gas state equations and the control volume equations. The governing equations may be combined into a single equation. We have

Mass:

$$\dot{m} = \rho A V = \frac{PAV}{RT} \tag{viii}$$

Energy:

$$T_t = T + \frac{V^2}{2 g_c c_p} \tag{ix}$$

Entropy:

$$P = P_t (T/T_t)^{\gamma/(\gamma-1)} \tag{x}$$

Equation (viii) can be written as

$$\frac{\dot{m}}{A} = \frac{PV}{RT} \tag{xi}$$

wherein

$$P = P_t \left(\frac{P}{P_t}\right) \qquad T = T_t \left(\frac{T}{T_t}\right)$$

and

$$V = \sqrt{2 g_c c_p (T_t - T)} = \left\{ 2 g_c c_p T_t \left[1 - \left(\frac{P}{P_t}\right)^{(\gamma-1)/\gamma} \right] \right\}^{1/2}$$

Substituting these expressions for P, T, and V in Eq. (xi) and simplifying, we obtain a single equation representing the simultaneous solution of

Eqs. (viii), (ix), and (x):

$$\frac{\dot{m}}{A} = \frac{P_t}{\sqrt{T_t}} \sqrt{\frac{2g_c}{R} \frac{\gamma}{\gamma - 1} \left[\left(\frac{P}{P_t} \right)^{2/\gamma} - \left(\frac{P}{P_t} \right)^{(\gamma+1)/\gamma} \right]} \tag{2.115}$$

If Eq. (2.115) is satisfied at every station of the flow through a nozzle, it follows that the conditions imposed on the flow by the thermal state equation and the mass, energy, and entropy control volume equations are satisfied. With P_c and T_c known in any given nozzle flow, we may effect a graphical solution of Eq. (2.115) by plotting $\dot{m}/A$ vs P/P_t. In a physical flow, P/P_t may vary from 1.0 in a storage chamber ($P = P_c = P_t$) to 0 in a vacuum ($P = 0$). A graph of $\dot{m}/A$ vs P/P_t is given in Fig. 2.35 for $P_c = 206$ psia and $T_c = 5000°\text{R}$. Because there is a unique value of M for each P/P_t, we show a Mach number scale along with the P/P_t axis. Notice that M increases as P/P_t decreases from left to right in the figure.

We note that for a given value of $\dot{m}/A$, there are two possible values of P/P_t in Fig. 2.35. In a particular problem, we can determine which value of P/P_t is applicable by examining the physical aspects of the flow.

Assume the nozzle depicted in Fig. 2.36 is discharging air isentropically from a storage chamber with $P_c = 206$ psia and $T_c = 5000°\text{R}$. Let us plot the nozzle

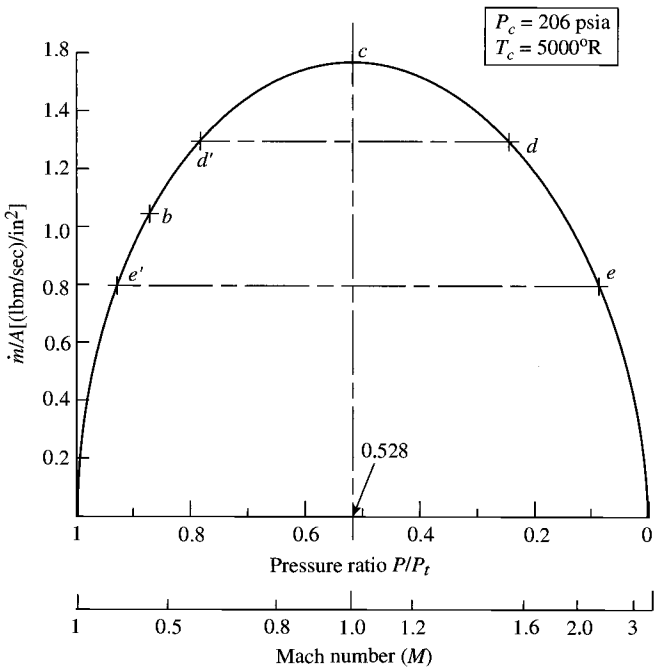

Fig. 2.35 $\dot{m}/A$ vs P/P_t and Mach number for air.

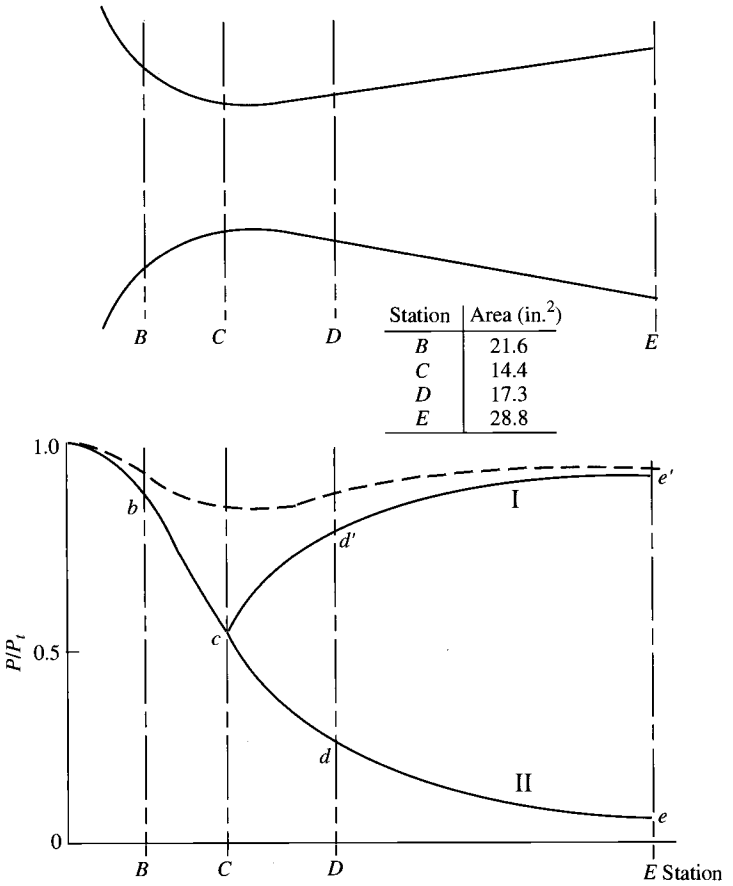

Fig. 2.36 Nozzle pressure distribution.

pressure distributions for various nozzle mass flows. We shall determine the pressure distribution for maximum mass flow first.

With the chamber pressure and temperature known, the $\dot{m}/A$ vs P/P_t plot of Fig. 2.35 is made. Then, because for maximum mass flow $M = 1$ at the nozzle throat, $\dot{m}_{\max}$ is determined by the relation

$$\dot{m}_{\max} = \left(\frac{\dot{m}}{A}\right)_{M=1} A_{\text{throat}}$$

$$= [1.55(\text{lbm/s})/\text{in.}^2](14.4\,\text{in.}^2) = 22.3\ \text{lbm/s}$$

With $\dot{m}$ and the areas at nozzle stations B, C, D, and E of Fig. 2.36 known, we determine $\dot{m}/A$ at these stations. With these values of $\dot{m}/A$, we locate state

points b, c, d, and e, as shown in Fig. 2.35, and read values of P/P_t corresponding to stations B, C, D, and E.

Beginning at the storage chamber, $P/P_t = 1$. Then as A decreases and $\dot{m}/A$ increases, P/P_t decreases from 1.0 to band c at the throat, as indicated in Figs. 2.35 and 2.36. After passing through the nozzle throat, A increases and $\dot{m}/A$ decreases. Now there may physically exist either value of the ratio P/P_t, corresponding to a given $\dot{m}/A$ with a continuous variation in pressure through the nozzle being maintained. Thus at section D, the pressure may be that corresponding to d or d' in Figs. 2.35 and 2.36. Whichever value exists depends on the nozzle pressure ratio $P_n = P_c/P_a$. The isentropic nozzle pressure distributions for maximum mass flow are the solid lines labeled I and II in the graph of Fig. 2.36. The dashed line represents a nozzle pressure distribution for a mass flow less than maximum and, hence, subsonic flow through the nozzle.

The nozzle pressure distribution corresponding to flow in I of Fig. 2.36 can be produced by nozzle pressure ratios other than the design value $P_{\tilde{n}}$. However, the nozzle exit plane pressure P_e and the exhaust region pressure P_a are equal only for the design nozzle pressure ratio $P_{\tilde{n}}$. At the off-design pressure ratios producing flow I, P_e remains the same, as given by

$$P_e = P_c/P_{\tilde{n}}$$

but is either greater than or less than the exhaust region pressure P_a.

When $P_e > P_a$, the nozzle is said to be *underexpanded.* Under these conditions, the gas in the nozzle has not expanded down to the exhaust region pressure. Similarly, when $P_e < P_a$, the nozzle is said to be *overexpanded* because the gas in the nozzle has expanded to a value below the exhaust region pressure.

We see from Fig. 2.36 that there are no solutions of the equation

$$\frac{\dot{m}}{A} = f\left(\frac{P}{P_t}\right)$$

which gives $P_e = P_a$ for exhaust region P_a between $P_{e'}$ and P_e. Physically, it is possible to have a discharge region pressure in this range. What happens when such an exhaust region pressure exists? To answer this question, let us discuss the operating characteristics of a nozzle that might be used as a high-speed wind tunnel.

2.9.3 Nozzle Flow and Shock Waves

Figure 2.37 shows a wind-tunnel nozzle that we shall use for purposes of discussion. The tunnel operates between an air storage chamber maintained at P_c and T_c and an evacuated receiver. The pressure of the receiver P_a increases as air flows from the storage chamber through the tunnel into the receiver. In this way, the nozzle pressure ratio $P_n = P_c/P_a$ decreases from a very high value (due to a low P_a initially) to a value of 1 when the receiver pressure becomes equal to the storage chamber pressure and flow ceases. A rocket engine nozzle

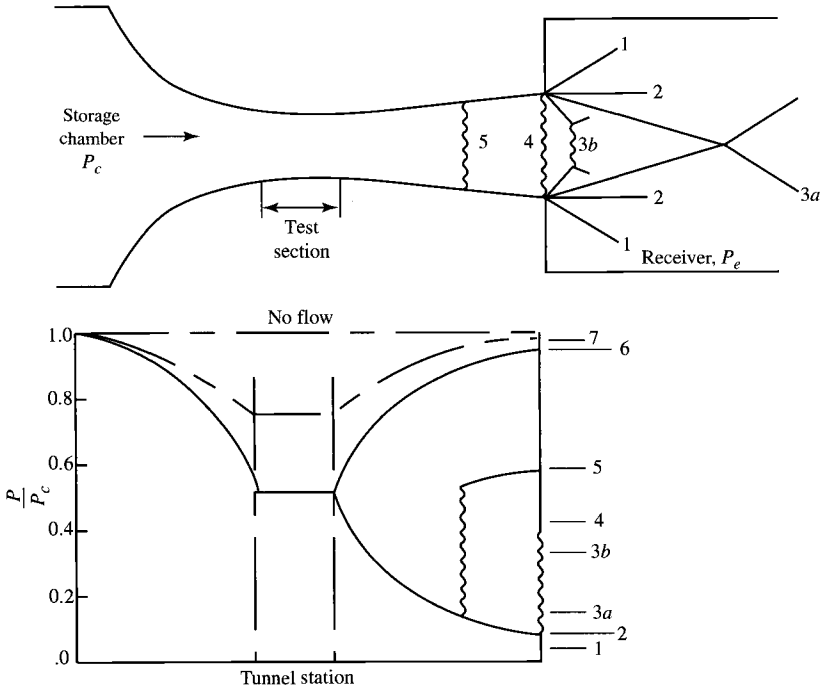

Fig. 2.37 Nozzle flow with shock waves.

descending through the atmosphere would experience a similar decrease in pressure ratio as P_a increases and P_c remains constant.

During the operation of the tunnel, the air flowing into the evacuated receiver raises the pressure in the nozzle exhaust region P_a and decreases the nozzle pressure ratio P_n. As a result, seven distinct nozzle pressure ratio operating conditions are present. They are depicted in Figs. 2.37 and 2.38 and tabulated in Table 2.3. The coordinates of the operating diagram in Fig. 2.38 are the nozzle pressure ratio and nozzle area ratio ε, where ε is the ratio of the nozzle exit area A_e to the nozzle throat area A_t. If we assume the tunnel of Fig. 2.37 has an area ratio of $\varepsilon = 2$, then the operating points of the tunnel all lie along the horizontal line $\varepsilon = 2$ in the nozzle operating diagram of Fig. 2.38. The following conditions are possible:

1) *Underexpanded,* $P_n > P_{\tilde{n}}$. The pressure in the evacuated receiver is less than the nozzle exit plane pressure, so that $P_e > P_a$. The nozzle is operating underexpanded with $P_n > P_{\tilde{n}}$. The flow *inside* the nozzle is the same as that corresponding to the design point pressure ratio $P_{\tilde{n}}$.The flow *outside* the nozzle *does not* correspond to that for $P_{\tilde{n}}$ since $P_e \neq P_a$. The transition of the nozzle exit plane pressure from P_e to the lower receiver pressure P_a occurs in the exhaust region, as depicted in the underexpanded portion of the nozzle operating diagram (Fig. 2.38).

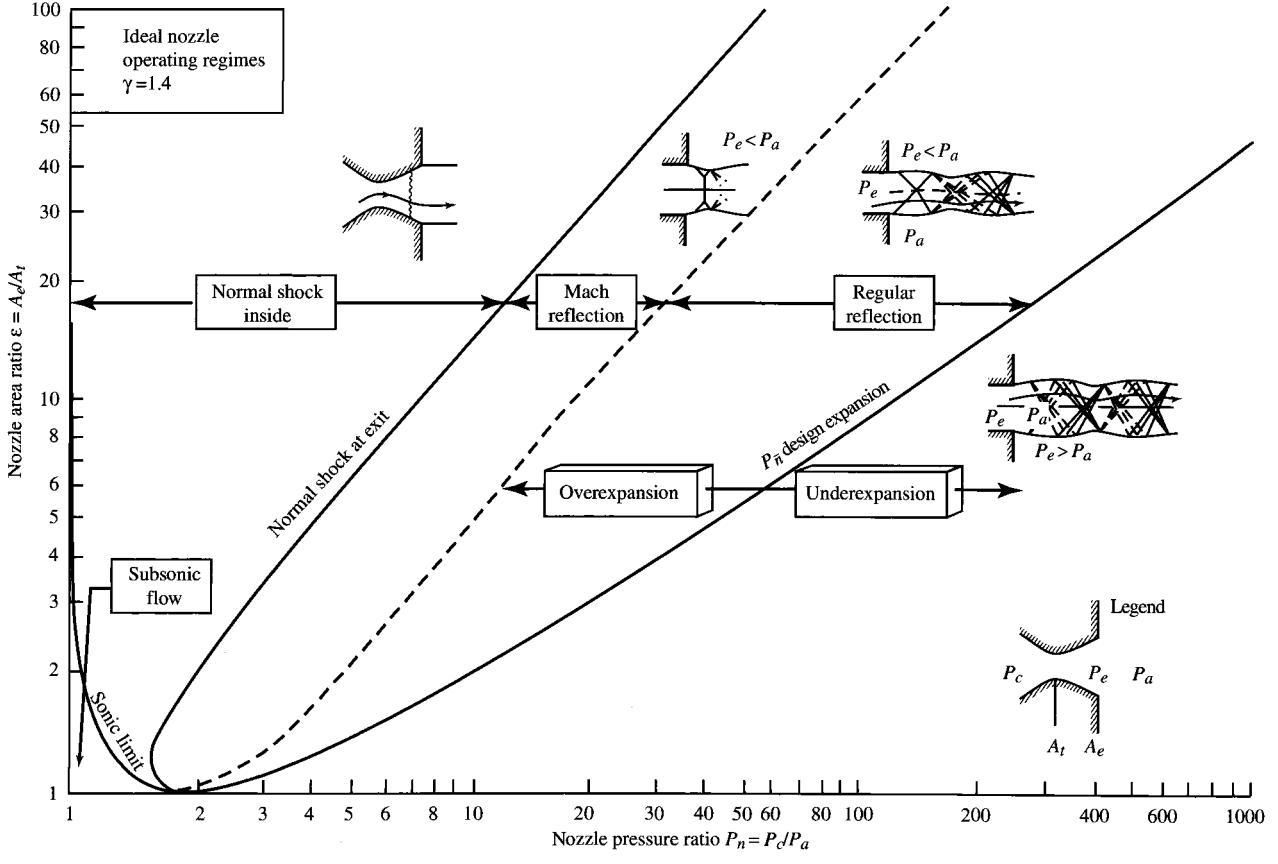

Fig. 2.38 Nozzle operating diagram.

Table 2.3 Nozzle operating points

Operand point	Exit section pressure P_e, $P_e = P_c/P_{\bar{n}}$	Nozzle pressure ratio $P_n = P_c/P_a$	Mass flow rate
1) Underexpanded	$P_e > P_a$	$P_n > P_{\bar{n}}$	Maximum
2) Design	$P_e = P_a$	$P_n = P_{\bar{n}}$	Maximum
3) Overexpanded	$P_e < P_a$	$P_n < P_{\bar{n}}$	Maximum
a) Regular reflection			
b) Mach reflection			
4) Normal shock at exit	$(P_e)_x < (P_e)_y = P_a$	$P_n < P_{\bar{n}}$	Maximum
5) Normal shock in divergent section	$P_e = P_a$	$P_n > P_{\bar{n}}$	Maximum
6) Sonic at throat subsonic elsewhere	$P_e = P_a$	$P_n < P_{\bar{n}}$	Maximum
7) Subsonic everywhere	$P_e = P_a$	$P_n < P_{\bar{n}}$	Less than maximum

2) *Design expansion,* $P_n = P_{\bar{n}}$. The pressure in the receiver has been increased to the nozzle exit plane pressure $P_e = P_a$ by the air flowing into the receiver. This is the nozzle design operating point with $P_n = P_{\bar{n}}$. No pressure disturbances occur in the jet issuing from the nozzle. This operating point is on the design expansion line of the nozzle operating diagram.

3) *Overexpanded,* $P_n < P_{\bar{n}}$. The pressure in the receiver is greater than the nozzle exit plane pressure $P_e < P_a$. The nozzle is operating overexpanded with $P_n < P_{\bar{n}}$. The transition from P_e to the higher receiver pressure is produced by either an oblique shock wave system (regular reflection 3a) or a combined oblique-normal shock wave system (Mach reflection pattern 3b). This nozzle operating condition lies between the design expansion line and normal-shock-at-exit line of the nozzle operating diagram.

4) *Normal shock at exit.* The pressure in the receiver has increased to a value that has moved the normal shock wave of condition 3b into the nozzle exit plane. The pressure of the gas entering the normal shock is $(P_e)_x$, and the pressure leaving is $(P_e)_y = P_a$. The loci of this operating condition are on the normal-shock-at-exit line of the nozzle operating diagram (Fig. 2.38).

5) *Normal shock inside.* The receiver pressure has increased to a value that has caused the normal shock to move into the diverging portion of the nozzle. Flow in the nozzle preceding the shock is unaffected. The flow through the shock is irreversible at constant T_t such that the total pressure decreases across the shock wave. The flow downstream of the shock is subsonic. This operating condition lies between the normal-shock-at-exit and sonic limit lines of the nozzle operating diagram.

6) *Sonic limit.* The receiver pressure has reached a value that produces isentropic shock-free flow throughout the nozzle with sonic throat conditions and

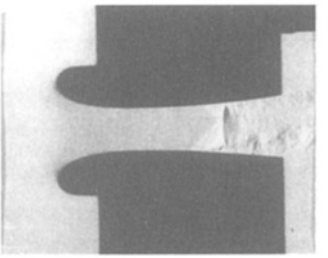

a) P_n=1.5, normal shock, inside

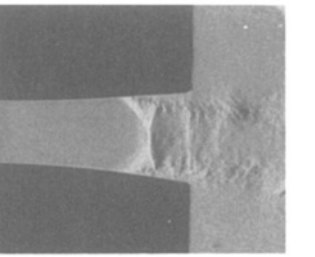

b) P_n=2.5, Mach reflection, overexpansion

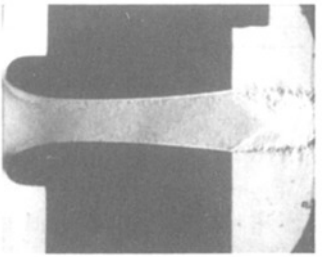

c) P_n=4.5, regular reflection, overexpansion

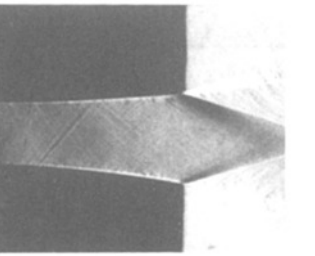

d) P_n=8.0, underexpansion

Fig. 2.39 Spark Schlieren photographs of nozzle exhaust flow patterns for an area ratio of 1.5. (Department of Aero-Mechanical Engineering, AFIT, WPAFB, Ohio.)

subsonic flow elsewhere. The nozzle pressure ratios corresponding to this operating condition lie on the sonic limit line of the nozzle operating diagram. This nozzle flow corresponds to flow I of Fig. 2.36.

7) *Subsonic flow.* The receiver pressure has risen to a value producing subsonic flow throughout with a reduced mass flow. This operating condition is bounded by the sonic limit and the $P_n = 1$ (no-flow) lines of the nozzle operating diagram.

Figure 2.39 is a picture of several nozzle exhaust flow patterns for a conical nozzle with an area ratio of $\varepsilon = 1.5$. For $P_n = 1.5$, the normal shock is located well within the nozzle. As P_n is increased to 2.5, the flow is overexpanded in the Mach reflection regime, as evidenced by the clearly defined normal shock internal to the flow. Further increase in P_n causes this normal shock in the Mach reflection pattern to move farther out and diminish in size. It disappears when the regular reflection pattern is obtained. For $P_n = 4.5$, the nozzle is overexpanded in the regular reflection regime. The photograph with $P_n = 8.0$ corresponds to an underexpanded operating point with the exhaust gas expanding down to the ambient pressure in the jet plume.

2.9.4 Nozzle Characteristics of Some Operational Engines

The operating point of a nozzle is determined by the nozzle pressure ratio P_n and area ratio ε. These ratios are presented in Table 2.4 along with other data for

Table 2.4 Some nozzle characteristics of rocket and turbojet engines

Engine	Chamber pressure P_c, psia	Area ratio ε	P_a	$(P_a)_{\text{operate}}$
Saturn				
F-1 without extension	965	10	140	Varies with
F-1 with extension	965	16	275	altitude P_a
J-2	763	27.5	610	
Atlas				
Booster	703	8	100	Varies with
Sustainer	543	25	528	altitude P_a
Subsonic airbreathing turbofan (40,000 ft)	8–14	1.0	1.9	3–5
Supersonic airbreathing turbofan (40,000 ft)	8–56	1–2	1.9–8	3–20

some operational nozzles. The data in Table 2.4 permit us to locate the operating points of the Saturn and Atlas engines at a given ε in the nozzle operating diagram (Fig. 2.38). In the Saturn F-1 engine, $\varepsilon = 16$ and $P_c = 965$ psia. Thus at 46,000 ft with $P_a = 2$ psia, we have $P_n = 965/2 = 482$ and a nozzle operating point of (482, 16). This operating point (assuming $\gamma = 1.4$) indicates that the F-1 nozzle is operating above the nozzle design point (underexpanded) at 46,000 ft. At sea level for the F-1, P_n is about 65, and the operating point of the engine nozzle (assuming $\gamma = 1.4$) is in the overexpanded regular reflection region. The turbojet engines of high-performance, airbreathing, subsonic aircraft generally use convergent nozzles ($\varepsilon = 1.0$) and operate with nozzle pressure ratios greater than the design value of 1.9 (assuming $\gamma = 1.4$). These nozzles therefore operate in the underexpanded operating regime. Turbojet/turbofan engines of supersonic aircraft, however, have converging-diverging nozzles.

2.10 One-Dimensional Gas Dynamics—Differential Control Volume Analysis

The steady one-dimensional flow of a chemically inert perfect gas with constant specific heats is conveniently described and governed by the following definitions and physical laws.

2.10.1 Definitions

Perfect gas:

$$P = \rho RT \tag{i}$$

Mach number:

$$M^2 = V^2/(\gamma R g_c T) \tag{ii}$$

Total temperature:

$$T_t = T\left(1 + \frac{\gamma - 1}{2} M^2\right) \tag{iii}$$

Total pressure:

$$P_t = P\left(1 + \frac{\gamma - 1}{2} M^2\right)^{\gamma/(\gamma-1)} \tag{iv}$$

2.10.2 Physical Laws

For one-dimensional flow through a control volume having a single inlet and exit sections 1 and 2, respectively, we have

One-dimensional mass flow:

$$\rho_1 A_1 V_1 = \rho_2 A_2 V_2 \tag{v}$$

Momentum:

$$F_{\text{frict}} = -\Delta\left(PA + \rho A V^2 / g_c\right) \tag{vi}$$

Energy equation (no shaft work):

$$q = c_p(T_{t2} - T_{t1}) \tag{vii}$$

Entropy equation (adiabatic flow):

$$s_2 \geq s_1 \tag{viii}$$

where F_{frict} is the frictional force of a solid control surface boundary on the flowing gas, and A is the flow cross-sectional area normal to the velocity V. The frictional force acting on a length L can be written as

$$F_{\text{frict}} = f\{\rho V^2/(2\, g_c)\} \text{ wetted perimeter } \times L$$

or

$$F_{\text{frict}} = f\left(\frac{\rho V^2}{2g_c}\right)\left(\frac{4A}{D}\right)L \tag{2.116}$$

where

f = frictional coefficient

D = hydraulic diameter $= \dfrac{4 \times A}{\text{wetted perimeter}}$

A = flow cross-sectional area

Now consider the differential element of duct with length dx, as shown in Fig. 2.40. The independent variables are the area change, total temperature change, and frictional force. The dependent variables are P, T, ρ, V, M^2, and P_t. The application of Eqs. (i–vi) to flow in Fig. 2.40, having the presence of the simultaneous effects of area change, heat interaction, and friction, results in the following set of equations for the infinitesimal element dx.

Perfect gas:

$$-\frac{dP}{P}+\frac{d\rho}{\rho}+\frac{dT}{T}=0 \tag{2.117a}$$

Total temperature:

$$\frac{dT}{T}+\frac{[(\gamma-1)/2]M^2}{1+[(\gamma-1)/2]M^2}\frac{dM^2}{M^2}=\frac{dT_t}{T_t} \tag{2.117b}$$

One-dimensional mass flow:

$$\frac{d\rho}{\rho}+\frac{dA}{A}+\frac{dV}{V}=0 \tag{2.117c}$$

Total pressure:

$$\frac{dP}{P}+\frac{(\gamma/2)M^2}{1+[(\gamma-1)/2]M^2}\frac{dM^2}{M^2}=\frac{dP_t}{P_t} \tag{2.117d}$$

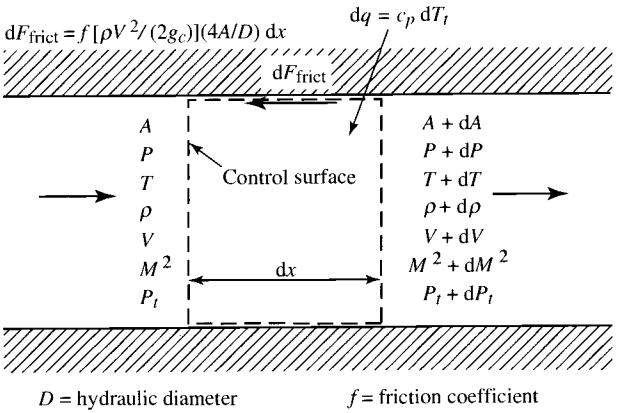

Fig. 2.40 Independent and dependent variables for one-dimensional flow.

Momentum:

$$\frac{dP}{P} + \gamma M^2 \frac{dV}{V} + 2\gamma M^2 f \frac{dx}{D} = 0 \tag{2.117e}$$

Mach number:

$$2\frac{dV}{V} - \frac{dT}{T} = \frac{dM^2}{M^2} \tag{2.117f}$$

With the exception of the momentum equation, these equations are obtained by taking the derivative of the natural log of Eqs. (i–v).

In these equations, heat interaction effects are measured in terms of the total temperature change according to Eq. (vii). The entropy condition of Eq. (viii) is also applicable if $dT_t = 0$. If dT_t is not zero, then the entropy requirement is $ds = dq/T$. The six dependent variables M^2, V, P, ρ, T, and P_t in the preceding set of six linear algebraic equations may be expressed in terms of the three independent variables A, T_t, and $4f\ dx/D$. The solution is given in Table 2.5. Note that D is the hydraulic diameter (= 4 × flow cross-sectional area/wetted perimeter).

General conclusions can be made relative to the variation of the stream properties of the flow with each of the independent variables by the relations of Table 2.5. As an example, the relationship given for dV/V at the bottom of the table indicates that, in a constant-area adiabatic flow, friction will increase the stream velocity in subsonic flow and will decrease the velocity in supersonic flow. Similar reasoning may be applied to determine the manner in which any dependent property varies with a single independent variable.

Example 2.12

Consider the one-dimensional flow of a perfect gas in a channel of circular cross section. The flow is adiabatic, and we wish to design the duct so that its area varies with x such that the velocity remains constant.

1) Show that in such a flow, the temperature must be a constant, hence the Mach number must be a constant.

2) Show that the total pressure varies inversely with the cross-sectional area.

3) Show that $2\ dA/C = \gamma M^2 f dx$, where C is the circumference.

4) For a constant f and a circular channel of diameter D, show that the diameter must vary in accordance with the following equation to keep the velocity constant:

$$D = D_1 + \gamma M^2 f x$$

Solution: This problem requires that we apply the relationships of Table 2.5 and other fundamental relationships.

1) Because the flow is adiabatic, the total temperature is constant. From the definition of the total temperature, we have $T_t = T + V^2/(2c_p g_c)$. Since T_t and

Table 2.5 Influence coefficients for steady one-dimensional flow

	Independent		
Dependent	$\frac{dA}{A}$	$\frac{dR}{T_t}$	$\frac{4f\,dx}{D}$
$\frac{dM^2}{M^2}$	$-\frac{2\left(1+\frac{\gamma-1}{2}M^2\right)}{1-M^2}$	$\frac{(1+\gamma M^2)\left(1+\frac{\gamma-1}{2}M^2\right)}{1-M^2}$	$\frac{\gamma M^2\left(1+\frac{\gamma-1}{2}M^2\right)}{1-M^2}$
$\frac{dV}{V}$	$-\frac{1}{1-M^2}$	$\frac{1+\frac{\gamma-1}{2}M^2}{1-M^2}$	$\frac{\gamma M^2}{2(1-M^2)}$
$\frac{dP}{P}$	$\frac{\gamma M^2}{1-M^2}$	$\frac{-\gamma M^2\left(1+\frac{\gamma-1}{2}M^2\right)}{1-M^2}$	$\frac{-\gamma M^2[1+(\gamma-1)M^2]}{2(1-M^2)}$
$\frac{dp}{p}$	$\frac{M^2}{1-M^2}$	$\frac{-\left(1+\frac{\gamma-1}{2}M^2\right)}{1-M^2}$	$\frac{-\gamma M^2}{2(1-M^2)}$
$\frac{dT}{T}$	$\frac{(\gamma-1)M^2}{1-M^2}$	$\frac{(1-\gamma M^2)\left(1+\frac{\gamma-1}{2}M^2\right)}{1-M^2}$	$\frac{-\gamma(\gamma-1)M^4}{2(1-M^2)}$
$\frac{dP_t}{P_t}$	0	$\frac{-\gamma M^2}{2}$	$\frac{-\gamma M^2}{2}$

This table is read:

$$\frac{dV}{V}=\left(-\frac{1}{1-M^2}\right)\frac{dA}{A}+\frac{1+\frac{\gamma-1}{2}M^2}{1-M^2}\frac{dT_t}{T_t}+\frac{\gamma M^2}{2(1-M^2)}\frac{4f\,dx}{D}$$

V are constant in the duct, the preceding equation requires that the static temperature remain constant. With the static temperature of the gas constant, the speed of sound will be constant ($a=\sqrt{\gamma R g_c T}$). With constant velocity and speed of sound, the Mach number will be constant.

2) Application of the continuity equation to the constant-velocity flow gives $A_i/A=\rho/\rho_i$. For a perfect gas with constant static temperature, we have $\rho/\rho_i=P/P_i$ and from Eq. (iv) for constant-Mach flow, we get $P_t/P_{ti}=P/P_i$. Thus $P_t/P_{ti}=A_i/A$.

3) To obtain this relationship, we need to get a relationship between two independent properties to keep the dependent property of velocity constant. Table 2.5 gives the basic relationships between dependent and independent properties for one-dimensional flow. We are interested in the case where velocity is constant,

and thus we write the equation listed as an example at the bottom of Table 2.5 for the case where both dV and dT_t are zero:

$$0 = \left(-\frac{1}{1-M^2}\right)\frac{dA}{A} + 0 + \frac{\gamma M^2}{2(1-M^2)}\frac{4f\,dx}{D}$$

The area of the duct is equal to the circumference C times one quarter of the diameter D. Thus $A = CD/4$, and the preceding relationship reduces to

$$2\,dA/C = \gamma M^2 f\,dx$$

4) For a circular cross section, $A = \pi D^2/4$ and $C = \pi D$. Thus $2dA/C = dD$. Substitution of this relationship into the preceding equation and integration give the desired result (at $x = 0$, $D = D_i$):

$$D = D_i + \gamma M^2 fx$$

2.11 Chemical Reactions

2.11.1 General Characteristics

A chemical reaction from reactants A and B to products C and D is generally represented by

$$N_A\mathrm{A} + N_B\mathrm{B} \rightarrow N_C\mathrm{C} + N_D\mathrm{D}$$

where N_A and N_B are the number of moles of reactants A and B, respectively. Likewise N_C and N_D are the number of moles of products C and D. An example reaction between one mole of methane (CH_4) and two moles of oxygen (O_2) can be written as

$$CH_4 + 2O_2 \rightarrow CO_2 + 2H_2O$$

and represents *complete combustion* between the fuel, methane, and oxidizer, oxygen. Combustion is complete when all of the carbon in the fuel burns to CO_2 and the hydrogen burns to H_2O. The combustion is incomplete when there is any unburned fuel or compounds such as carbon, hydrogen, CO, or OH. This *theoretical process* of complete combustion is very useful in our analysis because it represents the number of moles of each reactant that are needed for complete combustion to the number of moles of each product. The theoretical or complete combustion process is also referred to as a stoichiometric combustion process and is represented as

$$\nu_{CH_4}CH_4 + \nu_{O_2}O_2 \rightarrow \nu_{CO_2}CO_2 + \nu_{H_2O}H_2O$$

where ν_{CH_4} and ν_{O_2} are the number of moles of reactants CH_4 and O_2, and ν_{CO_2} and ν_{H_2O} are the number of moles of products CO_2 and H_2O. The ν_i in the

preceding equation are called the *stoichiometric coefficients* for the theoretical reaction. Thus the stoichiometric coefficients for the preceding reaction of methane and oxygen are

$$\nu_{CH_4} = 1 \qquad \nu_{O_2} = 2 \qquad \nu_{CO_2} = 1 \qquad \nu_{H_2O} = 2$$

The stoichiometric coefficients give the number of moles of each constituent required for complete combustion. Note that the units of both the mole number N_i and the stoichiometric coefficients ν_i can also be regarded as moles *per unit mass* of the gas mixture.

The *actual process* between reactants normally has different amounts of each reactant than that of the theoretical (stoichiometric) process. For example, consider one mole of methane reacting with three moles of oxygen. The stoichiometric coefficients of the theoretical reaction indicates that only two moles of oxygen are required for each mole of methane. Thus one mole of oxygen will not react and remains on the products side of the chemical equation as shown:

$$CH_4 + 3O_2 \rightarrow CO_2 + 2H_2O + O_2$$

2.11.2 Chemical Equilibrium

The chemical reactions represented so far were shown as complete reactions. In reality, the reactions go both forward and backward and the actual process is denoted as

$$N_A A + N_B B \rightleftharpoons N_C C + N_D D$$

Chemical equilibrium is reached when the forward rate of reaction of reactants A and B equals the backward rate of reaction of products C and D. It can be shown that chemical equilibrium corresponds to the minimum value of the Gibbs function ($G = H - TS$) for the entire gas mixture as shown in Fig. 2.41. Chemical equilibrium also corresponds to maximum entropy for an adiabatic system.

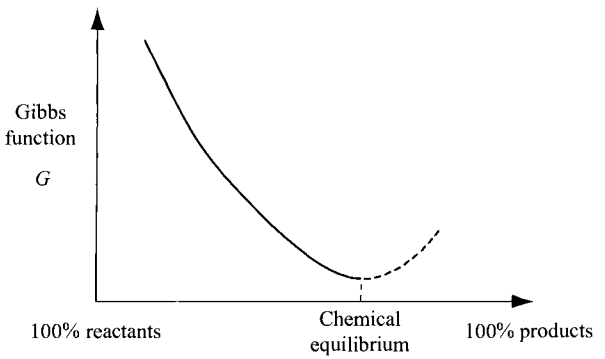

Fig. 2.41 Chemical equilibrium.

Chemical equilibrium for a stoichiometric (theoretical) reaction can be represented as

$$v_A A + v_B B \rightleftharpoons v_C C + v_D D \tag{2.118}$$

For solution of equilibrium problems, we define the *equilibrium constant* of a perfect gas as

$$K_P \equiv \frac{P_v^{v_C} P_D^{v_D}}{P_A^{v_A} P_B^{v_B}} \tag{2.119}$$

where P_A, P_B, P_C, and P_D are the partial pressures of components A, B, C, and D; v_A, v_B, v_C, and v_D are the stoichiometric coefficients shown in Eq. (2.118). For a perfect gas, K_P is only a function of temperature.

From Eq. (2.46), the partial pressure of constituent i can be written as

$$P_i = \frac{N_i}{N_{\text{total}}} P \tag{2.120}$$

where N_{total} is the total number of moles present in the reaction chamber. Using Eq. (2.120), Eq. (2.119) for the equilibrium constant can be rewritten as

$$K_P = \frac{N_C^{v_C} N_D^{v_D}}{N_A^{v_A} N_B^{v_B}} \left(\frac{P}{N_{\text{total}}}\right)^{\Delta v} \tag{2.121}$$

where $\Delta v = v_C + v_D - v_A - v_B$. Equation (2.121) can be used to verify equilibrium results from complex computer programs as will be done later in this section.

Example 2.13

One mole of hydrogen and one-half mole of oxygen are in equilibrium at a temperature of 2000 K and a pressure of 10 atm. Determine the number of moles of H_2O, H_2, and O_2 in the products (neglect other products such as OH, H, O, etc.).

Solution: We start by writing the chemical reaction equation for both the stoichiometric reaction and the actual reaction being modeled.

Stoichiometric:

$$H_2 + \frac{1}{2}O_2 \rightleftharpoons H_2O \quad (\text{thus } v_{H_2O} = 1,\ v_{H_2} = 1,\ v_{O_2} = 1/2)$$

Actual:

$$H_2 + \frac{1}{2}O_2 \longrightarrow xH_2 + yO_2 + zH_2O$$

Because there are the three unknowns (x, y, and z), three equations are required. Two equations come from the atom balance of each element (H and O) and the third from the chemical equilibrium coefficient (K_p):

Atom balance:

$$\text{H}: 2 = 2x + 2z \qquad \text{or } z = 1 - x$$
$$\text{O}: 1 = 2y + z \qquad \text{or } y = x/2$$

Now the actual reaction equation can be written with just one unknown:

$$\text{H}_2 + \frac{1}{2}\text{O}_2 \rightarrow x\text{H}_2 + \frac{x}{2}\text{O}_2 + (1 - x)\text{H}_2\text{O}$$

From the JANNAF tables in the Supporting Material, $\log K_p = 3.540$ at 2000 K for the reaction

$$\text{H}_2 + \frac{1}{2}\text{O}_2 \rightarrow \text{H}_2\text{O}$$

Thus

$$K_p = 10^{3.540} = 3467.4 = K_P = \frac{N_C^{\nu_{H_2O}}}{N_A^{\nu_{H_2}} N_B^{\nu_{O_2}}} \left(\frac{P}{N_{\text{total}}}\right)^{\Delta\nu}$$

where $N_A = x$, $N_B = x/2$, $N_C = 1 - x$, $\Delta\nu = -1/2$, and $N_{\text{total}} = 1 + x/2$. Thus

$$K_P = \frac{(1 - x)}{x^1\sqrt{x/2}} \left(\frac{10}{1 + x/2}\right)^{-1/2} = 3467.4$$

or

$$\frac{(1 - x)\sqrt{1 + x/2}}{x^{3/2}} = 3467.4\sqrt{10/2} = 7753.3$$

Solving for x gives $x = 0.002550$, and the reaction can be written as

$$\text{H}_2 + \frac{1}{2}\text{O}_2 \rightarrow 0.002550\text{H}_2 + 0.001275\text{O}_2 + 0.997450\text{H}_2\text{O}$$

Thus there are 0.002550 moles of hydrogen, 0.001275 moles of oxygen, and 0.997450 moles of water.

2.11.3 EQL Software

The included EQL software program by David T. Pratt uses the NASA Glenn thermochemical data and the Gordon-McBride equilibrium algorithm (see Ref. 18). This equilibrium calculation is based on finding the mixture composition that minimizes the Gibbs function, which allows rapid solution of reactions resulting in many products.

Example 2.14

The EQL software program gives the following result for one mole of hydrogen and one-half mole of oxygen at a temperature of 2000 K and a pressure of 10 atm:

$$H_2 + \frac{1}{2}O_2 \rightarrow 0.002717H_2 + 0.001118O_2 + 0.9952H_2O + 0.000974OH$$
$$+ 2.668 \times 10^{-5}H + 7.016 \times 10^{-6}O + 5.963 \times 10^{-7}HO_2 + 1.992 \times 10^{-7}H_2O_2$$

The 0.0022 moles less of H_2O are produced in this equilibrium mixture than Example 2.13, and these molecules show up in increases in the number of moles of H_2 and O_2.

The equilibrium constant can be determined from these data and Eq. (2.121):

$$K_P = \frac{N_C^{\nu_{H_2O}}}{N_A^{\nu_{H_2}} N_B^{\nu_{O_2}}} \left(\frac{P}{N_{\text{total}}}\right)^{\Delta\nu} = \frac{0.9952}{0.00271 \times \sqrt{0.001118}} \left(\frac{10}{0.9990}\right)^{-1/2} = 3471$$

or $\log K_p = 3.540$, which agrees with the JANNAF tables.

2.11.4 Enthalpy of Chemical Component, Enthalpy of Formation, Heat of Reaction, and Adiabatic Flame Temperature

For reacting systems, the enthalpy of each component must be written in a form that has the same reference state. The *enthalpy of chemical components* (products or reactants) can be calculated using Eq. (2.50) with $\bar{h}$ for a component written as

$$\bar{h} = \bar{h}_f^\circ + (\bar{h} - \bar{h}^\circ) = \bar{h}_f^\circ + \int_{T_d}^{T} \bar{c}_p \, dT' \tag{2.122}$$

where $\bar{h}_f^\circ$ is the *enthalpy of formation* (also called the heat of formation) at the reference state (datum) of 25°C (298 K), 1 atm $(\bar{h} - \bar{h}^\circ)$ is the enthalpy change due to the temperature change from the reference state (T_d), and $\bar{c}_p$ is the specific heat at constant pressure per mole. Typical values of $\bar{h}_f^\circ$ are given in Table 2.6 and values $(\bar{h} - \bar{h}^\circ)$ for typical gases are given in the JANNAF tables of the Supporting Material.

Table 2.6 Enthalpy of formation $\bar{h}_f^\circ$ for some reactants and product gases at datum temperature 536°R/298 K (Refs. 12, 13)

Gas	Btu/lbmol	kJ/kgmol
Methane, CH_4	−32,192	−74,883
Ethane, C_2H_6	−36,413	−84,701
Hexane, C_6H_{14}	−71,784	−166,978
Octane, C_8H_{18}	−89,600	−208,421
Jet-A, $C_{12}H_{23}$	−152,981	−355,853[a]
Carbon monoxide, CO	−47,520	−110,537
Carbon dioxide, CO_2	−169,181	−393,538
Atomic hydrogen, H	93,717	217,997
Hydrogen, H_2	0	0
Water vapor, H_2O	−103,966	−241,838
Atomic oxygen, O	107,139	249,218
Oxygen, O_2	0	0
Hydroxyl, OH	16,967	39,467
Atomic nitrogen, N	203,200	472,668
Nitrogen, N_2	0	0
Nitrous oxide, N_2O	35,275	82,053
Nitric oxide, NO	38,817	90,293
Nitrogen dioxide, NO_2	14,228	33,096

[a]For heating value $h_{PR} = 18{,}400$ Btu/lbm $= 42{,}800$ kJ/kg.

The enthalpy of both products and reactants in a reaction can be plotted vs temperature as shown in Fig. 2.41. A reaction typically causes a change in temperature. The *heat of reaction* ΔH is defined as the positive heat transfer to the products that is required to bring them back to the original temperature of the reactants. For ideal (perfect) gases, the heat of reaction ΔH at the standard reference temperature can be calculated using

$$\Delta H = H_P - H_R = \sum_{i=1}^{n_P} N_i \Delta \bar{h}_{fi}^\circ - \sum_{j=1}^{n_R} N_j \Delta \bar{h}_{fj}^\circ \tag{2.123}$$

where N_i and N_j are the number of moles of the products and reactants, respectively, and Δh_f° is the heat of formation per mole of species i and j, ΔH is the vertical difference between the enthalpy line of the reactants and that of the products in Fig. 2.42.

Consider the adiabatic flow through a combustion chamber like that of Fig. 2.4d. The reactants enter at a temperature denoted by 1 in Fig. 2.42 and the products leave at a temperature denoted by 2. Neglecting changes in kinetic energy, the energy balance for this process yields

$$H_1 = H_2 \qquad \text{or} \qquad H_P = H_R \tag{2.124}$$

The temperature at state 2 is called the *adiabatic flame temperature*. This temperature can be calculated by determining the equilibrium state with the

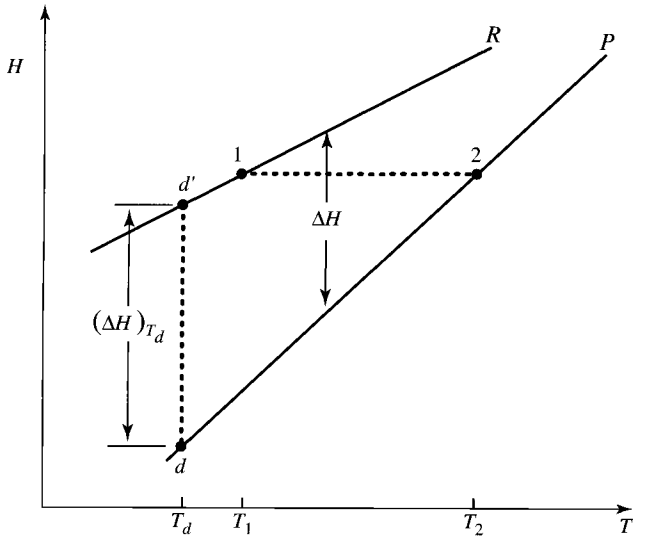

Fig. 2.42 Enthalpy states for a reaction.

same enthalpy H and pressure P as state 1. To facilitate calculation, we rewrite Eq. (2.124) in terms of the enthalpy difference $(\bar{h} - \bar{h}^\circ)$ and the heat of reaction at the datum (reference) state $([\Delta H]_{T_d}$. First we write

$$H_2 - [H_P]_{T_d} = H_1 - [H_R]_{T_d} + [\Delta H]_{T_d}$$

Since

$$H_2 - [H_P]_{T_d} = \sum_{j=1}^{n_P} N_j(\bar{h} - \bar{h}^\circ)_j$$

and

$$H_1 - [H_R]_{T_d} = \sum_{i=1}^{n_R} N_i(\bar{h} - \bar{h}^\circ)_i$$

then

$$H_2 - [H_P]_{T_d} = \sum_{j=1}^{n_P} N_j(\bar{h} - \bar{h}^\circ)_j = \sum_{i=1}^{n_R} N_i(\bar{h} - \bar{h}^\circ)_i + [\Delta H]_{T_d} \tag{2.125}$$

The following steps are used to calculate the adiabatic flame temperature:

1) Assume a final temperature T_2.
2) Calculate the mole fraction of the products for the resulting K_p at T_2.
3) Calculate $\sum_{i=1}^{n_R} N_i(\bar{h} - \bar{h}^\circ)_i + [\Delta H]_{T_d}$.
4) Calculate $\sum_{j=1}^{n_P} N_j(\bar{h} - \bar{h}^\circ)_j$. If its value is greater than that of step 3, reduce the value of T_2 and perform steps 2–4 again.

This calculation by hand is tedious and has been programmed for rapid calculation using computers. The EQL software calculates the adiabatic flame temperature for given reactants and inlet temperature T and pressure P as shown in Example 2.16.

Example 2.15

Calculate the heat of reaction for the reaction of Example 2.13.

Solution: We have

$$H_2 + \frac{1}{2}O_2 \rightarrow 0.002024H_2 + 0.001012O_2 + 0.997976H_2O$$

at 2000 K. From the JANNAF tables in the Supporting Materials, at 2000 K we have $\Delta\bar{h}^\circ_{fH_2} = 0$, $\Delta\bar{h}^\circ_{fO_2} = 0$, and $\Delta\bar{h}^\circ_{fH_2O} = -60.150$ kcal/mole. Eq. (2.78) gives

$$\Delta H = H_P - H_R$$
$$= \sum_{i=1}^{n_P} N_i \Delta\bar{h}^\circ_{fi} - \sum_{j=1}^{n_R} N_j \Delta\bar{h}^\circ_{fj} = 0.997976 \times -60.150 = -60.028 \text{ kcal}$$

Thus 60.028 kcal (251.28 kJ) of energy must be removed during the reaction to keep the temperature at 2000 K.

Example 2.16

Using the EQL software, determine the adiabatic flame temperature for one mole of oxygen and one-half mole of methane with the reactants at a temperature of 500 K and pressure of 800 kPa.

Solution: We first enter the reactants and inlet pressure and temperature into the opening screen of EQL. Next we select the Equilibrium Processes Tab, which displays the numerous possible combustion processes. We select 'Adiabatic Flame Temperature' and perform the calculations. The resulting adiabatic flame temperature is 3349.85 K, and the resulting principal products are listed below:

Compound	Mole fraction
H_2O	0.4093
CO	0.1540
CO_2	0.1190
OH	0.0989
O_2	0.0792
H_2	0.0681
H	0.0382
O	0.0330

Problems

2.1 Consider Fig. P2.1. A stream of air with velocity of 500 ft/s and density of 0.07 lbm/ft^3 strikes a stationary plate and is deflected 90 deg. Select an appropriate control volume and determine the force F_P necessary to hold the plate stationary. Assume that atmospheric pressure surrounds the jet and that the initial jet diameter is 1.0 in.

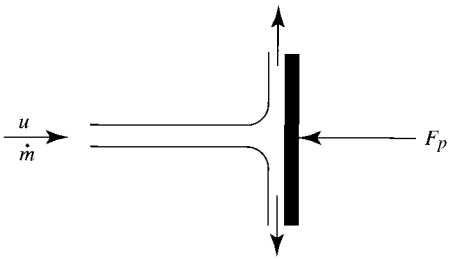

Fig. P2.1

2.2 Consider Fig. P2.1. An airstream with density of 1.25 kg/m^3 and velocity of 200 m/s strikes a stationary plate and is deflected 90 deg. Select an appropriate control volume and determine the force F_P necessary to hold the plate stationary. Assume that atmospheric pressure surrounds the jet and that the initial jet diameter is 1.0 cm.

2.3 Consider the flow shown in Fig. P2.2 of an incompressible fluid. The fluid enters (station 1) a constant-area circular pipe of radius r_0 with uniform velocity V_1 and pressure P_1. The fluid leaves (station 2) with the parabolic velocity profile V_2 given by

$$V_2 = V_{\max}\left[1 - \left(\frac{r}{r_0}\right)^2\right]$$

and uniform pressure P_2. Using the conservation of mass and momentum equations, show that the force F necessary to hold the pipe in place can be

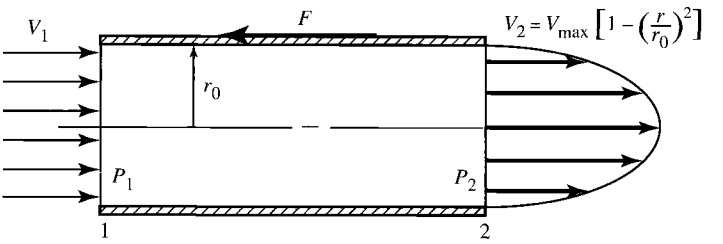

Fig. P2.2

expressed as

$$F = \pi r_0^2 \left(P_1 - P_2 + \frac{\rho V_1^2}{3g_c} \right)$$

2.4 Consider the flow of an incompressible fluid through a two-dimensional cascade as shown in Fig. P2.3. The airfoils are spaced at a distance s and have unit depth into the page. Application of the conservation of mass requires $V_t \cos \beta_t = V_e \cos \beta_e$.

(a) From the tangential momentum equation, show that

$$F_\theta = \frac{\dot{m}}{g_c}(V_t \sin \beta_t - V_e \sin \beta_e)$$

(b) From the axial momentum equation, show that

$$F_z = s(P_e - P_t)$$

(c) Show that the axial force can be written as

$$F_z = s\left[\frac{\rho}{2g_c}(V_t^2 \sin^2 \beta_t - V_e^2 \sin^2 \beta_e) - (P_{tt} - P_{te})\right]$$

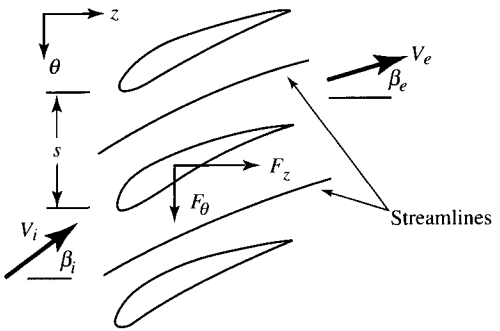

Fig. P2.3

2.5 When a freejet is deflected by a blade surface, a change of momentum occurs and a force is exerted on the blade. If the blade is allowed to move at a velocity, power may be derived from the moving blade. This is the basic principle of the impulse turbine. The jet of Fig. P2.4, which is initially horizontal, is deflected by a fixed blade. Assuming the same pressure surrounds the jet, show that the horizontal (F_x) and vertical forces (F_y) by the fluid on the blade are given by

$$F_x = \frac{\dot{m}(u_1 - u_2 \cos \beta)}{g_c} \qquad \text{and} \qquad F_y = \frac{\dot{m} u_2 \sin \beta}{g_c}$$

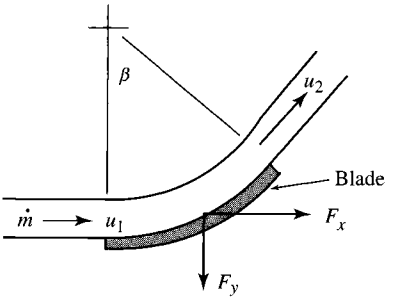

Fig. P2.4

Calculate the force F_y for a mass flow rate of 100 lbm/s, $u_1 = u_2 = 2000$ ft/s, and $\beta = 60$ deg.

2.6 One method of reducing an aircarft's landing distance is through the use of thrust reversers. Consider the turbofan engine in Fig. P2.5 with thrust reverser of the bypass airstream. It is given that 1500 lbm/s of air at 60°F and 14.7 psia enters the engine at a velocity of 450 ft/s and that 1250 lbm/s of bypass air leaves the engine at 60 deg to the horizontal, velocity of 890 ft/s, and pressure of 14.7 psia. The remaining 250 lbm/s leaves the engine core at a velocity of 1200 ft/s and pressure of 14.7 psia. Determine the force on the strut F_x. Assume the outside of the engine sees a pressure of 14.7 psia.

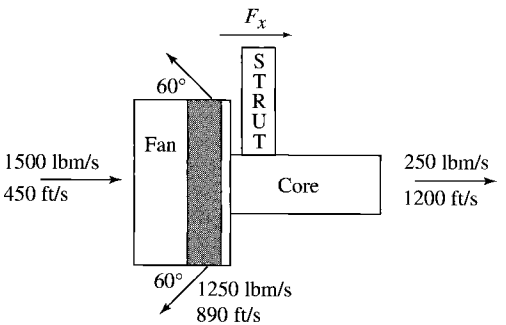

Fig. P2.5

2.7 Consider Fig. P2.6. Air with a density of 0.027 lbm/ft^3 enters a diffuser at a velocity of 2470 ft/s and a static pressure of 4 psia. The air leaves the diffuser at a velocity of 300 ft/s and a static pressure of 66 psia. The entrance area of the diffuser is 1.5 ft^2, and its exit area is 1.7 ft^2. Determine the magnitude and direction of the strut force necessary to hold the diffuser stationary when this diffuser is operated in an atmospheric pressure of 4 psia.

2.8 Consider Fig. P2.6. It is given that 50 kg/s of air enters a diffuser at a velocity of 750 m/s and a static pressure of 20 kPa. The air leaves the diffuser at a velocity of 90 m/s and a static pressure of 330 kPa. The entrance area of the diffuser is 0.25 m^2, and its exit area is 0.28 m^2. Determine the magnitude and direction of the strut force necessary to hold the diffuser stationary when this diffuser is operated in an atmospheric pressure of 20 kPa.

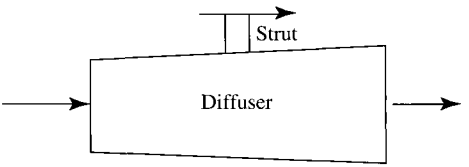

Fig. P2.6

2.9 Consider Fig. P2.7. It is given that 100 lbm/s of air enters a nozzle at a velocity of 600 ft/s and a static pressure of 70 psia. The air leaves the nozzle at a velocity of 4000 ft/s and static pressure of 2 psia. The entrance area of the nozzle is 14.5 ft^2, and its exit area is 30 ft^2. Determine the magnitude and direction of the strut force necessary to hold the nozzle stationary when this nozzle is operated in an atmospheric pressure of 4 psia.

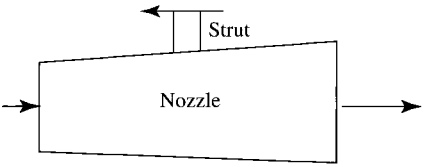

Fig. P2.7

2.10 Consider Fig. P2.7. Air with a density of 0.98 kg/m^3 enters a nozzle at a velocity of 180 m/s and a static pressure of 350 kPa. The air leaves the nozzle at a velocity of 1200 m/s and a static pressure of 10 kPa. The entrance area of the nozzle is 1.0 m^2, and its exit area is 2.07 m^2. Determine the magnitude and direction of the strut force necessary to hold the nozzle stationary when this nozzle is operated in an atmospheric pressure of 10 kPa.

2.11 For a calorically perfect gas, show that $P + \rho V^2/g_c$ can be written as $P(1 + \gamma M^2)$. Note that the Mach number M is defined as the velocity V divided by the speed of sound a.

2.12 Air at 1400 K, 8 atm, and 0.3 Mach expands isentropically through a nozzle to 1 atm. Assuming a calorically perfect gas, find the exit temperature and the inlet and exit areas for a mass flow rate of 100 kg/s.

2.13 It is given that 250 lbm/s of air at 2000°F, 10 atm, and 0.2 Mach expands isentropically through a nozzle to 1 atm. Assuming a calorically perfect gas, find the exit temperature and the inlet and exit areas.

2.14 Air at 518.7°R is isentropically compressed from 1 to 10 atm. Assuming a calorically perfect gas, determine the exit temperature and the compressor's input power for a mass flow rate of 150 lbm/s.

2.15 It is given that 50 kg/s of air at 288.2 K is isentropically compressed from 1 to 12 atm. Assuming a calorically perfect gas, determine the exit temperature and the compressor's input power.

2.16 Air at −55°F, 4 psia, and $M = 2.5$ enters an isentropic diffuser with an inlet area of 1.5 ft^2 and leaves at $M = 0.2$. Assuming a calorically perfect gas, determine:
(a) The mass flow rate of the entering air
(b) The pressure and temperature of the leaving air
(c) The exit area and magnitude and direction of the force on the diffuser (assume outside of diffuser sees 4 psia)

2.17 Air at 225 K, 28 kPa, and $M = 2.0$ enters an isentropic diffuser with an inlet area of 0.2 m^2 and leaves at $M = 0.2$. Assuming a calorically perfect gas, determine:
(a) The mass flow rate of the entering air
(b) The pressure and temperature of the leaving air
(c) The exit area and magnitude and direction of the force on the diffuser (assume outside of diffuser sees 28 kPa)

2.18 Air at 1800°F, 40 psia, and $M = 0.4$ enters an isentropic nozzle with an inlet area of 1.45 ft^2 and leaves at 10 psia. Assuming a calorically perfect gas, determine:
(a) The velocity and mass flow rate of the entering air
(b) The temperature and Mach number of the leaving air
(c) The exit area and magnitude and direction of the force on the nozzle (assume outside of nozzle sees 10 psia)

2.19 Air at 1500 K, 300 kPa, and M = 0.3 enters an isentropic nozzle with an inlet area of 0.5 m^2 and leaves at 75 kPa. Assuming a calorically perfect gas, determine:
(a) The velocity and mass flow rate of the entering air
(b) The temperature and Mach number of the leaving air
(c) The exit area and magnitude and direction of the force on the nozzle (assume outside of nozzle sees 75 kPa)

2.20 It is given that 100 lb/s of air enters a steady flow compressor at 1 atm and 68°F. It leaves at 20 atm and 800°F. If the process is adiabatic, find the input power, specific volume at exit, and change in entropy. Is the process reversible? (Assume a calorically perfect gas.)

2.21 It is given that 50 kg/s of air enters a steady flow compressor at 1 atm and 20°C. It leaves at 20 atm and 427°C. If the process is adiabatic, find the input power, specific volume at exit, and change in entropy. Is the process reversible? (Assume a calorically perfect gas.)

2.22 It is given that 200 lb/s of air enters a steady flow turbine at 20 atm and 3400°R. It leaves at 10 atm. For a turbine efficiency of 85%, determine the exit temperature, output power, and change in entropy. (Assume a calorically perfect gas.)

2.23 It is given that 80 kg/s of air enters a steady flow turbine at 30 atm and 2000 K. It leaves at 15 atm. For a turbine efficiency of 85%, determine the exit temperature, output power, and change in entropy. (Assume a calorically perfect gas.)

2.24 Rework Problem 2.13 for variable specific heats, using Appendix D or the program AFPROP. Compare your results to Problem 2.13.

2.25 Rework Problem 2.15 for variable specific heats, using Appendix D or the program AFPROP. Compare your results to Problem 2.15.

2.26 Rework Problem 2.16 for variable specific heats, using Appendix D or the program AFPROP. Compare your results to Problem 2.16.

2.27 Rework Problem 2.19 for variable specific heats, using Appendix D or the program AFPROP. Compare your results to Problem 2.19.

2.28 Rework Problem 2.20 for variable specific heats, using Appendix D or the program AFPROP. Compare your results to Problem 2.20.

2.29 Rework Problem 2.23 for variable specific heats, using Appendix D or the program AFPROP. Compare your results to Problem 2.23.

2.30 It is given that 100 lbm/s of air at total pressure of 100 psia, total temperature of 40°F, and static pressure of 20 psia flows through a duct. Find the static temperature, Mach number, velocity (ft/s), and flow area (ft^2).

2.31 Products of combustion ($\gamma = 1.3$) at a static pressure of 2.0 MPa, static temperature of 2000 K, and Mach number of 0.05 are accelerated in an isentropic nozzle to a Mach number of 1.3. Find the downstream static pressure and static temperature. If the mass flow rate is 100 kg/s and the gas constant R is 286 J/(kg · K), use the mass flow parameter (MFP) and find the flow areas for $M = 0.5$ and $M = 1.3$.

2.32 Data for the JT9D high-bypass-ratio turbofan engine are listed in Appendix B. If the gas flow through the turbines (from station 4 to 5) is 251 lbm/s with the total properties listed, what amount of power (kW and hp) is removed from the gas by the turbines? Assume the gas is calorically perfect with $\gamma = 1.31$ and $Rg_c = 1716\ \text{ft}^2/(\text{s}^2 \cdot {}^\circ\text{R})$.

2.33 At launch, the space shuttle main engine (SSME) has 1030 lbm/s of gas leaving the combustion chamber at $P_t = 3000$ psia and $T_t = 7350^\circ\text{R}$. The exit area of the SSME nozzle is 77 times the throat area. If the flow through the nozzle is considered to be reversible and adiabatic (isentropic) with $Rg_c = 3800\ \text{ft}^2/(\text{s}^2 \cdot {}^\circ\text{R})$ and $\gamma = 1.25$, find the area of the nozzle throat (in.^{2}) and the exit Mach number. *Hint*: Use the mass flow parameter to get the throat area and Eq. (3.14) to get the exit Mach number.

2.34 The experimental evaluation of a gas turbine engine's performance requires the accurate measurement of the inlet air mass flow rate into the engine. A bell-mouth engine inlet (shown schematically in Fig. P2.8) can be used for this purpose in the static test of an engine. The freestream velocity V_0 is assumed to be zero, and the flow through the bell mouth is assumed to be adiabatic and reversible. See Fig. P2.8.

Measurements are made of the freestream pressure P_{t0} and the static pressure at station 2 (P_2), and the exit diameter of the inlet D_2.

(a) For the bell-mouth inlet, show that the Mach number at station 2 is given by

$$M_2 = \sqrt{\frac{2}{\gamma - 1}\left[\left(\frac{P_{t0}}{P_{t0} - \Delta P}\right)^{(\gamma-1)/\gamma} - 1\right]}$$

and the inlet mass flow rate is given by

$$\dot{m} = \frac{P_{t0}}{\sqrt{T_{t0}}}\frac{\pi D_2^2}{4}\sqrt{\frac{2g_c}{R}\frac{\gamma}{\gamma - 1}\left[\left(\frac{P_{t0} - \Delta P}{P_{t0}}\right)^{2/\gamma} - \left(\frac{P_{t0} - \Delta P}{P_{t0}}\right)^{(\gamma+1)/\gamma}\right]}$$

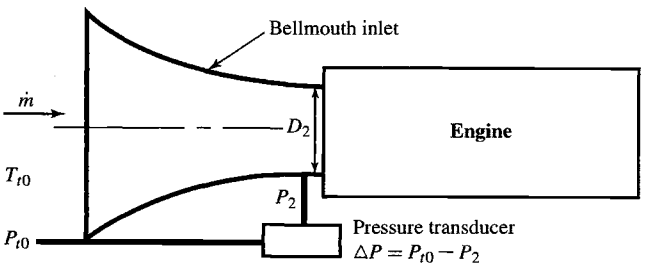

Fig. P2.8

(b) For the following measured data, determine the inlet air mass flow rate, Mach number M_2, static temperature T_2, and velocity V_2:

$$T_{t0} = 27°C \quad P_{t0} = 77.80\,\text{kPa}$$
$$\Delta P = 3.66\,\text{kPa} \quad D_2 = 0.332\,\text{m}$$

2.35 An ideal ramjet (see Fig. P2.9) is operated at 50,000-ft altitude with a flight Mach number of 3. The diffuser and nozzle are assumed to be isentropic, and the combustion is to be modeled as an ideal heat interaction at constant Mach number with constant total pressure. The cross-sectional area and Mach number for certain engine stations are given in Table P2.1. The total temperature leaving the combustor T_{t4} is 4000°R. Assume ambient pressure surrounding the engine flow passage.

(a) Determine the mass flow rate of air through the engine (lbm/s).
(b) Complete the table with flow areas, static pressures, static temperatures, and velocities.
(c) Find the thrust (magnitude and direction) of the diffuser, combustor, and nozzle.
(d) Find the thrust (magnitude and direction) of the ramjet.

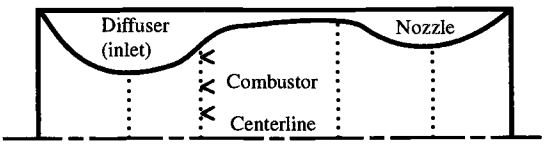

Fig. P2.9

2.36 If the flow enters the diffuser of Problem 2.7 at −55°F, is the process isentropic?

2.37 If the flow enters the nozzle of Problem 2.10 at 1250 K, is the process isentropic?

Table P2.1

Station	1	2	3	4	5	6
Area (ft^2)	4.235					
Mach	3	1	0.15	0.15	1	3
P (psia)						
T (°R)						
V (ft/s)						

2.38 Air at 20 kPa, 260 K, and Mach 3 passes through a normal shock. Determine:
(a) Total temperature and pressure upstream of the shock
(b) Total temperature and pressure downstream of the shock
(c) Static temperature and pressure downstream of the shock

2.39 Air upstream of a normal shock has the following properties: $P_t = 100$ psia, $T_t = 100°F$, and $M = 2$. Find the upstream static temperature, static pressure, and velocity (ft/s). Find the downstream total temperature, Mach number, total pressure, static temperature, static pressure, and velocity (ft/s).

2.40 If the diffuser of the ideal ramjet in Problem 2.35 has a normal shock in front of the inlet, determine:
(a) The total and static pressures and the static temperature downstream of the shock
(b) The mass flow rate through the engine (lbm/s) (assume choked flow at diffuser throat)
(c) The thrust of the engine

2.41 Air at a total pressure of 1.4 MPa, total temperature of 350 K, and Mach number of 0.5 is accelerated isentropically in a nozzle (see Fig. P2.10) to a Mach number of 3 (station x), passes through a normal shock (x to y), and then flows isentropically to the exit. Given a nozzle throat area of 0.05 m^2 and the exit area of 0.5 m^2:
(a) Find the area at the shock
(b) Find the static pressure and static temperature upstream of the shock (station x)
(c) Find the Mach number and the total and static pressures and temperatures downstream of the shock (station y)
(d) Find the Mach number, static pressure, and static temperature at the exit

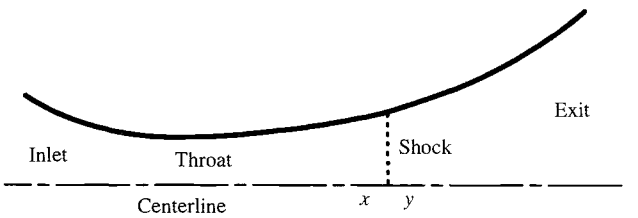

Fig. P2.10

2.42 Air flows through an isentropic nozzle with inlet conditions of $T_t = 2000°R$ and $P_t = 100$ psia. The throat area is 2 ft^2, and the exit area is 10.32 ft^2. If the flow is choked at the throat, find:
(a) Mass flow rate through the nozzle

(b) Mach number, static temperature, and static pressure at exit without a shock
(c) Mach number, static temperature, and static pressure at exit with a shock in the divergent section where the flow area is 4.06 ft^2 (see Fig. P2.10)

2.43 Air at a total pressure of 400 psia, total temperature of 500°R, and subsonic Mach number is accelerated isentropically in a nozzle (see sketch in Fig. P2.10) to a supersonic Mach number (station x), passes through a normal shock (x to y), and then flows isentropically to the exit. Given a nozzle inlet area of 3 ft^2, throat area of 1 ft^2, and exit area of 6 ft^2:
(a) Find the Mach number at the inlet
(b) Find the Mach number upstream of the shock (station x)
(c) Find the static pressure and static temperature upstream of the shock (station x)
(d) Find the Mach number and the total and static pressures and temperatures downstream of the shock (station y)
(e) Find the Mach number, static pressure, and static temperature at the exit

2.44 A 20-deg wedge (see Fig. P2.11) is to be used in a wind tunnel using air with test conditions of $M = 3$, $T_t = 500$°R, and $P_t = 100$ psia. Determine the angle of the oblique shocks and the downstream total and static properties (pressure and temperature). Use the GASTAB program.

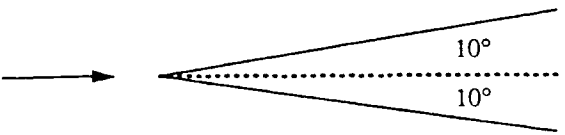

Fig. P2.11

2.45 A 15-deg ramp is used on a supersonic inlet at $M = 3.5$ and an altitude of 20 km. Use the GASTAB program.
(a) Determine the angle of oblique shock and flow properties (Mach number, total and static temperature, total and static pressure) upstream and downstream of the shock
(b) At what Mach number does the shock detach from the ramp?

2.46 Draw an H-K diagram for the J-79 afterburning turbojet engine of Fig. 1.6. Assume c_p is constant and T_{t0} is 518.7°R.

2.47 Draw an H-K diagram for the F-100 afterburning turbofan engine of Table B.4. Assume c_p is constant and T_{t0} is 518.7°R.

2.48 Show that dP/P is a constant for Example 2.12.

2.49 A calorically perfect gas undergoes an ideal heat interaction in a duct. The area of the duct is varied to hold the static pressure constant. Using the influence coefficients of Table 2.5, show the following:

(a) The area variation required to hold the static pressure constant is given by

$$\frac{dA}{A} = \left(1 + \frac{\gamma - 1}{2} M^2\right) \frac{dT_t}{T_t}$$

(b) The relationship between the Mach number and total temperature, for the preceding area variation, is given by

$$\frac{dM^2}{M^2} = -\left(1 + \frac{\gamma - 1}{2} M^2\right) \frac{dT_t}{T_t}$$

(c) The relationship for the area of the duct in terms of the Mach number is given by

$$A_2 = A_t \left(\frac{M_1}{M_2}\right)^2$$

where subscripts refer to states 1 and 2.

(d) Show V is CONSTANT.

2.50 You are required to design a nozzle to pass a given mass flow rate of air with minimum frictional losses between a storage pressure chamber P_c and an exhaust region P_c with a given variation in pressure between the two regions. The design conditions are

$$\dot{m} = 1000 \text{ lbm/s} \qquad P_c = 3000 \text{ psia} \qquad T_c = 3700^\circ\text{R}$$

Table P2.2

Station x, in.	P, psia	P/P_t	M	T/T_t	A/A^*	T, °R	a, ft/s	V, ft/s	A, in.^{2}	D, in.
0	2918									
2	2841									
4	2687									
6	2529									
8	2124									
10	1585									
(throat)										
12	727									
16	218									
24	19.8									
41	3.21									
60	1.17									

(a) Using the design conditions, complete Table P2.2
(b) Make a plot of the nozzle contour (see Fig. 2.33)
(c) Calculate the nozzle design pressure ratio $P_{\bar{n}}$ and the nozzle area ratio ε
(d) Using the altitude table, determine the design altitude for this nozzle ($P_c = P_a$)
(e) Determine the thrust of a rocket motor using this nozzle at its design altitude

2.51 A perfect gas enters a constant-area heater at a Mach number of 0.3, total pressure of 600 kPa, and total temperature of 500 K. A heat interaction of 500 kJ/kg into the gas occurs. Using the GASTAB software, determine the Mach number, total pressure, and total temperature after the heat interaction for the following gases:
(a) $\gamma = 1.4$ and $c_p = 1.004$ kJ/(kg · K)
(b) $\gamma = 1.325$ and $c_p = 1.171$ kJ/(kg · K)

2.52 A perfect gas enters a constant-area heater at a Mach number of 0.5, total pressure of 200 psia, and total temperature of 1000°R. A heat interaction of 100 Btu/lbm into the gas occurs. Using the GASTAB software, determine the Mach number, total pressure, and total temperature after the heat interaction for the following gases:
(a) $\gamma = 1.4$ and $c_p = 0.24$ Btu/(lbm · °R)
(b) $\gamma = 1.325$ and $c_p = 0.28$ Btu/(lbm · °R)

2.53 A convergent-only nozzle is to be used on an afterburning gas turbine engine as shown in Fig. P2.12. Model the afterburner (station 6 to station 7) as a constant-area duct ($A_6 = A_7$) with simple heat interaction q_{in} into the air. The flow through the nozzle (station 7 to station 8) is isentropic. The exit area of the nozzle A_8 is varied with the afterburner setting T_{t7} to keep sonic ($M = 1$) flow at station 8 and the inlet conditions (mass flow rate, P_t, and T_t) constant at station 6.
(a) Using the mass flow parameter, show that the area ratio A_8/A_6 is given by

$$\frac{A_8}{A_6} = \frac{P_{t6}}{P_{t7}}\sqrt{\frac{T_{t7}}{T_{t6}}}\frac{\text{MFP}(M_6)}{\text{MFP}(M=1)} = \frac{P_{t6}}{P_{t7}}\sqrt{\frac{T_{t7}}{T_{t6}}}\left(\frac{A^*}{A}\right)_{M_6}$$

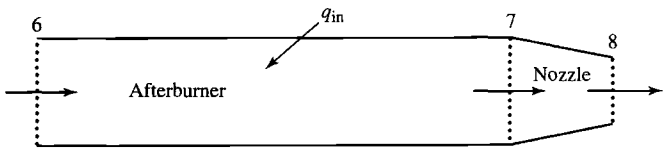

Fig. P2.12

(b) For $M_6 = 0.4$, determine the area ratio A_8/A_6 for the following values of T_{t7}/T_{t6}: 1.0, 1.1, 1.2, 1.3, 1.4, 1.5, 1.6, and $T_{t7} = T_t^*$

2.54 One mole of hydrogen and one mole of oxygen are in equilibrium at a temperature of 1500 K and a pressure of 5 atm. Determine the number of moles of H_2O, H_2, and O_2 in the products (neglect other products such as OH, H, O, etc.). Compare your results with that of the EQL program.

2.55 One mole of hydrogen and 0.45 moles of oxygen are in equilibrium at a temperature of 2200 K and a pressure of 20 atm. Determine the equilibrium constant from the results of the EQL program and compare to the JANNAF tables.

2.56 Calculate the heat of reaction for the reaction of Problem 2.54.

2.57 Using the EQL software, determine the adiabatic flame temperature for one mole of hydrogen and one-half mole of oxygen with the reactants at a temperature of 300 K and a pressure of 10 atm.

Page is intentionally blank

3
Rocket Propulsion

3.1 Introduction

The types of rocket propulsion and basic parameters used in performance evaluation of rocket propulsion are described in this chapter. First, the concepts of thrust, effective exhaust velocity, and specific impulse are presented for a gaseous continuum leaving a rocket engine. These concepts are covered in more detail than that contained in Chapter 1. To determine the requirements of rocket vehicles, some introductory mechanics of orbital flight are investigated along with rocket mass ratios, rocket acceleration, and multistage rockets. This section on requirements and capabilities is followed by a general discussion of the various sources of rocket propulsion and a summary of their capabilities. Following this general introduction to rocket propulsion and rocket flight is a discussion of rocket nozzle types, a study of the detailed performance parameters for rocket engines expelling a continuum, detailed example problems, and discussion of liquid- and solid-propellant rockets.

3.1.1 Rocket Thrust

The rocket thrust studied here will be applicable to rockets that eject a gaseous continuum material from a nozzle at a constant rate. Chemical and nuclear-H_2 rockets are examples of such rocket propulsion systems. The thrust of an ionic rocket that expels discrete ion particles at high speeds, on the other hand, is not related to properties of a continuum such as pressure and density. The thrust equation to be developed will not apply, therefore, to ionic rockets. The thrust of ion rockets, however, still depends on the same basic principle of operation as chemical or nuclear-H_2 rockets, i.e., the reaction force resulting from imparting momentum to a mass.

3.1.2 Ideal Thrust Equation

The ideal rocket thrust is defined as the force required to hold a rocket at rest as the rocket ejects a propellant rearward under the following assumed conditions:

1) Atmospheric pressure acts everywhere on the rocket's external surface. (There is no interaction between the jet issuing from the rocket nozzle and the air in contact with the external surface of the rocket.)

2) The propellant flows from the rocket at a constant rate in uniform one-dimensional flow at the nozzle exit section.

3) The rate of change of the momentum within the rocket is negligibly small and may be neglected.

The rocket of Fig. 3.1a is held in place by a reaction strut and is ejecting a propellant to the rear under the preceding conditions. The shear force at section B-B of the reaction strut is equal in magnitude to the ideal rocket thrust. As shown by the freebody diagram in Fig. 3.1a, the thrust is produced by the internal force on the rocket shell. In a vacuum, the thrust would be identical with F_{int}, but is less than the internal force in the atmosphere because of the ambient pressure forces acting on the external surface of the rocket. The external force is due to atmospheric pressure forces only and is given by

$$F_{\text{ext}} = P_a A_e$$

If we assume internal isentropic flow, the interior force is due to pressure forces only. It is the sum of all of the pressure forces exerted by the propellant on the interior wall surfaces. The internal force is readily evaluated in terms of propellant flow properties by application of the momentum equation to the control surface indicated in Fig. 3.1b, and by using the fact that the force of the propellant on

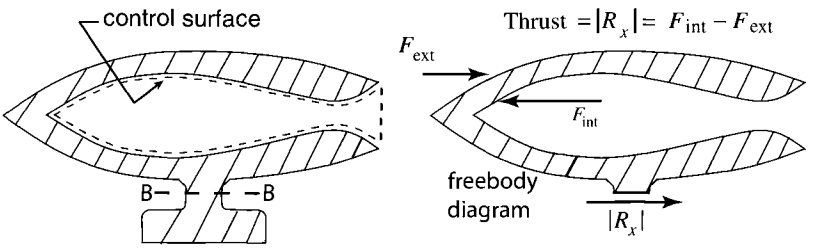

a) Forces on rocket shell

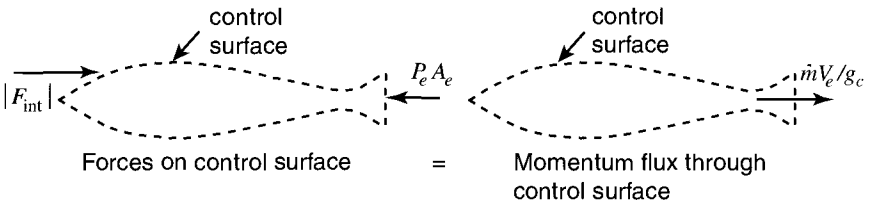

b) Evaluation of $|F_{\text{int}}|$ by momentum equation

Fig. 3.1 Ideal rocket thrust.

the internal walls equals, in magnitude, the force of the walls on the propellant. For the magnitude of the internal force, we obtain

$$|F_{\text{int}}| = P_e A_e + \frac{1}{g_c}\rho_e A_e V_e^2 = P_e A_e + \frac{\dot{m} V_e}{g_c}$$

The difference between F_{int} and F_{ext} is the ideal rocket thrust, F_i,

$$F_i = F_{\text{int}} - F_{\text{ext}}$$

$$F_i = \frac{\dot{m} V_e}{g_c} + (P_e - P_a)A_e \tag{3.1}$$

This equation gives the thrust in terms of the propellant flow properties, the exit area, and the ambient pressure. It is well to remember that only the term $P_a A_e$ on the right side of Eq. (3.1) represents *a real force acting on the rocket shell.*

3.1.3 Optimum Ideal Thrust

Let us consider a rocket ejecting a given propellant supersonically from a combustion chamber at a fixed temperature and pressure. Under these conditions, the mass flow through the rocket nozzle is constant at a value given by

$$\dot{m} = \frac{P_t A}{\sqrt{T_t}} \sqrt{\frac{2 g_c}{R} \frac{\gamma}{\gamma - 1} \left\{ \left(\frac{P}{P_t}\right)^{2/\gamma} - \left(\frac{P}{P_t}\right)^{(\gamma+1)/\gamma} \right\}} \tag{3.2}$$

Let us further assume that the nozzle exit area is adjustable and that the ambient pressure P_a is constant. Now notice that as we vary A_e, the pressure P_e and the velocity V_e will vary, but mass flow rate $\dot{m}$ and P_a will remain constant. The following question arises: For what value of A_e will the corresponding values of V_e and P_e make the thrust of Eq. (3.1) a maximum? The simplest way to demonstrate the optimum thrust condition is to deal with the *real forces* acting on the rocket shell, and to determine directly under what conditions these produce maximum thrust. First, we observe that as A_e is varied by adding a further divergent section on the nozzle exit, any change in thrust comes about by the net force acting on this added section. This follows from the fact that forces acting on the original surfaces of the rocket are not changed by the added section because atmospheric pressure still acts on the original external surfaces, and the original internal pressure distribution remains the same as long as supersonic flow exists at the nozzle exit. Because any thrust change, therefore, comes about by the action of the forces acting on the added surfaces introduced in changing A_e, we need only to examine the forces associated with the added surface to maximize thrust. Figure 3.2 shows an enlarged view of the pressure distribution on the external and internal surfaces near the exit of a rocket nozzle. The external

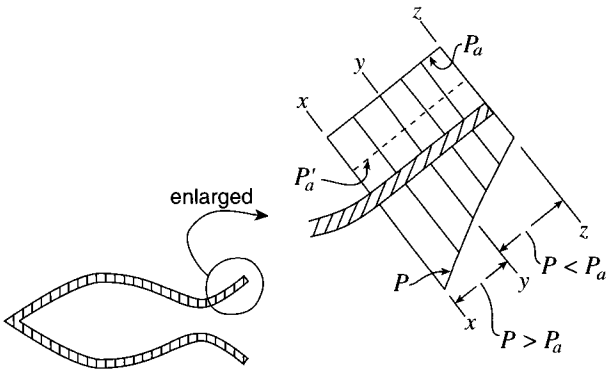

Fig. 3.2 Forces acting on rocket nozzle wall for optimum thrust consideration.

pressure is constant at P_a. The internal pressure decreases from a value greater than P_a at x to P_a at y, and to a value lower than P_a at z, corresponding to an overexpanded nozzle. Now, as A_e is increased by adding surfaces up to station y, we find the thrust is increased because the internal pressure on these added surfaces is greater than P_a. If A_e is increased beyond that value corresponding to y, the thrust is decreased because there is a net drag force acting on the surfaces beyond y because the internal pressure is less than P_a between y and z. To eliminate the wall surface producing a net drag and to not eliminate any wall surface producing a net thrust, the nozzle should be terminated at y where $P_e = P_a$. The exit velocity corresponding to this condition will be denoted $(V_e)_{\text{opt}}$ so that

$$(F_i)_{\text{opt}} = \frac{\dot{m}(V_e)_{\text{opt}}}{g_c} \tag{3.3a}$$

If the nozzle of Fig. 3.2 is at a higher altitude, the ambient pressure is reduced to a value of $P_{a'}$, indicated by the dashed line of Fig. 3.2. The pressure at this higher altitude is such that the internal pressure acting on the nozzle wall from y to z is greater than the new ambient pressure. At this higher altitude, then, the nozzle surface from y to z is a thrust-producing surface and should be retained. This means a higher nozzle area ratio at higher altitudes for optimum thrust.

3.1.4 Vacuum Ideal Thrust

In a vacuum (very high altitudes), $F_{\text{ext}} = 0$. Thus $(F_i)_{\text{vac}} = F_{\text{int}}$, where F_{int} can be evaluated by

$$(F_i)_{\text{vac}} = F_{\text{int}} = \frac{\dot{m}V_e}{g_c} + P_e A_e \tag{3.3b}$$

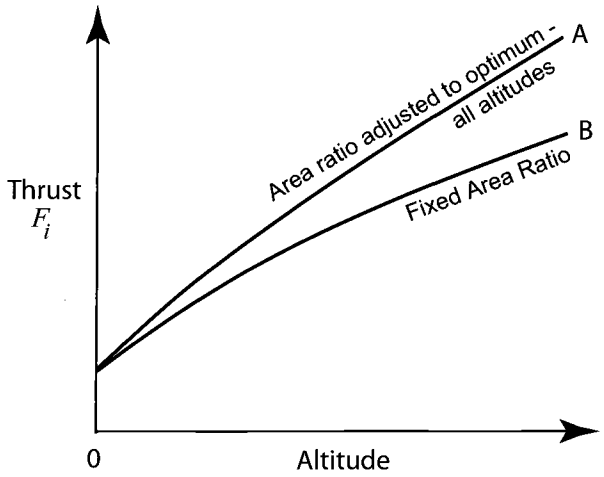

Fig. 3.3 Ideal thrust variation with altitude.

3.1.5 Thrust Variation with Altitude

To understand the variation of thrust with altitude, we consider two rockets, A and B. Rocket A has infinitely adjustable area ratio, whereas rocket B's area ratio is fixed (constant) at a value that gives optimum expansion at sea level.

For each rocket, $F_i = F_{\text{int}} - F_{\text{ext}}$. At higher than sea-level altitudes, rocket A's thrust increases because F_{int} remains the same, and F_{ext} decreases to zero as P_a approaches zero. The thrust of rocket A exceeds that of rocket B at altitudes since F_{ext} decreases the same as for rocket B. In addition, rocket A has thrust-producing surfaces (such as segment x–y of Fig. 3.2) added on to it as it climbs and expands to lower ambient pressures. The variation of thrust for rockets A and B is sketched in Fig. 3.3.

3.1.6 Effective Exhaust Velocity C and Specific Impulse (I_{sp})

The effective exhaust velocity C is defined in Chapter 1 by Eq. (1.53) as

$$C \equiv V_e + \frac{(P_e - P_a)A_e}{\dot{m}/g_c} \tag{3.4}$$

Using this definition of effective exhaust velocity in Eq. (3.1), the ideal thrust is simply

$$F_i = \frac{\dot{m}C}{g_c} \tag{3.5}$$

The values of a rocket's exhaust velocity V_e and exhaust pressure P_e depend on the type of rocket engine and its design and operation. For launch from the

surface of the Earth to Earth orbit, the atmospheric pressure P_a varies from a low of zero (vacuum) to a high of that at sea level. For a rocket engine where the mass flow rate and combustion chamber conditions are constant, the effective exhaust velocity C and ideal thrust F_i will vary from a low value for sea-level operation to a high value at vacuum conditions. Figure 1.42b shows the predicted variation of thrust with altitude for the space shuttle main engine (SSME) under these conditions. The variation of effective exhaust velocity C will be the same as the thrust times a constant. Even though the effective exhaust velocity C can vary, an average value of the effective exhaust velocity may be used for ease of analysis or calculation.

The specific impulse I_{sp} for a rocket is defined as the thrust per unit of propellant weight flow:

$$I_{sp} \equiv \frac{F}{\dot{w}} = \frac{F}{\dot{m}} \frac{g_c}{g_0} \tag{3.6}$$

where g_0 is the acceleration of gravity at sea level. Specific impulse has units of seconds. Using Eq. (3.5), the effective exhaust velocity is directly related to the specific impulse by

$$C = I_{sp} g_0 \tag{3.7}$$

As just discussed, the effective exhaust velocity can vary during operation. From Eq. (3.7), the specific impulse I_{sp} for a rocket engine will vary in direct proportion to its effective exhaust velocity C. For ease of analysis or calculation, an average value of specific impulse may be used.

Example 3.1

Appendix C lists the F-1 engine used on the Saturn V rocket as having a vacuum thrust of 1,726,000 lbf and vacuum I_{sp} of 305 s. Determine the mass flow rate at the vacuum conditions.

Solution: Solving Eq. (3.6) for the mass flow rate, we have

$$\dot{m} = \frac{F}{I_{sp}} \frac{g_c}{g_0} = \frac{1{,}726{,}000}{305} \frac{32.174}{32.174} = 5659 \text{ lbm/s}$$

3.2 Rocket Propulsion Requirements and Capabilities

3.2.1 Requirements

The propulsion requirements for space flight missions are usually expressed in terms of speed increment that the propulsion system must supply to the space vehicle. When the appropriate increment in speed is supplied to a vehicle, the vehicle's guidance system must adjust the direction of the speed to attain the orbit desired. As a simple example, the ideal speed increment to place a

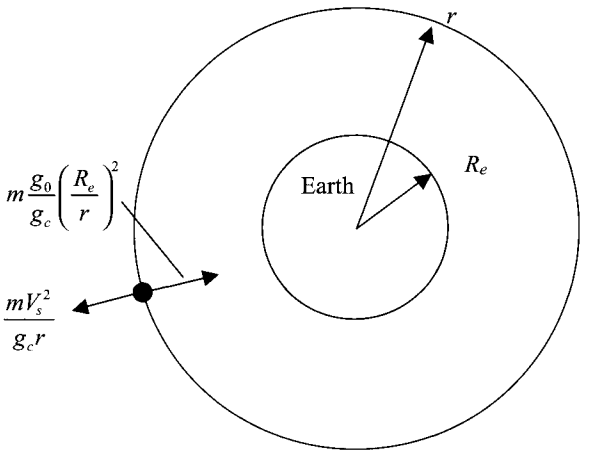

Fig. 3.4 Forces acting on near-Earth-orbiting mass.

vehicle in orbit about the Earth is that speed that will give a balance between the centrifugal and gravitational forces acting on the body in orbit. Considering the balance of these forces, we can determine the needed velocity increment. The force of gravity acting on a mass m at a distance r from the Earth's center is $m\frac{g_0}{g_c}\left(\frac{R_e}{r}\right)^2$, where R_e is the Earth's radius (3959 miles, 6370 km), and g_0 is the acceleration of gravity on the surface of the Earth (32.174 ft/s^2, 9.807 m/s^2). Referring to the force diagram of Fig. 3.4, we have

$$\frac{mV_s^2}{g_c r} = m\frac{g_0}{g_c}\left(\frac{R_e}{r}\right)^2$$

Solving for the satellite velocity V_s at a height h above the surface of the Earth ($r = R_e + h$) gives

$$V_s = \sqrt{g_0 \frac{R_e^2}{R_e + h}} \tag{3.8}$$

For a circular Earth orbit at 160 km (100 miles), Eq. (3.8) gives a satellite velocity of 7800 m/s (25,600 ft/s). Thus a rocket must increase the velocity from zero at launch to 7800 m/s at 160 km. The propulsion system's fuel is the original source of the kinetic energy and the higher potential energy possessed by the orbital mass of Fig. 3.4. The kinetic energy (KE) of the orbital mass is simply given by $\{mV_s^2/(2g_c)\}$, and the change in potential energy (ΔPE) is given by

$$\Delta\text{PE} = \int_{R_e}^{R_e+h} m\frac{g}{g_c}\,\mathrm{d}r = mR_e^2\frac{g_0}{g_c}\int_{R_e}^{R_e+h}\frac{\mathrm{d}r}{r^2} = m\frac{g_0}{g_c}\left(\frac{R_e}{R_e+h}\right) \tag{3.9}$$

The sum of the changes in potential and kinetic energies per unit mass $\{\Delta(\text{pe} + \text{ke})\}$ of the orbiting mass relative to sea-level launch is given by

$$\Delta(\text{pe} + \text{ke}) = \frac{\Delta(\text{PE} + \text{KE})}{m} = \frac{g_0}{g_c}\left(\frac{R_e}{R_e + h}\right) + \frac{V_s^2}{2\,g_c} \tag{3.10}$$

To place a mass in circular Earth orbit at 100 miles requires that the sum of the potential and kinetic energies be increased by 13,760 Btu/lbm (32 MJ/kg). This energy change is equal to the kinetic energy of a mass at a velocity of 26,250 ft/s (8000 m/s). In addition to this energy, the propulsion system must supply the energy that is delivered to the viscous atmosphere by the ascending vehicle due to aerodynamic drag forces. Thus the equivalent velocity increment requirement of a propulsion system to attain a near Earth orbit is greater than 26,250 ft/s (8000 m/s) due to aerodynamic drag. Taking these items into account gives an equivalent velocity increment requirement of approximately 30,000 ft/s (9140 m/s) for a near Earth orbit. Table 3.1 gives this velocity increment and those required for certain other space missions.

To escape the Earth's gravitational field ($h \to \infty$), solution of Eq. (3.9) gives the change in potential energy as Earth escape:

$$\Delta\text{pe} = \frac{g_0}{g_c} R_e \tag{3.11}$$

This potential energy change is equal to the kinetic energy corresponding to the escape velocity V_{escape} given by

$$V_{\text{escape}} = \sqrt{2\,g_0 R_e} \tag{3.12}$$

Comparison of Eq. (3.12) for the escape velocity to Eq. (3.8) for the satellite velocity evaluated for low Earth orbit gives

$$V_{\text{escape}} = \sqrt{2} V_s \tag{3.13}$$

This equation explains why the velocity increment of 42,000 ft/s (12,800 m/s) required for Earth escape (see Table 3.1) is 12,000 ft/s (3660 m/s) higher than that required for low Earth orbit.

Table 3.1 Mission equivalent velocity increment requirements

Mission	ΔV_{equiv} (m/s)	ΔV_{equiv} (ft/s)
Low Earth orbit	9,140	30,000
Earth escape-lunar hit	12,800	42,000
High Earth orbit	13,720	45,000
Lunar orbit		
Mars, Venus Probe		
Lunar soft landing	15,240	50,000
Lunar round trip	18,280	60,000
Escape from solar system		

The total mass of a rocket vehicle is the sum of its parts. For convenience, the vehicle mass is considered to be divided into three different masses: the payload mass m_{pl}, the propellant mass m_p, and the remaining mass, which will be called the dead weight mass m_{dw}. The mass of the structure includes the rocket engines, guidance and control system, tankage, rocket structure, etc. The initial mass of a rocket vehicle, m_o, can be expressed as

$$m_o = m_{\text{pl}} + m_p + m_{\text{dw}} \tag{3.14}$$

For convenience, we define the payload mass ratio λ and dead weight mass ratio δ as

$$\lambda \equiv \frac{m_{\text{pl}}}{m_o} \quad \text{and} \quad \delta \equiv \frac{m_{\text{dw}}}{m_o} \tag{3.15}$$

If all of the propellant is consumed during firing, the resulting vehicle mass is defined as the burnout mass m_{bo}, or

$$m_{\text{bo}} = m_o - m_p = m_{\text{pl}} + m_{\text{dw}} \tag{3.16}$$

In addition to the mass ratios of Eq. (3.15), the vehicle mass ratio (MR) is defined as the initial mass m_o divided by the burnout mass m_{bo}, or

$$\text{MR} \equiv \frac{m_o}{m_{\text{bo}}} \tag{3.17}$$

Using Eq. (3.16) and the mass ratio defined in Eq. (3.15), the MR can be written as

$$\text{MR} = \frac{1}{\lambda + \delta} \tag{3.18}$$

3.2.2 Equation of Motion for an Accelerating Rocket

In this section, the velocity increment ΔV of a rocket is related to the propulsion system's burning time t_b, the ejected mass velocity V_e, and the space vehicle's MR. The equation of motion for an accelerating rocket (see Fig. 3.5) rising from the Earth under the influence of gravity and drag as it expels matter was developed in Chapter 1. The analysis resulted in the general expression for the differential velocity change given by Eq. (1.58), or

$$\mathrm{d}V = -C\frac{\mathrm{d}m}{m} - \left(\frac{D}{m/g_c} + g\cos\theta\right)\mathrm{d}t \tag{3.19}$$

where C is the effective exhaust velocity. For launch from the surface of the Earth, the acceleration of gravity g can be written in terms of the radius from the center of the Earth, r, the acceleration of gravity at sea level, g_0, and the

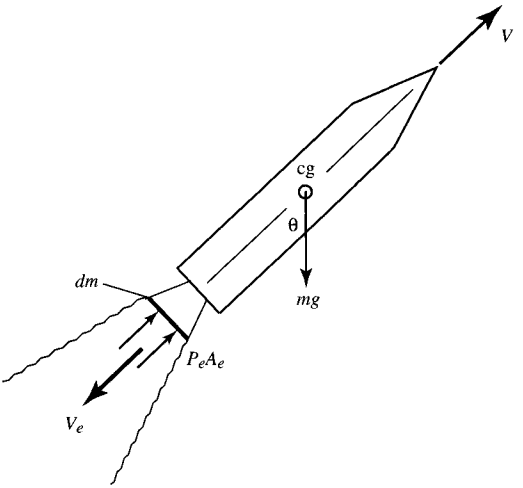

Fig. 3.5 Accelerating rocket.

radius of the Earth, R_e, as follows:

$$g = g_0\left(\frac{R_e}{r}\right)^2$$

Substitution of this expression into Eq. (3.19) yields

$$dV = -C\frac{dm}{m} - \left\{\frac{D}{m/g_c} + g_0\left(\frac{R_e}{r}\right)^2 \cos\theta\right\}dt \tag{3.20}$$

In this equation, dV is the velocity increment supplied to the vehicle of mass m in time dt as mass dm is expelled rearward at effective velocity C relative to the vehicle. Notice that dm is a negative quantity for leaving mass and hence $-C(dm/m)$ becomes a positive number exceeding the

$$\left\{\frac{D}{m/g_c} + g_0\left(\frac{R_e}{r}\right)^2 \cos\theta\right\}dt$$

when values of C are sufficiently high to produce a positive increment in V. When dm is zero (no burning), dV becomes a negative until the kinetic energy possessed by the vehicle at burnout is all converted into potential energy of the vehicle at zero velocity and maximum height. After this condition is reached, the vehicle begins to descend, and its potential energy is converted back into kinetic energy that, in turn, is dissipated into the atmosphere during reentry. To avoid this simple yo-yo motion, we assume that a guidance system has the rocket follow a specified trajectory. The trajectory is such that the vehicle's velocity vector is perpendicular to the radius r at the instant of burnout, and a near Earth orbit is established corresponding to the velocity of 26,000 ft/s.

Integration of Eq. (3.20) from liftoff to burnout gives us the desired relation between the vehicle's velocity increment ΔV and the propulsion system's burning time t_b, the effective exhaust velocity C, the drag D, the trajectory, and the vehicle's MR. Thus

$$\Delta V = \int_0^{V_\infty} \mathrm{d}V = -\int_{m_o}^{m_{\mathrm{bo}}} C\frac{\mathrm{d}m}{m} - g_o \int_{t=0}^{t_{\mathrm{bo}}} \left\{ \frac{D/m}{g_0/g_c} + \left(\frac{R_e}{r}\right)^2 \cos\theta \right\} \mathrm{d}t \tag{3.21}$$

where subscript bo denotes burnout conditions. Evaluation of this equation requires detailed knowledge of the trajectory and vehicle drag.

Using Eq. (3.21), the effective velocity increment $\Delta V_{\mathrm{effective}}$, the drag velocity increment ΔV_{drag}, and gravity velocity increment $\Delta V_{\mathrm{gravity}}$ are defined by

$$\begin{aligned} \Delta V_{\mathrm{effective}} &\equiv -\int_{m_o}^{m_{\mathrm{bo}}} C\frac{\mathrm{d}m}{m} \\ \Delta V_{\mathrm{drag}} &\equiv g_c \int_{t=0}^{t_{\mathrm{bo}}} \left\{\frac{D}{m}\right\} \mathrm{d}t \\ \Delta V_{\mathrm{gravity}} &\equiv g_o \int_{t=0}^{t_{\mathrm{bo}}} \left\{ \left(\frac{R_e}{r}\right)^2 \cos\theta \right\} \mathrm{d}t \end{aligned} \tag{3.22}$$

Note that the effective velocity increment $\Delta V_{\mathrm{effective}}$ is the specific vehicle impulse (engine thrust per unit mass of the vehicle integrated over time), or

$$\Delta V_{\mathrm{effective}} \equiv -\int_{m_o}^{m_{\mathrm{bo}}} C\frac{\mathrm{d}m}{m} \equiv \int_{t=0}^{t_{\mathrm{bo}}} \frac{\dot{m}C}{m}\,\mathrm{d}t \equiv g_c \int_{t=0}^{t_{\mathrm{bo}}} \frac{F}{m}\,\mathrm{d}t \tag{3.23}$$

Equation (3.21) for the vehicle's velocity increment can be rewritten as

$$\Delta V = \Delta V_{\mathrm{effective}} - \Delta V_{\mathrm{drag}} - \Delta V_{\mathrm{gravity}} \tag{3.24}$$

This equation shows the effect of drag and gravity on effective velocity increment that was discussed earlier in this section, namely, that the effective velocity increment $\Delta V_{\mathrm{effective}}$ is greater that the vehicle's velocity increment ΔV due to vehicle drag losses and gravity.

Assuming constant effective exhaust velocity C, Eq. (3.22) gives the following expression for effective velocity increment:

$$\Delta V_{\mathrm{effective}} = C\ell n\left(\frac{m_o}{m_{\mathrm{bo}}}\right) = C\ell n(\mathrm{MR}) = C\ell n\left(\frac{1}{\lambda+\delta}\right) \tag{3.25}$$

Equation (3.25) is plotted in Fig. 3.6, which shows the exponential relationship between the mass ratio and the effective velocity ratio ($\Delta V_{\mathrm{effective}}/C$). Both Fig. 3.6 and Eq. (3.25) show the extreme sensitivity of the mass ratio to the effective exhaust velocity for a given high energy mission (large $\Delta V_{\mathrm{effective}}$).

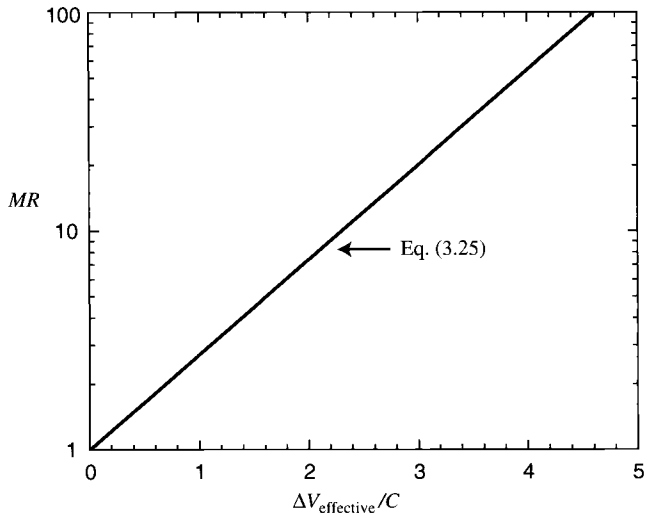

Fig. 3.6 Ideal rocket vehicle mass ratio.

Many space missions require multiple $\Delta V_{\text{effective}}$. Consider a mission from Earth orbit to the surface of the moon and return. This mission will require at least six ΔV: one to exit Earth orbit and reach transit speed; a second to enter lunar orbit; a third to land on the moon; a fourth to reach lunar orbit again; a fifth to exit lunar orbit and reach transit speed; and a sixth to enter Earth orbit. Additional ΔV will be required for trajectory corrections, vehicle orientation, etc. Each ΔV expends vehicle mass, and the mass ratio (m_o/m_{bo}) for the total mission of a single-stage vehicle can be obtained using Eq. (3.25) where $\Delta V_{\text{effective}}$ is the sum of all of the effective velocity changes $(\Delta V_{\text{effective}})$ in the mission.

For a near Earth orbit, R_e/r is close to unity ($R_e = 3959$ miles, $r = 3959 + 100 = 4059$ miles, and $R_e/r = 0.975$), and $\Delta V_{\text{gravity}}$ can be approximated as $\Delta V_{\text{gravity}} \approx g_0 t_{\text{bo}}$. Assuming constant effective exhaust velocity C and negligible drag ($\Delta V_{\text{drag}} = 0$), Eqs. (3.24) and (3.25) give

$$\Delta V = V_{\text{bo}} = C\ell n\left(\frac{m_o}{m_{\text{bo}}}\right) - g_0 t_{\text{bo}} \tag{3.26}$$

This simple equation provides a means of comparing the performance of different propulsion systems in terms of vehicle gross mass m_o required to put a given mass m_{bo} into a low Earth orbit requiring a vehicle velocity increment of V_{bo}.

Example 3.2

To demonstrate the importance of a high propellant exhaust velocity V_e, let us determine the orbital payload capabilities of various propulsion systems for a fixed initial vehicle gross weight. Table 3.2 gives approximate representative values of effective exhaust velocity C for four propulsion systems. The dead

Table 3.2 Performance of high-thrust rocket propulsion systems

Propulsion system fuel and propellant	Effective exhaust velocity, C		Assumed dead weight ratio (δ)
	m/s	ft/s	
Solid	2440	8000	0.03
Liquid O_2-kerosene (RP)	3050	10,000	0.03
Liquid O_2 and H_2	4110	13,500	0.06
Nuclear fuel using H_2 propellant	8230	27,000	0.10

weight ratio δ listed consists of tankage, pumps, and structural members excluding the payload.

As a reference point, we determine first the gross weight at liftoff for a 2000-lbm payload placed in a near Earth orbit by a liquid O_2-kerosene propulsion system. At burnout, the payload, m_{pl}, and the rocket dead weight, m_{dw}, have attained the velocity V_{bo} and both will orbit. Therefore,

$$m_{bo} = m_{pl} + m_{dw} = m_{pl} + \delta m_o = m_{pl} + 0.03\, m_o$$

We will assume for each propulsion system that the burning time is 100 s. We have, from Eq. (3.26),

$$\text{MR} = \frac{m_o}{m_{bo}} = \frac{m_o}{m_{pl} + 0.03\, m_o} = \exp\left\{\frac{V_{bo} + g_o t_{bo}}{C}\right\}$$

$$\text{MR} = \frac{m_o}{m_{bo}} = \frac{m_o}{2000 + 0.03\, m_o} = \exp\left\{\frac{30{,}000 + 3217}{10{,}000}\right\} = \exp\{3.32\} \approx 28$$

Thus

$$m_o = 28\{2000 + 0.03\, m_o\} = 56{,}000 + 0.84\, m_o$$

$$m_o = 56{,}000/0.16 = 350{,}000 \text{ lbm}$$

Thus to place a 2000-lbm payload in a near Earth orbit requires a sea-level liftoff gross weight of 350,000 lbf. With this gross weight as a reference point, let us evaluate the orbiting payload capabilities of the other propulsion systems of Table 3.2.

For the propulsion system using liquid O_2 and H_2, we find a pad weight of 350,000 lbf is capable of placing 8890 lbm into a near Earth orbit. The computation follows:

$$m_{pl} = m_{bo} - m_{dw} = m_o\left\{\exp\left(-\frac{V_{bo} + g_o t_{bo}}{C}\right) - 0.06\right\}$$

$$m_{pl} = 350{,}000\left\{\exp\left(-\frac{33{,}217}{13{,}500}\right) - 0.06\right\} = 350{,}000(0.0854 - 0.06)$$

$$m_o = 8890 \text{ lbm}$$

Table 3.3 Near-Earth orbital payload for 350,000 lbm (158,760 kg) launch mass

	Solid propellant	Liquid O_2-RP	Liquid H_2-O_2	Nuclear-H_2
C (ft/s)|(m/s)	8000|2440	10,000|3050	13,500|4115	27,000|8230
δ (dead weight ratio)	0.03	0.03	0.06	0.10
Payload (lbm)|(kg)	Nothing	2000|907	8890|4040	67,000|30,390
λ (payload ratio)	−0.0142	0.0057	0.0250	0.1914

Similar calculations give the results shown in Table 3.3. The solid-propellant propulsion system's performance is not sufficient to place any mass in orbit under the assumed conditions. The results in Table 3.3 indicate that a high value of effective exhaust velocity is extremely beneficial, if not mandatory. An increase in C by a factor of 2.7, in going from LOX-RP to nuclear-H_2, permits a 33-fold increase in the payload even though the dead weight of the nuclear-H_2 system is three times that of the LOX-RP propulsion unit. Obviously, it is advantageous to have a high exhaust velocity.

3.2.3 Rocket Vehicles in Free Space

When rockets are fired in "free space," there are no drag or gravitational penalties. Integration of Eq. (3.21) under these conditions and assuming constant effective exhaust velocity C yields

$$\Delta V/C = \ell n(\mathrm{MR}) = \ell n\left(\frac{1}{\lambda + \delta}\right) \tag{3.27a}$$

or

$$\mathrm{MR} = \frac{1}{\lambda + \delta} = \exp(\Delta V/C) \tag{3.27b}$$

For rocket vehicles in free space, the effective velocity increment $\Delta V_{\text{effective}}$ equals the vehicle's velocity increment ΔV, and thus Fig. 3.6 is also a plot of Eq. (3.27b).

3.2.4 Multiple-Stage Rocket Vehicles

The launch of a payload using single-stage rocket vehicles was investigated in the previous section. When large energy changes are required (large ΔV) for a given payload, the initial vehicle mass of a single-stage vehicle and its associated cost become very enormous. We consider a liquid H_2-O_2 chemical rocket ($C = 4115$ m/s, 13,500 ft/s) launching a 900-kg (2000-lbm) payload on a mission requiring a ΔV of 14,300 m/s (46,900 ft/s). From Fig. 3.6 or Eq. (3.27b), the required vehicle MR is 32.30. This high mass ratio for a payload of 900 kg and 3% dead weight results in an initial vehicle mass of 938,000 kg mass and

a vehicle dead weight mass of about 29,070 kg. This large initial vehicle mass can be dramatically reduced by using a multistage vehicle.

For a multistage vehicle with N stages, the payload of a lower stage, $[m_{pl}]_i$, is the mass of all higher stages, $[m_o]_{i+1}$, or

$$[m_{pl}]_i = [m_o]_{i+1} \qquad \text{for } i < N \tag{3.28}$$

From Eq. (3.27b), the initial mass of stage i and above (denoted by $[m_o]_i$) is given by

$$[m_o]_i = \frac{1}{\exp\{-(\Delta V/C)_i\} - \delta_i}[m_{pl}]_i \tag{3.29a}$$

and the payload ratio of stage i (denoted by λ_i) is given by

$$\lambda_i = \exp\{-(\Delta V/C)_i\} - \delta_i \tag{3.29b}$$

Using Eq. (3.27a), the total velocity change, ΔV_{total}, for an N-stage rocket can be written as

$$\Delta V_{\text{total}} = \sum_{i=1}^{N} C_i \ell n\left(\frac{1}{\lambda_i + \delta_i}\right) \tag{3.30}$$

The overall payload ratio λ_o for a multistage rocket is the product of all the λ_i and can be expressed as

$$\lambda_o = \prod_{i=1}^{N} \lambda_i \tag{3.31}$$

Equations (3.28) and (3.29) can be used to obtain the mass ratio required for each stage i of a multistage rocket.

Example 3.3

Consider both a two-stage vehicle and a three-stage vehicle for the launch of the 900-kg (2000-lbm) payload. Each stage uses a liquid H_2-O_2 chemical rocket ($C = 4115$ m/s, 13,500 ft/s), and the ΔV_{total} of 14,300 m/s (46,900 ft/s) is split evenly between the stages. Because each stage has the same ΔV and effective exhaust velocity C, the payload ratio λ_i of the stages of a multistage vehicle are the same. The payload ratio for a stage λ_i is 0.1460 for a two-stage vehicle and 0.2840 for a three-stage vehicle. Table 3.4 summarizes the results for one-, two-, and three-stage vehicles. Note that a very large reduction in initial vehicle mass is obtained when going from a single-stage vehicle to a two-stage vehicle (a two-stage vehicle is 4.5% of the mass of the single-stage vehicle), and only a slight reduction in mass is obtained going from a two-stage vehicle to a three-stage vehicle (a three-stage vehicle is 93% of the mass of the two-stage vehicle).

Table 3.4 Multistage vehicle sizes for a 900-kg payload at a ΔV of 14,300 m/s with liquid H_2-O_2

	Single-stage vehicle	Two-stage vehicle	Three-stage vehicle
Stage ΔV	14,300 m/s	7150 m/s	4,767 m/s
Stage δ_i	0.03	0.03	0.03
Stage λ_o	0.0009590	0.02130	0.02290
Vehicle m_o	938,480 kg	42,250 kg	39,300 kg
1st Stage m_{dw}	28,170 kg	1,270 kg	1,180 kg
1st Stage m_{pl}	900 kg	6,170 kg	11,200 kg
2nd Stage m_o		6,170 kg	11,200 kg
2nd Stage m_{dw}		185 kg	336 kg
2nd Stage m_{pl}		900 kg	3,180 kg
3rd Stage m_o			3,180 kg
3rd Stage m_{dw}			95 kg
3rd Stage m_{pl}			900 kg

3.3 Rocket Propulsion Engines

Figure 3.7 shows the basic features of any propulsion system. The function of the propulsion system is to combine energy with matter to produce a directed stream of high-speed particles. That portion of the propulsion system that performs this function may be called the accelerator. In most systems, it is necessary to transport the propellant to the accelerator, and this implies pumps and a certain amount of plumbing. In some systems, it is necessary to supply the propellant in a special form. For example, the ion accelerator requires the propellant in the form of an ionized gas. We lump all of these functions under the heading Propellant Feed System in Fig. 3.7. In all propulsion systems, it is necessary to convert the energy stored onboard the vehicle into a form that is compatible with the particular mechanisms used to accelerate the exhaust particles. Thus there must be an energy conversion system as shown in Fig. 3.7. The energy conversion system may range from a single combustion chamber, wherein the energy of chemical bonds is released, to a nuclear-electric power plant. For the purposes of further discussion, we divide propulsion systems into two broad categories: 1) thermal systems and 2) electric systems.

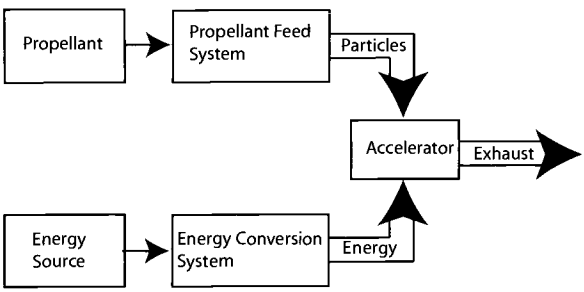

Fig. 3.7 Basic features of a rocket propulsion system.

3.3.1 Thermal Propulsion Systems

The basic principle of a thermal propulsion system is the paragon of simplicity. Energy from a chemical reaction, or from a nuclear reactor, or even from an electric arc discharge, is used to elevate the temperature of the propellant. The individual particles of the propellant thereby obtain considerable kinetic energy in the form of random thermal motion. The propellant is then expanded through a convergent-divergent nozzle whose purpose is to convert the random thermal energy of the propellant into a more or less unidirectional stream of high-speed particles. In this context, a thermal system is a hot gas generator with a nozzle for an accelerator. The nozzle-accelerator simply tries to make an ordered state of affairs out of the chaos of random thermal motion.

A key parameter in the analysis of propulsion systems in general is specific impulse I_{sp}. Thermodynamic analysis indicates, under some ideal assumptions, that the specific impulse of a thermal system is proportional to the quantity $T_c/\mathcal{M}$, where T_c is the propellant combustion chamber temperature and $\mathcal{M}$ is its molecular weight. To produce a high specific impulse in a thermal system, it is then desirable to have a high operating temperature in connection with a low molecular weight of exhaust products. The extent to which these two desirable objectives can be achieved is a rough basis for comparing thermal propulsion systems.

3.3.1.1 Chemical propulsion systems. Chemical propulsion systems are a subclass of thermal systems that use the energy released by exothermic chemical reaction in a combustion chamber. Chemical systems may be further divided into liquid-bipropellant engines, solid-propellant engines, and hybrid engines.

Figure 3.8a shows the essential features of a liquid rocket system. Two propellants (an oxidizer and a fuel) are pumped into the combustion chamber. The hybrid engine is shown in Fig. 3.8b, and the propellant is a solid fuel around the combustion chamber. We may summarize this system as follows:

1) Energy conversion system—combustion chamber,
2) Propellant feed system—fuel pump, oxidizer pump, and gas turbine (not required in hybrid system),
3) Accelerator—nozzle.

Figure 3.9 shows the essential features of a solid-propellant propulsion system. In this case, the fuel and oxidizer are mixed together and cast into a

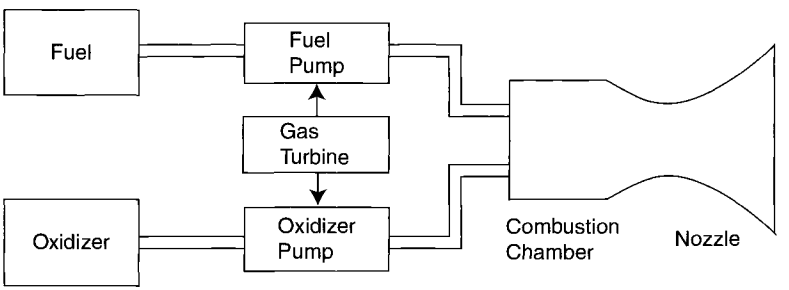

Fig. 3.8a Liquid-bipropellant rocket engine.

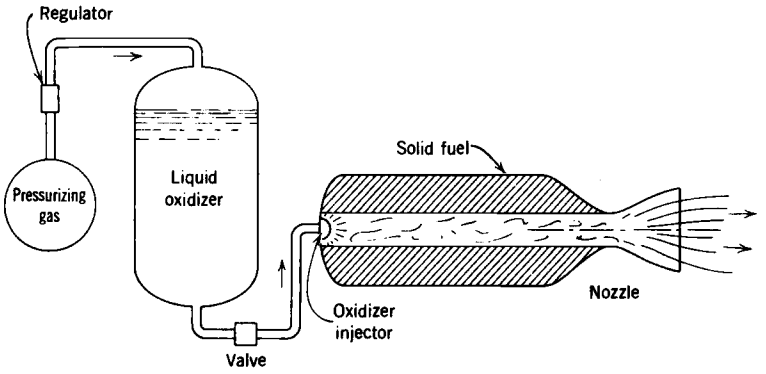

Fig. 3.8b Hybrid propulsion rocket engine.

solid mass called the grain. The grain is usually formed with a hole down the middle called the perforation and is firmly cemented to the inside of the combustion chamber. After ignition, the grain burns radially outward, and the hot combustion gases pass down the perforation and are exhausted through the nozzle.

We may summarize a solid-propellant system as follows:

1) Energy conversion system—combustion chamber
2) Propellant feed system—none
3) Accelerator—nozzle

The absence of a propellant feed system in the solid-propellant chemical rocket is one of its outstanding advantages.

Table 3.5 gives the pertinent characteristics of several different chemical propellants. It is important to note that the combustion temperature T_c and the molecular weight of exhaust products, $\mathcal{M}$, are largely determined by the specific chemical reaction taking place in the combustion chamber. It is possible to select different combinations and thereby achieve an increase in specific impulse, but there are limitations because the products of chemical combustion inherently tend to have relatively high molecular weights.

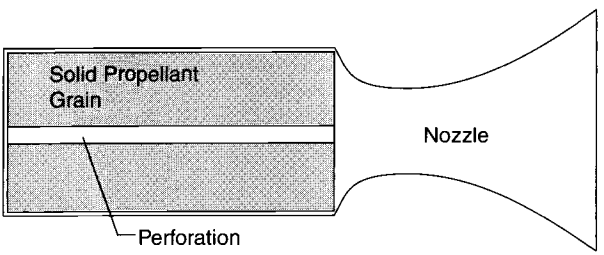

Fig. 3.9 Solid-propellant rocket engine.

Table 3.5 Characteristics of chemical propellants

Oxidizer and fuel	T_c, K	$\mathscr{M}$	I_{sp}, s
O_2-kerosene	3400	22	260
O_2-H_2	2800	9	360
F_2-H_2	3100	7.33	400
Nitrocellulose	2300–3100	22–28	200–230

This discussion serves to point out an important characteristic of chemical propulsion systems, namely, the oxidizer and fuel serve as both the source of energy and the source of particles for the propulsion system. Thus the process of supplying energy to the accelerator and the process of supplying particles to the accelerator are closely related. These fundamental facts place an upper bound of about 400 s on the specific impulse I_{sp} obtainable by chemical means.

3.3.1.2 Nuclear heat transfer propulsion systems. Figure 3.10 shows the essential features of the nuclear heat transfer propulsion system. As the name suggests, this system contains a nuclear reactor that serves two important purposes: 1) it produces the energy necessary to heat the propellant gas to a high temperature; 2) it transfers this energy to the propellant gas. Thus the reactor serves both as an energy source and a heat exchanger. Once heated in the reactor, the hot propellant gas is expanded through a nozzle in the manner characteristic of all thermal systems. The major components of this system are:

1) Energy conversion system—solid core nuclear reactor
2) Propellant feed system—pump and turbine
3) Accelerator—nozzle

An important feature of the nuclear heat transfer system is that the source of exhaust particles and the source of energy are independent. The propellant supplies the particles and the reactor supplies the energy. Thus the propellant need not be selected on the basis of its energy content, but can be selected on the basis of its suitability as exhaust material for a thermal propulsion system. In other words, the primary consideration in the selection of a propellant is low molecular weight.

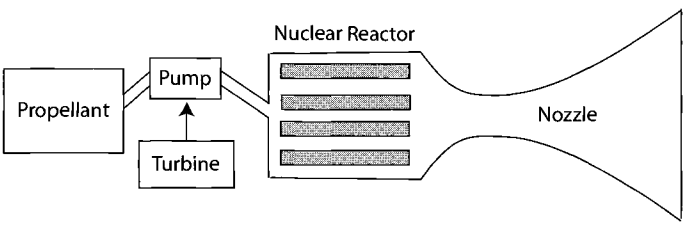

Fig. 3.10 Nuclear heat transfer propulsion system.

Table 3.6 Characteristics of propellants for nuclear propulsion

Propellant	T_c, K	$\mathcal{M}$	Max I_{sp}, s
H_2	2800	2	1000
C_3H_8 (propane)	2800	5.8	530
NH_3 (ammonia)	2800	8.5	460

Table 3.6 lists some important characteristics of different propellants for nuclear propulsion. Note that hydrogen produces the highest specific impulse because it has the lowest molecular weight. This fact is the primary reason that hydrogen is most often mentioned as the propellant for nuclear systems. Note also that the temperature T_c is the same for all three propellants listed in the table. The temperature T_c is determined primarily by the structural limitations of the reactor-heat exchanger and not by the nature of the propellant.

3.3.1.3 Electrothermal propulsion systems. Electrothermal propulsion systems use electric power to heat a propellant gas. One method of doing this is to pass the propellant around an electric arc as suggested by Fig. 3.11. The resulting propulsion system is sometimes called a thermal arcjet. A second possibility is to use tungsten heater elements (temperature increased by electrical energy) as a mechanism for imparting thermal energy to the propellant. In either case, the propellant can be heated to a rather high temperature, perhaps as high as 10,000 K. The temperature could be made higher, but beyond about 10,000 K, a significant portion of the input energy is used up in ionization and disassociation of the atoms of the propellant. This energy (called 'frozen flow' losses) is, therefore, not available for the basic purpose of the device, which is to impart kinetic energy to a directed stream of particles. We should also add that at very high temperatures, the exhaust stream would contain significant pieces of the electrodes and nozzle. These two effects alone tend to place an upper bound on the temperature to which the propellant may be heated, and hence there is an upper bound (~2500 s) on the specific impulse of the electrothermal devices. The major components of the system are:

1) Energy conversion system—electric plant and arc chamber
2) Propellant feed system—propellant pump
3) Accelerator—nozzle

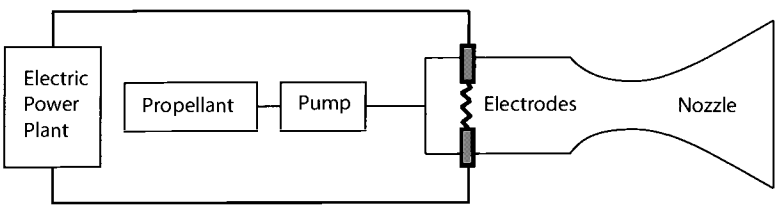

Fig. 3.11 Thermal arcjet propulsion system.

The electrothermal system is also characterized by the fact that the propellant plays no part in the process of supplying energy to the accelerator. The system also requires an electric power plant in the energy conversion system, and this feature is an important consideration in the design of vehicles propelled by electrothermal means. Because of the electric power plant, this system is often classified as an electric propulsion system. We have called it a thermal system because of the characteristic pattern of a high temperature gas plus expansion through a nozzle.

3.3.2 Electric Propulsion Systems

Electric propulsion systems are characterized by an accelerator that makes use of the interaction of electromagnetic fields and charged particles. In a rather crude sense, the electric charge on a particle provides a way for an electromagnetic field to regulate and direct the motion of the particle. In particular, it is possible to accelerate the particle to a high speed and eject it from a rocket vehicle. As should be clear by now, the ejection of high-speed particles is the very essence of rocket propulsion.

This simple picture of an electric propulsion system conceals some rather basic subtleties. First, the propellant feed system for such a system must do more than merely transport the propellant to the accelerator. It must also operate on the propellant to produce significant amounts of ionized particles at the entrance to the accelerator. Second, we note that electromagnetic fields are capable of accelerating charged particles to a very high specific impulse. However, it is necessary to supply the energy to the accelerator in electric form, and hence it is necessary to carry an electric power plant along on the mission. The electric power plant is the key to the problem because estimates of the power level for propulsion run into the megawatt range. In other words, the energy conversion system for an electric propulsion system is quite likely to be a very large and massive device. We will have more to say about this shortly.

3.3.2.1 Electromagnetic propulsion systems. Electromagnetic systems use a magnetic field to accelerate a collection of gas, called a plasma, to a speed on the order of 50,000 m/s (150,000 ft/s). A plasma is a fully or partially ionized gas containing essentially equal numbers of electrons and ions. Because the plasma is a rather good conductor of electricity, it will interact with electromagnetic fields. Because the plasma is also a gas, it displays the properties of a continuum or fluid. As a result, the basic description of the interaction of a magnetic field and a plasma combines all of the pleasantries of electromagnetic field theory and fluid mechanics into a whole new field of study called magnetohydrodynamics (MHD), or sometimes, magnetofluidmechanics.

In this new field, it is quite possible to write down the governing equations, but it is quite another matter to solve them. The factors involved in the study of MHD include the electrical and fluid properties of the plasma, the time history of the magnetic field (e.g., pulsed or continuous), and the geometry of the accelerator. The upshot of all of this is that there are MHD forces acting on the plasma. These

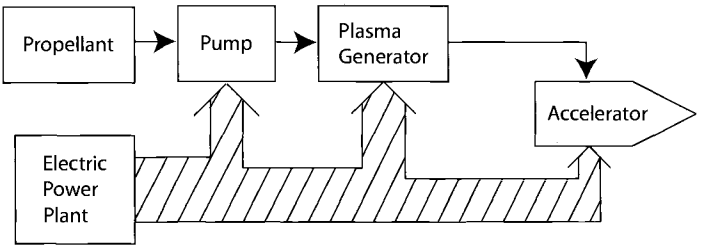

Fig. 3.12 Plasma propulsion system.

forces may act on the boundary of the plasma or may be distributed throughout the volume. In any case, the basic problem is to use these forces to drive the plasma out of the vehicle and thereby produce useful propulsive thrust.

Because of the variety of ways in which MHD forces can be made to act on a plasma, there is a bewildering array of plasma accelerators. The list of devices is constantly growing, and it is quite hopeless to try to classify them in any simple way that would do justice to the subject. In this case, we must be content with the schematic picture of the electromagnetic system shown in Fig. 3.12. We should recognize that the plasma generator and plasma accelerator shown in the figure represent a variety of possible devices. However, they are all united by the joint feature of using the action of a magnetic field on a macroscopically neutral plasma. The major components of the system are:

1) Energy conversion system—electric power plant
2) Propellant feed system—pump and plasma generator
3) Accelerator—plasma accelerator

The names MHD propulsion and plasma propulsion are often associated with this system. Although the specific impulse range for this system is not definitely established, the range 2,000–10,000 s is a reasonable consensus of the values given in open literature. Hydrogen, helium, and lithium are mentioned as propellants.

There is an important feature of the plasma system that is well worth mentioning at this point. The exhaust stream of this system is electrically neutral, and hence the neutralization problems of the ion engine, which we discuss next, are avoided in this case.

3.3.2.2 Electrostatic propulsion systems. The operating principle of this system is based on the static electric fields to accelerate and eject electrically charged particles. Figure 3.13 shows the main features of an ion engine. The propellant introduced into the engine is electrically neutral because charged particles cannot be stored in appreciable amounts. The ions are produced immediately before they are exposed to the accelerating field. This is accomplished by stripping off one or more electrons from the neutral propellant molecule, which is then a single- or multiple-charged positive ion. The positive ion is then accelerated by the electric field and ejected from the engine at a high speed. During this process of acceleration, it is necessary to focus and shape the ion beam to minimize the number of collisions between the ions and the structural members of the engine. Finally, both ions and electrons must be ejected from the engine to keep it

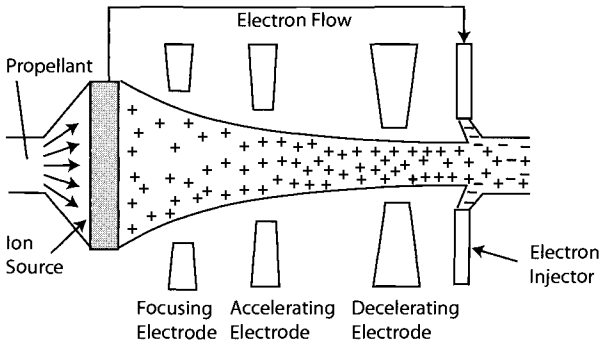

Fig. 3.13 Sketch of ion engine (electrostatic accelerator).

electrically neutral. This is accomplished by gathering up the electrons available at the ion source and transporting them to the engine exit where they are injected into the ion stream, thus hopefully producing an electrically neutral propulsive beam. The three major parts of an ion engine are the ion source, accelerator section, and beam neutralizer (electron injector).

In the simplest terms, a charged particle acquires a kinetic energy equal to its loss of electric potential energy when it "falls" through a difference in electric potential. This basic idea leads to the following expression for the exhaust speed on an ion engine:

$$\frac{1}{2}m_i V_e^2 = q\Delta v \tag{3.32}$$

where

Δv = net accelerating voltage, V
q = electric charge on the ion, C
m_i = mass of the ion, kg
V_e = exhaust speed, m/s

The factors affecting the exhaust speed are the net accelerating voltage Δv and the charge to mass ratio q/m_i of the exhausted particles.

To have a compact, efficient engine, it is desirable to have a rather high accelerating voltage, something on the order of several tens of thousands of volts. With this constraint in mind, we can investigate the influence of charge-to-mass ratio on the selection of the propellant.

Example 3.4

If we assume 1) that the ions are protons (disassociated and ionized hydrogen, $q/m_i = 0.91 \times 10^8$ C/kg) and 2) a reasonable accelerating voltage of 10,000 V, we obtain an exhaust speed of 1.34×10^6 m/s. This corresponds to a specific impulse of 134,000 s.

This value of specific impulse is several orders of magnitude higher than that obtainable from thermal systems. Thus it appears that the ion engine can produce incredibly high specific impulses.

However, several other considerations enter the picture to modify this apparently rosy situation. Performance analysis indicates there is an upper bound on the specific impulse so that the system has the capability of accomplishing useful missions. The reasons for this upper bound and the various factors involved will not emerge until one takes up the discussion of rocket performance. It suffices to say, at this point, that the ion engine is capable of producing specific impulses that are too high to be useful, and that a reasonable upper bound on specific impulse is something on the order of 100,000 s.

This situation points out one of the very profound differences between ion propulsion and thermal propulsion. In the latter, the propellant is often selected to make the specific impulse as high as possible. With ion propulsion, the problem is to select a propellant that will hold the specific impulse (at reasonable accelerator voltages) down to a useful value. For this reason, our interest centers on the heavier elements in the periodic table.

An additional consideration is the fact that the propellant must be supplied to the accelerator in ionized form, and this involves the expenditure of a certain amount of energy that is, therefore, not available for the purpose of propulsion. The amount of energy required for this purpose is measured by the ionization potential of an atom. Table 3.7 gives some important properties of the alkali metals. The alkali metals are the most promising propellants, because they combine the desirable features of low ionization potential together with reasonable accelerating voltages at useful specific impulses.

Figure 3.14 shows a schematic diagram of an electrostatic propulsion system. The major components may be identified as:

1) Energy conversion system—electric power plant
2) Propellant feed system—pump and ion source
3) Accelerator—ion engine

For obvious reasons, this system is also called an ion propulsion system. The preceding discussion points out there is an upper limit on the specific impulse for an ion system. It will also be difficult to obtain efficient operation at lower specific impulses as well. This lower limit arises due to a number of practical considerations such as electrode erosion at low accelerator voltages and

Table 3.7 Characteristics of propellants for electrostatic propulsion

Propellant	First ionization potential, ev	Atomic weight	Accelerating voltage at $I_{sp} = 10^5$ s
Sodium	5.14	23	12,000 V
Rubidium	4.18	85.4	45,000 V
Cesium	4.89	133.0	69,000 V

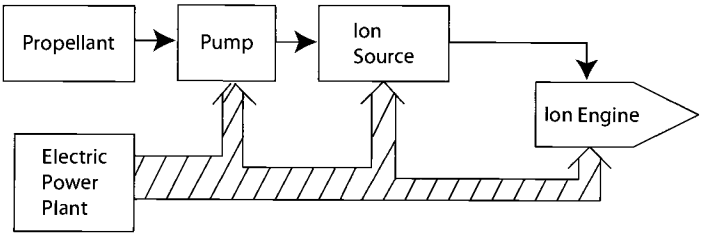

Fig. 3.14 Major features of an electrostatic (ion) propulsion system.

radiation from the hot surfaces of the ion source. The lower limit appears to be about 7500 s.

3.3.2.3 Electric power plants for space propulsion. A major component in any electric propulsion system is the electric power plant, and so we examine the situation regarding the generation of power in space. Electrical power will be required for a variety of reasons, including communication, control, life support, and propulsion. There are a great many methods of power generation that could satisfy some of these needs. Our interest is the generation of electric power for the purposes of propulsion. The very stringent requirements of electric propulsion narrow the field of interest.

One important factor is the power levels of interest in electric propulsion. For Earth satellite missions, such as altitude control, the power levels are on the order of 50–100 kW. More ambitious missions, such as lunar flight, require 1–3 MW. Manned interplanetary flight will require 20–100 MW of electric power. As a matter of perspective, we note that the installed capacity of Hoover Dam is 1200 MW. In other words, we are talking about electric power plants that are comparable to Earth-bound station applications that must operate for long periods of time in the rather unfriendly environs of space.

Our discussion will center on two parameters of space power plants: efficiency and specific mass α_c. Specific mass is defined as the mass of the power plant per unit output (electrical) power, or

$$\alpha_c = \frac{m_c}{P_c} \tag{3.33}$$

where

α_c = the specific mass, kg/W
P_c = the electrical output power, W
m_c = the total mass of the power plant, kg

All space power plants consist of at least three basic elements: an energy source, a conversion device, and a waste heat radiator. The only two energy sources that seem to offer much hope of producing the power levels of interest are the sun and the nuclear fission reactor. Solar collectors for the megawatt range become extremely large and must be constructed in a very sophisticated (i.e., flimsy) manner. Such

devices could stand only very small accelerations, and meteorite erosion of polished surfaces would be a problem. Nuclear power reactors are very powerful sources of energy. They have the important advantage that the power output is limited primarily by the capability of the reactor coolant to remove heat. They have a low specific mass and long life at high power levels. On the other hand, the reactor produces a radiation hazard for the crew and payload.

Both the solar collector and the nuclear reactor produce thermal energy. Among the possible methods of converting thermal energy into electrical energy are the following: thermionic, thermoelectric, and turboelectric. These three methods of conversion use vastly different mechanisms, but all three have one common feature—very low efficiency.

The inefficiency of power conversion schemes results in an increase in the specific mass of the power plant for two important reasons. First, the overall size and mass of the energy source must be increased to "supply" the losses. Second, the losses must somehow be dumped overboard by a waste heat rejection system. For the times of operation and power levels of interest in space propulsion, the only mechanism available for the rejection of heat waste is radiation into space. Because of the inherent low efficiency of the system, the waste heat radiator will be a very large and massive device. It will be susceptible to meteorite puncture and the attendant loss of working fluid from the system. For many designs, it appears that the waste heat radiator will be the dominant mass in the power plant for outputs exceeding a few hundred kilowatts.

Table 3.8 gives some projected characteristics of space power plants. As we have noted, all of the systems have low efficiency. The values of specific mass given in the table should be taken as tentative, particularly in the 1–10 MW range, because systems of this power level have not been built. Authorities differ widely in their estimate of the situation, and there is considerable uncertainty in the figures.

In all of this, we should not lose sight of the fact that the purpose of the propulsion system is to impart kinetic energy to a directed stream of particles. In electric propulsion, this energy first appears as thermal energy and then must be converted into electrical energy before it is in a form suitable for the basic task at hand. As we have suggested, the process of converting thermal energy into electricity in space is not noted for its efficiency. For the foreseeable future, it appears that electric propulsion will continue to pay a severe penalty for the several conversion processes involved in the generation of electric power. It is no exaggeration to state that the use of electric propulsion will be paced by the development of lightweight, efficient power conversion systems.

Table 3.8 Characteristics of space power systems

		Specific mass – α_c (kgm/W)	
System	Efficiency	10–100 kW	1–10 MW
Turboelectric	10–20%	0.02–0.04	0.003–0.004
Thermionic	5–10%	0.5–1.0	0.003–0.004
Thermoelectric	5–10%	0.5–1.0	—

3.3.3 Summary of Propulsion Systems

There are a number of ways in which propulsion systems can be classified to indicate certain fundamental features. In our discussion, we have used the classifications of *thermal* and *electric*. This classification is based on the mechanism used by the accelerator to impart kinetic energy to the exhaust stream. Thus propulsion systems may be summarized as follows.

Thermal:
1) Chemical
2) Nuclear heat transfer
3) Electrothermal (thermal arc jet)

Electric:
1) Electrostatic (ion)
2) Electromagnetic (plasma)

There are other fundamental features of propulsion systems of no less importance, and consideration of these leads to other possible classifications. For example, in our discussion, we noted that in certain systems, the propellant does not supply energy to the accelerator. That is, the source of energy and the source of particles are separate. Such propulsion systems are called separately powered. On the basis of this feature, we have the following classification.

Separately powered:
1) Nuclear heat transfer
2) Electrothermal (thermal arc jet)
3) Electromagnetic (plasma)
4) Electrostatic (ion)

Non-separately powered:
1) Chemical

Note that the chemical propulsion system is termed non-separately powered because the propellant supplies both energy and particles to the accelerator.

Propulsion systems can also be classified according to their performance capabilities as measured by the two key parameters, I_{sp} and thrust-to-weight (sea-level-weight) ratio. Table 3.9 presents typical values of these quantities for various propulsion systems.

The data in Table 3.9 offer several new ways to classify propulsion systems. For example, specific impulse values range over a fairly continuous spectrum from 200 (the lower end of the chemical range) up to 100,000 (the upper end

Table 3.9 Rocket performance summary

Propulsion system	I_{sp}, s	Thrust-to-weight ratio
Chemical	300–400	up to 10^2
Nuclear heat transfer	400–1000	up to 30
Electrothermal	400–2500	up to 10^{-2}
Electromagnetic	2000–10^4	up to 10^{-3}
Electrostatic	7500–10^5	up to 10^{-4}

of the ion range). Thus the order in which the systems are listed in Table 3.9 is a classification based on magnitude of specific impulse. There is, of course, some overlap, but in large measure, each of the systems fills a gap in the specific impulse spectrum.

A very important distinction between propulsion systems is found in Table 3.9. Note that there are several orders of magnitude difference between the thrust-to-weight ratio of electric propulsion systems and the chemical or nuclear propulsion systems. This leads to a classification of systems as either high thrust or low thrust.

High-thrust systems:
1) Chemical
2) Nuclear heat transfer

Low-thrust systems:
1) Electrothermal
2) Electromagnetic
3) Electrostatic

Note that all of the low-thrust systems require an electric power plant as the energy conversion system. This fact accounts for the low values of thrust-to-weight ratios for these systems. Significant increases in the thrust-to-weight capabilities of these systems can be achieved only by reducing the weight-per-unit power of space power plants.

Figure 3.15 is a summary of propulsion systems obtained by plotting the data in Table 3.9. Notice the very clear distinction between the high-thrust and low-thrust systems. Notice also that there is a fairly continuous range of specific impulse capability from 200 to 100,000 s with some significant overlapping among the electric propulsion systems.

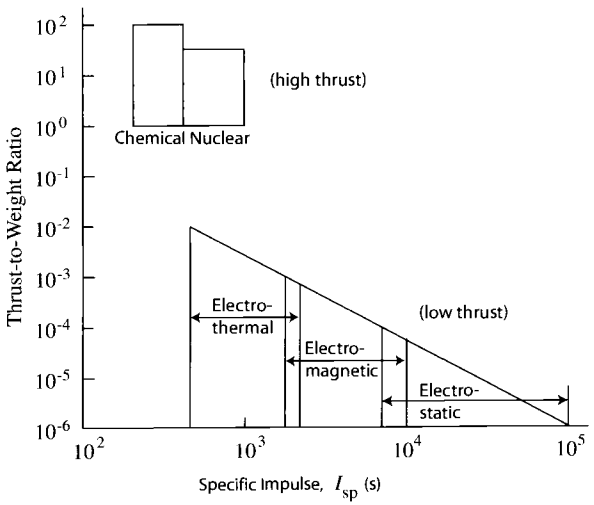

Fig. 3.15 Thrust-to-weight ratio vs specific impulse.

3.4 Types of Rocket Nozzles

The initial geometry of a circular-section rocket nozzle is fixed by the nozzle inlet, throat, and exit areas. The inlet area A_c is established by combustion chamber design considerations. The throat and exit areas are determined from a knowledge of the combustion chamber temperature and pressure, acceptable mean values of γ and R, the propellant mass flow rate, and the designed nozzle-pressure ratio $P_c/P_a = P_c/P_e$. With these data, the nozzle throat and exit areas can be obtained by application of the mass flow parameter (MFP). Having established A_c, A_t, and A_e (or the radii R_c, R_t, R_e), the problem of the nozzle contour design remains. Because of weight and space limitations, determination of the nozzle shape reduces to the problem of choosing a contour providing minimum length (a measure of volume and weight) and yielding maximum thrust. In addition, the selected contour must be sufficiently simple to manufacture.

3.4.1 Conical Nozzle

The conical nozzle represents a compromise of the length, thrust, and ease of manufacturing design criteria weighted somewhat in favor of the last factor. A conical nozzle consists of two truncated cones (Fig. 3.16), joined top to top along their axis by a suitable radius to form the nozzle throat. The combustion chamber is similarly faired into the convergent nozzle section. The converging contour of the nozzle is not critical as regards the flow, and a rather rapid change in cross section is permissible here with a conical apex half-angle on the order of 400 commonly used. The divergence angle of the supersonic portion of the nozzle, however, is limited by flow separation considerations and must not exceed a value of about 150. For divergence angles too much greater than 15 deg, the flow will separate from the nozzle walls short of the exit even though the nozzle is operating at design altitude $P_a = P_e$. Conversely, for a given divergence angle, the flow will separate if the nozzle back-pressure ratio P_a/P_e is too high ($P_a/P_e > 1$ when a nozzle is operating at an altitude lower than the design altitude). When separation occurs, oblique shock wave A (Fig. 3.17) is located inside the nozzle, and the gas flow is contained within the jet boundary or slip line shown. Figure 3.17 depicts the real flow situation that occurs (other than under ideal laboratory conditions) in place of normal shocks near the exit section as shown in Fig. 2.37.

Summerfield has established a criterion for judging whether or not separation is likely to occur in the exit section of a conical nozzle.[20] The criterion is based on

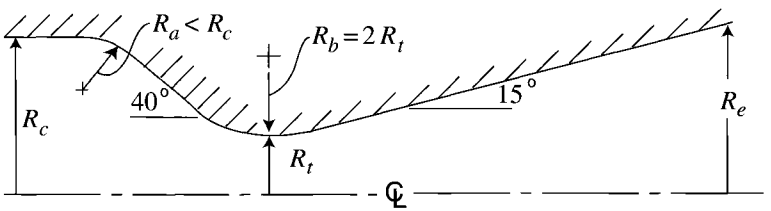

Fig. 3.16 Conical convergent-divergent nozzle.

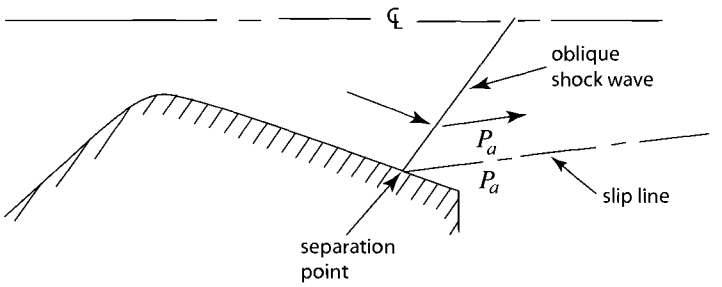

Fig. 3.17 Separation in overexpanded nozzle.

an accumulation of experimental separation data points from many sources. The experimental data give the pressure ratios P_a/P_{we} (P_{we} = wall pressure at exit = P_e for 15-deg conical nozzle) that produced flow separation in tests of 15-deg conical nozzles for various nozzle-pressure ratios. The data points are scattered throughout the cross-hatched region of Fig. 3.18. The Summerfield criterion states that for back-pressure ratios greater than 2.5, separation is likely to occur in the exit of a 15-deg conical nozzle for nozzle-pressure ratios in excess of 20. Current data on large rocket nozzles indicate that the critical back-pressure ratio for these large nozzles is 3.5. This increase in the permissible back-pressure ratio for no separation is to be expected as nozzle sizes increase because the boundary layer forms a smaller percentage of the total flow for larger nozzles. Using this modified Summerfield criterion value of 3.5, it should be noted that

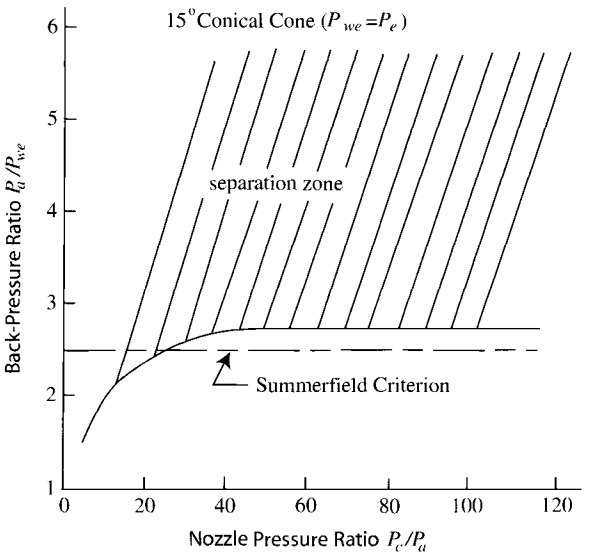

Fig. 3.18 Summerfield separation criterion.

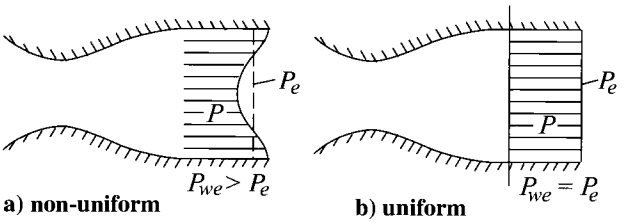

Fig. 3.19 Pressure profile at nozzle exit.

for large rocket nozzles, separation occurs when $P_a > 3.5\ P_{we}$. For a 15-deg conical nozzle, $P_{we} = P_e$ because the stream properties at the exit section are essentially uniform at the values determined by one-dimensional flow analysis. In some nozzles, the streams are not uniform across the exit section and $P_{we} > P_e$ (Fig. 3.19). Separation will occur sooner (at lower values of P_a) in a conical nozzle than in those of the same area ratio for which $P_{we} > P_e$.

3.4.2 Bell Nozzle

The bell-shaped nozzle of the Atlas sustainer engine (shown in Fig. 3.20) is designed to reduce the thrust and length disadvantages of a conical nozzle. To reduce length, a bell-shaped nozzle employs a high divergence angle at the throat with a very rapid expansion of the gases from the throat. The flow is then turned rather abruptly back toward the axial direction. The comparative lengths of a bell-shaped (L_B) and a conical (L_C) nozzle having the same expansion ratio are indicated in Fig. 3.20. The bell-shaped contour is used on several current engines. The bell-shaped nozzle on the H-1 Saturn 1B engine has a length 20%

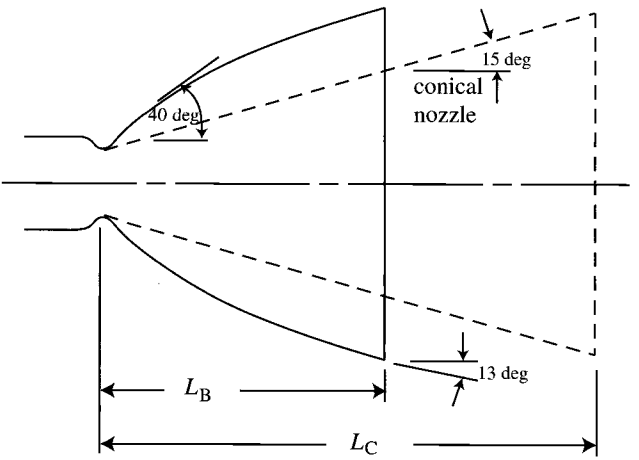

Fig. 3.20 Bell-shaped nozzle $A_e/A_t = 25$ (Atlas sustainer engine).

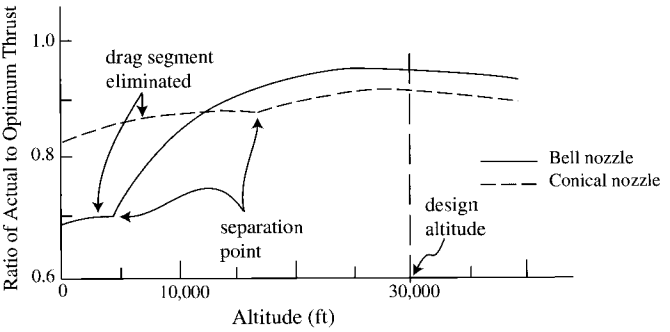

Fig. 3.21 Ratio of actual-to-optimum thrust for bell-shaped and conical nozzles vs altitude (pressure ratio).

less than the length that would be required for a 15-deg conical nozzle with the same 8:1 area ratio.

3.4.3 Free-Expansion (Plug) Nozzle

Figure 3.21 depicts the performance loss of conventional convergent-divergent (C-D) nozzles at off-design pressure ratios. To avoid the large penalties (Fig. 3.21) at liftoff pressure ratios, relatively low-area-ratio nozzles must be used. Note that high-area-ratio nozzles, however, improve performance at altitude. (Atlas booster—low-altitude operation—area ratio is 8:1. Atlas sustainer—high-altitude operation—area ratio is 25:1). Use of a high-altitude nozzle, such as the Atlas sustainer, at liftoff incurs a large performance degradation. To avoid such losses at off-design operation, a rocket nozzle with an adjustable area ratio that provides optimum expansion at each ascending altitude is needed. Obviously, a variable area C-D nozzle is not feasible because of hardware considerations. It is possible, however, to design a nozzle so that the expanding flow is not bound by immovable solid walls. In such free-expansion nozzles (Figs. 3.22 and 3.23), the expanding flow is bound by a solid surface and a free-to-move slip-line expansion surface. The adjustable slip-line boundary, in effect, produces a variable area ratio nozzle that accommodates itself to changing nozzle pressure ratios. Free-expansion nozzles, therefore, tend to operate at optimum expansion, with the ratio of thrust-to-optimum-thrust being quite insensitive to altitude variations (Fig. 3.24). The free-expansion nozzles shown in Fig. 3.22 have been dubbed "plug nozzles." The manner in which the flow adjusts to varying back-pressures for the two types of plug nozzles of Fig. 3.22 is shown in Figs. 3.25 and 3.26.

Note the performance gain of a free-expansion-type nozzle in the test data curves of Fig. 3.24 (ratio of actual thrust to optimum thrust plotted versus altitude). The improved performance of the free-expansion type of nozzle over the bell nozzle at lower off-design altitudes is evident. The absence of large thrust

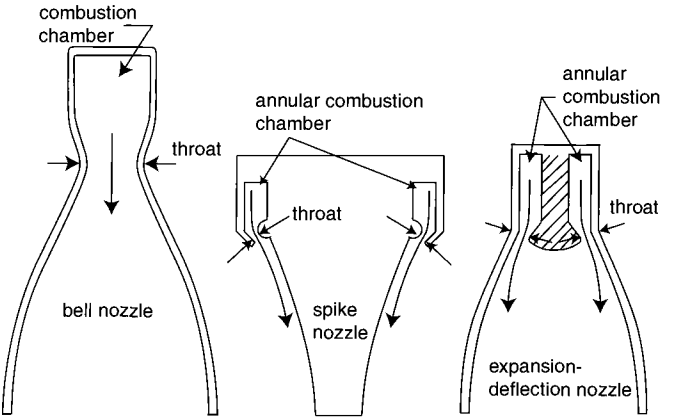

Fig. 3.22 Bounded and free-expansion nozzles.

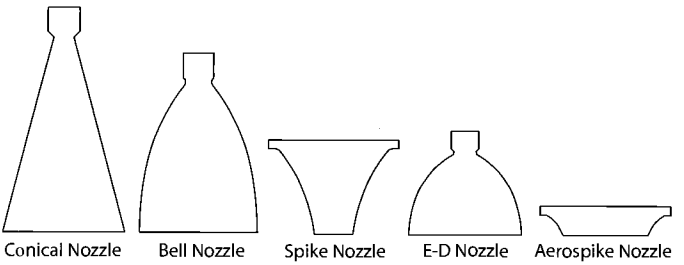

Fig. 3.23 Nozzle type and size comparison.

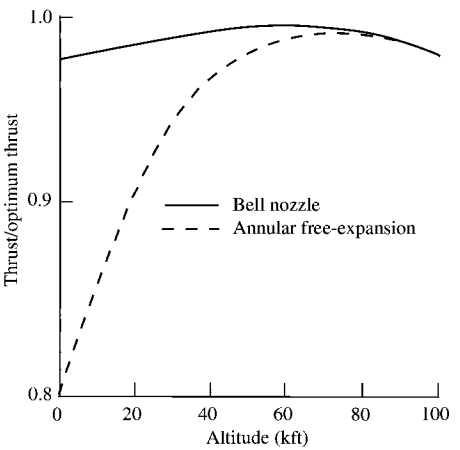

Fig. 3.24 Performance comparison of a bell nozzle and a free-expansion nozzle.

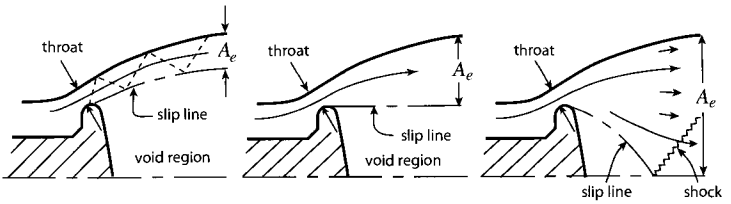

a) Low altitude **b) Intermediate altitude** **c) High altitude**

Fig. 3.25 Exhaust flow pattern from expansion-deflection (ED) plug nozzle.

losses at lower altitudes suggests that a free-expansion-type nozzle would be particularly suited for use in both boosters or in single-stage ballistic missiles.

3.5 Parameters for Chemical Rockets

The nozzle mass flow, ideal thrust equation, characteristic velocity, exit velocity, and area ratio for isentropic flow follow from the relations developed in Chapter 2. The purpose here is simply to write expressions for these quantities in forms that are particularly useful for substitution into the ideal chemical rocket-thrust coefficient equation to be developed later in this section. After deriving the mass flow and ideal thrust equations desired, the characteristic velocity C^* will be introduced. The expressions for mass flow rate, ideal thrust, C^*, V_e, and A_e/A_t will be written in terms of quantities relating to rocket nozzle hardware and gross parameters, such as chamber pressure and temperature. To identify the flow properties more closely with the physical hardware, the following notations will be adopted: the subscript 'c' will denote combustion chamber; thus, P_c and T_c will designate the combustion chamber temperature and pressure, which we will assume corresponds to the total pressure and temperature of the ideal flow; the nozzle throat conditions will be represented by a subscript 't' and exit section quantities by a subscript 'e.' Because the flow in the ideal rocket nozzle is isentropic, with sonic flow at the throat, we have $A_t = A^*$, $P_t = P^*$, etc.

3.5.1 Rocket Nozzle Mass Flow

The mass flow through a nozzle is conveniently determined by applying the mass flow parameter equation at the nozzle throat where $M_t = 1.0$. We have, from Eq. (2.76), using the notation just introduced,

$$\frac{\dot{m}\sqrt{T_c}}{P_c A_t} = \frac{(1)\sqrt{\gamma g_c/R}}{\left\{1 + \dfrac{\gamma - 1}{2}(1)^2\right\}^{\frac{\gamma+1}{2(\gamma-1)}}}$$

$$\frac{\dot{m}\sqrt{T_c}}{P_c A_t} = \sqrt{\frac{g_c}{R}\gamma\left\{\frac{\gamma+1}{2}\right\}^{-\frac{\gamma+1}{\gamma-1}}} = \frac{\Gamma}{\sqrt{R/g_c}} \tag{3.34}$$

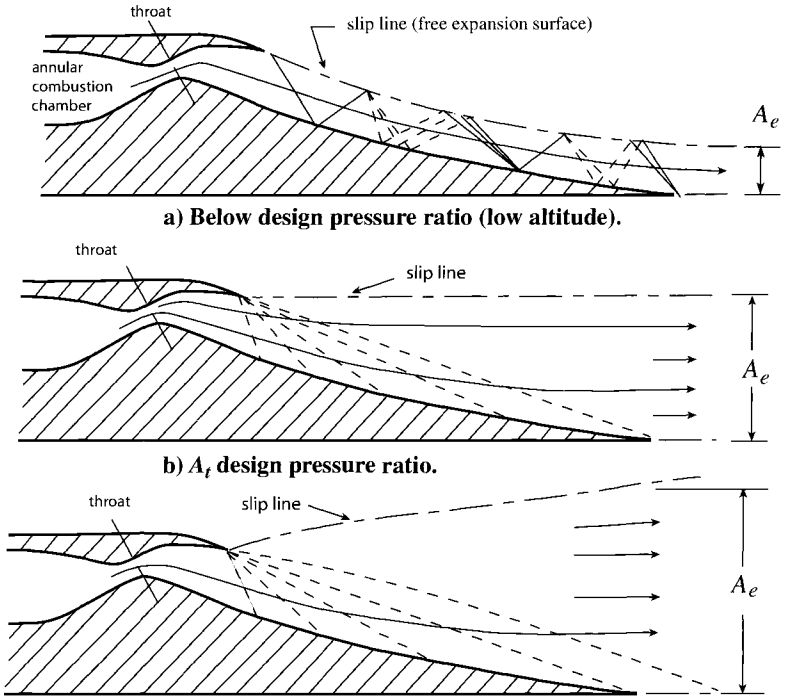

Fig. 3.26 Exhaust flow pattern from annular free-expansion nozzle.

where

$$\Gamma = \sqrt{\frac{\gamma}{\left\{\frac{\gamma+1}{2}\right\}^{\frac{\gamma+1}{\gamma-1}}}} \tag{3.35}$$

We introduce Γ because it is simpler to write than the square root of many exponential terms involving γ. Γ is a function of the combustion gases' specific heat ratio alone and is given in Table 3.10 for a range of γ values. The ratio Γevaluated for air should give the value of Fig. 2.20 at $M = 1.0$ and $\gamma = 1.4$.

To illustrate the use of Table 3.10 and the little-but-ever-with-us matter of units, let us evaluate $\Gamma/\sqrt{R/g_c}$ for $\gamma = 1.4$ and $R = 53.34$ ft-lbf/lbm-°R:

$$\frac{\dot{m}\sqrt{T_c}}{P_c A_t} = \frac{\Gamma}{\sqrt{R/g_c}} = \frac{0.6847}{\sqrt{53.34/32.174}} = 0.5318 \frac{\text{lbm-}\sqrt{^\circ R}}{\text{lbf-s}}$$

This value agrees with the GASTAB software.

Table 3.10 Γ tabulated vs γ

γ	Γ	γ	Γ	γ	Γ
1.14	0.6366	1.21	0.6505	1.28	0.6636
1.15	0.6386	1.22	0.6524	1.29	0.6654
1.16	0.6406	1.23	0.6543	1.30	0.6673
1.17	0.6426	1.24	0.6562	1.31	0.6691
1.18	0.6446	1.25	0.6581	1.32	0.6726
1.19	0.6466	1.26	0.6599	1.33	0.6779
1.20	0.6485	1.27	0.6618	1.34	0.6847

Solving Eq. (3.34) for the mass flow rate, we obtain the following simple expression for rocket nozzle mass flow:

$$\dot{m} = P_c A_t g_c \frac{\Gamma}{\sqrt{R g_c T_c}} \tag{3.36}$$

The mass flow rate is seen to be determined by the nozzle throat area, the combustion chamber pressure, and the quantity $(\Gamma/\sqrt{Rg_cT_c})$. The latter is determined by the combustion gas temperature T_c and the combustion gases' characteristics, γ and R.

Example 3.5

Determine the mass flow rate of a gas with a molecular weight of 18 and $\gamma = 1.25$ through a choked throat area of 2 ft^2 from a combustion chamber whose pressure is 2000 psia and temperature is 3000°R. From Eq. (3.35) or Table 3.10, $\Gamma = 0.6581$. For the gas, $R = \mathscr{R}/\mathscr{M} = 1545/18 = 85.83$ ft-lbf/(lbm-°R). Using Eq. (3.36), we have

$$\dot{m} = P_c A_t g_c \frac{\Gamma}{\sqrt{R g_c T_c}} = \frac{2000 \times 2 \times 144 \times 32.174 \times 0.6581}{\sqrt{85.83 \times 32.174 \times 3000}} = 4237 \text{ lbm/s}$$

3.5.2 Ideal Thrust Equation

The ideal thrust is given by Eq. (3.1). Using the one-dimensional isentropic relationship of Chapter 2 for V_e, we get

$$V_e = \sqrt{\frac{2\gamma}{\gamma - 1} R g_c T_c \left\{ 1 - \left(\frac{P_e}{P_c} \right)^{\frac{\gamma - 1}{\gamma}} \right\}}$$

Combining this equation for V_e and Eq. (3.36) for the mass flow rate with Eq. (3.1), we get the following ideal thrust equation in terms of areas, pressures, and γ:

$$F_i = P_c A_t \left\{ \Gamma \sqrt{\frac{2\gamma}{\gamma - 1}\left[1 - \left(\frac{P_e}{P_c}\right)^{\frac{\gamma-1}{\gamma}}\right]} + \left(\frac{P_e}{P_c} - \frac{P_a}{P_c}\right)\frac{A_e}{A_t} \right\} \tag{3.37}$$

3.5.3 Characteristic Velocity, C^*

The quantity $(\sqrt{Rg_c T_c}/\Gamma)$ of Eq. (3.36) has the dimensions of velocity, and as just noted, its value is determined by the combustion gas temperature T_c and the combustion gases' characteristics, γ and R. For a given propellant, therefore, the quantity $(\sqrt{Rg_c T_c}/\Gamma)$ is a characteristic of the reaction process of the propellant because the propellant's combustion process will establish the flame temperature T_c and the composition of the gas mixture making up the products of combustion.

The composition of the combustion gases in turn establishes γ and the molecular weight $\mathscr{M}$ (hence R, which equals $\mathscr{R}_u/\mathscr{M}$, where $\mathscr{R}_u$ is the universal gas constant). This quantity, which has the dimensions of velocity and a value characterized by the propellant combustion process, is called the characteristic velocity C^*. (The superscript star bears no relation to the star notation used for sonic flow properties.) Thus, by definition

$$C^* = \frac{\sqrt{Rg_c T_c}}{\Gamma} \tag{3.38}$$

The characteristic velocity can be determined theoretically by the methods of thermochemistry.[14] This theoretical value can be compared with an experimentally determined value of C^* to evaluate the actual combustion process against the "theoretical" combustion process. Experimental values of C^* can be obtained in a rocket motor test by measuring the propellant mass flow rate, the chamber pressure P_c, and the nozzle throat area A_t. These data and Eq. (3.36) give the experimental value C_x^*. Thus,

Experimental:

$$C_x^* = \frac{P_c A_t}{\dot{m}/g_c}$$

with P_c, A_t, and m obtained from measured data. Also, from Eq. (3.38) defining C_i^*

Theoretical:

$$C_i^* = \frac{\sqrt{Rg_c T_c}}{\Gamma}$$

with R, T_c, and Γ obtained from thermochemistry.

A well-designed combustion chamber should give a value of C_x^* in excess of 90% of the theoretical value computed by thermochemical means and Eq. (3.38). An experimental value of C_x^* less than 0.9 of the theoretical value would be evidence of a poorly designed combustion chamber or injector.

With present-day propellants, C^* ranges from 3000 to 7000 ft/s. The value of C^* for the design point operation of the Atlas sustainer rocket motor is 5440 ft/s.

3.5.4 Nozzle Exit Velocity, V_e

The expansion flow process through an ideal nozzle from a pressure P_c to P_e is shown on the temperature-entropy diagram of Fig. 3.27. The kinetic energy imparted to the expanding gas is proportional to the vertical distance indicated. There is also depicted the maximum possible kinetic energy that could be delivered to the expanding gas. This maximum corresponds to an expansion to zero absolute temperature.

It is seen from the diagram that $V_e^2/(2c_p) = T_c - T_e$. Using this and the perfect gas relations accompanying the T-s diagram of Fig. 3.27, we obtain

$$V_e = \sqrt{\frac{2\gamma}{\gamma - 1}\frac{\mathcal{R}}{\mathcal{M}} g_c T_c \left\{1 - \left(\frac{P_e}{P_c}\right)^{\frac{\gamma-1}{\gamma}}\right\}} \tag{3.39}$$

The ratio of the exit velocity to the maximum possible exit velocity is

$$\frac{V_e}{V_{\max}} = \sqrt{1 - \left(\frac{P_e}{P_c}\right)^{\frac{\gamma-1}{\gamma}}} \tag{3.40}$$

Because a high exit velocity means, for a given nozzle mass flow, a large momentum flux and, hence, thrust, let us examine the terms of Eq. (3.39) upon which V_e depends. These variables are 1) the pressure ratio P_c/P_e, 2) the chamber temperature T_c, and 3) the molecular weight $\mathcal{M}$.

Varying the specific heat ratio γ is of little practical use and will not be considered. Before discussing these factors, let us first note that for chemically

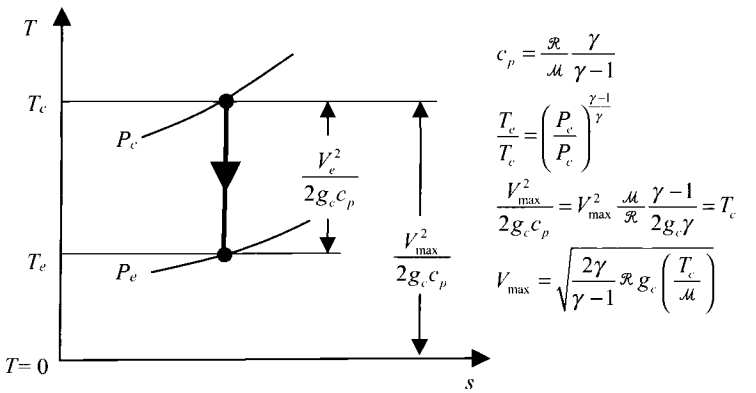

Fig. 3.27 Nozzle expansion process.

propelled rockets, the original source of kinetic energy V_e^2 is the ejected material itself, i.e., the propellant's chemical energy. For chemical rockets, therefore, the choice of propellant is fixed by the selection of fuel and oxidizer. If, on the other hand, the rocket combustion chamber is replaced with a nuclear reactor, then the reactor's fuel becomes the original source of the propellant's kinetic energy. In this case, the energy is supplied by a source independent of the propellant, and one can choose a propellant without consideration of its chemical energy. This is pointed out here because T_c and $\mathscr{M}$ are somewhat interdependent for a chemical rocket but can be completely independent in other cases.

Allowance can be made for these different situations in considering the influence of T_c and $\mathscr{M}$ on V_e in the following:

1) *Pressure Ratio* P_c/P_e. The pressure ratio determines what fraction of the maximum possible velocity is ideally attained. As P_c/P_e increases, V_e increases very rapidly (Fig. 3.28) up to a pressure ratio of 10. Above this value of P_c/P_e, the velocity increases less rapidly with pressure ratio. Increasing chamber pressure is thus seen to have a favorable influence on V_e. The favorable influence is limited, however, because a higher P_c means increased structural weight requirements and, for liquid chemical propellant rockets, increased propellant feed system weight. Note also that as P_c/P_e increases, the nozzle-area ratio must increase. The Atlas booster ($A_e/A_t = 8$) and sustainer ($A_e/A_t = 25$) operate with a pressure ratio (P_c/P_e) of 60 and 250, respectively.

2) *Chamber Temperature* T_c. The exit velocity V_e increases as the square root of the chamber temperature T_c. The upper limit on T_c is fixed by either structural (in the case of a nonchemical nuclear rocket) or chemical considerations. Usually, in a liquid chemical rocket, cooling alleviates the

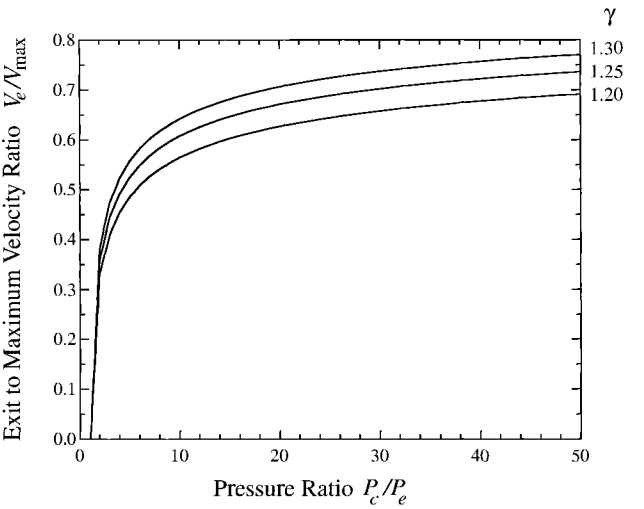

Fig. 3.28 Fraction of maximum velocity vs pressure ratio.

structural limitation so that T_c is limited by chemical considerations. From a chemical point of view, it would appear that fuels with greater chemical energy will give an increasingly higher temperature T_c. This is true up to a temperature where dissociation of the combustion products—CO_2 dissociating into C and O_2 for example—occur and absorb energy that would otherwise be available for increasing T_c. Thus we find that for the best fuels, dissociation sets an upper temperature limit of about 6000°R.

3) *Molecular Weight* $\mathscr{M}$. Since V_e varies inversely as the square root of $\mathscr{M}$, propellants with a low molecular weight are preferable. For chemical rockets, the molecular weight of the propellant is determined by the fuel and oxidizer and is on the order of 20. In a nuclear rocket, one has a freer choice of a propellant than in a chemical rocket, and hydrogen with a molecular weight of 2 can be used. A nuclear rocket, using H_2 for a propellant and having the same temperature T_c and pressure ratio P_c/P_e as a chemical rocket with $\mathscr{M} = 20$, would have a higher V_e factor $\sqrt{20/2} = \sqrt{10}$. This factor is approximately equal to the ratio of the exit velocities of the LOX-RP and the nuclear-H2 propulsion systems of Table 3.2. This is to be expected since the LOX-RP and the nuclear-H_2 systems each encounter the same structural limitations on T_c and P_c/P_e, so that the main difference in V_e between the two is due to the lower molecular weight of the nuclear system's propellant.

4) *Simultaneous Effect of Combustion Temperature and Molecular Weight on* V_e. Up to this point, we have considered the combustion temperature and molecular weight effects on exit velocity independent of each other. For a given fuel-oxidizer combination in a chemical rocket, the combustion temperature T_c and the molecular weight $\mathscr{M}$ of the propellant are interdependent. They vary simultaneously with mixture ratio and chamber pressure. Consequently, the influence of these two variables on V_e must, in this case, be considered together as the mixture ratio is varied for a given chamber pressure. Figure 3.29 shows the variation of T_c and $\mathscr{M}$, along with V_e, for a chamber pressure of 300 psia and a pressure ratio of $P_c/P_e = 20.4$ for a LOX-gasoline fuel combination. As the mixture ratio is increased from 1.5, we observe that the combustion temperature and molecular weight each increase. The former increases more rapidly initially so that the net effect of the ratio $T_c/\mathscr{M}$ on the velocity V_e [Eq. (3.39)] is to increase V_e as shown. As the mixture ratio is increased beyond 2.5, the molecular weight increases more rapidly than the temperature, thus producing lower values of the ratio $T_c/\mathscr{M}$ and, hence, V_e. The optimum mixture ratio for the LOX-gasoline system is, therefore, a value of 2.5. This compares with a stochiometric mixture ratio of 3.5 for LOX-gasoline. The mixture ratio of the LOX-RP-l combination used in the Atlas booster engine (YLR89-NA-7 model) is 2.38.

The curves of Fig. 3 .29 are for one chamber pressure. If a similar set of curves were drawn for a higher chamber pressure, the same general results would be obtained except that V_e would be higher due to the favorable effect of a higher pressure in reducing dissociation of the combustion products. Increasing the chamber pressure to obtain higher V_e, however, produces the unfavorable effect of increasing dead weight because of the higher stress levels introduced

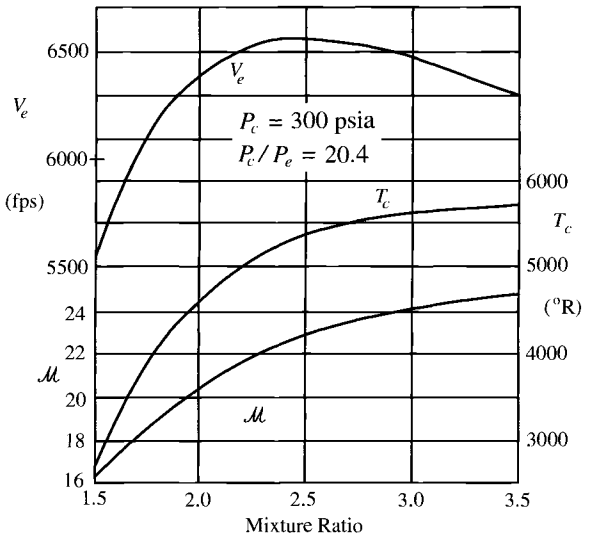

Fig. 3.29 LOX-gasoline performance vs mixture ratio.

and the added fuel feed system pressure requirements. In any particular application, the operating chamber pressure selected must be a compromise of the several interrelated factors that chamber pressure effects.

3.5.5 Area Ratio and Velocity Ratio in Terms of the Pressure Ratio

The isentropic area ratio A/A^*, calculated in program GASTAB and written as a function of the Mach number in Eq. (2.77), can be used to obtain the nozzle area ratio A_e/A_t when the exit Mach number is known. It is useful in rocket performance work to have the nozzle area expansion ratio A_e/A_t expressed in terms of the ratio of the rocket chamber pressure to the exit section pressure P_c/P_e for isentropic flow. This relation can be obtained rather directly by use of the mass flow parameter given in terms of $\Gamma/\sqrt{R/g_c}$ [Eq. (3.34)] and pressure ratio [Eq. (3.2)]. Thus with $P_t = P_c$ and $T_t = T_c$, we have from Eq. (3.34)

$$\frac{\dot{m}\sqrt{T_c}}{P_c A_t} = \frac{\Gamma}{\sqrt{R/g_c}}$$

Writing Eq. (3.2) for the exit station ($P = P_e$) and rearranging gives

$$\frac{\dot{m}\sqrt{T_c}}{P_c A_e} = \sqrt{\frac{2g_c}{R}\left(\frac{\gamma}{\gamma-1}\right)\left[\left(\frac{P_e}{P_c}\right)^{\frac{2}{\gamma}} - \left(\frac{P_e}{P_c}\right)^{\frac{\gamma+1}{\gamma}}\right]}$$

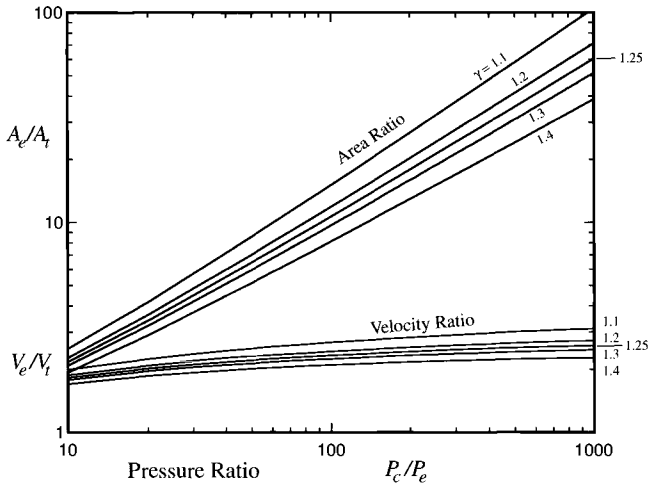

Fig. 3.30 Area and velocity ratios vs pressure ratio.

Dividing Eq. (3.34) by the preceding equation gives the desired expression for the area ratio A_e/A_t [Eq. (3.35)]:

$$\frac{A_e}{A_t} = \frac{\Gamma}{\sqrt{\dfrac{2\gamma}{\gamma-1}\left[\left(\dfrac{P_e}{P_c}\right)^{\frac{2}{\gamma}} - \left(\dfrac{P_e}{P_c}\right)^{\frac{\gamma+1}{\gamma}}\right]}} \tag{3.41}$$

Similarly, the ratio of the velocity at the exit, V_e, to the velocity at the throat, V_t, can be expressed as

$$\frac{V_e}{V_t} = \sqrt{\frac{\gamma+1}{\gamma-1}\left[1 - \left(\frac{P_e}{P_c}\right)^{\frac{\gamma-1}{\gamma}}\right]} \tag{3.42}$$

Equations (3.41) and (3.42) are plotted for several values of γ vs P_c/P_e on Fig. 3.30 as A_e/A_t and as V_e/V_t, respectively. Note that an area ratio (A_e/A_t) of 50 is required to obtain a value of two for V_e/V_t with $\gamma = 1.4$.

3.5.6 Thrust Coefficient

The thrust coefficient is defined as the thrust F divided by the product of the chamber pressure and throat area, P_cA_t, or

$$C_F \equiv \frac{F}{P_cA_t} \tag{3.43}$$

Why use thrust coefficient in place of thrust?

1) It is a dimensionless quantity.
2) Its numerical values have a convenient size that fall in range 0.6–2.2.
3) It provides a figure of merit that is independent of size of rocket and forms a common basis with which to compare different-sized rockets.

3.5.7 Ideal Thrust Coefficient, C_{Fi}

The proportionality factor between F_i and $P_c A_t$ is called ideal thrust coefficient. From Eqs. (3.37) and (3.43) we have

$$C_{Fi} = \Gamma \sqrt{\frac{2\gamma}{\gamma - 1}\left[1 - \left(\frac{P_e}{P_c}\right)^{\frac{\gamma-1}{\gamma}}\right]} + \left(\frac{P_e}{P_c} - \frac{P_a}{P_c}\right)\frac{A_e}{A_t} \tag{3.44}$$

C_{Fi} is a function of A_e/A_t and P_c/P_a—the nozzle area and pressure ratios—for given γ. Note that A_e/A_t determines P_e/P_c through Eq. (3.41). Using Eqs. (3.44) and (3.41), one can express the maximum value of the ideal thrust coefficient as

$$(C_{Fi})_{\max} = \Gamma \sqrt{\frac{2\gamma}{\gamma - 1}} \tag{3.45}$$

3.5.8 Optimum Thrust Coefficient, $(C_{Fi})_{opt}$

For optimum ideal thrust, $P_e = P_a$ and Eq. (3.44) gives

$$(C_{Fi})_{\text{opt}} = \Gamma \sqrt{\frac{2\gamma}{\gamma - 1}\left[1 - \left(\frac{P_e}{P_c}\right)^{\frac{\gamma-1}{\gamma}}\right]} \tag{3.46}$$

Note: It can be shown that

$$\frac{A_e}{A_t} = \frac{\gamma - 1}{2\gamma}\left(\frac{P_e}{P_c}\right)^{\frac{1}{\gamma}} \frac{(C_{Fi})_{\text{opt}}}{1 - \left(\frac{P_e}{P_c}\right)^{\frac{\gamma-1}{\gamma}}} \tag{3.47}$$

3.5.9 Vacuum Thrust Coefficient, $(C_{Fi})_{vac}$

For vacuum, $P_a = 0$ and Eqs. (3.44) and (3.46) give

$$(C_{Fi})_{\text{vac}} = (C_{Fi})_{\text{opt}} + \frac{P_e}{P_c}\frac{A_e}{A_t} \tag{3.48}$$

or

$$(C_{Fi})_{\text{vac}} = C_{Fi} + \frac{P_a}{P_c}\frac{A_e}{A_t} \tag{3.49}$$

3.5.10 Graphs for Determining Ideal Thrust Coefficient

Equation (3.44) can be solved conveniently by use of graphs. In Fig. 3.31 $(C_{Fi})_{\text{vac}}$ is plotted vs γ and nozzle area ratio ε. Figure 3.30, which gives a plot of nozzle area ratio and velocity ratio vs P_c/P_e, is handy in computational work when the area ratio or P_c/P_e is known and the value of the other is required. Figures 3.32–3.35 present C_{Fi} for various conditions. Figure 3.32 is a plot of $(C_{Fi})_{\text{opt}}$ vs nozzle pressure ratio with optimum expansion. The dashed curves in the lower right of Fig. 3.33 ($\gamma = 1.2$), Fig. 3.34 ($\gamma = 1.25$), and Fig. 3.35 ($\gamma = 1.3$) are plots of (C_{Fi}) with flow separation (Summerfield criterion for separation of $P_a > 3.5\ P_{\text{we}}$). The remaining curves present Eq. (3.44) for various values of P_c/P_a.

Example 3.6

We can illustrate the use of the graph of Fig. 3.31 with an example. Let us find C_{Fi} for a rocket at 100,000-ft altitude with an area ratio of 25, $\gamma = 1.29$, and a chamber pressure $P_c = 500$ psia. Because the value of γ is not one of the specific values plotted in Figs. 3.30 and 3.32–3.35, use of Fig. 3.31 presents a convenient

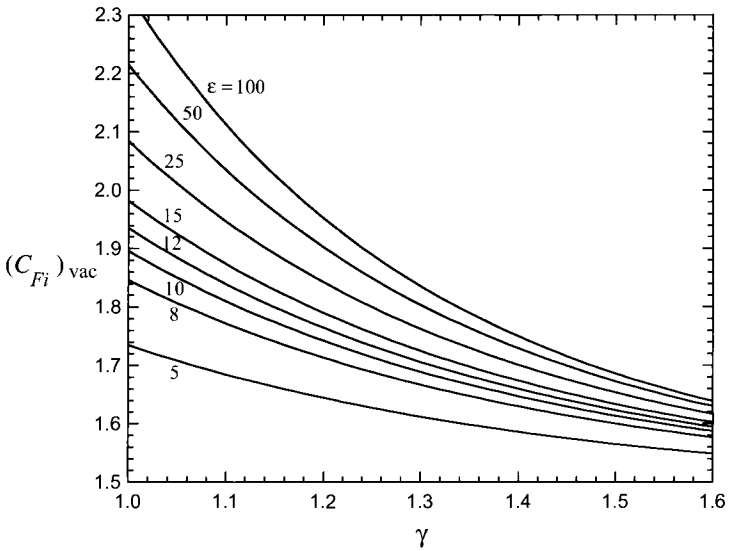

Fig. 3.31 Vacuum thrust coefficient, $(C_{Fi})_{\text{vac}}$.

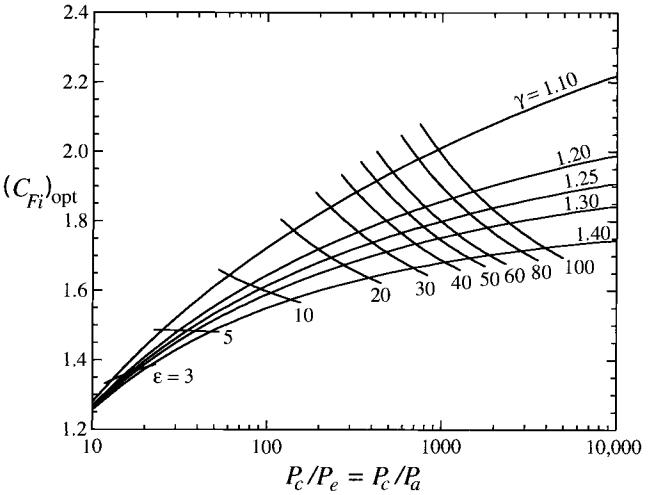

Fig. 3.32 Optimum thrust coefficient vs pressure ratio.

way of finding C_{Fi} without interpolation. First, we note that Eq. (3.45) can be written as

$$C_{Fi} = (C_{Fi})_{\text{vac}} - \frac{P_a}{P_c}\frac{A_e}{A_t}$$

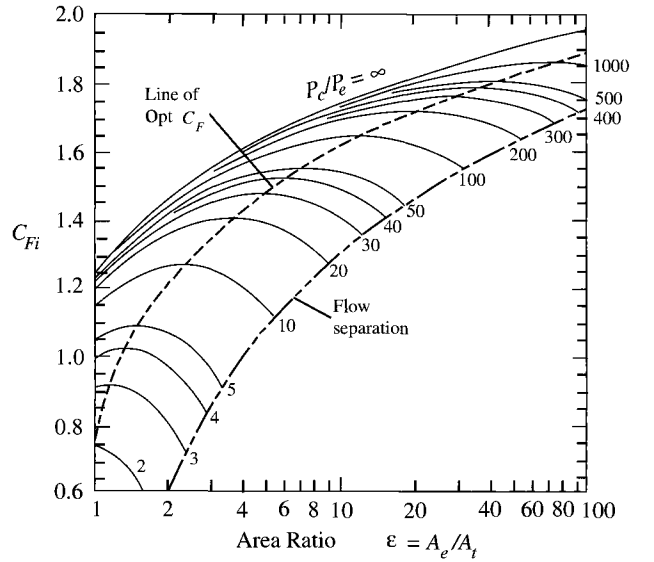

Fig. 3.33 Ideal thrust coefficient vs area ratio ($\gamma = 1.2$).

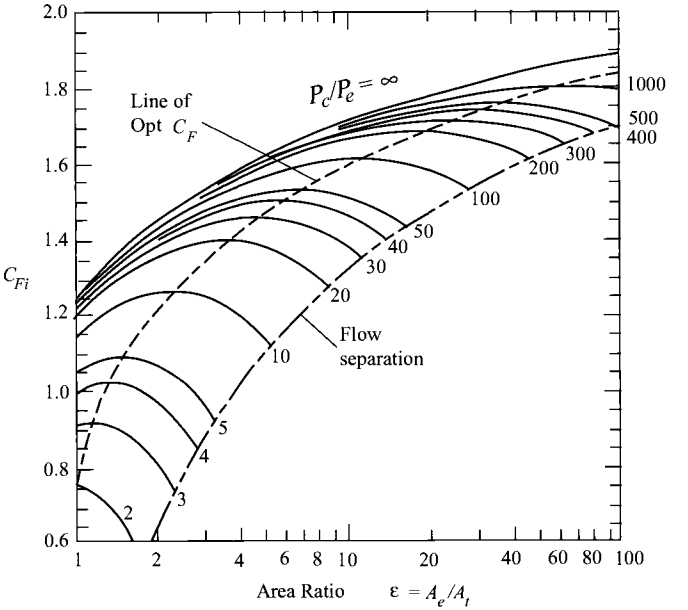

Fig. 3.34 Ideal thrust coefficient vs area ratio ($\gamma = 1.25$).

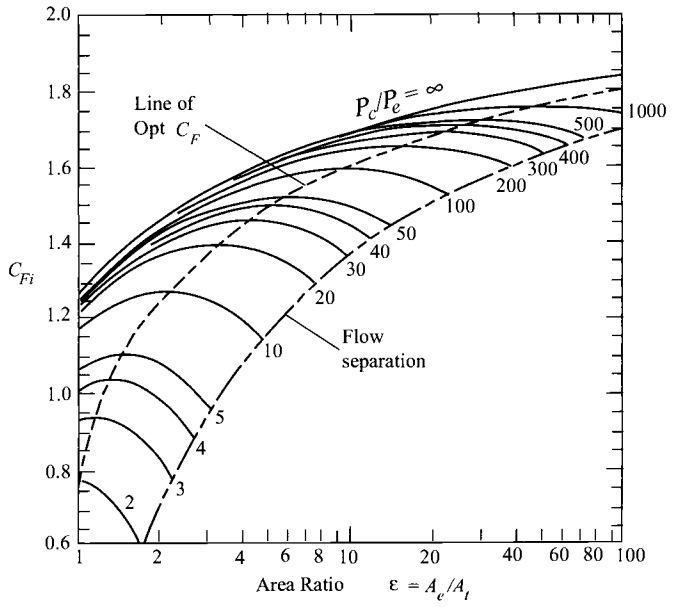

Fig. 3.35 Ideal thrust coefficient vs area ratio ($\gamma = 1.3$).

or

$$C_{Fi} = (C_{Fi})_{\text{vac}} - \Delta C_F \tag{3.50a}$$

where

$$\Delta C_F = \frac{P_a}{P_c}\frac{A_e}{A_t} \tag{3.50b}$$

Thus C_{Fi} can easily be found by getting the value of $(C_{Fi})_{\text{vac}}$ from Fig. 3.31 and calculating the value of ΔC_F provided that the nozzle flow is not separated. From the standard atmosphere data in Appendix A, the atmospheric pressure P_a at 100,000 ft is 23.28 lbf/ft^2 (2116 × 0.0110) or 0.162 psia. Using the given value for P_c and this value of P_a gives a value of 3086 for the ratio P_c/P_a. A quick check of Figs. 3.34 and 3.35, with this value of P_c/P_a and the given value for nozzle area ratio ε, shows that the nozzle is operating underexpanded, and flow is not separated in the nozzle. Thus Fig. 3.31 and Eqs. (3.50a) and (3.50b) can be used to determine the ideal thrust coefficient. We obtain $(C_{Fi})_{\text{vac}} = 1.770$ from Fig. 3.31 corresponding to $\gamma = 1.29$ and $\varepsilon = 25$. Using the value of P_a determined in the preceding and the given data for P_c and ε in Eq. (3.50b) gives

$$\Delta C_F = \frac{P_a}{P_c}\frac{P_e}{A_t} = \frac{0.162}{500}25 = 0.008$$

Thus

$$C_{Fi} = (C_{Fi})_{\text{vac}} - \Delta C_F = 1.770 - 0.008 = 1.762$$

3.5.11 Relationship Between C, C*, and C_{Fi}

Noting that from Eqs. (3.36) and (3.38), we can write

$$P_c A_t = \dot{m}C^*/g_c \tag{i}$$

from Eqs. (3.5) and (3.43), we have

$$C_{Fi} = \frac{F_i}{P_c A_t} = \frac{\dot{m}C/g_c}{P_c A_t} \tag{ii}$$

Substituting Eq. (i) into Eq. (ii) and solving for the effective exhaust velocity C gives

$$C = C_{Fi}C^* \tag{3.51}$$

This equation shows that the effective exhaust velocity C can be expressed as the product of the ideal thrust coefficient (dependent primarily on the nozzle area and pressure ratios) times the characteristic velocity (dependent on thermochemistry).

Example 3.7

The space shuttle main engine (SSME) operates for up to 520 s in one mission at altitudes over 100 miles. The nozzle expansion ratio ε is 77:1, and the inside exit diameter is 7.54 ft. Assume a calorically perfect gas with the following properties: $\gamma = 1.25$, $P_c = 3000$ psia, $T_c = 6890°$F, and $R = 112$ ft-lbf/(lbm-°R).

We want to calculate the following:

1) Characteristic velocity C^*.
2) Mass flow rate of gases through the nozzle.
3) Mach number at exit M_e.
4) Altitude that nozzle is "on-design."
5) Altitude that flow in nozzle is just separated (assume separation occurs when $P_a > 3.5\ P_{we}$).
6) Ideal thrust coefficient C_{Fi} and the ideal thrust F_i in 5000-ft increments from sea level to 40,000 ft; in 10,000-ft increments from 40,000 to 100,000 ft; and at vacuum.
7) $(I_{sp})_{vac}$ for the engine.
8) Actual exhaust velocity V_e and effective exhaust velocity C at sea level.

Solution: We assume isentropic flow of a perfect gas with constant specific heats.

a) Characteristic velocity C.*

$$C^* = \sqrt{Rg_cT_c}/\Gamma$$

where $\Gamma = 0.6581$ for $\gamma = 1.25$ and $T_c = 7350°$R. Thus

$$C^* = \sqrt{112 \times 32.174 \times 7350}/0.6581 = 7820 \text{ ft/s}$$

b) Mass flow rate.

$$\dot{m} = P_cA_tg_c/C^*$$

where

$$A_e = \frac{\pi D_e^2}{4} = \frac{\pi \times 7.54^2}{4} = 44.65 \text{ ft}^2$$

Then

$$A_t = \frac{A_e}{\varepsilon} = \frac{44.65}{77}144 = 83.50 \text{ in.}^2$$

Thus

$$\dot{m} = \frac{3000 \times 83.50 \times 32.174}{7820} = 1031 \text{ lbm/s}$$

c) Mach number at exit M_e. Using Eq. (2.27) for the flow between the throat and exit of the nozzle, we have

$$\frac{A_e}{A_t} = \frac{1}{M_e}\left\{\frac{2}{\gamma+1}\left(1+\frac{\gamma-1}{2}M_e^2\right)\right\}^{\frac{\gamma+1}{2(\gamma-1)}} \tag{3.52}$$

This equation cannot be solved directly for the exit Mach number in terms of the area ratio A_e/A_t; however, it can be set into a form that permits fast iteration to the solution. Because there are two Mach numbers (a subsonic value and a supersonic value) that can give the same area ratio, we must be careful that we get the correct value. Solving Eq. (3.52) for the Mach number in the denominator gives an equation that will yield the subsonic Mach number corresponding to the area ratio A_e/A_t, or

Subsonic solution:

$$M_e = \frac{1}{A_e/A_t}\left\{\frac{2}{\gamma+1}\left(1+\frac{\gamma-1}{2}M_e^2\right)\right\}^{\frac{\gamma+1}{2(\gamma-1)}} \tag{3.53}$$

Equation (3.53) can be used to iterate on a solution for the subsonic exit Mach number by starting with a guess (say 0.5) and substituting it into the right-hand side of the equation and then solving for a new exit Mach number. The new value of the Mach number is substituted into the equation and another value of Mach number calculated. This iterative process is repeated until successive values do not change very much (say about 0.001).

The supersonic iteration equation for the exit Mach number is obtained from Eq. (3.52) by solving for the Mach number within the brace, or

Supersonic solution:

$$M_e = \sqrt{\frac{\gamma+1}{\gamma-1}\left\{M_e\frac{A_e}{A_t}\right\}^{\frac{2(\gamma-1)}{\gamma+1}} - \frac{2}{\gamma-1}} \tag{3.54}$$

The nozzle pressure ratio P_c/P_e is great enough to give supersonic flow at the exit, and iterative use of Eq. (3.54) gives the results tabulated in Table 3.11 starting with a guess of 4.0 for the exit Mach.

d) Nozzle design altitude. The nozzle design altitude corresponds to that altitude where $P_c = P_a$. With both the exit Mach number and the chamber pressure known, the nozzle exit pressure can be determined using Eq. (2.73) for P_t/P written as

$$P_e = P_c\left(1+\frac{\gamma-1}{2}M_e^2\right)^{-\gamma/\gamma-1} \tag{3.55}$$

Thus $P_e = 2.187$ psia.

Table 3.11 Solution to exit Mach

Guess M_e	Eq. (3.54)
4.0	4.9148
4.9148	5.0657
5.0657	5.0881
5.0881	5.0913
5.0913	5.0918
5.0918	5.0919
5.0919	5.0919

Thus $M_e = 5.0919$ (this answer can be found quickly using the GASTAB program).

This exit pressure corresponds to a value for the atmospheric pressure ratio δ of 0.1488 (=2.187/14.696). Using the Standard Atmospheric data of Appendix A, the nozzle design altitude is about 44,700 ft.

e) Nozzle separation altitude. The nozzle separation altitude corresponds to that altitude where $P_a = 3.5 \times P_{we} = 7.655$ psia. This pressure corresponds to a value for δ of 0.5209 (= 7.655/14.696). Using the Standard Atmospheric data of Appendix A, the nozzle separation altitude is about 17,000 ft.

f) Ideal thrust and thrust coefficient. The ideal thrust coefficient C_{Fi} is given by Eq. (3.44) in terms of γ, P_c/P_e, A_e/A_t, and P_a/P_c. Equation (3.41) gives the nozzle expansion ratio A_e/A_t in terms of the nozzle pressure ratio P_c/P_e. When the flow in the nozzle is not separated, both the nozzle expansion ratio A_e/A_t and the nozzle pressure ratio P_c/P_e will remain constant at their design values of 77 and 1372 (=3000/2.187), respectively. At altitudes below 17,000 ft, the flow in the nozzle will separate, and the effective nozzle expansion ratio A_e/A_t and nozzle pressure ratio P_c/P_e will be less than their design values.

The ideal thrust coefficient C_{Fi} and ideal thrust F_i will be obtained using Eqs. (3.44) and (3.43), respectively, and Eq. (3.41) will be used, when needed, to obtain the effective nozzle expansion ratio A_e/A_t. The required equations are Eq. (3.41):

$$\frac{A_e}{A_t} = \frac{\Gamma}{\sqrt{\dfrac{2\gamma}{\gamma - 1}\left[\left(\dfrac{P_e}{P_c}\right)^{\frac{2}{\gamma}} - \left(\dfrac{P_e}{P_c}\right)^{\frac{\gamma+1}{\gamma}}\right]}}$$

Eq. (3.44):

$$C_{Fi} = \Gamma\sqrt{\frac{2\gamma}{\gamma - 1}\left[1 - \left(\frac{P_e}{P_c}\right)^{\frac{\gamma-1}{\gamma}}\right]} + \left(\frac{P_e}{P_c} - \frac{P_a}{P_c}\right)\frac{A_e}{A_t}$$

Eq. (3.43):

$$F_i = C_{Fi} P_c A_t$$

The values of C_{Fi} vs altitude are plotted in Fig. 3.36, and values of thrust are plotted in Fig. 1.42b. Note the change in slope of the plots at the separation altitude. As expected, the actual thrust is increased by the flow separation at altitudes below 17,000 ft. This is one of the few times when nature is kind. Table 3.12 shows the ideal thrust coefficient and ideal thrust vs altitude of the SSME.

g) Calculate specific impulse in vacuum, $(I_{sp})_{vac}$. Using the definition of specific impulse given by Eq. (3.6), we write

$$(I_{sp})_{vac} = \frac{(F_i)_{vac} g_c}{\dot{m} g_o} = \frac{469{,}790 \times 32.174}{1030 \times 32.174} = 456.1 \text{ s}$$

h) Actual exhaust velocity V_e and effective exhaust velocity C at sea level. From Eq. (1.52), we can solve for the effective exhaust velocity C in terms of the thrust and mass flow rate to get

$$C = \frac{F_i g_c}{\dot{m}} = \frac{404{,}880 \times 32.174}{1030} = 12{,}647 \text{ ft/s}$$

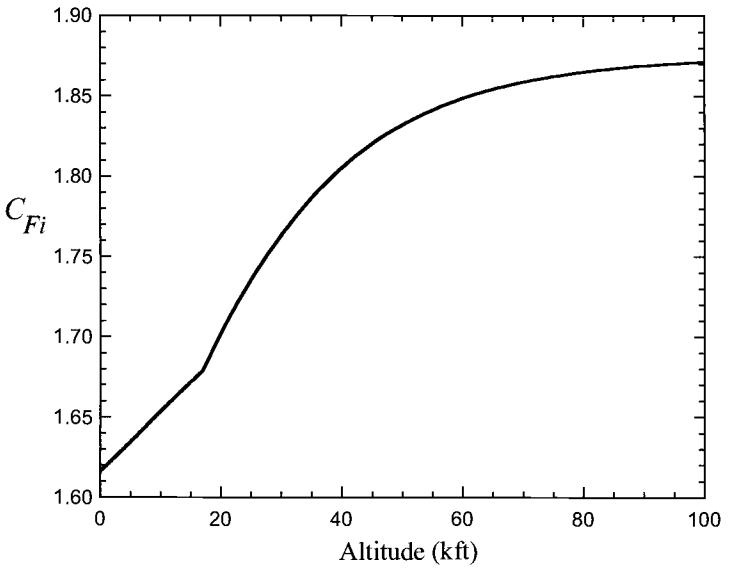

Fig. 3.36 Calculated ideal thrust coefficient of SSME.

Table 3.12 Ideal thrust coefficient and ideal thrust vs altitude of SSME

Altitude, ft	P_a, psia	P_e, psia	A_e/A_t	C_{Fi}	F_i, lbf
0	14.696	4.199	46.7	1.61627	404,880
5,000	12.228	3.494	53.8	1.63450	409,560
10,000	10.108	2.888	62.2	1.65345	414,190
15,000	8.297	2.371	72.4	1.67172	418,770
17,000	7.655	2.187	77.0	1.67892	420,570
20,000	6.759	2.187	77.0	1.70191	426,330
25,000	5.461	2.187	77.0	1.73523	434,670
30,000	4.373	2.187	77.0	1.76315	441,670
35,000	3.468	2.187	77.0	1.78638	447,490
40,000	2.730	2.187	77.0	1.80532	452,230
50,000	1.692	2.187	77.0	1.83197	458,910
60,000	1.049	2.187	77.0	1.84847	463,040
70,000	0.650	2.187	77.0	1.85871	465,610
80,000	0.404	2.187	77.0	1.86502	467,190
90,000	0.252	2.187	77.0	1.86893	468,170
100,000	0.160	2.187	77.0	1.87129	468,760
Vacuum	0	2.187	77.0	1.87540	469,790

Because we have determined the value of C_{Fi} at sea level and C^*, Eq. (3.51) can also be used to determine the effective exhaust velocity C at sea level. Substituting the values into Eq. (3.51) gives

$$C = C_{Fi}C^* = 1.61627 \times 7820 = 12{,}639 \text{ ft/s}$$

This value of C is about 0.06% lower than the value determined that can be attributed to roundoff.

The actual exhaust velocity V_e can be written in terms of the effective exhaust velocity using Eq. (1.51) as

$$V_e = C - (P_e - P_a)A_e g_c/\dot{m}$$

Using the value of C calculated and the values of P_e, P_a, and A_e/A_t determined in part f for sea level, the exhaust velocity can be calculated:

$$V_e = 12{,}647 - \frac{(4.199 - 14.696)(46.7 \times 83.50)32.174}{1030}$$

$$V_e = 12{,}647 + 1279 = 13{,}926 \text{ ft/s}$$

Example 3.8

Determine the C_{Fi} of the H-1 rocket engine at its design altitude of 80,000 ft using Fig. 3.31. The H-1 rocket engine has a chamber pressure P_c of 633 psia and a nozzle expansion ratio ε of 8. Assume $\gamma = 1.33$.

Solution: Using the standard atmosphere data in Appendix A at 80,000 ft, we get $P_a = 0.406$ psia and by calculation obtain $P_a/P_c = 0.00064$. Because the nozzle is at its design altitude, the flow is not separated in the nozzle. For $\varepsilon = 8$ and $\gamma = 1.33$, we have $(C_{Fi})_{\text{vac}} = 1.660$ from Fig. 3.31. For $\varepsilon = 8$ and $P_a/P_c = 0.00064$, we get $\Delta C_F = 0.005$. Thus,

$$C_{Fi} = (C_{Fi})_{\text{vac}} - \Delta C_F = 1.655$$

3.5.12 Liquid-Propellant Rockets

Liquid-propellant rockets can be classified into two general propellant categories: bipropellant (fuel and oxidizer) and monopropellant. Ordinarily, bipropellants are used for applications requiring high thrust, such as launch vehicles, and monopropellants are used for small control rockets. The focus in this section is on bipropellant rockets.

A typical liquid-propellant rocket consists of four main parts: rocket engine, propellants, propellant feed system, and propellant tanks. Figure 3.37 shows a schematic diagram of a bipropellant rocket with turbopump feed system. The turbopump feed system is usually used for high-thrust/long-duration rockets. In this system, fuel and oxidizer are burned in the gas generator. The resultant high temperature and pressure gas is expanded through the turbine before being exhausted. The turbine powers both the fuel and oxidizer pumps. This turbopump-fed rocket engine cycle is referred to as an *open cycle* because the working fluid exhausted from the turbine is discharged overboard. In *closed-cycle* turbopump feed systems, all of the working fluid exhausted from the turbine is injected into the combustion chamber of the rocket engine.

For a liquid-propellant rocket, the steady-state mass flow rate of propellant and combustion chamber pressure P_c are determined by a balance between mass flow rate entering the chamber from the fuel and oxidizer pumps and the mass flow rate leaving through the nozzle throat. The chamber pressure and mixture ratio of oxidizer to fuel directly affect the combustion process and its resultant products. For a given application, a high chamber pressure P_c is normally desirable because it permits higher nozzle thrust coefficient C_F and specific impulse I_{sp}. Most of the data presented in this section are for optimum expansion through a nozzle from a chamber pressure P_c of 1000 psia to an exhaust pressure P_e of 14.7 psia.

3.5.12.1 Propellants. Bipropellant liquid rockets use an oxidizer and a fuel. Typical oxidizers are liquid oxygen (O_2, also referred to as LOX), liquid fluorine (F), hydrogen peroxide (H_2O_2), chlorine trifluoride (ClF_3), nitric acid (HNO_3), and nitrogen tetroxide (N_2O_4). Common fuels include RP-1 (a hydrocarbon kerosene-like mixture), liquid hydrogen (H_2), hydrazine (N_2H_4), unsymmetrical dimethylhydrazine [$(CH_3)_2NNH_2$ also referred to as UDMH], monomethylhydrazine (CH_3NHNH_2), ethyl alcohol (C_2H_5OH), and liquid ammonia (NH_3). Table 3.13 shows some typical oxidizer/fuel combinations.

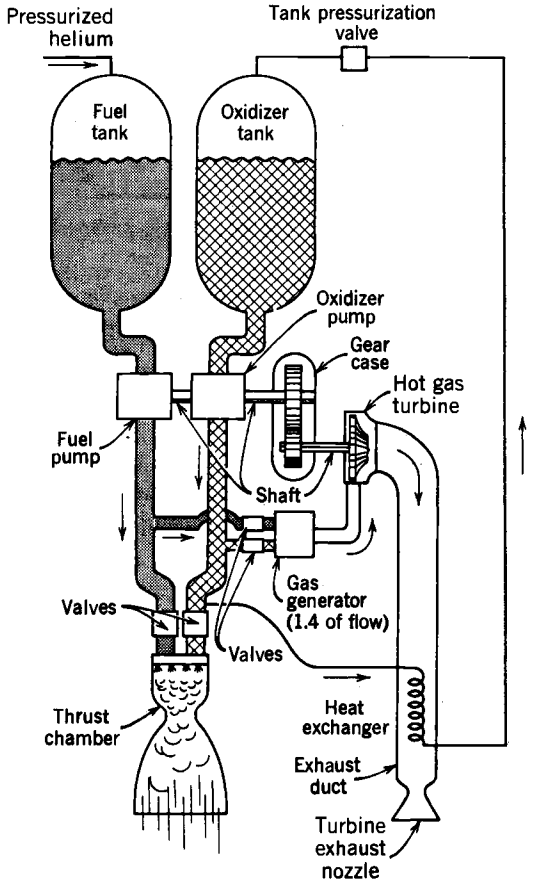

Fig. 3.37 Liquid-propellant rocket with turbopump feed system (from Ref. 19).

3.5.12.2 Performance calculations and results. It is beyond the scope of this chapter to cover the thermochemical theory and calculations required to determine the performance of a liquid-propellant rocket (see Chapter 2 for fundamentals). For the simple reaction between hydrogen (H_2) and oxygen (O_2), it is possible to form six products: water (H_2O), hydrogen (H_2), oxygen (H_2), hydroxyl (OH), atomic oxygen (O), and atomic hydrogen (H). The chemical equation for this reaction between a moles of hydrogen and b moles of oxygen can be written as

$$aH_2 + bO_2 \rightarrow n_{H_2O}H_2O + n_{H_2}H_2 + n_{O_2}O_2 + n_H H + n_O O + n_{OH}OH$$

Here n_{H_2O}, n_{H_2}, n_{O_2}, n_H, n_O, and n_{OH} are the molar quantities of the products.

Table 3.13 Theoretical performance[a] of liquid rocket propellant combinations[b] (from Ref. 19)

Oxidizer	Fuel	Mixture ratio		Chamber temperature, K	C^*, m/s	M, kg/mol	I_{sp}, s	γ
		By mass	By volume					
Oxygen:	75% Ethyl	1.30	0.98	3177	1641	23.4	267	1.22
	alcohol	1.43	1.08	3230	1670	24.1	279	
	Hydrazine	0.74	0.66	3285	1871	18.3	301	1.25
		0.90	0.80	3404	1892	19.3	313	
	Hydrogen	3.40	0.21	2959	2428	8.9	387	1.26
		4.02	0.25	2999	2432	10.0	390	
	RP-1	2.24	1.59	3571	1774	21.9	286	1.24
		2.56	1.82	3677	1800	23.3	300	
	UDMH	1.39	0.96	3542	1835	19.8	295	1.25
		1.65	1.14	3594	1864	21.3	310	
Fluorine:	Hydrazine	1.83	1.22	4553	2128	18.5	334	1.33
		2.30	1.54	4713	2208	19.4	363	
	Hydrogen	4.54	0.21	3080	2534	8.9	398	1.33
		7.60	0.35	3900	2549	11.8	410	
Nitrogen	Hydrazine	1.08	0.75	3258	1765	19.5	283	1.26
tetroxide:		1.34	0.93	3152	1782	20.9	292	
	50% UDMH	1.62	1.01	3242	1652	21.0	278	1.24
	50% hydrazine	2.00	1.24	3372	1711	22.6	288	
Red fuming	RP-1	4.10	2.12	3175	1594	24.6	258	1.22
nitric acid		4.80	2.48	3230	1609	25.8	268	
(15% NO_2):	50% UDMH-	1.73	1.00	2997	1682	20.6	272	1.22
	50% hydrazine	2.20	1.26	3172	1701	22.4	279	

[a]Conditions: $P_c = 1000$ psia, $P_e = 14.7$ psia, optimum nozzle expansion ratio, and frozen flow through nozzle.
[b]For every propellant combination, there are two sets of values listed: the upper line refers to frozen flow through the nozzle, the lower line to equilibrium flow through the nozzle.

An equilibrium solution of the preceding reaction in a combustion chamber can be obtained by use of the following principles:

1) Conservation of mass
2) Conservation of energy
3) Law of partial pressures

Figure 3.38 shows the results of these thermochemical calculations for liquid oxygen and the hydrocarbon fuel RP-1. Note that the concentration of carbon monoxide (CO) decreases and the oxidizer/fuel ratio is increased with a corresponding increase in carbon dioxide (CO_2). Also, note that the water (H_2O) reaches a maximum concentration for the given chamber pressure when the oxidizer/fuel ratio is about 2.7.

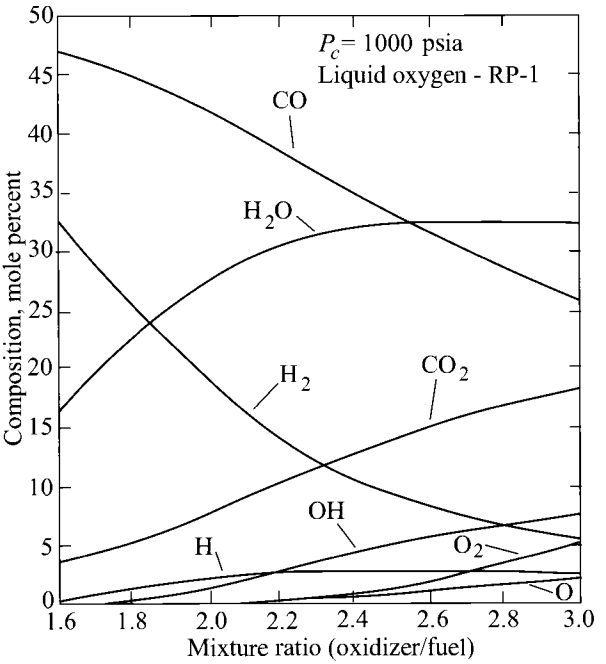

Fig. 3.38 Calculated chamber composition for liquid oxygen and RP-1 (from Ref. 19).

After reacting in the combustion chamber, the products then flow through the rocket nozzle. Two cases are considered for the flow of these products through the nozzle:

1) *Frozen flow*. The composition of the products do not change from those values determined for the combustion chamber. Here the mole fractions, molecular weight, etc., are the same at the nozzle exit as those at the exit of the combustion chamber.

2) *Equilibrium flow*. The composition of the products are maintained in chemical equilibrium as the pressure and temperature vary during the nozzle expansion process.

Figure 3.39 shows the equilibrium composition results leaving the nozzle for liquid oxygen and RP-1. Note that higher concentrations of carbon dioxide are shown in Fig. 3.39 leaving the nozzle than those shown leaving the combustion chamber in Fig. 3.38.

The actual flow through nozzles falls between these easily calculated cases. The products are able to stay in chemical equilibrium to some point downstream of the nozzle where their composition freezes. The equilibrium flow calculations give lower exhaust nozzle temperatures because of the recombination of dissociated species and thus give higher performance. Both frozen and equilibrium flow results are presented in Table 3.13.

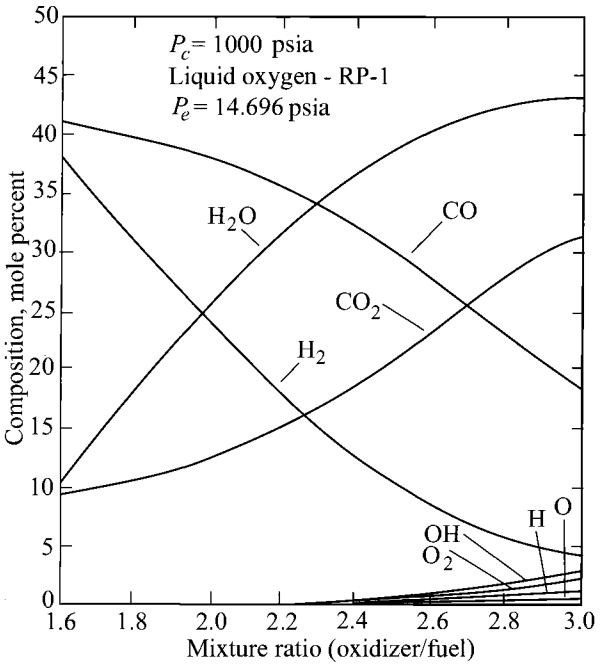

Fig. 3.39 Calculated nozzle exit equilibrium composition for liquid oxygen and RP-1 (from Ref. 19).

Example 3.9

Determine the I_{sp} of the oxygen-hydrogen rocket engine with a chamber temperature of 2960 K and an oxidizer-to-fuel mixture ratio by weight of 3.4:1 using the EQL software for both equilibrium and frozen flow through the nozzle. The rocket engine has a chamber pressure P_c of 1000 psia and an exit pressure P_e of 14.7 psia. Assume isentropic flow and perfect expansion.

Solution: The mixture ratio of 3.4:1 by weight equals a mole ratio of 0.214 (= 3.4 × 2.016/32). We use a pressure of 6893.2 kPa (= 1000 × 101.33/14.7) for the exit conditions from the combustion chamber. The nozzle inlet and exit states for both equilibrium and frozen flow are listed in Table 3.14. The exit velocity V_e follows from the definition of total enthalpy, Eq. (2.65).

3.5.13 Solid-Propellant Rockets

As shown in Fig. 3.40, solid-propellant rockets are relatively simple in construction. They contain the propellant to be burned within the combustion chamber or case. The propellant charge contains all of the chemical elements

Table 3.14 Oxygen–Hydrogen rocket engine results using EQL—Example 3.9

Property	Inlet	Exit, equilibrium flow	Exit, frozen flow
Pressure, kPa	6893.2	101.33	101.33
Temperature, K	2960.0	1308.3	1250.9
Molecular weight	8.80	8.87	8.80
Enthalpy, kJ/kg	371.3	−7835	−7651
V_e, m/s		4051	4006
I_{sp},		413	408

required for complete burning and is formed into a solid mass called the *grain.* Once the propellant is ignited, it burns on the surfaces of the propellant that are not inhibited by the case. The rate of burning is proportional to the exposed surface area.

3.5.13.1 Propellants. There are three general types of propellants for this type of rocket: double-base (homogeneous), composite (or heterogeneous), and composite modified double-base (CMDB). Table 3.15 gives representative formulations of these three types of propellants.

A homogeneous propellant has the fuel and oxidizer within the same molecule. The most common example of a homogeneous propellant is the double-base propellant of nitrocellulose and nitroglycerin with small amounts of additives. Figure 3.41 shows the variation in flame temperature and specific impulse with nitroglycerin (NG) concentration of the double-base propellant (JPN).

The composite propellant contains a heterogeneous mixture of oxidizer (as crystals) in a rubber-like binder. The binder is the fuel and must withstand a severe environment (high thermal and mechanical stresses). Hydroxyl terminated polybutaliene (HTPB) is a common binder. Common oxidizing crystals are ammonium perchlorate (AP), ammonium nitrate (AN), nitronium perchlorate (NP), potassium perchlorate (KP), potassium nitrate (KN), cyclotrimethylene trinitramine (RDX), and cyclotetramethylene tetranitramine (HMX).

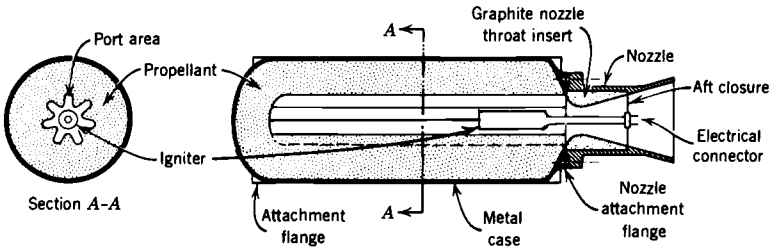

Fig. 3.40 Typical solid-propellant rocket motor (from Ref. 19).

Table 3.15 Representative propellant formulations in percent weight[a]

Propellant ingredient	Double-base (JPN)	Composite (PBAN)	Composite modified double-base (CMDB)
Nitrocellulose	51.5		21.9
Nitroglycerine	43.0		29.0
Ammonium perchlorate		70.0	20.4
Aluminum powder		16.0	21.1
Polybutadiene—acrylic acid—acrylonitrile		11.78	
Triacetin			5.1
Diethyl phthalate	3.2		
Epoxy curative		2.22	
Ethyl centralite	1.0		
Potassium sulfate	1.2		
Additives	0.1		
Stabilizers			

[a]Source: Air Force Wright Laboratory, Rocket Branch, Edwards, CA.

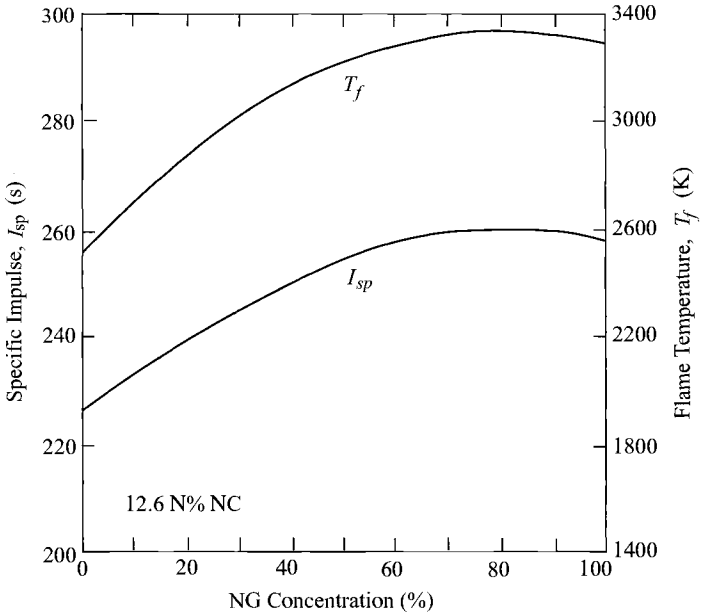

Fig. 3.41 Specific impulse and flame temperature vs nitroglycerin concentration of double-base propellants (from Ref. 21).

Figure 3.42 shows the variation in flame temperature, molecular weight, and specific impulse with oxidizer concentration for HTPB-based composite propellants. Maximum flame temperature for RDX and HMX are associated with 100% concentration, and these are commonly referred to as stoichiometrically balanced fuel-oxidizer combinations.

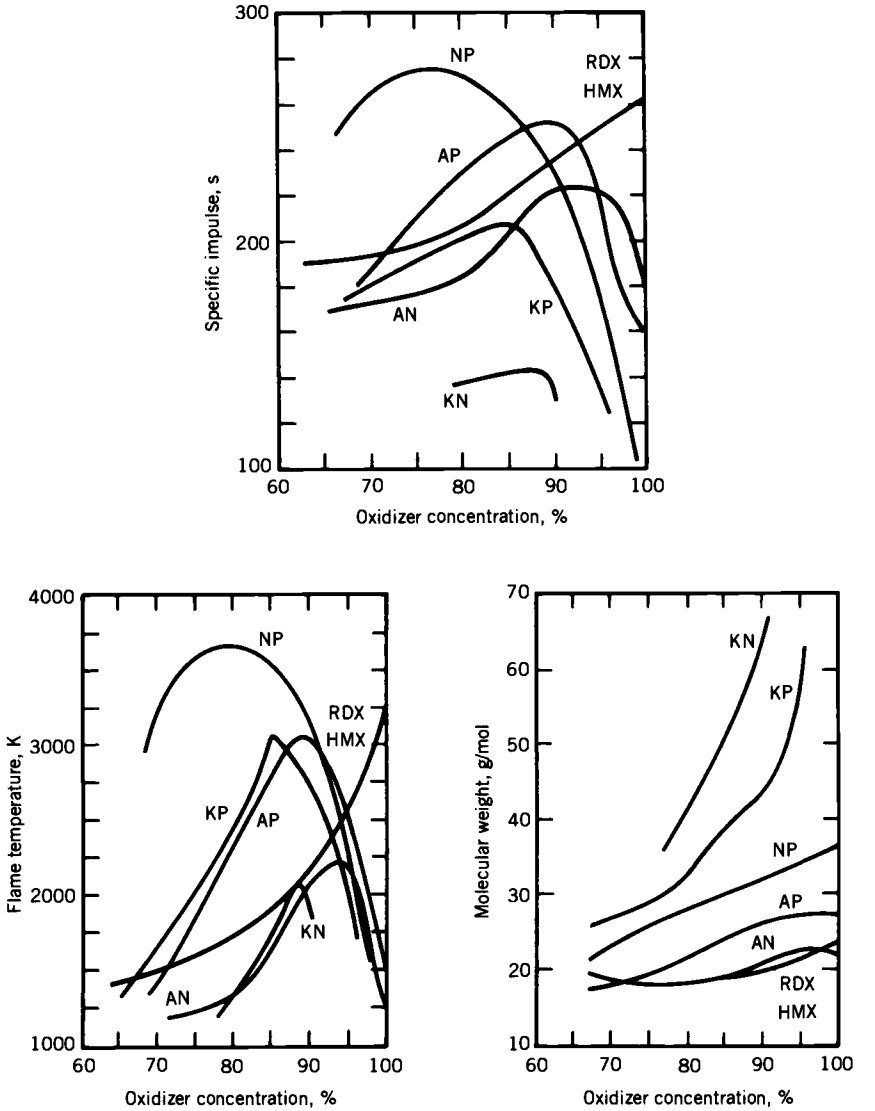

Fig. 3.42 HTPB-based composite propellants (from Ref. 21).

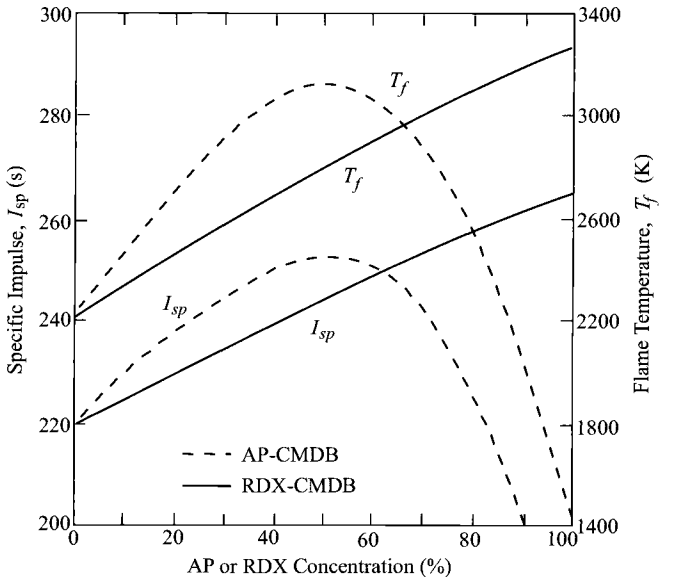

Fig. 3.43 Effects of percent concentration of AP or RDX on CMDB propellants (from Ref. 21).

The composite modified double-base (CMDB) propellant is a heterogeneous of the other two types of propellants. Figure 3.43 shows the variation in flame temperature and specific impulse vs the concentration of AP and RDX in AP-CMDB and RDX-CMDB propellants.

Metal powders are commonly added to solid propellants to increase specific impulse and fuel density. Aluminum powders that constitute 12–20% of the propellant mass have given the most successful experience.

The theoretical performances of three solid propellants are presented in Table 3.16. The results for specific impulse I_{sp} and effective exhaust velocity C are based on frozen flow through an optimum nozzle expansion ratio from a chamber pressure of 1000 psia to an exhaust pressure of 14.7 psia.

3.5.13.2 Burning rate. The burning rate r for a solid propellant is defined as the recession of the propellant surface per unit time (see Fig. 3.44). The burning rates of typical solid propellants are given in Fig. 3.45. For a given solid propellant, this rate is mainly a function of the chamber pressure P_c and is commonly written as

$$r = aP_c^n \tag{3.56}$$

where a is an empirical constant influenced by the ambient temperature of the propellant prior to ignition, and n is known as the *burning rate pressure exponent.*

Table 3.16 Theoretical performance of typical solid-rocket propellant combinations[a] (from Ref. 19)

Oxidizer	Fuel	Chamber temperature, K	C^*, m/s	$\mathcal{M}$, kg/mol	I_{sp}, s	γ
Ammonium nitrate	11% binder and 7% additives	1282	1209	20.1	192	1.26
Ammonium perchlorate 78–66%	18% organic polymer binder and 4–20% aluminum	2816	1590	25.0	262	1.21
Ammonium perchlorate 84–68%	12% polymer binder and 4–20% aluminum	3371	1577	29.3	266	1.17

[a]Conditions for I_{sp} and C: $P_c = 1000$ psia, $P_e = 14.7$ psia, optimum nozzle expansion ratio, and frozen flow through nozzle.

When a single value of the burning rate is given, this value corresponds to a propellant ambient temperature of 70°F and a combustion pressure of 1000 psia unless otherwise stated. For the composite ammonium nitrate propellant curve in Fig. 3.45, corresponding to an ambient temperature of −40°F, the empirical constants a and n are 0.0034 in./s and 0.445, respectively, for the chamber pressure P_c expressed in units of psia.

Accounting for both the density of the solid propellant and that of the propellant gas, the net mass flow rate of propellant gas being generated can be expressed as

$$\dot{m} = (\rho_s - \rho_g) r A_b \tag{3.57}$$

where A_b is the burning area of the propellant, r the burning rate, ρ_s the solid propellant density at ambient temperature, and ρ_g the propellant gas density. Since A_b and r vary with time and chamber pressure P_c, the thrust of a solid-propellant rocket changes with time. The variation in burning area of the propellant A_b designed into the grain determines the variation in thrust over time. Figure 3.46 shows six grain designs, their variations in thrust with time, and the corresponding general category of thrust variation.

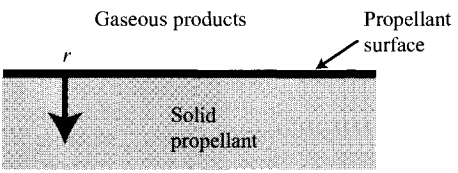

Fig. 3.44 Burning of a solid propellant.

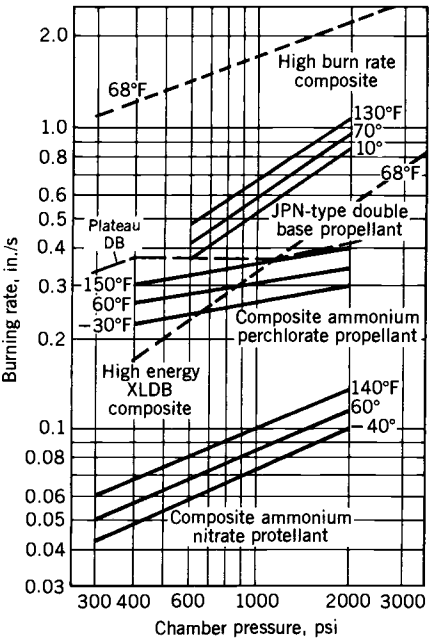

Fig. 3.45 Burning rates of typical solid propellants (from Ref. 19).

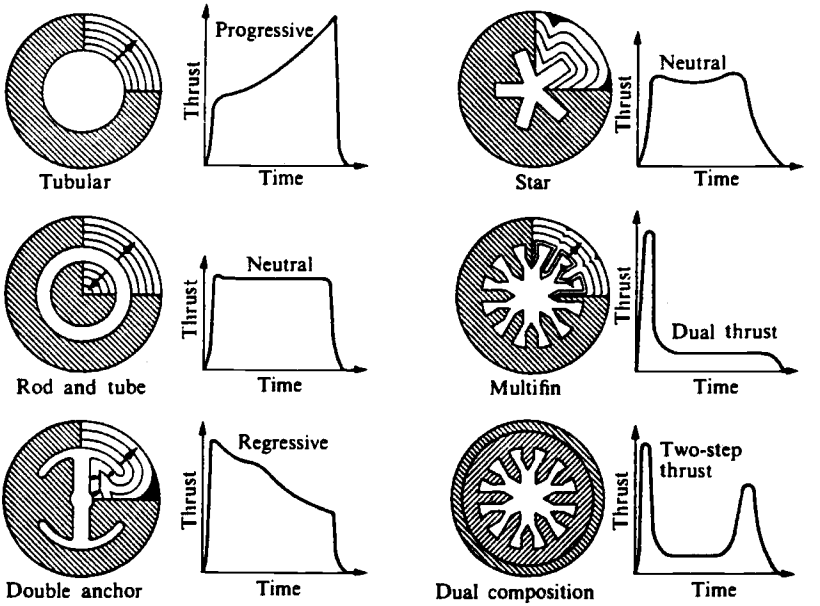

Fig. 3.46 Grain design and thrust vs time (from Ref. 22).

3.5.13.3 Chamber pressure and stability. A steady-state chamber pressure P_c is reached when the net mass flow of propellant gas being generated equals the mass flow rate of propellant gas leaving the nozzle. Using Eqs. (3.36), (3.38), and (3.57), we write

$$\dot{m} = \frac{P_c A_t g_c}{C^*} = (\rho_s - \rho_g) r A_b$$

where A_t is the nozzle throat area and C^* is the characteristic velocity given by Eq. (3.38). For solid-propellant rockets, the characteristic velocity C^* depends mainly on the propellant. Substituting the empirical relationship of Eq. (3.56) for the burning rate r into the preceding equation gives

$$\dot{m} = \frac{P_c A_t g_c}{C^*} = (\rho_s - \rho_g) a P_c^n A_b \tag{i}$$

Plotting the nozzle mass flow rate and propellant gas generation rate vs the chamber pressure gives the general curves shown in Fig. 3.47. Two curves are drawn for the propellant gas generation rate (mass burn rate): one for $n < 1$ and another for $n > 1$. *Stability requires that burning rate pressure exponent n be less than unity.* If n is greater than unity, increases in chamber pressure above operating point will cause the propellant gas generation to increase faster than the nozzle flow rate. The result would lead to a rapid rise in chamber pressure with an accompanying explosion.

From Eq. (i), the chamber pressure P_c can be expressed as

$$P_c = \left\{ \frac{a(\rho_s - \rho_g) C^*}{g_c} \frac{A_b}{A_t} \right\}^{\frac{1}{1-n}} \tag{3.58}$$

This equation can be used to determine the chamber pressure when data are available for the terms on the right-hand side of the equation. Because the density

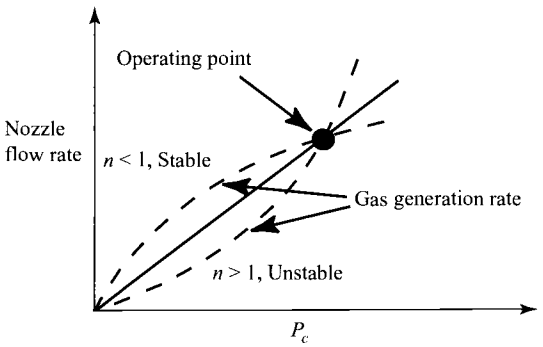

Fig. 3.47 Mass flow rate vs chamber pressure.

of the propellant gas is much smaller than that of the solid propellant, it is often neglected and Eq. (3.58), written as

$$P_c = \left\{ \frac{a\rho_s C^* A_b}{g_c A_t} \right\}^{\frac{1}{1-n}} \tag{3.59}$$

The sensitivity of the chamber pressure P_c to changes in the burn-to-throat area ratio A_b/A_t can be investigated with this equation. As an example, for a burning rate pressure exponent n of 0.75, the change in chamber pressure is proportional to A_b/A_t raised to the fourth power, which can lead to large variations in P_c over the burn. It is for this reason that most propellants have burning rate pressure exponent n in the range of 0.2 to 0.3.

As an example of the use of Eq. (3.59) to determine chamber pressure P_c, we consider a solid-propellant rocket with $A_b/A_t = 600$. The properties for the propellant are $\rho_s = 0.06$ lbm/in.^{3}, $n = 0.2$, $a = 0.05$ in./s, and $C^* = 5000$ ft/s. Using Eq. (3.59) gives

$$P_c = \left\{ \frac{0.05 \times 0.06 \times 5000}{32.174} 600 \right\}^{1.25} = 1144 \text{ psia}$$

Equation (3.59) can be used to determine the burn-to-throat area ratio A_b/A_t of a solid-propellant rocket when the other data are known. Solving Eq. (3.59) for this area ratio gives

$$\frac{A_b}{A_t} = \frac{g_c}{a\rho_s C^*} P_c^{1-n} \tag{3.60}$$

Consider that a chamber pressure 2000 psia is desired for the same propellant as used in the preceding. The required burn-to-throat area ratio is

$$\frac{A_b}{A_t} = \frac{32.174}{0.05 \times 0.06 \times 5000} 2000^{0.8} = 938$$

3.5.13.4 Total impulse and times. The total impulse I_t of a rocket is the integral of the thrust over the burning time t_b, or

$$I_t = \int_0^{t_b} F \, dt = \overline{F} t_b \tag{3.61}$$

where $\overline{F}$ is the average thrust over the burning time t_b, which is defined in Fig. 3.48, along with the action time t_a. Figure 3.48 shows representative plots of experimentally measured chamber pressure P_c vs time.

The specific impulse, effective exhaust velocity, and propellant mass flow rate cannot be measured directly in an experiment. The normal procedure is to determine the average specific impulse by finding the total impulse I_t and

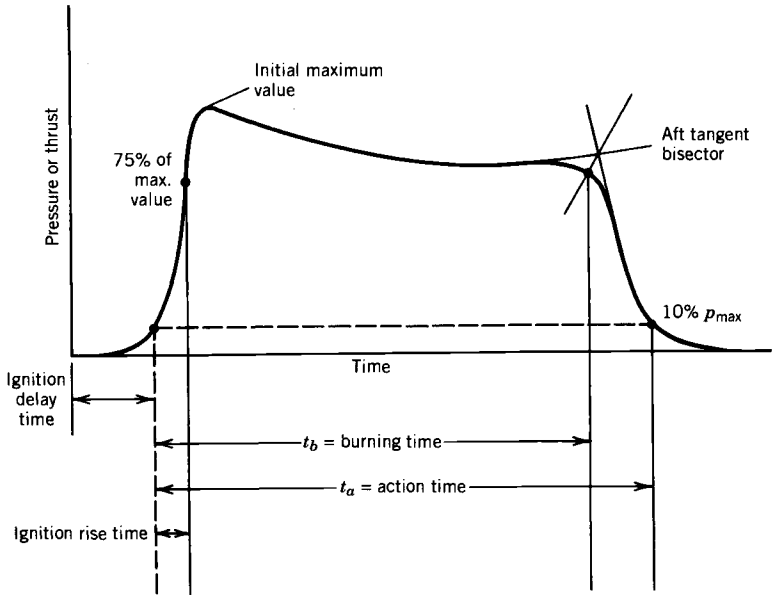

Fig. 3.48 Definition of burning time t_b and action time t_a (from Ref. 19).

weight of propellant w used for a rocket test. The average specific impulse ($\overline{I_{sp}}$) is then given by

$$\overline{I_{sp}} = \frac{I_t}{w} \tag{3.62}$$

The average effective exhaust velocity $\overline{C}$ and mass flow rate $\overline{\dot{m}}$ then follow from Eq. (3.6) and the values for the weight of propellant w used and burning time t_b. Thus we have

$$\overline{C} = \overline{I_{sp}} g_o \tag{3.63}$$

$$\overline{\dot{m}} = \frac{w}{t_b} \frac{g_c}{g_o} \tag{3.64}$$

Example 3.10

Two tests of a 5-in. diam, center-perforated, solid-propellant rocket was performed at the United States Air Force Academy. The first test used a convergent-only nozzle, and the second test used a convergent-divergent nozzle. Figure 3.49 shows a sketch of the test rocket motors. The rocket propellant grain burns on both ends and in the center. The following data were provided by the manufacturer:

1) Ammonium perchlorate composite propellant with aluminum (70% NH_4ClO_4, 15% Al, 15% binder),

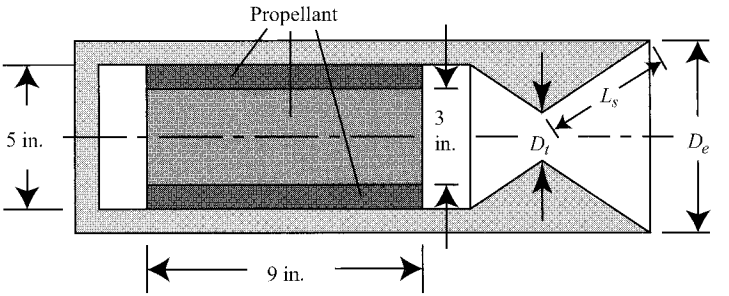

Fig. 3.49 Sketch of test rocket motor with convergent-divergent nozzle.

2) $C^* = 5118$ ft/s, $\mathcal{M} = 25.55$, $\gamma = 1.2$, $\rho_s = 0.064$ lbm/in.^{3},
3) Burning rate coefficients: $a = 0.0773$ in./s, $n = 0.21$, P_c in psia.

The test data for the two tests are presented in Table 3.17. The results for Case I are calculated and discussed in the following. The calculations for Case II are left as a homework problem.

Case I results:

$$\text{Average thrust} = \overline{F} = \frac{I_t}{t_b} = \frac{1257.6}{4.113} = 305.8 \text{ lbf}$$

$$\text{Average } P_c = \overline{P}_c = \int_0^{t_b} (P_c - P_a)\, dt/t_b + P_a$$

$$= 1161.6/4.113 + 23.16 \times 0.491 = 293.8 \text{ psia}$$

$$\text{Average } A_t = \overline{A_t} = \pi(1.1075)^2/4 = 0.963 \text{ in.}^2$$

$$\text{Burning rate} = r = a(\overline{P}_c)^n = 0.0773(293.8)^{0.21} = 0.255 \text{ in./s}$$

Table 3.17 Test data of two small solid-propellant rockets

Item	Case I	Case II
Barometric pressure P_a, in Hg	23.16	23.33
Initial rocket case weight, lbf	17.42	17.35
Final rocket case weight, lbf	10.10	10.10
Nozzle type	Convergent	Convergent-divergent
Initial throat diameter d_t, in.	1.107	0.852
Final throat diameter d_t, in.	1.108	0.866
Exit diameter d_e, in.	N/A	2.225
Nozzle slant length L_s, in.	N/A	3.0
Burning time t_b, s	4.113	3.64
$\int_0^{t_b} (P_c - P_a)\ dt$, psig-s	1161.6	1921.6
$I_t = \int_0^{t_b} F\ dt$, lbf-s	1257.6	1570.8

$$\text{Average burning rate} = \bar{r} = \frac{\text{Web thickness}}{t_b} = \frac{1.00}{4.113} = 0.243 \text{ in./s}$$

$$\text{Initial burning surface} = A_b = 2\pi(r_i L + r_o^2 - r_i^2)$$
$$= 2\pi(1.5 \times 9 + 2.5^2 - 1.5^2) = 110 \text{ in.}^2$$

$$\text{Initial propellant flow rate} = \dot{m} = r\rho_s A_b$$
$$= 0.255 \times 0.064 \times 110 = 1.795 \text{ lbm/s}$$

$$\text{Average propellant flow rate} = \bar{\dot{m}} = \frac{wg_c}{t_b g_o} = \frac{7.32}{4.113}\frac{32.174}{32.174} = 1.780 \text{ lbm/s}$$

$$\text{Experimental } C^* = \frac{\overline{P_c}\,\overline{A_t} g_c}{\bar{\dot{m}}} = \frac{293.8 \times 0.963 \times 32.174}{1.780} = 5114 \text{ ft/s}$$

$$\text{Experimental } C_F = \frac{\bar{F}}{\overline{P_c}\,\overline{A_t}} = \frac{305.8}{293.8 \times 0.963} = 1.081$$

$$\text{Experimental } I_{sp} = \frac{I_t}{w} = \frac{1257.6}{7.32} = 171.8 \text{ s}$$

$$\text{Experimental } C = I_{sp} g_o = 171.8 \times 32.174 = 5527 \text{ ft/s}$$

Theoretical thrust coefficient: $\gamma = 1.2$, $\varepsilon = 1$

$$\frac{P_c}{P_a} = \frac{293.8}{23.16 \times 0.491} = 25.84, \quad \frac{P_c}{P_e} = \left(\frac{\gamma+1}{2}\right)^{\gamma/(\gamma-1)} = \left(\frac{2.2}{2}\right)^6 = 1.772$$

Using these data with Eq. (3.44) gives $C_F = 1.185$, and

$$\text{Ideal } C = C_F C^* = 1.185 \times 5118 = 6065 \text{ ft/s}$$

$$\text{Ideal } I_{sp} = \frac{C}{g_o} = \frac{6065}{32.174} = 188.5 \text{ s}$$

The experimental and manufacturer's values of C^* are the same. The average and initial burning rates are within 5% of each other. The average and initial mass flow rates are within 1% of each other. Closer agreement between experimental and ideal results could be obtained with a higher γ.

Problems

3.1 For propellants having a specific impulse of 360 s, determine the mass flow rate through a rocket nozzle to obtain a thrust of 10,000 N.

3.2 For propellants having a specific impulse of 265 s, determine the mass flow rate through a rocket nozzle to obtain a thrust of 1,500,000 lbf.

3.3 Exhaust gas with $R = 0.375$ kJ/kg-K and $\gamma = 1.26$ flows through an isentropic nozzle. If the gas enters the nozzle at 100 atm and 4000 K and exits to a pressure of 1 atm, determine the following for a choked nozzle throat:
(a) the exhaust velocity V_e

(b) the specific impulse I_{sp}
(c) mass flow rate and ideal thrust for a throat area A_t of 0.1 m^2

3.4 Determine the area ratio of the nozzle in Problem 3.3.

3.5 Determine the gross weight at liftoff for a single-stage rocket with a 2000-kg payload placed in a low Earth orbit using a liquid O_2-H_2 propulsion system. Assume a burn time of 100 s and an average specific impulse of 400 s.

3.6 Determine the gross weight at liftoff for a single-stage rocket with a 1000-kg payload placed in a low Earth orbit using a liquid O_2-kerosene propulsion system. Assume a burn time of 120 s and an average specific impulse of 310 s.

3.7 Rework Example 3.3 with a liquid O_2-kerosene propulsion system having an average specific impulse of 310 s.

3.8 A calorically perfect gas with a molecular weight of 18 and $\gamma = 1.25$ has a combustion temperature T_c of 6000°R. Determine the characteristic velocity C^*.

3.9 Determine the characteristic velocity C^* for the data of Example 3.5.

3.10 Determine the area ratio (A_e/A_t) for a rocket nozzle operating at a pressure ratio (P_c/P_e) of 1000 with a calorically perfect gas where $\gamma = 1.2$.

3.11 A rocket nozzle has an ideal thrust coefficient C_{Fi} of 1.5, a chamber pressure P_c of 100 atm, and a throat area A_t of 0.15 m^2. Determine the ideal thrust F_i.

3.12 A rocket nozzle has an area ratio (A_e/A_t) of 25. If a calorically perfect gas with $\gamma = 1.25$ flows through the nozzle, determine its pressure ratio (P_c/P_e) and ideal thrust coefficient in a vacuum $(C_{Fi})_{vac}$.

3.13 Find the ideal thrust coefficient C_{Fi} for a rocket at 50-km altitude with an area ratio of 50, $\gamma = 1.28$, and a chamber pressure $P_c = 40$ atm.

3.14 Calculate the ideal thrust coefficient C_{Fi} and ideal thrust F_i for the space shuttle main engine (SSME) data of Example 3.7 at an altitude of 45,000 ft.

3.15 A chemical rocket motor has the following data during static testing at sea level:

$P_c = 225$ atm, $T_c = 2800$ K, $M_e = 5.3$
$\varepsilon = 62$, exit diameter = 2.15 m

Assume a calorically perfect gas with $\gamma = 1.3$ and $R = 0.317$ kJ/kg-K. Determine the throat area A_t, exit pressure P_e, exit temperature T_e, exit velocity V_e, mass flow rate $\dot{m}$, and thrust at both sea-level and design altitude.

3.16 A rocket booster using H_2-O_2 requires an ideal thrust of 100,000 lbf at a design altitude of 80 kft. The booster will have a chamber temperature of 4840°R and a throat area of 0.5 ft^2. Assuming a specific impulse of 400 s and a calorically perfect gas with $\gamma = 1.26$ and $R = 173.6$ ft-lbf/lbm-°R, determine the following:

(a) Mass flow rate
(b) Characteristic velocity C^*
(c) Chamber pressure P_c
(d) Effective exhaust velocity C at 80-kft altitude
(e) Ideal thrust coefficient C_{Fi} at 80-kft altitude
(f) Nozzle expansion ratio ε and exit diameter
(g) Altitude that flow in the nozzle is just separated (assume separation when $P_a > 3.5\ P_{we}$)
(h) Ideal thrust at sea level

3.17 Determine the I_{sp} of the oxygen-hydrogen rocket engine with a chamber temperature of 3200 K and an oxidizer-to-fuel mixture ratio by weight of 3.0:1 using the EQL software for both equilibrium and frozen flow through the nozzle. The rocket engine has a chamber pressure (P_c) of 100 atm and an exit pressure P_e of 1 atm. Assume isentropic flow and perfect expansion.

3.18 A solid-propellant rocket has $\rho_s = 0.06$ lbm/in.^{3}, $n = 0.2$, $a = 0.05$ in./s, and $C^* = 5000$ ft/s. Determine the burn-to-throat area ratio (A_b/A_t) for a chamber pressure of 1500 psia.

3.19 Determine the performance of Case II in Table 3.17. Compare your results to Case I (Example 3.10).

3.20 From a search of the Internet, find a thrust vs time plot for a solid-propellant motor (e.g., Estes Rocket Motors) and determine the burning time, action time, impulse, average mass flow rate, and average thrust.

3.21 Test firing of a 2.75-in. solid rocket at the U.S. Air Force Academy on May 8, 1992, gave the data plotted in Fig. P3.1.[23] The rocket motor used was the "Mighty Mouse" solid-propellant system used for the air-to-ground 2.75-in. folding fin aerial rocket. The motor uses a Class B propellant (MK43 MOD 1 propellant grain) with an internal burning eight-point star grain configuration. The motor has four straight, fixed, conical nozzles. The physical characteristics and published performance of the Mighty Mouse rocket motor based on 70°F sea-level operation are as follows:

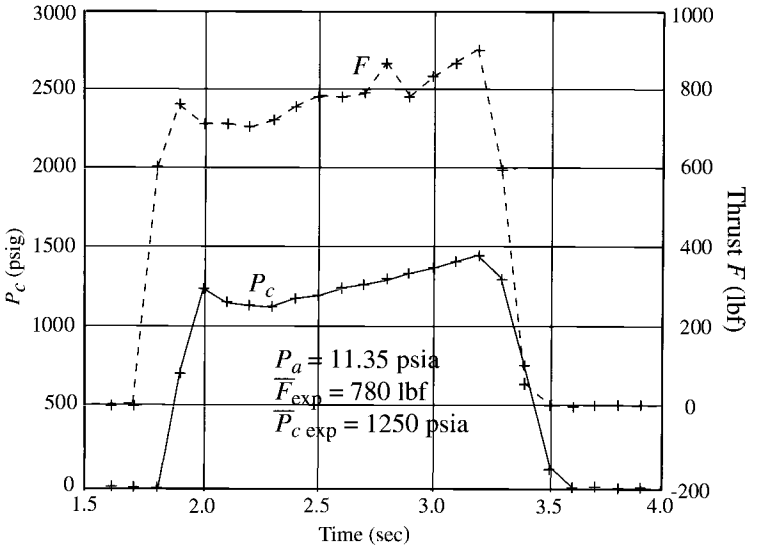

Fig. P3.1 Test firing of a 2.75-in. solid rocket at the U.S. Air Force Academy on May 8, 1992 (Ref. 23).

Size and mass:
Overall length = 39.4 in., nominal diameter = 2.75 in., loaded mass = 11.37 lbm, expended mass = 5.9 lbm, propellant mass = 6.40 lbm, and initial area of propellant burning surface = 160.83 in.^{2}

Manufacturer's performance characteristics (70°F sea-level operation):

Average chamber pressure P_c	1210 psia
Motor specific impulse	103 lbf-s/lbm
Action time impulse	1140 lbf-s
Total impulse	1170 lbf-s
Propellant	NC/NG/DEP/other (50/36/11/4%)
Propellant specific impulse I_{sp}	183 s
Propellant density ρ_p	0.056 lbm/in.^{3}
Propellant burn rate (1000 psia), r	0.48 in./s
Ratio of specific heat for gas, γ	1.17
Propellant mass fraction	0.563
Total nozzle throat area, A^*	0.444 in.^{2}
Expansion cone half angle	10°15′
Nozzle expansion ratio ε	3.75
Characteristic exhaust velocity C^*_{manuf}	4159 ft/s
Thrust coefficient, C_F	1.415

(a) Calculate the exit Mach number M_e.
(b) Using the experimental chamber pressure $P_{c\ exp}$ and calculated exit Mach number, calculate the exit pressure P_e.
(c) Describe the exit flow as underexpanded or overexpanded (see Figs. 2.37 and 2.38).
(d) Calculate the mass flow rate of the combustion products based on the initial area of propellant burning surface.
(e) Calculate the characteristic exhaust velocity C^*_{exp} based on the mass flow rate of item c and the experimental chamber pressure $P_{c\,exp}$.
(f) Calculate the thrust coefficient $C_{F\text{calc}}$ using the measured thrust and chamber pressure $P_{c\,exp}$.
(g) Calculate the thrust produced by the rocket using the calculated thrust coefficient, measured chamber pressure, and nozzle throat area.
(h) Calculate the experimental specific impulse $I_{sp\,exp}$.
(i) Compare calculated results to manufacturer's performance characteristics.

4
Aircraft Gas Turbine Engine

4.1 Introduction

The introductory fundamentals of aircraft propulsion systems are covered in this chapter. Emphasis is placed on propulsion systems that operate on the so-called Brayton cycle. Such systems include turbojets, turboprops, turbofans, ramjets, and combinations thereof. Before taking up the thermodynamic processes involved in these systems, we consider the forces acting on a propulsive duct and the effect of installation on the net propulsive force.

4.2 Thrust Equation

We define a *propulsion system* as a unit submerged in a fluid medium about and through which the fluid flows. The propulsion system contains an energy-transfer mechanism that increases the kinetic energy of the fluid passing through the system. This mechanism is called the *engine*. In Fig. 4.1, the engine is shown schematically in a nacelle housing that forms the second portion of the propulsion system. Thus the propulsion system contains:

1) An engine (the nozzle is considered to be part of the engine in our terminology),
2) Housing about the engine (nacelle or duct).

Several different aircraft systems may use the same engine submerged in different-shaped nacelles. Thus one propulsion system may use engine X in a pod installation hanging from a wing while, in another system, engine X may be surrounded by a nacelle that is, in fact, the airplane's fuselage—examples are the F-15 vs F-16 propulsion systems that use the F-100 turbofan engine. The thrust of a propulsion system will depend on 1) its engine and 2) its nacelle.

As a result, it is conventional to speak of *uninstalled engine thrust and installed engine thrust.* The uninstalled engine thrust should depend on the engine alone and hence must be independent of the nacelle. the installed engine thrust is the thrust produced by both the engine and the nacelle. Installed engine thrust T is defined as the shear force in the reaction strut of Fig. 4.1.

Uninstalled engine thrust F is defined as the force F_{int} acting on the internal surface of the propulsion system from 1 to 9 plus the force F'_{int} acting on the internal surface of the stream tube 0 to 1 that contains the air flowing into the engine. It will be shown that F is independent of the nacelle.

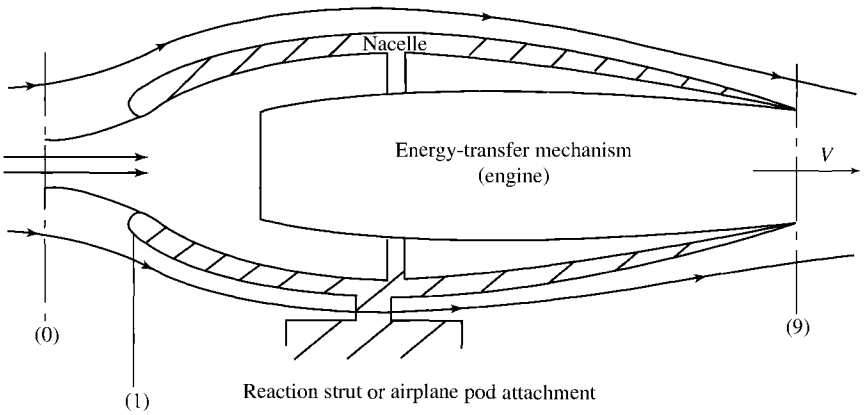

Fig. 4.1 Propulsion system.

To evaluate the uninstalled engine thrust, defined as $F_{\text{int}} + F'_{\text{int}}$, we apply the momentum equation to the control surface of Fig. 4.2. In so doing, we use the convention that all pressures used will be gauge pressures. We adopt this convention because it is used by the external aerodynamicist in computing the drag and lift forces on the airplane. To be consistent, then, the internal aerodynamicist must do the same. Figure 4.3 shows the momentum equation for assumed steady flow applied to flow through the control surface of Fig. 4.2.

Referring to Fig. 4.3 and equating forces to the change in momentum flux, we get

$$F'_{\text{int}} + F_{\text{int}} + (P_0 - P_0)A_0 - (P_9 - P_0)A_9 = \frac{\dot{m}_9 V_9 - \dot{m}_0 V_0}{g_c}$$

$$F + 0 - (P_9 - P_0)A_9 = \frac{\dot{m}_9 V_9 - \dot{m} V_0}{g_c}$$

$$\text{Uninstalled engine thrust} \quad F = \frac{\dot{m}_9 V_9 - \dot{m}_0 V_0}{g_c} + (P_9 - P_0)A_9 \tag{4.1}$$

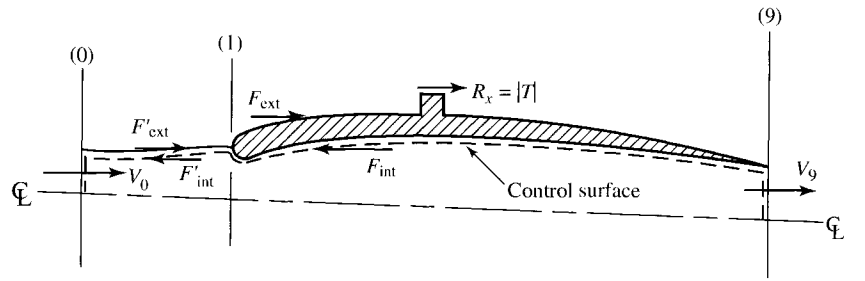

Fig. 4.2 Forces on propulsion system.

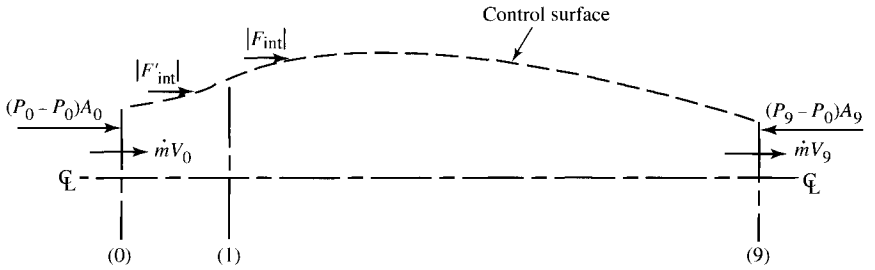

Fig. 4.3 Control surface forces and momentum fluxes for evaluating F (pressure referred to P_0).

This equation for the uninstalled engine thrust is seen to contain terms completely independent of the nacelle of the propulsion system. The terms $\dot{m}$, V_9, A_9, and P_9 are fixed by the engine while the terms V_0 and P_0 are fixed by the flight condition.

To obtain the installed engine thrust, we must "subtract" from the uninstalled engine thrust the drag forces F'_{ext} and F_{ext}. The first, F'_{ext}, is equal in magnitude to F'_{int} and adjusts the engine thrust for the force F'_{int}, which is credited to the uninstalled engine thrust but does not really contribute to the installed engine thrust. The second, F_{ext}, is the drag force acting on the external surface of the nacelle. Thus

F'_{ext} = pressure force on external stream tube surface from 0 to 1, which is called *additive drag* (Refs. 24, 25, and 26) or *preentry drag* (Ref. 27)

and

F_{ext} = pressure force on nacelle's external surface

In the accounting system of viscous and pressure forces acting on the airframe and engine, the viscous forces on the nacelle are included in the airframe drag, and the pressure forces on the nacelle are included in the installed engine thrust.

The installed engine thrust T is then

$$\text{Shear force in strut of Fig. 4.1} = T = F_{int} - F_{ext}$$
$$= F_{int} + F'_{int} - (F_{ext} + F'_{ext})$$

where $F_{int} + F'_{ext}$ is called the *drag* D and where, as in the preceding, $F_{int} + F'_{int}$ is called the *uninstalled engine thrust* F. Using this notation, we have

$$\text{Installed engine thrust } T = F - D \tag{4.2}$$

The two forces F_{ext} and F'_{ext} that make up the drag D are called the *nacelle drag* D_{nac} and the *additive drag* D_{add}, respectively. Thus the drag force can be written as

$$D = D_{nac} + D_{add} \tag{4.3}$$

In computing the pressure force in the drag term, we must reference all pressures to ambient pressure P_0. Thus the pressure drag on the external surface of the nacelle is

$$D_{nac} = \int_1^9 (P - P_0)\mathrm{d}A_y \tag{4.4}$$

where P is the absolute pressure on the nacelle surface $\mathrm{d}A$, which has a vertical component of $\mathrm{d}A_y$. The additive drag is the pressure drag on the stream tube bounding the internal flow between stations 0 and 1, or

$$D_{add} = \int_0^1 (P - P_0)\mathrm{d}A_y \tag{4.5}$$

Application of the momentum equation to the stream tube shown in Fig. 4.4 between stations 0 and 1 gives

Forces on stream tube = change in momentum flux

$$\int_0^1 (P - P_0)\mathrm{d}A_y - \int_1 (P - P_0)\mathrm{d}A_y = \int_1 \frac{\rho V^2}{g_c}\mathrm{d}A_y - \int_0 \frac{\rho V^2}{g_c}\mathrm{d}A_y$$

Thus

$$D_{add} = \int_1 \left(P + \frac{\rho V^2}{g_c}\right)\mathrm{d}A_y - \int_0 \frac{\rho V^2}{g_c}\mathrm{d}A_y - P_0 A_1$$

or

$$D_{add} = \int_1 \left(P + \frac{\rho V^2}{g_c}\right)\mathrm{d}A_y - \int_0 \left(P + \frac{\rho V^2}{g_c}\right)\mathrm{d}A_y - P_0(A_1 - A_0) \tag{4.6}$$

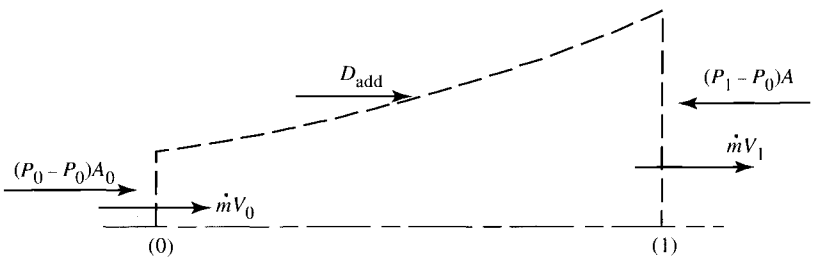

Fig. 4.4 Momentum equation applied to stream tube of engine air from 0 to 1.

The term $P + \rho V^2/g_c$ within the integrals is called the *total momentum flux*, and for a perfect gas

$$P + \frac{\rho V^2}{g_c} = P(1 + \gamma M^2) \tag{4.7}$$

Thus Eq. (4.6) can be expressed as

$$D_{\text{add}} = \int_1 P(1 + \gamma M^2)\mathrm{d}A_y - \int_0 \mathrm{P}(1 + \gamma M^2)\mathrm{d}A_y - P_0(A_1 - A_0)$$

For one-dimensional flow, this equation becomes

$$D_{\text{add}} = P_1A_1(1 + \gamma M_1^2) - P_0A_0(1 + \gamma M_0^2) - P_0(A_1 - A_0) \tag{4.8}$$

or

$$D_{\text{add}} = P_1A_1(1 + \gamma M_1^2) - P_0A_0\gamma M_0^2 - P_0A_1 \tag{4.9}$$

In the limit, as M_0 goes to zero, the $A_0M_0^2$ goes to zero, and Eq. (4.9) reduces to

$$(D_{\text{add}})_{M_0=0} = P_1A_1(1 + \gamma M_1^2) - P_0A_1 \tag{4.10}$$

Example 4.1

Two nacelles with inlet areas of (1) $A_1 = 0.20\,\text{m}^2$ and (2) $A_1 = 0.26\,\text{m}^2$ are being considered for use with a gas turbine engine X that produces an uninstalled thrust F of 20,000 N at sea level and $M_0 = 0.5$. Compare the installed engine thrust obtained with nacelle 1 and engine X to the installed engine thrust for nacalle 2 and engine X at $M_0 = 0.5$ and sea level. Engine X has a mass flow of 41.75 kg/s. Nacelles 1 and 2 each have the same nacelle drag of 900 N.

Solution: The installed engine thrust is given by

$$T = F - D = F - D_{\text{nac}} - D_{\text{add}}$$

Because both the uninstalled engine thrust F and nacelle drag D_{nac} are known, only the additive drag D_{add} need be determined for both nacelles. Either Eq. (4.8) or Eq. (4.9) can be used to calculate D_{add}, and both require the evaluation of P_1, M_1, and A_0. Because the mass flow rate into engine X is the same for both nacelles, A_0 will be determined first. The *mass flow parameter* (MFP) can

be used to find A_0 once the total temperature and pressure are known at station 0:

$$T_{t0} = T_0\left(1 + \frac{\gamma - 1}{2}M_0^2\right) = 288.2(1 + 0.2 \times 0.5^2) = 302.6\,\text{K}$$

$$P_{t0} = P_0\left(1 + \frac{\gamma - 1}{2}M_0^2\right)^{\gamma/(\gamma-1)} = 101{,}300(1 + 0.2 \times 0.5^2)^{35} = 120{,}160\,\text{Pa}$$

$$\text{MFP}(0.5)\sqrt{\frac{R}{g_c}} = \frac{\dot{m}\sqrt{T_{t0}}}{P_{t0}A_0}\sqrt{\frac{R}{g_c}} = 0.511053 \qquad \text{from Appendix E}$$

Thus

$$A_0 = \frac{\dot{m}\sqrt{T_{t0}}\sqrt{R/g_c}}{P_{t0}[\text{MFP}(0.5)\sqrt{R/g_c}]} = \frac{41.75\sqrt{302.6}(16.9115)}{120{,}160(0.511053)}$$
$$= 0.200\,\text{m}^2$$

With subsonic flow between stations 0 and 1, the flow between these two stations is assumed to be isentropic. Thus the total pressure and total temperature at station 1 are 120,160 Pa and 302.6 K. Because the mass flow rate, area, and total properties are known at station 1 for both nacelles, the Mach number M_1 and static pressure P_1 needed to calculate the additive drag can be determined as follows:

1) Calculate $\text{MFP}\sqrt{R/g_c}$ at station 1, and find M_1 from Appendix E.

2) Calculate P_1, using Eq. (3.10) or P/P_t from Appendix E.

Nacelle 1: Since the inlet area A_1 for nacelle 1 is the same as flow area A_0 and the flow process is isentropic, then $M_1 = 0.5$ and $P_1 = 101{,}300$ Pa. From Eq. (4.8), the additive drag is zero, and the installed thrust is

$$T = F - D_{\text{nac}} - D_{\text{add}} = 20{,}000 - 900 - 0 = 19{,}100\,\text{N}$$

Nacelle 2: Calculating $\text{MFP}\sqrt{R/g_c}$ at station 1, we find

$$\text{MFP}(M_1) = \frac{\dot{m}\sqrt{T_{t1}}}{P_{t1}A_1} = \frac{41.75\sqrt{302.6}}{120{,}160(0.26)}$$
$$= 0.0232465$$

From GASTAB, $M_1 = 0.3594$ and

$$P_1 = \frac{P_{t1}}{\{1 + [(\gamma - 1)/2]M_1^2\}^{\gamma/(\gamma-1)}} = \frac{120{,}160\,\text{Pa}}{1.09340} = 109.900\,\text{Pa}$$

Then, using Eq. (4.8), we have

$$\begin{aligned} D_{\text{add}} &= P_1A_1(1 + \gamma M_1^2) - P_0A_0(1 + \gamma M_0^2) - P_0(A_1 - A_0) \\ &= 109{,}900 \times 0.26(1 + 1.4 \times 0.3594^2) - 101{,}300 \\ &\quad \times 0.2(1 + 1.4 \times 0.5^2) - 101{,}300(0.26 - 0.20) \\ &= 33{,}741 - 27{,}351 - 6078 = 312\,\text{N} \\ T &= F - D_{\text{nac}} - D_{\text{add}} = 20{,}000 - 900 - 312 = 18{,}788\,\text{N} \end{aligned}$$

Conclusion: A comparison of the installed engine thrust T of nacelle 1 to that of nacelle 2 shows that nacelle 1 gives a higher installed engine thrust and is better than nacelle 2 at the conditions calculated.

Example 4.2

An inlet of about 48 ft^2 (a little larger than the inlet on one of the C5A's engines) is designed to have an inlet Mach number of 0.8 at sea level. Determine the variation of the additive drag with flight Mach number from $M_0 = 0$ to 0.9. Assume that M_1 remains constant at 0.8.

Solution: We will be using Eqs. (4.8) and (4.10) to solve this problem. The following values are known:

$$P_0 = 14.696\ \text{psia}, \quad M_1 = 0.8, \quad A_1 = 48\,\text{ft}^2, \quad \gamma = 1.4$$

Thus we must find values of A_0 and P_1 for each flight Mach number M_0. We assume isentropic flow between stations 0 and 1, and therefore P_t and A^* are constant. Using the relations for isentropic flow, We can write

$$P_1 = P_0 \frac{P_{t0}}{P_0} \frac{P_1}{P_{t1}} = P_0 \frac{(P/P_t)_1}{(P/P_t)_0}$$

$$A_0 = A_1 \frac{A_1^*}{A_1} \frac{A_0}{A_0^*} = A_1 \frac{(A/A^*)_0}{(A/A^*)_1}$$

We obtain values of P/P_t and A/A^* from the isentropic table (GASTAB program). At a flight Mach number of 0.9, we have

$$P_1 = P_0 \frac{(P/P_t)_1}{(P/P_t)_0} = 14.696\left(\frac{0.65602}{0.59126}\right) = 16.306\,\text{psia}$$

$$A_0 = A_1 \frac{(A/A^*)_0}{(A/A^*)_1} = 48\left(\frac{1.0089}{1.0382}\right) = 46.65\,\text{ft}^2$$

Table 4.1 Summary of additive calculations for Example 4.2

M_0	$\left(\frac{P}{P_t}\right)_0$	P_1, psia	$\left(\frac{A}{A^*}\right)_0$	A_0, ft^2	$1+\gamma M_0^2$	D_{add}, lbf
0.0	1.00000	9.641	—	—	1.000	24,768
0.1	0.99303	9.711	5.8218	269.16	1.014	17,711
0.2	0.97250	9.916	2.9635	137.01	1.056	12,135
0.3	0.93947	10.265	2.0351	94.09	1.126	7,857
0.4	0.89561	10.768	1.5901	73.52	1.224	4,687
0.5	0.84302	11.439	1.3398	61.94	1.350	2,453
0.6	0.78400	12.300	1.1882	54.94	1.504	1,017
0.7	0.72093	13.376	1.0944	50.60	1.686	258
0.8	0.65602	14.696	1.0382	48.00	1.896	0
0.9	0.59126	16.306	1.0089	46.65	2.134	164

Thus

$$\begin{aligned} D_{\text{add}} &= P_1A_1(1+\gamma M_1^2) - P_0A_0(1+\gamma M_0^2) - P_0(A_1 - A_0) \\ &= 16.306(144)(48)(1.896) - 14.696(144)(46.65)(2.134) \\ &\quad - 14.696(144)(1.35) \\ &= 213{,}693 - 210{,}672 - 2857 \\ &= 164 \text{ lbf} \end{aligned}$$

At a flight Mach number of 0, we have

$$(D_{\text{add}})_{M_0=0} = P_1A_1(1+\gamma M_1^2) - P_0A_1$$

$$P_t = (14.696)(0.65602) = 9.641 \text{ psia}$$

Thus

$$\begin{aligned} D_{\text{add}} &= 9.641(144)(48)(1.896) - 14.696(144)(48) \\ &= 126{,}347 - 101{,}579 \\ &= 24{,}768 \text{ lbf} \end{aligned}$$

Table 4.1 presents the results of this inlet's additive drag in the range of flight Mach numbers requested. As indicated in this table, the additive drag is largest at low flight Mach numbers for this fixed-area inlet.

As will be shown next, most of the additive drag D_{add} can be offset by the forebody portion of the nacelle drag (D_w, a negative drag or thrust), provided that the flow does not separate (in perfect flow, we will show that $D_{\text{add}} + D_w = 0$) with the large variation in M_0 and the fixed value of M_1,

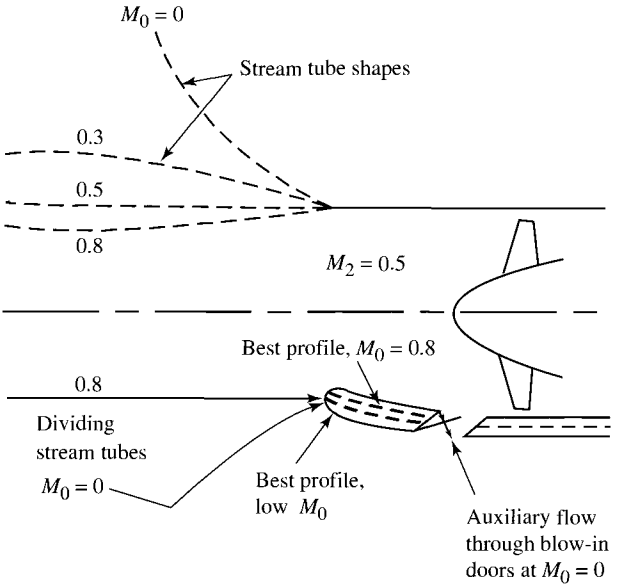

Fig. 4.5 Subsonic inlet at different flight Mach numbers (top) with auxiliary blow-in door (bottom) (from Ref. 28).

the path of the streamlines entering the inlet must go through large changes in geometry, as shown in Fig. 4.5. Boundary-layer separation on the forebody of the nacelle can occur when the inlet must turn the flow through large angles with a resulting decrease in the magnitude of the drag on the forebody portion of the nacelle and increase in the net drag $D_{\text{add}} + D_w$ on the front portion of the inlet. To reduce the additive drag at low flight Mach numbers, some subsonic inlets have blow-in doors or auxiliary inlets (see Fig. 4.5) that increase the inlet area at the low flight Mach numbers (full-throttle operation) and thus reduce the additive drag.

In the relationship between nacelle drag and additive drag, the nacelle drag and the additive drag are interdependent. We can learn something about this interdependence by considering a *perfect nacelle*, i.e., a nacelle with no external viscous drag or form drag.

We now consider a control volume for all of the fluid flowing external to the engine, i.e., all of the fluid outside the stream tube shown in Fig. 4.6. Because the flow is perfect (no shocks, no boundary layers, etc.), the fluid conditions are identical at the entrance 0 and exit 9 of our control volume.

Because the momentum of the fluid flowing through the control volume does not change, the sum of the pressure forces acting on the inside of the stream tube must equal zero. For perfect flow, we have

$$\int_0^1 (P - P_0)\mathrm{d}A_y + \int_1^9 (P - P_0)\mathrm{d}A_y + \int_9^\infty (P - P_0)\mathrm{d}A_y = 0$$

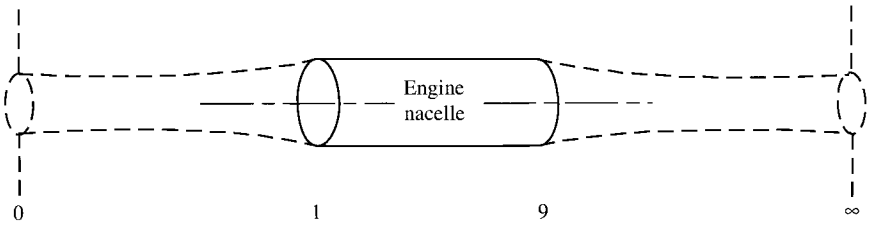

Fig. 4.6 Stream tube of flow through engine nacelle.

or

$$D_{\text{add}} + D_{\text{nac}} = -\int_{9}^{\infty} (P - P_0)\mathrm{d}A_y \tag{4.11}$$

For the case of a perfect fluid, we can combine Eqs. (4.11), (4.6), (4.3), and (4.2) to obtain

$$T = F + \int_{9}^{\infty} (P - P_0)\mathrm{d}A_y \tag{4.12}$$

For a perfectly expanded nozzle ($P_9 = P_0$) and a jet that is parallel to the free-stream ($\mathrm{d}A_y = 0$), the following conclusions can be made:

1) From Eq. (4.11), the sum of the additive drag and nacelle drag is zero.
2) From Eq. (4.12), the installed engine thrust T equals the uninstalled engine thrust F.

It is industry practice to break the nacelle drag into two components: the drag associated with the forebody (front half of nacelle) D_w and the drag associated with the afterbody (rear half of nacelle) D_b. This is usually a reasonable approach because often lip separation dominates near the inlet and boat-tail drag near the exit. Assuming the division of nacelle drag to be meaningful, we can interpret the two drag terms by considering the nacelle to be very long and parallel in the middle, as shown in Fig. 4.7.

In this case, perfect flow would give us P_0, etc., at the middle. Application of the momentum equation to a control volume from 0 to m containing all of the

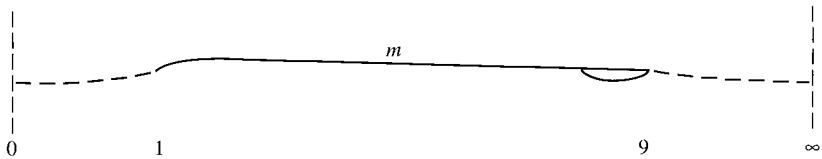

Fig. 4.7 Ideal long nacelle.

fluid outside the engine's stream tube will give

$$\int_0^1 (P - P_0)\mathrm{d}A_y + \int_1^m (P - P_0)\mathrm{d}A_y = 0$$

That is, in perfect flow,

$$D_{\text{add}} + D_{\text{w}} = 0 \tag{4.13}$$

similarly, application of the momentum equation to a control from m to ∞ containing all of the fluid outside the engine's stream tube will give

$$D_b + \int_9^\infty (P - P_0)\mathrm{d}A_y = 0 \tag{4.14}$$

4.3 Note on Propulsive Efficiency

The kinetic energy of the fluid flowing through an aircraft propulsion system is increased by an energy-transfer mechanism consisting of a series of processes constituting an engine cycle. From the point of view of an observer riding on the propulsion unit (see Fig. 4.8a), the engine cycle output is the increase of kinetic energy received by the air passing through the engine, which is $(V_9^2 - V_0^2)/(2g_c)$. From this observer's point of view, the total power output of the engine is the kinetic energy increase imparted to the air per unit time. On the other hand, from the point of view of an observer on the ground (see Fig. 4.8b), one sees the aircraft propulsion system's thrust moving at a velocity V_0 and observes the still air to receive an increase in kinetic energy, after passing through the engine, by an amount $(V_9 - V_0)^2/(2g_c)$. From this point of view, therefore, the total effect of the engine (and its output) is the sum of the propulsive power FV_0 and the kinetic energy per unit time imparted to the air passing through the engine. The sole purpose of the engine is to produce a propulsive power, and this is called the *useful power output* of the propulsion system. The ratio of the useful power output to the total power output of the propulsion system is called the *propulsive efficiency* [see Eq. (1.14)].

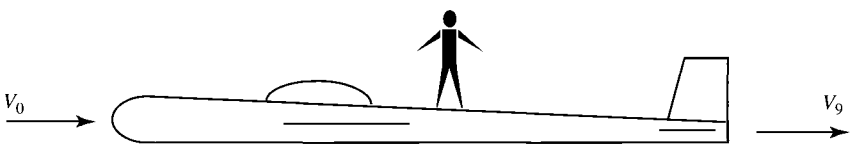

Fig. 4.8a Velocity change by observer on aircraft.

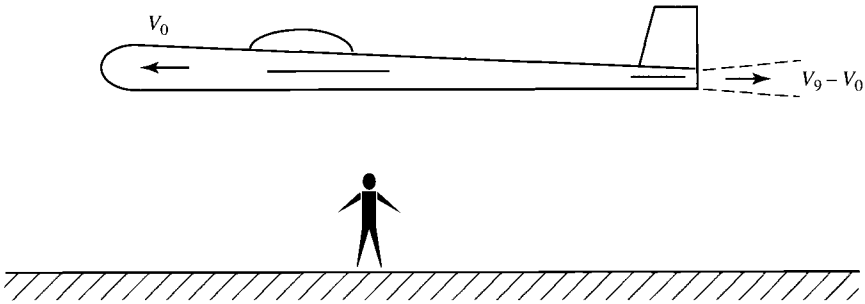

Fig. 4.8b Velocity change by observer on ground.

4.4 Gas Turbine Engine Components

The inlet, compressor, combustor, turbine, and nozzle are the main components of the gas turbine engine. The purpose and operation of these components and two thrust augmentation techniques are discussed in this section.

4.4.1 Inlets

An inlet reduces the entering air velocity to a level suitable for the compressor. The air velocity is reduced by a compression process that increases the air pressure. The operation and design of the inlet are described in terms of the efficiency of the compression process, the external drag of the inlet, and the mass flow into the inlet. The design and operation of the inlet depend on whether the air entering the duct is subsonic or supersonic. As the aircraft approaches the speed of sound, the air tends to be compressed more, and at Mach 1, shock waves occur. Shock waves are compression waves, and at higher Mach numbers, these compression waves are stronger. Compression by shock waves is inefficient. In subsonic flow, there are no shock waves, and the air compression takes place quite efficiently. In supersonic flow, there are shock waves present. Shock waves and the compressibility of air then influence the design of inlets.

4.4.1.1 Subsonic inlet. The subsonic inlet can be a divergent duct, as shown in Fig. 4.9. This duct is satisfactory until the Match number becomes greater than 1, at which time a shock wave occurs at the mouth and the compression process becomes inefficient. The subsonic divergent duct operates

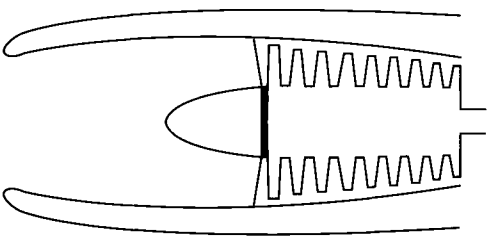

Fig. 4.9 Subsonic inlet.

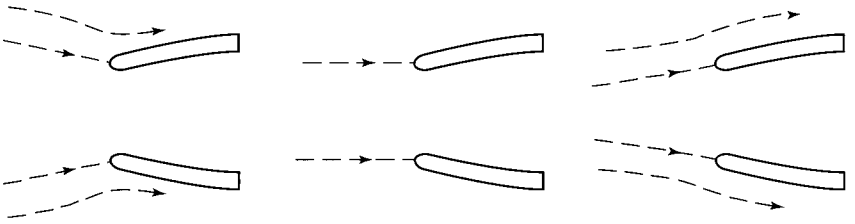

Fig. 4.10 Subsonic inlet flow patterns.

best at one velocity (design point), and at other velocities, the compression process is less efficient and the external drag is greater. The airflow patterns for the subsonic inlet are shown in Fig. 4.10.

4.4.1.2 Supersonic inlet. Because shock waves will occur in supersonic flow, the geometry of supersonic inlets is designed to obtain the most efficient compression with a minimum of weight. If the velocity is reduced from a supersonic speed to a subsonic speed with one normal shock wave, the compression process is relatively inefficient. If several oblique shock waves are employed to reduce the velocity, the compression process is more efficient. Two typical supersonic inlets are the *ramp* (two-dimensional wedge) and the *centerbody* (three-dimensional spike), which are shown in Fig. 4.11. The shock wave positions in Fig. 4.11 are for the design condition of the inlet. At off-design Mach numbers, the positions of the shock waves change, thus affecting the external drag and the efficiency of compression. A more efficient ramp or centerbody inlet can be designed by using more than two shock waves to compress the entering air. Also, if the geometry is designed to be variable, the inlet operates more efficiently over a range of Mach numbers.

4.4.2 Compressors

The function of the compressor is to increase the pressure of the incoming air so that the combustion process and the power extraction process after combustion can be carried out more efficiently. By increasing the pressure of the air, the volume of the air is reduced, which means that the combustion of the fuel/air mixture will occur in a smaller volume.

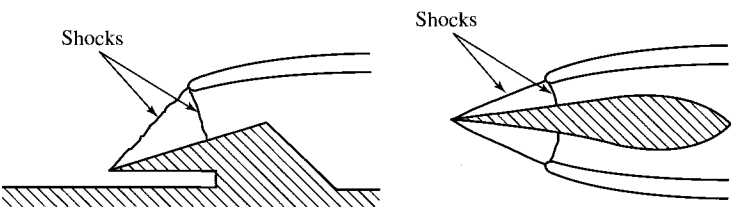

Fig. 4.11 Supersonic inlets.

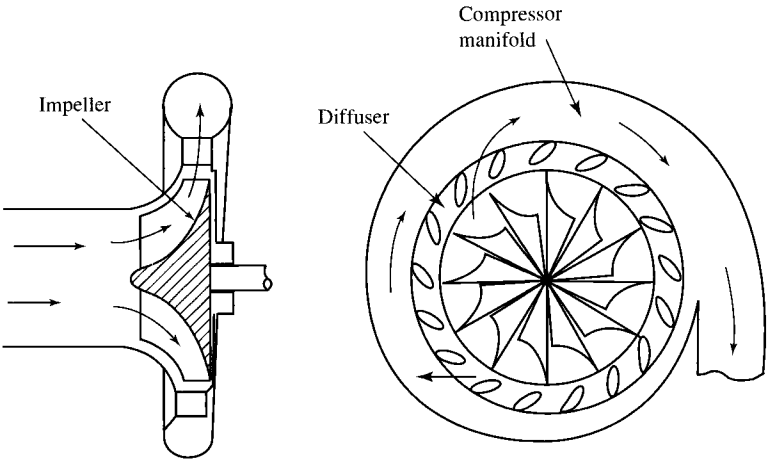

Fig. 4.12 Single-stage centrifugal compressor.

4.4.2.1 Centrifugal compressor. The compressor was the main stumbling block during the early years of turbojet engine development. Great Britain's Sir Frank Whittle solved the problem by using a centrifugal compressor. This type of compressor is still being used in many of the smaller gas turbine engines. A typical single-stage centrifugal compressor is shown in Fig. 4.12. The compressor consists of three main parts: an impeller, a diffuser, and a compressor manifold. Air enters the compressor near the hub of the impeller and is then compressed by the rotational motion of the impeller. The compression occurs by first increasing the velocity of the air (through rotation) and then diffusing the air where the velocity decreases and the pressure increases. The diffuser also straightens the flow, and the manifold serves as a collector to feed the air into the combustor. The single-stage centrifugal compressor has a low efficiency and a maximum compression ratio of 4:1 or 5:1. Multistage centrifugal compressors are somewhat better, but an axial compressor offers more advantages.

4.4.2.2 Axial compressors. An axial compressor is shown in Fig. 4.13. The air in an axial compressor flows in an axial direction through a series of rotating *rotor* blades and stationary *stator* vanes that are concentric with the axis of rotation. Each set of rotor blades and stator vanes is known as a *stage*. The flow

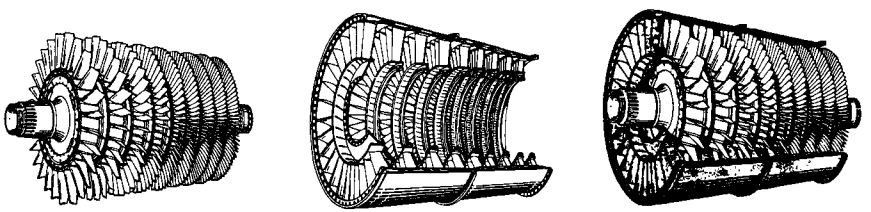

Fig. 4.13 Multistage axial compressor. (Courtesy of Pratt & Whitney.)

path in an axial compressor decreases in the cross-sectional area in the direction of flow. The decrease of area is in proportion to the increased density of the air as the compression progresses from stage to stage. Figure 4.13 contains a schematic of an axial compressor. Each stage of an axial compressor produces a small compression pressure ratio (1.1:1 to 1.2:1) at a high efficiency. Therefore, for high pressure ratios (12:1), multiple stages are used. Axial compressors are also more compact and have a smaller frontal area than a centrifugal compressor, which are added advantages. For the best axial compressor efficiency, the compressor operates at a constant axial velocity, as shown in Fig. 1.6. At high compression ratios, multistaging a single axial compressor does not produce as efficient an operation as a dual axial compressor would (see Fig. 1.4a). For a single rotational speed, there is a limit in the balance operation between the first and last stages of the compressor. To obtain more flexibility and a more uniform loading of each compressor stage, a dual compressor with two different rotational speeds is generally used in high-compression-ratio axial compressors.

4.4.3 Combustor or Main Burner

The combustor is designed to burn a mixture of fuel and air and to deliver the resulting gases to the turbine at a uniform temperature. The gas temperature must not exceed the allowable structural temperature of the turbine. A schematic of a combustor is shown in Fig. 4.14. About one-half of the total volume of air entering the burner mixes with the fuel and burns. The rest of the air—secondary air—is simply heated or may be thought of as cooling the products of combustion and cooling the burner surfaces. The ratio of total air to fuel varies among the different types of engines from 30 to 60 parts of air to 1 part of fuel by weight. The average ratio in new engine designs is about 40:1, but only 15 parts are used for burning (since the combustion process demands that the number of parts of air to fuel must be within certain limits at a given pressure for combustion to occur). Combustion chambers may be of the can, the annular, or the can-annular type, as shown in Fig. 4.15.

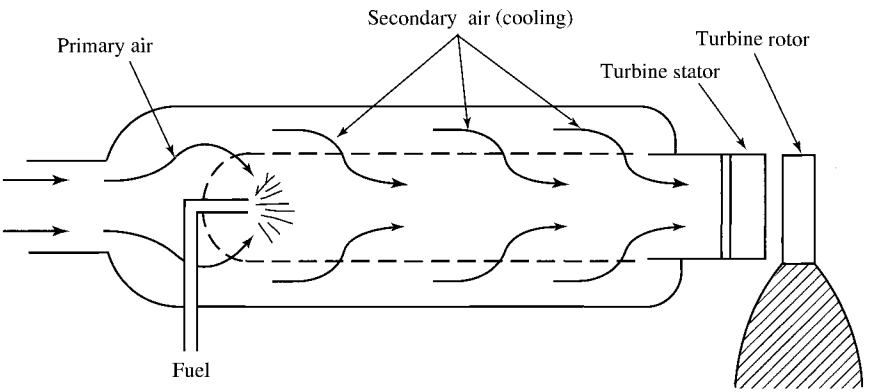

Fig. 4.14 Straight-through flow combustor.

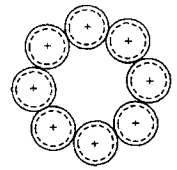

a) Can

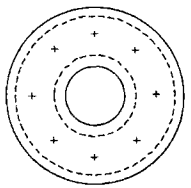

b) Annular

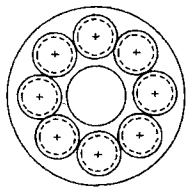

c) Can annular

Casing

Liner

Fuel inlet

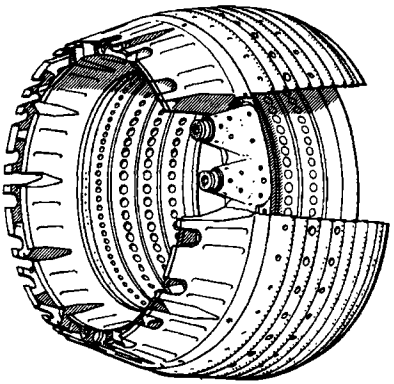

Typical annular-type combustion chamber

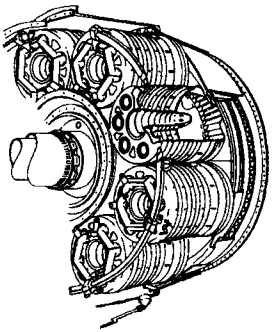

Typical can-annular-type combustion chamber

Fig. 4.15 Cross sections of combustion chambers. (Courtesy of Pratt & Whitney.)

For an acceptable burner design, the pressure loss as the gases pass through the burner must be held to a minimum, the combustion efficiency must be high, and there must be no tendency for the burner to blow out (flameout). Also, combustion must take place entirely within the burner.

4.4.4 Turbines

The turbine extracts kinetic energy from the expanding gases that flow from the combustion chamber. The kinetic energy is converted to shaft horsepower to drive the compressor and the accessories. Nearly three-fourths of all the energy available from the products of combustion is required to drive the compressor. The axial-flow turbine consists of a turbine wheel *rotor* and a set of stationary vanes *stator*, as shown in Fig. 4.16. The set of stationary vanes of the turbine is a plane of vanes (concentric with the axis of the turbine) that are set at an angle to form a series of small nozzles that discharge the gases onto the blades of the turbine wheel. The discharge of the gases onto the rotor

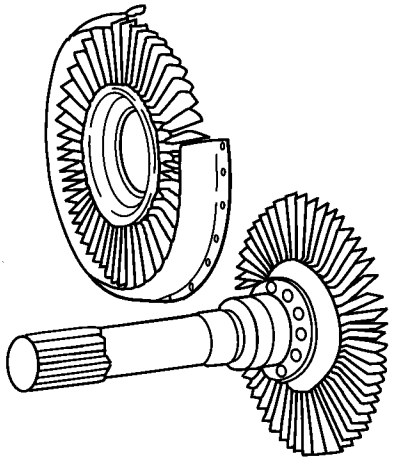

Fig. 4.16 Axial-flow turbine components.

allows the kinetic energy of the gases to be transformed to mechanical shaft energy.

Like the axial compressor, the axial turbine is usually multistaged. There are generally fewer turbine stages than compressor stages because in the turbine the pressure is decreasing (expansion process), whereas in the compressor the pressure is increasing (compression process). In each process (expansion or compression), the blades of the axial turbine or axial compressor act as airfoils, and the airflow over the airfoil is more favorable in the expansion process. The result is that one stage of turbine can power many compressor stages.

4.4.4.1 Impulse turbine. The impulse turbine and the reaction turbine are the two basic types of axial turbines, as shown in Fig. 4.17. In the impulse type, the relative discharge velocity of the rotor is the same as the relative inlet velocity because there is no net change in pressure between the rotor inlet and rotor exit. The stator nozzles of the impulse turbine are shaped to form passages that increase the velocity and reduce the pressure of the escaping gases.

4.4.4.2 Reaction turbine. In the reaction turbine, the relative discharge velocity of the rotor increases and the pressure decreases in the passages between rotor blades. The stator nozzle passages of the reaction turbine merely alter the direction of the flow.

Most turbines in jet engines are a combination of impulse and reaction turbines. In the design of turbines, the following items must be considered: 1) shaft rotational speed, 2) gas flow rate, 3) inlet and outlet temperatures, 4) inlet and outlet pressures, 5) exhaust velocity, and 6) required power output. If the jet engine is equipped with a dual compressor, the turbine must also be dual or split.

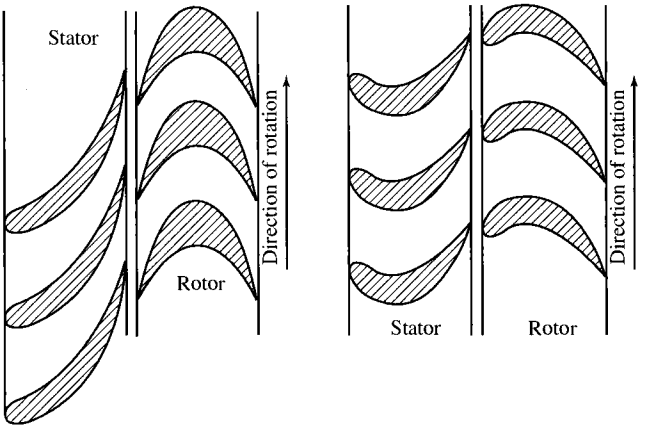

a) Impulse **b) Reaction**

Fig. 4.17 Impulse and reaction stages.

4.4.5 Exhaust Nozzle

The purpose of the exhaust nozzle is to increase the velocity of the exhaust gas before discharge from the nozzle and to collect and straighten gas flow from the turbine. In operating, the gas turbine engine converts the internal energy of the fuel to kinetic energy in the exhaust gas stream. The net thrust (or force) of the engine is the result of this operation, and it can be calculated by applying Newton's second law of motion (see Chapter 2). For large values of specific thrust, the kinetic energy of the exhaust gas must be high, which implies a high exhaust velocity. The nozzle supplies a high exit velocity by expanding the exhaust gas in an expansion process that requires a decrease in pressure. The pressure ratio across the nozzle controls the expansion process, and the maximum thrust for a given engine is obtained when the exit pressure equals the ambient pressure. Nozzles and their operation are discussed further in Chapters 2, 3, and 10. The two basic types of nozzles used in jet engines are the convergent and convergent-divergent nozzles.

4.4.5.1 Convergent nozzle. The convergent nozzle is a simple convergent duct, as shown in Fig. 4.18. When the nozzle pressure ratio (turbine exit pressure to nozzle exit pressure) is low (less than about 2), the convergent nozzle is used. The convergent nozzle has generally been used in low-thrust engines for subsonic aircraft.

4.4.5.2 Convergent-divergent nozzle. The convergent-divergent nozzle can be a convergent duct followed by a divergent duct. Where the cross-sectional area of the duct is a minimum, the nozzle is said to have a *throat* at that position. Most convergent-divergent nozzles used in supersonic aircraft are not simple

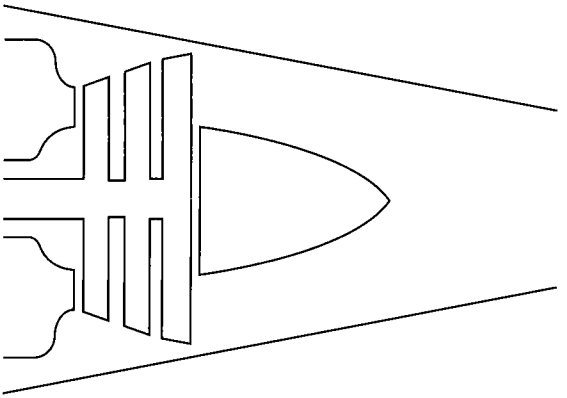

Fig. 4.18 Convergent exhaust nozzle.

ducts, but incorporate variable geometry and other aerodynamic features, as shown in Fig. 4.19. Only the throat area and exit area of the nozzle in Fig. 4.19 are set mechanically, the nozzle walls being determined aerodynamically by the gas flow. The convergent-divergent nozzle is used if the nozzle pressure ratio is high. High-specific-thrust engines in supersonic aircraft generally have some form of convergent-divergent nozzle. If the engine incorporates an afterburner, the nozzle throat and exit area must be varied to match the different flow conditions and to produce the maximum available thrust.

4.4.6 Thrust Augmentation

Thrust augmentation can be accomplished by either water injection or afterburning.

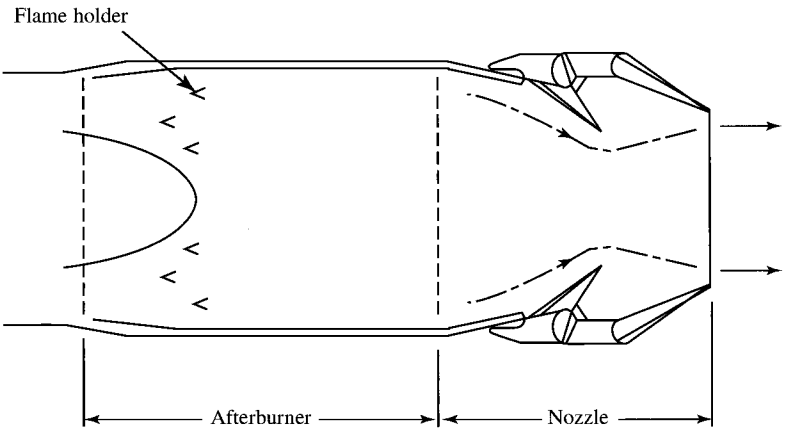

Fig. 4.19 Convergent-divergent ejector exhaust nozzle. (Courtesy of Pratt & Whitney.)

4.4.6.1 Water injection. Thrust augmentation by water injection (or by water/alcohol mixture) is achieved by injecting water into either the compressor or the combustion chamber. When water is injected into the inlet of the compressor, the mass flow rate increases and a higher combustion chamber pressure results if the turbine can handle the increased mass flow rate. The higher pressure and the increase in mass flow combine to increase the thrust. Injection of water into the combustion chamber produces the same effect, but to a lesser degree and with greater consumption of water. Water injection on a hot day can increase the takeoff thrust by as much as 50% because the original mass of air entering the jet engine is less for a hot day. The amount of air entering any turbomachine is determined by its volumetric constraints; therefore, it follows that the mass flow on a hot day will be less because the air is less dense on a hot day.

4.4.6.2 Afterburning. Another method of thrust augmentation is by burning additional fuel in the afterburner. The afterburner is a section of duct between the turbine and exhaust nozzle. The schematic diagram in Fig. 4.19 shows the afterburner section. The afterburner consists of the duct section, fuel injectors, and flame holders. It is possible to have afterburning because, in the main burner section, the combustion products are air-rich. The effect of the afterburning operation is to raise the temperature of the exhaust gases that, when exhausted through the nozzle, will reach a higher exit velocity. The pressure/temperature velocity profile for afterburning is also shown in Fig 1.6. The J79 for afterburner operation has a thrust of 17,900 lbf and a *thrust specific fuel consumption* (TSFC) of 1.965 [(lbm/h)/lbf]/h, and for military operation (no afterburning) it has a thrust of 11,870 lbf and a TSFC of 0.84 [(lbm/h)/lbf]/h. We then see that afterburning produces large thrust gains at the expense of fuel economy.

4.5 Brayton Cycle

The Brayton power cycle is a model used in thermodynamics for an ideal gas turbine power cycle. It is composed of the four following processes, which are also shown in Fig. 4.20a:

1) Isentropic compression (2 to 3)
2) Constant-pressure heat addition (3 to 4)
3) Isentropic expansion (4 to 9)
4) Constant-pressure heat rejection (9 to 2)

The basic components of the Brayton cycle are shown to the right in Fig. 4.20b. In the ideal cycle, the processes through both the compressor and the turbine are considered to be reversible and adiabatic (isentropic). The processes through the heater and cooler are considered to be constant-pressure in the ideal cycle.

For a calorically perfect gas, thermodynamic analysis of the ideal Brayton cycle gives the following equations for the rate of energy transfer of each

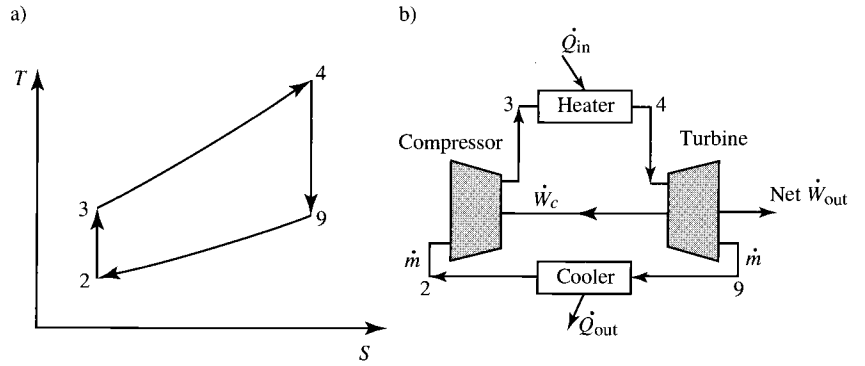

Fig. 4.20 Brayton cycle.

component:

$$\dot{W}_c = \dot{m}c_p(T_3 - T_2) \qquad \dot{Q}_{in} = \dot{m}c_p(T_4 - T_3)$$
$$\dot{W}_t = \dot{m}c_p(T_4 - T_9) \qquad \dot{Q}_{out} = \dot{m}c_p(T_9 - T_2)$$
$$\text{Net } \dot{W}_{out} = \dot{W}_t - \dot{W}_c = \dot{m}c_p[T_4 - T_9 - (T_3 - T_2)]$$

Now, the thermal efficiency of the cycle is $\eta_T = \text{net } \dot{W}_{out}/\dot{Q}_{in}$. Noting that $(P_3/P_2)^{(\gamma-1)/\gamma} = T_3/T_2 = T_4/T_9$, we see that the thermal efficiency for the ideal Brayton cycle can be shown to be given by

$$\eta_T = 1 - \left(\frac{1}{\text{PR}}\right)^{(\gamma-1)/\gamma} \tag{4.15}$$

where PR is the *pressure ratio* P_3/P_2. The thermal efficiency is plotted in Fig. 4.21 as a function of the compressor pressure ratio for two ratios of specific heats.

For an ideal Brayton cycle with fixed compressor inlet temperature T_2 and heater exit temperature T_4, simple calculus yields an expression for the pressure ratio P_3/P_2 and associated temperature ratio T_3/T_2 giving the maximum net work output per unit mass. This optimum compressor pressure, or temperature ratio, corresponds to the maximum area within the cycle on a *T-s* diagram, as shown in Fig. 4.22. One can show that the optimum compressor temperature ratio is given by

$$\left(\frac{T_3}{T_2}\right)_{\text{max work}} = \sqrt{\frac{T_4}{T_2}} \tag{4.16}$$

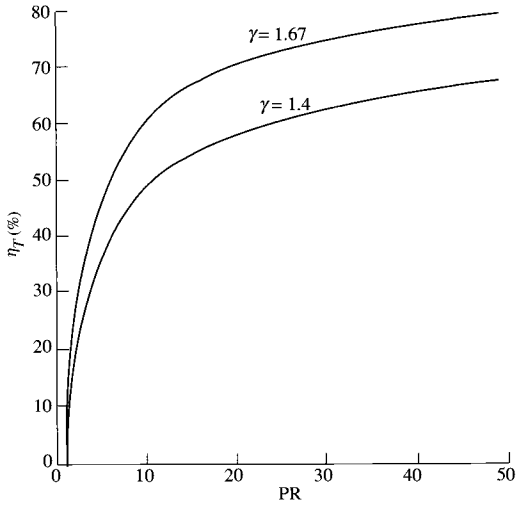

Fig. 4.21 Thermal efficiency of ideal Brayton cycle.

and the corresponding net work output per unit mass is given by

$$\frac{\text{Net } \dot{W}_{\text{out}}}{\dot{m}} = c_p T_2 \left(\sqrt{\frac{T_4}{T_2}} - 1 \right)^2 \tag{4.17}$$

which is plotted in Fig. 4.23 vs T_4 for air with $T_2 = 288$ K.

Three variations in the basic Brayton cycle are shown in Figs. 4.24–4.26. Figure 4.24 shows the cycle with a *high-pressure* (HP) turbine driving the compressor and a free-power turbine providing the output power. This cycle has the same thermal efficiency as the ideal Brayton cycle of Fig. 4.20. Figure 4.25 shows the Brayton cycle with reheat. Addition of reheat to the cycle increases the specific power of the free turbine and reduces the thermal efficiency.

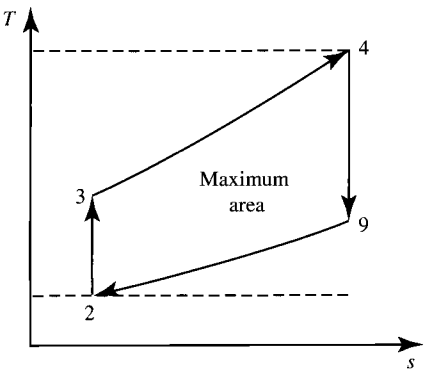

Fig. 4.22 Maxium-power-output Brayton cycle.

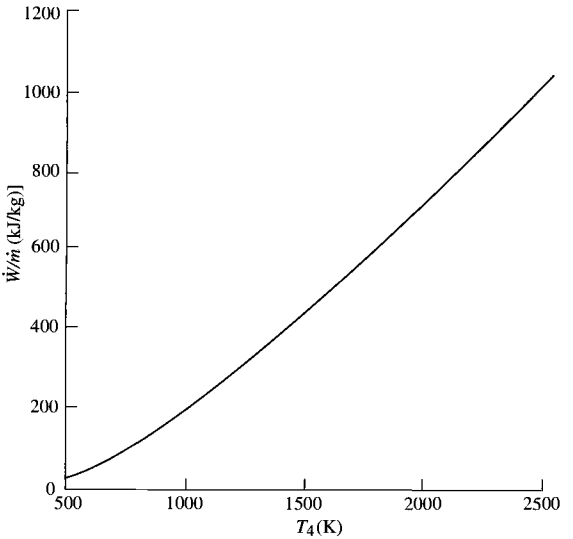

Fig. 4.23 Variation of maximum output power with T_4 for ideal Brayton cycle (T_2 = 288 K).

Figure 4.26 shows the ideal Brayton cycle with regeneration. When regeneration is added to the basic Brayton cycle, the energy input to the heater is reduced, which increases the cycle's thermal efficiency. For an ideal regenerator, we have

$$T_{3.5} = T_9 \qquad \text{and} \qquad T_{9.5} = T_3$$

Note that regeneration is possible only when T_9 is greater than T_3, which requires low cycle pressure ratios. The thermal efficiency of an ideal Brayton cycle with regeneration is shown in Fig. 4.27 for several values of T_4/T_2 along with the

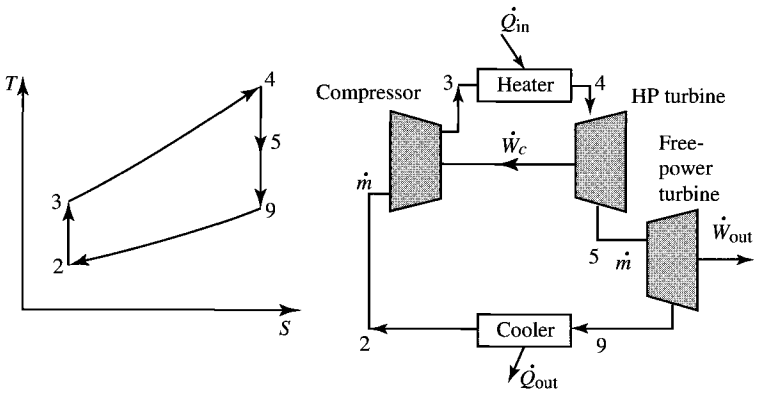

Fig. 4.24 Brayton cycle with free-power turbine.

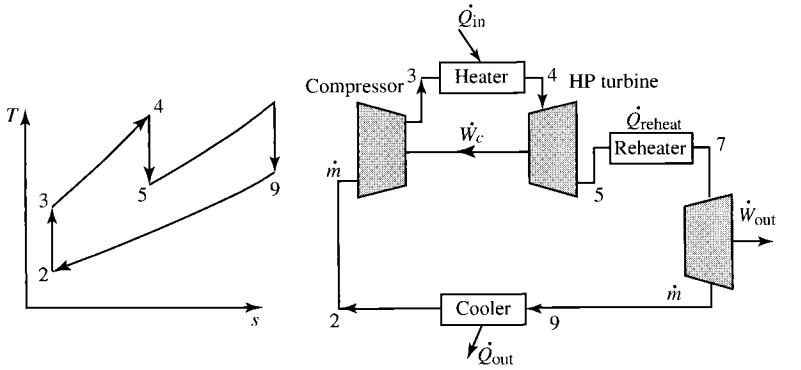

Fig. 4.25 Brayton cycle with reheat.

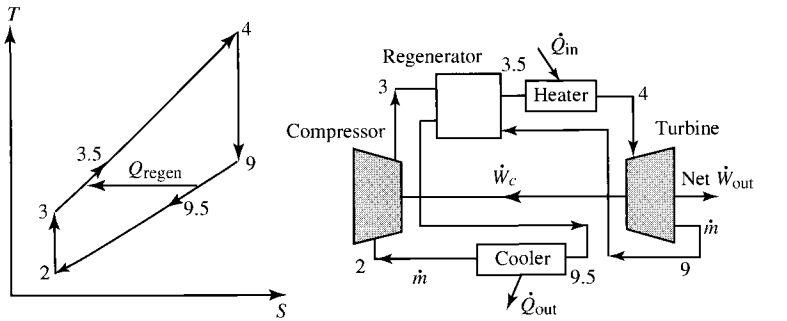

Fig. 4.26 Ideal Brayton cycle with regeneration.

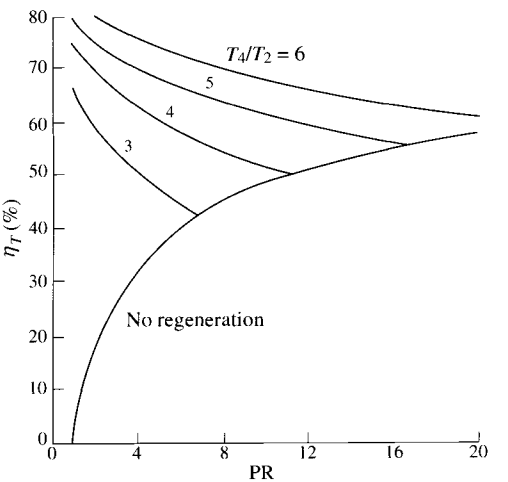

Fig. 4.27 Thermal efficiency of ideal Brayton cycle with regeneration.

thermal efficiency of the cycle without regeneration. The thermal efficiency of the ideal Brayton cycle with regeneration is given by

$$\eta_T = 1 - \frac{(\mathrm{PR})^{(\gamma-1)/\gamma}}{T_4/T_2} \tag{4.18}$$

4.6 Aircraft Engine Design

This introductory chapter to aircraft propulsion systems has presented the basic engine components and ideal engines. The following chapters present the cycle analysis (thermodynamic design-point study) of ideal and real engines, off-design performance, and an introduction to the aerodynamics of engine components. The design procedure for a typical gas turbine engine, shown in Fig. 4.28, requires that thermodynamic design-point studies (cycle analysis)

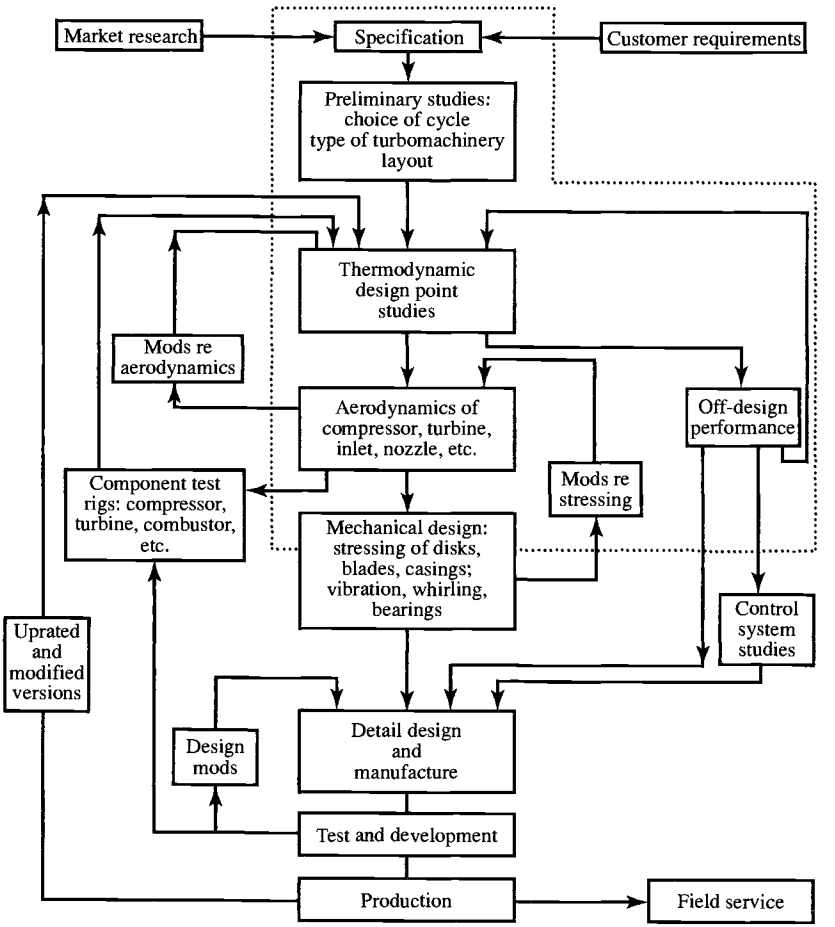

Fig. 4.28 Typical aircraft gas turbine design procedure (from Ref. 29).

and off-design performance be in the initial steps of design. The iterative nature of design is indicated in Fig. 4.28 by the feedback loops. Although only a few loops are shown, many more exist. Those items within the dashed lines of Fig. 4.28 are addressed within this textbook.

Problems

4.1 The inlet for a high-bypass-ratio turbofan engine has an area A_1 of 6.0 m^2 and is designed to have an inlet Mach number M_1 of 0.6. Determine the additive drag at the flight conditions of sea-level static test and Mach number of 0.8 at 12-km altitude.

4.2 An inlet with an area A_1 of 10 ft^2 is designed to have an inlet Mach number M_1 of 0.6. Determine the additive drag at the flight conditions of sea-level static test and Mach number of 0.8 at 40-kft altitude.

4.3 Determine the additive drag for an inlet having an area A_1 of 7000 $in.^2$ and a Mach number M_1 of 0.8 while flying at a Mach number M_0 of 0.4 at an altitude of 2000 ft.

4.4 Determine the additive drag for an inlet having an area A_1 of 5.0 m^2 and a Mach number M_1 of 0.7 while flying at a Mach number M_0 of 0.3 at an altitude of 1 km.

4.5 A turbojet engine under static test ($M_0 = 0$) has air with a mass flow of 100 kg/s flowing through an inlet area A_1 of 0.56 m^2 with a total pressure of 1 atm and total temperature of 288.8 K. Determine the additive drag of the inlet.

4.6 In Chapter 1, the loss in thrust due to the inlet is defined by Eq. (1.8) as $\phi_{\text{inlet}} = D_{\text{inlet}}/F$. Determine ϕ_{inlet} for the inlets of Example 4.1.

4.7 Determine the variation of inlet mass flow rate with Mach number M_0 for the inlet of Example 4.2

4.8 In Chapter 1, the loss in thrust due to the inlet is defined by Eq. (1.8) as $\phi_{\text{inlet}} = D_{\text{inlet}}/F$. For subsonic flight conditions, the additive drag D_{add} is a conservative estimate of D_{inlet}.

(a) Using Eq. (4.9) and isentropic flow relations, show that ϕ_{inlet} can be written as

$$\phi_{\text{inlet}} = \frac{D_{\text{add}}}{F} = \frac{(M_0/M_1)\sqrt{T_1/T_0}(1 + \gamma M_1^2) - (A_1/A_0 + \gamma M_0^2)}{(Fg_c/\dot{m}_0)(\gamma M_0/a_0)}$$

(b) Calculate and plot the variation of ϕ_{inlet} with flight Mach number M_0 from 0.2 to 0.9 for inlet Mach numbers M_1 of 0.6 and 0.8 with $(Fg_c/\dot{m}_0)(\gamma/a_0) = 4.5$.

4.9 A bell-mouth inlet (see Fig. P2.8) is installed for static testing of jet engines. Determine the force on the bell-mouth inlet with the data of Problem 2.34b for an inlet area that is 8 times the area at station 2 (assume that the inlet wall is a stream tube and that the outside of the bell-mouth inlet sees a static pressure equal to P_0.

4.10 The maximum power out of an ideal Brayton cycle operating between temperatures T_2 and T_4 is given by Eq. (4.17). By taking the derivative of the net work out of an ideal Brayton cycle with respect to the pressure ratio (PR) and setting it equal to zero, show that Eq. (4.16) gives the resulting compressor temperature ratio and Eq. (4.17) gives the net work out.

4.11 Show that Eq. (4.18) gives the thermal efficiency for the ideal Brayton cycle with regeneration.

4.12 For the ideal Brayton cycle with regeneration, regeneration is desirable when $T_9 \geq T_3$. Show that the maximum compressor pressure ratio $\mathrm{PR}_{\max}$ for regeneration ($T_9 = T_3$) is given by

$$\mathrm{PR}_{\max} = \left(\frac{T_4}{T_2}\right)^{\gamma/[2(\gamma-1)]}$$

Page is intentionally blank

5
Parametric Cycle Analysis of Ideal Engines

5.1 Introduction

Cycle analysis studies the thermodynamic changes of the working fluid (air and products of combustion in most cases) as it flows through the engine. It is divided into two types of analysis: *parametric cycle analysis* (also called *design-point* or *on-design)* and *engine performance analysis* (also called *off-design).* Parametric cycle analysis determines the performance of engines at different flight conditions and values of design choice (e.g., compressor pressure ratio) and design limit (e.g., combustor exit temperature) parameters. Engine performance analysis determines the performance of a specific engine at all flight conditions and throttle settings.

In both forms of analysis, the components of an engine are characterized by the change in properties they produce. For example, the compressor is described by a total pressure ratio and efficiency. A certain engine's behavior is determined by its geometry, and a compressor will develop a certain total pressure ratio for a given geometry, speed, and airflow. Because the geometry is not included in parametric cycle analysis, the plots of specific thrust $F/\dot{m}_0$, and thrust specific fuel consumption S vs, say, Mach number or compressor pressure ratio are not portraying the behavior of a specific engine. Each point on such plots represents a different engine. The geometry for each plotted engine will be different, and thus we say that parametric cycle analysis represents a "rubber engine." Parametric cycle analysis is also called *designpoint analysis* or *on-design analysis* because each plotted engine is operating at its so-called design point.[4,12,28,29]

The main objective of parametric cycle analysis is to relate the engine performance parameters (primarily thrust F and thrust specific fuel consumption S) to design choices (compressor pressure ratio, fan pressure ratio, bypass ratio, etc.), to design limitations (burner exit temperature, compressor exit pressure, etc.), and to flight environment (Mach number, ambient temperature, etc.). From parametric cycle analysis, we can easily determine which engine type (e.g., turbofan) and component design characteristics (range of design choices) best satisfy a particular need.

Supporting Material for this chapter is available electronically. See page 869 for instructions to download.

The value of parametric cycle analysis depends directly on the realism with which the engine components are characterized. For example, if a compressor is specified by the total pressure ratio and the isentropic efficiency, and if the analysis purports to select the best total pressure ratio for a particular mission, then the choice may depend on the variation of efficiency with pressure ratio. For the conclusions to be useful, a realistic variation of efficiency with total pressure ratio must be included in the analysis.

The parametric cycle analysis of engines will be developed in stages. First the general steps applicable to the parametric cycle analysis of engines will be introduced. Next these steps will be followed to analyze engines where all engine components are taken to be ideal. Trends of these ideal engines will be analyzed, given that only basic conclusions can be deduced. The parametric cycle analysis of ideal engines allows us to look at the characteristics of aircraft engines in the simplest possible ways so that they can be compared. Following this, realistic assumptions as to component losses will be introduced in Chapter 6 and the parametric cycle analysis repeated for the different aircraft engines in Chapter 7. Performance trends of these engines with losses (real engines) will also be analyzed in Chapter 8.

In the last chapter on engine cycle analysis, models will be developed for the performance characteristics of the engine components. The aerothermodynamic relationships between the engine components will be analyzed for several types of aircraft engines. Then the performance of specific engines at all flight conditions and throttle settings will be predicted.

5.2 Notation

The *total* or *stagnation temperature* is defined as that temperature reached when a steadily flowing fluid is brought to rest (stagnated) adiabatically. If T_t denotes the total temperature, T the static (thermodynamic) temperature, and V the flow velocity, then application of the first law of thermodynamics to a calorically perfect gas gives $T_t = T + V^2/(2g_c c_p)$. However, the Mach number $M = V/a = V/\sqrt{\gamma g_c RT}$ can be introduced into the preceding equation to give

$$T_t = T\left(1 + \frac{\gamma - 1}{2} M^2\right) \tag{5.1}$$

The *total or stagnation pressure* P_t is defined as the pressure reached when a steady flowing stream is brought to rest adiabatically and reversibly (i.e., isentropically). Since $P_t/P = (T_t/T)^{\gamma/(\gamma-1)}$ then

$$P_t = P\left(1 + \frac{\gamma - 1}{2} M^2\right)^{\gamma/(\gamma-1)} \tag{5.2}$$

Ratios of total temperatures and pressures will be used extensively in this text, and a special notation is adopted for them. We denote a *ratio of total pressures* across a component by π, with a subscript indicating the component: d for diffuser (inlet), c for compressor, b for burner, t for turbine, n for nozzle,

and f for fan:

$$\pi_a = \frac{\text{total pressure leaving component } a}{\text{total pressure entering component } a} \tag{5.3}$$

Similarly, the *ratio of total temperatures* is denoted by τ, and

$$\tau_a = \frac{\text{total temperature leaving component } a}{\text{total temperature entering component } a} \tag{5.4}$$

There are the following exceptions:

1) We define the total/static temperature and pressure ratios of the freestream (τ_r and π_r) by

$$\tau_r = \frac{T_{t0}}{T_0} = 1 + \frac{\gamma - 1}{2} M_0^2 \tag{5.5}$$

$$\pi_r = \frac{P_{t0}}{P_0} = \left(1 + \frac{\gamma - 1}{2} M_0^2\right)^{\gamma/(\gamma-1)} \tag{5.6}$$

Thus the total temperature and pressure of the freestream can be written as

$$T_{t0} = T_0 \tau_r \quad P_{t0} = P_0 \pi_r$$

2) Also, τ_λ is defined as the ratio of the burner exit enthalpy $c_p T_t$ to the ambient enthalpy $c_p T_0$:

$$\tau_\lambda = \frac{h_{t\ \text{burner exit}}}{h_0} = \frac{(c_p T_t)_{\text{burner exit}}}{(c_p T)_0} \tag{5.7}$$

Figure 5.1 shows the cross section and station numbering of a turbofan engine with both afterburning and duct burning. This station numbering is in accordance with Aerospace Recommended Practice (ARP) 755A (see Ref. 30). Note that

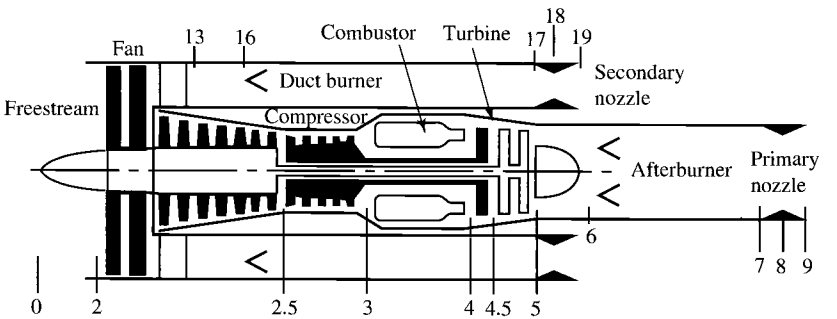

Fig. 5.1 Station numbering for gas turbine engines.

Table 5.1 Temperature and pressure relationships for all τ and π

Freestream			
$\tau_r = 1 + \frac{\gamma - 1}{2} M_0^2$		$\pi_r = \left(1 + \frac{\gamma-1}{2} M_0^2\right)^{\gamma/(\gamma-1)}$	
Core stream		Bypass stream	
$\tau_\lambda = \frac{c_{pt} T_{t4}}{c_{pc} T_0}$	$\tau_{\lambda AB} = \frac{c_{pAB} T_{t7}}{c_{pc} T_0}$	$\tau_{\lambda DB} = \frac{c_{pDB} T_{t17}}{c_{pc} T_0}$	
$\tau_d = \frac{T_{t2}}{T_{t0}}$	$\pi_d = \frac{P_{t2}}{P_{t0}}$	$\tau_f = \frac{T_{t13}}{T_{t2}}$	$\pi_f = \frac{P_{t13}}{P_{t2}}$
$\tau_c = \frac{T_{t3}}{T_{t2}}$	$\pi_c = \frac{P_{t3}}{P_{t2}}$	$\tau_{DB} = \frac{T_{t17}}{T_{t13}}$	$\pi_{DB} = \frac{P_{t17}}{P_{t13}}$
$\tau_b = \frac{T_{t4}}{T_{t3}}$	$\pi_b = \frac{P_{t4}}{P_{t3}}$	$\tau_{fn} = \frac{T_{t19}}{T_{t17}}$	$\pi_{fn} = \frac{P_{t19}}{P_{t17}}$
$\tau_t = \frac{T_{t5}}{T_{t4}}$	$\pi_t = \frac{P_{t5}}{P_{t4}}$		
$\tau_{AB} = \frac{T_{t7}}{T_{t5}}$	$\pi_{AB} = \frac{P_{t7}}{P_{t5}}$		
$\tau_n = \frac{T_{t9}}{T_{t7}}$	$\pi_n = \frac{P_{t9}}{P_{t7}}$		

the station numbers 13–19 are used for the bypass stream and decimal numbers such as station number 4.5 are used to indicate an intermediate station.

Table 5.1 contains most of the short-form notation temperature ratios τ and pressure ratios π that we will use in our analysis. (Note that the τ_λ are expressed for calorically perfect gases.) These ratios are shown in terms of the standard station numbering.[30]

5.3 Design Inputs

The total temperature ratios, total pressure ratios, etc., can be classified into one of four categories:

1) Flight conditions: P_0, T_0, M_0, c_p, τ_r, π_r
2) Design limits: $(c_p T_t)_{\text{burner exit}}$
3) Component performance: π_d, π_b, π_n, etc.
4) Design choices: π_c, π_f, etc.

5.4 Steps of Engine Parametric Cycle Analysis

The steps of engine parametric cycle analysis listed next are based on a jet engine with a single inlet and single exhaust. Thus these steps will use only the station numbers for the core engine flow (from 0 to 9) shown in Fig. 5.1. We will use these steps in this chapter and Chapter 7. When more than one

exhaust stream is present (e.g., high-bypass-ratio turbofan engine), the steps will be modified.

Parametric cycle analysis desires to determine how the engine performance (specific thrust and fuel consumption) varies with changes in the flight conditions (e.g., Mach number), design limits (e.g., main burner exit temperature), component performance (e.g., turbine efficiency), and design choices (e.g., compressor pressure ratio).

1) Starting with an equation for uninstalled engine thrust, we rewrite this equation in terms of the total pressure and total temperature ratios: the ambient pressure P_0, temperature T_0, and speed of sound a_0, and the flight
Mach number M_0 as follows:

$$F = \frac{1}{g_c}(\dot{m}_9 V_e - \dot{m}_0 V_0) + A_9(P_9 - P_0)$$

$$\frac{F}{\dot{m}_0} = \frac{a_0}{g_c}\left(\frac{\dot{m}_9}{\dot{m}_0}\frac{V_9}{a_0} - M_0\right) + \frac{A_9 P_9}{\dot{m}_0}\left(1 - \frac{P_0}{P_9}\right)$$

2) Next express the velocity ratio(s) V_9/a_0 in terms of Mach numbers, temperatures, and gas properties of states 0 and 9:

$$\left(\frac{V_9}{a_0}\right)^2 = \frac{a_9^2 M_9^2}{a_0^2} = \frac{\gamma_9 R_9 g_c T_9}{\gamma_0 R_0 g_c T_0} M_9^2$$

3) Find the exit Mach number M_9. Since

$$P_{t9} = P_9\left(1 + \frac{\gamma - 1}{2} M_9^2\right)^{\gamma/(\gamma-1)}$$

then

$$M_9^2 = \frac{2}{\gamma - 1}\left[\left(\frac{P_{t9}}{P_9}\right)^{(\gamma-1)/\gamma} - 1\right]$$

where

$$\frac{P_{t9}}{P_9} = \frac{P_0}{P_9}\frac{P_{t0}}{P_0}\frac{P_{t2}}{P_{t0}}\frac{P_{t3}}{P_{t2}}\frac{P_{t4}}{P_{t3}}\frac{P_{t5}}{P_{t4}}\frac{P_{t7}}{P_{t5}}\frac{P_{t9}}{P_{t7}}$$

$$= \frac{P_0}{P_9}\pi_r \pi_d \pi_c \pi_b \pi_t \pi_{AB} \pi_n$$

4) Find the temperature ratio T_9/T_0:

$$\frac{T_9}{T_0} = \frac{T_{t9}/T_0}{T_{t9}/T_9} = \frac{T_{t9}/T_0}{(P_{t9}/P_9)^{(\gamma-1)/\gamma}}$$

where

$$\frac{T_{t9}}{T_0} = \frac{T_{t0}}{T_0}\frac{T_{t2}}{T_{t0}}\frac{T_{t3}}{T_{t2}}\frac{T_{t4}}{T_{t3}}\frac{T_{t5}}{T_{t4}}\frac{T_{t7}}{T_{t5}}\frac{T_{t9}}{T_{t7}} = \tau_r\tau_d\tau_c\tau_b\tau_t\tau_{AB}\tau_n$$

5) Apply the first law of thermodynamics to the burner (combustor), and find an expression for the fuel/air ratio f in terms of τ's, etc.:

$$\dot{m}_0 c_p T_{t3} + \dot{m}_f h_{PR} = \dot{m}_0 c_p T_{t4}$$

6) When applicable, find an expression for the total temperature ratio across the turbine τ_t by relating the turbine power output to the compressor, fan, and/or propeller power requirements. This allows us to find τ_t in terms of other variables.

7) Evaluate the specific thrust, using the preceding results.

8) Evaluate the thrust specific fuel consumption S, using the results for specific thrust and fuel/air ratio:

$$S = \frac{f}{F/\dot{m}_0} \tag{5.8}$$

9) Develop expressions for the thermal and propulsive efficiencies.

5.5 Assumptions of Ideal Cycle Analysis

For analysis of ideal cycles, we assume the following:

1) There are isentropic (reversible and adiabatic) compression and expansion processes in the inlet (diffuser), compressor, fan, turbine, and nozzle. Thus we have the following relationships:

$$\tau_d = \tau_n = 1 \qquad \pi_d = \pi_n = 1 \qquad \tau_c = \pi_c^{(\gamma-1)/\gamma} \qquad \tau_t = \pi_t^{(\gamma-1)/\gamma}$$

2) Constant-pressure combustion ($\pi_b = 1$) is idealized as a heat interaction into the combustor. The fuel flow rate is much less than the airflow rate through the combustor such that

$$\frac{\dot{m}_f}{\dot{m}_c} \ll 1 \qquad \text{and} \qquad \dot{m}_c + \dot{m}_f \cong \dot{m}_c$$

3) The working fluid is air that behaves as a perfect gas with constant specific heats.

4) The engine exhaust nozzles expand the gas to the ambient pressure ($P_9 = P_0$).

5.6 Ideal Ramjet

A schematic diagram of a ramjet engine is shown in Fig. 5.2, and the ideal cycle is plotted on a temperature-entropy (T-s) diagram and H-K diagram in

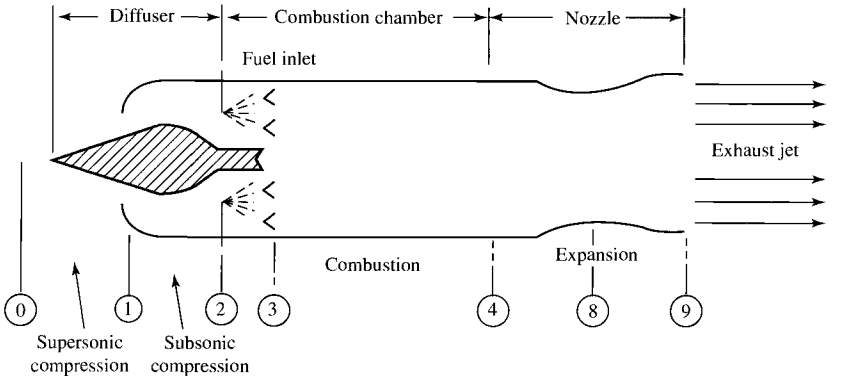

Fig. 5.2 Typical ramjet engine.

Fig. 5.3. A ramjet engine is conceptually the simplest aircraft engine and consists of an inlet or diffuser, a combustor or burner, and a nozzle. The inlet or diffuser slows the air velocity relative to the engine from the flight velocity V_0 to a smaller value V_2. This decrease in velocity increases both the static pressure P_2 and static temperature T_2. In the combustor or burner, fuel is added and its chemical energy is converted to thermal energy in the combustion process. This addition of thermal energy increases the static temperature T_4, and the combustion process occurs at a nearly constant pressure for $M_4 \ll 1$. The nozzle expands the gas to or near the ambient pressure, and

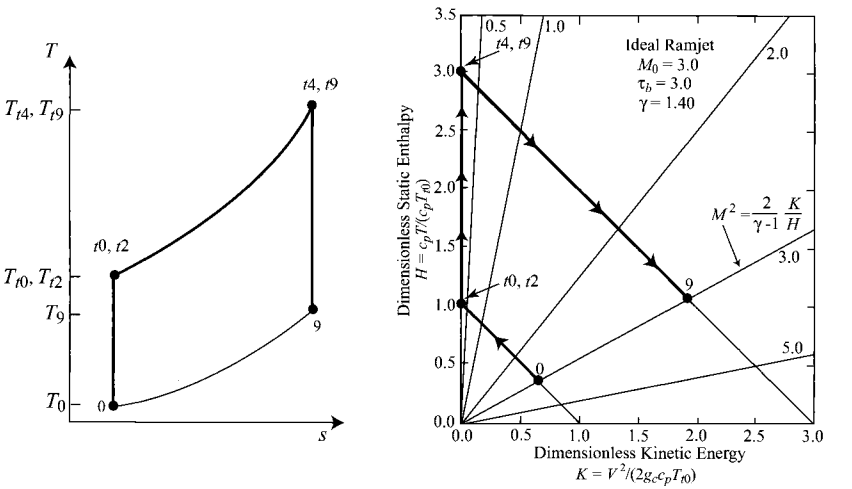

Fig. 5.3 The *T-s* diagram and *H-K* diagram of an ideal ramjet engine.

the temperature decreases from T_4 to T_9 with a corresponding increase in the kinetic energy per unit mass $(V_9^2 - V_4^2)/(2g_c)$.

5.6.1 Cycle Analysis

Application of the steps of cycle analysis to the ideal ramjet of Fig. 5.2 is presented next in the order listed in Section 5.4.

Step 1:

$$F = \frac{1}{g_c}(\dot{m}_9 V_9 - \dot{m}_0 V_0) + A_9(P_9 - P_0)$$

However, $P_9 = P_0$ and $\dot{m}_9 \cong \dot{m}_0$ for the ideal engine. Thus

$$F = \frac{\dot{m}_0}{g_c}(V_9 - V_0) = \frac{\dot{m}_0 a_0}{g_c}\left(\frac{V_9}{a_0} - M_0\right) \tag{5.9}$$

Step 2:

$$\left(\frac{V_9}{a_0}\right)^2 = \frac{a_9^2 M_9^2}{a_0^2} = \frac{\gamma_9 R_9 g_c T_9 M_9^2}{\gamma_0 R_0 g_c T_0}$$

However, $\gamma_9 = \gamma_0 = \gamma$ and $R_9 = R_0 = R$ for an ideal engine. Thus

$$\left(\frac{V_9}{a_0}\right)^2 = \frac{T_9}{T_0} M_9^2 \tag{5.10}$$

Step 3:

$$P_{t9} = P_0 \frac{P_{t0}}{P_0}\frac{P_{t2}}{P_{t0}}\frac{P_{t4}}{P_{t2}}\frac{P_{t9}}{P_{t4}} = P_0 \pi_r \pi_d \pi_b \pi_n$$

However, $\pi_d = \pi_b = \pi_n = 1$ for an ideal engine. Thus $P_{t9} = P_0 \pi_r$ and

$$\frac{P_{t9}}{P_9} = \frac{P_{t9}}{P_0}\frac{P_0}{P_9} = \pi_r \frac{P_0}{P_9} = \pi_r$$

$$M_9^2 = \frac{2}{\gamma - 1}\left[\left(\frac{P_{t9}}{P_9}\right)^{(\gamma-1)/\gamma} - 1\right] = \frac{2}{\gamma - 1}(\pi_r^{(\gamma-1)/\gamma} - 1)$$

However,

$$\pi_r^{(\gamma-1)/\gamma} = \tau_r$$

Thus

$$M_9^2 = \frac{2}{\gamma - 1}(\tau_r - 1) = M_0^2 \qquad \text{or} \qquad M_9 = M_0 \tag{5.11}$$

Step 4:

$$T_{t9} = T_0 \frac{T_{t0}}{T_0}\frac{T_{t2}}{T_{t0}}\frac{T_{t4}}{T_{t2}}\frac{T_{t9}}{T_{t4}} = T_0 \tau_r \tau_d \tau_b \tau_n = T_0 \tau_r \tau_b$$

$$\frac{T_{t9}}{T_0} = \left(\frac{P_{t9}}{P_9}\right)^{(\gamma-1)/\gamma}$$

$$\frac{T_9}{T_0} = \frac{T_{t9}/T_o}{T_{t9}/T_9} = \frac{\tau_r \tau_b}{(P_{t9}/P_9)^{(\gamma-1)/\gamma}} = \frac{\tau_r \tau_b}{\tau_r}$$

$$\frac{T_9}{T_0} = \tau_b \tag{5.12}$$

Step 5: Application of the steady flow energy equation (first law of thermodynamics) to the control volume about the burner or combustor shown in Fig. 5.4 gives

$$\dot{m}_0 h_{t2} + \dot{m}_f h_{PR} = (\dot{m}_0 + \dot{m}_f) h_{t4}$$

where h_{pR} is the thermal energy released by the fuel during combustion. For an ideal engine,

$$\dot{m}_0 + \dot{m}_f \cong \dot{m}_0 \qquad \text{and} \qquad c_{p2} = c_{p4} = c_p$$

Thus the preceding equation becomes

$$\dot{m}_0 c_p T_{t2} + \dot{m}_f h_{PR} = \dot{m}_0 c_p T_{t4}$$

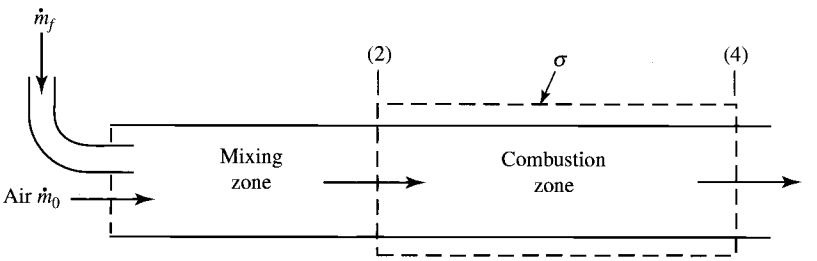

Fig. 5.4 Combustor model.

or

$$\dot{m}_f h_{PR} = \dot{m}_0 c_p (T_{t4} - T_{t2}) = \dot{m}_0 c_p T_{t2} \left(\frac{T_{t4}}{T_{t2}} - 1 \right)$$

The fuel/air ratio f is defined as

$$f \equiv \frac{\dot{m}_f}{\dot{m}_0} = \frac{c_p T_{t2}}{h_{PR}} \left(\frac{T_{t4}}{T_{t2}} - 1 \right) \tag{5.13a}$$

For the ideal ramjet, $T_{t0} = T_{t2} = T_0 \tau_r$ and $T_{t4}/T_{t2} = \tau_b$. Thus Eq. (5.13a) becomes

$$f = \frac{c_p T_0 \tau_r}{h_{PR}} (\tau_b - 1) \tag{5.13b}$$

However,

$$\tau_\lambda = \frac{c_{p4} T_{t4}}{c_{p0} T_0} = \frac{T_{t4}}{T_0} = \frac{T_{t2}}{T_0} \frac{T_{t4}}{T_{t2}} = \tau_r \tau_b$$

for the ramjet, and Eq. (5.13b) can be written as

$$f = \frac{c_p T_0}{h_{PR}} (\tau_\lambda - \tau_r) \tag{5.13c}$$

Step 6: This is not applicable for the ramjet engine.

Step 7: Since $M_9 = M_0$ and $T_9/T_0 = \tau_b$, then

$$\left(\frac{V_9}{a_0} \right)^2 = \frac{T_9}{T_0} M_9^2 = \tau_b M_0^2 \tag{5.14}$$

and the expression for thrust can be rewritten as

$$F = \frac{\dot{m}_0 a_0 M_0}{g_c} (\sqrt{\tau_b} - 1) = \frac{\dot{m}_0 a_0 M_0}{g_c} \left(\sqrt{\frac{\tau_\lambda}{\tau_r}} - 1 \right) \tag{5.15a}$$

or

$$\frac{F}{\dot{m}_0} = \frac{a_0 M_0}{g_c} (\sqrt{\tau_b} - 1) = \frac{a_0 M_0}{g_c} \left(\sqrt{\frac{\tau_\lambda}{\tau_r}} - 1 \right) \tag{5.15b}$$

Step 8:

$$S = \frac{f}{F/\dot{m}_0}$$

$$S = \frac{c_p T_0 g_c (\tau_\lambda - \tau_r)}{a_0 M_0 h_{PR} (\sqrt{\tau_\lambda/\tau_r} - 1)} \tag{5.16a}$$

or

$$S = \frac{c_p T_0 g_c \tau_r (\tau_b - 1)}{a_0 M_0 h_{PR} (\sqrt{\tau_b} - 1)} \tag{5.16b}$$

Step 9: Development of the following efficiency expressions is left to the reader.

Thermal efficiency:

$$\eta_T = 1 - \frac{1}{\tau_r} \tag{5.17a}$$

Propulsive efficiency:

$$\eta_P = \frac{2}{\sqrt{\tau_\lambda/\tau_r} + 1} \tag{5.17b}$$

Overall efficiency:

$$\eta_O = \eta_T \eta_P = \frac{2(\tau_r - 1)}{\sqrt{\tau_\lambda \tau_r} + \tau_r} \tag{5.17c}$$

5.6.2 Summary of Equations—Ideal Ramjet

INPUTS:

$$M_0,\ T_0(\mathrm{K},\ ^\circ\mathrm{R}),\ \gamma,\ c_p\left(\frac{\mathrm{kJ}}{\mathrm{kg}\cdot\mathrm{K}},\ \frac{\mathrm{Btu}}{\mathrm{lbm}\cdot{}^\circ\mathrm{R}}\right),\ h_{PR}\left(\frac{\mathrm{kJ}}{\mathrm{kg}},\ \frac{\mathrm{Btu}}{\mathrm{lbm}}\right),\ T_{t4}(\mathrm{K},\ ^\circ\mathrm{R})$$

OUTPUTS:

$$\frac{F}{\dot{m}_0}\left(\frac{\mathrm{N}}{\mathrm{kg/s}},\ \frac{\mathrm{lbf}}{\mathrm{lbm/s}}\right),\ f,\ S\left(\frac{\mathrm{mg/s}}{\mathrm{N}},\ \frac{\mathrm{lbm/h}}{\mathrm{lbf}}\right),\ \eta_T,\ \eta_P,\ \eta_O$$

EQUATIONS:

$$R = \frac{\gamma - 1}{\gamma} c_p \tag{5.18a}$$

$$a_0 = \sqrt{\gamma R g_c T_0} \tag{5.18b}$$

$$\tau_r = 1 + \frac{\gamma - 1}{2} M_0^2 \tag{5.18c}$$

$$\tau_\lambda = \frac{T_{t4}}{T_0} \tag{5.18d}$$

$$\frac{V_9}{a_0} = M_0 \sqrt{\frac{\tau_\lambda}{\tau_r}} \tag{5.18e}$$

$$\frac{F}{\dot{m}_0} = \frac{a_0}{g_c}\left(\frac{V_9}{a_0} - M_0\right) \tag{5.18f}$$

$$f = \frac{c_p T_0}{h_{PR}}(\tau_\lambda - \tau_r) \tag{5.18g}$$

$$S = \frac{f}{F/\dot{m}_0} \tag{5.18h}$$

$$\eta_T = 1 - \frac{1}{\tau_r} \tag{5.18i}$$

$$\eta_P = \frac{2}{\sqrt{\tau_\lambda/\tau_r} + 1} \tag{5.18j}$$

$$\eta_O = \eta_T \eta_P = \frac{2(\tau_r - 1)}{\sqrt{\tau_\lambda \tau_r} + \tau_r} \tag{5.18k}$$

Example 5.1

The performance of ideal ramjets is plotted in Figs. 5.5a–5.5d vs flight Mach number M_0 for different values of the total temperature leaving the combustor. Calculations were performed for the following input data:

$T_0 = 216.7\,\text{K}$, $\gamma = 1.4$, $c_p = 1.004\,\text{kJ/(kg} \cdot \text{K)}$, $h_{PR} = 42{,}800\,\text{kJ/kg}$

$T_{t4} = 1600$, 1900, and 2200 K

5.6.3 Optimum Mach Number

The plot of specific thrust vs Mach number (see Fig. 5.5a) shows that the maximum value of specific thrust is exhibited at a certain Mach number for each value of T_{t4}. An analytical expression for this optimum Mach number can be found by taking the partial derivative of the equation for specific thrust with respect to flight Mach number, setting this equal to zero, and solving as follows.

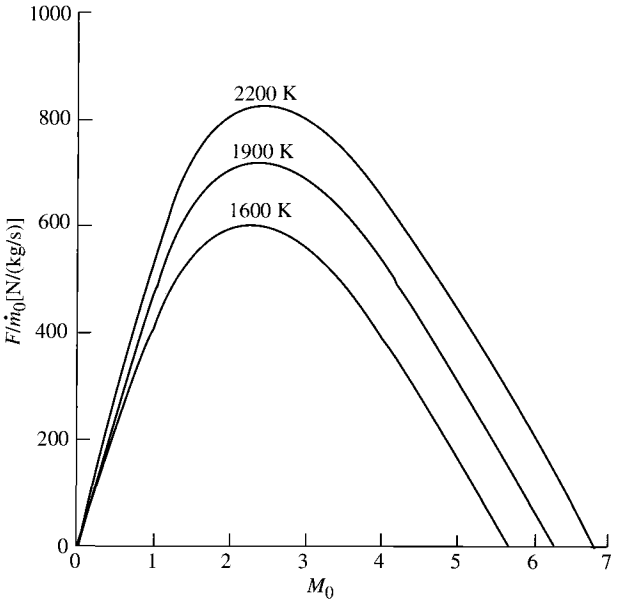

Fig. 5.5a Ideal ramjet performance vs Mach number: specific thrust.

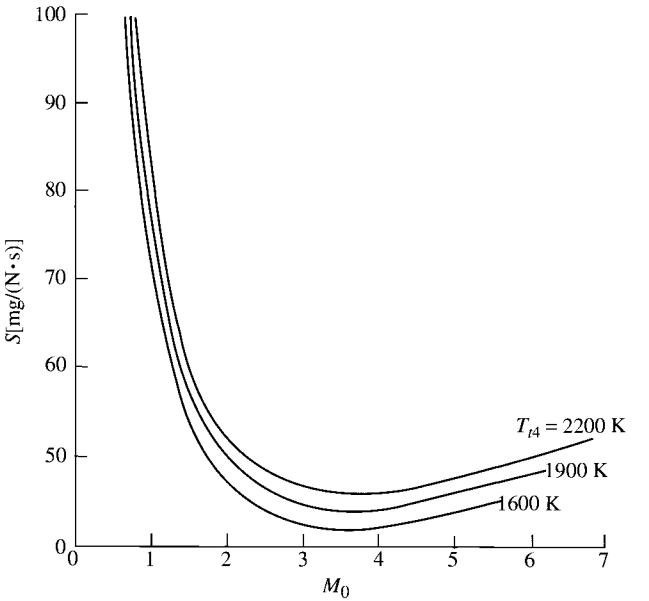

Fig. 5.5b Ideal ramjet performance vs Mach number: thrust-specific fuel consumption.

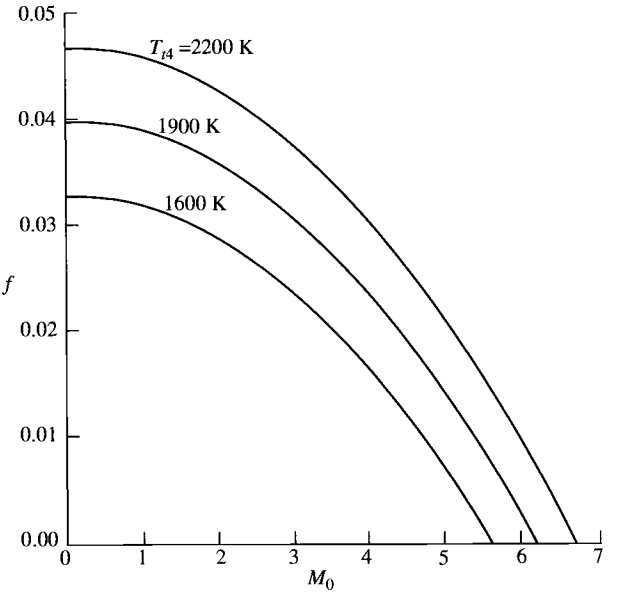

Fig. 5.5c Ideal ramjet performance vs Mach number: fuel/air ratio.

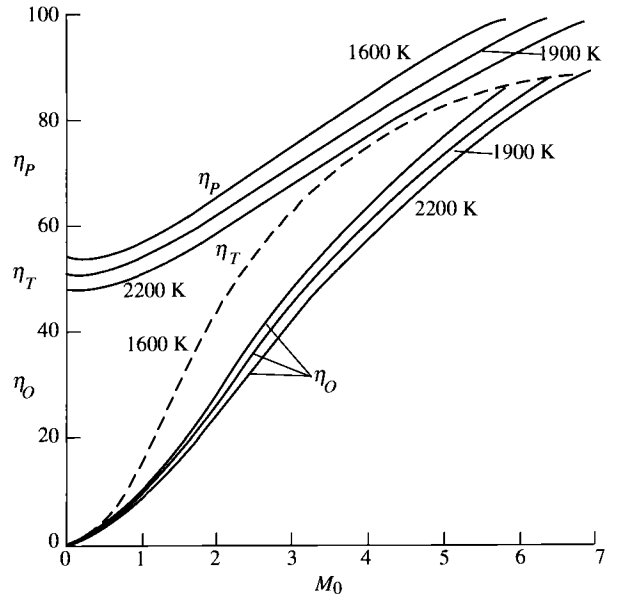

Fig. 5.5d Ideal ramjet performance vs Mach number: efficiencies.

Combining Eqs. (5.18e) and (5.18f) and differentiating gives

$$\frac{\partial}{\partial M_0}\left(\frac{F}{\dot{m}_0}\right) = \frac{a_0}{g_c}\frac{\partial}{\partial M_0}\left[M_0\left(\sqrt{\frac{\tau_\lambda}{\tau_r}} - 1\right)\right] = 0$$

$$\sqrt{\frac{\tau_\lambda}{\tau_r}} - 1 + M_0\sqrt{\tau_\lambda}\frac{\partial}{\partial M_0}\left(\frac{1}{\sqrt{\tau_r}}\right) = 0$$

Now

$$\frac{\partial}{\partial M_0}\left(\frac{1}{\sqrt{\tau_r}}\right) = -\frac{1}{2}\frac{1}{\tau_r^{3/2}}\frac{\partial \tau_r}{\partial M_0} = -\frac{1}{2\tau_r^{3/2}}\frac{\partial}{\partial M_0}\left(1 + \frac{\gamma - 1}{2}M_0^2\right)$$

$$= -\frac{(\gamma - 1)M_0}{2\tau_r^{3/2}}$$

Thus

$$\sqrt{\frac{\tau_\lambda}{\tau_r}} - 1 = M_0\sqrt{\tau_\lambda}\frac{(\gamma - 1)M_0}{2\tau_r^{3/2}}$$

or

$$\sqrt{\frac{\tau_\lambda}{\tau_r}} - 1 = \sqrt{\frac{\tau_\lambda}{\tau_r}}\frac{(\gamma - 1)M_0^2}{2\tau_r}$$

However,

$$\frac{\gamma - 1}{2}M_0^2 = \tau_r - 1$$

Then

$$\sqrt{\frac{\tau_\lambda}{\tau_r}} - 1 = \sqrt{\frac{\tau_\lambda}{\tau_r}}\frac{\tau_r - 1}{\tau_r} = \sqrt{\frac{\tau_\lambda}{\tau_r}} - \frac{\sqrt{\tau_\lambda}}{\tau_r^{3/2}} \quad \text{or} \quad \tau_r^3 = \tau_\lambda$$

Thus $F/\dot{m}_0$ is maximum when

$$\tau_{r\ \max\ F/\dot{m}_0} = \sqrt[3]{\tau_\lambda} \tag{5.19}$$

or

$$M_{0\ \max\ F/\dot{m}_0} = \sqrt{\frac{2}{\gamma - 1}(\sqrt[3]{\tau_\lambda} - 1)} \tag{5.20}$$

5.6.4 Mass Ingested by an Ideal Ramjet

Because the specific thrust of a ramjet has a maximum at the flight Mach number given by Eq. (5.20) and decreases at higher Mach numbers, one might question how the thrust of a given ramjet will vary with the Mach number. Does the thrust of a ramjet vary as its specific thrust? Because the thrust of a given ramjet will depend on its physical size (flow areas), the variation in thrust per unit area with Mach number will give the trend we seek. For a ramjet, the diffuser exit Mach number (station 2) is essentially constant over the flight Mach number operating range ($M_2 = 0.5$). Using this fact, we can find the engine mass flow rate in terms of A_2, M_0, M_2, and the ambient pressure and temperature. With this flow rate, we can then find the thrust per unit area at station 2 from

$$\frac{F}{A_2} = \frac{F}{\dot{m}_0}\frac{\dot{m}_0}{A_2}$$

As we shall see, the mass flow rate is a strong function of flight Mach number and altitude. For our case,

$$\frac{\dot{m}_0}{A_2} = \frac{\dot{m}_2}{A_2} = \frac{\dot{m}_2}{A_2^*}\frac{A_2^*}{A_2} = \frac{\dot{m}_2}{A_2^*}\left(\frac{A^*}{A}\right)_{M_2} \tag{i}$$

However, mass flow parameter (MFP),

$$\text{MFP}(M_i) = \frac{\dot{m}_i\sqrt{T_{ti}}}{A_i P_{ti}}$$

and

$$\text{MFP}^* = \text{MFF}(@M = 1) = \frac{\dot{m}\sqrt{T_t}}{A^* P_t}$$

Then

$$\frac{\dot{m}_2}{A_2^*} = \text{MFP}^*\frac{P_{t2}}{\sqrt{T_{t2}}}, \qquad T_{t2} = T_{t0}, \qquad \text{and} \qquad P_{t2} = \pi_d P_{t0} \tag{ii}$$

where

$$\frac{P_{t2}}{\sqrt{T_{t2}}} = \frac{\pi_d P_{t0}}{\sqrt{T_{t0}}} = \frac{\pi_d P_0}{\sqrt{T_0}}\frac{P_{t0}/P_0}{\sqrt{T_{t0}/T_0}} = \frac{\pi_d P_0}{\sqrt{T_0}}\frac{(T_{t0}/T_0)^{\gamma/(\gamma-1)}}{\sqrt{T_{t0}/T_0}}$$

or

$$\frac{P_{t2}}{\sqrt{T_{t2}}} = \frac{\pi_d P_0}{\sqrt{T_0}} \left(\frac{T_{t0}}{T_0}\right)^{\gamma/(\gamma-1)-1/2} = \frac{\pi_d P_0}{\sqrt{T_0}} (\tau_r)^{(\gamma+1)/[2(\gamma-1)]} \tag{iii}$$

For air, $\gamma = 1.4$ and $(\gamma + 1)/[2(\gamma - 1)] = 3$. Thus, combining Eqs. (i), (ii), and (iii), we get

$$\frac{\dot{m}_0}{A_2} = \text{MFP}^* \left(\frac{A^*}{A}\right)_{M_2} \frac{\pi_d P_0 \tau_r^3}{\sqrt{T_0}} \tag{5.21}$$

The variations of mass flow per unit area [Eq. (5.21)], specific thrust, and thrust per unit area at station 2 with flight Mach number are plotted in Fig. 5.6 for M_2 of 0.5, altitude of 12 km, T_{t4}, of 1900 K, and π_d of 1.0. Although the specific thrust variation with Mach number reaches a maximum at Mach 2.30 and then falls off, the thrust of an ideal ramjet continues to increase with flight Mach number until about Mach 5.25 due to the very rapid increase in mass flow per unit area.

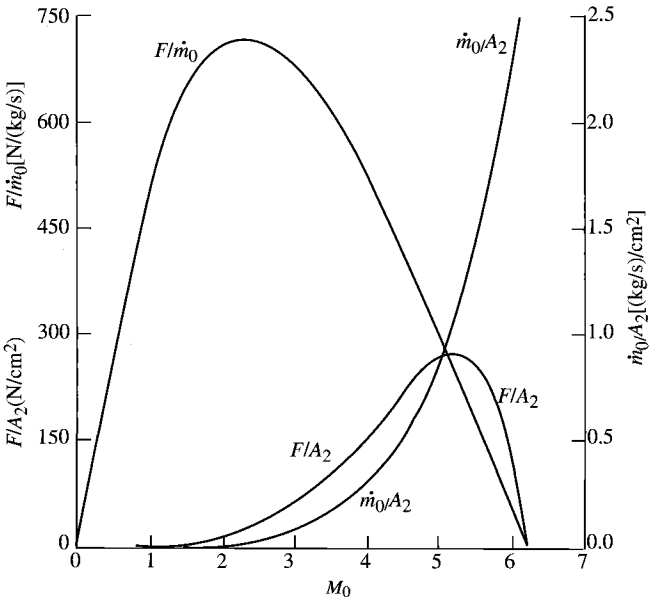

Fig. 5.6 Ideal ramjet thrust per unit area vs Mach number.

5.7 Ideal Turbojet

The thrust of a ramjet tends to zero as the Mach number goes to zero. This poor performance can be overcome by the addition of a compressor-turbine unit to the basic Brayton cycle, as shown in Fig. 5.7a. The thermal efficiency of this ideal cycle is now

$$\eta_T = 1 - \frac{T_0}{T_{t3}} = 1 - \frac{1}{\tau_r \tau_c} \tag{5.22}$$

Whereas an ideal ramjet's thermal efficiency is zero at Mach 0, a compressor having a pressure ratio of 10 will give a thermal efficiency of about 50% for the ideal turbojet at Mach 0.

For the ideal turbojet

$$\dot{W}_t = \dot{W}_c, \qquad T_{t4} > T_{t3}, \qquad \text{and} \qquad P_{t4} = P_{t3}$$

Thus the compressor-burner-turbine combination generates a higher pressure and temperature at its exit and is called, therefore, a *gas generator.* The gas leaving the gas generator may be expanded through a nozzle to form a turbojet, as depicted in Figs. 5.7a and 5.7b, or the gases may be expanded through a turbine to drive a fan (turbofan), a propeller (turboprop), a generator (gas turbine), an automobile (gas turbine), or a helicopter rotor (gas turbine).

We will analyze the ideal turbojet cycle as we did the ideal ramjet cycle and will determine the trends in the variation of thrust, thrust specific fuel consumption, and fuel/air ratio with compressor pressure ratio and flight Mach number.

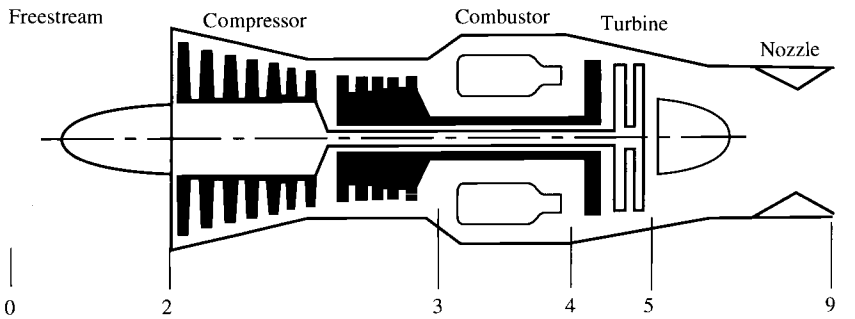

Fig. 5.7a Station numbering of ideal turbojet engine.

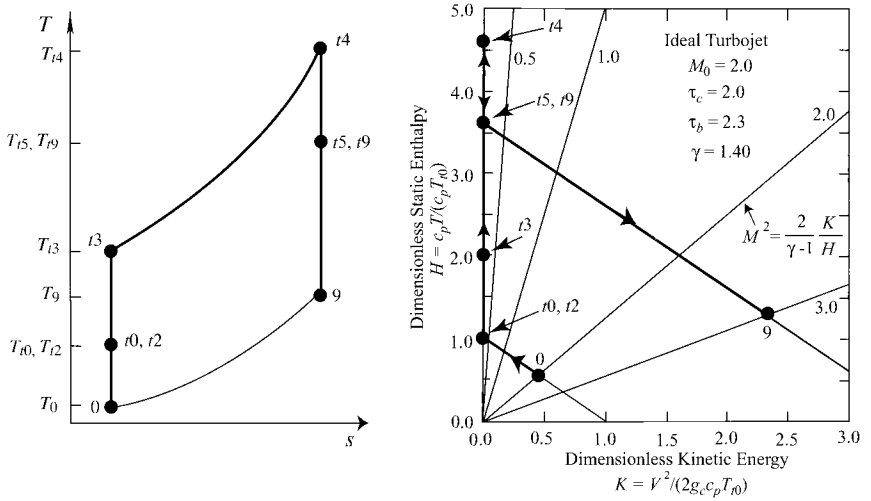

Fig. 5.7b The *T-s* diagram and *H-K* diagram of an ideal turbojet engine.

5.7.1 Cycle Analysis

Application of these steps of cycle analysis to the ideal turbojet engine is presented next in the order listed in Section 5.4.

Step 1:

$$\frac{F}{\dot{m}_0} = \frac{1}{g_c}(V_9 - V_0) = \frac{a_0}{g_c}\left(\frac{V_9}{a_0} - M_0\right)$$

Step 2:

$$\left(\frac{V_9}{a_0}\right)^2 = \frac{a_9^2 M_9^2}{a_0^2} = \frac{\gamma_9 R_9 g_c T_9 M_9^2}{\gamma_0 R_0 g_c T_0} = \frac{T_9}{T_0} M_9^2$$

Step 3:

$$P_{t9} = P_9\left(1 + \frac{\gamma - 1}{2} M_9^2\right)^{\gamma/(\gamma-1)}$$

and

$$P_{t9} = P_0 \frac{P_{t0}}{P_0}\frac{P_{t2}}{P_{t0}}\frac{P_{t3}}{P_{t2}}\frac{P_{t4}}{P_{t3}}\frac{P_{t5}}{P_{t4}}\frac{P_{t9}}{P_{t5}} = P_0 \pi_r \pi_d \pi_c \pi_b \pi_t \pi_n$$

However, $\pi_d = \pi_b = \pi_n = 1$; thus $P_{t9} = P_0 \pi_r \pi_c \pi_t$, and so

$$M_9^2 = \frac{2}{\gamma - 1}\left[\left(\frac{P_{t9}}{P_9}\right)^{(\gamma-1)/\gamma} - 1\right]$$

where

$$\frac{P_{t9}}{P_9} = \frac{P_{t9}}{P_0}\frac{P_0}{P_9} = \pi_r \pi_c \pi_t \frac{P_0}{P_9} = \pi_r \pi_c \pi_t$$

Then

$$M_9^2 = \frac{2}{\gamma - 1}[(\pi_r \pi_c \pi_t)^{(\gamma-1)/\gamma} - 1]$$

However, $\pi_r^{(\gamma-1)/\gamma} = \tau_r$ and for an ideal turbojet $\pi_c^{(\gamma-1)/\gamma} = \tau_c$ and $\pi_t^{(\gamma-1)/\gamma} = \tau_t$. Thus

$$M_9^2 = \frac{2}{\gamma - 1}(\tau_r \tau_c \tau_t - 1) \tag{5.23}$$

Step 4:

$$T_{t9} = T_0 \frac{T_{t0}}{T_0}\frac{T_{t2}}{T_{t0}}\frac{T_{t3}}{T_{t2}}\frac{T_{t4}}{T_{t3}}\frac{T_{t5}}{T_{t4}}\frac{T_{t9}}{T_{t5}} = T_0 \tau_r \tau_d \tau_c \tau_b \tau_t \tau_n = T_0 \tau_r \tau_c \tau_b \tau_t$$

Then

$$\frac{T_9}{T_0} = \frac{T_{t9}/T_0}{T_{t9}/T_9} = \frac{\tau_r \tau_c \tau_b \tau_t}{(P_{t9}/P_9)^{(\gamma-1)/\gamma}} = \frac{\tau_r \tau_c \tau_b \tau_t}{(\pi_r \pi_c \pi_t)^{(\gamma-1)/\gamma}} = \frac{\tau_r \tau_c \tau_b \tau_t}{\tau_r \tau_c \tau_t}$$

Thus

$$\frac{T_9}{T_0} = \tau_b \tag{5.24}$$

Step 5: Application of the steady flow energy equation to the burner gives

$$\dot{m}_0 h_{t3} + \dot{m}_f h_{PR} = (\dot{m}_0 + \dot{m}_f) h_{t4}$$

For an ideal cycle, $\dot{m}_0 + \dot{m}_f \cong \dot{m}_0$ and $c_{p3} = c_{p4} = c_p$. Thus

$$\dot{m}_0 c_p T_{t3} + \dot{m}_f h_{PR} = \dot{m}_0 c_p T_{t4}$$

$$\dot{m}_f h_{PR} = \dot{m}_0 c_p (T_{t4} - T_{t3}) = \dot{m}_0 c_p T_0 \left(\frac{T_{t4}}{T_0} - \frac{T_{t3}}{T_0}\right)$$

or

$$f = \frac{\dot{m}_f}{\dot{m}_0} = \frac{c_p T_0}{h_{PR}} \left(\frac{T_{t4}}{T_0} - \frac{T_{t3}}{T_0} \right)$$

However,

$$\tau_\lambda = \frac{T_{t4}}{T_0} \qquad \text{and} \qquad \tau_r \tau_c = \frac{T_{t3}}{T_0}$$

Then

$$f = \frac{\dot{m}_f}{\dot{m}_0} = \frac{c_p T_0}{h_{PR}} (\tau_\lambda - \tau_r \tau_c) \tag{5.25}$$

or

$$f = \frac{\dot{m}_f}{\dot{m}_0} = \frac{c_p T_0 \tau_r \tau_c}{h_{PR}} (\tau_b - 1) \tag{5.26}$$

Step 6: The power out of the turbine is

$$\dot{W}_t = (\dot{m}_0 + \dot{m}_f)(h_{t4} - h_{t5}) \cong \dot{m}_0 c_p (T_{t4} - T_{t5})$$
$$= \dot{m}_0 c_p T_{t4} \left(1 - \frac{T_{t5}}{T_{t4}} \right) = \dot{m}_0 c_p T_{t4} (1 - \tau_t)$$

The power required to drive the compressor is

$$\dot{W}_c = \dot{m}_0 (h_{t3} - h_{t2}) = \dot{m}_0 c_p (T_{t3} - T_{t2})$$
$$= \dot{m}_0 c_p T_{t2} \left(\frac{T_{t3}}{T_{t2}} - 1 \right) = \dot{m}_0 c_p T_{t2} (\tau_c - 1)$$

Since $\dot{W}_c = \dot{W}_t$ for the ideal turbojet, then

$$\dot{m}_0 c_p T_{t2} (\tau_c - 1) = \dot{m}_0 c_p T_{t4} (1 - \tau_t)$$

or

$$\tau_t = 1 - \frac{T_{t2}}{T_{t4}} (\tau_c - 1)$$

Thus

$$\tau_t = 1 - \frac{\tau_r}{\tau_\lambda} (\tau_c - 1) \tag{5.27}$$

Step 7:

$$\left(\frac{V_9}{a_0}\right)^2 = \frac{T_9}{T_0} M_9^2 = \frac{2}{\gamma - 1} \frac{\tau_\lambda}{\tau_r \tau_c} (\tau_r \tau_c \tau_t - 1) \tag{5.28}$$

However,

$$\frac{F}{\dot{m}_0} = \frac{a_0}{g_c} \left(\frac{V_9}{a_0} - M_0\right)$$

Thus

$$\frac{F}{\dot{m}_0} = \frac{a_0}{g_c} \left[\sqrt{\frac{2}{\gamma - 1} \frac{\tau_\lambda}{\tau_r \tau_c} (\tau_r \tau_c \tau_t - 1)} - M_0\right] \tag{5.29}$$

Step 8: According to Eq. (5.8),

$$S = \frac{f}{F/\dot{m}_0}$$

The thrust specific fuel consumption S can be calculated by first calculating the fuel/air ratio f and the thrust per unit of airflow $F/\dot{m}_0$, using Eqs. (5.25) and (5.29), respectively, and then substituting these values into the preceding equation. An analytical expression for S can be obtained by substituting Eqs. (5.25) and (5.29) into Eq. (5.8) to get the following:

$$S = \frac{c_p T_0 g_c (\tau_\lambda - \tau_r \tau_c)}{a_0 h_{PR} \left[\sqrt{\frac{2}{\gamma - 1} \frac{\tau_\lambda}{\tau_r \tau_c} (\tau_r \tau_c \tau_t - 1)} - M_0\right]} \tag{5.30}$$

Step 9: Again the development of these expressions is left to the reader.

Thermal efficiency:

$$\eta_T = 1 - \frac{1}{\tau_r \tau_c} \tag{5.31a}$$

Propulsive efficiency:

$$\eta_P = \frac{2M_0}{V_9/a_0 + M_0} \tag{5.31b}$$

Overall efficiency:

$$\eta_O = \eta_P \eta_T \tag{5.31c}$$

5.7.2 Summary of Equations—Ideal Turbojet

INPUTS:

$$M_0,\ T_0(\mathrm{K},\ ^\circ\mathrm{R}),\ \gamma,\ c_p\left(\frac{\mathrm{kJ}}{\mathrm{kg}\cdot\mathrm{K}},\ \frac{\mathrm{Btu}}{\mathrm{lbm}\cdot{}^\circ\mathrm{R}}\right),\ h_{PR}\left(\frac{\mathrm{kJ}}{\mathrm{kg}},\ \frac{\mathrm{Btu}}{\mathrm{lbm}}\right),\ T_{t4}(\mathrm{K},\ ^\circ\mathrm{R}),\ \pi_c$$

OUTPUTS:

$$\frac{F}{\dot{m}_0}\left(\frac{N}{\mathrm{kg/s}},\ \frac{\mathrm{lbf}}{\mathrm{lbm/s}}\right),\ f,\ S\left(\frac{\mathrm{mg/s}}{\mathrm{N}},\ \frac{\mathrm{lbm/h}}{\mathrm{lbf}}\right)\ \eta_T,\ \eta_P,\ \eta_O$$

EQUATIONS:

$$R = \frac{\gamma - 1}{\gamma} c_p \tag{5.32a}$$

$$a_0 = \sqrt{\gamma R g_c T_0} \tag{5.32b}$$

$$\tau_r = 1 + \frac{\gamma - 1}{2} M_0^2 \tag{5.32c}$$

$$\tau_\lambda = \frac{T_{t4}}{T_0} \tag{5.32d}$$

$$\tau_c = (\pi_c)^{(\gamma-1)/\gamma} \tag{5.32e}$$

$$\tau_t = 1 - \frac{\tau_r}{\tau_\lambda}(\tau_c - 1) \tag{5.32f}$$

$$\frac{V_9}{a_0} = \sqrt{\frac{2}{\gamma - 1}\frac{\tau_\lambda}{\tau_r \tau_c}(\tau_r \tau_c \tau_t - 1)} \tag{5.32g}$$

$$\frac{F}{\dot{m}_0} = \frac{a_0}{g_c}\left(\frac{V_9}{a_0} - M_0\right) \tag{5.32h}$$

$$f = \frac{c_p T_0}{h_{PR}}(\tau_\lambda - \tau_r \tau_c) \tag{5.32i}$$

$$S = \frac{f}{F/\dot{m}_0} \tag{5.32j}$$

$$\eta_T = 1 - \frac{1}{\tau_r \tau_c} \tag{5.32k}$$

$$\eta_P = \frac{2M_0}{V_9/a_0 + M_0} \tag{5.32l}$$

$$\eta_O = \eta_P \eta_T \tag{5.32m}$$

Example 5.2

In Figs. 5.8a–5.8d, the performance of ideal turbojets is plotted vs compressor pressure ratio π_c for different values of flight Mach number M_0. Figures 5.9a–5.9d plot the performance vs flight Mach number M_0 for different values of the compressor pressure ratio π_c. Calculations were performed for the following input data:

$$T_0 = 390°\text{R}, \qquad \gamma = 1.4, \qquad c_p = 0.24\,\text{Btu/(lbm} \cdot °\text{R)}$$
$$h_{PR} = 18{,}400\,\text{Btu/lbm}, \qquad T_{t4} = 3000°\text{R}$$

a) Figures 5.8a–5.8d. Figure 5.8a shows that for a fixed Mach number, there is a compressor pressure ratio that gives maximum specific thrust. The loci of the compressor pressure ratios that give maximum specific thrust are indicated by the dashed line in Fig. 5.8a. One can also see from Fig. 5.8a that a lower compressor pressure ratio is desired at high Mach numbers to obtain reasonable specific thrust. This helps explain why the compressor pressure ratio of a turbojet for a subsonic flight may be 24 and that for supersonic flight may be 10. Figure 5.8b shows the general trend that increasing the compressor pressure ratio will decrease the thrust specific fuel consumption. The decrease in fuel/air ratio with increasing compressor pressure ratio and Mach number is shown

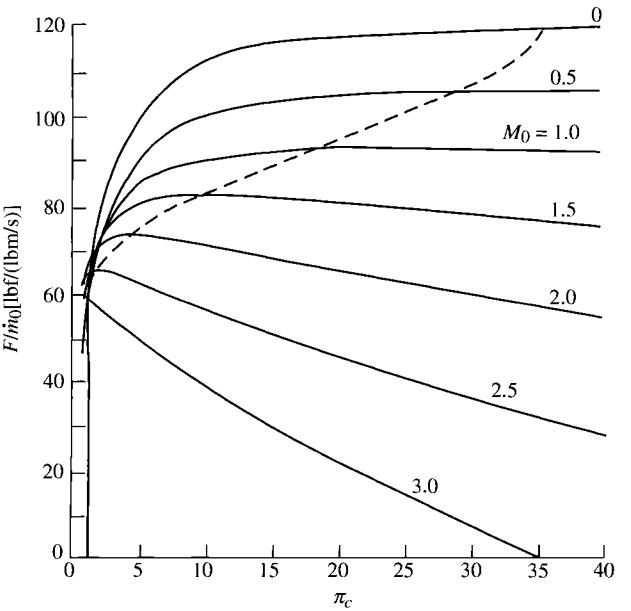

Fig. 5.8a Ideal turbojet performance vs compressor pressure ratio: specific thrust.

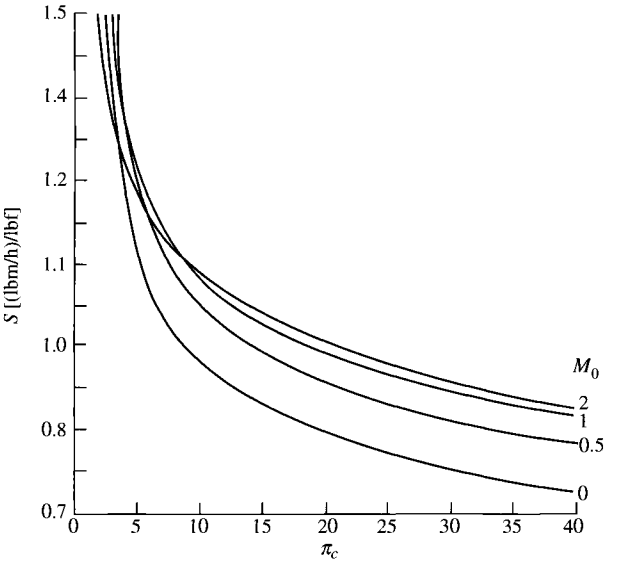

Fig. 5.8b Ideal turbojet performance vs compressor pressure ratio: thrust-specific fuel consumption.

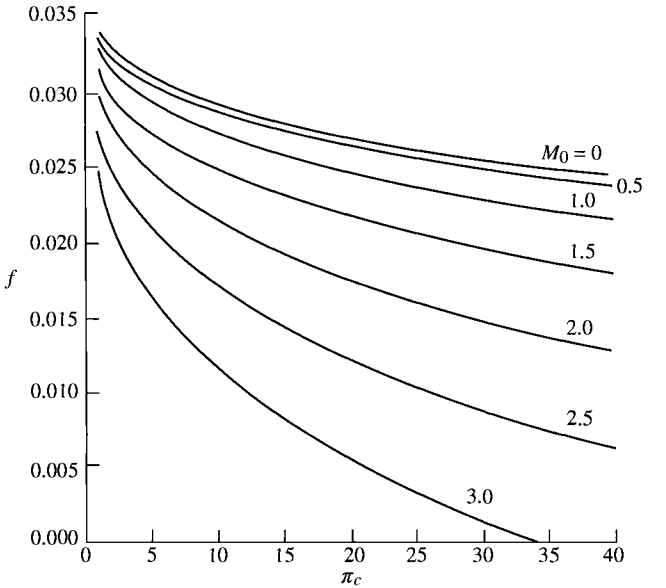

Fig. 5.8c Ideal turbojet performance vs compressor pressure ratio: fuel/air ratio.

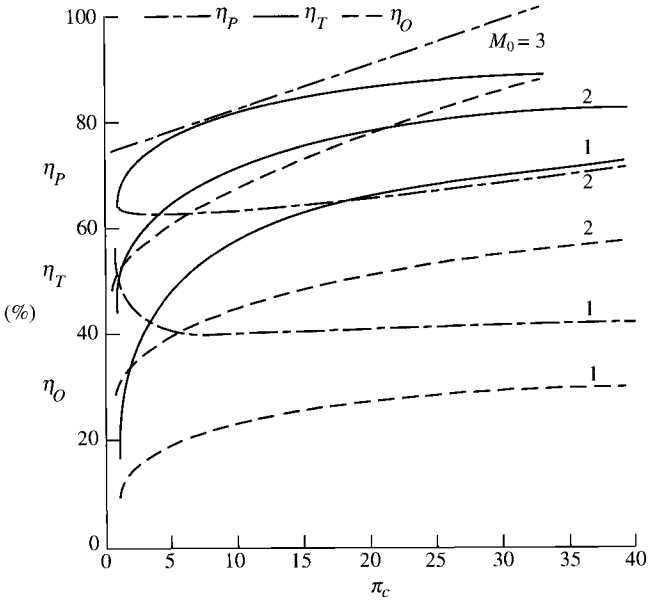

Fig. 5.8d Ideal turbojet performance vs compressor pressure ratio: efficiencies.

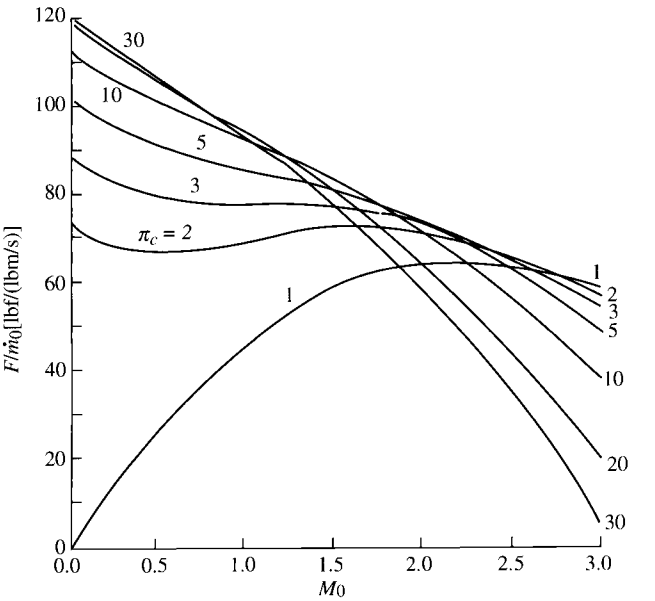

Fig. 5.9a Ideal turbojet performance vs flight Mach number: specific thrust.

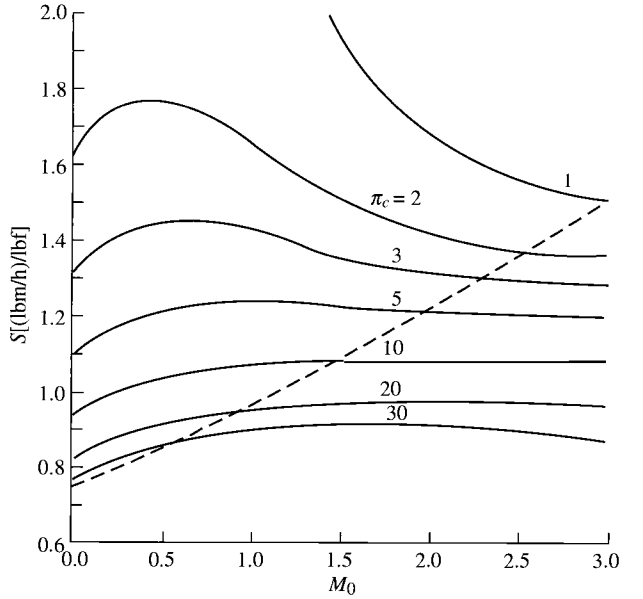

Fig. 5.9b Ideal turbojet performance vs flight Mach number: thrust-specific fuel consumption.

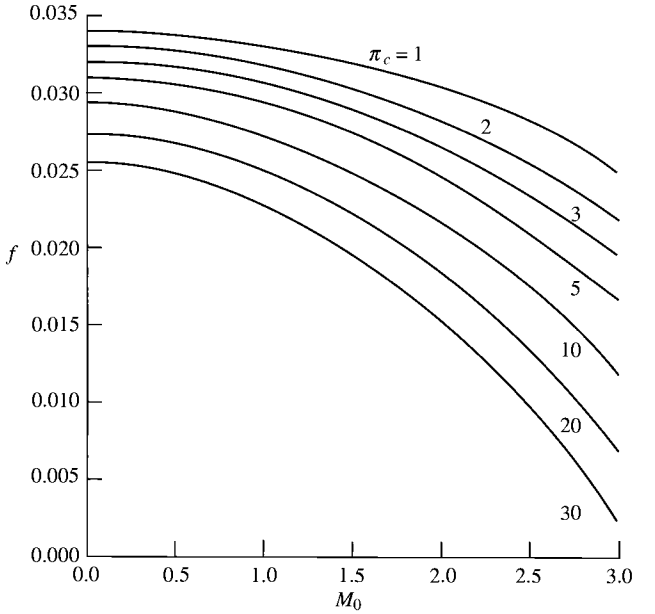

Fig. 5.9c Ideal turbojet performance vs flight Mach number: fuel/air ratio.

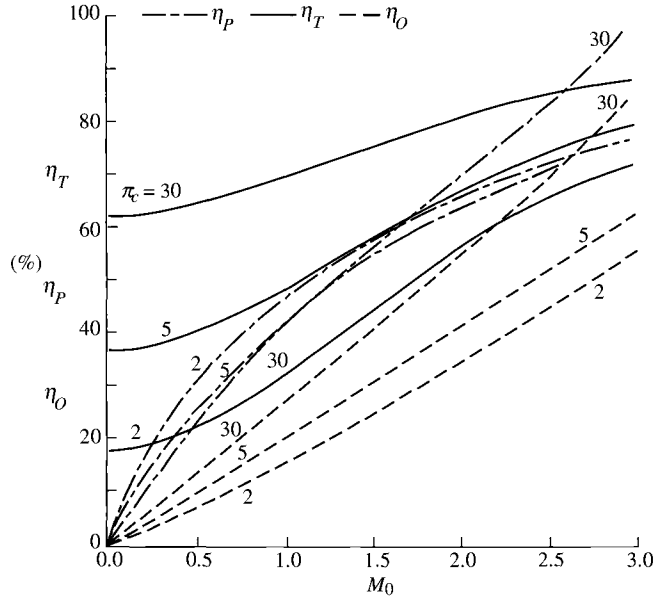

Fig. 5.9d Ideal turbojet performance vs flight Mach number: efficiencies.

in Fig. 5.8c. This is due to the increase in the total temperature entering the burner with increasing compressor pressure ratio and Mach number. Figure 5.8d shows the general increase in propulsive, thermal, and overall efficiencies with increasing compressor pressure ratio and flight Mach number.

b) Figures 5.9a–5.9d. These figures are another representation of the data of Figs. 5.8a–5.8d. Figures 5.9a and 5.9b show that a high compressor pressure ratio is desirable for subsonic flight for good specific thrust and low fuel consumption. However, some care must be used in selecting the compressor pressure ratio for the supersonic flight Mach number because of the rapid falloff in specific thrust with the compressor pressure ratio. The loci of the compressor pressure ratios that give maximum specific thrust are indicated by the dashed line in Fig. 5.9b. The decrease in fuel/air ratio with increasing Mach number and compressor pressure ratio is shown in Fig. 5.9c. Figure 5.9d shows the dominant influence of flight Mach number on propulsive efficiency. The performance of the ideal ramjet is shown in Figs. 5.9a–5.9c by curves for the compressor pressure ratio equal to 1.

5.7.3 Optimum Compressor Pressure Ratio

The plot of specific thrust vs the compressor pressure ratio (see Fig. 5.8a) shows that a maximum value is exhibited at a certain compressor pressure ratio at a given M_0, a_0, and τ_λ. The value of τ_c and hence of π_c to maximize

the specific thrust at a given M_0, a_0 and τ_λ can be found by differentiation. Because specific thrust will be maximum when V_9/a_0 is maximum, it is convenient to differentiate the expression for $(V_9/a_0)^2$ to find τ_c optimum. From Eq. (5.28), we have

$$\frac{\partial}{\partial \tau_c}\left[\left(\frac{V_9}{a_0}\right)^2\right] = \frac{2}{\gamma - 1}\frac{\partial}{\partial \tau_c}\left[\frac{\tau_\lambda}{\tau_r \tau_c}(\tau_r \tau_c \tau_t - 1)\right] = 0$$

Differentiating with respect to τ_c at constant M_0 (thus τ_r is constant) and constant τ_λ, we obtain

$$-\frac{\tau_\lambda}{\tau_r \tau_c^2}(\tau_r \tau_c \tau_t - 1) + \frac{\tau_\lambda}{\tau_r \tau_c}\left(\tau_r \tau_t + \tau_r \tau_c \frac{\partial \tau_t}{\partial \tau_c}\right) = 0$$

or

$$-\frac{\tau_\lambda \tau_t}{\tau_c} + \frac{\tau_\lambda}{\tau_r \tau_c^2} + \frac{\tau_\lambda \tau_t}{\tau_c} + \tau_\lambda \frac{\partial \tau_t}{\partial \tau_c} = 0$$

Then

$$\frac{1}{\tau_r \tau_c^2} + \frac{\partial \tau_t}{\partial \tau_c} = 0$$

where, using Eq. (5.27)

$$\frac{\partial \tau_t}{\partial \tau_c} = -\frac{\tau_t}{\tau_\lambda}$$

Thus

$$\frac{1}{\tau_r \tau_c^2} = \frac{\tau_t}{\tau_\lambda}$$

which results in

$$(\tau_c)_{\max F/\dot{m}_0} = \frac{\sqrt{\tau_\lambda}}{\tau_r} \tag{5.33a}$$

or

$$(\pi_c)_{\max F/\dot{m}_0} = (\tau_c)^{\gamma/(\gamma-1)}_{\max F/\dot{m}_0} \tag{5.33b}$$

An expression for the maximum V_9/a_0 can be found by substituting Eq. (5.33a) into Eqs. (5.28) and (5.27) to obtain

$$\frac{V_9}{a_0} = \sqrt{\frac{2}{\gamma - 1}\sqrt{\tau_\lambda}(\sqrt{\tau_\lambda}\tau_t - 1)}$$

and

$$\tau_t = 1 - \left(\frac{1}{\sqrt{\tau_\lambda}} - \frac{\tau_r}{\tau_\lambda}\right)$$

Thus

$$\frac{V_9}{a_0} = \sqrt{\frac{2}{\gamma - 1}[(\sqrt{\tau_\lambda} - 1)^2 + \tau_r - 1]} \tag{5.33c}$$

The specific thrust can then be written as

$$\frac{F}{\dot{m}_0} = \frac{a_0}{g_c}\left\{\sqrt{\frac{2}{\gamma - 1}[(\sqrt{\tau_\lambda} - 1)^2 + \tau_r - 1]} - M_0\right\} \tag{5.33d}$$

The fuel/air ratio f for the optimum turbojet can be written as

$$f = \frac{c_p T_0}{h_{PR}}(\tau_\lambda - \sqrt{\tau_\lambda}) \tag{5.33e}$$

and the thrust specific fuel consumption S as

$$S = \frac{c_p T_0 g_c(\tau_\lambda - \sqrt{\tau_\lambda})}{a_0 h_{PR}\{\sqrt{[2/(\gamma - 1)][(\sqrt{\tau_\lambda} - 1)^2 + \tau_r - 1]} - M_0\}} \tag{5.33f}$$

For the optimum ideal turbojet, it can be easily shown that $T_{t3} = T_9$. As the Mach number is changed in the optimum ideal turbojet at a fixed τ_λ and fixed altitude, the cycle and its enclosed area remain the same in the T-s diagram. The area enclosed by the cycle in the T-s diagram equals the net work output (kinetic energy change, for our case) of the cycle per unit mass flow. Even though this output is constant as M_0 increases, the thrust per unit mass flow decreases as M_0 increases. This can be shown as follows.

The kinetic energy change per unit mass is constant, and we can write

$$V_9^2 - V_0^2 = C$$

and therefore,

$$(V_9 - V_0)(V_9 + V_0) = C$$

or

$$\frac{F}{\dot{m}_0} = \frac{V_9 - V_0}{g_c} = \frac{C/g_c}{V_9 + V_0} \tag{5.34}$$

Referring to the T-s diagram of Fig. 5.7b, we see that as V_0 increases, T_{t2} increases and thus so does T_{t5}. However, if T_{t5} increases, V_9 increases also. Consequently $V_9 + V_0$ becomes larger as M_0 increases. Therefore, from Eq. (5.34), $V_9 - V_0$ must decrease as M_0 increases. It follows that the thrust per unit mass flow decreases with increasing M_0 even though the cycle work output per unit mass flow remains constant.

5.8 Ideal Turbojet with Afterburner

The thrust of a turbojet can be increased by the addition of a second combustion chamber, called an *afterburner*, aft of the turbine, as shown in Fig. 5.10. The total temperature leaving the afterburner has a higher limiting value than the total temperature leaving the main combustor because the gases leaving the afterburner do not have a turbine to pass through. The station numbering is indicated in Figs. 5.10, 5.11a, and 5.11b with 9′ representing the nozzle exit for the case of no afterburning.

5.8.1 Cycle Analysis

Rather than go through the complete steps of cycle analysis, we will use the results of the ideal turbojet and modify the equations to include afterburning. The gas velocity at the nozzle exit is given by

$$\frac{V_9^2}{2g_c c_p} = T_{t9} - T_9 = T_{t9}\left[1 - \left(\frac{P_9}{P_{t9}}\right)^{(\gamma-1)/\gamma}\right] \tag{5.35}$$

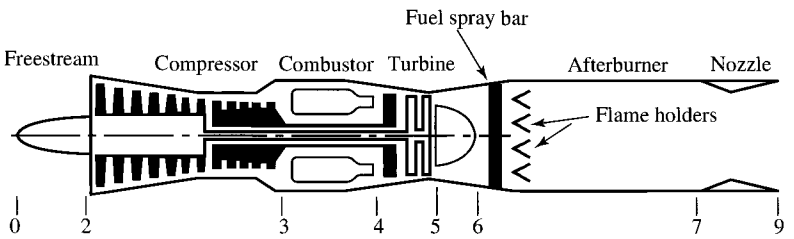

Fig. 5.10 Station numbering of an ideal afterburning turbojet engine.

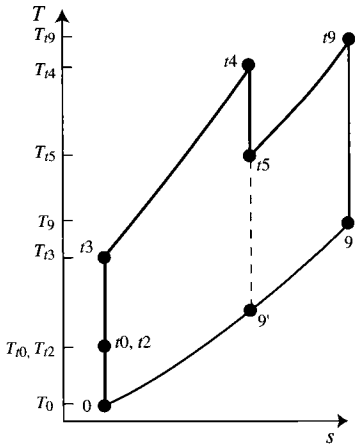

Fig. 5.11a The *T-s* diagram for an ideal afterburning turbojet engine.

and for the nonafterburning (subscript dry) and afterburning (subscript AB for afterburning) cases, we have

$$\frac{P_9}{P_{t9}} = \left(\frac{P_{9'}}{P_{t5}}\right)_{\text{dry}} = \left(\frac{P_9}{P_{t9}}\right)_{\text{AB}}$$

Thus we have

$$\left(\frac{V_9}{V_{9'}}\right)^2 = \frac{T_{t9}}{T_{t5}} \tag{5.36}$$

Equation (5.36) can be obtained directly from the *H-K* diagram in Fig. 5.11b. Since $(P_{9'}/P_{t5})_{\text{dry}} = (P_9/P_{t9})_{\text{AB}}$, $M_{9'} = M_9$. The triangle for the exit state of the turbojet with afterburner between points *t*9-9-origin is similar to that for the dry turbojet between points *t*5-9′-origin. Thus

$$\frac{K_9}{K_{9'}} = \frac{H_{t9}}{H_{t5}}$$

which can be rewritten as Eq. (5.36).

Consequently, we can find the velocity ratio $(V_9/a_0)^2$ for the afterburning turbojet by multiplying $(V_{9'}/a_0)^2$ from our nonafterburning turbojet analysis [Eq. (5.28)] by the total temperature ratio of the afterburner. That is,

$$\left(\frac{V_9}{a_0}\right)^2 = \frac{T_{t9}}{T_{t5}}\left(\frac{V_{9'}}{a_0}\right)^2 \tag{5.37}$$

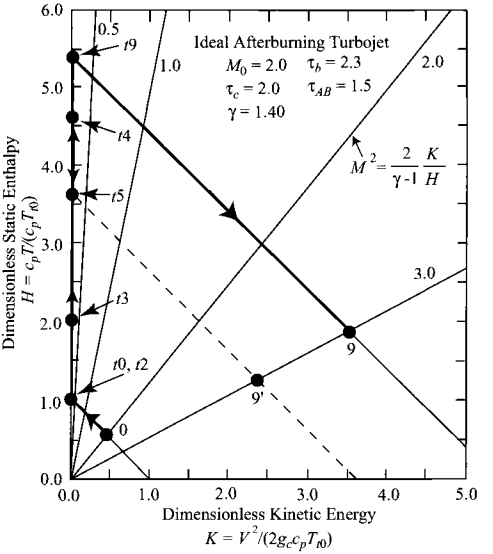

Fig. 5.11b *H-K* diagram for an ideal afterburning turbojet engine.

We define the temperature ratio $\tau_{\lambda AB}$ as

$$\tau_{\lambda AB} = \frac{T_{t7}}{T_0} \tag{5.38}$$

Thus we can write the total temperature ratio of the afterburner as

$$\frac{T_{t9}}{T_{t5}} = \frac{(T_{t9}/T_{t7})(T_{t7}/T_0)}{(T_{t5}/T_{t4})(T_{t4}/T_0)} = \frac{\tau_{\lambda AB}}{\tau_\lambda \tau_t} \tag{5.39}$$

Using Eqs. (5.27), (5.28), (5.37), and (5.39), we get the following expressions for V_9/a_0:

$$\left(\frac{V_9}{a_0}\right)^2 = \frac{2}{\gamma - 1}\frac{\tau_{\lambda AB}}{\tau_\lambda \tau_t}\frac{\tau_\lambda}{\tau_r \tau_c}(\tau_r \tau_c \tau_t - 1) = \frac{2}{\gamma - 1}\tau_{\lambda AB}\left(1 - \frac{1}{\tau_r \tau_c \tau_t}\right)$$

$$\left(\frac{V_9}{a_0}\right)^2 = \frac{2}{\gamma - 1}\tau_{\lambda AB}\left[1 - \frac{\tau_\lambda/(\tau_r \tau_c)}{\tau_\lambda - \tau_r(\tau_c - 1)}\right] \tag{5.40}$$

We find the total fuel flow rate to the burner and afterburner by an energy balance across the engine from station 0 to station 9, as sketched in Fig. 5.12.

The chemical energy of the fuel introduced between stations 0 and 9 is converted to thermal and kinetic energy of the gases, as measured by the total

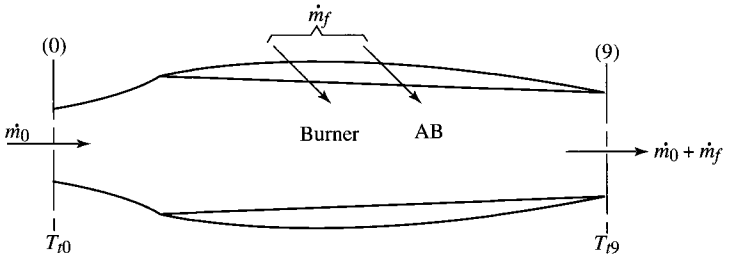

Fig. 5.12 Total fuel flow rate control volume.

temperature rise $T_{t9} - T_{t0}$. Thus we can write for this ideal engine

$$\dot{m}_{f\,\text{tot}} h_{PR} = \dot{m}_0 c_p (T_{t9} - T_{t0}) = \dot{m}_0 c_p T_0 \left(\frac{T_{t9}}{T_0} - \frac{T_{t0}}{T_0} \right)$$

Thus

$$f_{\text{tot}} = \frac{\dot{m}_f}{\dot{m}_0} = \frac{c_p T_0}{h_{PR}} (\tau_{\lambda \text{AB}} - \tau_r) \tag{5.41}$$

The thermal efficiency is given by

$$\eta_T = \frac{(\gamma - 1) c_p T_0 [(V_9/a_0)^2 - M_0^2]}{2 f_{\text{tot}} h_{PR}} \tag{5.42}$$

5.8.2 Summary of Equations—Ideal Turbojet with Afterburner

INPUTS:

$$M_0,\ T_0(\text{K, °R}),\ \gamma,\ c_p\left(\frac{\text{kJ}}{\text{kg} \cdot \text{K}}, \frac{\text{Btu}}{\text{lbm} \cdot \text{°R}}\right),\ h_{PR}\left(\frac{\text{kJ}}{\text{kg}}, \frac{\text{Btu}}{\text{lbm}}\right),$$

$$T_{t4}(\text{K, °R}),\ T_{t7}(\text{K, °R}),\ \pi_c$$

OUTPUTS:

$$\frac{F}{\dot{m}_0}\left(\frac{\text{N}}{\text{kg/s}}, \frac{\text{lbf}}{\text{lbm/s}}\right),\ f_{\text{tot}},\ S\left(\frac{\text{mg/s}}{\text{N}}, \frac{\text{lbm/h}}{\text{lbf}}\right),\ \eta_T,\ \eta_P,\ \eta_O$$

EQUATIONS:

Equations (5.32a–5.32f), (5.40), (5.32h), (5.41), (5.32j) with f replaced by f_{tot}, (5.42), (5.32l), and (5.32m).

Example 5.3

We consider the performance of an ideal turbojet engine with afterburner. For comparison with the nonafterburning (simple) turbojet of Example 5.2, we select the following input data:

$$T_0 = 390°\text{R}, \quad \gamma = 1.4, \quad c_p = 0.24\,\text{Btu/(lbm}\cdot°\text{R)}, \quad h_{PR} = 18{,}400\,\text{Btu/lbm}$$
$$T_{t4} = 3000°\text{R}, \quad T_{t7} = 4000°\text{R}$$

Figure 5.13 compares the performance of two turbojet engines with a compressor pressure ratio of 10, an afterburning turbojet and a simple turbojet. The graph of specific thrust vs M_0 indicates the thrust increase available by adding an afterburner to a simple turbojet. The afterburner increases the static thrust about 22% for the conditions shown and continues to provide significant thrust as the thrust of the simple turbojet goes to zero at about Mach 3.8. The graph of Fig. 5.13 also shows the cost in fuel consumption of the increased thrust provided by the afterburner. The cost is about a 20–30% increase in the fuel flow rate per unit thrust up to about $M_0 = 2.0$. In a nonideal turbojet, the same increase in S occurs up to about $M_0 = 2.0$. However, as the thrust of the simple turbojet approaches zero in the real case, its S rises above the afterburning engine's S so that the afterburning engine at the higher M_0 has a lower S and higher specific thrust than the simple turbojet.

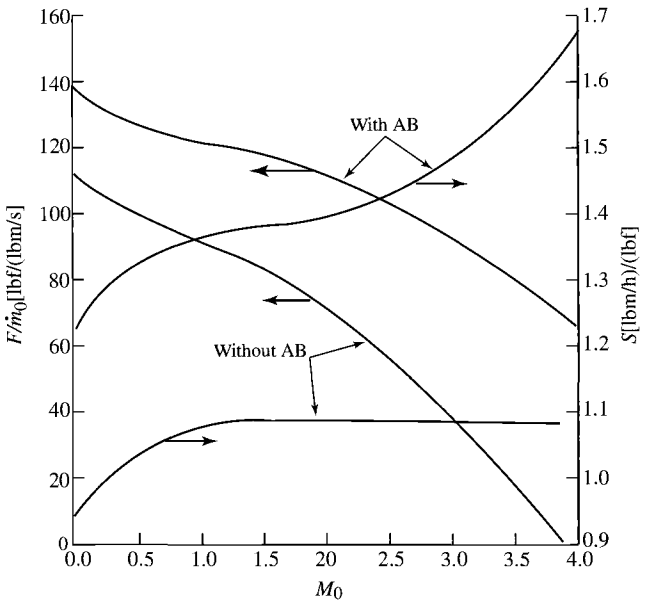

Fig. 5.13 Engine performance vs M_0 for an ideal afterburning turbojet.

Figures 5.14a–5.14d show the variation of engine performance with both Mach number and compressor pressure ratio for the afterburning turbojet. These should be compared to their counterparts in Figs. 5.8a–5.8d. For a fixed flight Mach number, the ideal afterburning turbojet has a compressor pressure ratio giving maximum specific thrust. The locus of these compressor pressure ratios is shown by a dashed line in Fig. 5.14a. Comparison of Figs. 5.14a–5.14d to Figs. 5.8a–5.8d yields the following general trends:

1) Afterburning increases both the specific thrust and the thrust specific fuel consumption.

2) Afterburning turbojets with moderate to high compressor pressure ratios give very good specific thrust at high flight Mach numbers.

3) The fuel/air ratio of the main burner f is unchanged. The afterburner fuel/air ratio f_{AB} increases with Mach number and compressor pressure ratio. The total fuel/air ratio decreases with Mach number and is not a function of π_c; see Eq. (5.41).

4) Thermal, propulsive, and overall efficiencies are reduced by afterburning.

5.8.3 Optimum Compressor Pressure Ratio with Afterburner

The value of the compressor pressure ratio to maximize the specific thrust at a given M_0, τ_r, τ_λ, and altitude can be found by differentiating V_9/a_0 with respect to

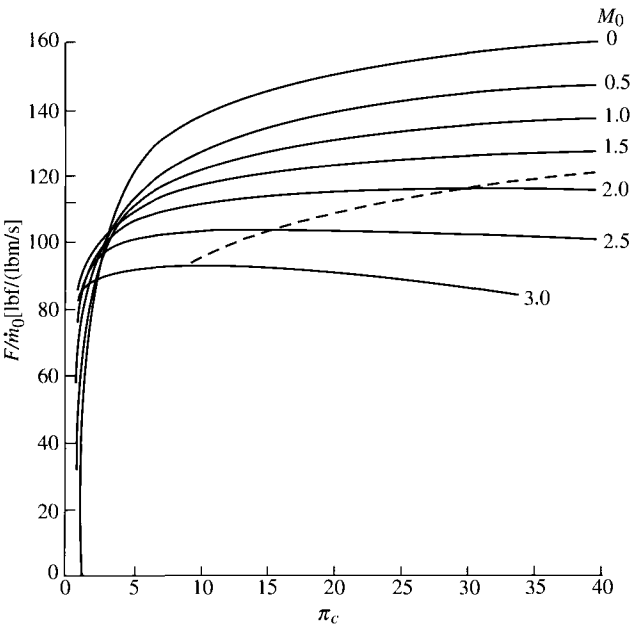

Fig. 5.14a Ideal afterburning turbojet engine performance vs compressor pressure ratio: specific thrust.

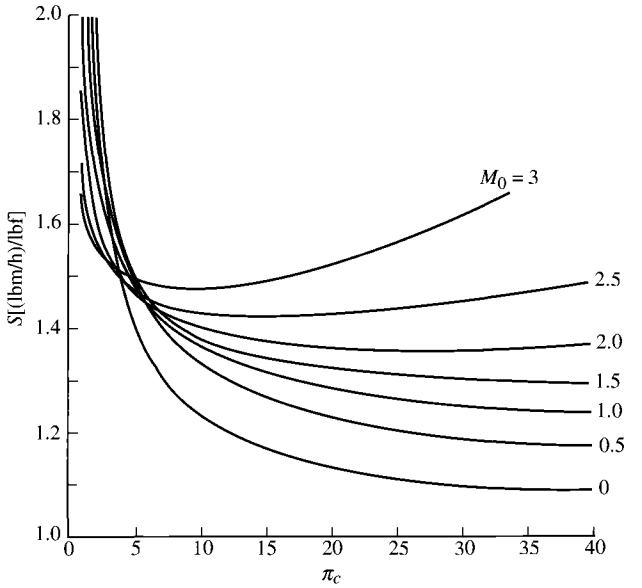

Fig. 5.14b Ideal afterburning turbojet engine performance vs compressor pressure ratio: thrust specific fuel consumption.

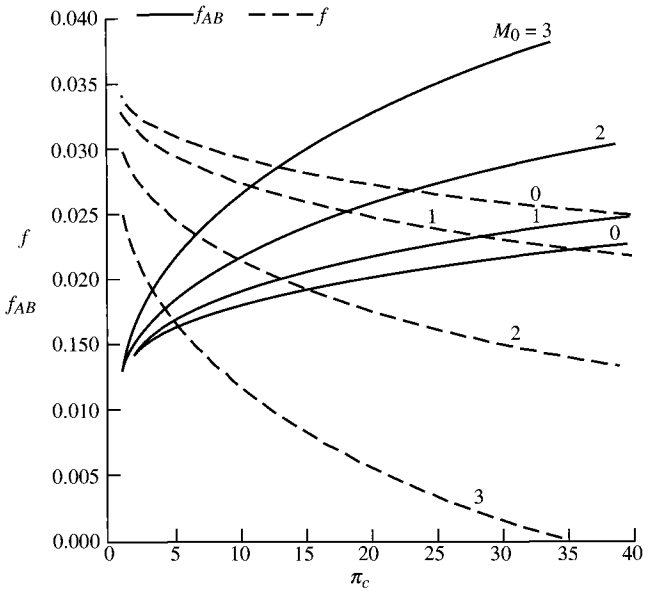

Fig. 5.14c Ideal afterburning turbojet engine performance vs compressor pressure ratio: fuel/air ratios.

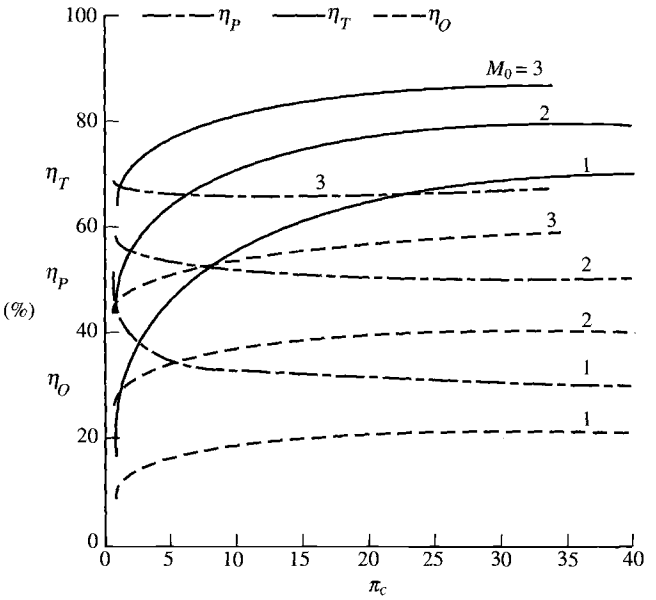

Fig. 5.14d Ideal afterburning turbojet engine performance vs compressor pressure ratio: efficiencies.

τ_c since the specific thrust depends on τ_c only through the ratio V_9/a_0 in the equation

$$\frac{F}{\dot{m}_0} = \frac{a_0}{g_c}\left(\frac{V_9}{a_0} - M_0\right)$$

We have for $(V_9/a_0)^2$, from Eq. (5.40),

$$\left(\frac{V_9}{a_0}\right)^2 = \frac{2}{\gamma - 1}\tau_{\lambda AB}\left[1 - \frac{\tau_\lambda/(\tau_r\tau_c)}{\tau_\lambda - \tau_r(\tau_c - 1)}\right]$$

Differentiating with respect to τ_c at constant M_0, τ_r, and τ_λ and setting it equal to zero, we get

$$\frac{\partial}{\partial\tau_c}\left[\left(\frac{V_9}{a_0}\right)^2\right] = \frac{2}{\gamma - 1}\tau_{\lambda AB}\frac{\partial}{\partial\tau_c}\left[1 - \frac{\tau_\lambda/(\tau_r\tau_c)}{\tau_\lambda - \tau_r(\tau_c - 1)}\right] = 0$$

Thus

$$\frac{\tau_\lambda}{\tau_r\tau_c^2}\frac{1}{\tau_\lambda - \tau_r(\tau_c - 1)} + \frac{\tau_\lambda/(\tau_r\tau_c)}{[\tau_\lambda - \tau_r(\tau_c - 1)]^2}(-\tau_r) = 0$$

or

$$\frac{1}{\tau_c} - \frac{\tau_r}{\tau_\lambda - \tau_r(\tau_c - 1)} = 0$$

which becomes

$$\tau_r\tau_c = \tau_\lambda - \tau_r(\tau_c - 1)$$

resulting in

$$\tau_{c\,\max F/\dot{m}\mathrm{AB}} = \frac{1}{2}\left(\frac{\tau_\lambda}{\tau_r} + 1\right) \tag{5.43}$$

Placing Eq. (5.43) into Eq. (5.40), we get

$$\left(\frac{V_9}{a_0}\right)^2 = \frac{2}{\gamma - 1}\tau_{\lambda\,\mathrm{AB}}\left[1 - \frac{4\tau_\lambda}{(\tau_\lambda + \tau_r)^2}\right] \tag{5.44}$$

so that

$$\frac{F}{\dot{m}_0} = \frac{a_0}{g_c}\left\{\sqrt{\frac{2}{\gamma - 1}\tau_{\lambda\,\mathrm{AB}}\left[1 - \frac{4\tau_\lambda}{(\tau_\lambda + \tau_r)^2}\right]} - M_0\right\} \tag{5.45}$$

The locus of specific thrust vs π_c and M_0 for optimum afterburning turbojets is plotted as a dashed line in Fig. 5.14a. Note that the pressure ratio giving the maximum specific thrust decreases with the flight Mach number.

5.8.4 Optimum Simple Turbojet and Optimum Afterburning Turbojet—Comparison

Figures 5.8a and 5.14a plot the thrust per unit mass flow vs the compressor pressure ratio for different values of the flight Mach number for the ideal turbojet without afterburner and the ideal turbojet with afterburner, respectively. These figures show that the thrust per unit mass flow is higher for the engine with afterburner and that the optimum compressor pressure ratio is also higher for the engine with afterburner. The thrust per unit mass flow, thrust specific fuel consumption, and compressor pressure ratio for an optimum simple and an optimum afterburning turbojet are shown vs the Mach number for representative conditions in Figs. 5.15 and 5.16. The optimum afterburning π_c and specific

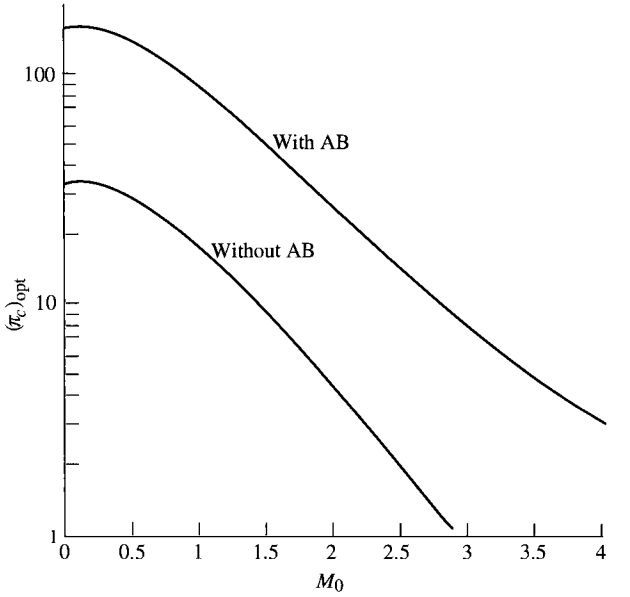

Fig. 5.15 Optimum ideal turbojet compressor pressure ratio ($\tau_\lambda = 7.5$).

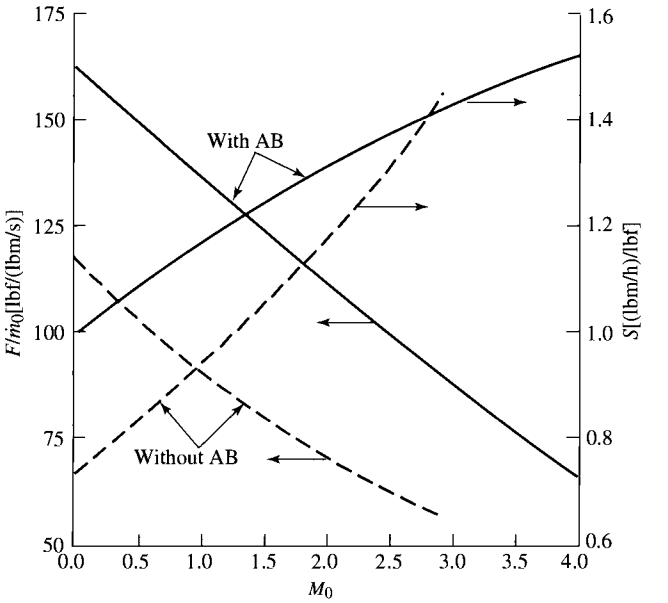

Fig. 5.16 Optimum ideal turbojet performance ($T_0 = 390°R$, $\tau_\lambda = 7.5$, $\tau_{\lambda AB} = 10$).

thrust are higher at all Mach numbers. Considering a given engine with, say, a compressor pressure ratio of 30, we see from Fig. 5.15 that it can operate optimally at Mach 2 with afterburning and near-optimum conditions subsonically without afterburning where less thrust is required and available and where the fuel consumption is much lower. Figure 5.16 shows that at $M_0 = 2.7$, the specific fuel consumption of an afterburning engine with $\pi_c = 12$ is the same as that of a simple turbojet with $\pi_c = 1.5$. From Fig. 5.16, we see that at $M_0 = 2.7$, the thrust per unit mass flow of the afterburning engine is 50% higher. Based on these data, which engine would you select for a supersonic transport (SST) to cruise at $M_0 = 2.7$?

The higher-pressure-ratio afterburning engine is the logical choice for cruise at $M_0 = 2.7$ because it provides a smaller engine with the same fuel consumption as the nonafterburning, low-pressure-ratio engine. The final choice of an engine depends on the engine's subsonic performance also.

The plots of Fig. 5.17 provide a comparison of the nonafterburning $\pi_c = 12$ and $\pi_c = 1.5$ engines at subsonic flight speeds. It is evident that the higher-pressure-ratio engine operating in the nonafterburning mode has the better subsonic performance. The higher-pressure-ratio engine is, therefore, the best choice overall.

Although our conclusions that an afterburning high-pressure-ratio ($\pi_c = 12$) turbojet engine is a proper engine for an SST are based on a simple ideal cycle analysis, they agree with practice. The Concorde uses four Olympus 593 afterburning turbojet engines (see Figs. 5.18a–5.18c) for supersonic cruise. In

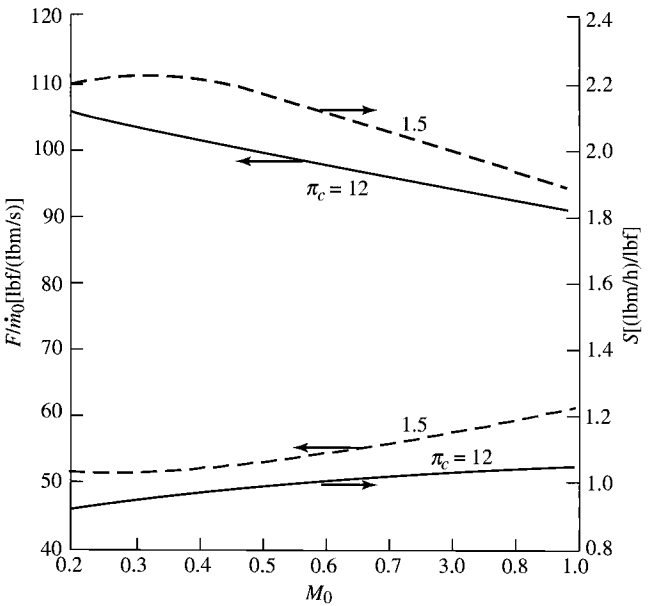

Fig. 5.17 Ideal turbojet without afterburning ($T_0 = 390°R$, $\tau_\lambda = 7.5$).

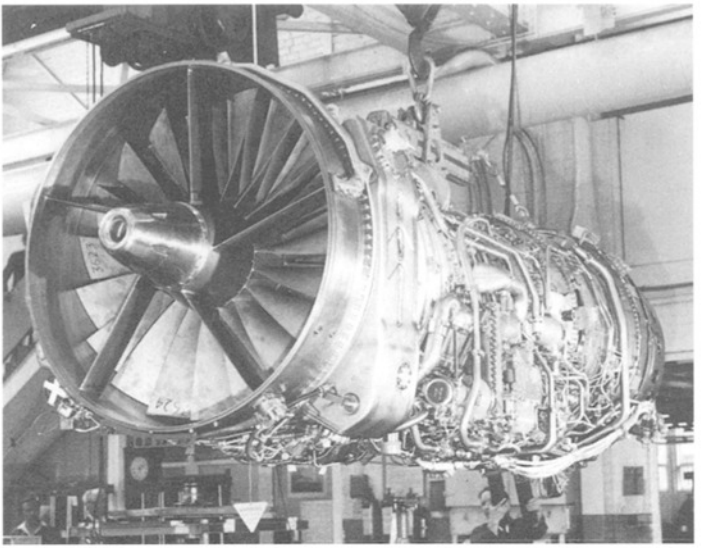

Fig. 5.18a Olympus 593 turbojet engine used in the Concorde. (Courtesy of Rolls-Royce.)

addition, the GE4 that was being developed by General Electric for the Boeing SST was an afterburning turbojet engine with a pressure ratio of about 12! This SST engine is shown in Fig. 5.19.

5.9 Ideal Turbofan

The propulsive efficiency of a simple turbojet engine can be improved by extracting a portion of the energy from the engine's gas generator to drive a ducted propeller, called a *fan*. The fan increases the propellant mass flow rate with an accompanying decrease in the required propellant exit velocity for a given thrust. Because the rate of production of "wasted" kinetic energy in the

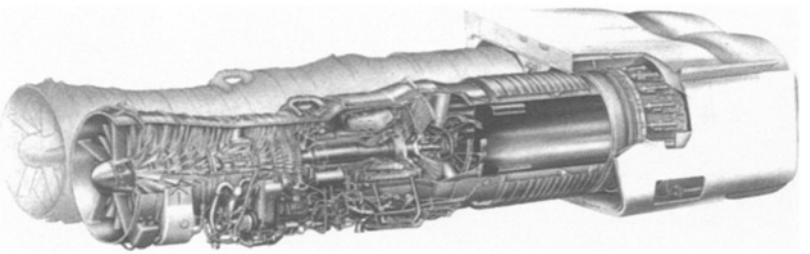

Fig. 5.18b Two Olympus engines, with thrust-reversing nozzles. (Courtesy of Rolls-Royce.)

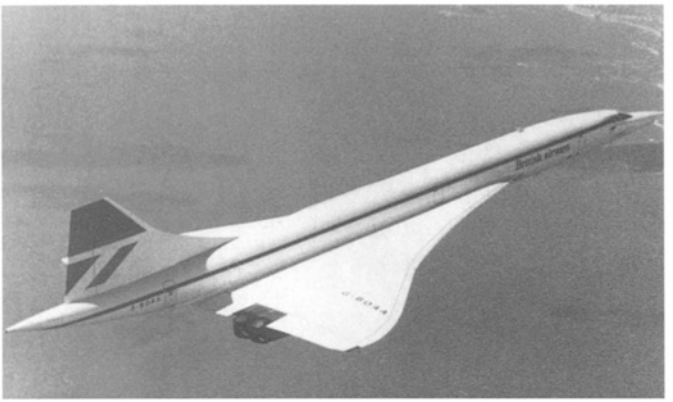

Fig. 5.18c Concorde supersonic transport. (Courtesy of Rolls-Royce.)

exit propellant gases varies as the first power with mass flow rate and as the square of the exit velocity, the net effect of increasing the mass flow rate and decreasing the exit velocity is to reduce the wasted kinetic energy production and to improve the propulsive efficiency.

Our station numbering for the turbofan cycle analysis is given in Fig. 5.20, and the *T-s* diagrams for ideal flow through the core engine and the fan are given in Figs. 5.21 and 5.22, respectively. The temperature drop through the turbine $(T_{t4} - T_{t5})$ is now greater than the temperature rise through the compressor $(T_{t3} - T_{t2})$ since the turbine drives the fan in addition to the compressor.

The fan exit is station 13, and the fan total pressure ratio and the fan total temperature ratio are π_f and τ_f, respectively. The fan flow nozzle exit is station

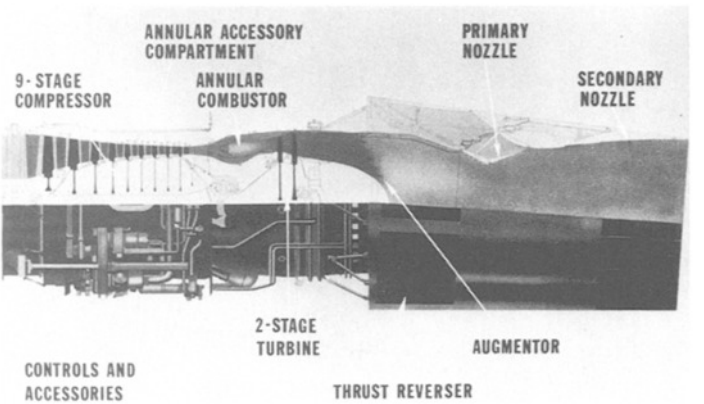

Fig. 5.19 General Electric GE4 turbojet engine (developed for Boeing SST). (Courtesy of General Electric.)

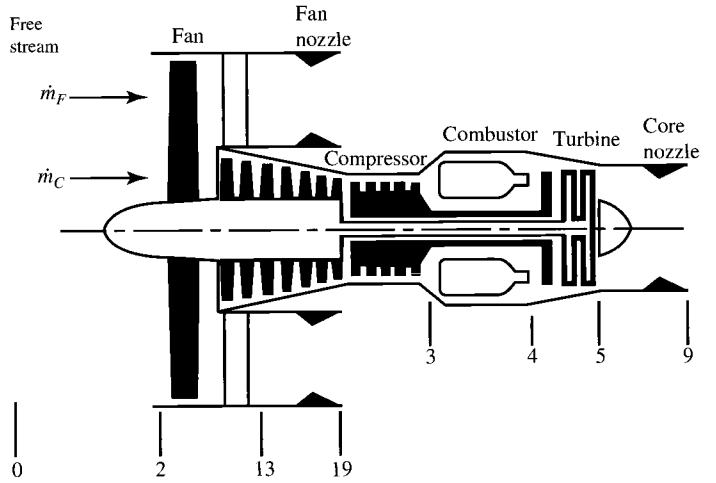

Fig. 5.20 Station numbering of a turbofan engine.

19, and the fan nozzle total pressure ratio and the fan nozzle total temperature ratio are π_{fn} and τ_{fn}, respectively. These four ratios are listed in the following:

$$\pi_f = \frac{P_{t13}}{P_{t2}} \qquad \tau_f = \frac{T_{t13}}{T_{t2}} \qquad \pi_{fn} = \frac{P_{t19}}{P_{t13}} \qquad \text{and} \qquad \tau_{fn} = \frac{T_{t19}}{T_{t13}}$$

The gas flow through the core engine is $\dot{m}_C$, and the gas flow through the fan is $\dot{m}_F$. The ratio of the fan flow to the core flow is defined as the *bypass ratio* and given the symbol alpha α. Thus

$$\text{Bypass ratio } \alpha = \frac{\dot{m}_F}{\dot{m}_C} \tag{5.46}$$

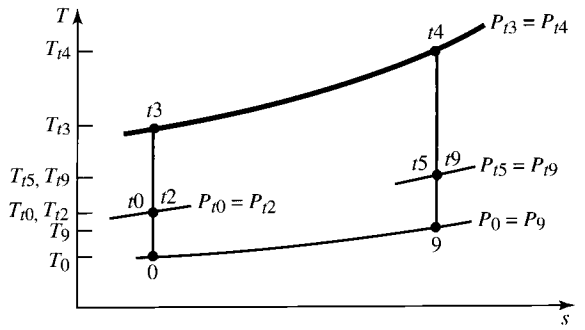

Fig. 5.21 The *T-s* diagram for core stream of ideal turbofan engine.

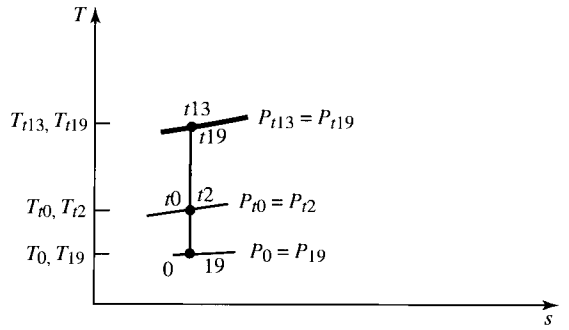

Fig. 5.22 The *T-s* diagram for fan stream of ideal turbofan engine.

The total gas flow is $\dot{m}_C + \dot{m}_F$, or $(1 + \alpha)\dot{m}_C$. We will also use $\dot{m}_0$ for the total gas flow. Thus

$$\dot{m}_0 = \dot{m}_C + \dot{m}_F = (1 + \alpha)\dot{m}_C \tag{5.47}$$

In the analysis of the ideal turbofan engine, we will assume that the mass flow rate of fuel is much less than the mass flow rate of gas through the engine core. We will also assume that both the engine core nozzle and the fan nozzle are designed so that $P_0 = P_9 = P_{19}$.

5.9.1 Cycle Analysis

Application of the steps of cycle analysis to the ideal turbofan engine of Figs. 5.20–5.22 is presented next in the order listed in Section 5.4.

Step 1: The thrust of the ideal turbofan engine is

$$F = \frac{\dot{m}_C}{g_c}(V_9 - V_0) + \frac{\dot{m}_F}{g_c}(V_{19} - V_0)$$

Thus

$$\frac{F}{\dot{m}_0} = \frac{a_0}{g_c}\frac{1}{1+\alpha}\left[\frac{V_9}{a_0} - M_0 + \alpha\left(\frac{V_{19}}{a_0} - M_0\right)\right] \tag{5.48}$$

Steps 2–4: First, the core stream of the turbofan encounters the same engine components as the ideal turbojet, and we can use its results. We have, from the analysis of the ideal turbojet,

$$\left(\frac{V_9}{a_0}\right)^2 = \frac{T_9}{T_0}M_9^2, \qquad \frac{T_9}{T_0} = \tau_b = \frac{\tau_\lambda}{\tau_r\tau_c}, \qquad \text{and} \qquad M_9^2 = \frac{2}{\gamma - 1}(\tau_r\tau_c\tau_t - 1)$$

Thus

$$\left(\frac{V_9}{a_0}\right)^2 = \frac{T_9}{T_0}M_9^2 = \frac{2}{\gamma - 1}\frac{\tau_\lambda}{\tau_r\tau_c}(\tau_r\tau_c\tau_t - 1) \tag{5.49}$$

Second, compared to the core stream, the fan stream of the turbofan contains a fan rather than a compressor and does not have either a combustor or a turbine. Thus the preceding equations for the core stream of the ideal turbofan can be adapted for the fan stream as follows:

$$\left(\frac{V_{19}}{a_0}\right)^2 = \frac{T_{19}}{T_0}M_{19}^2, \qquad T_{19} = T_0, \qquad \text{and} \qquad M_{19}^2 = \frac{2}{\gamma - 1}(\tau_r\tau_f - 1)$$

$$\left(\frac{V_{19}}{a_0}\right)^2 = M_{19}^2 = \frac{2}{\gamma - 1}(\tau_r\tau_f - 1) \tag{5.50}$$

Step 5: Application of the steady flow energy equation to the burner gives

$$\dot{m}_C c_p T_{t3} + \dot{m}_f h_{PR} = (\dot{m}_C + \dot{m}_f)c_p T_{t4}$$

We define the fuel/air ratio f in terms of the mass flow rate of air through the burner $\dot{m}_C$, and we obtain

$$f = \frac{\dot{m}_f}{\dot{m}_C} = \frac{c_p T_0}{h_{PR}}(\tau_\lambda - \tau_r\tau_c) \tag{5.51}$$

Step 6: The power out of the turbine is

$$\dot{W}_t = (\dot{m}_C + \dot{m}_f)c_p(T_{t4} - T_{t5}) \cong \dot{m}_C c_p T_{t4}(1 - \tau_t)$$

The power required to drive the compressor is

$$\dot{W}_c = \dot{m}_C c_p(T_{t3} - T_{t2}) = \dot{m}_C c_p T_{t2}(\tau_c - 1)$$

The power required to drive the fan is

$$\dot{W}_f = \dot{m}_F c_p(T_{t13} - T_{t2}) = \dot{m}_F c_p T_{t2}(\tau_f - 1)$$

Since $\dot{W}_t = \dot{W}_c + \dot{W}_f$ for the ideal turbofan, then

$$T_{t4}(1 - \tau_t) = T_{t2}(\tau_c - 1) + \alpha T_{t2}(\tau_f - 1)$$

$$\tau_t = 1 - \frac{T_{t2}}{T_{t4}}[\tau_c - 1 + \alpha(\tau_f - 1)]$$

$$\tau_t = 1 - \frac{\tau_r}{\tau_\lambda}[\tau_c - 1 + \alpha(\tau_f - 1)] \tag{5.52}$$

Step 7: Combining Eqs. (5.49) and (5.52), we get

$$\left(\frac{V_9}{a_0}\right)^2 = \frac{2}{\gamma - 1}\frac{\tau_\lambda}{\tau_r \tau_c}\left(\tau_r \tau_c \left\{1 - \frac{\tau_r}{\tau_\lambda}[\tau_c - 1 + \alpha(\tau_f - 1)]\right\} - 1\right)$$

which can be simplified to

$$\left(\frac{V_9}{a_0}\right)^2 = \frac{2}{\gamma - 1}\left\{\tau_\lambda - \tau_r[\tau_c - 1 + \alpha(\tau_f - 1)] - \frac{\tau_\lambda}{\tau_r \tau_c}\right\} \tag{5.53}$$

Thus the specific thrust of the ideal turbojet is given by Eqs. (5.48), (5.50), and (5.53).

Step 8:

$$S = \frac{\dot{m}_f}{F} = \frac{f}{F/\dot{m}_C} = \frac{f}{(\dot{m}_0/\dot{m}_C)(F/\dot{m}_0)}$$

$$S = \frac{f}{(1 + \alpha)(F/\dot{m}_0)} \tag{5.54}$$

Step 9: The thermal efficiency of an ideal turbofan engine is the same as that of an ideal turbojet engine. That is [Eq. (5.22)],

$$\eta_T = 1 - \frac{1}{\tau_r \tau_c}$$

This may seem surprising since the net power out of a turbojet is $\dot{m}_0(V_9^2 - V_0^2)/(2g_c)$, while for a turbofan it is $\dot{m}_C(V_9^2 - V_0^2)/(2g_c) + \dot{m}_F(V_{19}^2 - V_0^2)/(2g_c)$. The reason that the thermal efficiency is the same is that power extracted from the core stream of the turbofan engine is added to the bypass stream without loss in the ideal case. Thus the net power out remains the same.

One can easily show that the propulsive efficiency of the ideal turbofan engine is given by

$$\eta_P = 2\frac{V_9/V_0 - 1 + \alpha(V_{19}/V_0 - 1)}{V_9^2/V_0^2 - 1 + \alpha(V_{19}^2/V_0^2 - 1)} \tag{5.55}$$

A useful performance parameter for the turbofan engine is the ratio of the specific thrust per unit mass flow of the core stream to that of the fan stream. We give this *thrust ratio* the symbol FR and define

$$\text{FR} \equiv \frac{F_C/\dot{m}_C}{F_F/\dot{m}_F} \tag{5.56}$$

For the ideal turbofan engine, the thrust ratio FR can be expressed as

$$\text{FR} = \frac{V_9/a_0 - M_0}{V_{19}/a_0 - M_0} \tag{5.57}$$

We will discover in the analysis of optimum turbofan engines that we will want a certain thrust ratio for minimum thrust specific fuel consumption.

5.9.2 Summary of Equations—Ideal Turbofan

INPUTS:

$$M_0,\ T_0(\text{K},\ ^\circ\text{R}),\ \gamma,\ c_p\left(\frac{\text{kJ}}{\text{kg}\cdot\text{K}},\ \frac{\text{Btu}}{\text{lbm}\cdot{}^\circ\text{R}}\right),\quad h_{PR}\left(\frac{\text{kJ}}{\text{kg}},\ \frac{\text{Btu}}{\text{lbm}}\right)$$

$$T_{t4}(\text{K},\ ^\circ\text{R}),\ \pi_c,\ \pi_f,\ \alpha$$

OUTPUTS:

$$\frac{F}{\dot{m}_0}\left(\frac{\text{N}}{\text{kg/s}},\ \frac{\text{lbf}}{\text{lbm/s}}\right), f, S\left(\frac{\text{mg/s}}{\text{N}},\ \frac{\text{lbm/h}}{\text{lbf}}\right),\ \eta_T,\ \eta_P,\ \eta_O,\ \text{FR}$$

EQUATIONS:

$$R = \frac{\gamma - 1}{\gamma} c_p \tag{5.58a}$$

$$a_0 = \sqrt{\gamma R g_c T_0} \tag{5.58b}$$

$$\tau_r = 1 + \frac{\gamma - 1}{2} M_0^2 \tag{5.58c}$$

$$\tau_\lambda = \frac{T_{t4}}{T_0} \tag{5.58d}$$

$$\tau_c = (\pi_c)^{(\gamma-1)/\gamma} \tag{5.58e}$$

$$\tau_f = (\pi_f)^{(\gamma-1)/\gamma} \tag{5.58f}$$

$$\frac{V_9}{a_0} = \sqrt{\frac{2}{\gamma - 1}\left\{\tau_\lambda - \tau_r[\tau_c - 1 + \alpha(\tau_f - 1)] - \frac{\tau_\lambda}{\tau_r \tau_c}\right\}} \tag{5.58g}$$

$$\frac{V_{19}}{a_0} = \sqrt{\frac{2}{\gamma - 1}(\tau_r \tau_f - 1)} \tag{5.58h}$$

$$\frac{F}{\dot{m}_0} = \frac{a_0}{g_c}\frac{1}{1+\alpha}\left[\frac{V_9}{a_0} - M_0 + \alpha\left(\frac{V_{19}}{a_0} - M_0\right)\right] \tag{5.58i}$$

$$f = \frac{c_p T_0}{h_{PR}}(\tau_\lambda - \tau_r\tau_c) \tag{5.58j}$$

$$S = \frac{f}{(1+\alpha)(F/\dot{m}_0)} \tag{5.58k}$$

$$\eta_T = 1 - \frac{1}{\tau_r\tau_c} \tag{5.58l}$$

$$\eta_P = 2M_0\frac{V_9/a_0 - M_0 + \alpha(V_{19}/a_0 - M_0)}{V_9^2/a_0^2 - M_0^2 + \alpha(V_{19}^2/a_0^2 - M_0^2)} \tag{5.58m}$$

$$\eta_O = \eta_T\eta_P \tag{5.58n}$$

$$\text{FR} = \frac{V_9/a_0 - M_0}{V_{19}/a_0 - M_0} \tag{5.58o}$$

Example 5.4

The turbofan engine has three design variables: 1) compressor pressure ratio π_c, 2) fan pressure ratio π_f, and 3) bypass ratio α. Because this engine has two more design variables than the turbojet, this section contains many more plots of engine performance than were required for the turbojet. First, we will look at the variation of each of the three design variables for an engine that will operate at a flight Mach number of 0.9. Then we will look at the variation of design performance with flight Mach number. In all of the calculations for this section, the following values are held constant:

$$T_0 = 216.7\,\text{K}, \qquad \gamma = 1.4, \qquad c_p = 1.004\,\text{kJ/(kg}\cdot\text{K)}$$
$$h_{PR} = 42{,}800\,\text{kJ/kg}, \qquad T_{t4} = 1670\,\text{K}$$

a) Figures 5.23a–5.23e. Specific thrust and thrust specific fuel consumption are plotted vs the compressor pressure ratio for different values of the bypass ratio in Figs. 5.23a and 5.23b. The fan pressure ratio is held constant in these plots. Figure 5.23a shows that specific thrust remains essentially constant with respect to the compressor pressure ratio for values of π_c from 15 to 25, and that specific thrust decreases with increasing bypass ratio. Figure 5.23b shows that thrust-specific fuel consumption decreases with increasing compressor pressure ratio π_c and increasing bypass ratio α.

Figure 5.23c shows that the fuel/air ratio decreases with compressor pressure ratio, the thermal efficiency increases with compressor pressure ratio, and both are independent of the engine bypass ratio. From Fig. 5.23d, we can see that the propulsive efficiency increases with engine bypass ratio and varies very little with compressor pressure ratio. The overall efficiency, shown also in Fig. 5.23d, increases with both compressor pressure ratio and bypass ratio.

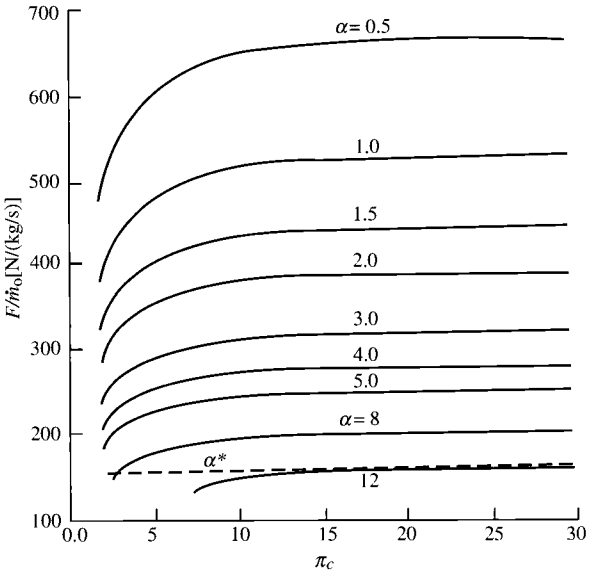

Fig. 5.23a Ideal turbofan performance vs π_c, for $\pi_f = 2$ and $M_0 = 0.9$: specific thrust.

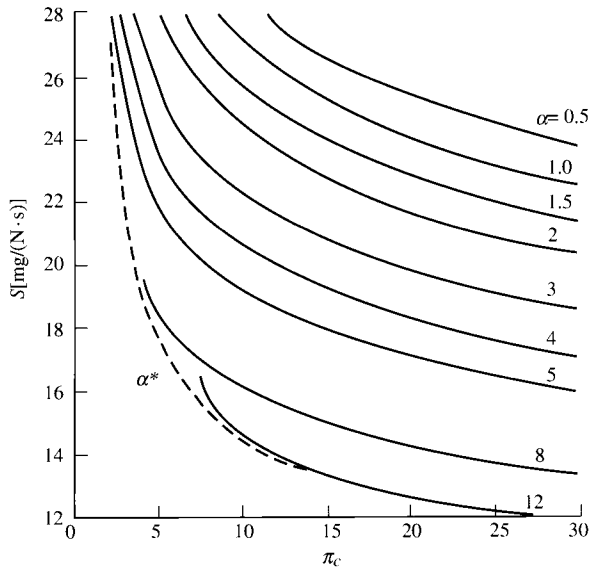

Fig. 5.23b Ideal turbofan performance vs π_c, for $\pi_f = 2$ and $M_0 = 0.9$: thrust-specific fuel consumption.

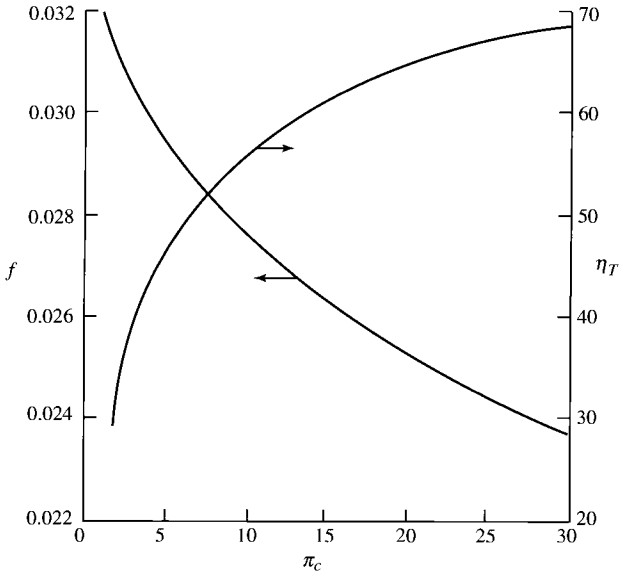

Fig. 5.23c Ideal turbofan performance vs π_c, for $\pi_f = 2$ and $M_0 = 0.9$: fuel/air ratio and thermal efficiency.

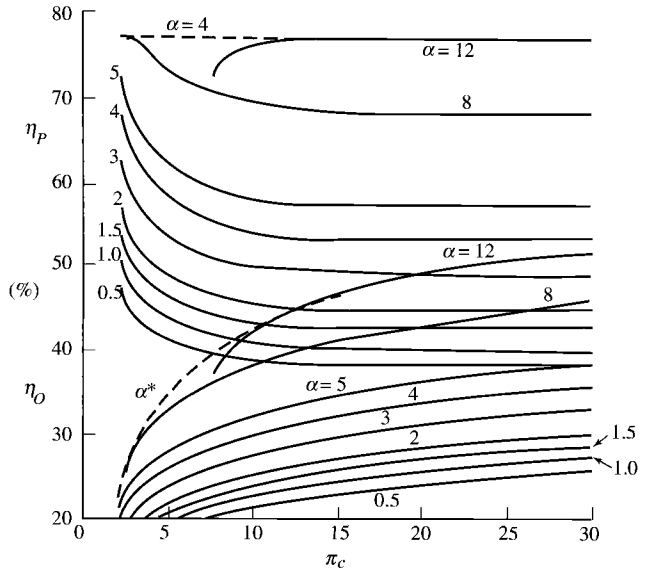

Fig. 5.23d Ideal turbofan performance vs π_c, for $\pi_f = 2$ and $M_0 = 0.9$: propulsive and overall efficiencies.

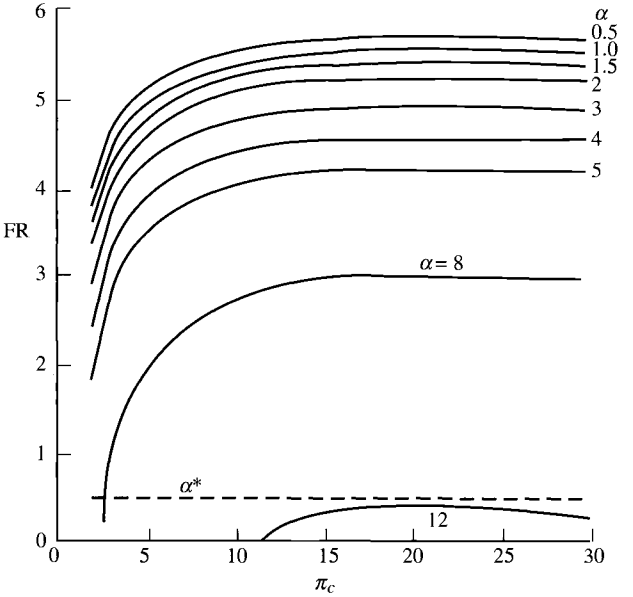

Fig. 5.23e Ideal turbofan performance vs π_c, for $\pi_f = 2$ and $M_0 = 0.9$: thrust ratio.

The thrust ratio is plotted vs compressor pressure ratio and bypass ratio in Fig. 5.23e. As can be seen, the thrust ratio decreases with increasing bypass ratio and varies very little with compressor pressure ratio.

b) Figures 5.24a–5.24e. Specific thrust and thrust-specific fuel consumption are plotted vs the compressor pressure ratio π_c for different values of the fan pressure ratio π_f. The bypass ratio α is held constant in these plots. Figure 5.24a shows that the specific thrust remains essentially constant with respect to the compressor pressure ratio for values of π_c from 15 to 25, and that the specific thrust has a maximum with respect to the fan pressure ratio π_f Figure 5.24b shows that thrust-specific fuel consumption decreases with increasing compressor pressure ratio π_c and that S has a minimum with respect to fan pressure ratio π_f. We will look at this optimum fan pressure ratio in more detail in another section of this chapter.

Propulsive and overall efficiencies are plotted vs compressor pressure ratio and fan pressure ratio in Figs. 5.24c and 5.24d. Figure 5.24c shows that propulsive efficiency increases with fan pressure ratio until a value of $\pi_f = 3.5$ and then decreases. There is a fan pressure ratio giving maximum propulsive efficiency. Propulsive efficiency is essentially constant for values of the compressor pressure ratio above 15. Also from Fig. 5.24d, we can see that overall efficiency increases with compressor pressure ratio and increases with fan pressure ratio until a value of $\pi_f = 3.5$ and then decreases. There is a fan pressure ratio giving maximum overall efficiency.

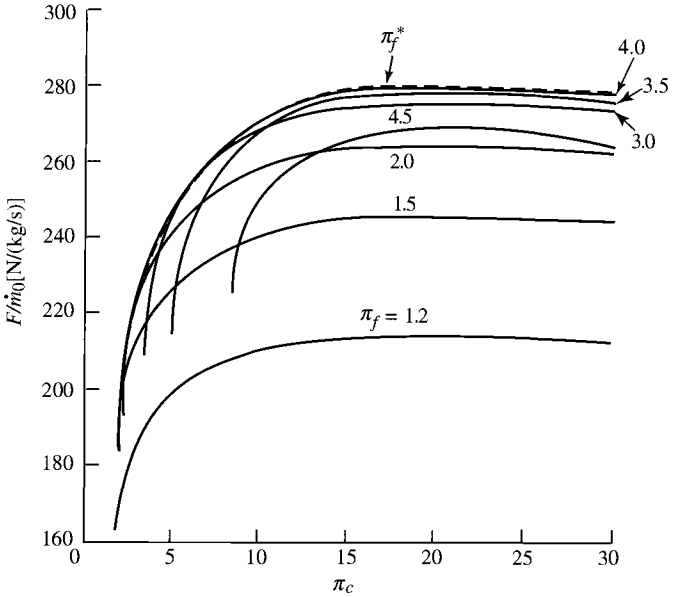

Fig. 5.24a Ideal turbofan performance vs π_c, for $\alpha = 5$ for $M_0 = 0.9$: specific thrust.

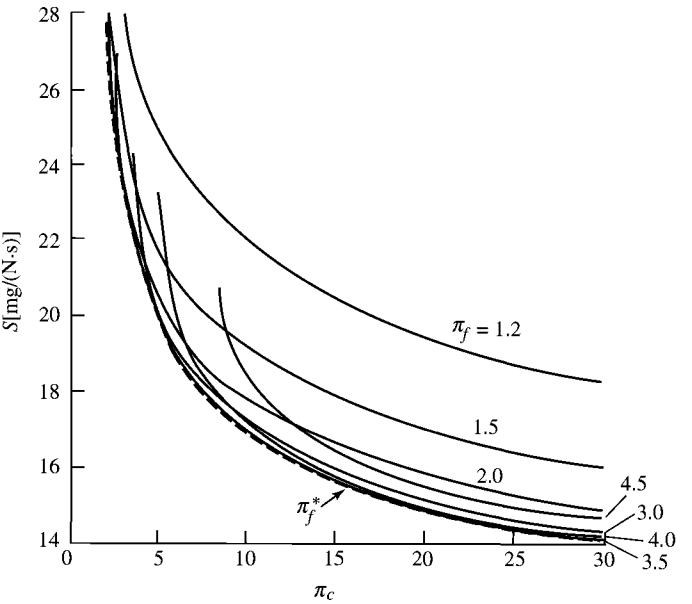

Fig. 5.24b Ideal turbofan performance vs π_c, for $\alpha = 5$ and $M_0 = 0.9$: thrust-specific fuel consumption.

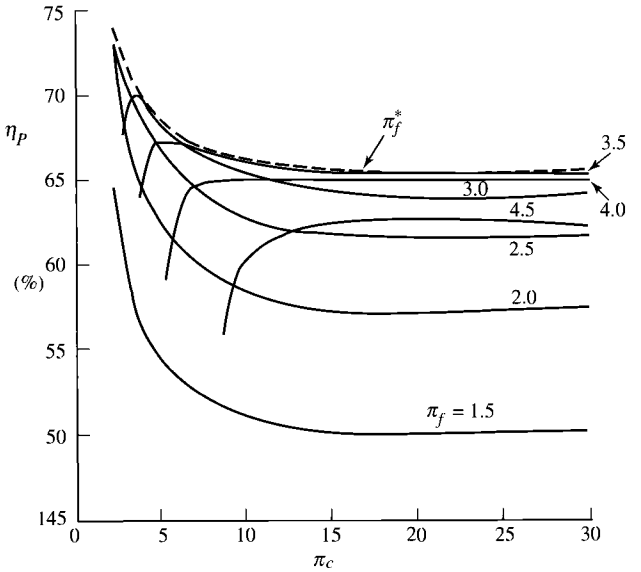

Fig. 5.24c Ideal turbofan performance vs π_c, for $\alpha = 5$ and $M_0 = 0.9$: propulsive efficiency.

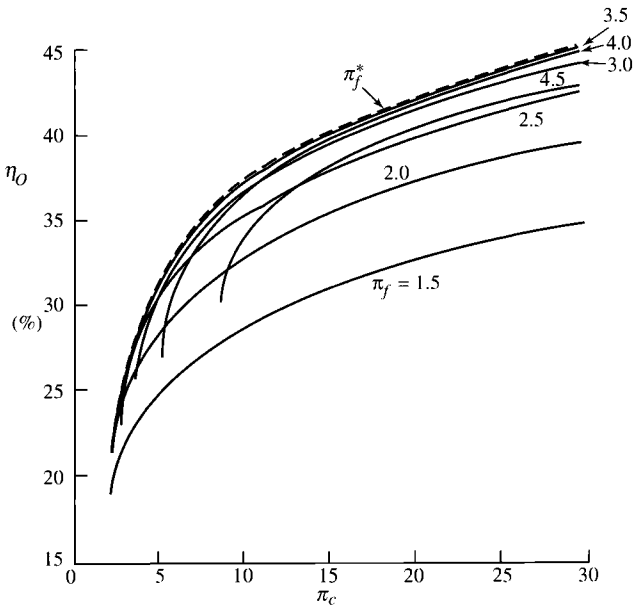

Fig. 5.24d Ideal turbofan performance vs π_c, for $\alpha = 5$ and $M_0 = 0.9$: overall efficiency.

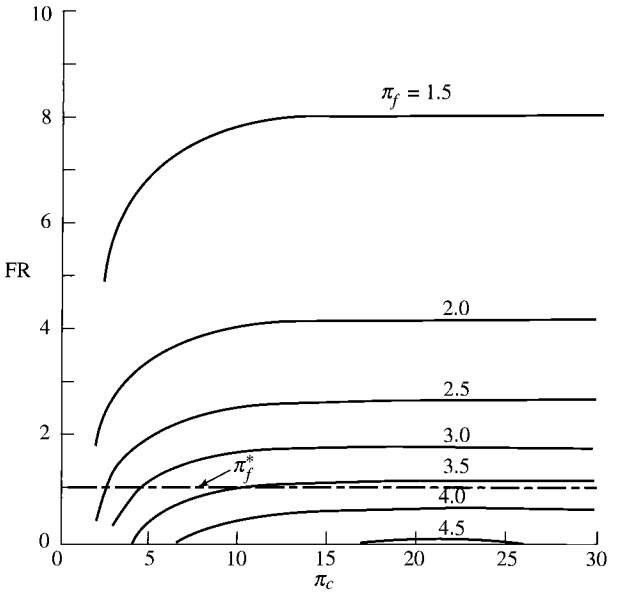

Fig. 5.24e Ideal turbofan performance vs π_c, for $\alpha = 5$ and $M_0 = 0.9$: thrust ratio.

The thrust ratio FR is plotted vs compressor pressure ratio and fan pressure ratio in Fig. 5.24e. As can be seen, the thrust ratio decreases with increasing fan pressure ratio and varies very little with compressor pressure ratio.

c) Figures 5.25a–5.25d. Specific thrust, thrust-specific fuel consumption, propulsive efficiency, and thrust ratio are plotted vs fan pressure ratio for different values of the bypass ratio in Figs. 5.25a, 5.25b, 5.25c, and 5.25d, respectively. The compressor pressure ratio is held constant in these plots. Figures 5.25a and 5.25b show there is an optimum fan pressure ratio for each bypass ratio that will maximize specific thrust while minimizing fuel consumption. Also Fig. 5.25c shows the optimum fan pressure ratio corresponds to maximum propulsive efficiency. We will look at this optimum fan pressure ratio in more detail in another section of this chapter. Figure 5.25d shows that thrust ratio decreases with increasing fan pressure ratio.

d) Figures 5.26a–5.26d. Specific thrust and thrust-specific fuel consumption are plotted vs the bypass ratio for different values of the fan pressure ratio in Figs. 5.26a and 5.26b. The compressor pressure ratio is held constant in these plots. Figure 5.26a shows the decreasing trend in specific thrust with increasing bypass ratio that is characteristic of turbofan engines. Figure 5.26b shows that there is an optimum bypass ratio for each fan pressure ratio that will minimize

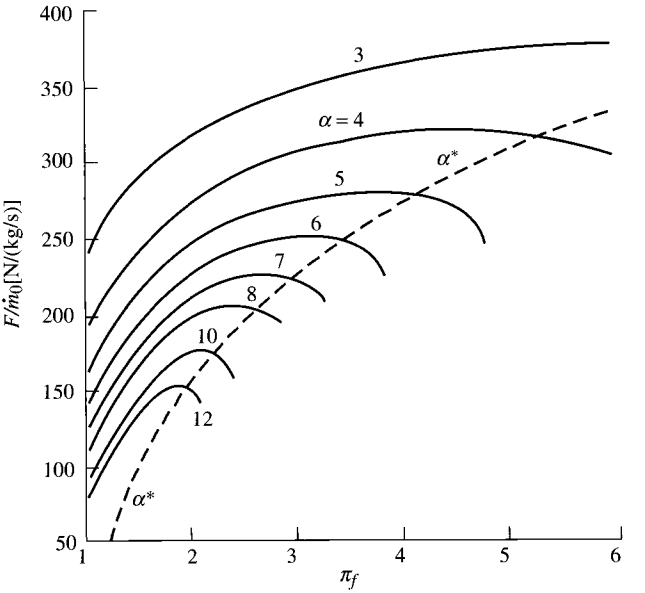

Fig. 5.25a Ideal turbofan performance vs π_f, for $\pi_c = 24$ and $M_0 = 0.9$: specific thrust.

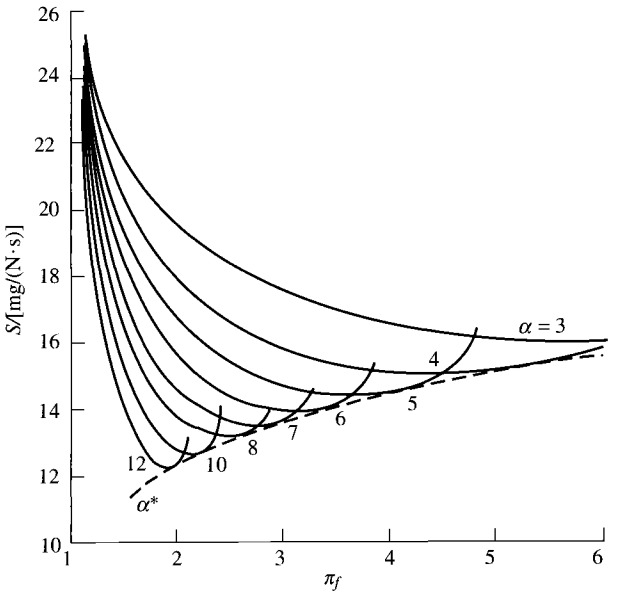

Fig. 5.25b Ideal turbofan performance vs π_f, for $\pi_c = 24$ and $M_0 = 0.9$: thrust-specific fuel consumption.

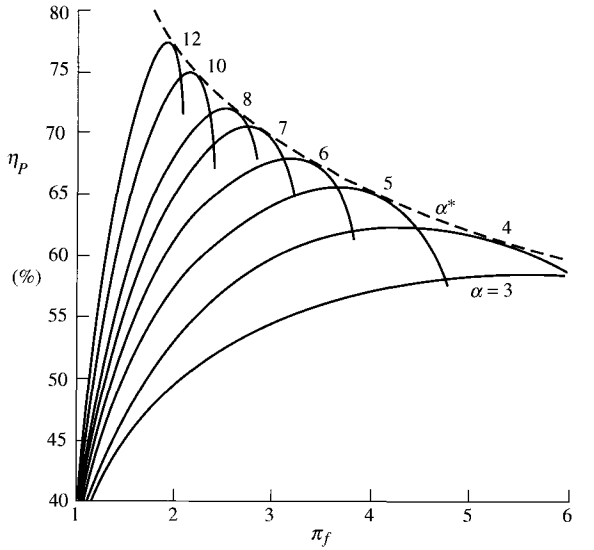

Fig. 5.25c Ideal turbofan performance vs π_f, for $\pi_c = 24$ and $M_0 = 0.9$: propulsive efficiency.

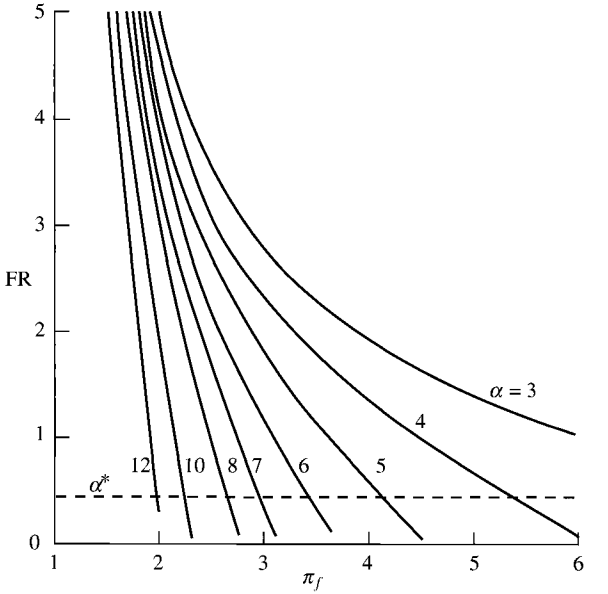

Fig. 5.25d Ideal turbofan performance vs π_f, for $\pi_c = 24$ and $M_0 = 0.9$: thrust ratio.

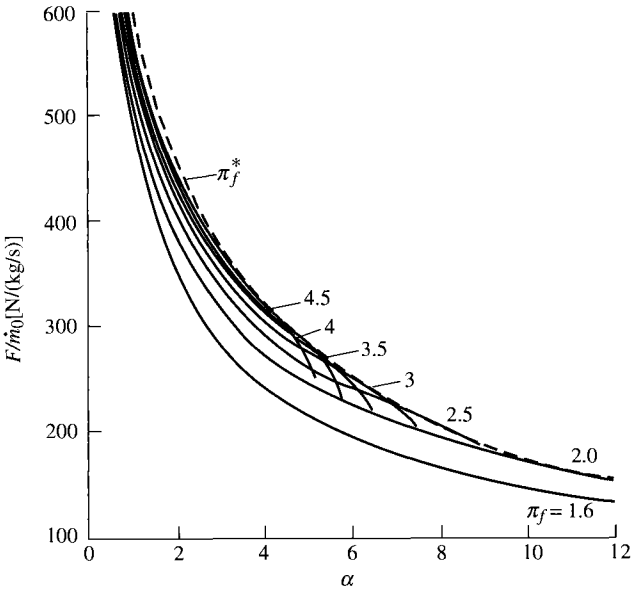

Fig. 5.26a Ideal turbofan performance vs α, for $\pi_c = 24$ and $M_0 = 0.9$: specific thrust.

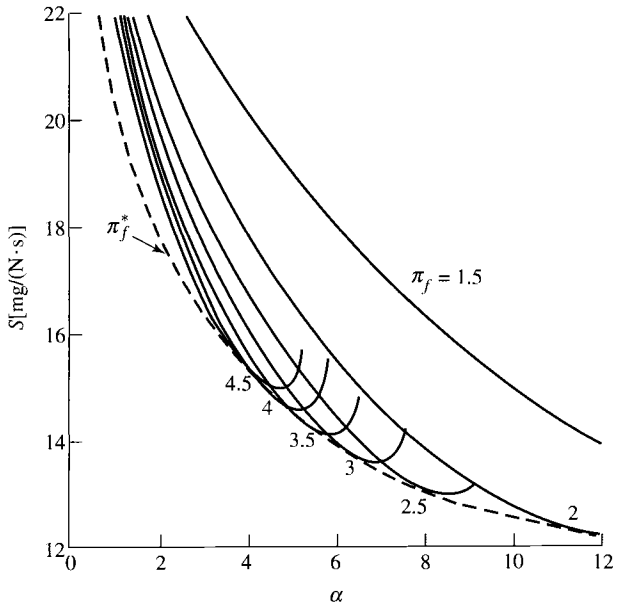

Fig. 5.26b Ideal turbofan performance vs α, for $\pi_c = 24$ and $M_0 = 0.9$: thrust-specific fuel consumption.

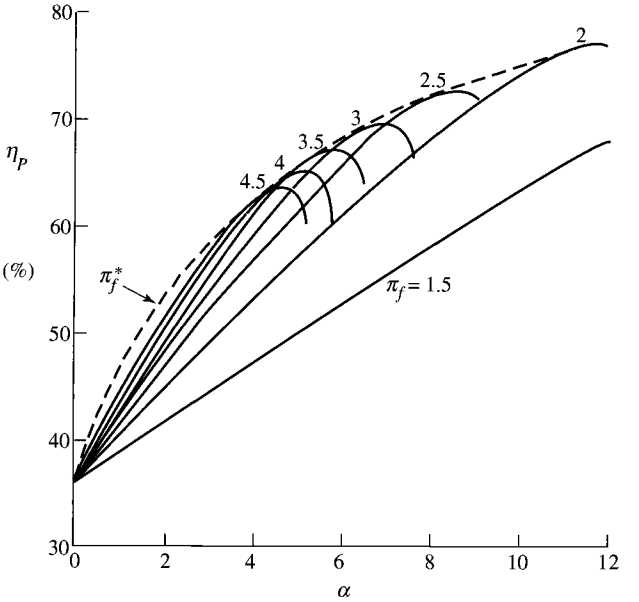

Fig. 5.26c Ideal turbofan performance vs α, for $\pi_c = 24$ and $M_0 = 0.9$: propulsive efficiency.

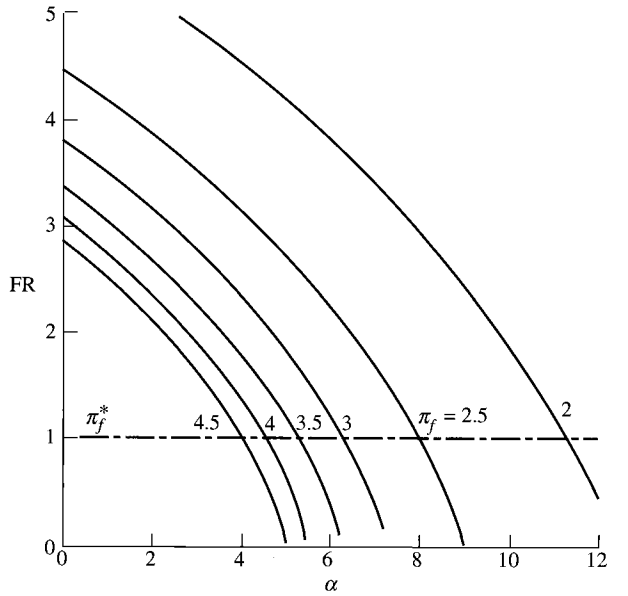

Fig. 5.26d Ideal turbofan performance vs α, for $\pi_c = 24$ and $M_0 = 0.9$: thrust ratio.

fuel consumption. We will look at this optimum bypass ratio in greater detail in another section of this chapter.

Propulsive efficiency and thrust ratio are plotted vs the bypass ratio in Figs. 5.26c and 5.26d, respectively. Figure 5.26c shows there is an optimum bypass ratio for each fan pressure ratio that will maximize propulsive efficiency. Figure 5.26d shows that thrust ratio decreases with both increasing bypass ratio and increasing fan pressure ratio.

e) Figures 5.27a–5.28e. Specific thrust and the specific fuel consumption are plotted vs the flight Mach number for different values of the bypass ratio in Figs. 5.27a, 5.27b, 5.28a, and 5.28b. The compressor pressure ratio has a value of 24 for all four plots, and the fan pressure ratio is held constant at a value of 2 for Figs. 5.27a and 5.27b and at a value of 3 for Figs. 5.28a and 5.28b. Figures 5.27a and 5.28a show that specific thrust decreases with increasing flight Mach number and with increasing bypass ratio. These four figures also show that the high-bypass-ratio engines are limited to lower flight Mach numbers and that a low-bypass-ratio engine is required for the higher flight Mach numbers.

Propulsive, thermal, and overall efficiencies are plotted vs the flight Mach number for different values of the bypass ratio in Figs. 5.27c, 5.27d, 5.28c, and 5.28d. We can see that propulsive efficiency increases with flight Mach number and that there is an optimum bypass ratio for each flight Mach number that gives maximum propulsive and overall efficiencies.

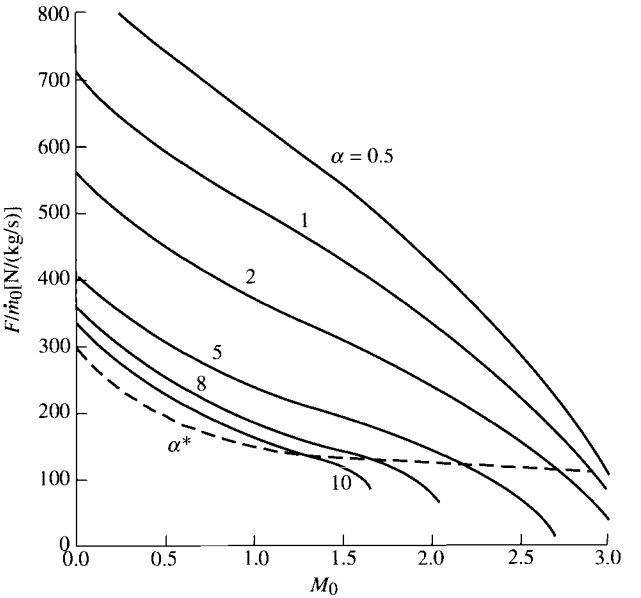

Fig. 5.27a Ideal turbofan performance vs M_0, for $\pi_c = 24$ and $\pi_f = 2$: specific thrust.

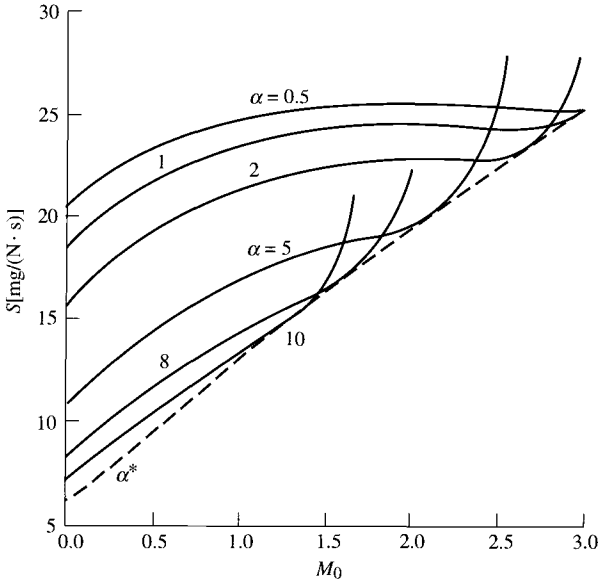

Fig. 5.27b Ideal turbofan performance vs M_0, for $\pi_c = 24$ and $\pi_f = 2$: thrust-specific fuel consumption.

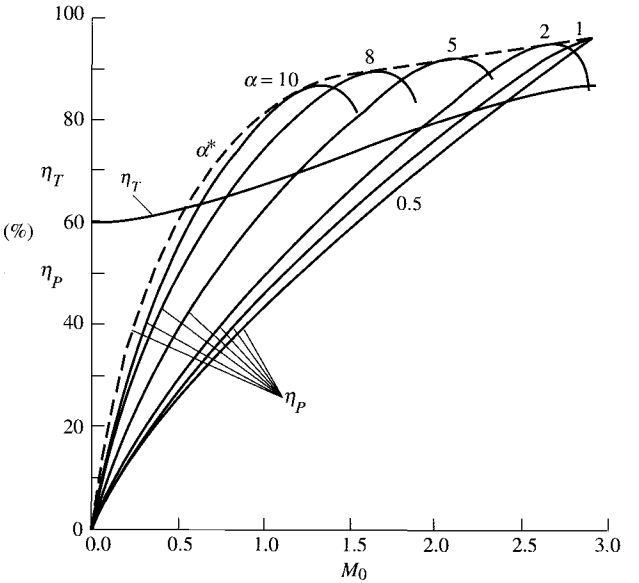

Fig. 5.27c Ideal turbofan performance vs M_0, for $\pi_c = 24$ and $\pi_f = 2$: thermal and propulsive efficiencies.

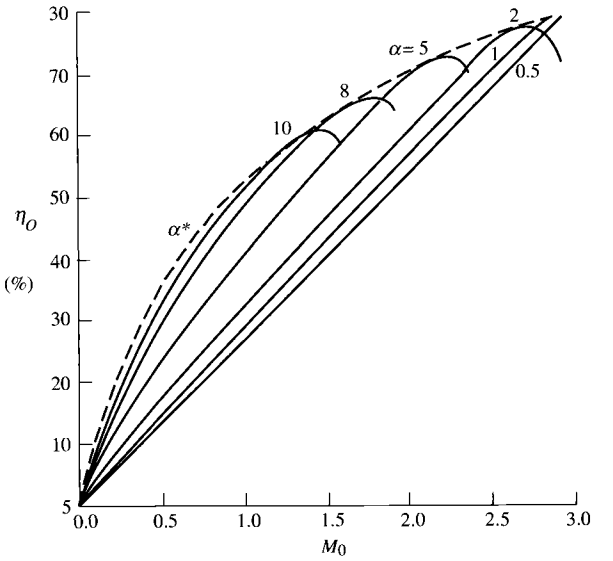

Fig. 5.27d Ideal turbofan performance vs M_0, for $\pi_c = 24$ and $\pi_f = 2$: overall efficiency.

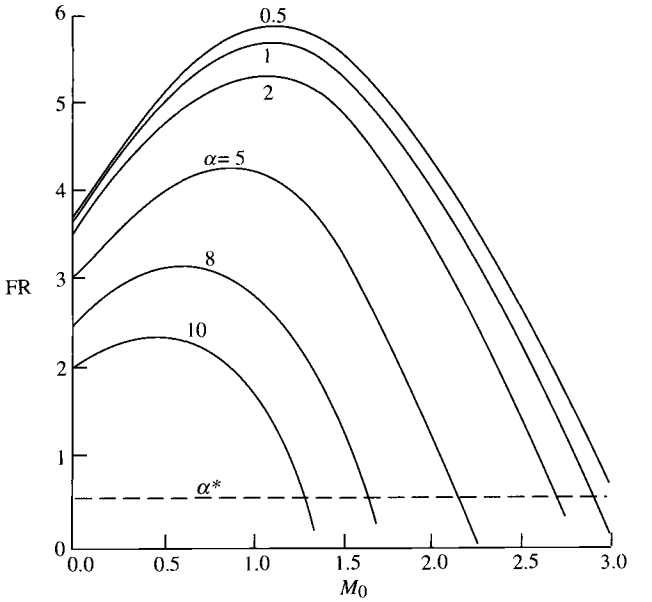

Fig. 5.27e Ideal turbofan performance vs M_0, for $\pi_c = 24$ and $\pi_f = 2$: thrust ratio.

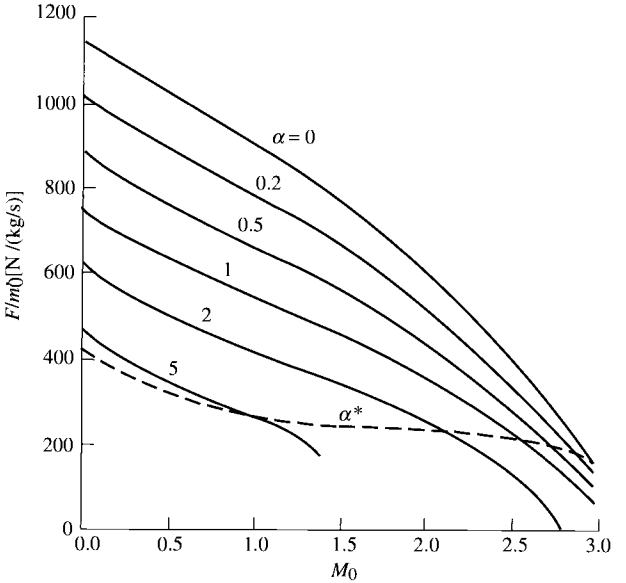

Fig. 5.28a Ideal turbofan performance vs M_0, for $\pi_c = 24$ and $\pi_f = 3$: specific thrust.

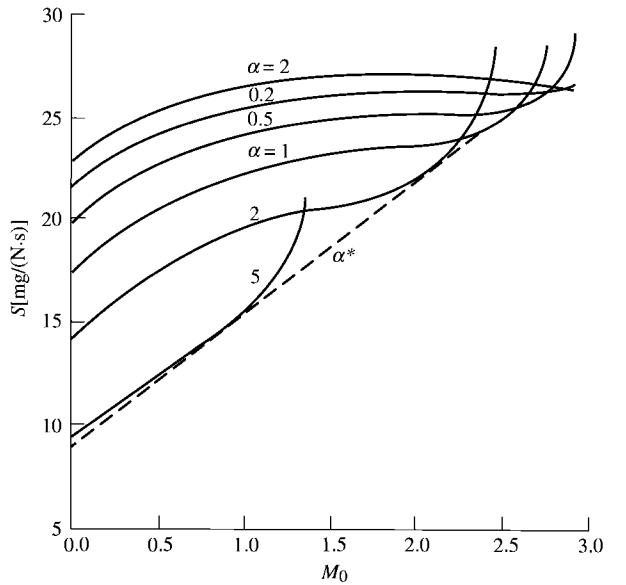

Fig. 5.28b Ideal turbofan performance vs M_0, for $\pi_c = 24$ and $\pi_f = 3$: thrust-specific fuel consumption.

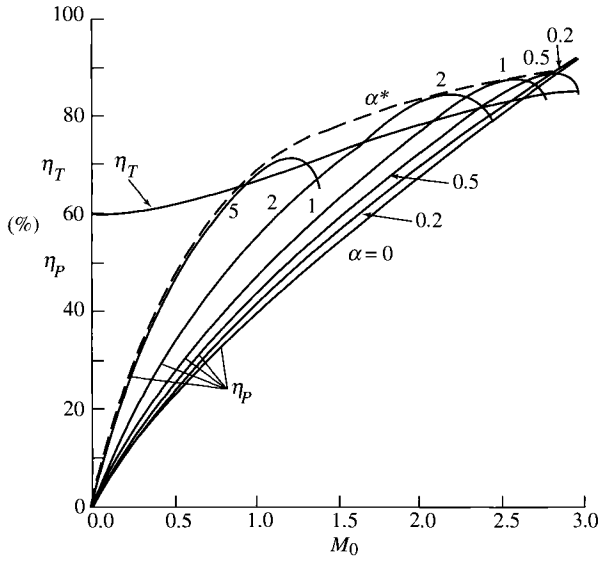

Fig. 5.28c Ideal turbofan performance vs M_0, for $\pi_c = 24$ and $\pi_f = 3$: thermal and propulsive efficiencies.

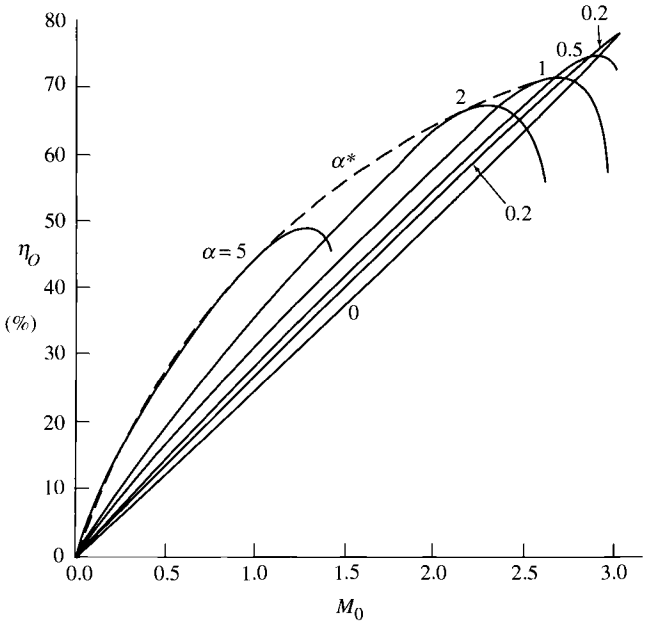

Fig. 5.28d Ideal turbofan performance vs M_0, for $\pi_c = 24$ and $\pi_f = 3$: overall efficiency.

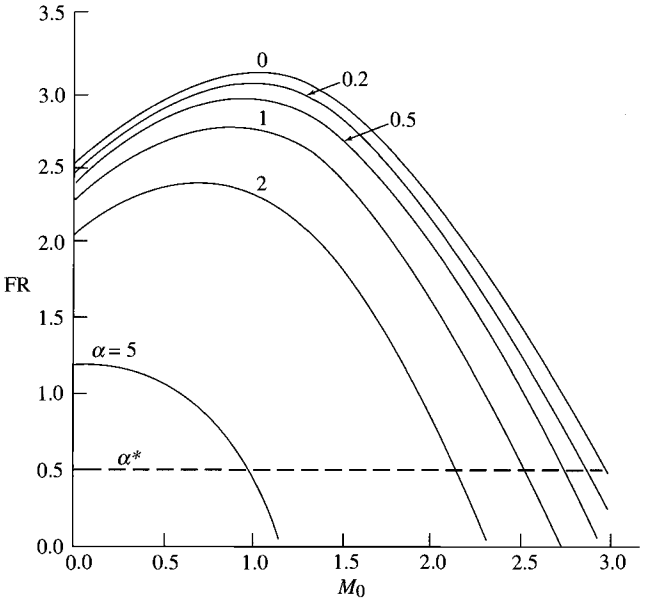

Fig. 5.28e Ideal turbofan performance vs M_0, for $\pi_c = 24$ and $\pi_f = 3$: thrust ratio.

The thrust ratio is plotted vs flight Mach number for different values of the bypass ratio in Figs. 5.27e and 5.28e. These plots show that thrust ratio decreases with increasing bypass ratio and generally decreases with increasing flight Mach number.

5.10 Ideal Turbofan with Optimum Bypass Ratio

For a given set of flight conditions T_0 and M_0 and design limit τ_λ, there are three design variables: π_c, π_f, and α. In Figs. 5.23a–5.23e and 5.24a–5.24e, we can see that by increasing the compressor ratio π_c we can increase the thrust per unit mass flow and decrease the thrust specific fuel consumption. For the data used in these figures, increases in the compressor pressure ratio above a value of 20 do not increase the thrust per unit mass flow but do decrease the thrust specific fuel consumption. In Figs. 5.25a–5.25d, we can see that an optimum fan pressure ratio exists for all other parameters fixed. This optimum fan pressure ratio gives both the maximum thrust per unit mass flow and minimum thrust specific fuel consumption. In Figs. 5.26a–5.26d, we see that an optimum bypass ratio exists for all other parameters fixed. This optimum bypass ratio gives the minimum thrust specific fuel consumption. We will look at this optimum bypass ratio first. The optimum fan pressure ratio will be analyzed in the next section of this chapter.

5.10.1 Optimum Bypass Ratio α^*

When Eq. (5.58j) for the fuel/air ratio and Eq. (5.58i) for specific thrust are inserted into the equation for specific fuel consumption [Eq. (5.58k)], an

expression in terms of the bypass ratio α and other prescribed variables results. For a given set of such prescribed variables (τ_r, π_c, π_f, τ_λ, V_0), we may locate the minimum S by taking the partial derivative of S with respect to the bypass ratio α. Because the fuel/air ratio f is not a function of the bypass ratio, we have

$$S = \frac{f}{(1+\alpha)(F/\dot{m}_0)}$$

$$\frac{\partial S}{\partial \alpha} = \frac{\partial}{\partial \alpha}\left[\frac{f}{(1+\alpha)(F/\dot{m}_0)}\right] = 0$$

$$\frac{\partial S}{\partial \alpha} = \frac{-f}{[(1+\alpha)(F/\dot{m}_0)]^2}\frac{\partial}{\partial \alpha}\left[(1+\alpha)\left(\frac{F}{\dot{m}_0}\right)\right] = 0$$

Thus $\partial S/\partial \alpha = 0$ is satisfied by

$$\frac{\partial}{\partial \alpha}\left[\frac{g_c}{V_0}(1+\alpha)\left(\frac{F}{\dot{m}_0}\right)\right] = 0$$

where, from Eq. (5.48),

$$\frac{g_c}{V_0}(1+\alpha)\left(\frac{F}{\dot{m}_0}\right) = \frac{V_9}{V_0} - 1 + \alpha\left(\frac{V_{19}}{V_0} - 1\right)$$

Then the optimum bypass ratio is given by

$$\frac{\partial}{\partial \alpha}\left[\frac{V_9}{V_0} - 1 + \alpha\left(\frac{V_{19}}{V_0} - 1\right)\right] = \frac{\partial}{\partial \alpha}\left(\frac{V_9}{V_0}\right) + \frac{V_{19}}{V_0} - 1 = 0. \tag{i}$$

However,

$$\frac{1}{2V_9/V_0}\frac{\partial}{\partial \alpha}\left[\left(\frac{V_9}{V_0}\right)^2\right] = \frac{\partial}{\partial \alpha}\left(\frac{V_9}{V_0}\right)$$

Thus Eq. (i) becomes

$$\frac{1}{2V_9/V_0}\frac{\partial}{\partial \alpha}\left[\left(\frac{V_9}{V_0}\right)^2\right] + \frac{V_{19}}{V_0} - 1 = 0 \tag{ii}$$

Since

$$\left(\frac{V_9}{V_0}\right)^2 = \frac{1}{M_0^2}\left(\frac{V_9}{a_0}\right)^2 = \frac{1}{[(\gamma-1)/2](\tau_r-1)}\left(\frac{V_9}{a_0}\right)^2$$
$$= \frac{\tau_\lambda - \tau_r[\tau_c - 1 + \alpha(\tau_f - 1)] - \tau_\lambda/(\tau_r\tau_c)}{\tau_r - 1}$$

then, using Eq. (5.53),

$$\frac{\partial}{\partial\alpha}\left[\left(\frac{V_9}{V_0}\right)^2\right] = \frac{\partial}{\partial\alpha}\left\{\frac{\tau_\lambda - \tau_r[\tau_c - 1 + \alpha(\tau_f - 1)] - \tau_\lambda/(\tau_r\tau_c)}{\tau_r - 1}\right\}$$

giving

$$\frac{\partial}{\partial\alpha}\left[\left(\frac{V_9}{V_0}\right)^2\right] = -\frac{\tau_r(\tau_f - 1)}{\tau_r - 1} \tag{iii}$$

Since, from Eq. (5.50),

$$\left(\frac{V_{19}}{V_0}\right)^2 = \frac{1}{M_0^2}\left(\frac{V_{19}}{a_0}\right)^2 = \frac{1}{[(\gamma-1)/2](\tau_r-1)}\left(\frac{V_{19}}{a_0}\right)^2 = \frac{\tau_r\tau_f - 1}{\tau_r - 1} \tag{iv}$$

then Eqs. (iii) and (iv), substituted into Eq. (ii), give

$$\frac{1}{2V_9/V_0}\left[-\frac{\tau_r(\tau_f - 1)}{\tau_r - 1}\right] + \sqrt{\frac{\tau_r\tau_f - 1}{\tau_r - 1}} - 1 = 0$$

Substitution of the preceding equation for V_9/V_0, and denoting the optimum bypass ratio as α^*, gives

$$\frac{1}{2}\frac{-\tau_r(\tau_f - 1)}{\sqrt{\{\tau_\lambda - \tau_r[\tau_c - 1 + \alpha^*(\tau_f - 1)] - \tau_\lambda/(\tau_r\tau_c)\}/(\tau_r - 1)}} + \sqrt{\frac{\tau_r\tau_f - 1}{\tau_r - 1}} - 1 = 0$$

or

$$\frac{1}{2}\frac{\tau_r(\tau_f - 1)}{\sqrt{\{\tau_\lambda - \tau_r[\tau_c - 1 + \alpha^*(\tau_f - 1)] - \tau_\lambda/(\tau_r\tau_c)\}/(\tau_r - 1)}} = \sqrt{\frac{\tau_r\tau_f - 1}{\tau_r - 1}} - 1$$

Squaring both sides, we have

$$\frac{1}{4}\frac{[\tau_r(\tau_f - 1)]^2}{\{\tau_\lambda - \tau_r[\tau_c - 1 + \alpha^*(\tau_f - 1)] - \tau_\lambda/(\tau_r\tau_c)\}/(\tau_r - 1)} = \left(\sqrt{\frac{\tau_r\tau_f - 1}{\tau_r - 1}} - 1\right)^2$$

or

$$\frac{1}{4}\frac{[\tau_r(\tau_f-1)]^2}{[\sqrt{(\tau_r\tau_f-1)/(\tau_r-1)}-1]^2}=\frac{\tau_\lambda-\tau_r[\tau_c-1+\alpha^*(\tau_f-1)]-\tau_\lambda/(\tau_r\tau_c)}{\tau_r-1} \quad \text{(v)}$$

An expression for the bypass ratio giving the minimum fuel consumption is obtained by solving Eq. (v) for α^*. Thus

$$\alpha^*=\frac{\tau_r-1}{\tau_r(\tau_f-1)}\left[\frac{\tau_\lambda-\tau_r(\tau_c-1)-\tau_\lambda/(\tau_r\tau_c)}{\tau_r-1}-\frac{1}{4}\left(\sqrt{\frac{\tau_r\tau_f-1}{\tau_r-1}}+1\right)^2\right]$$

or

$$\alpha^*=\frac{1}{\tau_r(\tau_f-1)}\left[\tau_\lambda-\tau_r(\tau_c-1)-\frac{\tau_\lambda}{\tau_r\tau_c}-\frac{1}{4}(\sqrt{\tau_r\tau_f-1}+\sqrt{\tau_r-1})^2\right] \quad (5.59)$$

Now note that we may write

$$\frac{\tau_r(\tau_f-1)}{\tau_r-1}=\frac{\tau_r\tau_f-\tau_r+1-1}{\tau_r-1}=\frac{\tau_r\tau_f-1}{\tau_r-1}-1$$

So then Eq. (v) becomes

$$\frac{1}{4}\left[\frac{\left(\sqrt{\frac{\tau_r\tau_f-1}{\tau_r-1}}\right)^2-1}{\sqrt{\frac{\tau_r\tau_f-1}{\tau_r-1}}-1}\right]^2=\frac{\tau_\lambda-\tau_r[\tau_c-1+\alpha^*(\tau_f-1]-\frac{\tau_\lambda}{\tau_r\tau_c}}{\tau_r-1}$$

Taking the square root of both sides of this equation gives

$$\frac{1}{2}\left(\sqrt{\frac{\tau_r\tau_f-1}{\tau_r-1}}+1\right)=\sqrt{\frac{\tau_\lambda-\tau_r[\tau_c-1+\alpha^*(\tau_f-1)]-\tau_\lambda/(\tau_r\tau_c)}{\tau_r-1}}$$

or

$$\frac{1}{2}\left(\sqrt{\frac{\tau_r\tau_f-1}{\tau_r-1}}-1\right)=\sqrt{\frac{\tau_\lambda-\tau_r[\tau_c-1+\alpha^*(\tau_f-1)]-\tau_\lambda/(\tau_r\tau_c)}{\tau_r-1}}-1 \quad \text{(vi)}$$

Noting from Eqs. (5.50) and (5.53) that the term within the square root on the left side of the equals sign is the velocity ratio V_{19}/V_0, and that the term within the

square root on the right side is the velocity ratio V_9/V_0, we see that Eq. (vi) becomes

$$\frac{1}{2}\left(\frac{V_{19}}{V_0} - 1\right) = \frac{V_9}{V_0} - 1 \qquad \text{or} \qquad V_9 - V_0 = \frac{1}{2}(V_{19} - V_0)$$

Thus

$$\text{FR} = \frac{V_9 - V_0}{V_{19} - V_0} = \frac{1}{2} \tag{5.60}$$

We thus note from Eq. (5.60) that when the bypass ratio is chosen to give the minimum specific fuel consumption, the thrust per unit mass flow of the engine core is one-half that of the fan. Thus the thrust ratio of an optimum-bypass-ratio ideal turbofan is 0.5. Using this fact, we may write the equation for the specific thrust simply as

$$\left(\frac{F}{\dot{m}_0}\right)_{\alpha^*} = \frac{a_0}{g_c}\frac{1 + 2\alpha^*}{2(1 + \alpha^*)}\left[\sqrt{\frac{2}{\gamma - 1}(\tau_r\tau_f - 1)} - M_0\right] \tag{5.61}$$

where α^* is obtained from Eq. (5.59).

One can easily show that the propulsive efficiency at the optimum bypass ratio is given by

$$(\eta_P)_{\min S} = \frac{4(1 + 2\alpha^*)V_0}{(3 + 4\alpha^*)V_0 + (1 + 4\alpha^*)V_{19}} \tag{5.62}$$

5.10.2 Summary of Equations—Optimum-Bypass-Ratio Ideal Turbofan

INPUTS:

$$M_0,\ T_0(\text{K, °R}),\ \gamma,\ c_p\left(\frac{\text{kJ}}{\text{kg} \cdot \text{K}}, \frac{\text{Btu}}{\text{lbm} \cdot \text{°R}}\right),\ h_{PR}\left(\frac{\text{kJ}}{\text{kg}}, \frac{\text{Btu}}{\text{lbm}}\right),$$

$$T_{t4}(\text{K, °R}),\ \pi_c,\ \pi_f$$

OUTPUTS:

$$\frac{F}{\dot{m}_0}\left(\frac{N}{\text{kg/s}}, \frac{\text{lbf}}{\text{lbm/s}}\right),\ f,\ S\left(\frac{\text{mg/s}}{\text{N}}, \frac{\text{lbm/h}}{\text{lbf}}\right),\ \eta_T,\ \eta_P,\ \eta_O,\ \alpha^*$$

EQUATIONS:

Equations (5.58a–5.58h) plus

$$\alpha^* = \frac{1}{\tau_r(\tau_f - 1)}\left[\tau_\lambda - \tau_r(\tau_c - 1) - \frac{\tau_\lambda}{\tau_r \tau_c} - \frac{1}{4}(\sqrt{\tau_r \tau_f - 1} + \sqrt{\tau_r - 1})^2\right] \tag{5.63a}$$

$$\frac{F}{\dot{m}_0} = \frac{a_0}{g_c}\frac{1 + 2\alpha^*}{2(1 + \alpha^*)}\left[\sqrt{\frac{2}{\gamma - 1}(\tau_r \tau_f - 1)} - M_0\right] \tag{5.63b}$$

$$\eta_P = \frac{4(1 + 2\alpha^*)M_0}{(3 + 4\alpha^*)M_0 + (1 + 4\alpha^*)(V_{19}/a_0)} \tag{5.63c}$$

and Eqs. (5.58j), (5.58k), (5.58l), (5.58n), and (5.60).

Example 5.5

The engine we looked at in Section 5.9 is used again in this section for an example. The following values are held constant for all plots:

$$T_0 = 216.7\,\text{K}, \qquad \gamma = 1.4, \qquad c_p = 1.004\,\text{kJ/(kg} \cdot \text{K)}$$
$$h_{PR} = 42{,}800\,\text{kJ/kg}, \qquad T_{t4} = 1670\,\text{K}$$

The optimum bypass ratio is plotted in Fig. 5.29a vs the compressor pressure ratio for a flight Mach number of 0.9 and fan pressure ratio of 2. From this plot,

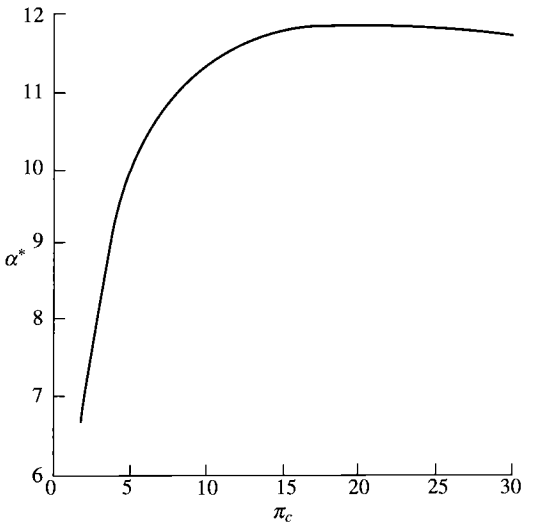

Fig. 5.29a α^* vs π_c, for $\pi_f = 2$ and $M_0 = 0.9$.

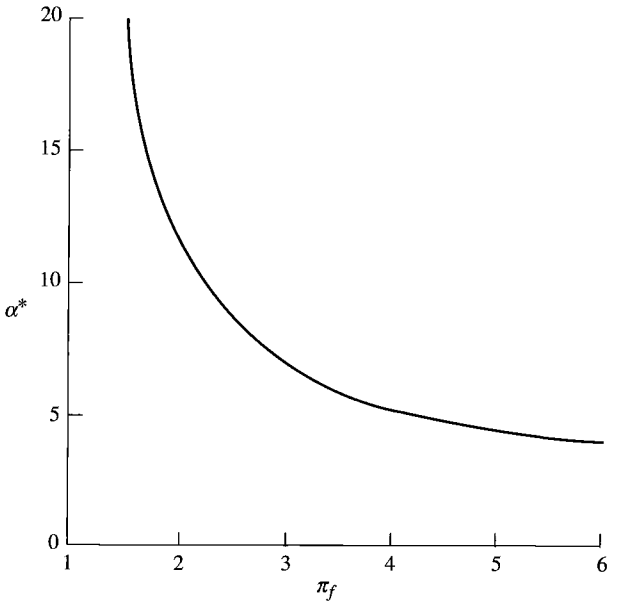

Fig. 5.29b α^* vs π_f, for $\pi_c = 24$ and $M_0 = 0.9$.

we can see that the optimum bypass ratio increases with the compressor pressure ratio. The optimum bypass ratio is plotted in Fig. 5.29b vs the fan pressure ratio, and this figure shows that optimum bypass ratio decreases with fan pressure ratio.

The optimum bypass ratio vs the flight Mach number is plotted in Fig. 5.29c for fan pressure ratios of 2 and 3. From these plots, we can see that the optimum bypass ratio decreases with the flight Mach number. Note that the optimum engine is a turbojet at a Mach number of about 3.0 for a fan pressure ratio of 3.

The plots of specific thrust and thrust specific fuel consumption for an ideal turbofan engine with optimum bypass ratio vs compressor pressure ratio are superimposed on Figs. 5.23a–5.23e by a dashed line marked α^*. The optimum-bypass-ratio ideal turbofan has the minimum thrust specific fuel consumption.

The plots of specific thrust and thrust specific fuel consumption for the optimum-bypass-ratio ideal turbofan vs fan pressure ratio are superimposed on Figs. 5.25a–5.25d by a dashed line marked α^*. As shown in these figures, the plot for α^* is the locus of the minimum value of S for each π_f.

The plots of specific thrust and thrust specific fuel consumption for the optimum-bypass-ratio ideal turbofan vs flight Mach number are superimposed on Figs. 5.27a–5.27e for a fan pressure ratio of 2 and on Figs. 5.28a–5.28e for a fan pressure ratio of 3. As shown in these figures, the plots for α^* are the locus of the minimum value of S for fixed values of π_c and π_f.

The thermal efficiency of an optimum-bypass-ratio ideal turbofan is the same as that of an ideal turbojet. The bypass ratio of an ideal turbofan affects only the

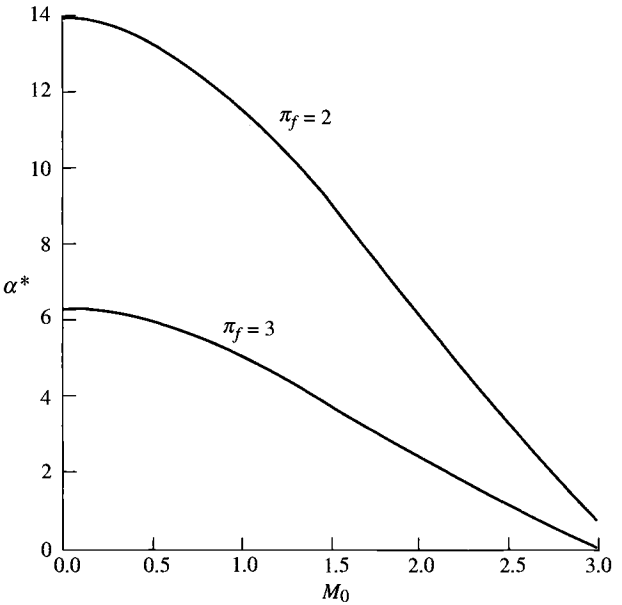

Fig. 5.29c α^* **vs** M_0**, for** $\pi_c = 24$ **and** $\pi_f = 2$ **and 3.**

propulsive efficiency. The propulsive efficiency of an optimum-bypass-ratio ideal turbofan is superimposed on those of Figs. 5.23d, 5.25c, 5.27c, and 5.28c. As can be seen, the optimum bypass ratio gives the maximum propulsive efficiency. Likewise, as shown in Figs. 5.23d, 5.25c, 5.27d, and 5.28d, the optimum bypass ratio gives the maximum overall efficiency. The thrust ratio of an optimum-bypass-ratio ideal turbofan is superimposed on those of Figs. 5.23e, 5.25d, 5.27e, and 5.28e and is equal to 0.5.

5.11 Ideal Turbofan with Optimum Fan Pressure Ratio

Figures 5.26a and 5.26b show that for given flight conditions T_0 and M_0, design limit τ_λ, compressor pressure ratio π_c, and bypass ratio α, there is an optimum fan pressure ratio π_f that gives the minimum specific fuel consumption and maximum specific thrust. As will be shown, the optimum fan pressure ratio corresponds to the exit velocity V_{19} of the fan stream, being equal to the exit velocity of the core stream V_9. It is left as a reader exercise to show that equal exit velocities ($V_9 = V_{19}$) correspond to maximum propulsive efficiency.

5.11.1 Optimum Fan Pressure Ratio π_f^*

For a given set of prescribed variables (τ_r, π_c, τ_λ, V_0, α), we may locate the optimum fan pressure ratio by taking the partial derivative of the specific

thrust with respect to the fan total temperature ratio. The derivation of an expression for the optimum fan total temperature ratio and, by Eq. (5.58f), the optimum fan pressure ratio follows. From Eq. (5.54), we have

$$\frac{\partial S}{\partial \tau_f} = \frac{-f}{[(1+\alpha)(F/\dot{m}_0)]^2} \frac{\partial}{\partial \tau_f}\left[(1+\alpha)\left(\frac{F}{\dot{m}_0}\right)\right] = 0$$

Thus

$$\frac{\partial S}{\partial \tau_f} = 0$$

is satisfied by

$$\frac{\partial}{\partial \tau_f}\left[\frac{g_c}{V_0}(1+\alpha)\left(\frac{F}{\dot{m}_0}\right)\right] = 0$$

where, from Eq. (5.48),

$$\frac{g_c}{V_0}(1+\alpha)\left(\frac{F}{\dot{m}_0}\right) = \frac{V_9}{V_0} - 1 + \alpha\left(\frac{V_{19}}{V_0} - 1\right)$$

Hence the optimum fan pressure ratio is given by solution of

$$\frac{\partial}{\partial \tau_f}\left[\frac{V_9}{V_0} - 1 + \alpha\left(\frac{V_{19}}{V_0} - 1\right)\right] = \frac{\partial}{\partial \tau_f}\left(\frac{V_9}{V_0}\right) + \alpha \frac{\partial}{\partial \tau_f}\left(\frac{V_{19}}{V_0}\right) = 0 \qquad \text{(i)}$$

Since

$$\frac{\partial}{\partial \tau_f}\left(\frac{V_9}{V_0}\right) = \frac{1}{2V_9/V_0} \frac{\partial}{\partial \tau_f}\left[\left(\frac{V_9}{V_0}\right)^2\right]$$

and

$$\frac{\partial}{\partial \tau_f}\left(\frac{V_{19}}{V_0}\right) = \frac{1}{2V_{19}/V_0} \frac{\partial}{\partial \tau_f}\left[\left(\frac{V_{19}}{V_0}\right)^2\right]$$

Eq. (i) becomes

$$\frac{1}{2V_9/V_0} \frac{\partial}{\partial \tau_f}\left[\left(\frac{V_9}{V_0}\right)^2\right] + \alpha \frac{1}{2V_{19}/V_0} \frac{\partial}{\partial \tau_f}\left[\left(\frac{V_{19}}{V_0}\right)^2\right] = 0 \qquad \text{(ii)}$$

To determine the first term of Eq. (ii), we start with

$$\left(\frac{V_9}{V_0}\right)^2 = \frac{1}{M_0^2}\left(\frac{V_9}{a_0}\right)^2 = \frac{1}{[(\gamma-1)/2](\tau_r-1)}\left(\frac{V_9}{a_0}\right)^2$$
$$= \frac{\tau_\lambda - \tau_r[\tau_c - 1 + \alpha(\tau_f - 1)] - \tau_\lambda/(\tau_r\tau_c)}{\tau_r - 1} \qquad \text{(iii)}$$

Thus

$$\frac{\partial}{\partial\tau_f}\left[\left(\frac{V_9}{V_0}\right)^2\right] = \frac{-\alpha\tau_r}{\tau_r - 1} \qquad \text{(iv)}$$

To determine the second term of Eq. (ii), we start with

$$\left(\frac{V_{19}}{V_0}\right)^2 = \frac{1}{M_0^2}\left(\frac{V_{19}}{a_0}\right)^2 = \frac{1}{[(\gamma-1)/2](\tau_r-1)}\left(\frac{V_{19}}{a_0}\right)^2 = \frac{\tau_r\tau_f - 1}{\tau_r - 1} \qquad \text{(v)}$$

Thus

$$\frac{\partial}{\partial\tau_f}\left[\left(\frac{V_{19}}{V_0}\right)^2\right] = \frac{\tau_r}{\tau_r - 1} \qquad \text{(vi)}$$

Substitution of Eqs. (iv) and (vi) into Eq. (ii) gives

$$\frac{1}{2V_9/V_0}\left(\frac{-\alpha\tau_r}{\tau_r - 1}\right) + \alpha\frac{1}{2V_{19}/V_0}\frac{\tau_r}{\tau_r - 1} = 0 \qquad \text{(vii)}$$

Thus we can conclude from Eq. (vii) that the optimum fan pressure ratio corresponds to that value of τ_f yielding

$$V_9 = V_{19} \qquad (5.64)$$

Also

$$\text{FR} = 1 \qquad (5.65)$$

To solve for the optimum fan temperature ratio, we equate Eqs. (iii) and (v):

$$\left(\frac{V_9}{V_0}\right)^2 = \frac{\tau_\lambda - \tau_r[\tau_c - 1 + \alpha(\tau_f - 1)] - \tau_\lambda/(\tau_r\tau_c)}{\tau_r - 1}$$
$$= \left(\frac{V_{19}}{V_0}\right)^2 = \frac{\tau_r\tau_f - 1}{\tau_r - 1}$$

giving

$$\tau_f^* = \frac{\tau_\lambda - \tau_r(\tau_c - 1) - \tau_\lambda/(\tau_r\tau_c) + \alpha\tau_r + 1}{\tau_r(1+\alpha)} \tag{5.66}$$

An equation for the specific thrust of an optimum-fan-pressure-ratio turbofan can be obtained by starting with the simplified expression

$$\left(\frac{F}{\dot{m}_0}\right)_{\tau_f^*} = \frac{a_0}{g_c}\left(\frac{V_{19}}{a_0} - M_0\right)$$

which becomes

$$\left(\frac{F}{\dot{m}_0}\right)_{\tau_f^*} = \frac{a_0}{g_c}\left[\sqrt{\frac{2}{\gamma-1}(\tau_r\tau_f^* - 1)} - M_0\right] \tag{5.67}$$

The propulsive efficiency for the optimum-fan-pressure-ratio turbofan engine is simply

$$(\eta_P)_{\tau_f^*} = \frac{2}{V_{19}/V_0 + 1} \tag{5.68}$$

5.11.2 Summary of Equations—Optimum-Fan-Pressure-Ratio Ideal Turbofan

INPUTS:

$$M_0,\ T_0(\mathrm{K},\ ^\circ\mathrm{R}),\ \gamma,\ c_p\left(\frac{\mathrm{kJ}}{\mathrm{kg}\cdot\mathrm{K}},\ \frac{\mathrm{Btu}}{\mathrm{lbm}\cdot{}^\circ\mathrm{R}}\right),\ hr_{PR}\left(\frac{\mathrm{kJ}}{\mathrm{kg}},\ \frac{\mathrm{Btu}}{\mathrm{lbm}}\right),\ T_{t4}(\mathrm{K},\ ^\circ\mathrm{R}),\ \pi_c,\ \alpha$$

OUTPUTS:

$$\frac{F}{\dot{m}_0}\left(\frac{\mathrm{N}}{\mathrm{kg/s}},\ \frac{\mathrm{lbf}}{\mathrm{lbm/s}}\right), f,\ S\left(\frac{\mathrm{mg/s}}{\mathrm{N}},\ \frac{\mathrm{lbm/h}}{\mathrm{lbf}}\right),\ \eta_T,\ \eta_P,\ \eta_O,\ \pi_f^*$$

EQUATIONS:

Equations (5.58a–5.58e), (5.58j), (5.58l), plus

$$\tau_f^* = \frac{\tau_\lambda - \tau_r(\tau_c - 1) - \tau_\lambda/(\tau_r\tau_c) + \alpha\tau_r + 1}{\tau_r(1+\alpha)} \tag{5.69a}$$

$$\pi_f^* = (\tau_f^*)^{\gamma/(\gamma-1)} \tag{5.69b}$$

$$\frac{V_{19}}{a_0} = \sqrt{\frac{2}{\gamma - 1}(\tau_r \tau_f^* - 1)} \tag{5.69c}$$

$$\frac{F}{\dot{m}_0} = \frac{a_0}{g_c}\left(\frac{V_{19}}{a_0} - M_0\right) \tag{5.69d}$$

$$\eta_P = \frac{2M_0}{V_{19}/a_0 + M_0} \tag{5.69e}$$

and Eqs. (5.58k), (5.58n), and (5.60).

5.11.3 Effect of Bypass Ratio on Specific Thrust and Fuel Consumption

Data for several turbofan engines are listed in Table 5.2. The bypass ratio ranges from 0.76 for the engine in the smaller A-7D fighter attack airplane to 5 for engines in the commercial transports, to 8 for the C-5A/B heavy logistics military transport engine. The specific thrust and specific fuel consumption for the fighter are about twice their values for the three transport-type airplanes. Let us look at the interrelationship between the bypass ratio, specific thrust, and specific fuel consumption to help explain the trends in the values of these quantities, as exhibited by the table.

We can examine how these quantities interact for the ideal turbofan with optimum fan pressure ratio by plotting specific thrust and thrust specific fuel consumption vs bypass ratio. Such plots are given in Fig. 5.30 for

$$M_0 = 0.8, \quad T_0 = 216.7 \text{ K}, \quad \tau_\lambda = 6.5, \quad \pi_c = 24, \quad h_{PR} = 42{,}800 \text{ kJ/kg}$$
$$\gamma = 1.4, \qquad c_p = 1.004 \text{ kJ/(kg} \cdot \text{K)}$$

Table 5.2 Data for several turbofan engines

Engine	Bypass ratio α	$F/\dot{m}_0$, [N/(kg/s)] [lbf/(lbm/s)]	S, [(mg/s)/N] [(lbm/h)/lbf]	π_f	π_c	Aircraft
TF-39	8.0	251.8 (25.68)	8.87 (0.313)	1.45	22.0	C5A/B
JT9D	5.1	253.4 (25.84)	9.80 (0.346)	1.54	22.3	Boeing 747
CF6	4.32	255.6 (26.06)	9.86 (0.348)	1.71	30.2	DC-10
TF-41	0.76	498.0 (50.78)	17.8 (0.629)	2.45	21.0	A-7D

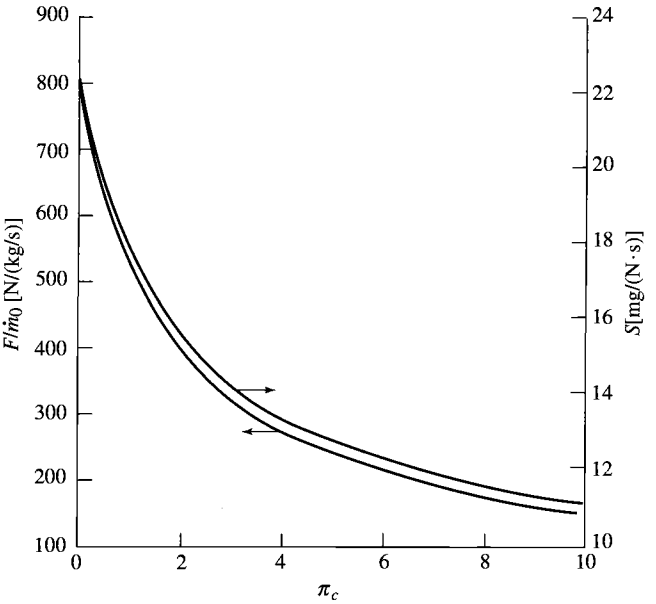

Fig. 5.30 Peformance at π_f^* vs α, for $\pi_c = 24$ and $M_0 = 0.8$.

The optimum fan pressure ratio that gives $V_9 = V_{19}$ is plotted vs the bypass ratio α in Fig. 5.31.

We can see, in Fig. 5.30, a sharp reduction in specific fuel consumption as α increases from zero. An equally marked, but unfavorable, decrease in thrust per unit mass flow occurs. A large fraction of the beneficial decrease in S is obtained by selecting an α of about 5, as was done for the engines in the DC-10 and 747 transports. At a bypass ratio of 8, corresponding to the C-5A engines, a further decrease in specific fuel consumption is realized. Because engine weight is a small fraction of the takeoff gross weight for these airplanes, it is of secondary importance compared to fuel weight and hence specific fuel consumption. Thus we find a relatively large bypass ratio for the engines in the transporters tabulated compared to the 0.76 value of the A-7D engine.

Example 5.6

The engine that we looked at in Section 5.9 is used again in this section for an example. The following values are held constant for all plots:

$$T_0 = 216.7\,\text{K}, \quad \gamma = 1.4, \quad c_p = 1.004\,\text{kJ/(kg K)}$$
$$h_{PR} = 42{,}800\,\text{kJ/kg}, \qquad T_{t4} = 1670\,\text{K}$$

The optimum fan pressure ratio is plotted vs the compressor pressure ratio in Fig. 5.32 and vs the bypass ratio in Fig. 5.33. From Fig. 5.32, we can see that the

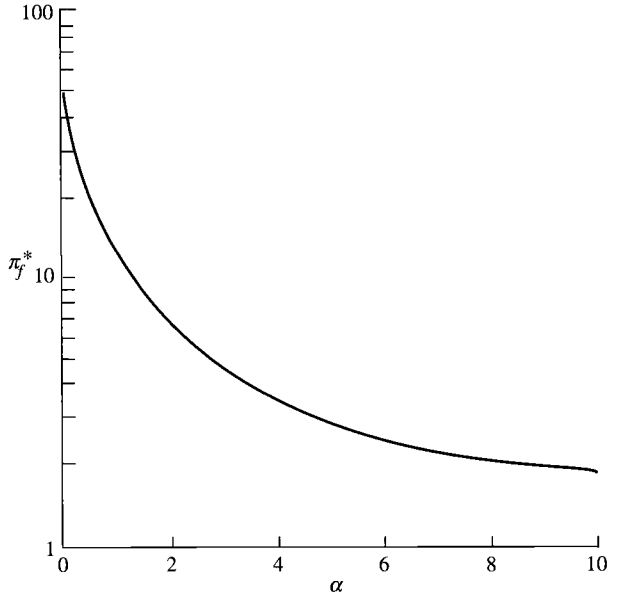

Fig. 5.31 π_f^* vs α, for $\pi_c = 24$ and $M_0 = 0.8$.

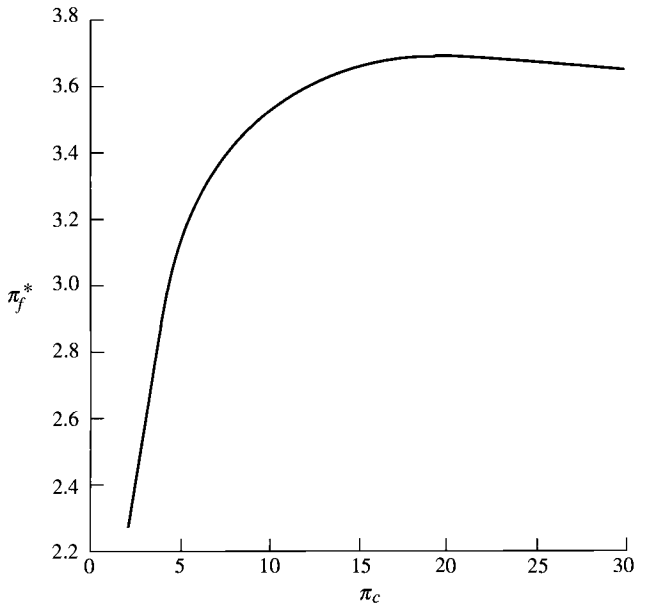

Fig. 5.32 π_f^* vs π_c, for $M_0 = 0.9$ and $\alpha = 5$.

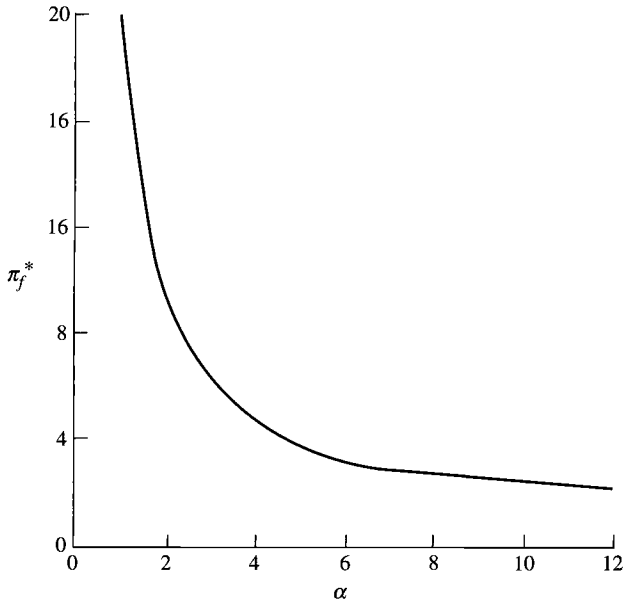

Fig. 5.33 π_f^* **vs** α, **for** $M_0 = 0.9$ **and** $\pi_c = 24$.

optimum fan pressure ratio increases with the compressor pressure ratio. Figure 5.33 shows that the optimum fan pressure ratio decreases with the bypass ratio.

Plots of specific thrust, thrust specific fuel consumption, propulsive efficiency, overall efficiency, and thrust ratio for the optimum-fan-pressure-ratio ideal turbofan engines are superimposed on Figs. 5.24 and 5.26 as dashed lines marked π_f^*. The plots for optimum fan pressure ratio are the loci of the optimums for specific thrust, thrust specific fuel consumption, propulsive efficiency, and overall efficiency. The thrust ratio of the optimum-fan-pressure-ratio ideal turbofan engines is equal to 1.

5.11.4 Comparison of Optimum Ideal Turbofans

A comparison of the two optimum ideal turbofan engines can be made by looking at contour plots of specific thrust $F/\dot{m}_0$ and thrust specific fuel consumption S vs fan pressure ratio π_f and bypass ratio α. For our example problem (Examples 5.4, 5.5, and 5.6), contours of constant specific thrust values and contours of constant thrust specific fuel consumption are plotted in Figs. 5.34a and 5.34b, respectively. Also plotted are the curves for π_f^* and α^* for each optimum engine. Figures 5.34a and 5.34b show that π_f^* is the fan pressure ratio giving maximum specific thrust and minimum thrust specific fuel consumption for a given bypass ratio. Figure 5.34b shows that α^* is the bypass ratio giving

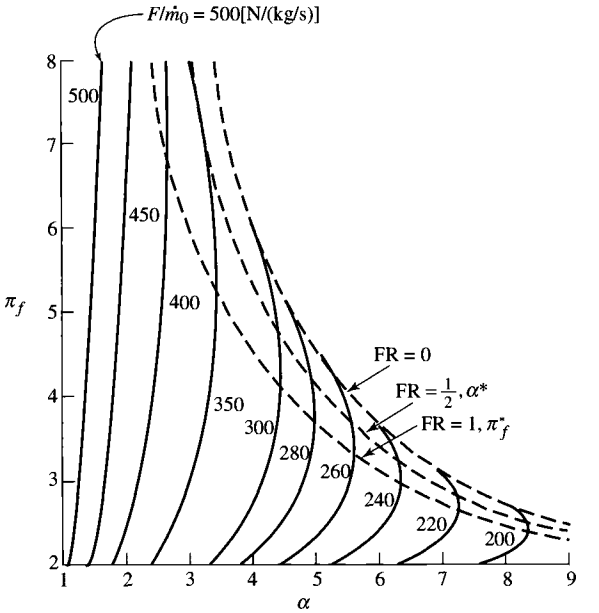

Fig. 5.34a Contours of constant specific thrust and curves for π_f^* and α^*.

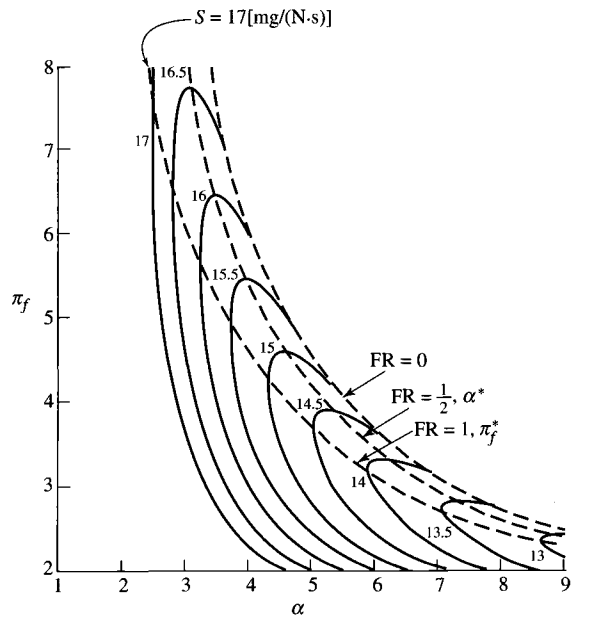

Fig. 5.34b Contours of constant fuel consumption and curves for π_f^* and α^*.

minimum thrust specific fuel consumption for a given fan pressure ratio. Also shown in Fig. 5.34b are that the α^* curve is the locus of horizontal tangents to contours of constant S and the π_f^* curve is the locus of vertical tangents to contours of constant S.

5.12 Ideal Pulse Detonation Engine

The classical, calorically perfect gas, closed thermodynamic cycle analysis should always be considered for the initial evaluation of ideal propulsion devices because it often provides transparent algebraic results that reveal fundamental behavior almost effortlessly. This is particularly true because the T-s diagram is not anchored in space or time, but represents the succession of states experienced by every element of the working fluid, and can therefore be applied equally well to steady (e.g., Brayton and Carnot) and unsteady (e.g., Diesel and Otto) cycles.

The pulse detonation engine (PDE) is a contemporary example of a novel propulsion cycle. Because of its inherently unsteady behavior, it has been difficult to conveniently classify and evaluate it relative to its steady-state counterparts by means of unsteady gas dynamic calculations alone. The classical, closed thermodynamic cycle analysis of the ideal PDE is identical to that of the ideal turbojet (see Section 5.7), except that the heat is released by a detonation wave that passes through the working fluid containing fuel that has been brought essentially to rest in the combustor. Please note that the compression process may include both ram compression due to forward flight and mechanical compression driven by the fluid leaving the combustor. The T-s diagram for an example PDE is shown in Fig. 5.35, where $\psi = T_3/T_0$ is the cycle thermal compression ratio, $\tilde{q}$ is the dimensionless heat release, and $\gamma = 1.36$. This approach takes advantage of the fact that entropy is a thermodynamic state property, independent of velocity reference frame, as opposed to, for example, the total pressure and total temperature. The complete version of this analysis can be found in Ref. 31.

We therefore direct our attention to the pulse detonation wave process. The reader is advised that the ensuing mathematical analyses will be straightforward, and is therefore encouraged to focus on the physical phenomena involved.

The generally accepted model of a normal detonation wave in PDP devices is that of a Zeldovich/von Neumann/Doering or ZND wave (see Refs. 32 and 33), a compound wave consisting of a normal shock wave progressing into the undisturbed fuel-air mixture, which is nearly at rest at the combustor entry condition (*point 3*), followed by release of sensible heat in a constant-area region (Rayleigh flow) terminating at *point 4*. The strength (Mach number, pressure ratio, or temperature ratio) of the leading shock wave, from point 3 to point 3a, is uniquely determined by the initial conditions and the amount of heat added. The entire process is constrained by the Chapman-Jouguet condition, which requires that the local Mach number at the termination of the heat addition region (point 4) be one (sonic or choked flow). The heat addition region is followed by a very complex constant-area region of nonsteady expansion waves, the most important

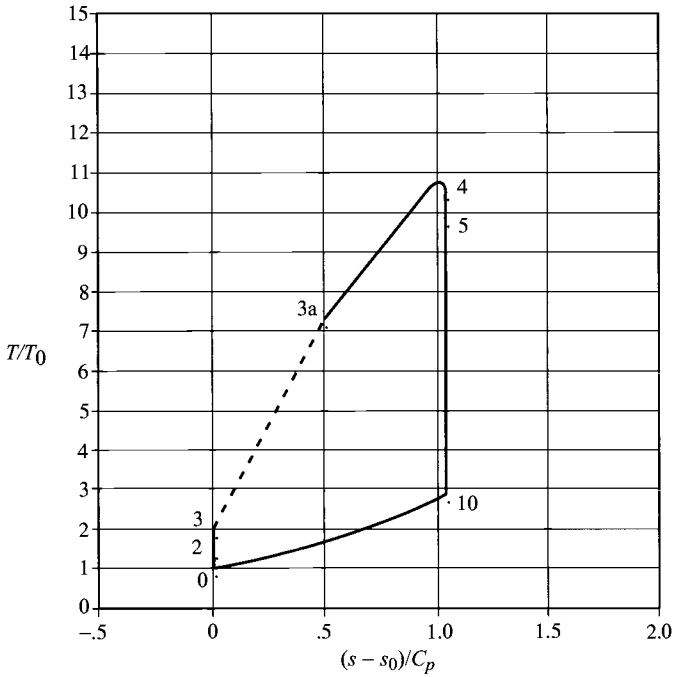

Fig. 5.35 Temperature-entropy diagram for the ideal PDE cycle, for $\psi = 2$, $\tilde{q} = 5$, and $\gamma = 1.36$.

property of which is that they are assumed to be isentropic. This ZND wave structure is stationary in detonation wave coordinates from the undisturbed flow to the end of the heat addition process. To ensure the greatest cycle performance, it is further assumed that 1) the nonsteady expansion (point 4 to point 10) of the detonated mixture is isentropic, 2) every fluid particle experiences the same normal detonation process, and 3) there is no energy penalty to the cycle for whatever spark or ignition torch may be required to initiate the detonation process.

Closed-form, algebraic solutions for the leading normal shock wave (Chapman-Jouguet) Mach number M_{CJ} and the entropy rise in the detonation wave have been derived by Shapiro[34] and others[33,35] for calorically perfect gases, and are given, respectively, by

$$M_{CJ}^2 = (\gamma+1)\frac{\tilde{q}}{\psi} + 1 + \sqrt{\left[(\gamma+1)\frac{\tilde{q}}{\psi} + 1\right]^2 - 1}$$

where

$$\tilde{q} \equiv \frac{q_{\text{supp}}}{c_p T_0} = \frac{f h_{PR}}{c_p T_0} \tag{5.70}$$

and

$$\frac{s_4 - s_3}{c_p} = -\ell n\left[M_{CJ}^2\left(\frac{\gamma+1}{1+\gamma M_{CJ}^2}\right)^{\frac{\gamma+1}{\gamma}}\right] \tag{5.71}$$

Consequently, the constant-pressure heat rejected and the cycle thermal efficiency become

$$\begin{aligned} q_{\text{rej}} &= h_{10} - h_0 = c_p(T_{10} - T_0) = c_p T_0\left(e^{\frac{s_{10}-s_0}{c_p}} - 1\right) \\ &= c_p T_0\left(e^{\frac{s_4-s_3}{c_p}} - 1\right) = c_p T_0\left[\frac{1}{M_{CJ}^2}\left(\frac{1+\gamma M_{CJ}^2}{\gamma+1}\right)^{\frac{\gamma+1}{\gamma}} - 1\right] \end{aligned} \tag{5.72}$$

and

$$\eta_{\text{th}} = 1 - \frac{\frac{1}{M_{CJ}^2}\left(\frac{1+\gamma M_{CJ}^2}{\gamma+1}\right)^{\frac{\gamma+1}{\gamma}} - 1}{\bar{q}} \tag{5.73}$$

Since

$$\frac{F}{\dot{m}_0} \equiv \frac{1}{g_c}\left[\sqrt{V_0^2 + 2\eta_{\text{th}} q_{\text{supp}}} - V_0\right] \tag{5.74}$$

and

$$S \equiv \frac{\dot{m}_f}{F} = \frac{f\dot{m}_0}{F} = \frac{f}{F/\dot{m}_0} \tag{5.75}$$

then generalized ideal PDE performance information, such as that shown in Figs. 5.36 and 5.37, are easily calculated. The ideal Brayton (ramjet/turbojet) is included for reference.

In summary, Figs. 5.36 and 5.37 clearly show that the thermal compression inherent in the PDE normal shock wave, albeit irreversible (see Fig. 5.35), leads to superior propulsion performance for the ideal PDE cycle vs the ideal Brayton cycle when $\psi = T_3/T_0$ is small. However, when $\psi \geq$ about 3 (due to combined ram and mechanical compression), the difference between PDE and Brayton performance is significantly reduced. Readers are now empowered to freely investigate comparisons of their own choice.

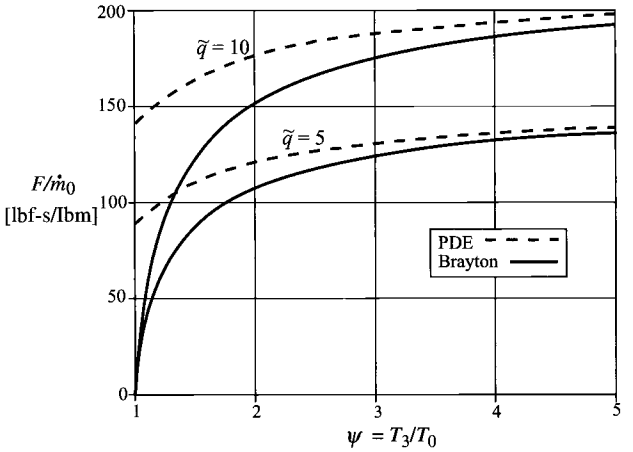

Fig. 5.36 Specific thrust $F/\dot{m}_0$ of ideal PDE and Brayton cycles as functions of ψ, for $\tilde{q} = 5$ and 10, $\gamma = 1.36$, and vehicle speed $V_0 = 0$.

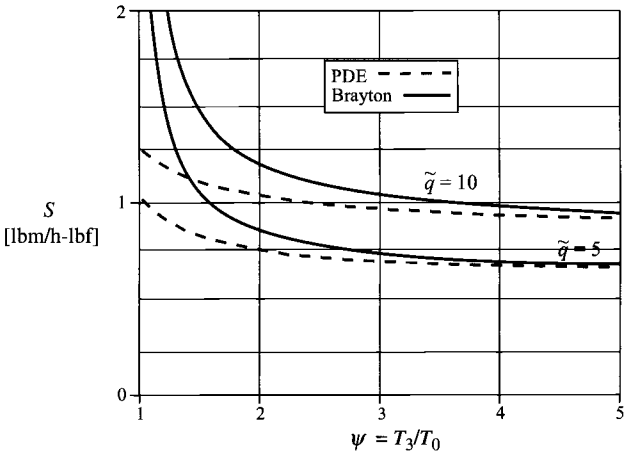

Fig. 5.37 Specific fuel consumption S of ideal PDE and Brayton cycles as functions of ψ, for $\tilde{q} = 5$ and 10, $\gamma = 1.36$, $h_{PR} = 19{,}000$ Btu/lbm, and $V_0 = 0$.

Problems

5.1 Show that the thermal and propulsive efficiencies for an ideal ramjet engine are given by Eqs. (5.17a) and (5.17b), respectively.

5.2 Calculate the variation with T_{t4} of exit Mach number, exit velocity, specific thrust, fuel/air ratio, and thrust specific fuel consumption of an ideal

turbojet engine for compressor pressure ratios of 10 and 20 at a flight Mach number of 2 and $T_0 = 390°R$. Perform calculations at T_{t4} values of 4400, 4000, 3500, and 3000°R. Use $h_{PR} = 18{,}400$ Btu/lbm, $c_p = 0.24$ Btu/(lbm · °R), and $\gamma = 1.4$. Compare your results with the output of the PARA computer program.

5.3 Calculate the variation with T_{t4} of exit Mach number, exit velocity, specific thrust, fuel/air ratio, and thrust specific fuel consumption of an ideal turbojet engine for compressor pressure ratios of 10 and 20 at a flight Mach number of 2 and $T_0 = 217$ K. Perform calculations at T_{t4} values of 2400, 2200, 2000, and 1800 K. Use $h_{PR} = 42{,}800$ kJ/kg, $c_P = 1.004$ kJ/(kg · K), and $\gamma = 1.4$. Compare your results with the output of the PARA computer program.

5.4 Show that the thermal efficiency for an ideal turbojet engine is given by Eq. (5.22).

5.5 Show that the thermal efficiency for an ideal afterburning turbojet is given by Eq. (5.42).

5.6 A major shortcoming of the ramjet engine is the lack of static thrust. To overcome this, it is proposed to add a compressor driven by an electric motor, as shown in the model engine in Fig. P5.1. For this new ideal engine configuration, show the following:

(a) The specific thrust is given by

$$\frac{F}{\dot{m}_0} = \frac{a_0}{g_c}\left[\sqrt{\frac{2}{\gamma - 1}\frac{\tau_\lambda}{\tau_r \tau_c}(\tau_r \tau_c - 1)} - M_0\right]$$

(b) The compressor power requirement is given by

$$\dot{W}_c = \dot{m}_0 c_p T_0 \tau_r (\tau_c - 1)$$

(c) Determine the static thrust of this engine at the following conditions:

$$T_0 = 518.7°R, \qquad T_{t4} = 3200°R, \qquad \pi_c = 4$$

$$c_P = 0.24\,\text{Btu/(lbm} \cdot °R), \qquad \gamma = 1.4$$

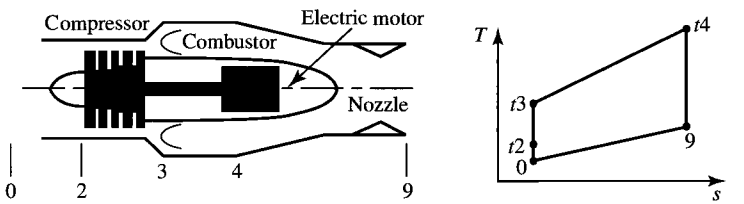

Fig. P5.1 Model engine.

5.7 Determine the optimum compressor pressure ratio, specific thrust, and thrust specific fuel consumption for an ideal turbojet engine giving the maximum specific thrust at the following conditions:

$$M_0 = 2.1,\ T_0 = 220\ \text{K}, \qquad T_{t4} = 1700\ \text{K}, \qquad h_{PR} = 42{,}800\ \text{kJ/kg}$$
$$c_p = 1.004\ \text{kJ/(kg} \cdot \text{K)}, \qquad \gamma = 1.4$$

5.8 Show that the thermal efficiency for an ideal turbojet engine with optimum compressor pressure ratio is given by $\eta_\tau = 1 - 1/\sqrt{\tau_\lambda}$.

5.9 Show that the thermal efficiency for an ideal turbofan engine is given by Eq. (5.22).

5.10 Compare the performance of three ideal turbofan engines with an ideal turbojet engine at two flight conditions by completing Table P5.1. The first flight condition (case 1) is at a flight Mach number of 0.9 at an altitude of 40,000 ft, and the second flight condition (case 2) is at a flight Mach number of 2.6 and an altitude of 60,000 ft. Note that the fuel/air ratio need be calculated only once for each case since it is not a function of α or π_f. The following design information is given:

$$\pi_c = 20, \qquad T_{t4} = 3000^\circ\text{R}, \qquad c_p = 0.24\ \text{Btu/(lbm} \cdot {}^\circ\text{R)}$$
$$\gamma = 1.4, \qquad h_{PR} = 18{,}400\ \text{Btu/lbm}$$

5.11 Repeat Problem 5.10 with the first flight condition (case 1) at a flight Mach number of 0.9 and altitude of 12 km and the second flight condition (case 2) at a flight Mach number of 2.6 and an altitude of 18 km. Use the following design information:

$$\pi_c = 20, \qquad T_{t4} = 1670\ \text{K}, \qquad c_p = 1.004\ \text{kJ/(kg} \cdot \text{K)}$$
$$\gamma = 1.4, \qquad h_{PR} = 42{,}800\ \text{kJ/kg}$$

Table P5.1

Engine	α	π_f	V_9/a_0	V_{19}/a_0	F/m_0	f	S
Turbofan							
(a) Case 1	1	4					
Case 2	1	4					
(b) Case 1, α^*		4					
Case 2, α^*		4					
(c) Case 1, π_f^*	1						
Case 2, π_f^*	1						
Turbojet							
(a) Case 1	0	n/a		n/a			
Case 2	0	n/a		n/a			

5.12 Show that the propulsive efficiency for an ideal turbofan engine with optimum bypass ratio is given by Eq. (5.62).

5.13 Show that the propulsive efficiency for an ideal turbofan engine with optimum fan pressure ratio is given by Eq. (5.68).

5.14 For an ideal turbofan engine, the maximum value of the bypass ratio corresponds to $V_9 = V_0$.

(a) Starting with Eq. (5.53), show that this maximum bypass ratio is given by

$$\alpha_{\max} = \frac{\tau_\lambda + 1 - \tau_r\tau_c - \tau_\lambda/(\tau_r\tau_c)}{\tau_r(\tau_f - 1)}$$

(b) Show that the propulsive efficiency for this maximum bypass ratio is given by

$$\eta_P = \frac{2}{\sqrt{(\tau_r\tau_f - 1)/(\tau_r - 1) + 1}}$$

5.15 Under certain conditions, it is desirable to obtain power from the freestream. Consider the ideal air-powered turbine shown in Fig. P5.2. This cycle extracts power from the incoming airstream. The incoming air is slowed down in the inlet and then heated in the combustor before going through the turbine. The cycle is designed to produce no thrust ($F = 0$), so that $V_9 = V_0$ and $P_9 = P_0$.

(a) Starting with Eq. (5.29), show that

$$\tau_t = \frac{1}{\tau_r} + \frac{1}{\tau_\lambda}\frac{\gamma - 1}{2}M_0^2$$

(b) Then show that the turbine output power is given by

$$\dot{W}_i = \dot{m}c_pT_0\left(\frac{\tau_\lambda}{\tau_r} - 1\right)\frac{\gamma - 1}{2}M_0^2$$

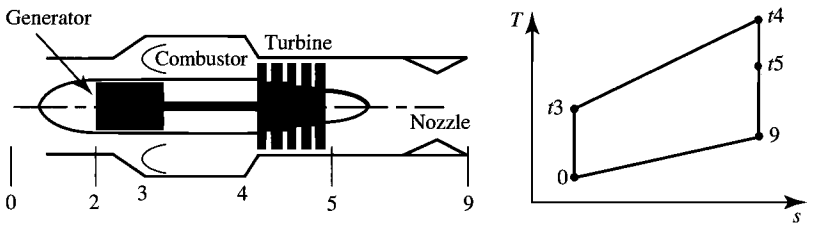

Fig. P5.2 Ideal air-powered turbine.

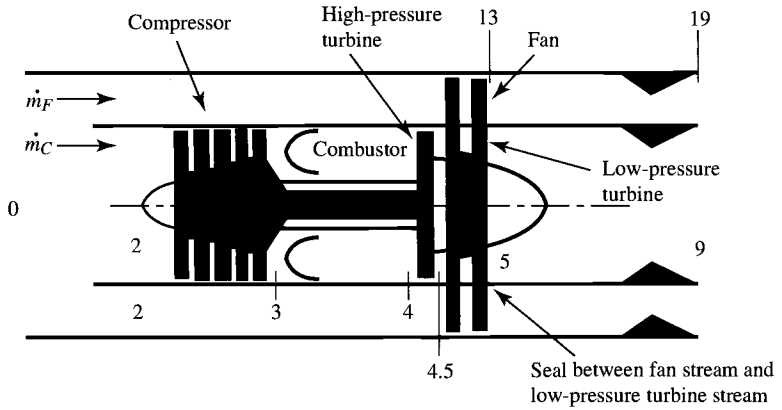

Fig. P5.3 Turbofan engine with aft fan.

5.16 In the early development of the turbofan engine, General Electric developed a turbofan engine with an aft fan, as shown in Fig. P5.3. The compressor is driven by the high-pressure turbine, and the aft fan is directly connected to the low-pressure turbine. Consider an ideal turbofan engine with an aft fan.

(a) Show that the high-pressure turbine temperature ratio is given by

$$\tau_{tH} = \frac{T_{t4.5}}{T_{t4}} = 1 - \frac{\tau_r}{\tau_\lambda}(\tau_c - 1)$$

(b) Show that the low-pressure-turbine temperature ratio is given by

$$\tau_{tL} = \frac{T_{t5}}{T_{t4.5}} = 1 - \frac{\alpha\tau_r}{\tau_\lambda \tau_{tH}}(\tau_f - 1)$$

5.17 Starting with Eq. (5.48), show that for known values of M_0, T_0, T_{t4}, π_c, and πf, the bypass ratio α giving a specified value of specific thrust $F/\dot{m}_0$ is given by the solution to the quadratic equation

$$A\alpha^2 + B\alpha + C = 0$$

where

$$A = \frac{\gamma - 1}{2} D^2$$

$$B = (\gamma - 1)\left(D^2 + D\frac{V_{19}}{a_0}\right) + \tau_r(\tau_f - 1)$$

$$C = \frac{\gamma - 1}{2}\left(D^2 + 2D\frac{V_{19}}{a_0}\right) - E$$

$$D = \frac{F}{\dot{m}_0}\frac{g_c}{a_0} - \left(\frac{V_{19}}{a_0} - M_0\right)$$

$$E = \tau_\lambda - \tau_r(\tau_c - 1) - \frac{\tau_\lambda}{\tau_r \tau_c} - (\tau_r \tau_f - 1)$$

$$\frac{V_{19}}{a_0} = \sqrt{\frac{2}{\gamma - 1}(\tau_r \tau_f - 1)}$$

5.18 Using the system of equations listed in Problem 5.17, determine the bypass ratio that gives a specific thrust of 400 N/(kg/s) for the following data:

$$T_0 = 216.7 \text{ K}, \quad T_{t4} = 1670 \text{ K}, \quad M_0 = 0.8, \quad \pi_c = 24, \quad \pi_f = 4$$
$$\text{with } \gamma = 1.4, \; c_p = 1.004 \text{ kJ/(kg} \cdot \text{K)}, \; h_{PR} = 42{,}800 \text{ kJ/kg}$$

5.19 Using the system of equations listed in Problem 5.17, determine the bypass ratio that gives a specific thrust of 40.0 lbf/(lbm/s) for the following data:

$$T_0 = 390°\text{R}, \quad T_{t4} = 3000°\text{R}, \quad M_0 = 2, \quad \pi_c = 16, \quad \pi_f = 5$$
$$\text{with } \gamma = 1.4, \quad c_p = 0.24 \text{ Btu/(lbm} \cdot °\text{R)}, \quad h_{PR} = 18{,}400 \text{ Btu/lbm}$$

Problems for Supporting Material

SM5.1 Considerable research and development effort is going into increasing the maximum T_{t4} in gas turbine engines for fighter aircraft. For a mixed-flow turbofan engine with $\pi_c = 16$ at a flight condition of $M_0 = 2.5$ and $T_0 = 216.7$ K, use the PARA computer program to determine and plot the required engine fan pressure, specific thrust, and specific fuel consumption vs T_{t4} over a range of 1600 to 2200 K for bypass ratios of 0.5 and 1. Use $h_{PR} = 42{,}800$ kJ/kg, $c_p = 1.004$ kJ/(kg · K), and $\gamma = 1.4$. Comment on your results in general. Why do the plots of specific fuel consumption vs specific thrust for these engines all fall on one line?

SM5.2 Considerable research and development effort is going into increasing the maximum T_{t4} in gas turbine engines for fighter aircraft. For a mixed-flow turbofan engine with $\pi_c = 20$ at a flight condition of $M_0 = 2$ and $T_0 = 390°$R, use the PARA computer program to determine and plot the required engine bypass ratio α, specific thrust, and specific fuel consumption vs T_{t4} over a range of 3000 to 4000°R for fan pressure ratios of 2 and 5. Use $h_{PR} = 18{,}400$ Btu/lbm, $c_p = 0.24$ Btu/(lbm · °R), and $\gamma = 1.4$. Comment on your results.

SM5.3 Show that the thermal efficiency of the afterburning mixed-flow turbofan engine given by Eq. (SM5.16) can be rewritten as

$$\eta_T = \frac{c_p T_0}{f_0 h_{PR}} \left[\tau_\lambda \text{AB} \left(1 - \frac{1}{\tau_r \tau_f} \right) - (\tau_r - 1) \right]$$

SM5.4 For an afterburning mixed-flow turbofan engine with $\pi_c = 16$ and $T_{t7} = 2200$ K at a flight condition of $M_0 = 2.5$ and $T_0 = 216.7$ K, use the PARA computer program to determine and plot the required engine fan pressure, specific thrust, and specific fuel consumption vs T_{t4} over a range of 1600 to 2200 K for bypass ratios of 0.5 and 1. Use $h_{PR} = 42{,}800$ kJ/kg, $c_p = 1.004$ kJ/(kg · K), and $\gamma = 1.4$. Comment on your results in general. Why do the plots of specific fuel consumption vs specific thrust for these engines all fall on one line? Compare these results to those for Problem SM5.1, and comment on the differences.

SM5.5 For an afterburning mixed-flow turbofan engine with $\pi_c = 20$ and $T_{t7} = 4000°$R at a flight condition of $M_0 = 2$ and $T_0 = 390°$R, use the PARA computer program to determine and plot the required engine bypass ratio α, specific thrust, and specific fuel consumption vs T_{t4} over a range of 3000 to 4000°R for fan pressure ratios of 2 and 5. Use $h_{PR} = 18{,}400$ Btu/lbm, $c_p = 0.24$ Btu/(lbm · °R), and $\gamma = 1.4$. Comment on your results. Compare these results to those for Problem SM5.2, and comment on the changes.

SM5.6 Use the PARA computer program to determine and plot the thrust specific fuel consumption vs specific thrust for the turboprop engine of Example SM5.2 over the same range of compressor pressure ratios for turbine temperature ratios of 0.8, 0.7, 0.6, 0.5, 0.4, and optimum.

SM5.7 Use the PARA computer program to determine and plot the thrust specific fuel consumption vs specific thrust for the turboprop engine over the range of compressor pressure ratios from 2 to 40 at $T_0 = 425°$R, $M_0 = 0.65$, $\gamma = 1.4$, $c_p = 0.24$ Btu/(lbm · °R), $h_{PR} = 18{,}400$ Btu/lbm, $T_{t4} = 2460°$R, and $\eta_{\text{prop}} = 0.8$ for turbine temperature ratios of 0.8, 0.7, 0.6, 0.5, 0.4, and optimum.

SM5.8 Use the PARA computer program to determine and plot the power specific fuel consumption vs specific power for the turboshaft engine with regeneration over compressor pressure ratios of 4 to 18 at $T_0 = 290$ K, $M_0 = 0$, $\gamma = 1.4$, $c_p = 1.004$ kJ/(kg · K), $h_{PR} = 42{,}800$ kJ/kg, and $x = 1.02$ for combustor exit temperatures T_{t4} of 1300, 1400, 1500, and 1600 K.

SM5.9 Use the PARA computer program to determine and plot the power specific fuel consumption vs specific power for the turboshaft engine with regeneration of Example SM5.3 at $x = 1.02$ over the same range of compressor ratios for combustor exit temperatures T_{t4} of 2400, 2600, 2800, and 3000°R.

Gas Turbine Design Problems

5.D1 You are to determine the range of compressor pressure ratios and bypass ratios for ideal turbofan engines that best meet the design requirements for the hypothetical passenger aircraft, the HP-1.

Hand-Calculate Ideal Performance (HP-1 Aircraft). Using the parametric cycle analysis equations for an ideal turbofan engine with $T_{t4} = 1560$ K, hand-calculate the specific thrust and thrust specific fuel consumption for an ideal turbofan engine with a compressor pressure ratio of 36, fan pressure ratio of 1.8, and bypass ratio of 10 at the 0.83 Mach, 11-km-altitude cruise condition. Assume $\gamma = 1.4$, $c_p = 1.004$ kJ/(kg · K), and $h_{PR} = 42{,}800$ kJ/kg. Compare your answers to results from the parametric cycle analysis program PARA.

Computer-Calculated Ideal Performance (HP-1 Aircraft). For the 0.83 Mach, 11-km-altitude cruise condition, determine the performance available from turbofan engines. This part of the analysis is accomplished by using the PARA computer program with $T_{t4} = 1560$ K. Specifically, you are to vary the compressor pressure ratio from 20 to 40 in increments of 2. Fix the fan pressure ratio at your assigned value of ___. Evaluate bypass ratios of 4, 6, 8, 10, 12, and the optimum value. Assume $\gamma = 1.4$, $c_p = 1.004$ kJ/(kg · K), and $h_{PR} = 42{,}800$ kJ/kg.

Calculate Minimum Specific Thrust at Cruise (HP-1 Aircraft). You can calculate the minimum uninstalled specific thrust at cruise based on the following information:

1) The thrust of the two engines must be able to offset drag at 0.83 Mach and 11-km altitude and have enough excess thrust for P_s of 1.5 m/s. Determine the required installed thrust to attain the cruise condition using Eq. (1.28). Assuming $\phi_{\text{inlet}} + \phi_{\text{noz}} = 0.02$, determine the required uninstalled thrust.

2) Determine the maximum mass flow into the 2.2-m-diam inlet for the 0.83 Mach, 11-km-altitude flight condition, using the equation given in the background section for this design problem in Chapter 1.

3) Using the results of steps 1 and 2, calculate the minimum uninstalled specific thrust at cruise.

4) Perform steps 2 and 3 for inlet diameters of 2.5, 2.75, 3.0, 3.25, and 3.5 m.

Select Promising Engine Cycles (HP-1 Aircraft). Plot thrust specific fuel consumption vs specific thrust (thrust per unit mass flow) for the engines analyzed in the preceding. Plot a curve for each bypass ratio, and cross-plot the values of the compressor pressure ratio (see Fig. P5.D1). The result is a *carpet plot* (a multivariable plot) for the cruise condition. Now draw a dashed horizontal line on the carpet plot corresponding to the maximum allowable uninstalled thrust specific fuel consumption $S_{\max}$ for the cruise condition (determined in the Chapter 1 portion of this design problem). Draw a dashed vertical line for each minimum uninstalled specific thrust

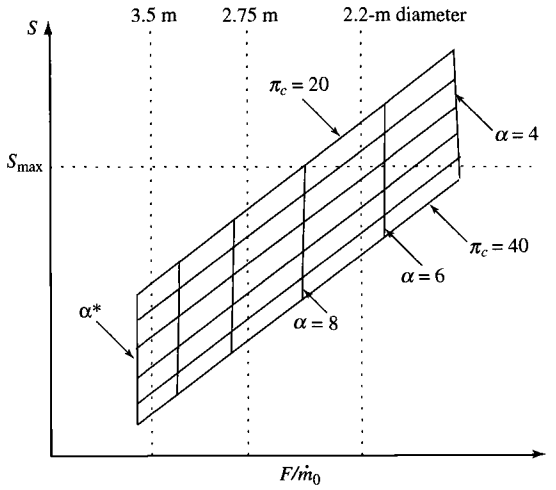

Fig. P5.D1 Example carpet plot for HP-1 aircraft engine.

determined in the preceding. Your carpet plots will look similar to the example shown in Fig. P5.D1. What ranges of bypass ratio and compressor pressure ratio look most promising?

5.D2 You are to determine the ranges of compressor pressure ratio and bypass ratio for ideal mixed-flow turbofan engines that best meet the design requirements for the hypothetical fighter aircraft, the HF-1.

Hand-Calculate Ideal Performance (HF-1 Aircraft). Using the parametric cycle analysis equations for an ideal mixed-flow turbofan engine with $T_{t4} = 3250°R$, hand-calculate the specific thrust and thrust-specific fuel consumption for an ideal turbofan engine with a compressor pressure ratio of 25 and bypass ratio of 0.5 at the 1.6 Mach, 40-kft-altitude supercruise condition. Assume $\gamma = 1.4$, $c_p = 0.24$ Btu/(lbm · °R), and $h_{PR} = 18{,}400$ Btu/lbm. Compare your answers to the results from the parametric cycle analysis program PARA.

Computer-Calculated Ideal Performance (HF-1 Aircraft). For the 1.6 Mach, 40-kft-altitude supercruise condition, determine the performance available from turbofan engines. This part of the analysis is accomplished by using the PARA computer program with $T_{t4} = 3250°R$. Specifically, you are to vary the bypass ratio from 0.1 to 1.0 in increments of 0.05. Evaluate compressor pressure ratios of 16, 18, 20, 22, 24, and 28. Assume $\gamma = 1.4$, $c_p = 0.24$ Btu/(lbm · °R), and $h_{PR} = 18{,}400$ Btu/lbm.

Calculate Minimum Specific Thrust at Cruise (HF-1 Aircraft). You can calculate the minimum uninstalled specific thrust at supercruise based on the following information:

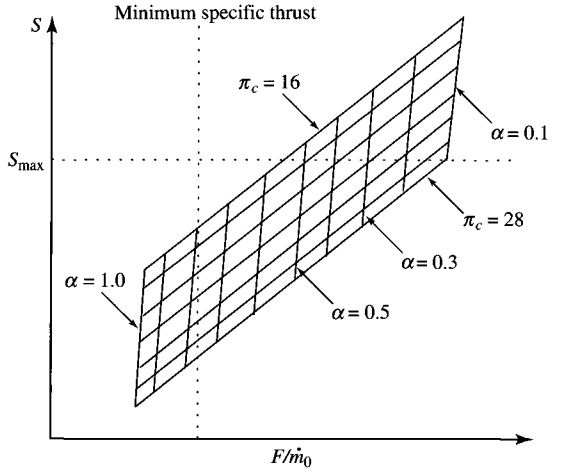

Fig. P5.D2 Example carpet plot for HF-1 aircraft engine.

1) The thrust of the two engines must be able to offset drag at 1.6 Mach, 40-kft altitude, and 92% of takeoff weight. Assuming $\phi_{inlet} + \phi_{noz} = 0.05$, determine the required uninstalled thrust for each engine.

2) The maximum mass flow into a 5-ft^2 inlet for the 1.6 Mach, 40-kft-altitude flight condition is $\dot{m} = \rho AV = \sigma\rho_{ref}AMa = (0.2471 - 0.07647)(5)\ (1.6 \times 0.8671 \times 1116) = 146.3$ lbm/s.

3) Using the results of steps 1 and 2, calculate the minimum uninstalled specific thrust at supercruise.

Select Promising Engine Cycles (HF-1 Aircraft). Plot the thrust specific fuel consumption vs specific thrust (thrust per unit mass flow) for the engines analyzed in the preceding. Plot a curve for each bypass ratio, and cross-plot the values of compressor pressure ratio (see Fig. P5.D2). The result is a carpet plot (a multivariable plot) for the supercruise condition. Now draw a dashed horizontal line on the carpet plot corresponding to the maximum allowable uninstalled thrust specific fuel consumption S_{max} for the cruise condition (determined in the Chapter 1 portion of this design problem). Draw a dashed vertical line for the minimum uninstalled specific thrust determined in the preceding section. Your carpet plots will look similar to the example shown in Fig. P5.D2. What ranges of bypass ratio and compressor pressure ratio look most promising?

Page is intentionally blank

6
Component Performance

6.1 Introduction

In Chapter 5, we idealized the engine components and assumed that the working fluid behaved as a perfect gas with constant specific heats. These idealizations and assumptions permitted the basic cycle analysis of several types of engines and the analysis of engine performance trends. In this chapter, we will develop the analytical tools that allow us to use realistic assumptions as to component losses and to include the variation of specific heats.

6.2 Variation in Gas Properties

The enthalpy h and specific heat at constant pressure c_p for air (modeled as a perfect gas) are functions of temperature. Also, the enthalpy h and specific heat at constant pressure c_p for a typical hydrocarbon fuel JP-8 and air combustion products (modeled as a perfect gas) are functions of temperature and the fuel/air ratio f. The variations of properties h and c_p for fuel/air combustion products vs temperature are presented in Figs. 6.1a and 6.1b, respectively. The ratio of specific heats γ for fuel/air combustion products is also a function of temperature and of fuel/air ratio. A plot of γ is shown in Fig. 6.2. These figures are based on Eq. (2.64) and the coefficients of Table 2.2. Note that both h and c_p increase and γ decreases with temperature and the fuel/air ratio. Our models of gas properties in the engines need to include changes in both c_p and γ across components where the changes are significant.

In Chapter 7, we will include the variation in c_p and γ through the engine. To simplify the algebra, we will consider c_p and γ to have constant representative values through all engine components except the burner (combustor). The values of c_p and γ will be allowed to change across the burner. Thus we will approximate c_p as c_{pc} (a constant for the engine upstream of the burner) and c_p as c_{pt} (a constant average value for the gases downstream of the burner). Likewise, γ will be γ_c upstream of the burner and γ_t downstream of the burner. The release of thermal energy in the combustion process affects the values of

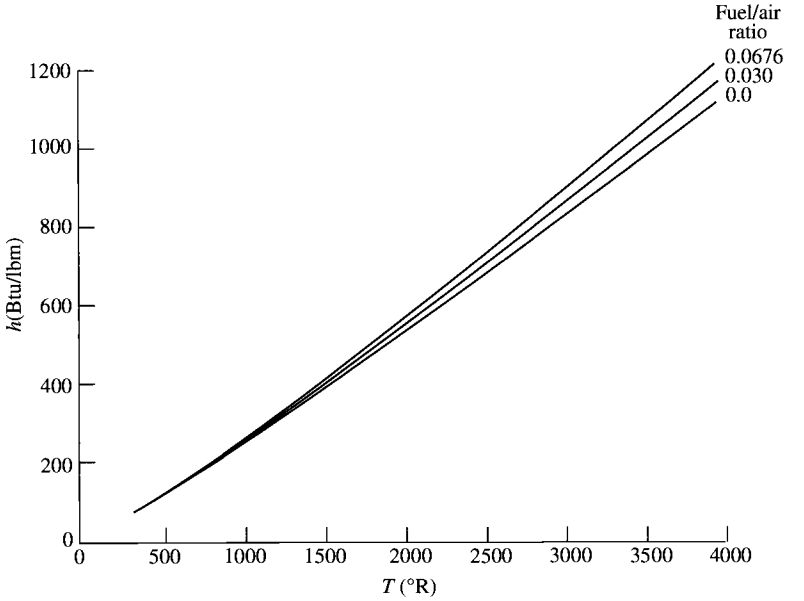

Fig. 6.1a Enthalpy vs temperature for JP-8 and air combustion products.

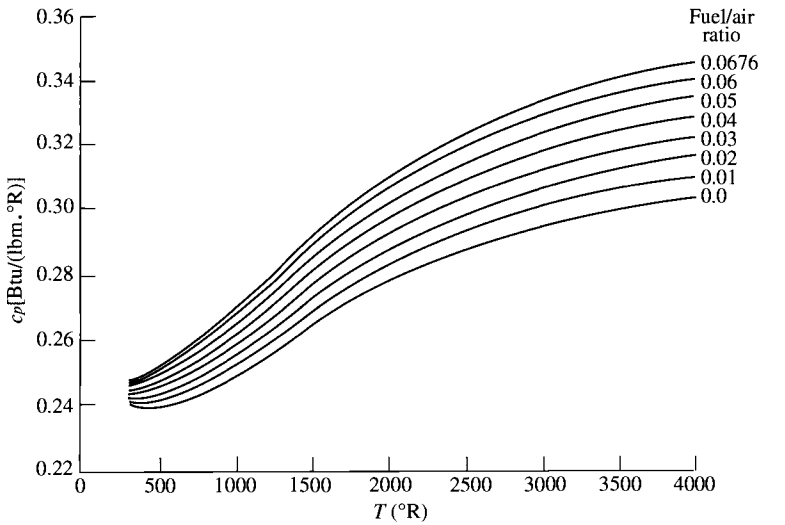

Fig. 6.1b Specific heat c_p vs temperature for JP-8 and air combustion products.

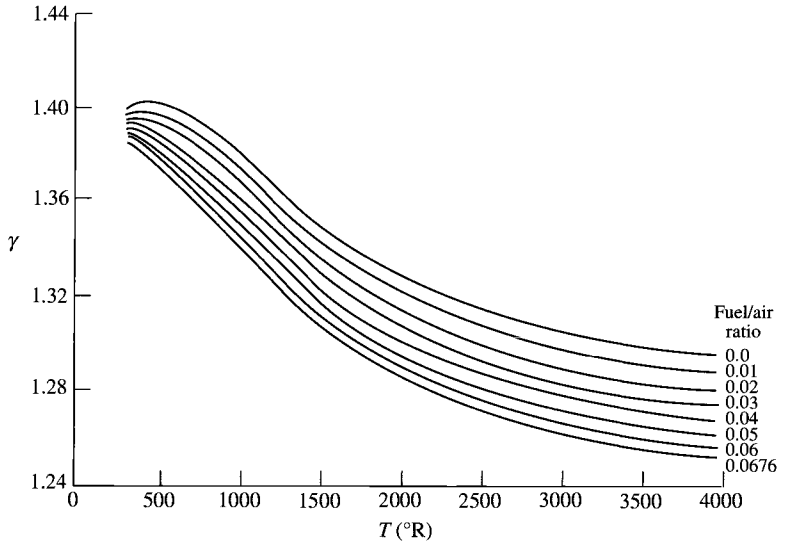

Fig. 6.2 Ratio of specific heats γ vs temperature for JP-8 and air combustion products.

c_{pt} and γ_t, but these two are related by

$$c_{pt} = \frac{\gamma_t}{\gamma_t - 1} R_t = \frac{\gamma_t}{\gamma_t - 1} \frac{\mathscr{R}_u}{\mathscr{M}} \tag{6.1}$$

where

$\mathscr{R}_u$ = universal gas constant
$\mathscr{M}$ = molecular weight

Thus if the chemical reaction causes the vibrational modes to be excited but does not cause appreciable dissociation, then the molecular weight $\mathscr{M}$ will be approximately constant. In this case, a reduction in γ is directly related to an increase in c_p by the formula

$$\frac{c_{pt}}{c_{pc}} = \frac{\gamma_t}{\gamma_t - 1} \frac{\gamma_c - 1}{\gamma_c} \tag{6.2}$$

6.3 Component Performance

In this chapter, each of the engine components will be characterized by *figures of merit* that model the component's performance and facilitate cycle analysis of real airbreathing engines. The total temperature ratio τ, the total pressure ratio π, and the interrelationship between τ and π will be used as much as possible in a component's figure of merit.

6.4 Inlet and Diffuser Pressure Recovery

Inlet losses arise because of the presence of wall friction and shock waves (in a supersonic inlet). Both wall friction and shock losses result in a reduction in total pressure so that $\pi_d < 1$. Inlets are adiabatic to a very high degree of approximation, and so we have $\tau_d = 1$. The inlet's figure of merit is defined simply as π_d.

The *isentropic efficiency* η_d of the diffuser is defined as (refer to Fig. 6.3)

$$\eta_d = \frac{h_{t2s} - h_0}{h_{t0} - h_0} \cong \frac{T_{t2s} - T_0}{T_{t0} - T_0} \tag{6.3}$$

This efficiency can be related to τ_r and π_d to give

$$\eta_d = \frac{\tau_{r(\pi_d)}^{(\gamma-1)/\gamma} - 1}{\tau_r - 1} \tag{6.4}$$

Figure 6.4 gives typical values of π_d for a subsonic inlet. The diffuser efficiency η_d was calculated from π_d by using Eq. (6.4).

In supersonic flight, the flow deceleration in inlets is accompanied by shock waves that can produce a total pressure loss much greater than, and in addition to, the wall friction loss. The inlet's overall pressure ratio is the product of the ram pressure ratio and the diffuser pressure ratio.

Because of shocks, only a portion of the ram total pressure can be recovered. We now define $\pi_{d\max}$ as that portion of π_d that is due to wall friction and define η_r as that portion of π_d due to ram recovery. Thus

$$\pi_d = \pi_{d\max}\eta_r \tag{6.5}$$

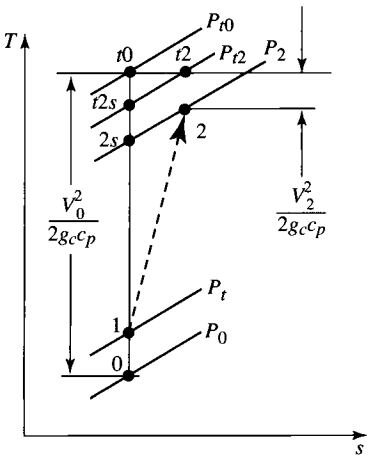

Fig. 6.3 Definition of inlet states.

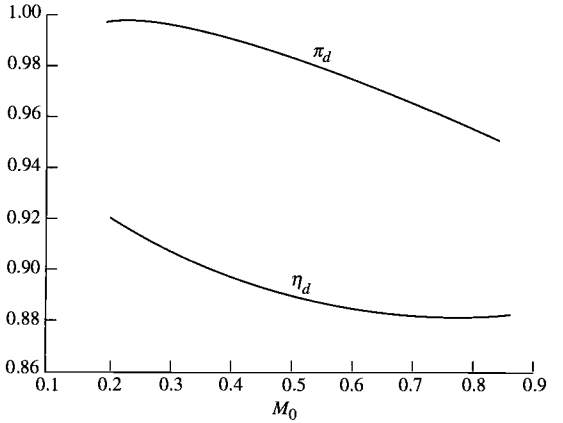

Fig. 6.4 Typical subsonic inlet π_d and η_d.

For subsonic and supersonic flow, a useful reference for the ram recovery η_r is Military Specification 5008B,[36] which is expressed as follows:

$$\eta_r = \begin{cases} 1 & M_0 \leq 1 \\ 1 - 0.075(M_0 - 1)^{1.35} & 1 < M_0 < 5 \\ \dfrac{800}{M_0^4 + 935} & 5 < M_0 \end{cases} \tag{6.6}$$

Because we often do not yet know the details of the inlet in cycle analysis, it is assumed that Military Specification 5008B applies as an ideal goal for ram recovery. The ram recovery of Military Specification 5008B is plotted in Fig. 6.5 vs M_0.

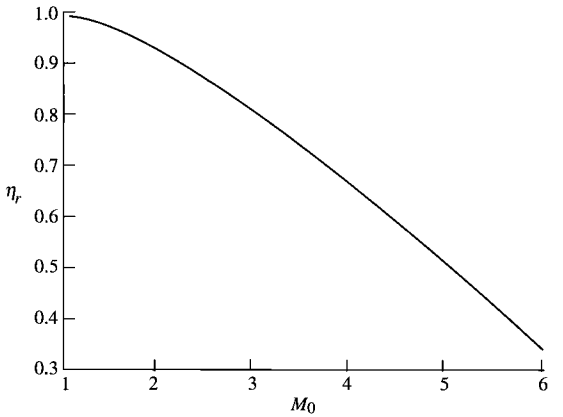

Fig. 6.5 Inlet total pressure recovery η_r of Military Specification 5008B.

6.5 Compressor and Turbine Efficiencies

6.5.1 Compressor Isentropic Efficiency

Compressors are, to a high degree of approximation, adiabatic. The overall efficiency used to measure a compressor's performance is the *isentropic efficiency* η_c, defined by

$$\eta_c = \frac{\text{ideal work of compression for given } \pi_c}{\text{actual work of compression for given } \pi_c} \tag{6.7}$$

Figure 6.6 shows both the ideal and actual compression processes for a given π_c on a T-s diagram. The actual work per unit mass w_c is $h_{t3} - h_{t2}$ $[=c_p\,(T_{t3} - T_{t2})]$, and the ideal work per unit mass w_{ct} is $h_{t3i} - h_{r2}$ $[=c_p(T_{t3i} - T_{t2})]$. Here, h_{t3i} is the ideal (isentropic) compressor leaving total enthalpy. Writing the isentropic efficiency of the compressor η_c in terms of the thermodynamic properties, we have

$$\eta_c = \frac{w_{ci}}{w_c} = \frac{h_{t3i} - h_{t2}}{h_{t3} - h_{t2}}$$

For a calorically perfect gas, we can write

$$\eta_c = \frac{w_{ci}}{w_c} = \frac{c_p(T_{t3\iota} - T_{t2})}{c_p(T_{t3} - T_{t2})} = \frac{\tau_{ci} - 1}{\tau_c - 1}$$

Here τ_{ci} is the ideal compressor temperature ratio that is related to the compressor pressure ratio π_c by the isentropic relationship

$$\tau_{ci} = \pi_{ci}^{(\gamma-1)/\gamma} = \pi_c^{(\gamma-1)/\gamma} \tag{6.8}$$

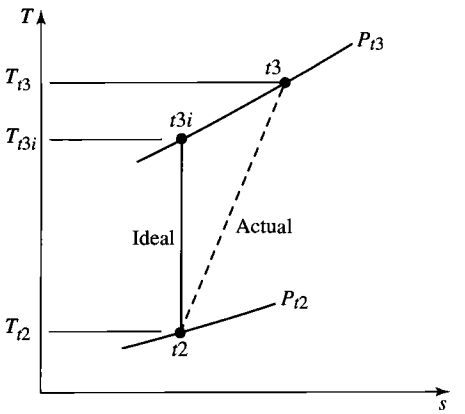

Fig. 6.6 Actual and ideal compressor processes.

Thus we have

$$\eta_c = \frac{\pi_c^{(\gamma-1)/\gamma} - 1}{\tau_c - 1} \tag{6.9}$$

6.5.2 Compressor Stage Efficiency

For a multistage compressor, each stage (set of rotor and stator) will have an isentropic efficiency. Let η_{sj} denote the isentropic efficiency of the jth stage. Likewise, π_{sj} and τ_{sj} represent the pressure ratio and temperature ratio, respectively, for the jth stage. From Eq. (6.9), we can write for the jth stage

$$\eta_{sj} = \frac{\pi_{sj}^{(\gamma-1)/\gamma} - 1}{\tau_{sj} - 1} \tag{6.10}$$

where $\tau_{sj} = T_{tj}/T_{tj-1}$ and $\pi_{sj} = P_{tj}/P_{tj-1}$.

Figure 6.7 shows the process for a multistage compressor. Here η_{sj} can be interpreted as the vertical height from A to B divided by the vertical height from A to C. For counting purposes, subscript 0 outside the parentheses is at the inlet, and subscript N is at the outlet of the compressor. Thus $(P_t)_0 = P_{t2}$, $(T_t)_0 = T_{t2}$, $P_{tN} = P_{tN} = P_3$, and $T_{TN} = T_{t3}$. From Eq. (6.9), we have for the overall compressor isentropic efficiency

$$\eta_c = \frac{(P_{t3}/P_{t2})^{(\gamma-1)/\gamma} - 1}{T_{t3}/T_{t2} - 1} = \frac{[P_{tN}/(P_t)_0]^{(\gamma-1)/\gamma} - 1}{T_{tN}/(T_t)_0 - 1} \tag{6.11}$$

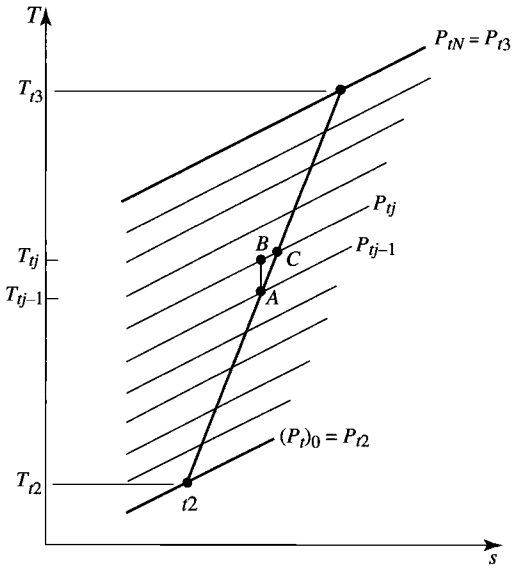

Fig. 6.7 Multistage compressor process and nomenclature.

From Eq. (6.10), we have

$$\frac{T_{tj}}{T_{tj-1}} = 1 + \frac{1}{\eta_{sj}}\left[\left(\frac{P_{tj}}{P_{tj-1}}\right)^{(\gamma-1)/\gamma} - 1\right]$$

and so

$$\frac{T_{tN}}{(T_t)_0} = \prod_{j=1}^{N}\left\{1 + \frac{1}{\eta_{sj}}\left[\left(\frac{P_{tj}}{P_{tj-1}}\right)^{(\gamma-1)/\gamma} - 1\right]\right\}$$

where $\prod$ means product. We note also the requirement that

$$\frac{P_{tN}}{(P_t)_0} = \prod_{j=1}^{N}\frac{P_{tj}}{P_{tj-1}}$$

where

$$\frac{P_{tN}}{(P_t)_0} \equiv \pi_c$$

Thus Eq. (6.11) becomes

$$\eta_c = \frac{[P_{tN}/(P_t)_0]^{(\gamma-1)/\gamma} - 1}{\prod_{j=1}^{N}\{1 + (1/\eta_{sj})[(P_{tj}/P_{tj-1})^{(\gamma-1)/\gamma} - 1]\} - 1} \tag{6.12}$$

We can see from Eq. (6.12) that the isentropic efficiency of a compressor is a function of the compressor pressure ratio, the pressure ratio of each stage, and the isentropic efficiency of each stage. This complex functional form makes the isentropic efficiency of the compressor undesirable for use in cycle analysis. We are looking for a simpler form of the figure of merit that will allow us to vary the compression ratio and still accurately predict the variation of η_c.

Let us consider the special case when each stage pressure ratio and each stage efficiency are the same. In this case

$$\pi_c = \prod_{j=1}^{N}\left(\frac{P_{tj}}{P_{tj-1}}\right) = \pi_s^N$$

Here η_s is the stage efficiency, and π_s is the stage pressure ratio. Also

$$\frac{T_{tj}}{T_{tj-1}} = 1 + \frac{1}{\eta_s}(\pi_s^{(\gamma-1)/\gamma} - 1)$$

and so

$$\frac{T_{tN}}{(T_t)_0} \equiv \tau_c = \left[1 + \frac{1}{\eta_s}(\pi_s^{(\gamma-1)/\gamma} - 1)\right]^N$$

or

$$\tau_c = \left[1 + \frac{1}{\eta_s}(\pi_c^{(\gamma-1)/(\gamma N)} - 1)\right]^N$$

and

$$\eta_c = \frac{\pi_c^{(\gamma-1)/\gamma} - 1}{[1 + (1/\eta_s)(\pi_c^{(\gamma-1)/(\gamma N)} - 1)]^N - 1} = \frac{\pi_s^{N(\gamma-1)/\gamma} - 1}{[1 + (1/\eta_s)(\pi_s^{(\gamma-1)/\gamma} - 1)]^N - 1} \tag{6.13}$$

Note: This is a relationship connecting η_c with η_s for an N-stage compressor with equal stage pressure ratios and equal stage efficiencies.

6.5.3 Compressor Polytropic Efficiency

The *polytropic efficiency* e_c is related to the preceding efficiencies and is defined as

$$e_c = \frac{\text{ideal work of compression for a differential pressure change}}{\text{actual work of compression for a differential pressure change}}$$

Thus

$$e_c = \frac{dw_i}{dw} = \frac{dh_{ti}}{dh_t} = \frac{dT_{ti}}{dT_t}$$

Note that for an ideal compressor, the isentropic relationship gives $T_{ti} = P_{ti}^{(\gamma-1)/\gamma} \times$ constant. Thus

$$\frac{dT_{ti}}{T_t} = \frac{\gamma - 1}{\gamma}\frac{dP_t}{P_t}$$

and

$$e_c = \frac{dT_{ti}}{dT_t} = \frac{dT_{ti}/T_t}{dT_t/T_t} = \frac{\gamma - 1}{\gamma}\frac{dP_t/P_t}{dT_t/T_t}$$

Assuming that the polytropic efficiency e_c is constant, we can obtain a simple relationship between τ_c and π_c as follows:

1) Rewrite the preceding equation as

$$\frac{dT_t}{T_t} = \frac{\gamma - 1}{\gamma e_c}\frac{dP_t}{P_t}$$

2) Integration between states $t2$ and $t3$ gives

$$\ell n \frac{T_{t3}}{T_{t2}} = \frac{\gamma - 1}{\gamma e_c} \ell n \frac{P_{t3}}{P_{t2}}$$

or

$$\tau_c = \pi_c^{(\gamma-1)/(\gamma e_c)} \tag{6.14}$$

For a state-of-the-art design, the polytropic efficiency is essentially constant. Substitution of Eq. (6.14) into Eq. (6.9) gives

$$\eta_c = \frac{\pi_c^{(\gamma-1)/\gamma} - 1}{\tau_c - 1} = \frac{\pi_c^{(\gamma-1)/\gamma} - 1}{\pi_c^{(\gamma-1)/(\gamma e_c)} - 1} \tag{6.15}$$

Equation (6.15) accurately predicts the relationship between the isentropic efficiency of a compressor and the compressor ratio for a given state-of-the-art polytropic efficiency. This relationship is plotted in Fig. 6.8 for a given value of e_c.

We will use the polytropic efficiency e_c as the figure of merit for the compressor. Equations (6.14) and (6.15) will be used to obtain the total temperature ratio and isentropic efficiency of the compressor, respectively, in the cycle analysis.

6.5.4 Relationship Between Compressor Efficiencies

We have, from Eqs. (6.13) and (6.15), relationships connecting η_c, η_s, and e_c. In this section, we wish to see if η_s formally approaches e_c as we let the number of stages get very large and the pressure ratio per stage get very small. To do this, first we note the relationship

$$1 - x^{1/N} = \frac{y}{N}$$

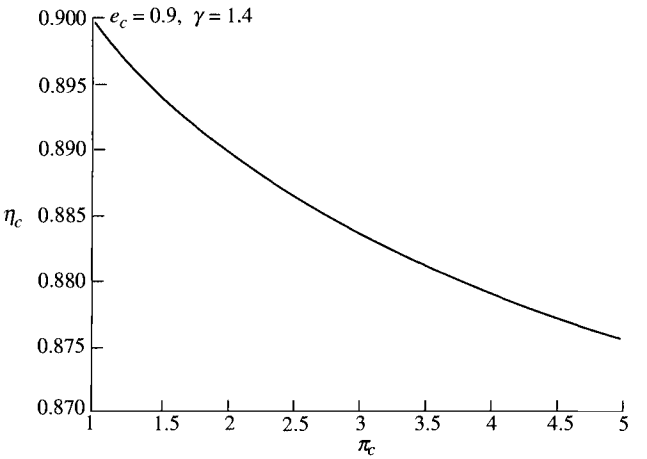

Fig. 6.8 Isentropic efficiency vs compressor pressure ratio for constant polytropic efficiency of 0.9.

then

$$x = \left(1 - \frac{y}{N}\right)^N$$

This may be expanded by the binomial expansion to give

$$x = \left(1 - \frac{y}{N}\right)^N = 1 + N\left(\frac{-y}{N}\right) + \frac{N(N-1)}{1 \cdot 2}\left(\frac{-y}{N}\right)^2 + \cdots \tag{i}$$

If N is very large, this becomes

$$x = 1 - y + \frac{y^2}{2!} - \frac{y^3}{3!} + \cdots = \exp(-y)$$

or

$$y = -\ell n\, x \tag{ii}$$

With these basic relationships established, we now write portions of Eq. (6.13) in the form given in Eq. (i). We consider

$$\left[1 + \frac{1}{\eta_s}(\pi_c^{(\gamma-1)/(\gamma N)} - 1)\right]^N \equiv \left[1 - \frac{1}{\eta_s}(1 - \pi_c^{(\gamma-1)(\gamma N)})\right]^N$$

Then

$$\frac{y}{N} = 1 - \pi_c^{(\gamma-1)/(\gamma N)} = 1 - x^{1/N}$$

where

$$x = \pi_c^{(\gamma-1)/\gamma}$$

Thus for N large, we approach

$$1 - \pi_c^{(\gamma-1)/(\gamma N)} \to \frac{y}{N} = -\frac{1}{N}\,\ell n\, x = -\frac{1}{N}\,\ell n\, \pi_c^{(\gamma-1)/\gamma}$$

Then

$$\left[1 - \frac{1}{\eta_s}(1 - \pi_c^{(\gamma-1)/(\gamma N)})\right]^N \to \left(1 + \frac{1}{\eta_s}\frac{1}{N}\ell n\, \pi_c^{(\gamma-1)/\gamma}\right)^N$$

$$= \left(1 + \frac{1}{N}\ell n\, \pi_c^{(\gamma-1)/(\gamma\eta_s)}\right)^N$$

However, as earlier, the expansion for $(1 - z/N)^N$ for large N is just e^{-z}. Here we let

$$z = -\ell n\, \pi_c^{(\gamma-1)/(\gamma N)}$$

and thus

$$e^{-z} = \pi_c^{(\gamma-1)/(\gamma N)}$$

Hence for large N

$$\left[1 - \frac{1}{\eta_s}(1 - \pi_c^{(\gamma-1)/(\gamma N)})\right]^N \to \pi_c^{(\gamma-1)/(\gamma\eta_s)}$$

Thus

$$\eta_c = \frac{\pi_c^{(\gamma-1)/\gamma} - 1}{\pi_c^{(\gamma-1)/(\gamma\eta_s)} - 1} \tag{6.16}$$

for a multistage machine. This expression is identical to Eq. (6.15) with e_c replaced by η_s. Thus for very large N, η_s approaches e_c.

Example 6.1

Say we plan to construct a 16-stage compressor, with each stage pressure ratio the same, given $\pi_c = 25$. Then we have $\pi_s = 25^{1/16} = 1.223$. Say η_s is measured at 0.93. Then, with Eq. (6.14) solved for e_c, we have

$$e_c = \frac{(\gamma - 1)/\gamma \, \ell n \, \pi_s}{\ell n[1 + (1/\eta_s)(\pi_s^{(\gamma-1)/\gamma} - 1)]}$$

$$= 0.9320 \tag{6.17}$$

Then we get two estimates for η_c, one based on constant η_s and another based on constant e_c. From Eq. (6.13), with $\pi_s = 1.223$, we obtain

$$\eta_c = \frac{\pi_c^{(\gamma-1)/\gamma} - 1}{[1 + (1/\eta_s)(\pi_s^{(\gamma-1)/\gamma} - 1)]^N - 1}$$

$$= \frac{25^{1/3.5} - 1}{[1 + (1/0.93)(1.223^{1/3.5} - 1)]^{16} - 1}$$

$$= 0.8965^-$$

From Eq. (6.15) we find, for comparison,

$$\eta_c = \frac{\pi_c^{(\gamma-1)/\gamma} - 1}{\pi_c^{(\gamma-1)/(\gamma e_c)} - 1} = 0.8965^+$$

More simply, if $e_c = \eta_s = 0.93$, then by either Eq. (6.15) or Eq. (6.16), we get $\eta_c = 0.8965$.

The point of all of this is that for a multistage machine, the simplicity and accuracy of using the polytropic efficiency make it a useful concept. Thus from now on we will use Eq. (6.15) to compute the compressor efficiency.

6.5.5 Compressor Stage Pressure Ratio

For a multistage compressor, the energy added is divided somewhat evenly per stage, and each stage increases the total temperature of the flow about the same amount. The total temperature ratio of a stage τ_s that has a total temperature change of ΔT_t can be written as

$$\tau_s = 1 + \frac{\Delta T_t}{T_{ti}}$$

Using the polytropic efficiency e_c to relate the stage pressure ratio π_s to its temperature ratio τ_s, we have

$$\pi_s = (\tau_s)^{(\gamma e_c)/(\gamma-1)} = \left(1 + \frac{\Delta T_t}{T_{ti}}\right)^{(\gamma e_c)/(\gamma-1)}$$

This equation gives the variation of the compressor stage pressure ratio with stage inlet temperature T_{ti} and total temperature change ΔT_t. This equation shows the decrease in stage pressure ratio with increases in stage inlet temperature for stages with the same total temperature change.

Stage pressure ratio results for $\gamma = 1.4$ and $e_c = 0.9$ are plotted in Fig. 6.9 vs $\Delta T_t/T_{ti}$. By using this figure, a 30 K change with 300 K inlet temperature gives a stage pressure ratio of about 1.35. Likewise, a 60°R change with 1000°R inlet temperature gives a stage pressure ratio of about 1.20. Figure 6.9 helps explain the change in stage pressure ratio through a compressor.

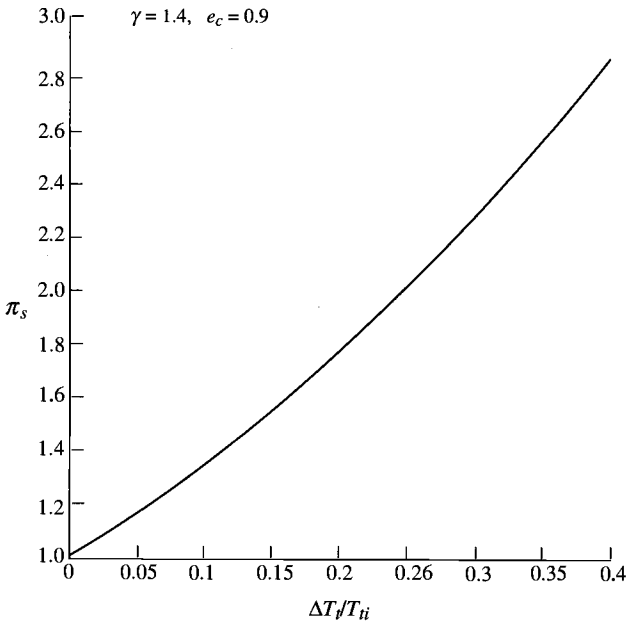

Fig. 6.9 Variation of compressor stage pressure ratio.

6.5.6 Turbine Isentropic Efficiency

Modern turbines are cooled by air taken from the compressors, passed through vanes and rotors, and then remixed with the main flow. From the point of view of the overall flow, the flow is adiabatic; but to be correct, a multiple-stream analysis would have to be applied. Such an analysis is straightforward conceptually, but it is difficult to estimate the various mixing losses, etc., that occur. The concept of isentropic efficiency is still utilized in most such analyses (for the mainstream portion of the flow), and in any case, the isentropic efficiency gives a reasonable approximation to the turbine performance when cooling flow rates are small. Hence, in this text, we consider only the adiabatic case.

In analogy to the compressor isentropic efficiency, we define the *isentropic efficiency* of the turbine by

$$\eta_t = \frac{\text{actual turbine work for a given } \pi_t}{\text{ideal turbine work for a given } \pi_t}$$

The actual and ideal expansion processes for a given π_t are shown in Fig. 6.10 on a T-s diagram. The actual turbine work per unit mass is $h_{t4} - h_{t5}$ $[=c_p(T_{t4} - T_{t5})]$, and the ideal turbine work per unit mass is $h_{t4} - h_{t5i}$ $[=c_p(T_{t4} - T_{t5i})]$. Here, T_{t5i} is the ideal turbine leaving total temperature. Writing the isentropic efficiency of the turbine in terms of the thermodynamic properties, we have

$$\eta_t = \frac{h_{t4} - h_{t5}}{h_{t4} - h_{t5i}} = \frac{T_{t4} - T_{t5}}{T_{t4} - T_{t5i}}$$

or

$$\eta_t = \frac{1 - \tau_t}{1 - \pi_t^{(\gamma-1)/\gamma}} \tag{6.18}$$

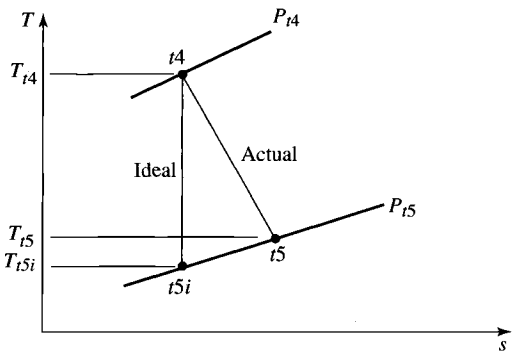

Fig. 6.10 Actual and ideal turbine processes.

6.5.7 Turbine Stage Efficiency

In a completely similar analysis to that for the compressor, the turbine isentropic efficiency can be written in terms of η_{sj} and π_{sj}:

$$\eta_t = \frac{1 - \prod_{j=1}^{N} [1 - \eta_{sj}(1 - \pi_{sj}^{(\gamma-1)/\gamma})]}{1 - \pi_t^{(\gamma-1)/\gamma}} \tag{6.19}$$

When all stages have the same π_s and η_s, the preceding equation reduces to

$$\eta_t = \frac{1 - [1 - \eta_s(1 - \pi_s^{(\gamma-1)/\gamma})]^N}{1 - \pi_t^{(\gamma-1)/\gamma}} \tag{6.20}$$

6.5.8 Turbine Polytropic Efficiency

The *polytropic turbine efficiency* e_t is defined similarly to the turbine isentropic efficiency as

$$e_t = \frac{\text{actual turbine work for a differential pressure change}}{\text{ideal turbine work for a differential pressure change}}$$

Thus

$$e_t = \frac{dw}{dw_i} = \frac{dh_t}{dh_{ti}} = \frac{dT_t}{dT_{ti}}$$

For the isentropic relationship, we have

$$\frac{dT_{ti}}{T_t} = \frac{\gamma - 1}{\gamma} \frac{dP_t}{P_t}$$

Thus

$$e_t = \frac{dT_t}{dT_{ti}} = \frac{dT_t/T_t}{dT_{ti}/T_t} = \frac{dT_t/T_t}{[(\gamma - 1)/\gamma]\, dP_t/P_t}$$

Assuming that the polytropic efficiency e_t is constant over the pressure ratio, we integrate the preceding equation to give

$$\pi_t = \tau_t^{\gamma/[(\gamma-1)e_t]} \tag{6.21}$$

and so

$$\eta_t = \frac{1 - \tau_t}{1 - \tau_t^{1/e_t}} \tag{6.22}$$

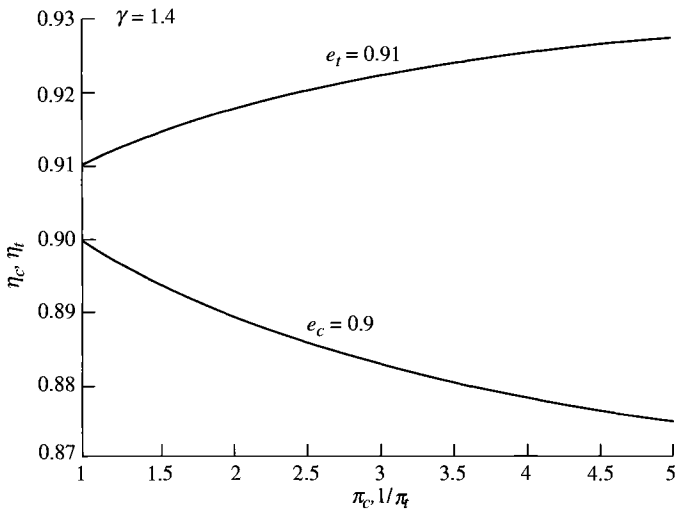

Fig. 6.11 Compressor and turbine efficiencies vs pressure ratio.

or

$$\eta_t = \frac{1 - \pi_t^{(\gamma-1)e_t/\gamma}}{1 - \pi_t^{(\gamma-1)/\gamma}} \tag{6.23}$$

This relationship is plotted in Fig. 6.11 along with Eq. (6.15) for the compressor. Note that the turbine efficiency increases with the turbine expression ratio $1/\pi_t$ for a constant e_t.

In cycle analysis, τ_t is usually first obtained from the work balance. Then π_t can be calculated for a known e_t by using Eq. (6.21), and η_t can be calculated by using either Eq. (6.22) or Eq. (6.23). We will use the polytropic efficiency e_t as the figure of merit for the turbine.

6.6 Burner Efficiency and Pressure Loss

In the burner, we are concerned with two efforts: incomplete combustion of the fuel and total pressure loss. *Combustion efficiency* η_b is defined by

$$\eta_b = \frac{(\dot{m} + \dot{m}_f)h_{t4} - \dot{m}h_{t3}}{\dot{m}_f h_{PR}} = \frac{(\dot{m} + \dot{m}_f)c_{p4}T_{t4} - \dot{m}c_{p3}T_{t3}}{\dot{m}_f h_{PR}}$$

We can approximate c_{p3} as c_{pc} (a constant for the engine upstream of the burner) and c_{p4} as c_{pt} (a constant average value for the gases downstream of the burner). Thus the combustion efficiency is

$$\eta_b = \frac{(\dot{m} + \dot{m}_f)c_{pt}T_{t4} - \dot{m}c_{pc}T_{t3}}{\dot{m}_f h_{PR}} \tag{6.24}$$

The total pressure losses arise from two effects: the viscous losses in the combustion chamber and the total pressure loss due to combustion at finite Mach number. These effects are combined for the purpose of performance analysis in

$$\pi_b = \frac{P_{t4}}{P_{t3}} < 1$$

We will use both η_b and π_b as the figures of merit for the burner. There are similar combustion efficiencies and total pressure ratios for afterburners (augmenters) and duct burners.

6.7 Exhaust Nozzle Loss

The primary loss due to the nozzle has to do with the over- or underexpansion of the nozzle. In addition, there will be a loss in total pressure from turbine to exit. Thus we may have

$$P_9 \neq P_0 \qquad \text{and} \qquad \pi_n = \frac{P_{t9}}{P_{t8}} < 1$$

We still have $\tau_n = 1$, because the nozzle is very nearly adiabatic. We will use π_n as the figure of merit for the nozzle.

6.8 Mechanical Efficiency of Power Shaft

We define the mechanical efficiency of a shaft to account for the loss or extraction of power on that shaft. The mechanical efficiency η_m is defined as the ratio of the power leaving the shaft that enters the compressor, $\dot{W}_c$, to the power entering the shaft from the turbine, $\dot{W}_t$. This can be written in equation form as

$$\eta_m = \frac{\text{power leaving shaft to compressor}}{\text{power entering shaft from turbine}} = \frac{\dot{W}_c}{\dot{W}_t}$$

The mechanical efficiency η_m is less than one due to losses in power that occur from shaft bearings and power extraction for driving engine acessories like oil and fuel pumps. For multishaft engines, each shaft will have a mechanical efficiency associated with the power transfer on the shaft.

6.9 Summary of Component Figures of Merit (Constant c_p Values)

Table 6.1 summarizes the ideal and actual behaviors of gas turbine engine components with calorically perfect gases. Note that for a compressor with constant polytropic efficiency, the isentropic efficiency follows from Eq. (6.15). We will use these figures of merit in the following chapter.

At a particular level of technological development, the polytropic efficiency e_c for the compressor can be considered to be a constant, and thus the compressor pressure ratio π_c determines the compressor efficiency η_c [see Eq. (6.16)]. Similarly, the polytropic efficiency e_t for the turbine can be considered to be a

Table 6.1 Summary of component figures of merit (constant c_p values)

Component	Ideal behavior	Actual behavior	Figure of merit
Inlet	Adiabatic and reversible (isentropic)	Adiabatic, not reversible	
	$\tau_d = 1,\ \pi_d = 1$	$\tau_d = 1,\ \pi_d < 1$	π_d
Compressor	Adiabatic and reversible (isentropic)	Adiabatic, not reversible	
	$w_c = c_p T_{t2}(\tau_c - 1)$	$w_c = c_{pc} T_{t2}(\tau_c - 1)$	
	$\pi_c = \tau_c^{\gamma/(\gamma-1)}$	$\pi_c = [1 + \eta_c(\tau_c - 1)]^{\gamma_c/(\gamma_c-1)}$	η_c
		$\tau_c = 1 + \frac{1}{\eta_c}(\pi_c^{(\gamma_c-1)/\gamma_c} - 1)$	
		$\tau_c = (\pi_c)^{(\gamma_c-1)/(\gamma_c e_c)}$	e_c
Burner	No total pressure loss, 100% combustion	Total pressure loss, combustion $<100\%$	
	$\pi_b = 1$	$\pi_b < 1$	π_b
	$\dot{m}c_p T_{t4} - \dot{m}c_p T_{t3} = \dot{m}_f h_{PR}$	$(\dot{m} + \dot{m}_f)c_{pt} T_{t4} - \dot{m}c_{pc} T_{t3}$ $= \eta_b \dot{m}_f h_{PR}$	η_b
Turbine	Adiabatic and reversible (isentropic)	Adiabatic, not reversible	
	$w_t = c_p T_{t4}(1 - \tau_t)$	$w_t = c_{pt} T_{t4}(1 - \tau_t)$	
	$\pi_t = \tau_t^{\gamma/(\gamma-1)}$	$\pi_t = [1 - \frac{1}{\eta_t}(1 - \tau_t)]^{\gamma_t/(\gamma_t-1)}$	η_t
		$\tau_t = 1 - \eta_t(1 - \pi_t^{(\gamma_t-1)/\gamma_t})$	
		$\pi_t = \tau_t^{\gamma_t/[(\gamma_t-1)e_t]}$	e_t
Nozzle	Adiabatic and reversible	Adiabatic, not reversible	
	$\tau_n = 1,\ \pi_n = 1$	$\tau_n = 1,\ \pi_n < 1$	π_n

constant, and thus the turbine temperature ratio τ_t determines the turbine efficiency η_t [see Eq. (6.22)]. For the analysis in the following chapter, we will use the polytropic efficiencies as input data and will calculate the resulting component efficiencies.

The values of these figures of merit have changed as technology has improved over the years. In addition, the values of the figures of merit for the diffuser and nozzle depend on the application. For example, a commercial airliner with engine nacelles and convergent, fixed-area exhaust nozzles will typically have much higher values of π_d and π_n than a supersonic fighter with its engines in the airframe and convergent-divergent, variable-area exhaust nozzles. Table 6.2 lists typical values for the figures of merit that correspond to different periods in the evolution of engine technology (called *levels of technology*) and the application.

Table 6.2 Component efficiencies, total pressure ratios, and temperature limits

Component	Figure of merit	Type[a]	Level of technology[b] 1	2	3	4
Diffuser	$\pi_{d\max}$	A	0.90	0.95	0.98	0.995
		B	0.88	0.93	0.96	0.98
		C	0.85	0.90	0.94	0.96
Compressor	e_c		0.80	0.84	0.88	0.90
Fan	e_f		0.78	0.82	0.86	0.89
Burner	π_b		0.90	0.92	0.94	0.95
	η_b		0.88	0.94	0.99	0.999
Turbine	e_t	Uncooled	0.80	0.85	0.89	0.90
		Cooled		0.83	0.87	0.89
Afterburner	π_{AB}		0.90	0.92	0.94	0.95
	η_{AB}		0.85	0.91	0.96	0.99
Nozzle		D	0.95	0.97	0.98	0.995
	π_n	E	0.93	0.96	0.97	0.98
		F	0.90	0.93	0.95	0.97
Mechanical shaft	η_m	Shaft only	0.95	0.97	0.99	0.995
		With power takeoff	0.90	0.92	0.95	0.97
Maximum T_{t4}		(K)	1110	1390	1780	2000
		(R)	2000	2500	3200	3600
Maximum T_{t7}		(K)	1390	1670	2000	2220
		(R)	2500	3000	3600	4000

[a]A = subsonic aircraft with engines in nacelles D = fixed-area convergent nozzle
B = subsonic aircraft with engine(s) in airframe E = variable-area convergent nozzle
C = supersonic aircraft with engine(s) in airframe F = variable-area convergent-divergent nozzle
[b]Notes: Stealth may reduce $\pi_{d\max}$, π_{AB}, and π_n. The levels of technology can be thought of as representing the technical capability for 20-yr increments in time beginning in 1945. Thus level 3 of technology presents typical component design values for the time period 1985–2005.

6.10 Component Performance with Variable c_p

In Section 2.6.6 of Chapter 2, we developed the relationships [Eqs. (2.53), (2.54), and (2.57)] for the thermodynamic properties h, ϕ, and s of a perfect gas with variable specific heat. In addition, the reduced pressure P_r and reduced volume v_r were defined by Eqs. (2.55) and (2.56), respectively. We will use these properties to describe the performance of engine components when the variation of specific heat is to be included. We will use Appendix D or the computer program AFPROP to obtain the thermodynamic properties.

The notation π_a [see Eq. (5.3)] represents a component's total pressure ratio. However, we will use a modified definition for τ_a to represent the ratio of total

enthalpies [see original definition given by Eq. (5.4)]. Thus

$$\tau_a = \frac{\text{total enthalpy leaving component } a}{\text{total enthalpy entering component } a} \tag{6.25}$$

6.10.1 Freestream Properties

From the definition of the total enthalpy and total pressure, we can write

$$\tau_r = \frac{h_{t0}}{h_0} = \frac{h_0 + V_0^2/(2g_c)}{h_0} \qquad \text{and} \qquad \pi_r = \frac{P_{r0}}{P_0} = \frac{P_{rt0}}{P_{r0}} \tag{6.26}$$

6.10.2 Inlet

Because the inlet is assumed to be adiabatic, then

$$\tau_d = \frac{h_{t2}}{h_{t0}} = 1 \tag{6.27}$$

By using Eq. (2.57), the inlet total pressure ratio can be expressed in terms of the entropy change as follows:

$$\pi_d = \frac{P_{t2}}{P_{r0}} - \exp\left(-\frac{s_2 - s_0}{R}\right) \tag{6.28}$$

6.10.3 Compressor

The variable τ_c represents the total enthalpy ratio of the compressor, and π_c represents its total pressure ratio, or

$$\tau_c = \frac{h_{t3}}{h_{t2}} \qquad \text{and} \qquad \pi_c = \frac{P_{t3}}{P_{t2}} \tag{6.29}$$

The polytropic efficiency of the compressor e_c can be written as

$$e_c = \frac{\mathrm{d}h_{ti}}{\mathrm{d}h_t} = \frac{\mathrm{d}h_{ti}/T_t}{\mathrm{d}h_t/T_t}$$

By using the Gibbs equation [Eq. (2.31)], the numerator in the preceding equation can be expressed as

$$\frac{\mathrm{d}h_{ti}}{T_t} = R\frac{\mathrm{d}P_t}{P_t}$$

Thus

$$e_c = R\frac{\mathrm{d}P_t/P_t}{\mathrm{d}h_t/T_t} \tag{6.30}$$

For a constant polytropic efficiency, integration of the preceding equation between states $t2$ and $t3$ gives

$$\phi_{t3} - \phi_{t2} = \frac{R}{e_c}\ell n\frac{P_{t3}}{P_{t2}}$$

Thus the compressor pressure ratio π_c can be written as

$$\pi_c = \frac{P_{t3}}{P_{t2}} = \exp\left(e_c \frac{\phi_{t3} - \phi_{t2}}{R}\right)$$

or

$$\pi_c = \left(\frac{P_{rt3}}{P_{rt2}}\right)^{e_c} \tag{6.31}$$

The reduced pressure at state $t2$ can be obtained from Appendix D or the computer program AFPROP, given the temperature at state $t2$. If the values of π_c and e_c are also known, one can get the reduced pressure at state $t3$ by using

$$P_{rt3} = P_{rt2}\pi_c^{1/e_c} \tag{6.32}$$

Given the reduced pressure at state $t3$, the total temperature and total enthalpy can be obtained from Appendix D or the computer program AFPROP.

The isentropic efficiency of a compressor can be expressed as

$$\eta_c = \frac{h_{t3i} - h_{t2}}{h_{t3} - h_{t2}} \tag{6.33}$$

This equation requires that the total enthalpy be known at states $t2$, $t3$, and $t3i$.

Example 6.2

Air at 1 atm and 540°R enters a compressor whose polytropic efficiency is 0.9. If the compressor pressure ratio is 15, determine the leaving total properties and compressor isentropic efficiency. From Appendix D for $f = 0$, we have

$$h_{t2} = 129.02\,\text{Btu/lbm} \qquad \text{and} \qquad P_{rt2} = 1.384$$

The exit total pressure is 15 atm. The reduced pressures at stations $t3$ and $t3i$ are

$$P_{rt3} = P_{rt2}\pi_c^{1/e_c} = 1.384 \times 15^{1/0.9} = 28.048$$
$$P_{rt3i} = P_{rt2}\pi_c = 1.384 \times 15 = 20.76$$

Linear interpolation of Appendix D, with $f = 0$ and using the preceding reduced pressures, gives the following values of total enthalpy and total temperature:

$$h_{t3} = 304.48\,\text{Btu/lbm} \qquad \text{and} \qquad T_{t3} = 1251.92°\text{R}$$
$$h_{t3i} = 297.67\,\text{Btu/lbm} \qquad \text{and} \qquad T_{t3i} = 1154.58°\text{R}$$

The compressor isentropic efficiency is

$$\eta_c = \frac{279.67 - 129.02}{304.48 - 129.02} = 0.8586$$

6.10.4 Burner

The τ_b represents the total enthalpy ratio of the burner, and π_b represents its total pressure ratio, or

$$\tau_b = \frac{h_{t4}}{h_{t3}} \qquad \text{and} \qquad \pi_b = \frac{P_{t4}}{P_{t3}} \tag{6.34}$$

From the definition of burner efficiency, we have

$$\eta_b = \frac{(\dot{m} + \dot{m}_f)h_{t4} - \dot{m}h_{t3}}{\dot{m}_f h_{PR}}$$

or

$$\eta_b = \frac{(1+f)h_{t4} - h_{t3}}{fh_{PR}} \tag{6.35}$$

where f is the ratio of the fuel flow rate to the airflow rate entering the burner, or $f = \dot{m}_f/\dot{m}$.

In the analysis of gas turbine engines, we determine the fuel/air ratio f and normally specify η_b, h_{PR}, and T_{t4}. The enthalpy at station t_3 (h_{t3}) will be known from analysis of the compressor. Equation (6.35) can be solved for the fuel/air ratio f, giving

$$f = \frac{h_{t4} - h_{t3}}{\eta_b h_{PR} - h_{t4}} \tag{6.36}$$

Note: The value of h_{t4} is a function of the fuel/air ratio f, and thus the solution of Eq. (6.36) is iterative.

6.10.5 Turbine

The τ_t represents the total enthalpy ratio of the turbine, and π_t represents its total pressure ratio or

$$\tau_t = \frac{h_{t5}}{h_{t4}} \qquad \text{and} \qquad \pi_t = \frac{P_{t5}}{P_{t4}} \tag{6.37}$$

The *polytropic efficiency of a turbine* is defined as

$$e_t = \frac{\mathrm{d}h_t}{\mathrm{d}h_{ti}}$$

which can be written as

$$e_t = \frac{1}{R}\frac{\mathrm{d}h_t/T_t}{\mathrm{d}P_t/P_t} \tag{6.38}$$

For constant polytropic efficiency, the following relationships are obtained by integration from state $t4$ to $t5$:

$$\pi_t = \frac{P_{t5}}{P_{t4}} = \exp\frac{\phi_{t5} - \phi_{t4}}{Re_t} \tag{6.39}$$

and

$$\pi_t = \left(\frac{P_{rt5}}{P_{rt4}}\right)^{1/e_t} \tag{6.40}$$

The *isentropic efficiency of the turbine* is defined as

$$\eta_t = \frac{h_{t4} - h_{t5}}{h_{t4} - h_{r5i}} \tag{6.41}$$

where each total enthalpy is a function of the total temperature T_t and fuel/air ratio f.

Example 6.3

Products of combustion ($f = 0.0338$) at 20 atm and 3000°R enter a turbine whose polytropic efficiency is 0.9. If the total enthalpy of the flow through the turbine decreases 100 Btu/lbm, determine the leaving total properties and turbine isentropic efficiency. From Appendix D for $f = 0.0338$, we have

$$h_{t4} = 828.75 \text{ Btu/lbm} \qquad \text{and} \qquad P_{rt4} = 1299.6$$

The exit total enthalpy is 728.75 Btu/lbm. From linear interpolation of Appendix D, the total temperature and reduced pressure at station $t5$ are

$$T_{t5} = 2677.52°\text{R} \qquad \text{and} \qquad P_{rt5} = 777.39$$

From Eq. (6.40), the turbine pressure ratio is

$$\pi_t = \left(\frac{P_{rt5}}{P_{rt4}}\right)^{1/e_t} = \left(\frac{777.39}{1299.6}\right)^{1/0.9} = 0.5650$$

and the reduced pressure at state $t5i$ is

$$P_{rt5i} = P_{rt4}\pi_t = 1299.6 \times 0.5650 = 734.3$$

Linear interpolation of Appendix D, with $f = 0.0338$ and using the preceding reduced pressure, gives the following values of total enthalpy and total temperature for state $t5i$:

$$h_{t5\iota} = 718.34 \text{ Btu/lbm} \qquad \text{and} \qquad T_{t5\iota} = 2643.64°\text{R}$$

The turbine isentropic efficiency is

$$\eta_t = \frac{828.75 - 728.75}{828.75 - 718.34} = 0.9057$$

6.10.6 Nozzle

Because the nozzle is assumed to be adiabatic, then

$$\tau_n = \frac{h_{t9}}{h_{t8}} = 1 \tag{6.42}$$

By using Eq. (2.57), the inlet total pressure ratio can be expressed in terms of the entropy change as follows:

$$\pi_n = \frac{P_{t9}}{P_{t8}} = \exp\left(-\frac{s_9 - s_8}{R}\right) \tag{6.43}$$

The exit velocity is obtained from the difference between the total and static enthalpies as follows:

$$V_9 = \sqrt{2g_c(h_{t9} - h_9)} \tag{6.44}$$

where h_9 is obtained from the reduced pressure at state 9 (P_{r9}) given by

$$P_{r9} = \frac{P_{rt9}}{P_{t9}/P_9} \tag{6.45}$$

Problems

6.1 Calculate the total pressure recovery η_r, using Eq. (6.6), and the total pressure ratio across a normal shock in air for Mach numbers 1.25, 1.50, 1.75, and 2.0. How do they compare?

6.2 The isentropic efficiency for a diffuser with a calorically perfect gas can be written as

$$\eta_d = \frac{(P_{t2}/P_0)^{(\gamma-1)/\gamma} - 1}{T_{t0}/T_0 - 1}$$

Show that this equation can be rewritten in terms τ_r and π_d as

$$\eta_d = \frac{\tau_r \pi_d^{(\gamma-1)/\gamma} - 1}{\tau_r - 1}$$

6.3 Starting from Eqs. (6.14) and (6.21), show that the polytropic efficiency for the compressor and turbine can be expressed as

$$e_c = \frac{\gamma_c - 1}{\gamma_c}\frac{\ell n\, \pi_c}{\ell n\, \tau_c} \qquad e_t = \frac{\gamma_t}{\gamma_t - 1}\frac{\ell n\, \tau_t}{\ell n\, \pi_t}$$

6.4 A J-57B afterburning turbojet engine at maximum static power on a sea-level, standard day ($P_0 = 14.696$ psia, $T_0 = 518.7°$R, and $V_0 = 0$) has the data listed in Appendix B.

(a) Calculate the adiabatic and polytropic efficiencies of the low-pressure and high-pressure compressors. Assume $\gamma = 1.4$ for the low-pressure compressor and $\gamma = 1.39$ for the high-pressure compressor.
(b) Calculate the adiabatic and polytropic efficiencies of the turbine. Assume $\gamma = 1.33$.
(c) Calculate π_b, τ_b, π_{AB}, and τ_{AB}.

6.5 A J-57B afterburning turbojet engine had 167 lbm/s of air at 167 psia and 660°F enter the combustor (station 3) and products of combustion at 158 psia and 1570°F leave the combustor (station 4). If the fuel flow into the combustor was 8520 lbm/h, determine the combustor efficiency η_b, assuming $h_{PR} = 18{,}400$ Btu/lbm, $c_{pc} = 0.25$ Btu/(lbm · °R), and $c_{pt} = 0.26$ Btu/(lbm · °R).

6.6 A J-57B afterburning turbojet engine had 169.4 lbm/s of air at 36 psia and 1013°F enter the afterburner (station 6) and products of combustion at 31.9 psia and 2540°F leave the afterburner (station 7). If the fuel flow into the afterburner was 25,130 lbm/h, determine the afterburner efficiency η_{AB}, assuming $h_{PR} = 18{,}400$ Btu/lbm, $c_{pt} = 0.27$ Btu/(lbm · °R), and $c_{PAB} = 0.29$ Btu/(lbm · °R).

6.7 A JT9D high-bypass-ratio turbofan engine at maximum static power on a sea-level, standard day ($P_0 = 14.696$ psia, $T_0 = 518.7$°R, and $V_0 = 0$) has the data listed in Appendix B.
(a) Calculate the adiabatic and polytropic efficiencies of the fan. Assume $\gamma = 1.4$.
(b) Calculate the adiabatic and polytropic efficiencies of both the low-pressure and high-pressure compressors. Assume $\gamma = 1.4$ for the low-pressure compressor and $\gamma = 1.39$ for the high-pressure compressor.
(c) Calculate the adiabatic polytropic efficiencies of the turbine. Assume $\gamma = 1.35$.
(d) Calculate the power (horsepower and kilowatts) into the fan and compressors. Assume $Rg_c = 1716$ ft^2/(s^2 · °R) and the γ of parts b and c.
(e) Calculate the power (horsepower and kilowatts) from the turbine for a mass flow rate of 251 lbm/s. Assume $\gamma = 1.31$ and $Rg_c = 1716$ ft^2/(s^2 · °R).
(f) How do the results of parts d and e compare?

6.8 The isentropic efficiency for a nozzle η_n is defined as

$$\eta_n = \frac{h_{t7} - h_9}{h_{t7} - h_{9s}}$$

where the states $t7$, 9, and $9s$ are shown in Fig. P6.1. For $P_9 = P_0$, show that the isentropic efficiency for the nozzle in a turbojet engine can be written

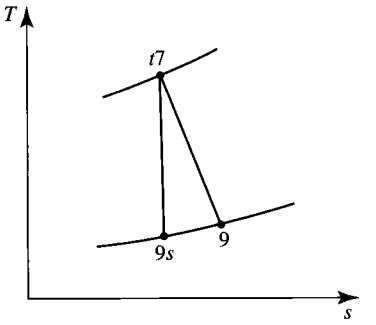

Fig. P6.1

for a calorically perfect gas as

$$\eta_n = \frac{\text{PIT}^{(\gamma-1)/\gamma} - 1}{\text{PIT}^{(\gamma-1)/\gamma} - (\pi_n)^{(\gamma-1)/\gamma}}$$

where $\text{PIT} = \pi_r \pi_d \pi_c \pi_b \pi_t \pi_n$.

6.9 Repeat Problem 6.4 with variable gas properties, using Appendix D or program AFPROP. Compare your results to those of Problem 6.4.

6.10 Repeat Problem 6.5 with variable gas properties, using Appendix D or program AFPROP. Compare your results to those of Problem 6.5.

6.11 Repeat Problem 6.6 with variable gas properties, using Appendix D or program AFPROP. Compare your results to those of Problem 6.6.

6.12 A JT9D high-bypass-ratio turbofan engine at maximum static power on a sea-level, standard day ($P_0 = 14.696$ psia, $T_0 = 518.7°\text{R}$, and $V_0 = 0$) has the data listed in Appendix B. Assuming 100% efficient combustion and $h_{PR} = 18{,}400$ Btu/lbm, calculate the fuel/air ratio, using Appendix D or program AFPROP and starting with an initial guess of 0.03. Now repeat Problem 6.7 with variable gas properties, using Appendix D or program AFPROP. Compare your results to those of Problem 6.7.

7
Parametric Cycle Analysis of Real Engines

7.1 Introduction

In Chapter 5, we idealized the engine components and assumed that the working fluid behaved as a perfect gas with constant specific heats. These idealizations and assumptions permitted the basic parametric analysis of several types of engine cycles and the analysis of engine performance trends. In Chapter 6, we looked at the variation of specific heat with temperature and fuel/air ratio and developed component models and figures of merit. This allows us to use realistic assumptions as to component losses and to include the variation of specific heats in engine cycle analysis. In this chapter, we develop the cycle analysis equations for many engine cycles, analyze their performance, and determine the effects of real components by comparison with the ideal engines of Chapter 5. We begin our analysis with the turbojet engine cycle and treat the simpler ramjet engine cycle as a special case of the turbojet ($\pi_c = 1,\ \tau_c = 1,\ \pi_t = 1,\ \tau_t = 1$).

7.2 Turbojet

We will now compute the behavior of the turbojet engine including component losses, the mass flow rate of fuel through the components, and the variation of specific heats. Our analysis still assumes one-dimensional flow at the entrance and exit of each component. The variation of specific heats will be approximated by assuming a perfect gas with constant specific heat c_{pc} upstream of the main burner (combustor) and a perfect gas with different constant specific heat c_{pt} downstream of the main burner.

The turbojet engine with station numbering is shown in Fig. 7.1, and the T-s diagram for this cycle with losses is plotted in Fig. 7.2. Figure 7.2 shows the total states for all engine stations along with the static states for stations 0 and 9.

7.2.1 Cycle Analysis

In this section we develop a system of equations to analyze the turbojet engine cycle. The steps of cycle analysis are applied to the turbojet engine and presented next in the order listed in Section 5.4.

Supporting Material for this chapter is available electronically. See page 869 for instructions to download.

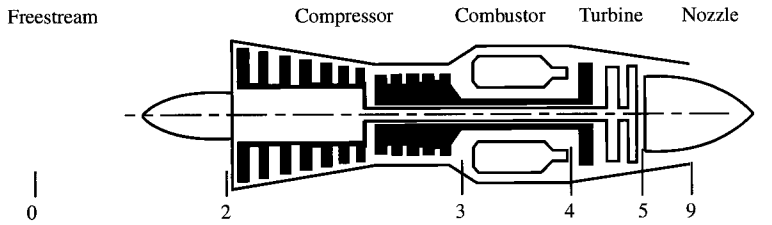

Fig. 7.1 Station numbering of turbojet engine.

Step 1: For uninstalled thrust,

$$F = \frac{1}{g_c}(\dot{m}_9 V_9 - \dot{m}_0 V_0) + A_9(P_9 - P_0)$$

$$\frac{F}{\dot{m}_0} = \frac{a_0}{g_c}\left(\frac{\dot{m}_9}{\dot{m}_0}\frac{V_9}{a_0} - M_0\right) + \frac{A_9 P_9}{\dot{m}_0}\left(1 - \frac{P_0}{P_9}\right) \tag{7.1}$$

We note that

$$\begin{aligned}
\frac{A_9 P_9}{\dot{m}_0}\left(1 - \frac{P_0}{P_9}\right) &= \frac{\dot{m}_9}{\dot{m}_0}\frac{A_9 P_9}{\rho_9 A_9 V_9}\left(1 - \frac{P_0}{P_9}\right) \\
&= \frac{\dot{m}_9}{\dot{m}_0}\frac{P_9}{[P_9/(R_9 T_9)]V_9}\left(1 - \frac{P_0}{P_9}\right) \\
&= \frac{\dot{m}_9}{\dot{m}_0}\frac{R_9 T_9}{V_9}\left(1 - \frac{P_0}{P_9}\right) \\
&= \frac{\dot{m}_9}{\dot{m}_0}\frac{R_9 T_9}{V_9}\frac{\gamma_0 R_0 g_c T_0}{\gamma_0 R_0 g_c T_0}\left(1 - \frac{P_0}{P_9}\right) \\
&= \frac{\dot{m}_9}{\dot{m}_0}\frac{R_9 T_9}{R_0 T_0}\frac{a_0^2}{\gamma_0 g_c V_9}\left(1 - \frac{P_0}{P_9}\right)
\end{aligned}$$

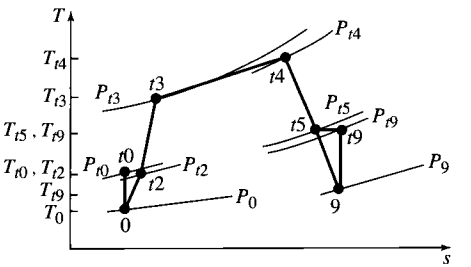

Fig. 7.2 The *T-s* diagram for turbojet engine.

$$\frac{A_9 P_9}{\dot{m}_0}\left(1-\frac{P_0}{P_9}\right)=\frac{a_0}{g_c}\left(\frac{\dot{m}_9}{\dot{m}_0}\frac{R_9}{R_0}\frac{T_9/T_0}{V_9/a_0}\frac{1-P_0/P_9}{\gamma_0}\right) \tag{7.2}$$

For the case of the turbojet cycle, the mass ratio can be written in terms of the fuel/air ratio f:

$$\frac{\dot{m}_9}{\dot{m}_0}=1+f$$

Using Eq. (7.2) with gas property subscripts c and t for engine stations 0 to 9, respectively, we can write Eq. (7.1) as

$$\frac{F}{\dot{m}_0}=\frac{a_0}{g_c}\left[(1+f)\frac{V_9}{a_0}-M_0+(1+f)\frac{R_t}{R_c}\frac{T_9/T_0}{V_9/a_0}\frac{1-P_0/P_9}{\gamma_c}\right] \tag{7.3}$$

Step 2:

$$\left(\frac{V_9}{a_0}\right)^2=\frac{a_9^2 M_9^2}{a_0^2}=\frac{\gamma_9 R_9 g_c T_9}{\gamma_0 R_0 g_c T_0}M_9^2$$

For the turbojet cycle, this equation becomes

$$\left(\frac{V_9}{a_0}\right)^2=\frac{\gamma_t R_t T_9}{\gamma_c R_c T_0}M_9^2 \tag{7.4}$$

Note: From the definition of τ_λ given in Eq. (5.7), we have

$$\tau_\lambda=\frac{c_{pt}T_{t4}}{c_{pc}T_0} \tag{7.5}$$

Step 3: We have

$$M_9^2=\frac{2}{\gamma_t-1}\left[\left(\frac{P_{t9}}{P_9}\right)^{(\gamma_t-1)/\gamma_t}-1\right] \tag{7.6}$$

where

$$\frac{P_{t9}}{P_9}=\frac{P_0}{P_9}\pi_r\pi_d\pi_c\pi_b\pi_t\pi_n \tag{7.7}$$

Step 4: We have

$$\frac{T_9}{T_0}=\frac{T_{t9}/T_0}{(P_{t9}/P_9)^{(\gamma_t-1)/\gamma_t}}$$

where

$$\frac{T_{t9}}{T_0} = \tau_r \tau_d \tau_c \tau_b \tau_t \tau_n \tag{7.8}$$

Step 5: Application of the first law of thermodynamics to the burner gives

$$\dot{m}_0 c_{pc} T_{t3} + \eta_b \dot{m}_f h_{PR} = \dot{m}_4 c_{pt} T_{t4} \tag{7.9}$$

Dividing the preceding equation by $\dot{m}_0 c_{pc} T_0$ and using the definitions of temperature ratios give

$$\tau_r \tau_c + f \frac{\eta_b h_{PR}}{c_{pc} T_0} = (1 + f)\tau_\lambda$$

Solving for the fuel/air ratio gives

$$f = \frac{\tau_\lambda - \tau_r \tau_c}{\eta_b h_{PR}/(c_{pc} T_0) - \tau_\lambda} \tag{7.10}$$

Step 6: The power balance between the turbine and compressor, with a mechanical efficiency η_m of the turbine compressor coupling, gives

$$\begin{gathered} \text{Power into compressor} = \text{net power from turbine} \\ \dot{m}_0 c_{pc}(T_{t3} - T_{t2}) = \eta_m \dot{m}_4 c_{pt}(T_{t4} - T_{t5}) \end{gathered} \tag{7.11}$$

Dividing the preceding equation by $\dot{m}_0 c_{pc} T_{t2}$ gives

$$\tau_c - 1 = \eta_m (1 + f) \frac{\tau_\lambda}{\tau_r} (1 - \tau_t)$$

Solving for the turbine temperature ratio gives

$$\tau_t = 1 - \frac{1}{\eta_m (1 + f)} \frac{\tau_r}{\tau_\lambda} (\tau_c - 1) \tag{7.12}$$

This expression enables us to solve for τ_t, from which we then obtain

$$\pi_t = \tau_t^{\gamma_t/[(\gamma_t - 1)e_t]} \tag{7.13}$$

We note that η_t will be given in terms of e_t by [Eq. (6.22)]

$$\eta_t = \frac{1 - \tau_t}{1 - \tau_t^{1/e_t}} \tag{7.14}$$

We also require the calculation of τ_c to allow determination of τ_t. Thus we note from Eq. (6.14)

$$\tau_c = \pi_c^{(\gamma_c - 1)/(\gamma_c e_t)} \tag{7.15}$$

Then also, from Eq. (6.15),

$$\eta_c = \frac{\pi_c^{(\gamma_c - 1)/\gamma_c} - 1}{\tau_c - 1} \tag{7.16}$$

Step 7: The equation for specific thrust cannot be simplified for this analysis.

Step 8: The equation for the thrust specific fuel consumption is

$$S = \frac{f}{F/\dot{m}_0} \tag{7.17}$$

Step 9: From the definitions of propulsive and thermal efficiency, one can easily show that for the turbojet engine

$$\eta_P = \frac{2g_c V_0 (F/\dot{m}_0)}{a_0^2[(1+f)(V_9/a_0)^2 - M_0^2]} \tag{7.18}$$

and

$$\eta_T = \frac{a_0^2[(1+f)(V_9/a_0)^2 - M_0^2]}{2g_c f h_{PR}} \tag{7.19}$$

Now we have all of the equations needed for analysis of the turbojet cycle. For convenience, this system of equations is listed (in the order of calculation) in the following section for easier calculation.

7.2.2 Summary of Equations—Turbojet Engine

INPUTS:

$$M_0,\ T_0(\mathrm{K},\ ^\circ\mathrm{R}),\ \gamma_c, c_{pc}\left(\frac{\mathrm{kJ}}{\mathrm{kg}\cdot\mathrm{K}}, \frac{\mathrm{Btu}}{\mathrm{lbm}\cdot{}^\circ\mathrm{R}}\right),\ \gamma_t,\ c_{pt}\left(\frac{\mathrm{kJ}}{\mathrm{kg}\cdot\mathrm{K}}, \frac{\mathrm{Btu}}{\mathrm{lbm}\cdot{}^\circ\mathrm{R}}\right)$$

$$h_{PR}\left(\frac{\mathrm{kJ}}{\mathrm{kg}}, \frac{\mathrm{Btu}}{\mathrm{lbm}}\right),\ \pi_{d\max},\ \pi_b,\ \pi_n,\ e_c,\ e_t,\ \eta_b,\ \eta_m,\ P_0/P_9,\ T_{t4}(\mathrm{K},\ ^\circ\mathrm{R},)\ \pi_c$$

OUTPUTS:

$$\frac{F}{\dot{m}_0}\left(\frac{\mathrm{N}}{\mathrm{kg/s}}, \frac{\mathrm{lbf}}{\mathrm{lbm/s}}\right), f, S\left(\frac{\mathrm{mg/s}}{\mathrm{N}}, \frac{\mathrm{lbm/h}}{\mathrm{lbf}}\right), \eta_T,\ \eta_P,\ \eta_O,\ \eta_c,\ \eta_t,\ \text{etc.}$$

EQUATIONS:

$$R_c = \frac{\gamma_c - 1}{\gamma_c} c_{pc} \tag{7.20a}$$

$$R_t = \frac{\gamma_t - 1}{\gamma_t} c_{pt} \tag{7.20b}$$

$$a_0 = \sqrt{\gamma_c R_c g_c T_0} \tag{7.20c}$$

$$V_0 = a_0 M_0 \tag{7.20d}$$

$$\tau_r = 1 + \frac{\gamma_c - 1}{2} M_0^2 \tag{7.20e}$$

$$\pi_r = \tau_r^{\gamma_t/(\gamma_t - 1)} \tag{7.20f}$$

$$\eta_r = 1 \quad \text{for } M_0 \leq 1 \tag{7.20g}$$

$$\eta_r = 1 - 0.075(M_0 - 1)^{1.35} \quad \text{for } M_0 > 1 \tag{7.20h}$$

$$\pi_d = \pi_{d\max} \eta_r \tag{7.20i}$$

$$\tau_\lambda = \frac{c_{pt} T_{t4}}{c_{pc} T_0} \tag{7.20j}$$

$$\tau_c = \pi_c^{(\gamma_c - 1)/(\gamma_c e_c)} \tag{7.20k}$$

$$\eta_c = \frac{\pi_c^{(\gamma_c - 1)/\gamma_c} - 1}{\tau_c - 1} \tag{7.20l}$$

$$f = \frac{\tau_\lambda - \tau_r \tau_c}{h_{PR} \eta_b / (c_{pc} T_0) - \tau_\lambda} \tag{7.20m}$$

$$\tau_t = 1 - \frac{1}{\eta_m (1 + f)} \frac{\tau_r}{\tau_\lambda} (\tau_c - 1) \tag{7.20n}$$

$$\pi_t = \tau_t^{\gamma_t [(\gamma_t - 1) e_t]} \tag{7.20o}$$

$$\eta_t = \frac{1 - \tau_t}{1 - \tau_t^{1/e_t}} \tag{7.20p}$$

$$\frac{P_{t9}}{P_9} = \frac{P_0}{P_9} \pi_r \pi_d \pi_c \pi_b \pi_t \pi_n \tag{7.20q}$$

$$M_9 = \sqrt{\frac{2}{\gamma_t - 1} \left[\left(\frac{P_{t9}}{P_9} \right)^{(\gamma_t - 1)/\gamma_t} - 1 \right]} \tag{7.20r}$$

$$\frac{T_9}{T_0} = \frac{\tau_\lambda \tau_t}{(P_{t9}/P_9)^{(\gamma_t - 1)/\gamma_t}} \frac{c_{pc}}{c_{pt}} \tag{7.20s}$$

$$\frac{V_9}{a_0} = M_9\sqrt{\frac{\gamma_t R_t T_9}{\gamma_c R_c T_0}} \tag{7.20t}$$

$$\frac{F}{\dot{m}_0} = \frac{a_0}{g_c}\left[(1+f)\frac{V_9}{a_0} - M_0 + (1+f)\frac{R_t T_9/T_0}{R_c V_9/a_0}\frac{(1-P_0/P_9)}{\gamma_c}\right] \tag{7.20u}$$

$$S = \frac{f}{F/\dot{m}_0} \tag{7.20v}$$

$$\eta_T = \frac{a_0^2[(1+f)(V_9/a_0)^2 - M_0^2]}{2g_c f h_{PR}} \tag{7.20w}$$

$$\eta_P = \frac{2g_c V_0(F/\dot{m}_0)}{a_0^2[(1+f)(V_9/a_0)^2 - M_0^2]} \tag{7.20x}$$

$$\eta_O = \eta_P \eta_T \tag{7.20y}$$

7.2.3 Examples—Turbojet Engine

We begin this section with a single example calculation for a turbojet engine. The other examples involve multiple calculations to investigate trends in engine performance.

Example 7.1

Consider a turbojet engine operating at high speed with the following input data.

INPUTS:

$$M_0 = 2,\ T_0 = 216.7\text{ K},\ \gamma_c = 1.4,\ c_{pc} = 1.004\text{ kJ/(kg}\cdot\text{K)},\ \gamma_t = 1.3$$
$$c_{pt} = 1.239\text{ kJ/(kg}\cdot\text{K)},\ h_{PR} = 42{,}800\text{ kJ/kg},\ \pi_{d\max} = 0.95,\ \pi_b = 0.94$$
$$\pi_n = 0.96,\ e_c = 0.9,\ e_t = 0.9,\ \eta_b = 0.98,\ \eta_m = 0.99,\ P_0/P_9 = 0.5$$
$$T_{t4} = 1800\text{ K},\ \pi_c = 10$$

EQUATIONS:

$$R_c = \frac{\gamma_c - 1}{\gamma_c}c_{pc} = \frac{0.4}{1.4}(1.004) = 0.2869\text{ kJ/(kg}\cdot\text{K)}$$

$$R_t = \frac{\gamma_t - 1}{\gamma_t}c_{pt} = \frac{0.3}{1.3}(1.239) = 0.2859\text{ kJ/(kg}\cdot\text{K)}$$

$$a_0 = \sqrt{\gamma_c R_c g_c T_0} = \sqrt{1.4 \times 286.9 \times 1 \times 216.7} = 295.0\text{ m/s}$$
$$V_0 = a_0 M_0 = 295.0 \times 2 = 590\text{ m/s}$$
$$V_0 = a_0 M_0 = 295.0 \times 2 = 590\text{ m/s}$$

$$\tau_r = 1 + \frac{\gamma_c - 1}{2} M_0^2 = 1 + 0.2 \times 2^2 = 1.8$$

$$\pi_r = \tau_r^{\gamma_c/(\gamma_c - 1)} = 1.8^{3.5} = 7.82445$$

$$\eta_r = 1 - 0.075(M_0 - 1)^{1.35} = 1 - 0.075(1^{1.35}) = 0.925$$

$$\pi_d = \pi_{d\max} \eta_r = 0.95 \times 0.925 = 0.87875$$

$$\tau_\lambda = \frac{c_{pt} T_{t4}}{c_{pc} T_0} = \frac{1.239 \times 1800}{1.004 \times 216.7} = 10.2506$$

$$\tau_c = \pi_c^{(\gamma_c - 1)/(\gamma_c e_c)} = 10^{1/(3.5 \times 0.9)} = 2.0771$$

$$\eta_c = \frac{\pi_c^{(\gamma_c - 1)/\gamma_c} - 1}{\tau_c - 1} = \frac{10^{1/3.5} - 1}{2.0771 - 1} = 0.8641$$

$$f = \frac{\tau_\lambda - \tau_r \tau_c}{h_{PR} \eta_b / (c_{pc} T_0) - \tau_\lambda}$$

$$= \frac{10.2506 - 1.8 \times 2.0771}{42{,}800 \times 0.98/(1.004 \times 216.7) - 10.2506} = 0.03567$$

$$\tau_t = 1 - \frac{1}{\eta_m (1 + f)} \frac{\tau_r}{\tau_\lambda} (\tau_c - 1)$$

$$= 1 - \frac{1}{0.99 \times 1.03567} \frac{1.8}{10.2506} (2.0771 - 1) = 0.8155$$

$$\pi_t = \tau_t^{\gamma_t/[(\gamma_t - 1)e_t]} = 0.8155^{1.3/(0.3 \times 0.9)} = 0.3746$$

$$\eta_t = \frac{1 - \tau_t}{1 - \tau_t^{1/e_t}} = \frac{1 - 0.8155}{1 - 0.8155^{1/0.9}} = 0.9099$$

$$\frac{P_{t9}}{P_9} = \frac{P_0}{P_9} \pi_r \pi_d \pi_c \pi_b \pi_t \pi_n$$

$$= 0.5 \times 7.824 \times 0.8788 \times 10 \times 0.94 \times 0.3746 \times 0.96 = 11.621$$

$$M_9 = \sqrt{\frac{2}{\gamma_t - 1} \left[\left(\frac{P_{t9}}{P_9} \right)^{(\gamma_t - 1)/\gamma_t} - 1 \right]}$$

$$= \sqrt{\frac{2}{0.3} (11.621^{0.3/1.3} - 1)} = 2.253$$

$$\frac{T_9}{T_0} = \frac{\tau_\lambda \tau_t}{(P_{t9}/P_9)^{(\gamma_t - 1)/\gamma_t}} \frac{c_{pc}}{c_{pt}} = \frac{10.2506 \times 0.8155}{11.621^{0.3/1.3}} \frac{1.004}{1.239} = 3.846$$

$$\frac{V_9}{a_0} = M_9\sqrt{\frac{\gamma_t R_t T_9}{\gamma_c R_c T_c}} = 2.253\sqrt{\frac{1.3 \times 0.2859}{1.4 \times 0.2869}(3.846)} = 4.250$$

$$\frac{F}{\dot{m}_0} = \frac{a_0}{g_c}\left[(1+f)\frac{V_9}{a_0} - M_0 + (1+f)\frac{R_t T_9/T_0}{R_c V_9/a_0}\frac{1-P_0/P_9}{\gamma_c}\right]$$

$$= \frac{295}{1}\left(1.03567 \times 4.250 - 2 + 1.03567\frac{0.2859}{0.2869}\frac{3.846}{4.250}\frac{0.5}{1.4}\right)$$

$$= 295(2.4016 + 0.3336) = 806.9 \text{ N/(kg/s)}$$

$$S = \frac{f}{F/\dot{m}_0} = \frac{0.03567}{806.9} \times 10^6 = 44.21(\text{mg/s})/\text{N}$$

$$\eta_T = \frac{a_0^2[(1+f)(V_9/a_0)^2 - M_0^2]}{2g_c f h_{PR}}$$

$$= \frac{295.0^2[(1.03835)4.250^2) - 2^2]}{2 \times 1 \times 0.03567 \times 42{,}800 \times 1000} = 41.92\%$$

$$\eta_P = \frac{2g_c V_0(F/\dot{m}_0)}{a_0^2[(1+f)(V_9/a_0)^2 - M_0^2]}$$

$$= \frac{2 \times 1 \times 590 \times 806.9}{295^2[1.03567(4.250^2) - 2^2]} = 74.39\%$$

$$\eta_O = \eta_P \eta_T = 0.4192 \times 0.7439 = 31.18\%$$

Example 7.2

Now we consider the turbojet cycle with losses over the same range of Mach numbers and compressor pressure ratios as analyzed for the ideal turbojet cycle and plotted in Figs. 5.8, 5.9, and 5.10.

INPUTS:

$M_0 = 0 \rightarrow 3$, $T_0 = 390°\text{R}$, $\gamma_c = 1.4$, $c_{pc} = 0.24$ Btu/(lbm · °R)
$\gamma_t = 1.35$, $c_{pt} = 0.262$ Btu/(lbm · °R), $h_{PR} = 18{,}400$ Btu/lbm
$\pi_{d\max} = 0.98$, $\pi_b = 0.98$, $\pi_n = 0.98$, $e_c = 0.92$, $e_t = 0.91$
$\eta_b = 0.99$, $\eta_m = 0.98$, $P_0/P_9 = 1$, $T_{t4} = 3000°\text{R}$, $\pi_c = 1 \rightarrow 30$

The results of the analysis are plotted vs compressor pressure ratio in Figs. 7.3a–7.3d and vs flight Mach number in Figs. 7.4a–7.4d. When compared to the corresponding figures for the ideal turbojet cycle, the following can be concluded for the turbojet cycle with losses:

a) Specific thrust $F/\dot{m}_0$. Comparing Fig. 7.3a to Fig. 5.8a and Fig. 7.4a to Fig. 5.9a, one can see that the variation of specific thrust with compressor pressure ratio or Mach number is not appreciably changed and the magnitudes are nearly equal. At high Mach numbers, the effect of the losses causes the

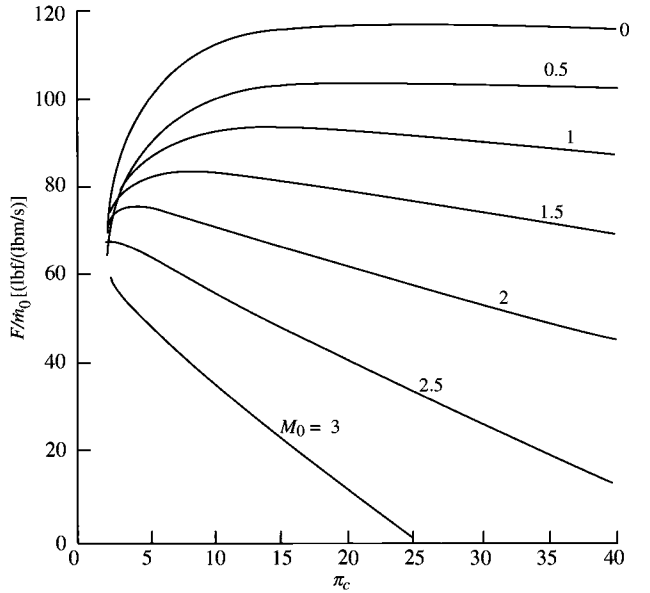

Fig. 7.3a Turbojet performance vs π_c: specific thrust.

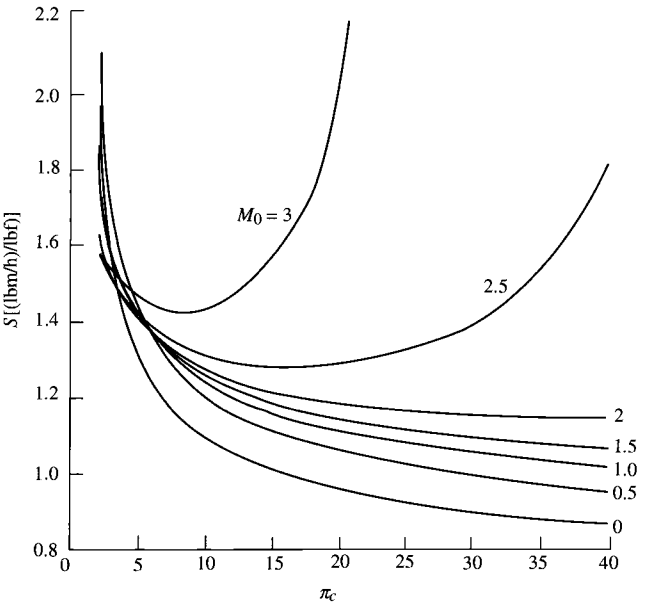

Fig. 7.3b Turbojet performance vs π_c: thrust-specific fuel consumption.

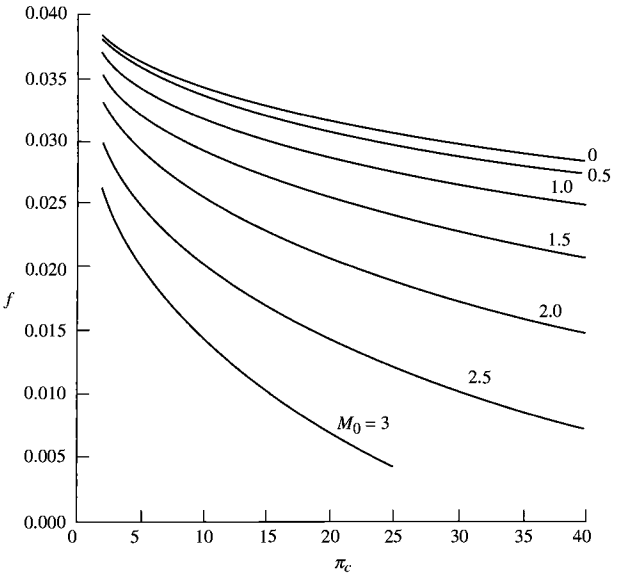

Fig. 7.3c Turbojet performance vs π_c: fuel/air ratio.

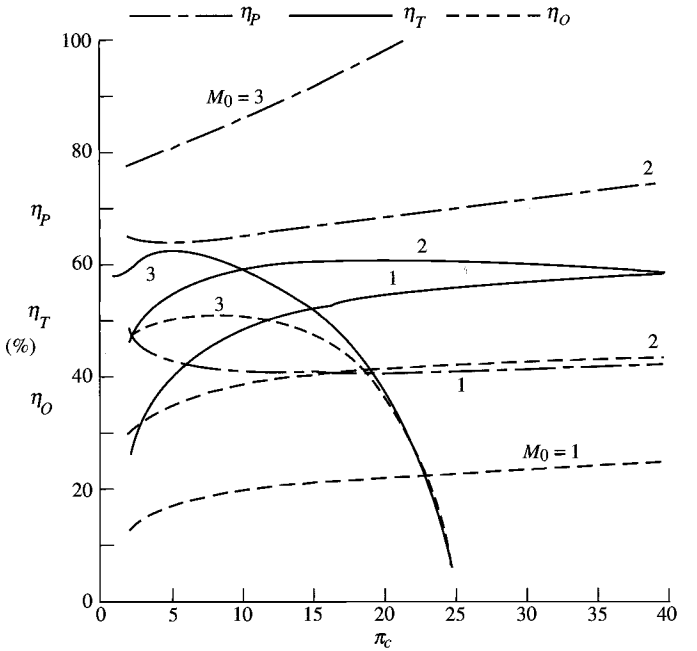

Fig. 7.3d Turbojet performance vs π_c: efficiencies.

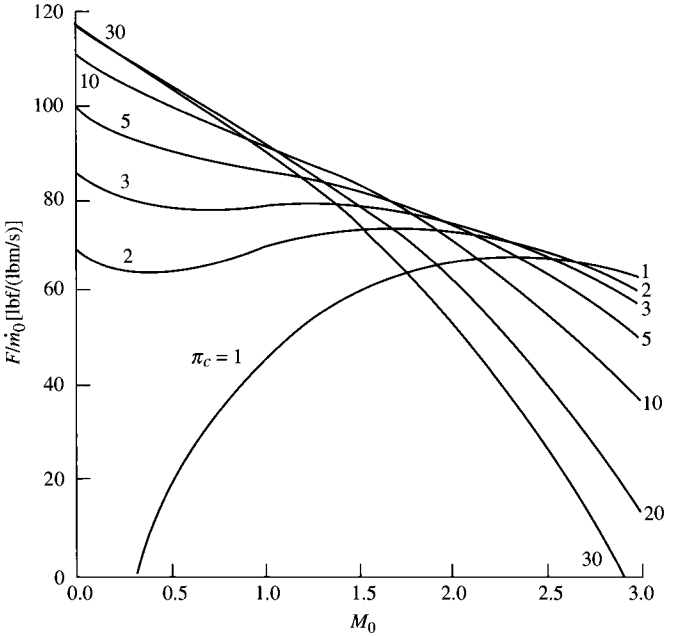

Fig. 7.4a Turbojet performance vs M_0: specific thrust.

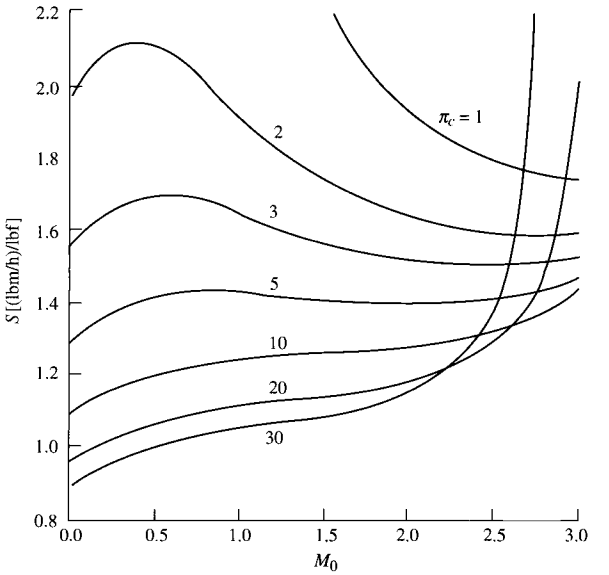

Fig. 7.4b Turbojet performance vs M_0: thrust-specific fuel consumption.

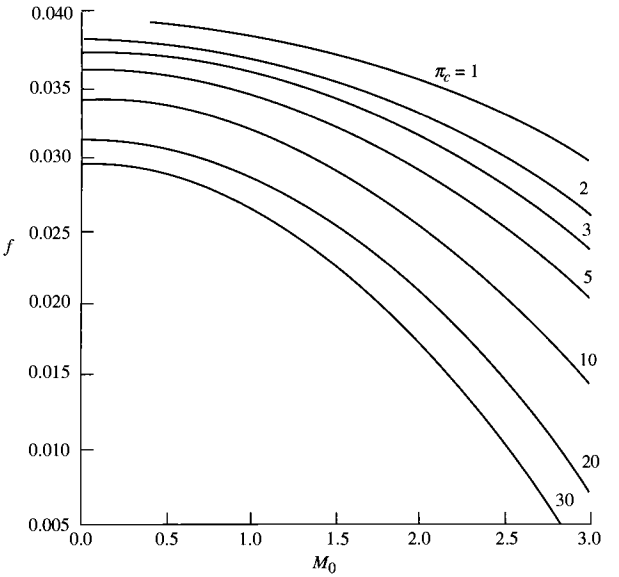

Fig. 7.4c Turbojet performance vs M_0: fuel/air ratio.

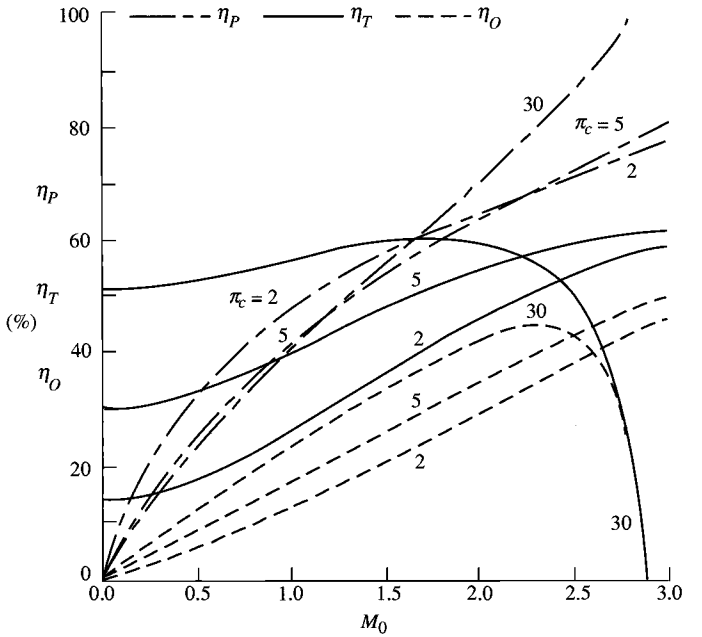

Fig. 7.4d Turbojet performance vs M_0: efficiencies.

thrust to go to zero at a lower compressor pressure ratio. For a Mach number, the compressor pressure ratio that gives maximum specific thrust is lower than that of the ideal turbojet. Also, the ramjet cycle ($\pi_c = 1$) does not have thrust for Mach numbers less than 0.3.

b) Thrust specific fuel consumption S. Comparison of Fig. 7.3b to Fig. 5.8b and Fig. 7.4b to Fig. 5.9b shows that the values of fuel consumption are larger for the engine with losses. The thrust specific fuel consumption no longer continues to decrease with increasing compressor pressure ratio, and there is now a compressor pressure ratio giving minimum fuel consumption for a given Mach number.

c) Fuel/air ratio f. Comparing Fig. 7.3c to Fig. 5.8c and Fig. 7.4c to Fig. 5.9c, we see that the values of the fuel/air ratio are larger for the turbojet with losses. The main reasons for this increase in fuel/air ratio are the increase in specific heat across the main burner, the inefficiency of the combustion process, and the larger mass flow rate exiting the main burner.

d) Propulsive efficiency η_P. Comparison of Fig. 7.3d to Fig. 5.8d and Fig. 7.4d to Fig. 5.9d shows that the propulsive efficiencies are a little larger for the turbojet with losses. This is due mainly to the decrease in exhaust velocity for the engine with losses.

e) Thermal efficiency η_T. Comparing Fig. 7.3d to Fig. 5.8d and Fig. 7.4d to Fig. 5.9d, we can see that the engines with losses have lower thermal efficiency. Also, the thermal efficiency of high-compressor-pressure-ratio engines at high Mach go toward zero because the thrust goes to zero before the fuel flow rate.

f) Overall efficiency η_O. One can see that the overall efficiencies are lower for the turbojet engines with losses by comparison of Fig. 7.3d to Fig. 5.8d and Fig. 7.4d to Fig. 5.9d. This is mainly due to the decrease in thermal efficiency of the engines with losses.

Example 7.3

The effect of compressor efficiency on the performance of a turbojet engine cycle at Mach 2.0 is investigated in the following. The compressor pressure ratio was varied over the range of 1 to 40 for two different compressor polytropic efficiencies to give the results indicated in Fig. 7.5. Also included on this plot are the results of ideal cycle analysis. The input data for this analysis are listed here.

INPUTS:

$$M_0 = 2,\ T_0 = 390°\text{R},\ \gamma_c = 1.4,\ c_{pc} = 0.24\ \text{Btu/(lbm} \cdot °\text{R)}$$

$$\gamma_t = 1.33,\ c_{pt} = 0.276\ \text{Btu/(lbm} \cdot °\text{R)},\ h_{PR} = 18{,}400\ \text{Btu/lbm}$$

$$\pi_{d\max} = 0.98,\ \pi_b = 0.98,\ \pi_n = 0.98,\ e_c = 0.92 \text{ and } 0.89,\ e_t = 0.91$$

$$\eta_b = 0.99,\ \eta_m = 0.98,\ P_0/P_9 = 1,\ T_{t4} = 3000°\text{R},\ \pi_c = 1 \rightarrow 40$$

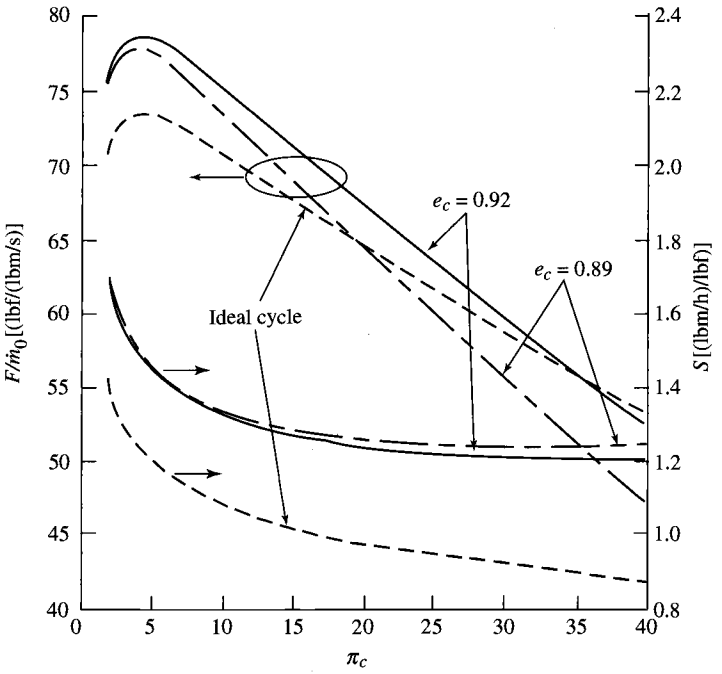

Fig. 7.5 Effect of compressor polytropic efficiency of turbojet cycle.

It can be seen from Fig. 7.5 that the ideal turbojet analysis gives the basic trends for the lower values of the compressor pressure ratio. As the compressor pressure ratio increases, the effect of engine losses increases. At low compressor pressure ratio, the ideal analysis predicts a lower value of specific thrust than the engine with losses because the momentum of the fuel is neglected in the ideal case.

It can also be seen from Fig. 7.5 that a prospective designer would be immediately confronted with a design choice, because the compressor pressure ratio leading to maximum specific thrust is far from that leading to minimum fuel consumption. Clearly, a short-range interceptor would better suit a low compressor pressure ratio with the resultant high specific thrust and lightweight (small compressor) engine. Conversely, the designer of a long-range transport would favor an engine with high compressor pressure ratio and low specific fuel consumption. Thus we see what should be obvious—before an engine can be correctly designed, the mission (use) for which it is being designed must be precisely understood.

Another aspect of the designer's dilemma becomes apparent when the curves obtained for the two different compressor polytropic efficiencies in Fig. 7.5 are compared. For example, if a designer chooses a compressor pressure ratio of 35 for use in a supersonic transport because the compressor design group has promised a compressor with $e_c = 0.92$, and then the group delivers a compressor with $e_c = 0.89$, clearly the choice $\pi_c = 35$ would be quite inappropriate. That is, such a compressor would have a higher pressure ratio than that leading to minimum fuel consumption. Thus the designer would have a compressor that

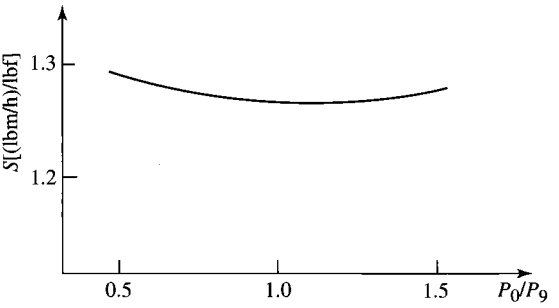

Fig. 7.6 Effect of nozzle off-design conditions on thrust-specific fuel consumption.

was heavier (and more expensive) than that leading to a minimum specific fuel consumption, he or she would also have lower specific thrust, and finally the designer would have an acute need to change employers.

The effect of nozzle off-design conditions can be invesigated by considering the engine to have the same parameters as those indicated previously, but with various values of P_0/P_9. As an example, we consider an engine with $\pi_c = 16$ and $e_c = 0.92$ to obtain the thrust specific fuel consumption information plotted in Fig. 7.6.

It is apparent that for small exit nozzle off-design conditions ($0.8 < P_0/P_9 < 1.2$), the thrust and thrust specific fuel consumption vary only slightly with the exit pressure mismatch. This result indicates that the best nozzle design should be determined by considering the external flow behavior (boattail drag, etc.). Note also that for a long-range transport or passenger aircraft, a 1% change in specific fuel consumption is very significant.

Example 7.4

Let's consider another example in which we let the Mach number vary and see how the engine performance changes. The flight conditions, design limits, component performance figures of merit, and design choices are listed in the following. We will compare the turbojet engine with losses with the corresponding ideal engine. The trends that were obtained for the ideal engine are generally true for the engine with losses; exceptions are noted in the following discussion.

INPUTS:

$$M_0 = 1 \rightarrow 4,\ T_0 = 216.7\ \text{K},\ \gamma_c = 1.4,\ c_{pc} = 1.004\ \text{kJ/(kg} \cdot \text{K)},\ \gamma_t = 1.35$$
$$c_{pt} = 1.096\ \text{kJ/(kg} \cdot \text{K)},\ h_{PR} = 42{,}800\ \text{kJ/kg},\ \pi_{d\max} = 0.98,\ \pi_b = 0.98$$
$$\pi_n = 0.96,\ e_c = 0.89,\ e_t = 0.91,\ \eta_b = 0.99,\ \eta_m = 0.98$$
$$P_0/P_9 = 1,\ T_{t4} = 1670\ \text{K},\ \pi_c = 8 \text{ and } 24$$

The specific thrust vs Mach number is plotted in Fig. 7.7a for both compressor pressure ratios. The specific thrust is approximately the same as that for the ideal

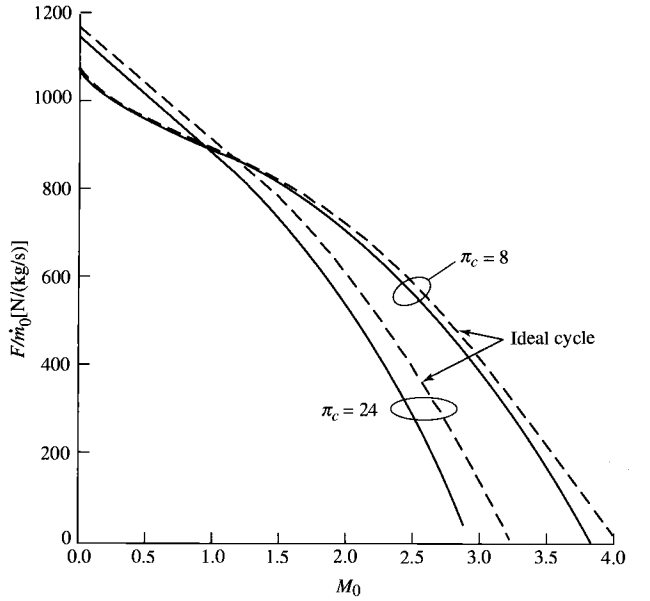

Fig. 7.7a Specific thrust for two compressor pressure ratios.

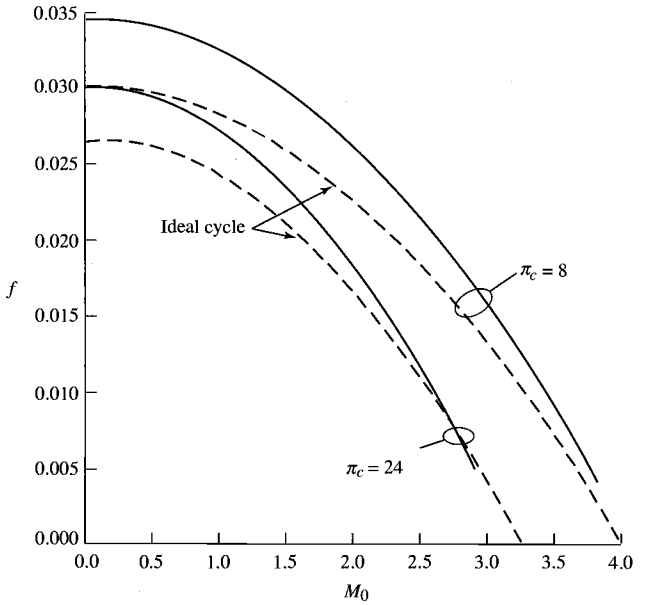

Fig. 7.7b Fuel/air ratio for two compressor pressure ratios.

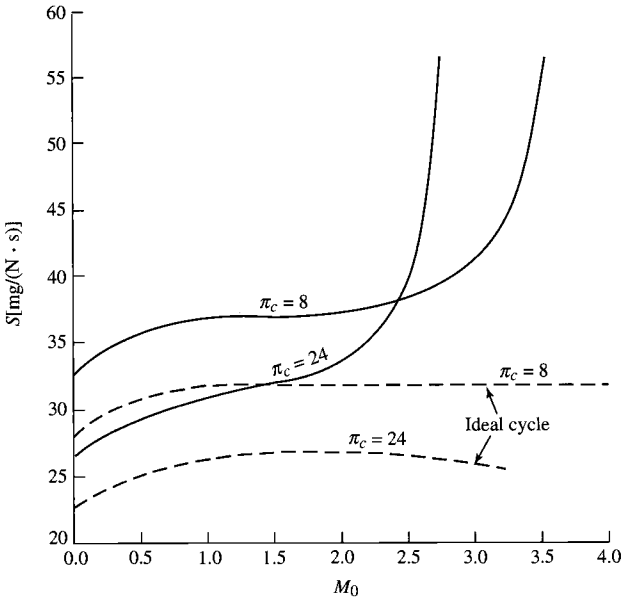

Fig. 7.7c Specific fuel consumption for two compressor pressure ratios.

engine. While the exit velocity decreases slightly for the engine with losses, this is compensated by the extra mass flow leaving the engine due to fuel addition.

The fuel/air ratio f vs Mach number is plotted in Fig. 7.7b for both compressor pressure ratios. The fuel/air ratio is considerably higher for the engine with losses. There are three reasons for this:

1) The extra mass due to fuel addition, neglected in the ideal case, must be heated to the temperature of the products of combustion leaving the burner. This requires extra fuel.

2) The combustion process is not 100% efficient, and so extra fuel is required.

3) Most important, the change in gas properties, i.e., the increase in the specific heat at constant pressure c_P, means that more energy is needed to increase the temperature of the products of combustion than if the gas remained as air with the low-temperature properties. This is true since $h_t = c_p T_t$ and the fuel burned goes to increasing h_t directly and T_t only indirectly.

The thrust-specific fuel consumption S vs Mach number is plotted in Fig. 7.7c for both compressor pressure ratios. Because the thrust is approximately the same for the ideal engine and the corresponding engine with losses, and because the required fuel/air ratio is higher for the engine with losses, the thrust-specific fuel consumption is considerably higher for the engine with losses. For the example given here, the value for the engine with losses is generally higher by 30–40%. However, the two values really diverge for high flight Mach numbers. The thrust specific fuel consumption starts increasing toward infinity

at $M_0 > 2.0$ for a compressor pressure ratio of 8 and at $M_0 > 1.5$ for a compressor pressure ratio of 24. This follows from the definition of the thrust specific fuel consumption—the fuel flow rate divided by the thrust. For the engine with losses, the thrust goes to zero before the fuel flow rate does. This indicates that the thermal efficiency for the turbojet at high speeds goes to zero; i.e., there is a heat input from the fuel, but no net power output because of the component inefficiencies. This is not the case for the ideal engines where the thermal efficiency always increases with flight Mach number.

7.3 Turbojet with Afterburner

The turbojet engine with afterburner is shown in Fig. 7.8, and the temperature-entropy plot of this engine with losses is shown in Fig. 7.9. The numbering system indicated in these figures is the industry standard.[30]

For the analysis of this engine, we remind the reader of the following definitions for the afterburner:

$$\pi_{AB} = \frac{P_{t7}}{P_{t6}} \quad f_{AB} = \frac{\dot{m}_{fAB}}{\dot{m}_0}$$

$$\tau_{AB} = \frac{T_{t7}}{T_{t6}} \quad \tau_{\lambda AB} = \frac{c_{pAB}}{c_{pc}} \frac{T_{t7}}{T_0} \tag{7.21}$$

$$\eta_{AB} = \frac{(\dot{m}_0 + \dot{m}_f + \dot{m}_{fAB}) c_{pAB} T_{t7} - (\dot{m}_0 + \dot{m}_f) c_{pt} T_{t6}}{\dot{m}_{fAB} h_{PR}}$$

Note that stations 6 and 7 are used for these afterburner parameters. We assume isentropic flow from station 5 to station 6 in the following analysis. Thus Fig. 7.9 shows the afterburning process going from station 5 to 7.

We also note that

$$\tau_{\lambda AB} = \frac{c_{pAB}}{c_{pc}} \frac{T_{t4}}{T_0} \frac{T_{t5}}{T_{t4}} \frac{T_{t8}}{T_{t5}} = \frac{c_{pAB}}{c_{pc}} \tau_\lambda \tau_t \tau_{AB} \tag{7.22}$$

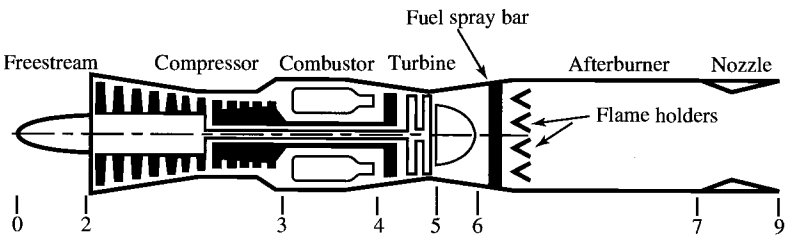

Fig. 7.8 Ideal afterburning turbojet engine with station numbering.

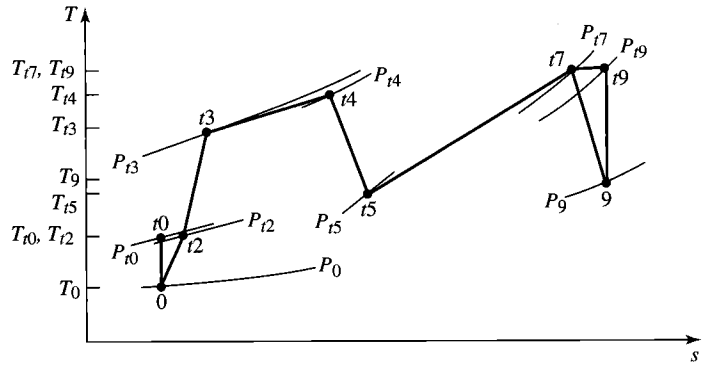

Fig. 7.9 The *T-s* diagram for afterburning turbojet engine.

and

$$\frac{\dot{m}_9}{\dot{m}_0} = \frac{\dot{m}_0 + \dot{m}_f + \dot{m}_{f\text{AB}}}{\dot{m}_0} = 1 + f + f_{\text{AB}} \tag{7.23}$$

7.3.1 Cycle Analysis

The expression for the thrust will be the same as that already obtained for the turbojet without afterburning except that the effects of fuel addition in the afterburner must be included. Application of the steps of cycle analysis (see Section 5.4) is listed next.

Step 1: The specific thrust equation becomes

$$\frac{F}{\dot{m}_0} = \frac{a_0}{g_c}\left[(1 + f + f_{\text{AB}})\frac{V_9}{a_0} - M_0 + (1 + f + f_{\text{AB}}) \times \frac{R_{\text{AB}}}{R_c}\frac{T_9/T_0}{V_9/a_0}\frac{1 - P_0/P_9}{\gamma_c}\right] \tag{7.24}$$

Step 2: As before,

$$\left(\frac{V_9}{a_0}\right)^2 = \frac{\gamma_{\text{AB}} R_{\text{AB}} T_9}{\gamma_c R_c T_0} M_9^2 \tag{7.25}$$

Step 3: We have

$$M_9^2 = \frac{2}{\gamma_{\text{AB}} - 1}\left[\left(\frac{P_{t9}}{P_9}\right)^{(\gamma_{\text{AB}}-1)/\gamma_{\text{AB}}} - 1\right] \tag{7.26}$$

where

$$\frac{P_{t9}}{P_9} = \frac{P_0}{P_0}\pi_r\pi_d\pi_c\pi_b\pi_t\pi_{AB}\pi_n \tag{7.27}$$

Step 4: We have

$$\frac{T_9}{T_0} = \frac{T_{t9}/T_0}{(P_{t9}/P_9)^{(\gamma_{AB}-1)/\gamma_{AB}}}$$

where

$$\frac{T_{t9}}{T_0} = \tau_{\lambda AB}\frac{c_{pc}}{c_{pAB}} \tag{7.28}$$

Step 5: Application of the steady flow energy equation to the main combustor gives, [Eq. (7.10)]

$$f = \frac{\tau_\lambda - \tau_r\tau_c}{\eta_b h_{PR}/(c_{pc}T_0) - \tau_\lambda}$$

Application of the steady flow energy equation to the afterburner gives

$$(\dot{m}_0 + \dot{m}_f)c_{pt}T_{t6} + \eta_{AB}\dot{m}_{fAB}h_{PR} = (\dot{m}_0 + \dot{m}_f + \dot{m}_{fAB})c_{pAB}T_{t7}$$

This equation can be solved for the afterburner fuel/air ratio f_{AB}, giving

$$f_{AB} = (1+f)\frac{\tau_{\lambda AB} - \tau_\lambda\tau_t}{\eta_{AB}h_{PR}/(c_{pc}T_0) - \tau_{\lambda AB}} \tag{7.29}$$

Step 6: The power balance between the turbine and compressor is unaffected by the addition of the afterburner. Thus Eqs. (7.12)–(7.16) apply to this engine cycle.

Step 7: Not used in this analysis.

Step 8: The thrust specific fuel consumption S is expressed in terms of both the main burner and afterburner fuel/air ratios as

$$S = \frac{f + f_{AB}}{F/\dot{m}_0} \tag{7.30}$$

Step 9: From the definitions of propulsive and thermal efficiency, one can easily show that for the afterburning turbojet engine

$$\eta_P = \frac{2g_c V_0(F/\dot{m}_0)}{a_0^2[(1+f+f_{AB})(V_9/a_0)^2 - M_0^2]} \tag{7.31}$$

$$\eta_T = \frac{a_0^2[(1+f+f_{AB})(V_9/a_0)^2 - M_0^2]}{2g_c(f+f_{AB})h_{PR}} \tag{7.32}$$

Now we have all of the equations needed for analysis of the afterburning turbojet cycle. For convenience, this system of equations is listed (in the order of calculation) in the following section for easier calculation.

7.3.2 Summary of Equations—Afterburning Turbojet Engine

INPUTS:

$$M_0,\ T_0(\mathrm{K},^\circ\mathrm{R}),\ \gamma_c,\ c_{pc}\left(\frac{\mathrm{kJ}}{\mathrm{kg}\cdot\mathrm{K}},\frac{\mathrm{Btu}}{\mathrm{lbm}\cdot{}^\circ\mathrm{R}}\right),\ \gamma_t,\ c_{pt}\left(\frac{\mathrm{kJ}}{\mathrm{kg}\cdot\mathrm{K}},\frac{\mathrm{Btu}}{\mathrm{lbm}\cdot{}^\circ\mathrm{R}}\right)$$

$$h_{PR}\left(\frac{\mathrm{kJ}}{\mathrm{kg}},\frac{\mathrm{Btu}}{\mathrm{lbm}}\right),\ \gamma_{AB},\ c_{pAB}\left(\frac{\mathrm{kJ}}{\mathrm{kg}\cdot\mathrm{K}},\frac{\mathrm{Btu}}{\mathrm{lbm}\cdot{}^\circ\mathrm{R}}\right),\ \pi_{d\max},\ \pi_b,\ \pi_{AB},\ \pi_n,\ e_c,\ e_t$$

$$\eta_b,\ \eta_{AB},\eta_m,\ P_0/P_9,\ T_{t4}(\mathrm{K},^\circ\mathrm{R}),\ T_{t7}(\mathrm{K},^\circ\mathrm{R}),\ \pi_c$$

OUTPUTS:

$$\frac{F}{\dot{m}_0}\left(\frac{\mathrm{N}}{\mathrm{kg/s}},\frac{\mathrm{lbf}}{\mathrm{lbm/s}}\right), f, f_{AB}, S\left(\frac{\mathrm{mg/s}}{N},\frac{\mathrm{lbm/h}}{\mathrm{lbf}}\right),\ \eta_T,\ \eta_P,\ \eta_O,\ \eta_c,\eta_t,\ \text{etc.}$$

EQUATIONS:

Equations (7.20a–7.20p) and the following:

$$R_{AB} = \frac{\gamma_{AB}-1}{\gamma_{AB}} c_{pAB} \tag{7.33a}$$

$$\tau_{\lambda AB} = \frac{c_{pAB}}{c_{pc}}\frac{T_{t7}}{T_0} \tag{7.33b}$$

$$f_{AB} = (1+f)\frac{\tau_{\lambda AB} - \tau_\lambda \tau_t}{\eta_{AB} h_{PR}/(c_{pc}T_0) - \tau_{\lambda AB}} \tag{7.33c}$$

$$\frac{P_{t9}}{P_9} = \frac{P_0}{P_9}\pi_r\pi_d\pi_c\pi_b\pi_t\pi_{AB}\pi_n \tag{7.33d}$$

$$\frac{T_9}{T_0} = \frac{T_{t7}/T_0}{(P_{t9}/P_9)^{(\gamma_{AB}-1)/\gamma_{AB}}} \tag{7.33e}$$

$$M_9^2 = \frac{2}{\gamma_{AB}-1}\left[\left(\frac{P_{t9}}{P_9}\right)^{(\gamma_{AB}-1)/\gamma_{AB}} - 1\right] \tag{7.33f}$$

$$\frac{V_9}{a_0} = M_9\sqrt{\frac{\gamma_{AB}R_{AB}T_9}{\gamma_c R_c T_0}} \tag{7.33g}$$

$$\frac{F}{\dot{m}_0} = \frac{a_0}{g_c}\left[(1+f+f_{AB})\frac{V_9}{a_0} - M_0 + (1+f+f_{AB}) \times \frac{R_{AB}}{R_c}\frac{T_9/T_0}{V_9/a_0}\frac{1-P_0/P_9}{\gamma_c}\right] \tag{7.33h}$$

$$S = \frac{f+f_{AB}}{F/\dot{m}_0} \tag{7.33i}$$

$$\eta_P = \frac{2g_c V_0(F/\dot{m}_0)}{a_0^2[(1+f+f_{AB})(V_9/a_0)^2 - M_0^2]} \tag{7.33j}$$

$$\eta_T = \frac{a_0^2[(1+f+f_{AB})(V_9/a_0)^2 - M_0^2]}{2g_c(f+f_{AB})h_{PR}} \tag{7.33k}$$

$$\eta_O = \eta_P\eta_T \tag{7.33l}$$

Example 7.5

We consider an example similar to that considered for the "dry" turbojet of Example 7.3 so that we can directly compare the effects of afterburning. Thus we have the following input data.

INPUTS:

$$M_0 = 2,\ T_0 = 390°\text{R},\ \gamma_c = 1.4,\ c_{pc} = 0.24\ \text{Btu/(lbm}\cdot°\text{R)}$$
$$\gamma_t = 1.33,\ c_{pt} = 0.276\ \text{Btu/(lbm}\cdot°\text{R)},\ h_{PR} = 18{,}400\ \text{Btu/lbm}$$
$$\gamma_{AB} = 1.30,\ c_{pAB} = 0.295\ \text{Btu/(lbm}\cdot°\text{R)},\ \pi_{d\max} = 0.98,\ \pi_b = 0.98$$
$$\pi_{AB} = 0.98,\ \pi_n = 0.98,\ e_c = 0.89,\ e_t = 0.91,\ \eta_b = 0.99$$
$$\eta_{AB} = 0.96,\ \eta_m = 0.98,\ P_0/P_9 = 1,\ T_{t4} = 3000°\text{R}$$
$$T_{t7} = 3500°\text{R},\ \pi_c = 2 \rightarrow 14$$

In this example, we limit the maximum compressor pressure ratio to 14 because the total temperature leaving the compressor T_{t3} will exceed 1200°F

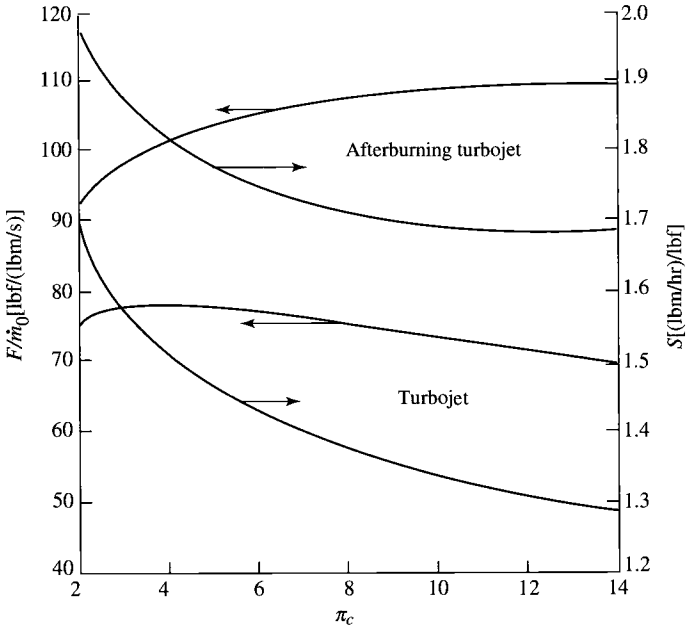

Fig. 7.10 Performance of turbojet engine with and without afterburner.

(temperature limit of current compressor materials) at higher pressure ratios. For the afterburning turbojet, we take

$$\pi_n \pi_{AB} = 0.98^2 \quad \text{afterburner on}$$
$$\pi_n \pi_{AB} = 0.98 \quad \text{afterburner off}$$

The results are indicated in Fig. 7.10. Note that operation of the afterburner will increase both the specific thrust and the fuel consumption. The magnitude of the increases depends on the compressor pressure ratio. A compressor pressure ratio of 12 gives good specific thrust and fuel consumption for afterburner operation and reasonable performance without the afterburner.

The design compressor pressure ratio will depend on the aircraft and its mission (use), which requires an in-depth analysis.

7.4 Turbofan—Separate Exhaust Streams

A turbofan engine with station numbering is shown in Fig. 7.11. A temperature vs entropy plot for the flow through the fan and the engine core is shown in Fig. 7.12. The effect of engine losses can be seen by comparing Fig. 7.12 with Figs. 5.21 and 5.22. The exit velocity of both the fan stream and the engine core stream is reduced by engine losses.

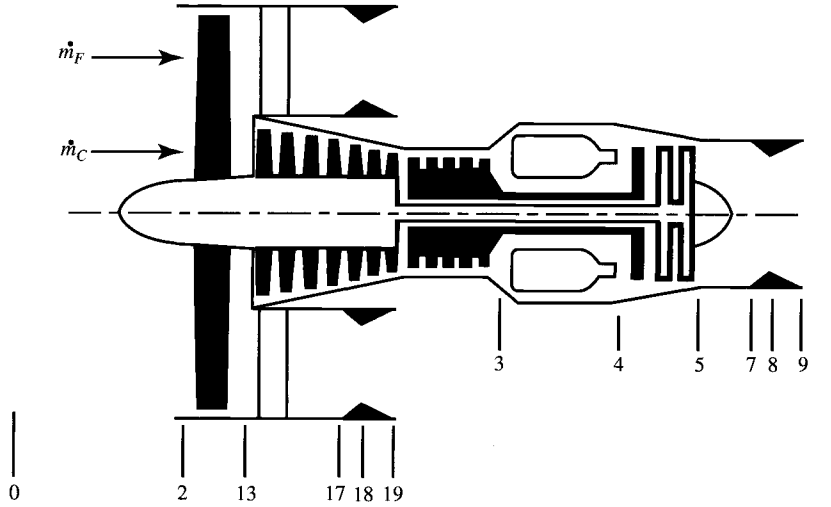

Fig. 7.11 Station numbering of turbofan engine.

7.4.1 Cycle Analysis

The assumptions for the analysis of the turbofan engine cycle with losses are as follows:

1) Perfect gas upstream of main burner with constant properties γ_c, R_c, c_{pc}, etc.
2) Perfect gas downstream of main burner with constant properties γ_t, R_t, c_{pt}, etc.
3) All components are adiabatic (no turbine cooling).

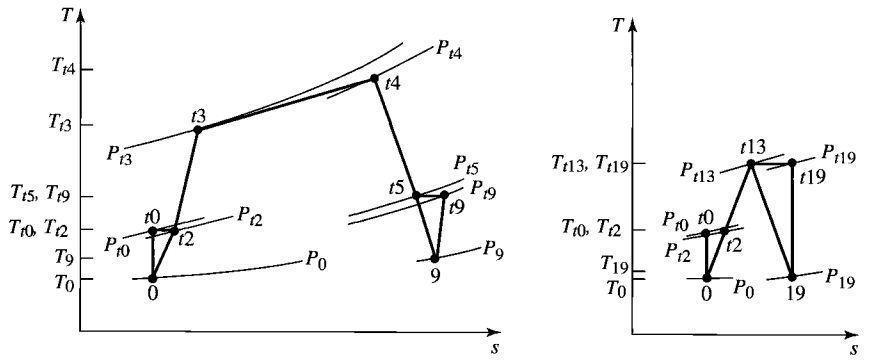

Fig. 7.12 The *T*-*s* diagram of turbofan engine with losses (not to scale).

4) The efficiencies of the compressor, fan, and turbine are described through the use of (constant) polytropic efficiencies e_c, e_f, and e_t, respectively.

The steps of cycle analysis are applied to the turbofan engine and presented next in the order listed in Section 5.4. We will apply the steps of cycle analysis to both the fan stream and the engine core stream.

7.4.1.1 Fan stream. Steps 1–4 are as follows.

Step 1: Uninstalled thrust of fan stream F_F:

$$F_F = \frac{\dot{m}_F}{g_c}(V_{19} - V_0) + A_{19}(P_{19} - P_0)$$

Using Eq. (7.2) for the fan stream gives

$$\frac{F_F}{\dot{m}_F} = \frac{a_0}{g_c}\left(\frac{V_{19}}{a_0} - M_0 + \frac{T_{19}/T_0}{V_{19}/a_0}\frac{1 - P_0/P_{19}}{\gamma_c}\right) \tag{7.34}$$

Step 2:

$$\left(\frac{V_{19}}{a_0}\right)^2 = \frac{T_{19}}{T_0}M_{19}^2 \tag{7.35}$$

Step 3: We have

$$M_{19}^2 = \frac{2}{\gamma_c - 1}\left[\left(\frac{P_{t19}}{P_{19}}\right)^{(\gamma_c - 1)/\gamma_c} - 1\right] \tag{7.36a}$$

where

$$\frac{P_{t19}}{P_{19}} = \frac{P_0}{P_{19}}\pi_r\pi_d\pi_f\pi_{fn} \tag{7.36b}$$

Step 4: We have

$$\frac{T_{19}}{T_0} = \frac{T_{t19}/T_0}{(P_{t19}/P_{19})^{(\gamma_c - 1)/\gamma_c}} \tag{7.37a}$$

where

$$\frac{T_{t19}}{T_0} = \tau_r\tau_f \tag{7.37b}$$

7.4.1.2 Engine core stream. Steps 1–5 are the same as for the turbojet engine cycle with losses.

Step 1: Uninstalled thrust:

$$F_C = \frac{1}{g_c}(\dot{m}_9 V_9 - \dot{m}_C V_0) + A_9(P_9 - P_0)$$

or

$$\frac{F_C}{\dot{m}_C} = \frac{a_0}{g_c}\left[(1+f)\frac{V_9}{a_0} - M_0 + (1+f)\frac{R_t}{R_c}\frac{T_9/T_0}{V_9/a_0}\frac{1-P_0/P_9}{\gamma_c}\right] \tag{7.38}$$

where the fuel/air ratio for the main burner is defined as

$$f \equiv \frac{\dot{m}_f}{\dot{m}_C} \tag{7.39}$$

Step 2:

$$\left(\frac{V_9}{a_0}\right)^2 = \frac{\gamma_t R_t T_9}{\gamma_c R_c T_0} M_9^2 \tag{7.40}$$

Step 3: We have

$$M_9^2 = \frac{2}{\gamma_t - 1}\left[\left(\frac{P_{t9}}{P_9}\right)^{(\gamma_t-1)/\gamma_t} - 1\right] \tag{7.41a}$$

where

$$\frac{P_{t9}}{P_9} = \frac{P_0}{P_9}\pi_r\pi_d\pi_c\pi_b\pi_t\pi_n \tag{7.41b}$$

Step 4: We have

$$\frac{T_9}{T_0} = \frac{T_{t9}/T_0}{(P_{t9}/P_9)^{(\gamma_t-1)/\gamma_t}} \tag{7.42a}$$

where

$$\frac{T_{t9}}{T_0} = \tau_r\tau_d\tau_c\tau_b\tau_t\tau_n = \frac{c_{pc}}{c_{pt}}\tau_\lambda\tau_t \tag{7.42b}$$

Step 5: Application of the first law of thermodynamics to the burner gives

$$\dot{m}_C c_{pc} T_{t3} + \eta_b \dot{m}_f h_{PR} = \dot{m}_4 c_{pt} T_{t4}$$

By using the definitions of the temperature ratios and fuel/air ratio, the preceding equation becomes

$$\tau_r\tau_c + f\frac{\eta_b h_{PR}}{c_{pc}T_0} = (1+f)\tau_\lambda$$

Solving for f, we get

$$f = \frac{\tau_\lambda - \tau_r\tau_c}{\eta_b h_{PR}/(c_{pc}T_0) - \tau_\lambda} \tag{7.43}$$

Step 6: The power balance between the turbine, compressor, and fan, with a mechanical efficiency η_m of the coupling between the turbine and compressor and fan, gives

$$\dot{m}_C c_{pc}(T_{t3} - T_{t2}) + \dot{m}_F c_{pc}(T_{t13} - T_{t2}) = \eta_m \dot{m}_4 c_{pt}(T_{t4} - T_{t5}) \tag{7.44}$$

power into compressor | power into fan | net power from turbine

Dividing the preceding equation by $\dot{m}_C c_{pc} T_{t2}$ and using the definitions of temperature ratios, fuel/air ratio, and the bypass ratio [α, Eq. (5.46)], we obtain

$$\tau_c - 1 + \alpha(\tau_f - 1) = \eta_m(1 + f)\frac{\tau_\lambda}{\tau_r}(1 - \tau_t)$$

Solving for the turbine temperature ratio gives

$$\tau_t = 1 - \frac{1}{\eta_m(1+f)}\frac{\tau_r}{\tau_\lambda}[\tau_c - 1 + \alpha(\tau_f - 1)] \tag{7.45}$$

Equations (7.13–7.16) are used to obtain the unknown pressure or temperature ratio and efficiencies of the turbine and compressor. For the fan, the following equations apply:

$$\tau_f = \pi_f^{(\gamma_c - 1)/(\gamma_c e_f)} \tag{7.46}$$

$$\eta_f = \frac{\pi_f^{(\gamma_c - 1)/\gamma_c} - 1}{\tau_f - 1} \tag{7.47}$$

Step 7: Combining the thrust equations for the fan stream and the engine core stream, we obtain

$$\frac{F}{\dot{m}_0} = \frac{1}{1+\alpha}\frac{a_0}{g_c}\left[(1+f)\frac{V_9}{a_0} - M_0 + (1+f)\frac{R_t T_9/T_0}{R_c V_9/a_0}\frac{1 - P_0/P_9}{\gamma_c}\right] + \frac{\alpha}{1+\alpha}\frac{a_0}{g_c}\left(\frac{V_{19}}{a_0} - M_0 + \frac{T_{19}/T_0}{V_{19}/a_0}\frac{1 - P_0/P_{19}}{\gamma_c}\right) \tag{7.48}$$

Step 8: The thrust specific fuel consumption S is

$$S = \frac{\dot{m}_f}{F} = \frac{\dot{m}_f/\dot{m}_C}{(\dot{m}_0/\dot{m}_C)F/\dot{m}_0}$$

or

$$S = \frac{f}{(1+\alpha)F/\dot{m}_0} \tag{7.49}$$

Step 9: Expressions for the propulsive efficiency η_p and thermal efficiency η_T are listed next for the case of $P_9 = P_{19} = P_0$. Development of these equations is left as an exercise for the reader.

$$\eta_P = \frac{2M_0[(1+f)(V_9/a_0) + \alpha(V_{19}/a_0) - (1+\alpha)M_0]}{(1+f)(V_9/a_0)^2 + \alpha(V_{19}/a_0)^2 - (1+\alpha)M_0^2} \tag{7.50}$$

$$\eta_T = \frac{a_0^2[(1+f)(V_9/a_0)^2 + \alpha(V_{19}/a_0)^2 - (1+\alpha)M_0^2]}{2g_c f h_{PR}} \tag{7.51}$$

7.4.2 Summary of Equations—Separate-Exhaust-Stream Turbofan Engine

INPUTS:

$$M_0,\ T_0(\mathrm{K},\ ^\circ\mathrm{R}),\ \gamma_c,\ c_{pc}\left(\frac{\mathrm{kJ}}{\mathrm{kg}\cdot\mathrm{K}},\ \frac{\mathrm{Btu}}{\mathrm{lbm}\cdot{}^\circ\mathrm{R}}\right),\ \gamma_t,\ c_{pt}\left(\frac{\mathrm{kJ}}{\mathrm{kg}\cdot K},\ \frac{\mathrm{Btu}}{\mathrm{lbm}\cdot{}^\circ\mathrm{R}}\right)$$

$$h_{PR}\left(\frac{\mathrm{kJ}}{\mathrm{kg}},\ \frac{\mathrm{Btu}}{\mathrm{lbm}}\right),\ \pi_{d\max},\ \pi_b,\ \pi_n,\ \pi_{fn},\ e_c,\ e_f,\ e_t,\ \eta_b$$

$$\eta_m,\ P_0/P_9,\ P_0/P_{19},\ T_{t4}(\mathrm{K},\ ^\circ\mathrm{R}),\ \pi_c,\ \pi_f,\ \alpha$$

OUTPUTS:

$$\frac{F}{\dot{m}_0}\left(\frac{\mathrm{N}}{\mathrm{kg/s}},\ \frac{\mathrm{lbf}}{\mathrm{lbm/s}}\right),\ f,\ S\left(\frac{\mathrm{mg/s}}{\mathrm{N}},\ \frac{\mathrm{lbm/h}}{\mathrm{lbf}}\right),\ \eta_T,\ \eta_P,\ \eta_O,\ \eta_c,\ \eta_t,\ \text{etc.}$$

EQUATIONS:

$$R_c = \frac{\gamma_c - 1}{\gamma_c} c_{pc} \tag{7.52a}$$

$$R_t = \frac{\gamma_t - 1}{\gamma_t} c_{pt} \tag{7.52b}$$

$$a_0 = \sqrt{\gamma_c R_c g_c T_0} \tag{7.52c}$$

$$V_0 = a_0 M_0 \tag{7.52d}$$

$$\tau_r = 1 + \frac{\gamma_c - 1}{2} M_0^2 \tag{7.52e}$$

$$\pi_r = \tau_r^{\gamma_c/(\gamma_c-1)} \tag{7.52f}$$

$$\eta_r = 1 \quad \text{for } M_0 \leq 1 \tag{7.52g}$$

$$\eta_r = 1 - 0.075(M_0 - 1)^{1.35} \quad \text{for } M_0 > 1 \tag{7.52h}$$

$$\pi_d = \pi_{d\max}\eta_r \tag{7.52i}$$

$$\tau_\lambda = \frac{c_{pt}T_{t4}}{c_{pc}T_0} \tag{7.52j}$$

$$\tau_c = \pi_c^{(\gamma_c-1)/(\gamma_c e_c)} \tag{7.52k}$$

$$\eta_c = \frac{\pi_c^{(\gamma_c-1)/\gamma_c} - 1}{\tau_c - 1} \tag{7.52l}$$

$$\tau_f = \pi_f^{(\gamma_c-1)/(\gamma_c e_f)} \tag{7.52m}$$

$$\eta_f = \frac{\pi_f^{(\gamma_c-1)/\gamma_c} - 1}{\tau_f - 1} \tag{7.52n}$$

$$f = \frac{\tau_\lambda - \tau_r\tau_c}{\eta_b h_{PR}/(c_{pc}T_0) - \tau_\lambda} \tag{7.52o}$$

$$\tau_t = 1 - \frac{1}{\eta_m(1+f)}\frac{\tau_r}{\tau_\lambda}[\tau_c - 1 + \alpha(\tau_f - 1)] \tag{7.52p}$$

$$\pi_t = \tau_t^{\gamma_t/[(\gamma_t-1)e_t]} \tag{7.52q}$$

$$\eta_t = \frac{1 - \tau_t}{1 - \tau_t^{1/e_t}} \tag{7.52r}$$

$$\frac{P_{t9}}{P_9} = \frac{P_0}{P_9}\pi_r\pi_d\pi_c\pi_b\pi_t\pi_n \tag{7.52s}$$

$$M_9 = \sqrt{\frac{2}{\gamma_t - 1}\left[\left(\frac{P_{t9}}{P_9}\right)^{(\gamma_t-1)/\gamma_t} - 1\right]} \tag{7.52t}$$

$$\frac{T_9}{T_0} = \frac{\tau_\lambda\tau_t}{(P_{t9}/P_9)^{(\gamma_t-1)/\gamma_t}}\frac{c_{pc}}{c_{pt}} \tag{7.52u}$$

$$\frac{V_9}{a_0} = M_9\sqrt{\frac{\gamma_t R_t T_9}{\gamma_c R_c T_0}} \tag{7.52v}$$

$$\frac{P_{t19}}{P_{19}} = \frac{P_0}{P_{19}}\pi_r\pi_d\pi_f\pi_{fn} \tag{7.52w}$$

$$M_{19} = \sqrt{\frac{2}{\gamma_c - 1}\left[\left(\frac{P_{t19}}{P_{19}}\right)^{(\gamma_c-1)/\gamma_c} - 1\right]} \tag{7.52x}$$

$$\frac{T_{19}}{T_0} = \frac{\tau_r \tau_f}{(P_{t19}/P_{19})^{(\gamma_c-1)/\gamma_c}} \tag{7.52y}$$

$$\frac{V_{19}}{a_0} = M_{19}\sqrt{\frac{T_{19}}{T_0}} \tag{7.52z}$$

$$\frac{F}{\dot{m}_0} = \frac{1}{1+\alpha}\frac{a_0}{g_c}\left[(1+f)\frac{V_9}{a_0} - M_0 + (1+f) \times \frac{R_t T_9/T_0}{R_c V_9/a_0}\frac{1 - P_0/P_9}{\gamma_c}\right] + \frac{\alpha}{1+\alpha}\frac{a_0}{g_c} \times \left(\frac{V_{19}}{a_0} - M_0 + \frac{T_{19}/T_0}{V_{19}/a_0}\frac{1 - P_0/P_{19}}{\gamma_c}\right) \tag{7.52aa}$$

$$S = \frac{f}{(1+\alpha)F/\dot{m}_0} \tag{7.55ab}$$

$$\text{Thrust ratio (FR)} = \frac{(1+f)\dfrac{V_9}{a_0} - M_0 + (1+f)\dfrac{R_t T_9/T_0}{R_c V_9/a_0}\dfrac{1 - P_0/P_9}{\gamma_c}}{\dfrac{V_{19}}{a_0} - M_0 + \dfrac{T_{19}/T_0}{V_{19}/a_0}\dfrac{1 - P_0/P_{19}}{\gamma_c}} \tag{7.52ac}$$

$$\eta_P = \frac{2M_0[(1+f)V_9/a_0 + \alpha(V_{19}/a_0) - (1+\alpha)M_0]}{(1+f)(V_9/a_0)^2 + \alpha(V_{19}/a_0)^2 - (1+\alpha)M_0^2} \tag{7.52ad}$$

$$\eta_T = \frac{a_0^2[(1+f)(V_9/a_0)^2 + \alpha(V_{19}/a_0)^2 - (1+\alpha)M_0^2]}{2g_c f h_{PR}} \tag{7.52ae}$$

$$\eta_O = \eta_P \eta_T \tag{7.52af}$$

7.4.3 Exit Pressure Conditions

Separate-stream turbofan engines are generally used with subsonic aircraft, and the pressure ratio across both primary and secondary nozzles is not very large. As a result, often convergent-only nozzles are utilized. In this case, if the nozzles are choked, we have

$$\frac{P_{t19}}{P_{19}} = \left(\frac{\gamma_c + 1}{2}\right)^{\gamma_c/(\gamma_c-1)} \quad \text{and} \quad \frac{P_{t9}}{P_9} = \left(\frac{\gamma_t + 1}{2}\right)^{\gamma_t/(\gamma_t-1)} \tag{7.53}$$

Thus

$$\frac{P_0}{P_{19}} = \frac{P_{t19}/P_{19}}{P_{19}/P_0} = \frac{[(\gamma_c + 1)/2]^{\gamma_c/(\gamma_c - 1)}}{\pi_r \pi_d \pi_f \pi_{fn}} \tag{7.54}$$

and

$$\frac{P_0}{P_9} = \frac{P_{t9}/P_9}{P_9/P_0} = \frac{[(\gamma_t + 1)/2]^{\gamma_t/(\gamma_t - 1)}}{\pi_r \pi_d \pi_c \pi_b \pi_t \pi_n} \tag{7.55}$$

Note that these two expressions are valid only when both P_9 and P_{19} are greater than P_0. If these expressions predict P_9 and P_{19} less than P_0, the nozzles will not be choked. In this case, we take $P_{19} = P_0$ and/or $P_9 = P_0$.

Example 7.6

As our first example for the turbofan with losses, we calculate the performance of a turbofan engine cycle with the following input data.

INPUTS:

$$M_0 = 0.8,\ T_0 = 390°\text{R},\ \gamma_c = 1.4,\ c_{pc} = 0.240\ \text{Btu/(lbm} \cdot °\text{R)}$$
$$\gamma_t = 1.33,\ c_{pt} = 0.276\ \text{Btu/(lbm} \cdot °\text{R)},\ h_{PR} = 18{,}400\ \text{Btu/lbm}$$
$$\pi_{d\max} = 0.99,\ \pi_b = 0.96,\ \pi_n = 0.99,\ \pi_{fn} = 0.99,\ e_c = 0.90,\ e_f = 0.89$$
$$\pi_t = 0.89,\ \eta_b = 0.99,\ \eta_m = 0.99,\ P_0/P_9 = 0.9,\ P_0/P_{19} = 0.9$$
$$T_{t4} = 3000°\text{R},\ \pi_c = 36,\ \pi_f = 1.7,\ \alpha = 8$$

EQUATIONS:

$$R_c = \frac{\gamma_c - 1}{\gamma_c} c_{pc} = \frac{0.4}{1.4}(0.24 \times 778.16) = 53.36\ \text{ft} \cdot \text{lbf/(lbm} \cdot °\text{R)}$$

$$R_t = \frac{\gamma_t - 1}{\gamma_t} c_{pt} = \frac{0.33}{1.33}(0.276 \times 778.16) = 53.29\ \text{ft} \cdot \text{lbf/(lbm} \cdot °\text{R)}$$

$$a_0 = \sqrt{1.4 \times 53.36 \times 32.174 \times 390} = 968.2\ \text{ft/s}$$

$$V_0 = a_0 M_0 = 968.2 \times 0.8 = 774.6\ \text{ft/s}$$

$$\tau_r = 1 + \frac{\gamma_c - 1}{2} M_0^2 = 1 + 0.2 \times 0.8^2 = 1.128$$

$$\pi_r = \tau_r^{\gamma_c/(\gamma_c - 1)} = 1.128^{3.5} = 1.5243$$

$$\eta_r = 1 \quad \text{since } M_0 < 1$$

$$\pi_d = \pi_{d\max} \eta_r = 0.99$$

$$\tau_\lambda = \frac{c_{pt} T_{t4}}{c_{pc} T_0} = \frac{0.276 \times 3000}{0.240 \times 390} = 8.846$$

$$\tau_c = \pi_c^{(\gamma_c - 1)/(\gamma_c e_c)} = 36^{1/(3.5 \times 0.9)} = 3.119$$

$$\eta_c = \frac{\pi_c^{(\gamma_c - 1)/\gamma_c} - 1}{\tau_c - 1} = \frac{36^{1/3.5} - 1}{3.119 - 1} = \frac{1.784}{2.119} = 84.2\%$$

$$\tau_f = \pi_f^{(\gamma_c - 1)/\gamma_c e_f)} = 1.7^{1/(3.5 \times 0.89)} = 1.1857$$

$$\eta_f = \frac{\pi_f^{(\gamma_c - 1)/\gamma_c} - 1}{\tau_f - 1} = \frac{1.7^{1/35} - 1}{1.1857 - 1} = \frac{0.1637}{0.1857} = 88.2\%$$

$$f = \frac{\tau_\lambda - \tau_r \tau_c}{h_{PR} \eta_b / (c_p T_0) - \tau_\lambda}$$

$$= \frac{8.846 - 1.128 \times 3.119}{18{,}400 \times 0.99/(0.24 \times 390) - 8.846} = 0.02868$$

$$\tau_t = 1 - \frac{1}{\eta_m (1 + f)} \frac{\tau_r}{\tau_\lambda} [\tau_c - 1 + \alpha(\tau_f - 1)]$$

$$= 1 - \frac{1}{0.99(1.02868)} \frac{1.128}{8.846} [3.119 - 1 + 8(1.1857 - 1)]$$

$$= 0.54866$$

$$\pi_t = \tau_t^{\gamma_t / [(\gamma_t - 1) e_t]} = 0.54866^{1.33/(0.33 \times 0.89)} = 0.06599$$

$$\eta_t = \frac{1 - \tau_t}{1 - \tau_t^{1/e_t}} = \frac{1 - 0.54866}{1 - 0.54866^{1/0.89}} = 92.0\%$$

$$\frac{P_{t9}}{P_9} = \frac{P_0}{P_9} \pi_r \pi_d \pi_c \pi_b \pi_t \pi_n$$

$$= 0.9 \times 1.5243 \times 0.99 \times 36 \times 0.96 \times 0.06599 \times 0.99 = 3.066$$

$$M_9 = \sqrt{\frac{2}{\gamma_t - 1} \left[\left(\frac{P_{t9}}{P_9} \right)^{(\gamma_t - 1)/\gamma_t} - 1 \right]}$$

$$= \sqrt{\frac{2}{0.33} (3.066^{0.33/1.33} - 1)} = 1.394$$

$$\frac{T_9}{T_0} = \frac{8.846 \times 0.54866}{3.066^{0.33/1.33}} \frac{0.240}{0.276} = 3.196$$

$$\frac{V_9}{a_0} = M_9 \sqrt{\frac{\gamma_t R_t T_9}{\gamma_c R_c T_0}} = 1.394 \sqrt{\frac{1.33 \times 53.29}{1.40 \times 53.36} (3.196)} = 2.427$$

$$M_{19} = \sqrt{\frac{2}{\gamma_c - 1}\left[\left(\frac{P_{t19}}{P_{19}}\right)^{(\gamma_c-1)/\gamma_c} - 1\right]}$$

$$= \sqrt{\frac{2}{0.4}(2.286^{1/3.5} - 1)} = 1.154$$

$$\frac{T_{19}}{T_0} = \frac{\tau_r \tau_f}{(P_{t19}/P_{19})^{(\gamma_c-1)/\gamma_c}} = \frac{1.128 \times 1.1857}{2.286^{1/3.5}} = 1.0561$$

$$\frac{V_{19}}{a_0} = M_{19}\sqrt{\frac{T_{19}}{T_0}} = 1.154\sqrt{1.0561} = 1.186$$

$$\frac{F}{\dot{m}_0} = \frac{1}{1+\alpha}\frac{a_0}{g_c}\left[(1+f)\frac{V_9}{a_0} - M_0 + (1+f)\frac{R_t T_9/T_0}{R_c V_9/A_0}\frac{1 - P_0/P_9}{\gamma_c}\right]$$

$$+ \frac{\alpha}{1+\alpha}\frac{a_0}{g_c}\left(\frac{V_{19}}{a_0} - M_0 + \frac{T_{19}/T_0}{V_{19}/a_0}\frac{1 - P_0/P_{19}}{\gamma_c}\right)$$

$$= \frac{968.2}{9 \times 32.174}\left(1.02868 \times 2.427 - 0.8 + 1.02868\frac{53.29}{53.36}\frac{3.196}{2.427}\frac{0.1}{1.4}\right)$$

$$+ \frac{8 \times 968.2}{9 \times 32.174}\left(1.186 - 0.8 + \frac{1.0561}{1.186}\frac{0.1}{1.4}\right)$$

$$= 3.3436(1.79324 + 3.59684) = 18.02 \text{ lbf/(lbm/s)}$$

$$S = \frac{f}{(1+\alpha)F/\dot{m}_0} = \frac{3600 \times 0.02868}{9 \times 18.02} = 0.6366 \text{ (lbm/h)/lbf}$$

$$FR = \frac{1.79324}{3.59684/8} = 3.988$$

$$\eta_P = \frac{2M_0[(1+f)V_9/a_0 + \alpha(V_{19}/a_0) - (1+\alpha)M_0]}{(1+f)(V_9/a_0)^2 + \alpha(V_{19}/a_0)^2 - (1+\alpha)M_0^2}$$

$$= \frac{2 \times 0.8(1.02868 \times 2.427 + 8 \times 1.186 - 9 \times 0.8)}{1.02868 \times 2.427^2 + 8 \times 1.186^2 - 9 \times 0.8^2}$$

$$\eta_T = \frac{a_0^2[(1+f)(V_9/a_0)^2 + \alpha(V_{19}/a_0)^2 - (1+\alpha)M_0^2]}{2g_c f h_{PR}}$$

$$= \frac{968.2^2(1.02868 \times 2.427^2 + 8 \times 1.186^2 - 9 \times 0.8^2)}{2 \times 32.174 \times 0.02868 \times 18{,}400 \times 778.16} = 40.98\%$$

$$\eta_O = \eta_T \eta_P = 0.4098 \times 0.6627 = 27.16\%$$

Example 7.7

Because the turbofan cycle has three design variables, its performance with losses can be understood by performing a parametric analysis, plotting the

results vs values of the design variables, and comparing results to the performance of the ideal turbofan. Figures 7.13–7.16 are plots for turbofan engines with $P_9 = P_{19} = P_0$ and the following input values. Unless shown otherwise, the Mach number, compressor pressure ratio, and fan pressure ratio are the values listed under *Baseline*:

$T_0 = 216.7$ K	$\pi_{d\max} = 0.98$	$e_c = 0.90$	*Baseline*
$\gamma_c = 1.4$	$\pi_b = 0.98$	$e_t = 0.91$	$M_0 = 0.9$
$c_{pc} = 1.004$ kJ/(kg · K)	$\pi_n = \pi_{fn} = 0.98$	$e_f = 0.88$	$\pi_c = 24$
$\gamma_t = 1.35$	$\eta_b = 0.99$	$h_{PR} = 42{,}800$ kJ/kg	$\pi_f = 2$
$c_{pt} = 1.096$ kJ/(kg · K)	$\eta_m = 0.98$	$T_{t4} = 1670$ K	

Figures 7.13a, 7.13b, and 7.13c show the influence of compressor pressure ratio and bypass ratio on engine performance. As the bypass ratio increases, the difference in specific thrust between the engine cycle with losses and the "ideal" engine cycle increases. The major difference between the engine cycle's thrust specific fuel consumption for the two models is due to the much higher "fuel/air" ratio for the "real" engine.

Figures 7.14a and 7.14b show the influence of Mach number and bypass ratio on engine performance. The engine's specific thrust is reduced more than that of the ideal engine at high Mach number because of the increasing inlet total pressure loss. The limiting Mach number for economical operation of a turbofan engine with a specific bypass ratio is much lower for the engine with losses than for the ideal engine.

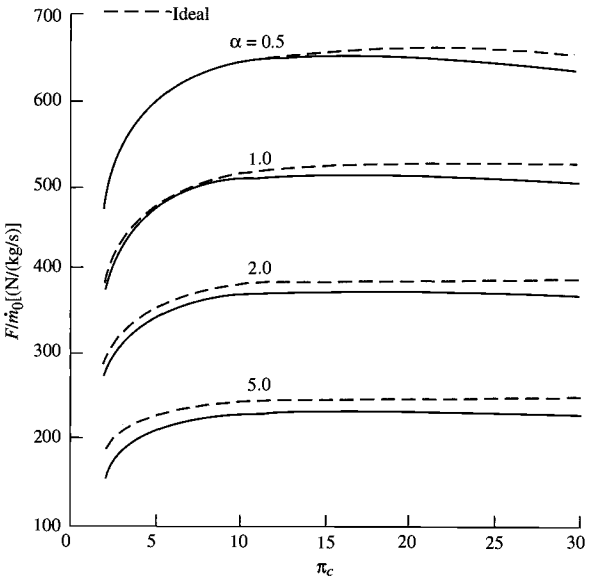

Fig. 7.13a Turbofan engine with losses vs compressor pressure ratio: specific thrust.

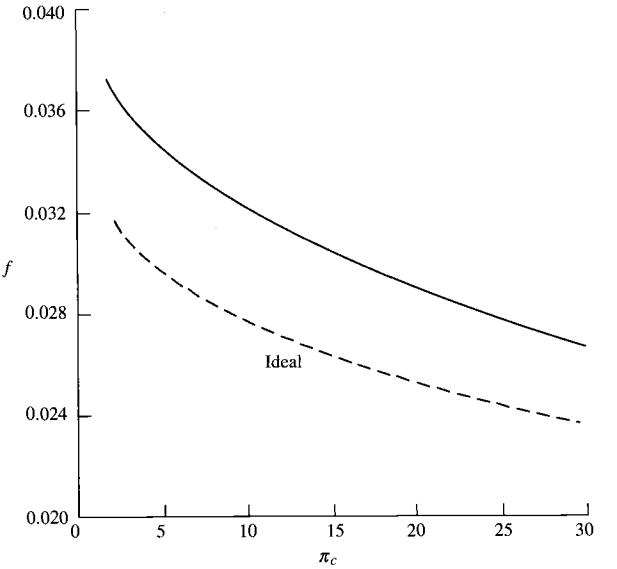

Fig. 7.13b Turbofan engine with losses vs compressor pressure ratio: fuel/air ratio.

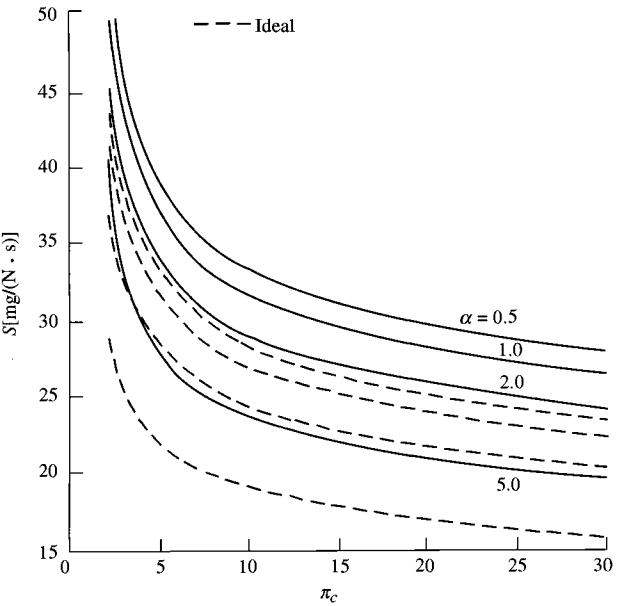

Fig. 7.13c Turbofan engine with losses vs compressor pressure ratio: thrust-specific fuel consumption.

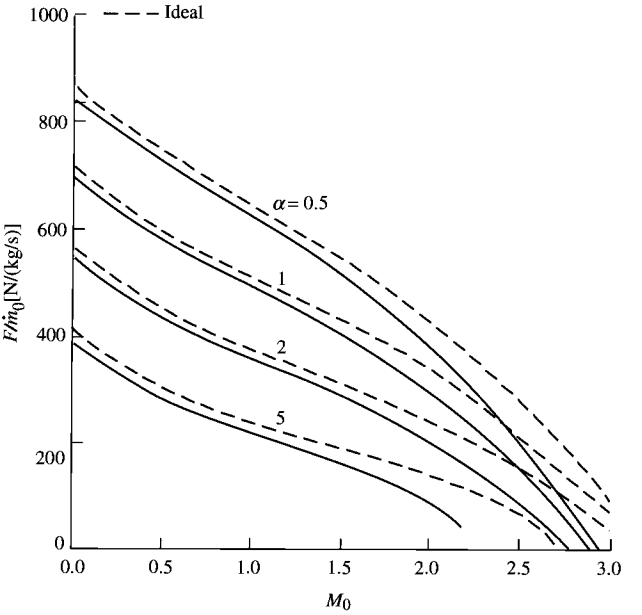

Fig. 7.14a Turbofan engine with losses vs flight Mach number: specific thrust.

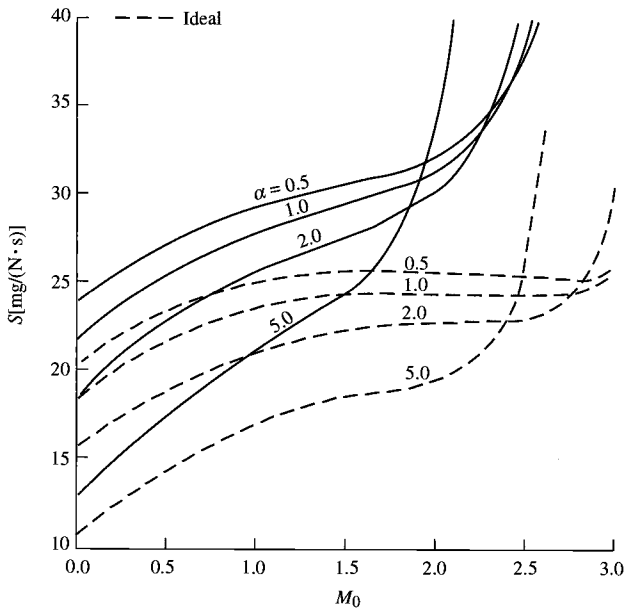

Fig. 7.14b Turbofan engine with losses vs flight Mach number: thrust-specific fuel consumption.

Figures 7.15a and 7.15b show the influence of fan pressure ratio and bypass ratio on engine performance. An optimum fan pressure ratio still exists for the turbofan with losses, and the value of the optimum fan pressure ratio is much lower than that for the ideal turbofan.

Figures 7.16a and 7.16b show the variation in specific thrust and thrust specific fuel consumption with bypass ratio and fan pressure ratio. An optimum bypass ratio still exists for the turbofan with losses, and the value of the optimum bypass ratio is much less than that for the ideal turbofan.

7.4.4 Optimum Bypass Ratio α^*

As was true for the turbofan with no losses, we may obtain an expression that allows us to determine the bypass ratio α^* that leads to minimum thrust specific fuel consumption. For a given set of such prescribed variables (τ_r, π_c, π_f, τ_λ, V_0), we may locate the minimum S by taking the partial derivative of S with respect to the bypass ratio α. We consider the case where the exhaust pressures of both the fan stream and the core stream equal the ambient pressure $P_0 = P_9 = P_{19}$. Because the fuel/air ratio is not a function of bypass ratio, we have

$$S = \frac{f}{(1+\alpha)(F/\dot{m}_0)}$$

$$\frac{\partial S}{\partial \alpha} = \frac{\partial}{\partial \alpha}\left[\frac{f}{(1+\alpha)(F/\dot{m}_0)}\right] = 0$$

$$\frac{\partial S}{\partial \alpha} = \frac{-f}{[(1+\alpha)(F/\dot{m}_0)]^2}\frac{\partial}{\partial \alpha}\left[(1+\alpha)\left(\frac{F}{\dot{m}_0}\right)\right] = 0$$

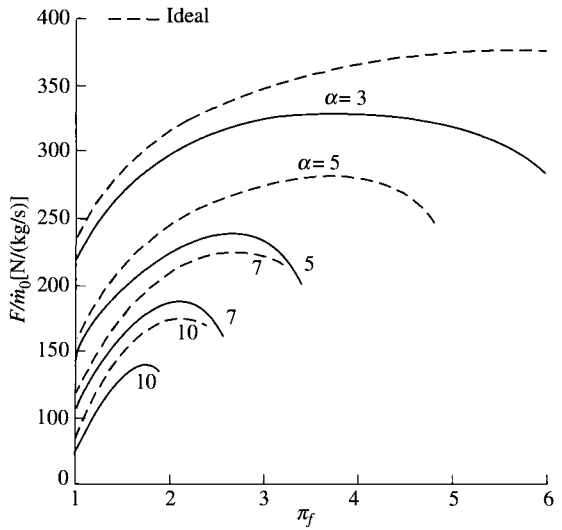

Fig. 7.15a Turbofan engine with losses vs fan pressure ratio: specific thrust.

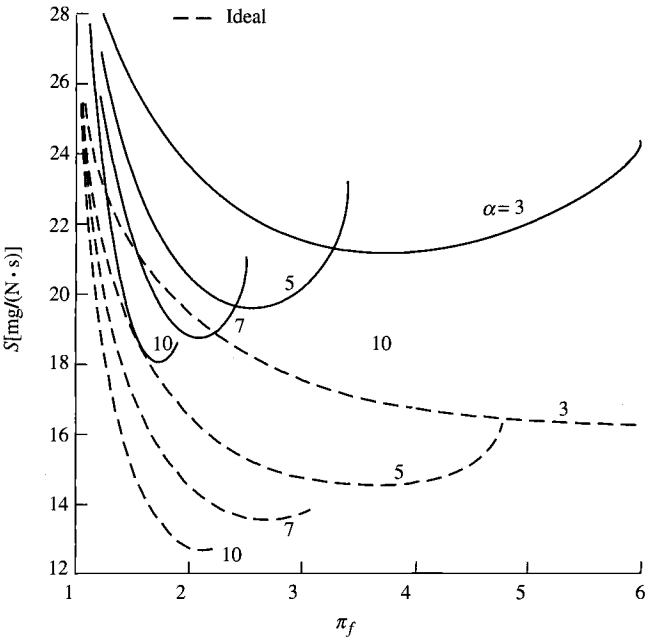

Fig. 7.15b Turbofan engine with losses vs fan pressure ratio: thrust-specific fuel consumption.

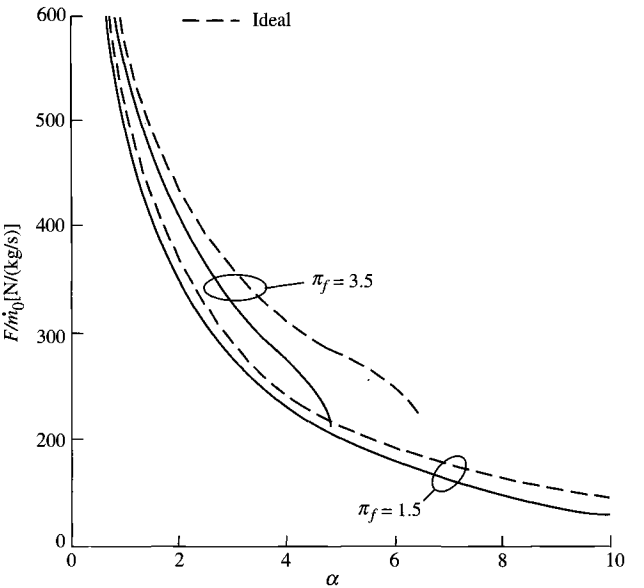

Fig. 7.16a Turbofan engine with losses vs bypass ratio: specific thrust.

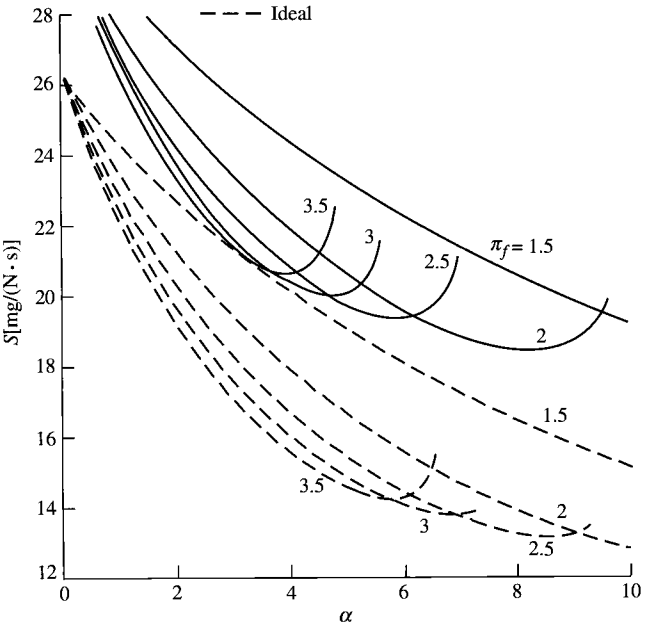

Fig. 7.16b Turbofan engine with losses vs bypass ratio: thrust-specific fuel consumption.

Thus $\partial S/\partial\alpha = 0$ is satisfied by

$$\frac{\partial}{\partial\alpha}\left[\frac{g_c}{V_0}(1+\alpha)\left(\frac{F}{\dot{m}_0}\right)\right] = 0$$

where

$$\frac{g_c}{V_0}(1+\alpha)\left(\frac{F}{\dot{m}_0}\right) = (1+f)\left(\frac{V_9}{V_0}-1\right) + \alpha\left(\frac{V_{19}}{V_0}-1\right)$$

Then the optimum bypass ratio is given by the following expression:

$$\frac{\partial}{\partial\alpha}\left[(1+f)\left(\frac{V_9}{V_0}-1\right) + \alpha\left(\frac{V_{19}}{V_0}-1\right)\right]$$
$$= (1+f)\frac{\partial}{\partial\alpha}\left(\frac{V_9}{V_0}\right) + \frac{V_{19}}{V_0} - 1 = 0 \qquad \text{(i)}$$

However,

$$\frac{1}{2V_9/V_0}\frac{\partial}{\partial\alpha}\left[\left(\frac{V_9}{V_0}\right)^2\right]=\frac{\partial}{\partial\alpha}\left(\frac{V_9}{V_0}\right)$$

Thus Eq. (i) becomes

$$\left(\frac{V_9}{V_0}\right)_{\alpha^*}=-\frac{1+f}{2}\frac{\partial/\partial\alpha[(V_9/V_0)^2]}{V_{19}/V_0-1} \tag{ii}$$

Note that

$$\left(\frac{V_9}{V_0}\right)^2=\frac{1}{M_0^2}\left(\frac{V_9}{a_0}\right)^2=\frac{1}{[2/(\gamma_c-1)](\tau_r-1)}\left(\frac{V_9}{a_0}\right)^2$$
$$=\frac{1}{[2/(\gamma_c-1)](\tau_r-1)}M_9^2\frac{\gamma_t R_t T_9}{\gamma_c R_c T_0}$$

Using Eqs. (7.41) and (7.42), we have

$$\left(\frac{V_9}{V_0}\right)^2=\frac{\tau_\lambda\tau_t}{\tau_r-1}\left[1-\left(\frac{P_{t9}}{P_9}\right)^{-(\gamma_t-1)/\gamma_t}\right] \tag{iii}$$

where

$$\frac{P_{t9}}{P_9}=\pi_r\pi_d\pi_c\pi_b\pi_t\pi_n \tag{iv}$$

Combining Eqs. (iii) and (iv), we obtain

$$\left(\frac{V_9}{V_0}\right)^2=\frac{\tau_\lambda\tau_t}{\tau_r-1}\left[1-\frac{1}{\Pi(\pi_t)^{(\gamma_t-1)/\gamma_t}}\right] \tag{v}$$

where

$$\Pi=(\pi_r\pi_d\pi_c\pi_b\pi_n)^{(\gamma_t-1)/\gamma_t} \tag{7.56}$$

Noting that

$$\pi_t^{(\gamma_t-1)/\gamma_t}=\tau_t^{1/e_t}$$

we see that then Eq. (v) becomes

$$\left(\frac{V_9}{V_0}\right)^2 = \frac{\tau_\lambda}{\tau_r - 1}\left(\tau_t - \frac{1}{\Pi}\tau_t^{-(1-e_t)/e_t}\right) \tag{vi}$$

To evaluate the partial derivative of Eq. (ii), we apply the chain rule to Eq. (vi) as follows:

$$\frac{\partial}{\partial\alpha}\left[\left(\frac{V_9}{V_0}\right)^2\right] = \frac{\partial\tau_t}{\partial\alpha}\frac{\partial}{\partial\tau_t}\left[\left(\frac{V_9}{V_0}\right)^2\right]$$

$$= \frac{\partial\tau_t}{\partial\alpha}\frac{\tau_\lambda}{\tau_r - 1}\left(1 + \frac{1 - e_t}{e_t}\frac{\tau_t^{-1/e_t}}{\Pi}\right) \tag{vii}$$

Since

$$\tau_t = 1 - \frac{1}{\eta_m(1+f)}\frac{\tau_r}{\tau_\lambda}[\tau_c - 1 + \alpha(\tau_f - 1)]$$

then

$$\frac{\partial\tau_t}{\partial\alpha} = -\frac{\tau_r(\tau_f - 1)}{\eta_m\tau_\lambda(1+f)} \tag{viii}$$

Combining Eqs. (ii), (vii), and (viii) yields

$$\left(\frac{V_9}{V_0}\right)_{\alpha^*} = \frac{1}{2\eta_m(\tau_r - 1)}\frac{\tau_r(\tau_f - 1)}{V_{19}/V_0 - 1}\left(1 + \frac{1 - e_t}{e_t}\frac{\tau_t^{-1/e_t}}{\Pi}\right)$$

An expression for τ_t is obtained by squaring the preceding equation, substituting for $(V_9/V_0)^2$ by using Eq. (vi), and then solving for the first τ_t within parentheses on the right side of Eq. (vi). The resulting expression for the turbine temperature ratio τ_t^* corresponding to the optimum bypass ratio α^* is

$$\tau_t^* = \frac{\tau_t^{-(1-e_t)/e_t}}{\Pi} + \frac{1}{\tau_\lambda(\tau_r - 1)}\left[\frac{1}{2\eta_m}\frac{\tau_r(\tau_f - 1)}{V_{19}/V_0 - 1}\left(1 + \frac{1 - e_t}{e_t}\frac{\tau_t^{-1/e_t}}{\Pi}\right)\right]^2 \tag{7.57}$$

Because Eq. (7.57) is an equation for τ_t^* in terms of itself, in addition to other known values, an iterative solution is required. A starting value of τ_t^*, denoted by τ_{ti}^*, is obtained by solving Eq. (7.57) for the case when $e_t = 1$, which gives

$$\tau_{ti}^* = \frac{1}{\Pi} + \frac{1}{\tau_\lambda(\tau_r - 1)}\left[\frac{1}{2\eta_m}\frac{\tau_r(\tau_f - 1)}{V_{19}/V_0 - 1}\right]^2 \tag{7.58}$$

This starting value can be substituted into the right-hand side of Eq. (7.57), yielding a new value of τ_t^*. This new value of τ_t^* is then substituted into Eq. (7.57), and another new value of τ_t^* is calculated. This process continues until the change in successive calculations of τ_t^* is less than some small number (say, 0.0001). Once the solution for τ_t^* is found, the optimum bypass ratio α^* is calculated by using Eq. (7.45), solved for α:

$$\alpha^* = \frac{\eta_m(1+f)\tau_\lambda(1-\tau_t^*) - \tau_r(\tau_c - 1)}{\tau_r(\tau_f - 1)} \tag{7.59}$$

When the optimum bypass ratio α^* is desired in calculating the parametric engine cycle performance, Eqs. (7.56), (7.57), (7.58), and (7.59) replace the equation for τ_t contained in the summary of equations and α^* is an output.

Example 7.8

Because the optimum-bypass-ratio turbofan cycle has two design variables, its performance with losses can be understood by performing a parametric analysis, plotting the results vs values of the design variables, and comparing results to the performance of the optimum-bypass-ratio ideal turbofan. Figures 7.17–7.19 are plots for optimum-bypass-ratio turbofan engines with the following input values (the same input used for the parametric analysis of the turbofan engine with losses in Example 7.7). The results for the ideal optimum-bypass-ratio turbofan engine cycle are shown in dashed lines. Unless shown otherwise, the Mach number, compressor pressure ratio, and fan pressure ratio are the values listed under *Baseline*:

$T_0 = 216.7$ K	$\pi_{d\max} = 0.98$	$e_c = 0.90$	*Baseline*
$\gamma_c = 1.4$	$\pi_b = 0.98$	$e_t = 0.91$	$M_0 = 0.9$
$c_{pc} = 1.004$ kJ/(kg · K)	$\pi_n = \pi_{fn} = 0.98$	$e_f = 0.88$	$\pi_c = 24$
$\gamma_t = 1.35$	$\eta_b = 0.99$	$h_{PR} = 42{,}800$ kJ/kg	$\pi_f = 2$
$c_{pt} = 1.096$ kJ/(kg · K)	$\eta_m = 0.98$	$T_{t4} = 1670$ K	
$\frac{P_0}{P_9} = 1$	$\frac{P_0}{P_{19}} = 1$		

Figures 7.17a and 7.17b show the following characteristics of the optimum bypass-ratio turbofan engine:

1) The compressor pressure ratio has very little effect on the specific thrust.
2) Increasing the fan pressure ratio increases the specific thrust.
3) The optimum bypass ratio increases with π_c and decreases with π_f.
4) Specific fuel consumption decreases with increasing π_c.
5) Specific fuel consumption increases with increasing π_f.

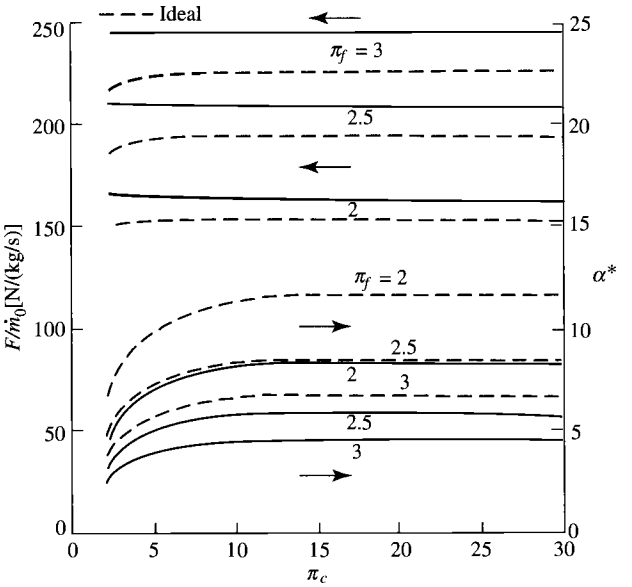

Fig. 7.17a Optimum-bypass-ratio turbofan engine vs π_c: specific thrust and optimum bypass ratio.

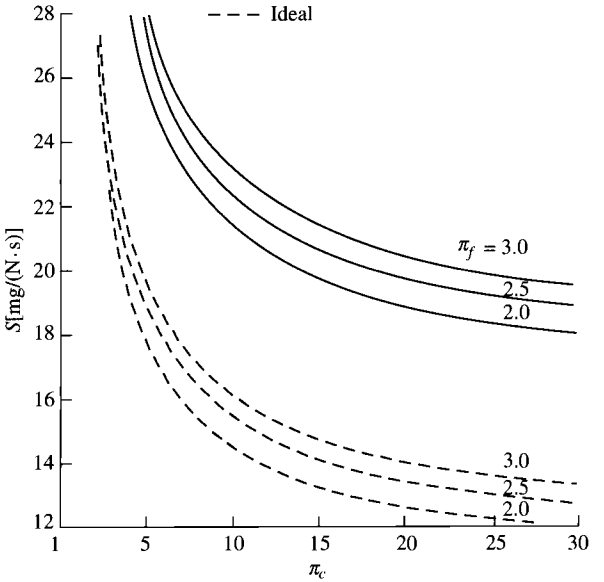

Fig. 7.17b Optimum-bypass-ratio turbofan engine vs π_c: thrust-specific fuel consumption.

The effect of flight Mach number on the performance of the optimum-bypass-ratio turbofan engine as shown in Figs. 7.18a and 7.18b has the following characteristics:

1) The specific thrust decreases with Mach number up to a Mach number of about 1.5.
2) Increasing the fan pressure ratio increases the specific thrust.
3) The optimum bypass ratio decreases with increasing M_0 and π_f.
4) The optimum turbofan is a turbojet engine at a Mach number of about 2.5.
5) Specific fuel consumption increases with increasing M_0 and π_f.

Figures 7.19a and 7.19b show the following characteristics of the optimum-bypass-ratio turbofan engine with respect to fan pressure ratio and flight Mach number:

1) Increasing the fan pressure ratio increases the specific thrust.
2) Increasing the flight Mach number decreases the specific thrust.
3) The optimum bypass ratio decreases with π_f and increases with M_0.
4) Specific fuel consumption increases with increasing π_f.
5) Specific fuel consumption increases with increasing M_0.

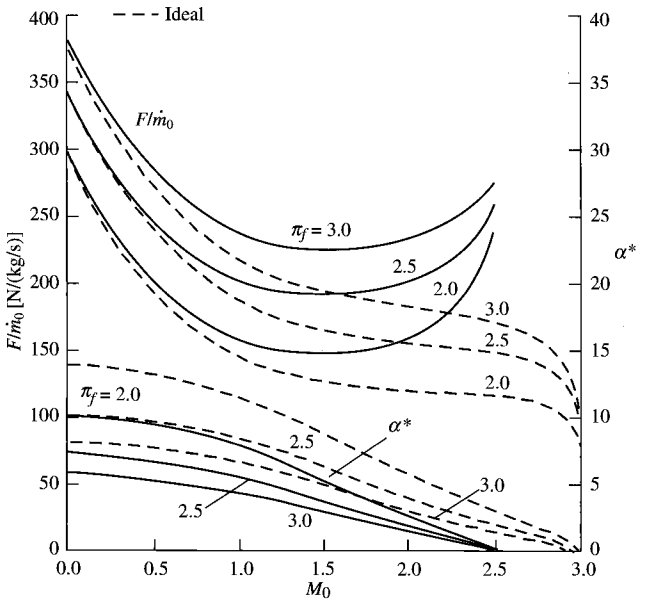

Fig. 7.18a Optimum-bypass-ratio turbofan engine vs Mach number: specific thrust and optimum bypass ratio.

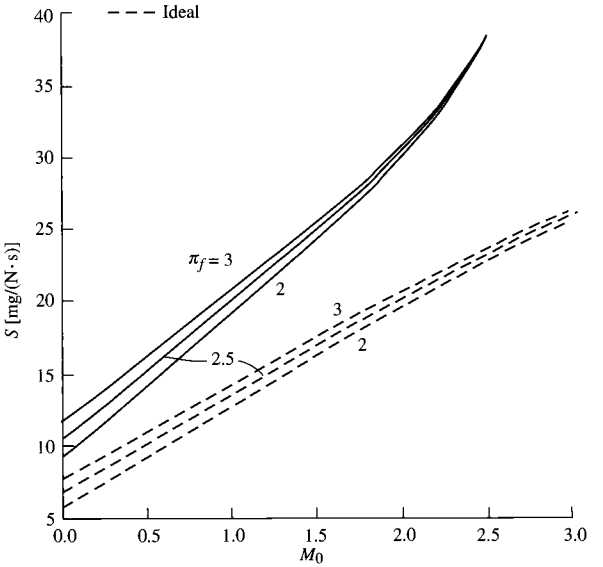

Fig. 7.18b Optimum-bypass-ratio turbofan engine vs Mach number: thrust-specific fuel consumption.

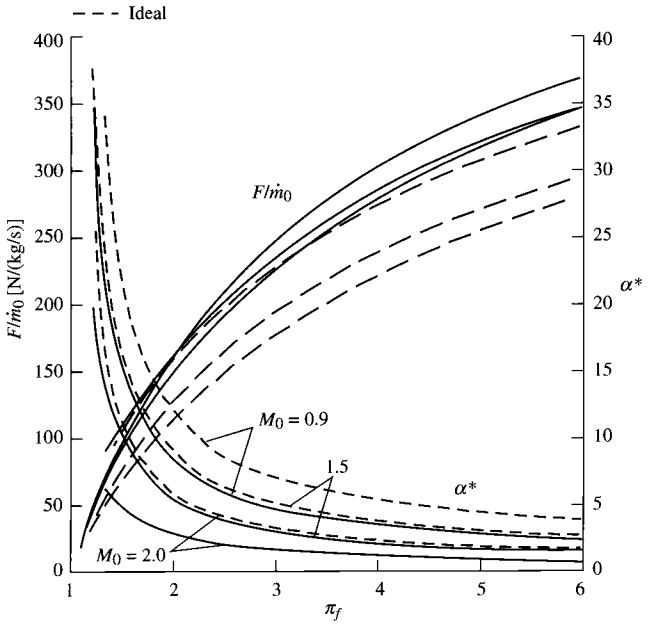

Fig. 7.19a Optimum-bypass-ratio turbofan engine vs τ_f: specific thrust and optimum bypass ratio.

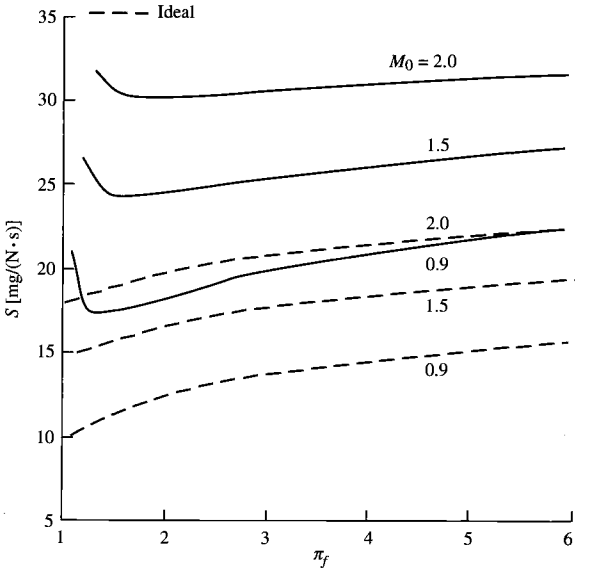

Fig. 7.19b Optimum-bypass-ratio turbofan engine vs π_f: thrust specific fuel consumption.

Problems

7.1 Develop a set of equations for parametric analysis of a ramjet engine with losses. Calculate the performance of a ramjet with losses over a Mach number range of 1 to 3 for the following input data:

$$\pi_{d\max} = 0.95 \quad T_0 = 217 \text{ K} \quad \gamma_c = 1.4 \quad c_{pc} = 1.004 \text{ kJ/(kg} \cdot \text{K)}$$
$$\pi_b = 0.94 \quad \eta_b = 0.96 \quad \gamma_t = 1.3 \quad c_{pt} = 1.235 \text{ kJ/(kg} \cdot \text{K)}$$
$$\pi_n = 0.95 \quad \frac{P_0}{P_9} = 1 \quad T_{14} = 1800 \text{ K} \quad h_{PR} = 42{,}800 \text{ kJ/kg}$$

Compare your results to those obtained from the PARA computer program.

7.2 Why are the polytropic efficiencies used for the fans, compressors, and turbines in parametric engine cycle analysis rather than the isentropic efficiencies?

7.3 Calculate and compare the performance of turbojet engines with the basic data of Example 7.1 for components with technology level 2 values in Table 6.2 (assume cooled turbine and the same diffuser and nozzle values as in Example 7.1). Comment on the changes in engine performance.

7.4 Using the PARA computer program, compare the performance of turbojet engines with the basic data of Example 7.1 for the polytropic efficiencies of component technology levels 1, 2, 3, and 4 in Table 6.2 (assume uncooled turbine). Comment on the improvements in engine performance.

7.5 Using the PARA computer program, compare the performance of turbojet engines with the basic data of Example 7.3 for the polytropic efficiencies of component technology levels 1, 2, 3, and 4 in Table 6.2 (assume uncooled turbine). Comment on the changes in optimum compressor pressure ratio and improvements in engine performance.

7.6 Using the PARA computer program, find the range of compressor pressure ratios that give turbojet engines with specific thrust greater than 88 lbf/(lbm/s) and thrust specific fuel consumption below 1.5 (lbm/h)/lbf at $M_0 = 1.5$, $T_0 = 390°R$, and component performance of technology level 3 in Table 6.2 (assume type C diffuser, cooled turbine, and type F nozzle). Determine the compressor pressure ratio giving maximum specific thrust. Assume $\eta_m = 0.99$, $\gamma_c = 1.4$, $c_{pc} = 0.24$ Btu/(lbm · °R), $\gamma_t = 1.3$, $c_{pt} = 0.296$ Btu/(lbm · °R), $h_{PR} = 18{,}400$ Btu/lbm, and $P_0/P_9 = 1$.

7.7 Using the PARA computer program, find the range of compressor pressure ratios that give turbojet engines with specific thrust greater than 950 N/(kg/s) and thrust specific fuel consumption below 40 (mg/s)/N at $M_0 = 0.9$, $T_0 = 216.7$ K, and component performance of technology level 3 in Table 6.2 (assume type C diffuser, cooled turbine, and type F nozzle). Determine the compressor pressure ratio giving maximum specific thrust. Assume $\eta_m = 0.99$, $\gamma_c = 1.4$, $c_{pc} = 1.004$ kJ/(kg · K), $\gamma_t = 1.3$, $c_{pt} = 1.239$ kJ/(kg · K), $h_{PR} = 42{,}800$ kJ/kg, and $P_0/P_9 = 1$.

7.8 For a single-spool turbojet engine with losses, determine the compressor exit T_t and P_t, the turbine exit T_t and P_t, and the nozzle exit Mach number M_9 for the following input data:

$M_0 = 0.8$	$\pi_c = 9$	$T_{t4} = 1780$ K	$h_{PR} = 42{,}800$ kJ/kg
$P_0 = 29.92$ kPa	$T_0 = 229$ K	$\gamma_c = 1.4$	$c_{pc} = 1.004$ kJ/(kg · K)
$\pi_{d\max} = 0.95$	$\pi_b = 0.904$	$\gamma_t = 1.3$	$c_{pt} = 1.239$ kJ/(kg · K)
$e_c = 0.85$	$e_t = 0.88$	$\eta_b = 0.99$	$\eta_m = 0.98$
$\pi_n = 0.98$	$\dfrac{P_0}{P_9} = 0.8$		

Compare your results with those obtained from the PARA computer program.

7.9 Products of combustion enter the afterburner (station 6) at a rate of 230 lbm/s with the following properties: $T_{t6} = 1830°R$, $P_{t6} = 38$ psia, $M_6 = 0.4$, $\gamma = 1.33$, $c_P = 0.276$ Btu/(lbm · °R), and $R = 53.34$ ft · lbf/

(lbm · °R). Assume a calorically perfect gas and $\eta_{AB} = 0.95$.

(a) Determine the flow area at station 6 in square feet.

(b) With the afterburner off, determine the area (ft^2) of the exhaust nozzle's choked throat (station 8) for $P_{t8}/P_{t6} = 0.97$.

(c) With the afterburner on, determine the afterburner fuel flow rate (lbm/s) and the area (ft^2) of the exhaust nozzle's choked throat (station 8) for $P_{t8}/P_{t6} = 0.94$ and $T_{t8} = 3660°R$. *Assume* that the gas leaving the operating afterburner is a calorically perfect gas with $\gamma = 1.3$, $c_p = 0.297$ Btu/(lbm · °R), and the same gas constant. Also assume the properties at station 6 do not change and $h_{PR} = 18{,}400$ Btu/lbm.

7.10 Calculate and compare the performance of afterburning turbojet engines with the basic data of Example 7.5 but with combustion temperatures of level 4 in Table 6.2 for compressor pressure ratios of 4, 8, and 12. Comment on the improvements in engine performance.

7.11 Using the PARA computer program, find the range of compressor pressure ratios that give afterburning turbojet engines with specific thrust greater than 118 lbf/(lbm/s) and thrust specific fuel consumption below 1.7 (lbm/h)/lbf at $M_0 = 1.5$, $T_0 = 390°R$, and component performance of technology level 3 in Table 6.2 (assume type C diffuser, cooled turbine, and type F nozzle). Determine the compressor pressure ratio giving maximum specific thrust. Assume $\eta_m = 0.99$, $\gamma_c = 1.4$, $c_{pc} = 0.24$ Btu/(lbm · °R), $\gamma_t = 1.3$, $c_{pc} = 0.296$ Btu/(lbm · °R), $\gamma_{AB} = 1.3$, $c_{pAB} = 0.296$ Btu/(lbm · °R), $h_{PR} = 18{,}400$ Btu/lbm, and $P_0/P_9 = 1$.

7.12 Using the PARA computer program, find the range of compressor pressure ratios that give afterburning turbojet engines with specific thrust greater than 1250 N/(kg/s) and thrust specific fuel consumption below 45 (mg/s)/N at $M_0 = 0.9$, $T_0 = 216.7$ K, and component performance of technology level 3 in Table 6.2 (assume type C diffuser, cooled turbine, and type F nozzle). Determine the compressor pressure ratio giving maximum specific thrust. Assume $\eta_m = 0.99$, $\gamma_c = 1.4$, $c_{pt} = 1.004$ kJ/(kg · K), $\gamma_t = 1.3$, $c_{pt} = 1.239$ kJ/(kg · K), $\gamma_{AB} = 1.3$, $c_{pAB} = 0.239$ kJ/(kg · K), $h_{PR} = 42{,}800$ kJ/kg, and $P_0/P_9 = 1$.

7.13 Using the PARA computer program, calculate and compare the performance of afterburning turbojet engines with the basic data of Example 7.5 for the different combustion temperatures and component technologies of levels 2, 3, and 4 in Table 6.2 (assume cooled turbine, type B diffuser, and type F nozzle). Comment on the improvements in engine performance.

7.14 Show that the propulsive efficiency and thermal efficiency of a turbofan engine with separate exhausts are given by Eqs. (7.50) and (7.51), respectively.

7.15 Calculate the performance of a turbofan engine with the basic data of Example 7.6 but with a fan pressure ratio of 1.65 and a bypass ratio of 10. Comment on the improvement in engine performance. Compare your results to those of the PARA computer program.

7.16 Using the PARA computer program, compare the performance of turbofan engines with the basic data of Example 7.6 for the polytropic efficiencies of component technology levels 2, 3, and 4 in Table 6.2 (assume cooled turbine, type A diffuser, and type D nozzle). Comment on the improvement in engine performance.

7.17 Using the PARA computer program, find the range of compressor pressure ratios and fan pressure ratios that give optimum-bypass-ratio, separate-exhaust turbofan engines with specific thrust greater than 13 lbf/(lbm/s) and thrust specific fuel consumption below 1.0 (lbm/h)/lbf at $M_0 = 0.9$, $T_0 = 390°\text{R}$, and component performance of technology level 2 in Table 6.2 (assume type A diffuser, uncooled turbine, and type D nozzle). Assume $\eta_m = 0.99$, $\gamma_c = 1.4$, $c_{pc} = 0.24$ Btu/(lbm · °R), $\gamma_t = 1.3$, $c_{pt} = 0.296$ Btu/(lbm · °R), $h_{PR} = 18{,}400$ Btu/lbm, and $P_0/P_9 = 1$.

7.18 Using the PARA computer program, find the range of compressor pressure ratios and fan pressure ratios that give optimum-bypass-ratio, separate-exhaust turbofan engines with specific thrust greater than 130 N/(kg/s) and thrust specific fuel consumption below 28 (mg/s)/N at $M_0 = 0.8$, $T_0 = 216.7$ K, and component performance of technology level 2 in Table 6.2 (assume type A diffuser, uncooled turbine, and type D nozzle). Assume $\eta_m = 0.99$, $\gamma_c = 1.4$, $c_{pc} = 1.004$ kJ/(kg · K), $\gamma_t = 1.3$, $c_{pt} = 1.239$ kJ/(kg · K), $h_{PR} = 42{,}800$ kJ/kg, and $P_0/P_9 = 1$.

7.19 Calculate the performance of an optimum-bypass-ratio turbofan engine with the basic data of Example 7.8 but with a compressor pressure ratio of 30 and fan pressure ratio of 1.7. Compare your results to those of the PARA computer program.

7.20 Using the PARA computer program, compare the performance of optimum-bypass-ratio turbofan engines with the basic data of Example 7.8 for the polytropic efficiencies of component technology levels 2, 3, and 4 in Table 6.2 (assume cooled turbine, type A diffuser, and type D nozzle). Comment on the improvement in engine performance.

7.21 A stationary gas turbine engine with regeneration is shown in Fig. P7.1. The effectiveness of a regenerator η_{rg} is defined by

$$\eta_{rg} = \frac{T_{t3.5} - T_{t3}}{T_{t5} - T_{t3}}$$

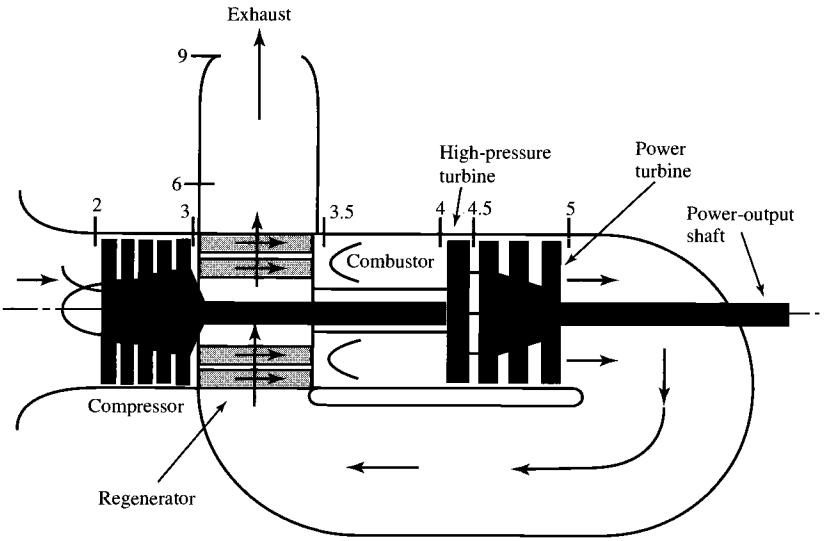

Fig. P7.1

The total pressure ratios across the cold and hot gas paths of the regenerator are defined by

$$\pi_{\text{rg cold}} = \frac{P_{t3.5}}{P_{t3}} \qquad \pi_{\text{rg hot}} = \frac{P_{t6}}{P_{t5}}$$

Using these definitions and others, develop a set of equations for parametric analysis of this turboshaft engine with regeneration and losses.

Problems for Supporting Material

SM7.1 Calculate the performance of an afterburning mixed-flow turbofan engine with the basic data of Example SM7.2 at $M_0 = 0.9$ for a compressor pressure ratio of 30 and a fan pressure ratio of 4. Compare your results to those of the PARA computer program.

SM7.2 Using the PARA computer program, find the range of compressor pressure ratios and corresponding fan pressure ratios that give mixed-flow turbofan engines of 0.5 bypass ratio a specific thrust greater than 55 lbf/(lbm/s) and thrust specific fuel consumption below 1.3 (lbm/h)/lbf at $M_0 = 1.8$, $T_0 = 390°\text{R}$, and component performance of technology level 3 in Table 6.2 (assume type C diffuser, cooled turbine, and type F nozzle). Assume $\eta_m = 0.99$, $\gamma_c = 1.4$, $c_{pc} = 0.24$ Btu/(lbm · °R), $\gamma_t = 1.3$, $c_{pt} = 0.296$ Btu/(lbm · °R), $M_6 = 0.5$, $\pi_{M\max} = 0.95$, $h_{PR} = 18{,}400$ Btu/lbm, and $P_0/P_9 = 1$.

SM7.3 Using the PARA computer program, find the range of compressor pressure ratios and corresponding fan pressure ratios that give mixed-flow turbofan engines of 0.4 bypass ratio a specific thrust greater than 550 N/(kg/s) and thrust specific fuel consumption below 39 (mg/s)/N at $M_0 = 2.0$, $T_0 = 216.7$ K, and component performance of technology level 3 in Table 6.2 (assume type C diffuser, cooled turbine, and type F nozzle). Assume $\eta_m = 0.99$, $\gamma_c = 1.4$, $c_{pc} = 1.004$ kJ/(kg · K), $\gamma_t = 1.3$, $c_{pt} = 1.239$ kJ/(kg · K), $M_6 = 0.5$, $\pi_{M\max} = 0.95$, $h_{PR} = 42{,}800$ kJ/kg, and $P_0/P_9 = 1$.

SM7.4 Using the PARA computer program, find the range of compressor pressure ratios and corresponding fan pressure ratios that give afterburning mixed-flow turbofan engines of 0.5 bypass ratio a specific thrust greater than 105 lbf/(lbm/s) and thrust specific fuel consumption below 1.845 (lbm/h)/lbf at $M_0 = 1.8$, $T_0 = 390°$R, and component performance of technology level 3 in Table 6.2 (assume type C diffuser, cooled turbine, and type F nozzle). Assume $\eta_m = 0.99$, $\gamma_c = 1.4$, $c_{pc} = 0.24$ Btu/(lbm · °R), $\gamma_t = 1.3$, $c_{pt} = 0.296$ Btu/(lbm · °R), $\gamma_{AB} = 1.3$, $c_{pAB} = 0.296$ Btu/(lbm · °R), $M_6 = 0.5$, $\pi_{M\max} = 0.95$, $h_{PR} = 18{,}400$ Btu/lbm, and $P_0/P_9 = 1$.

SM7.5 Using the PARA computer program, find the range of compressor pressure ratios and corresponding fan pressure ratios that give afterburning mixed-flow turbofan engines of 0.4 bypass ratio a specific thrust greater than 1000 N/(kg/s) and thrust specific fuel consumption below 52.25 (mg/s)/N at $M_0 = 2.0$, $T_0 = 216.7$ K, and component performance of technology level 3 in Table 6.2 (assume type C diffuser, cooled turbine, and type F nozzle). Assume $\eta_m = 0.99$, $\gamma_c = 1.4$, $c_{pc} = 1.004$ kJ/(kg · K), $\gamma = 1.3$, $c_{pt} = 1.239$ kJ/(kg · K), $\gamma_{AB} = 1.3$, $c_{pAB} = 1.239$ kJ/(kg · K), $M_6 = 0.5$, $\pi_{M\max} = 0.95$, $h_{PR} = 42{,}800$ kJ/kg, $M_6 = 0.5$, and $P_0/P_9 = 1$.

SM7.6 Using the PARA computer program, compare the performance of afterburning mixed-flow turbofan engines with the basic data of Example SM7.2 at $M_0 = 0.9$, $\pi_c = 24$, and $\pi_f = 3.5$ for the different combustion temperatures and component technologies of levels 2, 3, and 4 in Table 6.2 (assume cooled turbine, type C diffuser, and type F nozzle). Also assume the same γ, c_p, η_m, and $\pi_{M\max}$. Comment on the improvement in engine performance.

SM7.7 For the mixed-flow turbofan engine with the bypass ratio specified, show that the following functional iteration equation for the fan temperature ratio with matched total pressures entering the mixer can be obtained from Eqs. (SM7.31) and (SM7.32):

$$(\tau_f)_{i+1} = \frac{\tau_r[\alpha - (\tau_c - 1)] + \eta_m(1+f)\tau_\lambda}{\tau_r\alpha + [\eta_m(1+f)\tau_\lambda/(\pi_c\pi_b)^{(\gamma_t-1)e_t/\gamma_t}]^{(\gamma_t-1)/(\gamma_c-1)(\gamma_c/\gamma_t)e_te_j-1}}$$

with the first value of the fan temperature ratio given by

$$(\tau_f)_1 = \frac{\tau_r[\alpha - (\tau_c - 1)] + \eta_m(1+f)\tau_\lambda}{\tau_r\alpha + \eta_m(1+f)\tau_\lambda/(\pi_c\pi_b)^{(\gamma_t-1)e_t/\gamma_t}}$$

SM7.8 Calculate the performance of a turboprop engine with the basic data of Example SM7.4 at a compressor pressure ratio of 20 and turbine temperature ratio of 0.5. Compare your results to those of Example SM7.4 and the PARA computer program.

SM7.9 Using the PARA computer program, find the range of compressor pressure ratios that give turboprop engines with optimum turbine temperature ratio τ_t^* a specific thrust greater than 120 lbf/(lbm/s) and thrust specific fuel consumption below 0.8 (lbm/h)/lbf at $M_0 = 0.7$, $T_0 = 447°\text{R}$, and component performance of technology level 2 in Table 6.2 (assume type A diffuser, uncooled turbine, and type D nozzle). Assume $\eta_{\text{prop}} = 0.83$, $\eta_g = 0.99$, $\eta_{mH} = 0.99$, $\eta_{mL} = 0.99$, $\gamma_c = 1.4$, $c_{pc} = 0.24$ Btu/(lbm · °R), $\gamma_t = 1.35$, $c_{pt} = 0.265$ Btu/(lbm · °R), and $h_{PR} = 18{,}400$ Btu/lbm.

SM7.10 Using the PARA computer program, find the range of compressor pressure ratios that give turboprop engines with optimum turbine temperature ratio τ_t^* a specific thrust greater than 1300 N/(kg/s) and thrust specific fuel consumption below 18 (mg/s)/N at $M_0 = 0.6$, $T_0 = 250$ K, and component performance of technology level 2 in Table 6.2 (assume type A diffuser, uncooled turbine, and type D nozzle). Assume $\eta_{\text{prop}} = 0.83$, $\eta_g = 0.99$, $\eta_{mH} = 0.995$, $\eta_{mL} = 0.995$, $\gamma_e = 1.4$, $c_{pc} = 1.004$ kJ/(kg · K), $\gamma_t = 1.35$, $c_{pt} = 1.108$ kJ/(kg · K), and $h_{PR} = 42{,}800$ kJ/kg.

SM7.11 Using the PARA computer program, compare the performance of turboprop engines with the basic data of Example SM7.4 with component technologies of levels 1, 2, 3, and 4 in Table 6.2. Comment on the improvement in engine performance.

Gas Turbine Design Problems

7.D1 You are to determine the range of compressor pressure ratios and bypass ratios for turbofan engines with losses that best meet the design requirements for the hypothetical passenger aircraft HP-1.

Hand-Calculate Performance with Losses (HP-1 Aircraft). Using the parametric cycle analysis equations for a turbofan engine with losses and component technology level 4 in Table 6.2 (assume cooled turbine, type A diffuser, and type D nozzle) with $T_{t4} = 1560$ K, hand-calculate the specific thrust and thrust specific fuel consumption for a turbofan engine with a compressor pressure ratio of 36, fan pressure ratio of

1.8, and bypass ratio of 10 at the 0.83 Mach and 11-km altitude cruise condition. Assume $\gamma_c = 1.4$, $c_{pc} = 1.004$ kJ/(kg · K), $\gamma_t = 1.3$, $c_{pt} = 1.235$ kJ/(kg · K), $h_{PR} = 42{,}800$ kJ/kg, and $\eta_m = 0.99$. Compare your answers to results from the parametric cycle analysis program PARA and Design Problem 5.D1.

Computer-Calculated Performance with Losses (HP-1 Aircraft). For the 0.83 Mach and 11-km altitude cruise condition, determine the performance available from turbofan engines with losses. This part of the analysis is accomplished by using the PARA computer program with component technology level 4 in Table 6.2 (assume cooled turbine, type A diffuser, and type D nozzle) and $T_{t4} = 1560$ K. Specifically, you are to vary the compressor pressure ratio from 20 to 40 in increments of 2. Fix the fan pressure ratio at your assigned value of_____. Evaluate bypass ratios of 4, 6, 8, 10, 12, and the optimum value. Assume $\gamma_c = 1.4$, $c_{pc} = 1.004$ kg/(kg · K), $\gamma_t = 1.3$, $c_{pt} = 1.235$ kJ/(kg · K), $h_{PR} = 42{,}800$ kJ/kg, and $\eta_m = 0.99$.

Calculate Minimum Specific Thrust at Cruise (HP-1 Aircraft). You can calculate the minimum uninstalled specific thrust at cruise based on the following information:

1) The thrust of the two engines must be able to offset drag at 0.83 Mach and 11-km altitude and have enough excess thrust for P_s of 1.5 m/s. Determine the required installed thrust to attain the cruise condition, using Eq. (1.28). Assuming $\phi_{\text{inlet}} + \phi_{\text{noz}} = 0.02$, determine the required uninstalled thrust.

2) Determine the maximum mass flow into the 2.2-m-diam inlet for the 0.83 Mach and 11-km altitude flight condition, using the equation given in the background section for this design problem in Chapter 1.

3) Using the results of steps 1 and 2, calculate the minimum uninstalled specific thrust at cruise.

4) Perform steps 2 and 3 for inlet diameters of 2.5, 2.75, 3.0, 3.25, and 3.5 m.

Select Promising Engine Cycles (HP-1 Aircraft). Plot thrust specific fuel consumption vs specific thrust (thrust per unit mass flow) for the engines analyzed in the preceding. Plot a curve for each bypass ratio and cross-plot the values of the compressor pressure ratio (see Fig. P5.D1). The result is a carpet plot (a multivariable plot) for the cruise condition. Now draw a dashed horizontal line on the carpet plot corresponding to the maximum allowable uninstalled thrust specific consumption ($S_{\max}$) for the cruise condition (determined in the Chapter 1 portion of this design problem). Draw a dashed vertical line for each minimum uninstalled specific thrust determined in the preceding. Your carpet plots will look similar to the example shown in Fig. P5.D1. What ranges of bypass ratio and compressor pressure ratio look most promising? Compare to the results of Design Problem 5.D1.

7.D2 You are to determine the ranges of compressor pressure ratio and bypass ratio for mixed-flow turbofan engines with losses that best meet the design requirements for the hypothetical fighter aircraft HF-1.

Hand-Calculate Performance with Losses (HF-1 Aircraft). Using the parametric cycle analysis equations for a mixed-flow turbofan engine with losses and component technology level 4 in Table 6.2 (assume cooled turbine, type C diffuser, and type F nozzle) with $T_{t4} = 3250°R$, hand-calculate the specific thrust and thrust specific fuel consumption for an ideal turbofan engine with a compressor pressure ratio of 25 and bypass ratio of 0.5 at the 1.6-Mach and 40-kft altitude supercruise condition. Because the bypass ratio is given, you will need to use the system of equations given in Problem 7.27 to calculate the temperature ratio of the fan. Assume $\gamma_c = 1.4$, $c_{pc} = 0.240$ Btu/(lbm · °R), $\gamma_t = 1.3$, $c_{pt} = 0.296$ Btu/(lbm · °R), $h_{PR} = 18{,}400$ Btu/lbm, $M_6 = 0.4$, $\pi_{M\max} = 0.96$, and $\eta_m = 0.99$. Compare your answers to results from the parametric cycle analysis program PARA and Design Problem 5.D2.

Computer-Calculated Performance with Losses (HF-1 Aircraft). For the 1.6-Mach and 40-kft altitude supercruise condition, determine the performance available from mixed-flow turbofan engines with losses. This part of the analysis is accomplished by using the PARA computer program with component technology level 4 in Table 6.2 (assume cooled turbine, type C diffuser, and type F nozzle) and $T_{t4} = 3250°R$. Specifically, you are to vary the bypass ratio from 0.1 to 1.0 in increments of 0.05. Evaluate compressor pressure ratios of 16, 18, 20, 22, 24, and 28. Assume $\gamma_c = 1.4$, $c_{pc} = 0.240$ Btu/(lbm · °R), $\gamma_t = 1.3$, c_{pt}, $= 0.296$ Btu/(lbm · °R), $h_{PR} = 18{,}400$ Btu/lbm, $M_6 = 0.4$, $\pi_{M\max}$ $=0.96$, and $\eta_m = 0.99$.

Calculate Minimum Specific Thrust at Cruise (HF-1 Aircraft). You can calculate the minimum uninstalled specific thrust at supercruise based on the following information:

1) The thrust of the two engines must be able to offset drag at 1.6-Mach number and 40-kft altitude and 92% of takeoff weight. Assuming $\phi_{\text{inlet}} + \phi_{\text{noz}} = 0.05$, determine the required uninstalled thrust for each engine.

2) The maximum mass flow into a 5-ft^2 inlet for the 1.6-Mach number and 40-kft altitude flight condition is $\dot{m} = \rho AV = \sigma\rho_{\text{ref}} AMa = (0.2471 \times 0.07647)(5)(1.6 \times 0.8671) \times 1116) = 146.3$ lbm/s.

3) Using the results of steps 1 and 2, calculate the minimum uninstalled specific thrust at supercruise.

Select Promising Engine Cycles (HF-1 Aircraft). Plot thrust specific fuel consumption vs specific thrust (thrust per unit mass flow) for the engines analyzed in the preceding. Plot a curve for each bypass ratio, and cross-plot the values of compressor pressure ratio (see Fig. P5.D2). The result is a carpet plot (a multivariable plot) for the supercruise condition. Now draw a dashed horizontal line on the carpet plot

corresponding to the maximum allowable uninstalled thrust specific fuel consumption (S_{max}) for the cruise condition (determined in the Chapter 1 portion of this design problem). Draw a dashed vertical line for the minimum uninstalled specific thrust determined in the preceding. Your carpet plots will look similar to the example shown in Fig. P5.D2. What ranges of bypass ratio and compressor pressure ratio look most promising? Compare to the results of Design Problem 5.D2.

8
Engine Performance Analysis

8.1 Introduction

This chapter is concerned with predicting the performance of a gas turbine engine and obtaining performance data similar to Figs. 1.14a–1.14e, 1.15a, and 1.15b and the data contained in Appendix B. The analysis required to obtain engine performance is related to, but very different from, the parametric cycle analysis of Chapters 5 and 7. In parametric cycle analysis of a turbojet engine, we independently selected values of the compressor pressure ratio, main burner exit temperature, flight condition, etc. The analysis determined the turbine temperature ratio—it is dependent on the choices of compressor pressure ratio, main burner exit temperature, and flight condition, as shown by Eq. (7.12). In engine performance analysis, we consider the performance of an engine that was built (constructed physically or created mathematically) with a selected compressor pressure ratio and its corresponding turbine temperature ratio. As will be shown in this chapter, the turbine temperature ratio remains essentially constant for a turbojet engine (and many other engine cycles), and its compressor pressure ratio is dependent on the throttle setting (main burner exit temperature T_{t4}) and flight condition (M_0 and T_0). The basic independent and dependent variables of the turbojet engine are listed in Table 8.1 for both parametric cycle analysis and engine performance analysis.

In parametric cycle analysis, we looked at the variation of gas turbine engine cycles where the main burner exit temperature and aircraft flight conditions were specified via the design inputs: T_{t4}, M_0, T_0, and P_0, In addition, the engine cycle was selected along with the compressor pressure ratio, the polytropic efficiency of turbomachinery components, etc. For the combination of design input values, the resulting calculations yielded the specific performance of the engine (specific thrust and thrust specific fuel consumption), required turbine temperature ratio, and the efficiencies of the turbomachinery (fan, compressor, and turbine). The specific combination of design input values is referred to as the engine *design point* or *reference point.* The resulting specific engine thrust and fuel consumption are valid only for the given engine cycle and values of T_{t4}, M_0, T_0, π_c, τ_t, η_c, etc. When we changed any of these values in parametric cycle analysis,

Supporting Material for this chapter is available electronically. See page 869 for instructions to download.

Table 8.1 Comparison of analysis variables

Variable	Parametric cycle	Engine performance
Flight condition (M_0, T_0, and P_0)	Independent	Independent
Compressor pressure ratio π_c	Independent	Dependent
Main burner exit temperature T_{t4}	Independent	Independent
Turbine temperature ratio τ_t	Dependent	Constant

we were studying a "rubber" engine, i.e., one that changes its shape and component design to meet the thermodynamic, fluid dynamic, etc., requirements.

When a gas turbine engine is designed and built, the degree of variability of an engine depends on available technology, the needs of the principal application for the engine, and the desires of the designers. Most gas turbine engines have constant-area flow passages and limited variability (variable T_{t4}; and *sometimes variable* T_{t7} and exhaust nozzle throat area). In a simple constant-flow-area turbojet engine, the performance (pressure ratio and mass flow rate) of its compressor depends on the power from the turbine and the inlet conditions to the compressor. As we will see in this chapter, a simple analytical expression can be used to express the relationship between the compressor performance and the independent variables: throttle setting (T_{t4}) and flight condition (M_0, T_0, P_0).

When a gas turbine engine is installed in an aircraft, its performance varies with flight conditions and throttle setting and is limited by the engine control system. In flight, the pilot controls the operation of the engine directly through the throttle and indirectly by changing flight conditions. The thrust and fuel consumption will thereby change. In this chapter, we will look at how specific engine cycles perform at conditions other than their design (or reference) point.

There are several ways to obtain this engine performance. One way is to look at the interaction and performance of the compressor-burner-turbine combination, known as the *pumping characteristics* of the gas generator. In this case, the performance of the components is known because the gas generator exists. However, in a preliminary design, the gas generator has not been built, and the pumping characteristics are not available. In such a case, the gas generator performance can be estimated by using first principles and estimates of the variations in component efficiencies. In reality, the principal effects of engine performance occur because of the changes in *propulsive efficiency* and *thermal efficiency* (rather than because of changes in component efficiency). Thus a good approximation of an engine's performance can be obtained by simply assuming that the component efficiencies remain constant.

The analysis of engine performance requires a model for the behavior of each engine component over its actual range of operation. The more accurate and complete the model, the more reliable the computed results. Even though the approach (constant efficiency of rotating components and constant total pressure ratio of the other components) used in this textbook gives answers that are perfectly adequate for preliminary design, it is important to know that the usual industrial practice is to use data or correlations having greater accuracy and definition in the form of component "maps." The principal values of the maps are to

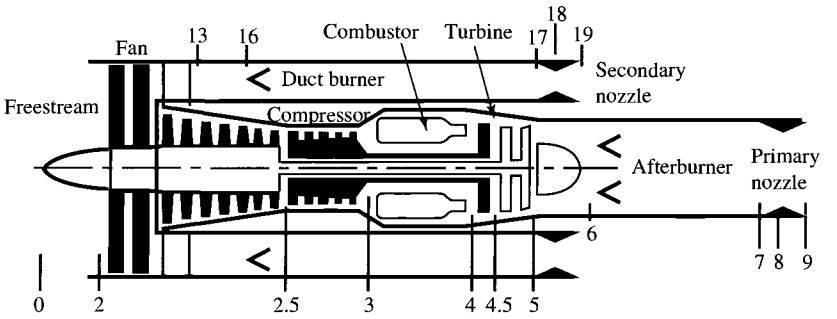

Fig. 8.1 Station numbering for two-spool gas turbine engine.

improve the understanding of component behavior and to slightly increase the accuracy of the results.

8.1.1 Nomenclature

The station numbering used for the performance analysis of the turbojet and turbofan is shown in Fig. 8.1. Note that the turbine is divided into a high-pressure turbine (station 4 to 4.5) and a low-pressure turbine (station 4.5 to 5). The high-pressure turbine drives the high-pressure compressor (station 2.5 to 3), and the low-pressure turbine drives the fan (station 2 to 13) and low-pressure compressor (station 2 to 2.5).

The assembly containing the high-pressure turbine, high-pressure compressor, and connecting shaft is called the *high-pressure spool.* That containing the low-pressure turbine, fan or low-pressure compressor, and connecting shaft is called the *low-pressure spool.* In addition to the τ and π values defined in Table 5.1, the component total temperature ratios and total pressure ratios listed in Table 8.2 are required for analysis of the gas turbine engine with high- and low-pressure spools.

8.1.2 Reference Values and Engine Performance Analysis Assumptions

Functional relationships are used to predict the performance of a gas turbine engine at different flight conditions and throttle settings. These relationships are based on the application of mass, energy, momentum, and entropy considerations to the one-dimensional steady flow of a perfect gas at an engine

Table 8.2 Additional temperature and pressure relationships

$\tau_{cH} = \dfrac{T_{t3}}{T_{t2.5}}$	$\pi_{cH} = \dfrac{P_{t3}}{P_{t2.5}}$	$\tau_{tH} = \dfrac{T_{t4.5}}{T_{t4}}$	$\pi_{tH} = \dfrac{P_{t4.5}}{T_{t4}}$
$\tau_{cL} = \dfrac{T_{t2.5}}{T_{t2}}$	$\pi_{cL} = \dfrac{P_{t2.5}}{P_{t2}}$	$\tau_{tL} = \dfrac{T_{t5}}{T_{t4.5}}$	$\pi_{tL} = \dfrac{P_{t5}}{P_{t4.5}}$
$\tau_c = \tau_{cL}\tau_{cH}$	$\pi_c = \pi_{cL}\pi_{cH}$	$\tau_t = \tau_{tH}\tau_{tL}$	$\pi_t = \pi_{tH}\pi_{tL}$

steady-state operating point. Thus, if

$$f(\tau, \pi) = \text{const}$$

represents a relationship between the two engine variables τ and π at a steady-state operating point, then the constant can be evaluated at a reference condition (subscript R) so that

$$f(\tau, \pi) = f(\tau_R, \pi_R) = \text{const}$$

since $f(\tau, \pi)$ applies to the engine at all operating points. *Sea-level static (SLS) is the normal reference condition (design point) for the value of the gas turbine engine variables.* This technique for replacing constants with reference conditions is frequently used in the analysis to follow.

For conventional turbojet, turbofan, and turboprop engines, we will consider the simple case where the high-pressure turbine entrance nozzle, low-pressure turbine entrance nozzle, and primary exit nozzle (and bypass duct nozzle for the separate-exhaust turbofan) are choked. In addition, we assume that the throat areas where choking occurs in the high-pressure turbine entrance nozzle and the low-pressure turbine entrance nozzle are constant. This type of turbine is known as a *fixed-area turbine* (FAT) engine. These assumptions are true over a wide operating range for modern gas turbine engines. The following performance analyses also include the case(s) of unchoked engine exit nozzle(s).

The following assumptions will be made in the turbojet and turbofan performance analysis:

1) The flow is choked at the high-pressure turbine entrance nozzle, low-pressure turbine entrance nozzle, and the primary exit nozzle. Also the bypass duct nozzle for the turbofan is choked.

2) The total pressure ratios of the main burner, primary exit nozzle, and bypass stream exit nozzle (π_b, π_n, and π_{fn}) do not change from their reference values.

3) The component efficiencies (η_c, η_f, η_b, η_{tH}, η_{tL}, η_{mH}, and η_{mL}) do not change from their reference values.

4) Turbine cooling and leakage effects are neglected.

5) No power is removed from the turbine to drive accessories (or alternately, η_{mH} or η_{mL} includes the power removed but is still constant).

6) Gases will be assumed to be calorically perfect both upstream and downstream of the main burner, and γ_t and c_{pt} do not vary with the power setting (T_{t4}).

7) The term unity plus the fuel/air ratio $(1+f)$ will be considered as a constant.

Assumptions 4 and 5 are made to simplify the analysis and increase understanding. Reference 12 includes turbine cooling air, compressor bleed air, and power takeoff in the performance analysis. Assumptions 6 and 7 permit easy analysis that results in a set of algebraic expressions for an engine's performance. The performance analysis of an engine with variable gas properties is covered in the Supporting Material Section SM8.3.

8.1.3 Dimensionless and Corrected Component Performance Parameters

Dimensional analysis identifies correlating parameters that allow data taken under one set of conditions to be extended to other conditions. These parameters are useful and necessary because it is always impractical to accumulate experimental data for the bewildering number of possible operating conditions, and because it is often impossible to reach many of the operating conditions in a single, affordable facility.

The quantities of pressure and temperature are normally made dimensionless by dividing each by its respective standard sea-level static values. The dimensionless pressure and temperature are represented by δ and θ, respectively, and given in Eqs. (1.2) and (1.3) When total (stagnation) properties are nondimensionalized, a subscript is used to indicate the station number of that property. The only static properties made dimensionless are freestream, the symbols for which carry no subscripts. Thus

$$\delta_i \equiv \frac{P_{ti}}{P_{\text{ref}}} \tag{8.1a}$$

and

$$\theta_i \equiv \frac{T_{ti}}{T_{\text{ref}}} \tag{8.1b}$$

where $P_{\text{ref}} = 14.696$ psia (101,300 Pa) and $T_{\text{ref}} = 518.69°\text{R}$ (288.2 K).

Dimensionless analysis of engine components yields many useful dimensionless and/or modified component performance parameters. Some examples of these are the compressor pressure ratio, adiabatic efficiency, Mach number at the compressor face, ratio of blade (tip) speed to the speed of sound, and the Reynolds number.

The *corrected mass flow rate* at engine station i used in this analysis is defined as

$$\dot{m}_{ci} \equiv \frac{\dot{m}_i \sqrt{\theta_i}}{\delta_i} \tag{8.2}$$

and is related to the Mach number at station i as shown in the following. From the definition of the mass flow parameter [Eq. (2.75)], we can write the mass flow at station i as

$$\dot{m}_i = \frac{P_{ti}}{\sqrt{T_{ti}}} A_i \times \text{MFP}(M_i)$$

Then

$$\frac{\dot{m}_{ci}}{A_i} = \frac{\dot{m}_{ci}\sqrt{T_{ti}}}{A_i P_{ti}} \frac{P_{\text{ref}}}{\sqrt{T_{\text{ref}}}} = \frac{P_{\text{ref}}}{\sqrt{T_{\text{ref}}}} \text{MFP}(M_i) \tag{8.3}$$

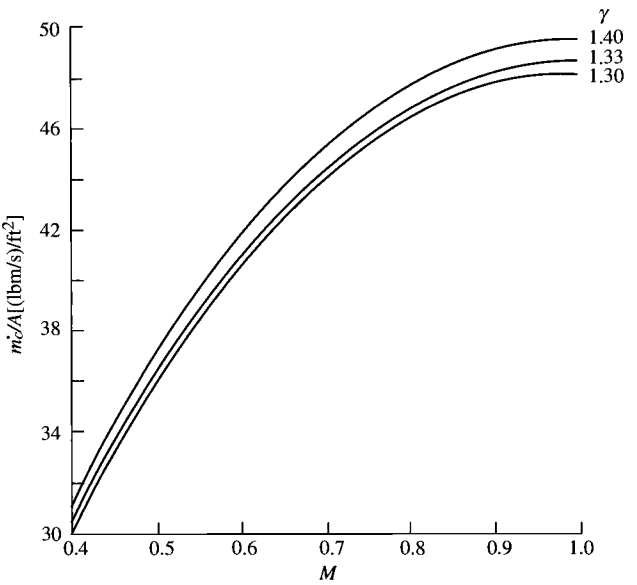

Fig. 8.2 Variation of corrected mass flow per area.

and the corrected mass flow rate per unit area is a function of the Mach number alone for a gas. Equation (8.3) is plotted vs Mach number in Fig. 8.2 for three different γ values. Aircraft gas turbine engines need high thrust or power per unit weight that requires high corrected mass flow rates per unit area.

At the entrance to the fan or compressor (station 2), the design Mach number is about 0.56, which corresponds to a corrected mass flow rate per unit area of about 40 lbm/(s · ft^2). A reduction in engine power will lower the corrected mass flow rate and the corresponding Mach number into the fan or compressor.

The flow is normally choked at the entrance to the turbine (station 4) and the throat of the exhaust nozzle (station 8) for most steady-state operating conditions of interest (the flow is typically unchoked at these stations during engine startup). When the flow is choked at station 4, the corrected mass flow rate per unit area entering the turbine is constant, which helps define the pumping characteristics of the gas generator. As shown later in this chapter, choked flow at both stations 4 and 8 limits the turbine operation. Even if the flow unchokes at a station and the Mach number drops from 1.0 to 0.9, the corrected mass flow rate is reduced less than 1%. Thus the corrected mass flow rate is considered constant when the flow is near or at choking conditions.

Choked flow at station 8 is desired in convergent-only exhaust nozzles to obtain high exit velocity and is required in a convergent-divergent exhaust nozzle to reach supersonic exit velocities. When the afterburner is operated on a turbojet or turbofan engine with choked exhaust nozzle, T_{t8} increases—this requires an increase in the nozzle throat area A_8 to maintain the correct mass

flow rate/area ratio corresponding to choked conditions. If the nozzle throat is not increased, the pressure increases and the mass flow rate decreases, which can adversely impact the upstream engine components.

The *corrected engine speed* at engine station i used in this analysis is defined as

$$N_{ci} \equiv \frac{N}{\sqrt{\theta_i}} \tag{8.4}$$

and is related to the *blade* Mach number.

These four parameters represent a first approximation of the complete set necessary to reproduce nature for the turbomachinery. These extremely useful parameters have become a standard in the gas turbine industry and are summarized in Table 8.3.

Three additional corrected quantities have found common acceptance for describing the performance of gas turbine engines: corrected thrust F_c, corrected thrust specific fuel consumption S_c, and corrected fuel mass flow rate $\dot{m}_{fc}$.

The *corrected thrust* is defined as

$$F_c \equiv \frac{F}{\delta_0} \tag{8.5}$$

For many gas turbine engines operating at maximum T_{t4}, the corrected thrust is essentially a function of only the corrected freestream total temperature θ_0.

The *corrected thrust-specific fuel consumption* is defined as

$$S_c \equiv \frac{S}{\sqrt{\theta_0}} \tag{8.6}$$

Table 8.3 Corrected parameters

Parameter	Symbol	Corrected parameter
Total pressure	P_{ti}	$\delta_i = \frac{P_{ti}}{P_{\text{ref}}}$
Total temperature	T_{ti}	$\theta_i = \frac{T_{ti}}{T_{\text{ref}}}$
Rotational speed	$N = \text{RPM}$	$N_{ci} = \frac{N}{\sqrt{\theta_i}}$
Mass flow rate	$\dot{m}_i$	$\dot{m}_{ci} = \frac{\dot{m}_i\sqrt{\theta_i}}{\delta_i}$
Thrust	F	$F_c = \frac{F}{\delta_0}$
Thrust-specific fuel consumption	S	$S_c = \frac{S}{\sqrt{\theta_0}}$
Fuel mass flow rate	$\dot{m}_f$	$\dot{m}_{fc} = \frac{\dot{m}_f}{\delta_2\sqrt{\theta_2}}$

and the *corrected fuel mass flow rate is* defined as

$$\dot{m}_{fc} \equiv \frac{\dot{m}_f}{\delta_2 \sqrt{\theta_2}} \tag{8.7}$$

Like the corrected thrust, these two corrected quantities collapse the variation in fuel consumption with flight condition and throttle setting.

These three corrected quantities are closely related. By using the equation for thrust-specific fuel consumption

$$S = \frac{\dot{m}_f}{F}$$

$\pi_d = P_{t2}/P_{t0}$, and the fact that $\theta_2 = \theta_0$, the following relationship results between these corrected quantities:

$$S_c = \pi_d \frac{\dot{m}_{fc}}{F_c} \tag{8.8}$$

These extremely useful corrected engine performance parameters have also become a standard in the gas turbine industry and are included in Table 8.3.

8.1.4 Component Performance Maps

8.1.4.1 Compressor and fan performance maps. The performance of a compressor or fan is normally shown by using the total pressure ratio, corrected mass flow rate, corrected engine speed, and component efficiency. Most often this performance is presented in one map showing the interrelationship of all four parameters, like that depicted in Fig. 8.3. Sometimes, for clarity, two maps are used, with one showing the pressure ratio vs corrected mass flow rate/corrected

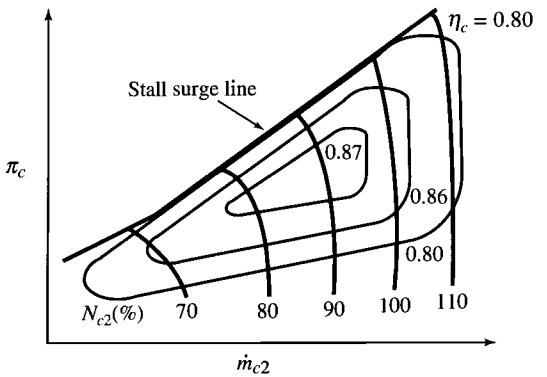

Fig. 8.3 Typical compressor performance map.

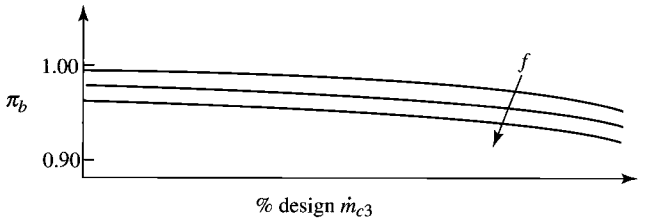

Fig. 8.4a Combustor pressure ratio.

speed and the other showing compressor efficiency vs corrected mass flow rate/corrected speed.

A limitation on fan and compressor performance of special concern is the *stall* or *surge line.* Steady operation above the line is impossible, and entering the region even momentarily is dangerous to the gas turbine engine.

8.1.4.2 Main burner maps. The performance of the main burner is normally presented in terms of its performance parameters that are most important to engine performance: total pressure ratio of the main burner π_b and its combustion efficiency η_b. The total pressure ratio of the main burner is normally plotted vs the corrected mass flow rate through the burner ($\dot{m}_3\sqrt{\theta_3}/\delta_3$) for different fuel/air ratios f, as shown in Fig. 8.4a. The efficiency of the main burner can be represented as a plot vs the temperature rise in the main burner $T_{t4} - T_{t3}$ or fuel/air ratio f for various values of inlet pressures P_{t3}, as shown in Fig. 8.4b.

8.1.4.3 Turbine maps. The flow through a turbine first passes through stationary airfoils (often called *inlet guide vanes* or *nozzles*) that turn and accelerate the fluid, increasing its tangential momentum. The flow then passes through rotating airfoils (called *rotor blades*) that remove energy from the fluid as they

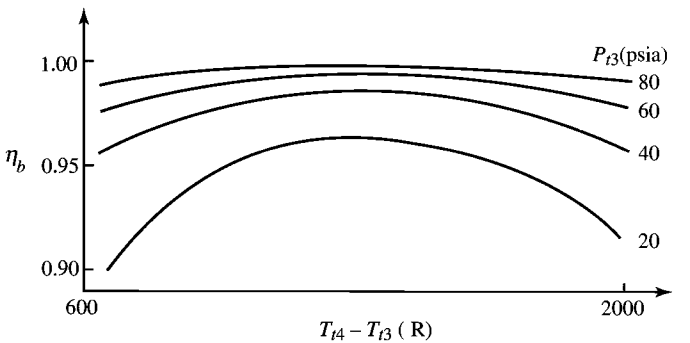

Fig. 8.4b Combustor efficiency.

change its tangential momentum. Successive pairs of stationary airfoils followed by rotating airfoils remove additional energy from the fluid. To obtain a high output power/weight ratio from a turbine, the flow entering the first-stage turbine rotor is normally supersonic, which requires the flow to pass through sonic conditions at the minimum passage area in the inlet guide vanes (nozzles). By using Eq. (8.3), the corrected inlet mass flow rate based on this minimum passage area (throat) will be constant for fixed-inlet-area turbines. This flow characteristic is shown in the typical turbine flow map (Fig. 8.5a) when the expansion ratio across the turbine $[(P_{t4}/P_{t5}) = 1/\pi_t)]$ is greater than about 2 and the flow at the throat is choked.

The performance of a turbine is normally shown by using the total pressure ratio, corrected mass flow rate, corrected turbine speed, and component efficiency. This performance can be presented in two maps or a combined map (similar to that shown for the compressor in Fig. 8.3). When two maps are used, one map shows the interrelationship of the total pressure ratio, corrected mass flow rate, and corrected turbine speed, like that depicted in Fig. 8.5a. The other map shows the interrelationship of turbine efficiency vs corrected mass flow rate/expansion ratio, like that shown in Fig. 8.5b. When a combined map is used, the total pressure ratio of the turbine is plotted vs the product of corrected mass flow rate and the corrected speed, as shown in Fig. 8.5c. This spreads out the lines of constant corrected speed from those shown in Fig. 8.5a, and the turbine efficiency can now be shown. If we tried to add these lines of constant turbine efficiency to Fig. 8.5a, many would coincide with the line for choked flow.

For the majority of aircraft gas turbine engine operation, the turbine efficiency varies very little. In the analysis of this chapter, we consider that the turbine efficiency is constant.

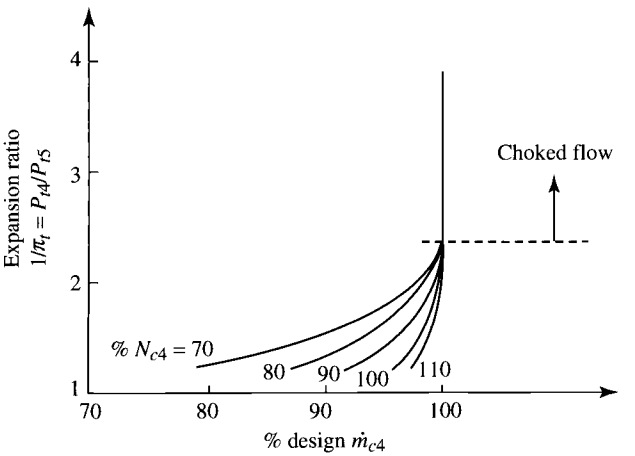

Fig. 8.5a Typical turbine flow map.

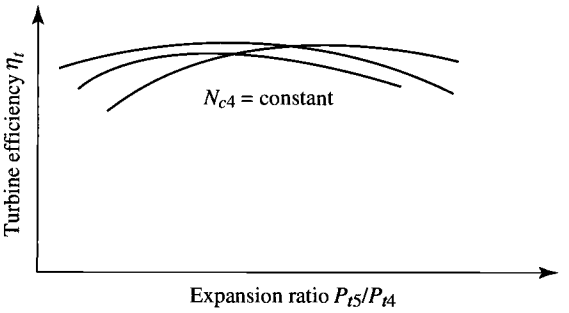

Fig. 8.5b Typical turbine efficiency map.

8.2 Gas Generator

The performance of a gas turbine engine depends on the operation of its gas generator. In this section, algebraic expressions for the pumping characteristics of a simple gas turbine engine are developed.

8.2.1 Conservation of Mass

We consider the flow through a single-spool turbojet engine with constant inlet area to the turbine (A_4 = constant). The mass flow rate into the turbine is equal to the sum of the mass flow rate through the compressor and the fuel flow rate into the main burner. Using the *mass flow parameter* (MFP), we can write

$$\dot{m}_2 + \dot{m}_f = (1+f)\dot{m}_2 = \dot{m}_4 = \frac{P_{t4}A_4}{\sqrt{T_{t4}}}\text{MFP}(M_4)$$

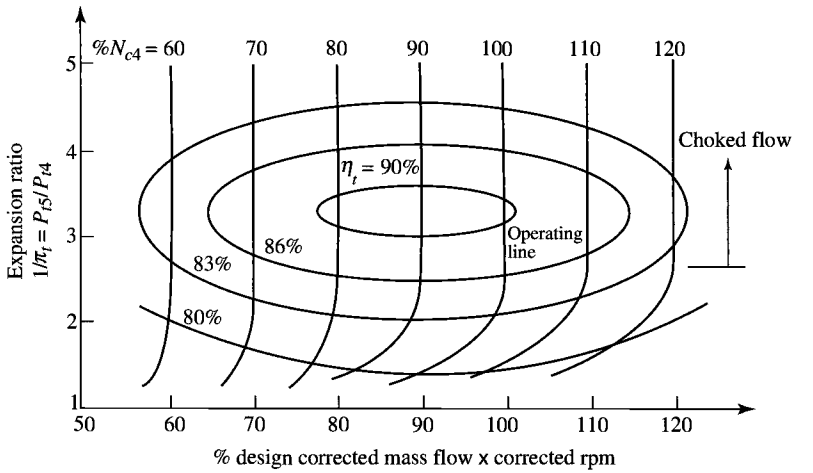

Fig. 8.5c Combined turbine performance map.

With the help of Eq. (8.3), the preceding equation yields the following expression for the compressor corrected mass flow rate:

$$\dot{m}_{c2} = \sqrt{\frac{T_{t2}}{T_{\text{ref}}}} \frac{P_{\text{ref}}}{P_{t2}} \frac{P_{t4}}{\sqrt{T_{t4}}} \frac{A_4}{1+f} \text{MFP}(M_4)$$

Noting that $P_{t4} = \pi_c \pi_b P_{t2}$, we see that

$$\dot{m}_{c2} = \left(\frac{T_{t2}}{T_{t4}}\right)^{1/2} \pi_c \pi_b \frac{P_{\text{ref}}}{\sqrt{T_{\text{ref}}}} \frac{A_4}{1+f} \text{MFP}(M_4) \tag{8.9}$$

Equation (8.9) is a straight line on a compressor map for constant values of T_{t4}/T_{t2}, A_4, f, and M_4. Lines of constant T_{t2}/T_{t4} are plotted on a typical compressor map in Figs. 8.6a and 8.6b for constant values of A_4 and f. Note that these lines start at a pressure ratio of 1 and corrected mass flow rate of 0 and are curved for low compressor pressure ratios (see Fig. 8.6b) because station 4 is unchoked. Station 4 chokes at a pressure ratio of about 2. At pressure ratios above 2, these lines are straight and appear to start at the origin (pressure ratio of 0 and mass

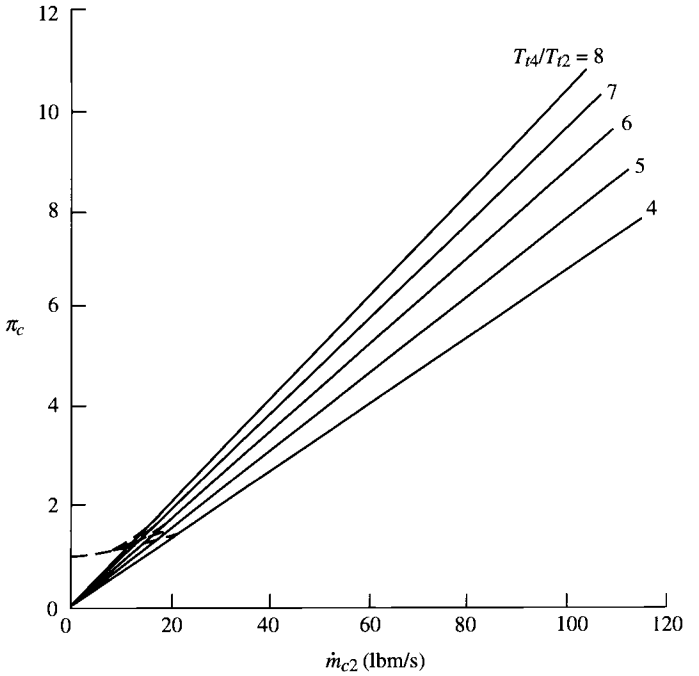

Fig. 8.6a Compressor map with lines of constant T_{t4}/T_{t2}.

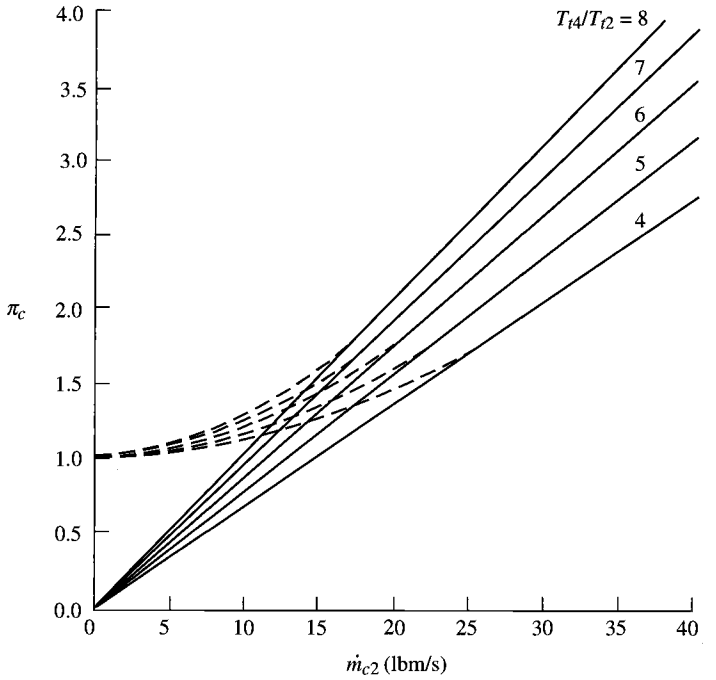

Fig. 8.6b Compressor map origin with lines of constant T_{t4}/T_{t2}.

flow rate of 0). The lines of constant T_{t2}/T_{t4} show the general characteristics required to satisfy conservation of mass and are independent of the turbine. For a given T_{t4}/T_{t2}, any point on that line will satisfy mass conservation for engine stations 2 and 4. The actual operating point of the compressor depends on the turbine and exhaust nozzle.

Equation (8.9) can be written simply for the case when station 4 is choked (the normal situation in gas turbine engines) as

$$\dot{m}_{c2} = C_1 \frac{\pi_c}{\sqrt{T_{t4}/T_{t2}}} \tag{8.10}$$

For an engine or gas generator, the specific relationship between the compressor pressure ratio and corrected mass flow rate is called the *compressor operating line* and depends on the characteristics of the turbine. The equation for the operating line is developed later in this section.

8.2.2 Turbine Characteristics

Before developing the equations that predict the operating characteristics of the turbine, we write the mass flow parameter at any station i in terms of

the mass flow rate, total pressure, total temperature, area, and Mach number. Since

$$\frac{\dot{m}_i\sqrt{T_{ti}}}{P_{ti}A_i} = \text{MFP}(M_i) = \sqrt{\frac{\gamma_i g_c}{R_i}} M_i \left(1 + \frac{\gamma_i - 1}{2} M_i^2\right)^{-(\gamma_i+1)/[2(\gamma_i-1)]}$$

Then, for $M_i = 1$,

$$\frac{\dot{m}_i\sqrt{T_{ti}}}{P_{ti}A_i} = \text{MFP}(M_i = 1) = \sqrt{\frac{\gamma_i g_c}{R_i}} \left(\frac{2}{\gamma_i + 1}\right)^{(\gamma_i+1)/[2(\gamma_i-1)]} = \frac{\Gamma_i}{\sqrt{R_i/g_c}} \tag{8.11a}$$

where

$$\Gamma_i \equiv \sqrt{\gamma_i} \left(\frac{2}{\gamma_i + 1}\right)^{(\gamma_i+1)/[2(\gamma_i-1)]} \tag{8.11b}$$

For a turbojet engine, the flow is choked ($M = 1$) in the turbine inlet guide vanes (station 4) and nearly at the throat of the exhaust nozzle (station 8). Thus the corrected mass flow rate per unit area is constant at station 4 and

$$\dot{m}_4 = \frac{P_{t4}A_4}{\sqrt{T_{t4}}} \frac{\Gamma_4}{\sqrt{R_4/g_c}} \qquad \dot{m}_8 = \frac{P_{t8}A_8}{\sqrt{T_{t8}}} \text{MFP}(M_8) \tag{i}$$

For a simple turbojet engine, the mass flow rate through the turbine is equal to that through the exhaust nozzle, or

$$\dot{m}_8 = \dot{m}_4$$

Using Eq. (i) then, we have

$$\frac{\sqrt{T_{t8}/T_{t4}}}{P_{t8}/P_{t4}} = \frac{A_8}{A_4} \frac{\text{MFP}(M_8)}{\Gamma_4/\sqrt{R_4/g_c}}$$

or

$$\frac{\sqrt{\tau_t}}{\pi_t} = \frac{A_8}{A_4} \frac{\text{MFP}(M_8)}{\Gamma_4/\sqrt{R_4/g_c}} \tag{8.12a}$$

where

$$\pi_t = \left(1 - \frac{1 - \tau_t}{\eta_t}\right)^{\gamma_t/(\gamma_t-1)} \tag{8.12b}$$

For constant turbine efficiency η_t, constant values of R and Γ, constant areas at stations 4 and 8, and choked flow at station 8, Eqs. (8.12a) and (8.12b) can be satisfied only by constant values of the turbine temperature ratio τ_t and the turbine pressure ratio π_t. Thus we have

$$\tau_t,\ \pi_t \text{ constant} \qquad \text{for } M_8 = 1 \text{ and constant } A_4 \text{ and } A_8$$

If the exhaust nozzle unchokes and/or its throat area is changed, then both τ_t and π_t will change. Consider a turbine with reference values of $\eta_t = 0.90$ and $\tau_t = 0.80$ when the exhaust nozzle is choked and the gas has $\gamma = 1.33$. From Eqs. (8.12a) and (8.12b), $\pi_t = 0.363174$ and $A_8/A_4 = 2.46281$ at reference conditions. Figure 8.7a shows plots of Eq. (8.12a) for different values of the area ratio A_8/A_4 times the mass flow parameter at station 8 [MFP(M_8)] and Eq. (8.12b). Because of the relative slopes of these equations, the changes of both τ_t and π_t with A_8 and M_8 can be found by using the following functional iteration scheme, starting with an initial value of τ_t: 1) solve for π_t, using Eq. (8.12a); 2) calculate a new τ_t, using Eq. (8.12b); 3) repeat steps 1 and 2 until successive values of τ_t are within a specified range (say, ± 0.0001). The results of this iteration, plotted in Figs. 8.7b and 8.7c, show that when the Mach number M_8 is

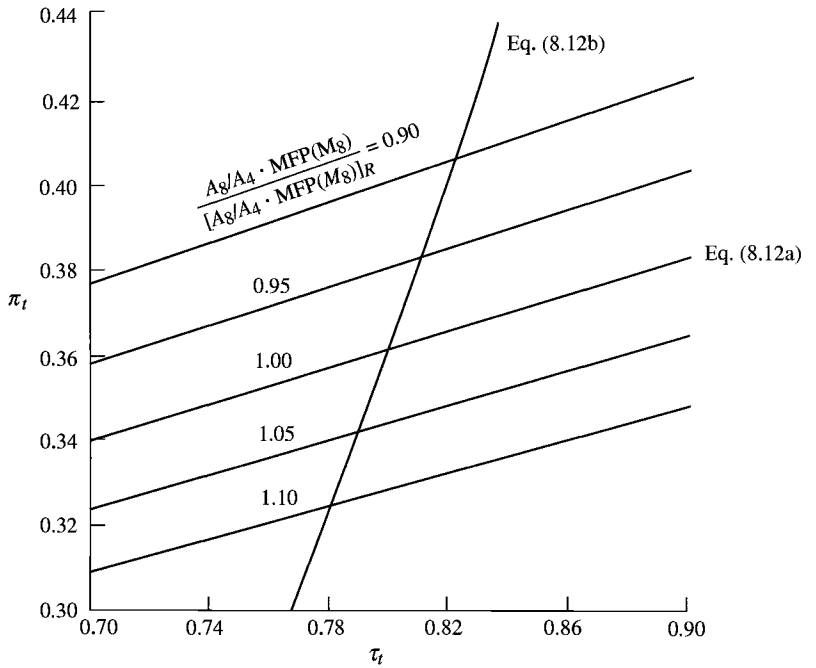

Fig. 8.7a Plot of turbine performance Eqs. (8.12a) and (8.12b).

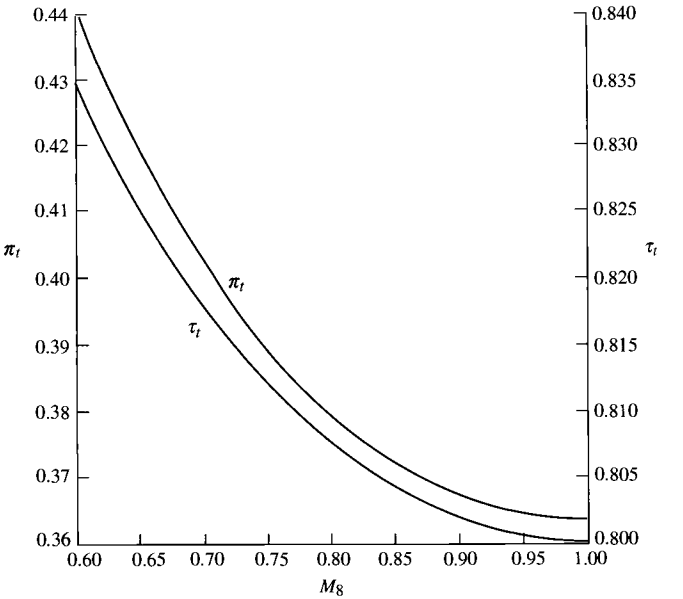

Fig. 8.7b Variation of turbine performance with exhaust nozzle Mach number.

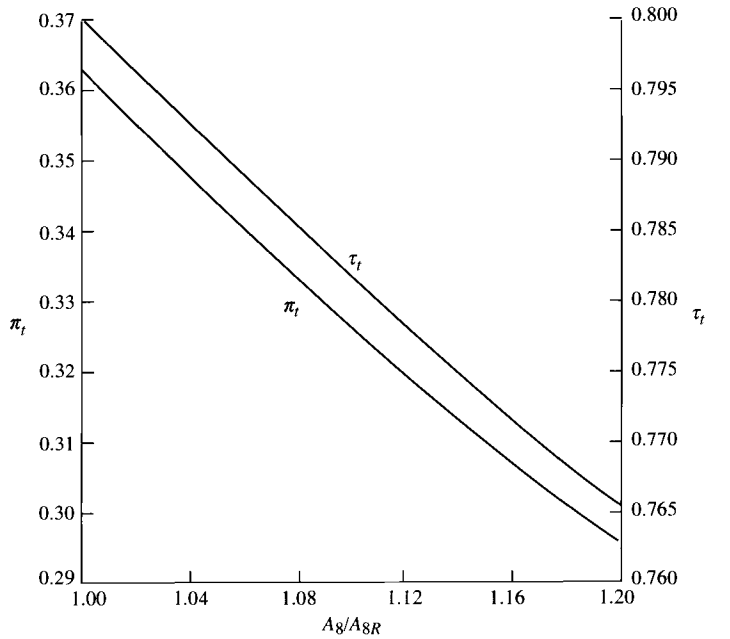

Fig. 8.7c Variation of turbine performance with exhaust nozzle area.

reduced from choked conditions ($M_8 = 1$), both τ_t and π_t increase; and when the exhaust nozzle throat area A_8 is increased from its reference value, both τ_t and π_t decrease. A decrease in τ_t, with its corresponding decrease in π_t, will increase the turbine power per unit mass flow and change the pumping characteristics of the gas generator.

8.2.3 Compressor Operating Line

From a work balance between the compressor and turbine, we write

$$\dot{m}_2 c_{pc}(T_{t3} - T_{t2}) = \eta_m \dot{m}_2(1+f)c_{pt}(T_{t4} - T_{t5})$$

or

$$\tau_c = 1 + \frac{T_{t4}}{T_{t2}}\frac{c_{pt}}{c_{pc}}\eta_m(1+f)(1-\tau_t) \tag{8.13}$$

where

$$\pi_c = [1 + \eta_c(\tau_c - 1)]^{\gamma_c/(\gamma_c - 1)} \tag{ii}$$

Combining Eqs. (8.13) and (ii) gives

$$\pi_c = \left\{1 + \frac{T_{t4}}{T_{t2}}\left[\frac{c_{pt}}{c_{pc}}\eta_c\eta_m(1+f)(1-\tau_t)\right]\right\}^{\gamma_c/(\gamma_c-1)} \tag{8.14}$$

where the term in square brackets can be considered a constant when τ_t is constant. Solving Eq. (8.14) for the temperature ratio gives

$$\frac{T_{t4}}{T_{t2}} = C_2[(\pi_c)^{(\gamma_c-1)/\gamma_c} - 1]$$

where C_2 represents the reciprocal of the constant term within the square brackets of Eq. (8.14). Combining this equation with Eq. (8.10) gives an equation for the *compressor operating line* that can be written as

$$\dot{m}_{c2} = \frac{\pi_c}{\sqrt{\pi_c^{(\gamma_c-1)/\gamma_c} - 1}}\frac{C_1}{\sqrt{C_2}} \qquad \text{for constant } \tau_t \tag{8.15}$$

We can plot the *compressor operating line*, using Eq. (8.15), on the compressor map of Fig. 8.6a, giving the compressor map with operating line shown in Fig. 8.8. This compressor operating line shows that for each value of the temperature ratio T_{t2}/T_{t4} there is one value of compressor pressure ratio and corrected

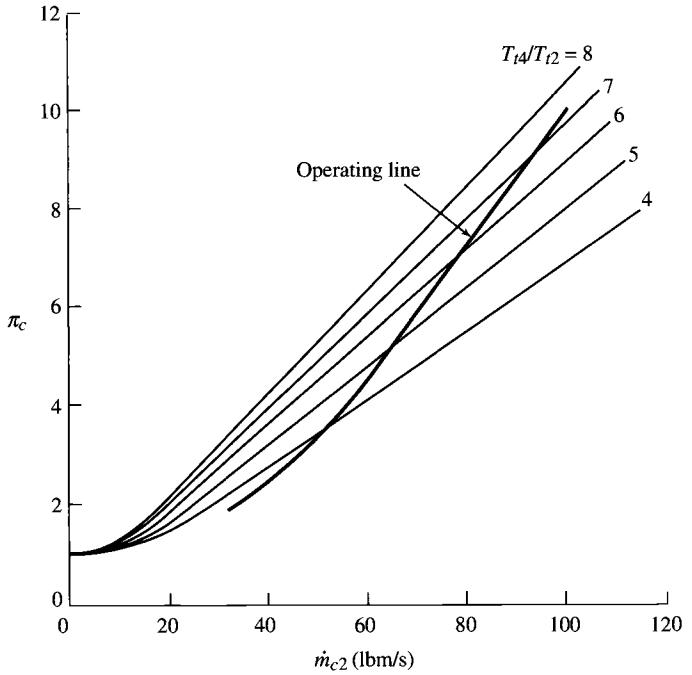

Fig. 8.8 Compressor map with operating line.

mass flow rate. One can also see that for a constant value of T_{t2}, both the compressor pressure ratio and the corrected mass flow rate will increase with increases in throttle setting (increases in T_{t4}). In addition, when at constant T_{t4}, the compressor pressure ratio and corrected mass flow rate will decrease with increases in T_{t2} due to higher speed and/or lower altitude (note: $T_{t2} = T_{t0} = T_0\tau_r$). The curving of the operating line in Fig. 8.8 at pressure ratios below 4 is due to the exhaust nozzle being unchoked ($M_8 < 1$), which increases the value of τ_t (see Fig. 8.7b).

The compressor operating line defines the pumping characteristics of the gas generator. As mentioned earlier, changing the throat area of the exhaust nozzle A_8 will change these characteristics. It achieves this change by shifting the compressor operating line. Increasing A_8 will decrease τ_t (see Fig. 8.7c). This decrease in τ_t will increase the term within the square brackets of Eq. (8.14) that corresponds to the reciprocal of constant C_2 in Eq. (8.15). Thus an increase in A_8 will decrease the constant C_2 in Eq. (8.15). For a constant T_{t4}/T_{t2}, this shift in the operating line will increase both the corrected mass flow rate and the pressure ratio of the compressor, as shown in Fig. 8.9 for a 20% increase in A_8. For some compressors, an increase in the exhaust nozzle throat area A_8 can keep engine operation away from the surge.

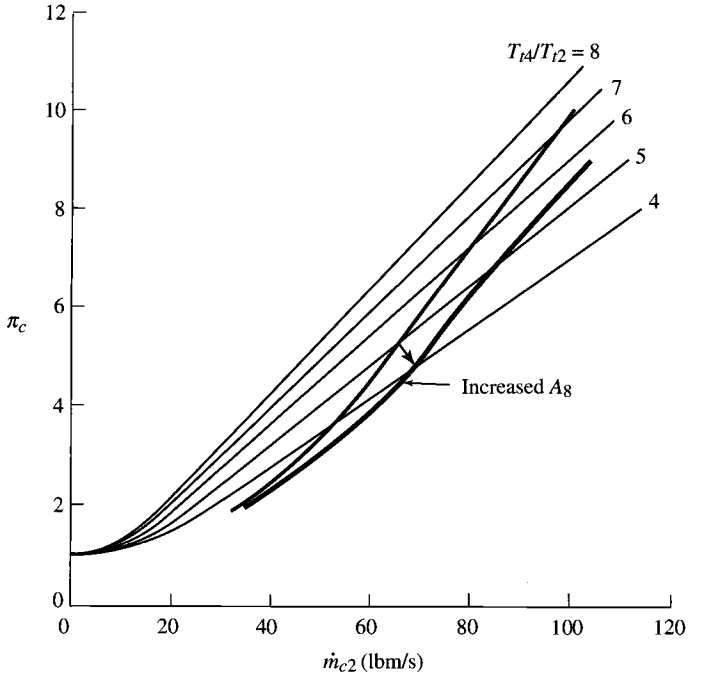

Fig. 8.9 Effect of exhaust nozzle area on compressor operating line.

8.2.4 Engine Controls

The engine control system will control the gas generator operation to keep the main burner exit temperature T_{t4}, the compressor's pressure ratio π_c, rotational speed N, exit total pressure T_{t3}, and exit total pressure P_{t3} from exceeding specific maximum values. Limiting T_{t4} and π_c has the most dominating effect and is included in the following analysis. An understanding of the influence of the engine control system on compressor performance during changing flight conditions and throttle settings can be gained by recasting Eqs. (8.10) and (8.14) in terms of the dimensionless total temperature at station 0 (θ_0). We note that

$$T_{t0} = T_{\text{ref}} \frac{T_{t0}}{T_{\text{ref}}} = T_{\text{ref}} \theta_0$$

and

$$\theta_0 = \frac{T_0}{T_{\text{ref}}} \tau_r = \frac{T_0}{T_{\text{ref}}} \left(1 + \frac{\gamma - 1}{2} M_0^2\right) \tag{8.16}$$

Equation (8.16) and Figs. 8.10 and 8.11 show that θ_0 includes the influence of both the altitude (through the ambient temperature T_0) and the flight Mach number. Although Fig. 8.10 shows the direct influence of Mach number and

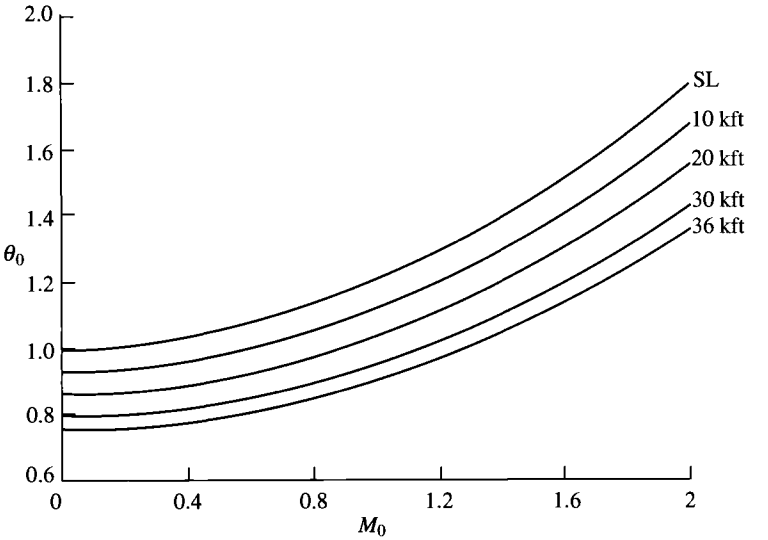

Fig. 8.10 θ_0 **vs Mach number at different altitudes (standard day).**

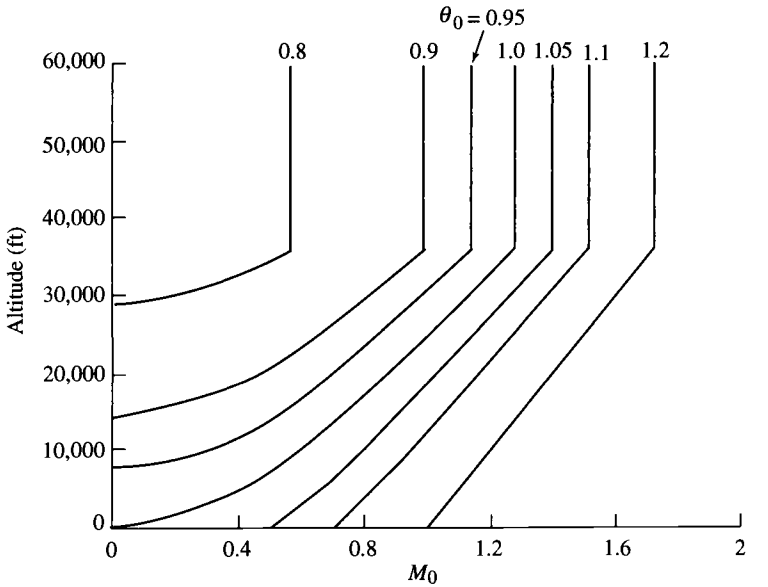

Fig. 8.11 θ_0 **vs Mach number and altitude (standard day).**

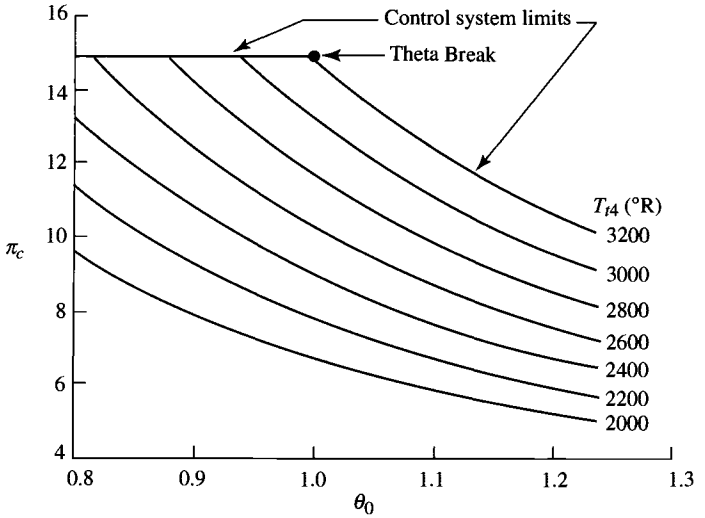

Fig. 8.12 Compressor pressure ratio vs θ_0 and T_{t4}.

altitude on θ_0, Fig. 8.11 is an easier plot to understand in terms of aircraft flight conditions (Mach number and altitude).

Using Eq. (8.16) and the fact that $T_{t2} = T_{t0}$, we can write Eq. (8.14) as

$$\pi_c = \left(1 + \frac{T_{t4}}{\theta_0} K_1\right)^{\gamma_c/(\gamma_c - 1)} \tag{8.17}$$

where K_1 is a constant. Equation (8.17) is plotted in Fig. 8.12 for the turbojet engine of Example 8.1.

By using Eqs. (8.17) and (8.10), the corrected mass flow rate through the compressor can be expressed as

$$\dot{m}_{c2} = \left(\frac{\theta_0}{T_{t4}}\right)^{1/2} \left(1 + \frac{T_{t4}}{\theta_0} K_1\right)^{\gamma_c/(\gamma_c - 1)} K_2 \tag{8.18}$$

where K_2 is a constant. Equation (8.18) is plotted in Fig. 8.13 for the turbojet engine of Example 8.1.

8.2.5 Theta Break

This concept is explained in Appendix D of *Aircraft Engine Design*, by Mattingly et al. (Ref. 12, pp. 525, 526) and is reprinted here with permission of the publisher:

> The unique point, so visually striking in [Fig. 8.12], at which the control logic must switch from limiting π_c to limiting T_{t4}, is known as the theta break, or $\theta_{0\ \text{break}}$.

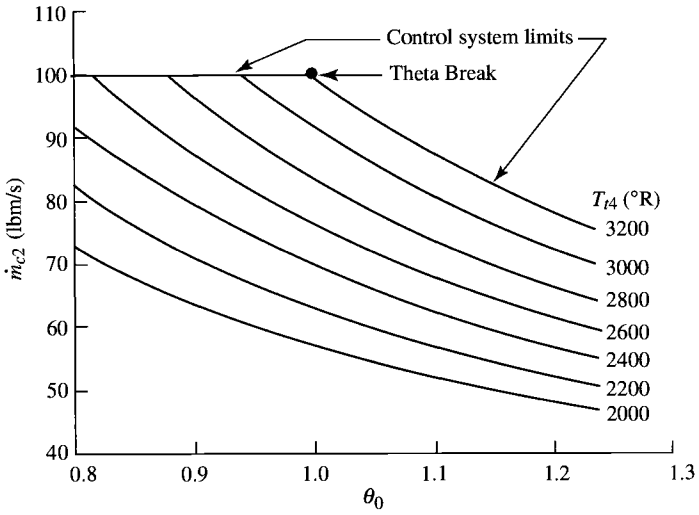

Fig. 8.13 Compressor corrected mass flow rate vs θ_0 and T_{t4}.

Returning briefly to [Fig. 8.12], you will find it very convenient to visualize that at any point in the flight envelope to the left of the theta break $\pi_c = \pi_{c\,\max}$ and $T_{t4} < T_{t4\,\max}$, while at any point in the right of the theta break $\pi_c < \pi_{c\,\max}$ and $T_{t4} = T_{t4\,\max}$. The relationship of the instantaneous value of θ_0 to $\theta_{0\,\text{break}}$ has important consequences to engine cycle performance. On the one hand, when $\theta_0 < \theta_{0\,\text{break}}$ and $T_{t4} < T_{t4\,\max}$, the specific thrust of the engine is less than its inherent material capabilities would make possible. On the other hand, when $\theta_0 > \theta_{0\,\text{break}}$ and $\pi_c < \pi_{c\,\max}$, the specific fuel consumption is more than its inherent thermal efficiency would make possible.

The designer would therefore strongly prefer to have the engine always operate at or very near $\theta_0 = \theta_{0\,\text{break}}$, but this is impossible because every aircraft has a flight envelope with a range of θ_0 [see Fig. 8.11]. The best available compromise is to choose a $\theta_{0\,\text{break}}$ that provides the best balance of engine performance over the expected range of flight conditions.

It is interesting to note that, since early commercial and military aircraft primarily flew at or near $\theta_0 = 1$, they were successfully designed with $\theta_{0\,\text{break}} = 1$. Consequently, several generations of propulsion engineers took it for granted that aircraft engines always operated at $\pi_{c\,\max}$ and $T_{t4\,\max}$ under standard sea-level static conditions. However, the special requirements of more recent aircraft such as [the F-22 Raptor ($\theta_0 > 1.2$ at supercruise)] have forced designers to select theta breaks different from 1.0. These engines may operate either at $\pi_{c\,\max}$ or $T_{t4\,\max}$ at standard sea-level static conditions, but never both.

Example 8.1

We now consider compressor operation at different T_{t4} and θ_0, specifically a compressor that has a pressure ratio of 15 and corrected mass flow rate of 100 lbm/s for T_{t2} of 518.7°R (sea-level standard) and T_{t4} of 3200°R. At these

conditions, θ_0 is 1, and constants K_1 and K_2 in Eqs. (8.17) and (8.18) are 3.649×10^{-4} and 377-1, respectively. In addition, we assume that an engine control system limits π_c to 15 and T_{t4} to 3200°R. By using Eqs. (8.17) and (8.18), the compressor pressure ratio and corrected mass flow rate are calculated for various values of T_{t4} and θ_0. Figures 8.12 and 8.13 show the resulting variation of compressor pressure ratio and corrected mass flow rate, respectively, with flight condition θ_0 and throttle setting T_{t4}. Note that at θ_0 above 1.0, the compressor pressure ratio and corrected mass flow rate are limited by the maximum combustor exit temperature T_{t4} of 3200°R. The compressor pressure ratio limits performance at θ_0 below 1.0. Thus $\theta_{0\,\text{break}} = 1.0$.

8.2.6 Variation in Engine Speed

As will be shown in Chapter 9, the change in total enthalpy across a fan or compressor is proportional to the rotational speed N squared. For a calorically perfect gas, we can write

$$T_{t3} - T_{t2} = K_1 N^2$$

or

$$\tau_c - 1 = \frac{K_1}{T_{\text{ref}}} N_{c2}^2 \tag{i}$$

where N_{c2} is the compressor corrected speed. The compressor temperature ratio is related to the compressor pressure ratio through the efficiency, or

$$\tau_c - 1 = (\pi_c^{(\gamma_c - 1)/\gamma_c} - 1)/\eta_c$$

Combining this equation with Eq. (i), rewriting the resulting equation in terms of pressure ratio and corrected speed, rearranging into variable and constant terms, and equating the constant to reference values give for constant compressor efficiency

$$\frac{\pi_c^{(\gamma_c - 1)/\gamma_c} - 1}{N_{c2}^2} = \frac{\eta_c K_1}{T_{\text{ref}}} = \frac{\pi_{cR}^{(\gamma_c - 1)/\gamma_c} - 1}{N_{c2R}^2} \tag{ii}$$

Solving Eq. (ii) for the corrected speed ratio N_{c2}/N_{c2R}, we have

$$\frac{N_{c2}}{N_{c2R}} = \sqrt{\frac{\pi_c^{(\gamma_c - 1)/\gamma_c} - 1}{\pi_{cR}^{(\gamma_c - 1)/\gamma_c} - 1}} \tag{8.19a}$$

This equation can also be used to estimate the variation in engine speed N with flight condition. Equation (8.19a) is plotted in Fig. 8.14 for a reference compressor pressure ratio of 16. Note that a reduction in compressor pressure ratio from 16 to 11 requires only a 10% reduction in corrected speed N_c. Equation (8.19a)

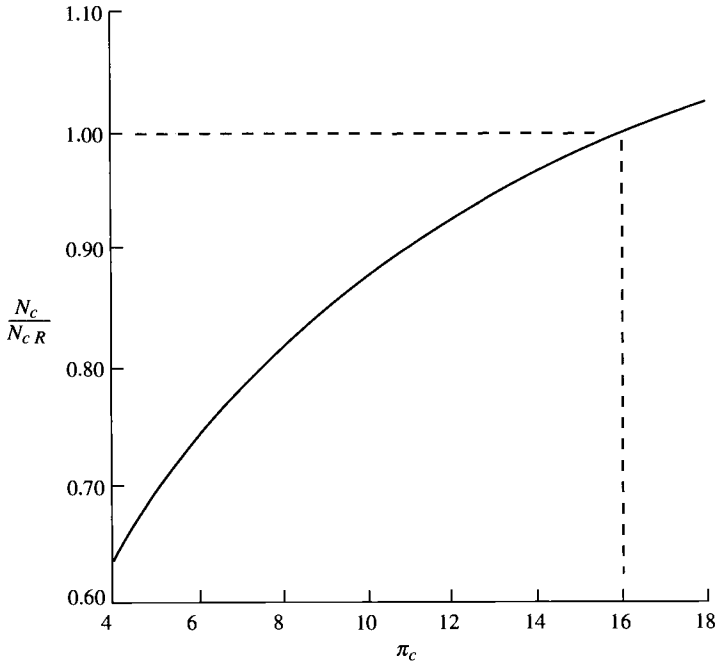

Fig. 8.14 Variation in corrected speed with compressor pressure ratio.

can be written in terms of T_{t4}/θ_0 by using Eq. (8.17), yielding

$$\frac{N_{c2}}{N_{c2R}} = \sqrt{\frac{T_{t4}/\theta_0}{(T_{t4}/\theta_0)_R}} \tag{8.19b}$$

Because the compressor and turbine are connected to the same shaft, they have the same rotational speed N, and we can write the following relationship between their corrected speeds:

$$N_{c2} = \frac{1}{\sqrt{T_{\text{ref}}}} \sqrt{\frac{T_{t4}}{\theta_0}} N_{c4} \tag{8.20}$$

Comparison of Eqs. (8.19b) and (8.20) gives the result that the corrected turbine speed is constant, or

$$N_{c4} = \text{const} \tag{8.21}$$

This result may surprise one at first. However, given that the turbine's temperature ratio τ_t, pressure ratio π_t, and efficiency η_t are considered constant in this analysis, the turbine's corrected speed must be constant (see Fig. 8.5c).

8.2.7 Gas Generator Equations

The pumping characteristics of a simple gas generator can be represented by the variation of the gas generator's parameter ratios with corrected compressor speed. The equations for the gas generator's pressure and temperature ratios, corrected air mass flow and fuel flow rates, compressor pressure ratio, and corrected compressor speed can be written in terms of T_{t4}/T_{t2}, reference values (subscript R), and other variables. The gas generator's pressure and temperature ratios are given simply by

$$\frac{P_{t6}}{P_{t2}} = \pi_c \pi_b \pi_t \tag{8.22}$$

$$\frac{T_{t6}}{T_{t2}} = \frac{T_{t4}}{T_{t2}} \tau_t \tag{8.23}$$

From Eq. (8.10) and referencing, the corrected mass flow rate can be written as

$$\frac{\dot{m}_{c2}}{\dot{m}_{c2R}} = \frac{\pi_c}{\pi_{cR}} \sqrt{\frac{(T_{t4}/T_{t2})_R}{T_{t4}/T_{t2}}} \tag{8.24}$$

where the compressor pressure ratio is given by Eq. (8.17), rewritten in terms of T_{t4}/T_{t2}, or

$$\pi_c = \left[1 + \frac{T_{t4}/T_{t2}}{(T_{t4}/T_{t2})_R} (\pi_{cR}^{(\gamma_c - 1)/\gamma_c} - 1) \right]^{\gamma_c/(\gamma_c - 1)} \tag{8.25}$$

Equation (8.19b) for the corrected speed can be rewritten in terms of T_{t4}/T_{t2} as

$$\frac{N_{c2}}{N_{c2R}} = \sqrt{\frac{T_{t4}/T_{t2}}{(T_{t4}/T_{t2})_R}} \tag{8.26}$$

An expression for the corrected fuel flow rate results from Eqs. (7.9), (8.2), and (8.7) as follows. Solving Eq. (7.9) for the fuel flow rate gives

$$\dot{m}_f = \dot{m}_0 \frac{c_{pt} T_{t4} - c_{pc} T_{t3}}{\eta_b h_{PR} - c_{pt} T_{t4}}$$

From Eqs. (8.2) and (8.7), this equation becomes

$$\dot{m}_{fc} = \frac{\dot{m}_{c2}}{\theta_2} \frac{c_{pt} T_{t4} - c_{pc} T_{t3}}{\eta_b h_{PR} - c_{pt} T_{t4}}$$

or

$$\dot{m}_{fc} = \dot{m}_{c2} \frac{T_{t4}/T_{t2} - \tau_c (c_{pc}/c_{pt})}{\eta_b h_{PR}/(c_{pt} T_{\text{ref}}) - T_{t4}/T_{\text{ref}}} \tag{8.27}$$

where by using Eq. (8.13) and referencing, τ_c is given by

$$\tau_c = 1 + (\tau_{cR} - 1)\frac{T_{t4}/T_{t2}}{(T_{t4}/T_{t2})_R} \tag{8.28}$$

Equations (8.22–8.28) constitute a set of equations for the pumping characteristics of a simple gas generator in terms of T_{t4}/T_{t2} and reference values. Only Eq. (8.27) for the corrected fuel flow rate has the term T_{t4}/T_{ref} that is not strictly a function of T_{t4}/T_{t2}. The first term in the denominator of Eq. (8.27) has a magnitude of about 130, and T_{t4}/T_{ref} has a value of about 6 or smaller. Thus the denominator of Eq. (8.28) does not vary appreciably, and the corrected fuel flow rate is a function of T_{t4}/T_{t2} and reference values. In summary, the pumping characteristics of the gas generator are a function of only the temperature ratio T_{t4}/T_{t2}.

Example 8.2

We want to determine the characteristics of a gas generator with a maximum compressor pressure ratio of 15, a compressor corrected mass flow rate of 100 lbm/s at T_{t2} of 518.7°R (sea-level standard), and a maximum T_{t4} of 3200°R. This is the same compressor we considered in Example 8.1 (see Figs. 8.12 and 8.13). We assume the compressor has an efficiency η_c of 0.8572 ($e_c = 0.9$), and the burner has an efficiency η_b of 0.995 and a pressure ratio π_b of 0.96. In addition, we assume the following gas constants: $\gamma_c = 1.4$, $c_{pc} = 0.24$ Btu/(lbm · °R), $\gamma_t = 1.33$, and $c_{pt} = 0.276$ Btu/(lbm · °R).

By using Eq. (7.10), the reference fuel/air ratio f_R is 0.03381 for $h_{PR} = 18{,}400$ Btu/lbm, and the corrected fuel flow rate is 12,170 lb/h. From Eq. (7.12), the turbine temperature ratio τ_t is 0.8124. Assuming $e_t = 0.9$, Eqs. (7.13) and (7.14) give the turbine pressure ratio π_t as 0.3943 and the turbine efficiency η_t, as 0.910. The reference compressor temperature ratio τ_{cR} is 2.3624.

Calculations were done over a range of T_{t4} with $T_{t2} = 518.7$°R and using Eqs. (8.22–8.28). The resulting gas generator pumping characteristics are plotted in Fig. 8.15. We can see that the compressor pressure ratio and corrected fuel flow rate decrease more rapidly with decreasing corrected speed than corrected airflow rate. As discussed previously, the gas generator's pumping characteristics are a function of only T_{t4}/T_{t2}, and Fig. 8.15 shows this most important relationship in graphical form.

Because the maximum T_{t4} is 3200°R and the maximum pressure ratio is 15, the operation of the gas generator at different inlet conditions (T_{t2}, P_{t2}) and/or different throttle setting (T_{t4}) can be obtained from Fig. 8.15. For example, consider a 100°F day (T_{t2}) at sea level with maximum power. Here $T_{t2} = 560$°R, $P_{t2} = 14.7$ psia, and $T_{t4} = 3200$°R; thus $T_{t4}/T_{t2} = 5.71$, and Fig. 8.15 gives the following data: $N_c/N_{cR} = 0.96$, $\dot{m}_c/\dot{m}_{cR} = 0.88$, $\pi_c/\pi_{cR} = 0.84$, $\dot{m}_{fc}/\dot{m}_{fcR} = 0.78$, $T_{t6}/T_{t2} = 4.6$, and $P_{t6}/P_{t2} = 4.8$. With these data, the pressures,

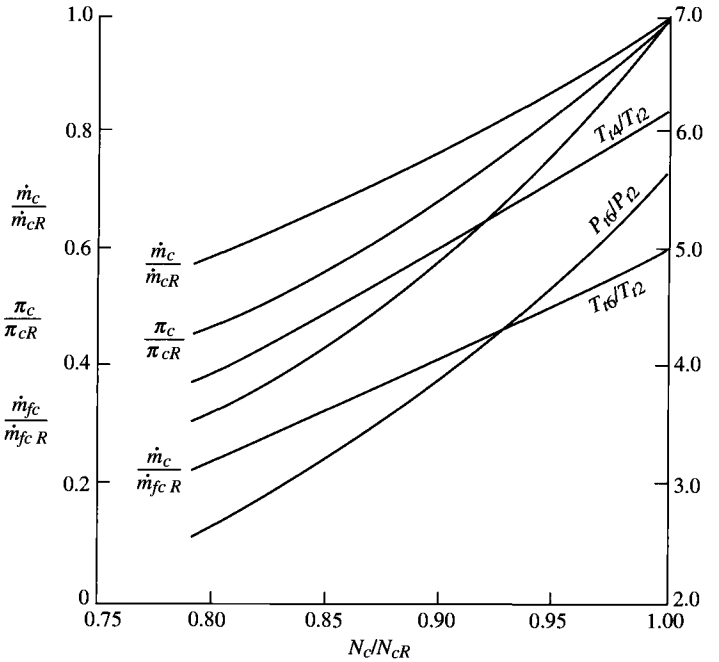

Fig. 8.15 Gas generator pumping characteristics.

temperatures, and flow rates can be calculated as follows:

$$\dot{m} = \left(\frac{P_{t2}}{P_{t2R}}\sqrt{\frac{T_{t2R}}{T_{t2}}}\right)\left(\frac{\dot{m}_c}{\dot{m}_{cR}}\right)\dot{m}_{cR} = 1 \times \sqrt{\frac{518.7}{560}}\,(0.88)(100) = 84.7 \text{ lbm/s}$$

$$\dot{m}_f = \frac{P_{t2}}{P_{t2R}}\sqrt{\frac{T_{t2}}{T_{t2R}}\frac{\dot{m}_{fc}}{\dot{m}_{fcR}}}\dot{m}_{fcR} = 1 \times \sqrt{\frac{560}{518.6}}\,(0.78)(12{,}170) = 9860 \text{ lbm/h}$$

$$T_{t6} = \frac{T_{t6}}{T_{t2}}T_{t2} = 4.6(560) = 2576°\text{R}$$

$$P_{t6} = \frac{P_{t6}}{P_{t2}}P_{t2} = 4.8(14.7) = 70.6 \text{ psia}$$

$$\pi_c = \frac{\pi_c}{\pi_{cR}}\pi_{cR} = 0.84(15) = 12.6$$

As another example, consider flight at Mach 0.6 and 40 kft ($\theta = 0.7519$, $\delta = 0.1858$) with maximum throttle. Since T_{t2} ($= 418.1°\text{R}$) is less than T_{t2R},

the maximum value for T_{t4} is 2579.4°R (= 3200 × 418.1/518.7), and the compressor has a pressure ratio of 15 and corrected mass flow rate of 100 lbm/s. The air mass flow rate is reduced to 20.7 lbm/s and the mass fuel flow rate is reduced to 2030 lbm/h.

8.3 Turbojet Engine

In this section, the performance equations of the single-spool turbojet engine, shown in Fig. 8.16, are developed and the results are studied. We assume choked flow at stations 4 and 8. In addition, the throttle (T_{t4}), flight conditions (M_0, T_0, and P_0), and the ambient pressure/exhaust pressure ratio P_0/P_9 can be independently varied for this engine. The performance equations for this turbojet can be obtained easily by adding inlet and exhaust nozzle losses to the single-spool gas generator studied in the previous section.

This engine has five independent variables (T_{t4}, M_0, T_0, P_0, and P_0/P_9). The performance analysis develops analytical expressions for component performance in terms of these independent variables. We have six dependent variables for the single-spool turbojet engine: engine mass flow rate, compressor pressure ratio, compressor temperature ratio, burner fuel/air ratio, exit temperature ratio T_9/T_0, and exit Mach number. A summary of the independent variables, dependent variables, and constants or knowns for this engine is given in Table 8.4.

The thrust for this engine is given by

$$\frac{F}{\dot{m}_0} = \frac{a_0}{g_c}\left[(1+f)\frac{V_9}{a_0} - M_0 + (1+f)\frac{R_t}{R_c}\frac{T_9/T_0}{V_9/a_0}\frac{1-P_0/P_9}{\gamma_c}\right] \tag{i}$$

where

$$\frac{T_9}{T_0} = \frac{T_{t4}\tau_t}{(P_{t9}/P_9)^{(\gamma_t-1)/\gamma_t}} \tag{ii}$$

$$\frac{P_{t9}}{P_9} = \frac{P_0}{P_9}\pi_r\pi_d\pi_c\pi_b\pi_t\pi_n \tag{iii}$$

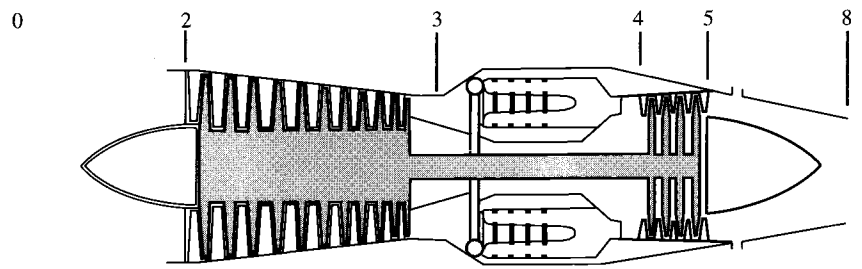

Fig. 8.16 Single-spool turbojet engine. (Courtesy of Pratt & Whitney.)

Table 8.4 Performance analysis variables for single-spool turbojet engine

	Variables		
Component	Independent	Constant or known	Dependent
Engine	M_0, T_0, P_0		$\dot{m}_0$
Diffuser		$\pi_d = f(M_0)$	
Compressor		η_c	π_c, τ_c
Burner	T_{t4}	π_b, η_b	f
Turbine		π_t, τ_t	
Nozzle	P_9/P_0	π_n	$M_9, T_9/T_0$
Total number	5		6

$$M_9 = \sqrt{\frac{2}{\gamma_t - 1}\left[\left(\frac{P_{t9}}{P_9}\right)^{(\gamma_t - 1)/\gamma_t} - 1\right]} \tag{iv}$$

and

$$\frac{V_9}{a_0} = M_9\sqrt{\frac{\gamma_t R_t T_9}{\gamma_c R_c T_0}} \tag{v}$$

The thrust-specific fuel consumption for this engine is given by

$$S = \frac{f}{F/\dot{m}_0} \tag{vi}$$

where

$$f = \frac{\tau_\lambda - \tau_r \tau_c}{h_{PR}\eta_b/(c_{pc}T_0) - \tau_\lambda} \tag{vii}$$

Equations (i–vii) can be solved for given T_{t4}, M_0, T_0, P_0, P_0/P_9, gas properties with expressions for τ_λ, π_r, τ_r, π_d, π_c, τ_c, and engine mass flow rate in terms of the five independent variables and other dependent variables. In the previous section, we developed Eq. (8.28), repeated here, for the compressor's temperature ratios in terms of T_{t4}/T_{t2} and reference values:

$$\tau_c = 1 + (\tau_{cR} - 1)\frac{T_{t4}/T_{t2}}{(T_{t4}/T_{t2})_R}$$

The compressor pressure ratio is related to its temperature ratio by its efficiency.

An equation for the engine mass flow rate follows from the mass flow parameter (MFP) written for station 4 with choked flow and the definitions of

component π values. We write

$$\dot{m}_0 = \frac{P_{t4}}{\sqrt{T_{t4}}} \frac{A_4}{1+f} \text{MFP}(1) = \frac{P_0 \pi_r \pi_d \pi_c}{\sqrt{T_{t4}}} \left[\frac{\pi_b A_4}{1+f} \text{MFP}(1) \right]$$

Because the terms within the square brackets are considered constant, we move the variable terms to the left side of the equation, and, using referencing, equate the constant to reference values:

$$\frac{\dot{m}_0 \sqrt{T_{t4}}}{P_0 \pi_r \pi_d \pi_c} = \frac{\pi_b A_4}{1+f} \text{MFP}(1) = \left(\frac{\dot{m}_0 \sqrt{T_{t4}}}{P_0 \pi_r \pi_d \pi_c} \right)_R$$

Solving for the engine mass flow rate, we get

$$\dot{m}_0 = \dot{m}_{0R} \frac{P_0 \pi_r \pi_d \pi_c}{(P_0 \pi_r \pi_d \pi_c)_R} \sqrt{\frac{T_{t4R}}{T_{t4}}} \tag{8.29}$$

Relationships for τ_λ, π_r, τ_r, and π_d follow from their equations in Chapter 7.

The throat area of the exhaust nozzle is assumed to be constant. With P_0/P_9 an independent variable, the exit area of the exhaust nozzle A_9 must correspond to the nozzle pressure ratio P_{t9}/P_9. An expression for the exhaust nozzle exit area follows from the mass flow parameter and other compressible flow properties. The subscript t is used in the following equations for the gas properties (γ, R, and Γ) at stations 8 and 9. Using Eq. (8.11) for choked flow at station 8 gives

$$\dot{m}_8 = \frac{P_{t9} A_8}{\sqrt{T_{t8}}} \frac{\Gamma_t}{\sqrt{R_t/g_c}} \tag{i}$$

From the equation for the mass flow parameter [Eq. (2.76)], the mass flow rate at station 9 is

$$\dot{m}_9 = \frac{P_{t9} A_9}{\sqrt{T_{t9}}} \frac{\sqrt{\gamma_t}}{\sqrt{R_t/g_c}} M_9 \left(1 + \frac{\gamma_t - 1}{2} M_9^2 \right)^{-(\gamma_t+1)/2(\gamma_t-1)} \tag{ii}$$

Using the nozzle relationships $T_{t8} = T_{t9}$ and $\pi_n = P_{t9}/P_{t8}$ and equating the mass flow rate at station 8 [Eq. (i)] to that at station 9 [Eq. (ii)] give

$$\frac{A_9}{A_8} = \frac{\Gamma_t}{\sqrt{\gamma_t}} \frac{1}{\pi_n} \frac{1}{M_9} \left(1 + \frac{\gamma_t - 1}{2} M_9^2 \right)^{(\gamma_t+1)/[2(\gamma_t-1)]}$$

Replacing the Mach number at station 9 by using

$$M_9 = \sqrt{\frac{2}{\gamma_t - 1}\left[(P_{t9}/P_9)^{(\gamma_t - 1)/\gamma_t} - 1\right]}$$

gives

$$\frac{A_9}{A_8} = \Gamma_t \sqrt{\frac{\gamma_t - 1}{2\gamma_t}} \frac{1}{\pi_n} \frac{(P_{t9}/P_9)^{(\gamma_t + 1)/(2\gamma_t)}}{\sqrt{(P_{t9}/P_9)^{(\gamma_t - 1)/\gamma_t} - 1}} \tag{8.30}$$

Because the throat area A_8 is constant, Eq. (8.30) can be used to obtain the ratio of the exit area A_9 to a reference exit area A_{9R} that can be written as

$$\frac{A_9}{A_{9R}} = \left[\frac{P_{t9}/P_9}{(P_{t9}/P_9)_R}\right]^{(\gamma_t + 1)/(2\gamma_t)} \sqrt{\frac{(P_{t9}/P_9)_R^{(\gamma_t - 1)/\gamma_t} - 1}{(P_{t9}/P_9)^{(\gamma_t - 1)/\gamma_t} - 1}} \tag{8.31}$$

8.3.1 Summary of Performance Equations—Single-Spool Turbojet Without Afterburner

INPUTS:

Choices	
Flight parameters:	M_0, T_0 (K, °R), P_0 (kPa, psia)
Throttle setting:	T_{t4} (K, °R)
Exhaust nozzle setting:	P_0/P_9
Design constants	
π:	$\pi_{d\max}$, π_b, π_t, π_n
τ:	τ_t
η:	η_c, η_b, η_m
Gas properties:	γ_c, γ_t, c_{pc}, c_{pt} [kJ/(Kg · K), Btu/(lbm · °R)]
Fuel:	h_{PR}, (kJ/kg, Btu/lbm)
Reference conditions	
Flight parameters:	M_{0R}, T_{0R} (K, °R), P_{0R} (kPa, psia), τ_{rR}, π_{rR}
Throttle setting:	T_{tAR} (K, °R)
Component behavior:	T_{dR}, π_{cR}, τ_{cR}

OUTPUTS:

Overall performance:	F(N, lbf), $\dot{m}_0$ (kg/s, lbm/s), f, $S\left(\frac{\text{mg/s}}{\text{N}}, \frac{\text{lbm/h}}{\text{lbf}}\right)$, η_P, η_T, η_O
Component behavior:	π_d, π_c, τ_c, f, M_9, N/N_R

EQUATIONS:

$$R_c = \frac{\gamma_c - 1}{\gamma_c} c_{pc} \tag{8.32a}$$

$$R_t = \frac{\gamma_t - 1}{\gamma_t} c_{pt} \tag{8.32b}$$

$$a_0 = \sqrt{\gamma_c R_c g_c T_0} \tag{8.32c}$$

$$V_0 = a_0 M_0 \tag{8.32d}$$

$$\tau_r = 1 + \frac{\gamma_c - 1}{2} M_0^2 \tag{8.32e}$$

$$\pi_r = \tau^{\gamma_c/(\gamma_c - 1)} \tag{8.32f}$$

$$\eta_r = 1 \qquad \text{for } M_0 \le 1 \tag{8.32g}$$

$$\eta_r = 1 - 0.075(M_0 - 1)^{1.35} \qquad \text{for } M_0 > 1 \tag{8.32h}$$

$$\pi_d = \pi_{d\max} \eta_r \tag{8.32i}$$

$$T_{t2} = T_0 \tau_r \tag{8.32j}$$

$$\tau_c = 1 + (\tau_{cR} - 1) \frac{T_{t4}/T_{t2}}{(T_{t4}/T_{t2})_R} \tag{8.32k}$$

$$\pi_c = [1 + \eta_c(\tau_c - 1)]^{\gamma_c/(\gamma_c - 1)} \tag{8.32l}$$

$$\tau_\lambda = \frac{c_{pt} T_{t4}}{c_{pc} T_0} \tag{8.32m}$$

$$f = \frac{\tau_\lambda - \tau_r \tau_c}{h_{PR} \eta_b / (c_p T_0) - \tau_\lambda} \tag{8.32n}$$

$$\dot{m}_0 = \dot{m}_{0R} \frac{P_0 \pi_r \pi_d \pi_c}{(P_0 \pi_r \pi_d \pi_c)_R} \sqrt{\frac{T_{t4R}}{T_{t4}}} \tag{8.32o}$$

$$\frac{P_{t9}}{P_9} = \frac{P_0}{P_9} \pi_r \pi_d \pi_c \pi_b \pi_t \pi_n \tag{8.32p}$$

$$M_9 = \sqrt{\frac{2}{\gamma_t - 1} \left[\left(\frac{P_{t9}}{P_9} \right)^{(\gamma_t - 1)/\gamma_t} - 1 \right]} \tag{8.32q}$$

$$\frac{T_9}{T_0} = \frac{T_{t4} \tau_t / T_0}{(P_{t9}/P_0)^{(\gamma_t - 1)/\gamma_t}} \tag{8.32r}$$

$$\frac{V_9}{a_0} = M_9 \sqrt{\frac{\gamma_t R_t}{\gamma_c R_c} \frac{T_9}{T_0}} \tag{8.32s}$$

$$\frac{F}{\dot{m}_0} = \frac{a_0}{g_c}\left[(1+f)\frac{V_9}{a_0} - M_0 + (1+f)\frac{R_t}{R_c}\frac{T_9/T_0}{V_9/a_0}\frac{1-P_0/P_9}{\gamma_c}\right] \tag{8.32t}$$

$$F = \dot{m}_0\left(\frac{F}{\dot{m}_0}\right) \tag{8.32u}$$

$$S = \frac{f}{F/\dot{m}_0} \tag{8.32v}$$

$$\eta_T = \frac{a_0^2[(1+f)(V_9/a_0)^2 - M_0^2]}{2g_c f h_{PR}} \tag{8.32w}$$

$$\eta_P = \frac{2g_c V_0(F/\dot{m}_0)}{a_0^2[(1+f)(V_0/a_0)^2 - M_0^2]} \tag{8.32x}$$

$$\eta_o = \eta_P \eta_T \tag{8.32y}$$

$$\frac{N}{N_R} = \sqrt{\frac{T_0\tau_r}{T_{0R}\tau_{rR}}\frac{\pi_c^{(\gamma_c-1)/\gamma_c} - 1}{\pi_{cR}^{(\gamma_c-1)/\gamma_c} - 1}} \tag{8.32z}$$

$$\frac{A_9}{A_{9R}} = \left[\frac{P_{t9}/P_9}{(P_{t9}/P_9)_R}\right]^{(\gamma_t+1)/(2\gamma_t)}\sqrt{\frac{(P_{t9}/P_9)_R^{(\gamma_t-1)/\gamma_t} - 1}{(P_{t9}/P_9)^{(\gamma_t-1)/\gamma_t} - 1}} \tag{8.32aa}$$

Example 8.3

We consider the performance of the turbojet engine of Example 7.1 sized for a mass flow rate of 50 kg/s at the reference condition and altitude of 12 km. We are to determine this engine's performance at an altitude of 9 km, Mach number of 1.5, reduced throttle setting ($T_{t4} = 1670°\text{R}$), and exit to ambient pressure ratio (P_0/P_9) of 0.955.

REFERENCE:

$$T_0 = 216.7\text{ K}, \quad \gamma_c = 1.4, \quad c_{pc} = 1.004\text{ kJ/(kg·K)}, \quad \gamma_t = 1.3$$
$$c_{pt} = 1.239\text{ kJ/(kg·K)}, \quad T_{t4} = 1800\text{ K}, \quad M_0 = 2, \quad \pi_c = 10$$
$$\tau_c = 2.0771, \quad \eta_c = 0.8641, \quad \pi_t = 0.8155, \quad \pi_t = 0.3746$$
$$\pi_{d\max} = 0.95, \quad \pi_d = 0.8788, \quad \pi_b = 0.94, \quad \pi_n = 0.96$$
$$\eta_b = 0.98, \quad \eta_m = 0.99, P_0/P_9 = 0.5, \quad h_{PR} = 42{,}800\text{ kJ/kg}$$
$$f = 0.03567, \quad P_{t9}/P_9 = 11.62, \quad F/\dot{m}_0 = 806.9\text{ N/(kg/s)}$$
$$S = 44.21\text{ (mg/s)/N}, \quad P_0 = 19.40\text{ kPa (12 km)}, \quad \dot{m}_0 = 50\text{ kg/s}$$
$$F = \dot{m}_0 \times (F/\dot{m}_0) = 50 \times 806.9 = 40{,}345\text{ N}$$

OFF-DESIGN CONDITION:

$$T_0 = 229.8\text{ K}, \quad P_0 = 30.8\text{ kPa (9 km)}, \quad M_0 = 1.5$$
$$P_0/P_9 = 0.955, \quad T_{t4} = 1670\text{ K}$$

EQUATIONS:

$$R_c = \frac{\gamma_c - 1}{\gamma_c} c_{pc} = \frac{0.4}{1.4}(1.004) = 0.2869\,\text{kJ/(kg} \cdot \text{K)}$$

$$R_t = \frac{\gamma_t - 1}{\gamma_t} c_{pt} = \frac{0.3}{1.3}(1.239) = 0.2859\,\text{kJ/(kg} \cdot \text{K)}$$

$$a_0 = \sqrt{\gamma_c R_c g_c T_0} = \sqrt{1.4 \times 286.9 \times 1 \times 229.8} = 303.8\ \text{m/s}$$

$$V_0 = a_0 M_0 = 303.8 \times 1.5 = 455.7\,\text{m/s}$$

$$\tau_r = 1 + \frac{\gamma_c - 1}{2} M_0^2 = 1 + 0.2 \times 1.5^2 = 1.45$$

$$\pi_r = \tau_r^{\gamma_c/(\gamma_c - 1)} = 1.45^{3.5} = 3.671$$

$$\eta_r = 1 - 0.075(M_0 - 1)^{1.35} = 1 - 0.075(0.5)^{1.35} = 0.9706$$

$$\pi_d = \pi_{d\max} \eta_r = 0.95 \times 0.9706 = 0.9220$$

$$\tau_\lambda = \frac{c_{pt} T_{t4}}{c_{pc} T_0} = \frac{1.2329 \times 1670}{1.004 \times 229.8} = 8.9682$$

$$T_{t2} = T_0 \tau_r = 229.8 \times 1.45 = 333.2\,\text{K}$$

$$\tau_{rR} = 1 + \frac{\gamma_c - 1}{2} M_{0R}^2 = 1 + 0.2 \times 2^2 = 1.80$$

$$T_{t2R} = T_{0R} \tau_{rR} = 216.7 \times 1.8 = 390.1\,\text{K}$$

$$\pi_{rR} = \tau_{rR}^{\gamma_c/(\gamma_c - 1)} = 1.8^{3.5} = 7.824$$

$$\tau_c = 1 + (\tau_{cR} - 1)\frac{T_{t4}/T_{t2}}{(T_{t4}/T_{t2})_R}$$

$$= 1 + (2.0771 - 1)\frac{1670/333.2}{1800/390.1} = 2.170$$

$$\pi_c = [1 + \eta_c(\tau_c - 1)]^{\gamma_c/(\gamma_c - 1)} = [1 + 0.8641(2.170 - 1)]^{3.5} = 11.53$$

$$f = \frac{\tau_\lambda - \tau_r \tau_c}{h_{PR}\eta_b/(c_{pc} T_0) - \tau_\lambda}$$

$$= \frac{8.9682 - 1.45 \times 2.170}{42{,}800 \times 0.98/(1.004 \times 229.8) - 8.9682} = 0.03368$$

$$\frac{P_{t9}}{P_9} = \frac{P_0}{P_9} \pi_r \pi_d \pi_c \pi_b \pi_t \pi_n$$

$$= 0.955 \times 3.671 \times 0.9220 \times 11.53 \times 0.94 \times 0.3746 \times 0.96 = 12.60$$

$$M_9 = \sqrt{\frac{2}{\gamma_t - 1}[(P_{t9}/P_9)^{(\gamma_t - 1)/\gamma_t} - 1]} = \sqrt{\frac{2}{0.3}(12.60^{0.3/1.3} - 1)} = 2.301$$

$$\frac{T_9}{T_0} = \frac{\tau_\lambda \tau_t}{(P_{t9}/P_9)^{(\gamma_t-1)/\gamma_t}} \frac{c_{pc}}{c_{pt}} = \frac{8.9682 \times 0.8155}{12.60^{0.3/1.3}} \frac{1.004}{1.239} = 3.303$$

$$\frac{V_9}{a_0} = M_9 \sqrt{\frac{\gamma_t R_t T_9}{\gamma_c R_c T_0}} = 2.301 \sqrt{\frac{1.3 \times 285.9}{1.4 \times 286.9}(3.303)} = 4.023$$

$$\frac{F}{\dot{m}_0} = \frac{a_0}{g_c}\left[(1+f)\frac{V_9}{a_0} - M_0 + (1+f)\frac{R_t}{R_c}\frac{T_9/T_0}{V_9/a_0}\frac{1 - P_0/P_9}{\gamma_c}\right]$$

$$= 303.8\left(1.03368 \times 4.023 - 1.5 + 1.03368 \frac{285.9}{286.9}\frac{3.303}{4.023}\frac{0.045}{1.4}\right)$$

$$= 303.8(2.6585 + 0.0272) = 815.9\,\text{N/(kg/s)}$$

$$S = \frac{f}{F/\dot{m}_0} = \frac{0.03368 \times 10^6}{815.9} = 41.28\,\text{(mg/s)/N}$$

$$\dot{m}_0 = \dot{m}_{0R} \frac{P_0 \pi_r \pi_d \pi_c}{(P_0 \pi_r \pi_d \pi_c)_R} \sqrt{\frac{T_{t4R}}{T_{t4}}}$$

$$\dot{m}_0 = 50 \frac{30.8 \times 3.671 \times 0.9220 \times 11.53}{19.4 \times 7.824 \times 0.8788 \times 10} \sqrt{\frac{1800}{1670}} = 46.78\,\text{kg/s}$$

$$F = \dot{m}_0 \frac{F}{\dot{m}_0} = 46.78 \times 815.9 = 38{,}170\,\text{N}$$

$$\eta_T = \frac{a_0^2[(1+f)(V_9/a_0)^2 - M_0^2]}{2 g_c f h_{PR}}$$

$$= \frac{303.8^2[(1.03368)(4.023^2) - 1.5^2]}{2 \times 1 \times 0.03368 \times 42{,}800 \times 1{,}000} = 46.36\%$$

$$\eta_P = \frac{2 g_c V_0 (F/\dot{m}_0)}{a_0^2[(1+f)(V_9/a_0)^2 - M_0^2]}$$

$$= \frac{2 \times 1 \times 455.7 \times 815.9}{303.8^2[(1.03368)(4.023^2) - 1.5^2]} = 55.64\%$$

$$\eta_O = \eta_P \eta_T = 0.4635 \times 0.5564 = 25.79\%$$

$$\frac{N}{N_R} = \sqrt{\frac{T_0 \tau_r}{T_{0R} \tau_{rR}} \frac{\pi_c^{(\gamma_c-1)/\gamma_c} - 1}{\pi_{cR}^{(\gamma_c-1)/\gamma_c} - 1}}$$

$$= \sqrt{\frac{229.8 \times 1.45}{216.7 \times 1.8} \frac{11.53^{0.4/1.4} - 1}{10^{0.4/1.4} - 1}} = 0.9278$$

$$\frac{\dot{m}_{c2}}{\dot{m}_{c2R}} = \frac{\pi_c}{\pi_{cR}} \sqrt{\frac{(T_{t4}/T_{t2})_R}{T_{t4}/T_{t2}}} = \frac{11.53}{10} \sqrt{\frac{1800/390.1}{1670/333.2}} = 1.106$$

$$\frac{A_9}{A_{9R}} = \left[\frac{P_{t9}/P_9}{(P_{t9}/P_9)_R}\right]^{(\gamma_t+1)/(2\gamma_t)} \sqrt{\frac{(P_{t9}/P_9)_R^{(\gamma_t-1)/\gamma_t} - 1}{(P_{t9}/P_9)^{(\gamma_t-1)/\gamma_t} - 1}}$$

$$\frac{A_9}{A_{9R}} = \left(\frac{12.60}{11.62}\right)^{2.3/1.3} \sqrt{\frac{11.62^{0.3/1.3} - 1}{12.60^{0.3/1.3} - 1}} = 1.052$$

Example 8.4

Consider a turbojet engine composed of the gas generator of Example 8.2, an inlet with $\pi_{d\max} = 0.99$, and an exhaust nozzle with $\pi_n = 0.99$ and $P_0/P_9 = 1$. The reference engine has the following values.

REFERENCE:

$$T_0 = 518.7°R, \quad \gamma_c = 1.4, \quad c_{pc} = 0.24 \text{ Btu/(lbm} \cdot °\text{R)}, \quad \gamma_t = 1.33$$

$$c_{pt} = 0.276 \text{ Btu/(lbm} \cdot °\text{R)}, \quad T_{t4} = 3200°\text{R}, \quad M_0 = 0$$

$$\pi_c = 15, \quad \eta_c = 0.8572, \quad \tau_t = 0.8124, \quad \pi_t = 0.3943$$

$$\pi_{d\max} = 0.99, \quad \pi_b = 0.96, \quad \pi_n = 0.99, \quad \eta_b = 0.995$$

$$\eta_m = 0.99, \quad P_0/P_9 = 1, \quad P_0 = 14.696 \text{ psia (sea level)}$$

$$P_{t9}/P_9 = 5.5653, \quad \dot{m}_0 = 100 \text{ lbm/s}, \quad F/\dot{m}_0 = 113.42 \text{ lbf/(lbm/s)}$$

$$F = \dot{m}_0 \times (F/\dot{m}_0) = 100 \times 113.42 = 11{,}342 \text{ lbf}$$

This engine has a control system that limits the compressor pressure ratio π_c to 15 and the combustor exit total temperature T_{t4} to 3200°R. Calculation of engine performance using Eqs. (8.32a–8.32aa) with full throttle at altitudes of sea level, 20 kft, and 40 kft over a range of flight Mach numbers gives the results shown in Figs. 8.17–8.22. Note the breaks in the plots of thrust, engine mass flow rate, compressor pressure ratio, and station 2 corrected mass flow rate at a Mach/altitude combination of about 0.9/20 kft and 1.3/40 kft. To the left of these breaks, the combustor exit temperature T_{t4} is below its maximum of 3200°R, and the compressor pressure ratio π_c is at its maximum of 15. To the right of these breaks, the combustor exit temperature T_{t4} is at its maximum of 3200°R, and the compressor pressure ratio π_c is below its maximum of 15. At the break, both the compressor pressure ratio and combustor exit temperature are at their maximum values. This break corresponds to the engine's theta break of 1.0.

The designer of a gas generator's turbomachinery needs to know the maximum power requirements of the compressor and turbine. Because the turbine drives the compressor, the maximum requirements of both occur at the same conditions. Consider the following power balance between the compressor and turbine:

$$\dot{W}_c = \eta_m \dot{W}_t$$

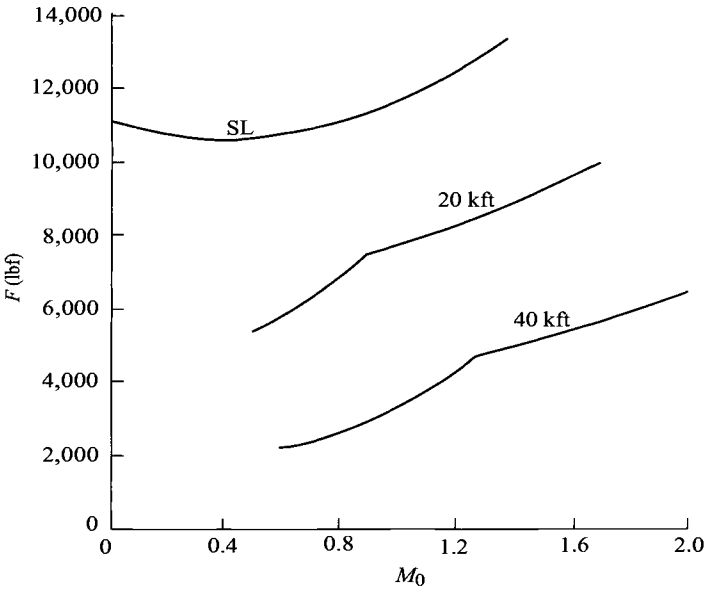

Fig. 8.17 Maximum thrust F of a turbojet vs M_0.

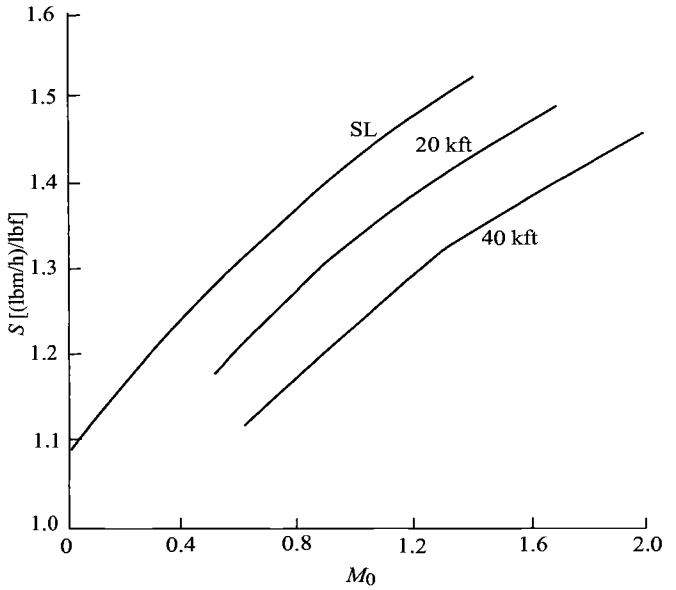

Fig. 8.18 Thrust-specific fuel consumption S of a turbojet vs M_0.

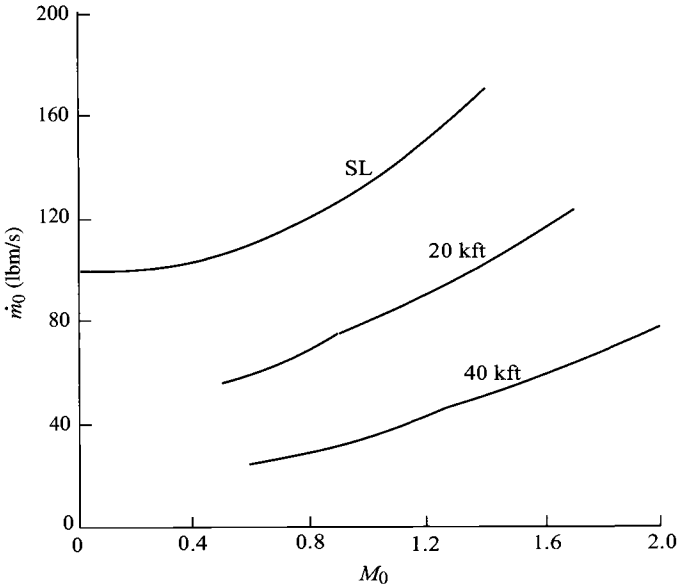

Fig. 8.19 Engine mass flow rate of a turbojet vs M_0.

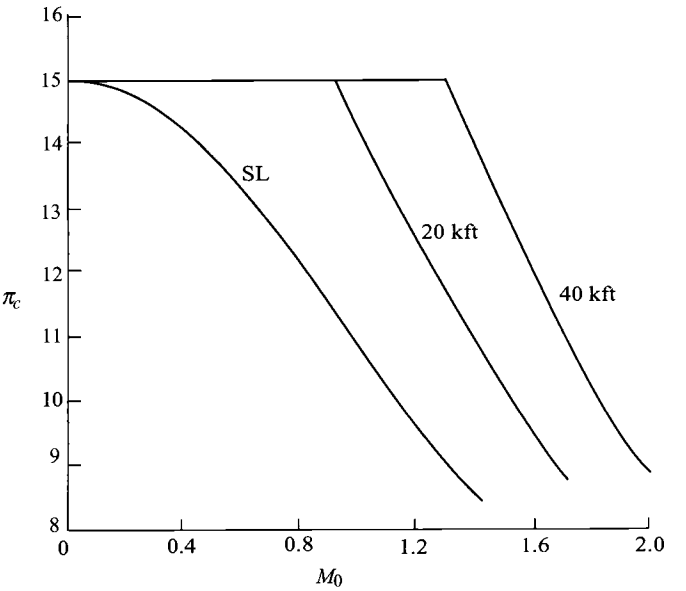

Fig. 8.20 Compressor pressure ratio of a turbojet vs M_0.

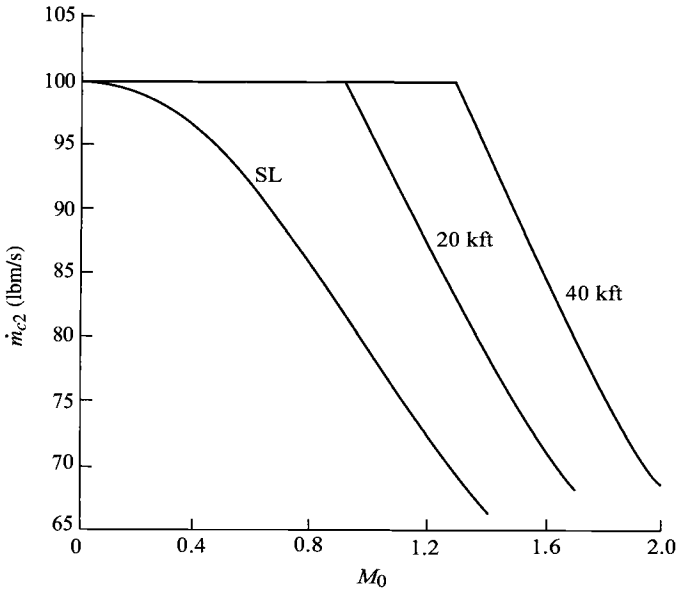

Fig. 8.21 Compressor corrected mass flow rate of a turbojet vs M_0.

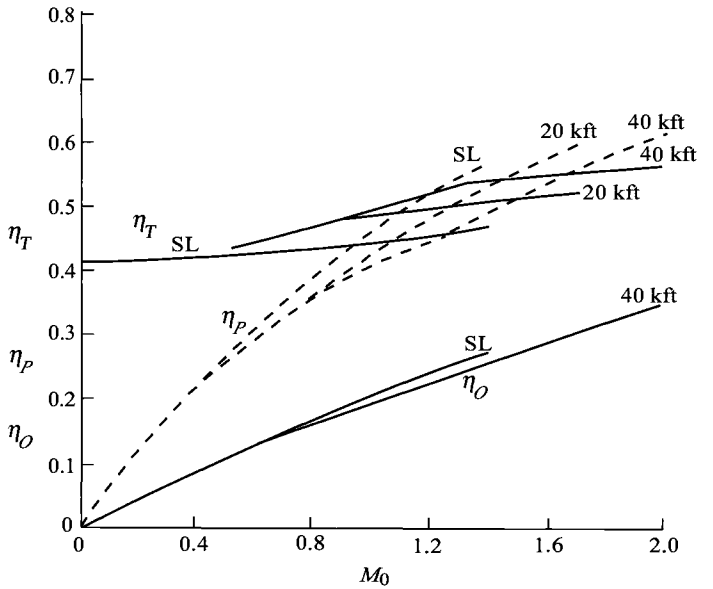

Fig. 8.22 Turbojet efficiencies vs M_0.

Rewriting turbine power in terms of its mass flow rate, total temperatures, etc., gives

$$\dot{W}_c = \eta_m \dot{m}_0 (1 + f) c_{pt} (T_{t4} - T_{t5})$$

or

$$\dot{W}_c = \dot{m}_0 T_{t4} [\eta_m (1 + f) c_{pt} (1 - \tau_t)]$$

Because the terms within the square braces of the preceding equation are considered constant, the maximum compressor power will be at the flight condition having maximum engine mass flow rate at maximum T_{t4}. From Fig. 8.19, the maximum compressor or turbine power corresponds to the maximum engine mass flow rate at sea level and Mach 1.4.

At an altitude of 20 kft and a Mach number of 0.8, engine performance calculations at reduced throttle (T_{t4}) using Eqs. (8.32a–8.32aa) were performed, and some of these results are given in Fig. 8.23. The typical variation in thrust specific fuel consumption S with thrust F is shown in this figure. As the throttle is reduced, the thrust specific fuel consumption first reduces before increasing. This plot of thrust specific fuel consumption S vs thrust F is commonly called the *throttle hook* because of its shape.

We stated at the beginning of this chapter that the principal efficiencies that affect engine performance are the thermal efficiency and the propulsive

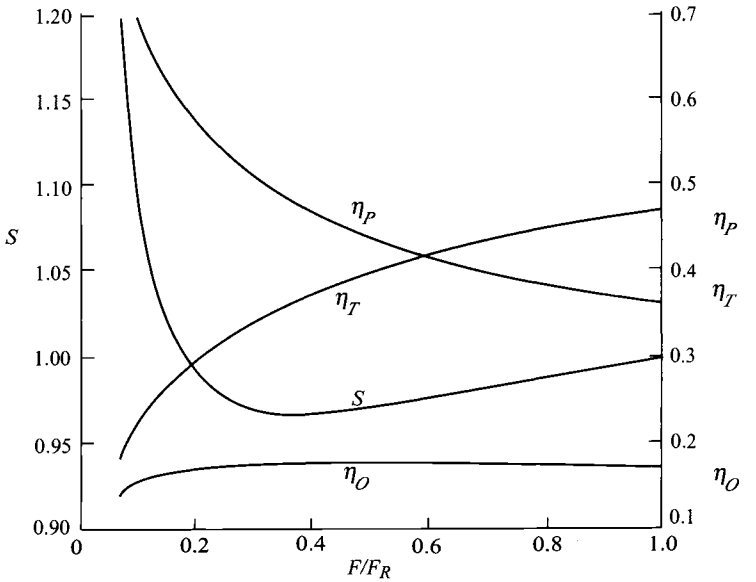

Fig. 8.23 Turbojet performance at partial throttle.

efficiency. Figure 8.23 shows the very large changes in both propulsive and thermal efficiency with engine thrust. Note that as thrust is reduced from its maximum, the increase in propulsive efficiency more than offsets the decrease in thermal efficiency such that the overall efficiency increases and the thrust specific fuel consumption decreases until about 40% of maximum thrust. Below 40% thrust, the decrease in thermal efficiency dominates the increase in propulsive efficiency and the overall efficiency decreases, and the thrust specific fuel consumption increases with reduced thrust.

8.3.2 Corrected Engine Performance

The changes in maximum thrust of a simple turbojet engine can be presented in a corrected format that essentially collapses the thrust data. Consider the thrust equation for the turbojet engine as given by

$$F = \frac{\dot{m}_0}{g_c}[(1+f)V_9 - V_0]$$

where

$$V_9 = \sqrt{2g_c c_{pt} T_{t4} \tau_t [1 - (\pi_r \pi_d \pi_c \pi_b \pi_t \pi_n)^{(-\gamma_t - 1)/\gamma_t}]}$$

and

$$V_0 = M_0 a_0 = M_0 \sqrt{\gamma_c R_c T_0}$$

Note that the engine mass flow rate is related to the compressor corrected mass flow rate by

$$\dot{m}_0 = \dot{m}_{c0} = \frac{\delta_0}{\sqrt{\theta_0}} = \dot{m}_{c2} \frac{\delta_2}{\sqrt{\theta_2}} = \dot{m}_{c2} \frac{\pi_d \delta_0}{\sqrt{\theta_0}}$$

The engine thrust can now be written as

$$F = \frac{\dot{m}_{c2}}{g_c} \frac{\pi_d \delta_0}{\sqrt{\theta_0}} [(1+f)V_9 - V_0]$$

Dividing the thrust by the dimensionless total pressure at station 0 gives

$$\frac{F}{\delta_0} = \frac{\dot{m}_{c2} \pi_d}{g_c} \left[(1+f) \frac{V_9}{\sqrt{\theta_0}} - \frac{V_0}{\sqrt{\theta_0}} \right] \tag{8.33a}$$

where

$$\frac{V_9}{\sqrt{\theta_0}} = \sqrt{\frac{T_{t4}}{T_{t2}}} \sqrt{2g_c c_{pt} T_{\text{ref}} \tau_t [1 - \pi_r \pi_d \pi_c \pi_b \pi_t \pi_n)^{-(\gamma_t - 1)/\gamma_t}]} \tag{8.33b}$$

and

$$\frac{V_0}{\sqrt{\theta_0}} = \frac{M_0}{\sqrt{\tau_r}} a_{SL} \tag{8.33c}$$

The maximum thrust for the turbojet engine of Example 8.4 can be determined by using the preceding equations. Figures 8.17, 8.20, and 8.21 show the variation of the maximum thrust F, compressor pressure ratio, and corrected mass flow rate from this turbojet engine at full throttle vs flight Mach number M_0. The corrected thrust F/δ_0 of this engine is plotted vs flight condition θ_0 in Fig. 8.24. The variation of T_{t4}/T_{t2}, compressor pressure ratio, corrected mass flow rate, and corrected fuel flow rate are plotted vs θ_0 in Fig. 8.25. The representation of the engine thrust, as corrected thrust vs θ_0, essentially collapses the thrust data into one line for θ_0 greater than 1.0. The discussion that follows helps one see why the plot in Fig. 8.24 behaves as shown. When θ_0 is less than 1.0, we observe the following:

1) The compressor pressure ratio is constant at its maximum value of 15 (see Fig. 8.25).
2) The compressor corrected mass flow rate is constant at its maximum value of 100 lbm/s (see Fig. 8.25).
3) The value of T_{t4}/T_{t2} is constant at its maximum value of 6.17 (see Fig. 8.25).
4) The corrected exit velocity given by Eq. (8.33b) is essentially constant.

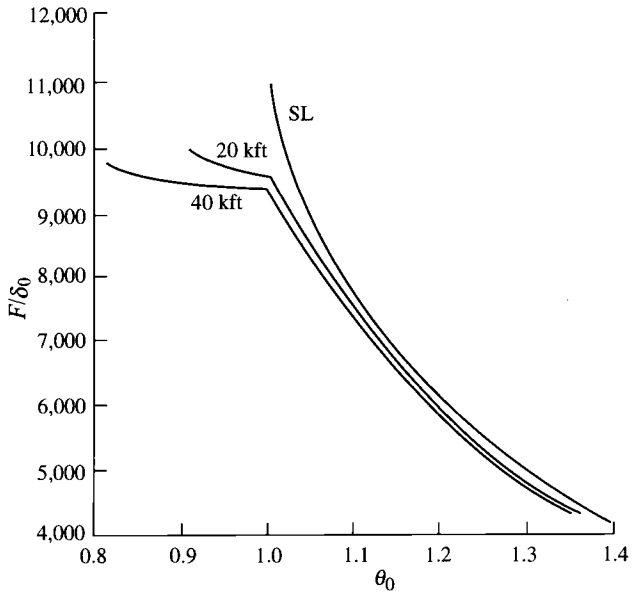

Fig. 8.24 Maximum corrected thrust (F/δ_0) of a turbojet vs θ_0.

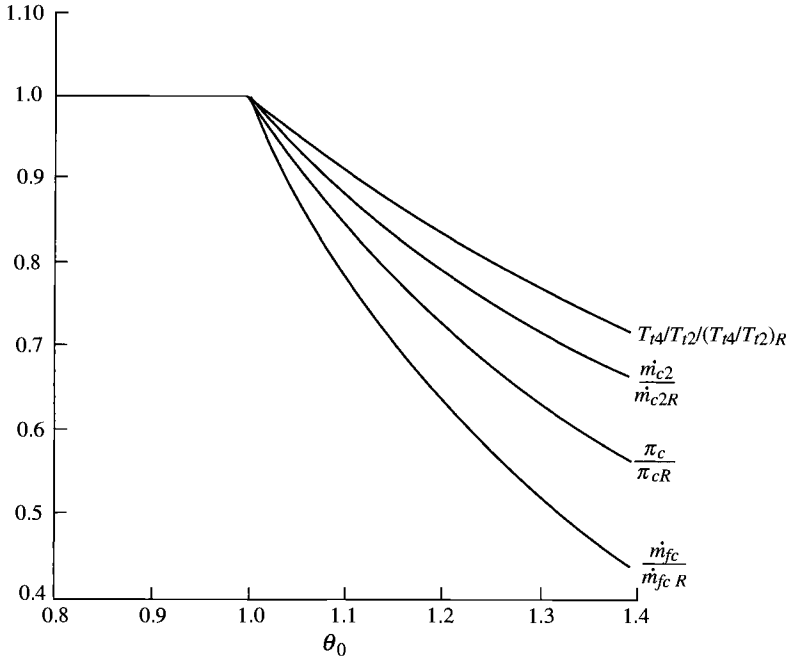

Fig. 8.25 Maximum throttle characteristics of a turbojet vs θ_0.

5) The corrected flight velocity [Eq. (8.33c)] increases in a nearly linear manner with M_0.
6) The corrected thrust [Eq. (8.33a)] decreases slightly with increasing θ_0.

When θ_0 is greater than 1.0, we observe the following:

1) The compressor pressure ratio decreases with increasing θ_0.
2) The compressor corrected mass flow rate decreases with increasing θ_0.
3) The value of T_{t4} is constant at its maximum value of 3200°R.
4) The corrected exit velocity given by Eq. (8.33b) decreases with increasing θ_0.
5) The corrected flight velocity [Eq. (8.33c)] increases in a nearly linear manner with M_0.
6) The corrected thrust [Eq. (8.33a)] decreases substantially with increasing θ_0.

As shown in Fig. 8.24, the trend in maximum corrected thrust F/δ_0 of this turbojet dramatically changes at the $\theta_{0\text{break}}$ value of 1.0. Both the compressor pressure ratio π_c and combustor exit temperature T_{t4} are at their maximum values when θ_0 is 1.0. The engine control system varies the fuel flow to the combustor to keep π_c and T_{t4} under control. The control system maintains π_c at its maximum for θ_0 values less than 1.0, and T_{t4} at its maximum for θ_0 values greater than 1.0. These same kinds of trends are observed for many other gas turbine aircraft engines.

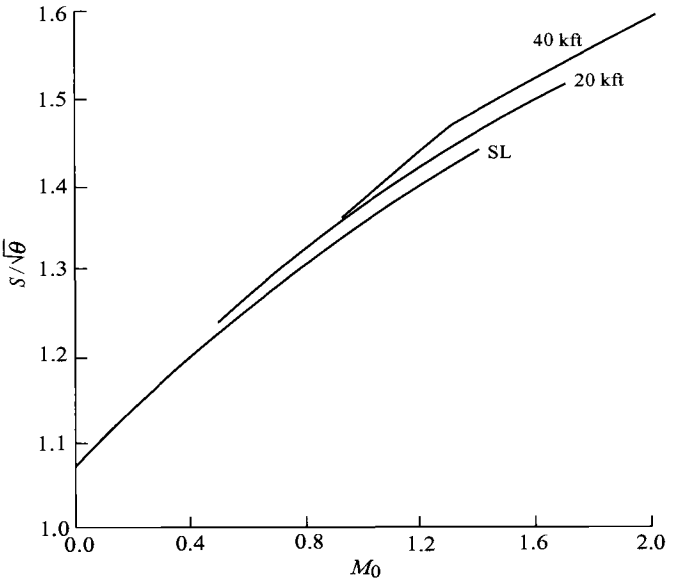

Fig. 8.26 $S/\sqrt{\theta}$ **of a turbojet vs** M_0.

The thrust-specific fuel consumption S of this turbojet at maximum thrust is plotted vs Mach number in Fig. 8.18. If the values of S are divided by the square root of the corrected ambient temperature, then the curves for higher altitudes are shifted up and we get Fig. 8.26. Note that these curves could be estimated by a straight line. Equations (1.36a–1.36f) are based on this nearly linear relationship with flight Mach number M_0. When the corrected thrust-specific fuel consumption [S_c, see Eq. (8.8)] is plotted vs θ_0, the spread in fuel consumption data is substantially reduced, as shown in Fig. 8.27. One could estimate that the corrected thrust specific fuel consumption has a value of about 1.24 for most flight conditions.

8.3.3 Throttle Ratio

The *throttle ratio* (TR) is defined as the ratio of the maximum value of T_{t4} to the value of T_{t4} at sea-level static (SLS) conditions. In equation form, the throttle ratio is

$$\text{TR} \equiv \frac{(T_{t4})_{\max}}{(T_{t4})_{\text{SLS}}} \tag{8.34a}$$

The throttle ratio for the simple turbojet engine and compressor of Figs. 8.17–8.27 has a value of 1.0. Both the compressor performance and engine performance curves change shape at a θ_0 value of 1.0. This change in shape of the performance curves occurs at the simultaneous maximum of π_c and T_{t4}. The fact that both the throttle ratio and dimensionless total temperature

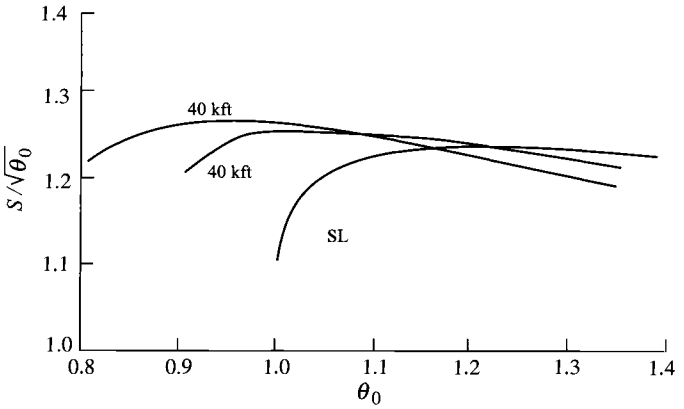

Fig. 8.27 $S/\sqrt{\theta_0}$ of a turbojet vs θ_0.

θ_0 have a value of 1.0 at the simultaneous maximum is not a coincidence but is a direct result of compressor-turbine power balance given by Eq. (8.17). At the simultaneous maximum of π_c and T_{t4}, the throttle ratio equals θ_0:

$$\text{TR} = \theta_0 \qquad \text{at max } \pi_c \text{ and max } T_{t4}$$

or

$$\text{TR} = \theta_{0\,\text{break}} \tag{8.34b}$$

High-performance fighters want gas turbine engines whose thrust does not drop off as fast with increasing θ_0 as that of Fig. 8.24. The value of θ_0, where the corrected maximum thrust F/δ_0 curves change slope, can be increased by increasing the maximum T_{t4} of the preceding example turbojet engine.

Example 8.5

Again, we consider the example turbojet engine with a compressor that has a compressor pressure ratio of 15 and corrected mass flow rate of 100 lbm/s for T_{t2} of 518.7°R and T_{t4} of 3200°R. The maximum π_c is maintained at 15, and the maximum T_{t4} is increased from 3200 to 3360°R (TR = 1.05). The variation in thrust, thrust-specific fuel consumption, compressor pressure ratio, and corrected mass flow rate of this turbojet engine at full throttle are plotted vs flight Mach number M_0 in Figs. 8.28, 8.29, 8.30, and 8.31, respectively. Figure 8.32 shows the corrected thrust F/δ_0 plotted vs θ_0. Comparing Figs. 8.17 and 8.28, we note that the thrust of both engines are the same at sea-level static, and the engine with a throttle ratio of 1.05 has higher thrust at high Mach numbers. Figures 8.24 and 8.32 show that changing the throttle ratio from 1.0 to 1.05 changes the θ_0 value at which the curves change shape $\theta_{0\,\text{break}}$ and increases the corrected thrust at θ_0 values greater than 1.0.

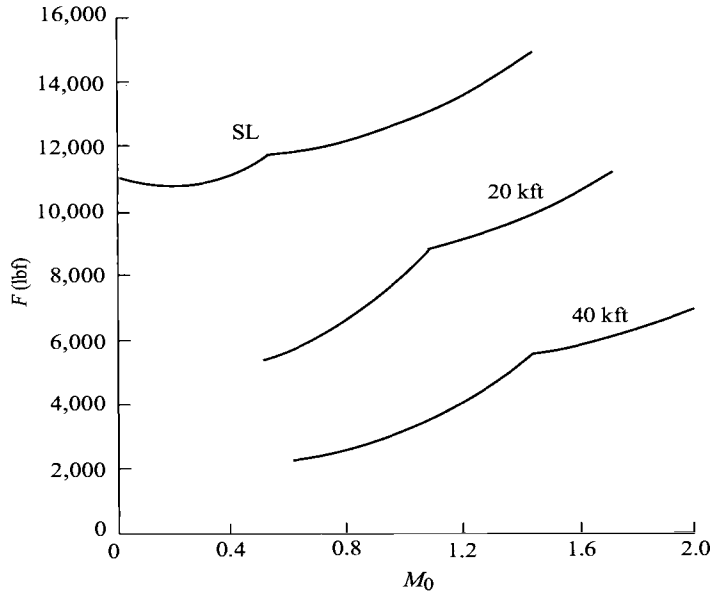

Fig. 8.28 Maximum thrust F of improved turbojet vs M_0.

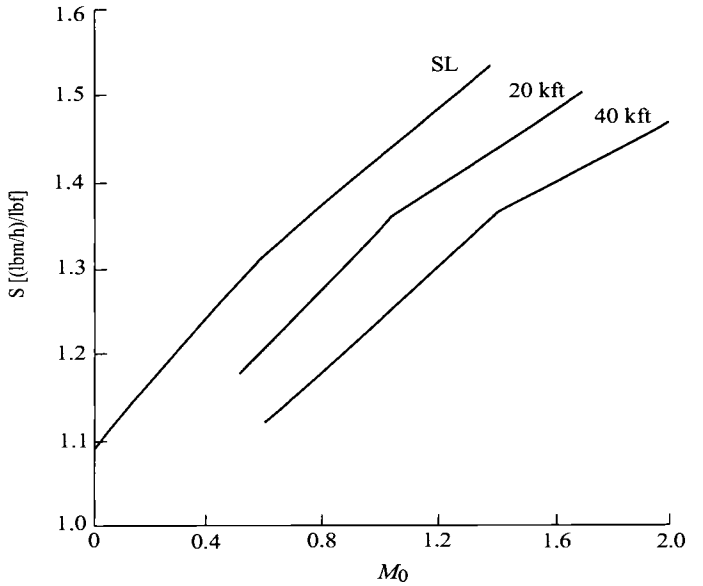

Fig. 8.29 Thrust-specific fuel consumption S of improved turbojet vs M_0.

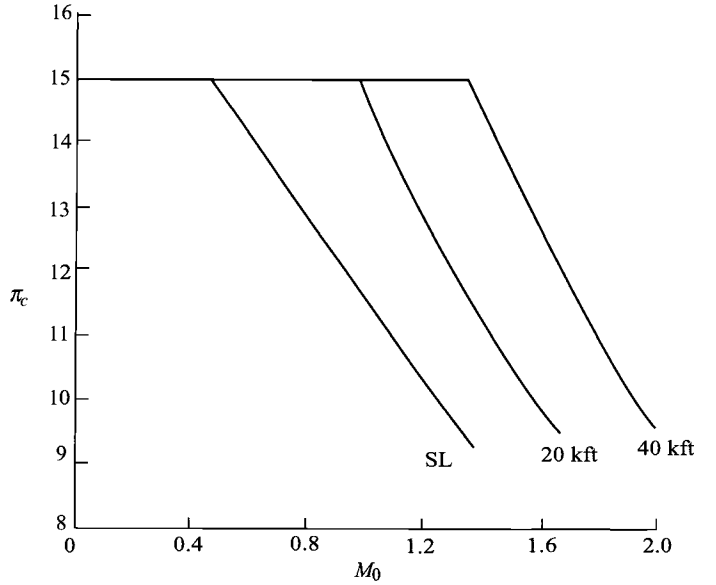

Fig. 8.30 Compressor pressure ratio of improved turbojet vs M_0.

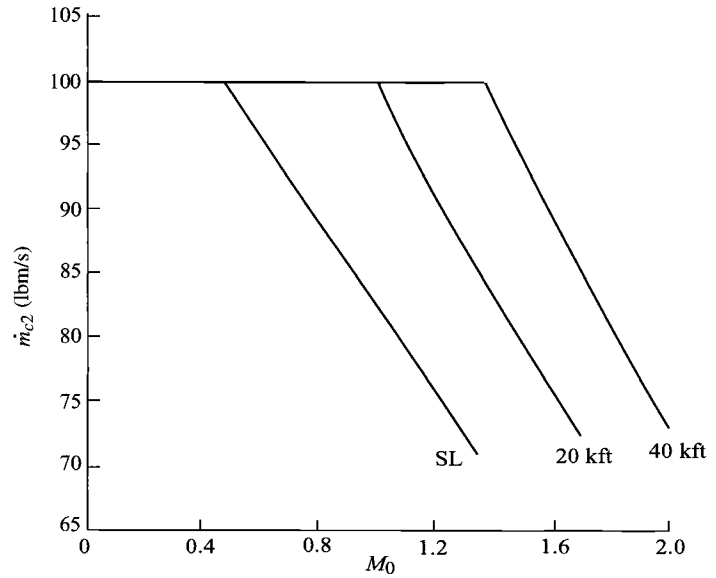

Fig. 8.31 Compressor corrected mass flow rate of improved turbojet vs M_0.

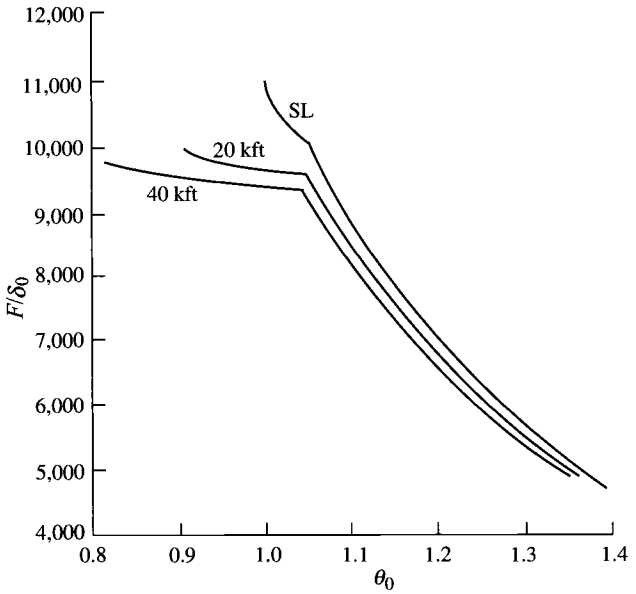

Fig. 8.32 Maximum corrected thrust F/δ_0 of improved turbojet vs θ_0.

Because the compressor and turbine are connected to the same shaft, they have the same rotational speed N, and we can write the following relationship between their corrected speeds:

$$N_{c2} = 1/\sqrt{T_{\text{ref}}}\sqrt{T_{t4}/\theta_0}\, N_{c4} \tag{8.35}$$

Recall that for constant turbine efficiency and choked flow at stations 4 and 8, the correct turbine speed N_{c4} was found to be constant. For maximum thrust engine conditions where θ_0 is less than the throttle ratio, the corrected rotational speed of the compressor N_{c2} and the ratio T_{t4}/θ_0 are constant. Equation (8.35) shows that the corrected speed of the turbine N_{c4} must also be constant at these engine conditions. At $\theta_0 = \text{TR}$, T_{t4} is maximum, the corrected rotational speed of the compressor N_{c2} is constant, and the shaft rotational speed N increases by the square root of θ_0. Thus an engine with a throttle ratio of 1.05 can have a shaft rotational speed at $\theta_0 = \text{TR}$ that is 1.0247 times the maximum speed at sea-level static conditions. This is commonly referred to as an *overspeed* of 2.47%.

8.3.4 Turbine Performance Relationships—Dual-Spool Engines

Two-spool engines, like the turbojet engine shown in Fig. 8.33 and the turbofan engine of Fig. 8.1, are designed with choked flow at engine

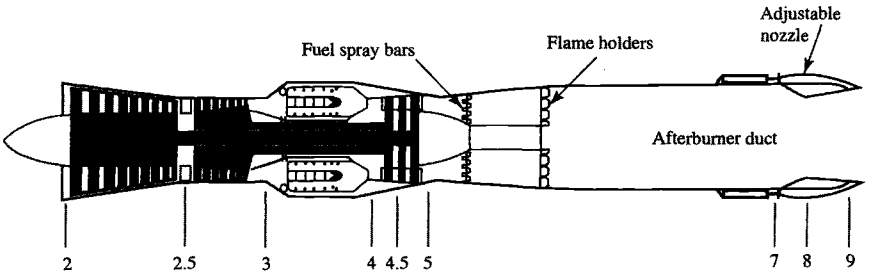

Fig. 8.33 Dual-spool afterburning turbojet engine. (Courtesy of Pratt & Whitney.)

stations 4, 4.5, and 8. Under some operating conditions, the flow may unchoke at station 8. The resulting high-pressure turbine and low-pressure turbine performance relationships are developed in this section for later use.

8.3.4.1 High-pressure turbine. Because the mass flow rate at the entrance to the high-pressure turbine equals that entering the low-pressure turbine,

$$\dot{m}_4 = \frac{P_{t4}}{\sqrt{T_{t4}}} A_4 \text{MFP}(M_4) = \dot{m}_{4.5} = \frac{P_{t4.5}}{\sqrt{T_{t4.5}}} A_{4.5} \text{MFP}(M_{4.5})$$

We assume that the areas are constant and the flow is choked at stations 4 and 4.5. Then

$$\frac{P_{t4}/P_{t4.5}}{\sqrt{T_{t4}/T_{t4.5}}} = \frac{\sqrt{\tau_{tH}}}{\pi_{tH}} = \text{const}$$

Thus for constant η_{tH}, we have

$$\text{constant values of } \pi_{tH},\ \tau_{tH},\ \dot{m}_{c4}, \text{ and } \dot{m}_{c4.5} \tag{8.36}$$

8.3.4.2 Low-pressure turbine. Because the mass flow rate at the entrance to the low-pressure turbine equals that at the exit nozzle throat,

$$\dot{m}_{4.5} = \frac{P_{t4.5}}{\sqrt{T_{t4.5}}} A_{4.5} \text{MFP}(M_{4.5}) = \dot{m}_8 = \frac{P_{t8}}{\sqrt{T_{t8}}} A_8 \text{MFP}(M_8)$$

We assume that the areas are constant at stations 4.5 and 8 and the flow is choked at station 4.5, and so

$$\frac{P_{t4.5}/P_{t5}}{\sqrt{T_{t4.5}/T_{t8}}} \frac{1}{\text{MFP}(M_8)} = \frac{\sqrt{\tau_{tL}}/\pi_{tL}}{\text{MFP}(M_8)} = \frac{A_8 \pi_{\text{AB}}}{A_{4.5} \text{MFP}(M_{4.5})}$$

Using the reference condition to evaluate the constant on the right-hand side of the preceding equation gives

$$\pi_{tL} = \pi_{tLR}\sqrt{\frac{\tau_{tL}}{\tau_{tL\ R}}}\frac{\text{MFP}(M_{8R})}{\text{MFP}(M_8)} \tag{8.37}$$

where

$$\tau_{tL} = 1 - \eta_{tL}(1 - \pi_{tL}^{(\gamma_t-1)/\gamma_t}) \tag{8.38}$$

If station 8 is choked at the reference condition and at the current operating point, then π_{tL} and τ_{tL} are constant and equal their reference values.

8.4 Turbojet Engine with Afterburning

The dual-spool afterburning turbojet engine (Fig. 8.33) is normally designed with choked flow at stations 4, 4.5, and 8. For the afterburning turbojet engine, the variable-area exhaust nozzle is controlled by the engine control system so that the upstream turbomachinery is unaffected by the afterburner operation. In other words, the exhaust nozzle throat area A_8 is controlled during afterburner operation such that the turbine exit conditions (P_{t5}, T_{t5}, and M_5) remain constant. Because the exhaust nozzle has choked flow at its throat at all operating conditions of interest, Eqs. (8.37) and (8.38) for constant efficiency of the low-pressure turbine require that π_{tL} and τ_{tL} be constant:

$$\text{constant values of } \pi_{tL} \text{ and } \tau_{tL} \tag{8.39}$$

This engine has six independent variables (T_{t4}, T_{t7}, M_0, T_0, P_0, and P_0/P_9) and nine dependent variables. These performance analysis variables are summarized in Table 8.5.

Table 8.5 Performance analysis variables for dual-spool afterburning turbojet engine

	Variables		
Component	Independent	Constant or known	Dependent
Engine	M_0, T_0, P_0	$\dot{m}_0$	
Diffuser		$\pi_d = f(M_0)$	
Fan		η_{cL}	π_{cL}, τ_{cL}
High-pressure compressor		η_{cH}	π_{cH}, τ_{cH}
Burner	T_{t4}	π_b, η_b	f
High-pressure turbine		π_{tH}, τ_{tH}	
Low-pressure turbine		π_{tL}, τ_{tL}	
Afterburner	T_{t7}	π_{AB}, η_{AB}	f_{AB}
Nozzle	$\frac{P_9}{P_0}$	π_n	M_9, $\frac{T_9}{T_0}$
Total number	6		9

8.4.1 Analysis of Compressors

8.4.1.1 High-pressure compressor (τ_{cH}, π_{cH}). The power balance between the high-pressure turbine and the high-pressure compressor (high-pressure spool) gives

$$\eta_{mH}\dot{m}_4 c_{pt}(T_{t4} - T_{t4.5}) = \dot{m}_2 c_{pc}(T_{t3} - T_{t2.5})$$

Rewriting this equation in terms of temperature ratios, rearranging into variable and constant terms, and equating the constant to reference values give

$$\frac{\tau_r \tau_{cL}(\tau_{cH} - 1)}{T_{t4}/T_0} = \eta_{mH}(1+f)(1 - \tau_{tH}) = \left[\frac{\tau_r \tau_{cL}(\tau_{cH} - 1)}{T_{t4}/T_0}\right]_R$$

Solving for τ_{cH} gives

$$\tau_{cH} = 1 + \frac{T_{t4}/T_0}{(T_{t4}/T_0)_R}\frac{(\tau_r \tau_{cL})_R}{\tau_r \tau_{cL}}(\tau_{cH} - 1)_R \tag{8.40}$$

From the definition of compressor efficiency, π_{cH} is given by

$$\pi_{cH} = [1 + \eta_{cH}(\tau_{cH} - 1)]^{\gamma_c/(\gamma_c - 1)} \tag{8.41}$$

8.4.1.2 Low-pressure compressor (τ_{cL}, π_{cL}). From a power balance between the low-pressure compressor and low-pressure turbine, we get

$$\eta_{mL}\dot{m}_{4.5} c_{pt}(T_{t4.5} - T_{t5}) = \dot{m}_2 c_{pc}(T_{t2.5} - T_{t2})$$

Rewriting this equation in terms of temperature ratios, rearranging into variable and constant terms, and equating the constant to reference values give

$$\frac{\tau_r(\tau_{cL} - 1)}{T_{t4}/T_0} = \eta_{mL}(1+f)\tau_{tH}(1 - \tau_{tL}) = \left[\frac{\tau_r(\tau_{cL} - 1)}{T_{t4}/T_0}\right]_R$$

Solving for τ_{cL} gives

$$\tau_{cL} = 1 + \frac{T_{t4}/T_0}{(T_{t4}/T_0)_R}\frac{(\tau_r)_R}{\tau_r}(\tau_{cL} - 1)_R \tag{8.42}$$

where

$$\pi_{cL} = [1 + \eta_{cL}(\tau_{cL} - 1)]^{\gamma_c/(\gamma_c - 1)} \tag{8.43}$$

8.4.2 Mass Flow Rate

Since

$$\dot{m}_4 = \dot{m}_0 + \dot{m}_f = \dot{m}_0(1+f)$$

and

$$\dot{m}_4 = \frac{P_{t4}}{\sqrt{T_{t4}}} A_4 \,\mathrm{MFP}(M_4)$$

thus

$$\dot{m}_0 = \frac{P_{t4}}{\sqrt{T_{t4}}} \frac{A_4 \,\mathrm{MFP}(M_4)}{1+f} = \frac{P_0 \pi_r \pi_d \pi_{cL} \pi_{cH} \pi_b}{\sqrt{T_{t4}}} \frac{A_4 \,\mathrm{MFP}(M_4)}{1+f}$$

For A_4, M_4, $1+f$, and π_b essentially constant, the preceding expression can be rewritten as

$$\frac{\dot{m}_0 \sqrt{T_{t4}}}{P_0 \pi_r \pi_d \pi_{cL} \pi_{cH}} = \frac{\pi_b A_4 \,\mathrm{MFP}(M_4)}{1+f} = \left(\frac{\dot{m}_0 \sqrt{T_{t4}}}{P_0 \pi_r \pi_d \pi_{cL} \pi_{cH}} \right)_R$$

or

$$\frac{\dot{m}_0}{\dot{m}_{0R}} = \frac{P_0 \pi_r \pi_d \pi_{cL} \pi_{cH}}{(P_0 \pi_r \pi_d \pi_{cl} \pi_{cH})_R} \sqrt{\frac{T_{t4R}}{T_{t4}}} \tag{8.44}$$

8.4.3 Summary of Performance Equations—Turbojet With and Without Afterburner

INPUTS:

Choices	
Flight parameters:	M_0, T_0(K, °R), P_0(kPa, psia)
Throttle setting:	T_{t4} (K, °R), T_{t7} (K, °R)
Exhaust nozzle setting:	P_0/P_9
Design constants	
π:	$\pi_{d\,\max}$, π_b, π_{tH}, π_{tL}, π_{AB}, π_n
τ:	τ_{tH}, τ_{tL}
η:	η_{cL}, η_{cH}, η_b, η_{AB}, η_{mH}, η_{mL}
Gas properties:	γ_c, γ_t, γ_{AB}, c_{pc}, c_{pt}, $c_{p\mathrm{AB}}$ [kJ/(kg · K), Btu/(lbm · °R)]
Fuel:	h_{PR} (kJ/kg, Btu/lbm)
Reference conditions	
Flight parameters:	M_{0R}, T_{0R} (K, °R), P_{0R} (kPa, psia) τ_{rR}, π_{rR}
Throttle setting:	T_{t4R} (K, °R)
Component behavior:	π_{dR}, π_{cLR}, π_{cHR}, τ_{cLR}, τ_{cHR}

OUTPUTS:

Overall performance:	F(N, lbf), $\dot{m}_0$ (kg/s, lbm/s), f_O, $S\left(\frac{\mathrm{mg/s}}{N}, \frac{\mathrm{lbm/h}}{\mathrm{lbf}}\right)$, η_P, η_T, η_O
Component behavior:	π_{cL}, π_{cH}, τ_{cL}, τ_{cH}, f, f_{AB}, M_9, $(N/N_R)_{\mathrm{LPspool}}$, $(N/N_R)_{\mathrm{HPspool}}$

EQUATIONS:

$$R_c = \frac{\gamma_c - 1}{\gamma_c} c_{pc} \tag{8.45a}$$

$$R_t = \frac{\gamma_t - 1}{\gamma_t} c_{pt} \tag{8.45b}$$

$$a_0 = \sqrt{\gamma_c R_c g_c T_0} \tag{8.45c}$$

$$V_0 = a_0 M_0 \tag{8.45d}$$

$$\tau_r = 1 + \frac{\gamma_c - 1}{2} M_0^2 \tag{8.45e}$$

$$\pi_r = \tau_r^{\gamma_c/(\gamma_c - 1)} \tag{8.45f}$$

$$\eta_r = 1 \qquad \text{for } M_0 \le 1 \tag{8.45g}$$

$$\eta_r = 1 - 0.075(M_0 - 1)^{1.35} \qquad \text{for } M_0 > 1 \tag{8.45h}$$

$$\pi_d = \pi_{d\max} \eta_r \tag{8.45i}$$

$$\tau_{cL} = 1 + \frac{T_{t4}/T_0}{(T_{t4}/T_0)_R} \frac{(\tau_r)_R}{\tau_r} (\tau_{cL} - 1)_R \tag{8.45j}$$

$$\pi_{cL} = [1 + \eta_{cL}(\tau_{cL} - 1)]^{\gamma_c/(\gamma_c - 1)} \tag{8.45k}$$

$$\tau_{cH} = 1 + \frac{T_{t4}/T_0}{(T_{t4}/t_0)_R} \frac{(\tau_r \tau_{cL})_R}{\tau_r \tau_{cL}} (\tau_{cH} - 1)_R \tag{8.45l}$$

$$\pi_{cH} = [1 + \eta_{cH}(\tau_{cH} - 1)]^{\gamma_c/(\gamma_c - 1)} \tag{8.45m}$$

$$\tau_\lambda = \frac{c_{pt} T_{t4}}{c_{pc} T_0} \tag{8.45n}$$

$$f = \frac{\tau_\lambda - \tau_r \tau_{cL} \tau_{cH}}{h_{PR} \eta_b / (c_{pc} T_0) - \tau_\lambda} \tag{8.45o}$$

$$\dot{m}_0 = \dot{m}_{0R} \frac{P_0 \pi_r \pi_d \pi_{cL} \pi_{cH}}{(P_0 \pi_r \pi_d \pi_{cL} \pi_{cH})_R} \sqrt{\frac{T_{t4R}}{T_{t4}}} \tag{8.45p}$$

Without afterburner:

$$R_{AB} = R_t \quad c_{pAB} = c_{pt} \quad \gamma_{AB} = \gamma_t \quad T_{t7} = T_{t4} \tau_{tH} \tau_{tL} \quad \pi_{AB} = 1 \quad f_{AB} = 0 \tag{8.45q}$$

With afterburner:

$$R_{AB} = \frac{\gamma_{AB} - 1}{\gamma_{AB}} c_{pAB} \tag{8.45r}$$

$$\tau_{\lambda AB} = \frac{c_{pAB} T_{t7}}{c_{pc} T_0} \tag{8.45s}$$

$$f_{AB} = \frac{\tau_{\lambda AB} - \tau_\lambda \tau_{tH} \tau_{tL}}{h_{PR} \eta_{AB} / (c_{pc} T_0) - \tau_{\lambda AB}} \tag{8.45t}$$

Remainder of equations:

$$\frac{P_{t9}}{P_9} = \frac{P_0}{P_9} \pi_r \pi_d \pi_{cL} \pi_{cH} \pi_b \pi_{tH} \pi_{tL} \pi_{AB} \pi_n \tag{8.45u}$$

$$M_9 = \sqrt{\frac{2}{\gamma_{AB-1}} \left[\left(\frac{P_{t9}}{P_9} \right)^{(\gamma_{AB}-1)/\gamma_{AB}} - 1 \right]} \tag{8.45v}$$

$$\frac{T_9}{T_0} = \frac{T_{t7}/T_0}{(P_{t9}/P_9)^{(\gamma_{AB}-1)/\gamma_{AB}}} \tag{8.45w}$$

$$\frac{V_9}{a_0} = M_9 \sqrt{\frac{\gamma_{AB} R_{AB}}{\gamma_c R_c} \frac{T_9}{T_0}} \tag{8.45x}$$

$$f_O = f + f_{AB} \tag{8.45y}$$

$$\frac{F}{\dot{m}_0} = \frac{a_0}{g_c} \left[(1 + f_0) \frac{V_9}{a_0} - M_0 + (1 + f_O) \frac{R_{AB}}{R_c} \frac{T_9/T_0}{V_9/a_0} \frac{1 - P_0/P_9}{\gamma_c} \right] \tag{8.45z}$$

$$F = \dot{m}_0 \left(\frac{F}{\dot{m}_0} \right) \tag{8.45aa}$$

$$S = \frac{f_O}{F/\dot{m}_0} \tag{8.45ab}$$

$$\eta_T = \frac{a_0^2 [(1 + f_O)(V_9/a_0)^2 - M_0^2]}{2 g_c f_O h_{PR}} \tag{8.45ac}$$

$$\eta_P = \frac{2 g_c V_0 (F/\dot{m}_0)}{a_0^2 [(1 + f_O)(V_9/a_0)^2 - M_0^2]} \tag{8.45ad}$$

$$\eta_O = \eta_P \eta_T \tag{8.45ae}$$

$$\left(\frac{N}{N_R} \right)_{\text{LPspool}} = \sqrt{\frac{T_0 \tau_r}{T_{0R} \tau_{rR}} \frac{\pi_{cL}^{(\gamma-1)/\gamma} - 1}{\pi_{cLR}^{(\gamma-1)/\gamma} - 1}} \tag{8.45af}$$

$$\left(\frac{N}{N_R} \right)_{\text{HPspool}} = \sqrt{\frac{T_0 \tau_r \tau_{cL}}{T_{0R} \tau_{rR} \tau_{cLR}} \frac{\pi_{cH}^{(\gamma-1)/\gamma} - 1}{\pi_{cHR}^{(\gamma-1)/\gamma} - 1}} \tag{8.45ag}$$

$$\frac{A_9}{A_{9R}} = \left[\frac{P_{t9}/P_9}{(P_{t9}/P_9)_R} \right]^{(\gamma_t+1)/(2\gamma_t)} \sqrt{\frac{(P_{t9}/P_9)_R^{(\gamma_t-1)/\gamma_t} - 1}{(P_{t9}/P_9)^{(\gamma_t-1)/\gamma_t} - 1}} \tag{8.45ah}$$

Example 8.6

In this example, we consider the variation in engine performance of the dry turbojet in Example 8.3 with Mach number M_0, altitude, ambient temperature T_0, ambient pressure P_0, and throttle setting T_{t4}. The compressor pressure ratio is limited to 12.3, and the combustor exit temperature T_{t4} is limited to 1800 K. Figures 8.34, 8.35, 8.36, 8.37, and 8.38 show the variations of thrust, thrust specific fuel consumption S, engine mass flow, engine corrected mass flow, and compressor pressure ratio with Mach number, respectively.

At θ_0 values below 1.2, the engine is at the maximum compressor pressure ratio of 12.3 and T_{t4} is below its maximum value of 1800 K. At θ_0 values above 1.2, the engine is at its maximum T_{t4} value of 1800 K and the compressor pressure ratio is below its maximum value of 12. This engine has a throttle ratio ($\theta_{0\,\text{break}}$) of 1.2.

The corrected engine mass flow, shown in Fig. 8.37, is used in sizing the engine inlet area. For this engine, the maximum corrected engine mass flow is constant for subsonic Mach numbers and decreases with increasing supersonic Mach numbers.

The effect of the inlet total pressure loss on the engine mass flow rate can be seen by comparison of the variations of corrected engine mass flow and compressor pressure ratio, shown in Figs. 8.37 and 8.38. The compressor corrected mass flow rate is constant when the compressor pressure ratio is constant. The drop-off in corrected engine mass flow rate (Fig. 8.37) at Mach numbers greater than 1 is due to the decrease from unity of the inlet total pressure recovery.

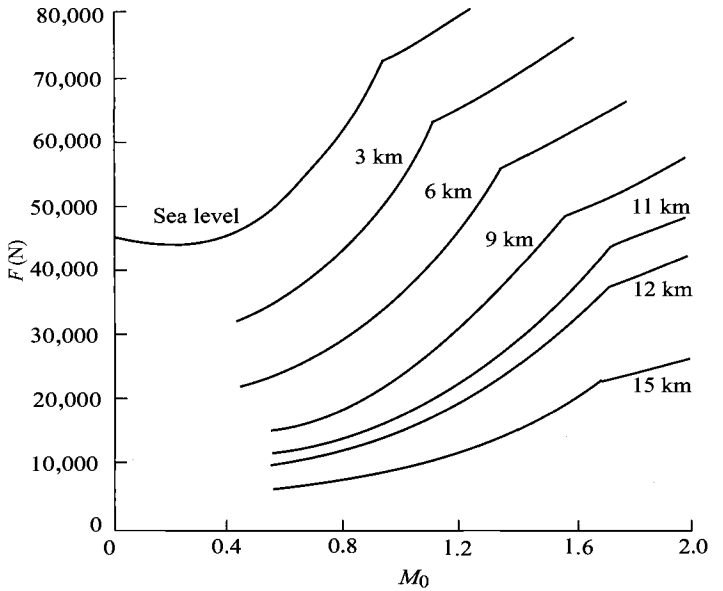

Fig. 8.34 Maximum thrust of dry turbojet.

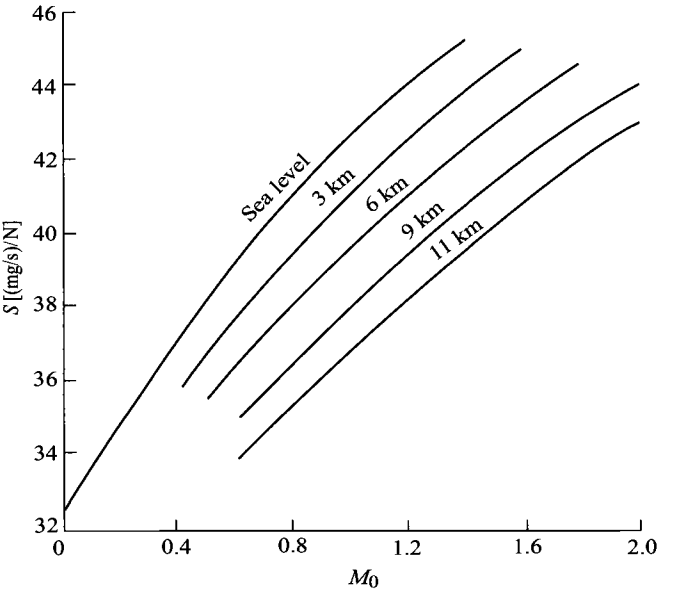

Fig. 8.35 Thrust-specific fuel consumption of dry turbojet at maximum thrust.

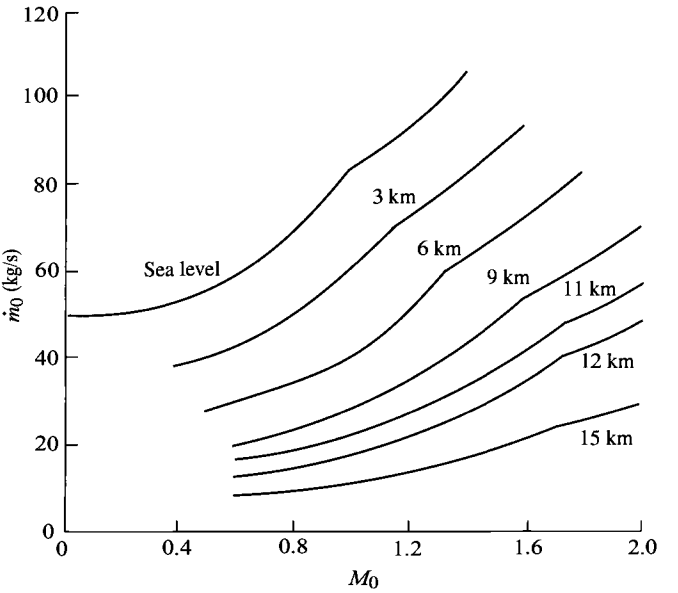

Fig. 8.36 Mass flow rate of dry turbojet at maximum thrust.

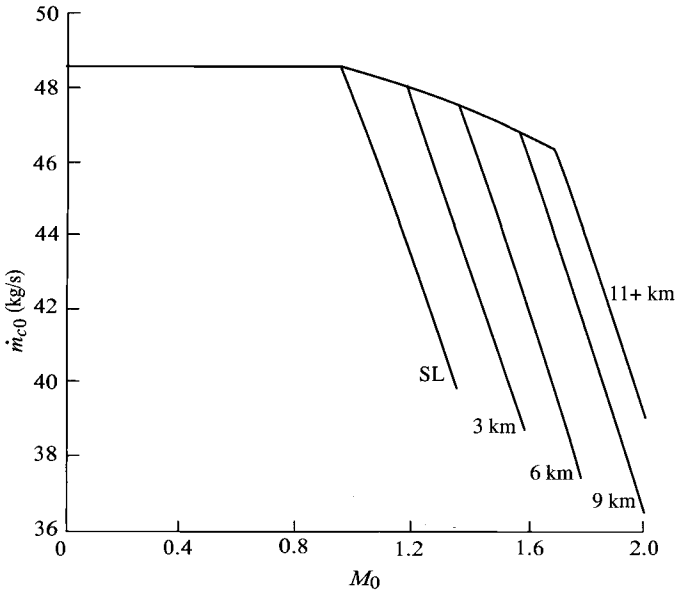

Fig. 8.37 Corrected mass flow rate of dry turbojet at maximum thrust.

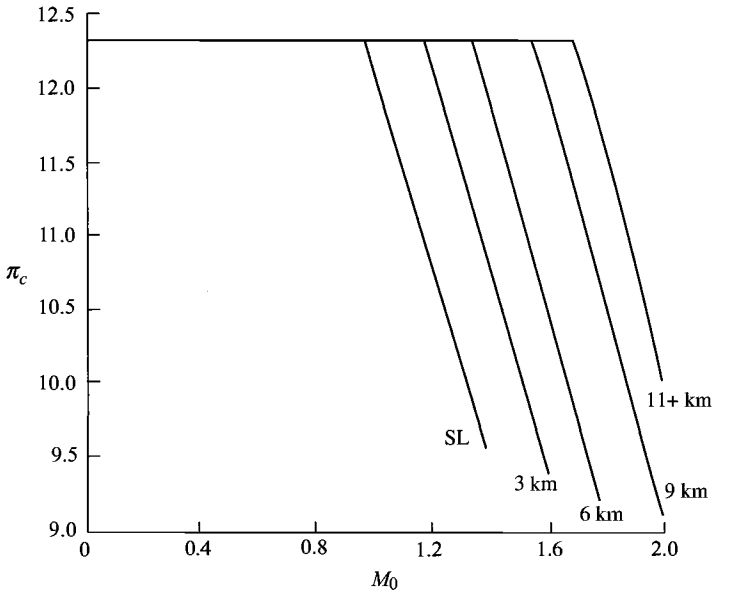

Fig. 8.38 Compressor pressure ratio of dry turbojet at maximum thrust.

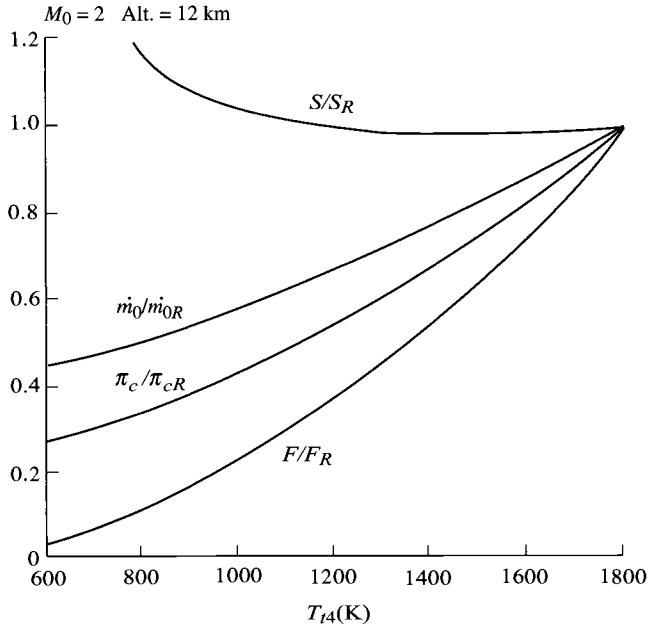

Fig. 8.39 Performance of dry turbojet at partial throttle.

Figure 8.39 shows the variation of engine performance with reduction in engine throttle T_{t4}. Here each engine parameter is compared to its value at the reference condition. As T_{t4} is reduced, the thrust specific fuel consumption initially decreases a little and then increases substantially. The thrust, mass flow rate, and compressor pressure ratio decrease as T_{t4} is reduced.

Figures 8.40 and 8.41 show the variations of engine performance with changes in ambient temperature T_0 and pressure P_0, respectively. Note that decreases in temperature improve thrust F and thrust specific fuel consumption S. The combined effect of ambient temperature and pressure T_0 and P_0 can be seen in the plot vs altitude shown in Fig. 8.42.

Example 8.7

The performance of an afterburning turbojet with a throttle ratio of 1 is considered. The engine performance, when the afterburner is operating at its maximum exit temperature, is commonly referred to as *maximum* or *wet*. This afterburning turbojet engine has a maximum thrust of 25,000 lbf. The terms *military* and *dry* refer to the engine's performance when the afterburner is off (not operating) and the engine core is at maximum operating conditions. The reference conditions and operating limits for the afterburning turbojet engine are as follows.

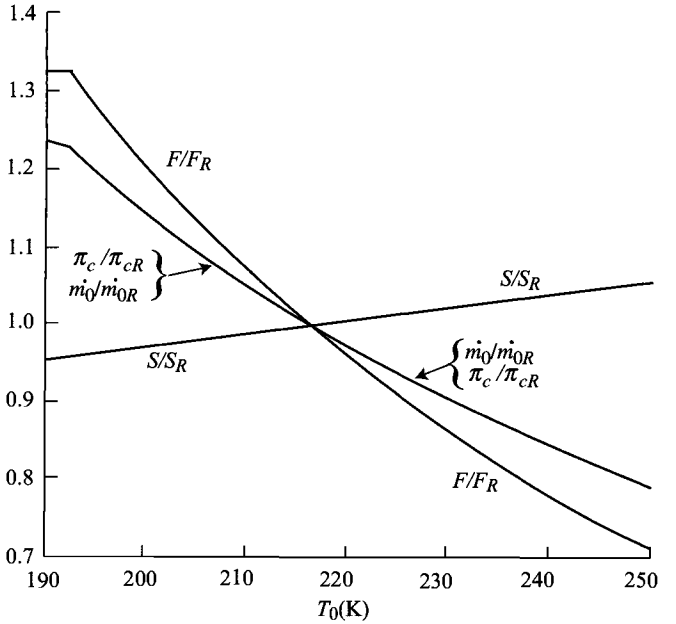

Fig. 8.40 Performance of dry turbojet at maximum thrust vs T_0.

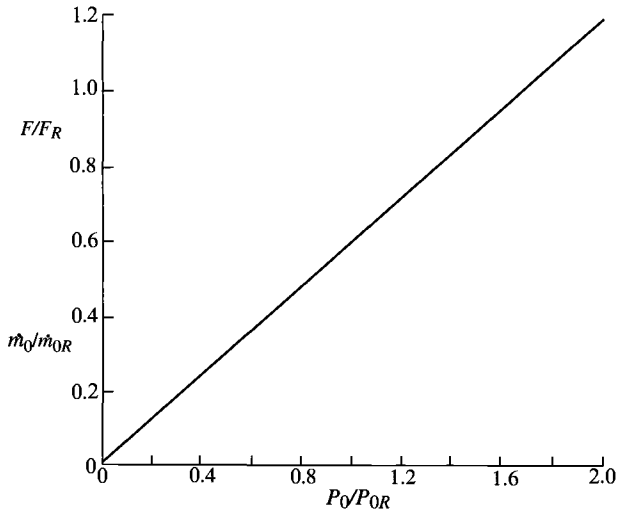

Fig. 8.41 Performance of dry turbojet at maximum thrust vs P_0.

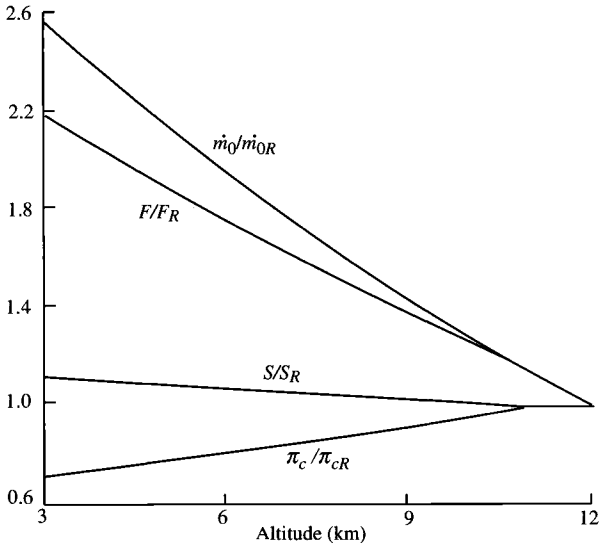

Fig. 8.42 Performance of dry turbojet at maximum thrust vs altitude.

REFERENCE:

Sea-level static ($T_0 = 518.7°\text{R}$, $P_0 = 14.696$ psia)

$$\pi_c = 20, \quad \pi_{cL} = 5, \quad \pi_{cH} = 4, \quad e_{cL} = 0.9$$

$$e_{cH} = 0.9, \quad e_{tH} = 0.9, \; e_{tL} = 0.9, \quad \pi_{d\,\max} = 0.98$$

$$\pi_b = 0.96, \quad \pi_n = 0.98, \quad T_{t4} = 3200°\text{R}$$

$$c_{pc} = 0.24 \text{ Btu/(lbm} \cdot °\text{R)}, \quad \gamma_c = 1.4, \quad c_{pt} = 0.295 \text{ Btu/(lbm} \cdot °\text{R)}$$

$$\gamma_t = 1.3, \quad \eta_b = 0.995, \quad \eta_{mL} = 0.995, \quad \eta_{mH} = 0.995$$

$$h_{PR} = 18{,}400 \text{ Btu/lbm}, \quad T_{t7} = 3600°\text{R}, \quad c_{p\text{AB}} = 0.295 \text{ Btu/(lbm} \cdot °\text{R)}$$

$$\gamma_{\text{AB}} = 1.3, \quad \pi_{\text{AB}} = 0.94, \quad \eta_{\text{AB}} = 0.95, \quad \eta_{cL} = 0.8755$$

$$\eta_{cH} = 0.8791, \quad \eta_{tH} = 0.9062, \quad \eta_{tL} = 0.9050, \quad \pi_{tH} = 0.5466$$

$$\tau_{tH} = 0.8821, \quad \pi_{tL} = 0.6127, \quad \tau_{tL} = 0.9033, \quad M_8 = 1$$

$$M_9 = 1.85, \quad f = 0.0358, \quad f_{\text{AB}} = 0.0195, \quad f_O = 0.0554$$

$$F = 25{,}000 \text{ lbf}, \quad S = 1.4473 \text{ (lbm/h)/lbf}, \quad \dot{m}_0 = 181.57 \text{ lbm/s}$$

OPERATION:

Maximum $T_{t4} = 3200°R$	Maximum $T_{t7} = 3600°R$
Mach number: 0 to 2	Altitudes (kft): 0, 20, and 40

The wet and dry performances of this afterburning turbojet are compared in Figs. 8.43 and 8.44. Note that the wet thrust is about 20% greater than the dry thrust, and the thrust at 40-kft altitude is about 25% of its sea-level value. The thrust specific fuel consumption at 40-kft altitude is much higher than expected for Mach numbers below about 1.3. This high S is due to the reduction in T_{t4} below maximum for $\theta_0 < \text{TR}$, which lowers the temperature of the gas entering the afterburner and increases the temperature rise across the afterburner.

The partial-throttle performance of the afterburning turbjoet is shown in Fig. 8.45 at flight conditions of sea-level static and Mach 1.5 at 40 kft. These curves are commonly called *throttle hooks* because of their shape. At sea-level static conditions, the minimum thrust specific fuel consumption of about 1.02 (lbm/h)/lbf occurs at a thrust of about 4300 lbf (about 20% of dry thrust). At partial-power levels this low, the change in component efficiency can cause the fuel consumption of a real engine to be very different from that predicted here. Because the engine models used to generate these curves are based on constant component efficiencies, the results at significantly reduced throttle settings can be misleading. Comparison of this figure with the

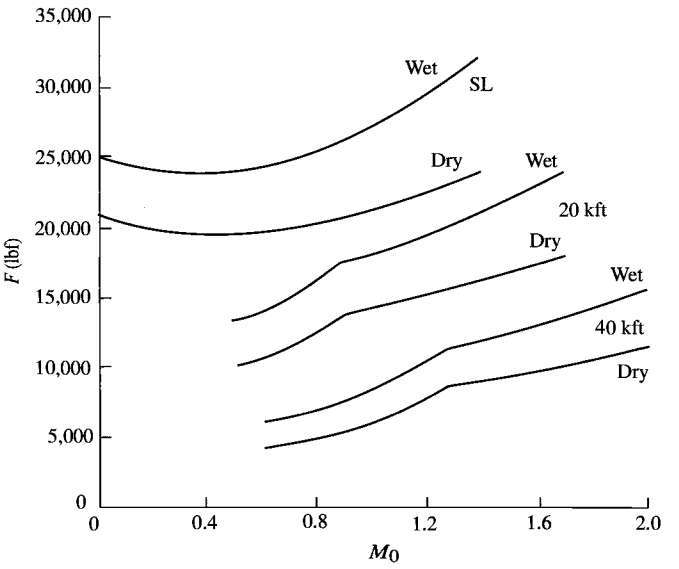

Fig. 8.43 Maximum wet and dry thrust of afterburning turbojet.

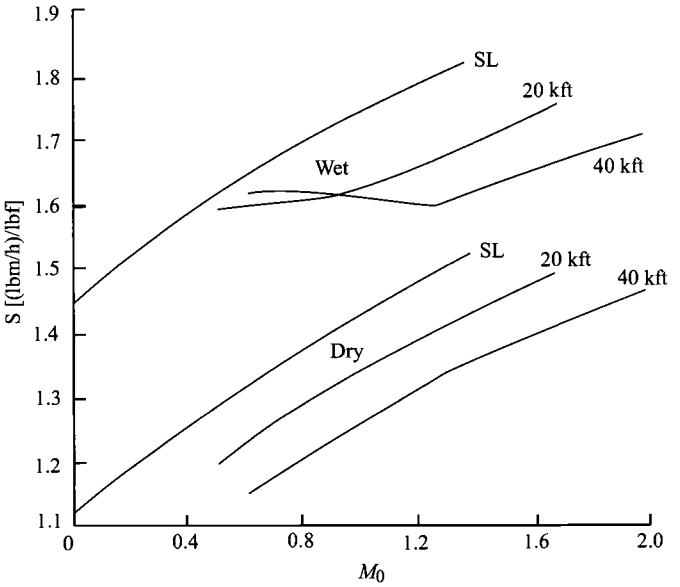

Fig. 8.44 Maximum wet and dry thrust-specific fuel consumption of afterburning turbojet.

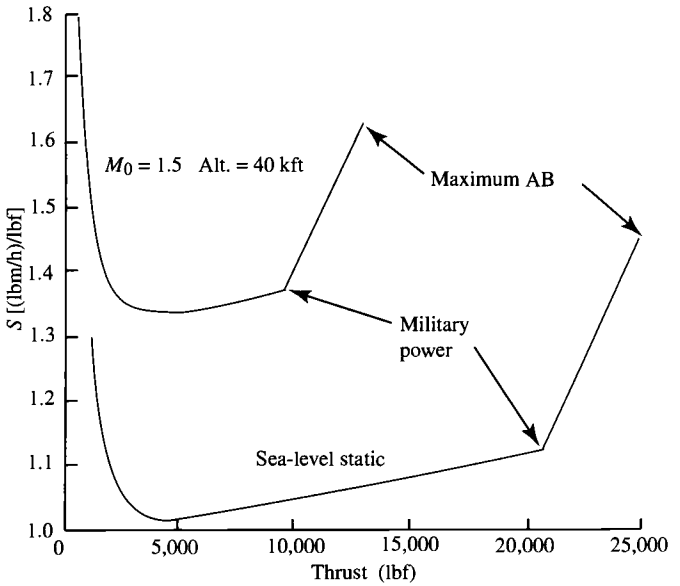

Fig. 8.45 Partial-throttle performance of afterburning turbojet.

partial-power performance of the advanced fighter engine of Fig. 1.14e shows that the trends are correct. The advanced turbofan engine of Fig. 1.14e has lower thrust specific fuel consumption mainly because it is a low-bypass-ratio turbofan engine.

8.5 Turbofan Engine—Separate Exhausts and Convergent Nozzles

The turbofan engines used on commercial subsonic aircraft typically have two spools and separate exhaust nozzles of the convergent type, as shown in Fig. 8.46. For ease of analysis, we will consider a turbofan engine whose fan exit state (13) is the same as the low-pressure compressor exit state (2.5). Thus

$$\tau_f = \tau_{cL} \qquad \text{and} \qquad \pi_f = \pi_{cL}$$

The exhaust nozzles of these turbofan engines have fixed throat areas that will be choked when the exhaust total pressure/ambient static pressure ratio is equal to or larger than $[(\gamma+1)/2]^{\gamma/(\gamma-1)}$. When an exhaust nozzle is unchoked, the nozzle exit pressure equals the ambient pressure and the exit Mach number is subsonic.

Choked flow at stations 4 and 4.5 of the high-pressure spool during engine operation requires [Eq. (8.36)]

$$\text{constant values of } \pi_{tH},\ \tau_{tH},\ \dot{m}_{c4}, \text{ and } \dot{m}_{c4.5}$$

Because the exhaust nozzles have fixed areas, this gas turbine engine has 4 independent variables (T_{t4}, M_0, T_0, and P_0). We will consider the case when both exhaust nozzles may be unchoked, resulting in 11 dependent variables. The performance analysis variables and constants are summarized in Table 8.6.

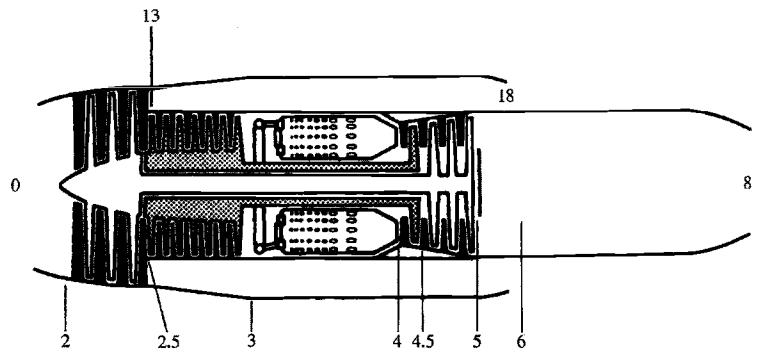

Fig. 8.46 Turbofan engine with separate exhausts. (Courtesy of Pratt & Whitney.)

Table 8.6 Performance analysis variables for separate-exhaust turbofan engine

	Variables		
Component	Independent	Constant or known	Dependent
Engine	M_0, T_0, P_0		$\dot{m}_0, \alpha$
Diffuser		$\pi_d = f(M_0)$	
Fan			π_f, τ_f
High-pressure compressor			π_{cH}, τ_{cH}
Burner	T_{t4}	π_b, η_b	f
High-pressure turbine		π_{tH}, τ_{tH}	
Low-pressure turbine			π_{tL}, τ_{tL}
Core exhaust nozzle		π_n	M_9
Fan exhaust nozzle		π_{fn}	M_{19}
Total number	4		11

8.5.1 Engine Analysis

8.5.1.1 Low-pressure turbine (τ_{tL}, π_{tL}). Equations (8.37) and (8.38) apply for the low-pressure turbine temperature and pressure ratios of this turbofan engine:

$$\pi_{tL} = \pi_{tLR}\sqrt{\frac{\tau_{tL}}{\tau_{tLR}}}\frac{\text{MFP}(M_{9R})}{\text{MFP}(M_9)}$$

where

$$\tau_{tL} = 1 - \eta_{tL}(1 - \pi_{tL}^{(\gamma_t - 1)/\gamma_t})$$

If station 9 is choked at the reference condition and at off-design conditions, then π_{tL} and τ_{tL} are constant.

8.5.1.2 Bypass ratio α. An expression for the engine bypass ratio at any operating condition is obtained by first relating the mass flow rates of the core and fan streams to their reference values. For the engine core, we have

$$\dot{m}_C = \frac{\dot{m}_4}{1+f} = \frac{P_{t4}A_4}{\sqrt{T_{t4}}}\frac{\text{MFP}(M_4)}{1+f}$$

Thus

$$\frac{\dot{m}_C}{\dot{m}_{CR}} = \frac{P_{t4}}{P_{t4R}}\sqrt{\frac{T_{t4R}}{T_{t4}}} \qquad \text{(i)}$$

For the fan stream, we have

$$\dot{m}_F = \frac{P_{t19}A_{19}}{\sqrt{T_{t19}}}\text{MFP}(M_{19})$$

Thus

$$\frac{\dot{m}_F}{\dot{m}_{FR}} = \frac{P_{t19}}{P_{t19R}}\sqrt{\frac{T_{t19R}}{T_{t19}}}\frac{\text{MFP}(M_{19})}{\text{MFP}(M_{19R})} \tag{ii}$$

Combining Eqs. (i) and (ii) to obtain the equation for the bypass ratio α yields

$$\alpha = \alpha_R \frac{\pi_{cHR}}{\pi_{cH}}\sqrt{\frac{\tau_\lambda/(\tau_r\tau_f)}{[\tau_\lambda/(\tau_r\tau_f)]_R}}\frac{\text{MFP}(M_{19})}{\text{MFP}(M_{19R})} \tag{8.46}$$

8.5.1.3 Engine mass flow $\dot{m}_0$. The engine mass flow rate can be written simply as

$$\dot{m}_0 = (1+\alpha)\dot{m}_C$$

Then from Eq. (i), we have

$$\dot{m}_0 = \dot{m}_{0R}\frac{1+\alpha}{1+\alpha_R}\frac{P_0\pi_r\pi_d\pi_f\pi_{cH}}{(P_0\pi_r\pi_d\pi_f\pi_{cH})_R}\sqrt{\frac{T_{t4R}}{T_{t4}}} \tag{8.47}$$

8.5.1.4 High-pressure compressor (τ_{cH}, π_{cH}). The power balance between the high-pressure turbine and the high-pressure compressor [high-pressure (HP) spool] gives

$$\eta_{mH}\dot{m}_4 c_{pt}(T_{t4} - T_{t4.5}) = \dot{m}_{2.5}c_{pc}(T_{t3} - T_{t2.5})$$

Rewriting this equation in terms of temperature ratios, rearranging into variable and constant terms, and equating the constant to reference values give

$$\frac{\tau_r\tau_f(\tau_{cH}-1)}{T_{t4}/T_0} = \eta_{mH}(1+f)(1-\tau_{tH}) = \left[\frac{\tau_r\tau_f(\tau_{cH}-1)}{T_{t4}/T_0}\right]_R$$

Solving for τ_{cH} gives

$$\tau_{cH} = 1 + \frac{T_{t4}/T_0}{(T_{t4}/T_0)_R}\frac{(\tau_r\tau_f)_R}{\tau_r\tau_f}(\tau_{cH}-1)_R \tag{8.48}$$

From the definition of compressor efficiency, π_{cH} is given by

$$\pi_{cH} = [1 + \eta_{cH}(\tau_{cH} - 1)]^{\gamma_c/(\gamma_c - 1)} \tag{8.49}$$

8.5.1.5 Fan (τ_f, π_f). From a power balance between the fan and low-pressure turbine, we get

$$\eta_{mL}\dot{m}_{4.5}c_{pt}(T_{t4.5} - T_{t5}) = (\dot{m}_C + \dot{m}_F)c_{pc}(T_{t13} - T_{t2})$$

Rewriting this equation in terms of temperature ratios, rearranging variable and constant terms, and equating the constant to reference values give

$$(1 + \alpha)\frac{\tau_r(\tau_f - 1)}{T_{t4}/T_0} = \eta_{mL}(1 + f)\tau_{tH}(1 - \tau_{tL}) = \left[(1 + \alpha)\frac{\tau_r(\tau_f - 1)}{T_{t4}/T_0}\right]_R$$

Solving for τ_f gives

$$\tau_f = 1 + \frac{1 - \tau_{tL}}{(1 - \tau_{tL})_R}\frac{\tau_\lambda/\tau_r}{(\tau_\lambda/\tau_r)_R}\frac{1 + \alpha_R}{1 + \alpha}(\tau_{fR} - 1) \tag{8.50}$$

where

$$\pi_f = [1 + (\tau_f - 1)\eta_f]^{\gamma_c/(\gamma_c - 1)} \tag{8.51}$$

8.5.2 Solution Scheme

The principal dependent variables for the turbofan engine are π_{tL}, τ_{tL}, α, τ_{cH}, π_{cH}, τ_f, π_f, M_9, and M_{19}. These variables are dependent on each other plus the engine's independent variables—throttle setting and flight condition. The functional interrelationship of the dependent variables can be written as

$$\begin{aligned}
\tau_{cH} &= f_1(\tau_f) & M_9 &= f_6(\pi_f, \pi_{cH}, \pi_{tL}) \\
\pi_{cH} &= f_2(\tau_{cH}) & \pi_{tL} &= f_7(\tau_{tL}, M_9) \\
\tau_f &= f_3(\tau_{tL}, \alpha) & \tau_{tL} &= f_8(\pi_{tL}) \\
\pi_f &= f_4(\tau_f) & \alpha &= f_9(\tau_f, \pi_{cH}, M_{19}) \\
M_{19} &= f_5(\pi_f)
\end{aligned}$$

This system of nine equations is solved by functional iteration, starting with reference quantities as initial values for π_{tL}, τ_{tL}, and τ_f. The following equations are calculated for the nine dependent variables in the order

listed until successive values of τ_{tL} do not change more than a specified amount (say, 0.0001):

$$\tau_{cH} = 1 + \frac{T_{t4}/T_0}{(T_{t4}/T_0)_R} \frac{(\tau_r \tau_f)_R}{\tau_r \tau_f} (\tau_{cH} - 1)_R \tag{i}$$

$$\pi_{cH} = \left[1 + \eta_{cH}(\tau_{cH} - 1)\right]^{\gamma_c/(\gamma_c - 1)} \tag{ii}$$

$$\pi_f = \left[1 + (\tau_f - 1)\eta_f\right]^{\gamma_c/(\gamma_c - 1)} \tag{iii}$$

$$P_{t19}/P_0 = \pi_r \pi_d \pi_f \pi_{\text{fn}} \tag{iv}$$

$$\text{If} \quad \frac{P_{t19}}{P_0} < \left(\frac{\gamma_c + 1}{2}\right)^{\gamma_c/(\gamma_c - 1)} \quad \text{then} \quad \frac{P_{t19}}{P_{19}} = \frac{P_{t19}}{P_0}$$

$$\text{else} \quad \frac{P_{t19}}{P_{19}} = \left(\frac{\gamma_c + 1}{2}\right)^{\gamma_c/(\gamma_c - 1)} \tag{v}$$

$$M_{19} = \sqrt{\frac{2}{\gamma_c - 1}\left[\left(\frac{P_{t19}}{P_{19}}\right)^{(\gamma_c - 1)/\gamma_c} - 1\right]} \tag{vi}$$

$$\frac{P_{t9}}{P_0} = \pi_r \pi_d \pi_f \pi_{cH} \pi_b \pi_{tH} \pi_{tL} \pi_n \tag{vii}$$

$$\text{If} \quad \frac{P_{t9}}{P_0} < \left(\frac{\gamma_t + 1}{2}\right)^{\gamma_t/(\gamma_t - 1)} \quad \text{then} \quad \frac{P_{t9}}{P_9} = \frac{P_{t9}}{P_0}$$

$$\text{else} \quad \frac{P_{t9}}{P_9} = \left(\frac{\gamma_t + 1}{2}\right)^{\gamma_t/(\gamma_t - 1)} \tag{viii}$$

$$M_9 = \sqrt{\frac{2}{\gamma_t - 1}\left[\left(\frac{P_{t9}}{P_9}\right)^{(\gamma_t - 1)/\gamma_t} - 1\right]} \tag{ix}$$

$$\alpha = \alpha_R \frac{\pi_{cHR}}{\pi_{cH}} \sqrt{\frac{\tau_\lambda/(\tau_r \tau_f)}{[\tau_\lambda/(\tau_r \tau_f)]_R}} \frac{\text{MFP}(M_{19})}{\text{MFP}(M_{19R})} \tag{x}$$

$$\tau_f = 1 + \frac{1 - \tau_{tL}}{(1 - \tau_{tL})_R} \frac{\tau_\lambda/\tau_r}{(\tau_\lambda/\tau_r)_R} \frac{1 + \alpha_R}{1 + \alpha} (\tau_{fR} - 1) \tag{xi}$$

$$\tau_{tL} = 1 - \eta_{tL}(1 - \pi_{tL}^{(\gamma_t - 1)/\gamma_t}) \tag{xii}$$

$$\pi_{tL} = \pi_{tLR} \sqrt{\frac{\tau_{tL}}{\tau_{tLR}}} \frac{\text{MFP}(M_{9R})}{\text{MFP}(M_9)} \tag{xiii}$$

8.5.3 Summary of Performance Equations—Turbofan Engine with Separate Exhausts and Convergent Nozzles

INPUTS:

Choices

Flight parameters:	M_0, T_0 (K, °R), P_0 (kPa, psia)
Throttle setting:	T_{t4} (K, °R)

Design constants

π:	$\pi_{d\max}$, π_b, π_{tH}, π_n, π_{fn}
τ:	τ_{tH}
η:	η_f, η_{cH}, η_b, η_{mH}, η_{mL}
Gas properties:	γ_c, γ_t, c_{pc}, c_{pt} [kJ/(kg · K), Btu/(lbm · °R)]
Fuel:	h_{PR} (kJ/kg, Btu/lbm)

Reference conditions

Flight parameters:	M_{0R}, T_{0R} (K, °R), P_{0R} (kPa, psia), τ_{rR}, π_{rR}
Throttle setting:	T_{t4R} (K, °R)
Component behavior:	π_{dR}, π_{fR}, π_{cHR}, π_{tL}, τ_{fR}, τ_{cHR}, τ_{rLR}, α_R, M_{9R}, M_{19R}

OUTPUTS:

Overall performance:	F(N, lbf), $\dot{m}_0$ (kg/s, lbm/s), f, $S\left(\frac{\text{mg/s}}{\text{N}}, \frac{\text{lbm/h}}{\text{lbf}}\right)$, η_P, η_T, η_O
Component behavior:	α, π_f, π_{cH}, π_{tL}, τ_f, τ_{cH}, τ_{tL}, f, M_9, M_{19}, N_{fan}, N_{HPspool}
Exhaust nozzle pressure:	P_0/P_9, P_0/P_{19}

EQUATIONS:

$$R_c = \frac{\gamma_c - 1}{\gamma_c} c_{pc} \tag{8.52a}$$

$$R_t = \frac{\gamma_t - 1}{\gamma_t} c_{pt} \tag{8.52b}$$

$$a_0 = \sqrt{\gamma_c R_c g_c T_0} \tag{8.52c}$$

$$V_0 = a_0 M_0 \tag{8.52d}$$

$$\tau_r = 1 + \frac{\gamma_c - 1}{2} M_0^2 \tag{8.52e}$$

$$\pi_r = \tau_r^{\gamma_c/(\gamma_c - 1)} \tag{8.52f}$$

$$\eta_r = 1 \qquad \text{for } M_0 \leq 1 \tag{8.52g}$$

$$\eta_r = 1 - 0.075(M_0 - 1)^{1.35} \qquad \text{for } M_0 > 1 \tag{8.52h}$$

$$\pi_d = \pi_{d\max}\eta_r \tag{8.52i}$$

$$\tau_\lambda = \frac{c_{pt}T_{t4}}{c_{pc}T_0} \tag{8.52j}$$

Initial values:

$$\tau_{tL} = \tau_{tLR} \qquad \tau_f = \tau_{fR} \qquad \tau_{tL} = \tau_{tLR}$$

$$\tau_{cH} = 1 + \frac{\tau_\lambda/\tau_r}{(\tau_\lambda/\tau_r)_R}\frac{\tau_{fR}}{\tau_f}(\tau_{cHR} - 1) \tag{8.52k}$$

$$\pi_{cH} = [1 + (\tau_{cH} - 1)\eta_{cH}]^{\gamma_c/(\gamma_c-1)} \tag{8.52l}$$

$$\pi_f = [1 + (\tau_f - 1)\eta_f]^{\gamma_c/(\gamma_c-1)} \tag{8.52m}$$

Exhaust nozzles:

$$\frac{P_{t19}}{P_0} = \pi_r\pi_d\pi_f\pi_{\text{fn}} \tag{8.52n}$$

$$\text{If} \quad \frac{P_{t19}}{P_0} < \left(\frac{\gamma_c + 1}{2}\right)^{\gamma_c/(\gamma_c-1)} \quad \text{then} \quad \frac{P_{t19}}{P_{19}} = \frac{P_{t19}}{P_0}$$

$$\text{else} \quad \frac{P_{t19}}{P_{19}} = \left(\frac{\gamma_c + 1}{2}\right)^{\gamma_c/(\gamma_c-1)} \tag{8.52o}$$

$$M_{19} = \sqrt{\frac{2}{\gamma_c - 1}\left[\left(\frac{P_{t19}}{P_{19}}\right)^{(\gamma_c-1)/\gamma_c} - 1\right]} \tag{8.52p}$$

$$\frac{P_{t9}}{P_0} = \pi_r\pi_d\pi_f\pi_{cH}\pi_b\pi_{tH}\pi_{tL}\pi_n \tag{8.52q}$$

$$\text{If} \quad \frac{P_{t9}}{P_0} < \left(\frac{\gamma_t + 1}{2}\right)^{\gamma_t/(\gamma_t-1)} \quad \text{then} \quad \frac{P_{t9}}{P_9} = \frac{P_{t9}}{P_0}$$

$$\text{else} \quad \frac{P_{t9}}{P_9} = \left(\frac{\gamma_t + 1}{2}\right)^{\gamma_t/(\gamma_t-1)} \tag{8.52r}$$

$$M_9 = \sqrt{\frac{2}{\gamma_t - 1}\left[\left(\frac{P_{t9}}{P_9}\right)^{(\gamma_t-1)/\gamma_t} - 1\right]} \tag{8.52s}$$

$$\alpha = \alpha_R\frac{\pi_{cHR}}{\pi_{cH}}\sqrt{\frac{\tau_\lambda/(\tau_r\tau_f)}{[\tau_\lambda/(\tau_r\tau_f)]_R}}\frac{\text{MFP}(M_{19})}{\text{MFP}(M_{19R})} \tag{8.52t}$$

$$\tau_f = 1 + \frac{1 - \tau_{tL}}{(1 - \tau_{tL})_R} \frac{\tau_\lambda/\tau_r}{(\tau_\lambda/\tau_r)_R} \frac{1 + \alpha_R}{1 + \alpha} (\tau_{fR} - 1) \tag{8.52u}$$

$$\tau_{tL} = 1 - \eta_{tL}(1 - \pi_{tL}^{(\gamma_t - 1)/\gamma_t}) \tag{8.52v}$$

$$\pi_{tL} = \pi_{tLR} \sqrt{\frac{\tau_{tL}}{\tau_{tLR}}} \frac{\text{MFP}(M_{9R})}{\text{MFP}(M_9)} \tag{8.52w}$$

If τ_{tL} is not within 0.0001 of its previous value, return to Eq. (8.52k) and perform another iteration.

Remainder of calculations:

$$\dot{m}_0 = \dot{m}_{0R} \frac{1 + \alpha}{1 + \alpha_R} \frac{P_0 \pi_r \pi_d \pi_f \pi_{cH}}{(P_0 \pi_r \pi_d \pi_f \pi_{cH})_R} \sqrt{\frac{T_{t4R}}{T_{t4}}} \tag{8.52x}$$

$$f = \frac{\tau_\lambda - \tau_r \tau_f \tau_{cH}}{h_{PR} \eta_b / (c_p T_0) - \tau_\lambda} \tag{8.52y}$$

$$\frac{T_9}{T_0} = \frac{\tau_\lambda \tau_{tH} \tau_{tL}}{(P_{t9}/P_9)^{(\gamma_t - 1)/\gamma_t}} \frac{c_{pc}}{c_{pt}} \tag{8.52z}$$

$$\frac{V_9}{a_0} = M_9 \sqrt{\frac{\gamma_t R_t T_9}{\gamma_c R_c T_0}} \tag{8.52aa}$$

$$\frac{T_{19}}{T_0} = \frac{\tau_r \tau_f}{(P_{t19}/P_{19})^{(\gamma_c - 1)/\gamma_c}} \tag{8.52ab}$$

$$\frac{V_{19}}{a_0} = M_{19} \sqrt{\frac{T_{19}}{T_0}} \tag{8.52ac}$$

$$\frac{F}{\dot{m}_0} = \frac{1}{1 + \alpha} \frac{a_0}{g_c} \left[(1 + f) \frac{V_9}{a_0} - M_0 + (1 + f) \frac{R_t}{R_c} \frac{T_9/T_0}{V_9/\alpha_0} \frac{1 - P_0/P_9}{\gamma_c} \right] + \frac{\alpha}{1 + \alpha} \frac{a_0}{g_c} \left[\frac{V_{19}}{a_0} - M_0 + \frac{T_{19}/T_0}{V_{19}/a_0} \frac{1 - P_0/P_{19}}{\gamma_c} \right] \tag{8.52ad}$$

$$S = \frac{f}{(1 + \alpha)(F/\dot{m}_0)} \tag{8.52ae}$$

$$F = \dot{m}_0 \left(\frac{F}{\dot{m}_0} \right) \tag{8.52af}$$

$$\left(\frac{N}{N_R} \right)_{\text{fan}} = \sqrt{\frac{T_0 \tau_r}{T_{0R} \tau_{rR}} \frac{\pi_f^{(\gamma_c - 1)/\gamma_c} - 1}{\pi_{fR}^{(\gamma_c - 1)/\gamma_c} - 1}} \tag{8.52ag}$$

$$\left(\frac{N}{N_R} \right)_{\text{HPspool}} = \sqrt{\frac{T_0 \tau_r \tau_f}{(T_0 \tau_r \tau_f)_R} \frac{\pi_{cH}^{(\gamma_c - 1)/\gamma_c} - 1}{\pi_{cHR}^{(\gamma_c - 1)/\gamma_c} - 1}} \tag{8.52ah}$$

$$\eta_T = \frac{a_0^2[(1+f)(V_9/a_0)^2 + \alpha(V_{19}/a_0)^2 - (1+\alpha)M_0^2]}{2g_c f h_{PR}} \tag{8.52ai}$$

$$\eta_P = \frac{2g_c V_0(1+\alpha)(F/\dot{m}_0)}{a_0^2[(1+f)(V_9/a_0)^2 + \alpha(V_{19}/a_0)^2 - (1+\alpha)M_0^2]} \tag{8.52aj}$$

$$\eta_O = \eta_P \eta_T \tag{8.52ak}$$

Example 8.8

Given the reference engine (see data) sized for a mass flow rate of 600 lbm/s at 40 kft and Mach 0.8, determine the performance at sea-level static conditions with $T_{t4} = 3000°\text{R}$.

REFERENCE:

$$T_0 = 390°\text{R}, \quad \gamma_c = 1.4, \quad c_{pc} = 0.24\ \text{Btu/(lbm}\cdot°\text{R)}, \quad \gamma_t = 1.33$$

$$c_{pt} = 0.276\ \text{Btu/(lbm}\cdot°\text{R)}, \quad T_{t4} = 3000°\text{R}, \quad M_0 = 0.8$$

$$\pi_c = 36, \quad \pi_f = 1.7, \quad \alpha = 8, \quad \eta_f = 0.8815$$

$$\eta_{cH} = 0.8512, \quad \tau_{tH} = 0.7580, \quad \pi_{tH} = 0.2851, \quad \tau_{tL} = 0.7262$$

$$\pi_{tL} = 0.2349, \quad \eta_{tL} = 0.9068, \quad \eta_b = 0.99, \quad \pi_{d\max} = 0.99$$

$$\pi_b = 0.96, \quad \pi_n = 0.99, \quad \pi_{\text{fn}} = 0.99, \quad \eta_{mH} = 0.9915$$

$$\eta_{mL} = 0.997, \quad P_0 = 2.730\ \text{psia (40 kft)}, \quad \dot{m}_0 = 600\ \text{lbm/s}$$

$$F/\dot{m}_0 = 17.92\ \text{lbf/(lbm/s)}, \quad F = 10{,}750\ \text{lbf}$$

PERFORMANCE CONDITIONS:

$T_0 = 518.7°\text{R}$ $P_0 = 14.696$ psia (sea level) $T_{t4} = 3000°\text{R}$ $M_0 = 0$

EQUATIONS:

$$R_c = \frac{\gamma_c - 1}{\gamma_c} c_{pc} = \frac{0.4}{1.4}(0.24 \times 778.16) = 53.36\ \text{ft}\cdot\text{lbf/(lbm}\cdot°\text{R)}$$

$$R_t = \frac{\gamma_t - 1}{\gamma_t} c_{pt} = \frac{0.33}{1.33}(0.276 \times 778.16) = 53.29\ \text{ft}\cdot\text{lbf/(lbm}\cdot°\text{R)}$$

$$a_0 = \sqrt{\gamma_c R_c g_c T_0} = \sqrt{1.4 \times 53.36 \times 32.174 \times 518.7} = 1116.6\ \text{ft/s}$$

$$V_0 = a_0 M_0 = 1116.6 \times 0 = 0\ \text{ft/s}$$

$$\tau_r = 1 \quad \text{and} \quad \pi_r = 1$$

$$\pi_d = \pi_{d\max}\eta_r = 0.99 \times 1 = 0.99$$

$$\tau_\lambda = \frac{c_{pt}T_{t4}}{c_{pc}T_0} = \frac{0.276 \times 3000}{0.240 \times 518.7} = 6.651$$

Initial values:

$$\tau_{tL} = \tau_{tLR} = 0.7262 \qquad \tau_f = \tau_{fR} = 1.1857 \qquad \pi_{tL} = \pi_{tLR} = 0.2349$$

Eq. (A)
$$\tau_{cH} = 1 + \frac{\tau_\lambda/\tau_r}{(\tau_\lambda/\tau_r)_R}\frac{\tau_{fR}}{\tau_f}(\tau_{cHR} - 1)$$
$$= 1 + \frac{6.651/1.0}{8.846/1.128}\frac{1.1857}{1.1857}(2.636 - 1) = 2.3875$$
$$\pi_{cH} = [1 + (\tau_{cH} - 1)\eta_{cH}]^{\gamma_c/(\gamma_c-1)}$$
$$= [1 + (2.3875 - 1)(0.8512)]^{3.5} = 15.322$$
$$\pi_f = [1 + (\tau_f - 1)\eta_f]^{\gamma_c/(\gamma_c-1)}$$
$$= [1 + (1.1857 - 1)(0.8815)]^{3.5} = 1.70$$

Exhaust nozzles:

$$\frac{P_{t19}}{P_0} = \pi_r\pi_d\pi_f\pi_{\text{fn}} = 1 \times 0.99 \times 1.70 \times 0.99 = 1.6662$$

Since $\dfrac{P_{t19}}{P_0} < 1.893$ then $P_{19} = P_0$

$$M_{19} = \sqrt{\frac{2}{\gamma_c - 1}\left[\left(\frac{P_{t19}}{P_{19}}\right)^{(\gamma_c-1)/\gamma_c} - 1\right]} = \sqrt{\frac{2}{0.4}(1.6662^{1/3.5} - 1)} = 0.8861$$

$$\frac{P_{t9}}{P_0} = \pi_r\pi_d\pi_f\pi_{cH}\pi_b\pi_{tH}\pi_{tL}\pi_n$$
$$= 1 \times 0.99 \times 1.70 \times 15.322 \times 0.96 \times 0.2851 \times 0.2349 \times 0.99 = 1.6413$$

Since $\dfrac{P_{t9}}{P_0} < 1.851$ then $P_9 = P_0$

$$M_9 = \sqrt{\frac{2}{\gamma_t - 1}\left[\left(\frac{P_{t9}}{P_9}\right)^{(\gamma_t-1)/\gamma_t} - 1\right]}$$
$$= \sqrt{\frac{2}{0.33}(1.6413^{0.33/1.33} - 1)} = 0.8904$$

$$\alpha = \alpha_R \frac{\pi_{cHR}}{\pi_{cH}} \sqrt{\frac{\tau_\lambda/(\tau_r\tau_f)}{\tau_\lambda/(\tau_r\tau_f)]_R}} \frac{\text{MFP}(M_{19})}{\text{MFP}(M_{19R})}$$

$$= 8\frac{21.177}{15.322}\sqrt{\frac{6.651/1.1857}{8.846/(1.128 \times 1.1857)}}\left(\frac{0.5257}{0.5318}\right) = 10.066$$

$$\tau_f = 1 + \frac{1-\tau_{tL}}{(1-\tau_{tL})_R}\frac{\tau_\lambda/\tau_r}{(\tau_\lambda/\tau_r)_R}\frac{1+\alpha_R}{1+\alpha}(\tau_{fR}-1)$$

$$= 1 + \frac{1-0.7262}{1-0.7262}\frac{6.651/1}{8.846/1.128}\frac{1+8}{1+10.066}(1.1857-1) = 1.1281$$

$$\tau_{tL} = 1 - \eta_{tL}(1 - \pi_{tL}^{(\gamma_t-1)/\gamma_t}) = 1 - 0.9068(1 - 0.2349^{0.33/1.33}) = 0.7262$$

$$\pi_{tL} = \pi_{tLR}\sqrt{\frac{\tau_{tL}}{\tau_{tLR}}}\frac{\text{MFP}(M_{9R})}{\text{MFP}(M_9)} = 0.2349\sqrt{\frac{0.7262}{0.7262}}\frac{0.5224}{0.5167} = 0.2375$$

Since τ_{tL} is not within 0.0001 of its previous value, return to **Eq. (A)** and do another iteration. These data required 10 iterations, which are summarized in Table 8.7.

Remainder of calculations:

$$\dot{m}_0 = \dot{m}_{0R}\frac{1+\alpha}{1+\alpha_R}\frac{P_0\pi_r\pi_d\pi_f\pi_{cH}}{(P_0\pi_r\pi_d\pi_f\pi_{cH})_R}\sqrt{\frac{T_{t4R}}{T_{t4}}}$$

$$= 600\frac{1+9.103}{1+8}\frac{14.696 \times 1.0 \times 0.99 \times 1.4973 \times 16.555}{2.730 \times 1.524 \times 0.99 \times 1.7 \times 21.176}\sqrt{\frac{3000}{3000}}$$

$$= 1638 \text{ lbm}$$

$$f = \frac{\tau_\lambda - \tau_r\tau_f\tau_{cH}}{h_{PR}\eta_b/(c_pT_0) - \tau_\lambda}$$

$$= \frac{6.651 - 1 \times 1.1387 \times 2.448}{18{,}400 \times 0.99/(0.24 \times 518.7) - 6.651} = 0.02769$$

$$\frac{T_9}{T_0} = \frac{\tau_\lambda\tau_{tH}\tau_{tL}}{(P_{t9}/P_9)^{(\gamma_t-1)/\gamma_t}}\frac{c_{pc}}{c_{pt}}$$

$$= \frac{6.651 \times 0.7580 \times 0.7293}{1.5932^{0.33/1.33}}\frac{0.240}{0.276} = 2.848$$

$$\frac{V_9}{a_0} = M_9\sqrt{\frac{\gamma_tR_tT_9}{\gamma_cR_cT_0}} = 0.8617\sqrt{\frac{1.33 \times 53.29}{1.40 \times 53.36}}(2.848) = 1.4165$$

$$\frac{T_{19}}{T_0} = \frac{\tau_r\tau_f}{(P_{t19}/P_{19})^{(\gamma_c-1)/\gamma_c}} = \frac{1.0 \times 1.1387}{1.4675^{1/3.5}} = 1.0205$$

Table 8.7 Summary of internal iterations

i	τ_{cH}	π_{cH}	π_f	M_{19}	M_9	α	τ_f	τ_{tL}	π_{tL}
1	2.3875	15.322	1.7000	0.8861	0.8904	10.07	1.1281	0.7262	0.2375
2	2.4584	16.857	1.4542	0.7299	0.8419	8.833	1.1441	0.7279	0.2408
3	2.4379	16.403	1.5199	0.7766	0.8719	9.233	1.1376	0.7301	0.2391
4	2.4461	16.585	1.4930	0.7580	0.8586	9.077	1.1387	0.7290	0.2398
5	2.4448	16.556	1.4972	0.7609	0.8623	9.102	1.1389	0.7294	0.2396
...	...	...	...	...	...	...	...	...	...
10	2.4448	16.555	1.4973	0.7610	0.8617	9.103	1.1387	0.7293	0.2396

$$\frac{V_{19}}{a_0} = M_{t9}\sqrt{\frac{T_{19}}{T_0}} = 0.7610\sqrt{1.0205} = 0.7688$$

$$\frac{F}{\dot{m}_0} = \frac{a_0}{(1+\alpha)g_c}\left[(1+f)\frac{V_9}{a_0} - M_0 + \alpha\left(\frac{V_{19}}{a_0} - M_0\right)\right]$$

$$= \frac{1116.6/32.174}{1+9.1039}[1.02769(1.4165) + 9.103(0.7688)]$$

$$= 29.04 \text{ lbf/(lbm/s)}$$

$$S = \frac{3600 \times 0.02769}{10.103 \times 29.04}\frac{32.174}{32.174} = 0.3398 \text{ (lbm/h)/lbf}$$

$$F = 1639 \times 29.04 = 47{,}570 \text{ lbf}$$

$$\left(\frac{N}{N_R}\right)_{\text{fan}} = \sqrt{\frac{T_0\tau_r}{T_{0R}\tau_{rR}}\frac{\pi_f^{(\gamma-1)/\gamma} - 1}{\pi_{fR}^{(\gamma-1)/\gamma} - 1}}$$

$$= \sqrt{\frac{518.7 \times 1.0}{390 \times 1.128}\frac{1.4973^{0.4/1.4} - 1}{1.7^{0.4/1.4} - 1}} = 0.938$$

$$\left(\frac{N}{N_R}\right)_{\text{HPspool}} = \sqrt{\frac{T_0\tau_r\tau_f}{(T_{0R}\tau_r\tau_f)_R}\frac{\pi_{cH}^{(\gamma-1)/\gamma} - 1}{\pi_{cHR}^{(\gamma-1)/\gamma} - 1}}$$

$$= \sqrt{\frac{518.7 \times 1.0 \times 1.1387}{390 \times 1.128 \times 1.1857}\frac{16.555^{0.4/1.4} - 1}{21.176^{0.4/1.4} - 1}} = 1.00$$

Example 8.9

In this example, we consider the variation in engine performance of a 270,000-N thrust, high-bypass-ratio turbofan engine with Mach number M_0, altitude, ambient temperature T_0, and throttle setting T_{t4}. The engine reference flight condition is sea-level static with the following values:

$$\alpha = 8 \qquad \pi_f = 1.77 \qquad \pi_{cH} = 20.34 \qquad T_{t4} = 1890\,\text{K} \qquad \dot{m}_0 = 760\,\text{kg/s}$$

For the performance curves drawn in solid lines, the compressor pressure ratio was limited to 36, the combustor exit temperature T_{t4} was limited to 1890 K, and the compressor exit temperature T_{t3} was limited to 920 K. This engine has a throttle ratio TR of 1. At θ_0 values below 1.0, the engine is at the maximum compressor pressure ratio of 36 and T_{t4} is below its maximum value of 1890 K. For these conditions, the flow in the bypass stream is unchoked at sea level and does not choke at altitude until a Mach number of 0.34.

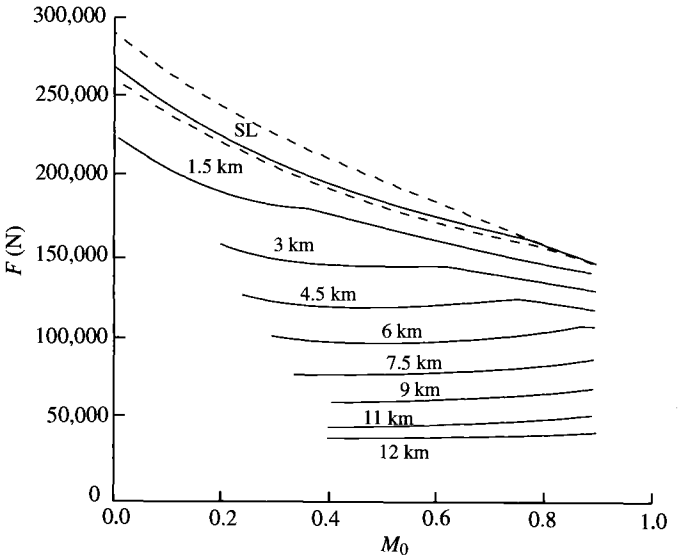

Fig. 8.47 Maximum thrust of high-bypass-ratio turbofan.

Figures 8.47–8.53 show the variations of thrust, thrust specific fuel consumption S, engine mass flow, corrected engine mass flow, bypass ratio, fan pressure ratio π_f, and high-pressure (HP) compressor pressure ratio π_{cH} with Mach number and altitude, respectively. The dashed lines in these figures show the engine performance with the combustor exit temperature T_{t4} limited to 1940 K.

The corrected engine mass flow rate of Fig. 8.50 has the same trend with Mach number and altitude as the fan pressure ratio of Fig. 8.52 and the HP compressor pressure ratio of Fig. 8.53. Both the corrected mass flow rate and the HP compressor pressure ratio reach their maximum values when the bypass stream chokes (flight Mach of 0.34). Figure 8.51 shows that the engine bypass ratio at maximum thrust has a constant minimum value of about 8 when the bypass stream is choked.

The effects of ambient temperature T_0 and altitude on engine performance at maximum thrust are shown in Figs. 8.54 and 8.55, respectively. For ambient temperatures below the reference value of 288.2 K ($\theta_0 < 1.0$), Fig. 8.54 shows that the limit of 36 for the compressor pressure ratio ($\pi_c = \pi_f \pi_{cH}$) holds the engine thrust, bypass ratio, and fan pressure ratio constant. Engine thrust drops off rapidly with T_0 for $\theta_0 > 1.0$. The decreases in engine thrust, fuel consumption, and air mass flow rate with altitude are shown in Fig. 8.55 for a flight Mach number of 0.5. The decrease in engine thrust with altitude for the high-bypass-ratio turbofan engine is much greater than that of the dry turbojet (see Fig. 8.42). If both a high-bypass-ratio turbofan engine and a dry turbojet engine were sized to produce the same thrust at 9 km and 0.8 Mach, the high-bypass-ratio turbofan engine would have much greater thrust at sea-level static conditions. This helps explain the decrease in takeoff length between the

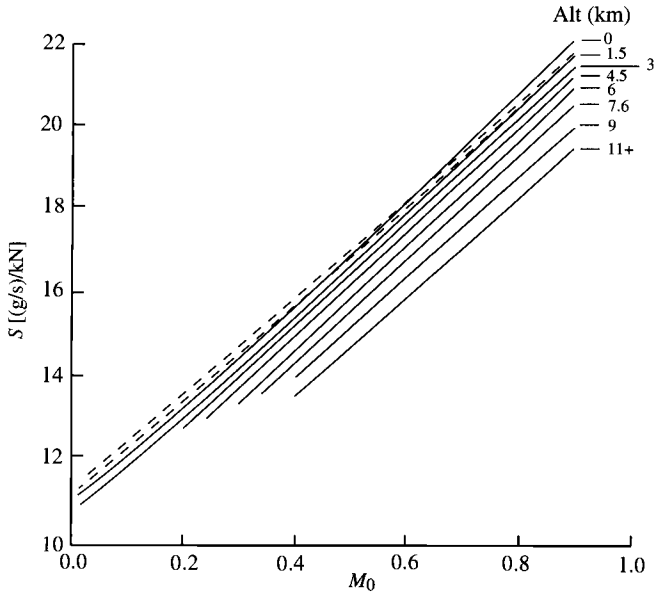

Fig. 8.48 Thrust-specific fuel consumption of high-bypass-ratio turbofan at maximum thrust.

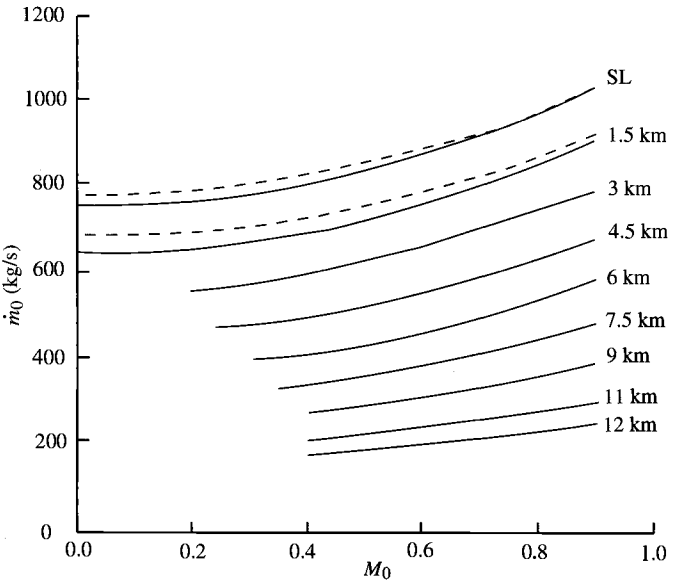

Fig. 8.49 Mass flow rate of high-bypass-ratio turbofan at maximum thrust.

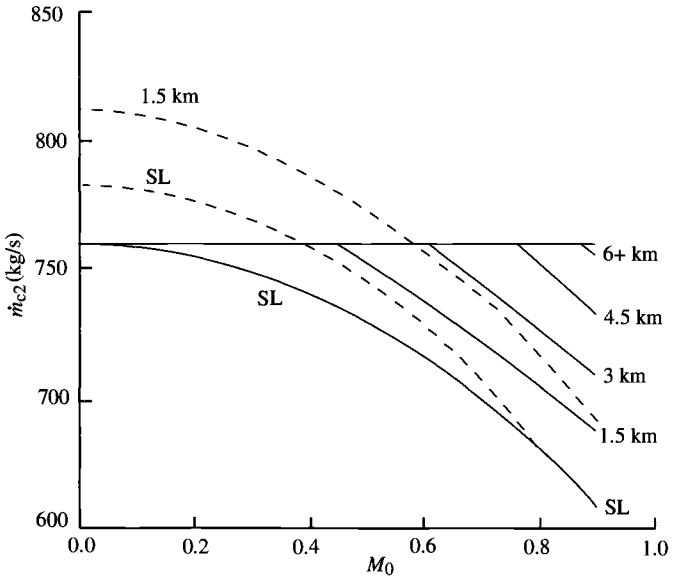

Fig. 8.50 Corrected mass flow rate of high-bypass-ratio turbofan at maximum thrust.

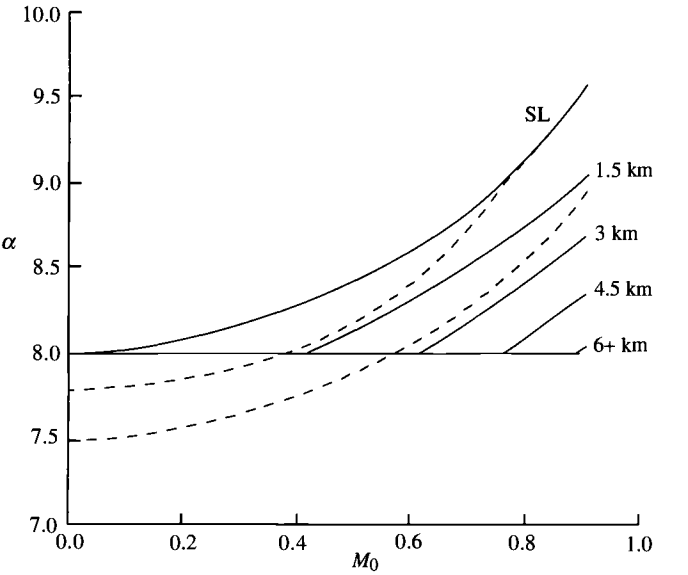

Fig. 8.51 Bypass ratio of high-bypass-ratio turbofan at maximum thrust.

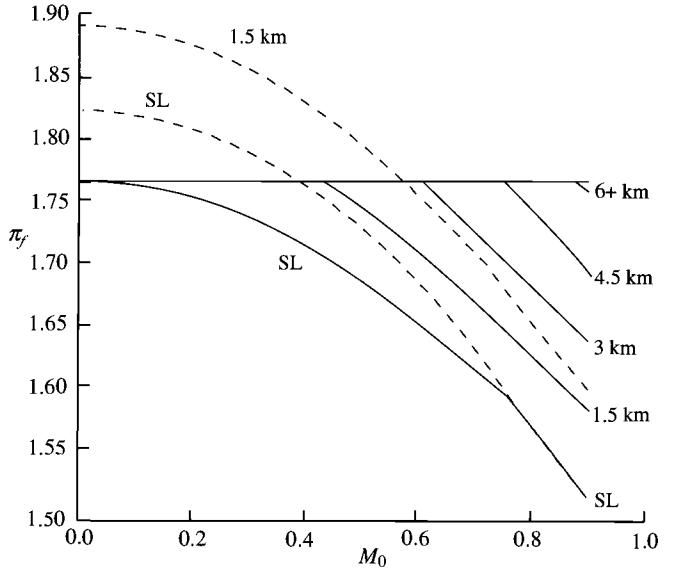

Fig. 8.52 Fan pressure ratio of high-bypass-ratio turbofan at maximum thrust.

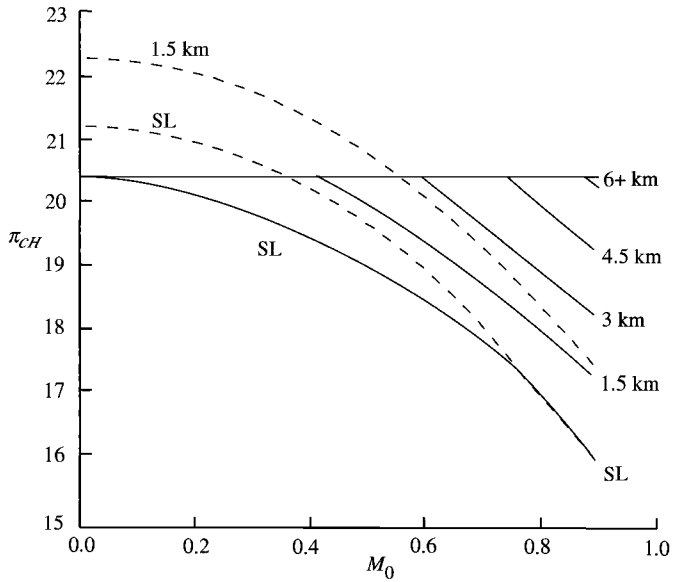

Fig. 8.53 High-pressure compressor pressure ratio of high-bypass-ratio turbofan at maximum thrust.

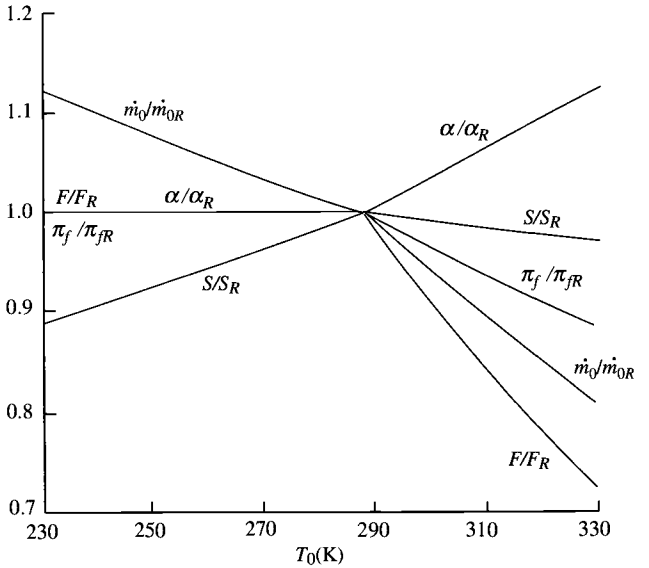

Fig. 8.54 Performance of high-bypass-ratio turbofan vs T_0 at sea-level static, maximum thrust.

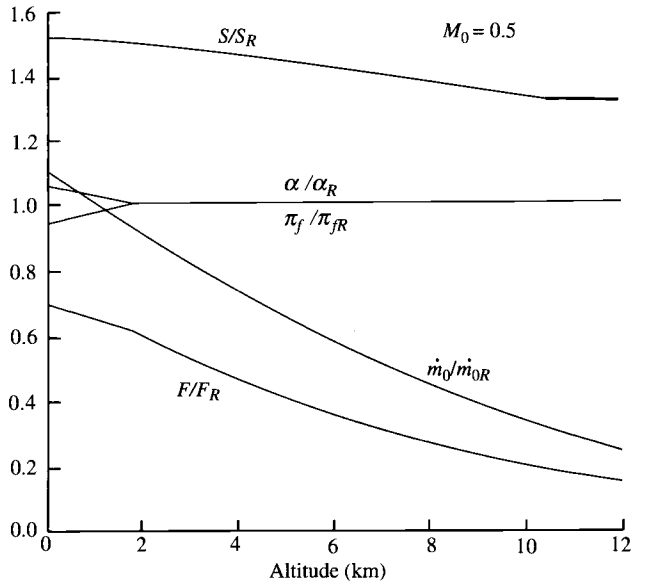

Fig. 8.55 Performance of high-bypass-ratio turbofan at maximum thrust vs altitude.

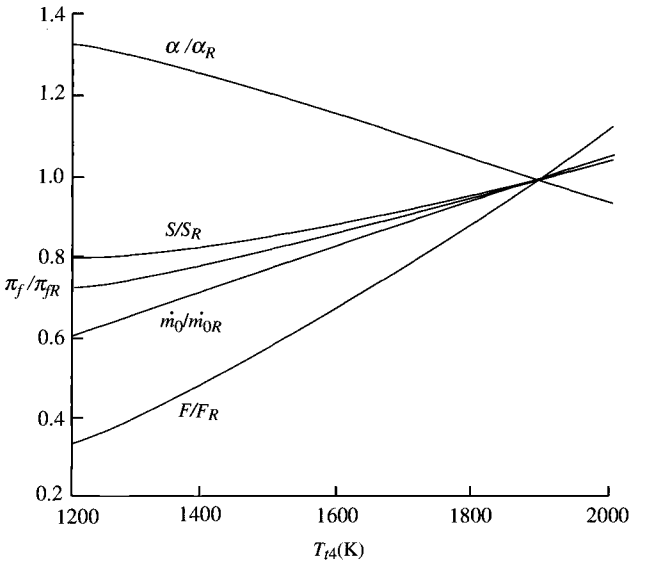

Fig. 8.56 Performance of high-bypass-ratio turbofan vs T_{t4} at sea-level static conditions.

early turbojet-powered passenger aircraft and the modern high-bypass-ratio turbofan-powered passenger aircraft of today.

Figures 8.56 and 8.57 show the effects that changes in combustor exit temperature T_{t4} have on engine performance. As shown in Fig. 8.56, all engine performance parameters except the bypass ratio decrease with reduction in engine throttle T_{t4}. If the throttle were reduced further, the thrust specific fuel consumption S would start to increase. The thrust specific fuel consumption S vs thrust F at partial throttle (partial power) is shown in Fig. 8.57 for two different values of altitude and Mach number. These curves have the classical hook shape that gives them their name of *throttle hook.* Minimum S occurs at about 50% of maximum thrust. At lower throttle settings, the thrust specific fuel consumption rapidly increases.

The characteristics of the low-pressure spool and high-pressure spool for this high-bypass-ratio turbofan engine are shown in Figs. 8.58 and 8.59, respectively. The core flow and/or bypass flow may be choked ($M_9 = 1$ and/or $M_{19} = 1$) at its respective exhaust nozzles, which influences the low-pressure spool. Figure 8.58 shows the characteristics of the low-pressure spool at the flight condition of 9 km and $M_0 = 0.8$ with solid lines, and at the sea-level static flight condition with dashed lines. At sea-level static conditions, the bypass stream is unchoked for all operating conditions of the low-pressure spool, and the core exhaust nozzle unchokes at about 95% of N_{cL}. However, at 9 km and $M_0 = 0.8$, the core exhaust nozzle unchokes at about 78% of N_{cL}, and the bypass stream unchokes at about 61% of N_{cL}. The variation of fan pressure ratio and corrected fuel flow with the corrected speed of the low-pressure spool is unaffected by the

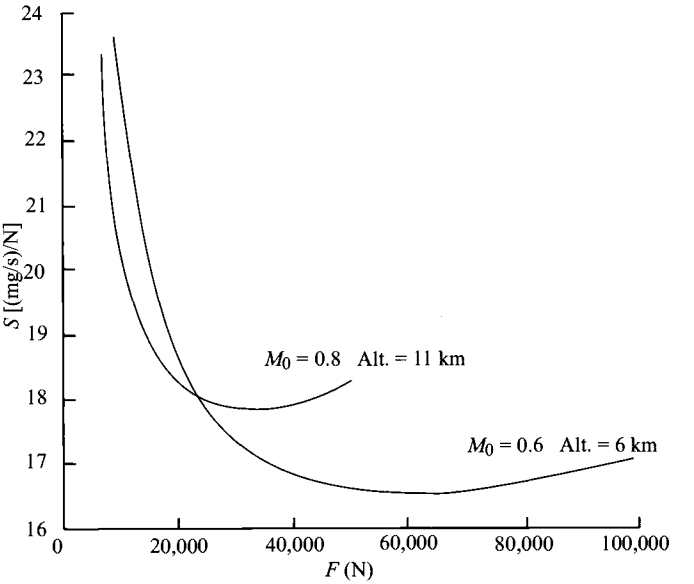

Fig. 8.57 Partial-throttle performance of high-bypass-ratio turbofan.

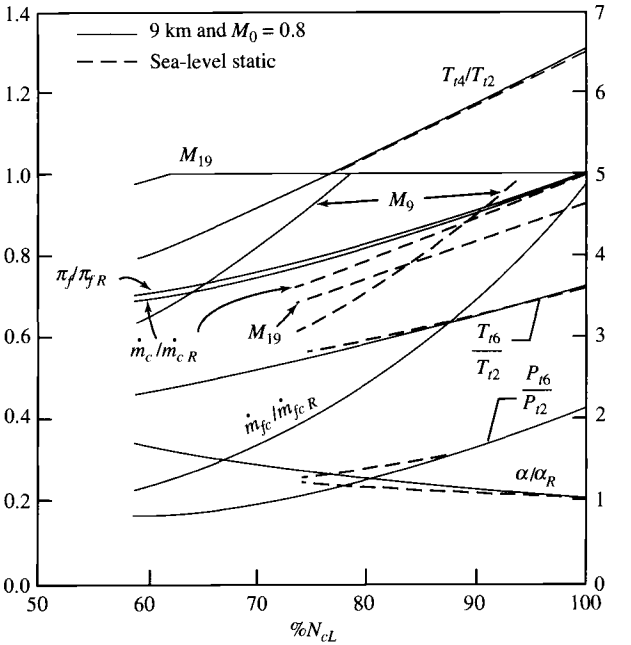

Fig. 8.58 Partial-throttle characteristics of low-pressure spool.

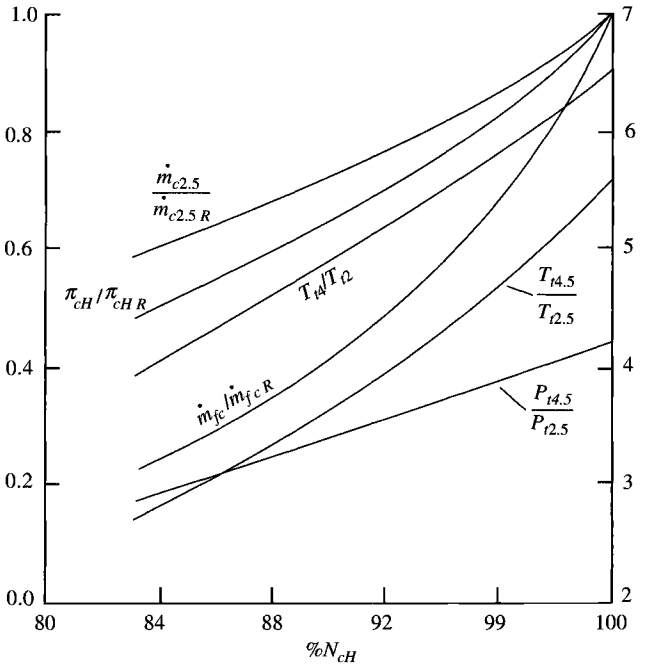

Fig. 8.59 Partial-throttle characteristics of high-pressure spool.

flight condition. The variations in T_{t6}/T_{t2}, P_{t6}/P_{t2}, and α/α_R with corrected speed are small above 80% of N_{cL}. As in the single-spool engine, there is a one-to-one correspondence of the temperature ratio T_{t4}/T_{t2} with the corrected speed of the spool.

The pumping characteristics of the high-pressure spool are shown in Fig. 8.59. These are the same characteristic curves that we found for the gas generator of the single-spool turbojet (Fig. 8.15).

8.5.4 Compressor Stages on Low-Pressure Spool

Modern high-bypass-ratio turbofan engines and other turbofan engines are constructed with compressor stages on the low-pressure spool as shown in Fig. 8.60. This addition of compressor stages to the spool that powers the fan gives a better balance between the high- and low-pressure turbines. This change in engine layout also adds two dependent variables to the nine we had for the performance analysis of the turbofan engine in the previous section. These two new variables are the low-pressure compressor's total temperature ratio τ_{cL} and total pressure ratio π_{cL}.

Because the low-pressure compressor and the fan are on the same shaft, the enthalpy rise across the low-pressure compressor will be proportional to the

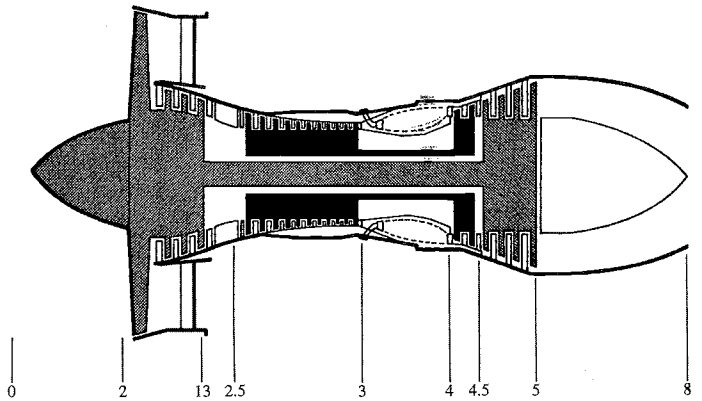

Fig. 8.60 Turbofan engine with compressor stages on low-pressure spool. (Courtesy of Pratt & Whitney.)

enthalpy rise across the fan during normal operation. For a calorically perfect gas, we can write

$$T_{t2.5} - T_{t2} = K(T_{t13} - T_{t2})$$

or

$$\tau_{cL} - 1 = K(\tau_f - 1)$$

Using reference conditions to replace the constant K, we can solve the preceding equation for τ_{cL} as

$$\tau_{cL} = 1 + (\tau_f - 1)\frac{\tau_{cLR} - 1}{\tau_{fR} - 1} \tag{8.53}$$

The pressure ratio for the low-pressure compressor is given by Eq. (8.43):

$$\pi_{cL} = [1 + \eta_{cL}(\tau_{cL} - 1)]^{\gamma_c/(\gamma_c - 1)}$$

In a manner like that used to obtain Eq. (8.46), the following equation for the bypass ratio results:

$$\alpha = \alpha_R \frac{\pi_{cLR}\pi_{cHR}/\pi_{fR}}{\pi_{cL}\pi_{cH}/\pi_f} \sqrt{\frac{\tau_\lambda/(\tau_r\tau_f)}{[\tau_\lambda/(\tau_r\tau_f)]_R}} \frac{\text{MFP}(M_{19})}{\text{MFP}(M_{19R})} \tag{8.54}$$

By rewriting Eq. (8.47) for this engine configuration, the engine mass flow rate is given by

$$\dot{m}_0 = \dot{m}_{0R} \frac{1 + \alpha}{1 + \alpha_R} \frac{P_0\pi_r\pi_d\pi_{cL}\pi_{cH}}{(P_0\pi_r\pi_d\pi_{cL}\pi_{cH})_R} \sqrt{\frac{T_{t4R}}{T_{t4}}} \tag{8.55}$$

Equation (8.40) applies to the high-pressure compressor of this engine and is

$$\tau_{cH} = 1 + \frac{T_{t4}/T_0}{(T_{t4}/T_0)_R} \frac{(\tau_r \tau_{cL})_R}{\tau_r \tau_{cL}} (\tau_{cH} - 1)_R$$

Equations (8.36), (8.37), and (8.38) apply to the high- and low-pressure turbines.

From a power balance between the fan, low-pressure compressor, and low-pressure turbine, we get

$$\eta_{mL} \dot{m}_{4.5} c_{pt} (T_{t4.5} - T_{t5}) = \dot{m}_F c_{pc} (T_{t13} - T_{t2}) + \dot{m}_C c_{pc} (T_{t2.5} - T_{t2})$$

Rewriting this equation in terms of temperature ratios, rearranging into variable and constant terms, and equating the constant to reference values give

$$\frac{\tau_r[(\tau_{cL} - 1) + \alpha(\tau_f - 1)]}{(T_{t4}/T_0)(1 - \tau_{tL})} = \eta_{mL}(1 + f)\tau_{tH} = \left\{ \frac{\tau_r[\tau_{cL} - 1 + \alpha(\tau_f - 1)]}{(T_{t4}/T_0)(1 - \tau_{tL})} \right\}_R$$

Using Eq. (8.53), we substitute for τ_{cL} on the left side of the preceding equation, solve for τ_f, and get

$$\tau_f = 1 + (\tau_{fR} - 1)\left[\frac{1 - \tau_{tL}}{(1 - \tau_{tL})_R} \frac{\tau_\lambda/\tau_r}{(\tau_\lambda/\tau_r)_R} \frac{\tau_{cLR} - 1 + \alpha_R(\tau_{fR} - 1)}{\tau_{cLR} - 1 + \alpha(\tau_{fR} - 1)} \right] \tag{8.56}$$

8.5.5 Solution Scheme

The principal dependent variables for the turbofan engine are π_{tL}, τ_{tL}, α, τ_{cL}, π_{cL}, τ_{cH}, π_{cH}, τ_f, π_f, M_9, and M_{19}. These variables are dependent on each other plus the engine's independent variables—throttle setting and flight condition. The functional interrelationship of the dependent variables can be written as

$$\begin{aligned}
\tau_{cH} &= f_1(\tau_{cL}) & M_{19} &= f_7(\pi_f) \\
\pi_{cH} &= f_2(\tau_{cH}) & M_9 &= f_8(\pi_f, \pi_{cH}, \pi_{tL}) \\
\tau_f &= f_3(\tau_{rL}, \alpha) & \pi_{tL} &= f_9(\tau_{tL}, M_9) \\
\pi_f &= f_4(\tau_f) & \tau_{tL} &= f_{10}(\pi_{tL}) \\
\tau_{cL} &= f_5(\tau_f) & \alpha &= f_{11}(\tau_f, \pi_{cH}, M_{19}) \\
\pi_{cL} &= f_6(\tau_{cL})
\end{aligned}$$

This system of 11 equations is solved by functional iteration, starting with reference quantities as initial values for π_{tL}, τ_{tL}, and τ_f. The following equations are calculated for the 11 dependent variables in the order listed until successive values of τ_{tL} do not change more than a specified amount

(say, 0.0001):

$$\tau_{cH} = 1 + \frac{T_{t4}/T_0}{(T_{t4}/T_0)_R}\frac{(\tau_r\tau_{cL})_R}{\tau_r\tau_{cL}}(\tau_{cH} - 1)_R \tag{8.57a}$$

$$\pi_{cH} = [1 + \eta_{cH}(\tau_{cH} - 1)]^{\gamma_c/(\gamma_c-1)} \tag{8.57b}$$

$$\pi_f = [1 + (\tau_f - 1)\eta_f]^{\gamma_c/(\gamma_c-1)} \tag{8.57c}$$

$$\frac{P_{t19}}{P_0} = \pi_r\pi_d\pi_f\pi_{\text{fn}} \tag{8.57d}$$

If $\dfrac{P_{t19}}{P_0} < \left(\dfrac{\gamma_c + 1}{2}\right)^{\gamma_c/(\gamma_c-1)}$ then $\dfrac{P_{t19}}{P_{19}} = \dfrac{P_{t19}}{P_0}$

else $\dfrac{P_{t19}}{P_{19}} = \left(\dfrac{\gamma_c + 1}{2}\right)^{\gamma_c/(\gamma_c-1)}$ (8.57e)

$$M_{19} = \sqrt{\frac{2}{\gamma_c - 1}\left[\left(\frac{P_{t19}}{P_{19}}\right)^{(\gamma_c-1)/\gamma_c} - 1\right]} \tag{8.57f}$$

$$\frac{P_{t9}}{P_0} = \pi_r\pi_d\pi_{cL}\pi_{cH}\pi_b\pi_{tH}\pi_{tL}\pi_n \tag{8.57g}$$

If $\dfrac{P_{t9}}{P_0} < \left(\dfrac{\gamma_t + 1}{2}\right)^{\gamma_t/(\gamma_t-1)}$ then $\dfrac{P_{t9}}{P_9} = \dfrac{P_{t9}}{P_0}$

else $\dfrac{P_{t9}}{P_9} = \left(\dfrac{\gamma_t + 1}{2}\right)^{\gamma_t/(\gamma_t-1)}$ (8.57h)

$$M_9 = \sqrt{\frac{2}{\gamma_t - 1}\left[\left(\frac{P_{t9}}{P_9}\right)^{(\gamma_t-1)/\gamma} - 1\right]} \tag{8.57i}$$

$$\alpha = \alpha_R\frac{\pi_{cLR}\pi_{cHR}/\pi_{fR}}{\pi_{cL}\pi_{cH}/\pi_f}\sqrt{\frac{\tau_\lambda/(\tau_r\tau_f)}{[\tau_\lambda/(\tau_r\tau_f)]_R}}\frac{\text{MFP}(M_{19})}{\text{MFP}(M_{19R})} \tag{8.57j}$$

$$\tau_f = 1 + (\tau_{fR} - 1)\left[\frac{1 - \tau_{tL}}{(1 - \tau_{tL})_R}\frac{\tau_\lambda/\tau_r}{(\tau_\lambda/\tau_r)_R}\frac{\tau_{cLR} - 1 + \alpha_R(\tau_{fR} - 1)}{\tau_{cLR} - 1 + \alpha(\tau_{fR} - 1)}\right] \tag{8.57k}$$

$$\tau_{cL} = 1 + (\tau_f - 1)\frac{\tau_{cLR} - 1}{\tau_{fR} - 1} \tag{8.57l}$$

$$\pi_{cL} = [1 + \eta_{cL}(\tau_{cL} - 1)]^{\gamma_c/(\gamma_c-1)} \tag{8.57m}$$

$$\tau_{tL} = 1 - \eta_{tL}(1 - \pi_{tL}^{(\gamma_t-1)/\gamma_t}) \tag{8.57n}$$

$$\pi_{tL} = \pi_{tLR}\sqrt{\frac{\tau_{tL}}{\tau_{tLR}}}\frac{\text{MFP}(M_9R)}{\text{MFP}(M_9)} \tag{8.57o}$$

8.5.6 Summary of Performance Equations—Turbofan Engine with Compressor Stages on Low-Pressure Spool

INPUTS:

Choices	
Flight parameters:	M_0, T_0 (K, °R), P_0 (kPa, psia)
Throttle setting:	T_{t4} (K, °R)
Design constants	
π:	$\pi_{d\,\max}$, π_b, π_{tH}, π_{AB}, π_n, π_{fn}
τ:	τ_{tH}
η:	η_f, η_{cL}, η_{cH}, η_b, η_{AB}, η_{mH}, η_{mL}
Gas properties:	γ_c, γ_t, c_{pc}, c_{pt} [kJ/(Kg · K), Btu/(lbm · °R)]
Fuel:	h_{PR} (kJ/kg, Btu/lbm)
Reference conditions	
Flight parameters:	M_{0R}, T_{0R} (K, °R), P_{0R} (kPa, psia), τ_{rR}, τ_{rR}
Throttle setting:	T_{t4R} (K, °R)
Component behavior:	π_{dR}, π_{fR}, π_{cLR}, π_{cHR}, π_{tL}, τ_{fR}, τ_{cHR}, τ_{tLR}, α_R, M_{9R}, M_{19R}

OUTPUTS:

Overall performance:	F (N, lbf), $\dot{m}_0$ (kg/s, lbm/s), f, $S\left(\frac{\text{mg/s}}{\text{N}}, \frac{\text{lbm/h}}{\text{lbf}}\right)$ η_P, η_T, η_O
Component behavior:	α, π_f, π_{cL}, π_{cH}, π_{tL}, τ_f, τ_{cH}, τ_{tL}, f, M_9, M_{19}, N_{fan}, N_{HPspool}
Exhaust nozzle pressure:	P_0/P_9, P_0/P_{19}

EQUATIONS (in order of calculation):

Equations (8.52a–8.52j)
Set initial values: $\tau_{tL} = \tau_{tLR}$ $\tau_f = \tau_{fR}$ $\tau_{cL} = \tau_{cLR}$ $\pi_{tL} = \pi_{tL\,R}$
Equations (8.57a–8.57o)

$$\dot{m}_0 = \dot{m}_{0R} \frac{1+\alpha}{1+\alpha_R} \frac{P_0 \pi_r \pi_d \pi_{cL} \pi_{cH}}{(P_0 \pi_r \pi_d \pi_{cL} \pi_{cH})_R} \sqrt{\frac{T_{t4R}}{T_{t4}}} \tag{8.57p}$$

$$f = \frac{\tau_\lambda - \tau_r \tau_{cL} \tau_{cH}}{h_{PR}\eta_b/(c_p T_0) - \tau_\lambda} \tag{8.57q}$$

Equations (8.52z–8.52ag)

$$\left(\frac{N}{N_R}\right)_{\text{HPspool}} = \sqrt{\frac{T_0 \tau_r \tau_{cL}}{(T_0 \tau_r \tau_{cL})_R} \frac{\pi_{cH}^{(\gamma-1)/\gamma} - 1}{\pi_{cHR}^{(\gamma-1)/\gamma} - 1}} \tag{8.57r}$$

Equations (8.52ai–8.52ak)

Problems

8.1 The flow in a typical single-spool turbojet engine is choked in two locations. This fact is used in performance analysis to predict the variations of the compressor and turbine with changes in T_{t4} and T_{t2}. As a result, the turbine temperature and pressure ratios are constant for all operating conditions.

(a) Identify the two locations where the flow is choked in the engine.
(b) Describe the basic engineering principle that gives the equation for the lines of constant $T_{t4}//T_{t2}$, sketched in Fig. P8.1 and in Figs. 8.6a and 8.6b.
(c) Sketch the operating line of a typical turbojet on the compressor map of Fig. P8.1.
(d) Describe the advantage of a turbojet engine having a throttle ratio greater than 1.

8.2 If the compressor of a single-spool turbojet has a maximum compressor ratio of 8 with a corrected mass flow rate of 25 kg/s for $T_{t4} = 1800$ K and $\theta_0 = 1$, determine the following (assume $\gamma_c = 1.4$):

(a) Constants K_1 and K_2 of Eqs. (8.17) and (8.18).
(b) Compressor pressure ratio and corrected mass flow rate for $T_{t4} = 1200$ K and $\theta_0 = 1.1$.
(c) The maximum T_{t4} and corresponding compressor pressure ratio and corrected mass flow rate at $\theta_0 = 0.9$ and 1.1 for a throttle ratio of 1.0.
(d) The maximum T_{t4} and corresponding compressor pressure ratio and corrected mass flow rate at $\theta_0 = 0.9$ and 1.1 for a throttle ratio of 1.05.

8.3 The typical operation of the single-spool turbojet engine at maximum throttle for flight conditions where $\theta_0 < \text{TR}$ is such that $T_{t4}/T_{t2} = \text{constant}$. Show that π_c, T_{t5}/T_{t2}, P_{t5}/P_{t2}, and $\dot{m}_{c2}$ are also constant.

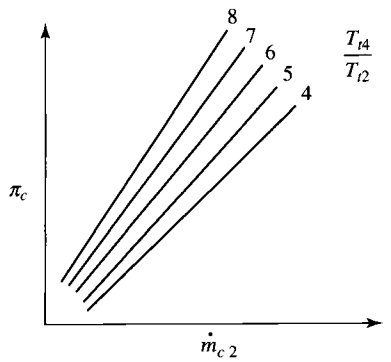

Fig. P8.1

8.4 Show that the total temperature ratios for the compressors of the two-spool turbojet engine [Eqs. (8.42) and (8.40)] can be written as

$$\tau_{cL} = 1 + \frac{T_{t4}/\theta_0}{(T_{t4}/\theta_0)_R}(\tau_{cL} - 1)_R$$

$$\tau_{cH} = 1 + \frac{T_{t4}/\theta_0}{(T_{t4}/\theta_0)_R}\frac{\tau_{cLR}}{\tau_{cL}}(\tau_{cH} - 1)_R$$

8.5 In terms of reference conditions (subscript R), show that the following equations apply for the operation of an *ideal* single-spool turbojet engine:

(a) The compressor pressure ratio is given by

$$\pi_c = \left\{1 + [(\pi_{cR})^{(\gamma-1)/\gamma} - 1]\frac{T_{t4}/T_{t2}}{(T_{t4}/T_{t2})_R}\right\}^{\gamma/(\gamma-1)}$$

(b) The engine mass flow rate is given by

$$\dot{m}_0 = \dot{m}_{0R}\frac{P_{t2}}{P_{t2R}}\frac{\pi_c}{\pi_{cR}}\sqrt{\frac{T_{t4R}}{T_{t4}}}$$

(c) The corrected mass flow rate at station 2 is given by

$$\dot{m}_{c2} = \dot{m}_{c2R}\frac{\pi_c}{\pi_{cR}}\sqrt{\frac{(T_{t4}/T_{t2})_R}{(T_{t4}/T_{t2})}}$$

(d) Given $(T_{t4}//T_{t2})_R = 4$, $\pi_{cR} = 12$, $\dot{m}_{cR} = 200$ lbm/s, and $\gamma = 1.4$, calculate the engine operating line by completing the following table of data; plot the results.

T_{t4}/T_{t2}	4.0	3.6	3.2	2.8	2.4	2.0	1.6
π_c	12						
$\dot{m}_c$ (lbm/s)	200						

8.6 For a ramjet engine with a constant nozzle throat area A_8, develop the performance equations and calculate the performance of the ramjet with the reference data of Problem 7.1.

(a) Show that the engine mass flow rate can be written as

$$\dot{m}_0 = \dot{m}_{0R}\frac{P_0\pi_r\pi_d}{(P_0\pi_r\pi_d)R}\sqrt{\frac{T_{t4R}}{T_{t4}}}\frac{\text{MFP}(M_8)}{\text{MFP}(M_{8R})}$$

where the Mach number at station 8 is determined by the value of P_{t8}/P_0.

(b) Show that the remainder of the performance equations are given by those developed to answer Problem 7.1.
(c) If the ramjet of Problem 7.1 has a reference mass flow rate of 20 kg/s at 15 km and $M_0 = 2$, determine its performance at 20 km, $M_0 = 3$, and $T_{t4} = 1600$ K. Assume $P_9 = P_0$.

8.7 A turbojet engine operated at a flight Mach number of 2.0 and an altitude of 15 km has the following compressor performance with $T_{t4} = 1860$ K: $\pi_c = 8$, $\tau_c = 1.9$, and $\eta_c = 0.9$. Determine τ_c, π_c, and $\dot{m}_2/\dot{m}_{2R}$ for $M_0 = 0.8$, 11-km altitude, and $T_{t4} = 1640$ K. Assume that $\pi_d = 0.88$ at $M_0 = 2$, $\pi_d = 0.98$ at $M_0 = 0.8$, and $\gamma_c = 1.4$.

8.8 Calculate the thrust of the turbojet engine in Example 7.1 at $M_0 = 0.8$, 9-km altitude, reduced throttle ($T_{t4} = 1100$ K), and $P_0/P_9 = 1$ for a reference air mass flow rate of 50 kg/s at a reference altitude of 12 km.

8.9 Given a single-spool turbojet engine that has the following reference values.

REFERENCE:

$$\dot{m}_{c2} = 100 \text{ lbm/s}, \quad \pi_c = 6, \quad M_0 = 0, \quad T_{t2} = 518.7^\circ\text{R}$$

$$T_{t4} = 3200^\circ\text{R}, \quad P_0 = 1 \text{ atm}, \quad \pi_d = 0.97, \quad \pi_b = 0.96$$

$$\pi_n = 0.98, \quad \eta_b = 0.995, \quad \eta_m = 0.99, \quad P_0/P_9 = 1$$

$$\eta_c = 0.8725, \quad \pi_t = 0.6098, \quad \tau_t = 0.9024, \quad \eta_t = 0.9051$$

$$f = 0.041895, \quad V_9/a_0 = 2.8876, \quad P_{t9}/P_9 = 3.3390, \quad M_9 = 1.4624$$

$$F/\dot{m}_0 = 104.41 \text{ lbf (lbm/s)}, \quad \gamma_c = 1.4, \quad c_{pc} = 0.24 \text{ Btu/(lbm} \cdot {}^\circ\text{R)}$$

$$\gamma_t = 1.3, \; c_{pt} = 0.296 \text{ Btu/(lbm} \cdot {}^\circ\text{R)}, \quad h_{PR} = 18{,}400 \text{ Btu/lbm}$$

(a) Determine $\dot{m}_0$, P_{t5}/P_{t2}, T_{t5}/T_{t2}, V_9, F, and S at the reference condition.
(b) If this engine has a throttle ratio of 1.0 and is operating at maximum T_{t4} at a flight condition where $\theta_0 = 1.2$, determine π_c, $\dot{m}_{c2}$, P_{t5}/P_{t2}, T_{t5}/T_{t2}, and N_c/N_{cR} at this operating point.
(c) If this engine has a throttle ratio of 1.1 and is operating at maximum T_{t4} at a flight condition where $\theta_0 = 1.2$, determine π_c, $\dot{m}_{c2}$, P_{t5}/P_{t2}, T_{t5}/T_{t2}, and N_c/N_{cR} at this operating point.
(d) Determine the percentage change in performance parameters between parts b and c.

8.10 Given a single-spool turbojet engine that has the following reference values.

REFERENCE:

$$\dot{m}_{c2} = 50 \text{ kg/s}, \quad \pi_c = 8, M_0 = 0, \quad T_{t2} = 288.2 \text{ K}$$

$$T_{t4} = 1780 \text{ K}, \quad P_0 = 1 \text{ atm}, \quad \pi_d = 0.97, \quad \pi_b = 0.96$$

$$\pi_n = 0.98, \quad \eta_b = 0.995, \quad \eta_m = 0.99, \quad P_0/P_9 = 1$$

$$\eta_c = 0.8678, \quad \pi_t = 0.5434, \quad \tau_t = 0.8810, \quad \eta_t = 0.9062$$

$$f = 0.040796, \quad V_9/a_0 = 3.0256, \quad P_{t9}/P_9 = 3.9674, \quad M_9 = 1.5799$$

$$F/\dot{m}_0 = 1071 \text{ N/(kg/s)}, \quad \gamma_c = 1.4, \quad c_{pc} = 1.004 \text{ kJ/(kg} \cdot \text{K)}$$

$$\gamma_t = 1.3, \quad c_{pt} = 1.24 \text{ kJ/(kg} \cdot \text{K)}, \quad h_{PR} = 42{,}800 \text{ kJ/kg}$$

(a) Determine $\dot{m}_0$, P_{t5}/P_{t2}, T_{t5}/T_{t2}, V_9, F, and S at the reference condition.

(b) If this engine has a throttle ratio of 1.0 and is operating at maximum T_{t4} at a flight condition where $\theta_0 = 1.4$, determine π_c, $\dot{m}_{c2}$, P_{t5}/P_{t2}, T_{t5}/T_{t2}, and N_c/N_{cR} at this operating point.

(c) If this engine has a throttle ratio of 1.15 and is operating at maximum T_{t4}, at a flight condition where $\theta_0 = 1.4$, determine π_c, $\dot{m}_{c2}$, P_{t5}/P_{t2}, T_{t5}/T_{t2}, and N_c/N_{cR} at this operating point.

(d) Determine the percentage change in performance parameters between parts b and c.

8.11 Calculate the thrust of the afterburning turbojet engine in Example 8.7 at $M_0 = 2.0$, 40-kft altitude, maximum afterburner ($T_{t7} = 3600°\text{R}$), and $P_0/P_9 = 1$ for throttle ratios of 1.0, 1.05, 1.1, 1.15, and 1.2. Comment on the variation in performance with throttle ratio.

8.12 Calculate the thrust and fuel consumption of the afterburning turbojet engine in Example 8.7 at $M_0 = 0.8$, 40-kft altitude, $P_0/P_9 = 1$, a throttle ratio of unity, and a range of T_{t7} from 3600°R down to T_{t5}. Compare your results to those of the PERF computer program.

8.13 Using the PERF computer program, find the performance of the afterburning turbojet engine in Example 8.7 for throttle ratios of 1.1 and 1.2 over the same range of Mach numbers and altitudes. Compare these results to those of Example 8.7.

8.14 Calculate the thrust of the high-bypass-ratio turbofan engine in Example 8.8 at $M_0 = 0.8$, 40-kft altitude, and partial throttle ($T_{t4} = 2600°\text{R}$). Assume convergent-only exhaust nozzles. Compare your results to those of the PERF computer program.

8.15 Calculate the thrust of the high-bypass-ratio turbofan engine in Example 8.8 at $M_0 = 0$, sea-level altitude, and increased throttle ($T_{t4} = 3500°\text{R}$). Assume convergent-only exhaust nozzles. Compare your results to those of the PERF computer program.

8.16 Using the PERF computer program, find the performance of the high-bypass-ratio turbofan engine in Example 8.8 for a throttle ratio of 1.0 over the range of Mach numbers from 0 to 0.8 and altitudes of sea level, 20 kft, and 40 kft. Use 3200°R for maximum T_{t4}.

8.17 Early jet aircraft for passenger service used turbojet engines (e.g., Boeing 707) and the newer aircraft use high-bypass-ratio turbofan engines (e.g., Boeing 777). The early turbojets required a much longer takeoff distance than the newer turbofan-powered aircraft. This difference is due mainly to the variation in thrust of these different engine types with Mach number and altitude. To get a better understanding, use the PERF computer program to design two engines and determine their variations in thrust with Mach number and altitude. Consider a turbojet with the component performance of technology level 3 in Table 6.2 (assume type A diffuser, uncooled turbine, and type D nozzle), $T_{t4} = 2500$°R, compressor pressure ratio of 12, and sea-level static thrust of 10,000 lbf. Determine the turbojet's performance for TR = 1 at maximum T_{t4}, Mach 0.8, and 30-kft altitude. Now consider a high-bypass-ratio turbofan with the component performance of technology level 3 in Table 6.2 (assume type A diffuser, uncooled turbine, and type D nozzle), $T_{t4} = 3000$°R, compressor pressure ratio of 22, fan pressure ratio of 1.54, bypass ratio of 5, and sea-level static thrust of 56,000 lbf. Determine the turbofan's performance for TR = 1 at maximum T_{t4}, Mach 0.8, and 30-kft altitude, and compare to the turbojet.

8.18 Develop a set of performance equations for the stationary gas turbine engine with regeneration (see Problem 7.26) depicted in Fig. P8.2 based on the following assumptions:

(a) Flow is choked at engine stations 4 and 4.5.
(b) Constant component efficiencies (η_c, η_b, η_c, η_{rg}, etc.).
(c) Exit pressure equals the ambient pressure ($P_9 = P_0$).
(d) Constant specific heat c_{pc} and ratio of specific heats γ_c from stations 0 to 3.5.
(e) Constant specific heat c_{pt} and ratio of specific heats γ_t from stations 4 to 9.

8.19 Calculate the corrected fuel flow rate [see Eq. (8.7)] and corrected thrust specific fuel consumption [see Eq. (8.6)] for the turbojet engine of Example 8.4 at an altitude of 40 kft and Mach numbers of 0.6, 0.8, 1.0, and 1.2 with maximum T_{t4}. Comment on your results.

8.20 For a single-spool turbojet engine, show that the maximum corrected fuel flow rate is essentially constant for $\theta_0 \leq$ TR. See Eq. (8.27) for a starting point.

8.21 Consider the dual-spool afterburning turbojet engine modeled in Section 8.4 of the textbook. In this development, the area of station 4.5 was modeled as fixed. If this area changes from its reference value, the temperature and pressure ratios of the high- and low-pressure turbines vary from their reference values. As a result, changes occur in the operating

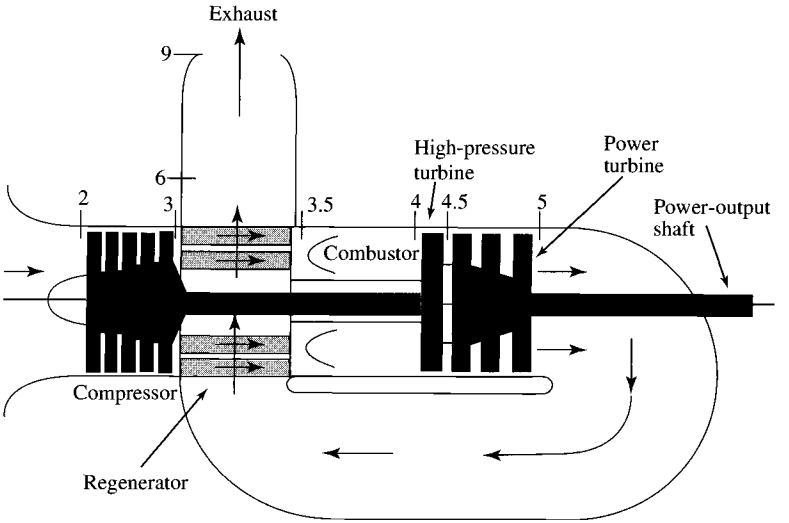

Fig. P8.2

points for both the low- and high-pressure compressors. To better understand this, you are asked to

(a) Redevelop the turbine and compressor relationships influenced by variation in the area at station 4.5. Consider all other assumptions remain valid.

(b) For the reference conditions of Example 8.7, determine the changes in the temperature and pressure ratios of the turbomachinery (compressors and turbines) for a 5% increase in the flow area at station 4.5.

8.22 Variable area turbojet (VAT) engine: The partial throttle (reduced T_{t4}) performance of the typical turbojet engine (see Fig. 8.8) results in reduced compressor pressure ratio π_c and compressor corrected mass flow rate $\dot{m}_{c2}$. The thermal efficiency of the engine is reduced by the lower compressor pressure ratio. Reduced compressor corrected mass flow rate results in increased installation loss from inlet spillage drag (see Chapter 10). We desire to keep compressor mass flow rate $\dot{m}_{c2}$ and compressor total pressure ratio π_c constant at reduced throttle T_{t4} by varying the areas at stations 4 and 8 in a single-spool turbojet engine.

(a) Starting from Eq. (8.9) and assuming $M_4 = 1$ and π_b and $(1+f)$ are con stants, show that constant $\dot{m}_{c2}$ and π_c requires that the area at station 4 (A_4) be varied in the following way:

$$\frac{A_4}{A_{4R}} = \sqrt{\frac{T_{t4}/T_{t2}}{(T_{t4}/T_{t2})_R}} \qquad \text{(VAT.1)}$$

(b) Starting with the work balance between the turbine and compressor of Eq (8.13), show that for τ_c constant then the turbine total

temperature will vary as

$$\tau_t = 1 - (1 - \tau_{tR})\frac{(T_{t4}/T_{t2})_R}{T_{t4}/T_{t2}} \qquad \text{(VAT.2)}$$

(c) Using conservation of mass between stations 4 and 8 (with $M_4 = 1$ and $M_8 = 1$), show that

$$\frac{\sqrt{\tau_t}}{\pi_t} = \frac{A_8}{A_4}$$

and the area at station 8 must be varied in the following way:

$$\frac{A_8}{A_{8R}} = \frac{A_8}{A_{4R}}\sqrt{\frac{\tau_t}{\tau_{tR}}}\frac{\pi_{tR}}{\pi_t} = \sqrt{\frac{T_{t4}/T_{t2}}{(T_{t4}/T_{t2})_R}}\sqrt{\frac{\tau_t}{\tau_{tR}}}\frac{\pi_{tR}}{\pi_t} \qquad \text{(VAT.3)}$$

where, assuming constant turbine efficiency η_t, the turbine total pressure ratio is given by Eq. (8.12b).

(d) Because the corrected mass flow rate into the compressor is constant, show that the engine mass flow rate can be written as

$$\frac{\dot{m}_0}{\dot{m}_{0R}} = \frac{P_0\pi_r\pi_d}{(P_0\pi_r\pi_d)_R}\sqrt{\frac{(T_0\tau_r)_R}{T_0\tau_r}} \qquad \text{(VAT.4)}$$

Problems for Supporting Material

SM8.1 Calculate the maximum thrust of the afterburning mixed-flow exhaust turbofan engine in Example SM8.1 at $M_0 = 2$ and 40-kft altitude for throttle ratios of 1.1 and 1.2 using the PERF computer program.

SM8.2 Using the PERF computer program, find the performance of the afterburning mixed-flow exhaust turbofan engine in Example 8.10 for throttle ratios of 1.0 and 1.2 over the range of Mach numbers from 0 to 2 and altitude of sea level, 10 kft, 20 kft, 30 kft, 36 kft, 40 kft, and 50 kft. Compare your results to those of Example SM8.1 for a throttle ratio of 1.1.

SM8.3 Calculate the thrust and fuel consumption of the turboprop engine in Example 8.11 at $M_0 = 0.5$, a 6-km altitude, and reduced throttle ($T_{t4} = 1400$ K). Assume a convergent-only exhaust nozzle. Compare your results to those of the PERF computer program.

SM8.4 Using the PERF computer program, find the performance of the turboprop engine in Example SM8.2 at partial throttle at $M_0 = 0.5$ and altitudes of sea level, 3 km, and 6 km. Compare these results to those of Example SM8.2.

Gas Turbine Design Problems

8.D1 Find the best high-bypass-ratio turbofan engine for the HP-1 aircraft from those engines showing promise in Design Problem 7.D1. You are to determine the best engine, sized to meet the required engine thrust at takeoff and/or single engine out (0.45 Mach at 16 kft), and whose fuel consumption is minimum.

Hand-Calculate Engine Performance (HP-1 Aircraft). Using the performance analysis equations for a high-bypass-ratio turbofan engine, hand-calculate the performance of the turbofan engine hand-calculated in Design Problem 7.D1 at the flight condition of 0.83 Mach and 11-km altitude at $T_{t4} = 1500$ K.

Required Thrust at Different Flight Conditions (HP-1 Aircraft). Determine both the required installed thrust and the required uninstalled engine thrust for each of the following flight conditions (assume $\phi_{noz} = 0.01$):

1) Uninstalled thrust of 267 kN for each engine at sea-level static while at takeoff power setting ($T_{t4} = 1890$ K). Assume $\phi_{inlet} = 0.05$.
2) Start of Mach 0.83 cruise, 11-km altitude, $P_s = 1.5$ m/s, 95.95% of takeoff weight; $\phi_{inlet} = 0.01$.
3) Mach 0.45, 5-km altitude, engine out, $P_s = 1.5$ m/s, 88% of takeoff weight; $\phi_{inlet} = 0.02$. Assume a drag coefficient increment for engine out = 0.0035 (based on wing area).
4) Loiter at 9-km altitude, 64% of takeoff weight; $\phi_{inlet} = 0.03$.

Computer-Calculated Engine Performance (HP-1 Aircraft). For each of the engines showing promise in Design Problem 7.D1, systematically perform the following analysis:

1) Design the reference engine at sea-level static conditions. Size the engine to provide the required uninstalled thrust (engine size normally will be determined by either the takeoff flight condition or the engine-out flight condition listed previously). Check engine operation at takeoff and make sure that $T_{t3} < 920$ K.
2) Determine the uninstalled fuel consumption at the start of Mach 0.83 cruise, 11-km altitude, and $P_s = 0$. You can do this by input of "% thrust" in the PERF computer program and calculate for the required uninstalled thrust. Assuming cruise climb with constant range factor (RF), calculate the weight at the end of the Mach 0.83 cruise, using the Breguet range equation, Eq. (1.45a or b).
3) Determine the loiter Mach number at 9-km altitude for the current aircraft weight at the start of loiter. Find the engine fuel consumption at start of loiter. Assuming a constant endurance factor (EF), calculate the weight at the end of the 9-km loiter. Some engines may not throttle down to the required uninstalled thrust due to the model used in the computer program, and the uninstalled thrust specific fuel consumption will have to be obtained by *extrapolation*. To extrapolate, use the performance analysis computer

program and iterate on T_{t4} in steps of 25 K to the lowest value giving results. Then plot S vs F as shown in Fig. P8.D1a, and draw a tangent line to obtain the extrapolated value of S at the desired uninstalled thrust.

Fuel Consumption (HP-1 Aircraft). During this preliminary analysis, you can assume that the fuel consumption changes only for the Mach 0.83 cruise and 9-km loiter. For every one of the engines you investigate, you must determine whether it can satisfy the fuel consumption requirements by calculating the amount of fuel consumed during the Mach 0.83 cruise climb and 9-km loiter and adding these to that consumed for other parts of the flight. During your analysis of the engines, make a plot of fuel consumed vs the reference bypass ratio like that shown in Fig. P8.D1b. Starting with one compressor pressure ratio π_{c1}, and a low-bypass-ratio engine, calculate the total fuel consumed for the flight. Now increase the bypass ratio, size the engine, and determine this engine's performance.

Engine Selection (HP-1 Aircraft). Select one of your engines that, according to your criteria, best satisfies the mission requirements. Your criteria *must include* at least the following items (other items may be added based on knowledge gained in other courses and any additional technical sources):

Thrust requirement
Fuel consumption
Aircraft performance
Operating cost (assume 10,000-h engine life and fuel cost of \$1.00/lb)
First cost
Size and weight
Complexity

Determine Engine Thrust vs Mach Number and Altitude (HP-1 Aircraft). For the engine you select, determine and plot the uninstalled thrust F at maximum power vs Mach number at sea level, 5-km altitude, and 11-km altitude and at takeoff power at sea level (see Fig. 8.47). Use $T_{t4} = 1780$ K for maximum power and $T_{t4} = 1890$ K for takeoff power.

Summary. Summarize the final choice for the selected engine including a list of design conditions and choices, performance during the mission, and overall mission performance. Include suggestions, if necessary, for

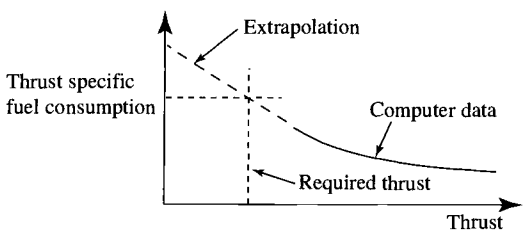

Fig. P8.D1a

overcoming any of the performance shortcomings that may exist in any of the mission legs. In addition, make meaningful comments about the feasibility of building such an engine.

8.D2 Find the best mixed-flow turbofan engine with afterburner for the HF-1 aircraft from those engines showing promise in Design Problem 7.D2. You are to determine the best engine, sized to meet the required engine thrust at takeoff, supercruise, and/or 5-g turns, and whose cruise fuel consumption over the maximum mission (see Design Problem 1.D2) is minimum.

Hand-Calculate Engine Performance (HP-1 Aircraft). Using the performance analysis equations for a mixed-flow turbofan engine with afterburner, hand-calculate the performance of the mixed-flow turbofan engine hand-calculated in Design Problem 7.D2 at the flight condition of 1.6 Mach and 40-kft altitude at $T_{t4} = 3200°R$ with the afterburner turned off.

Required Thrust at Different Flight Conditions (HP-1 Aircraft). Determine both the required installed thrust and the required uninstalled engine thrust for each of the following flight conditions (assume $\phi_{noz} = 0.01$):

1) For takeoff, an installed thrust of 23,500 lbf for each engine at sea level, 0.1 Mach while at maximum power setting (afterburner on with $T_{t7} = 3600°R$). Assume $\phi_{inlet} = 0.10$.

2) Start of Mach 1.6 supercruise, 40-kft altitude, 92% of takeoff weight W_{TO}; $\phi_{inlet} = 0.04$.

3) Start of 5-g turn at Mach 1.6, 30-kft altitude, 88% of W_{TO}; $\phi_{inlet} = 0.04$.

4) Start of 5-g turn at Mach 0.9, 30-kft altitude, 88% of W_{TO}; $\phi_{inlet} = 0.04$.

Computer-Calculated Engine Performance (HP-1 Aircraft). Develop a reference mixed-flow turbofan engine with afterburner based on the data used in Design Problem 7.D2. For the afterburner, use $\gamma_{AB} = 1.3$, $c_{pAB} = 0.296$ Btu/(lbm·°R), $\pi_{AB} = 0.96$, $\eta_{AB} = 0.97$, and $T_{t7} = 3600°R$.

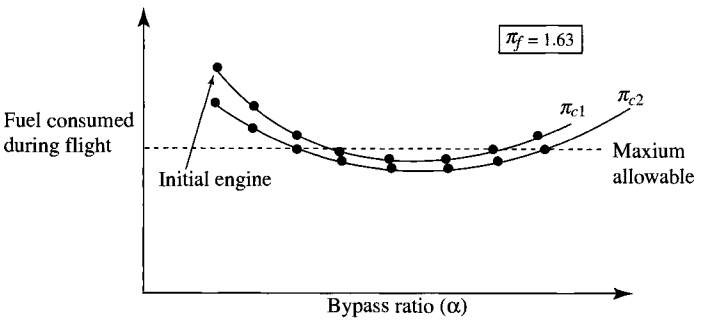

Fig. P8.D1b

For each of the engines showing promise in Design Problem 7.D2, systematically perform the following analysis:

1) Design the reference engine at sea-level static conditions. Size the engine to provide the required uninstalled thrust (engine size will normally be determined by the takeoff flight condition, by the start of supercruise flight condition, or by the 5-g turn at Mach 1.6 listed previously). Check engine operation at takeoff, and make sure that $T_{t3} < 1600°\text{R}$ and that the compressor pressure is within a specified limit.

2) Determine uninstalled fuel consumption at the start of the Mach 1.6 supercruise, 40-kft altitude. You can do this by input of "% thrust" in the PERF computer program and calculate for the required uninstalled thrust. Your engine should be able to deliver the required thrust with the afterburner off. Assuming cruise climb with constant range factor (RF), calculate the weight at the end of the Mach 1.6 supercruise, using the Breguet range equation, Eq. (1.45a or b).

3) Calculate the aircraft weight at the start of the Mach 0.9 cruise and the corresponding best cruise altitude (maximum C_L/C_D) and aircraft drag. Calculate the uninstalled required thrust at start of Mach 0.9 cruise, assuming $\phi_{\text{inlet}} = 0.05$ and $\phi_{\text{noz}} = 0.01$. Now determine the uninstalled fuel consumption at the start of Mach 0.9 cruise. Assuming cruise climb with constant range factor (RF), calculate the weight at the end of the Mach 0.9 cruise, using the Breguet range equation, Eq. (1.45a,b).

4) Determine the loiter Mach number at 30-kft altitude for the current aircraft weight at the start of loiter. Find the engine fuel consumption at the start of loiter. Assuming constant endurance factor (EF), calculate the weight at the end of the 30-kft loiter. Some engines may not throttle down to the required uninstalled thrust due to the model used in the computer program, and the uninstalled thrust specific fuel consumption will have to be obtained by *extrapolation*. To extrapolate, use the performance analysis computer program and iterate on T_{t4} in steps of 50°R to the lowest value giving results. Then plot S vs F as shown in Fig. P8.D1a, and draw a tangent line to obtain the extrapolated value of S at the desired uninstalled thrust.

Fuel Consumption (HP-1 Aircraft). During this preliminary analysis, you can assume that the fuel consumption changes only for the Mach 1.6 supercruise, Mach 0.9 cruise, and 30-kft loiter. For every one of the engines you investigate, you must determine whether it can satisfy the fuel consumption requirements by calculating the amount of fuel consumed during the Mach 1.6 supercruise, Mach 0.9 cruise, and 30-kft loiter and adding these values to that consumed for other parts of the maximum mission. During your analysis of the engines, make a plot of fuel consumed vs the reference bypass ratio like that shown in Fig. P8.D1b. Starting with one compressor pressure ratio π_{c1} and a low-bypass-ratio engine, calculate the total fuel consumed for the mission. Now increase the bypass ratio, size the engine, and determine this engine's performance.

Engine Selection (HP-1 Aircraft). Select one of your engines that, according to your criteria, best satisfies the mission requirements. Your criteria *must include* at least the following items (other items may be added based on knowledge gained in other courses and any additional technical sources):

Thrust required
Fuel consumption
Aircraft performance
Operating cost (assume 10,000-h engine life and fuel cost of \$1.00/lb)
First cost
Size and weight
Complexity

Determine Engine Thrust vs Mach Number and Altitude (HP-1 Aircraft). For the engine you select, determine and plot the uninstalled thrust F and thrust specific fuel consumption at both maximum power (afterburner on) and military power (afterburner off) vs Mach number at altitudes of sea level, 10 kft, 20 kft, 30 kft, 36 kft, and 40 kft (see Figs. 8.65, 8.66, 8.67, and 8.68). Use $T_{t4\max} = 3250°\text{R}$ and the throttle ratio TR for your engine. Also determine and plot the partial-throttle performance (see Fig. 8.69) of your engine at sea-level static, 1.6 Mach and 40 kft, 1.6 Mach and 30 kft, and 0.9 Mach and 30 kft.

Summary. Summarize the final choice for the selected engine including a list of design conditions and choices, performance during the mission, and overall mission performance. Include suggestions, if necessary, for overcoming any of the performance shortcomings that may exist in any of the mission legs. In addition, make meaningful comments about the feasibility of building such an engine.

Page is intentionally blank

9
Turbomachinery

9.1 Introduction

In general, turbomachinery is classified as all those devices in which energy is transferred either to or from a continuously flowing fluid by the dynamic action of one or more moving blade rows.[37] The word *turbo or turbinis* is of Latin origin and implies that which spins or whirls around. Essentially, a rotating blade row or rotor changes the total enthalpy of the fluid moving through it by either doing work on the fluid or having work done on it by the fluid, depending on the effect required of the machine. These enthalpy changes are intimately linked with the pressure changes occurring simultaneously in the fluid.

This definition of turbomachinery embraces both open and enclosed turbomachines.[37] Open turbomachinery (such as propellers, windmills, and unshrouded fans) influence an indeterminate quantity of fluid. In enclosed turbomachinery (such as centrifugal compressors, axial-flow turbines, etc.), a finite quantity of fluid passes through a casing in unit time. In this chapter, we will focus on the enclosed turbomachinery used in gas turbine engines: fans, compressors, and turbines. There are many excellent references on enclosed turbomachinery, such as Refs. 4, 12, 22, 28, 29, and 37–47. Open turbomachines are covered in aeronautics textbooks such as Refs. 48, 49, and 50.

Turbomachines are further categorized according to the nature of the flow path through the passages of the rotor. When the path of the throughflow is wholly or mainly parallel to the axis of rotation, the device is termed an *axial-flow turbomachine*. When the path of the throughflow is wholly or mainly in a plane perpendicular to the rotation axis, the device is termed a *radial-flow turbomachine*. When the direction of the throughflow at the rotor outlet has both radial and axial velocity components present in significant amounts, the device is termed a *mixed-flow turbomachine*.

9.2 Euler's Turbomachinery Equations

In turbomachinery, power is added to or removed from the fluid by the rotating components. These rotating components exert forces on the fluid that change both the energy and the tangential momentum of the fluid. In this section, we will develop Euler's equations for turbomachinery that relate the change in energy to the change in tangential momentum.

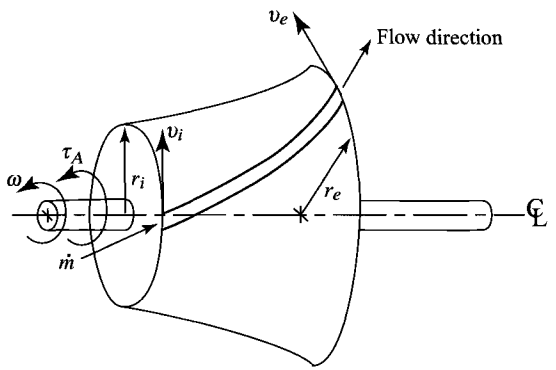

Fig. 9.1 Control volume for a general turbo-machine.

Consider the adiabatic flow of a fluid as shown in Fig. 9.1. The fluid in a stream tube enters a control volume at radius r_i with tangential velocity v_i and exits at r_e with tangential velocity v_e. For a compressor or pump with steady flow, the applied torque τ_A is equal to the change in angular momentum of the fluid, or

$$\tau_A = \frac{\dot{m}}{g_c}(r_e v_e - r_i v_i)$$

The input power is $\dot{W}_c = \omega \tau_A$, or

$$\dot{W}_c = \frac{\dot{m}\omega}{g_c}(r_e v_e - r_i v_i) \tag{9.1}$$

This equation is often referred to as the *Euler pump equation.* Application of the first law of thermodynamics to the flow through the control volume gives

$$\dot{W}_c = \dot{m}(h_{te} - h_{ti})$$

Combining this expression with Eq. (9.1) gives

$$h_{te} - h_{ti} = \frac{\omega}{g_c}(r_e v_e - r_i v_i) \tag{9.2}$$

Likewise, for a steady-flow turbine, the output torque τ_O is equal to the change in angular momentum of the fluid, or

$$\tau_O = \frac{\dot{m}}{g_c}(r_i v_i - r_e v_e)$$

The output power is

$$\dot{W}_t = \omega \tau_O$$

or

$$\dot{W}_t = \frac{\dot{m}\omega}{g_c}(r_i v_i - r_e v_e) \tag{9.3}$$

This equation is often referred to as the *Euler turbine equation*. Application of the first law of thermodynamics to the flow through the control volume gives

$$\dot{W}_t = \dot{m}(h_{ti} - h_{te})$$

Combining this expression with Eq. (9.3) gives

$$h_{ti} - h_{te} = \frac{\omega}{g_c}(r_i v_i - r_e v_e) \tag{9.4}$$

which is the same as Eq. (9.2).

In the design of turbomachinery for a compressible gas, the gas is often modeled as having constant specific heats. For this case, we can write Eq. (9.4) as

$$c_p(T_{ti} - T_{te}) = \frac{\omega}{g_c}(r_i v_i - r_e v_e) \tag{9.5}$$

This equation is also referred to as the *Euler turbine equation*. We will be using this equation throughout the analysis of turbomachinery for a compressible gas. Component efficiencies and the isentropic relationships will be used to relate total temperature changes to total pressure changes.

9.3 Axial-Flow Compressor Analysis

The axial-flow compressor is one of the most common compressor types in use today. It finds its major application in large gas turbine engines like those that power today's jet aircraft. A cutaway view of an axial-flow compressor is shown in Fig. 9.2. The compressor is made up of two major assemblies: the rotor with its blades, as shown in Fig. 9.2a, and the casing with its stationary blades (called *stators*), as shown in Fig. 9.2b.

This chapter investigates the relationships of the desired performance parameters to the related blade loading and resultant fluid flow angles. Because the flow is inherently three-dimensional, the problem of analysis seems almost

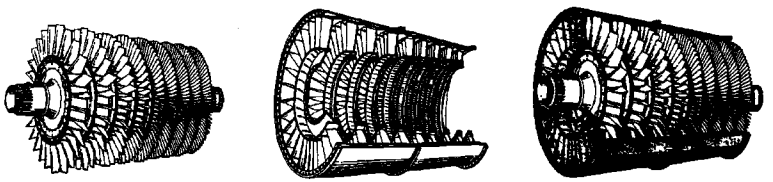

a) b) c)

Fig. 9.2 Axial-flow compressor: a) rotor with blades, b) case with stators, and c) compressor assembly. (Courtesy of Pratt & Whitney).

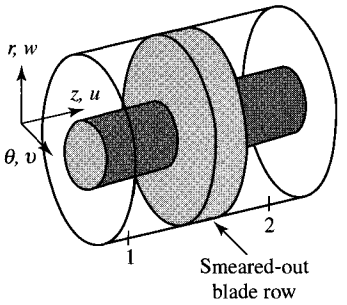

Fig. 9.3 Coordinate system and throughflow representation.

incomprehensible. *Do not fear*! This most complex flow can be understood by dividing the three-dimensional flowfield into three two-dimensional flowfields. The complete flowfield will be the "sum" of these less complex two-dimensional flows. The two-dimensional flowfields are normally called the *throughflow field*, the *cascade field* (or *blade-to-blade field*), and the *secondary flowfield*. Each of these fields is described in more detail next.

The *throughflow field* is concerned with the variation in fluid properties in only the radial r and axial z directions (see Fig. 9.3). No variations in the θ direction occur. A row of blades is modeled as a thin disk that affects the flowfield uniformly in the θ direction. If you imagine that the forces of the blades had been distributed among an infinite number of very thin blades, then you can begin to see the throughflow field model. As a result of throughflow field analysis, one will obtain the axial, tangential, and radial velocities as a function of r and z. Typical axial velocity profiles as a result of throughflow analysis are shown in Fig. 9.4a.

When the axial velocity changes, like that shown in Fig. 9.4a, conservation of mass requires that a downward flow of the fluid occur between stations 1 and 2. This downward flow could be shown by the stream surface as drawn in Fig. 9.4b.

The *cascade field* considers the flow behavior along stream surfaces (s coordinate) and tangentially through blade rows. Unwrapping the stream surface

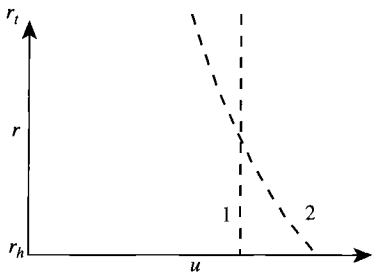

Fig. 9.4a Typical axial velocity profiles.

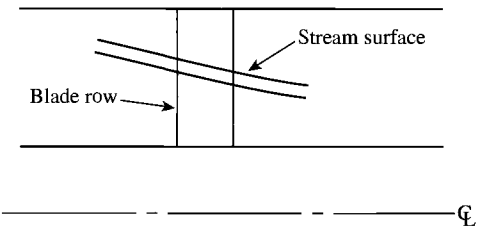

Fig. 9.4b Typical stream surface.

(like that shown in Fig. 9.5) gives the meridional projection of blade profiles, as shown in Fig. 9.6—a two-dimensional flowfield in the θ and the meridional (almost z) coordinates. If the curvature of the stream surfaces in the throughflow field is not too great, the flow at a radial location may be modeled as a meridional projection and a suitable blade profile determined for the flow conditions. By considering a number of such projections, the blade profiles for selected radial locations on the blade are determined. The complete blade shape necessary to describe the full three-dimensional blade can be obtained by blending in the desired blade profiles.

The most common method of obtaining performance data for different blade profiles is to run cascade tests. A set of airfoils of the desired blade shape is mounted in a conditioned flow stream, and the performance is experimentally measured. Figure 9.7 shows the complete flowfield about a typical cascade with the blades spaced a distance s apart.

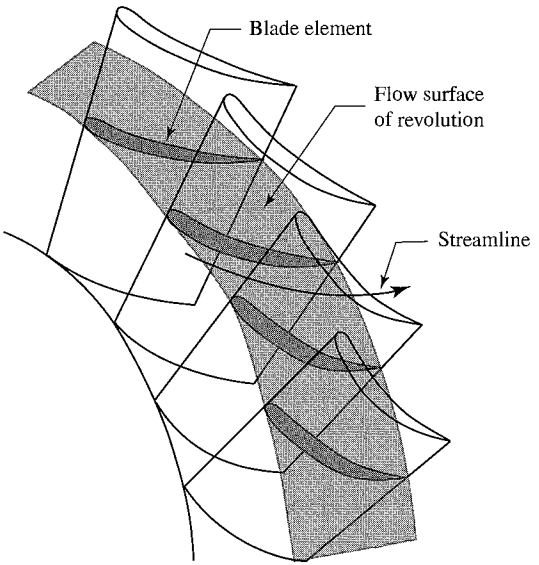

Fig. 9.5 Stream surface and streamlines.

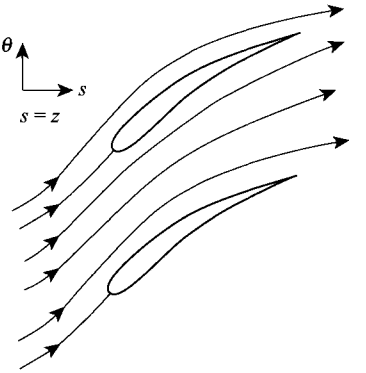

Fig. 9.6 Meridional projections of blade profiles.

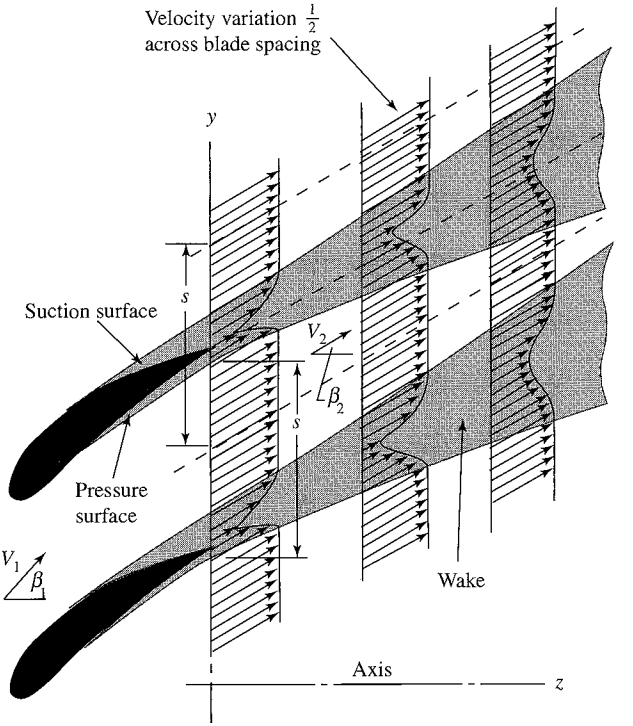

Fig. 9.7 Flowfield about cascade.

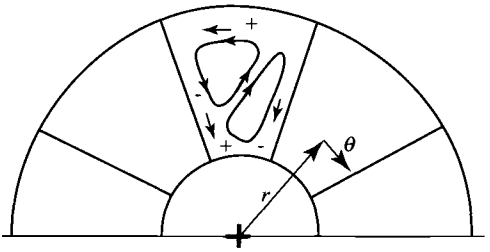

Fig. 9.8 Secondary flowfield within a stator row.

The *secondary flowfield* exists because the fluid near the solid surfaces (in the boundary layer) of the blades and passage walls has a lower velocity than that in the *freestream* (external to the boundary layer). The pressure gradients imposed by the freestream will cause the fluid in the boundary layers to flow from regions of higher pressure to regions of lower pressure. Figure 9.8 shows the possible secondary flowfield within a stator row.

9.3.1 Two-Dimensional Flow Through Blade Rows

A cross section and a top view of a typical axial-flow compressor are shown in Fig. 9.9. Depending on the design, an inlet guide vane (IGV) may be used to deflect the incoming airflow to a predetermined angle toward the direction of rotation of the rotor. The rotor increases the angular velocity of the fluid, resulting in increases in total temperature, total pressure, and static pressure. The following stator decreases the angular velocity of the fluid, resulting in an increase in the static pressure, and sets the flow up for the following rotor. A compressor stage is made up of a rotor and a stator.

The basic building block of the aerodynamic design of axial-flow compressors is the *cascade*, an endless repeating array of airfoils (Fig. 9.10) that results from the "unwrapping" of the stationary (stators) and rotating (rotor) airfoils. Each cascade passage acts as a small diffuser, and it is said to be well designed or

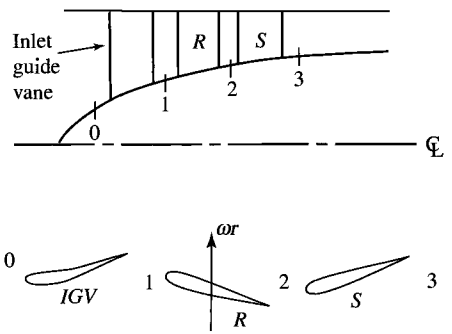

Fig. 9.9 Cross section and top view of a typical axial-flow compressor.

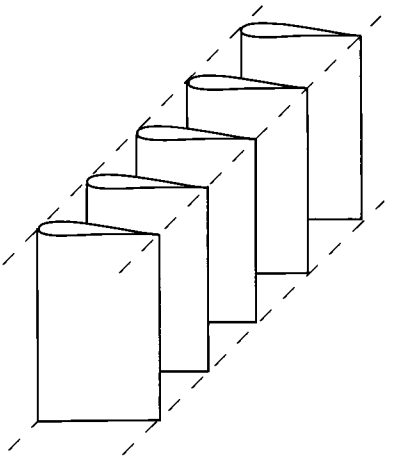

Fig. 9.10 Rectilinear cascade.

"behaved" when it provides a large static pressure rise without incurring unacceptable total pressure losses and/or flow instabilities due to shock waves and/or boundary-layer separation.

The changes in fluid velocity induced by the blade rows are related to changes in the fluid's thermodynamic properties in this section. The analysis is concerned with only the flow far upstream and far downstream of a cascade—the regions where the flowfields are uniform. In this manner, the details about the flowfield are not needed, and performance can be related to just the changes in fluid properties across a blade row.

In the analysis that follows, two different coordinate systems are used: one fixed to the compressor housing (absolute) and the other fixed to the rotating blades (relative). The static (thermodynamic) properties *do not* depend on the reference frame. However, the *total properties do depend on the reference frame*. The velocity of a fluid in one reference frame is easily converted to the other frame by the following equation:

$$\boldsymbol{V} = \boldsymbol{V}_R + \boldsymbol{U} \tag{9.6}$$

where

$\boldsymbol{V}$ = velocity in stationary coordinate system
$\boldsymbol{V}_R$ = velocity in moving coordinate system
$\boldsymbol{U}$ = velocity of moving coordinate system ($=\omega r$)

Consider the compressor stage made up of a rotor followed by a stator as shown in Fig. 9.11. The flow enters the rotor with velocity V_1 (relative velocity V_{1R}) and leaves with velocity V_2 (relative velocity V_{2R}). The rotor is moving upward at velocity ωr (the symbol $\boldsymbol{U}$ is also used). The flow enters the stator with velocity V_2 and leaves with velocity V_3. Rather than keep the axial velocity

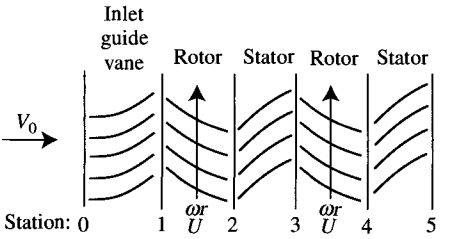

Fig. 9.11 Two repeating compressor stages with inlet guide vane.

constant, as is done in many textbooks, the following analysis permits variation in axial velocity from station to station.

Euler's equation:

$$c_p(T_{t2} - T_{t1}) = \frac{\omega}{g_c}(r_2 v_2 - r_1 v_1)$$

For $r_2 \cong r_1$,

$$c_p(T_{t2} - T_{t1}) = \frac{\omega r}{g_c}(v_2 - v_l) = \frac{U}{g_c}(v_2 - v_1)$$

Since

$$v_2 = \omega r - v_{2R} = \omega r - u_2 \tan \beta_2 = u_2 \tan \alpha_2$$

and

$$v_1 = \omega r - v_{1R} = \omega r - u_1 \tan \beta_1 = u_1 \tan \alpha_1$$

then

$$c_p(T_{t2} - T_{t1}) = \frac{(\omega r)^2}{g_c}\frac{u_1}{\omega r}\left(\tan \beta_1 - \frac{u_2}{u_1}\tan \beta_2\right)$$

$$= \frac{U^2}{g_c}\frac{u_1}{U}\left(\tan \beta_1 - \frac{u_2}{u_1}\tan \beta_2\right) \tag{9.7a}$$

or

$$c_p(T_{t2} - T_{t1}) = \frac{(\omega r)^2}{g_c}\frac{u_1}{\omega r}\left(\frac{u_2}{u_1}\tan \alpha_2 - \tan \alpha_1\right)$$

$$= \frac{U^2}{g_c}\frac{u_1}{U}\left(\frac{u_2}{u_1}\tan \alpha_2 - \tan \alpha_1\right) \tag{9.7b}$$

Hence the work done per unit mass flow can be determined from the rotor speed ($U = \omega r$), the velocity ratios (u_1/U and u_2/u_1), and either the rotor cascade flow angles (β_1 and β_2) or the absolute rotor flow angles (α_1 and α_2). Equations (9.7a) and (9.7b) are useful forms of the Euler equation for compressor stage design and show the dependence of the stage work on the rotor speed squared (U^2).

9.3.2 Velocity Diagrams

An axial-flow compressor stage consists of a rotor followed by a stator as shown in Fig. 9.12a. Two compressor stages (which are identical in geometry) are shown in Fig. 9.12b preceded by inlet guide vanes. The velocity diagrams depicted in Fig. 9.12b show the absolute velocities entering and leaving the guide vanes, rotor, and stator (solid vectors). In addition, for the rotors, the entering and leaving relative velocities (dashed vectors) and the rotor tangential velocity are shown. We have assumed, in the diagram, that the axial velocity component is constant.

Referring to Fig. 9.12b, we see that the guide vanes act as nozzles through which the static pressure decreases as the air velocity increases, and the fluid is given a tangential (swirl) component in the direction of the rotor velocity. The air leaves the inlet guide vanes with velocity V_1.

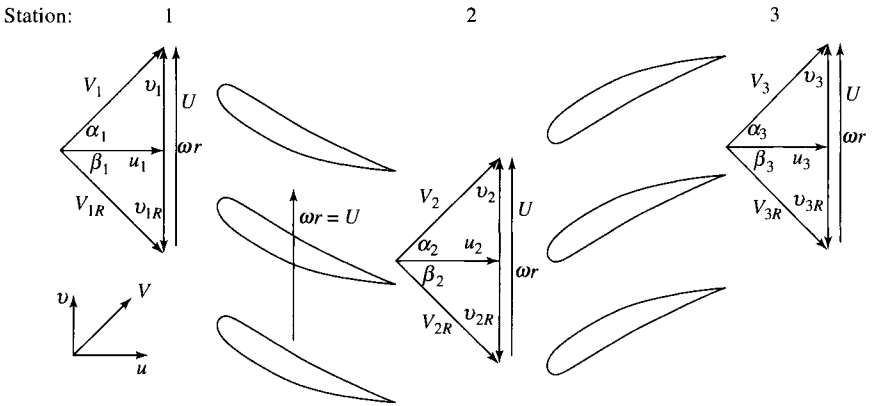

	Rotor	Stator
Velocities	$\mathbf{V}_1 = \mathbf{V}_{1R} + \mathbf{U}$	$\mathbf{V}_2 = \mathbf{V}_{2R} + \mathbf{U}$
	$u_1 = V_1 \cos \alpha_1$	$u_2 = V_2 \cos \alpha_2$
	$v_1 = V_1 \sin \alpha_1$	$v_2 = V_2 \sin \alpha_2$
	$u_1 = V_{1R} \cos \beta_1$	$u_2 = V_{2R} \cos \beta_2$
	$v_{1R} = V_{1R} \sin \beta_1 = u_1 \tan \beta_1$	$v_{2R} = V_{2R} \sin \beta_2 = u_2 \tan \beta_2$
	$v_1 + v_{1R} = \omega r = U$	$v_2 + v_{2R} = \omega r = U$

Fig. 9.12a Blade rows of a typical compressor.

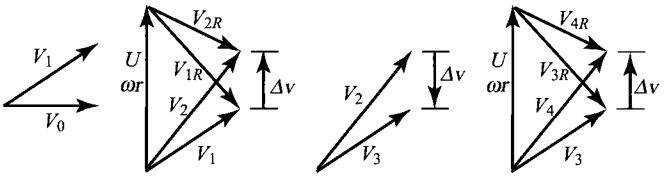

Fig. 9.12b Velocity diagrams for typical compressor.

The absolute velocity entering the rotor at station 1 is V_1. Subtracting the rotor speed ωr from V_1 vectorially, we obtain the relative velocity V_{1R} entering the rotor. In the rotor blade row, the blade passages act as diffusers, reducing the relative velocity from V_{1R} to V_{2R} as the static pressure is increased from P_1 to P_2. The relative velocity leaving the rotor is V_{2R}. Combining V_{2R} vectorially with ωr, we get their sum V_2—the absolute velocity leaving the rotor.

The velocity of the air leaving the rotor and entering the stator at station 2 is V_2. The stator diffuses the velocity to V_3 as the static pressure rises from P_2 to P_3. Because the velocity V_3 entering the rotor at station 3 is identical with V_1 entering the first-stage rotor, we find the velocity triangle for the second-stage rotor is a repeat of the triangle for the first stage.

The effects occurring in each compressor component are summarized in Table 9.1, where +, 0, and − mean increase, unchanged, and decrease, respectively. The table entries assume isentropic flow. In making entries in the table, it is important to distinguish between absolute and relative values. Because total pressure and total temperature depend on the speed of the gas, they have different values "traveling with the rotor" than for an observer not riding on the rotor. In particular, an observer on the rotor sees a force F (rotor on gas), but it is stationary; hence, in the rider's reference system, the force does no work on the gas. Consequently, the total temperature and total pressure do not change relative to an observer on the rotor as the gas passes through the rotor. An observer not on the rotor sees the force F (rotor on gas) moving at the rate ωr. Hence, to the stationary observer, work is done on the gas passing through the rotor, and the total temperature and total pressure increase.

Table 9.1 Property changes[a] in an isentropic compressor

Property	Inlet guide vanes	Rotor	Stator
Absolute velocity	+	+	−
Relative velocity	n/a	−	n/a
Static pressure	−	+	+
Absolute total pressure	0	+	0
Relative total pressure	n/a	0	n/a
Static temperature	−	+	0
Absolute total temperature	0	+	0
Relative total temperature	n/a	0	n/a

[a] + = increase, − = decrease, 0 = unchanged, n/a = not applicable.

9.3.3 Flow Annulus Area

For uniform total properties at a station i, the area of the flow annulus A_i can be obtained from the mass flow parameter (MFP) by using

$$A_t = \frac{\dot{m}\sqrt{T_{ti}}}{P_{ti}(\cos\alpha_i)\mathrm{MFP}(M_i)} \tag{9.8}$$

where α_i is the angle that the velocity V_i makes with the centerline of the annulus.

Example 9.1

Consider mean radius stage calculation—isentropic flow.

Given:

$$T_{t1} = 518.7°\mathrm{R}, \quad P_{t1} = 14.70\ \mathrm{psia}, \quad \omega = 1000\ \mathrm{rad/s}, \quad r = 12\ \mathrm{in.}$$
$$\alpha_1 = \alpha_3 = 40\ \mathrm{deg}, \quad \dot{m} = 50\ \mathrm{lbm/s}, \quad M_1 = M_3 = 0.7$$
$$u_2/u_1 = 1.1, \quad P_{t3}/P_{t1} = 1.3$$

Gas is air.

Note: For air, $\gamma = 1.4$, $c_p = 0.24\ \mathrm{Btu/(lbm \cdot °R)}$, $Rg_c = 1716\ \mathrm{ft^2/(s^2 \cdot °R)}$ $c_p g_c = 6006\ \mathrm{ft^2/(s^2 \cdot °R)}$

Solution:

$$T_1 = \frac{T_{t1}}{1 + [(\gamma - 1)/2]M_1^2} = -\frac{518.7°\mathrm{R}}{1 + 0.2 \times 0.7^2} = 472.4°\mathrm{R}$$

$$a_1 = \sqrt{\gamma R g_c T_1} = \sqrt{1.4 \times 1716 \times 472.4} = 1065.3\ \mathrm{ft/s}$$

$$V_1 = M_1 a_1 = 0.7 \times 1065.3\ \mathrm{ft/s} = 745.71\ \mathrm{ft/s}$$

$$u_1 = V_1 \cos\alpha_1 = 745.71\ \mathrm{ft/s} \times 0.766 = 571.21\ \mathrm{ft/s}$$

$$v_1 = V_1 \sin\alpha_1 = 745.71\ \mathrm{ft/s} \times 0.6428 = 479.34\ \mathrm{ft/s}$$

$$P_1 = \frac{P_{t1}}{\{1 + [(\gamma - 1)/2]M_1^2\}^{\gamma/(\gamma-1)}} = \frac{14.70\ \mathrm{psia}}{(1 + 0.2 + 0.7^2)^{3.5}} = 10.60\ \mathrm{psia}$$

$$\mathrm{MFP}(M_1) = 0.4859$$

$$A_1 = \frac{\dot{m}\sqrt{T_{t1}}}{P_{t1}(\cos\alpha_1)\mathrm{MFP}(M_1)} = \frac{50\sqrt{518.7}}{14.70 \times 0.7660 \times 0.4859} = 207.2\ \mathrm{in.}^2$$

$$\omega r = 1000 \times \frac{12}{12} = 1000\ \mathrm{ft/s}$$

$$v_{1R} = \omega r - v_1 = 1000 - 479.34 = 520.66\ \mathrm{ft/s}$$

$$\beta_1 = \tan^{-1}\frac{v_{1R}}{u_1} = \tan^{-1} 0.9114 = 42.35\ \mathrm{deg}$$

$$V_{1R} = \sqrt{u_1^2 + v_{1R}^2} = \sqrt{571.21^2 + 520.66^2} = 772.90 \text{ ft/s}$$

$$M_{1R} = \frac{V_{1R}}{a_1} = \frac{772.90}{1065.3} = 0.7255$$

$$T_{t1R} = T_1\left(1 + \frac{\gamma - 1}{2} M_{1R}^2\right) = 472.4(1 + 0.2 \times 0.7255^2) = 522.2^\circ\text{R}$$

$$P_{t1R} = P_1\left(\frac{T_{t1R}}{T_1}\right)^{\gamma/(\gamma-1)} = 10.60\left(\frac{522.1}{472.4}\right)^{3.5} = 15.04 \text{ psia}$$

$$P_{t2} = P_{t3} = 1.3 \times 14.70 = 19.11 \text{ psia}$$

$$T_{t3} = T_{t2} = T_{t1}\left(\frac{P_{t2}}{P_{t1}}\right)^{(\gamma-1)/\gamma} = 518.7(1.3)^{1/3.5} = 559.1^\circ\text{R}$$

$$\tan\beta_2 = \frac{u_1}{u_2}\left[\tan\beta_1 - \frac{g_c c_p}{\omega r\, u_1}(T_{t2} - T_{t1})\right]$$

$$= \frac{1}{1.1}\left[\tan 42.35 - \frac{6006}{1000 \times 571.21}(559.1 - 518.7)\right] = 0.4425$$

$$\beta_2 = 23.87 \text{ deg}$$

$$u_2 = \frac{u_2}{u_1} u_1 = 1.1 \times 571.21 = 628.33 \text{ ft/s}$$

$$v_{2R} = u_2 \tan\beta_2 = 628.33 \times 0.4425 = 278.04 \text{ ft/s}$$

$$V_{2R} = \sqrt{u_2^2 + v_{2R}^2} = \sqrt{628.33^2 + 278.04^2} = 687.10 \text{ ft/s}$$

$$v_2 = \omega r - v_{2R} = 1000 - 278.04 = 721.96 \text{ ft/s}$$

$$\alpha_2 = \tan^{-1}\frac{v_2}{u_2} = \tan^{-1}\frac{721.96}{628.33} = 48.97 \text{ deg}$$

$$V_2 = \sqrt{u_2^2 + v_2^2} = \sqrt{628.33^2 + 721.96^2} = 957.10 \text{ ft/s}$$

$$T_{t2R} = T_{t1R} = 552.5^\circ\text{R}$$

$$P_{t2R} = P_{t1R} = 15.04 \text{ psia}$$

$$T_2 = T_{t2} - \frac{V_2^2}{2 g_c c_p} = 559.1 - \frac{957.10^2}{2 \times 6006} = 482.8^\circ\text{R}$$

$$P_2 = P_{t2}\left(\frac{T_2}{T_{t2}}\right)^{\gamma/(\gamma-1)} = 19.11\left(\frac{482.8}{559.1}\right)^{3.5} = 11.43 \text{ psia}$$

$$a_2 = \sqrt{\gamma R g_c T_2} = \sqrt{1.4 \times 1746 \times 482.8} = 1077.0 \text{ ft/s}$$

$$M_2 = \frac{V_2}{a_2} = \frac{957.10}{1077.0} = 0.8887$$

$$M_{2R} = \frac{V_{2R}}{a_2} = \frac{687.10}{1077.0} = 0.6380$$

$$\text{MFP}(M_2) = 0.5260$$

$$A_2 = \frac{\dot{m}\sqrt{T_{t2}}}{P_{t2}(\cos\alpha_2)\text{MFP}(M_2)} = \frac{50\sqrt{559.1}}{19.11 \times 0.6566 \times 0.5260} = 179.1 \text{ in.}^2$$

$$T_3 = \frac{T_{t3}}{1 + [(\gamma - 1)/2]M_3^2} = \frac{559.1^\circ\text{R}}{1 + 0.2 \times 0.7^2} = 509.2^\circ\text{R}$$

$$P_3 = P_{t3}\left(\frac{T_3}{T_{t3}}\right)^{\gamma/(\gamma-1)} = 19.11\left(\frac{509.2}{559.1}\right)^{3.5} = 13.77 \text{ psia}$$

$$a_3 = \sqrt{\gamma R g_c T_3} = \sqrt{1.4 \times 1716 \times 509.2} = 1106.03 \text{ ft/s}$$

$$V_3 = M_3 a_3 = 0.7 \times 1106.03 = 774.22 \text{ ft/s}$$

$$u_3 = V_3 \cos\alpha_3 = 593.09 \text{ ft/s}$$

$$v_3 = V_3 \sin\alpha_3 = 497.66 \text{ ft/s}$$

$$A_3 = \frac{\dot{m}\sqrt{T_{t3}}}{P_{t3}(\cos\alpha_3)\text{MFP}(M_3)} = \frac{50\sqrt{559.1}}{19.11 \times 0.766 \times 0.4859} = 165.3 \text{ in.}^2$$

The results of this stage calculation for isentropic flow are summarized in Table 9.2, with the given data shown in bold type (SI results are shown within parentheses). Note that the flow through the rotor is adiabatic in the relative reference frame and, through the stator, is adiabatic in the absolute reference frame. Figure 9.13 is a representation of the flow properties for an isentropic stage on a *T-s* diagram.

9.3.4 Stage Parameters

9.3.4.1 Efficiencies. Several efficiencies are used to compare the performance of compressor stage designs. The two efficiencies most commonly used are stage efficiency and polytropic efficiency. The *stage efficiency* of an adiabatic compressor is defined as the ratio of the ideal work per unit mass to the actual work per unit mass between the same total pressures, or

$$\eta_s = \frac{h_{t3s} - h_{t1}}{h_{t3} - h_{t1}} \tag{9.9}$$

Table 9.2 Results for Example 9.1 axial-flow compressor stage calculation, insentropic flow

Property		Station 1	1*R*	2*R*	2	3
T_1	°R	**518.7**	522.1	522.1	559.1	559.1
	(K)	**(288.2)**	(290.1)	(290.1)	(310.6)	(310.6)
T	°R	472.4	472.4	482.8	482.8	509.2
	(K)	(262.4)	(262.4)	(268.2)	(268.2)	(282.9)
P_t	psia	**14.70**	15.04	15.04	19.11	**19.11**
	(kPa)	**(101.3)**	(103.7)	(103.7)	(131.7)	**(131.7)**
P	psia	10.60	10.60	11.43	11.43	13.77
	(kPa)	(73.05)	(73.05)	(78.85)	(78.85)	(94.96)
M		**0.700**	0.7255	0.6380	0.8887	0.700
V	ft/s	745.71	772.90	687.10	957.10	774.22
	(m/s)	(227.30)	(235.58)	(209.43)	(291.73)	(235.99)
u	ft/s	571.21	571.21	628.33	628.33	593.09
	(m/s)	(174.11)	(174.11)	(191.53)	(191.52)	(180.78)
v	ft/s	479.34	520.66	278.04	721.96	497.66
	(m/s)	(146.10)	(158.70)	(84.75)	(220.06)	(151.69)
α	deg	**40.00**	——	——	48.97	**40.00**
β	deg	——	42.35	23.87	——	——

For a calorically perfect gas, this simplifies to

$$\eta_s = \frac{T_{t3s} - T_{t1}}{T_{t3} - T_{t1}} = \frac{(P_{t3}/P_{t1})^{(\gamma-1)/\gamma} - 1}{T_{t3}/T_{t1} - 1} \tag{9.10}$$

where the states used in this equation for stage efficiency are plotted on the *T-s* diagram of Fig. 9.14a.

The *polytropic efficiency* of an adiabatic compressor is defined as the ratio of the ideal work per unit mass to the actual work per unit mass for a differential

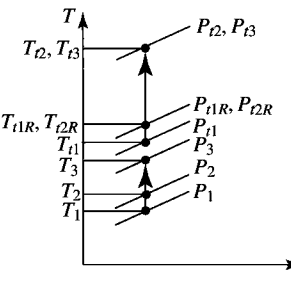

Fig. 9.13 Property changes of an isentropic compressor stage.

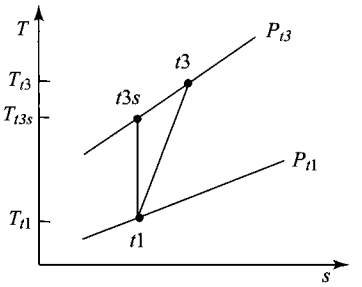

Fig. 9.14a Stages for definition of compressor stage efficiency.

pressure change, or

$$e_c = \frac{dh_{ti}}{dh_t} = \frac{dT_{ti}}{dT_t} = \frac{dT_{ti}/T_t}{dT_t/T_t} = \frac{\gamma - 1}{\gamma}\frac{dP_t/P_t}{dT_t/T_t}$$

For a constant polytropic efficiency e_c, integration between states $t1$ and $t3$ gives

$$e_c = \frac{\gamma - 1}{\gamma}\frac{\ell n\,(P_{t3}/P_{t1})}{\ell n\,(T_{t3}/T_{t1})} \tag{9.11}$$

A useful expression for stage efficiency, in terms of the pressure ratio and polytropic efficiency, can be easily obtained by using Eqs. (9.10) and (9.11). Solving Eq. (9.11) for the temperature ratio and substituting into Eq. (9.10) give

$$\eta_s = \frac{(P_{t3}/P_{t1})^{(\gamma-1)/\gamma} - 1}{(P_{t3}/P_{t1})^{(\gamma-1)/(\gamma e_c)} - 1} \tag{9.12}$$

In the limit, as the pressure ratio approaches 1, the stage efficiency approaches the polytropic efficiency. The variation in stage efficiency with stage pressure ratio is plotted in Fig. 9.14b for constant polytropic efficiency.

The compressor polytropic efficiency is useful in preliminary design of compressors for gas turbine engines to predict the compressor efficiency for a given level of technology. The value of the polytropic efficiency is mainly a

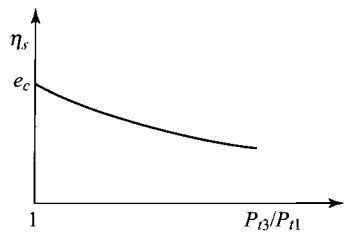

Fig. 9.14b Variation of stage efficiency with pressure ratio.

function of the technology level (see Table 6.2). Axial-flow compressors designed in the 1980s have a polytropic efficiency of about 0.88, whereas the compressors being designed today have a polytropic efficiency of about 0.9.

9.3.4.2 Degree of reaction. For compressible flow, the *degree of reaction* is defined as

$$^{\circ}R_c = \frac{\text{rotor static enthalpy rise}}{\text{stage static enthalpy rise}} = \frac{h_2 - h_l}{h_3 - h_1} \tag{9.13a}$$

For a calorically perfect gas, the static enthalpy rises in the equation become static temperature rises, and the degree of reaction is

$$^{\circ}R_c = \frac{T_2 - T_1}{T_3 - T_1} \tag{9.13b}$$

In the general case, it is desirable to have the degree of reaction in the vicinity of 0.5 because the rotor and stator rows then will "share the burden" of increasing the enthalpy of the flow. The degree of reaction for the stage data of Example 9.1 is approximately 0.28, which means the majority of the static temperature rise occurs in the stator.

9.3.4.3 Cascade airfoil nomenclature and loss coefficient. Figure 9.15 shows the cascade airfoil nomenclature and the airfoil and flow angles. Subscripts i and e are used for the inlet and exit states, respectively. The ratio of the airfoil chord c to the airfoil spacing s is called the *solidity* σ, which typically is near unity. At design, the incidence angle is nearly zero. The exit deviation can be determined by using Carter's rule:

$$\delta_c = \frac{\gamma_i - \gamma_e}{4\sqrt{\sigma}} \tag{9.14}$$

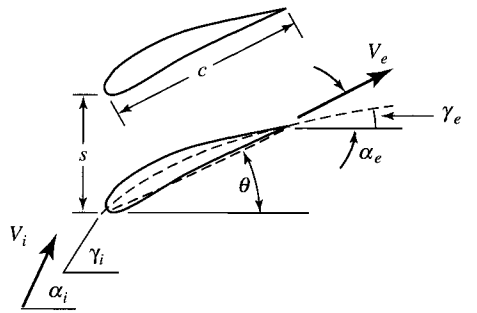

$\alpha_i - \alpha_e$ = turning angle
$\gamma_i - \gamma_e$ = airfoil camber angle
$\alpha_i - \gamma_i$ = incidence angle
$\alpha_e - \gamma_e = \delta_c$ = exit deviation
$\sigma = c/s$ = solidity
θ = stagger angle

Fig. 9.15 Cascade airfoil nomenclature.

The airfoil angles of both the rotor and the stator can be calculated from the flow angles, given the incidence angle and solidity for each. To obtain the exit airfoil angle, Eq. (9.14) is rearranged to give

$$\gamma_e = \frac{4\alpha_e\sqrt{\sigma} - \gamma_i}{4\sqrt{\sigma} - 1}$$

For the data of Example 9.1, we obtain the following airfoil angles, assuming a solidity of 1 and a zero incidence angle for both rotor and stator:

Rotor	$\gamma_i = 42.35\,\text{deg}$	$\gamma_e = 17.71\,\text{deg}$
Stator	$\gamma_i = 48.97\,\text{deg}$	$\gamma_e = 37.01\,\text{deg}$

Losses in cascade airfoils are normally quantified in terms of the drop in total pressure divided by the dynamic pressure of the incoming flow. This ratio is called the *total pressure loss coefficient* and is defined as

$$\phi_c \equiv \frac{P_{ti} - P_{te}}{\rho V_i^2/(2g_c)} \tag{9.15}$$

Figure 9.16 shows the typical total pressure loss behavior of compressor airfoils obtained from cascade tests. Note that these losses increase with Mach number and incidence angle. The loss coefficients shown in Fig. 9.16 include only the two-dimensional or "profile" losses and must be increased in compressor stage design to account for end losses (e.g., tip leakage, wall boundary layer, or cavity leakage).

9.3.4.4 Diffusion Factor. The total pressure loss of a cascade depends on many factors. The pressure and velocity distribution about a typical cascade airfoil is shown in Fig. 9.17. The upper (suction) side of the compressor blade has a large static pressure rise (due to the deceleration from $V_{\max}$ to V_e), which

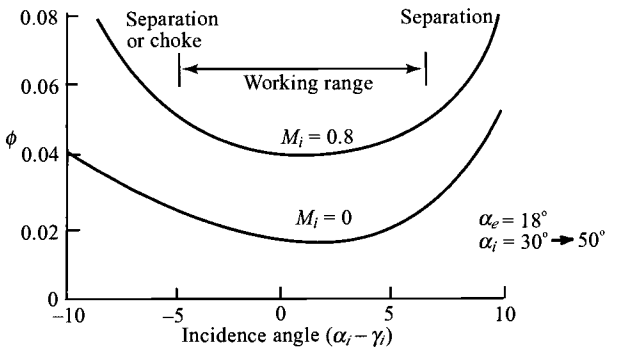

Fig. 9.16 Compressor cascade experimental behavior.

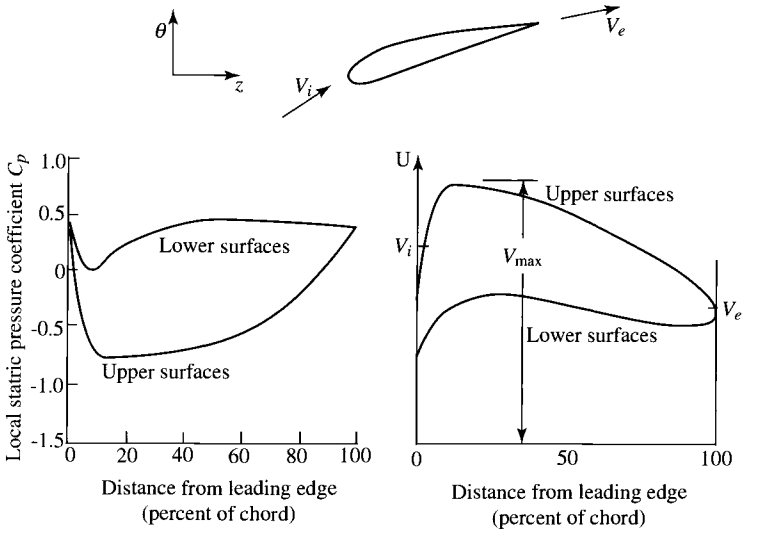

Fig. 9.17 Compressor airfoil pressure and velocity distribution (Ref. 41).

can cause the viscous boundary layer to separate. Boundary-layer separation is not desirable because of the associated higher losses in total pressure.

Cascade test results (see Fig. 9.18) show a direct correlation between total pressure loss and the deceleration (diffusion) on the upper (suction) side of blades. The amount of diffusion is measured by the diffusion factor D. The expression for the diffusion factor is based on the fact that the diffusion of the flow on the suction surface is approximated as

$$D \approx \frac{V_{\max} - V_e}{V_{\text{av}}} \approx \frac{V_{\max} - V_e}{V_i}$$

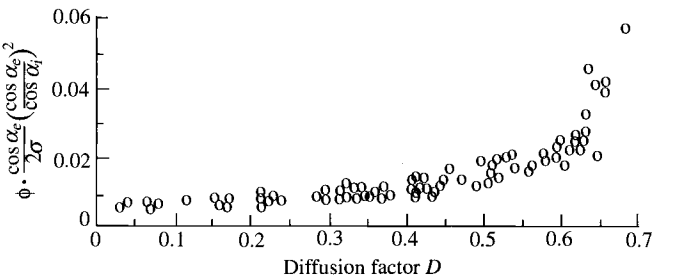

Fig. 9.18 Total pressure loss vs diffusion factor for typical compressor airfoil (Ref. 41).

where

$$V_{\max} \approx V_i + f\left(\frac{\Delta v}{\sigma}\right) \approx V_i + \frac{|\Delta v|}{2\sigma}$$

Thus the *diffusion factor D* is defined by

$$D \equiv 1 - \frac{V_e}{V_i} + \frac{|v_i - v_e|}{2\sigma V_i} \tag{9.16}$$

where the subscripts i and e refer to the inlet and exit, respectively. Note that for a compressor stage, there is a diffusion factor for the rotor and another for the stator.

The diffusion factor for the rotor D_r is in terms of the relative velocities at stations 1 and 2, or

$$D_r = 1 - \frac{V_{2R}}{V_{1R}} + \frac{|v_{1R} - v_{2R}|}{2\sigma V_{1R}} \tag{9.17}$$

The diffusion factor for the stator D_s is in terms of the absolute velocities at stations 2 and 3, or

$$D_s = 1 - \frac{V_3}{V_2} + \frac{|v_2 - v_3|}{2\sigma V_2} \tag{9.18}$$

Figure 9.18 shows a loss parameter vs diffusion factor for typical compressor cascade airfoils. This figure is useful for estimating total pressure losses during preliminary design. Because the total pressure loss increases dramatically for diffusion factors above 0.6, *designs of axial compressors are limited to diffusion factors less than or equal to 0.6*. The diffusion factors for the data of Example 9.1, with a solidity of 1, are

$$D_r = 1 - \frac{V_{2R}}{V_{1R}} + \frac{|v_{1R} - v_{2R}|}{2\sigma V_{1R}} = 1 - \frac{687.10}{772.90} + \frac{|520.66 - 278.04|}{2 \times 1 \times 772.90} = 0.2680$$

$$D_s = 1 - \frac{V_3}{V_2} + \frac{|v_2 - v_3|}{2\sigma V_2} = 1 - \frac{774.22}{957.10} + \frac{|721.96 - 497.66|}{2 \times 1 \times 957.10} = 0.3083$$

These values of diffusion factor show that both the rotor and stator of the example problem are lightly loaded.

9.3.4.5 Stage loading and flow coefficients. The ratio of the stage work to rotor speed squared is called the *stage loading coefficient* and is defined as

$$\psi \equiv \frac{g_c \Delta h_t}{(\omega r)^2} = \frac{g_c \Delta h_t}{U^2} \tag{9.19}$$

For a calorically perfect gas, the stage loading coefficient can be written as

$$\psi = \frac{g_c c_p \, \Delta T_t}{(\omega r)^2} = \frac{g_c c_p \, \Delta T_t}{U^2} \tag{9.20}$$

Modern axial-flow compressors used for aircraft gas turbine engines have stage loading coefficients in the range of 0.3–0.35 at the mean radius. For Example 9.1, the stage loading coefficient is 0.24, a low value.

The ratio of the axial velocity to the rotor speed is called the *flow coefficient* and is defined as

$$\Phi \equiv \frac{u_1}{\omega r} = \frac{u_1}{U} \tag{9.21}$$

The flow coefficients for modern axial-flow compressors of aircraft gas turbine engines are in the range of 0.45–0.55 at the mean radius. For Example 9.1, the flow coefficient is 0.57, a high value.

Equations (9.20) and (9.21) can be substituted into Eqs. (9.7a) and (9.7b), respectively, to give

$$\frac{\psi}{\Phi} = \tan\beta_1 - \frac{u_2}{u_1}\tan\beta_2 \quad \text{and} \quad \frac{\psi}{\Phi} = \frac{u_2}{u_1}\tan\alpha_2 - \tan\alpha_1 \tag{9.22}$$

Equation (9.22) is plotted in Fig. 9.19 for the case of constant axial velocity ($u_1 = u_2$). This figure can be used to determine the ratio of the stage loading

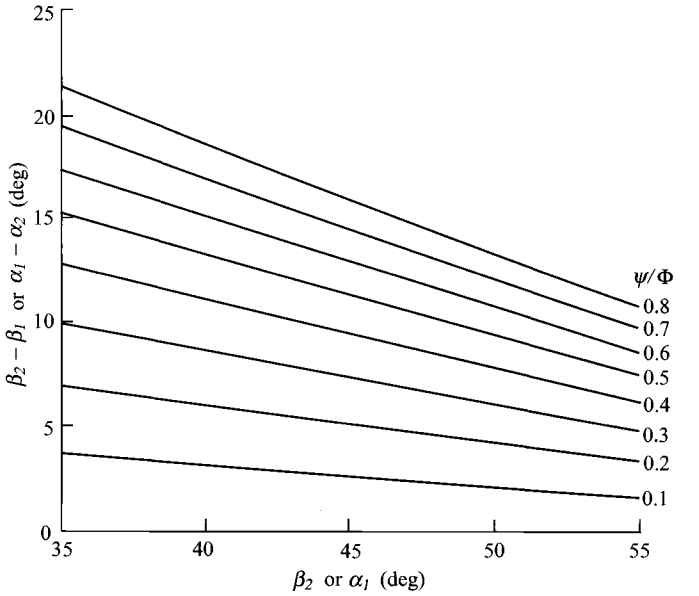

Fig. 9.19 Stage flow angles vs Ψ/Φ for constant axial velocity.

coefficient to the flow coefficient from stage flow angles. This figure also gives the combinations of flow angles that will give a desired value of ψ/Φ.

The flow coefficient can be expressed in terms of the flow angles (α_1 and β_1). From the velocity triangles, we have

$$U = u_1 \tan \alpha_1 + u_1 \tan \beta_1$$

Solving for the ratio u_1/U, we get

$$\Phi = \frac{1}{\tan \alpha_1 + \tan \beta_1} \tag{9.23}$$

This equation is plotted in Fig. 9.20. Given the flow angles (α_1 and, β_1), one can use Eq. (9.23) or Fig. 9.20 to determine the flow coefficient. On the other hand, Fig. 9.20 can be used to find the combination of the flow angles (α_1 and β_1) that gives a desired flow coefficient.

9.3.4.6 Stage pressure ratio. Equation (9.10) can be rewritten as

$$\frac{P_{t3}}{P_{t1}} = \left(1 + \eta_s \frac{\Delta T_t}{T_{t1}}\right)^{\gamma/(\gamma-1)} \tag{9.24}$$

Likewise, Eq. (9.11) can be rewritten as

$$\frac{P_{t3}}{P_{t1}} = \left(\frac{T_{t2}}{T_{t1}}\right)^{\gamma e_c/(\gamma-1)} = \left(1 + \frac{\Delta T_t}{T_{t1}}\right)^{\gamma e_c/(\gamma-1)} \tag{9.25}$$

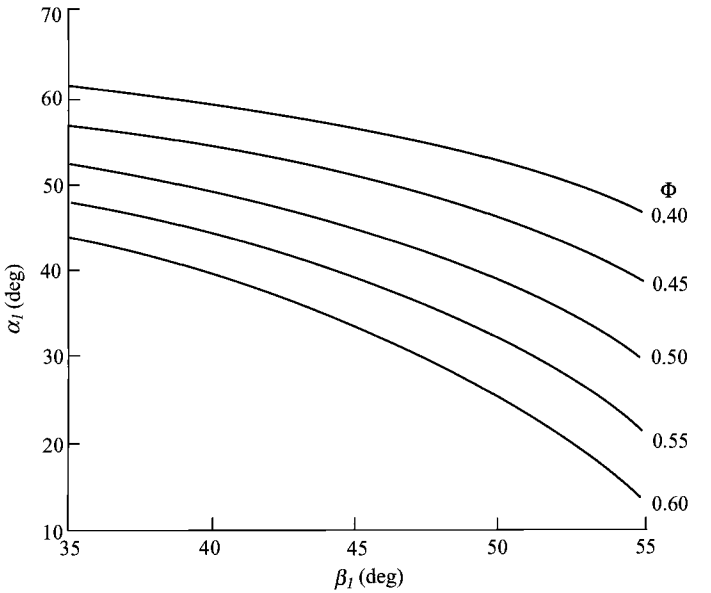

Fig. 9.20 Flow coefficient Φ vs flow angles α_1 and β_1.

The stage pressure ratio can be calculated given the stage total temperature rise and the stage efficiency or polytropic efficiency from Eq. (9.24) or (9.25), respectively. We can see from these equations and Eq. (9.20) that a high stage pressure ratio requires high work loading (change in T_t).

When the stage efficiency and polytropic efficiency are unknown, the stage pressure ratio can be determined by using loss coefficients based on cascade data and other losses. The total pressure for a compressor stage can be written in terms of loss coefficients of the rotor ϕ_{cr} and stator ϕ_{cs}. Noting that the total pressure loss of the rotor is based on the relative velocity, we write

$$\phi_{cr} \equiv \frac{P_{t1R} - P_{t2R}}{\rho_1 V_{1R}^2/(2g_c)} \tag{9.26}$$

Then

$$\frac{P_{t2R}}{P_{t1R}} = 1 - \phi_{cr}\frac{\rho_1 V_{1R}^2}{2g_c P_{t1R}} = 1 - \phi_{cr}\frac{\gamma P_1 M_{1R}^2}{2P_{t1R}}$$

or

$$\frac{P_{t2R}}{P_{t1R}} = 1 - \phi_{cr}\frac{\gamma M_{1R}^2/2}{\{1 + [(\gamma - 1)/2]M_{1R}^2\}^{\gamma/(\gamma-1)}} \tag{9.27}$$

Likewise,

$$\phi_{cs} \equiv \frac{P_{t2} - P_{t3}}{\rho_2 V_2^2/(2g_c)} \tag{9.28}$$

then

$$\frac{P_{t3}}{P_{t2}} = 1 - \phi_{cs}\frac{\gamma M_2^2/2}{\{1 + [(\gamma - 1)/2]M_2^2\}^{\gamma/(\gamma-1)}} \tag{9.29}$$

The total pressure ratio of a stage can be written in the following form:

$$\frac{P_{t3}}{P_{t1}} = \left(\frac{P_{t3}}{P_{t2}}\right)_{\phi_{cs},\, M_2}\left(\frac{P_{t2}}{P_2}\right)_{M_2}\left(\frac{P_2}{P_{t2R}}\right)_{M_{2R}}\left(\frac{P_{t2R}}{P_{t1R}}\right)_{\phi_{cr},\, M_{1R}} \times \left(\frac{P_{t1R}}{P_1}\right)_{M_1 R}\left(\frac{\rho_1}{P_{t1}}\right)_{M_1} \tag{9.30}$$

where the subscripts for the ratio inside the parentheses indicate the variables of the ratio. The loss coefficient of the rotor ϕ_{cr} required in Eq. (9.27) is obtained from cascade data with allowance for other losses (tip leakage, side wall boundary layer, etc.) and can range in value from 0.05 to 0.12. Likewise, the stator's loss coefficient ϕ_{cs} required in Eq. (9.28) is also obtained from cascade data with allowance for other losses and can range in value from 0.03 to 0.06.

Figure 9.21 is a *T-s* diagram of a compressor stage with losses. It shows the losses in total pressure in the rotor and the stator. Comparison with the *T-s* diagram for an ideal compressor stage (Fig. 9.13) can help one see the effects of losses on the process through a compressor stage.

9.3.4.7 Blade Mach number M_b. Equation (9.7) can be written in terms of the flow angles (α_1 and β_2) and rearranged to give

$$\frac{\Delta T_t}{T_{t1}} = \frac{(\omega r)^2}{g_c c_p T_{t1}} \left[1 - \frac{u_2}{\omega r} \left(\tan \beta_2 + \frac{u_1}{u_2} \tan \alpha_1 \right) \right]$$

or

$$\frac{\Delta T_t}{T_{t1}} = \frac{(\omega r)^2}{g_c c_p T_1} \frac{T_1}{T_{t1}} \left[1 - \frac{u_2}{\omega r} \left(\tan \beta_2 + \frac{u_1}{u_2} \tan \alpha_1 \right) \right]$$

Note that

$$\frac{(\omega r)^2}{g_c c_p T_1} = \frac{\gamma R}{c_p} \frac{(\omega r)^2}{\gamma R g_c T_1} = (\gamma - 1) \frac{(\omega r)^2}{a_1^2} = (\gamma - 1) M_b^2$$

where M_b is the blade tangential Mach number based on the upstream speed of sound a_1,

$$\frac{T_1}{T_{t1}} = \frac{1}{1 + [(\gamma - 1)/2] M_1^2} \quad \text{and} \quad \frac{u_2}{\omega r} = (\cos \alpha_1) \frac{M_1}{M_b} \frac{u_2}{u_1}$$

Then

$$\frac{\Delta T_t}{T_{t1}} = \frac{(\gamma - 1) M_b^2}{1 + [(\gamma - 1)/2] M_1^2} \left[1 - (\cos \alpha_1) \frac{M_1}{M_b} \left(\frac{u_2}{u_1} \tan \beta_2 + \tan \alpha_1 \right) \right] \tag{9.31}$$

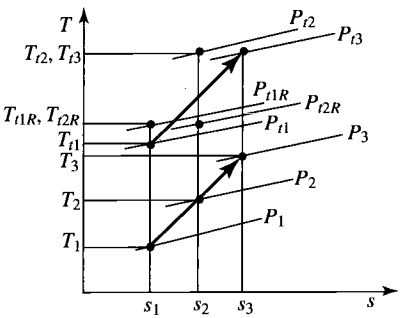

Fig. 9.21 The *T-s* diagram of a typical compressor stage with losses.

If we consider that the flow angles and the velocity ratio u_2/u_1 are functions of the geometry, then the stage temperature rise is mainly a function of M_b and the ratio M_1/M_b. From Eq. (9.31), we can see that high M_b is desirable to give higher stage temperature rise. The blade Mach number for Example 9.1 is about 0.94.

Example 9.2

Consider mean radius stage calculation—flow with losses.

Given:

$$T_{t1} = 288.16\ \text{K}, \quad P_{t1} = 101.3\ \text{kPa}, \quad \omega = 1000\ \text{rad/s}$$
$$r = 0.3048\ \text{m}, \quad \alpha_1 = \alpha_3 = 40\ \text{deg}, \quad \sigma = 1$$
$$\dot{m} = 22.68\ \text{kg/s}, \quad M_1 = M_3 = 0.7, \quad u_2/u_1 = 1.1$$
$$\Delta T_t = 22.43\ \text{K}, \quad \phi_{cr} = 0.09, \quad \phi_{cs} = 0.03$$

Gas is air. The input data are the same as in Example 9.1 with the same ΔT_t specified.

Note: For air, $\gamma = 1.4$, $c_p = 1.004\ \text{kJ/(kg} \cdot \text{K)}$, and $R = 0.287\ \text{kJ/(kg} \cdot {}^\circ\text{R)}$.

Solution:

$$T_1 = \frac{T_{t1}}{1 + [(\gamma - 1)/2]M_1^2} = \frac{288.16\ \text{K}}{1 + 0.2 \times 0.7^2} = 262.44\ \text{K}$$

$$a_1 = \sqrt{\gamma R g_c T_1} = \sqrt{1.4 \times 287 \times 1 \times 262.44} = 324.73\ \text{m/s}$$

$$V_1 = M_1 a_1 = 0.7 \times 324.73 = 227.31\ \text{m/s}$$

$$u_1 = V_1 \cos\alpha_1 = 227.31 \times 0.7660 = 174.13\ \text{m/s}$$

$$v_1 = V_1 \sin\alpha_1 = 227.31 \times 0.6428 = 146.11\ \text{m/s}$$

$$P_1 = \frac{P_{t1}}{\{1 + [(\gamma - 1)/2]M_1^2\}^{\gamma/(\gamma-1)}}$$

$$= \frac{101.3\ \text{kPa}}{(1 + 0.2 \times 0.7^2)^{3.5}} = 73.03\ \text{kPa}$$

$$\text{MFP}(M_1) = 0.03700$$

$$A_1 = \frac{\dot{m}\sqrt{T_{t1}}}{P_{t1}(\cos\alpha_1)\text{MFP}(M_1)} = \frac{22.68\sqrt{288.16}}{101,300 \times 0.7660 \times 0.0370}$$

$$= 0.134\ \text{m}^2$$

$$\omega r = 1000 \times 0.3048 = 304.8\ \text{m/s}$$

$$v_{1R} = \omega r - v_1 = 304.80 - 146.11 = 158.69\ \text{m/s}$$

$$\beta_1 = \tan^{-1}\frac{v_{1R}}{u_1} = \tan^{-1} 0.9113 = 42.34 \text{ deg}$$

$$V_{1R} = \sqrt{u_1^2 + v_{1R}^2} = \sqrt{174.13^2 + 158.69^2} = 235.59 \text{ m/s}$$

$$M_{1R} = \frac{V_{1R}}{a_1} = \frac{235.59}{324.73} = 0.7255$$

$$T_{t1R} = T_1\left(1 + \frac{\gamma - 1}{2}M_{1R}^2\right) = 262.44(1 + 0.2 \times 0.7255^2) = 290.07 \text{ K}$$

$$P_{t1R} = P_1\left(\frac{T_{t1R}}{T_1}\right)^{\gamma/(\gamma-1)} = 73.03\left(\frac{290.07}{262.44}\right)^{3.5} = 103.67 \text{ kPa}$$

$$P_{t2R} = P_{t1R}\left(\frac{P_{t2R}}{P_{t1R}}\right)_{\phi_{cr}, M_{1R}}$$

$$= P_{t1R}\left(1 - \phi_{cr}\frac{\gamma M_{1R}^2/2}{\{1 + [(\gamma - 1)/2]M_{1R}^2\}^{\gamma/(\gamma-1)}}\right)$$

$$P_{t2R} = 103.67\left[1 - \frac{0.09 \times 0.7 \times 0.7255^2}{(1 + 0.2 \times 0.7255^2)^{3.5}}\right]$$

$$= 103.67 \times 0.9766 = 101.24 \text{ kPa}$$

$$T_{t2R} = T_{t1R} = 290.07 \text{ K}$$

$$T_{t2} = T_{t1} + \Delta T_t = 288.16 + 22.43 = 310.59 \text{ K}$$

$$\tan\beta_2 = \frac{u_1}{u_2}\left[\tan\beta_1 - \frac{g_c c_p}{\omega r u_1}(T_{t2} - T_{t1})\right]$$

$$\tan\beta_2 = \frac{1}{1.1}\left[\tan 42.34 - \frac{1004}{304.8 \times 174.13}(310.59 - 288.16)\right]$$

$$= 0.4426$$

$$\beta_2 = 23.87 \text{ deg}$$

$$u_2 = \frac{u_2}{u_1}u_1 = 1.1 \times 174.13 = 191.54 \text{ m/s}$$

$$v_{2R} = u_2 \tan\beta_2 = 191.54 \times 0.4426 = 84.78 \text{ m/s}$$

$$V_{2R} = \sqrt{u_2^2 + v_{2R}^2} = \sqrt{191.54^2 + 84.78^2} = 209.46 \text{ m/s}$$

$$v_2 = \omega r - v_{2R} = 304.80 - 84.78 = 220.02 \text{ m/s}$$

$$\alpha_2 = \tan^{-1}\frac{v_2}{u_2} = \tan^{-1}\frac{220.02}{191.54} = 48.96 \text{ deg}$$

$$V_2 = \sqrt{u_2^2 + v_2^2} = \sqrt{191.54^2 + 220.02^2} = 291.71\,\text{m/s}$$

$$T_2 = T_{t2} - \frac{V_2^2}{2g_c c_p} = 310.59 - \frac{291.71^2}{2 \times 1 \times 1004} = 268.21\,\text{K}$$

$$P_2 = P_{t2R}\left(\frac{T_2}{T_{t2R}}\right)^{\gamma/(\gamma-1)} = 101.24\left(\frac{268.21}{290.07}\right)^{3.5} = 76.96\,\text{kPa}$$

$$a_2 = \sqrt{\gamma R g_c T_2} = \sqrt{1.4 \times 287 \times 268.21} = 328.28\,\text{m/s}$$

$$M_2 = \frac{V_2}{a_2} = \frac{291.71}{328.28} = 0.8886$$

$$M_{2R} = \frac{V_{2R}}{a_2} = \frac{209.46}{328.28} = 0.6381$$

$$P_{t2} = P_2\left(\frac{T_{t2}}{T_2}\right)^{\gamma/(\gamma-1)} = 76.96\left(\frac{310.59}{268.21}\right)^{3.5} = 128.61\,\text{kPa}$$

$$\text{MFP}(M_2) = 0.04004$$

$$A_2 = \frac{\dot{m}\sqrt{T_{t2}}}{P_{t2}(\cos\alpha_2)\text{MFP}(M_2)} = \frac{22.68\sqrt{310.59}}{128{,}610 \times 0.65659 \times 0.04004}$$
$$= 0.118\,\text{m}^2$$

$$T_{t3} = T_{t2} = T_{t1} + \Delta T_t = 310.59\,\text{K}$$

$$T_3 = \frac{T_{t3}}{1 + [(\gamma-1)/2]M_3^2} = \frac{310.59\,\text{K}}{1 + 0.2 \times 0.7^2} = 282.87\,\text{K}$$

$$P_{t3} = P_{t2}\left(\frac{P_{t3}}{P_{t2}}\right)_{\phi_{cs}, M_2}$$
$$= P_{t2}\left(1 - \phi_{cs}\frac{\gamma M_2^2/2}{\{1 + [(\gamma-1)/2]M_2^2\}^{\gamma/(\gamma-1)}}\right)$$
$$= 128.61\left[1 - \frac{0.03 \times 0.7 \times 0.8887^2}{(1 + 0.2 \times 0.8887^2)^{3.5}}\right]$$
$$= 128.61 \times 0.09900 = 127.32\,\text{kPa}$$

$$P_3 = P_{t3}\left(\frac{T_3}{T_{t3}}\right)^{\gamma/(\gamma-1)} = 127.32\left(\frac{282.87}{310.59}\right)^{3.5} = 91.79\,\text{kPa}$$

$$a_3 = \sqrt{\gamma R g_c T_3} = \sqrt{1.4 \times 287 \times 282.87} = 337.13\,\text{m/s}$$

$$V_3 = M_3 a_3 = 0.7 \times 337.13 = 235.99\,\text{m/s}$$

$$u_3 = V_3 \cos \alpha_3 = 180.78 \text{ m/s}$$

$$v_3 = V_3 \sin \alpha_3 = 151.69 \text{ m/s}$$

$$A_3 = \frac{\dot{m}\sqrt{T_{t3}}}{P_{t3}(\cos \alpha_3)\text{MFP}(M_3)} = \frac{22.68\sqrt{310.59}}{127{,}320 \times 0.7660 \times 0.0370} = 0.111 \text{ m}^2$$

$$^{\circ}R_c = \frac{T_2 - T_1}{T_3 - T_1} = \frac{268.21 - 262.44}{282.87 - 262.44} = 0.2824$$

$$D_r = 1 - \frac{V_{2R}}{V_{1R}} + \frac{|v_{1R} - v_{2R}|}{2\sigma V_{1R}} = 1 - \frac{209.46}{235.59} + \frac{|158.69 - 84.78|}{2 \times 1 \times 235.59} = 0.2678$$

$$D_s = 1 - \frac{V_3}{V_2} + \frac{|v_2 - v_3|}{2\sigma V_2} = 1 - \frac{235.99}{291.71} + \frac{|220.02 - 151.69|}{2 \times 1 \times 291.71} = 0.3081$$

$$\eta_s = \frac{(P_{t3}/P_{t1})^{(\gamma-1)/\gamma} - 1}{T_{t3}/T_{t1} - 1} = \frac{(127.32/101.30)^{1/3.5} - 1}{310.59/288.16} = 0.8672$$

$$e_c = \frac{\gamma - 1}{\gamma} \frac{\ell n(P_{t3}/P_{t1})}{\ell n(T_{t3}/T_{t1})} = \frac{1}{3.5} \frac{\ell n(127.32/101.30)}{\ell n(310.59/288.16)} = 0.8714$$

$$\psi = \frac{g_c c_p \Delta T_t}{(\omega r)^2} = \frac{1 \times 1004 \times 22.43}{304.8^2} = 0.2424$$

$$\Phi = \frac{u_1}{\omega r} = \frac{174.13}{304.8} = 0.5713$$

The results of this example stage calculation with losses are summarized in Table 9.3, with the given data listed in boldface type (results in English units are shown within parentheses). One sees, by comparison with the isentropic flow results of Example 9.1 (see Table 9.2), that all the properties are the same except the total and static pressures at stations $2R$, 2, and 3. One might also want to compare the change in flow properties listed in Table 9.3 with those sketched in Fig. 9.21.

With losses, the resulting stage pressure ratio of Example 9.2 is 1.257. Without losses, the same amount of work per unit mass gives a pressure ratio of 1.300 for Example 9.1. Also note that the flow areas at stations 2 and 3 are larger in Example 9.2 than in Example 9.1 because of the lower total pressures resulting from losses.

9.3.5 Repeating-Stage, Repeating-Row, Mean-Line Design

The analysis and design of an axial-flow compressor is complex with many design choices. To simplify the design, we will consider a stage (Fig. 9.22) whose exit velocity and flow angle equal those at its inlet (repeating stage), made up of "repeating" (i.e., mirror-image) rows of airfoils. The analysis will

Table 9.3 Results for Example 9.2 axial-flow compressor stage calculation, flow with loss

Property		Station 1	1*R*	2*R*	2	3
T_t	K	**288.2**	290.1	290.1	310.6	**310.6**
	(°R)	(518.7)	(522.1)	(522.1)	(559.1)	(559.1)
T	K	262.4	262.4	268.2	268.2	282.9
	(°R)	(472.4)	(472.4)	(482.8)	(482.8)	(509.2)
P_t	kPa	**101.3**	103.7	101.2	128.6	127.3
	(psia)	(14.69)	(15.04)	(14.68)	(18.65)	(18.46)
P	kPa	73.03	73.03	76.96	76.96	91.79
	(psia)	(10.59)	(10.59)	(11.16)	(11.16)	(13.31)
M		**0.700**	0.7255	0.6381	0.8886	**0.700**
V	m/s	227.31	235.59	209.46	291.71	235.99
	(ft/s)	(745.76)	(772.92)	(687.20)	(957.04)	(774.24)
u	m/s	174.13	174.13	191.54	191.54	180.78
	(ft/s)	(571.29)	(571.29)	(628.40)	(628.40)	(593.10)
v	m/s	146.11	158.69	84.78	220.02	151.69
	(ft/s)	(479.36)	(520.63)	(278.15)	(721.84)	(497.66)
α	deg	**40.00**	——	——	48.96	**40.00**
β	deg	——	42.34	23.87	——	——

be based on the behavior of the flow at the *average radius* (halfway between the hub radius and the tip radius), known henceforth as the *mean radius*. With this introduction in mind, the development of design tools for compressors follows.

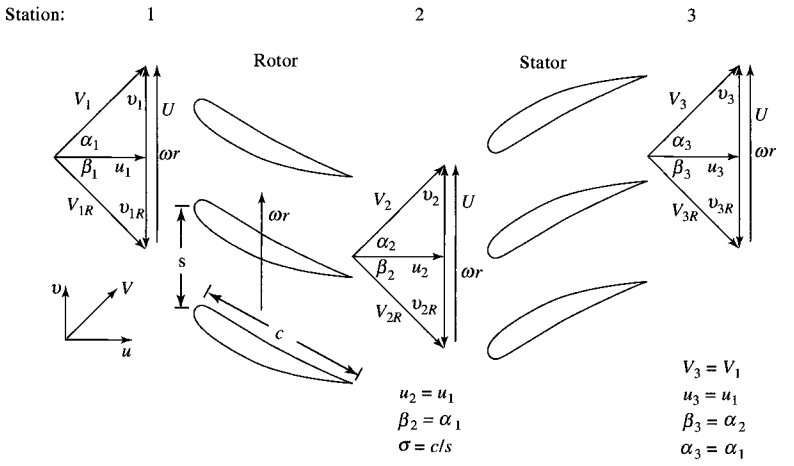

Fig. 9.22 Repeating-row compressor stage nomenclature.

9.3.5.1 Assumptions. We make the following assumptions for this analysis:

1) Repeating-row, repeating-airfoil cascade geometry ($\alpha_1 = \beta_2 = \alpha_3$, $\beta_1 = \alpha_2 = \beta_3$, $u_1 = u_2 = u_3$)
2) Two-dimensional flow (i.e., no variation or component of velocity normal to the page)
3) Polytropic efficiency e_c representing stage losses
4) Constant mean radius

9.3.5.2 Analysis. We assume that the following data are given: $D, M_1, \gamma, \sigma, e_c$. The analysis of the repeating-row, repeating-stage, mean-line design follows.

Conservation of mass: Application of this law for steady one-dimensional flow gives

$$\rho_1 u_1 A_1 = \rho_2 u_2 A_2 = \rho_3 u_3 A_3$$

or

$$\rho_1 A_1 = \rho_2 A_2 = \rho_3 A_3 \tag{9.32}$$

Repeating-row constraint: Since $\beta_2 = \alpha_1$, then

$$v_{2R} = v_1 = \omega r - v_2$$

or

$$v_1 + v_2 = \omega r \tag{9.33}$$

Also, since $\beta_3 = \alpha_2$, then $v_{3R} = v_2$ and $v_3 = v_1$; thus, the stage exit conditions are indeed identical to those at the stage entrance.

Diffusion factor: Since both

$$D = 1 - \frac{V_{2R}}{V_{1R}} + \frac{v_{1R} - v_{2R}}{2\sigma V_{1R}} = 1 - \frac{V_3}{V_2} + \frac{v_2 - v_3}{2\sigma V_2}$$

and

$$D = 1 - \frac{\cos \alpha_2}{\cos \alpha_1} + \frac{\tan \alpha_2 - \tan \alpha_1}{2\sigma} \cos \alpha_2 \tag{9.34}$$

are the same for both the rotor and stator, D is evaluated only once for the stage. Rearranging Eq. (9.34) to solve for α_2, we find that

$$\cos \alpha_2 = \frac{2\sigma(1 - D)\Gamma + \sqrt{\Gamma^2 + 1 - 4\sigma^2(1 - D)^2}}{\Gamma^2 + 1} \tag{9.35}$$

where

$$\Gamma \equiv \frac{2\sigma + \sin \alpha_1}{\cos \alpha_1} \tag{9.36}$$

In other words, Eq. (9.35) shows that there is *only* one value of α_2 that corresponds to the chosen values of D and σ for each α_1. Thus the entire flowfield geometry is indicated by those choices.

Stage total temperature ratio: From the Euler equation, we have for constant radius

$$c_p(T_{t3} - T_{t1}) = \frac{\omega r}{g_c}(v_2 - v_1)$$

From Eq. (9.33)

$$\omega r = v_1 + v_2$$

then

$$c_p(T_{t3} - T_{t1}) = \frac{1}{g_c}(v_2 + v_1)(v_2 - v_1)$$
$$= \frac{v_2^2 - v_1^2}{g_c} = \frac{V_2^2 - V_1^2}{g_c}$$

Thus

$$\frac{T_{t3}}{T_{t1}} - 1 = \frac{V_2^2 - V_1^2}{c_p g_c T_{t1}}$$

or

$$\tau_s \equiv \frac{T_{t3}}{T_{t1}} = \frac{(\gamma - 1)M_1^2}{1 + [(\gamma - 1)/2]M_1^2}\left(\frac{\cos^2 \alpha_1}{\cos^2 \alpha_2} - 1\right) + 1 \tag{9.37}$$

Stage pressure ratio: From Eq. (9.11), we can write

$$\pi_s \equiv \frac{P_{t3}}{P_{t1}} = \left(\frac{T_{t3}}{T_{r1}}\right)^{\gamma e_c/(\gamma - 1)}$$

or

$$\pi_s = (\tau_s)^{\gamma e_c/(\gamma - 1)} \tag{9.38}$$

Degree of reaction: A special characteristic of repeating-stage, repeating-row compressor stages is that the degree of reaction must be exactly 0.5, as shown in the following:

$$^{\circ}R_c = \frac{T_2 - T_1}{T_3 - T_1} = 1 - \frac{T_3 - T_2}{T_3 - T_1} = 1 - \frac{(V_2^2 - V_3^2)/(2g_c c_p)}{T_{t3} - T_{t1}}$$
$$= 1 - \frac{(V_2^2 - V_1^2)/(2g_c c_p)}{(V_2^2 - V_1^2)/(g_c c_p)} = \frac{1}{2}$$

Stage efficiency: From Eq. (9.10), we have

$$\eta_s = \frac{\pi_s^{(\gamma-1)/\gamma} - 1}{\tau_s - 1} \tag{9.39}$$

Stage exit Mach number: Since

$$V_3 = V_1 \quad \text{and} \quad V^2 = M^2 \gamma R g_c T$$

then

$$\frac{M_3}{M_1} = \sqrt{\frac{T_1}{T_3}}$$

$$= \sqrt{\frac{1}{\tau_s\{1 + [(\gamma-1)/2]M_1^2\} - [(\gamma-1)/2]M_1^2}} \leq 1 \tag{9.40}$$

Inlet velocity/wheel speed ratio $V_1/(\omega r)$: One of the most important trigonometric relationships for the stage is that between the total cascade inlet velocity V_1 and the mean wheel speed ωr. Since

$$V_1 = \frac{u_1}{\cos \alpha_1}$$

and

$$\omega r = v_1 + v_2 = u_1(\tan \alpha_1 + \tan \alpha_2)$$

then u_1 can be eliminated to yield

$$\frac{\omega r}{V_1} = (\cos \alpha_1)(\tan \alpha_1 + \tan \alpha_2) \tag{9.41}$$

Stage loading and flow coefficients: The stage loading coefficient ψ for the repeating-stage, repeating-row, mean-line design can be expressed in terms of the flow angles α_1 and α_2 as

$$\psi = \frac{g_c c_p \Delta T_t}{(\omega r)^2} = \frac{\tan \alpha_2 - \tan \alpha_1}{\tan \alpha_1 + \tan \alpha_2} \tag{9.42a}$$

Likewise, the flow coefficient can be expressed in terms of the flow angles α_1 and α_2 as

$$\Phi = \frac{u_1}{\omega r} = \frac{1}{\tan \alpha_1 + \tan \alpha_2} \tag{9.42b}$$

9.3.5.3 General solution. The behavior of all possible repeating-row compressor stages with given values of D, M_1, γ, σ, and e_c can now be computed. This is done by selecting any α_1 and using the following sequence of equations, expressed as functional relationships:

$$\alpha_2 = f(D, \sigma, \alpha_1) \tag{9.35}$$

$$\Delta\alpha = \alpha_2 - \alpha_1$$

$$\tau_s = f(M_1, \gamma, \alpha_1, \alpha_2) \tag{9.37}$$

$$\pi_s = f(\tau_s, \gamma, e_c) \tag{9.38}$$

$$\eta_s = f(\tau_s, \pi_s, \gamma, e_c) \tag{9.39}$$

$$\frac{\omega r}{V_1} = f(\alpha_1, \alpha_2) \tag{9.41}$$

In most cases, T_{t1} is also known, so that selecting M_1 fixes V_1 and ωr is known.

We can now generate plots of α_2, $\Delta\alpha$, π_s, η_s, and $V_1/(\omega r)$ vs α_1. Note that only π_s depends on M_1 and that the process may be repeated to cover the entire range of reasonable values of α_1.

These calculations have been carried out for $D = 0.6$; $M_1 = 0.45$, 0.5, 0.55, 0.6, 0.65, and 0.7; $\gamma = 1.4$; $e_c = 0.9$; and $0\,\text{deg} < \alpha_1 < 70$ deg. The results are presented on Fig. 9.23. The most notable characteristics of these data are that the most direct way to increase π_s is to increase M_1 and that to operate at higher values of α_1, a large wheel speed is required.

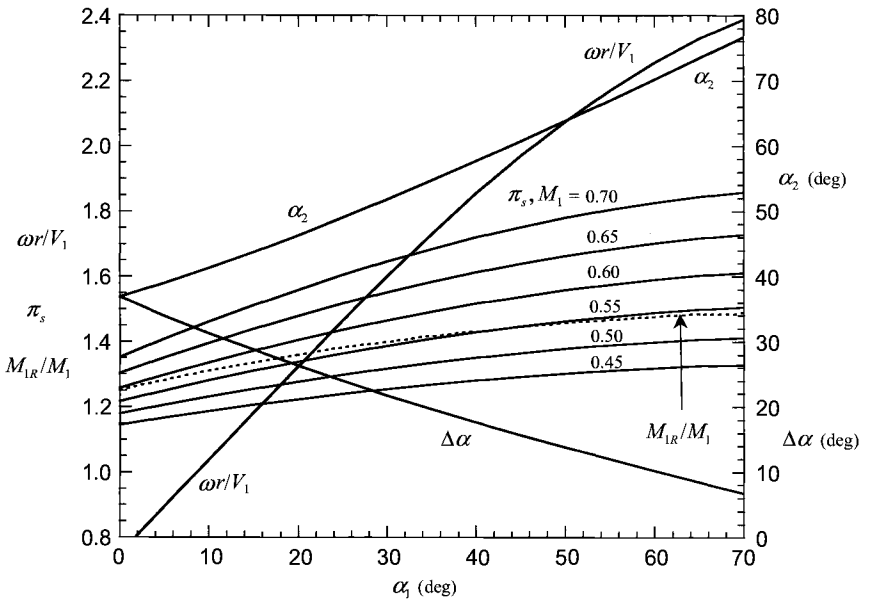

Fig. 9.23 Repeating compressor stage ($D = 0.5$, $\sigma = 1$, and $e_c = 0.9$).

The following two simple examples illustrate the use of this method and are based on the parameters of Fig. 9.23.

Example 9.3

Given:

$$M_1 = 0.6,\ a_1 = 360\,\text{m/s},\ \text{and}\ \omega r = 300\,\text{m/s}$$

Then

$$\frac{\omega r}{V_1} = \frac{\omega r}{a_1 M_1} = 1.39$$

$$\alpha_1 = 22\,\text{deg} \quad \Delta\alpha = 25\,\text{deg}$$

$$\alpha_2 = 47\,\text{deg} \quad \pi_s = 1.42$$

Example 9.4

Given:

$$a_1 = 320\,\text{m/s and } M_1/\alpha_1 = 0.5/20\,\text{deg and } 0.6/30\,\text{deg}$$

Then

M_1	α_1	$\frac{\omega r}{V_1}$	$\frac{\omega r}{a_1}$	π_s
0.5	40 deg	1.852	0.926	1.351
0.6	50 deg	2.075	1.245	1.558

Since a_1 is unaffected by the cascade and affected only slightly by M_1, the price of higher π_s is a greatly increased ωr (that is, $1.245/0.926 = 1.344$).

Figures 9.24 and 9.25 show how the performance of repeating compressor stages changes with diffusion factor and solidity, respectively. For a given inlet flow angle α_1 and inlet velocity V_1, we can see from Fig. 9.24 that increasing the diffusion factor D will increase the exit flow angle α_2, stage pressure ratio π_s, and wheel speed ωr. Likewise, for a given inlet flow angle α_1 and inlet velocity V_1, Fig. 9.25 shows that increasing the solidity σ will increase the exit flow angle α_2, stage pressure ratio π_s, and wheel speed ωr.

For a multistage compressor composed of numerous stages designed by using the repeating-stage, repeating-row, mean-line design, the total temperature change across each of these stages will be the same. Also the mean-line radius for each of these stages is the same. Because the ratio of M_3/M_1 is less than 1, the pressure ratio of any downstream repeating stages will be lower.

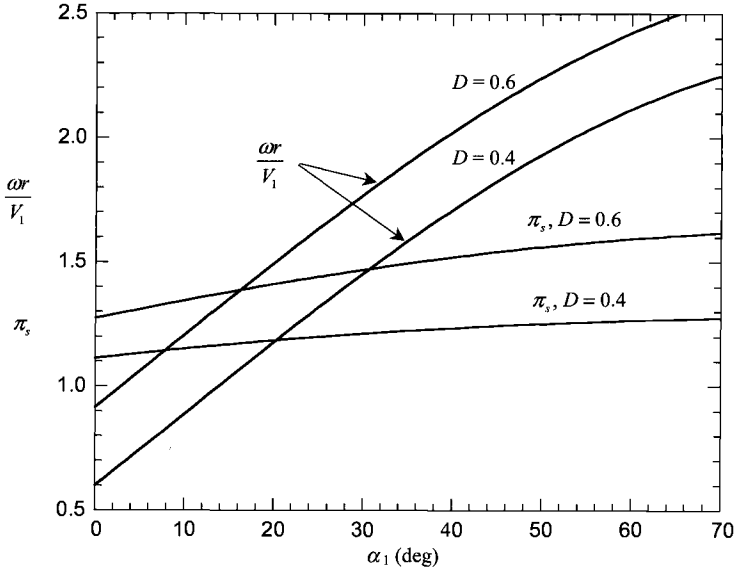

Fig. 9.24 Repeating compressor stage—variation with D ($M_1 = 0.5$, $\sigma = 1$, and $e_c = 0.9$).

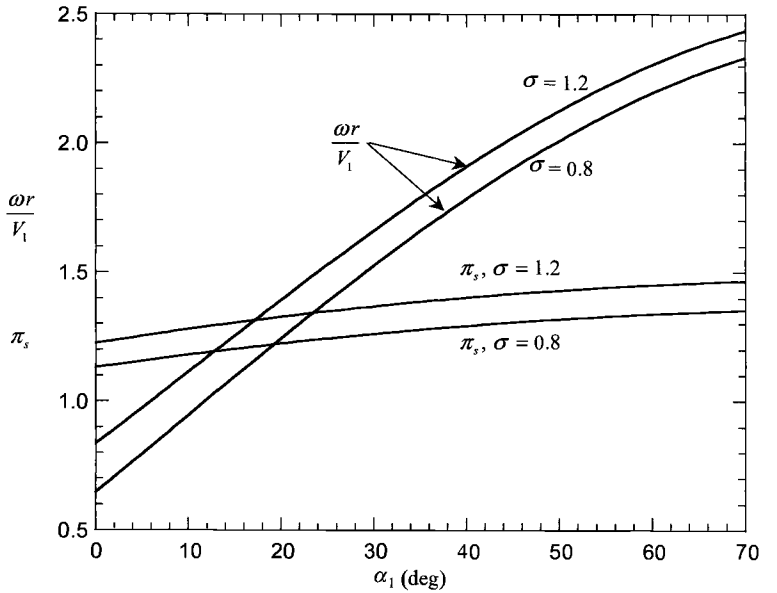

Fig. 9.25 Repeating compressor stage—variation with σ ($M_1 = 0.5$, $D = 0.5$, and $e_c = 0.9$).

Example 9.5

Given:

$$\alpha_1 = 40\,\text{deg}, \quad D = 0.6, \quad \sigma = 1, \quad \gamma = 14, \quad M_1 = 0.5, \quad e_c = 0.9$$

Solution:

$$\Gamma = \frac{2\sigma + \sin\alpha_1}{\cos\alpha_1} = \frac{2 + \sin 40\,\text{deg}}{\cos 40\,\text{deg}} = 3.4499$$

$$\cos\alpha_2 = \frac{2 \times 0.4 \times 3.4499 + \sqrt{3.4499^2 + 1 - 4 \times 1^2 \times 0.4^2}}{3.4499^2 + 1} = 0.4853$$

$$\alpha_2 = 60.966\,\text{deg}$$

$$\tau_s = \frac{0.4 \times 0.5^2}{1 + 0.2 \times 0.5^2}\left(\frac{\cos^2 40\,\text{deg}}{\cos^2 60.966\,\text{deg}} - 1\right) + 1 = 1.142$$

$$\pi_s = 1.142^{3.5 \times 0.9} = 1.519$$

$$\eta_s = \frac{1.519^{1/3.5} - 1}{1.142 - 1} = 0.893$$

$$\frac{M_3}{M_1} = \sqrt{\frac{1}{1.142(1 + 0.2 \times 0.5^2) - 0.4 \times 0.5^2}} = 0.954$$

$$\frac{M_{1R}}{M_1} = \frac{\cos 40\,\text{deg}}{\cos 60.966\,\text{deg}} = 1.578$$

$$M_{1R} = 0.789$$

$$\frac{\omega r}{V_1} = (\cos 40\,\text{deg})(\tan 40\,\text{deg} + \tan 60.966\,\text{deg}) = 2.023$$

$$\psi = \frac{\tan 60.966\,\text{deg} - \tan 40\,\text{deg}}{\tan 40\,\text{deg} + \tan 60.966\,\text{deg}} = 0.364$$

$$\Phi = \frac{1}{\tan 40\,\text{deg} + \tan 60.966\,\text{deg}} = 0.379$$

The flow angles and Mach numbers of a repeating-stage, repeating-row, mean-line design are defined by the preceding calculations. The velocities and temperatures throughout this stage can now be determined by knowing either a velocity or a temperature at any station in the stage. For example, if $T_{t1} = 288.16$ K, then simple calculations give

$$a_1 = 332\,\text{m/s}, \quad V_1 = V_{2R} = V_3 = 166\,\text{m/s}, \quad \omega r = 336\,\text{m/s}$$
$$V_{1R} = V_2 = 261.9\,\text{m/s}, \quad \text{and} \quad \Delta T_t = 40.9\,\text{K}$$

9.3.6 Flow Path Dimensions

9.3.6.1 Annulus area. The preliminary design of multistage axial-flow compressors is typically based on determining each stage's flow properties along the compressor mean line (line along compressor axis that corresponds to the mean radius). The annulus area at any station is based on the flow properties (T_t, P_t, Mach number, and flow angle) at the mean radius and the total mass flow rate. Equation (9.8) is the easiest equation to calculate the flow area at any station i:

$$A_i = \frac{\dot{m}\sqrt{T_{ti}}}{P_{ti}(\cos \alpha_i)\text{MFP}(M_i)}$$

The *mean radius* of a flow annulus is defined as the average of the tip radius and hub radius. Consider Fig. 9.26, which shows a typical annulus area.

In many calculations, the flow area can be calculated and the mean radius is tied to the required rotor speed at the mean radius ωr_m. The designer can select ω and calculate the required mean radius. Then the root radius and tip radius are calculated directly from the mean radius and flow area. In some calculations, the designer may want to select the ratio of the hub radius to the tip radius r_h/r_t. The hub/tip ratio at the inlet to a multistage compressor normally is between 0.6 and 0.75, whereas that at the compressor exit is in the range of 0.9 to 0.92. Then the tip, hub, and mean radii directly follow from the geometry:

$$A = (r_t^2 - r_h^2) = \pi r_t^2 \left[1 - \left(\frac{r_h}{r_t}\right)^2\right]$$

$$r_t = \sqrt{\frac{A}{\pi[1 - (r_h/r_t)^2]}} \qquad r_h = r_t\left(\frac{r_h}{r_t}\right) \qquad r_m = \frac{r_t + r_h}{2}$$

The variation of the flow area and the associated dimensions of the flow path from one station to the next can be calculated easily by using the preceding relationships and the results sketched. Figure 9.27 is a sketch of typical results. The calculation of the axial dimensions requires additional data.

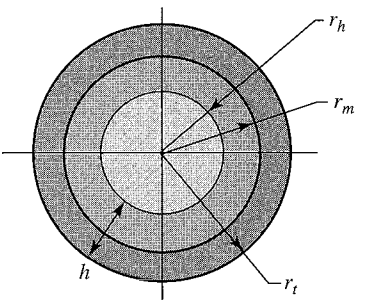

$$r_m = \frac{r_t + r_h}{2}$$

$$A = \pi(r_t^2 - r_h^2)$$

$$A = \pi(r_t + r_h) \times (r_t - r_h)$$

$$A = 2\pi\left(\frac{r_t + r_h}{2}\right) \times (r_t - r_h)$$

$$A = 2\pi r_m \times h, \text{ where } h = r_t - r_h$$

Fig. 9.26 Flow annulus dimensions.

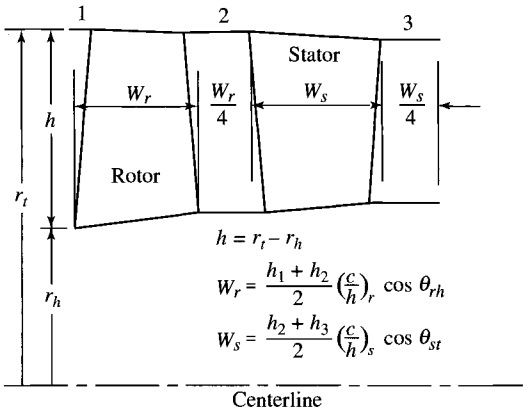

Fig. 9.27 Typical axial dimensions of a compressor stage.

9.3.6.2 Axial dimensions. The axial dimensions of a typical stage are also shown in Fig. 9.27, and these can be used to estimate the axial length of a stage. Blade axial widths (W_r and W_s) of a stage are calculated in the program COMPR along with the blade spacings ($W_r/4$ and $W_s/4$) based on user-input chord-to-height ratios c/h for the rotor and stator blades and assuming a constant chord length for each blade. A minimum width of $\frac{1}{4}$ in. (0.006 m) and a minimum spacing of $\frac{1}{8}$ in. (0.003 m) are used in the plot of compressor cross section and calculation of axial length.

The value of the chord/height ratio c/h selected for a blade depends on such factors as the stage loading coefficient, diffusion factor, etc. Typical values of c/h range from 0.2 to 0.8. Higher values of c/h lead to longer stages and fewer blades.

The chord of a blade c is obtained by multiplying its height h by the user-input chord/height ratio c/h. The blade width (W_r or W_s) is the maximum value of the axial chord c_x for that blade, which depends on the stagger angle θ as shown in Fig. 9.15. The maximum axial chord c_x normally occurs at the hub for a rotor blade and at the tip for a stator blade.

9.3.6.3 Number of blades. The COMPR program calculates the number of blades n_b for the rotor and stator of a stage based on the user-input values of the solidity σ along the mean line. For a rotor or stator, the blade spacing s along the mean line is equal to the blade chord c divided by its solidity ($\sigma = c/s$). The number of blades is simply the circumference of the mean line divided by the blade spacing, rounded up to the next integer.

9.3.6.4 Blade profile. The shapes of compressor rotor and stator blades are based on airfoil shapes developed specifically for compressor applications. One such airfoil shape is the symmetric NACA 65A010 compressor airfoil whose profile shape is shown in Fig. 9.28 and specified in Table 9.4. This airfoil has a thickness that is 10% of its chord c.

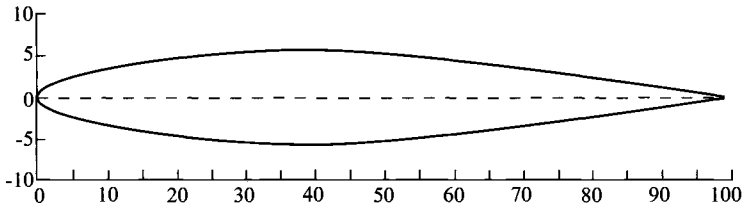

Fig. 9.28 NACA 65A010 blade shape.

To obtain the desired change in fluid flow direction, the airfoil's chamber line is curved and the symmetric shape of the airfoil profile is distributed about the chamber line. The curved chamber line of the airfoil and nomenclature used for flow through a compressor cascade are shown in Fig. 9.15. Normally, the curved chamber line is that of a circular arc or a parabola. If a circular arc is used, then the stagger angle of the airfoil θ is the average of the chamber line's inlet angle γ_i and exit angle γ_e. From Fig. 9.29 and basic trigonometry, the radius of the chamber line is given by

$$r = \frac{c \sin \theta}{\cos \gamma_e - \cos \gamma_i} \tag{9.43}$$

The COMPR computer program uses the NACA 65A010 compressor profile with circular arc chamber line to sketch the blade shapes for a stage. The user can change the blade thickness for the rotor or stator blades, select the desired stage, specify the number of blades to be sketched, and specify the percentage of chord

Table 9.4 NACA 65A010 compressor airfoil[a,b]

x/c, %	y/c, %	x/c, %	y/c, %
0.0	0.0	40	4.995
0.5	0.765	45	4.983
0.75	0.928	50	4.863
1.25	1.183	55	4.632
2.5	1.623	60	4.304
5	2.182	65	3.809
7.5	2.65	70	3.432
10	3.04	75	2.912
15	3.658	80	2.352
20	4.127	85	1.771
25	4.483	90	1.188
30	4.742	95	0.604
35	4.912	100	0.0

[a]Leading-edge radius = 0.00636c. Trailing-edge radius = 0.00023c.
[b]Source: Ref. 51.

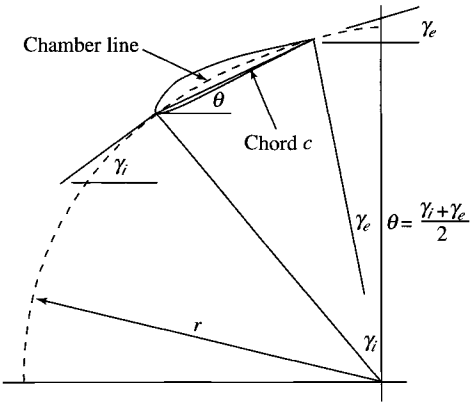

Fig. 9.29 Circular arc chamber line.

for stacking blade profiles. The user can view one or more blades in the rotor and stator at a time.

If the user selects to view just one blade, the program initially sketches the blade shape at the mean radius as a solid, and the shapes at the hub and tip are drawn in dashed outline stacked over the other profile at the user-selected stacking location. Figure 9.30 is a copy of the blade profile plot screen for one blade. The user can move the slider for percentage of blade height by using the up and down arrows and replot the blade shape at a new height (radial location).

If the user selects to view more than one blade, the program initially sketches the blade shapes at the mean radius. Figure 9.31 is a copy of the blade profile plot screen for three blades. The user can move the slider for percentage of blade height by using the up and down arrows and replot the blade shape at a new height (radial location).

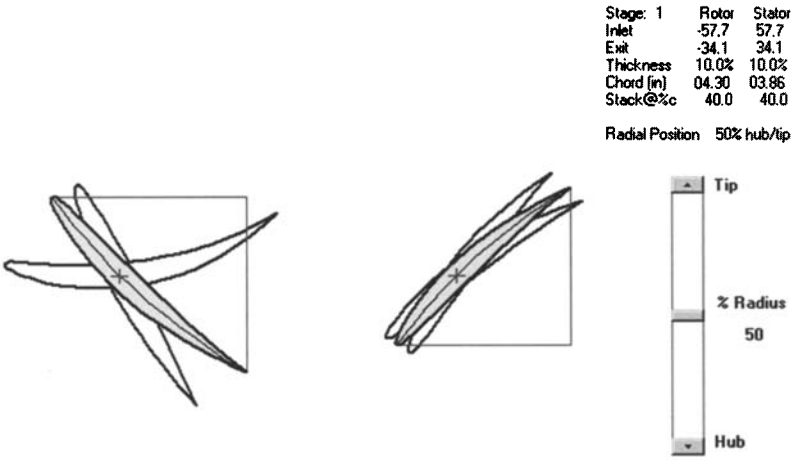

Fig. 9.30 Single-blade profile sketch from COMPR.

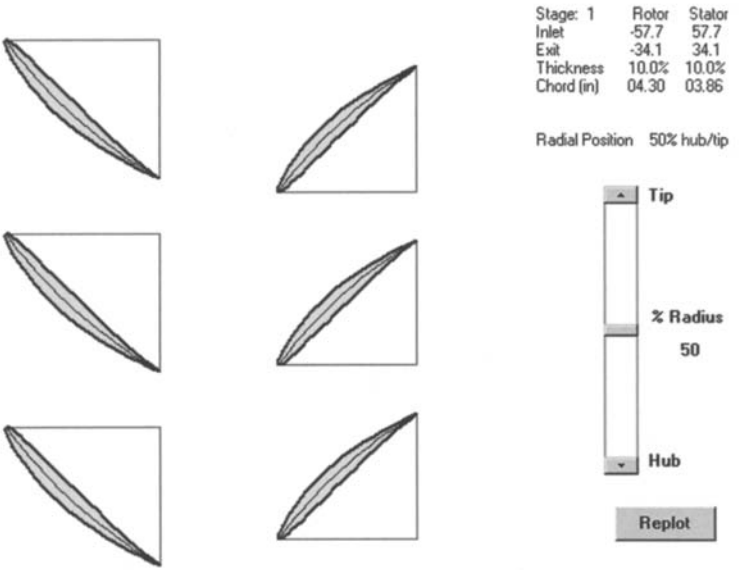

Fig. 9.31 Three-blade profile sketch from COMPR.

9.3.7 Radial Variation

A practical goal of a design is to do a constant amount of work on the fluid passing through a stage that is independent of radius. For this to occur, the Euler pump equation [Eq. (9.1)] reveals that less "turning" of the fluid will be required as the radius increases. In addition, the static pressure must increase with the radius to maintain the radial equilibrium of the swirling flow. All airfoil and flow properties must, therefore, vary with radius.

In the following analysis, the relationships are developed for the radial variation of flow between the rows of airfoils (stage stations 1, 2, and 3). Initially, a general equation for radial equilibrium is developed, assuming no radial velocity. Then specific radial variations of the velocity are analyzed for the case of constant work on the fluid.

9.3.7.1 Radial equilibrium equation. The main features of the radial variation of flow *between* the rows of airfoils are accounted for in the following analysis. These equations are valid at stations 1, 2, and 3 at any radius. We assume the following:

1) Constant losses (entropy s = constant with respect to radius)
2) No circumferential variations
3) No radial velocity

The definition of total (stagnation) enthalpy with no radial velocity gives

$$dh_t = dh + \frac{d(u^2 + v^2)}{2g_c} \tag{i}$$

Gibbs' equation can be written as

$$T\,\mathrm{d}s = \mathrm{d}h - \frac{\mathrm{d}P}{\rho}$$

With s = constant, Gibbs' equation becomes

$$\mathrm{d}h = \frac{\mathrm{d}P}{\rho} \tag{ii}$$

Equations (i) and (ii) can be combined to give

$$\mathrm{d}h_t = \frac{\mathrm{d}P}{\rho} + \frac{u\,\mathrm{d}u}{g_c} + \frac{v\,\mathrm{d}v}{g_c}$$

When h_t is a constant, this equation becomes the well-known Bernoulli equation. We rewrite the preceding equation as

$$\frac{\mathrm{d}h_t}{\mathrm{d}r} = \frac{1}{\rho}\frac{\mathrm{d}P}{\mathrm{d}r} + \frac{1}{g_c}\left(u\frac{\mathrm{d}u}{\mathrm{d}r} + v\frac{\mathrm{d}v}{\mathrm{d}r}\right) \tag{iii}$$

For radial equilibrium, the pressure gradient in the radial direction must balance the centrifugal acceleration, or

$$\frac{\mathrm{d}P}{\mathrm{d}r} = \frac{\rho v^2}{r g_c} \tag{iv}$$

Equations (iii) and (iv) may be combined to yield

$$\frac{\mathrm{d}h_t}{\mathrm{d}r} = \frac{1}{g_c}\left(u\frac{\mathrm{d}u}{\mathrm{d}r} + v\frac{\mathrm{d}v}{\mathrm{d}r} + \frac{v^2}{r}\right) \tag{9.44}$$

This general form of the radial equilibrium equation prescribes the relationship between the radial variations of the three variables: h_t, u, and v. The designer can specify the radial variation of any two variables, and Eq. (9.44) specifies the radial variation of the third variable.

9.3.7.2 Free-vortex variation of swirl. We consider the case where the axial velocity u and total enthalpy h_t do not vary with radius. For this case, Eq. (9.44) becomes

$$v\frac{\mathrm{d}v}{\mathrm{d}r} + \frac{v^2}{r} = 0 \quad \text{or} \quad \frac{\mathrm{d}v}{v} + \frac{\mathrm{d}r}{r} = 0$$

for which the integrated solution is

$$rv = \text{const}$$

or

$$v = v_m \frac{r_m}{r} \tag{9.45}$$

where the subscript m refers to values at the mean radius. Because v varies inversely with radius, this is known as *free-vortex* flow. Thus, if the flow at station 1 has $v_1 r = v_{m1} r_m$ and the rotor airfoils modify the flow to $v_2 r = v_{m2} r_m$, then the Euler equation confirms that this is a constant-work machine because

$$\begin{aligned} \omega r(v_2 - v_1) &= \omega r\left(\frac{v_{m2} r_m}{r} - \frac{v_{m1} r_m}{r}\right) \\ &= \omega r_m (v_{m2} - v_{m1}) \\ &= \text{const} \end{aligned}$$

Equation (9.45) also shows that as long as r does not vary substantially from r_m (say, $\pm 10\%$), the airfoil and flow properties will not vary much from those of the original mean-line design.

If the compressor has constant axial velocity and repeating stages (not rows) for which $v_1 = v_3$, then the degree of reaction can be shown to be

$$^{\circ}R_c = 1 - \frac{v_1 + v_2}{2\omega r} \tag{9.46}$$

which, for a free-vortex machine, becomes

$$^{\circ}R_c = 1 - \frac{v_{m1} r_m + v_{m2} r_m}{2\omega r^2} = 1 - \frac{\text{const}}{(r/r_m)^2} \tag{9.47}$$

For a stage whose degree of reaction is 50% at the mean radius (where $(\omega r = v_1 + v_2)$, it becomes more difficult to design rotor airfoils at $r > r_m$ and stator airfoils at $r < r_m$. In fact, since $^{\circ}R_c = 0$ at $r = r_m/\sqrt{2}$, the rotor will actually experience accelerating flow for smaller radii, whereas this is never the case for the stator. Because of these problems, compressor designers have looked at other swirl distributions.

9.3.7.3 Swirl distributions. We now consider the case where the total enthalpy does not vary with the radius and where the swirl velocity at the inlet and exit to the rotor has the following general variation with radius:

$$v_1 = a\left(\frac{r}{r_m}\right)^n - b\frac{r_m}{r} \quad \text{and} \quad v_2 = a\left(\frac{r}{r_m}\right)^n + b\frac{r_m}{r} \tag{9.48}$$

where a, b, and r_m are constants. From the Euler equation, the work per unit mass flow is

$$\Delta h_t = \frac{\omega r(v_2 - v_1)}{g_c} = \frac{2b\omega r_m}{g_c} \tag{9.49}$$

which is independent of the radius. Note from the preceding relationship that the constant b in Eq. (9.48) is determined by the total enthalpy rise across the rotor and the mean rotor speed. As will be shown next, constant a in Eq. (9.48) is related to the degree of reaction at the mean radius. Three cases of the swirl distribution of Eq. (9.48) are considered: $n = -1$, $n = 0$, and $n = 1$.

1) For $n = -1$:

$$v_1 = a\frac{r_m}{r} - b\frac{r_m}{r} \quad \text{and} \quad v_2 = a\frac{r_m}{r} + b\frac{r_m}{r} \tag{9.50}$$

which is the *free-vortex* swirl distribution. For this case and constant h_t, Eq. (9.44) required that the axial velocity u not vary with the radius. Using Eq. (9.46) for a repeating stage ($v_3 = v_1$), we see that the degree of reaction is

$$^{\circ}R_c = 1 - \frac{a}{\omega r_m}\left(\frac{r_m}{r}\right)^2 \tag{9.51}$$

An equation for the constant a in Eq. (9.48) is obtained by evaluating the preceding equation at the mean radius. Thus

$$a = \omega r_m(1 - {}^{\circ}R_{cm}) \tag{9.52}$$

2) For $n = 0$:

$$v_1 = a - b\frac{r_m}{r} \quad \text{and} \quad v_2 = a + b\frac{r_m}{r} \tag{9.53}$$

This is called the *exponential* swirl distribution. Before solving for the axial velocity distribution, we rewrite Eq. (9.44) for constant total enthalpy h_t in terms of the dimensionless radius r/r_m as

$$u\,\mathrm{d}u + v\,\mathrm{d}V + v^2\frac{\mathrm{d}(r/r_m)}{r/r_m} = 0$$

Integration of the preceding equation from the mean radius to any radius r gives

$$\frac{1}{2}(u^2 - u_m^2) = -\frac{1}{2}(v^2 - v_m^2) - \int_1^{r/r_m} v^2\frac{\mathrm{d}(r/r_m)}{r/r_m} \tag{9.54}$$

At the entrance to the rotor (station 1), substitution of the equation for v_1 into Eq. (9.54) and integration give the axial velocity profile

$$u_1^2 = u_{1m}^2 - 2\left(a^2\ell n\frac{r}{r_m} + \frac{ab}{r/r_m} - ab\right) \tag{9.55}$$

Likewise, at the exit from the rotor (station 2), we obtain

$$u_2^2 = u_{2m}^2 - 2\left(a^2 \ell n \frac{r}{r_m} - \frac{ab}{r/r_m} + ab\right) \tag{9.56}$$

Because the axial velocity is not constant, we must start with Eq. (9.13b) to obtain an expression for the degree of reaction for the velocity distribution given by Eqs. (9.53), (9.55), and (9.56). We start by noting for repeating stages ($V_3 = V_1$) that

$$\begin{aligned} {}^{\circ}R_c &= \frac{T_2 - T_1}{T_3 - T_1} = \frac{T_{t2} - T_{t1}}{T_{t3} - T_{t1}} - \frac{V_2^2 - V_1^2}{2g_c c_p (T_{t3} - T_{t1})} \\ &= 1 - \frac{V_2^2 - V_1^2}{2g_c c_p (T_{t3} - T_{t1})} = 1 - \frac{u_2^2 - u_1^2}{2g_c c_p (T_{t3} - T_{t1})} - \frac{v_2^2 - v_1^2}{2g_c c_p (T_{t3} - T_{t1})} \end{aligned}$$

From the Euler equation, we write $g_c c_p (T_{t3} - T_{t1}) = \omega r (v_2 - v_1)$, and the preceding becomes

$$\begin{aligned} {}^{\circ}R_c &= 1 - \frac{u_2^2 - u_1^2}{2\omega r (v_2 - v_1)} - \frac{v_2^2 - v_1^2}{2\omega r (v_2 - v_1)} \\ {}^{\circ}R_c &= 1 + \frac{u_1^2 - u_2^2}{2\omega r (v_2 - v_1)} - \frac{v_2 + v_1}{2\omega r} \end{aligned} \tag{9.57}$$

For the case where $u_{1m} = u_{2m}$, Eqs. (9.55) and (9.56) give

$$u_1^2 - u_2^2 = 4ab\left(1 - \frac{r_m}{r}\right)$$

and from the swirl distribution of Eq. (9.53), we have

$$v_2 + v_1 = 2a \quad \text{and} \quad v_2 - v_1 = 2b\frac{r_m}{r}$$

Thus the degree of reaction for the exponential swirl distribution is given by

$${}^{\circ}R_c = 1 + \frac{a}{\omega r_m} - \frac{2a}{\omega r} \tag{9.58}$$

3) For $n = 1$:

$$v_1 = a\frac{r}{r_m} - b\frac{r_m}{r} \quad \text{and} \quad v_2 = a\frac{r}{r_m} + b\frac{r_m}{r} \tag{9.59}$$

This is called *first-power* swirl distribution. At the entrance to the rotor (station 1), substitution of the equation for v_1 into Eq. (9.54) and integration give the

axial velocity profile

$$u_1^2 = u_{1m}^2 - 2\left[a^2\left(\frac{r}{r_m}\right)^2 + 2ab\,\ell n\frac{r}{r_m} - a^2\right] \tag{9.60a}$$

Likewise, at the exit from the rotor (station 2), we obtain

$$u_2^2 = u_{2m}^2 - 2\left[a^2\left(\frac{r}{r_m}\right)^2 - 2ab\,\ell n\frac{r}{r_m} - a^2\right] \tag{9.60b}$$

An equation for the degree of reaction for the case of $u_{1m} = u_{2m}$ is obtained in the same manner. The resulting relationship is

$$^{\circ}R_c = 1 + \frac{2a\,\ell n(r/r_m)}{\omega r_m} - \frac{a}{\omega r_m} \tag{9.61}$$

9.3.7.4 Comparison. Equations (9.51), (9.58), and (9.61) give the radial variation of the degree of reaction for the free-vortex, exponential, and first-power swirl distributions, respectively. The value of the constant a is evaluated at the mean radius and is given by Eq. (9.52) for all three cases. Consider the case where the degree of reaction at the mean radius is 0.5. Results from Eqs. (9.51), (9.58), and (9.61) are plotted in Fig. 9.32 for the range $0.5 < r/r_m < 1.5$. Note that at any radius other than the mean, the free-vortex swirl distribution results in the lowest value for the degree of reaction, and the first-power swirl distribution gives the highest value.

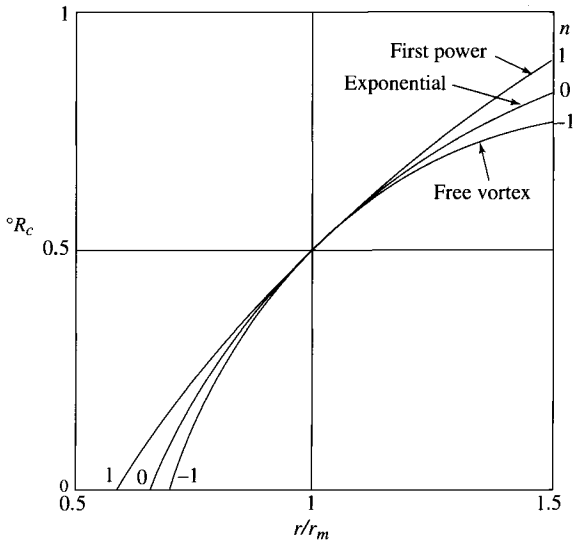

Fig. 9.32 Radial variation of degree of reaction (from Ref. 29).

The low (nonzero) values for the degree of reaction can occur at the hub for stages having small hub/tip ratios r_h/r_t. The variation with the radius ratio r/r_t for the degree of reaction can be obtained from Eqs. (9.51), (9.58), and (9.61) and the following relationship between r/r_t and r/r_m:

$$\frac{r}{r_m} = \frac{r}{r_m}\frac{1 + r_h/r_t}{2} \tag{9.62}$$

For the free-vortex swirl distribution with 0.5 degree of reaction at the mean radius, the degree of reaction is 0 at $r/r_m = 0.707$, which corresponds to the hub radius for a stage having a hub/tip ratio of 0.547. It is not uncommon for the initial stages of a compressor to have a hub/tip ratio of 0.4. The degree of reaction at the hub can be increased by increasing the degree of reaction at the mean radius for stages with low hub/tip ratios. Another way to increase the degree of reaction at the hub is to change the swirl distribution.

For the first-power swirl distribution with 0.5 degree of reaction at the mean radius, the degree of reaction is 0 at $r/r_m = 0.6065$, which corresponds to the hub radius for a stage having a hub/tip ratio of 0.435. Even with this improvement over the free-vortex distribution, the degree of reaction at the mean radius will have to be greater than 0.5 to have a positive degree of reaction at the hub of a stage with a hub/tip ratio of 0.4.

Because of the problems encountered with the preceding swirl distribution, modern compressor designers have looked to nonconstant work machines. However, these are absolutely dependent on large computers for their definition.

Example 9.6

Consider the results using program COMPR. The program COMPR can perform the calculations for repeating-row, repeating-stage, mean-line stage design. To have values for the total pressure and static pressures at stations 2 and 2*R*, the program requires a value of the stator loss coefficient ϕ_{cs} in addition to the polytropic efficiency for repeating-row, repeating-stage calculations. The program assumes that the solidity σ varies inversely with radius (constant chord length) for calculation of the radial variation in the diffusion factor. The free-vortex swirl distribution is used for the radial variation of the tangential velocity v in this example.

Given:

$$\dot{m} = 22.68\,\text{kg/s}\ (50\,\text{lbm/s}), \qquad P_t = 101.3\,\text{kPa}\ (14.70\,\text{psia})$$
$$T_t = 288.16\,\text{K}\ (518.7^\circ\text{R}), \quad \omega = 900\,\text{rad/s}, \quad e_c = 0.9, \quad \phi_{cs} = 0.03$$
$$\text{on mean line: } \sigma = 1, \quad \alpha_1 = 45\,\text{deg}, \quad D = 0.5, \quad M_1 = 0.5$$

Solution: Tables 9.5a and 9.5b summarize the results obtained from COMPR. Note that the Mach numbers at the hub of stations 1, 2, and 3 are higher than on

Table 9.5a Flow property results for Example 9.6

Property		Station										
		$1/h$	$1m$	$1t$	$1Rm$	$2Rm$	$2h$	$2m$	$2t$	$3h$	$3m$	$3t$
T_t	K	288.2	288.2	288.2	303.1	303.1	318.1	318.1	318.1	318.1	318.1	318.1
	(°R)	(518.7)	(518.7)	(518.7)	(545.6)	(545.6)	(572.6)	(572.6)	(572.6)	(572.6)	(572.6)	(572.6)
T	K	272.7	274.4	275.7	274.4	289.4	284.5	289.4	293.1	303.0	304.4	305.4
	(°R)	(490.8)	(494.0)	(496.3)	(494.0)	(520.9)	(512.1)	(520.9)	(527.6)	(545.4)	(547.9)	(549.8)
P_t	kPa	101.3	101.3	101.3	120.9	117.7	139.3	139.3	139.3	138.3	138.3	138.3
	(psia)	(14.70)	(14.70)	(14.70)	(17.55)	(17.08)	(20.21)	(20.21)	(20.21)	(20.06)	(20.06)	(20.06)
P	kPa	83.5	85.4	86.8	85.4	100.1	94.3	100.1	104.6	116.7	118.5	119.9
	(psia)	(12.11)	(12.39)	(12.59)	(12.39)	(14.52)	(13.67)	(14.52)	(15.18)	(16.93)	(17.19)	(17.40)
M		0.533	0.500	0.475	0.723	0.487	0.769	0.704	0.653	0.499	0.475	0.456
V	m/s	176	166	158	240	166	260	240	224	174	166	160
	(ft/s)	(578)	(545)	(519)	(788)	(545)	(853)	(788)	(735)	(571)	(545)	(524)
u	m/s	117	117	117	117	117	117	117	117	117	117	117
	(ft/s)	(385)	(385)	(385)	(385)	(385)	(385)	(385)	(385)	(385)	(385)	(385)
v	m/s	132	117	106	209	117	232	209	191	128	117	108
	(ft/s)	(432)	(385)	(348)	(687)	(385)	(761)	(687)	(626)	(421)	(385)	(355)
α	deg	48.25	45.00	42.08	——	——	63.14	60.72	58.41	47.57	45.00	42.64
β	deg	——	——	——	60.72	45.00	——	——	——	——	——	——
radii	m	0.324	0.363	0.402	0.363	0.363	0.328	0.363	0.398	0.332	0.363	0.394
	(in.)	(12.76)	(14.30)	(15.83)	(14.30)	(14.30)	(12.91)	(14.30)	(15.68)	(13.07)	(14.30)	(15.52)

Table 9.5b Stage results for Example 9.6

Hub	$^{\circ}R_c = 0.3888$	$D_r = 0.5455$	$D_s = 0.5101$
Mean	$^{\circ}R_c = 0.5000$	$D_r = 0.5000$	$D_s = 0.5000$
Tip	$^{\circ}R_c = 0.5850$	$D_r = 0.4476$	$D_s = 0.4906$

$\Delta T_t = 29.93\,\text{K}$ $\eta_s = 89.55\%$ $AN^2 = 1.184 \times 10^7\,\text{m}^2 \cdot \text{rpm}^2$

$$\psi = \frac{g_c c_p \Delta T_t}{(\omega r)^2} = 0.281 \qquad \Phi = \frac{u_1}{\omega r} = 0.359$$

the mean radius due to the swirl distribution. This affects both the static temperatures and the static pressures at the hub.

The cross section of this stage, as created by COMPR, is shown in Fig. 9.33. The stage length of 0.099 m is based on a chord/height ratio of 0.75 for both the rotor and stator blades.

The variation in tangential and axial velocities with radius across the rotor is shown in Fig. 9.34 for the free-vortex swirl distribution. To obtain the 30.5°C (54.9°F) temperature rise across the rotor, the tangential velocity is increased 92 m/s (302 ft/s).

9.3.8 Design Process

The theory and design tools presented in previous sections can now be applied to the design of a multistage axial-flow compressor. The design process requires

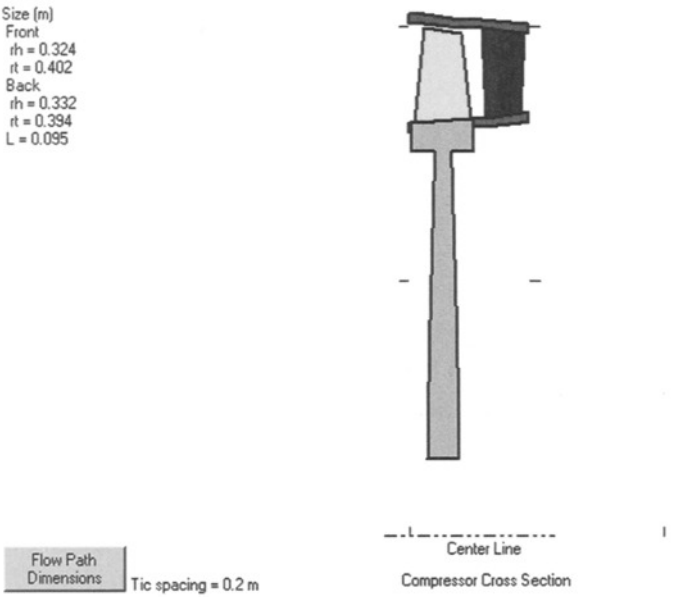

Fig. 9.33 Cross section of a single stage from COMPR.

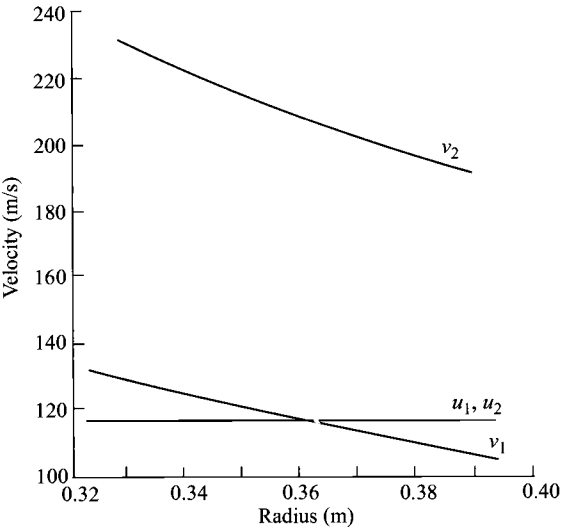

Fig. 9.34 Axial and swirl velocity profiles at stations 1 and 2.

both engineering judgment and knowledge of typical design values. We will consider the design of a compressor suitable for a simple turbojet gas turbine engine. It is assumed that such a compressor will require inlet guide vanes.

From engine cycle calculations, a suitable design point for the compressor of such an engine at sea-level, standard-day conditions [$P/T = 14.70$ psia/518.7°R ($P/T = 101.3$ kPa/288.2 K)] may emerge as

Compressor pressure ratio	10.2
Air mass flow rate	150 lbm/s (68.04 kg/s)
Temperature entering turbine	3200°R (1778 K)

From these specified data, we will now investigate the aerodynamic design of an axial-flow compressor.

The complete design process for the compressor will include the following items:

1) Selection of rotational speed and annulus dimensions
2) Selection of the number of stages
3) Calculation of airflow angles for each stage at the mean radius
4) Calculation of airflow angle variations from the hub to tip for each stage
5) Selection of blading using experimental cascade data
6) Verification of compressor efficiency based on cascade loss data
7) Prediction of off-design performance
8) Rig testing of design

Items 1–4 will be covered in this section. Many of the remaining steps will be discussed in following sections. The design process is inherently iterative, often requiring return to an earlier step when prior assumptions are found to be

Table 9.6 Range of axial-flow compressor design parameters

Parameter	Design range
Fan or low-pressure compressor	
Pressure ratio for one stage	1.5–2.0
Pressure ratio for two stages	2.0–3.5
Pressure ratio for three stages	3.5–4.5
Inlet corrected mass flow rate	40–42 lbm/(s · ft^2) [195–205 kg/(s · m^2)]
Tip speed	1400–1500 ft/s (427–457 m/s)
Diffusion factor	0.50–0.55
High-pressure compressor	
Inlet corrected mass flow rate	36–38 lbm/(s · ft^2) [175–185 kg/(s · m^2)]
Hub/tip ratio at inlet	0.60–0.75
Hub/tip ratio at exit	0.90–0.92
Maximum rim speed at exit	1300–1500 ft/s (396–457 m/s)
Flow coefficient	0.45–0.55
Stage loading coefficient	0.30–0.35
Diffusion factor	0.50–0.55

invalid. Table 9.6 lists ranges for some design parameters of axial-flow compressors and can be used as a guide.

Many technical specialities are interwoven in a design, e.g., an axial-flow air compressor involves at least thermodynamics, aerodynamics, structures, materials, manufacturing processes, and controls. Design requires the active participation and disciplined communication by many technical specialists.

9.3.8.1 Selection of rotational speed and annulus dimensions. Selection of the rotational speed is not a simple matter. For a simple turbojet engine, it depends on a balance of the requirements of both components on the common shaft—the compressor and the turbine. Typically, the rotational speed can be found by assuming values for the rotor blade-tip speed, the hub/tip ratio, and axial velocity of the first stage. A check of the magnitude of AN^2 (related to blade stress) is also made. For the first stage of typical compressors, the hub/tip ratio is between 0.6 and 0.75, the axial Mach number is between 0.48 and 0.6, and the rotor blade-tip speed is between 1150 and 1500 ft/s (350 to 460 m/s) (higher values for first-stage fans without inlet guide vanes).

Initially, we select a modest value for the axial Mach number M_0 of 0.5 entering the inlet guide vanes. Because the inlet guide vanes will accelerate and turn the flow to an angle of 30–45 deg, we will start with a compressor inlet Mach number M_1 of 0.6 and a high tip speed U_t of 1400 ft/s (426.7 m/s). From the

definition of mass flow parameter, we can write

$$A = \frac{\dot{m}\sqrt{T_t}}{(\cos\alpha)(P_t)\text{MFP}(M)}$$

For the given mass flow rate and the inlet total pressure, total temperature, and Mach number, we can determine the flow annulus area at the entrance to the inlet guide vanes:

$$\text{MFP}(M_0) = 0.3969$$

$$A_0 = \frac{\dot{m}\sqrt{T_{t0}}}{P_{t0}\text{MFP}(M_0)} = \frac{150\sqrt{518.7}}{14.70 \times 0.3969}$$

$$= 585.7\,\text{in.}^2\ (0.3780\,\text{m}^2)$$

Likewise, the area at the face of the first-stage rotor, assuming a flow angle of 40 deg, is

$$\text{MFP}(M_1) = 0.4476$$

$$A_1 = \frac{\dot{m}\sqrt{T_t}}{(\cos\alpha_1)(P_t)\text{MFP}(M)} = \frac{150\sqrt{518.7}}{0.7660 \times 14.70 \times 0.4476}$$

$$= 677.8\ \text{in.}^2\ (0.4375\,\text{m}^2)$$

The tip radius r_t and mean radius r_m are directly related to the flow area A and hub/tip ratio r_h/r_t by

$$r_t = \sqrt{\frac{A}{\pi[1 - (r_h/r_t)^2]}}$$

$$r_m = r_t \frac{1 + r_h/r_t}{2}$$

The rotational speeds ω and N are related to the rotor tip speed by

$$\omega = \frac{U_t}{r_t} \quad \text{and} \quad N = \frac{30}{\pi}\omega$$

From the preceding relationships, we can calculate r_t, ω, N, and AN^2 over the hub/tip ratio range and obtain the data in Table 9.7a for a tip speed of 1400 ft/s (426.7 m/s).

With the information in Table 9.7a, it is most appropriate for the compressor designer to get together with the turbine designer to select a rotational speed. The first stages of turbines typically have tip speeds of about 1400 ft/s (426.7 m/s),

Table 9.7a Variation of first-stage size and speed for a tip speed of 1400 ft/s

$\frac{r_h}{r_t}$	r_t, in.	r_m, in.	ω, rad/s	N, rpm	AN^2, in.^{2} · rpm^2
0.60	18.36	14.69	914.8	8735.7	5.17×10^{10}
0.65	19.33	15.95	869.0	8298.2	4.67×10^{10}
0.70	20.57	17.49	816.6	7798.2	4.12×10^{10}
0.75	22.21	19.44	756.4	7222.7	3.54×10^{10}

a hub/tip ratio of 0.85 to 0.9, and Mach number entering the rotor of 1.2 at 60 deg to the centerline of the turbine. Assuming a fuel/air ratio of 0.04, the turbine mass flow rate is 156 lbm/s. For $\gamma = 1.3$ and a 5% total pressure loss through the combustor, the annulus area at the turbine rotor is

$$\text{MFP}(M) = 0.5021$$

$$A = \frac{\dot{m}\sqrt{T_t}}{(\cos\alpha)(P_t)\text{MFP}(M)} = \frac{156\sqrt{3200}}{\cos 60\,\text{deg} \times 142.40 \times 0.5021}$$

$$= 246.8\,\text{in.}^2\,(0.1593\,\text{m}^2)$$

For a hub/tip ratio of 0.9, the tip radius is 20.3 in. (0.516 m). The rotor speed of 1400 ft/s (426.7 m/s) requires a rotational speed of 826 rad/s. For a hub/tip ratio of 0.85, the tip radius is 16.8 in. (0.427 m), and the corresponding rotational speed is 998 rad/s. At this time, *we select a rotor speed of 800 rad/s for the compressor* to keep the AN^2 of the compressor and turbine low. This value will be used in the preliminary design of the compressor stages. The corresponding hub, mean, and tip radii of the compressor's first stage will be 15, 18, and 21 in., respectively.

9.3.8.2 Inlet guide vanes. We will now consider the inlet guide vanes. The inlet guide vanes change both the direction of flow and its Mach number. For isentropic flow through the inlet guide vanes, the following relationship can be written with stations 0 and 1 corresponding to the inlet and exit, respectively:

$$(\cos\alpha_1)(A_1)\text{MFP}(M_1) = A_0\text{MFP}(M_0) \tag{9.63}$$

For our case, where the entrance Mach number is 0.5, the preceding relationship can be used to calculate α_1 vs M_1 for different values of A_1/A_0. Results for $A_1/A_0 = 1.15$, 1.10, 1.05, and 1.0 are plotted in Fig. 9.35. Because the inlet guide vane sets up the flow for the first stage of the compressor, we will use this plot in conjunction with the repeating-stage design curves to help select the area ratio A_1/A_0 for the desired inlet Mach number M_1 and flow angle α_1.

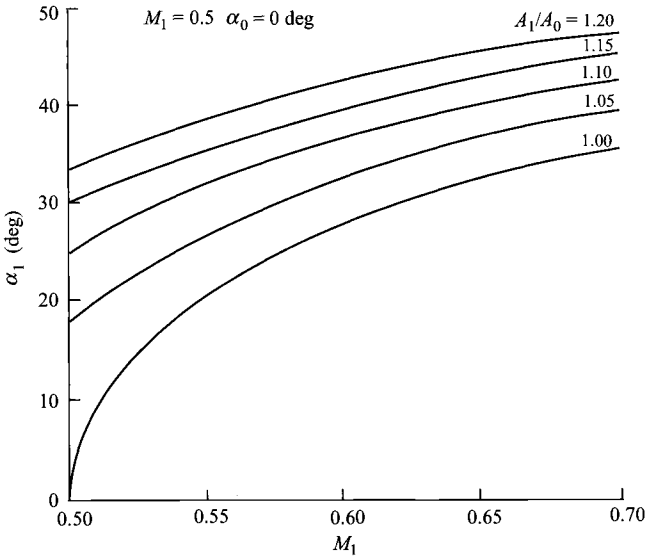

Fig. 9.35 Mean exit conditions from inlet guide vanes.

9.3.8.3 Selection of the number of stages. The number of compressor stages depends on the overall pressure ratio and the change in total temperature of each stage. Normally the changes in total temperature of the first and last stages are less than those of the other stages. In the absence of inlet guide vanes, the inlet flow to the first stage is axial, and less work can be done than in a stage whose inlet flow has swirl. The exit flow from the last stage is normally axial, which reduces the work of this stage.

The preliminary compressor design is based on repeating-row, repeating stage design. Thus the repeating-row, repeating-stage design equations and Figs. 9.23, 9.24, and 9.25 can be used to estimate the number of compressor stages. We will base the design on a mean-line diffusion factor D of 0.5, a mean-line solidity σ of 1, and a polytropic efficiency e_c of 0.9.

Because the stage inlet Mach number decreases through the compressor, the stage pressure ratio of a repeating-row, repeating-stage design will decrease. However, *the change in total temperature across each stage will remain constant* for this type of design.

For $M_1 = 0.6$ and α_1 between 30 and 40 deg, the data in Table 9.7b for the first stage can be obtained from the equations for repeating-row, repeating-stage design. Thus, for the assumed value of M_1 and range of α_1, we see from Table 9.7b that the total temperature change for a stage will be between 66.9 and 73.3°R. The total temperature rise for the whole compressor will be approximately

$$\Delta T_t = T_{ti}[(\pi_c)^{(\gamma-1)/(\gamma e_c} - 1] = 518.7[(10.2)^{1/(3.5\times0.9)} - 1] = 565.5°\text{R}$$

Table 9.7b Variation in repeating-row, repeating-stage designs with inlet flow angle

α_1, deg	α_2, deg	τ_s	π_s	ΔT_t, °R	$V_1/(\omega r)$	M_{1R}	ψ	Φ
30.0	51.79	1.1290	1.465	66.9	0.6250	0.840	0.375	0.541
32.0	52.94	1.1316	1.476	68.3	0.6051	0.844	0.359	0.513
34.0	54.10	1.1342	1.487	69.6	0.5867	0.848	0.344	0.486
36.0	55.28	1.1367	1.497	70.9	0.5697	0.852	0.330	0.461
38.0	56.47	1.1390	1.507	72.1	0.5541	0.856	0.318	0.437
40.0	57.67	1.1413	1.516	73.3	0.5396	0.859	0.306	0.413

The number of stages will then be either 9 (565.5/66.9 = 8.45) or 8 (565.5/73.3 = 7.71). *We select eight stages for this design.* Because the first stage has inlet guide vanes, we will use the same change in total temperature for this stage as for the other compressor stages. In addition, we will allow the last stage to have exit swirl (this can be removed by an additional set of stators) and will use the same change in total temperature for the last stage as for the other compressor stages. Thus each stage will have an equal temperature rise of 70.7°R (565.5/8). For the first stage, this corresponds to a temperature ratio of 1.136, which requires α_1 of about 36 deg and $V_1/(\omega r)$ of 0.57.

We select an inlet flow angle of 36 deg. The inlet air at $T_t = 518.7$°R and $M = 0.6$ has a velocity of 647 ft/s. The resulting stage loading coefficient is 0.3302 and flow coefficient is 0.4609, both within the range of these coefficients for modern axial-flow compressors. For a rotor speed of 800 rad/s, the mean radius is about 17 in. The inlet annulus area of the first stage will be

$$\text{MFP}(M_1) = 0.44757$$

$$A_1 = \frac{\dot{m}\sqrt{T_{t1}}}{(\cos\alpha_1)(P_{t1})\text{MFP}(M_1)} = \frac{150\sqrt{518.7}}{\cos 36\,\text{deg} \times 14.70 \times 0.4475}$$

$$= 641.8\,\text{in.}^2\ (0.4142\,\text{m}^2)$$

This area is 1.1 times the inlet area of the guide vanes. The corresponding tip radius and hub radius at the inlet to the first stage are about 20 and 14 in., respectively, giving a first-stage hub/tip ratio of 0.7.

Example 9.7

Consider the preliminary design of mean line. The COMPR program was used to perform the following analysis of a repeating-row, repeating-stage, mean-line design with a free-vortex swirl distribution. The following input data were entered:

Number of stages: 8
Rotor angular speed ω: 800 rad/s
Inlet total temperature T_t: 518.7°R
Mass flow rate: 150 lbm/s
Inlet total pressure P_t: 14.70 psia
Inlet flow angle α_1: 36 deg

Table 9.8a Summary of eight-stage compressor design

Stage	1	2	3	4	5	6	7	8
M_1	0.600	0.560	0.528	0.500	0.476	0.456	0.438	0.422
π_s	1.497	1.430	1.379	1.338	1.306	1.279	1.256	1.237
P_{t1}, psia	14.70	22.01	31.47	43.39	58.07	75.81	96.9	121.8
T_{r1}, °R	518.7	589.6	660.5	731.4	802.3	873.1	944.0	1014.9
r_h, in.	14.03	14.80	15.32	15.67	15.93	16.12	16.27	16.38
r_t, in.	20.03	19.26	18.75	18.39	18.14	17.94	17.80	17.68
A_1, in.^{2}	641.8	476.9	367.4	291.1	236.0	194.9	163.5	139.0

Inlet Mach number M_1: 0.6
Solidity σ: 1.0
Rotor c/h: 0.6
Gas constant: 53.34 ft . lbf/(lbm · °R)
Diffusion factor D: 0.5
Polytropic efficiency e_c: 0.9
Stator c/h: 0.6
Ratio of specific heats γ: 1.4

The results from COMPR are summarized in Table 9.8a for the mean-line design. The mean radius is 17.032 in. and the flow angle at the entrance to the stator α_2 is 55.28 deg. A cross-sectional sketch of the eight stages as plotted by COMPR and captured on a laser printer is shown in Fig. 9.36a. The estimated length of the compressor is 25.53 in. The resulting number of blades and blade chord lengths are given in Table 9.8b based on the input chord/height ratio of 0.6 for both the rotor and stator of all stages.

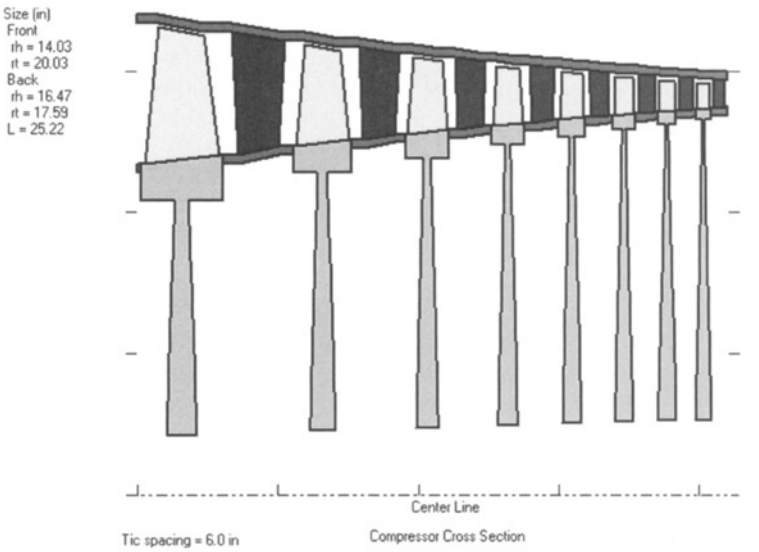

Fig. 9.36a Sketch of compressor cross section from COMPR with constant c/h.

Table 9.8b Number of blades with same c/h value for each row

Stage	1	2	3	4	5	6	7	8
Rotor								
c/h	0.60	0.60	0.60	0.60	0.60	0.60	0.60	0.60
Blades	33	43	56	70	86	103	122	143
Chord, in.	3.362	2.518	1.953	1.555	1.266	1.050	0.883	0.753
Stator								
c/h	0.60	0.60	0.60	0.60	0.60	0.60	0.60	0.60
Blades	38	49	63	77	94	112	132	154
Chord, in.	2.899	2.211	1.739	1.401	1.151	0.962	0.814	0.698

The number of blades in a rotor or stator now can be reduced by increasing its chord/height ratio. Because COMPR uses the same chord/height ratio for each blade row, for repeating-row, repeating-stage design, the user must select and run the program with the constant-mean-radius design. To obtain the same stage loss coefficients, the program is first run with the repeating-row, repeating-stage design. Then the user selects the constant mean-line design, inputs the desired chord/height ratios in the stage data screen for the rotor and stator of each stage, and performs the new calculations with a mean radius of 17.032 in. This procedure was used to reduce the number of blades in a row of stages 3 through 8, and the results are shown in Table 9.8c and Fig. 9.36b. For these stages, note that the number of blades is reduced and that the chord lengths are increased (see Table 9.8c). In addition, the estimated length of the compressor has increased to 30.36 in. (see Fig. 9.36b).

The AN^2 and estimated rim speed (assuming a rim height equal to the blade chord) at the inlet to each rotor are listed in Table 9.8d along with the relative total temperature on the mean line. These data values are related to the stresses in the turbomachinery (see Appendix J), and they can be used as a guide in blade and rim material selection and determining disk requirements. Based on

Table 9.8c Number of blades with different c/h values for each row

Stage	1	2	3	4	5	6	7	8
Rotor								
c/h	0.60	0.60	0.63	0.73	0.83	0.93	1.03	1.13
Blades	33	43	53	58	62	67	72	76
Chord, in.	3.362	2.518	2.050	1.892	1.752	1.627	1.516	1.418
Stator								
c/h	0.60	0.60	0.60	0.70	0.80	0.90	1.00	1.10
Blades	38	49	63	66	71	75	80	85
Chord, in.	2.899	2.211	1.739	1.634	1.535	1.442	1.357	1.280

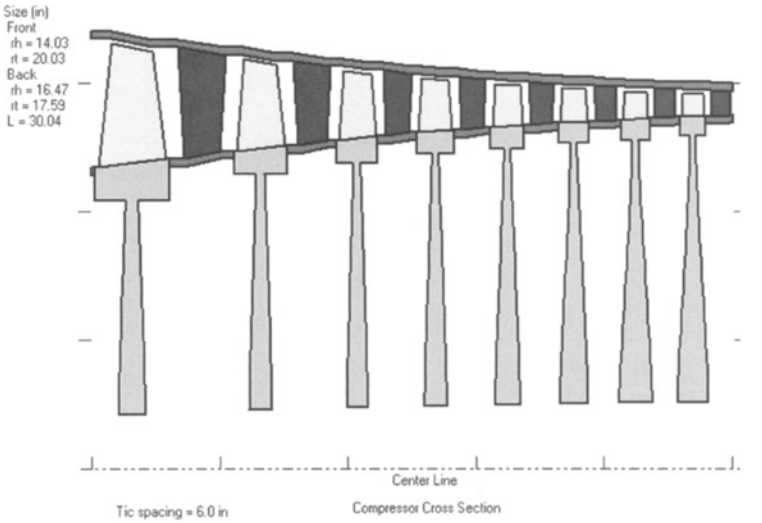

Fig. 9.36b Sketch of compressor cross section from COMPR with variable c/h.

the analytical tools and material properties of Appendix J, the rotor blades of stages 1–8 will require material 2 (a titanium alloy). The rim stress requirements can be met for these eight stages by using the same type of material as the blade. Since W_d/W_{dr} is greater than zero for each stage, each stage requires a disk.

The resulting total pressure and total temperature leaving the eight-stage compressor are 150.6 psia and 1086°R, respectively. The compressor efficiency is 86.32%. For axial flow at the exit with $M = 0.4$, an exit area of 98.15 in.^{2} (0.0633 m^2) is required for this compressor.

COMPR program calculates the variation in flow angle, diffusion factor, degree of reaction, Mach number, etc., of each stage for the selected swirl distribution. The minimum and maximum results and their location are listed in Table 9.9 for the free-vortex swirl distribution.

For this design, the inlet guide vanes have an inlet Mach number of 0.5, an exit Mach number of 0.6, and a flow angle of 36 deg. From Eq. (9.63), the flow area must increase from 585.7 to 639.4 in.^{2} For the same means radius as in the compressor stages, the entrance to the guide vanes will have a tip radius of 19.59 in. and a hub radius of 14.05 in.

The swirl velocity distributions v and flow angles β at the inlet and exit of the rotor are plotted in Fig. 9.37. Note the significant variation with radius of the swirl velocity and flow angles for the first stage ($14 < r < 20$) and very little for the last stage ($16.4 < r < 17.7$). In the first-stage rotor, the relative flow turns about 30 deg at the hub and only about 10 deg at the tip. The large radial variation in the rotor inlet flow angle for the first stage requires that its rotor blades have a lot of twist in them, whereas most of the relative flow in the last-stage rotor is turned about 20 deg and its rotor blades do not require a lot of twist.

Table 9.8d Material selection calculations for rotor blades, rims, and disks

Stage	1	2	3	4	5	6	7	8
AN^2 ($\times 10^{10}$ in.$^2 \cdot$ rpm^2)	3.2530	2.4598	1.9209	1.5389	1.2587	1.0474	0.88422	0.75579
σ_c/ρ, ksi/(slug/ft^3)[a]	2.7377	1.0702	1.6166	1.2951	1.0593	0.8815	0.7442	0.6361
T_{t1R}, °R	554	625	696	767	838	909	979	1050
T_{t1R}, °F	94	165	236	307	378	449	519	590
Blade material	← Material 2 →							
r_h, in.	14.03	14.80	15.32	15.67	15.93	16.12	16.27	16.38
ωr_h ft/s	953.33	986.67	1021.3	1044.7	1062.0	1074.7	1084.7	1092.0
h_r[b] in.	3.362	2.518	2.050	1.892	1.752	1.627	1.516	1.418
r_r, in.	10.668	12.282	13.270	13.778	14.178	14.493	14.754	14.962
Rim material	← Material 2 →							
σ_r/ρ, ksi/(slug/ft^3)	4	4	4	4	4	4	4	4
$\rho\,(\omega r)^2/\sigma_r$	1.5188	1.6901	1.8110	1.8947	1.9581	2.0050	2.0425	2.0702
W_{dr}/W_r[c]	0.4578	0.3367	0.2856	0.2735	0.2616	0.2500	0.2395	0.2299
ωr, ft/s	711.20	818.80	884.67	918.53	945.20	966.20	983.60	997.47
σ_d/ρ, ksi/(slug/ft^3)[d]	0.8781	1.1639	1.3587	1.4648	1.5510	1.6207	1.6796	1.7273
Disk material	← Material 2 →							

[a]Based on Eq. (E.6) and a blade taper ratio of 1.0.
[b]Based on h_r equal to blade chord.
[c]Based on Eq. (E.10) and $\bar{\sigma}_{\text{blades}}/\sigma_r = 0.1$.
[d]Based on Eq. (E.12).

Table 9.9 Extreme values in eight-stage compressor design

Item	Value	Location
Maximum α_1, deg	41.41	Hub at entrance to first-stage rotor
Minimum α_1, deg	31.71	Tip at entrance to first-stage rotor
Maximum β_1, deg	62.68	Tip at entrance to first-stage rotor
Minimum β_1, deg	42.15	Hub at entrance to first-stage rotor
Maximum M	0.943	Hub at exit of first-stage rotor
Maximum M_R	1.053	Tip at entrance to first-stage rotor
Maximum D	0.526	Hub of first-stage stator
Minimum D	0.450	Tip of first-stage rotor
Maximum reaction	0.625	Tip of first stage
Minimum reaction	0.309	Hub of first stage

9.3.9 Compressor Performance

The pumping characteristics of axial-flow compressors are best represented by a plot (based on experimental data) called the *compressor map*. The data are presented in terms of *corrected quantities* that are related to the performance of the compressor. A compressor is tested in a rig similar to the sketch of Fig. 9.38. The rotational speed is controlled by the electric motor and the mass flow rate by the valve. The inlet and exit conditions are measured along with the rotational speed and input power. These data are reduced to give the resulting compressor map.

9.3.9.1 Corrected quantities. For a compressor, the four corrected quantities shown in Table 9.10 are normally used to map its performance. The corrected rotational speed is directly proportional to the ratio of the axial to rotational velocity. The corrected mass flow rate is directly proportional to the Mach number of the entering flow. We note that

$$\dot{m}_i = \frac{P_{ti}}{\sqrt{T_{t_i}}} A_i \, \mathrm{MFP}(M_i)$$

Table 9.10 Compressor corrected quantities

Item	Symbol	Corrected
Pressure	P_{t_i}	$\delta_t = \dfrac{P_{ti}}{P_{\text{ref}}}$ where $P_{\text{ref}} = 14.696$ psia
Temperature	T_{t_i}	$\theta_t = \dfrac{T_{t_i}}{T_{\text{ref}}}$ where $T_{\text{ref}} = 518.7°\text{R}$
Rotational speed	$N = \text{RPM}$	$\dfrac{N}{\sqrt{\theta_t}}$
Mass flow rate	$\dot{m}_t$	$\dot{m}_{ct} = \dfrac{\dot{m}_t \sqrt{\theta_t}}{\delta_t}$

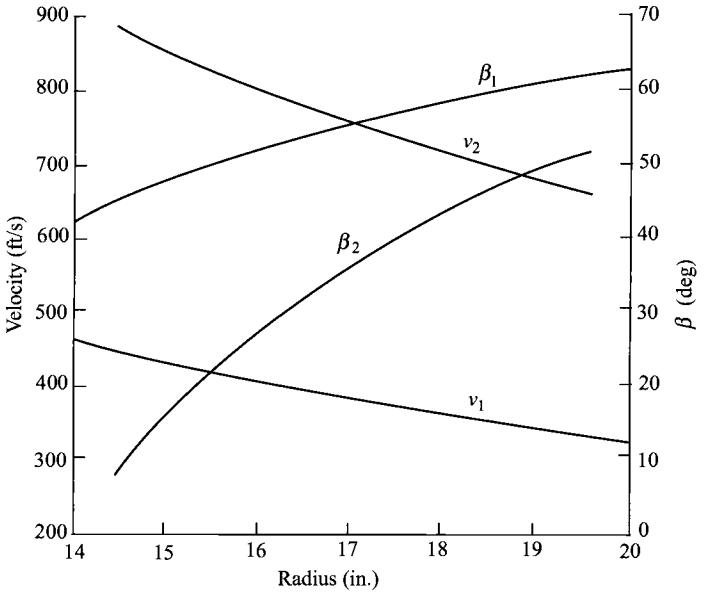

Fig. 9.37 Swirl velocity distribution and variation of rotor flow angles.

Then

$$\dot{m}_{ci} = \frac{\dot{m}_i\sqrt{T_{ti}}}{P_{ti}}\frac{P_{\text{ref}}}{\sqrt{T_{\text{ref}}}} = \frac{P_{\text{ref}}}{\sqrt{T_{\text{ref}}}}A_i\,\text{MFP}(M_i)$$

Therefore,

$$\dot{m}_{ci} = f(M_i)$$

At engine station 2 (entrance to compressor or fan)

$$\dot{m}_{c2} = \frac{P_{\text{ref}}}{\sqrt{T_{\text{ref}}}}A_2\,\text{MFP}(M_2) \tag{9.64}$$

Thus the corrected mass flow rate is directly proportional to a the Mach number at the entrance to the compressor.

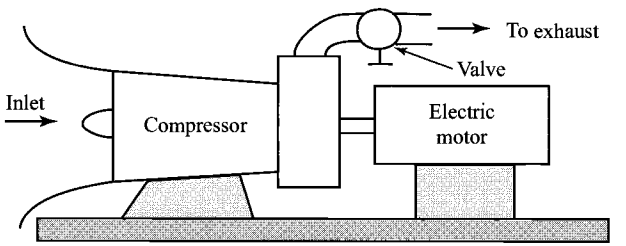

Fig. 9.38 Sketch of compressor test rig.

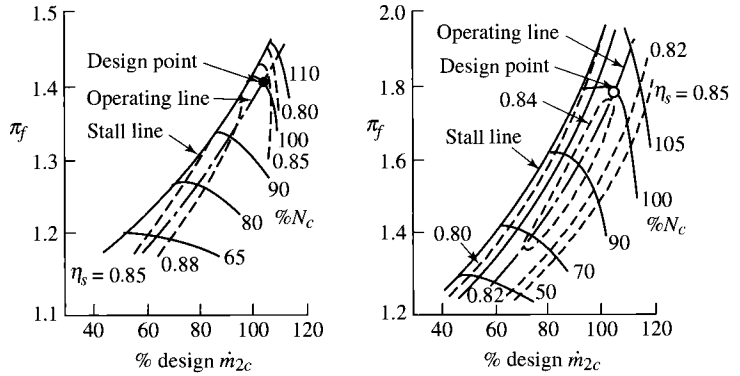

a) Subsonic tangential Mach **b) Supersonic tangential Mach**

Fig. 9.39 Typical fan stage maps (Ref. 52).

9.3.9.2 Compressor map. The performance of two modern high-performance fan stages is shown in Fig. 9.39. They have no inlet guide vanes. One has a low tangential Mach number (0.96) to minimize noise. The other has supersonic tip speed and a considerably larger pressure ratio. Both have high axial Mach numbers.

Variations in the axial-flow velocity in response to changes in pressure cause the multistage compressor to have quite different mass flow vs pressure ratio characteristics from those of one of its stages. The performance map of a typical high-pressure-ratio compressor is shown in Fig. 9.40.

A limitation on fan and compressor performance of special concern is the stall or surge line. Steady operation above the line is impossible, and entering the region even momentarily is dangerous to the compressor and its application.

9.3.9.3 Compressor starting problems. The cross section of a multistage compressor is shown in Fig. 9.41. Also shown (in solid lines) at three locations in the machine are mean-line rotor inlet velocity diagrams for on-design operation. The design shown here has a constant mean radius, a constant axial velocity, and zero swirl at the rotor-inlet stations.

Let us apply the continuity equation, which states that the mass flow rate is the same at all stations in the compressor. Then, at the inlets to the first and last stages,

$$\dot{m} = \rho_1 A_1 u_1 = \rho_3 A_3 u_3$$

or

$$\frac{u_1}{u_3} = \frac{\rho_3 A_3}{\rho_1 A_1} \tag{9.65}$$

At the design point, since $u_3 = u_1$, then $\rho_3/\rho_1 = A_1/A_3$. When the compressor is operating at a lower speed, however, it is not able to produce as high a density

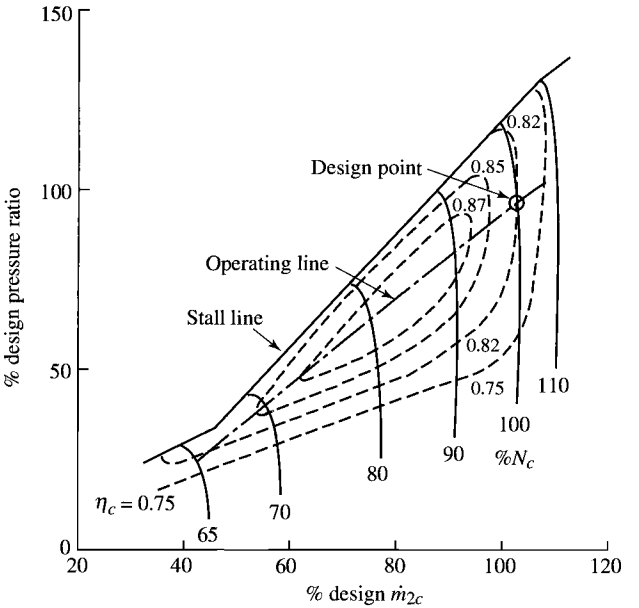

Fig. 9.40 Typical compressor map.

ratio (or pressure ratio) as at design speed, and because the area ratio remains fixed, it follows from Eq. (9.65) that the inlet/outlet axial velocity ratio must have a value less than that at design. In Fig. 9.41, the velocity diagrams shown (in dashed lines) indicate the rotor inlet conditions at partial speed. For each of the three stages represented, the blade speed is the same, but the inlet stage axial velocity is shown less than that for the outlet stage in accordance with

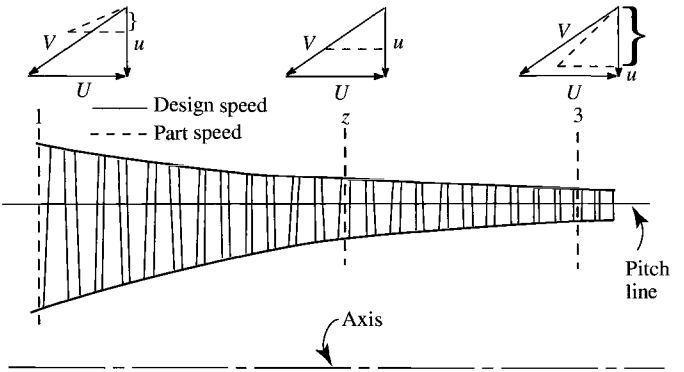

Fig. 9.41 Cross section of a multistage compressor. Rotor-inlet velocity diagrams are shown for inlet, middle, and exit stages.

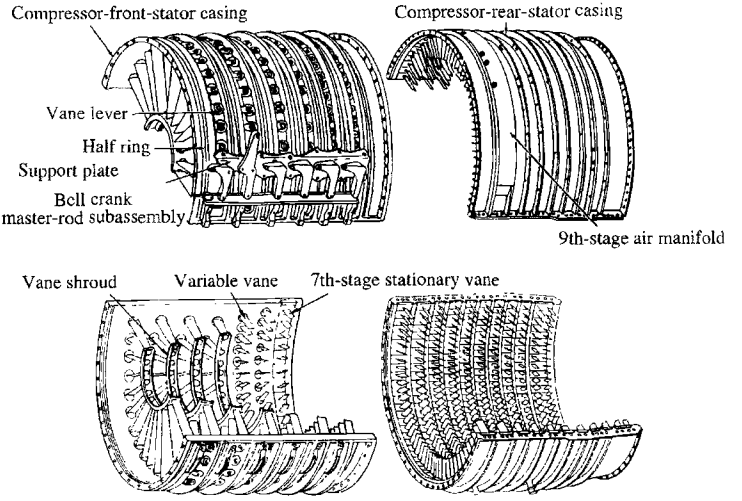

Fig. 9.42 Compressor case for the General Electric J-79 turbojet engine. (Courtesy of General Electric.)

Eq. (9.65). Because of the varying axial velocity, it is possible for only one stage near the middle of the machine (called the *pivot stage*) to operate with the same angle of attack at all speeds. At lower speeds, the blading forward of the pivot stage is pushed toward stall, and the blading aft of the pivot stage is windmilling with a tendency toward choking. At speeds higher than the design value, these trends are reversed.

Several techniques have been utilized to reduce the low-speed and starting effects:

1) Use bleed valves. Release air from the middle stages, reducing the tendency to windmill in later stages.

2) Use multispool compressors. Run different spools at their own suitable speeds.

3) Use variable stators in the early rows.

4) Use combinations of the preceding techniques.

An example of an early high-performance compressor is that used in the General Electric J-79 turbojet engine. This compressor has 17 stages on a single spool that results in a pressure ratio of 13.5. Figure 9.42 shows the compressor case of this engine with the variable stators used on the first six stages and the manifold for the bleed valves on the ninth stage. Most modern engines have compressors with multiple spools and bleed valves. The need for variable stators in the early rows is less for the multispool compressors.

9.4 Centrifugal-Flow Compressor Analysis

The centrifugal compressor has been around for many years. It was used in turbochargers before being used in the first turbojet engines of Whittle and von

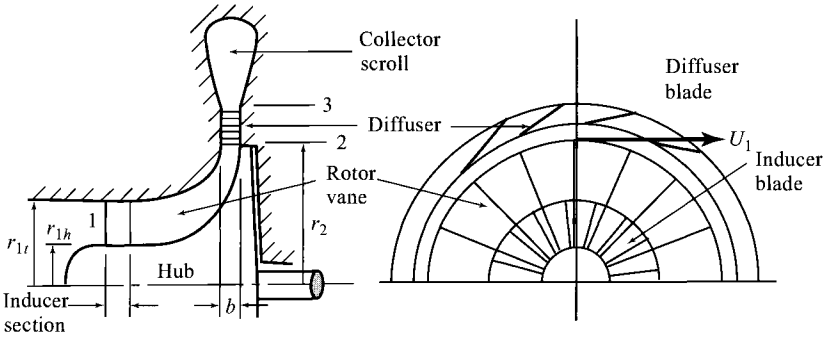

a) Cross-sectional view **b) View of rotor and diffuser**

Fig. 9.43 Centrifugal-flow compressor.

Ohain. Figure 9.43 shows a sketch of a centrifugal-flow compressor with radial rotor (or impeller) vanes. Flow passes through the annulus between r_{1h} and r_{1t} at station 1 and enters the inducer section of the rotor (also called *rotating guide vanes*). Flow leaves the rotor at station 2 through the cylindrical area of radius r_2 and width b. The flow then passes through the diffuser, where it is slowed and then enters the collector scroll at station 3.

The velocity diagrams at the entrance and exit of the rotor (impeller) are shown in Fig. 9.44. The inlet flow is assumed to be axial of uniform velocity u_1. The relative flow angle of the flow entering the rotor increases from hub to tip and thus the twist of the inlet to the inducer section of the rotor. The flow leaves the rotor with a radial component of velocity w_2 that is approximately equal to the inlet axial velocity u_1 and a swirl (tangential) component of velocity v_2 that is about 90% of the rotor velocity U_t. The diffuser (which may be vaneless) slows the velocity of the flow v_3 to about 90 m/s (300 ft/s).

Application of the Euler equation to flow of a calorically perfect gas through a centrifugal-flow compressor with axial flow entering gives

$$T_{t3} - T_{t1} = \frac{v_2 U_t}{g_c c_p} \tag{9.66}$$

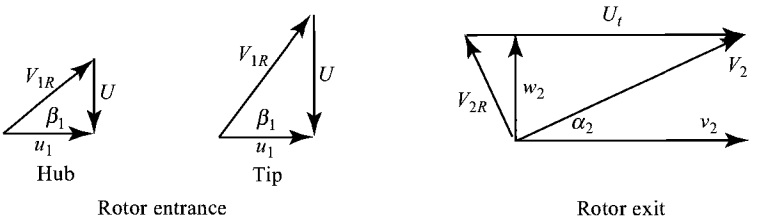

Fig. 9.44 Velocity diagrams for radial vaned centrifugal compressor.

Ideally, the fluid leaving the rotor wheel has a swirl velocity v_2 equal to the rotor speed U_t. Because of slip between the rotor and fluid, the fluid leaving the rotor wheel attains only a fraction of the rotor speed. The ratio of the exit swirl velocity to the rotor speed is called the *slip factor* ε:

$$\varepsilon = \frac{v_2}{U_t} \tag{9.67}$$

The slip factor is related to the number of vanes on the rotor. As the number of vanes n is increased, the slip factor approaches 1 and the frictional losses of the rotor increase. Selection of the number of vanes is a balance between high slip factor and reasonable losses, which usually results in a slip factor of 0.9. A useful correlation between the slip factor ε and number of vanes n *is*

$$\varepsilon = 1 - \frac{2}{n} \tag{9.68}$$

Substitution of Eq. (9.67) into Eq. (9.66) gives a relationship for the compressor temperature rise in terms of the rotor speed U_t and slip factor ε:

$$T_{t3} - T_{t1} = \frac{\varepsilon U_t^2}{g_c c_p} \tag{9.69}$$

By using the polytropic compressor efficiency e_c and Eq. (9.69), the compressor pressure ratio can be expressed as

$$\pi_c = \frac{P_{t3}}{P_{t1}} = \left(1 + \frac{\varepsilon U_t^2}{g_c c_p T_{t1}}\right)^{\gamma e_c/(\gamma-1)} \tag{9.70}$$

From Eq. (9.70), compressor pressure ratio π_c is plotted vs rotor speed U_t in Fig. 9.45 for air [$\gamma = 1.4$, $c_p = 1.004$ kJ/(kg · K)] at standard conditions ($T_{t1} = 288.16$ K) with a slip factor ε of 0.9. For rotors with light alloys, U_t is limited to about 450 m/s (1500 ft/s) by the maximum centrifugal stresses of the rotor, which corresponds to compressor pressure ratios of about 4. More extensive materials permit higher speeds and pressure ratios up to about 8.

Equation (9.70) can also be written in terms of the compressor adiabatic efficiency η_c as

$$\pi_c = \frac{P_{t3}}{P_{t1}} = \left(1 + \frac{\eta_c \varepsilon U_t^2}{g_c c_p T_{t1}}\right)^{\gamma/(\gamma-1)} \tag{9.71}$$

The *T-s* diagram for the centrifugal compressor is shown in Fig. 9.46. This diagram is very useful during the analysis of centrifugal-flow compressors. Even though the rotor exit velocity v_2 may be supersonic, the flow leaving the rotor will choke only when the radial exit velocity w_2 is sonic. For determining the total pressure at station 2, an estimate must be made of the split in total

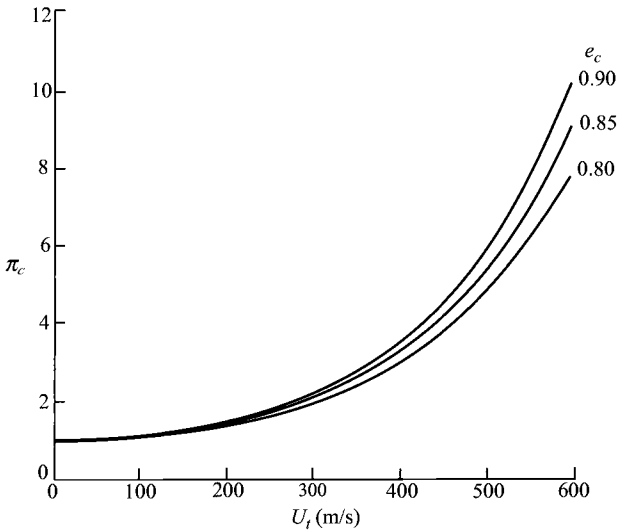

Fig. 9.45 Compressor pressure ratio vs rotor speed.

pressure loss between the rotor and diffuser. As an estimate, we equate the total pressure ratio of the diffuser P_{t3}/P_{t2} to the actual/ideal total pressure ratio leaving the rotor P_{t2}/P_{t3s}, or

$$\frac{P_{t2}}{P_{t3s}} = \frac{P_{t3}}{P_{t2}} = \sqrt{P_{t3}/P_{t3s}} \tag{9.72}$$

The radial component of velocity leaving the rotor w decreases with radius due to the increase in radial flow area. If frictional losses are neglected, the tangential

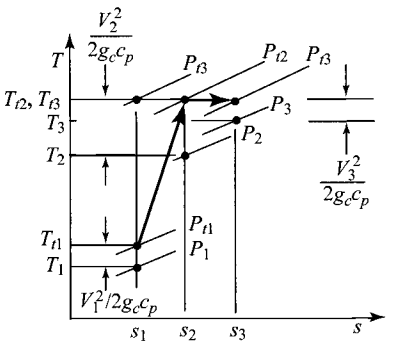

Fig. 9.46 The *T-s* diagram for centrifugal compressor.

momentum rv will remain constant, or

$$rv = \text{const} = r_2 v_2$$

As a result of the decreases in both the radial and tangential velocities, the velocity entering the diffuser is less than that leaving the rotor.

The diffuser further decreases the velocity and may turn the flow with blades. The flow leaving the diffuser is collected in the scroll (see Fig. 9.43). The flow area of the scroll A_θ must increase in proportion to the mass flow being added to keep the flow properties constant. We can write

$$\frac{dA_\theta}{d\theta} = \frac{1}{\rho_3 V_3} \frac{d\dot{m}}{d\theta} = r_3 b_3 \tag{9.73}$$

Centrifugal-flow compressors are used in gas turbine engines when the corrected mass flow rate is small (less than about 10 kg/s). For small corrected mass flow rates, the rotor blades of axial-flow compressors are very short, and the losses are high. The performance of a centrifugal compressor for low flow rates can be as good as or better than that of the axial-flow compressor.

The performance of a centrifugal-flow compressor is presented as a compressor map (similar to the map of an axial-flow compressor). The map of a typical centrifugal compressor is shown in Fig. 9.47. Note that the overall pressure ratio is limited to about 4. Gas turbine engine cycles normally require a pressure ratio greater than 4 and additional stages of compression are needed. For engines with entering corrected mass flow rates greater than 10 kg/s, additional compression is obtained from axial-flow stages in front of the centrifugal compressor. When the corrected mass flow is less than 10 kg/s, higher cycle pressure ratios are obtained by using two or more centrifugal compressors in series.

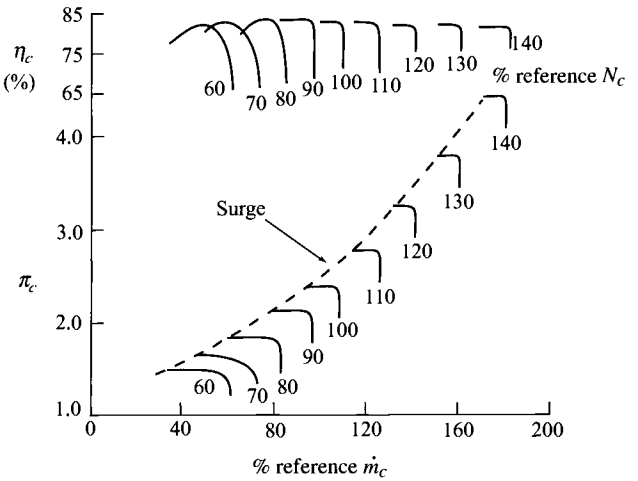

Fig. 9.47 Performance map of typical centrifugal compressor.

Example 9.8

Consider a centrifugal compressor.

Given:

Mass flow rate = 8 kg/s
Pressure ratio $\pi_c = 4.0$
Polytropic efficiency $e_c = 0.85$
Inlet root diameter = 15 cm
Outlet diameter of impeller = 50 cm
$V_3 = 90$ m/s
$P_{t1} = 101.3$ kPa
$T_{t1} = 288.16$ K
Slip factor $\varepsilon = 0.9$
Inlet tip diameter = 30 cm
$w_2 = u_1$

Find:

1) Rotational speed and rpm of the rotor
2) Rotor inlet Mach number, velocity, and relative flow angles at hub and tip
3) Rotor exit velocity, Mach number, total temperature, total pressure, and direction
4) Depth of rotor exit s
5) Diffuser exit Mach number, area, total temperature, and total pressure

Solution:

$$U_t^2 = \frac{g_c c_p T_{t1}}{\varepsilon}(\pi_c^{(\gamma-1)/(\gamma e_c)} - 1)$$

$$= \frac{1004 \times 288.16}{0.9}(4^{1/(3.5\times 0.85)} - 1)$$

$$U_t = 436.8 \text{ m/s}$$

$$N = \frac{60U_t}{\pi d_2} = \frac{60(436.8)}{\pi(0.5)} = 16{,}685 \text{ rpm}$$

$$\text{MFP}(M_1) = \frac{\dot{m}\sqrt{T_n}}{P_{t1}A_1} = \frac{8\sqrt{288.16}}{101{,}300 \times \pi(0.15^2 - 0.075^2)} = 0.025287$$

$$M_1 = 0.3966$$

$$u_1 = V_1 = \sqrt{2g_c c_p T_{t1}\left\{1 - \frac{1}{1 + [(\gamma-1)/2]M_1^2}\right\}}$$

$$= \sqrt{2 \times 1004 \times 288.16\left(1 - \frac{1}{1 + 0.2 \times 0.3966^2}\right)} = 132.8 \text{ m/s}$$

$$v_{1Rh} = \frac{d_{1h}}{d_2}U_t = \frac{15}{50}(436.8) = 131.0 \text{ m/s}$$

$$v_{1R_t} = \frac{d_{1t}}{d_2}U_t = \frac{30}{50}(436.8) = 262.1 \text{ m/s}$$

$$\beta_{1h} = \tan^{-1}\frac{v_{1Rh}}{u_1} = 44.6\,\text{deg}$$

$$\beta_{1t} = \tan^{-1}\frac{v_{1Rt}}{u_1} = 63.1\,\text{deg}$$

$$T_{t3} = T_{t2} = T_{t1} + \frac{\varepsilon U_t^2}{g_c c_p} = 288.16 + \frac{0.9 \times 436.8^2}{1004} = 459.19\,\text{K}$$

$$\eta_c = \frac{(P_{t3}/P_{t1})^{\gamma/(\gamma-1)} - 1}{T_{t3}/T_{t1} - 1} = \frac{4^{1/3.5} - 1}{459.19/288.16 - 1} = 81.9\%$$

$$v_2 = \varepsilon U_t = 0.9 \times 436.8 = 393.1\ \text{m/s}$$

$$w_2 = u_1 = 132.8\ \text{m/s}$$

$$V_2 = \sqrt{w_2^2 + v_2^2} = \sqrt{132.8^2 + 393.1^2} = 414.9\,\text{m/s}$$

$$\alpha_2 = \tan^{-1}\frac{w_2}{v_2} = 18.67\,\text{deg}$$

$$M_2 = \sqrt{\frac{2}{\gamma - 1}\left[\frac{T_{t2}}{T_{t2} - V_2^2/(2g_c c_p)} - 1\right]}$$

$$= \sqrt{5\left(\frac{459.19}{459.19 - 85.73} - 1\right)} = 1.071$$

$$\frac{P_{t3s}}{P_{t1}} = \left(\frac{T_{t3}}{T_{t1}}\right)^{\gamma/(\gamma-1)} = 5.108$$

$$\frac{P_{t2}}{P_{t3s}} = \frac{P_{t3}}{P_{t2}} = \sqrt{\frac{P_{t3}/P_{t1}}{P_{t3s}/P_{t1}}} = 0.8849$$

$$P_{t2} = 0.8849 \times 5.108 \times 101.3 = 457.9\,\text{kPa}$$

$$P_{t3} = 4.0 \times 101.3 = 405.2\,\text{kPa}$$

$$\text{MFP}(M_2) = 0.040326$$

$$A_2 = \frac{\dot{m}\sqrt{T_{t2}}}{P_{t2}\text{MFP}(M_2)(\cos\alpha_2)} = \frac{8\sqrt{459.19}}{457{,}900 \times 0.040326 \times 0.9474} = 0.0098\,\text{m}^2$$

$$b = \frac{A_2}{\pi d_2} = \frac{0.0098}{\pi \times 0.5} = 0.624\,\text{cm}$$

Table 9.11 Results for Example 9.8 centrifugal compressor

Property		Station 1	1*R*	2*R*	2	3
T_t	K	**288.16**	296.70/322.36 (hub/tip)	383.23	459.19	459.19
T	K	279.37	279.37	272.50	373.50	455.16
P_t	kPa	**101.3**	112.2/150.0	243.1	457.9	**405.2**
P	kPa	90.9	90.9	222.2	222.2	392.9
M		0.3966	0.557/0.877	0.361	1.071	0.2105
V	m/s	132.8	186.54/293.82	139.8	414.9	90
u/w	m/s	132.8	132.8	132.8	132.8	
v	m/s	0	131.0/262.1	43.7	393.1	
r	cm		**15/30**	**50.0**	**50.0**	
α	deg	0	——	——	18.67	
β	deg	——	44.6/63.1	69.1	——	

$$M_3 = \sqrt{\frac{2}{\gamma - 1}\left[\frac{T_{t3}}{T_{t3} - V_3^2/(2g_c c_p)} - 1\right]}$$

$$= \sqrt{5\left(\frac{459.19}{459.19 - 4.034} - 1\right)} = 0.2105$$

$$\text{MFP}(M_3) = 0.014343$$

$$A_3 \cos \alpha_3 = \frac{\dot{m}\sqrt{T_{t3}}}{P_{t3}\text{MFP}(M_3)} = \frac{8\sqrt{459.196}}{405{,}200 \times 0.014343} = 0.0295 \text{ m}^2$$

The results of this example are summarized in Table 9.11. Note that different values of flow properties are listed for the hub and tip at station 1*R* and that M_2 is supersonic while M_{2R} is subsonic.

9.5 Axial-Flow Turbine Analysis

The mass flow of a gas turbine engine, which is limited by the maximum permissible Mach number entering the compressor, is generally large enough to require an axial turbine (even for centrifugal compressors). The axial turbine is essentially the reverse of the axial compressor except for one essential difference: the turbine flow operates under a favorable pressure gradient. This permits greater angular changes, greater pressure changes, greater energy changes, and higher efficiency. However, there is more blade stress involved because of the higher work and temperatures. *It is this latter fact that generally dictates the blade shape.*

Conceptually, a turbine is a very simple device because it is fundamentally no different from a pinwheel that spins rapidly when air is blown against it. The pinwheel will turn in one direction or the other, depending on the direction of the impinging air, and a direction can be found for the air that causes no rotation at all. Thus it is important to properly direct the airstream if the desired motion and speed are to be obtained.

A modern turbine is merely an extension of these basic concepts. Considerable care is taken to establish a directed flow of fluid of high velocity by means of stator blades, and then similar care is used in designing the blades on the rotating wheel (the vanes on the pinwheel) so that the fluid applies the required force to these rotor blades most efficiently. Conceptually, the turbine is a cousin to the pinwheel, but such an analogy gives no appreciation for the source of the tremendous power outputs that can be obtained in a modern turbine. The appreciation comes when one witnesses a static test of the stator blades that direct a gas stream to the rotor of a modern aircraft gas turbine. Such a stream exhausting into the quiescent air of a room will literally rip the paint off the wall at a point 6 ft away in line with the jet direction. When blades of the rotating element are pictured in place immediately at the exit of these directing blades, it then becomes difficult to imagine that the rotor could be constrained from turning and producing power.

Terminology can be a problem in the general field of turbomachinery. Compressor development grew out of aerodynamics and aircraft wing technology, while turbines have historically been associated with the mechanical engineers who developed the steam turbine. The symbols as well as the names used in these two fields differ, but for consistency and to minimize problems for the reader, the turbine will be presented using the nomenclature already established in the beginning of this chapter. Where a term or symbol is in such common use that to ignore it would mean an incomplete education, it will be indicated as an alternate. Thus turbine stator blades are usually called *nozzles* and rotor blades are *buckets.*

In the gas turbine, the high-pressure, high-temperature gas from the combustion chamber flows in an annular space to the stationary blades (called *stators, vanes*, or *nozzles*) and is directed tangentially against the rotating blade row (called *rotor blades* or *buckets*). A simple single-stage turbine configuration with nomenclature is shown in Fig. 9.48a. It is convenient to "cut" the blading on a cylindrical surface and look at the section of the stator and rotor blades in two dimensions. This leads to the construction of a vector or velocity diagram for the stage (see Fig. 9.48a) that shows the magnitude and direction of the gas velocities within the stage on the cylindrical surface.

In the stator or nozzle, the fluid is accelerated while the static pressure decreases and the tangential velocity of the fluid is increased in the direction of rotation. The *rotor* decreases the tangential velocity in the direction of rotation, tangential forces are exerted by the fluid on the rotor blades, and a resulting torque is produced on the output shaft. The absolute velocity of the fluid is reduced across the rotor. Relative to the moving blades, typically there is acceleration of the fluid with the associated decrease in static pressure and static temperature. A multistage turbine is made up of consecutive stages, each stage consisting of first a nozzle row followed by a rotor row. Figure 9.48b shows an

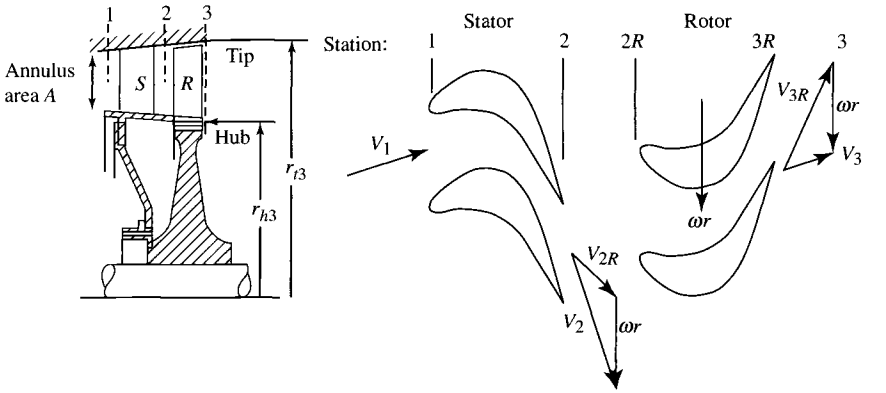

Fig. 9.48a Typical single-stage turbine and velocity diagram.

isometric section of the four-stage turbine for a two-spool, low-bypass-ratio turbofan engine.

The following analysis of the axial-flow turbine stage is performed along the mean radius with radial variations being considered. In many axial-flow turbines, the hub and tip diameters vary little through a stage, and the hub/tip ratio approaches unity. There can be no large radial components of velocity between the annular walls in such stages, there is little variation in static pressure from root to tip, and the flow conditions are little different at each radius.

For these stages of high hub/tip ratio, the two-dimensional analysis is sufficiently accurate. The flow velocity triangles are drawn for the mean-radius

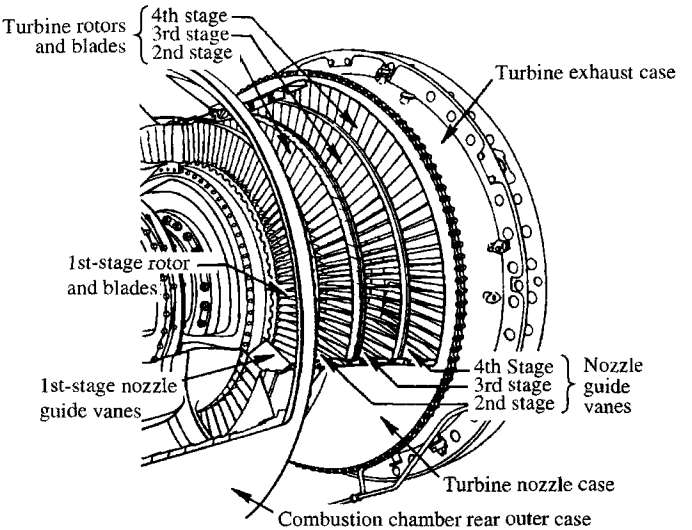

Fig. 9.48b Isometric section of multistage turbine. (Courtesy of Pratt & Whitney.)

condition, but these triangles are assumed to be valid for the other radial sections. The mean-radius analysis presented in this section applies to the total flow for such *two-dimensional* stages: the flow velocity, blade speed, and pressures being assumed constant along the blade length.

From the Euler turbine equation, [Eq. (9.4)], the energy per unit mass flow exchanged between fluid and rotor for $r_2 = r_3$ is

$$h_{t2} - h_{t3} = c_p(T_{t2} - T_{t3}) = \frac{\omega r}{g_c}(v_2 + v_3) \tag{9.74}$$

Inspection of the velocity triangles (Fig. 9.49) shows that because of the large angle α_2 at the stator exit and the large turning possible in the rotor, the value of v_3 is often positive (positive α_3). As a result, the two swirl velocity terms on the right side of Eq. (9.74) add, giving large power output.

The large turning in stator and rotor is possible because, usually, the flow is accelerating through each blade row, that is, $v_2 > v_1$ and $v_{3R} > v_{2R}$. This means that the static pressure drops across both stator and rotor and, under such circumstances, a favorable pressure gradient exists for the boundary layers on the blade and wall surfaces, and separation can be avoided. Accelerating flow is an inherent feature of turbines and means that no general flow breakdown similar to compressor stall will occur.

Note that the vector diagram establishes the characteristics of a stage, and geometrically similar diagrams have the same characteristics. The angles of the vector diagram determine its shape and, therefore, become important design parameters. The velocity magnitudes are not important as performance parameters except in relation to the sonic velocity, i.e., except in terms of the Mach number. The angles may be used directly as design parameters or may be implied through the use of velocity ratios. Thus the magnitude of, say,

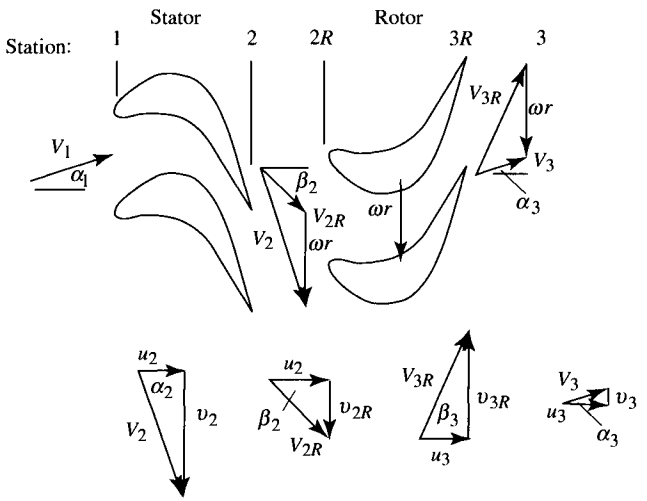

Fig. 9.49 Velocity triangles for a typical turbine stage.

$v_2 + v_3 = \Delta v$, although proportional to the absolute output, is not significant in defining the vector diagram, whereas the ratio $\Delta v/(\omega r)$ helps establish the vector diagram angles and, therefore, the stage characteristics.

The stage analysis in the following sections neglects the influence of cooling air. Thus the flow through the turbine nozzle is assumed to be adiabatic ($T_{t2} = T_{t1}$), as is the flow through the rotor in the relative reference frame ($T_{t3R} = T_{t2R}$). Turbine cooling is discussed at the end of this chapter.

Example 9.9

Consider mean-radius stage calculation—isentropic flow.

Given:

$$T_{t1} = 3200°\text{R}, \quad P_{t1} = 300 \text{ psia}, \quad \alpha_2 = 60 \text{ deg}$$
$$\alpha_3 = 0 \text{ deg}, \quad M_2 = 1.1, \quad \omega r = 1400 \text{ ft/s}$$
$$u_3 = u_2, \quad \gamma = 1.3, \quad R = 53.40 \text{ ft} \cdot \text{lbf/(lbm} \cdot °\text{R)}$$

Find the flow properties for this isentropic turbine stage.

Solution:

$$T_{t2} = T_{t1} = 3200°\text{R}$$

$$T_2 = \frac{T_{t2}}{1 + [(\gamma - 1)/2]M_2^2} = \frac{3200}{1 + 0.15 \times 1.1^2} = 2708.4°\text{R}$$

$$g_c c_p = g_c \left(\frac{\gamma}{\gamma - 1}\right) R = 32.174 \left(\frac{1.3}{0.3}\right) 53.40 = 7445 \text{ ft}^2/(\text{s}^2 \cdot °\text{R})$$

$$V_2 = \sqrt{2 g_c c_p (T_{t2} - T_2)} = \sqrt{2(7445)(3200 - 2708.4)} = 2705.5 \text{ ft/s}$$

$$u_2 = V_2 \cos \alpha_2 = 2705.5 \cos 60 \text{ deg} = 1352.8 \text{ ft/s}$$

$$v_2 = V_2 \sin \alpha_2 = 2705.5 \sin 60 \text{ deg} = 2343.0 \text{ ft/s}$$

$$v_{2R} = v_2 - \omega r = 2343.0 - 1400 = 943.0 \text{ ft/s}$$

$$V_{2R} = \sqrt{u_2^2 + v_{2R}^2} = \sqrt{1352.8^2 + 943.0^2} = 1649.0 \text{ ft/s}$$

$$\beta_2 = \tan^{-1} \frac{v_{2R}}{u_2} = \tan^{-1} \frac{943.0}{1352.8} = 34.88 \text{ deg}$$

$$M_{2R} = M_2 \frac{V_{2R}}{V_2} = 1.1 \left(\frac{1649.0}{2705.5}\right) = 0.670$$

$$T_{t2R} = T_2 + \frac{V_{2R}^2}{2 g_c c_p} = 2708.4 + \frac{1649.0^2}{2(7445)} = 2891.0°\text{R}$$

$$v_3 = 0$$

$$V_3 = u_3 = u_2 = 1352.8 \text{ ft/s}$$

$$v_{3R} = v_3 + \omega r = 0 + 1400 = 1400\,\text{ft/s}$$

$$V_{3R} = \sqrt{u_3^2 + v_{3R}^2} = \sqrt{1352.8^2 + 1400^2} = 1946.8\,\text{ft/s}$$

$$\beta_3 = \tan^{-1}\frac{v_{3R}}{u_3} = \tan^{-1}\frac{1400}{1352.8} = 45.98\,\text{deg}$$

$$T_{t3} = T_{t2} - \frac{\omega r}{g_c c_p}(v_2 + v_3) = 3200 - \frac{1400}{7445}(2343.0 + 0) = 2759.4^\circ\text{R}$$

$$T_3 = T_{t3} - \frac{V_3^2}{2g_c c_p} = 2759.4 - \frac{1352.8^2}{2(7445)} = 2636.5^\circ\text{R}$$

$$M_3 = \sqrt{\frac{2}{\gamma - 1}\left(\frac{T_{t3}}{T_3} - 1\right)} = \sqrt{\frac{2}{0.3}\left(\frac{2759.8}{2636.5} - 1\right)} = 0.558$$

$$M_{3R} = M_3\frac{V_{3R}}{V_3} = 0.558\left(\frac{1946.8}{1352.8}\right) = 0.803$$

$$T_{t3R} = T_{t2R} = 2891.0^\circ\text{R}$$

$$P_{t2} = P_{t1} = 300\,\text{psia}$$

$$P_2 = P_{t2}\left(\frac{T_2}{T_{t2}}\right)^{\gamma/(\gamma-1)} = 300\left(\frac{2708.4}{3200}\right)^{1.3/0.3} = 145.6\,\text{psia}$$

$$P_{t2R} = P_2\left(\frac{T_{t2R}}{T_2}\right)^{\gamma/(\gamma-1)} = 145.6\left(\frac{2891.0}{2708.4}\right)^{1.3/0.3} = 193.2\,\text{psia}$$

$$P_{t3R} = P_{t2R} = 193.2\,\text{psia}$$

$$P_{t3} = P_{t2}\left(\frac{T_{t3}}{T_{t2}}\right)^{\gamma/(\gamma-1)} = 300\left(\frac{2759.4}{3200}\right)^{1.3/0.3} = 157.9\,\text{psia}$$

$$P_3 = P_{t3}\left(\frac{T_3}{T_{t3}}\right)^{\gamma/(\gamma-1)} = 157.9\left(\frac{2636.5}{2759.4}\right)^{1.3/0.3} = 129.6\,\text{psia}$$

Table 9.12 is a summary of the results for this axial-flow turbine stage with isentropic flow. The given data are listed in boldface type. Even though the flow leaving the nozzle (station 2) is supersonic, the relative flow entering the rotor is subsonic. The flow through the rotor is turned 80.8 deg. Figure 9.50 shows the change in temperature and pressure for an isentropic turbine stage.

9.5.1 Stage Parameters

9.5.1.1 Adiabatic efficiency. The adiabatic efficiency (the most common definition of efficiency for turbines) is the ratio of the actual energy output to the

Table 9.12 Results for Example 9.9 axial-flow turbine stage calculation, isentropic flow

Property		Station 1	2	2*R*	3*R*	3
T_t	°R	**3200**	3200.0	2891.0	2891.0	2759.4
	(K)	(1778)	(1777.8)	(1606.1)	(1606.1)	(1533.0)
T	°R		2708.4	2708.4	2636.5	2636.5
	(K)		(1504.7)	(1504.7)	(1464.7)	(1464.7)
P_t	psia	**300**	300	193.2	193.2	157.9
	(kPa)	(2068)	(2068)	(1332)	(1332)	(1089)
P_t	psia		145.6	145.6	129.6	129.6
	(kPa)		(1004)	(1004)	(893.6)	(893.6)
M			**1.10**	0.670	0.803	0.558
V	ft/s		2705.5	1649.0	1946.8	1352.8
	(m/s)		(824.6)	(502.6)	(593.4)	(412.3)
u	ft/s		1352.8	1352.8	1352.8	1352.8
	(m/s)		(412.3)	(412.3)	(412.3)	(412.3)
v	ft/s		2343.0	943.0	1400.0	0
	(m/s)		(714.2)	(287.4)	(426.7)	(0)
α	deg		**60.0**	——	——	**0**
β	deg			34.88	45.98	——

theoretical isentropic output (see Fig. 9.51a) for the same input total state and same exit total pressure:

$$\eta_t = \frac{\text{actual } \Delta h_t}{\text{ideal } \Delta h_t} = \frac{h_{t1} - h_{t3}}{h_{t1} - h_{t3s}} \tag{9.75}$$

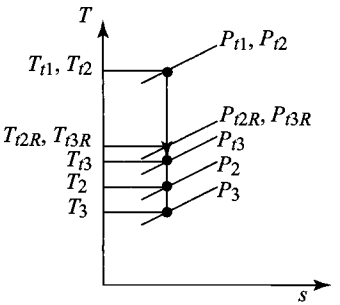

Fig. 9.50 Property changes of an isentropic turbine stage.

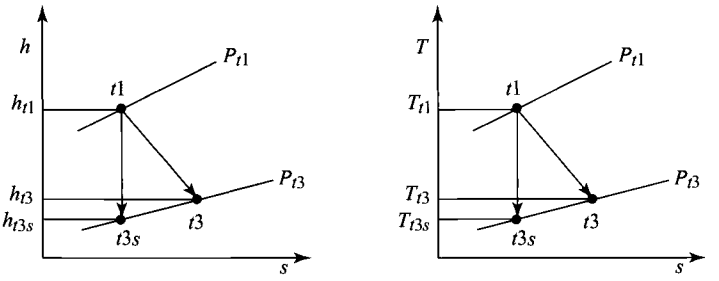

a) *h-s* diagram **b) *T-s* diagram**

Fig. 9.51 Definition of turbine adiabatic efficiency.

For a calorically perfect gas, the efficiency can be written in terms of total temperatures and total pressures (see Fig. 9.51b) as follows:

$$\eta_t = \frac{h_{t1} - h_{t3}}{h_{t1} - h_{t3s}} = \frac{c_p(T_{t1} - T_{t3})}{c_p(T_{t1} - T_{t3s})}$$

$$\eta_t = \frac{1 - T_{t3}/T_{t1}}{1 - (P_{t3}/P_{t1})^{(\gamma-1)/\gamma}} \tag{9.76}$$

The preceding definition is sometimes called the *total-to-total turbine efficiency* η_t, since the theoretical output is based on the leaving total pressure.

9.5.1.2 Exit swirl angle. The absolute angle of the leaving flow α_3 is called the *swirl angle* and, by convention, is positive when opposite to wheel speed direction (*backward*-running). The angle is important for two reasons. It is difficult in any fluid dynamic situation to efficiently convert kinetic energy to pressure or potential energy, and the kinetic energy in the flow leaving a turbine stage can be minimized by having $v_3 = u_3$, that is, by having zero swirl. Conversely, we see that the higher the swirl angle (if backward-running), the higher in magnitude v_3 will be, which generally means higher output from the stage [see Eq. (9.74) and Fig. 9.49].

9.5.1.3 Stage loading and flow coefficients. The *stage loading coefficient*, defined by Eq. (9.19), is the ratio of the stage work per unit mass to the rotor speed squared, or

$$\psi \equiv \frac{g_c \Delta h_t}{(\omega r)^2} = \frac{g_c \Delta h_t}{U^2}$$

For a calorically perfect gas, we write [Eq. (9.20)]

$$\psi = \frac{g_c c_p \Delta T_t}{(\omega r)^2} = \frac{g_c c_p \Delta T_t}{U^2}$$

The ratio of the axial velocity entering the rotor to the rotor speed is called the flow *coefficient* and is defined as

$$\Phi \equiv \frac{u_2}{\omega r} = \frac{u_2}{U} \tag{9.77}$$

The stage loading coefficient and flow coefficient for a turbine stage have a range of values. Figure 9.52 shows the range of these coefficients for several types of turbines. For Example 9.9 data, the stage loading coefficient is 1.67, and the flow coefficient is 0.962, which is well within the range for high-efficiency axial-flow turbines. Both the stage loading and flow coefficients affect the turbine stage efficiency, as shown in Fig. 9.53. Modern high-pressure turbines used for aircraft gas turbine engines have stage loading coefficients in the range of 1.3–2.2 and flow coefficients in the range of 0.5–1.1.

From Fig. 9.49 and Eqs. (9.74), (9.20), and (9.77), we obtain the stage loading coefficient in terms of the flow coefficient, the axial velocity ratio u_3/u_2, and flow angles as

$$\psi = \frac{g_c c_p \Delta T}{(\omega r)^2} = \frac{v_2 + v_3}{\omega r} = \Phi\left(\tan\alpha_2 + \frac{u_3}{u_2}\tan\alpha_3\right) \tag{9.78a}$$

or

$$\psi = \frac{g_c c_p \Delta T}{(\omega r)^2} = \frac{v_2 + v_3}{\omega r} = \Phi\left(\tan\beta_2 + \frac{u_3}{u_2}\tan\beta_3\right) \tag{9.78b}$$

By using Fig. 9.49, the flow coefficient can be expressed in terms of the flow angles as

$$\Phi = (\tan\alpha_2 - \tan\beta_2)^{-1} \tag{9.79}$$

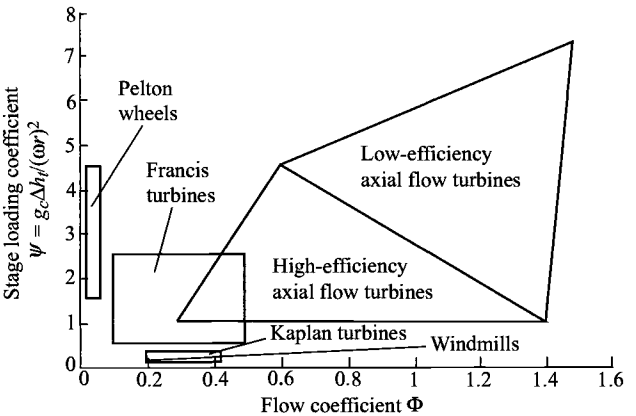

Fig. 9.52 Stage loading vs flow coefficient for different turbine types (Ref. 40).

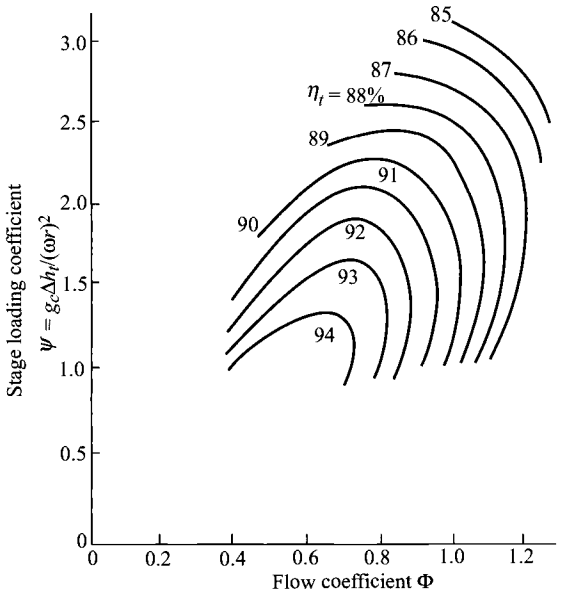

Fig. 9.53 Stage efficiency vs stage loading and flow coefficients, corrected for zero tip leakage (Ref. 40).

We obtain the following expression for the stage loading coefficient in terms of flow angles and u_3/u_2 by combining Eqs. (9.78a) and (9.79):

$$\psi = \frac{\tan \alpha_2 + (u_3/u_2)(\tan \alpha_3)}{\tan \alpha_2 - \tan \beta_2} \tag{9.80}$$

Equations (9.79) and (9.80) are plotted in Fig. 9.54 for constant axial velocity over a range of α_2 and β_2 and specific values of Φ, ψ, and α_3. This figure shows the effect of changing flow angles on Φ and ψ. Increasing α_3 with α_2 and β_2 held constant increases ψ and decreases Φ. Figure 9.54 also can be used to approximately determine the flow coefficient Φ from flow angles α_2 and β_2 and/or the stage loading coefficient ψ from flow angles α_2, β_2, and α_3. For example, given $\alpha_2 = 65$, $\beta_2 = 40$, and $\alpha_3 = 10$, Fig. 9.49 gives Φ of about 0.77 and ψ of about 1.8. More accurate results can be obtained by using Eqs. (9.79) and (9.80).

Figure 9.55 shows the rotor turning ($\varepsilon = \beta_2 + \beta_3$) for constant axial velocity as a function of the flow angle β_2 for different values of the ratio ψ/Φ. This figure can be used in conjunction with Fig. 9.54 to determine the rotor turning ε and the flow angle β_3.

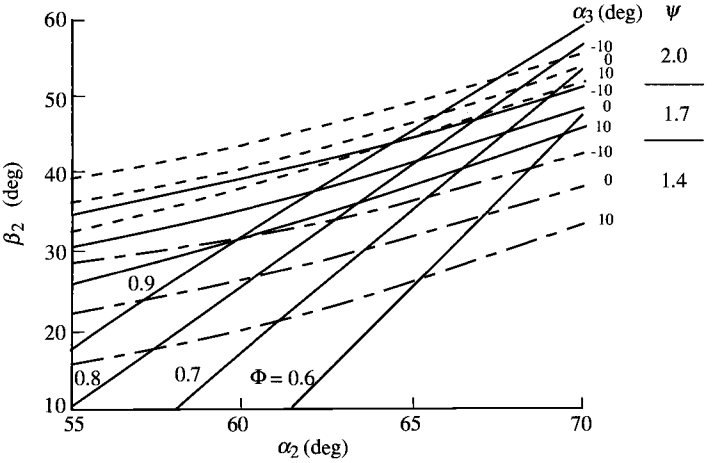

Fig. 9.54 Stage loading and flow coefficients vs flow angles (constant axial velocity).

9.5.1.4 Degree of reaction. The *degree of reaction* is defined as

$$^{\circ}R_t = \frac{h_2 - h_3}{h_{t1} - h_{t3}} \tag{9.81a}$$

For a calorically perfect gas, we can write

$$^{\circ}R_t = \frac{T_2 - T_3}{T_{t1} - T_{t3}} \tag{9.81b}$$

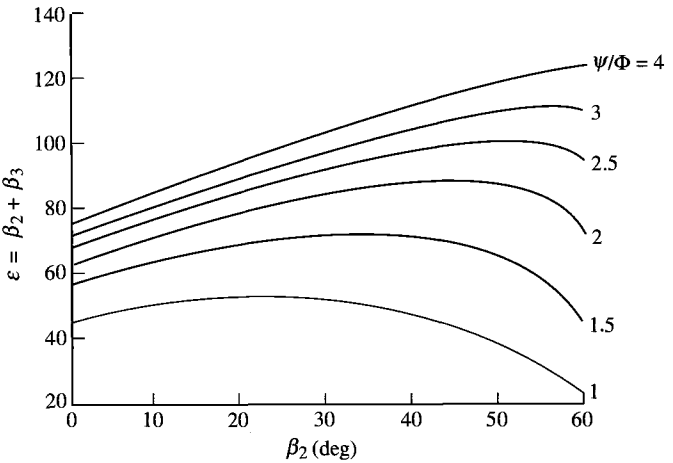

Fig. 9.55 Rotor turning ε vs Ψ/Φ and β_2 (constant axial velocity).

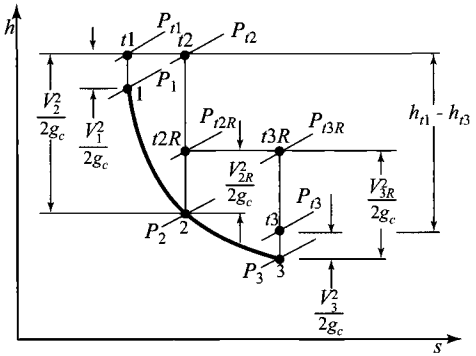

Fig. 9.56 The *h-s* diagram for general turbine stage.

That is, the degree of reaction is the ratio of the static enthalpy drop in the rotor to the drop in total enthalpy across both the rotor and stator. Figure 9.56 gives a complete picture for a general turbine stage. For Example 9.9, the degree of reaction is 0.166.

It can be shown that the degree of reaction may be related to the flow angles for the case of constant axial velocity ($u_3 = u_2$) by

$$^{\circ}R_t = \frac{u_2}{\omega r}\frac{\tan\beta_3 - \tan\beta_2}{2} = \Phi\frac{\tan\beta_3 - \tan\beta_2}{2} \tag{9.82}$$

By using Eq. (9.82), plots of $^{\circ}R_t/\Phi$ were added to Fig. 9.55, giving Fig. 9.57. One can see from this figure that zero reaction corresponds to maximum rotor turning ε for fixed value of ψ/Φ.

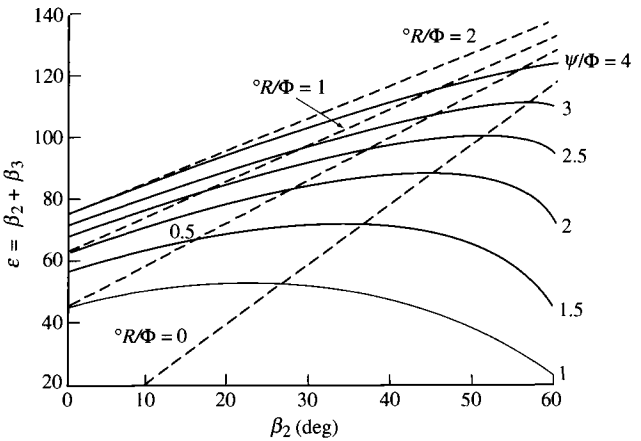

Fig. 9.57 Degree of reaction, stage loading coefficient, and flow coefficient vs rotor flow angles.

Three important basic designs of turbine are related to the choice of reaction—zero reaction, 50% reaction, and axial leaving velocity (variable reaction). It should be emphasized, however, that the designer is not limited to these three types and that in a three-dimensional turbine design, the reaction may vary continuously along the blades.

Zero reaction: From the definition of reaction, if the reaction is selected as zero for the case of constant axial velocity, then

$$h_3 = h_2 \quad \text{and} \quad \tan \beta_3 = \tan \beta_2$$

Therefore,

$$\beta_3 = \beta_2 \quad \text{and} \quad V_{3R} = V_{2R}$$

Velocity triangles for this zero reaction stage are shown in Fig. 9.58a, and the *h-s* diagram is drawn in Fig. 9.58b.

If the flow is isentropic and the fluid is a perfect gas, then the condition of zero enthalpy drop ($h_3 - h_2 = 0$) implies no change in pressure across the rotor. The turbine is then *called* an impulse turbine, with the tangential load arising from impulsive forces only. *It is important to note that reaction is defined here not on the basis of pressure drops, but in terms of static enthalpy changes.* Note, however, that there is a pressure drop from P_2 to P_3 across the rotor, and the

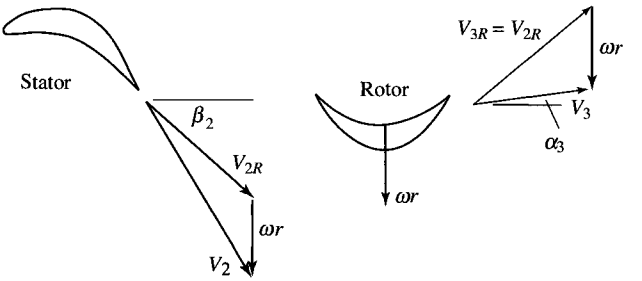

Fig. 9.58a Zero-reaction velocity diagram.

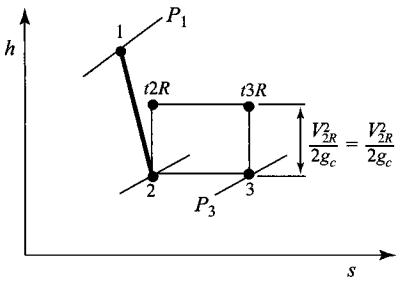

Fig. 9.58b Zero-reaction *h-s* diagram.

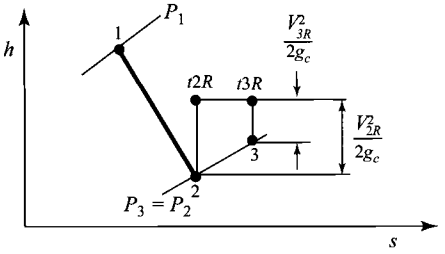

Fig. 9.59 Impulse turbine *h-s* diagram.

stage is not, therefore, truly impulse. The *h-s* diagram for an "impulse" stage of zero pressure drop is shown in Fig. 9.59. There is an enthalpy increase from h_2 to h_3 across the rotor, and the relative velocity decreases. Thus, *the impulse stage is actually one of negative reaction*!

The stage loading coefficient for the impulse stage with constant axial velocity is

$$\psi = \frac{g_c c_p \, \Delta T_t}{(\omega r)^2} = \frac{\omega r \Delta v}{(\omega r)^2} = \frac{\Delta v}{\omega r}$$

with

$$v_2 = u_2 \tan \alpha_2$$
$$v_3 = u_2 \tan \alpha_3 = u_2 \tan \alpha_2 - 2\omega r$$

then

$$\psi = 2(\Phi \tan \alpha_2 - 1) = 2\Phi \tan \beta_2 \tag{9.83}$$

We desire α_2 to be large. However, this leads to large v_2 and large v_{2R}, which lead to large losses. Thus α_2 is generally limited to less than 70 deg.

Also, if (see Fig. 9.58a) $\alpha_3 = 0$ (no exit swirl), then $\tan \alpha_2 = 2\omega r / u_2$ and

$$\psi = 2 \qquad \text{no exit swirl} \tag{9.84}$$

Thus we see that the rotor speed ωr is proportional to $\sqrt{\Delta h_t}$. If the resultant blade speed is too high, we must go to a multistage turbine.

50% reaction: If there is equal enthalpy drop across rotor and stator, then $R_t = 0.5$ and the velocity triangles are symmetrical, as shown in Fig. 9.60. Then, $\alpha_2 = \beta_3$, $\alpha_3 = \beta_2$, and

$$\tan \beta_3 - \tan \beta_2 = \tan \alpha_2 - \tan \alpha_3 = \frac{\omega r}{u_2} = \frac{1}{\Phi}$$

The stage loading coefficient for this turbine with constant axial velocity is

$$\psi = \frac{\Delta v}{\omega r} = 2\Phi \tan \alpha_2 - 1 = 2\Phi \tan \beta_3 - 1 \tag{9.85}$$

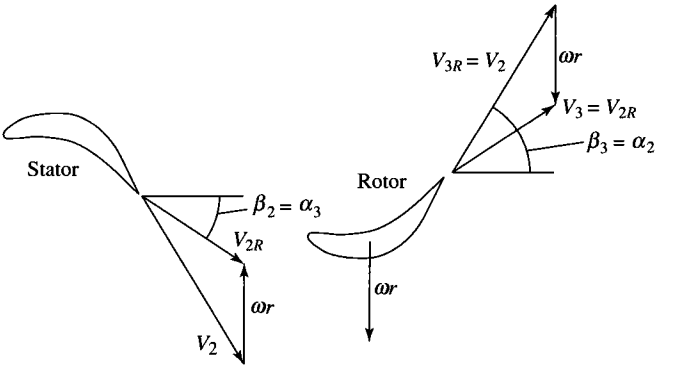

Fig. 9.60 Diagram of 50% reaction turbine velocity.

Again, α_2 should be high but is limited to less than 70 deg. For *zero exit swirl*

$$\tan \beta_3 = \tan \alpha_2 = \frac{\omega r}{u}, \quad \beta_2 = 0, \quad \psi = 1 \tag{9.86}$$

Thus, for the same ωr and $v_3 = 0$, the work per unit mass from a zero-reaction turbine is twice that from the 50% reaction turbine [compare Eqs. (9.84) and (9.86)].

General zero-swirl case (constant axial velocity): If the exit swirl is to be zero (Fig. 9.61), then $\alpha_3 = 0$, $v_3 = 0$, and $\tan \beta_3 = \omega r/u$. From Eq. (9.82), the reaction is then

$$^{\circ}R_t = \frac{u}{2\omega r}\left(\frac{\omega r}{u} - \tan \beta_2\right) = \frac{1}{2} - \frac{u \tan \beta_2}{2\omega r} = 1 - \frac{v_2}{2\omega r}$$

$$^{\circ}R_t = 1 - \frac{v_2}{2\omega r} = 1 - \frac{\psi}{2} \tag{9.87}$$

This equation can be rewritten as

$$\psi = 2(1 - {}^{\circ}R_t) \tag{9.88}$$

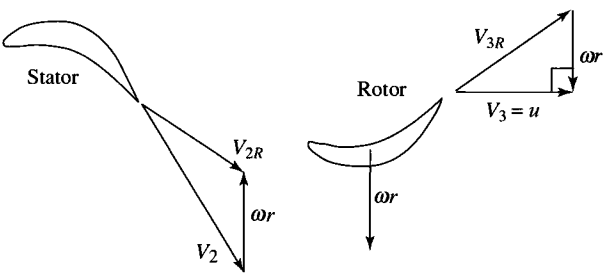

Fig. 9.61 Zero-exit-swirl turbine.

Thus high stage loadings give a low degree of reaction. In aircraft gas turbine engines, engine weight and performance must be balanced. Weight can be reduced by increasing stage loading (reduces the number of turbine stages), but this normally leads to a loss in stage efficiency (see Fig. 9.53).

9.5.1.5 Turbine airfoil nomenclature and design metal angles. The nomenclature for turbine airfoil cascades is presented in Fig. 9.62. The situation in unchoked turbines is similar to that in compressors except that the deviations are markedly smaller because of the thinner boundary layers. Hence

$$\delta_t = \frac{\gamma_i + \gamma_e}{8\sqrt{\sigma}} \tag{9.89}$$

is a good estimate of the turbine exit deviation. More importantly, however, when the turbine airfoil cascade exit Mach number is near unity, the deviation is usually negligible because the cascade passage is similar to a nozzle. In fact, the suction (or convex) surface of the airfoils often has a flat stretch before the trailing edge, which evokes the name *straight-backed.* Finally, the simple concept of deviation loses all meaning at large supersonic exit Mach numbers because expansion or compression waves emanating from the trailing edge can dramatically alter the final flow direction. This is a truly fascinating field of aerodynamics, but one that requires considerable study.

9.5.1.6 Stage temperature ratio τ_s. The stage temperature ratio ($\tau_s = T_{t1}/T_{t3}$) can be expressed as follows, by using the definition of the stage loading coefficient:

$$\tau_s = \frac{T_{t3}}{T_{t1}} = 1 - \psi \frac{(\omega r)^2}{g_c c_p T_{t1}} \tag{9.90}$$

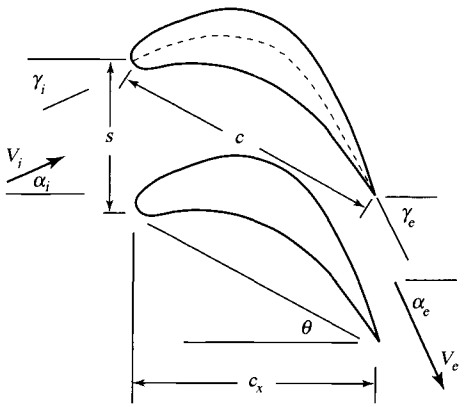

$\alpha_i - \gamma_i$ = incidence angle
$\alpha_i + \alpha_e$ = turning angle
$\gamma_e - \alpha_e = \delta_t$ = exit deviation
$\gamma_i + \gamma_e$ = blade chamber
$\sigma = c/s$ = solidity
θ = stagger angle
c_x = axial chord

Fig. 9.62 Turbine airfoil nomenclature.

Thus, for a given T_{t1} and ωr, the zero-reaction turbine stage will have the lower stage temperature ratio (greater work output per unit mass) than a 50% reaction turbine stage.

9.5.1.7 Stage pressure ratio π_s. Once the stage temperature ratio, flowfield, and airfoil characteristics are established, several avenues are open to predict the stage pressure ratio. The most simple and direct method is to employ the polytropic efficiency e_t. Recall that the polytropic efficiency is

$$e_t = \frac{dh_t}{dh_{t\,\text{ideal}}} = \frac{\gamma}{\gamma - 1}\frac{dT_t/T_t}{dP_t/P_t}$$

Integration with constant γ and e_t yields the following equation for the stage pressure ratio

$$\pi_s = \frac{P_{t3}}{P_{t1}} = \left(\frac{T_{t3}}{T_{t1}}\right)^{\gamma/[(\gamma-1)e_t]} = \tau_s^{\gamma/[(\gamma-1)e_t]} \tag{9.91}$$

where the stage temperature ratio can be obtained from the total temperatures or an equation like Eq. (9.90).

Another approach involves the use of experimental or empirical cascade loss correlations, such as those shown in Figs. 9.63 and 9.64, to the stator and rotor in order to determine the total pressure loss. The *total pressure loss coefficient* for turbine cascade data is defined as

$$\phi_t \equiv \frac{P_{ti} - P_{te}}{P_{te} - P_e} \tag{9.92}$$

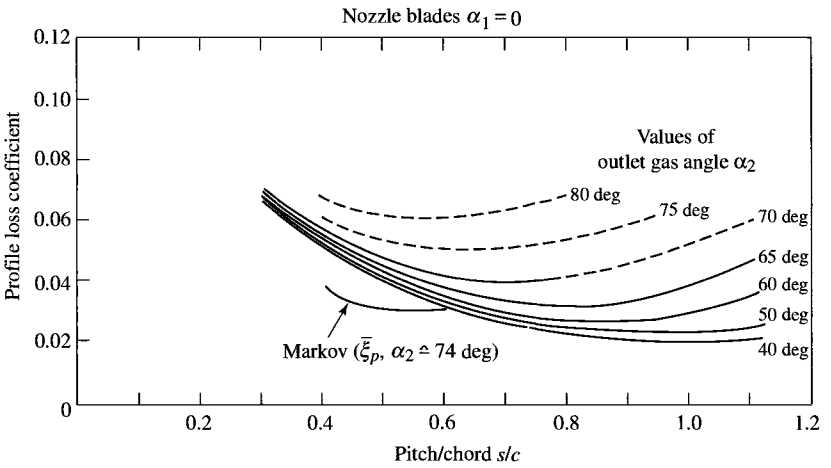

Fig. 9.63 Turbine stator cascade loss coefficient ($\alpha_1 = 0$) (Ref. 40).

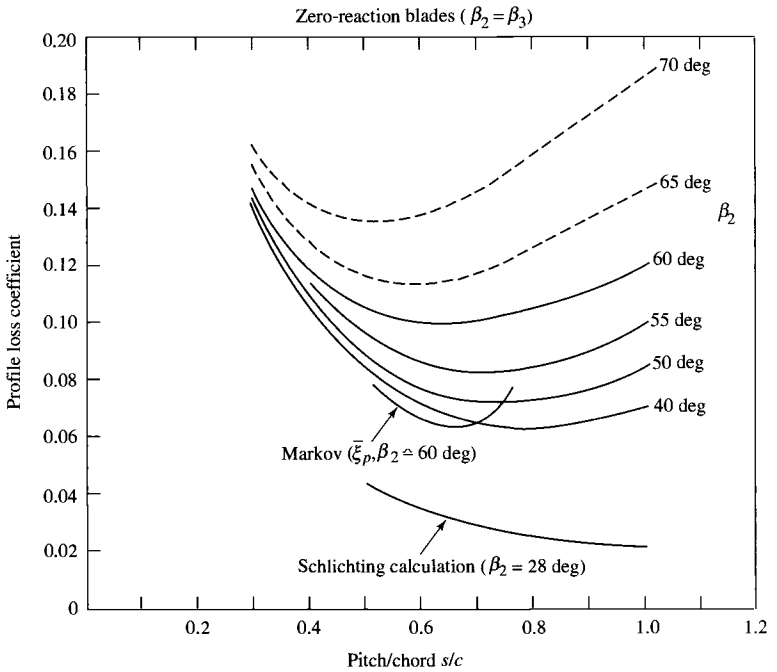

Fig. 9.64 Turbine rotor cascade loss coefficient ($\beta_2 = \beta_3$) (Ref. 40).

where subscripts i and e refer to the inlet and exit states, respectively. This equation can be rewritten for the cascade total pressure ratio as

$$\frac{P_{te}}{P_{ti}} = \frac{1}{1 + \phi_t(1 - P_e/P_{te})} \tag{9.93}$$

where P_e/P_{te} depends only on the usually known airfoil cascade exit Mach number M_e. Note that the total pressure loss coefficient for the rotor is based on the relative total states. The stage total pressure ratio can be written as

$$\frac{P_{t3}}{P_{t1}} = \left(\frac{P_{t2}}{P_{t1}}\right)_{\phi_{t\,\text{stator}},\, M_2} \frac{P_{t2R}}{P_{t2}} \left(\frac{P_{t3R}}{P_{t2R}}\right)_{\phi_{t\,\text{rotor}},\, M_{3R}} \frac{P_{t3}}{P_{t3R}} \tag{9.94}$$

where $\phi_{t\,\text{stator}}$ and $\phi_{t\,\text{rotor}}$ are the loss coefficients for the stator and rotor, respectively, and the subscripted total pressure ratios are obtained from Eq. (9.93) and cascade data. Additional losses are associated with tip leakage, annulus boundary layers, and secondary flows. Then, with all the stator, rotor, and stage properties computed, the stage efficiency can be computed from Eq. (9.76).

9.5.1.8 Blade spacing. The momentum equation relates the tangential force of the blades on the fluid to the change in tangential momentum of the fluid. This force is equal and opposite to that which results from the difference in pressure between the pressure side and the suction side of the airfoil. Figure 9.65 shows the variation in pressure on both the suction and pressure surfaces of a typical turbine airfoil from cascade tests. On the pressure surface, the pressure is nearly equal to the inlet total pressure for 60% of the length before the fluid is accelerated to the exit pressure condition. However, on the suction surface, the fluid is accelerated in the first 60% of the length to a low pressure and then is decelerated to the exit pressure condition. The deceleration on the suction surface is limited and controlled since it can lead to boundary-layer separation.

Enough airfoils must be present in each row that the sum of the tangential force on each is equal to the change in tangential momentum of the fluid. A simple expression for the relationship of the blade spacing to the fluid flow angles is developed in this section based on an incompressible fluid. This same expression correlates to the required blade spacing in a turbine stator or rotor row.

Referring to the cascade nomenclature in Fig. 9.62, we see that the tangential force per unit depth of blades spaced a distance s apart is

$$F_t = \frac{\rho u_i s(v_i + v_e)}{g_c} = \frac{\rho u_i^2 s}{g_c}\left(\tan \alpha_i + \frac{u_e}{u_i}\tan \alpha_e\right) \tag{9.95}$$

Zweifel[53] defines a tangential force coefficient that is the ratio of the force given by Eq. (9.95) to the maximum tangential force $F_{t\ \max}$ that can be achieved efficiently, and $F_{t\ \max}$ is obtained when

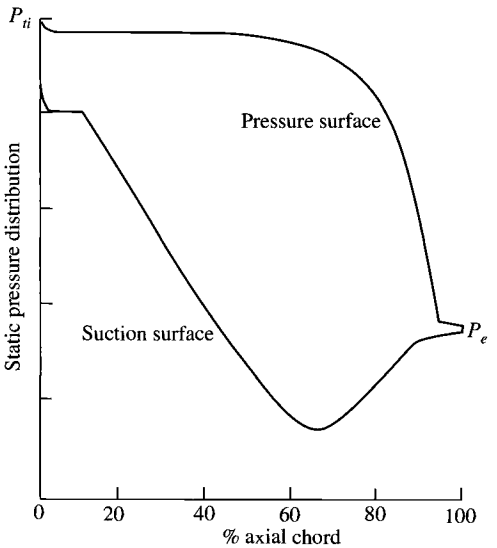

Fig. 9.65 Pressure distribution on a turbine cascade airfoil.

1) The pressure on the pressure surface is maintained at the inlet total pressure and drops to the exit static pressure at the trailing edge.

2) The pressure on the suction surface drops to the exit static pressure at the leading edge and remains at this value.

Thus the maximum tangential force is $F_{t\,\max} = (P_{ti} - P_e)c_x$, where c_x is the axial chord of the blade (see Fig. 9.62). For reversible flow of an incompressible fluid, $F_{t\,\max}$ can be written as

$$F_{t\,\max} = \frac{\rho V_e^2 c_x}{2g_c} = \frac{\rho u_e^2 c_x}{2g_c \cos^2 \alpha_e} \tag{9.96}$$

The *Zweifel tangential force coefficient* Z is defined as

$$Z \equiv \frac{F_t}{F_{t\,\max}} \tag{9.97}$$

From Eqs. (9.95) and (9.96), the equation of Z for a cascade airfoil becomes

$$Z = \frac{2s}{c_x}(\cos^2 \alpha_e)\left(\tan \alpha_t + \frac{u_e}{u_i}\tan \alpha_e\right)\left(\frac{u_i}{u_e}\right)^2$$

For the stator, we write

$$Z_s = \frac{2s}{c_x}(\cos^2 \alpha_2)\left(\tan \alpha_1 + \frac{u_2}{u_1}\tan \alpha_2\right)\left(\frac{u_1}{u_2}\right)^2 \tag{9.98a}$$

Likewise for the rotor, we write

$$Z_r = \frac{2s}{c_x}(\cos^2 \beta_3)\left(\tan \beta_2 + \frac{u_3}{u_2}\tan \beta_3\right)\left(\frac{u_2}{u_3}\right)^2 \tag{9.98b}$$

Because suction surface pressures can be less than the exit static pressure along the blade (see Fig. 9.65), *Z values near unity are attainable*. By using Eq. (9.98b), lines of constant $Z_r c_x/s$ are plotted in Fig. 9.66 vs the relative rotor angles β_2 and β_3. High β_2 and zero reaction (high stage loading ψ, see Fig. 9.57) give high values of $Z_r c_x/s$ (see Fig. 9.66) and require high values of solidity $[\sigma = c/s = (c_x/s)/\cos\theta]$. High solidity at high β_2 and zero reaction can lead to high total pressure losses (see Fig. 9.64). For no exit swirl ($\alpha_3 = 0$), the 50% reaction stage ($\psi = 1$) corresponds to $\beta_2 = 0$, the required solidity is low (Fig. 9.66), and the total pressure losses are low (Fig. 9.64). Thus the turbine design for aircraft engines will be a balance between the number of stages (stage loadings) and the turbine efficiency (total pressure losses).

9.5.1.9 Radial variations. Because the mass flow rate per unit area [that is, $\dot{m}/A = P_t/(\mathrm{MFP}\sqrt{T_t})$] is higher in turbines than in compressors, turbine

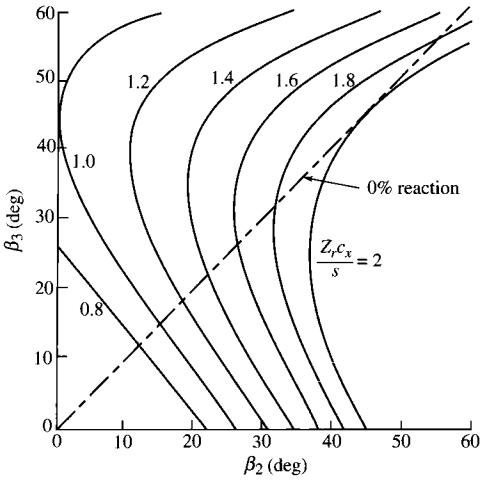

Fig. 9.66 Zc_x/s **of rotor vs** β_2 **and** β_3**.**

airfoils are correspondingly shorter. The result is little radial variation of aerodynamic properties from hub to tip except in the last few stages of the low-pressure turbine. Figure 9.67 is the rotor blade of a low-pressure turbine that shows radial variation from hub to tip. Typically, the degree of reaction varies from near zero at the hub to about 40% at the tip.

If the aerodynamic design of these stages began as free vortex, the swirl distribution with radius is the same as for compressors, given by [Eq. (9.45)]

$$v = v_m \frac{r_m}{r}$$

For constant axial velocity ($u_2 = u_3$), the degree of reaction is

$$^{\circ}R_t = \frac{T_2 - T_3}{T_{t1} - T_{t3}} = \frac{T_2 - T_3}{T_{t2} - T_{t3}} = 1 - \frac{V_2^2 - V_3^2}{2g_c c_p (T_{t1} - T_{t3})} = 1 - \frac{v_2^2 - v_3^2}{2\omega r (v_2 + v_3)}$$

$$= 1 - \frac{v_2 - v_3}{2\omega r}$$

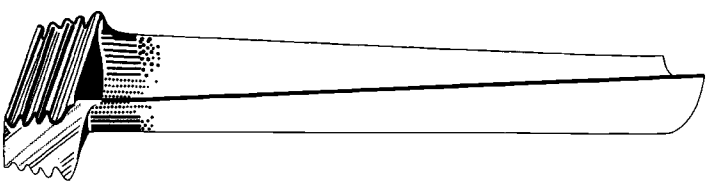

Fig. 9.67 Low-pressure turbine rotor blade. (Courtesy of Pratt & Whitney.)

Substituting Eq. (9.44), we write the degree of reaction at any radius in terms of the degree of reaction at the mean radius as

$$^{\circ}R_t = 1 - \frac{v_{m2} - v_{m3}}{2\omega r}\frac{r_m}{r} = 1 - \frac{v_{m2} - v_{m3}}{2\omega r_m}\left(\frac{r_m}{r}\right)^2$$

$$^{\circ}R_t = 1 - (1 - {}^{\circ}R_{tm})\left(\frac{r_m}{r}\right)^2 \tag{9.99}$$

This is the same result as for compressors [Eqs. (9.51) and (9.52)]. Consequently, the most difficult airfoil contours to design would be at the hub of the rotating airfoils and at the tips of the stationary airfoils where the degree of reaction is low. It is, therefore, possible to find portions of some airfoils near the rear of highly loaded (i.e., high work per stage), low-pressure turbines where the static pressure actually rises across the cascade and boundary-layer separation is hard to avoid. In these cases, turbine designers have used their computers to develop nonfree or controlled vortex machines without these troublesome regions in order to maintain high efficiency at high loading.

Because of radial variations, the degree of reaction is lowest at the hub. Hence the Zweifel tangential force coefficient of the rotor Z_r times c_x/s will be maximum at the hub. Although the blade spacing varies directly with radius, $Z_r c_x/s$ is greatest at the hub and decreases faster than $1/r$ with increasing radius. Thus the value of $Z_r c_x/s$ at the rotor hub determines the spacing and number of rotor blades. For the stator, $Z_s c_x/s$ will be greatest at the tip, and its value determines the spacing and number of stator blades.

9.5.1.10 Velocity ratio. The *velocity ratio* (VR) is defined as the ratio of the rotor speed ($U = \omega r$) to the velocity equivalent of the change in stage total enthalpy, or

$$\text{VR} \equiv \frac{U}{\sqrt{2g_c\,\Delta h_t}} = \frac{\omega r}{\sqrt{2g_c\,\Delta h_t}} \tag{9.100}$$

The velocity ratio is used by some turbine designers rather than the stage loading coefficient ψ, and one can show that

$$\text{VR} = \frac{1}{\sqrt{2\psi}} \tag{9.101}$$

The VR at the mean radius ranges between 0.5 and 0.6 for modern aircraft gas turbine engines. This range corresponds to stage loading coefficients ψ between 1.4 and 2.

9.5.2 Axial-Flow Turbine Stage

Consider the flow through a single-stage turbine as shown in Fig. 9.68. For generality, we will allow the axial velocity to change from station 2 to 3. The

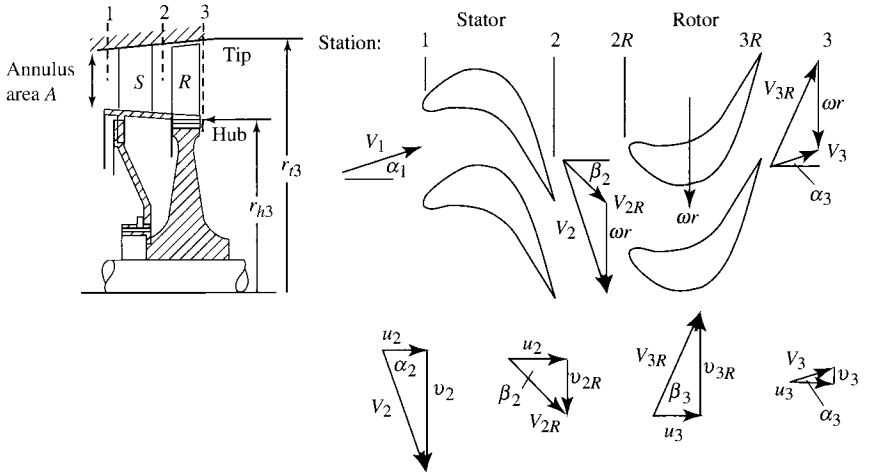

Fig. 9.68 Axial-flow turbine stage (after Ref. 29).

flows through the nozzle (stator) and rotor are assumed to be adiabatic. For solution, we assume that the following data are known: M_2, T_{t1}, T_{t3}, ωr, α_3, c_p, γ, and u_3/u_2. We will develop and write the equations for a general axial-flow turbine based on these known data.

To solve for the flow angle at station $2(\alpha_2)$, we first write the Euler turbine equation

$$c_p(T_{t2} - T_{t3}) = \frac{\omega r}{g_c}(v_2 + v_3) \tag{9.102}$$

Solving for v_2, we have

$$v_2 = \frac{g_c c_p \, \Delta T_t}{\omega r} - v_3$$

Then

$$\sin \alpha_2 = \frac{v_2}{V_2} = \frac{g_c c_p \, \Delta T_t}{\omega r V_2} - \frac{v_3}{V_2} \tag{i}$$

However,

$$\frac{v_3}{V_2} = \frac{u_3}{V_2}\tan \alpha_3 = \frac{u_3}{u_2}\frac{u_2}{V_2}\tan \alpha_3 = \frac{u_3}{u_2}\cos \alpha_2 \tan \alpha_3$$

Thus, Eq. (i) becomes

$$\sin \alpha_2 = \frac{v_2}{V_2} = \frac{g_c c_p \, \Delta T_t}{\omega r V_2} - \frac{u_3}{u_2}\cos \alpha_2 \tan \alpha_3 \tag{ii}$$

By using the stage loading parameter ψ, Eq. (ii) can be written as

$$\sin \alpha_2 = \psi \frac{\omega r}{V_2} - \frac{u_3}{u_2} \cos \alpha_2 \tan \alpha_3 \tag{9.103}$$

The velocity at station 2 can be found from

$$V_2 = M_2 a_2 = \sqrt{\frac{2 g_c c_p T_{t2}}{1 + 2/[(\gamma - 1) M_2^2]}} \tag{9.104}$$

If $\alpha_3 = 0$, then Eq. (9.103) simplifies to

$$\sin \alpha_2 = \psi \frac{\omega r}{V_2} \tag{9.105}$$

If α_3 is not zero, Eq. (9.103) can be solved by substituting $\sqrt{1 - \sin^2 \alpha_2}$ for $\cos \alpha_2$, squaring both sides of the equation, and solving the resulting quadratic equation for $\sin \alpha_2$. The solution is

$$\sin \alpha_2 = \frac{\left(\psi \dfrac{\omega r}{V_2}\right) - \left(\dfrac{u_3}{u_2} \tan \alpha_3\right) \sqrt{1 + \left(\dfrac{u_3}{u_2} \tan \alpha_3\right)^2 - \left(\psi \dfrac{\omega r}{V_2}\right)^2}}{1 + \left(\dfrac{u_3}{u_2} \tan \alpha_3\right)^2} \tag{9.106}$$

The velocity at station 3 can be written in terms of that at station 2 and the two flow angles α_2 and α_3:

$$V_3 = \frac{u_3}{u_2} \frac{\cos \alpha_2}{\cos \alpha_3} V_2 \tag{9.107}$$

The degree of reaction can be written in terms of the given data as follows:

$$\begin{aligned} {}^{\circ}R_t &= \frac{T_2 - T_3}{T_{t2} - T_{t3}} = \frac{T_{t2} - T_{t3} - (T_{t2} - T_2) + T_{t3} - T_3}{T_{t2} - T_{t3}} \\ &= 1 - \frac{V_2^2 - V_3^2}{2 g_c c_p (T_{t2} - T_{t3})} = 1 - \frac{V_2^2 - V_3^2}{2 \psi (\omega r)^2} \\ &= 1 - \frac{1}{2 \psi (\omega r)^2} \left(\frac{u_2^2}{\cos^2 \alpha_2} - \frac{u_3^2}{\cos^2 \alpha_3} \right) \\ {}^{\circ}R_t &= 1 - \frac{1}{2\psi} \left(\frac{V_2}{\omega r} \right)^2 \left[1 - \left(\frac{u_3}{u_2} \frac{\cos \alpha_2}{\cos \alpha_3} \right)^2 \right] \end{aligned} \tag{9.108}$$

The Mach number at station 3 can be found from

$$M_3 = M_2 \frac{V_3}{V_2} \sqrt{\frac{T_2}{T_3}} \tag{9.109}$$

where

$$\frac{T_3}{T_2} = 1 - {}^{\circ}R_t \frac{\Delta T_t}{T_{t2}} \left(1 + \frac{\gamma - 1}{2} M_2^2\right) \tag{9.110}$$

An equation for the Mach number at station $2R$ can be developed as follows:

$$M_{2R} = M_2 \frac{V_{2R}}{V_2}$$

where

$$V_{2R} = \sqrt{u_2^2 + (v_2 - \omega r)^2} = V_2 \sqrt{\cos^2 \alpha_2 + \left(\sin \alpha_2 - \frac{\omega r}{V_2}\right)^2}$$

Thus

$$M_{2R} = M_2 \sqrt{\cos^2 \alpha_2 + \left(\sin \alpha_2 - \frac{\omega r}{V_2}\right)^2} \tag{9.111}$$

Likewise, an equation for the Mach number at station $3R$ is developed as follows:

$$M_{3R} = M_3 \frac{V_{3R}}{V_3}$$

where

$$V_{3R} = \sqrt{u_3^2 + (v_3 + \omega r)^2} = V_3 \sqrt{\cos^2 \alpha_3 + \left(\sin \alpha_3 + \frac{\omega r}{V_3}\right)^2}$$

Thus

$$M_{3R} = M_3 \sqrt{\cos^2 \alpha_3 + \left(\sin \alpha_3 + \frac{\omega r}{V_3}\right)^2} \tag{9.112}$$

An equation for the rotor relative total temperature ($T_{t2R} = T_{t3R}$) can be developed by noting that

$$T_3 = T_{t3} - \frac{V_3^2}{2g_c c_p} = T_{t3R} - \frac{V_{3R}^2}{2g_c c_p}$$

Then

$$T_{t3R} = T_{t3} + \frac{V_{3R}^2 - V_3^2}{2g_c c_p}$$

or

$$T_{t3R} = T_{t3} + \frac{V_3^2}{2g_c c_p}\left[\cos^2\alpha_3 + \left(\sin\alpha_3 + \frac{\omega r}{V_3}\right)^2 - 1\right] \tag{9.113}$$

9.5.3 Summary of Equations—Axial-Flow Turbine Stage

INPUTS:

T_{t1}, T_{t3}, ωr, P_{t1}, M_1, M_2, α_1, α_3, c_p, γ, u_3/u_2, and e_t or $\phi_{t\,\text{stator}}$ and $\phi_{t\,\text{rotor}}$

OUTPUTS:

$\alpha_2, V_2, u_2, v_2, T_2, P_{t2}, P_2, M_{2R}, V_3, u_3, v_3, T_3, P_{t3}, P_3, M_3, M_{3R}, \psi$, VR, ${}^\circ R_t, Z_s c_x/s$, $Z_r c_x/s$, π_s, and η_s

EQUATIONS:

$$T_1 = \frac{T_{t1}}{1 + [(\gamma - 1)/2]M_1^2}$$

$$V_1 = \sqrt{\frac{2g_c c_p T_{t1}}{1 + 2/[(\gamma - 1)M_1^2]}}$$

$$u_1 = V_1 \cos\alpha_1$$

$$T_{t2} = T_{t1}$$

$$T_2 = \frac{T_{t2}}{1 + [(\gamma - 1)/2]M_2^2}$$

$$V_2 = \sqrt{\frac{2g_c c_p T_{t2}}{1 + 2/[(\gamma - 1)M_2^2]}}$$

$$\psi = \frac{g_c c_p (T_{t1} - T_{t3})}{(\omega r)^2}$$

$$\text{VR} = \frac{1}{\sqrt{2\psi}}$$

$$\alpha_2 = \sin^{-1}\frac{\psi\dfrac{\omega r}{V_2} - \dfrac{u_3}{u_2}\tan\alpha_3\sqrt{1 + \left(\dfrac{u_3}{u_2}\tan\alpha_3\right)^2 - \left(\psi\dfrac{\omega r}{V_2}\right)^2}}{1 + \left(\dfrac{u_3}{u_2}\tan\alpha_3\right)^2}$$

$$u_2 = V_2 \cos\alpha_2$$

$$v_2 = V_2 \sin\alpha_2$$

$$V_3 = \frac{u_3}{u_2}\frac{\cos\alpha_2}{\cos\alpha_3}V_2$$

$$u_3 = V_3 \cos \alpha_3$$

$$v_3 = V_3 \sin \alpha_3$$

$$^{\circ}R_t = 1 - \frac{1}{2\psi}\left(\frac{V_2}{\omega r}\right)^2\left[1 - \left(\frac{u_3}{u_2}\frac{\cos \alpha_2}{\cos \alpha_3}\right)^2\right]$$

$$T_3 = T_2 - {}^{\circ}R_t(T_{t1} - T_{t3})$$

$$M_3 = M_2 \frac{V_3}{V_2}\sqrt{\frac{T_2}{T_3}}$$

$$M_{2R} = M_2\sqrt{\cos^2 \alpha_2 + \left(\sin \alpha_2 - \frac{\omega r}{V_2}\right)^2}$$

$$M_{3R} = M_3\sqrt{\cos^2 \alpha_3 + \left(\sin \alpha_3 + \frac{\omega r}{V_3}\right)^2}$$

$$T_{t3R} = T_{t3} + \frac{V_3^2}{2g_c c_p}\left[\cos^2 \alpha_3 + \left(\sin \alpha_3 + \frac{\omega r}{V_3}\right)^2 - 1\right]$$

$$T_{t2R} = T_{t3R}$$

$$P_2 = P_{t1}\left(\frac{T_1}{T_{t1}}\right)^{\gamma/(\gamma-1)}$$

$$\tau_s = \frac{T_{t3}}{T_{t1}}$$

$$\frac{Z_s c_x}{s} = (2\cos^2 \alpha_2)\left(\tan \alpha_1 + \frac{u_2}{u_1}\tan \alpha_2\right)\left(\frac{u_1}{u_2}\right)^2$$

$$\beta_2 = \tan^{-1}\frac{v_2 - \omega r}{u_2}$$

$$\beta_3 = \tan^{-1}\frac{v_3 + \omega r}{u_3}$$

$$\frac{Z_r c_x}{s} = (2\cos^2 \beta_3)\left(\tan \beta_2 + \frac{u_3}{u_2}\tan \beta_3\right)\left(\frac{u_2}{u_3}\right)^2$$

I. $\phi_{r\,\text{stator}}$ and $\phi_{t\,\text{rotor}}$ given:

$$P_{t2} = \frac{P_{t1}}{1 + \phi_{t\,\text{stator}}[1 - (T_2/T_{t2})^{\gamma/(\gamma-1)}]}$$

$$P_2 = P_{t2}\left(\frac{T_2}{T_{t2}}\right)^{\gamma/(\gamma-1)}$$

$$P_{t2R} = P_2\left(\frac{T_{t2R}}{T_2}\right)^{\gamma/(\gamma-1)}$$

$$P_{t3R} = \frac{P_{t2R}}{1 + \phi_{t\,\text{rotor}}[1 - (T_3/T_{t3R})^{\gamma/(\gamma-1)}]}$$

$$P_3 = P_{t3R}\left(\frac{T_3}{T_{t3R}}\right)^{\gamma/(\gamma-1)}$$

$$P_{t3} = P_3\left(\frac{T_{t3}}{T_3}\right)^{\gamma/(\gamma-1)}$$

$$\pi_s = \frac{P_{t3}}{P_{t1}}$$

$$\eta_t = \frac{1 - \tau_s}{1 - \pi_s^{(\gamma-1)/\gamma}}$$

II. e_t given:

$$P_{t3} = P_{t1}\left(\frac{T_{t3}}{T_{t1}}\right)^{\gamma/[(\gamma-1)e_t]}$$

$$\pi_s = \frac{P_{t3}}{P_{t1}}$$

$$\eta_s = \frac{1 - \tau_s}{1 - \pi_s^{(\gamma-1)/\gamma}}$$

$$P_3 = P_{t3}\left(\frac{T_3}{T_{t3}}\right)^{\gamma/(\gamma-1)}$$

$$P_{t3R} = P_3\left(\frac{T_{t3R}}{T_3}\right)^{\gamma/(\gamma-1)}$$

With polytropic efficiency specified, P_2, P_{t2}, and P_{t2R} cannot be calculated without an additional relationship for either P_2 or P_{t2}. For estimation of P_{t2}, the program TURBN has as the user input a value of $\phi_{t\,\text{stator}}$.

Example 9.10

Consider mean-radius stage calculation—flow with losses.

Given:

$$T_{t1} = 1850\ \text{K}, \quad P_{t1} = 1700\ \text{kPa}, \quad M_1 = 0.4, \quad \alpha_1 = 0\ \text{deg}$$

$$T_{t3} = 1560\ \text{K}, \quad M_2 = 1.1, \quad \omega r = 450\ \text{m/s}, \quad \alpha_3 = 10\ \text{deg}$$

$$u_3/u_2 = 0.9, \quad \phi_{t\,\text{stator}} = 0.06, \quad \phi_{t\,\text{rotor}} = 0.15$$

$$\gamma = 1.3, \quad R = 0.2873\ \text{kJ/(kg}\cdot\text{K)}\ [c_p = 1.245\ \text{kJ/(kg}\cdot\text{K)}]$$

Solution:

$$T_1 = \frac{T_{t1}}{1 + [(\gamma - 1)/2]M_1^2} = \frac{1850\,\text{K}}{1 + 0.15 \times 0.4^2} = 1806.6\,\text{K}$$

$$V_1 = \sqrt{\frac{2g_c c_p T_{t1}}{1 + 2/[(\gamma - 1)M_1^2]}} = \sqrt{\frac{2 \times 1 \times 1245 \times 1850}{1 + 2/(0.3 \times 0.4^2)}} = 328.6\,\text{m/s}$$

$$u_1 = V_1 \cos \alpha_1 = 328.6\,\text{m/s}$$

$$v_1 = V_1 \sin \alpha_1 = 0$$

$$T_{t2} = T_{t1} = 1850\,\text{K}$$

$$T_2 = \frac{T_{t2}}{1 + [(\gamma - 1)/2]M_2^2} = \frac{1850\,\text{K}}{1 + 0.15 \times 1.1^2} = 1565.8\,\text{K}$$

$$V_2 = \sqrt{\frac{2g_c c_p T_{t2}}{1 + 2/[(\gamma - 1)M_2^2]}}$$

$$= \sqrt{\frac{2 \times 1 \times 1245 \times 18}{1 + 2/(0.3 \times 1.1^2)}} = 841.2\,\text{m/s}$$

$$\psi = \frac{g_c c_p (T_{t1} - T_{t3})}{(\omega r)^2} = \frac{1245(1850 - 1560)}{450^2} = 1.78296$$

$$\text{VR} = \frac{1}{\sqrt{2\psi}} = \frac{1}{\sqrt{2 \times 1.78296}} = 0.5296$$

$$\alpha_2 = \sin^{-1} \frac{\left(\psi \dfrac{\omega r}{V_2}\right) - \left(\dfrac{u_3}{u_2} \tan \alpha_3\right) \sqrt{1 + \left(\dfrac{u_3}{u_2} \tan \alpha_3\right)^2 - \left(\psi \dfrac{\omega r}{V_2}\right)^2}}{1 + \left(\dfrac{u_3}{u_2} \tan \alpha_3\right)^2}$$

$$\psi \frac{\omega r}{V_2} = 1.78296 \left(\frac{450}{841.2}\right) = 0.95379$$

$$\frac{u_3}{u_2} \tan \alpha_3 = 0.9 \tan 10\,\text{deg} = 0.15869$$

$$\alpha_2 = \sin^{-1} \frac{0.95379 - 0.15869\sqrt{1 + 0.15869^2 - 0.95379^2}}{1.015869^2}$$

$$= \sin^{-1} 0.87776 = 61.37\,\text{deg}$$

$$u_2 = V_2 \cos \alpha_2 = 841.2 \cos 61.37\,\text{deg} = 403.1\,\text{m/s}$$

$$v_2 = V_2 \sin \alpha_2 = 841.2 \sin 61.37 \text{ deg} = 738.3 \text{ m/s}$$

$$\Phi = \frac{u_2}{\omega r} = \frac{403.1}{450} = 0.8958$$

$$V_3 = \frac{u_3}{u_2} \frac{\cos \alpha_2}{\cos \alpha_3} V_2 = 0.9 \left(\frac{\cos 61.37 \text{ deg}}{\cos 10 \text{ deg}} \right) (841.2) = 368.4 \text{ m/s}$$

$$u_3 = V_3 \cos \alpha_3 = 368.4 \cos 10 \text{ deg} = 362.8 \text{ m/s}$$

$$v_3 = V_3 \sin \alpha_3 = 368.4 \sin 10 \text{ deg} = 64.0 \text{ m/s}$$

$$^{\circ}R_t = 1 - \frac{1}{2\psi} \left(\frac{V_2}{\omega r} \right)^2 \left[1 - \left(\frac{u_3 \cos \alpha_2}{u_2 \cos \alpha_3} \right)^2 \right]$$

$$= 1 - \frac{1}{2 \times 1.78296} \left(\frac{841.2}{450} \right)^2 \left[1 - \left(0.9 \frac{\cos 61.37 \text{ deg}}{\cos 10 \text{ deg}} \right)^2 \right] = 0.2080$$

$$T_3 = T_2 - {}^{\circ}R_t (T_{t1} - T_{t3}) = 1565.8 - 0.2080(1850 - 1560) = 1505.5 \text{ K}$$

$$M_3 = M_2 \frac{V_3}{V_2} \sqrt{\frac{T_2}{T_3}} = 1.1 \left(\frac{368.4}{841.2} \right) \sqrt{\frac{1565.8}{1505.5}} = 0.4913$$

$$M_{2R} = M_2 \sqrt{\cos^2 \alpha_2 + \left(\sin \alpha_2 - \frac{\omega r}{V_2} \right)^2}$$

$$= 1.1 \sqrt{\cos^2 61.37 \text{ deg} + \left(\sin 61.37 \text{ deg} - \frac{450}{841.2} \right)^2} = 0.6481$$

$$M_{3R} = M_3 \sqrt{\cos^2 \alpha_3 + \left(\sin \alpha_3 + \frac{\omega r}{V_3} \right)^2}$$

$$= 0.4913 \sqrt{\cos^2 10 \text{ deg} + \left(\sin 10 \text{ deg} + \frac{450}{368.4} \right)^2} = 0.8390$$

$$T_{t3R} = T_{t3} + \frac{V_3^2}{2 g_c c_p} \left[\cos^2 \alpha_3 + \left(\sin \alpha_3 + \frac{\omega r}{V_3} \right)^2 - 1 \right]$$

$$= 1560 + \frac{368.4^2}{2 \times 1 \times 1245} \left[\cos^2 10 \text{ deg} + \left(\sin 10 \text{ deg} + \frac{450}{368.4} \right)^2 - 1 \right]$$

$$= 1664.4 \text{ K}$$

$$T_{t2R} = T_{t3R} = 1664.4 \text{ K}$$

$$\tau_s = \frac{T_{t3}}{T_{t1}} = \frac{1560}{1850} = 0.8432$$

$$\frac{Z_s c_x}{s} = (2\cos^2\alpha_2)\left(\tan\alpha_1 + \frac{u_2}{u_1}\tan\alpha_2\right)\left(\frac{u_1}{u_2}\right)^2$$

$$= (2\cos^2 61.371\,\text{deg})\left(\tan 0\,\text{deg} + \frac{403.1}{328.6}\tan 61.37\,\text{deg}\right)\left(\frac{328.6}{403.1}\right)^2$$

$$= 0.6857$$

$$\beta_2 = \tan^{-1}\frac{v_2 - \omega r}{u_2} = \tan^{-1}\frac{738.3 - 450}{403.1} = 35.57\,\text{deg}$$

$$\beta_3 = \tan^{-1}\frac{v_3 + \omega r}{u_3} = \tan^{-1}\frac{64.0 + 450}{362.8} = 54.78\,\text{deg}$$

$$\frac{Z_r c_x}{s} = (2\cos^2\beta_3)\left(\tan\beta_2 + \frac{u_3}{u_2}\tan\beta_3\right)\left(\frac{u_2}{u_3}\right)^2$$

$$= (2\cos^2 54.78\,\text{deg})(\tan 35.573\,\text{deg} + 0.9\tan 54.78\,\text{deg})\left(\frac{1}{0.9}\right)^2$$

$$= 1.6330$$

$$P_1 = P_{t1}\left(\frac{T_1}{T_{t1}}\right)^{\gamma/(\gamma-1)} = 1700\left(\frac{1806.6}{1850}\right)^{1.3/0.3} = 1533.8\,\text{kPa}$$

$$P_{t2} = \frac{P_{t1}}{1 + \phi_{t\,\text{stator}}[1 - (T_2/T_{t2})^{\gamma/(\gamma-1)}]}$$

$$= \frac{1700}{1 + 0.06[1 - (1565.8/1850)^{1.3/0.3}]} = 1649.1\,\text{kPa}$$

$$P_2 = P_{t2}\left(\frac{T_2}{T_{t2}}\right)^{\gamma/(\gamma-1)} = 1649.1\left(\frac{1565.8}{1850}\right)^{1.3/0.3} = 800.5\,\text{kPa}$$

$$P_{t2R} = P_2\left(\frac{T_{t2R}}{T_2}\right)^{\gamma/(\gamma-1)} = 800.5\left(\frac{1664.4}{1565.8}\right)^{1.3/0.3} = 1043.0\,\text{kPa}$$

$$P_{t3R} = \frac{P_{t2R}}{1 + \phi_{t\,\text{rotor}}[1 - (T_3/T_{t3R})^{\gamma/(\gamma-1)}]}$$

$$= \frac{1043.0}{1 + 0.15[1 - (1505.5/1664.4)^{1.3/0.3}]} = 990.6\,\text{kPa}$$

$$P_3 = P_{t3R}\left(\frac{T_3}{T_{t3R}}\right)^{\gamma/(\gamma-1)} = 990.6\left(\frac{1505.5}{1664.4}\right)^{1.3/0.3} = 641.3\,\text{kPa}$$

$$P_{t3} = P_3\left(\frac{T_{t3}}{T_3}\right)^{\gamma/(\gamma-1)} = 641.3\left(\frac{1560}{1505.5}\right)^{1.3/0.3} = 748.1\,\text{kPa}$$

$$\pi_s = \frac{P_{t3}}{P_{t1}} = \frac{748.1}{1700} = 0.441$$

$$\eta_s = \frac{1 - \tau_s}{1 - \pi_s^{(\gamma-1)/\gamma}} = \frac{1 - 0.8432}{1 - 0.4401^{0.3/1.3}} = 90.87\%$$

9.5.4 Flow Path Dimensions

9.5.4.1 Annulus area. The annulus area (see Fig. 9.26) at any station of a turbine stage is based on the flow properties (T_t, P_t, Mach number, and flow angle) at the mean radius and the total mass flow rate. Equation (9.8) is the easiest equation to use to calculate the flow area at any station i:

$$A_i = \frac{\dot{m}\sqrt{T_{ti}}}{P_{ti}(\cos \alpha_i)\text{MFP}(M_i)}$$

By using the relationships of Fig. 9.26, the radii at any station i can be determined, given the flow annulus area [Eq. (9.8)] and either the mean radius r_m or the hub/tip ratio r_h/r_t.

9.5.4.2 Axial dimensions and number of blades. Figure 9.69 shows the cross section of a typical turbine stage that can be used to estimate its axial length. The chord/height ratio c/h of turbine blades varies from about 0.3 to 1.0. Assuming constant chord length and circular arc chamber line, the program TURBN calculates the axial blade widths W_s and W_r of a stage, the blade spacings $W_s/4$ and $W_r/4$, and the number of blades based on user inputs of the tangential force coefficient Z and chord/height ratio c/h for both the stator and rotor blades. A minimum width of $\frac{1}{4}$ in. (0.6 cm) and spacing of $\frac{1}{8}$ in. (0.3 cm) are used in the plot of a turbine cross section and calculation of axial length.

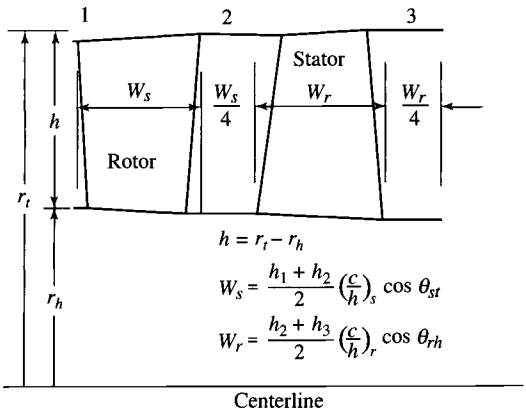

Fig. 9.69 Typical axial dimensions of a turbine stage.

The stagger angle θ of a blade depends on the shape of the chamber line and blade angles γ_i and γ_e (see Fig. 9.62). For a circular arc chamber line, the stagger angle θ is simply given by $\theta = (\gamma_e - \gamma_i)/2$. For constant-chord blades, the axial chord (and axial blade width) is greatest where the stagger angle is closest to zero. This normally occurs at the tip of the stator and hub of the rotor blades. For estimation purposes, a turbine blade's incidence angle is normally small and can be considered to be zero. Thus $\gamma_i = \alpha_i$. The blade's exit angle γ_e can be obtained using Eq. (9.89) for the exit deviation. However, Eq. (9.89) requires that the solidity ($\sigma = c/s$) be known. For known flow conditions (α_1, α_2, u_2/u_1, α_2, α_3, and u_3/u_2) and given tangential force coefficients (Z_s and Z_r), Eqs. (9.98a) and (9.98b) will give the required axial chord/spacing ratio c_x/s for the stator and rotor, respectively. An initial guess for the blade's solidity σ is needed to obtain the stagger angle θ from c_x/s.

After the solidities are determined at the hub, mean, and tip that give the desired tangential force coefficient Z, the number of required blades follows directly from the chord/height ratio c/h, the circumference, and the blade spacing at each radius. The following example shows the calculations needed to find the axial blade width and number of blades.

Example 9.11

Here we consider the turbine stator of Example 9.10 with a mass flow rate of 60 kg/s, a mean radius of 0.3 m, a tangential force coefficient Z_s of 0.9, and a chord/height ratio c/h of 1.0. The flow annulus areas and radii at stations 1 and 2 are as follows.

Station 1:

$$\text{MFP}(M_1) = 0.024569$$

$$A_1 = \frac{\dot{m}\sqrt{T_{t1}}}{P_{t1}\text{MFP}(M_1)(\cos\alpha_1)} = \frac{60\sqrt{1850}}{1{,}700{,}00 \times 0.024569 \times 1}$$

$$= 0.0617788\ \text{m}^2$$

$$h_1 = \frac{A_1}{2\pi r_m} = \frac{0.061788}{0.6\pi} = 0.03278\ \text{m}$$

$$r_{t1} = 0.3164\ \text{m} \qquad r_{h1} = 0.2836\ \text{m}$$

$$v_{1h} = v_{1m} = v_{1t} = 0$$

Station 2:

$$\text{MFP}(M_2) = 0.039042$$

$$A_2 = \frac{\dot{m}\sqrt{T_{t2}}}{P_{t2}\text{MFP}(M_2)(\cos\alpha_2)}$$

$$= \frac{60\sqrt{1850}}{1{,}649{,}100 \times 0.039042 \times \cos 61.37\ \text{deg}} = 0.083654\ \text{m}^2$$

$$h_2 = \frac{A_2}{2\pi r_m} = \frac{0.083654}{0.6\pi} = 0.04438\,\text{m}$$

$$r_{t2} = 0.3222\,\text{m} \qquad r_{h2} = 0.2778\,\text{m}$$

$$v_{2h} = v_{2m}\frac{r_m}{r_{2h}} = 738.3\left(\frac{0.3}{0.2778}\right) = 797.3\,\text{m/s}$$

$$\alpha_{2h} = \tan^{-1}\frac{v_{2h}}{u_2} = \tan^{-1}\frac{797.3}{403.1} = 63.18\,\text{deg}$$

$$v_{2t} = v_{2m}\frac{r_m}{r_{2t}} = 738.3\left(\frac{0.3}{0.3222}\right) = 687.4\,\text{m/s}$$

$$\alpha_{2t} = \tan^{-1}\frac{v_{2t}}{u_2} = \tan^{-1}\frac{687.4}{403.1} = 59.61\,\text{deg}$$

The chord of the stator is

$$c = \frac{c}{h}\frac{h_1 + h_2}{2} = 1.0\frac{0.03278 + 0.04438}{2} = 0.03858\,\text{m}$$

For the specified tangential force coefficient Z_s, we calculate the stagger angle, solidity, and spacing of the stator at the mean line, hub, and tip.

Mean line:

$$Z_s\left(\frac{c_x}{s}\right)_m = (2\cos^2\alpha_{2m})\left(\tan\alpha_{1m} + \frac{u_2}{u_1}\tan\alpha_{2m}\right)\left(\frac{u_1}{u_2}\right)^2$$

$$= (2\cos^2 61.37\,\text{deg})\left(\tan 0\,\text{deg} + \frac{403.1}{328.6}\tan 61.37\,\text{deg}\right)$$

$$\times\left(\frac{328.6}{403.1}\right)^2 = 0.6857$$

$$\left(\frac{c_x}{s}\right)_m = \frac{0.6857}{0.9} = 0.7619$$

$$\gamma_{1m} = \alpha_{1m} = 0$$

Initially, we assume a solidity σ of 1.0. Then,

$$\gamma_{2m} = \frac{\gamma_{1m} + 8\sqrt{\sigma_m}\alpha_{2m}}{8\sqrt{\sigma_m} - 1} = \frac{0 + 8\sqrt{1}61.37}{8\sqrt{1} - 1} = 70.14\,\text{deg}$$

$$\theta_m = \frac{\gamma_{2m} - \gamma_{1m}}{2} = \frac{70.14}{2} = 35.07\,\text{deg}$$

$$\sigma_m = \frac{(c_x/s)_m}{\cos\theta_m} = \frac{0.7619}{\cos 35.07\,\text{deg}} = 0.9309$$

After several iterations, the results are $\gamma_{2m} = 70.49$ deg, $\theta_m = 35.25$ deg, and $\sigma_m = 0.9329$. The blade spacing s is 0.04135 m, and the axial chord is 0.03150 m.

Hub:

$$Z_s\left(\frac{c_x}{s}\right)_h = (2\cos^2\alpha_{2h})\left(\tan\alpha_{1h} + \frac{u_2}{u_1}\tan\alpha_{2h}\right)\left(\frac{u_1}{u_2}\right)^2$$

$$= (2\cos^2 63.18\,\text{deg})\left(\tan 0\,\text{deg} + \frac{403.1}{328.6}\tan 63.18\,\text{deg}\right)$$

$$\times \left(\frac{328.6}{403.1}\right)^2 = 0.6565$$

$$\left(\frac{c_x}{s}\right)_h = \frac{0.6565}{0.9} = 0.7294$$

$$\gamma_{1h} = \alpha_{1h} = 0$$

Initially, we assume a solidity σ of 1.0. Then,

$$\gamma_{2h} = \frac{\gamma_{1h} + 8\sqrt{\sigma_h}\alpha_{2h}}{8\sqrt{\sigma_h} - 1} = \frac{0 + 8\sqrt{1}63.18}{8\sqrt{1} - 1} = 72.21\,\text{deg}$$

$$\theta_h = \frac{\gamma_{2h} - \gamma_{1h}}{2} = \frac{72.21}{2} = 36.10\,\text{deg}$$

$$\sigma_h = \frac{(c_x/s)_h}{\cos\theta_h} = \frac{0.7294}{\cos 361.0\,\text{deg}} = 0.9027$$

After several iterations, the results are $\gamma_{2h} = 72.73$ deg, $\theta_h = 36.37$ deg, and $\sigma_h = 0.9058$. The blade spacing s is 0.04259 m, and the axial chord is 0.03107 m.

Tip:

$$Z_x\left(\frac{c_x}{s}\right)_t = (2\cos^2\alpha_{2t})\left(\tan\alpha_{1t} + \frac{u_2}{u_1}\tan\alpha_{2t}\right)\left(\frac{u_1}{u_2}\right)^2$$

$$= (2\cos^2 59.61\,\text{deg})\left(\tan 0\,\text{deg} + \frac{403.1}{328.6}\tan 59.61\,\text{deg}\right)$$

$$\times \left(\frac{328.6}{403.1}\right)^2 = 0.7115$$

$$\left(\frac{c_x}{s}\right)_t = \frac{0.7115}{0.9} = 0.7905$$

$$\gamma_{1t} = \alpha_{1t} = 0$$

Table 9.13 Summary of Example 9.11 results

Location	Average radius, m	Solidity	Spacing, m	Number of blades	Axial chord, m
Tip	0.3193	0.9555	0.04038	49.7	0.03192
Mean	0.3000	0.9329	0.04135	45.6	0.03150
Hub	0.2807	0.9058	0.04259	41.4	0.03107

Initially, we assume a solidity σ of 1.0:

$$\gamma_{2t} = \frac{\gamma_{1t} + 8\sqrt{\sigma_t}\alpha_{2t}}{8\sqrt{\sigma_t} - 1} = \frac{0 + 8\sqrt{1}59.61}{8\sqrt{1} - 1} = 68.13 \text{ deg}$$

$$\theta_t = \frac{\gamma_{2t} - \gamma_{1t}}{2} = \frac{68.13}{2} = 34.06 \text{ deg}$$

$$\sigma_t = \frac{(c_x/s)_t}{\cos\theta_t} = \frac{0.7905}{\cos 34.06 \text{ deg}} = 0.9542$$

After several iterations, the results are $\gamma_{2t} = 68.35$ deg, $\theta_t = 34.18$ deg, and $\sigma_t = 0.9555$. The blade spacing s is 0.04038 m, and the axial chord is 0.03192 m.

For this stator blade with a chord of 0.03858 m, we require the information in Table 9.13. Thus the number of required stator blades is 50, which will have a mean-radius spacing s of 0.03770 m and solidity σ of 1.023 (= 0.03858/0.03770) on the mean radius. The blade has an axial width W_s of 0.03192 m (see Fig. 9.69).

9.5.4.3 Blade profile. The shapes of turbine stator and rotor blades are based on airfoil shapes developed specifically for turbine applications. Two airfoil shapes are included in the program TURBN to sketch the blade shapes for a stage: the C4 and T6 British profiles. The base profile of the C4 airfoil is listed in Table 9.14 and shown in Fig. 9.70 for a 10% thickness. Table 9.15 and Fig. 9.71 give the base profile of the T6 airfoil for a 10% thickness. The program TURBN assumes a circular arc mean line for sketching the blade shapes.

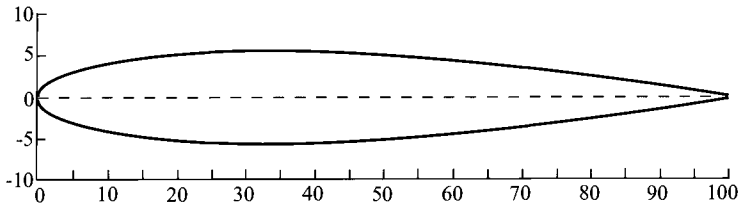

Fig. 9.70 The C4 turbine airfoil base profile.

Table 9.14 C4 airfoil profile ($t/c = 0.10$)[a,b]

x/c, %	y/c, %	x/c, %	y/c, %
0.0	0.0	40	4.89
1.25	1.65	50	4.57
2.5	2.27	60	4.05
5	3.08	70	3.37
7.5	3.62	80	2.54
10	4.02	90	1.60
15	4.55	95	1.06
20	4.83	100	0.0
30	5.00		

[a]Leading-edge radius = $0.12t$.
[b]Trailing-edge radius = $0.06t$.

Table 9.15 T6 airfoil profile ($t/c = 0.10$)[a,b]

x/c, %	y/c, %	x/c, %	y/c, %
0.0	0.0	40	5.00
1.25	1.17	50	4.67
2.5	1.54	60	3.70
5	1.99	70	2.51
7.5	2.37	80	1.42
10	2.74	90	0.85
15	3.4	95	0.72
20	3.95	100	0.0
30	4.72		

[a]Leading-edge radius = $0.12t$.
[b]Trailing-edge radius = $0.06t$.

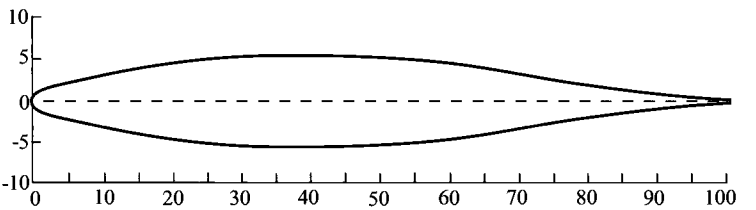

Fig. 9.71 The T6 turbine airfoil base profile.

Example 9.12

Consider a single-stage turbine using the computer program TURBN.

Given:

$$\dot{m} = 200\ \text{lbm/s}, \quad M_1 = 0.4, \quad T_{t1} = 3400°\text{R}$$

$$T_{t3} = 2860°\text{R}, \quad M_2 = 1.1, \quad \omega r = 1500\ \text{ft/s}, \quad r_m = 12\ \text{in.}$$

$$P_{t1} = 250\ \text{psia}, \quad \alpha_1 = 0\ \text{deg}, \quad \alpha_3 = 0\ \text{deg}, \quad \gamma = 1.3$$

$$R = 53.40\ \text{ft} \cdot \text{lbf/(lbm} \cdot °\text{R)}, \quad u_3/u_2 = 0.90, \quad \psi_{t\,\text{stator}} = 0.06, \quad \phi_{t\,\text{rotor}} = 0.15$$

Solution: The program TURBN is run with α_2 as the unknown. The results are given in Table 9.16 with the hub and tip tangential velocities based on free-vortex swirl distribution. The cross section of the stage sketched by the computer program is shown in Fig. 9.72 for stator $c/h = 0.8$ and rotor $c/h = 0.6$. The very high AN^2 of 4.18×10^{10} in.$^2 \cdot$ rpm^2 at a relative total temperature of 3052°R is not possible with current materials unless the blades are cooled. Also, the high rim speed of about 1206 ft/s would require existing materials to be cooled.

9.5.5 Axial-Flow Turbine Stage—α_2 Known

The preceding method of calculation assumed that α_2 was unknown. The program TURBN will handle the case when any one of the following four variables is unknown:

$$\alpha_2,\ T_{t3},\ \alpha_3,\ \text{or}\ M_2$$

When T_{t3} is unknown, Eqs. (9.20) and (9.103) are solved for T_{t3}, giving

$$T_{t3} = T_{t1} - \frac{\omega r V_2}{g_c c_p}\left(\sin\alpha_2 + \frac{u_3}{u_2}\cos\alpha_2 \tan\alpha_3\right) \tag{9.114}$$

When α_3 is unknown, Eqs. (9.20) and (9.103) are solved for α_3, giving

$$\tan\alpha_3 = \frac{1}{u_3/u_2}\left(\frac{\psi}{\cos\alpha_2}\frac{\omega\gamma}{V_2} - \tan\alpha_2\right) \tag{9.115}$$

When M_2 is unknown, the velocity at station 2 (v_2) is obtained from Eq. (9.103), giving

$$V_2 = \frac{\psi\,\omega r}{\sin\alpha_2 + (u_3/u_2)\cos\alpha_2 \tan\alpha_3} \tag{9.116}$$

Then M_2 is obtained from Eq. (9.104) rewritten as

$$M_2 = \frac{V_2}{\sqrt{(\gamma-1)g_c c_p T_{t2} - [(\gamma-1)/2]V_2^2}} \tag{9.117}$$

9.5.6 Axial-Flow Turbine Stage Analysis—No Exit Swirl

Consider the flow through a single-stage turbine as shown in Fig. 9.73 with zero exit swirl. We will consider the case where there is no exit swirl ($v_3 = 0$,

Table 9.16 Results for Example 9.12 axial-flow turbine stage calculation using TURBN

Property		Station										
		1*h*	1*m*	1*t*	2*h*	2*m*	2*t*	2*Rm*	3*Rm*	3*h*	3*m*	3*t*
T_t	°R	3400	3400	3400	3400	3400	3400	3052	3052	2860	2860	2860
T	°R	3320	3320	3320	2767	2878	2957	2878	2768	2767	2768	2769
P_t	psia	250.0	250.0	250.0	242.5	242.5	242.5	151.9	144.4	109.0	109.0	109.0
P	psia	225.6	225.6	225.6	99.2	117.7	132.4	117.7	94.6	94.4	94.6	94.7
M		0.400	0.400	0.400	1.236	1.100	1.100	0.636	0.827	0.474	0.471	0.469
V	ft/s	1089	1089	1089	3071	2789	2569	1611	2057	1178	1171	1167
u	ft/s	1089	1089	1089	1282	1282	1282	1282	1153	1153	1153	1153
v	ft/s	0	0	0	2791	2477	2226	977	1703	239	203	177
α	deg	0	0	0	65.34	62.64	60.07	——	——	11.68	10.00	8.74
β	deg	——	——	——	——	——	——	37.32	55.90	——	——	——
Radii	in.	11.04	12.00	12.96	10.65	12.00	13.35	12.00	12.00	10.20	12.00	13.80

Hub: $^\circ R_t = -0.0005$ $A_1 = 144.31$ in.^{2}

Mean: $^\circ R_t = 0.2034$ $A_2 = 203.72$ in.^{2}

Tip: $^\circ R, = 0.3487$ $A_3 = 271.04$ in.^{2}

$\tau_s = 0.8412$ $\pi_s = 0.4359$ RPM = 14,324 $\psi = 1.7868$ $\phi = 0.8544$

$\eta_s = 91.08\%$ and AN^2 at $2 = 4.18 \times 10^{10}$ in.$^2 \cdot$ rpm^2

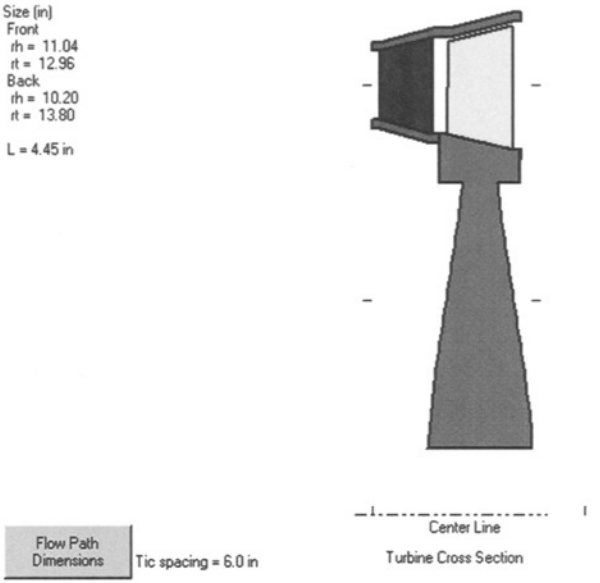

Fig. 9.72 Sketch of cross section for turbine stage of Example 9.12 from TURBN.

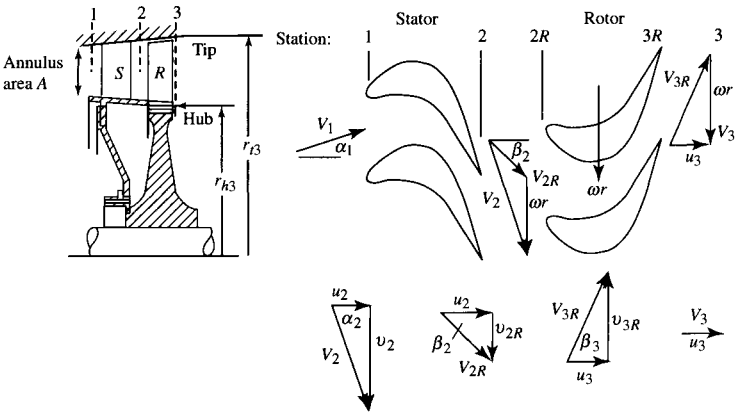

Fig. 9.73 Generalized turbine stage, zero exit swirl.

$\alpha_3 = 0$) and the axial velocities at stations 2 to 3 are the same ($u_2 = u_3$). The flows through the nozzle (stator) and rotor are assumed to be adiabatic. For solution, we assume the following data are known:

$$M_2,\ T_{t1},\ T_{t3},\ \omega r,\ c_p, \text{ and } \gamma$$

The equations for solution of a zero exit swirl, axial-flow turbine based on these known data are developed in this section.

At station 2, v_2 is given by

$$V_2 = \sqrt{\frac{2g_c c_p T_{t2}}{1 + 2/[(\gamma - 1)M_2^2]}}$$

$$= \omega r \sqrt{\frac{2\psi/(1 - \tau_s)}{1 + 2/[(\gamma - 1)M_2^2]}} \tag{9.118}$$

and α_2 by

$$\sin \alpha_2 = \psi \frac{\omega \gamma}{V_2} = \sqrt{(1 - \tau_s)\frac{\psi}{2}\left[1 + \frac{2}{(\gamma - 1)M_2^2}\right]} \tag{9.119}$$

Because the axial velocities at stations 2 and 3 are equal, the velocity at station 3 is given by

$$V_3 = V_2 \cos \alpha_2 \tag{9.120}$$

The degree of reaction is given by Eq. (9.87):

$$^{\circ}R_t = 1 - \frac{\psi}{2}$$

The stage exit Mach number M_3 is derived as follows. Given that

$$\frac{M_3}{M_2} = \frac{u_3/a_3}{V_2/a_2} = \frac{u_2}{V_2}\frac{a_2}{a_3} = \cos \alpha_2 \sqrt{\frac{T_2}{T_3}}$$

Then from Eq. (9.81b), we write

$$^{\circ}R_t = \frac{T_2 - T_3}{T_{t1} - T_{t3}} = 1 - \frac{\psi}{2}$$

which allows the temperature ratio T_2/T_3 to be written as

$$\frac{T_2}{T_3} = \frac{1}{1 - (T_{t2}/T_2)(1 - \tau_s)(1 - \psi/2)} \tag{9.121}$$

Thus the Mach number M_3 can be written as

$$M_3 = \frac{M_2 \cos \alpha_2}{\sqrt{1 - (1 - \tau_s)(1 - \psi/2)\{1 + (\gamma - 1)/2]M_2^2\}}} \tag{9.122}$$

A compact equation for the rotor exit relative Mach number M_{3R} is developed as follows. Since

$$\frac{M_{3R}}{M_2} = \frac{V_{3R}}{a_3}\frac{a_2}{V_2} = \frac{V_{3R}}{V_2}\sqrt{\frac{T_2}{T_3}}$$

the velocity ratio is obtained by first writing

$$V_{3R}^2 = u^2 + (\omega r)^2 = V_2^2 - v_2^2 + (\omega r)^2$$

Thus

$$\frac{V_{3R}^2}{V_2^2} = 1 - \frac{v_2^2}{V_2^2} + \frac{(\omega r)^2}{V_2^2} = 1 - \left(\frac{\omega r}{V_2}\right)^2\left[\left(\frac{v_2}{\omega r}\right)^2 - 1\right]$$

$$= 1 - \left(\frac{\omega r}{V_2}\right)^2(\psi^2 - 1)$$

Since

$$\frac{M_{3R}}{M_2} = \frac{V_{3R}}{V_2}\sqrt{\frac{T_2}{T_3}}$$

then by using Eq. (9.121), the Mach number ratio is found by

$$\frac{M_{3R}}{M_2} = \sqrt{\frac{1 - (\omega r/V_2)^2(\psi^2 - 1)}{1 - (T_{t2}/T_2)(1 - \tau_s)(1 - \psi/2)}} \tag{9.123}$$

which with Eq. (9.119) becomes (and is actually used as)

$$\frac{M_{3R}}{M_2} = \sqrt{\frac{1 - (1 - \tau_s)\dfrac{\psi^2 - 1}{2\psi}\left[1 + \dfrac{2}{(\gamma - 1)M_2^2}\right]}{1 - (1 - \tau_s)\left(1 - \dfrac{\psi}{2}\right)\left(1 + \dfrac{\gamma - 1}{2}M_2^2\right)}} \tag{9.124}$$

This equation contains an interesting and unexpected piece of guidance for the design of turbine stages. To ensure that stator cascade choking controls the turbine mass flow rate, M_2 should be greater than unity and M_{3R} should be less than unity. Equation (9.124) reveals, however, that when the stage loading coefficient is unity (degree of reaction is 0.5), the opposite must be true. Therefore, even though it would appear preferable to aim for a degree of reaction near 0.5 to balance the difficulty of designing the stator and rotor airfoils, the requirement to reduce M_{3R} translates to lower allowable values of the degree of reaction and correspondingly higher stage loadings. In actual practice, the degree of reaction is usually found in the range of 0.2 to 0.4, so that a substantial, but minority, fraction of the overall static enthalpy (and static presssure) drop still takes place across the rotor and is available to prevent the separation of the suction surface boundary layer. It is important to bear in mind that even turbine airfoil boundary layers can separate, and when they do, the effect on efficiency (and heat transfer) is usually disastrous.

The rotor relative total temperature ($T_{t2R} = T_{t3R}$), which is useful for heat transfer and structural analyses, is given by Eq. (9.113). For our case of zero exit swirl and constant axial velocity ($u_3 = u_2$), this equation reduces to

$$\frac{T_{t3R}}{T_{t2}} = \tau_s + \frac{1 - \tau_s}{2\psi} \tag{9.125}$$

Example 9.13

To illustrate the application of this method, a single-stage turbine with zero exit swirl will be designed for the following conditions:

$M_1 = 0.4$	$M_2 = 1.10$
$\omega r = U = 300$ m/s	$T_{t2} = T_{t1} = 1400$ K
$R = 0.2872$ kJ/(kg · K)	$g_c c_p = 1.158$ KJ/(kg · K)
$T_{t3} = 1260$ K	$\gamma = 1.33$
$\tau_s = \dfrac{T_{t3}}{T_{t1}} = 0.900$	$\psi = 1.8006$ Eq. (9.20)

If one chooses to assume $e_t = 0.90$, the results are

$^{\circ}R_t = 0.0997$	Eq. (9.87)	$M_{3R} = 0.8756$	Eq. (9.124)
$\alpha_2 = 47.35$ deg	Eq. (9.119)	$T_{t3R} = 1299$ K	Eq. (9.125)
$M_3 = 0.7498$	Eq. (9.122)	$\Phi = 1.6586$	Eq. (9.78a)
$\pi_s = 0.6239$	Eq. (9.91)	$\eta_t = 0.9053$	Eq. (9.76)

These results provide the basis for step-by-step calculations leading to the summary of flow properties given in Table 9.17.

Table 9.17 Results for Example 9.13 axial-flow turbine state calculation with zero exit swirl

	Station				
Property	1	2	2R	3R	3
T_t	1400.0	1400.0	1298.9	1298.9	1260.0
T	1364.0	1167.0	1167.0	2012.7	2012.7
$\dfrac{P_t}{P_{t1}}$	1.0000	?	?	0.7053	0.6239
$\dfrac{P}{P_{t1}}$	0.9003	?	?	0.4364	0.4364
M	0.400	1.100	0.8586	0.8756	0.7498
V m/s	288.7	734.4	552.5	581.0	497.6
u m/s	288.7	497.6	497.6	497.6	497.6
v m/s	0	540.2	240.2	300.0	0
α deg	0	47.35	——	——	0
β deg	——	——	25.76	31.09	——

9.5.6.1 General solution. When γ and e_t are fixed, closer examination of the turbine stage design equation set reveals that the results depend only on the dimensionless quantities M_2, τ_s, and ψ. Under these conditions, it is therefore possible to generate graphical representations that reveal the general tendencies of such turbine stages and serve the important purpose of defining the limits of reasonable stage designs.

This has been done for typical ranges of the prevailing dimensionless parameters and γ values of 1.33 and 1.3; the results are presented in Figs. 9.74 and 9.75, respectively. These charts may be used to obtain initial ballpark-stage design estimates and also reveal some important trends. If values of M_{3R} less than 1 and stage loading coefficients ψ less than or equal to 2.0 are taken as reasonable limits, it is clear that better (i.e., lower) values of ψ are available for the same ΔT_t as τ_s decreases (lower inlet temperatures) and/or ωr increases (higher wheel speeds). By noting that ψ does not depend on M_2 [Eq. (9.87)], it is also clear that M_2 determines only M_{3R}. Larger values of M_2 are desirable because they reduce the annulus flow area A and the rotating airfoil centrifugal stresses, and ensure choking of the stator airfoil passages over a wider turbine operating range; but Figs. 9.74 and 9.75 show that increasing M_2 reduces the number of acceptable solutions. Finally, all other things being equal, stages having lower τ_s (i.e., more energy extraction) suffer the dual disadvantages of increased stage loading coefficient ψ and increased annulus flow area A.

Figures 9.74 and 9.75 exhibit an extremely interesting mathematical behavior in the region where all the curves for a value of M_2 appear to, and indeed do, pass through a single point. This fact may be verified by equating the numerator and denominator on the right side of the equals sign in Eq. (9.124), and this reveals that $M_{3R} = M_2$ is independent of either M_2 or τ_s provided only that

$$\psi^2 - 1 = \frac{\gamma - 1}{2}(2\psi - \psi^2)M_2^2$$

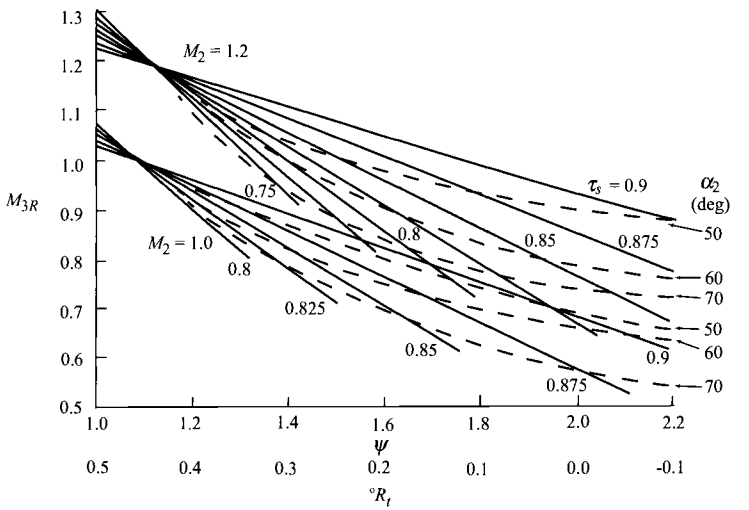

Fig. 9.74 Generalized turbine stage behavior, zero exit swirl ($\gamma = 1.33$).

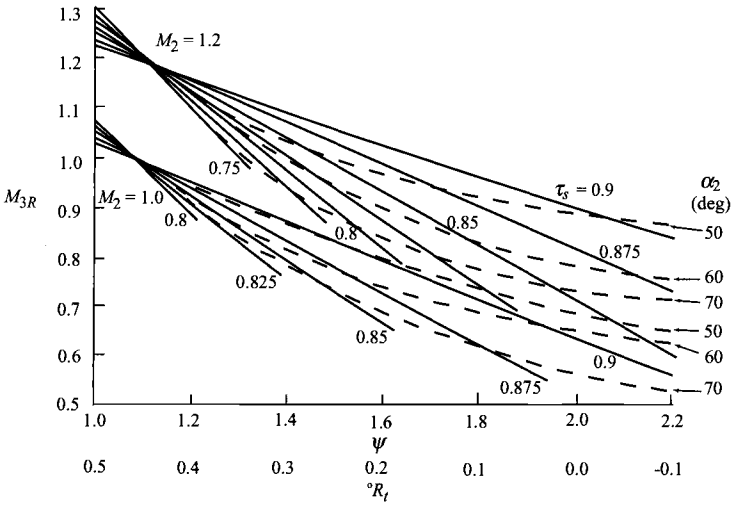

Fig. 9.75 Generalized turbine stage behavior, zero exit swirl ($\gamma = 1.3$).

Hence, for each γ, there are two values of ψ that satisfy this condition. When $M_{3R} = M_2 = 1.0$ and $\gamma = 1.3$, they are 1.072 and -0.82, the former obviously being the one that appears in Fig. 9.75 and the latter having no practical use. For $M_{3R} = M_2 = 1.2$ and $\gamma = 1.3$, they are 1.102 and -0.746. The physical meaning of this convenient convergence is clear enough, namely, that near $M_{3R} = M_2$, where the stator and rotor airfoil exit conditions are similar, the stage loading parameter ψ must be near unity regardless of the other stage parameters.

9.5.6.2 Multistage turbine design. When the required stage loading coefficient ψ for a design is greater than 2.0, a single-stage design would require a hopeless negative reaction [Eq. (9.87)] and would be impossible to design with high aerodynamic efficiency. A desirable multistage design would have the total temperature difference distributed evenly among the stages:

$$(\Delta T_t)_{\text{turbine}} = (\text{number of stages}) \times (\Delta T_t)_{\text{stage}}$$

This would result in stages with the same stage loading coefficients [Eq. (9.20)] and same degree of reaction [Eq. (9.87)] for the same rotor speed U. For a three-stage design, we get

$$\psi_{s1} = \psi_{s2} = \psi_{s3} \quad \text{and} \quad (^\circ R_t)_{s1} = (^\circ R_t)_{s2} = (^\circ R_t)_{s3}$$

To obtain the choked flow in the first-stage stator (nozzle), the Mach number entering the rotor M_2 is slightly supersonic. The Mach numbers in the remaining stages are kept subsonic. The net result is that the stage loading of the first stage is larger than the loading of any of the other stages. For a three-stage design, the

stage loading coefficient and degree of reaction of the second and third stages are nearly equal.

9.5.7 Shaft Speed

The design rotational speed of a spool (shaft) having stages of compression driven by a turbine is initially determined by that component that limits the speed because of high stresses. For a low-pressure spool, the first stage of compression, since it has the greatest AN^2, normally dictates the rotational speed. The first stage of turbine on the high-pressure spool normally determines that spool's rotational speed because of its high AN^2 or high disk rim speed at elevated temperature.

9.5.8 Design Process

The design process requires both engineering judgment and knowledge of typical design values. Table 9.18a gives the range of design parameters for axial-flow turbines that can be used for guidance. The comparison of turbines for Pratt & Whitney engines in Table 9.18b shows typical turbine design values and the leading trends in turbine technology. Note the increases over the years in inlet temperature, mass flow rate, and output power.

From Table 9.18b, comparison of the JT3D and JT9D high-pressure turbines shows that the stage loading coefficient did not appreciably change between the designs. However, the turbine inlet temperature increased to a value above the working temperature of available materials, requiring extensive use of cooling air. The stage loading coefficient for the low-pressure turbine increased dramatically, reducing the number of stages to four. If the stage loading coefficient of the low-pressure turbine of the JT3D were not increased significantly in the design of the JT9D, about six or seven stages of low-pressure turbine would have been required—increasing both cost and weight.

Table 9.18a Range of axial-flow turbine design parameters

Parameter	Design range
High-pressure turbine	
Maximum AN^2	$4-5 \times 10^{10}$ in.$^2 \cdot$ rpm^2
Stage loading coefficient	1.4–2.0
Exit Mach number	0.40–0.50
Exit swirl angle, deg	0–20
Low-pressure turbine	
Inlet corrected mass flow rate	40–44 lbm/(s $\cdot$ ft^2)
Hub/tip ratio at inlet	0.35–0.50
Maximum stage loading at hub	2.4
Exit Mach number	0.40–0.50
Exit swirl angle, deg	0–20

Table 9.18b Comparison of Pratt & Whitney engines

Parameter	JT3D	JT9D
Year of introduction	1961	1970
Engine bypass ratio	1.45	4.86
Engine overall pressure ratio	13.6	24.5
Core engine flow, lb/s	187.7	272.0
High-pressure turbine		
Inlet temperature, °F	1745	2500
Power output, hp	24,100	71,700
Number of stages	1	2
Average stage loading coefficient	1.72	1.76
Coolant plus leakage flow, %	2.5	16.1
Low-pressure turbine		
inlet temperature, °F	1410	1600
Power output, hp	31,800	61,050
Number of stages	3	4
Average stage loading coefficient	1.44	2.47
Coolant plus leakage flow, %	0.7	1.4

9.5.8.1 Steps of design. The material presented in previous sections can now be applied to the design of an axial-flow turbine. The complete design process for a turbine will include the following items:

1) Selection of rotational speed and annulus dimensions
2) Selection of the number of stages
3) Calculation of airflow angles for each stage at the mean radius
4) Calculation of airflow angle variations from the hub to tip for each stage
5) Selection of blade material
6) Selection of blading using experimental cascade data
7) Selection of turbine cooling, if needed
8) Verification of turbine efficiency based on cascade loss data
9) Prediction of off-design performance
10) Rig testing of design

Items 1–5 will be covered in this section. The other steps are covered in Refs. 42, 43, 22, and 29. The design process is inherently iterative, often requiring the return to an earlier step when prior assumptions are found to be invalid. Many technical specialities are interwoven in a design, e.g., an axial-flow turbine involves at least thermodynamics, aerodynamics, structures, materials, heat transfer, and manufacturing processes. Design requires the active participation and disciplined communication by many technical specialists.

Example 9.14

We will consider the design of a turbine suitable to power the eight-stage, axial-flow compressor designed earlier in this chapter for a simple turbojet gas turbine

engine (see Example 9.7). From engine cycle and compressor design calculations, a suitable design point for the turbine of such an engine at sea-level, standard-day conditions ($P = 14.696$ psia and $T = 518.7°R$) may emerge as follows:

Compressor pressure ratio: 10.41	Rotor speed ω: 800 rad/s
Compressor flow rate: 150 lbm/s	Turbine flow rate: 156 lbm/s
Compressor efficiency: 86.3%	T_t entering turbine: 3200°R
Compressor exit T_t: 1086°R	P_t entering turbine: 143.1 psia
Compressor γ: 1.4	Turbine γ: 1.3
Compressor R: 53.34 ft · lbf/(lbm · °R)	Turbine R: 53.40 ft · lbf/(lbm · °R)

From these specified data, we now investigate the aerodynamic design of an axial-flow turbine.

The compressor input power is

$$\dot{W}_c = \dot{m}c_p(T_{te} - T_{ti}) = (150 \times 0.240)(1086 - 518.7) = 20{,}423 \text{ Btu/s}$$
$$= 21.55 \text{ MW}$$

Assuming that the compressor input power is 0.98 of the turbine output power (the other 2% of turbine power goes to shaft takeoff power and bearing losses), the required output power of the turbine is 22.0 MW (21.55 MW/0.98). The total temperature leaving the turbine is

$$T_{tc} = T_{ti} - \frac{\dot{W}_t}{\dot{m}c_p} = 3200 - \frac{22{,}000/1.055}{156 \times 0.297} = 3200 - 450.1 = 2749.9°R$$

The turbine temperature ratio ($\tau_t = T_{te}/T_{ti}$) is 0.8593. If the flow entering the rotor has a Mach number of 1.2 at 60 deg to the centerline of the turbine and a 1 % total pressure loss through the turbine stator (nozzle), the annulus area entering the rotor is

$$A_2 = \frac{\dot{m}\sqrt{T_{t2}}}{(\cos \alpha_2)(P_{t2})\text{MFP}(M_2)}$$
$$= \frac{156\sqrt{3200}}{\cos 60 \text{ deg} \times 143.1 \times 0.99 \times 0.502075\sqrt{53.34/53.40}} = 248.3 \text{ in.}^2$$

For a rotor angular speed ω of 800 rad/s, AN^2 for the rotor is 1.45×10^{10} in.$^2 \cdot$ rpm^2—this blade stress is within the capability of modern cooled turbine materials (about 2 to 3×10^{10} in.$^2 \cdot$ rpm^2).

Calculation of the stage loading coefficient for the turbine helps in determining the number of turbine stages. For the turbine mean radius equal to that of the compressor, the stage loading coefficient on the mean line is

$$\psi = \frac{g_c c_p \Delta T_t}{(\omega r_m)^2} = \frac{7455 \times 450.1}{(800 \times 17.04/12)^2} = 2.600$$

Using Fig. 9.73, we see that this value of stage loading coefficient is larger than that possible for a single-stage turbine. Either the mean rotor speed ωr_m must be

Table 9.19 Variation of stage loading, radii, and rim speed with mean radius for Example 9.14 single-stage design

r_m, in.	ψ	r_t, in.	r_h, in.	r_h/r_t	U_r, ft/s
16.00	2.949	17.23	14.77	0.857	918
17.04	2.600	18.20	15.88	0.873	992
18.00	2.330	19.10	16.90	0.885	1060
19.00	2.091	20.04	17.96	0.896	1131
20.00	1.887	20.99	19.01	0.906	1201
21.00	1.712	21.94	20.06	0.914	1271

increased to reduce the stage loading coefficient for a single-stage turbine, or a two-stage turbine will be required. Because increasing the rotor angular speed ω will increase the blade stress AN^2 and because only a little margin exists, we will investigate the effect of increasing the mean radius on stage loading coefficient, annulus radii (r_t and r_h), and rim speed (U_r—assuming the rim radius is 1 in. smaller than that of the hub). From the results given in Table 9.19, we can see that a single-stage turbine would require a mean radius of 19 to 20 in. to reduce the stage loading coefficient and keep the rim speed below about 1200 ft/s. This would result in a tip radius equal to or larger than the compressor's inlet radius. In addition, the tip radius of 20 to 21 in. is much larger than current turbines for gas turbine engines that range between 10 and 17 in. Although a single-stage turbine is desirable because of the reduced weight, the low rotor angular speed of 800 rad/s makes this size undesirable.

For a smaller turbine, the designer might consider increasing the rotor angular speed and redesigning the compressor. A rotor angular speed of 1000 rad/s for a turbine with a 16-in. mean radius has a stage loading coefficient for the mean radius of 1.885 and a rim speed of 1148 ft/s, which is possible for a single stage.

The designs of both a single-stage turbine and a two-stage turbine are performed in the following sections. The computer program TURBN is used to ease the calculational burden in both designs.

9.5.8.2 Single-stage design. We consider a single-stage turbine with the following characteristics:

Rotor angular speed ω: 800 rad/s
T_t entering turbine: 3200°R
T_t leaving turbine: 2749.1°R
Turbine R: 53.40 ft · lbf/(lbm · °R)
Turbine mass flow rate: 156 lbm/s
P_t entering turbine: 143.1 psia
Ratio of specific heats: 1.3

To keep the degree of reaction at the hub from being too negative at a reasonable value of the stage loading coefficient ψ, we consider a nonzero exit swirl angle α_3 for a stage with a hub speed of about 1200 ft/s (this corresponds to a rim speed of about 1130 ft/s, which will limit the disk stress). This hub speed corresponds to a hub radius of 18 in. and a tip radius of about 20.1 in. The

computer program TURBN was run with the exit swirl angle α_3 unknown, the data just listed, and the following additional input data:

Mean rotor speed ωr: 1270 ft/s	ω: 800 rad/s
M_2: 1.1	α_2: 60 deg
M_1: 0.4	α_1: 0 deg
u_3/u_2: 1.0	$\phi_{t\,\text{stator}} = 0.06$ and $\phi_{t\,\text{rotor}} = 0.15$
Z_s: 0.9	$(c/h)_s$: 1.0
Z_r: 0.9	$(c/h)_r$: 1.0

Computer calculations yield the single-stage turbine summarized in Table 9.20 with hub and tip tangential velocities based on free-vortex swirl distribution. This is a viable single-stage design with moderate exit swirl α_3, positive reaction, and subsonic M_{3R} at the tip.

This design gives a blade AN^2 of 1.44×10^{10} in.$^2 \cdot$rpm ^{2} and hub speed of 1201 ft/s. This AN^2 value is well within the limits of cooled turbine materials, and the low hub speed is below the limiting speed of turbine disk materials.

A cross-sectional sketch of the single-stage turbine just designed and plotted by the computer program TURBN is shown in Fig. 9.76. Note that this sketch does not show the required exit guide vanes that will turn the flow back to axial. The estimated axial length L shown in Fig. 9.76 is based on the input values of Z and c/h for the stator and rotor blades and the scaling relationships of Fig. 9.69. For the input values of Z and c/h, the resulting solidity at the mean radius, number of blades, and chord length for the stator and rotor are as shown in Table 9.21.

The selected axial chord and number of blades for the stator or rotor depend on many factors (e.g., flow through the blades, vibration, blade attachment). Figure 9.77 shows the computer sketch of the blades at the mean radius, using C4 base profiles.

9.5.8.3 Two-stage design. In a two-stage design, the stage loading coefficients ψ are lower and the temperature ratios τ_s are higher than those for a single-stage design. This results in higher reactions, less turning of the flow, and lower loss coefficients. For good flow control of the turbine, the first-stage stator (nozzle) should be choked, which requires that M_2 for this stage be supersonic. Inspection of Fig. 9.75 shows that at low ψ and high τ_s, the value of M_{3R} is a little less than M_2—thus, we will want to select a low supersonic value of M_2 (about 1.05) for the first stage. A balanced design would have about the same α_2 values for both stages with the first-stage M_{3Rt} below 0.9.

The two-stage turbine will be designed with a 17.04-in. mean radius (same as multistage compressor) at an rpm of 7640 ($\omega = 800$ rad/s), giving a mean rotor speed $U_m = \omega r_m$ of 1136 ft/s. An initial starting point for the design of this two-stage turbine is constant axial velocity through the rotor ($u_3 = u_2$), zero exit swirl ($\alpha_3 = 0$), and a second-stage M_2 of 0.7. The stage loading coefficients and other flow properties depend on the split in temperature drop between the stages. Calculations were performed by using the computer program TURBN

Table 9.20 Results for Example 9.14 single-stage axial-flow turbine design

Property		Station										
		1*h*	1*m*	1*t*	2*h*	2*m*	2*t*	2*Rm*	3*Rm*	3*h*	3*m*	3*t*
T_1	°R	3200	3200	3200	3200	3200	3200	2909	2909	2750	2750	2750
T	°R	3125	3125	3125	2665	2708	2745	2708	2621	2620	2621	2622
Pt	psia	143.1	143.1	143.1	138.8	138.8	138.8	91.8	87.0	68.3	68.3	68.3
P	psia	129.1	129.1	129.1	62.8	67.4	71.5	67.4	55.4	55.4	55.4	55.5
M		0.400	0.400	0.400	1.157	1.100	1.051	0.702	0.855	0.574	0.572	0.571
V	ft/s	1057	1057	1057	2823	2705	2602	1727	2069	1389	1385	1381
u	ft/s	1057	1057	1057	1353	1353	1353	1353	1353	1353	1353	1353
v	ft/s	0	0	0	2477	2343	2222	1073	1566	316	296	278
α	deg	0	0	0	61.36	60.00	58.67	——	——	13.14	12.33	11.61
β	deg	——	——	——	——	——	——	38.42	49.17	——	——	——
Radii	in.	18.25	19.05	19.85	18.02	19.05	20.08	19.05	19.05	17.83	19.05	20.27

Hub: $^{\circ}R_t = 0.0990$ $A_1 = 190.78$ in.^{2}
Mean: $^{\circ}R_t = 0.1939$ $A_2 = 247.52$ in.^{2}
Tip: $^{\circ}R_t = 0.2746$ $A_3 = 291.11$ in.^{2}

$M_{3Rt} = 0.875$ $\tau_s = 0.8593$ $\pi_s = 0.4770$ $\psi = 2.0776$ $\Phi = 1.0652$

$\eta_s = 89.57\%$ AN^2 at $2 = 1.44 \times 10^{10}$ in.$^2 \cdot$rpm^2

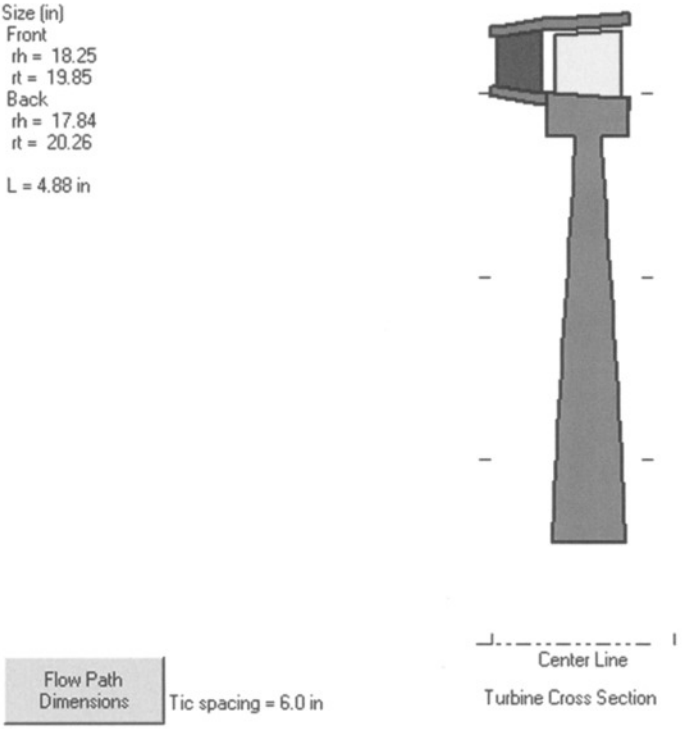

Fig. 9.76 Sketch of cross section for single-stage turbine design.

with α_2 unknown at different values of the temperature leaving the first-stage turbine. The resulting α_2 and M_{3Rt} values are listed in Table 9.22. An interstage temperature of 2925°R gives a balance design for α_2 values with the first stage M_{3Rt}, above 0.9. The value of M_{3Rt} can be reduced by selecting a value for the axial velocity ratio u_3/u_2 less than unity.

A design with an interstage temperature of 2925°R and first-stage u_3/u_2 of 0.9 is selected to reduce M_{3Rt}. The losses for the first stage and second stage are estimated by using polytropic efficiencies of 0.9 and 0.92, respectively, and stator loss coefficients of 0.06 and 0.02, respectively. For all blades, a value of 0.9 is used for the tangential force coefficient Z, and a value of 1.0 is used for the chord/height ratio c/h. Results for both stages are presented in Tables 9.23

Table 9.21 Blade results for single-stage turbine

	Solidity	Number of blades	Chord, in.
Stator	0.979	64	1.831
Rotor	1.936	103	2.250

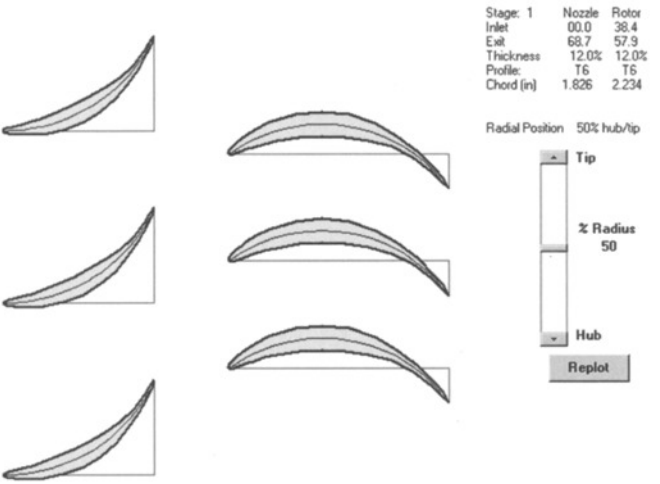

Fig. 9.77 Sketch of blades for single-stage turbine design.

and 9.24 with hub and tip tangential velocities based on free-vortex swirl distribution.

A cross-sectional sketch of the two-stage turbine just designed and plotted by TURBN is shown in Fig. 9.78. The sketch shows the stator and rotor for both stages. Note that the turbine exit stator is not shown in the sketch. For the input values of Z and c/h, the resulting solidity at the mean radius, number of blades, and chord length for the stator and rotor blades of the two stages are as shown in Table 9.25.

The selected axial chord and number of blades for the stator and rotor depend on many factors (e.g., flow through the blades, vibration, blade attachment). Figures 9.79 and 9.80 show the computer sketch of the blades at the mean radius, using C4 base profiles for the first and second stages, respectively.

Table 9.22 Variation of stage parameters with interstage temperature for Example 9.14 two-stage design

	Stage 1				Stage 2		
T_{t3}, °R	ψ	τ_s	α_2, deg	M_{3Rt}	ψ	τ_s	α_2, deg
2875	1.8750	0.8984	55.0	0.7774	1.0034	0.9565	28.61
2900	1.7307	0.9063	49.12	0.8467	0.8659	0.9482	34.90
2925	1.5865	0.9141	43.88	0.9068	1.0102	0.9401	41.65
2950	1.4423	0.9219	39.06	0.9587	1.1544	0.9322	49.13
2975	1.2981	0.9297	34.55	1.0034	1.2986	0.9243	57.90

Table 9.23 Results for Example 9.14, first stage of two-stage axial-flow turbine design

Property		Station										
		1*h*	1*m*	1*t*	2*h*	2*m*	2*t*	2*Rm*	3*Rm*	3*h*	3*m*	3*t*
T_t	°R	3200	3200	3200	3200	3200	3200	3012	3012	2925	2925	2925
T	°R	3125	3135	3125	2724	2746	2765	2746	2734	2734	2734	2734
P_t	psia	143.1	143.1	143.1	139.1	139.1	139.1	106.9	105.4	92.8	92.8	92.8
P	psia	129.1	129.1	129.1	69.2	71.6	73.8	71.6	69.3	69.3	69.3	69.3
M		0.400	0.400	0.400	1.079	1.050	1.024	0.803	0.823	0.683	0.683	0.683
V	ft/s	1057	1057	1057	2662	2600	2545	1989	2034	1687	1687	1687
u	ft/s	1057	1057	1057	1874	1874	1874	1874	1687	1687	1687	1687
v	ft/s	0	0	0	1891	1802	1722	666	1136	0	0	0
α	deg	0	0	0	45.25	43.88	42.57	——	——	0	0	0
β	deg	——	——	——	——	——	——	19.57	33.96	——	——	——
Radii	in.	16.15	17.04	17.93	16.24	17.04	17.84	17.04	17.04	16.13	17.04	17.95

Hub: $^\circ R_t = 0.0359$ $A_1 = 190.78$ in.^{2}
Mean: $^\circ R_t = 0.0437$ $A_2 = 170.34$ in.^{2}
Tip: $^\circ R_t = 0.1129$ $A_3 = 194.88$ in.^{2}

$M_{3Rt} = 0.8370$ $\tau_s = 0.9141$ $\pi_s = 0.6488$ $\psi = 1.5865$ $\Phi = 1.650$

$\eta_s = 90.44\%$ AN^2 at 2 $= 9.94 \times 10^{10}$ in.$^2 \cdot$ rpm^2

Table 9.24 Results for Example 9.14 second stage of two-stage axial-flow turbine design

Property		Station										
		1*h*	1*m*	1*t*	2*h*	2*m*	2*t*	2*Rm*	3*Rm*	3*h*	3*m*	3*t*
T_t	°R	2925	2925	2925	2925	2925	2925	2837	2837	2750	2750	2750
T	°R	2734	2734	2734	2711	2725	2736	2725	2638	2638	2638	2638
P_t	psia	92.84	92.84	92.84	92.35	92.35	92.35	80.85	79.41	69.42	69.42	69.42
P	psia	69.27	69.27	69.27	66.41	67.92	69.15	67.92	57.99	57.99	57.99	57.99
M		0.683	0.683	0.683	0.726	0.700	0.678	0.523	0.708	0.532	0.532	0.532
V	ft/s	1687	1687	1687	1786	1727	1677	1290	1719	1290	1290	1290
u	ft/s	1687	1687	1687	1290	1290	1290	1290	1290	1290	1290	1290
v	ft/s	0	0	0	1235	1148	1072	12	1136	0	0	0
α	deg	0	0	0	43.75	41.65	39.71	—	—	0	0	0
β	deg	—	—	—	—	—	—	0.51	41.36	—	—	—
Radii	in.	16.13	17.04	17.95	15.83	17.04	18.25	17.04	17.04	15.67	17.04	18.41

Hub: $^\circ R_t = 0.4148$ $A_1 = 194.88$ in.^{2}
Mean: $^\circ R_t = 0.4949$ $A_2 = 258.99$ in.^{2}
Tip: $^\circ R_t = 0.5596$ $A_3 = 293.69$ in.^{2}

$M_{3Rt} = 0.7337$ $\tau_s = 0.9401$ $\pi_s = 0.7477$ $\psi = 1.0102$ $\Phi = 1.136$

$\eta_s = 92.24\%$ AN^2 at 2 $= 1.51 \times 10^{10}$ in.$^2 \cdot$ rpm^2

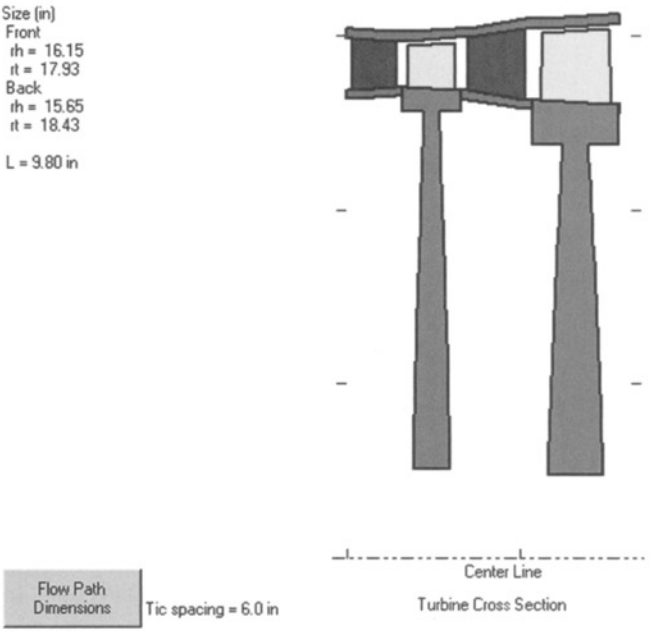

Fig. 9.78 Sketch of cross section for two-stage turbine design.

For the first stage, this design gives a blade AN^2 of 9.94×10^9 in.$^2 \cdot$ rpm^2 and disk speed of about 1020 ft/s. This AN^2 is well within the limits of cooled turbine materials, and the low rim speed is below the limiting speed of turbine disk materials.

9.5.9 Turbine Cooling

The turbine components are subjected to much higher temperatures in the modern gas turbine engines being designed and built today than was possible 60 years ago. This is due mainly to improvements in metallurgy and cooling of turbine components. The cooling air to cool the turbine is bleed air from the compressor. A schematic of a typical turbine cooling system is shown in

Table 9.25 Blade results for two-stage turbine

	Stage 1		Stage 2	
	Stator	Rotor	Stator	Rotor
Solidity	0.725	1.880	1.643	1.254
Blades	46	118	83	52
Chord, in.	1.686	1.706	2.120	2.581

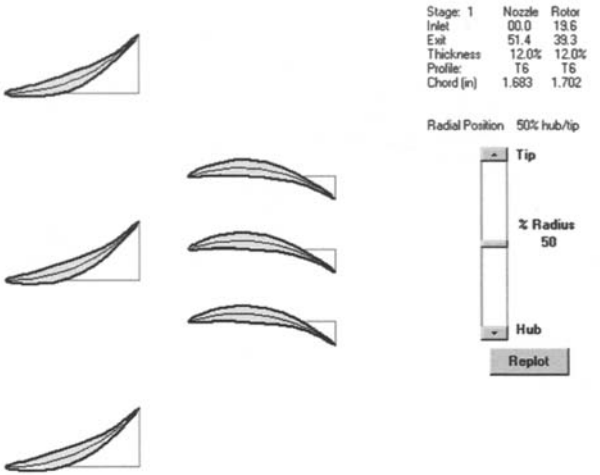

Fig. 9.79 Sketch of blades for first stage of two-stage turbine design.

Fig. 9.81. The stator blades and the outer wall of the turbine flow passage use cooling air that travels from the compressor between the combustor and outer engine case. The turbine rotor blades, disks, and inner wall of the turbine flow passage use cooling air that is routed through inner passageways.

The first-stage stator blades (nozzles) are exposed to the highest turbine temperatures (including the hot spots from the combustor). The first-stage rotor blades are exposed to a somewhat lower temperature because of circumferential averaging, dilution of turbine gases with first-stage stator cooling air, and relative

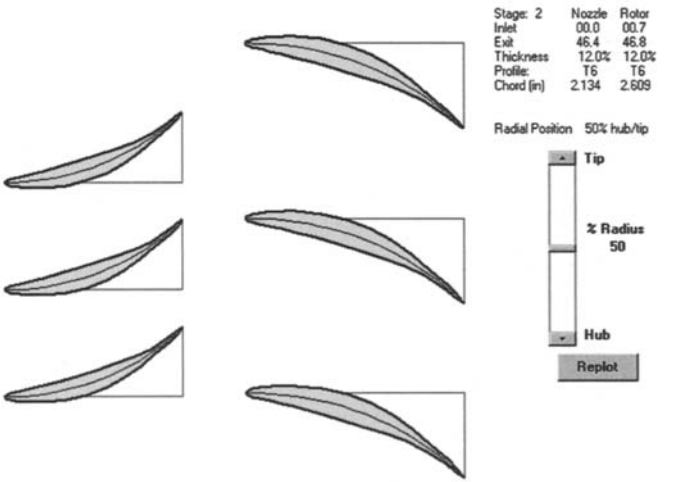

Fig. 9.80 Sketch of blades for second stage of two-stage turbine design.

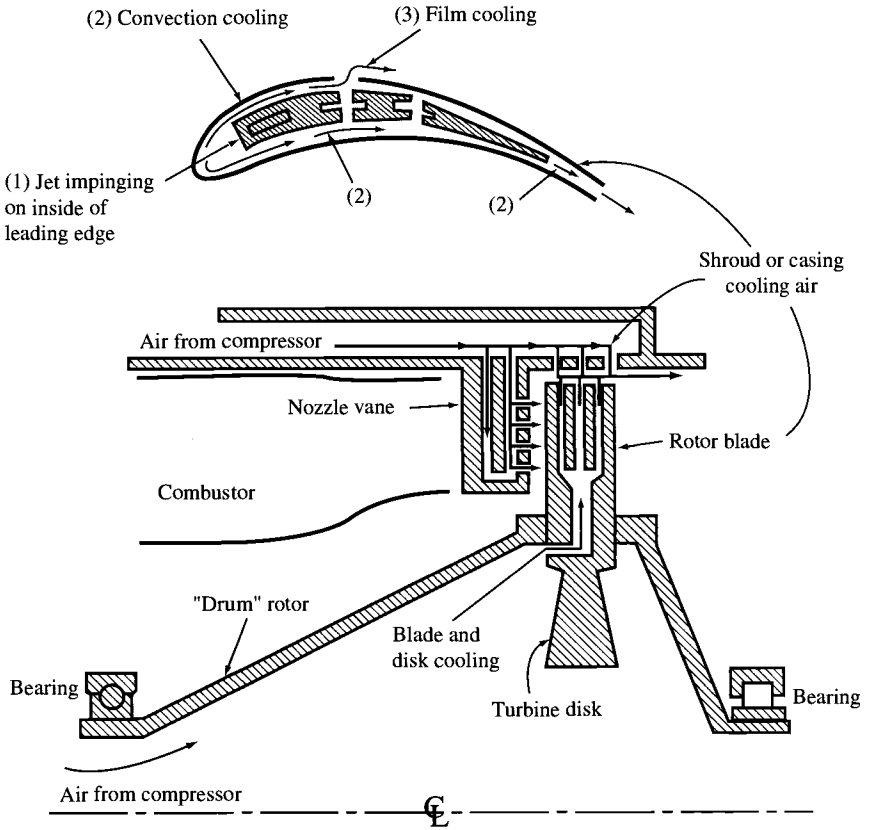

Fig. 9.81 Schematic of air-cooled turbine (from Ref. 28).

velocity effects. The second-stage stator blades are exposed to an even lower temperature because of additional cooling air dilution and power extraction from the turbine gases. The turbine temperature decreases in a like manner through each blade row.

The cooling methods used in the turbine are illustrated in Fig. 9.82 and can be divided into the following categories:

1) Convection cooling
2) Impingement cooling
3) Film cooling
4) Full-coverage film cooling
5) Transpiration cooling

Applications of these five methods of cooling to turbine blades are shown in Fig. 9.83.

Figure 9.84 shows a typical first-stage stator (nozzle) blade with cooling. This stator has cooling holes along its nose (leading edge) and pressure surface (gill

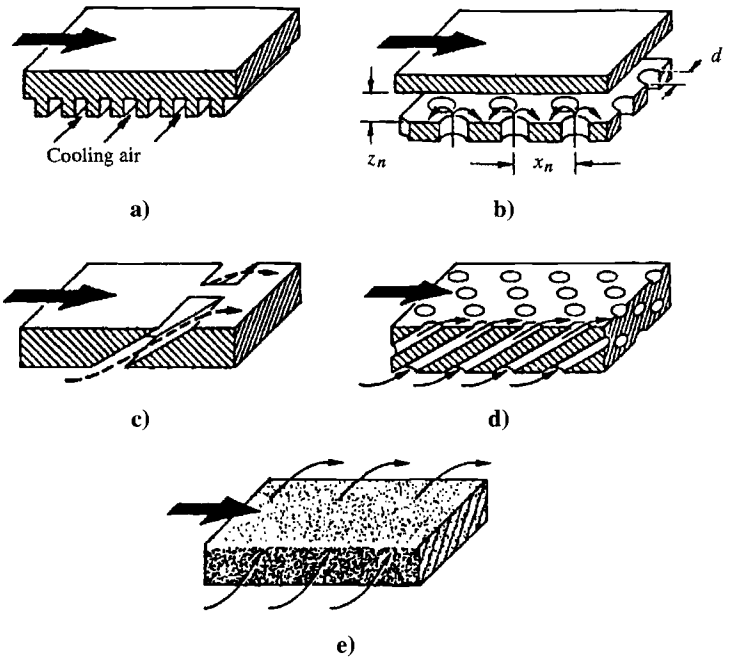

Fig. 9.82 Methods of turbine cooling (Ref. 42): a) convection cooling, b) impingement cooling, c) film cooling, d) full-coverage film cooling, e) transpiration cooling.

holes) in addition to cooling flow exiting at its trailing edge. The cooling holes on the inside wall are also shown.

A rotor blade of the General Electric CF6-50 engine is shown in Fig. 9.85. The cross section of the blade shows the elaborate internal cooling and flow exiting the blade tip (through its cap) and along the trailing edge. The blade isometric shows flow through the gill holes on the pressure surface in addition to the tip and trailing-edge cooling flows.

9.5.10 Turbine Performance

The flow enters a turbine through stationary airfoils (often called *stator blades* or *nozzles*) that turn and accelerate the fluid, increasing its tangential momentum. Then the flow passes through rotating airfoils (called *rotor blades*) that remove energy from the fluid as they change its tangential momentum. Successive pairs of stationary airfoils followed by rotating airfoils remove additional energy from the fluid. To obtain high output power to weight from a turbine, the flow entering the first-stage turbine rotor is normally supersonic, which requires the flow to pass through sonic conditions at the minimum passage area in the first-stage stators (nozzles). From Eq. (8.3), the corrected inlet mass flow rate based on this minimum passage area (throat) will be constant for fixed-inlet-area turbines. This flow characteristic is shown in the typical turbine flow map (Fig. 9.86) when the expansion ratio across the turbine (ratio

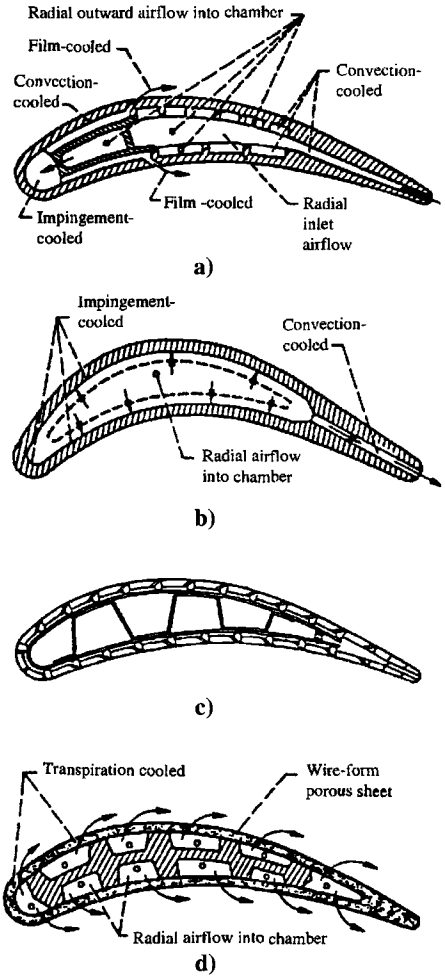

Fig. 9.83 Turbine blade cooling (Ref. 42): a) convection-, impingement-, and film-cooled blade configuration, b) convection- and impingement-cooled blade configuration, c) full-coverage film-cooled blade configuration, d) transpiration-cooled blade configuration.

of total pressure at exit to total pressure at entrance $P_{t4}/P_{t5} = 1/\pi_t$ is greater than about 2 and the flow at the throat is choked.

The performance of a turbine is normally shown by using the total pressure ratio, corrected mass flow rate, corrected turbine speed, and component efficiency. This performance is presented in either two maps or one consolidated map. One map shows the interrelationship of the total pressure ratio, corrected mass flow rate, and corrected turbine speed, like that depicted in Fig. 9.86 for a single-stage turbine. Because the corrected-speed lines collapse into one line when the turbine is choked, the turbine efficiency must be shown in a

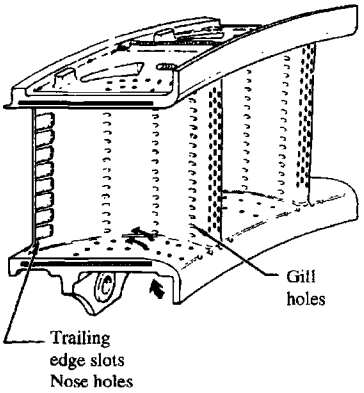

Fig. 9.84 Typical cooled turbine nozzle. (Courtesy of General Electric.)

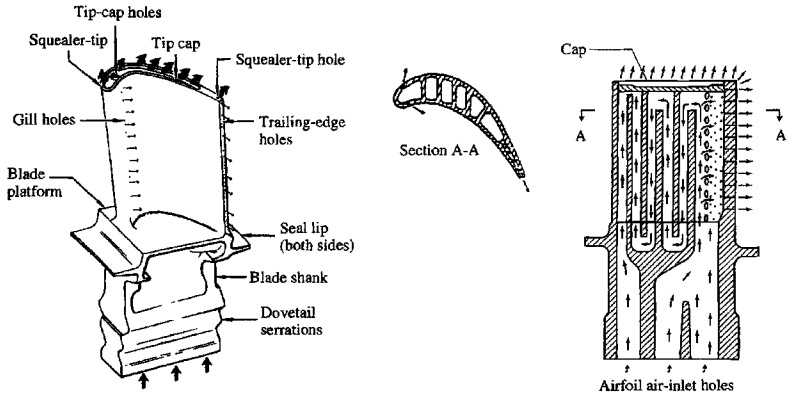

Fig. 9.85 Construction features of air-cooled turbine blade. (Courtesy of General Electric.)

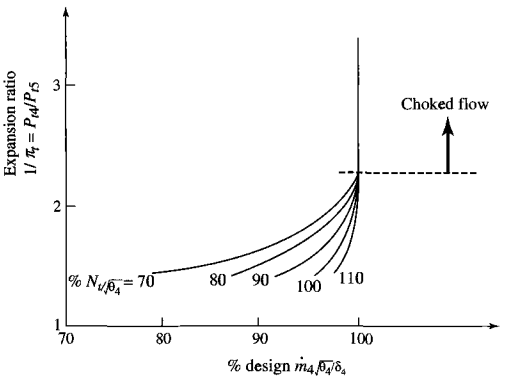

Fig. 9.86 Typical turbine flow map.

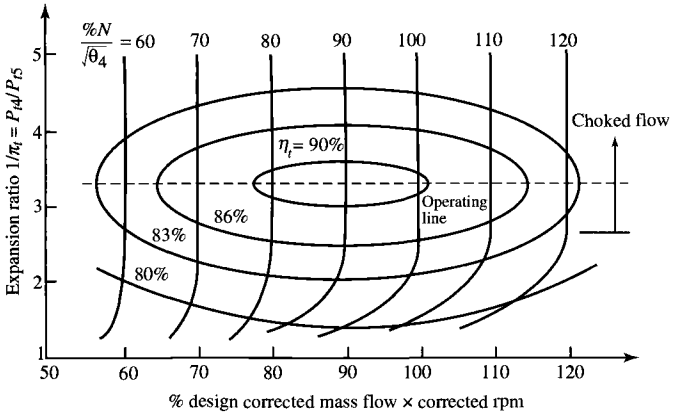

Fig. 9.87 Typical turbine consolidated performance map.

separate map (see Fig. 8.5b). The constant corrected speed lines of Fig. 9.86 can be spread out horizontally by multiplying the corrected mass flow rate by the percentage of corrected speed. Now the turbine efficiency lines can be superimposed without cluttering the resulting performance map. Figure 9.87 shows the consolidated turbine performance map of a multistage turbine with all four performance parameters: total pressure ratio, corrected mass flow rate, corrected turbine speed, and efficiency.

For the majority of aircraft gas turbine engine operation, the turbine expansion ratio is constant and the turbine operating line can be drawn as a horizontal line in Fig. 9.87 (it would collapse to an operating point on the flow map of Fig. 9.86). At off-design conditions, the corrected speed and efficiency of a turbine change very little from their design values. In the analysis of gas turbine engine performance of Chapter 8, we considered that the turbine efficiency was constant.

9.6 Centrifugal-Flow Turbine Analysis

The flow through the stators (nozzles) and rotor of a centrifugal flow turbine is shown in Fig. 9.88. The stators accelerate the flow and increase its tangential velocity. The rotor decreases the tangential velocity of the flow as it removes energy from the flow. Flow exiting the rotor is normally axial, but some tangential (swirl) velocity may still be present. This type of turbine was used in the turbojet engine of von Ohain and is used extensively in turbochargers and very small gas turbine engines.

Figure 9.89 shows the station numbering used in the analysis of the centrifugal-flow turbine. The flow enters the stators at station 1 and leaves at station 2. It then passes through the rotor and leaves at station 3. Normally the flow leaving the rotor is axial ($V_3 = u_3$). Application of the Euler turbine equation to the flow through the stator and rotor, assuming adiabatic stator, gives

$$h_{t1} - h_{t3} = \frac{U_t v_2}{g_c} \tag{9.126}$$

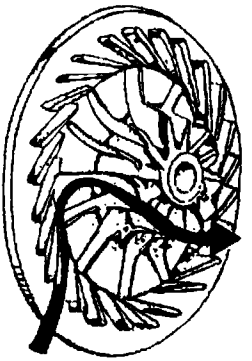

Fig. 9.88 Flow through a centrifugal-flow turbine.

The relative velocity V_{2R} at the entrance to the rotor is designed to be radial ($v_{2R} = 0$, $V_{2R} = w_2$); thus, the tangential velocity at station 2 (v_2) equals the rotor speed at its tip U_t. For this case, Eq. (9.126) becomes

$$h_{t1} - h_{t3} = \frac{U_t^2}{g_c} \tag{9.127}$$

For a calorically perfect gas, Eq. (9.127) can be written in terms of the total temperature change, or

$$T_{t1} - T_{t3} = \frac{U_t^2}{g_c c_p} \tag{9.128}$$

Note that the temperature drop through a centrifugal turbine is directly proportional to the rotor speed squared. Using the polytropic turbine efficiency e_t

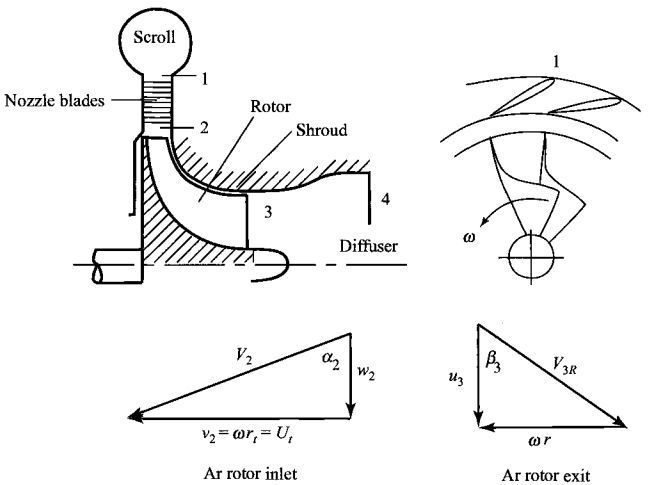

Fig. 9.89 Station numbering for centrifugal-flow turbine (after Dixon, Ref. 37).

and Eq. (9.128), we can express the turbine pressure ratio π_t as

$$\pi_t = \frac{P_{t3}}{P_{t1}} = \left(\frac{T_{t3}}{T_{t1}}\right)^{\gamma/[(\gamma-1)e_t]} = \left(1 - \frac{U_t^2}{g_c c_p T_{t1}}\right)^{\gamma/[(\gamma-1)e_t]} \tag{9.129}$$

The tip speed U_t can be written in terms of T_{t2}, M_2, and α_2. From the velocity triangle at station 2, we can write

$$U_t = v_2 = V_2 \sin \alpha_2 \tag{9.130}$$

V_2 can be expressed in terms of T_{t1} and M_2 as

$$V_2 = \sqrt{\frac{2g_c c_p T_{t2}}{1 + 2/[(\gamma - 1)M_2^2]}}$$

$$= \sqrt{\frac{2g_c c_p T_{t1}}{1 + 2/[(\gamma - 1)M_2^2]}}$$

Thus

$$U_t = \sin \alpha_2 \sqrt{\frac{2g_c c_p T_{t1}}{1 + 2/[(\gamma - 1)M_2^2]}} \tag{9.131}$$

The rotor speed U_t is plotted vs T_{t1}, α_2, and M_2 in Fig. 9.90 by using Eq. (9.131). The maximum swirl angle at station 2 (α_2) is normally 70 deg. The maximum rotor tip speed is limited to between 350 and 500 m/s by the

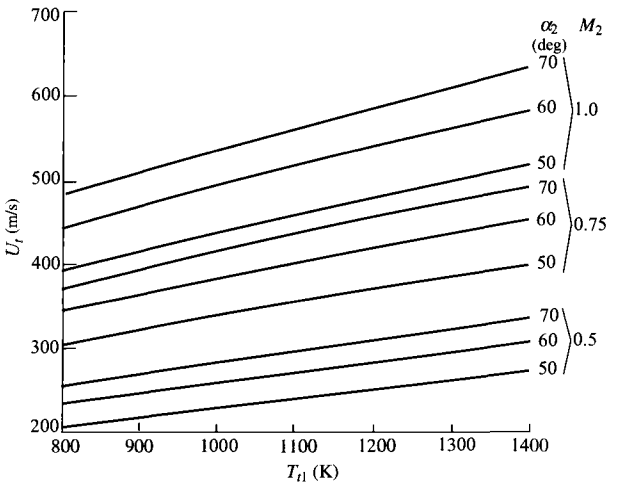

Fig. 9.90 Rotor speed U_t vs T_{t1}, M_2, and α_2 [$\gamma = 1.33$, $c_p = 1.158$ kJ/(kg · K)].

maximum centrifugal stresses of the rotor. These stresses are a function of the relative total temperature T_{t2R} of the rotor; T_{t2R} can be written as

$$T_{t2R} = T_{t2} - \frac{U_t^2}{2g_c c_p} \tag{9.132}$$

Example 9.15

Consider a radial-flow turbine.

Given:

Mass flow rate = 2.5 kg/s
$T_{t1} = 1100$ K
Polytropic efficiency $e_t = 0.85$
$\alpha_2 = 70$ deg
$\gamma = 1.33$
Hub/tip ratio at 3 = 0.4
$P_{t2} = 0.99\ P_{t1}$
$P_{t1} = 400$ kPa
$T_{t3} = 935$ K
Rotor diameter = 0.40 m
$u_3 = w_2$
$R = 0.2872$ kJ/(kg · K)
$g_c c_p = 1.158$ kJ/(kg · K)

Find:

1) Tip speed, rotational speed, and rpm of rotor
2) Mach number, velocities, rotor depth, and T_{tR} at station 2
3) Total pressure, Mach number, and hub and tip radius at station 3
4) Values of V_{3R}, T_{t3R}, β_3, and M_{3R} at mean radius
5) Variation of M_{3R} and β_3 with radius

Solution:

$$U_t = \sqrt{g_c c_p (T_{t1} - T_{t3})} = \sqrt{1158(1100 - 935)} = 437.1 \text{ m/s}$$

$$\omega = \frac{U_t}{r_t} = \frac{437.1}{0.20} = 2185.5 \text{ rad/s}$$

$$\text{RPM} = \frac{30}{\pi}\omega = \frac{30}{\pi}(2185.5) = 20{,}870 \text{ rpm}$$

$$M_2 = \sqrt{\frac{2/(\gamma - 1)}{2g_c c_p T_{t1} \sin^2 \alpha_2 / U_t^2 - 1}}$$

$$= \sqrt{\frac{2/0.33}{2 \times 1158 \times 1100 \sin^2 70 \text{ deg}/437.1^2 - 1}}$$

$$= 0.750$$

$$V_2 = \frac{U_t}{\sin \alpha_2} = \frac{437.1}{\sin 70 \text{ deg}} = 465.2 \text{ m/s}$$

$$w_2 = V_2 \cos \alpha_2 = 465.2 \cos 70 \text{ deg} = 159.1 \text{ m/s}$$

$$\text{MFP}(M_2) = 0.03731$$

$$A_2 = \frac{\dot{m}\sqrt{T_{t2}}}{(P_{t2})(\cos\alpha_2)\text{MFP}(M_2)}$$

$$= \frac{2.5\sqrt{1100}}{(0.99 \times 400{,}000)(\cos 70\,\text{deg})(0.03731)} = 0.01641\,\text{m}^2$$

$$b = \frac{A_2}{2\pi r_t} = \frac{0.01641}{2\pi \times 0.2} = 0.01306\,\text{m}$$

$$T_{t2R} = T_{t2} - \frac{U_t^2}{2g_c c_p} = 1100 - \frac{437.1^2}{2 \times 1158} = 1017.5\,\text{K}$$

$$\pi_t = \frac{P_{t3}}{P_{t1}} = \left(\frac{T_{t3}}{T_{t1}}\right)^{\gamma/[(\gamma-1)e_t]}$$

$$= \left(\frac{935}{1100}\right)^{1.33/(0.33\times 0.85)} = 0.4627$$

$$P_{t3} = 0.4627 P_{t1} = 0.4627 \times 400 = 185.1\,\text{kPa}$$

$$V_3 = u_3 = w_2 = 159.1\,\text{m/s}$$

$$M_3 = \sqrt{\frac{2/(\gamma-1)}{2g_c c_p T_{t3}/V_3^2 - 1}}$$

$$= \sqrt{\frac{2/0.33}{2 \times 1158 \times 935/159.1^2 - 1}} = 0.2677$$

$$\text{MFP}(M_3) = 0.01748$$

$$A_3 = \frac{\dot{m}\sqrt{T_{t3}}}{P_{t3}\text{MFP}(M_3)}$$

$$= \frac{2.5\sqrt{935}}{185{,}100 \times 0.01748} = 0.02363\,\text{m}^2$$

$$r_{3t} = \sqrt{\frac{A_3}{\pi[1 - (r_h/r_t)^2]}} = \sqrt{\frac{0.02363}{\pi(1 - 0.4^2)}} = 0.09463\,\text{m}$$

$$r_{3h} = 0.4 r_{3t} = 0.4 \times 0.09463 = 0.03785\,\text{m}$$

$$r_{3m} = \frac{r_{3t} + r_{3h}}{2} = 0.06624\,\text{m}$$

$$v_{3Rm} = \omega r_{3m} = 2185.5 \times 0.06624 = 144.8\,\text{m/s}$$

Table 9.26 Results for Example 9.15 radial-flow turbine

Property		Station				
		1	2	$2R$	$3Rm$	$3m$
T_t	K	**1100.0**	1100.0	1017.5	944.1	**935.0**
T	K		1006.6	1006.6	924.1	924.1
P_t	kPa	**400.0**	**396.0**	289.2	192.4	185.1
P	kPa		276.9	276.9	176.5	176.5
M			0.7500	0.2565	0.3619	0.2677
V	m/s		465.2	159.1	215.1	159.1
u/w	m/s		159.1	159.1	159.1	159.1
v	m/s	0	437.1	0	144.8	0
r	m		0.2000	0.2000	0.06624	
α	deg	0	**70.0**	——	——	0
β	deg		——	0	42.31	——

$$V_{3Rm} = \sqrt{u_3^2 + v_{3Rm}^2} = \sqrt{159.1^2 + 144.8^2} = 215.1 \text{ m/s}$$

$$T_{t3Rm} = T_3 + \frac{V_{3Rm}^2}{2g_c c_p} = T_{t3} + \frac{v_{3Rm}^2}{2g_c c_p}$$

$$= 935 + \frac{144.8^2}{2 \times 1158} = 944.1 \text{ K}$$

$$M_{3Rm} = M_3 \frac{V_{3Rm}}{V_3} = 0.2677\left(\frac{215.1}{159.1}\right) = 0.3619$$

$$\beta_{3m} = \tan^{-1}\frac{v_{3Rm}}{u_3} = \tan^{-1}\frac{144.8}{159.1} = 42.31 \text{ deg}$$

The results of this example are summarized in Table 9.26. The radial variation of β_3 and M_{3R} are given in Fig. 9.91, using the following relationships:

$$\beta_3 = \tan^{-1}\frac{v_{3R}}{u_3} = \tan^{-1}\frac{\omega r_3}{u_3}$$

$$M_{3R} = M_3\sqrt{1 + \tan^2\beta_3}$$

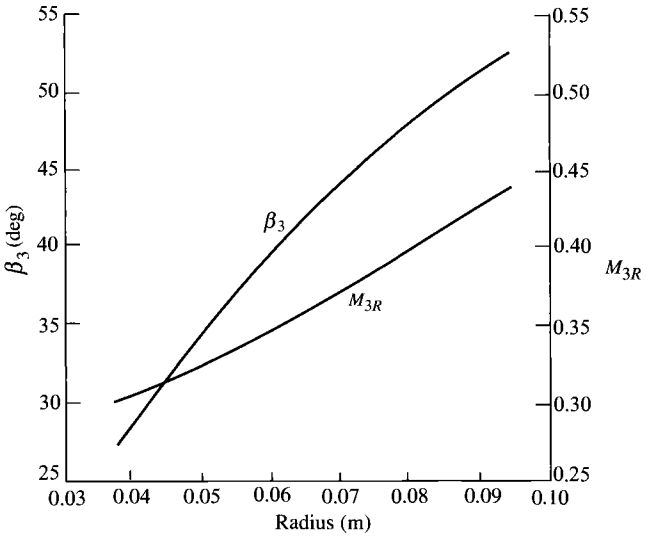

Fig. 9.91 β_3 and M_{3R} vs radius for Example 9.15.

Problems

9.1 Relative velocities are an important concept in the analysis of turbomachines. To help understand relative velocity, consider that a baseball is thrown at a moving train as shown in Fig. P9.1. If the baseball has a velocity of 60 mph and the train is traveling at 80 mph, find the magnitude and direction of the baseball velocity relative to the train.

9.2 A small fan used to circulate air in a room is shown in Fig. P9.2. The fan blades are twisted and change their angle relative to the centerline of the fan as the radius increases. If the relative velocity of the air makes the same angle to the centerline of the fan as the blades and if the blade at a radius of 0.2 m has an angle of 60 deg, determine the speed of the air for fan speeds of 1725 and 3450 rpm.

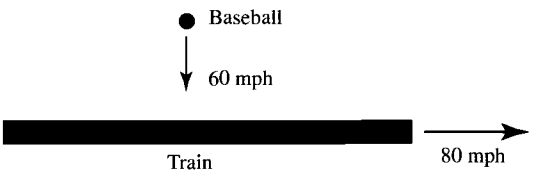

Fig. P9.1

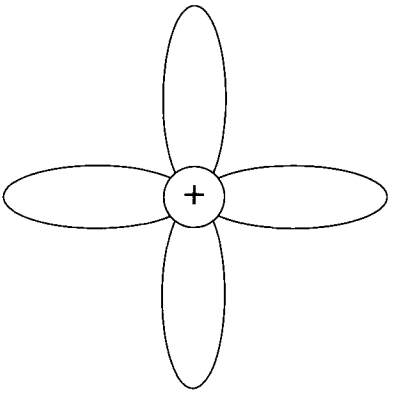

Fig. P9.2

9.3 Air flows through an axial compressor stage with the following properties:

$$T_{t1} = 300 \text{ K}, \quad u_2/u_t = 1.0, \quad v_1 = 120 \text{ m/s}, \quad \alpha = 0 \text{ deg}$$
$$\beta_2 = 45 \text{ deg}, \quad U = \omega r_m = 240 \text{ m/s}$$

Note: For air, use $\gamma = 1.4$ and $R = 0.286 \text{ kJ/(kg} \cdot \text{ K)}$. Determine the change in tangential velocity and the total pressure ratio of the stage for a stage efficiency of 0.88.

9.4 Air flows through an axial compressor stage with the following properties:

$$T_{t1} = 540 \text{ deg R}, \quad u_2/u_1 = 1.0, \quad v_1 = 400 \text{ ft/s}$$
$$\alpha_1 = 0 \text{ deg}, \quad \beta_2 = 45 \text{ deg}, \quad U = \omega r_m = 800 \text{ ft/s}$$

Note: For air, use $\gamma = 1.4$ and $R = 53.34 \text{ ft} \cdot \text{lbf/(lbm} \cdot {}^\circ\text{R)}$. Determine the change in tangential velocity and the total pressure ratio of the stage for a stage efficiency of 0.9.

9.5 Air flows through an axial compressor stage with the following properties:

$$T_{t1} = 290 \text{ K}, \quad P_{t1} = 101.3 \text{ kPa}, \quad u_2/u_1 = 1.0$$
$$M_1 = 0.6, \quad \alpha_1 = 40 \text{ deg}, \quad \alpha_2 = 57.67 \text{ deg}, \quad U = \omega r_m = 360 \text{ m/s}.$$

Note: For air, use $\gamma = 1.4$ and $R = 0.286 \text{ kJ/(kg} \cdot \text{K)}$. Determine the following:

(a) V_1, u_1, and v_1
(b) u_2, V_2, and V_2
(c) ΔT_t and τ_s for the stage
(d) π_s and P_{t3} for a polytropic efficiency of 0.88

9.6 Air flows through an axial compressor stage with the following properties:

$$T_{t1} = 518.7°R, \quad P_{t1} = 14.696 \text{ psia}, \quad u_2/u_1 = 1.0, \quad M_1 = 0.6$$

$$\alpha_1 = 40 \text{ deg}, \quad \alpha_2 = 57.67 \text{ deg}, \quad U = \omega r_m = 1200 \text{ ft/s}$$

Note: For air, use $\gamma = 1.4$ and $R = 53.34 \text{ ft} \cdot \text{lbf}/(\text{lbm} \cdot °R)$. Determine the following:

(a) V_1, u_1, and v_1
(b) u_2, v_2, and V_2
(c) ΔT_t and τ_s for the stage
(d) π_s and P_{t3} for a polytropic efficiency of 0.9

9.7 Air enters a compressor stage that has the following properties:

$$\dot{m} = 50 \text{ kg/s}, \quad \omega = 800 \text{ rad/s}, \quad r = 0.5 \text{ m}$$

$$M_1 = M_3 = 0.5, \quad \alpha_1 = \alpha_3 = 45 \text{ deg}, \quad T_{t1} = 290 \text{ K}$$

$$P_{t1} = 101.3 \text{ kPa}, \quad u_2/u_1 = 1.0, \quad T_{t3} - T_{t1} = 45 \text{ K}$$

$$\phi_{cr} = 0.10, \quad \phi_{cs} = 0.03, \quad \sigma = 1$$

Note: For air, use $\gamma = 1.4$ and $R = 0.286 \text{ kJ}/(\text{kg} \cdot \text{K})$. Make and fill out a table of flow properties like Table 9.3, and determine the diffusion factors, degree of reaction, stage efficiency, polytropic efficiency, and flow areas and associated hub and tip radii at stations 1, 2, and 3.

9.8 Air enters a compressor stage that has the following properties:

$$\dot{m} = 100 \text{ lbm/s}, \quad \omega = 1000 \text{ rad/s}, \quad r = 12 \text{ in.}, \quad M_1 = M_3 = 0.6$$

$$\alpha_1 = \alpha_3 = 42 \text{ deg}, \quad T_{t1} = 518.7°R, \quad P_{t1} = 14.7 \text{ psia}, \quad u_2/u_1 = 1.0$$

$$T_{t3} - T_{t1} = 50°R, \quad \phi_{cr} = 0.12, \quad \phi_{cs} = 0.03, \quad \sigma = 1$$

Note: For air, use $\gamma = 1.4$ and $R = 53.34 \text{ ft} \cdot \text{lbf}/(\text{lbm} \cdot °R)$. Make and fill out a table of flow properties like Table 9.3, and determine the diffusion factors, degree of reaction, stage efficiency, polytropic efficiency, and flow areas and associated hub and tip radii at stations 1, 2, and 3.

9.9 Some axial-flow compressors have inlet guide vanes to add tangential velocity to the axial flow and thus set up the airflow for the first-stage rotor.

(a) Assuming reversible, adiabatic flow through the inlet guide vanes, use the continuity equation and the mass flow parameter to show that

$$(\cos \alpha_1)(A_1)\text{MFP}(M_1) = A_0\text{MFP}(M_0)$$

where the subscripts 0 and 1 refer to the inlet and exit of the inlet guide vanes and the areas are those normal to the centerline of the axial-flow compressor.

(b) For $A_0/A_1 = 1$ and 1.1, plot a curve of α_1 vs M_1 for $M_0 = 0.3$, 0.4, and 0.5 (see Fig. 9.35).

9.10 In the analysis of turbomachinery, many authors use the dimensionless stage loading coefficient ψ, defined as

$$\psi = \frac{g_c c_p \Delta T_t}{(\omega r)^2}$$

For a repeating-stage, repeating-row compressor stage, show that the stage loading coefficient can be written as

$$\psi = \frac{g_c c_p \Delta T_t}{(\omega r)^2} = \frac{\tan \alpha_2 - \tan \alpha_1}{\tan \alpha_2 + \tan \alpha_1} = 1 - \frac{2 \tan \alpha_1}{\tan \alpha_2 + \tan \alpha_1}$$

9.11 Air enters a repeating-row, repeating-stage compressor that has the following properties:

$$\dot{m} = 40\,\text{kg/s}, \quad T_{t1} = 290\,\text{K}, \quad P_{t1} = 101.3\,\text{kPa}, \quad M_1 = 0.5$$
$$\alpha_1 = 38\ \text{deg}, \quad D = 0.5, \quad e_c = 0.9$$
$$\omega = 1000\ \text{rad/s}, \quad \phi_{cs} = 0.03, \quad \sigma = 1$$

Note: For air, use $\gamma = 1.4$ and $R = 0.286\,\text{kJ/(kg} \cdot \text{K)}$. Make and fill out a table of flow properties like Table 9.3, and determine the temperature rise, pressure ratio, mean radius, and flow areas and associated hub and tip radii at stations 1, 2, and 3.

9.12 Air enters a repeating-row, repeating-stage compressor that has the following properties:

$$\dot{m} = 50\,\text{lbm/s}, \quad T_{t1} = 518.7^\circ\text{R}, \quad P_{t1} = 14.7\,\text{psia}, \quad M_1 = 0.5$$
$$\alpha_1 = 35\ \text{deg}, \quad D = 0.5, \quad e_c = 0.9$$
$$\omega = 1200\ \text{rad/s}, \quad \phi_{cs} = 0.03, \quad \sigma = 1$$

Note: For air, use $\gamma = 1.4$ and $R = 53.34\,\text{ft} \cdot \text{lbf/(lbm} \cdot {}^\circ\text{R)}$. Make and fill out a table of flow properties like Table 9.3, and determine the temperature rise, pressure ratio, mean radius, and flow areas and associated hub and tip radii at stations 1, 2, and 3.

9.13 For an exponential swirl distribution and the data of Problem 9.11, calculate and plot the variation of u_1, v_1, u_2, and v_2 vs radius from hub to tip (see Fig. 9.34).

9.14 For an exponential swirl distribution and the data of Problem 9.12, calculate and plot the variation of u_1, v_1, u_2, and v_2 vs radius from hub to tip (see Fig. 9.34).

9.15 For the data of Problem 9.11, determine the shape of both the rotor and the stator blades on the mean radius, using NACA 65-series airfoils with circular camber line. Assume $c/h = 0.3$ and 10% thickness.

9.16 For the data of Problem 9.12, determine the shape of both the rotor and the stator blades on the mean radius, using NACA 65-series airfoils with circular camber line. Assume $c/h = 0.3$ and 10% thickness.

9.17 For the data of Problem 9.11, determine AN^2 at station 1.

9.18 For the data of Problem 9.12, determine AN^2 at station 1.

9.19 A 0.4-m-diam rotor of a centrifugal compressor for air is needed to produce a pressure ratio of 3.8. Assuming a polytropic efficiency of 0.85, determine the angular speed ω, total temperature rise, and adiabatic efficiency. Determine the input power for a mass flow rate of 2 kg/s at 1 atm and 288.2 K. Assume a slip factor of 0.9.

9.20 A 12-in. diam rotor of a centrifugal compressor for air is needed to produce a pressure ratio of 4. Assuming a polytropic efficiency of 0.86, determine the angular speed ω, total temperature rise, and adiabatic efficiency. Determine the input power for a mass flow rate of 10 lbm/s at 1 atm and 518.7°R. Assume a slip factor of 0.9.

9.21 Products of combustion flow through an axial turbine stage with the following properties:

$$T_{t1} = 1800 \text{ K}, \quad P_{t1} = 1000 \text{ kPa}, \quad u_3/u_2 = 1, \quad M_2 = 1.1$$

$$U = \omega r_m = 360 \text{ m/s}, \quad \alpha_2 = 45 \text{ deg}, \quad \alpha_3 = 5 \text{ deg}$$

Note: For the gas, use $\gamma = 1.3$ and $R = 0.287$ kJ/(kg · K). Determine the following:

(a) V_2, u_2, and v_2
(b) u_3, v_3, and V_3
(c) ΔT_t and τ_s for the stage
(d) π_s and P_{t3} for a polytropic efficiency of 0.89

9.22 Products of combustion flow through an axial turbine stage with the following properties:

$$T_{t1} = 3200°\text{R}, \quad \text{P}_{t1} = 200 \text{ psia}, \quad u_3/u_2 = 1$$

$$M_2 = 1.05, \quad U = \omega r_m = 1200 \text{ ft/s}, \quad \alpha_2 = 40 \text{ deg}, \quad \alpha_3 = 25 \text{ deg}$$

Note: For the gas, use $\gamma = 1.3$ and $R = 53.4$ ft · lbf/(lbm · °R). Determine the following:

(a) V_2, u_2, and v_2
(b) u_3, v_3, and V_3
(c) ΔT_t and τ_s for the stage
(d) π_s and P_{t3} for a polytropic efficiency of 0.9

9.23 In the preliminary design of turbines, many designers use the dimensionless work coefficient ψ, defined as

$$\psi \equiv \frac{g_c c_p \Delta T_t}{(\omega r)^2}$$

(a) For a turbine stage with $\alpha_3 = 0$, show that the degree of reaction can be written as

$$^{\circ}R_t = 1 - \frac{\psi}{2}$$

(b) For a turbine stage with $\alpha_3 = 0$, $\gamma = 1.3$, $R = 0.287$ kJ/(kg · K), and $\psi = 1$ and 2, plot ΔT_t vs ωr for $250 < \omega r < 450$ m/s.

9.24 Products of combustion enter a turbine stage with the following properties:

$$\dot{m} = 40\,\text{kg/s}, \quad T_{t1} = 1780\,\text{K}, \quad P_{t1} = 1.40\,\text{MPa}, \quad M_1 = 0.3$$
$$M_2 = 1.15, \quad \omega r = 400\,\text{m/s}, \quad T_{t3} = 1550\,\text{K}, \quad \alpha_1 = \alpha_3 = 0$$
$$r_m = 0.4\,\text{m}, \quad u_3/u_2 = 1.0, \quad \phi_{t\,\text{stator}} = 0.04, \quad \phi_{t\,\text{rotor}} = 0.08$$

Note: For the gas, use $\gamma = 1.3$ and $R = 0.287$ kJ/(kg · K). Make and fill out a table of flow properties like Table 9.12 for the mean line, and determine the degree of reaction, total temperature change, stage efficiency, polytropic efficiency, and flow areas and associated hub and tip radii at stations 1, 2, and 3.

9.25 Products of combustion enter a turbine stage with the following properties:

$$\dot{m} = 105\,\text{lbm/s}, \quad T_{t1} = 3200^{\circ}\text{R}, \quad P_{t1} = 280\,\text{psia}, \quad M_1 = 0.3$$
$$M_2 = 1.2, \quad \omega r = 1400\,\text{ft/s}, \quad T_{t3} = 2700^{\circ}\text{R}, \quad \alpha_1 = \alpha_3 = 0$$
$$r_m = 14\,\text{in.}, \quad u_3/u_2 = 1.0, \quad \phi_{t\,\text{stator}} = 0.04, \quad \phi_{t\,\text{rotor}} = 0.08$$

Note: For the gas, use $\gamma = 1.3$ and $R = 53.34$ ft · lbf/(lbm · °R). Make and fill out a table of flow properties like Table 9.12 for the mean line, and determine the degree of reaction, total temperature change, stage efficiency, polytropic efficiency, and flow areas and associated hub and tip radii at stations 1, 2, and 3.

9.26 For the data of Problem 9.24, determine the shape of both the nozzle and the rotor blades on the mean radius, using a C4 profile with circular camber line for the nozzle blades and T6 profile with circular camber line for the rotor blades. Assume $c/h = 1$, $Z = 0.9$, and 10% thickness for both nozzle and rotor blades.

9.27 For the data of Problem 9.25, determine the shape of both the nozzle and the rotor blades on the mean radius, using a C4 profile with circular camber line for the nozzle blades and a T6 profile with circular camber line for the rotor blades. Assume $c/h = 1$, $Z = 0.9$, and 10% thickness for both nozzle and rotor blades.

9.28 For the data of Problem 9.24, determine AN^2 at station 2.

9.29 For the data of Problem 9.25, determine AN^2 at station 2.

9.30 Products of combustion [$\gamma = 1.3$, $R = 0.287$ kJ/(kg · K)] exit from a set of axial-flow turbine nozzles at a swirl angle of 60 deg, $M = 1.1$, $P_t = 2.0$ MPa, and $T_t = 1670$ K. This gas then enters, the turbine rotor.

(a) For a mass flow rate of 150 kg/s, determine the area of the flow annulus upstream of the turbine rotor.

(b) If the maximum centrifugal load on the turbine blade is 70 MPa, determine the maximum shaft speed (rpm, N). Assume a blade taper factor of 0.9 and material density of 8700 kg/m^3.

(c) For the shaft speed determined in part b, the turbine disk designer has determined that the maximum radius of the hub is 0.6 m. Determine the tip radius, mean radius, and the total temperature drop through the turbine rotor based on the mean rotor velocity and zero exit swirl.

9.31 Products of combustion [$\gamma = 1.3$, $R = 53.34$ ft · lbf/(lbm · °R)] exit from a set of axial-flow turbine nozzles at a swirl angle of 65 deg, $M = 1.2$, $P_t = 300$ psia, and $T_t = 3000$°R. This gas then enters the turbine rotor.

(a) For a mass flow rate of 325 lbm/s, determine the area of the flow annulus upstream of the turbine rotor.

(b) If the maximum centrifugal load on the turbine blade is 10,000 psia, determine the maximum shaft speed (rpm, N). Assume a blade taper factor of 0.9 and material density of 0.25 lb/in.^{3}

(c) For the shaft speed determined in part b, the turbine disk designer has determined that the maximum radius of the hub is 15 in. Determine the tip radius, mean radius, and the total temperature drop through the turbine rotor based on the mean rotor velocity and zero exit swirl.

9.32 A centrifugal turbine has products of combustion [$\gamma = 1.33$, $R = 0.287$ kJ/(kg · K)] entering at 1200 K and 1.5 MPa and leaving at 1000 K. For a rotor diameter of 0.3 m, flow angle α_2 of 60 deg, and polytropic efficiency of 0.9, determine the following:

(a) Rotor tip speed and angular speed ω

(b) Mach number at station 2

(c) Total pressure at the exit

(d) Adiabatic efficiency

9.33 A centrifugal turbine has products of combustion [$\gamma = 1.33$, $R = 53.34$ ft · lbf/(lbm · °R)] entering at 2100°R and 200 psia and leaving at 1800°R. For

an 8-in. rotor diameter, flow angle α_2 of 55 deg, and polytropic efficiency of 0.85, determine the following:
(a) Rotor tip speed and angular speed ω
(b) Mach number at station 2
(c) Total pressure at the exit
(d) Adiabatic efficiency

9.34 At a total pressure of 1 atm and total temperature of 288.2 K, 2.0 kg/s of air enters the centrifugal compressor of a turbocharger and leaves the compressor at a total pressure of 1.225 atm. This compressor is directly driven by a radial-flow turbine. Products of combustion with a mass flow rate of 2.06 kg/s enter the turbine at a total temperature of 900 K and leave the turbine at a total pressure of 1.02 atm. Assume adiabatic flow through both compressor and turbine, no loss of power to bearings from the drive shaft that connects the compressor and turbine, $e_c = 0.80$, $e_t = 0.82$, a slip factor of 0.9 for the compressor, and the following gas properties:

For air	$\gamma = 1.40$ and $c_p = 1.004$ kJ/ (kg · K)
For products of combustion	$\gamma = 1.33$ and $c_p = 1.157$ kJ/ (kg · K)

Determine the following:
(a) Compressor rotor tip speed U_t m/s and exit total temperature in Kelvins
(b) Turbine rotor tip speed U_t m/s and inlet total pressure in atmospheres
(c) Turbine exit total temperatures in Kelvins
(d) Tip radius of compressor rotor and tip radius of turbine rotor for $N = 20{,}000$ rpm

9.35 At a total pressure of 14.696 psia and total temperature of 518.7°R, 2.0 lbm/s of air enters the centrifugal compressor of a turbocharger and leaves the compressor at a total pressure of 18 psia. This compressor is directly driven by a radial-flow turbine. Products of combustion with a mass flow rate of 2.06 lbm/s enter the turbine at a total temperature of 1600°R and leave the turbine at a total pressure of 15.0 psia. Assume adiabatic flow through both compressor and turbine, no loss of power to bearings from the drive shaft that connects the compressor and turbine, $e_c = 0.80$, $e_t = 0.82$, a slip factor of 0.9 for the compressor, and the following gas properties:

For air	$\gamma = 1.40$ and $g_c c_p = 6000$ ft^2/(s^2 · °R)
For products of combustion	$\gamma = 1.33$ and $g_c c_p = 6860$ ft^2/(s^2 · °R)

Determine the following:
(a) Compressor rotor tip speed U_t ft/s and exit total temperature in degrees Rankine
(b) Turbine rotor tip speed U_t ft/s and inlet total pressure in pounds per square inch absolute
(c) Turbine exit total temperatures in degrees Rankine
(d) Tip radius of compressor rotor and tip radius of turbine rotor for $N = 20{,}000$ rpm

Table P9.D1 Compressor and turbine design data for a 25,000-lb turbojet[a]

π_c	T_{t3}, °R	P_{t3}, psia	T_{t5}, °R	P_{t4}, psia	P_{t5}, psia	$\dot{m}_{\text{compr}}$, lbm/s	$\dot{m}_{\text{turb}}$, lbm/s	$\dot{W}_c$, kW	$\dot{W}_t$, kW
7.0	962.06	102.87	2853.21	98.76	56.85	200.28	208.66	22,298	22,523
7.5	983.36	110.22	2836.44	105.81	59.20	197.79	206.01	23,079	23,312
8.0	1003.72	117.57	2820.41	112.87	61.45	195.61	203.68	23,824	24,065
8.5	1023.22	124.92	2805.04	119.92	63.60	193.69	201.63	24,539	24,786
9.0	1041.96	132.26	2790.27	126.97	65.65	191.97	199.79	25,225	25,480
9.5	1060.00	139.61	2776.04	134.03	67.61	190.44	198.15	25,886	26,147
10.0	1077.40	146.96	2762.31	141.08	69.49	189.05	196.66	26,523	26,791
10.5	1094.22	154.31	2749.03	148.14	71.29	187.80	195.31	27,140	27,415
11.0	1110.50	161.66	2736.18	155.19	73.02	186.65	194.08	27,738	28,018
11.5	1126.28	169.00	2723.71	162.24	74.68	185.61	192.95	28,318	28,605
12.0	1141.60	176.35	2711.60	169.30	76.27	184.65	191.91	28,882	29,174
12.5	1156.49	183.70	2699.82	176.35	77.80	183.77	190.96	29,431	29,729
13.0	1170.98	191.05	2688.36	183.41	79.27	182.95	190.07	29,966	30,269

[a]Air entering compressor has $T_t = 518.7$°R and $P_t = 14.696$ psia. Gas enters turbine at 3200°R and P_{t4}. Polytropic efficiencies: $e_c = 0.90$ and $e_t = 0.90$. Also, $\dot{W}_t = \dfrac{\dot{W}_c}{0.99}$ $P_{t4} = 0.96\,P_{t3}$.

Axial Flow Turbomachinery Design Problems

9.D1 Perform the preliminary design of the turbomachinery for a turbojet engine having a thrust of 25,000 lbf at sea-level static conditions. Based on polytropic efficiencies of 0.9 for both compressor and turbine, the engineers in the engine cycle analysis group have determined the compressor and turbine inlet and exit conditions for a range of compressor pressure ratios that will give the required engine thrust. The results of their analysis are presented in Table P9.D1. Note that the mass flow rate through the compressor and turbine decreases with increasing compressor pressure ratio. To minimize on engine weight, it is desirable to have the maximum compressor pressure that can be driven by a single-stage turbine with exit guide vanes. The number of compressor stages depends on both the compressor design and the turbine design. As you can see, there are many sets of compressor/turbine designs that meet the thrust need; however, some of the designs cannot be done with one turbine stage or may be too large (high mass flow rate). Data for other compressor pressure ratios between 7 and 13 not listed in the table can be obtained by interpolation.

Assume that a turbine disk material exists that permits a rim speed of 1200 ft/s and that the turbine rotor airfoils can withstand an AN^2 of 5×10^{10} in.$^2 \cdot$ rpm^2. Use Fig. E.8 from Appendix E and computed AN^2 stresses to select material for each compressor stage.

For the compressor, use

$$\gamma = 1.4 \quad \text{and} \quad R = 53.34\,\text{ft} \cdot \text{lbf}/(\text{lbm} \cdot {}^\circ\text{R})$$

For the turbine, use

$$\gamma = 1.3 \quad \text{and} \quad R = 53.39\,\text{ft} \cdot \text{lbf}/(\text{lbm} \cdot {}^\circ\text{R})$$

Suggested Design Process.

1) Select a set of compressor and turbine design data from Table P9.D1.
2) For the design turbine rim speed, estimate the mean turbine rotor speed ωr_m and determine the variation of turbine radii (hub, mean, and tip) and AN^2 vs rpm. Select a shaft speed (rpm).
3) Determine the turbine mean-line design, using TURBN. Make sure the turbine meets the design criteria listed below.
4) For the selected shaft speed (rpm) and compressor pressure ratio, determine the number of compressor stages and the compressor mean-line design, using the repeating-row, repeating-stage design choice in COMPR. Make sure the compressor meets the design criteria listed below.
5) Check that 99% of power from turbine equals the power required by the compressor.
6) Check alignment of compressor and turbine. If the mean radii are not more than 2 in. apart, go back to item 2 and select a new rpm.
7) Determine the inlet and exit flow conditions for the turbine exit guide vanes (include estimate of losses).

8) Determine the inlet and exit flow conditions for the inlet guide vanes (include estimate of losses).
9) Specify compressor material for each stage based on the rotor's relative total temperature and blade AN^2.
10) Make a combined scale drawing of the compressor and turbine flow path. Allow 12 in. between the compressor exit and turbine inlet for the combustor. Show the shaft centerline.

Compressor Design Criteria.
1) Axial flow entering inlet guide vanes and leaving compressor
2) Reactions at all radii >0
3) Diffusion at all radii <0.6
4) M_{1R} at tip of first stage <1.05
5) M_2 at hub of first stage <1
6) Flow coefficient at mean radius between 0.45 and 0.55
7) Stage loading coefficient at mean radius between 0.3 and 0.35
8) Number of blades for rotor or stator of any stage <85
9) Number of blades for inlet guide vanes <85
10) AN^2 at entrance of rotor within material limits

Turbine Design Criteria.
1) Axial flow entering turbine nozzle at $M = 0.3$
2) Axial flow leaving exit guide vanes of turbine
3) Reaction at all radii >-0.15
4) Number of blades for nozzle, rotor, or exit guide vanes <85
5) $M_2 < 1.2$ at hub and >1 at tip
6) M_{3R} at tip of rotor <0.9
7) Velocity ratio at mean radius between 0.5 and 0.6
8) AN^2 at entrance of rotor within material limits
9) Tangential force coefficient Z for stator or rotor <1.0

9.D2 Perform the preliminary design of the turbomachinery for a turbojet engine of Problem 9.D1 but with no inlet guide vanes for the compressor or exit guide vanes from the turbine. Thus the turbine must have zero exit swirl.

9.D3 Perform the preliminary design of the turbomachinery for a turbojet engine of Problem 9.D1 scaled for a thrust of 16,000 lbf at sea-level, static conditions. Thus the mass flow rates and powers will be 64% of the values listed in Table P9.D1.

9.D4 You are to perform the preliminary design of the turbomachinery for a turbojet engine of Problem 9.D3 but with no inlet guide vanes for the compressor or exit guide vanes from the turbine. Thus the turbine must have zero exit swirl.

10
Inlets, Nozzles, and Combustion Systems

10.1 Introduction to Inlets and Nozzles

The inlet and exhaust nozzle are the two engine components that directly interface with the internal airflow and the flow about the aircraft. In fact, integration of the engine and the airframe is one of the most complex problems and has a major impact on the performance of the aircraft system. Many technical books, reports, articles, etc., are available in open literature (public domain) that concentrate on only small parts of this major technical challenge. This chapter identifies the major design considerations of inlets and exhaust nozzles and presents basic analysis tools for their preliminary sizing and design.

The results of the engine performance analysis provide a wealth of information about the required performance of both the inlet and the exhaust nozzle. For example, the required full-throttle, corrected engine airflow vs both Mach number and altitude can be obtained from the engine performance analysis program PERF (see Figs. 8.21, 8.31, 8.50, and 8.74b). Likewise, the engine airflow at specific partial-throttle conditions (corresponding to cruise, loiter, etc.) and the assumed inlet total pressure ratio vs Mach number can be obtained. The design information defines the requirements of the inlet in terms of total pressure ratio and mass flow rate, and preliminary design of the inlet starts with this information.

The simplest and most powerful design tool available for preliminary design of these components is one-dimensional compressible flow. Both the inlet and the exhaust nozzle can be modeled as simple one-dimensional adiabatic flows or a series of these flows. The following sections of this chapter present the basic principles of operation for each component, the major design considerations, and the basic design tools. Starting at the front of the engine, we consider the inlet first.

10.2 Inlets

The inlet interchanges the organized kinetic and random thermal energies of the gas in an essentially adiabatic process. The perfect (no-loss) inlet would thus correspond to an isentropic process. The primary purpose of the inlet is to bring the air required by the engine from freestream conditions to the conditions required at the entrance of the fan or compressor with minimum total pressure loss. The fan or compressor works best with a uniform flow of air at a Mach

number of about 0.5. Also, because the installed engine performance depends on the inlet's installation losses (additive drag, forebody or cowl drag, bypass air, boundary-layer bleed air, etc.), the design of the inlet should minimize these losses. The performance of an inlet is related to the following characteristics: high total pressure ratio π_d, controllable flow matching of requirements, good uniformity of flow, low installation drag, good starting and stability, low signatures (acoustic, radar, etc.), and minimum weight and cost while meeting life and reliability goals. An inlet's overall performance must be determined by simultaneously evaluating all of these characteristics because improvement in one is often achieved at the expense of another.

The design and operation of subsonic and supersonic inlets differ considerably due to the characteristics of the flow. For the subsonic inlets, near-isentropic internal diffusion can be easily achieved, and the inlet flow rate adjusts to the demand. The internal aerodynamic performance of a supersonic inlet is a major design problem, because achieving efficient and stable supersonic diffusion over a wide range of Mach numbers is very difficult. In addition, the supersonic inlet must be able to capture its required mass flow rate, which may require variable geometry to minimize inlet loss and drag and provide stable operation. Because of these differences, in the following sections we consider the subsonic and supersonic inlets separately, beginning with the subsonic inlet.

10.3 Subsonic Inlets

Most subsonic aircraft have their engines placed in nacelles; thus, in this section we do not deal with the inlet alone but include the nacelle at subsonic Mach numbers. The cross section of a typical subsonic inlet and its geometric parameters are shown in Fig. 10.1. The inlet area A_1 is based on the flow cross section at the inlet highlight. Because the subsonic inlet can draw in airflow whose freestream area A_0 is larger than the inlet area A_1, variable inlet geometry

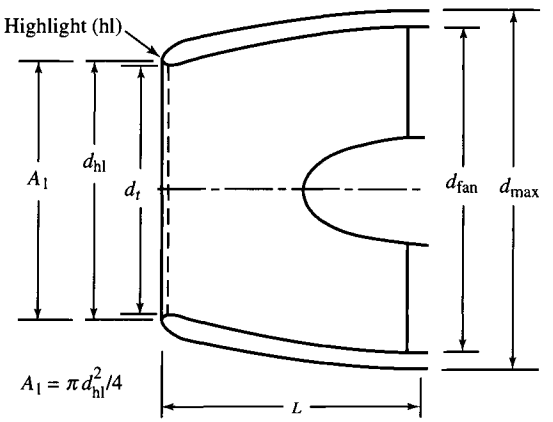

Fig. 10.1 Subsonic inlet nomenclature.

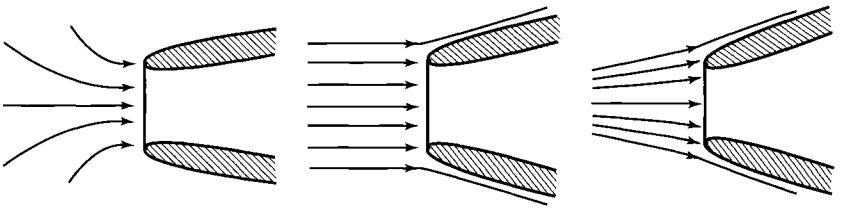

a) Static operation (or insufficient air for engine)

b) Low-speed operation (correct engine air)

c) High-speed operation (more air than the engine needs)

Fig. 10.2 Typical streamline patterns for subsonic inlet (Ref. 55).

is not required (except sometimes blow-in doors or auxiliary inlets are used to reduce installation drag during takeoff). The material in this section on subsonic inlets is based on a fixed-geometry inlet.

The operating conditions of an inlet depend on the flight velocity and mass flow demanded by the engine. Figure 10.2 shows the streamline pattern for three typical subsonic conditions. Figure 10.2a shows acceleration of the fluid external to the inlet that will occur when the inlet operates at a velocity lower than the design value or at a mass flow higher than the design value. Figure 10.2c shows deceleration of the fluid external to the inlet that will occur at a velocity higher than design or a mass flow lower than design.

A list of the major design variables for the inlet and nacelle includes the following:

1) Inlet total pressure ratio and drag at cruise
2) Engine location on wing or fuselage (avoidance of foreign-object damage, inlet flow upwash and downwash, exhaust gas reingestion, ground clearance)
3) Aircraft attitude envelope (angle of attack, yaw angle, cross-wind takeoff)
4) Inlet total pressure ratio and distortion levels required for engine operation
5) Engine-out windmilling airflow and drag (nacelle and engine)
6) Integration of diffuser and fan flow path contour
7) Integration of external nacelle contour with thrust reverser and accessories
8) Flowfield interaction between nacelle, pylon, and wing
9) Noise suppression requirements

Basic design tools for many of these items will be identified in this section. The reader is encouraged to research open literature (public domain) for a more in-depth analysis of any single item. Special attention is drawn to Refs. 54 and 55, which are textbooks on the aerodynamics of inlets.

10.3.1 Inlet Total Pressure Ratio π_d

In the cycle analysis used in the earlier chapters, the inlet total pressure ratio π_d was assumed to be constant for subsonic inlets and equal to $\pi_{d\max}$ (the total pressure ratio due to friction). Because of the complexity of the flow, we do not present a method for calculating the inlet total pressure ratio. However,

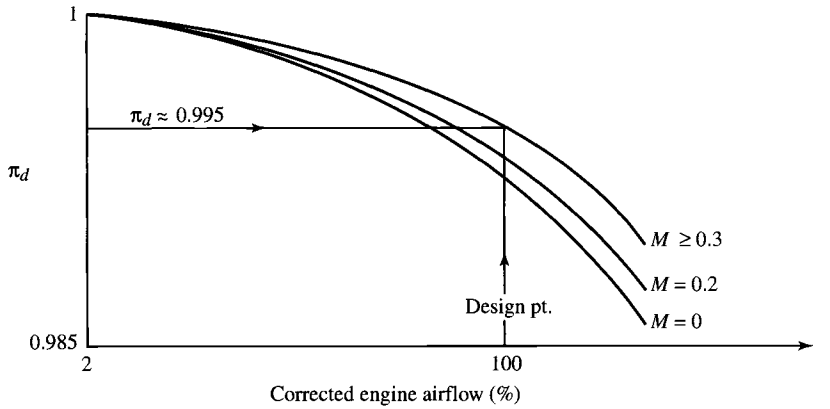

Fig. 10.3 Typical subsonic inlet total pressure ratio (after Younghans, Ref. 57).

Fig. 10.3 presents attainable π_d and its variation with flight Mach number and engine mass flow. The impact of the varying π_d on engine performance can be estimated by using this figure in concert with the performance analysis program and mission profile.

10.3.2 Inlet Sizing—Throat Diameter d_t

The diameter at the throat of the subsonic inlet is sized such that the Mach number at this location (based on one-dimensional flow) does not exceed 0.8. This will provide some margin for growth or error because the one-dimensional Mach number at the throat corresponding to actual inlet choke is about 0.9. The maximum corrected engine mass flow that the throat must pass will then correspond to this limiting Mach number, and the diameter is easily calculated by using

$$d_t = \sqrt{\frac{4}{\pi} A_{\text{th max}}} = \sqrt{\frac{4}{\pi}\left(\frac{\dot{m}_0\sqrt{T_{t0}}}{P_{t0}}\right)_{\max} \frac{1}{\text{MFP@}M = 0.8}}$$

which can be expressed in terms of the corrected mass flow as

$$d_t = \sqrt{\frac{4}{\pi}\frac{\sqrt{518.7}}{2116}\frac{\dot{m}_{c0\,\max}}{MFP@M = 0.8}}$$

and reduces to

$$d_t = 0.1636\sqrt{\dot{m}_{c0\,\max}} \qquad \text{or} \qquad d_t = 1.105\sqrt{A^*_{0\max}} \tag{10.1}$$

where $\dot{m}_{c0\,\max}$ has units of pound-mass per second, d_t has units of feet, and $A^*_{0\,\max}$ has units of square feet. Figure 10.4 is a representative output from

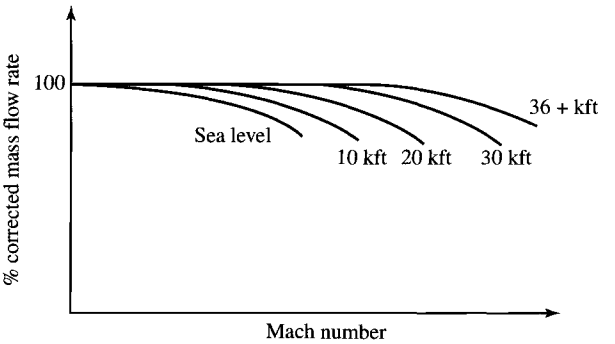

Fig. 10.4 Typical subsonic engine airflow requirements.

the engine performance computer program PERF of the corrected mass flow for a high-bypass-ratio turbofan engine. A figure like this can be used for selecting the point of maximum corrected mass flow that determines the throat diameter d_t.

10.3.3 Inlet Flow Distortion

Inlets operated with high angles of flow incidence are susceptible to flow separation from the inside contour of the inlet. This flow separation causes large regions of low total pressure, as shown in Fig. 10.5. The magnitude of

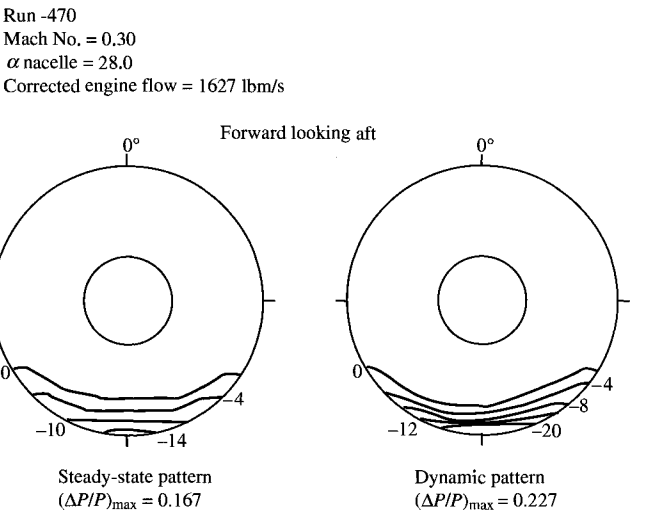

Fig. 10.5 Typical steady-state and dynamic total pressure distortion patterns (from Younghans, Ref. 56).

this distortion from the desired uniform flow is measured by the term called *inlet distortion* and is calculated by

$$\text{Inlet distortion} = \frac{P_{t\,\max} - P_{t\,\min}}{P_{t\,\text{av}}} \tag{10.2}$$

Both the instantaneous (dynamic) and time-averaged (steady-state) distortion levels are used to measure the quality of an inlet's flow. When Eq. (10.2) is used for calculation of the dynamic inlet distortion, the average total pressure in the denominator is the spatial average at an instant in time, and the maximum and minimum total pressures are for that same instant in time. Determination of the steady-state inlet distortion requires time-averaging of the total pressures in the inlet. The average total pressure $P_{t\,\text{av}}$ of Eq. (10.2) is the spatial average of the time-averaged total pressures.

The magnitude of the inlet distortion is a function of the inlet's geometry, mass flow rate, flight Mach number, and flow incidence angle. The effect of high distortion is to shift the fan or compressor surge line to values of higher mass flow rate, as shown in Fig. 10.6. This shift in surge line may result in compressor surge.

10.3.4 Inlet Drag

In Chapter 4, we looked at the additive drag that occurs when the area of the freestream air A_0 is different from the area of the entrance to the inlet A_1. Figure 4.5 shows a subsonic inlet at various flight Mach numbers and the use of "blow-in" doors at low Mach numbers to increase the inlet entrance area and thus reduce the additive drag. These blow-in doors were used in the turbofan-powered B-707 and in the early model of the B-747. Boeing deleted the use of

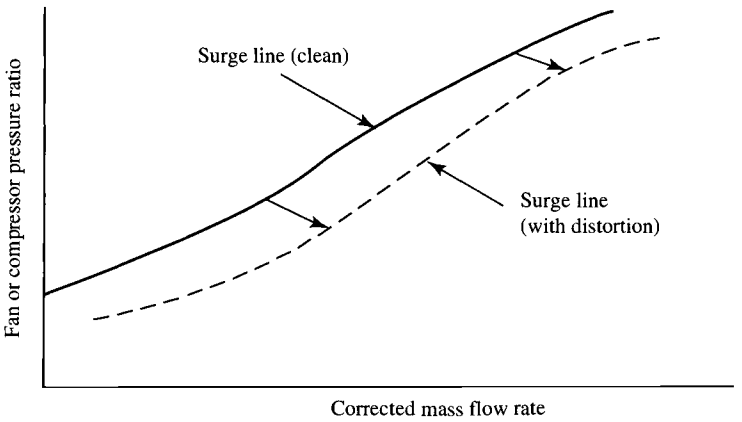

Fig. 10.6 Effect of inlet distortion on the fan or compressor.

blow-in doors in later models of the B-747 because of the nonuniform flow they created into the fan during takeoff and the resulting unacceptable fan noise. Elimination of blow-in doors required an increase in the entrance area, a more rounded lip, and a somewhat higher additive drag at cruise conditions. Most subsonic inlets operate as shown in Fig. 10.2c at cruise conditions.

At an engine inlet, flow separation can occur on the external surface of the nacelle due to local high velocities and subsequent deceleration. Flow separation can also occur on the internal surface of the inlet due to the flow deceleration, which causes an adverse pressure gradient (static pressure increase in the direction of flow). We will discuss the flow inside the inlet subsequently.

The size of the nacelle forebody [d_{h1}/d_{max} and L/d_{max} (see Fig. 10.1)] is a design compromise between the requirement of low cruise drag and avoiding catastrophes when one or more engines are out. The nacelle forebody size that gives minimum drag at cruise may not give good engine-out drag. In Chapter 4, the additive drag given by Eq. (4.8) was used as a conservative estimate of the inlet drag for engine sizing. A portion of the additive drag can be recovered along the forebody portion of the engine nacelle if the flow does not separate. This is indicated by the suction pressures near the lip of the nacelle in Fig. 10.7. The resulting pressure force on the outside of the nacelle forebody is called the *forebody drag*. The sum of the additive drag and the forebody drag is called the *inlet drag*.

Because flow around a curved surface accelerates the flow, then (at high subsonic Mach numbers) the local velocity can become supersonic adjacent to a nacelle. A shock then occurs, and a rise in static pressure across the shock reduces the negative pressure, thereby reducing the thrust component. This phenomenon is the same as that for an airfoil on which the local sonic velocity appears at the critical flight Mach number. At higher subsonic speeds, therefore, the curve of the inlet must be reduced in order to reduce the drag forces. The result is that for high subsonic Mach numbers, the inlet lip becomes very thin with little or no external curvature.

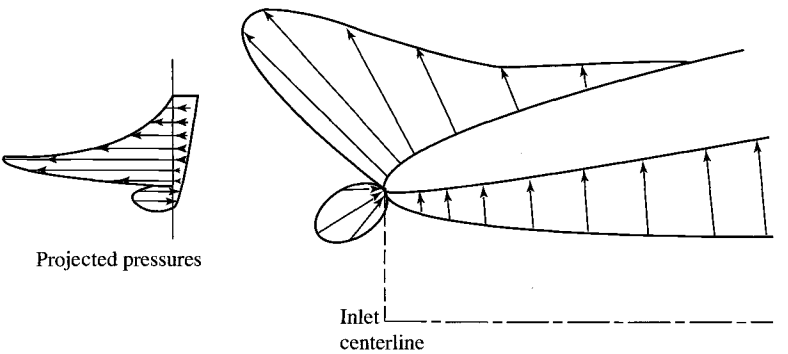

Fig. 10.7 Pressure distribution around a subsonic inlet lip (Ref. 57).

10.3.5 Nacelle and Interference Drag

The minimum drag for a nacelle does not necessarily occur when the inlet is designed for minimum inlet drag. The influences of the afterbody drag, interference drag, and aircraft trim drag need to be included in the integration and design of an engine nacelle. The inlet and afterbody drag of a typical nacelle is shown in Fig. 10.8 as a function of forebody diameter d_{h1}/d_{max} and flight Mach number. Note that the design value of d_{h1}/d_{max} corresponding to minimum inlet drag does not correspond to minimum inlet-plus-afterbody drag. Also note that the design value of d_{h1}/d_{max} corresponding to minimum inlet-plus-afterbody drag changes with flight Mach number. Thus the selection of d_{h1}/d_{max} for an inlet will depend on the design flight Mach number and may require the compromise of an individual component design goal to achieve the best overall system performance.

The engine location on the wing that provides the best integration of engine and airframe depends on the nacelle design, wing design, and resulting interference drag. Considerable analytical and experimental work is needed in the design of each installation. The resulting difference in best engine location on three aircraft is shown in Fig. 10.9.

10.3.6 Diffuser

The flow within the inlet is required to undergo diffusion in a divergent duct. This reduction in flow velocity creates an increase in static pressure that interacts with the boundary layer. If the pressure rise due to diffusion occurs more rapidly than turbulent mixing can reenergize the boundary layer, the boundary layer will

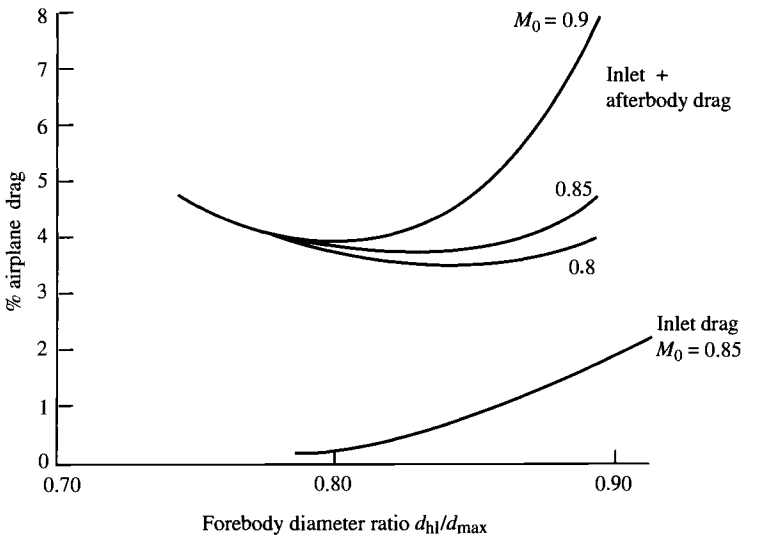

Fig. 10.8 Typical inlet and afterbody drag (from Younghans, Ref. 56).

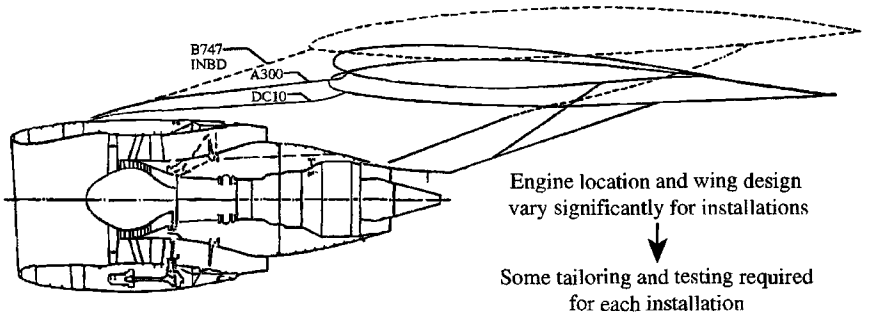

Fig. 10.9 The CF6-50 installation on three aircraft. (Courtesy of GE Aircraft Engines.)

assume the configurations shown in Fig. 10.10. If the flow in an inlet separates, the total and static pressures are reduced from their corresponding nonseparated flow values.

The rate of area increase in a diffuser has a direct effect on the behavior of flow in the diffuser, as shown in Fig. 10.11. If the rate of area increase is greater than that needed to keep the boundary layer energized and attached, the flow may be characterized by unsteady zones of stall. The turbulent mixing is no longer able to overcome the pressure forces at all points in the flow, and local separation occurs at some points. The total pressure decreases markedly due to the irreversible mixing of a fairly large portion of low-velocity fluid with the main flow. If the diffuser walls diverge rapidly, the flow will separate completely and behave much as a jet, as shown in Fig. 10.11d.

The rate of area increase without stall for a diffuser depends on the characteristics of the flow at the entrance and on the length of the divergent section. Figure 10.12a shows the results for two-dimensional straight-walled diffusers as presented by Kline in Ref. 58. Kline's results are for incompressible flow, and they do not give a qualitatively valid indication of the sensitivity of any diffuser to rapid divergence of flow area.

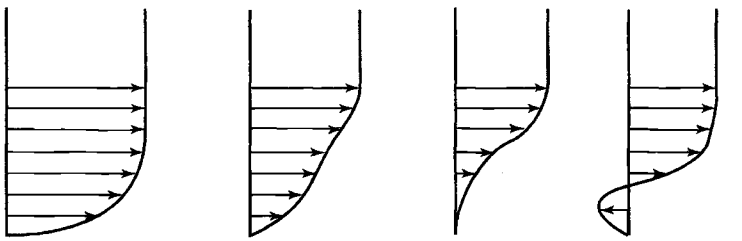

a) Turbulent **b) Intermediate** **c) Separation** **d) Reversed flow**

Fig. 10.10 Boundary layer with an adverse pressure gradient (Ref. 57).

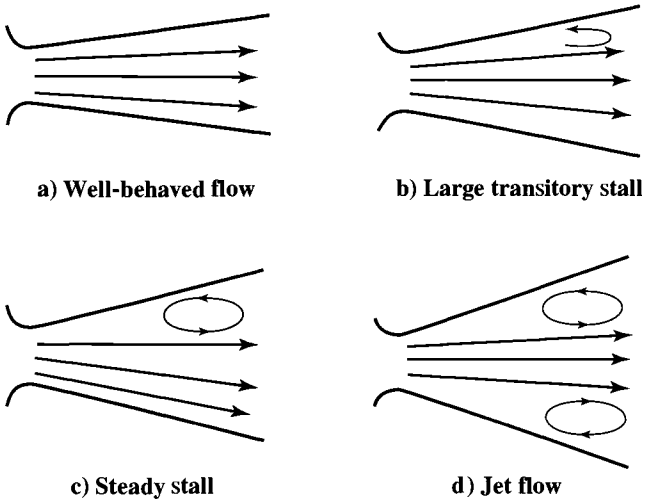

Fig. 10.11 Types of flow in straight-walled diffusers (Ref. 41).

For the design of an optimum diffuser, research has shown that the boundary-layer profile should maintain a constant shape, although the boundary-layer thickness will, of course, increase as the flow moves down the diffuser. The stipulation of a constant shape for the boundary-layer profile implies the assumption that mixing reenergizes the profile at the same rate as the static pressure depletes it.

In the presence of an adverse pressure gradient (static pressure increasing in the direction of flow), boundary layers tend to separate when the boundary layer is not reenergized rapidly enough by turbulent mixing. In Ref. 59, Taylor proposed the use of vortex generators as a mechanical mixing device to supplement the turbulent mixing. If vortices are generated by vortex generators in pairs, regions of inflow and outflow exist. These carry high-energy air into the boundary layer and low-energy air out. Figure 10.12b shows how vortex generators reenergize a boundary layer.

By using vortex generators together with a short, wide-angle diffuser, it may be possible to have a lower total pressure loss than with a long diffuser without vortex generators. Here, the reduced skin friction losses associated with flow

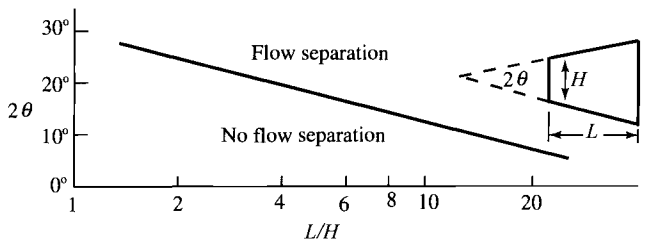

Fig. 10.12a Flow separation limits in two-dimensional straight-walled diffusers (Ref. 58).

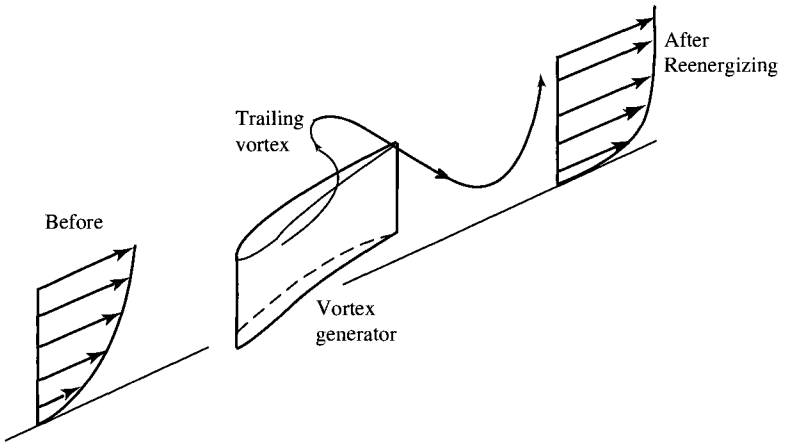

Fig. 10.12b Vortex generators reenergize a boundary layer.

separation are traded against vortex losses. The use of shorter diffusers may reduce weight and facilitate engine installation.

The rotating blades of an engine are a large source of an easily detected reflected radar signature. To reduce this signature, every effort is used to hide the engine face from direct (line-of-sight) view and thus reduce reflected radar. A serpentine-shaped diffuser with radar-absorbing material (RAM) can reduce the inlet's signature. Figure 10.13 shows some of the challenges facing designers—the energy transmission is at least a function of the shape of the duct (e.g., the number of reflections) and the wavelength-to-duct-width ratio. The F-117A Nighthawk stealth fighter uses a gridded inlet with 1.5-cm pitch between elements to keep out X-band and below radiation.[60]

10.4 Supersonic Inlets

The supersonic inlet is required to provide the proper quantity and uniformity of air to the engine over a wider range of flight conditions than the subsonic inlet is. In addition, the nature of supersonic flow makes this inlet more difficult to design and integrate into the airframe. In supersonic flight, the flow is decelerated by shock waves that can produce a total pressure loss much greater than, and in addition to, the boundary-layer losses. Indeed, at $M_0 = 3$, a simple pitot-type inlet preceded by a normal shock wave would have a total pressure recovery η_r of 0.32 due to the normal shock alone!

An engine overall compression ratio is the product of the engine's ram, diffuser, and compressor pressure ratios:

$$\text{Cycle compression ratio} \frac{P_{t3}}{P_0} = \pi_r \pi_d \pi_c \tag{10.3}$$

Because the product $\pi_r \pi_d$ is a major fraction of the cycle compression ratio at high supersonic Mach numbers, the engine thrust specific fuel consumption and

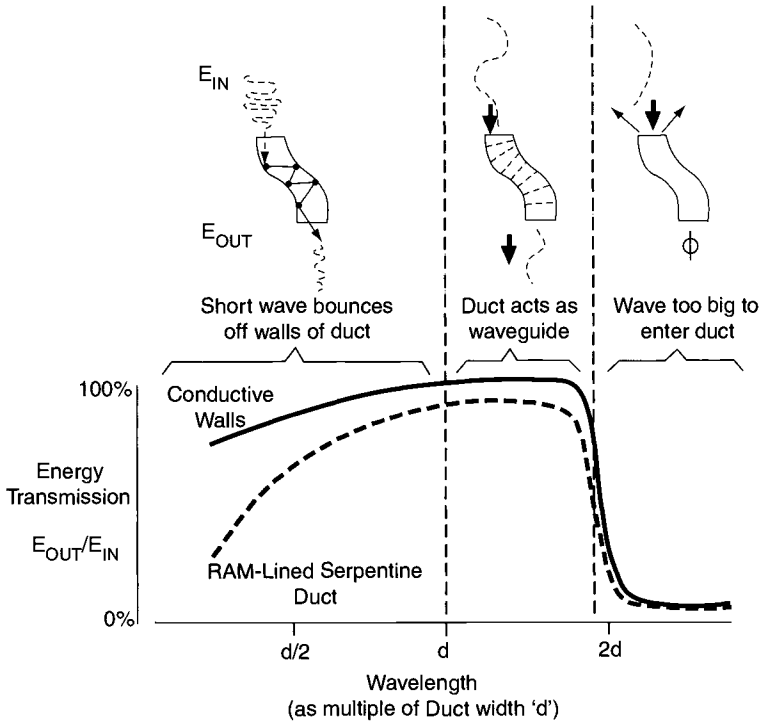

Fig. 10.13 Radar attenuation of engine inlet duct. (From Ref. 60. Copyright © 2001, McGraw-Hill Companies, Inc. Reproduced with permission.)

thrust per unit mass flow are very sensitive to the diffuser pressure ratio π_d. For supersonic cruise flight, therefore, the design of the inlet becomes of paramount importance. For this reason, we shall now examine the basic principles and operating characteristics of supersonic aircraft inlets (or diffusers).

The study of supersonic inlets is not new, and many excellent books and reports have been written for the benefit of students and practicing professionals (see Refs. 54–59 and 61–67). Special attention should be paid to Ref. 55, a textbook that covers the aerodynamics of inlets.

10.4.1 Basics of One-Dimensional Inlet Flow

First, we review some one-dimensional perfect gas flow ideas that are basic to understanding a supersonic diffuser operation.

10.4.1.1 Total and sonic state points and A/A^*. Consider the one-dimensional perfect gas flow of Fig. 10.14. The static state point of the gas at station 1 of the flow is designated as 1 in the T-s diagram of Fig. 10.14. Associated with static state point 1 at the same entropy are the total state point $t1$, where $M = 0$, and the sonic state point ^{*1}, where $M = 1$. The sonic and total state points can be attained by imagining a duct at station 1 decelerating the supersonic flow

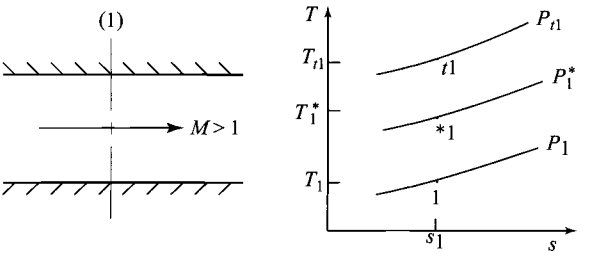

Fig. 10.14 States for supersonic flow.

isentropically to a sonic throat *1 followed by a subsonic deceleration to zero speed $t1$ in an infinitely large storage reservoir.

Treating station 1 as any general station in the flow with no subscripts, we can write the area ratio A/A^* as [Eq. (2.77)]

$$\frac{A}{A^*} = \frac{1}{M}\left[\frac{2}{\gamma+1}\left(1+\frac{\gamma-1}{2}M^2\right)\right]^{(\gamma+1)/[2(\gamma-1)]}$$

Since P and T in a given isentropic flow are also functions of the Mach number, this equation connects A to P, T, and other flow properties. In Fig. 10.15, A/A^*, P/P_t, and T/T_t are plotted vs the Mach number. Note that A/A^* varies from a minimum of 1 to 4.23 at $M = 3$. This large variation tends to complicate supersonic inlet design.

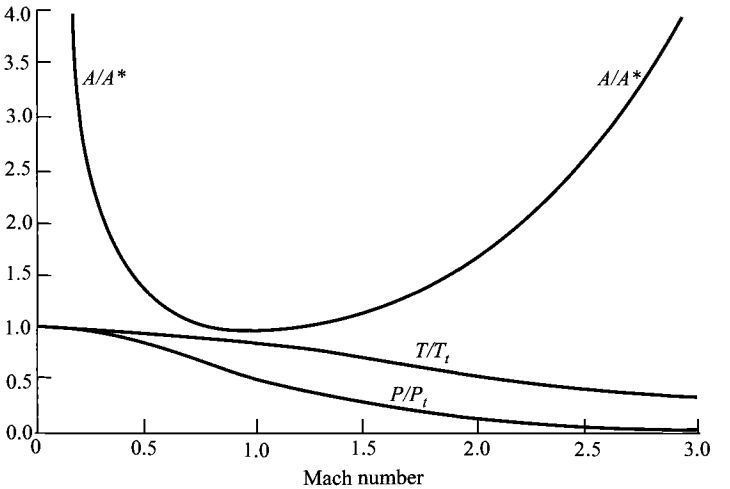

Fig. 10.15 Compressible flow functions vs Mach number.

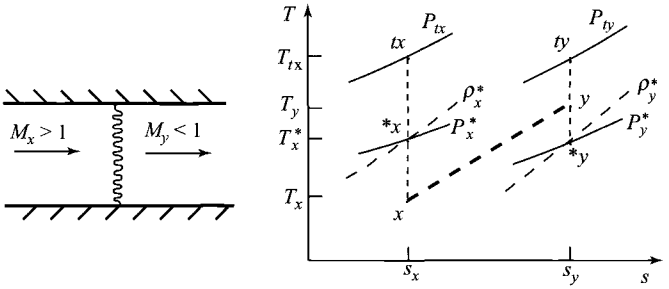

Fig. 10.16 Normal shock wave.

10.4.1.2 Normal shock wave. Consider the perfect gas flow through a normal shock wave depicted in Fig. 10.16, with subscripts x and y denoting shock upstream and downstream flow conditions, respectively. The static, sonic, and total state points of the gas entering and leaving the shock wave are shown in the T-s diagram of the figure with $s_y > s_x$ since the flow through a normal shock is irreversible and adiabatic at constant T_t. It follows that $T_x^* = T_y^*$, $P_{ty} < P_{tx}$, $V_x^* = V_y^*$, and $\rho_y^* < \rho_x^*$, as indicated in the T-s diagram.

Given the inlet conditions to a normal shock wave in a perfect gas, the exit conditions can be found since $P_y/P_x = f_1(M_x)$, $M_y = f_2(M_x)$, $P_{ty}/P_{tx} = f_3(M_x)$, etc. The total pressure ratio across a normal shock is of particular interest in supersonic diffuser studies and is plotted in Fig. 10.17 along with A/A^* from Fig. 10.15.

Suppose, now, that the flow of Fig. 10.16 passes through sonic throats of areas A_x^* and A_y^*, as in Fig. 10.18. What is the ratio of the area of the first throat to that of the second throat A_x^*/A_y^*? Conservation of mass and one-dimensional

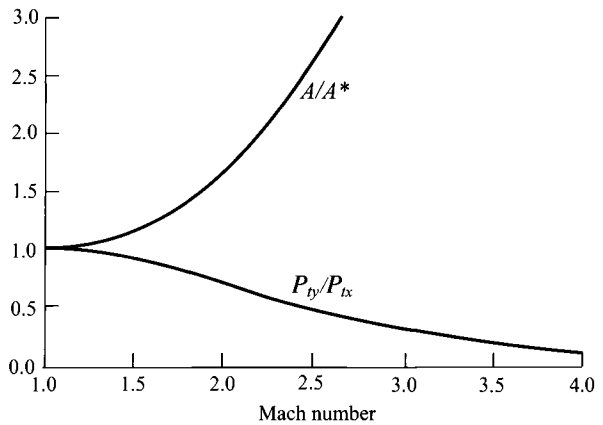

Fig. 10.17 A/A^* and P_{ty}/P_{tx} vs Mach number.

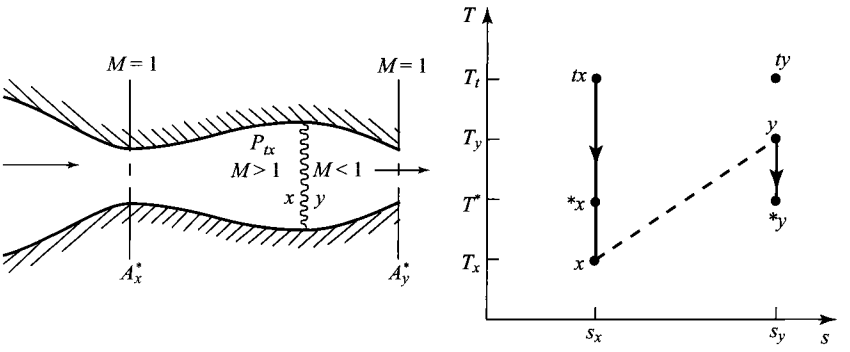

Fig. 10.18 A/A^* **and shock wave.**

flow give

$$(\rho VA)_x^* = (\rho VA)_y^*$$

Since in this equation $V_x^* = V_y^*$ and $\rho_x^* > \rho_y^*$, the second throat area must be larger than the first to compensate for the lower-density gas passing through it, and

$$\frac{A_x^*}{A_y^*} = \frac{\rho_y^*}{\rho_x^*}$$

With $T_x^* = T_y^*$, we can write

$$\frac{\rho_y^*}{\rho_x^*} = \frac{P_y^*}{P_x^*} = \frac{P_{ty}}{P_{tx}} \frac{(P^*/P_t)_y}{(P^*/P_t)_x} \quad \text{(the ratio equals 1)}$$

Therefore,

$$\frac{A_x^*}{A_y^*} = \frac{\rho_y^*}{\rho_x^*} = \frac{P_{ty}}{P_{tx}} \tag{10.4}$$

and the plot of P_{ty}/P_{tx} in Fig. 10.17 can also be interpreted as A_x^*/A_x^* or ρ_y^*/ρ_x^* vs Mach number.

Example 10.1

Let us illustrate the preceding ideas with an example involving a supersonic inlet. The stream tube of air captured by the ideal shock-free inlet in Fig. 10.19 has an area A_0 equal to the inlet capture area A_c. Since $A_0 = A_c$, no

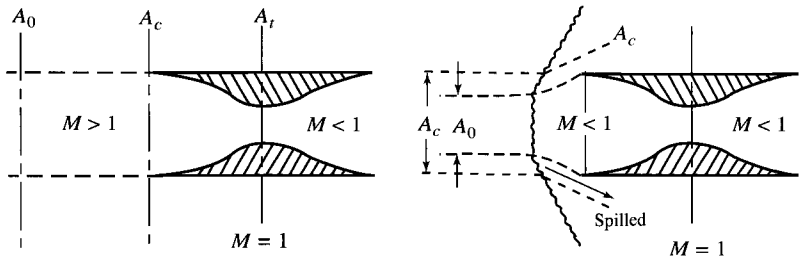

Fig. 10.19 Inlet spillage.

air is spilled by the inlet. The inlet on the right is preceded by a shock wave and capture air contained in a stream tube of area $A_0 < A_c$. The freestream airflow contained in the projected area A_c that does not enter the inlet is said to be spilled as shown. The fraction of air spilled is

$$\text{Fraction spilled} = \frac{(\rho V)_0 A_c - (\rho V)_0 A_0}{(\rho V)_0 A_c}$$

$$\text{Fraction spilled} = \frac{A_c - A_0}{A_c} = \frac{A_c/A_t - A_0/A_t}{A_c/A_t} \tag{10.5}$$

Consider a fixed-geometry inlet operating in a freestream flow with $M_0 = 2$ and with a normal shock, as in Fig. 10.19. If the inlet capture/throat area ratio is $A_c/A_t = 1.34$, determine the fraction of air spilled.

Solution: We have

$$\text{Fraction spilled} = \frac{A_c/A_t - A_0/A_t}{A_c/A_t} = \frac{1.34 - A_0/A_t}{1.34}$$

and so we must find A_0/A_t. Using y for the exit state of the normal shock, we have the flow state points and path line shown in the T-s diagram of Fig. 10.20. By using the sonic state points ^{*0} and $^*y$, we can find A_0/A_t thus. Since $A_t = A_y^*$,

$$\frac{A_0}{A_t} = \left(\frac{A}{A^*}\right)_0 \frac{A_0^*}{A_y^*}$$

From Eq. (10.4),

$$\frac{A_0^*}{A_y^*} = \frac{(\rho V)_y^*}{(\rho V)_0^*} = \frac{\rho_y^*}{\rho_0^*} = \frac{P_{ty}}{P_{t0}}$$

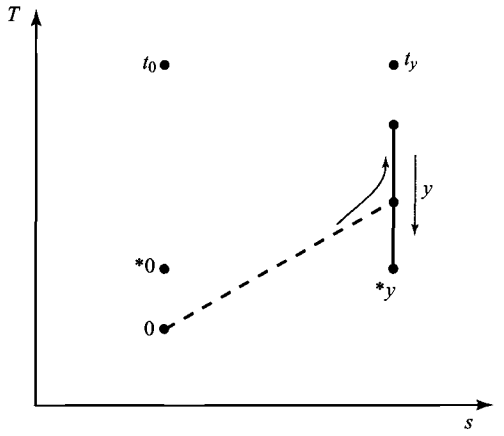

Fig. 10.20 Stages of inlet flow across shock.

where P_{ty}/P_{t0} is the total pressure ratio of a normal shock wave. Hence

$$\frac{A_0}{A_t} = \left[\left(\frac{A}{A^*}\right)\frac{P_{ty}}{P_{t0}}\right]_{M_0} \tag{10.6}$$

The right-hand side of this equation is the product of points lying on the two curves of Fig. 10.17 at a given M_0. Thus, at $M_0 = 2$, $A/A^* = 1.688$ and $P_{ty}/P_{t0} = 0.721$ (GASTAB), so that

$$\frac{A_0}{A_t} = (1.688)(0.721) = 1.218$$

and

$$\text{Fraction spilled} = \frac{1.34 - 1.218}{1.34} = 9.1\%$$

As M_0 increases above 2, the shock wave will move closer to the inlet and less air is spilled. Finally, when M_0 reaches the critical value M_{0c}, the shock is at the lip of the inlet and $A_0 = A_c$. (The shock is immediately swallowed by the inlet once it gets to the inlet lips because this is an unstable condition.)

10.4.2 Ideal One-Dimensional Internal Compression Inlet

One would think initially that a supersonic inlet could operate shock-free as a simple converging-diverging nozzle in reverse. Although this is feasible in principle, a starting problem arises that prevents the attainment of this condition in a constant-geometry inlet. To fix ideas in the arguments to follow, consider a

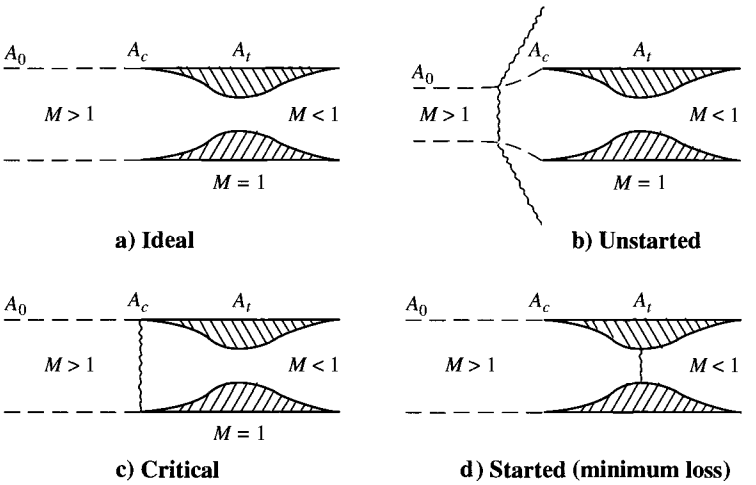

Fig. 10.21 Operation of ideal internal compression inlet.

supersonic inlet with a capture/throat area ratio of $A_0/A_t = 1.34$. Assuming no viscous boundary-layer losses, as we do throughout our treatment of inlets, this inlet could, in theory, operate free at $M_0 = 1.7$, corresponding to $A_0/A^* = A_c/A_t = 1.34$ with $A_0 = A_c$, as in Fig. 10.21a. This flow condition cannot be attained, however, by increasing M_0 from a lower value up to $M_0 = 1.7$ with a fixed-geometry inlet. This is the reason: $A_0/A^* < A_c/A_t$ if $M_0 < 1.7$ (Fig. 10.17), and in shock-free flow with $A_t = A_0^*$, it follows that $A_c > A_0$ so that the inlet captures more flow than the throat can pass. Consequently, air piles up in the inlet, causing, almost instantaneously, a shock to form ahead of the inlet, as in Fig. 10.21b). The excess airflow spills around the inlet in the subsonic flow behind the shock wave. To find the fraction of air spilled in the unstarted condition, we must find A_0/A_t in the expression

$$\text{Fraction spilled} = \frac{A_c - A_0}{A_c} = \frac{A_c/A_t - A_0/A_t}{A_c/A_t}$$

This can be done by using the identity

$$\frac{A_0}{A_t} = \frac{A_0}{A_0^*}\frac{A_0^*}{A_y^*}$$

Here, A_0^* is smaller than A_y^* because the mass flows through the two sonic throats *0 and *y (Fig. 10.22) are equal

$$(\rho A V)_0^* = (\rho A V)_y^*$$

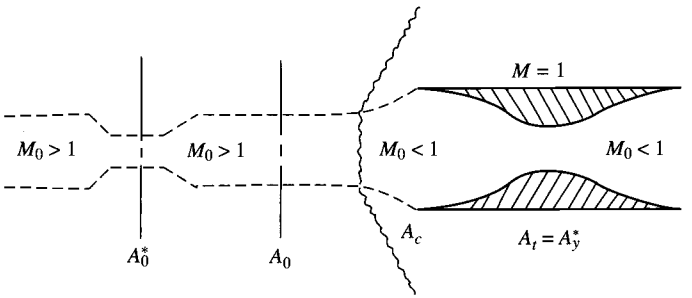

Fig. 10.22 Area relationships.

and $V_0^* = V_y^*$, but $\rho_x^* > \rho_y^*$. In fact, by Eq. (10.4),

$$\frac{A_0^*}{A_y^*} = \frac{\rho_y^*}{\rho_0^*} = \frac{P_{ty}}{P_{t0}}$$

hence

$$\frac{A_0}{A_t} = \left[\left(\frac{A}{A^*}\right)\frac{P_{ty}}{P_{t0}}\right]_{M_0} = f(M_0) \tag{10.7}$$

This ratio of actual captured stream-tube area to inlet throat area is plotted vs M_0 in Fig. 10.23. The curve of A_0/A_t in Fig. 10.23 is the product of the A/A^* and

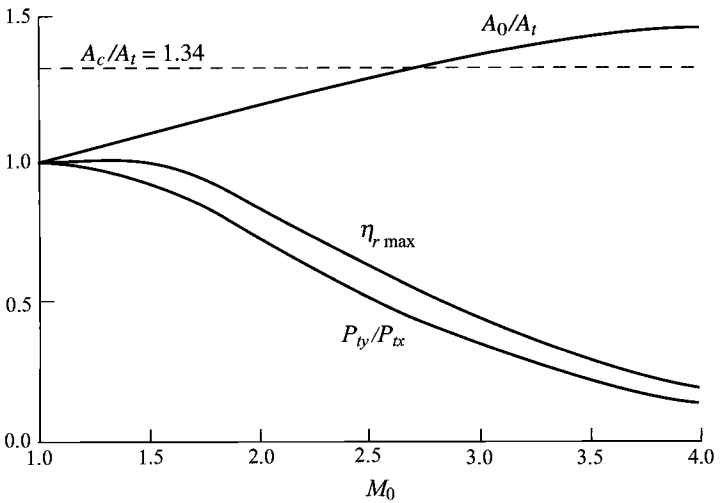

Fig. 10.23 Performance of ideal internal compression inlet.

P_{ty}/P_{t0} curves in accordance with Eq. (10.7). We show, in Fig. 10.23, a horizontal line representing $A_c/A_t = 1.34$. The vertical distance between this line and the A_0/A_t curve (to the left of their intersection) is proportional to the amount of air spilled by the inlet [Eq. (10.5)]. As M_0 is increased from $M_0 = 1$, this vertical distance decreases so that less and less air is spilled until at $M_{0c} = 2.66$, the shock is on the inlet lips. This is an unstable position, and the shock will move precipitously through the converging portion of the inlet if perturbed.

This can be explained as follows: The mass flow through the throat is proportional to ρ_y^*, which, in turn, is proportional to P_{ty}. If the shock moves into the inlet, M_x decreases so that P_{ty} and the throat mass flow increase. Because the flow at the lips continues to be at freestream conditions, the throat passes more air than is captured by the inlet. To make the throat mass flow equal to the flow captured, the density at the throat must decrease. This lower density is attained by the shock passing through the throat with supersonic flow at the throat as in the started condition of Fig. 10.16d. Once started, the inlet backpressure can be adjusted (e.g., by closing bypass doors downstream of the throat) to place the shock at the throat for minimum M_x and least total pressure loss.

The throat Mach number of a started inlet with area ratio $A_c/A_t = A_0/A_t$ is that corresponding to the value of $(A/A^*)_t$ obtained from

$$\left(\frac{A}{A^*}\right)_{M_t} = \left(\frac{A}{A^*}\right)_{M_0}\left(\frac{A_t}{A_0}\right)_{M_0} = \left(\frac{A}{A^*}\frac{1}{A_0/A_t}\right)_{M_0}$$

where A_0/A_t and A/A^* on the right-hand side of this equation are each a function of M_0 as given in Figs. 10.23 and 10.17, respectively. For example, at $M_0 = 2$

$$\left(\frac{A}{A^*}\right)_{M_t} = \left(\frac{A}{A^*}\frac{1}{A_0/A_t}\right)_{M_0} = \frac{1.688}{1.216} = 1.388$$

and

$$M_t = 1.75$$

The value of M_t corresponding to each flight Mach number can be found in this manner. Then, for each M_t, the corresponding normal shock total pressure loss can be determined to obtain the curve labeled $\eta_{r\max}$ in Fig. 10.23. For example, at $M_0 = 2$ and $M_t = 1.75$, the total pressure recovery of the inlet with a normal shock at the throat with $M_x = M_t = 1.75$ is $P_{ty}/P_{t0} = \eta_{r\max} = 0.835$.

Example 10.2

Design a fixed-area internal compression inlet that will start at $M_0 = 2.9$ for an aircraft that will cruise at $M_0 = 2.4$.

1) Determine the capture/throat area ratio A_c/A_t.

2) Determine both $\eta_{r\max}$ of the inlet after starting at $M_0 = 2.9$ and the shock located at the throat.

3) Determine $\eta_{r\max}$ of the inlet after starting at $M_0 = 2.4$ and the shock located at the throat.

4) Determine the Mach number at which the inlet will "unstart."

Solution:

1) Design an inlet to start at $M_0 = 2.9$. Thus $A_0 = A_c$ at $M_0 = 2.9$. Using Eq. (10.7), we have

$$\frac{A_c}{A_t} = \frac{A_0}{A_t}\left(\frac{A}{A^*}\frac{P_{ty}}{P_{tx}}\right)_{M_0} = 3.8498 \times 0.35773 = 1.377$$

Or, using Fig. 10.23, we read $A_c/A_t = 1.38$.

2) After starting, $A_c = A_0$; thus, we want to determine the area ratio A_t/A^* to get the Mach number at the throat and $\eta_{r\max}$ for $M_0 = 2.9$.

$$\frac{A_t}{A^*} = \frac{A_0/A^*}{A_c/A_t} = \frac{3.8498}{1.377} = 2.796$$

From GASTAB, $M_t = 2.56$. Then $P_{ty}/P_{tx} = \eta_{r\max} = 0.4754$. Or, using Fig. 10.23, we read $\eta_{r\max} = 0.48$.

3) For this inlet $A_c = A_0$,

$$\frac{A_t}{A^*} = \frac{A_0/A^*}{A_c/A_t} = \frac{2.4031}{1.377} = 1.745$$

From GASTAB, $M_t = 2.04$. Then $P_{ty}/P_{tx} = \eta_{r\max} = 0.702$.

4) The inlet will "unstart" when $M_t = 1$. We are looking for an M_0 whose A_0/A^* is equal to the inlet's A_c/A_t. For $A_0/A^* = 1.377$, $M_0 = 1.74$ from GASTAB or Fig. 10.17.

10.4.3 Inlet Types

As discussed in Chapter 4, supersonic inlets are classified into three basic types, characterized by the location of the supersonic compression wave system: internal compression, external compression, and mixed compression.

10.4.3.1 Internal compression inlet. The internal compression inlet shown in Fig. 10.24a achieves compression through a series of internal oblique shock waves followed by a terminal normal shock positioned downstream of the throat (its stable location). This type of inlet requires variable throat area to allow the inlet to swallow the normal shock (during starting). Fast reaction bypass doors are also required downstream of the throat to permit proper positioning of the normal shock under varying flight and engine conditions.

Figure 10.24a shows an internal compression inlet with an area contraction ratio A_1/A_t of 2.56 (corresponding to $M_1 = 2.5$ and $M_t = 1.2$) operating at design. With the terminal normal shock positioned downstream of the throat for stable operation, where the Mach number is 1.3, this inlet's ideal total

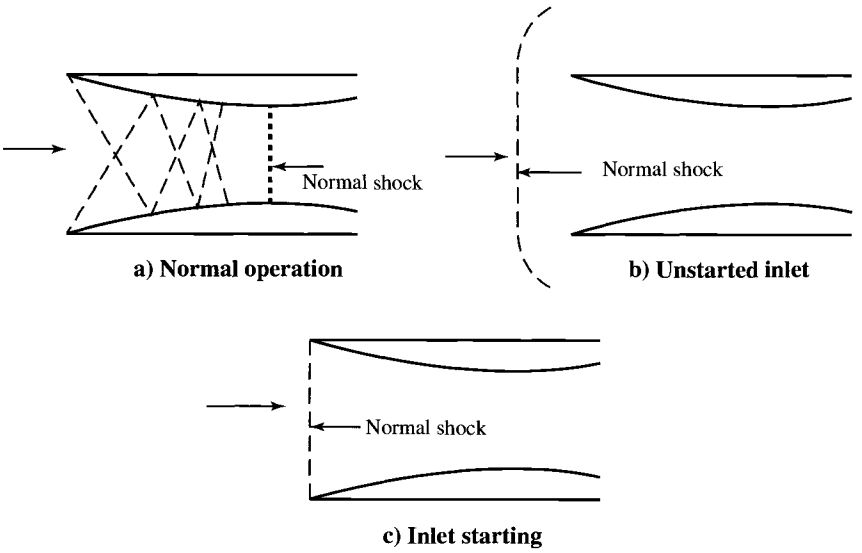

a) Normal operation

b) Unstarted inlet

c) Inlet starting

Fig. 10.24 Internal compression inlet.

pressure ratio (total pressure recovery η_r) corresponds to that across a normal shock at Mach 1.3, or $\eta_r = 0.9794$ when $\gamma = 1.4$. Reduction in the flight Mach number to 2.47 or movement of the terminal shock to the throat (which is an unstable location) will cause the total internal flow pattern to be completely disrupted (inlet unstarting), followed by formation of a normal shock ahead of the inlet and its associated low total pressure ratio (about 0.52), reduced mass flow through the inlet, high spillage drag, and possible engine flameout. The unstarted inlet is shown in Fig. 10.24b. This unstarted condition of the inlet can also be achieved by bringing the freestream Mach number from subsonic up to 2.5 without changing the throat area sufficiently to start the inlet (swallow the normal shock).

Starting of the inlet can be achieved when the area of the throat (flow is choked at the throat) is made large enough for the normal shock to move back and touch the inlet tip (critical operation), as shown in Fig. 10.24c. The ratio of the throat area required to start the inlet A_{ts} to the throat area required at normal operation A_{tr}, (corresponding to $M_t = 1.2$) is obtained from basic one-dimensional flow, plotted in Fig. 10.25 and expressed as

$$\frac{A_{ts}}{A_{tr}} = \frac{1}{1.030(P_{ty}/P_{tx})_{M_0}} \tag{10.8}$$

where 1.030 is the value of A/A^* corresponding to $M_t = 1.2$ and $(P_{ty}/P_{tx})_{M_0}$ is the total pressure ratio across a normal shock with upstream Mach number of M_0. As can be seen in Fig. 10.25, the internal compression inlet has a large throat area variation required to start the inlet at Mach numbers greater

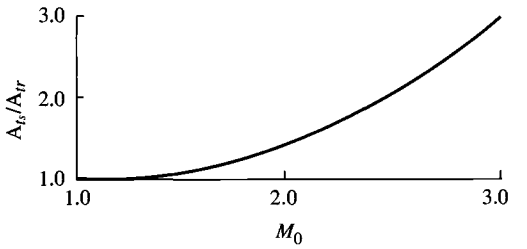

Fig. 10.25 Throat area variation required of an internal compression inlet.

than 2. For example, the throat area required to start an inlet at a Mach number of 2.4 is about 1.8 times the throat area required for normal operation. This large area variation, the problem of inlet upstart, the poor performance at angles of attack, and many other problems have led to the demise of the internal compression inlet.

10.4.3.2 External compression inlet. The compression of the external compression inlet (Fig. 10.26) is achieved through either one or a series of oblique shocks followed by a normal shock, or simply through one normal shock. As shown in Fig. 10.26, A_{0i}, A_{0e}, $A_{0\,\mathrm{bl}}$, and $A_{0\,\mathrm{bp}}$ are the freestream tube areas containing the inlet, engine, boundary-layer bleed, and bypass airflows, respectively.

The external compression inlet that achieves compression through only a single normal shock is called a *pitot inlet or normal shock inlet* and is shown in Fig. 10.27. The pitot inlet is simple, short, lightweight, and inexpensive. The total pressure recovery η_r of this inlet corresponds to the total pressure ratio across a normal shock, shown in Fig. 10.23. The total pressure recovery of this inlet is acceptable for flight Mach numbers up to about 1.6. Above this Mach number, the total pressure recovery of the inlet is too low and another, more efficient inlet design must be used.

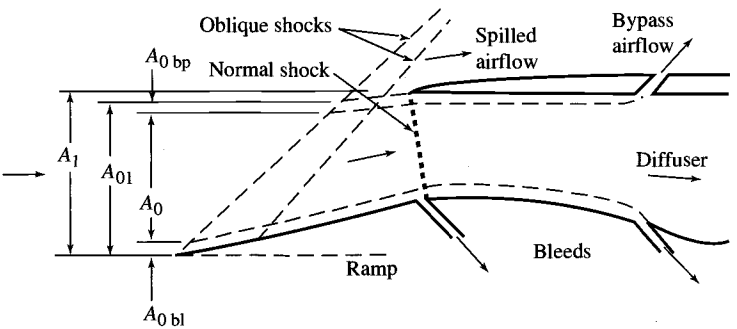

Fig. 10.26 External compression inlet and flow areas.

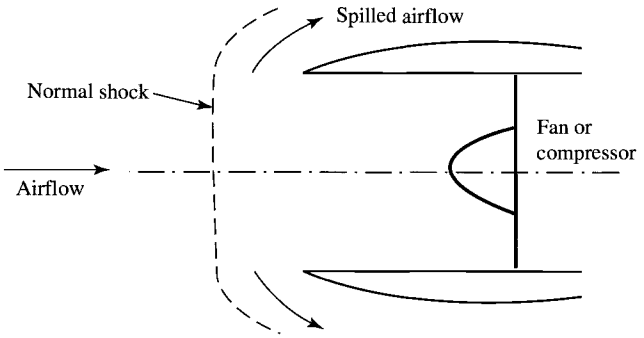

Fig. 10.27 Pilot or normal shock inlet.

The external compression inlet with one or more oblique shocks (Fig. 10.26) has its inlet throat at or very near the cowl leading edge. Desired operation of this inlet is with the normal shock positioned at or very near the cowl lip (critical operation).

The total pressure recovery η_r across n oblique shocks of equal strength (same total pressure ratio) followed by a normal shock is shown in Fig. 10.28. Increasing the number of oblique shocks increases η_r for any given freestream Mach number. However, the ramp of the external compression inlet turns the flow away from the axial direction; thus, the subsonic diffuser duct must turn the flow back to the axial direction, which may add weight and length to the inlet. Figure 10.29 shows the total turning angle of an external compression shock system that attains the total pressure recovery of MIL-E-5008B as a function of freestream Mach number. As the freestream Mach number increases, the

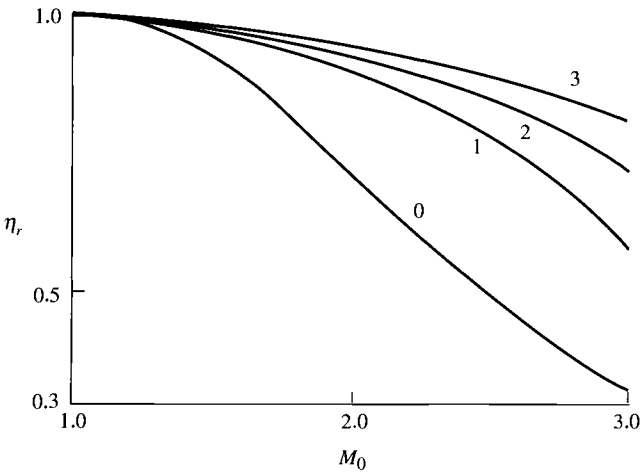

Fig. 10.28 Total pressure recovery of oblique shocks.

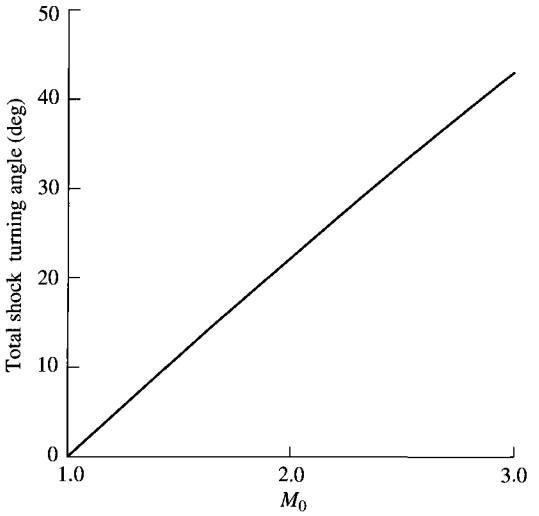

Fig. 10.29 Turning angle of external compression shock system (Ref. 61).

total shock-turning angle of the external ramp increases, resulting in increases in cowl angle and cowl drag. External compression inlets can maintain a balance between an acceptable total pressure ratio and cowl drag up to a flight Mach number of about 2.5.

10.4.3.3 Mixed compression inlet. At flight Mach numbers above 2.5, the mixed compression inlet is used to obtain an acceptable total pressure ratio (by utilizing the required number of oblique shocks) while obtaining acceptable cowl drag. The mixed compression inlet is more complex, heavier, and costlier than the external compression inlet. The typical mixed compression inlet (Fig. 10.30) achieves compression through the external oblique shocks, the internal reflected oblique shocks, and the terminal normal shock. The ideal location of the normal shock is just downstream of the inlet throat, to minimize total pressure loss while maintaining a stable operating location of this shock. Similar to the internal compression inlet, the mixed compression inlet requires

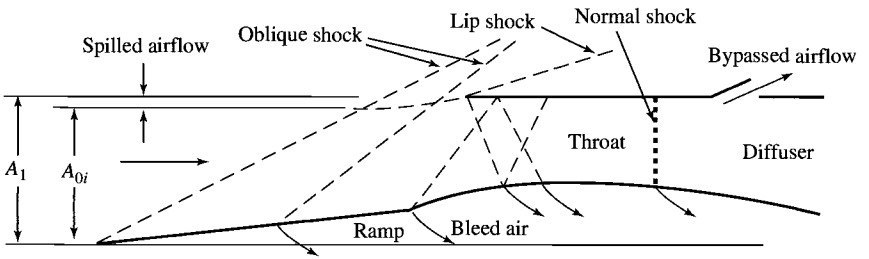

Fig. 10.30 Two-dimensional mixed compression inlet.

both fast-reacting bypass doors (to maintain the normal shock in a stable location) and variable throat area (to allow the inlet to start by swallowing the normal shock). However, the variation in inlet throat area of the mixed compression inlet is considerably less than that of the internal compression inlet because of the mixed compression inlet's external oblique shock system.

Supersonic inlets can also be classified further as *two-dimensional* (rectangular) and *axisymmetric* (circular or a portion of a circle). Figure 10.30 shows a typical two-dimensional mixed compression inlet. Axisymmetric inlets have a slight advantage over two-dimensional inlets with respect to weight and total pressure ratio. However, the two-dimensional inlets have an advantage in design simplicity and in providing a larger variation in inlet airflow. Furthermore, axisymmetric inlets have the added design problem of getting sufficient boundary-layer bleed air out from the centerbody through the support struts.

The improved performance of variable-geometry mixed compression inlets and external compression inlets at high Mach numbers comes with some reduced performance at low supersonic Mach numbers due to the increased frictional losses. Figures 10.31 and 10.32 show the total pressure recovery of past and current aircraft and the supersonic transport (SST) model. Note, in Fig. 10.32, the reduced total pressure recovery of the complex SST mixed compression inlet at subsonic and low supersonic Mach numbers when compared to the simple pitot intake. The message of these two figures is that a supersonic inlet can be designed for good performance at supersonic or subsonic flight Mach numbers, but not at both.

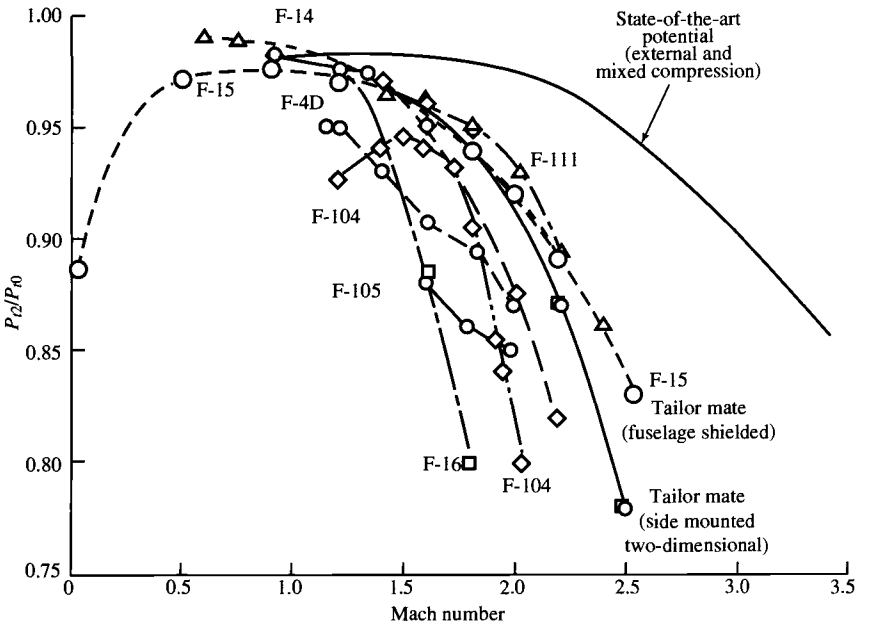

Fig. 10.31 Total pressure ratio survey (Refs. 62–64).

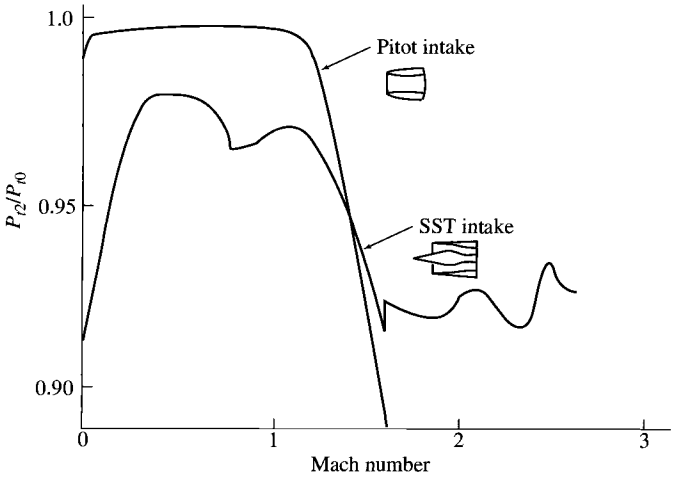

Fig. 10.32 Total pressure ratio—SST model (Ref. 63).

10.4.4 Total Pressure Recovery η_r

In the engine cycle analysis of this textbook, the total pressure recovery of the supersonic inlet was estimated by [Eq. (6.6)]

$$\eta_r = \begin{cases} 1 & M_0 \leq 1 \\ 1 - 0.075(M_0 - 1)^{1.35} & 1 < M_0 < 5 \\ \dfrac{800}{M_0^4 + 935} & 5 < M_0 \end{cases}$$

the ram recovery of military specification MIL-E-5008B. This design inlet total pressure recovery has been added to Fig. 10.28 to give Fig. 10.33, a very useful design tool for selection of inlet type and preliminary number of oblique shocks required. As an example, consider an inlet for flight at Mach 2.5. Equation (6.6) or Fig. 10.33 gives an allowable total pressure ratio for the shock system of 0.87. Figure 10.33 shows that more than two oblique shocks of equal strength followed by a normal shock are required. This could be obtained by an external compression inlet with three oblique shocks or a mixed compression inlet.

Example 10.3

Consider an external compression inlet (part 1). The total pressure recovery of the external compression inlet shown in Fig. 10.34 can be determined by using the normal and oblique shock tables of GASTAB. Applying the normal and oblique shock equations to this inlet with $\theta_a = \theta_b = 5$ deg yields the results

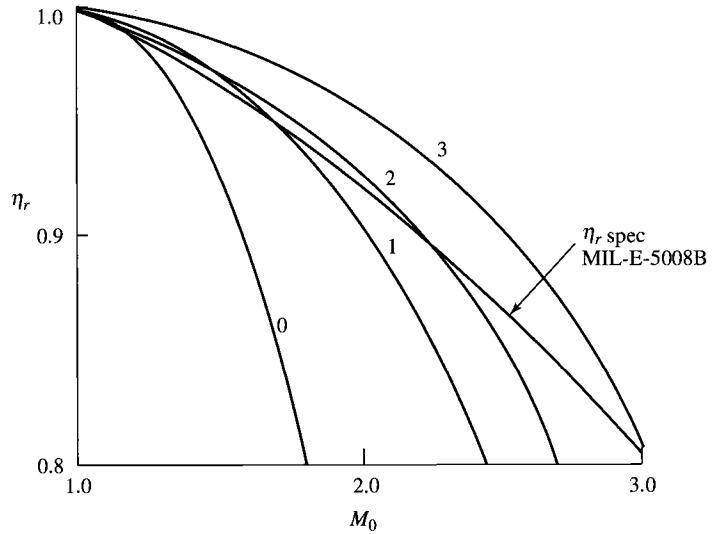

Fig. 10.33 Total pressure recovery required.

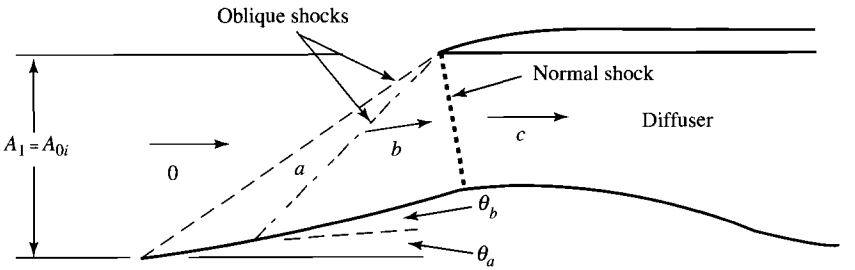

a) On-design operation

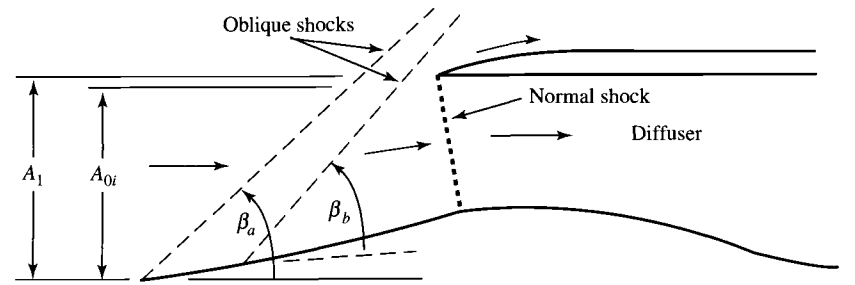

b) Off-design operation

Fig. 10.34 External compression inlet of Example 10.3.

shown in Table 10.1 and plotted in Fig. 10.35. The total pressure recovery η_r of the inlet is the product of the total pressure ratio across each shock. This inlet exceeds the total pressure recovery required by Eq. (6.6) at Mach 1.7 (0.9654 vs 0.9537) but not at Mach 1.8 (0.9396 vs 0.9445).

Note that for M_0 between 1.42 and 1.26, the second oblique shock becomes the terminal normal shock because its ramp angle θ is larger than θ_{max} for M_0 between 1.238 and 1.023. Likewise, the first oblique shock becomes the terminal normal shock for M_0 between 1.23 and 1.0. Also note that the total pressure recovery goes through local maxima and minima as these oblique shocks become normal shocks.

Table 10.1 External compression inlet of Fig. 10.34 with $\theta_a = \theta_b = 5$ deg

M_0	β_a	P_{ta}/P_{t0}	M_a	β_b	P_{tb}/P_{ta}	M_b	P_{tc}/P_{tb}	η_r
2.00	34.30	0.9979	1.821	37.95	0.9982	1.649	0.8765	0.8731
1.95	35.23	0.9980	1.773	39.09	0.9983	1.602	0.8945	0.8912
1.90	36.23	0.9981	1.725	40.34	0.9983	1.554	0.9117	0.9084
1.85	37.30	0.9982	1.677	41.70	0.9984	1.506	0.9278	0.9246
1.80	38.44	0.9982	1.628	43.19	0.9984	1.457	0.9428	0.9396
1.75	39.68	0.9983	1.579	44.84	0.9985	1.407	0.9563	0.9533
1.70	41.03	0.9984	1.529	46.69	0.9985	1.356	0.9684	0.9654
1.65	42.50	0.9984	1.480	48.78	0.9985	1.303	0.9788	0.9758
1.60	44.11	0.9985	1.429	51.21	0.9985	1.248	0.9873	0.9842
1.55	45.89	0.9985	1.378	54.11	0.9984	1.190	0.9937	0.9906
1.50	47.89	0.9985	1.325	57.77	0.9982	1.125	0.9980	0.9947
1.45	50.16	0.9985	1.272	63.05	0.9976	1.045	0.9999	0.9960
1.44	50.65	0.9985	1.261	64.59	0.9973	1.024	1	0.9958
1.43	51.16	0.9985	1.250	66.59	0.9969	0.9974	1	0.9953
1.42	51.68	0.9984	1.238	90	0.9886	0.8192	1	0.9870
1.41	52.22	0.9984	1.227	90	0.9899	0.8257	1	0.9884
1.40	52.78	0.9984	1.216	90	0.9912	0.8325	1	0.9896
1.35	55.93	0.9983	1.156	90	0.9963	0.8705	1	0.9946
1.30	59.96	0.9980	1.090	90	0.9992	0.9195	1	0.9972
1.29	60.95	0.9979	1.075	90	0.9995	0.9316	1	0.9974
1.28	62.04	0.9977	1.059	90	0.9998	0.9450	1	0.9975
1.27	63.26	0.9976	1.042	90	0.9999	0.9602	1	0.9975
1.26	64.69	0.9973	1.023	90	1	0.9782	1	0.9973
1.25	66.50	0.9969	0.9986	0	1	0.9986	1	0.9969
1.24	69.90	0.9957	0.9554	0	1	0.9554	1	0.9957
1.23	90	0.9896	0.8241	0	1	0.8241	1	0.9896
1.22	90	0.9907	0.8300	0	1	0.8300	1	0.9907
1.21	90	0.9918	0.8360	0	1	0.8360	1	0.9918
1.20	90	0.9928	0.8422	0	1	0.8422	1	0.9928
1.15	90	0.9967	0.8750	0	1	0.8750	1	0.9967
1.10	90	0.9989	0.9118	0	1	0.9118	1	0.9989
1.05	90	0.9999	0.9531	0	1	0.9531	1	0.9999

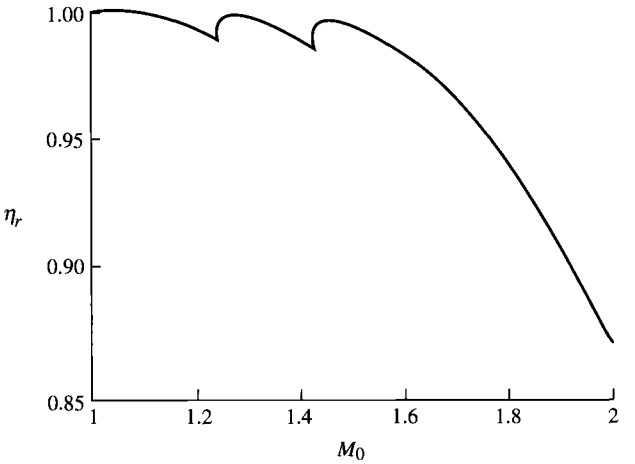

Fig. 10.35 Total pressure recovery η_r of external compression inlet (Fig. 10.36) with $\theta_a = \theta_b = 5$ deg.

10.4.5 Mass Flow Characteristics

The *inlet mass flow ratio* is the ratio of the actual mass flow rate of the inlet $\dot{m}_i$ to the mass flow rate that could be captured $\dot{m}_1$ by the inlet (see Fig. 10.36), and from the conservation of mass equation

$$\frac{\dot{m}_i}{\dot{m}_1} = \frac{\rho_0 V_0 A_{0i}}{\rho_0 V_0 A_1} = \frac{A_{0i}}{A_1} \tag{10.9}$$

which is the inlet area ratio. Thus the inlet mass flow ratio and the inlet area ratio are used interchangeably. The difference between $\dot{m}_i$ and $\dot{m}_1$ is the air that is spilled around the inlet. The *engine mass flow ratio* is defined similarly to that

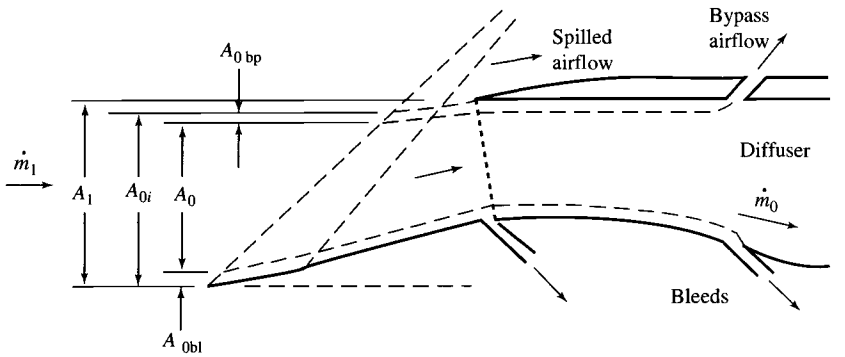

Fig. 10.36 Critical inlet operation.

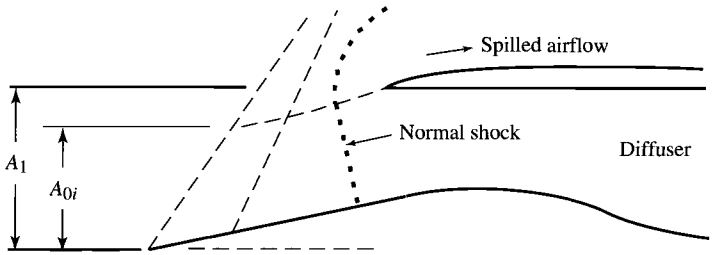

Fig. 10.37 Subcritical inlet operation.

of the inlet, as the ratio of the required engine mass flow rate $\dot{m}_0$ to the mass flow rate that the inlet could capture $\dot{m}_1$, or

$$\frac{\dot{m}_0}{\dot{m}_1} = \frac{\rho_0 V_0 A_0}{\rho_0 V_0 A_1} = \frac{A_0}{A_1} \tag{10.10}$$

The difference between $\dot{m}_i$ and $\dot{m}_0$ is the air that enters the inlet but is removed through boundary-layer bleed, the bypass system, or the secondary air system.

When the inlet can accept the mass flow rate of air required to position the terminal shock just inside the cowl lip (*critical* operation), the fraction of air spilled around the inlet is a minimum and the inlet is said to be *matched* to the engine. When the inlet is not matched, as shown in Fig. 10.37, the normal shock moves upstream (*subcritical* operation) and the fraction of air spilled is increased. This increase in air spillage has associated with it an increase in *spillage drag*, or drag due to the change in momentum of the spilled air and the pressure forces on its stream tube.

When the inlet cannot capture the mass flow rate required by the engine and the other systems, the terminal normal shock is sucked down into the diffuser (*supercritical* operation), as shown in Fig. 10.38, which strengthens the shock and increases the *corrected* mass flow rate to the engine. At a specific operating point on the fan or compressor map, the engine operates as a constant corrected mass flow device. Thus, when the inlet cannot provide the required corrected mass flow rate at critical operation, the engine causes supercritical

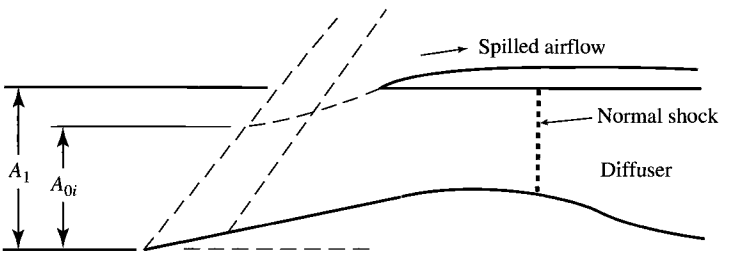

Fig. 10.38 Supercritical inlet operation.

operation and attains the required corrected mass flow rate. Note that supercritical operation has a lower inlet total pressure recovery associated with it, thus, a reduction in engine performance (lower thrust and higher specific fuel consumption). Supercritical operation of the inlet is to be avoided when possible because of poor engine performance.

A common way of presenting the mass flow rate characteristics of an inlet is through a map of the total pressure recovery vs the inlet mass flow ratio, as shown in Fig. 10.39. The performance of a typical external compression inlet is presented in Fig. 10.39 for a specific freestream Mach number. The critical operation point and the subcritical and supercritical operating regimes are also shown on this figure.

The engine mass flow ratio $\dot{m}_0/\dot{m}_1$ can be expressed in terms of corrected mass flow rates and the inlet total pressure ratio as

$$\frac{\dot{m}_0}{\dot{m}_1} = \frac{\dot{m}_{c0}}{\dot{m}_{c1}}\pi_d = \frac{\dot{m}_{c0}}{\dot{m}_{c1}}\eta_r \pi_{d\max} \tag{10.11}$$

where $\dot{m}_{c0}$ is the corrected mass flow rate of the engine and $\dot{m}_{c1}$ is the corrected mass flow rate based on the capture area, a constant for fixed capture area and flight condition. Variation in the engine corrected mass flow rate $\dot{m}_{c0}$ due to a change in engine throttle can be presented on the inlet mass flow map of Fig. 10.39 for the case where the boundary-layer bleed and bypass flows are essentially constant. A line of constant $\dot{m}_{c0}$ is shown on Fig. 10.39 along with the direction of increasing $\dot{m}_{c0}$. When the engine's requirement for air decreases below that required for critical inlet operation, the inlet operating point moves

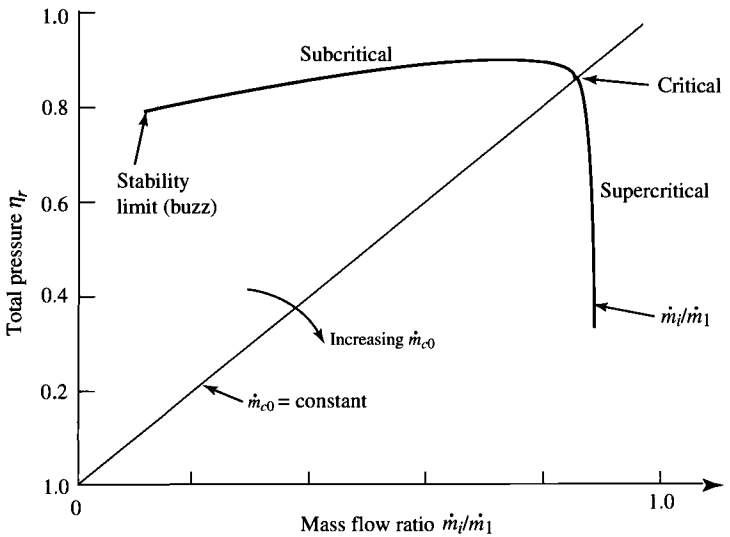

Fig. 10.39 External compression inlet performance characteristics.

into the subcritical region as the engine mass flow rate decreases and the fraction of air spilled increases. When the engine's requirement for air increases above that required for critical operation, the inlet operating point moves into the supercritical region as the engine mass flow ratio remains constant and the total pressure recovery of the inlet decreases with the strengthening of the terminal normal shock in the diffuser.

Two supersonic flow phenomena associated with the stability of the shock structure in external and mixed compression inlets require consideration at this point. One is called inlet *buzz*, and the other is associated with the location of the terminal normal shock.

Buzz is a low-frequency, high-amplitude pressure oscillation that is linked to shock/boundary layer and/or shock/shock interaction at relatively low inlet mass flow ratio. As an example of a flow condition leading to inlet buzz, consider the external compression inlet of Fig. 10.40. When this inlet is operated in the subcritical regime, the terminal normal shock will impinge on the boundary layer formed along the wall of the ramp, causing the boundary layer to separate. If the separated boundary layer produces a large enough low-velocity flow region, the inlet will choke, reducing the inlet mass flow rate and moving the normal shock forward along the ramp. The boundary layer at this forward location is thinner; its separated mass flow region does not choke the inlet. Thus the inlet mass flow increases, moving the normal shock back up the ramp toward its original location, to be repeated again and again, creating buzz. When buzz occurs on a mixed compression inlet, the inlet will "unstart" and engine flameout is possible.

The stability of the terminal normal shock in a mixed compression inlet is important during operation of the inlet near its design point. Design for stability of the terminal normal shock requires that the need for higher total pressure recovery be compromised, and the design throat Mach number be 1.2, with the normal shock positioned downstream where the Mach number is 1.3. Thus the mixed compression inlet is designed to operate in the supercritical regime. When the engine needs less air than provided by this inlet, the excess air must bypass the engine to maintain the terminal normal shock at its stable location and prevent the inlet from "unstarting" (expelling the normal shock). When the engine wants more air than the inlet can provide, the terminal normal shock is

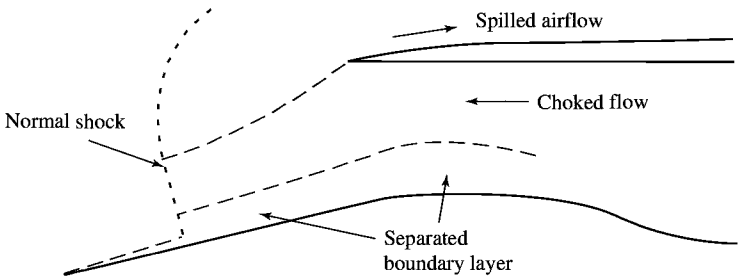

Fig. 10.40 Condition leading to inlet "buzz."

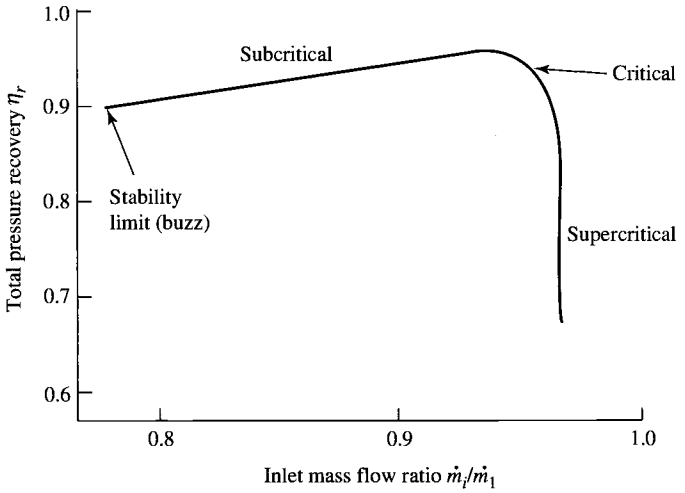

Fig. 10.41 Mixed compression inlet performance characteristics.

drawn downstream into the diffuser, strengthening the shock and increasing the corrected mass flow rate to the engine. When the normal shock is drawn downstream into the diffuser, flow separation and flow distortion become dominant design considerations. To limit this problem, the inlet needs to be designed to provide the required engine mass flow rate with the terminal normal shock positioned where the Mach number in the diffuser is 1.3.

The total pressure recovery vs mass flow ratio of a typical mixed compression inlet is shown in Fig. 10.41. Note that this inlet has a much smaller allowable variation in mass flow ratio before onset of buzz than does the external compression inlet of Fig. 10.39. This reduction in the range for the inlet mass ratio $\dot{m}_i/\dot{m}_1$ corresponds to a larger change in the amount of inlet air that is required to be bypassed $\dot{m}_{bp}$ to prevent buzz (maintain $\dot{m}_i/\dot{m}_1$ above the stability limit), with a corresponding smaller variation in the amount of air spilled.

10.4.6 Inlet Design and Sizing

The design and sizing for a supersonic inlet are considerably more difficult than for the subsonic inlet due mainly to differences in the nature of supersonic and subsonic flows. The supersonic inlet is designed to operate at both subsonic and supersonic flight Mach numbers. The capture and throat areas of the inlet must be large enough not to choke the airflow required by the engine, boundary-layer bleed system, etc. For supersonic flight conditions, the inlet's capture area A_1 is sized to capture the required airflow. Because this airflow varies with both flight Mach number and engine throttle setting, variable-geometry inlet design is sometimes needed to meet the total pressure recovery goal of military specification MIL-E-5008B and/or to keep the installation losses low (spillage drag and/or bypass air drag).

The required values of engine airflow $\dot{m}_0$ and the corresponding values of the freestream area A_0, calculated by the engine performance analysis of Chapter 8 and/or the associated engine performance computer program PERF, are based on the total pressure recovery given by military specification MIL-E-5008B, where

$$\eta_{r\,\text{spec}} = \begin{cases} 1 & M_0 \le 1 \\ 1 - 0.075(M_0 - 1)^{1.35} & 1 < M_0 < 5 \\ \dfrac{800}{M_0^4 + 935} & 5 < M_0 \end{cases} \tag{10.12}$$

This same reference inlet total pressure recovery is used by many others. [Note: Because the total pressure recovery η_r of an inlet design may be different from $\eta_{r\text{spec}}$ given by Eq. (10.12), the required values of engine airflow $\dot{m}_0$ and the corresponding values of freestream area A_0 will be different from those calculated in the engine performance analyses. Thus the values of $\dot{m}_0$ and A_0 determined by using the total pressure recovery of Eq. (10.12) will be referred to as $\dot{m}_{0\,\text{spec}}$ and $A_{0\,\text{spec}}$ respectively, from this point on.]

Inlet design and sizing begin with an analysis of airflow requirements. Figure 10.42 shows the typical variation in inlet airflow requirements at different altitudes from engine performance analyses $A_{0\,\text{spec}}$ with flight Mach number for an advanced supersonic engine. Variable boundary-layer bleed and a safety margin of 4% have been added to the maximum full-throttle engine airflow to obtain the required inlet airflow $A_{0i\,\text{spec}}$.

The engine airflow requirements ($\dot{m}_0$, A_0) for a given inlet design η_r can be estimated based on the engine airflow requirements ($\dot{m}_{0\,\text{spec}}$, $A_{0\,\text{spec}}$) obtained by using a known inlet total pressure recovery $\eta_{r\,\text{spec}}$. Because the engine operates essentially as a constant corrected mass flow device ($\dot{m}_{c2}$ = constant) when the

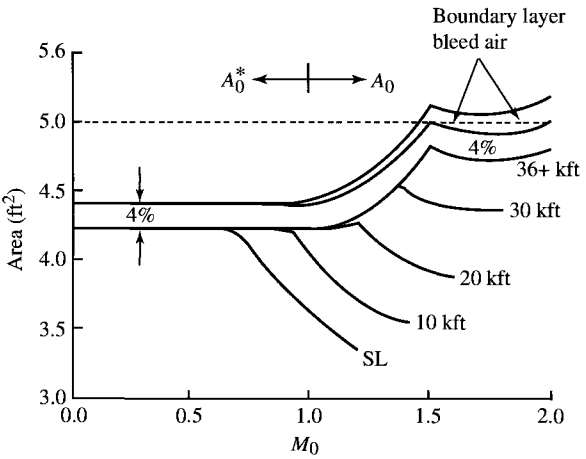

Fig. 10.42 Typical engine airflow requirements.

throttle and flight conditions are constant, then the required engine airflow $\dot{m}_0$ for a specific inlet design η_r can be determined from required engine airflow data ($\dot{m}_{0\,\text{spec}}$, $A_{0\,\text{spec}}$) based on a reference inlet total pressure recovery $\eta_{r\,\text{spec}}$ by using

$$\frac{\dot{m}_0}{\dot{m}_{0\,\text{spec}}} = \frac{A_0}{A_{0\,\text{spec}}} = \frac{\eta_r}{\eta_{r\,\text{spec}}} \tag{10.13a}$$

Likewise, for the inlet air

$$\frac{\dot{m}_i}{\dot{m}_{i\,\text{spec}}} = \frac{A_{0i}}{A_{0i\,\text{spec}}} = \frac{\eta_r}{\eta_{r\,\text{spec}}} \tag{10.13b}$$

10.4.6.1 Inlet performance. Consider the generalized inlet of Fig. 10.43 with capture area A_1 and area A_s at location s. The inlet mass flow ratio can be written as

$$\frac{A_{0i}}{A_1} = \frac{A_{0i}}{A_s}\frac{A_s}{A_1} \tag{10.14a}$$

where A_s/A_1 is determined by the geometry of the inlet. The shock system determines the area ratio A_{0i}/A_s as follows. Conservation of mass gives $\dot{m}_i = \dot{m}_s$ or $\rho_0 V_0 A_{0i} = \rho_s V_s A_s$; thus

$$\frac{A_{0i}}{A_s} = \frac{\dot{m}_s/A_s}{\dot{m}_i/A_{0i}} = \frac{\rho_s V_s}{\rho_0 V_0}$$

and for adiabatic flow in the inlet ($T_{ts} = T_{t0}$), the mass flow rate per unit area in the preceding equation can be written in terms of total pressure and mass flow parameter as

$$\frac{A_{0i}}{A_s} = \frac{P_{ts}}{P_{t0}}\frac{\text{MFP}(M_s)}{\text{MFP}(M_0)} \tag{10.14b}$$

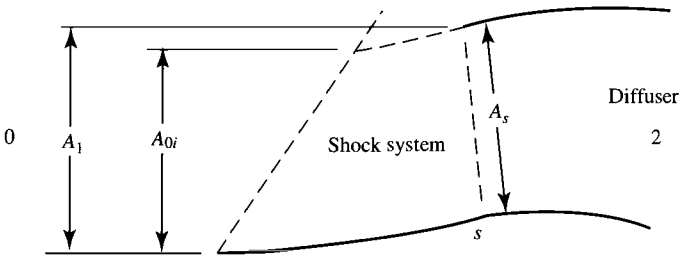

Fig. 10.43 External compression inlet.

Equations (10.14a) and (10.14b) provided the tools to estimate the inlet mass flow ratio A_{0i}/A_1 of an inlet. The area ratio A_s/A_1 is a geometric function of the inlet design, whereas the area ratio A_{0i}/A_s is a function of the flow properties at stations 0 and s. The previous section on total pressure recovery presented the analytical tools for determining both M_s and P_{ts}/P_{t0} of a general inlet, as shown in Example 10.3. Reference 54 contains exact solutions for one and two oblique shock inlets designed for critical operation.

10.4.6.2 Inlet size. The ratio of the inlet capture area A_1 to the engine's area at state 0* for the cycle reference point $A^*_{0\,\mathrm{ref}}$ is referred to as the *inlet size* $A_1/A^*_{0\,\mathrm{ref}}$, since this ratio is the size of the inlet relative to the engine. The required inlet size $(A_1/A^*_{0\,\mathrm{ref}})_{\mathrm{req}}$ at a flight condition can be calculated from the required inlet airflow $A_{0i\,\mathrm{req}}/A^*_{0\,\mathrm{ref}}$ and the inlet mass flow ratio $A^*_{0\,\mathrm{ref}}/A_1$ by using

$$\left(\frac{A_1}{A^*_{0\,\mathrm{ref}}}\right)_{\mathrm{req}} = \frac{(A_{0i}/A^*_{0\,\mathrm{ref}})_{\mathrm{req}}}{A_{0i}/A_1} \tag{10.15}$$

For an inlet with fixed capture area A_1, the flight condition requiring the largest inlet size $(A_1/A^*_{0\,\mathrm{ref}})_{\mathrm{req}}$ is used to size the inlet capture area A_1.

Care must be taken that the inlet does not choke the flow to the engine at subsonic flight conditions. This can be ensured by having the inlet capture area A_1 larger than the maximum required one-dimensional inlet area A^*_{0i} by about 4% ($A/A^* = 1.038$ at $M = 0.8$) and/or providing additional air inlet area for very low-velocity engine airflow requirements.

Example 10.4

Consider an external compression inlet (part 2). We consider the double-ramp external compression inlet of Fig. 10.34 with $\theta_a = \theta_b = 5$ deg to be used with the engine whose required airflow is plotted as $A_0/A^*_{0\,\mathrm{ref}}$ in Fig. 10.44. These data are based on the airflow requirements of Fig. 10.42 at 40-kft altitude and an $A^*_{0\,\mathrm{ref}}$ of 4.22 ft^2 at sea-level static conditions. The inlet is to be capable of operating up to Mach 2 at 40 kft with efficient operation ($\eta_r > \eta_{r\ \mathrm{spec}}$) at Mach numbers less than 1.7. The inlet size and mass flow characteristics of the inlet and engine are considered.

a) Inlet performance. The total pressure recovery of this inlet η_r is tabulated in Table 10.1, is plotted in Fig. 10.35, and meets the requirement for efficient total pressure recovery ($\eta_r > \eta_{r\ \mathrm{spec}}$) at Mach numbers less than 1.75. Analysis of the mass flow characteristics of the inlet and the engine is required before this inlet can be sized. As long as the normal shock between stations b and c touches the lip of the inlet, either station b or c of Fig. 10.34 can be equated to station s of Fig. 10.43. From Eq. (10.14b), we have

$$\frac{A_{0t}}{A_s} = \frac{P_{tb}}{P_{t0}}\frac{\mathrm{MFP}(M_b)}{\mathrm{MFP}(M_0)} = \frac{P_{tc}}{P_{t0}}\frac{\mathrm{MFP}(M_c)}{\mathrm{MFP}(M_0)} \tag{10.16a}$$

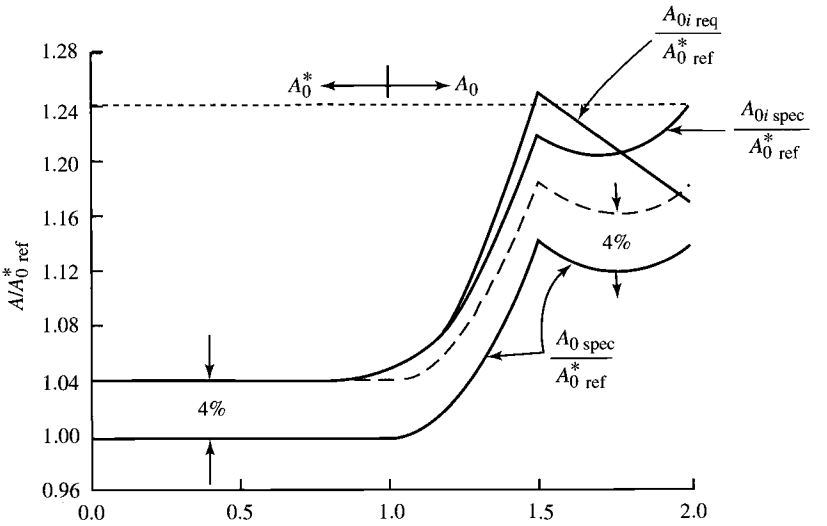

Fig. 10.44 Airflow requirement for example inlet at altitude.

and

$$\frac{P_{tc}}{P_{t0}} = \eta_r \quad \frac{P_{tb}}{P_{t0}} = \frac{\eta_r}{P_{tc}/P_{tb}} \tag{10.16b}$$

The area ratio A_{0t}/A_s can be calculated by using the results of Table 10.1, assuming that $M_s = M_b$ at subsonic values of M_b (no local flow acceleration or deceleration). For subsonic M_0, a reasonable approximation is for choked flow at station s; thus, $A^*_{0i} = A_s$.

The results of the area ratio A_{0i}/A_s calculations for this example inlet are plotted in Fig. 10.45. Note that this plot has a minimum value of 1 at $M_0 = 1$. Also note the jumps in value of A_{0i}/A_s corresponding to the transition between normal and oblique shocks at each ramp (these also correspond to the jumps in total pressure shown in Fig. 10.35).

The selected design point of an external compression inlet sets the value of A_s/A_1. Since $A_{0i} = A_1$ at an inlet's supersonic design point, then $A_s/A_1 = 1/(A_{0i}/A_s)$ evaluated at this design point. For this example, the inlet design point is the maximum M_0 of 2.0. Thus $A_s/A_1 = 0.7681$ and the resulting values of A_{0i}/A_1, from using Eq. (10.14a), are tabulated in Table 10.2.

b) Inlet size. Now that the mass flow ratio of the inlet has been determined, the inlet mass flow rate requirements must be established before it can be sized. By using these data, the maximum calculated value of the inlet size ($A_1/A^*_{0\ \text{ref}}$), from Eq. (10.15), sets the size of this fixed-geometry inlet. Comparison of Figs. 10.44 and 10.45 indicates that the two most demanding operating points will most likely be at $M_0 = 1.23$ and $M_0 = 1.42$. Sizing calculations at the two Mach

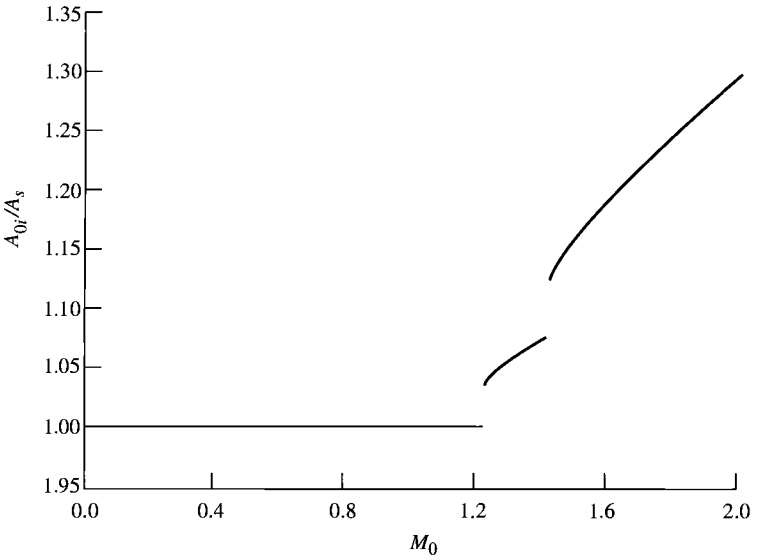

Fig. 10.45 Area ratio of Example 10.4 inlet (Fig. 10.34).

numbers are presented in Table 10.3. The flight condition at $M_0 = 1.42$ determines the inlet size as $A_1 = 1.425A^*_{0\text{ref}}$.

The resulting flow ratios of the sized inlet and its required performance are plotted for altitudes between 36 and 60 kft in Fig. 10.46. This plot shows the difference in flow behavior of the inlet between actual and required flows. As the flight Mach number increases above 1.5, the inlet mass flow rate A_{0i}/A_1

Table 10.2 Example 10.4 inlet performance

M_0	A_{0i}/A_1
0.9	0.7749
1.0	0.7681
1.1	0.7681
1.2	0.7681
1.3	0.8121
1.4	0.8259
1.5	0.8895
1.6	0.9151
1.7	0.9378
1.8	0.9592
1.9	0.9798
2.0	1.0

Table 10.3 Example 10.4 inlet sizing

M_0	$A_0/A_{0\,\text{ref}}^*$	$A_{0i\,\text{req}}/A_{0\,\text{ref}}^*$	A_{0i}/A_1	$A_{1\,\text{req}}/A_{0\,\text{ref}}^*$
1.23	1.0290	1.0854	0.7681	1.413
1.42	1.1004	1.1803	0.8283	1.425

increases while the required inlet mass flow rate $(A_{0i}/A_1)_{\text{req}}$ decreases. The difference between these mass flow rates is airflow that is accepted by the inlet and then bypassed about the engine back to the atmosphere, or spilled about the inlet, or is a combination of bypassed and spilled. The large quantity of excess air for this inlet will correspond to a high inlet installation loss at Mach numbers above 1.5. If a better match of inlet and engine is needed, the inlet will require variable geometry.

10.4.7 Examples of Existing Inlet Designs

Three examples of supersonic inlet designs are shown in Figs. 10.47a, 10.47b, 10.48, and 10.49. Figure 10.47a shows the fixed double-ramp (6-deg ramp followed by a 6.67-deg isentropic ramp) external compression inlet with a throat slot bleed system developed in the J-79 engine installation in the F-16 aircraft. The total pressure recovery of this inlet is shown in Fig. 10.47b.

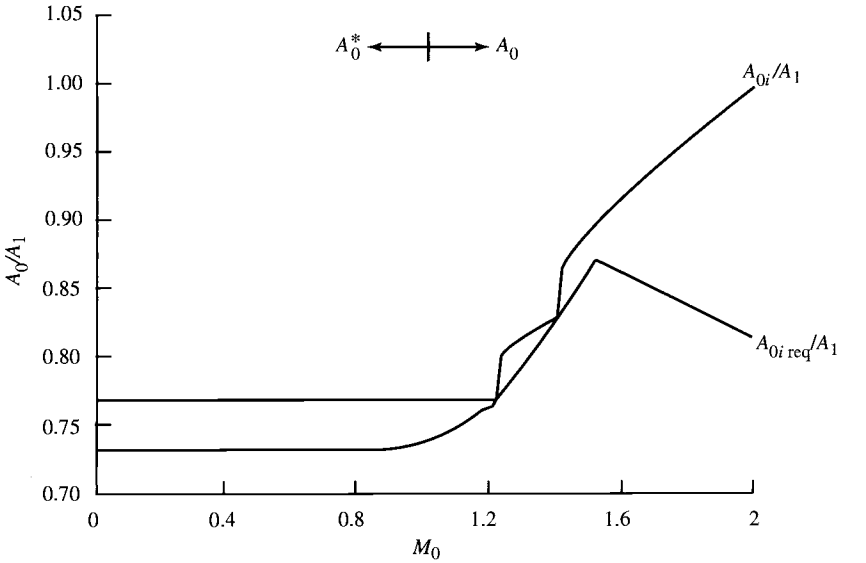

Fig. 10.46 Mass flow performance of sized Example 10.4 inlet at altitude and full engine throttle.

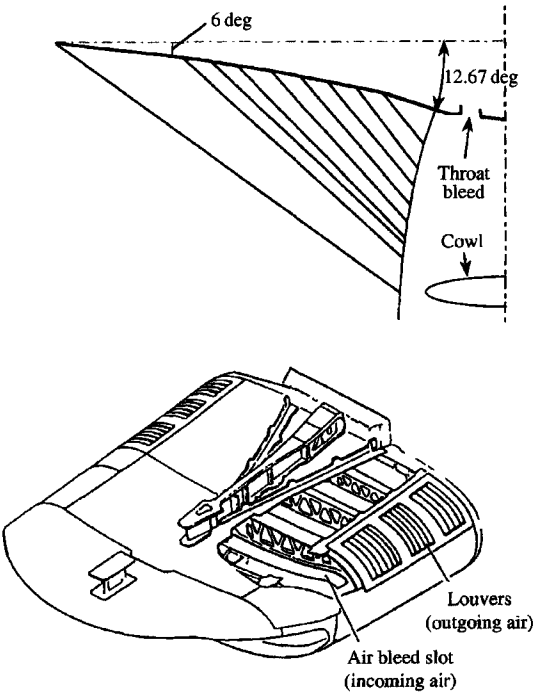

Fig. 10.47a The F-16/J-79 inlet: side and isometric views (Ref. 65).

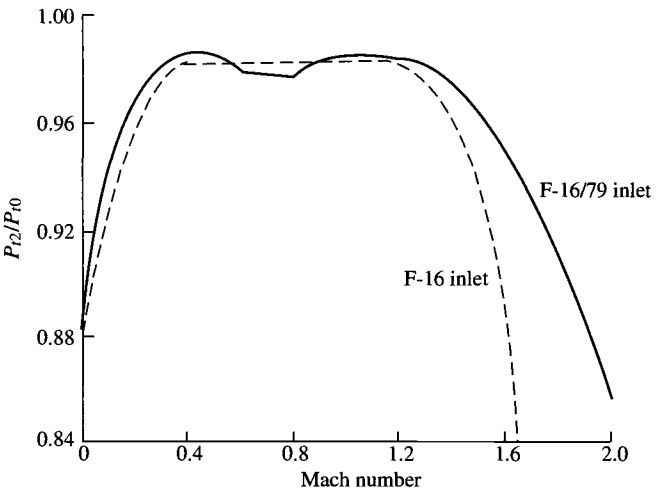

Fig. 10.47b The F-16/J-79 inlet: inlet pressure recovery comparison (Ref. 65).

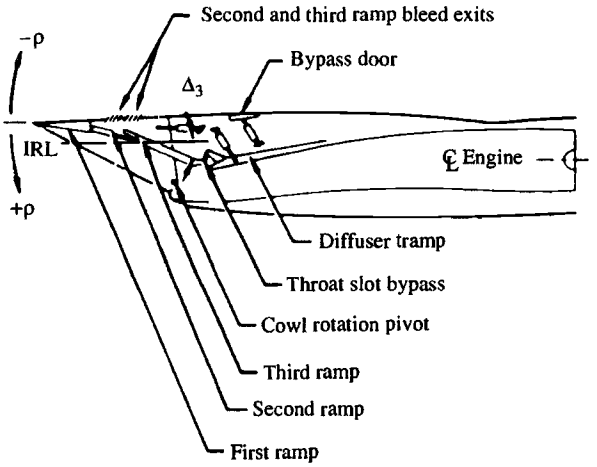

Note: Sideplate bleed not shown

Fig. 10.48 The F-15 inlet system (Ref. 66).

The variable triple-ramp external compression inlet of the F-15 aircraft is shown in Fig. 10.48. This side view of the inlet shows the ramps as they would be positioned when operating at the supersonic design point (ramp angles of 7, 8, and 8 deg for the first, second, and third ramps, respectively). The first ramp angle is fixed, and the second and third ramp angles are variable. The capture area of this inlet is variable with movement of the first ramp/top of inlet assembly from −4 to +11 deg (this assembly is shown at 0 deg).

The takeoff, transonic acceleration, and supersonic cruise modes of operation for the Concorde propulsion system are shown in Fig. 10.49. It has a complex variable-geometry inlet to satisfy the engine mass flow rate requirements at many diverse flight conditions. Note that the supersonic cruise dump control (3) is opened as an auxiliary inlet for takeoff.

10.5 Exhaust Nozzles

The purpose of the exhaust nozzle is to increase the velocity of the exhaust gas before discharge from the nozzle and to collect and straighten the gas flow. For large values of specific thrust, the kinetic energy of the exhaust gas must be high, which requires a high exhaust velocity. The pressure ratio across the nozzle controls the expansion process, and the maximum thrust for a given engine is obtained when the exit pressure P_e equals the ambient pressure P_0. Nozzles and their operation are discussed in many textbooks. The two basic types of nozzles used in jet engines are the *convergent* and *convergent-divergent* (C-D) nozzles.

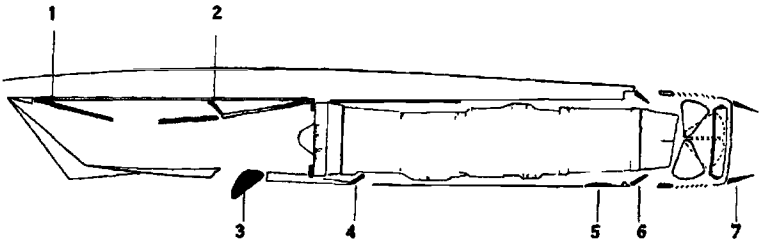

Engine variable geometry. The takeoff settings: 1-ramp sections retracted: 2-secondary control valve closed; 3-dump control open as auxiliary inlet; 4-engine bay cooling air flap open; 5-after spill flap closed; 6-tertiary doors open; 7-secondary nozzle in convergent position

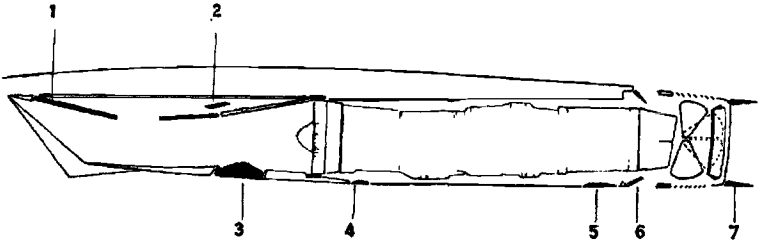

Transonic acceleration: 1-ramp section retracted; 2-secondary control valve open; 3-dump control closed; 4-cooling air flap closed; 5-spill flap closed; 6-tertiary doors open; 7-secondary nozzle trailing

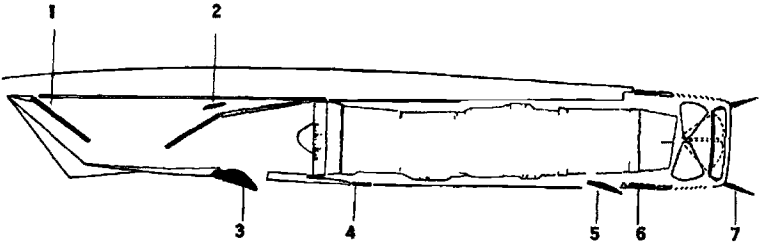

Cruise at Mach 2.2: 1-ramp sections extended; 2-secondary control valve open; 3-dump control open to dump; 4-cooling air flap closed; 5-spill flap open; 6-tertiary doors closed; 7-secondary nozzle divergent.

Fig. 10.49 Concorde propulsion system, modes of operation.

The functions of an exhaust nozzle may be summarized as follows:

1) Accelerate the flow to a high velocity with minimum total pressure loss.
2) Match exit and atmospheric pressures as closely as desired.
3) Permit afterburner operation without affecting main engine operation—this function requires a variable-area nozzle.

4) Allow for cooling of walls if necessary.
5) Mix core and bypass streams of turbofan if necessary.
6) Allow for thrust reversing if desired.
7) Suppress jet noise and infrared radiation (IR) if desired.
8) Thrust vector control if desired.

Do all of these with minimal cost, weight, and boattail drag while meeting life and reliability goals.

10.5.1 Nozzle Types

10.5.1.1 Convergent nozzle. The convergent nozzle is a simple convergent duct, as shown in Fig. 10.50. When the nozzle pressure ratio P_{te}/P_0 is low (less than about 4), the convergent nozzle is used. The convergent nozzle has generally been used in engines for subsonic aircraft.

10.5.1.2 Convergent-divergent (C-D) nozzle. The convergent-divergent nozzle is a convergent duct followed by a divergent duct. Where the cross-sectional area of the duct is at a minimum, the nozzle is said to have a *throat*. Most convergent-divergent nozzles used in aircraft are not simple ducts, but incorporate variable geometry and other aerodynamic features. The convergent-divergent nozzle is used if the nozzle pressure ratio P_{te}/P_0 is high (greater than about 6). High-performance engines in supersonic aircraft generally have some form of a convergent-divergent nozzle. If the engine incorporates an afterburner, the nozzle throat is usually scheduled to leave the operating conditions of the engine upstream of the afterburner unchanged (in other words, vary the exit nozzle area so that the engine does not know that the afterburner is operating). Also, the exit area must be varied to match the different flow conditions and to produce the maximum available thrust.

Earlier supersonic aircraft used ejector nozzles (Fig. 10.51) with their high-performance turbojets. Use of the ejector nozzle permitted bypassing varying amounts of inlet air around the engine, providing engine cooling, good inlet recovery, and reduced boattail drag. Ejector nozzles can also receive air from outside the nacelle directly into the nozzle for better overall nozzle matching—these are called *two-stage ejector nozzles*. For the modern high-performance afterburning turbofan engines, simple convergent-divergent nozzles are used without secondary air, as shown in Fig. 10.52 for the F100 engine.

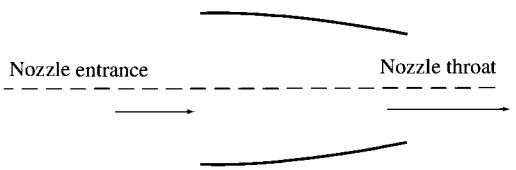

Fig. 10.50 Convergent exhaust nozzle.

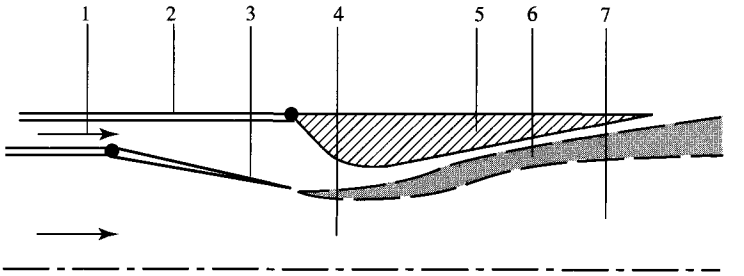

Supersonic nozzle configuration with afterburning: (1) secondary flow; (2) outer case engine; (3) movable primary nozzle shown at maximum area; (4) primary flow, effective throat; (5) movable secondary nozzle shown at maximum exit area; (6) mixing layer between primary and secondary streams; and (7) supersonic primary flow

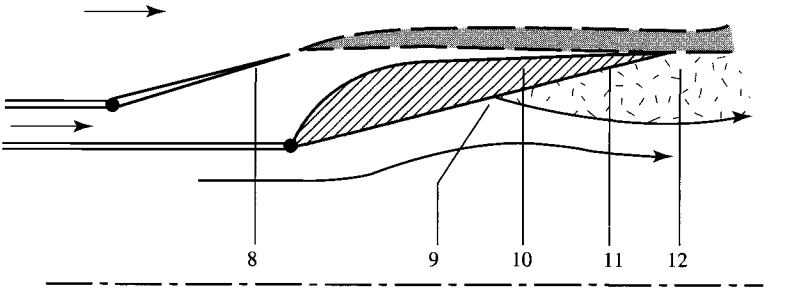

Subsonic nozzle configuration with no afterburning: (8) primary nozzle at minimum area; (9) separation point of external flow; (10) secondary nozzle at minimum area; (11) sonic primary stream; and (12) region of separated flow in external flow

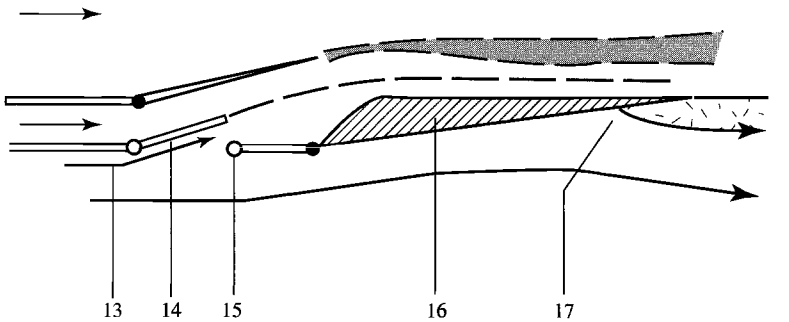

Subsonic nozzle configuration, not afterburning, and blow-in door in use: (13) tertiary flow of ambient gas into nozzle; (14) blow-in door and inflow configuration; (15) reversible hinge/latch; (16) movable secondary nozzle; and (17) separation point of external flow.

Fig. 10.51 Ejector nozzle configuration (Ref. 67).

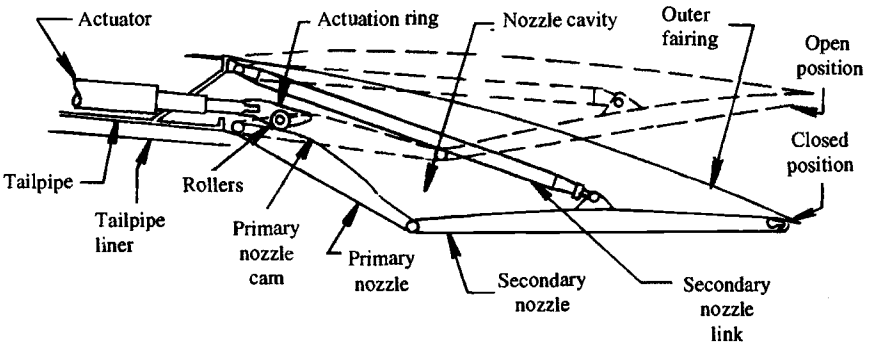

Fig. 10.52 Convergent-divergent exhaust nozzle schematic (Ref. 67).

10.5.2 Nozzle Functions

One can think of the exhaust nozzle as dividing the power available from the main burner exit gas between the requirements of the turbine and the jet power.[67] Thus the nozzle serves as a backpressure control for the engine and an acceleration device converting gas thermal energy to kinetic energy. A secondary function of the nozzle is to provide required thrust reversing and/or thrust vectoring.

10.5.2.1 Engine backpressure control. The throat area of the nozzle is one of the main means available to control the thrust and fuel consumption characteristics of an existing engine. In preliminary engine cycle analysis, selection of specific values for the engine design parameters and the design mass flow rate fixes the throat area of the nozzle. The engine performance methods of Chapter 8 assume that the nozzle throat area and the other internal flow areas of the engine remain constant. This assumption of constant areas establishes the off-design operating characteristics of the engine and the resulting operating lines for each major component. Changing the nozzle throat area from its original design value will change the engine design and the operating characteristics of the engine at both on- and off-design conditions.

At times, it is necessary to change the off-design operation of an engine in only a few operating regions, and variation of the throat area of the exhaust nozzle may provide the needed change. At reduced engine corrected mass flow rates (normally corresponding to reduced engine throttle settings), the operating line of a multistage compressor moves closer to the stall or surge line (see Fig. 10.53). Steady-state operation close to the stall or surge line is not desirable because transient operation may cause the compressor to stall or surge. The operating line can be moved away from the stall or surge line by increasing the exhaust nozzle throat area, as shown in Fig. 10.53. This increase in nozzle throat area reduces the engine backpressure and increases the corrected mass flow rate through the compressor (see Figs. 8.9 and 10.53).

Large changes in the exhaust nozzle throat area are required for afterburning engines to compensate for the large changes in total temperature leaving the

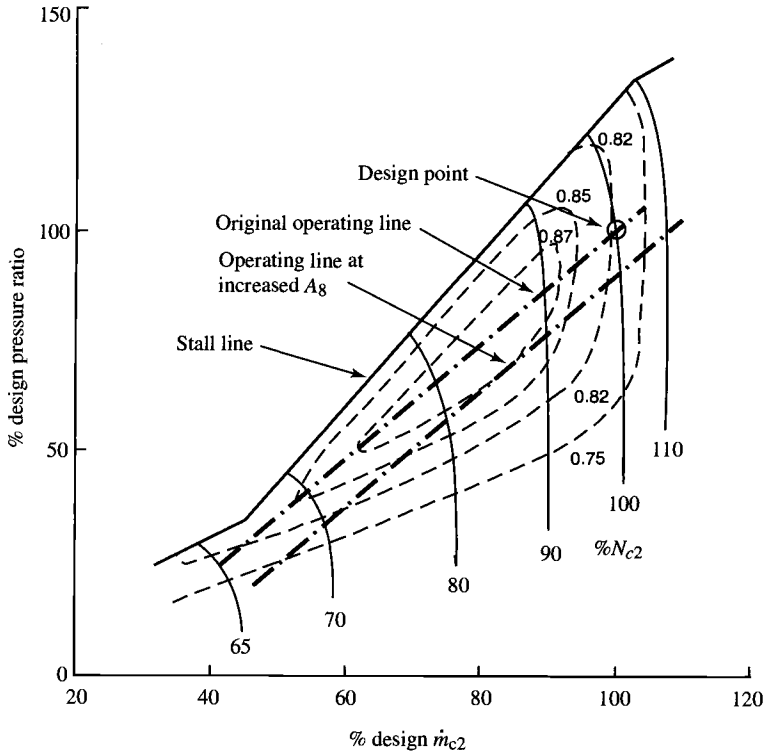

Fig. 10.53 Compressor map with exhaust nozzle area change.

afterburner. The variable-area nozzle required for an afterburning engine can also be used for back pressure control at its nonafterburning settings.

One advantage of the variable-area exhaust nozzle is that it improves the starting of the engine. Opening the nozzle throat area to its maximum value reduces the backpressure on the turbine and increases its expansion ratio. Thus the necessary turbine power for starting operation may be produced at a lower turbine inlet temperature. Also, because the backpressure on the gas generator is reduced, the compressor may be started at a lower engine speed, which reduces the required size of the engine starter.

10.5.2.2 Exhaust nozzle area ratio. Maximum engine thrust is realized for ideal flow when the exhaust nozzle flow is expanded to ambient pressure ($P_e = P_0$). When the nozzle pressure ratio is above choking, supersonic expansion occurs between aft-facing surfaces. A small amount of underexpansion is less harmful to aircraft and engine performance than overexpansion. Overexpansion can produce regions of separated flow in the nozzle and on the aft end of the aircraft, reducing aircraft performance.

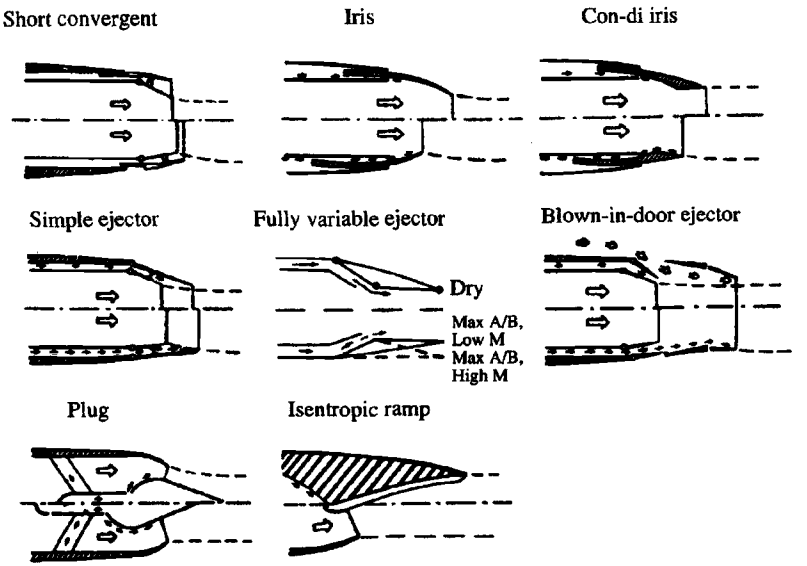

Fig. 10.54 Typical nozzle concepts for afterburning engines (Ref. 67).

The exhaust nozzle pressure ratio P_{te}/P_0 is a strong function of flight Mach number. Whereas convergent nozzles are usually used on subsonic aircraft, convergent-divergent nozzles are usually used for supersonic aircraft. When afterburning engine operation is required, complex variable-geometry nozzles must be used (see Fig. 10.52). Most of the nozzles shown in Fig. 10.54 are convergent-divergent nozzles with variable throat and exit areas. The throat area of the nozzle is controlled to satisfy engine backpressure requirements, and the exit area is scheduled with the throat area. The sophisticated nozzles of the F-15 and B-1 aircraft have two schedules: a low-speed mode and a high-speed mode.[67]

10.5.2.3 Thrust reversing and thrust vectoring. The need for thrust reversing and thrust vectoring is normally determined by the required aircraft and engine system performance. Thrust reversers are used on commercial transports to supplement the brakes. In-flight thrust reversal has been shown to enhance combat effectiveness of fighter aircraft.[67]

Two basic types of thrust reversers are used: the cascade-blocker type and the clamshell type (Fig. 10.55). In the cascade-blocker type, the primary nozzle exit is blocked off, and cascades are opened in the upstream portion of the nozzle duct to reverse the flow. In the clamshell type, the exhaust jet is split and reversed by the clamshell. Because both types usually provide a change in effective throat area during deployment or when deployed, most reversers are designed such that the effective nozzle throat area increases during the brief transitory period, thus preventing compressor stall. High bypass turbofan engines use cascade-blocker type thrust reverser in the fan nozzle.

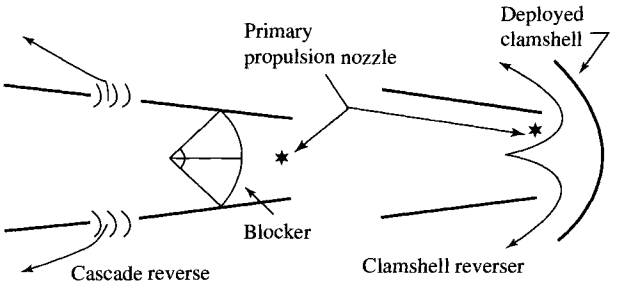

Fig. 10.55 Thrust reversers (Ref. 67).

The exhaust system for the Concorde is shown in Fig. 10.56a. There are two nozzles, a primary nozzle and a secondary nozzle. The secondary nozzle is positioned as a convergent nozzle for takeoff and as a divergent nozzle for supersonic cruise. The modes of operation for this exhaust system are shown in Fig. 10.49 along with the inlet.

Development of thrust vectoring nozzles for combat aircraft has increased in the last decade. Vectoring nozzles have been used on vertical takeoff and landing (VTOL) aircraft, such as the AV-8 Harrier and F-35 Joint Strike Fighter, and are proposed for future fighters to improve maneuvering and augment lift in combat.

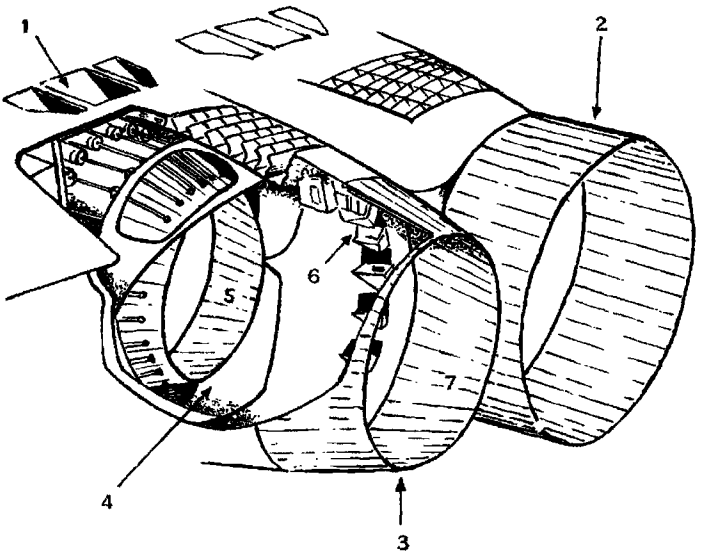

Details of the exhaust system: (1) tertiary doors; (2) nozzle in supersonic configuration; (3) subsonic configuration; (4) thrust reverse buckets; (5) primary nozzle; (6) silencer lobes; (7) secondary nozzle

Fig. 10.56a Concorde exhaust system.

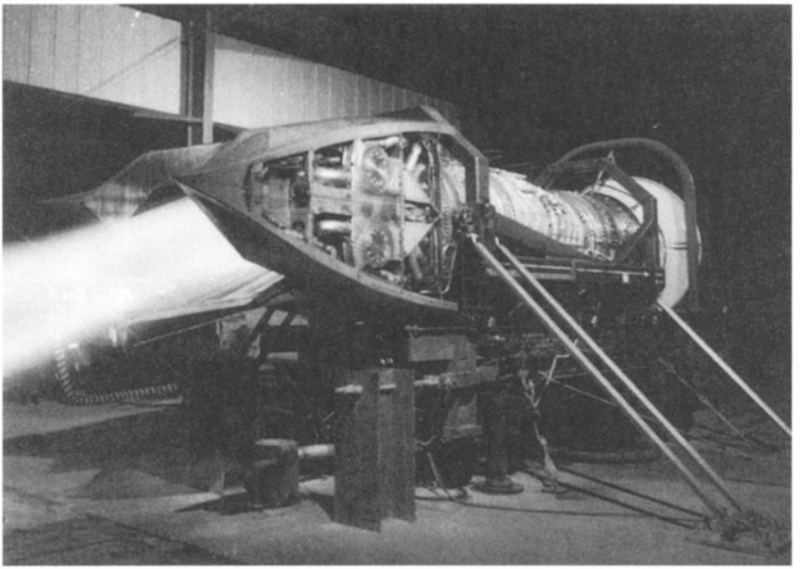

Fig. 10.56b Pratt & Whitney F119-PW-100 turbofan engine with two-dimensional thrust vectoring nozzle. (Courtesy of Pratt & Whitney.)

Thrust vectoring at augmented power settings is being developed for use in future fighters. However, cooling of the nozzle walls in contact with the hot turning or stagnating flows is very difficult and will require increased amounts of nozzle-cooling airflow. The operation of the Pratt & Whitney F119-PW-100 augmented turbofan engine's thrust vectoring nozzle is shown in Fig. 10.56b. This two-dimensional nozzle was developed for use in the F-22 Advanced Tactical Fighter.

Figure 10.57 shows the schematic of a two-dimensional convergent-divergent nozzle with thrust vectoring of ± 15 deg and thrust reversing. This is typical of the capabilities sought for use in future fighter aircraft.

10.5.2.4 Infrared signature. The rear of the engine is very hot and can produce a large infrared signature. Considerable effort is being used in modern military aircraft to reduce this signature. Most effective methods involve hiding the exit of the low-pressure turbine from direct view. Shown in Fig. 10.58 is a platypus exhaust duct used on the F-117A Nighthawk stealth fighter. This exhaust nozzle is canted up 10 deg to prevent ling-of-sight to the turbine face.[60,68] For afterburning engines, the nozzle in concert with the devices (e.g., flameholders) downstream of the turbine can hide the turbine exit and thus reduce high temperature signatures. Generally speaking, reduced engine performance is the cost of stealth.

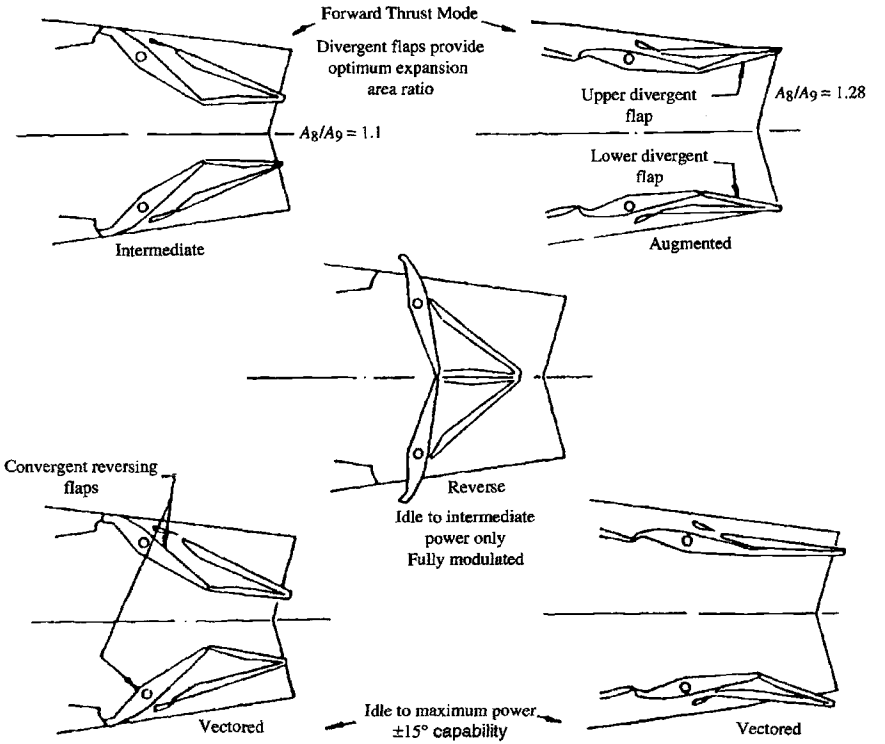

Fig. 10.57 Typical two-dimensional thrust vectoring nozzle with thrust reversing (Ref. 68).

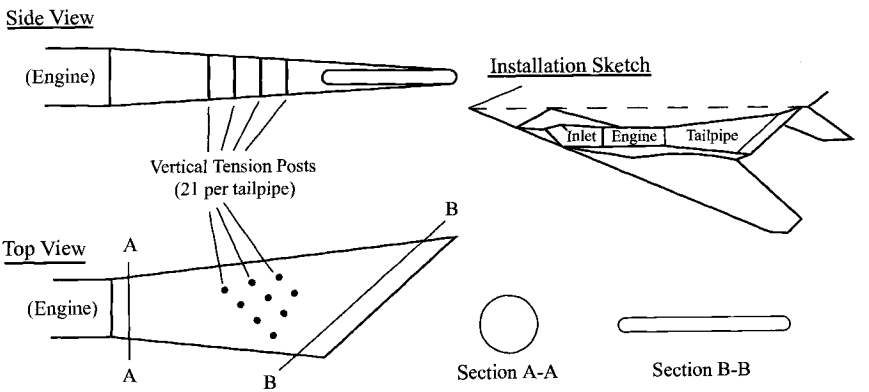

Fig. 10.58 Exhaust nozzle of F-117A (from Ref. 68).

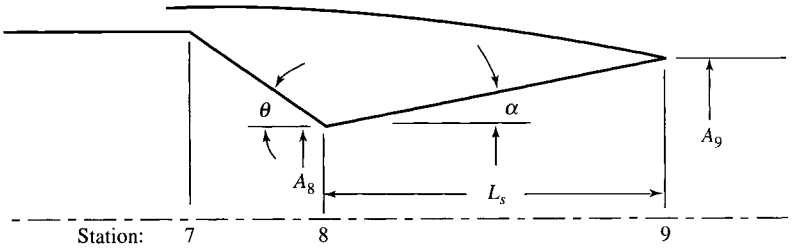

A_8 = Primary nozzle throat area
A_9 = Secondary nozzle exit area
α = Secondary nozzle half-angle
θ = Primary nozzle half-angle
L_s = Secondary nozzle length

Fig. 10.59 Nozzle geometric parameters.

10.5.3 Nozzle Coefficients

Nozzle performance is ordinarily evaluated by two dimensionless coefficients: the gross thrust coefficient and the discharge or flow coefficient. Figure 10.59 shows a convergent-divergent exhaust nozzle with the geometric parameters used in the following definitions of nozzle coefficients. Only total pressure losses downstream of station 8 are included in the gross thrust coefficient.

10.5.3.1 Gross thrust coefficient. The *gross thrust coefficient* C_{fg} is the ratio of the actual gross thrust $F_{g\,\text{actual}}$ to the ideal gross thrust $F_{g\,\text{ideal}}$, or

$$C_{fg} \equiv \frac{F_{g\,\text{actual}}}{F_{g\,\text{ideal}}} \tag{10.17}$$

Empirically derived coefficients are applied to Eq. (10.17) to account for the losses and directionality of the actual nozzle flow. Each engine organization uses somewhat different coefficients, but each of the following basic losses is accounted for:

1) Thrust loss due to exhaust velocity vector angularity
2) Thrust loss due to the reduction in velocity magnitude caused by friction in the boundary layers
3) Thrust loss due to loss of mass flow between stations 7 and 9 from leakage through the nozzle walls
4) Thrust loss due to flow nonuniformities

10.5.3.2 Discharge or flow coefficient. The ratio of the actual mass flow $\dot{m}_8$ to the ideal mass flow $\dot{m}_{8i}$ is called the *discharge coefficient* C_D:

$$C_D \equiv \frac{\dot{m}_8}{\dot{m}_{8i}} \tag{10.18}$$

This coefficient can be shown to be identically equal to the ratio of the effective one-dimensional flow area required to pass the total actual nozzle flow A_{8e} to the nozzle physical throat area A_8 as follows:

$$C_D = \frac{\dot{m}_8}{\dot{m}_{8i}} = \frac{\rho_8 V_8 A_{8e}}{\rho_8 V_8 A_8} = \frac{A_{8e}}{A_8}$$

The variation of the discharge coefficient with nozzle pressure ratio is shown in Fig. 10.60a for a conic convergent nozzle. When the nozzle is choked, the

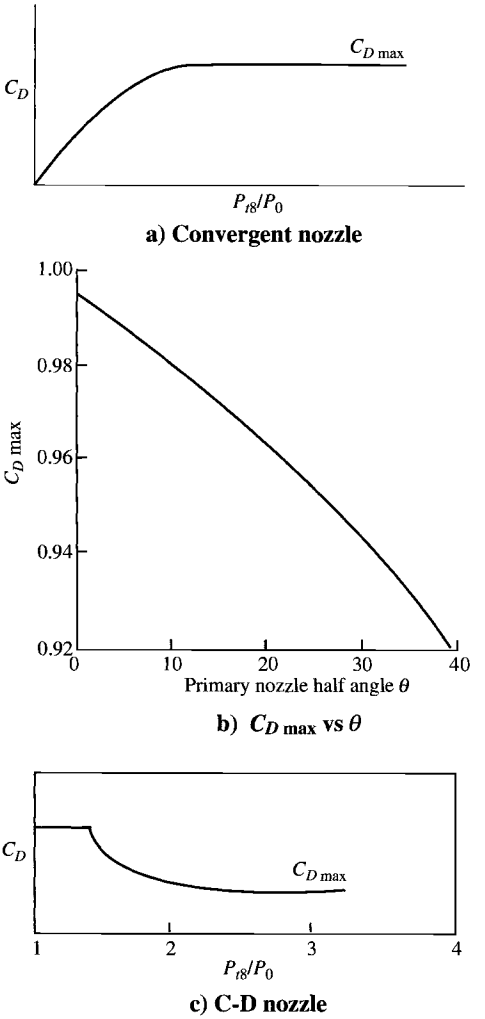

a) Convergent nozzle

b) $C_{D\,max}$ vs θ

c) C-D nozzle

Fig. 10.60 Nozzle discharge coefficient (Ref. 67).

discharge coefficient reaches a maximum value $C_{D\max}$. The value of $C_{D\max}$ is a function of the primary nozzle half-angle θ, as shown in Fig. 10.60b. Figure 10.60c shows the variation in discharge coefficient for a convergent-divergent nozzle with nozzle pressure ratio. Note the change in behavior of C_D between that of the convergent-divergent nozzle and that of the convergent nozzle as the nozzle pressure ratio drops below choking. This is due to the venturi behavior of the convergent-divergent nozzle.

The discharge coefficient is used to size the nozzle throat area to pass the desired mass flow rate. For example, consider a nozzle with

$$\dot{m}_8 = 200\,\text{lbm/s}, \quad P_{t8} = 30\,\text{psia}, \quad T_{t8} = 2000^\circ\text{R}, \quad \gamma = 1.33$$
$$R = 53.34\,\text{ft} \cdot \text{lbf/(lbm} \cdot {}^\circ\text{R)}, \quad \theta = 20\,\text{deg}$$

At $M_8 = 1$, GASTAB with $\gamma = 1.33$ and $\mathscr{M} = 28.97$, then MFP = 0.5224, and thus $A_{8e} = 570.7\,\text{in.}^2$. Figure 10.60b gives $C_{D\max} = 0.96$ for $\theta = 20\,\text{deg}$ and thus the required throat area is $594.5\,\text{in.}^2$.

10.5.3.3 Velocity coefficient. The *velocity coefficient* C_V is the ratio of the actual exit velocity V_9 to the ideal exit velocity V_{9i} corresponding to $P_{t9} = P_{t8}$, or

$$C_V \equiv \frac{V_9}{V_{9i}} \tag{10.19}$$

and represents the effect of frictional loss in the boundary layer of the nozzle. It is mainly a function of the nozzle ratio A_8/A_9 and the half-angle α, as shown in Fig. 10.61.

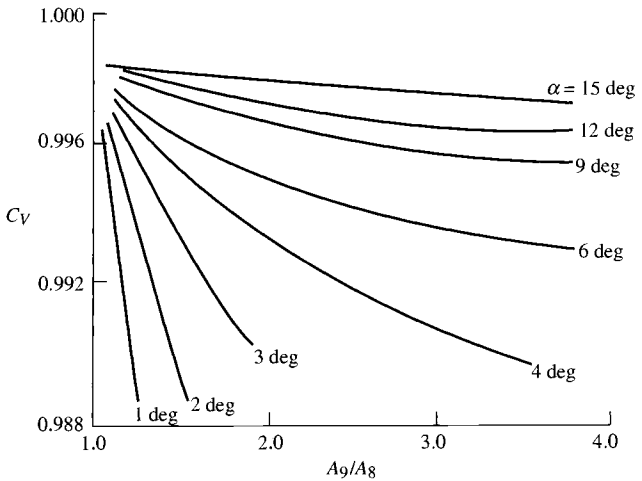

Fig. 10.61 C-D nozzle velocity coefficient (Ref. 67).

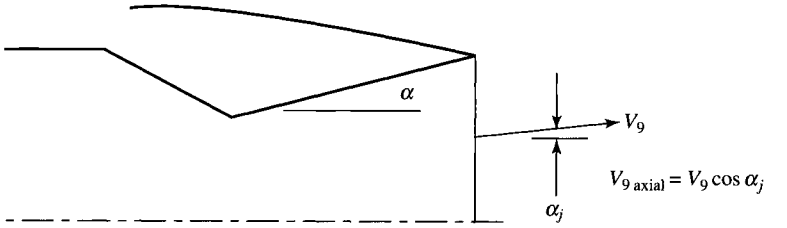

Fig. 10.62 Local angularity coefficient.

10.5.3.4 Angularity coefficient. The *angularity coefficient* C_A represents the axial friction of the nozzle momentum; thus it is proportional to the thrust loss due to the nonaxial exit of the exhaust gas (see Fig. 10.62). For a differential element of flow, this coefficient is the cosine of the local exit flow angle α_j.

The local flow angle α_j varies from zero at the centerline to α at the outer wall; thus, the nozzle angularity coefficient is the integral of α_j across the nozzle:

$$C_A \equiv \frac{1}{\dot{m}} \int \cos \alpha_j \, d\dot{m} \tag{10.20}$$

Figure 10.63 presents the correlation of the angularity coefficient with the nozzle area ratio A_8/A_9 and half-angle α. This figure is based on analytical evaluations of the inviscid flowfield in convergent-divergent nozzles for a range of practical nozzle geometries.

10.5.4 Nozzle Performance

Many nozzle coefficients simplify to algebraic expressions or become unity for the special case of *one-dimensional adiabatic flow*. This is a useful

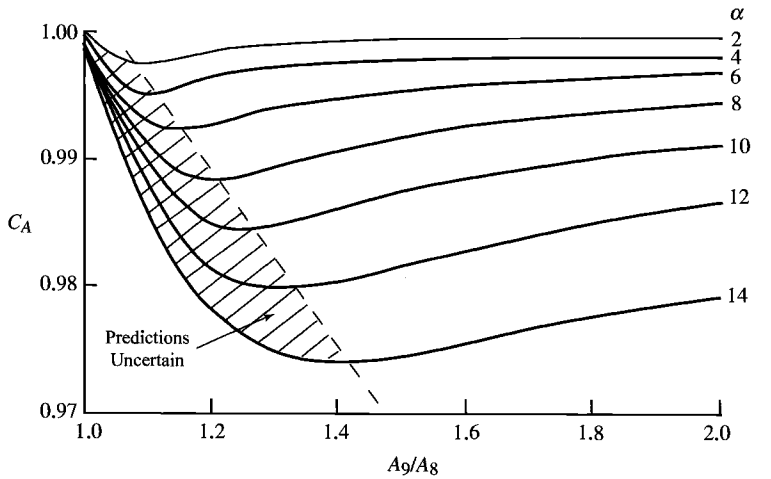

Fig. 10.63 C-D nozzle angularity coefficient (Ref. 67).

limit for understanding each coefficient and for preliminary analysis of nozzle performance using engine cycle performance data.

For one-dimensional adiabatic flow, $C_A = 1$,

$$C_D = \frac{\dot{m}_8}{\dot{m}_{8i}} = \frac{A_{8e}}{A_8} = \frac{P_{t8}}{P_{t7}}$$

and the velocity coefficient C_V is given by [Eq. (10.19)]

$$C_V \equiv \frac{V_9}{V_{9i}}$$

where V_9 is the exit velocity corresponding to T_{t8} and $(A/A^*)_9 = (P_{t9}/P_{t8}) \times [A_9/(C_D A_8)]$ and V_{9i} is the ideal exit velocity corresponding to T_{t8} and $(A/A^*)_{9i} = A_9/(C_D A_8)$.

The gross thrust for a one-dimensional flow can be expressed as

$$F_{g\,\text{actual}} = \frac{\dot{m}_8 V_9}{g_c} + (P_9 - P_0)A_9 \tag{10.21}$$

and the ideal gross thrust (corresponds to $P_9 = P_0$) as

$$F_{g\,\text{ideal}} = \frac{\dot{m}_{8i} V_s}{g_c} \tag{10.22}$$

where V_s is the isentropic exit velocity based on P_{t8}/P_0 and T_{t8}.

For one-dimensional flow of a calorically perfect gas, Eq. (10.21) can be written as

$$F_{g\,\text{actual}} = \frac{\dot{m}_8 V_9}{g_c}\left[1 + \frac{\gamma - 1}{2\gamma}\frac{1 - P_0/P_9}{(P_{t9}/P_9)^{(\gamma-1)/\gamma} - 1}\right] \tag{10.23}$$

The gross thrust coefficient for one-dimensional flow of a calorically perfect gas can be obtained by substituting Eqs. (10.22) and (10.23) into Eq. (10.17), giving

$$C_{fg} = C_D C_V \sqrt{\frac{1 - (P_{9i}/P_{t8})^{(\gamma-1)/\gamma}}{1 - (P_0/P_{t8})^{(\gamma-1)/\gamma}}}\left[1 + \frac{\gamma - 1}{2\gamma}\frac{1 - P_0/P_9}{(P_{t9}/P_9)^{(\gamma-1)/\gamma} - 1}\right] \tag{10.24}$$

This equation reduces to $C_{fg} = C_D C_V$ for the ideal expansion ($P_9 = P_{9i} = P_0$). For isentropic flow, $P_9 = P_{9i}$, $P_{t9} = P_{t8}$, $C_V = 1$, and $C_D = 1$.

Equation (10.24) is plotted in Fig. 10.64 for isentropic flow vs the nozzle area ratio A_9/A_8 for different nozzle pressure ratios P_{t8}/P_0. Note that ideal expansion ($P_9 = P_0$) gives a gross thrust coefficient of unity and that both underexpansion

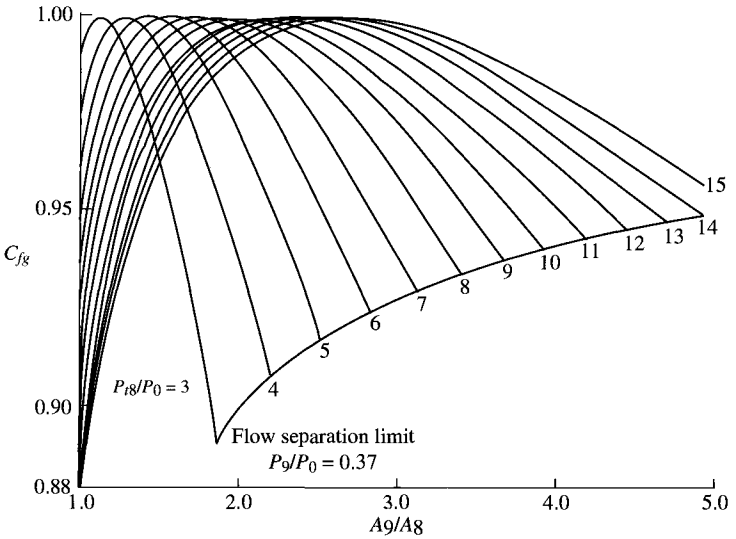

Fig. 10.64 Thrust coefficient for one-dimensional isentropic flow ($\gamma = 1.3$).

($P_9 > P_0$) and overexpansion ($P_9 < P_0$) reduces the gross thrust coefficient below unity.

The extent of overexpansion in nozzles is limited by flow separation resulting from the interaction of the nozzle boundary layer and the strong oblique shock waves at the exit of the nozzle. In extreme overexpansion, Summerfield et al.[20] noted that the oblique shock waves moved from the exit lip into the nozzle (see Fig. 3.17), the flow downstream of the shock waves was separated in the vicinity of the wall, and as a result, the wall static pressure downstream of the shock waves was nearly equal to the ambient pressure P_0. A simple estimate for the ratio of the pressure just preceding the shock waves P_s to the ambient pressure P_0, suggested by Summerfield et al.,[20] is given by

$$\frac{P_s}{P_0} \approx 0.37 \tag{10.25}$$

This flow separation limit can be included in the one-dimensional gross thrust coefficient of Eq. (10.24) for isentropic flow by considering the effective exit pressure ($P_9 = P_{9i}$) to be the pressure just preceding the shock wave (P_s). Equations (10.24) and (10.25) were used to obtain the flow separation limit shown in Fig. 10.64. The design area ratio A_9/A_8 of convergent-divergent nozzles is selected such that the nozzle flow does not separate due to overexpansion for most throttle settings. This is because the increase in gross thrust coefficient associated with flow separation does not normally offset the accompanying increase in installation loss.

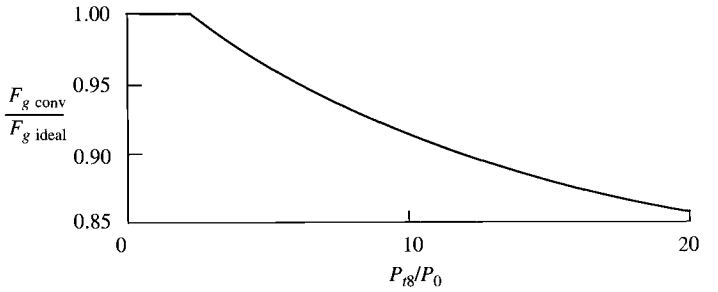

Fig. 10.65 Ratio of convergent nozzle gross thrust to ideal gross thrust vs pressure ratio ($\gamma = 1.3$).

Nozzle pressure ratios are 3 to 5 in the subsonic cruise speed range of turbofan and turbojet engines. Typically, a subsonic engine uses a convergent exhaust nozzle. This is because, in the nozzle pressure range of 3 to 5, the convergent gross thrust (interception of lines with vertical axis, $A_9/A_8 = 1$) is 1–3% below the peak gross thrust ($P_9 = P_0$). Consequently, there may be insufficient gross thrust increase available in going to a convergent-divergent nozzle on a subsonic cruise turbofan or turbojet engine to pay for the added drag and weight of such a nozzle. In some applications, this loss in gross thrust coefficient of a convergent nozzle is too much, and a C-D nozzle is used.

The design pressure ratio across the nozzle increases rapidly with supersonic flight Mach number. At Mach 2, a pressure ratio of about 12 is typical. At this pressure ratio, the convergent nozzle gross thrust penalty is about 9%, as shown in Fig. 10.65. This figure is a plot of the ratio of the gross thrust in Fig. 10.64 of a convergent nozzle ($A_9/A_8 = 1$) to the peak thrust ($P_9 = P_0$) vs P_{t8}/P_0. Substitution of convergent-divergent nozzles for convergent nozzles provides large thrust gains for supersonic aircraft.

Example 10.5

Consider the calculation based on one-dimensional flow.

Given:

$$\dot{m}_8 = 200 \text{ lbm/s} \quad P_{t8} = 30 \text{ psia} \quad T_{t8} = 2000^\circ\text{R}$$

$$\frac{A_9}{A_8} = 2.0 \quad \gamma = 1.33 \quad R = 53.34 \text{ ft} \cdot \text{lbf/(lbm} \cdot {}^\circ\text{R)}$$

$$\frac{P_{t9}}{P_{t8}} = 0.98 \quad C_D = 0.98 \quad P_0 = 5 \text{ psia}$$

Find the dimensions of an axisymmetric nozzle and the vaues of C_{fg}, F_g, and C_V.

Solution: At $M_8 = 1$ GASTAB with $\gamma = 1.33$ and $\mathscr{M} = 28.97$, then MFP = 0.5224, thus

$$A_{8e} = \frac{\dot{m}_8\sqrt{T_{t8}}}{P_{t8}\text{MFP}(M_8 = 1)} = \frac{200\sqrt{2000}}{30 \times 0.5224} = 570.7 \text{ in.}^2$$

With $C_D = 0.98$, thus $A_8 = 582.3$ in.^{2} and $r_8 = 13.61$ in. Since $A_9/A_8 = 2.0$, then $A_9 = 1165$ in.^{2} and $r_9 = 19.25$ in.:

$$\left(\frac{A}{A^*}\right)_{9i} = \frac{A_9}{C_D A_8} = \frac{2.0}{0.98} = 2.041 \longrightarrow M_{9i} = 2.168 \quad \text{and} \quad \frac{P_{9i}}{P_{t9i}} = 0.0990$$

Thus, $P_{9i} = (0.0990)(30 \text{ psia}) = 2.970$ psia,

$$V_{9i} = \sqrt{Rg_c T_{t8}}\sqrt{\frac{2\gamma}{\gamma - 1}\left[1 - \left(\frac{P_{9i}}{P_{t8}}\right)^{(\gamma-1)/\gamma}\right]}$$

$$V_{9i} = \sqrt{(1716)(2000)}\sqrt{\frac{2(1.33)}{0.33}[1 - (0.0990)^{0.33/1.33}]} = 3475 \text{ ft/s}$$

$$\left(\frac{A}{A^*}\right)_9 = \frac{P_{t9}}{P_{t8}}\frac{A_9}{C_D A_8} = \frac{0.98 \times 2.0}{0.98} = 2.0 \longrightarrow M_9 = 2.146 \quad \text{and} \quad \frac{P_9}{P_{t9}} = 0.1025$$

Thus, $P_9 = (0.1025)(0.98)(30 \text{ psia}) = 3.014$ psia,

$$V_9 = \sqrt{(1716)(2000)}\sqrt{\frac{2(1.33)}{0.33}[1 - (0.1025)^{0.33/1.33}]} = 3456 \text{ ft/s}$$

$$C_V = \frac{V_9}{V_{9_i}} = 0.9945$$

$$C_{fg} = (0.98)(0.9945)\sqrt{\frac{1 - (2.97/30)^{0.33/1.33}}{1 - (5.0/30)^{0.33/1.33}}} \times \left[1 + \frac{0.33}{2 \times 1.33}\frac{1 - 5.0/3.014}{(29.4/3.014)^{0.33/1.33} - 1}\right]$$

$$= 0.9593$$

Figure 10.3b gives $\theta = 10$ deg for $C_D = 0.98$. Likewise, Fig. 10.64 gives $\alpha = 6$ deg for $C_V = 0.9945$ and $A_9/A_8 = 2$. Thus $L_s = 54$ in. and the dimensions of the exhaust nozzle are shown in Fig. 10.66. The gross thrust can be calculated

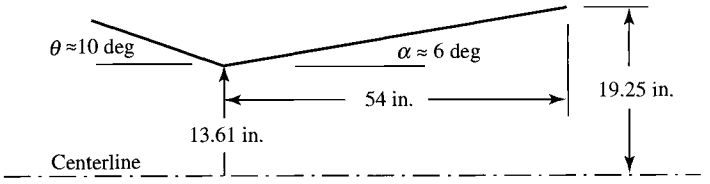

Fig. 10.66 Dimensions of Example 10.5 exhaust nozzle.

in several ways: directly from Eq. (10.23),

$$F_{g\,\text{actual}} = \frac{\dot{m}_8 V_9}{g_c} + (P_9 - P_0)A_9$$

$$= \frac{(200)(3456)}{32.174} + (3.014 - 5.0)(1165) = 19{,}170 \text{ lbf}$$

or from the ideal gross thrust and C_{fg} with

$$V_s = \sqrt{(1716)(2000)}\sqrt{\frac{2(1.33)}{0.33}\left[1 - \left(\frac{5}{30}\right)^{0.33/1.33}\right]} = 3151 \text{ ft/s}$$

then

$$F_{g\,\text{ideal}} = \frac{\dot{m}_{8t} V_s}{g_c} = \frac{(200/0.98)(3151)}{32.174} = 19{,}990 \text{ lbf}$$

$$F_{g\,\text{actual}} = C_{fg} F_{g\,\text{ideal}} = (0.9593)(19{,}990) = 19{,}170 \text{ lbf}$$

10.6 Introduction to Combustion Systems

Combustion systems of aircraft gas turbine engines largely encompass the main burners (also called *burners or combustors*) and afterburners (also called *augmenters or reheaters*). Both main burners and afterburners are covered in this section because they have many basic principles in common. The basic principles of the combustion process, combustion stability, total pressure ratio, length scaling, diffusers, and fuels are presented in the following sections and provide the means for understanding the design of the main burner and afterburner.

The thermal energy of the air/fuel mixture (reactants) flowing through an airbreathing engine is increased by the combustion process. The fuel must be vaporized and mixed with the air before this chemical reaction can occur. Once this is done, the combustion process can occur and thus increase the thermal energy of the mixture (products of combustion). All of this takes time and space.

The design of the main burner and afterburner of an airbreathing engine differs in many ways from that of conventional combustion devices. Space (especially length) is at a premium in aircraft applications, and the length of the combustion chamber is reduced by hastening completion of the combustion process. The combustion intensity (rate of energy released per unit volume) is much higher for the main burner of a turbojet [40,000 Btu/(s · ft^3) or 11,150 MW/m^3] compared to a typical steam power plant [10 Btu/(s · ft^3) or 2.8 MW/m^3]. The following properties of the combustion chambers are desired:

1) Complete combustion
2) Low total pressure loss
3) Stability of combustion process
4) Proper temperature distribution at exit with no "hot spots"
5) Short length and small cross section
6) Freedom from flameout
7) Relightability
8) Operation over a wide range of mass flow rates, pressures, and temperatures

However, many of these desirable properties are in competition. For example, both complete combustion and low total pressure loss are contrary to small size. Hence the design of a main burner or afterburner is a compromise. We examine many of these desirable combustion properties in order to understand the design and operation of main burners and afterburners, starting with the combustion process.

10.6.1 Combustion Process

The combustion processes occur with the vaporized fuel and air mixed on a molecular scale. The rate of this reaction depends on both the static pressure P and temperature T in a very complex way. For many situations, the reaction rate can be approximated by a form of the Arrhenius equation[67,69] written for the mass rate of reaction as

$$\text{Reaction rate} \propto P^n f(T) \exp \frac{-E}{\mathscr{R}T} \tag{10.26}$$

where n is an exponent that depends on the number of molecules involved in a reactive collision (for example, $n = 2$ for two molecules, $n = 3$ for three molecules); $f(T)$ is a function that relates the reaction rate to the forms of energy (translation, rotation, and vibration) the molecules have; the term $\exp[-E/(\mathscr{R}T)]$ accounts for the number of molecular collisions in which the energy of one molecule relative to another exceeds the activation energy E; and $\mathscr{R}$ is the universal gas constant.

For hydrocarbon-air combustion, $n = 1.8$. At low pressures, the reaction rate becomes slow and can become limiting for aircraft engines at very high altitudes. However, under most operating conditions, the rate of combustion is limited by the rate at which the fuel is vaporized and mixed with air. In most combustors, the fuel is injected as an atomized liquid-droplet spray into the hot reaction zone where it mixes with air and hot combustion gases. The atomized fuel vaporizes,

and then the vapor is mixed with air. If the temperature and pressure in the reaction zone are sufficiently high, the reaction rate will be fast and the fuel vapor will react as it comes in contact with sufficient oxygen.

The stoichiometric fuel/air ratio for the typical hydrocarbon fuel can be estimated by assuming octane as a representative hydrocarbon and writing the stoichiometric chemical reaction:

$$2C_8H_{18} + 25\left(O_2 + \frac{79}{21}N_2\right) \longrightarrow 16CO_2 + 18H_2O + 25\left(\frac{79}{21}\right)N_2$$

For this reason, the stoichiometric fuel/air ratio is found to be

$$f_{\text{stoich}} = \frac{2(96 + 18)}{25[32 + (79/21)28]} = 0.0664$$

The *equivalence ratio* ϕ is the actual fuel/air ratio divided by the fuel/air ratio required for complete combustion (stoichiometric fuel/air ratio), or

$$\phi \equiv \frac{f}{f_{\text{stoich}}} \tag{10.27}$$

The equivalence ratio ϕ is greater than 1.0 for rich fuel/air ratio and less than 1.0 for a lean fuel/air mixture. To prevent excessive temperatures at the exit of the main burner or afterburner and protect its walls, the overall fuel/air ratio must be much less than stoichiometric with $\phi < 1.0$.

As an example, an engine being flown at Mach 0.9, a 12-km altitude, and full throttle with a compressor pressure ratio of 20 and 85% isentropic efficiency will have a compressor pressure outlet temperature of about 653 K. If the turbine inlet temperature is limited to 1670 K, h_{PR} is 42,800 kJ/kg, and c_{pc} and c_{pt} are 1.004 and 1.235 kJ/(kg · K), then the fuel/air ratio for 100% efficient combustion in the main burner is, from Eq. (7.9),

$$f = \frac{1.235 \times 1670 - 1.004 \times 653}{42{,}800 - 1.235 \times 1670} = 0.0346$$

which corresponds to an overall equivalence ratio of 0.519 for a main burner using JP-8 fuel ($f_{\text{stoich}} = 0.0667$).

Figure 10.67 shows the flammability characteristics of a kerosene-type fuel. The 0.52 equivalence ratio of the preceding example is at the lower limit of flammability shown in Fig. 10.67. This presents a design problem at the full-throttle value of ϕ and at the engine's partial-throttle values of ϕ. The problem of lean mixtures in a burner can be overcome by mixing and burning a rich fuel/air mixture in a small region where the local equivalence ratio is near unity. By using only a portion of the total air in a region, a locally rich mixture can be efficiently burned and then the products of combustion diluted and cooled to an acceptable turbine inlet temperature by the remaining air (see Fig. 10.77).

At usual pressures and temperatures, hydrocarbon/air mixtures will react over only a rather narrow range of ϕ—from approximately 0.5 to 3 and not at all below

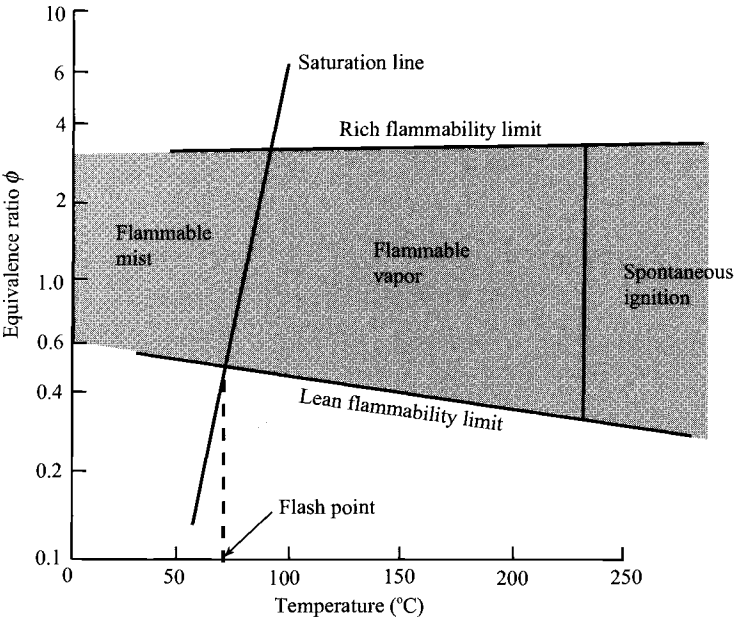

Fig. 10.67 Flammability characteristics for a kerosene type fuel in air at atmospheric pressure (Refs. 38 and 67).

0.2 atm at standard temperature. Hydrogen has much wider flammability limits than do hydrocarbons—approximately $0.25 < \phi < 6$ at standard temperature and 1 atm. Some special, rather expensive fuels have flammability limits intermediate between hydrogen and hydrocarbons. These special fuels have been used at times for testing and for extending the altitude limits of engines for special applications.

A limitation is imposed by the combustion because it is necessary to maintain a stationary flame within a high-velocity airstream. Imagine the flame as propagating through the combustible mixture at the flame speed, while the mixture is carried downstream. To have a stable flame, the velocity of the mixture must be maintained within certain limits: If the velocity is too high, the flame will be "blown out" the exit; if it is too low, the flame will travel upstream and be extinguished. This problem of holding the combustion flame within the combustion system is solved by establishing regions of recirculation at the front of the main burner (see Fig. 10.77) or behind a bluff body, called a *flame holder*, at the front of an afterburner (see Fig. 10.87). These regions of recirculation create areas of local low velocity that "hold" the flame, and at the same time, the resulting turbulence gently increases the rate of energy transfer from these regions.

Provided stable combustion is attained, complete combustion in the case of lean mixtures is virtually ensured since, with excess oxygen, local fuel-rich areas are unlikely. On the other hand, combustion of a near-stoichiometric

mixture requires an essentially uniform distribution of constituents to avoid wasting some fuel in local fuel-rich (oxygen-poor) regions.

10.6.2 Ignition

Ignition of a fuel/air mixture in a turbine engine combustion system requires inlet air and fuel conditions within flammability limits, sufficient residence time of a combustible mixture, and location of an effective ignition source in the vicinity of the combustible mixture. The flammability limits for a kerosene-type fuel are shown in Fig. 10.67. Note that the flammability region is further subdivided into two regions separated by the *spontaneous ignition temperature* (SIT). The spontaneous ignition temperature is the lowest temperature at which visible or audible evidence of combustion is observed. Typical values of SIT are presented in Table 10.4.

When the temperature in the combustion system is below the SIT, an ignition source is required to bring the local temperature above the spontaneous ignition temperature. The minimum amount of energy necessary to achieve ignition is shown in Fig. 10.68. Note that the minimum amount of energy is not always at a stoichiometric mixture ratio. For heavy fuels, such as C_7H_{16}, the minimum is nearer $\phi = 2$.

Once the flammability limits and SIT requirements are met, then the ignition delay time becomes the key combustion characteristic. The ignition delay time t_{ign} is related to the initial temperature T by

$$t_{ign} \propto \exp \frac{E}{\mathcal{R}T} \tag{10.28}$$

Table 10.4 Spontaneous-ignition temperatures

Fuel	SIT, K
Propane	767
Butane	678
Pentane	558
Hexane	534
Heptane	496
Octane	491
Nonane	479
Decane	481
Hexadecane	478
Isooctane	691
Kerosene (JP-8 or jet A)	501
JP-3	511
JP-4	515
JP-5	506

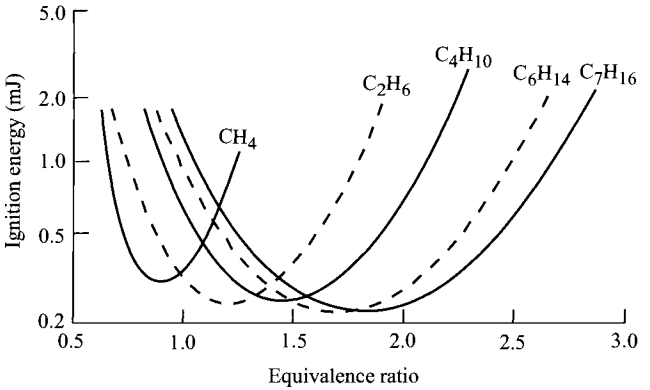

Fig. 10.68 Minimum ignition energies at standard temperature and pressure (Refs. 67 and 70).

The variation of ignition delay time with pressure has been experimentally observed to follow $t_{ign} \propto 1/P$. Ignition delay times for typical fuels are shown in Fig. 10.69.

10.6.3 Combustion Stability

The ability of the combustion process to sustain itself in a continuous manner is called *combustion stability*. Stable, efficient combustion can be upset by the fuel/air mixture becoming too lean or too rich such that the temperatures and reaction rates drop below the level necessary to effectively heat and vaporize the incoming fuel and air. Such a situation causes blowout of the combustion process. The effects of mass flow rate, combustion volume, and pressure on the stability of the combustion process are combined into the *combustor loading parameter* (CLP), defined as

$$\text{CLP} \equiv \frac{\dot{m}}{P^n(\text{combustion volume})} \tag{10.29}$$

Because the denominator of the combustor loading parameter is based on the rate of the combustion process, the pressure component n will correspond to 2 for a simple bimolecular reaction. Because of the complex set of reactions occurring when a hydrocarbon is burned in air, n has been experimentally determined to be about 1.8, and this value of n is applied for most situations. However, under high-pressure conditions, a value of 1 for n is more realistic because the chemical reaction rate is not the limiting factor and physical mixing processes play a more important role.

The method of presenting the stability characteristics of a combustion process for a gas turbine engine is based on stirred reactor theory[67,69,71,72] and shows the stable and unstable operation regions in a plot of the equivalence ratio vs the combustor loading parameter, as shown in Fig. 10.70. Spalding[72] reports

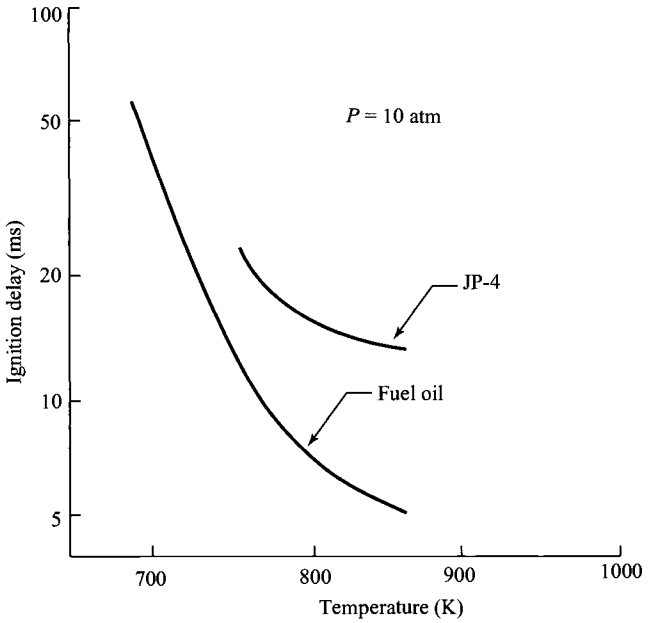

Fig. 10.69 Ignition delay times for practical fuels (Refs. 38 and 67).

the loading parameter stability limit of a stirred reactor with $n = 1.8$ as 90 lbm/$(s \cdot atm^{1.8} \cdot ft^3)$ at $\phi = 1$ and 10 lbm/$(s \cdot atm^{1.8} \cdot ft^3$ at $\phi = 0.5$ and 1.7.

10.6.4 Length Scaling

An estimate of the size of the main burner and/or afterburner is required during the engine's preliminary design. The cross-sectional area can be easily

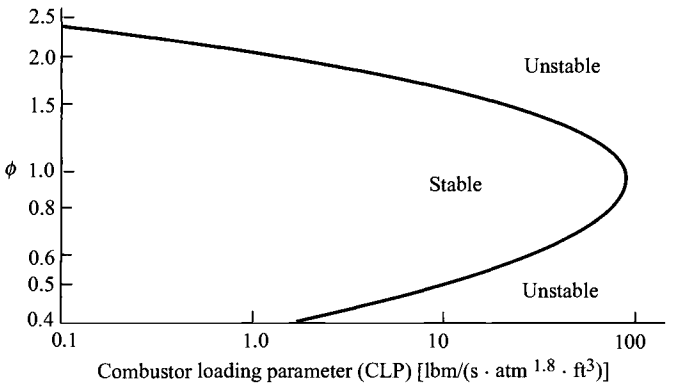

Fig. 10.70 Combustion stability characteristics (Refs. 67 and 73).

determined based on one-dimensional gas dynamics, but the length requires scaling laws. The length of a main burner is primarily based on the distance required for combustion to come to near completion. Equation (10.26) gives the reaction rate in terms of pressure and temperature and will be used to develop the length-scaling equation for main burners.

The residence time t_{res} in the main burner is given by

$$t_{\text{res}} = \frac{L}{V_{\text{av}}} \approx \frac{L}{V_{\text{ref}}} = \frac{\rho_{t3} A_{\text{ref}} L}{\dot{m}_3} \tag{10.30}$$

where V_{ref} is based on the air mass flow rate entering the combustor; A_{ref} is the cross-sectional area normal to the airflow (case to case) of the combustion chamber; L is the length of the main burner; the density of the air entering the combustion chamber is approximated by ρ_{t3}; and the other variables have their normal meanings. Assuming an isentropic compression process, the total density at state 3 is proportional to the total pressure at this state as given by

$$\rho_{t3} \propto P_{t3}^{1/\gamma_c}$$

Substituting the preceding relationship into Eq. (10.30) and solving for the main burner length yield

$$L \propto \frac{\dot{m}_3}{A_{\text{ref}}} \frac{t_{\text{res}}}{P_{t3}^{1/\gamma_c}}$$

Noting that

$$\frac{\dot{m}_3}{A_{\text{ref}}} = \frac{\dot{m}_3 A_4}{A_4 A_{\text{ref}}} = \frac{P_{t4}}{\sqrt{T_{t4}}} \frac{A_4}{A_{\text{ref}}} \frac{\text{MFP}(M_4 = 1, \gamma_4)}{1 + f}$$

(where station 4 is in the high-pressure turbine inlet stators and this flow is choked) and P_{t4} is approximately equal to P_{t3}, we see that the preceding equation for L becomes

$$L \propto \frac{P_{t3}^{(\gamma_c - 1)/\gamma_c}}{\sqrt{T_{t4}}} \frac{A_4}{A_{\text{ref}}} t_{\text{res}} \tag{10.31}$$

The reaction time t_{rea} is inversely proportional to the reaction rate. Thus from Eq. (10.26)

$$t_{\text{rea}} \propto P_{t3}^{-n} \tag{10.32}$$

Table 10.5 Contemporary main burners

Engine type	TF39 Annular	TF41 Cannular	J79 Cannular	JT9D Annular	F100 Annular	T63 Can
Mass flow						
Air, lb/s	178	135	162	242	135	3.3
Fuel, lb/h	12,850	9965	8350	16,100	10,580	235
Size						
Length, in.	20.7	16.6	19.0	17.3	18.5	9.5
Diameter, in.	33.3	5.3/24.1[a]	6.5/32.0[a]	38.0	25.0	5.4
P_{t3}, psia	382	314	198	316	366	92
$T_{t4\ \max}$, °R	2915	2620	2160	2865	3025	1840

[a]Can diameter/annulus diameter.

For the main burner, the residence time t_{res} is proportional to the reaction time t_{rea}. Thus t_{res} in Eq. (10.31) can be replaced by Eq. (10.32), giving

$$L \propto \frac{A_4}{A_{ref}\sqrt{T_{t4}}} P_{t3}^{-[n-(\gamma_c-1)/\gamma_c]} \tag{10.33}$$

For the main burners of similar design, the area ratio A_4/A_{ref} is constant and

$$L \propto P_{t3}^{-r}/\sqrt{T_{t4}} \tag{10.34}$$

where $r = 1.51$ for $n = 1.8$ and $r = 0.714$ for $n = 1$. Thus the length of main burners having similar design varies with the pressure and temperature and is unaffected by the size of the engine. This explains both the shortening of the main burner length with increases in compressor pressure ratio and the reduction in the ratio of the main burner length to engine diameter as engine size increases.

Equation (10.34) can be used to obtain a preliminary estimate of the main burner length based on a known-reference similar design. The size and sea-level operating conditions for contemporary main burners are provided in Table 10.5, and this information may be used as a reference in estimating main burner length.

As an example of estimating main burner length, consider a design similar to the JT9D but with $P_{t3} = 350$ psia at sea level and $T_{t4} = 2900$°R. Use of Eq. (10.34) with $n = 1$ ($r = 0.714$) gives a length that is 92.4% of the JT9D, or 16.0 in.

10.6.5 Combustion System Total Pressure Ratio

An estimate of the total pressure loss resulting from increasing the gas total temperature and frictional loss of a combustion system can be obtained by modeling the combustion system as a constant-area duct (Fig. 10.71) with simple heating (increase in total temperature) and internal drag proportional to

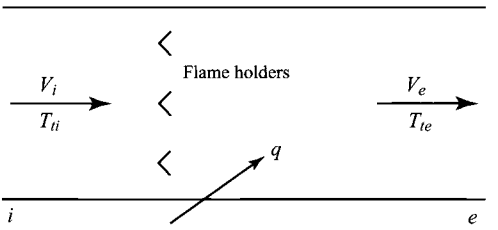

Fig. 10.71 Model of combustion system.

the incoming dynamic pressure (drag $= 0.5\rho_i V_i^2 C_D A$). The gas is assumed to be calorically perfect at inlet i and exit e, and the mass addition of fuel neglected in comparison to the air mass flow.

The basic conservation equations are the following.

Mass:

$$\rho_i V_i = \rho_e V_e$$

Momentum:

$$P_i + \frac{\rho_i V_i^2}{g_c} = P_e + \frac{\rho_e V_e^2}{g_c} + C_D\left(\frac{1}{2}\rho_i V_i^2\right)$$

Energy:

$$q = c_{pe}T_{te} - c_{pi}T_{ti}$$

Solution of these equations[4] gives

$$\frac{T_{te}}{T_{ti}} = \frac{q + c_{pi}T_{ti}}{c_{pe}T_{ti}}$$

$$\Phi = \frac{\gamma_i}{\gamma_e}\frac{M_i^2\{1 + [(\gamma_i - 1)/2]M_i^2\}}{[1 + \gamma_i M_i^2(1 - C_D/2)]^2}\frac{T_{te}}{T_{ti}} \tag{10.35}$$

$$M_e^2 = \frac{2\Phi}{1 - 2\gamma_e\Phi + \sqrt{1 - 2(\gamma_e + 1)\Phi}} \tag{10.36}$$

$$\frac{P_e}{P_i} = \frac{1 + \gamma_i M_i^2(1 - C_D/2)}{1 + \gamma_e M_e^2} \tag{10.37}$$

$$\frac{P_{te}}{P_{ti}} = \frac{P_e}{P_i}\frac{\{1 + [(\gamma_e - 1)/2]M_e^2\}^{\gamma_e/(\gamma_e - 1)}}{\{1 + [(\gamma_i - 1)/2]M_i^2\}^{\gamma_i/(\gamma_i - 1)}} < 1 \tag{10.38}$$

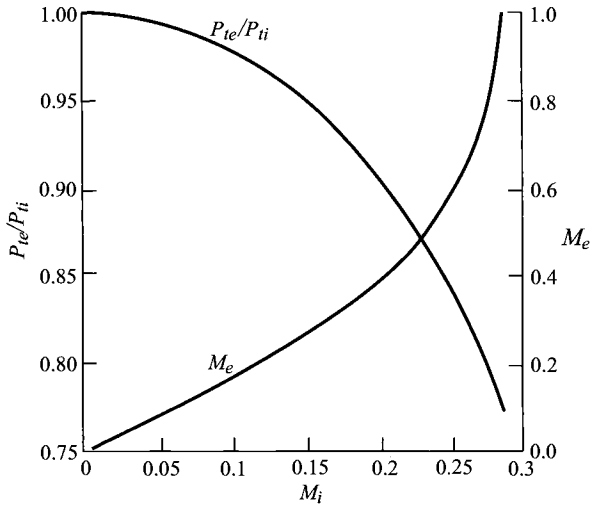

Fig. 10.72 Main burner total pressure loss.

Example 10.6

Consider the following data for a turbojet's main burner:

$$T_{t4} = 3000^\circ\text{R} \quad \gamma_t = 1.3 \quad C_D = 1.5 \quad \tau_r = 1.162\,(M_0 = 0.9)$$

$$T_0 = 540^\circ\text{R} \quad \gamma_c = 1.4 \quad \tau_c = 1.92 \quad (\pi_c = 7.55 \text{ and } \eta_c = 0.85)$$

For convenience, the equation for the total temperature ratio can be written in terms of engine temperature ratios as

$$\frac{T_{te}}{T_{ti}} = \frac{T_{t4}}{T_{t3}} = \frac{T_{t4}/T_0}{(T_{t2}/T_0)(T_{t3}/T_{t_2})} = \frac{T_{t_4}/T_0}{\tau_r \tau_c} = \frac{3000/540}{1.162 \times 1.92} = 2.49$$

Thus $T_{t4}/T_{t3} = 2.49$ and calculations using Eqs. (10.35–10.38) yield the results of Fig. 10.72. These results show that the inlet Mach number to the combustion zone of a main burner must be kept below 0.10 to achieve a reasonable total pressure ratio ($P_{te}/P_{ti} > 0.975$) resulting from increasing gas total temperature and frictional loss.

10.6.6 Diffusers

Many instances arise in the design of engine components when the flow velocity must be decreased; a diffuser is used to perform this important function. One such instance is the flow entering the main burner where the flow leaving the

compressor must be slowed from a high subsonic Mach number to a very low Mach number.[72] Another instance is the flow entering the afterburner where the flow leaving the turbine must be slowed from a high subsonic Mach number to a Mach number of about 0.2.

Because the flow is being slowed in the diffuser, an adverse pressure exists and flow separation from the walls is possible. Figure 10.12 presents the standard diffuser flow regimes. Main burner and afterburner diffusers are designed to fall below the flow separation boundary line.

The pressure recovery coefficient C_P and the pressure recovery effectiveness η are two performance parameters used to describe diffuser performance. The *pressure recovery coefficient* C_P is a measure of the diffuser's ability to recover dynamic pressure and is defined by

$$C_P \equiv \frac{P_e - P_i}{\rho V_i^2/2} \tag{10.39}$$

where P_i and P_e are the static pressure at the inlet and exit, respectively, and $\rho V_i^2/2$ is the inlet dynamic pressure. For the ideal diffuser (incompressible flow with constant total pressure), C_P can be expressed in terms of the area ratio

$$C_{P\,\text{ideal}} \equiv 1 - \left(\frac{A_i}{A_e}\right)^2 \tag{10.40}$$

where A_i and A_e are the inlet and exit areas, respectively. The *pressure recovery effectiveness* η of the diffuser is the ratio of the actual pressure recovery coefficient to the ideal pressure recovery coefficient:

$$\eta \equiv \frac{C_P}{C_{P\,\text{ideal}}} \equiv \frac{P_e - P_i}{(\rho V_i^2/2)[1 - (A_i/A_e)^2]} \tag{10.41}$$

The total pressure ratio of the diffuser can, therefore, be expressed in terms of the pressure recovery effectiveness η and other convenient flow properties as

$$\frac{P_{te}}{P_{ti}} = 1 - \frac{\rho V_i^2}{2P_{ti}}(1 - \eta)\left[1 - \left(\frac{A_i}{A_e}\right)^2\right] \tag{10.42a}$$

or

$$\frac{P_{te}}{P_{ti}} = 1 - \frac{(\gamma/2)M_i^2(1 - \eta)[1 - (A_i/A_e)^2]}{\{1 + [(\gamma - 1)/2]M_i^2\}^{\gamma/(\gamma-1)}} \tag{10.42b}$$

The diffuser performance characteristics for preliminary design are presented in Fig. 10.73. This figure relates diffuser area ratio A_e/A_i and length/height ratio L/H to the pressure recovery effectiveness η. Maintaining high pressure recovery effectiveness often leads to long diffusers that are undesirable.

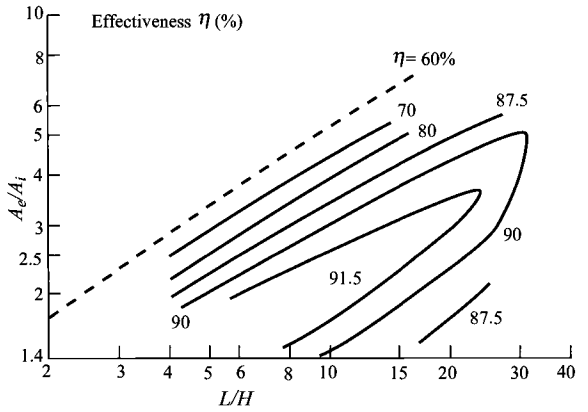

Fig. 10.73 Straight-wall diffuser performance (Ref. 67).

Dump diffusers are often used in conjunction with straight-walled diffusers to meet design goals. The pressure loss for a dump diffuser, as depicted in Fig. 10.74, was investigated by Barclay[74] and can be estimated in the range $0.2 < A_i/A_e < 1$ by

$$\frac{P_{te}}{P_{ti}} = \exp\left\{-\frac{\gamma}{2}M_i^2\left[\left(1-\frac{A_i}{A_e}\right)^2+\left(1-\frac{A_i}{A_e}\right)^6\right]\right\} \tag{10.43}$$

Example 10.7

Find the total pressure ratio of a straight wall diffuser with the following data: $A_e/A_i = 4.0$, $M_i = 0.5$, $\gamma = 1.4$, and $L/H = 15$. Using Fig. 10.73 and Eq. (10.42b) gives $\eta = 0.9$ and $P_{te}/P_{ti} = 0.9858$.

Example 10.8

Find the total pressure ratio for a dump diffuser with the following data: $A_e/A_i = 5.0$, $M_i = 0.5$, and $\gamma = 1.4$. Using Eq. (10.43) gives $P_{te}/P_{ti} = 0.8540$.

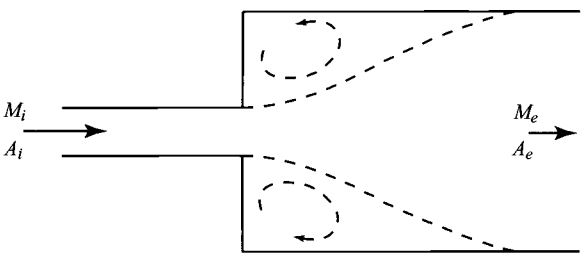

Fig. 10.74 Model dump diffuser.

10.6.7 Fuels

In the early development of the gas turbine engine, it was common belief that this engine could use any fuel that would burn. This is true in theory, but not in practice. The modern turbojet engine is quite particular about the fuel used due to the high rate of fuel flow and wide temperature and pressure variations.

Jet fuel is refined from crude oil petroleum. A typical pound of jet fuel might be composed of 16% hydrogen atoms, 84% carbon atoms, and a small amount of impurities, such as sulfur, nitrogen, water, and sediment. Various grades of jet fuel have evolved during the development of jet engines in an effort to ensure both satisfactory performance and adequate supply. JP-8 is the most commonly used fuel for U.S. Air Force jet engines. The U.S. Navy uses JP-5, a denser, less volatile fuel than JP-8, which allows it to be safely stored in the skin tanks of ships. The most common commercial aircraft fuels are Jet A and Jet A-1. They are alike except Jet A has a freezing point below $-40°$F and Jet A-1 has a freezing point below $-58°$F. Table 10.6 gives specifications for some of the most commonly used jet fuels. The heating value h_{PR} used for most jet fuels is 18,400 Btu/lbm or 42,800 kJ/kg (=10,222 cal/g).

Many aircraft engines are built to operate on any of these fuels. To do so, they must have a special switch on the fuel control to allow it to compensate for differences in specific gravity that is used in fuel metering calculations.

There are many other fuels of interest for use in aircraft gas turbine engines. High-Mach-number aircraft like the SR-71 uses JP-7, a fuel with a very high boiling point. Hydrogen is often considered a fuel because of its very high heating value (h_{PR} of approximately 49,900 Btu/lb or 116,000 kJ/kg) and its capacity to absorb the thermal loads of high-Mach-number flight.

10.7 Main Burners

10.7.1 Types

Turbine engine burners have undergone continuing development over the past 50 years, resulting in the evolution of a variety of basic combustor configurations. Contemporary main burner systems may be broadly classified into one of the three types schematically illustrated in Fig. 10.75: can, cannular, or annular.

A can system consists of one or more cylindrical burners, each contained in a burner case. Because of its modular design, the can system was used during the early development of the turbojet engine. The cannular system consists of a series of cylindrical burners arranged within a common annulus—hence, the name *cannular*. This burner type was the most common in the aircraft turbine engine population, but has been replaced with the annular type in most modern engines. Most modern main burner systems employ the annular design wherein a single burner having an annular cross section supplies gas to the turbine. The improved combustion zone uniformity, design simplicity, reduced linear surface area, and shorter system length provided by the common combustion annulus have made the annular burner the leading contender for all future propulsion systems.

Table 10.6 Jet engine fuels[a]

Property	JP-4		JP-5		JP-8 (Jet A-1)	
	Specification requirement	Typical value	Specification requirement	Typical value	Specification requirement	Typical value
Vapor pressure, atm @ 38°C (100°F)	0.13–0.2	0.18	—	0.003	—	0.007
Initial boiling point, °C	—	60	—	182	—	169
Endpoint, °C	—	246	288	260	288	265
Flash point, °C	—	−25	>63	65	>49	52
Aromatic content, % vol.	<25	12	<25	16	<20	16
Olefinic content, % vol.	<5	1	—	1	—	1
Saturates content, % vol.	—	87	—	83	—	83
Net heat of combustion, cal/g	>10,222	10,388	>10,166	10,277	>10,222	10,333
Specific gravity	0.751	0.758	0.788	0.818	0.755	0.810
U.S. yearly consumption, 10^9 gal		5		1		12

[a]Source: Refs. 12, 15.

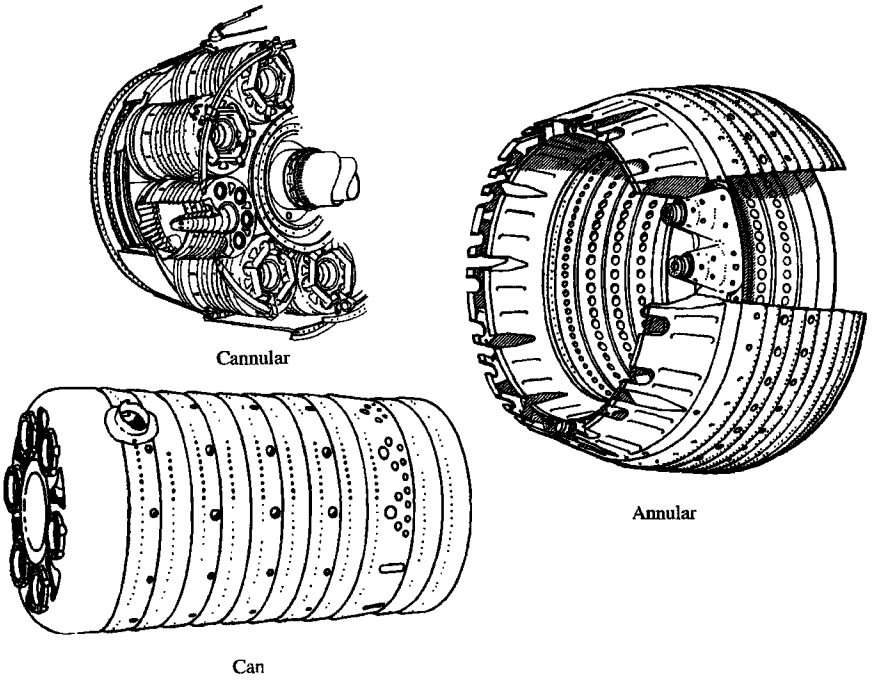

Fig. 10.75 Main burner type. (Courtesy of Pratt & Whitney.)

10.7.2 Main Burner Components

The turbine engine main burner system consists of three principal elements: the inlet diffuser, the dome and snout or cowl, and the liner. In addition, important subcomponents are necessary: the fuel injector, igniter, burner case, and primary swirler, if used. The term *combustion zone* is used to designate that portion of the main burner within the dome and liner. These elements are illustrated in Fig. 10.76.

The purpose of the inlet diffuser is to reduce the velocity of the air exiting the compressor and deliver the air to the combustion zone as a stable, uniform flowfield while recovering as much of the dynamic pressure as possible. The inlet diffuser represents a design and performance compromise relative to required compactness, low-pressure loss, and good flow uniformity. Early inlet diffuser designs were of the smooth curved wall or contoured wall type. Because of the wide variations in the characteristics of the flowfield exiting the compressor, however, the curved wall diffuser cannot always provide uniform, nonseparated flow at all operating conditions. This can become a critical problem in the short-length diffusers required of many current systems. Consequently, a trend toward dump, or combination curved wall and dump, diffuser designs is occurring. Although this design results in somewhat higher total pressure losses, it provides a known and constant point of flow separation at the dump plane, which prevents stalled operation at all diffuser entrance conditions.

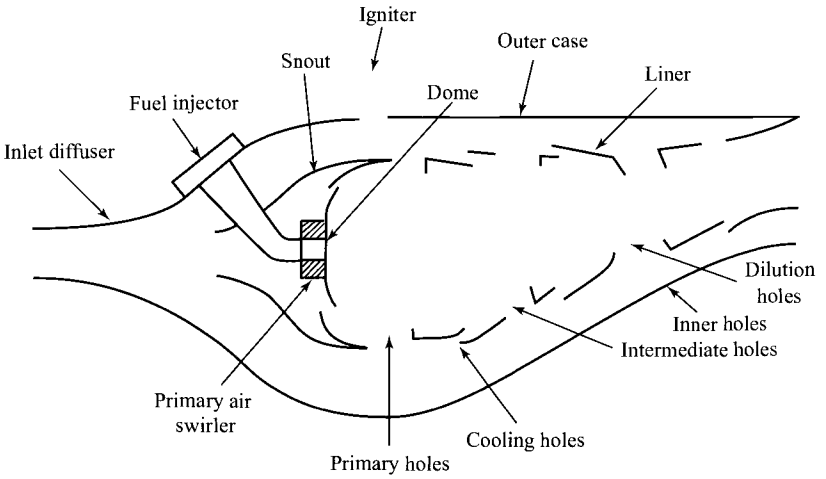

Fig. 10.76 Main burner components (Ref. 67).

The snout divides the incoming air into two streams: primary air and the other airflows (intermediate, dilution, and cooling air). The snout streamlines the combustor dome and permits a larger diffuser divergence angle and reduced overall diffuser length.

The combustor dome is designed to produce an area of high turbulence and flow shear in the vicinity of the fuel nozzle to finely atomize the fuel spray and promote rapid fuel/air mixing. There are two basic types of combustor domes: bluff body and swirl-stabilized. The bluff-body domes were used in early main burners, but swirl-stabilized domes are used in most modern main burners.

The combustion process is contained by the liner. The liner also allows introduction of intermediate and dilution airflow and the liner's cooling airflow. The liner must be designed to support forces resulting from pressure drop and must have high thermal resistance capable of continuous and cyclic high-temperature operation. This requires use of high-strength, high-temperature, oxidation-resistant materials (e.g., Hastalloy X) and cooling air.

Fuel injectors can be classified into four basic types according to the injection method utilized: pressure-atomizing, air blast, vaporizing, and premix/prevaporizing. The first two methods are the most common and are described next, but the reader is directed to other references (e.g., Ref. 38) for a description of the other two methods. In past main burner designs, the most common method of fuel injection was pressure atomizing, which can provide a large flow range with excellent fuel atomization when fuel system pressures are high (500 psi above main burner pressure). The pressure-atomized system is susceptible to fuel leaks (due to high fuel pressures) and plugging of orifices from fuel contaminants. Most modern main burner designs incorporate the air-blast atomizing fuel injector, which achieves fuel atomization and mixing through the use of primary air momentum with strong swirling motion. The air-blast atomizing fuel injector requires lower fuel pressures (50–200 psi above main burner pressure) than the pressure-atomizing type.

Spark igniters, similar to automotive spark plugs, are used to ignite the cold, flowing fuel/air mixture in main burners. These spark igniters produce 4–12 J of ignition energy and require several thousand volts at the plug tip. Main burner starting redundancy is typically provided by use of at least two spark lighters.

10.7.3 Airflow Distribution and Cooling Air

This section identifies and briefly describes the airflow distribution terminology in, around, and through the main burner, resulting in the four basic airflow regions illustrated in Fig. 10.77. Effective control of this air distribution is vital to the attainment of complete combustion, stable operation, correct burner exit temperature profile, and acceptable liner temperatures for long life.

Primary air is the combustion air introduced through the dome or head plate of the burner and through the first row of liner airholes. This air mixes with the incoming fuel, producing the locally near-stoichiometric mixture necessary for optimum stabilization and operation. To complete the reaction process and consume the high levels of primary zone CO, H^-, and unburned fuel, intermediate air is introduced through a second row of liner holes. The reduced temperature and excess oxygen cause CO and H^- concentrations to decrease. In contemporary systems, the dilution air is introduced at the rear of the burner to reduce the high temperature of the combustion gases. The dilution air is used to carefully tailor exit temperature radial and circumferential profiles to ensure acceptable turbine durability and performance. This requires minimum temperatures at the turbine root (where stresses are highest) and at the turbine tip (to protect seal materials). However, modern and future main burner exit temperature requirements are necessitating increased combustion air in the primary and intermediate zones; thus, dilution zone airflow is necessarily reduced or eliminated to permit these increases.

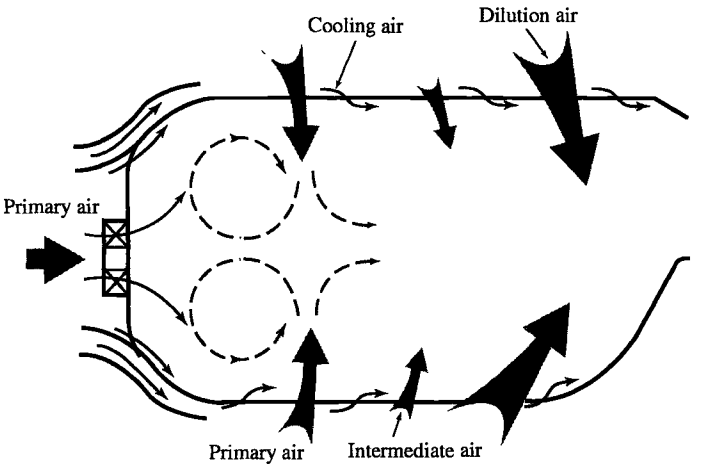

Fig. 10.77 Main burner airflow distribution (Ref. 67).

Cooling air must be used to protect the burner liner and dome from the high radiative and convective heat loads produced within the burner. This air is normally introduced through the liner such that a protective blanket or film of air is formed between the combustion gases and the liner hardware (see Fig. 10.78).

The effectiveness of the cooling technique is quantified by the *cooling effectiveness* Φ, defined by

$$\Phi \equiv \frac{T_g - T_m}{T_g - T_c} \tag{10.44}$$

where T_g, T_m, and T_c, are the mainstream gas, average metal, and cooling air temperatures, respectively.

Figure 10.79 provides design data for the amount of coolant flow required to achieve the desired cooling effectiveness and, thus, desired metal temperature of a combustor liner. Hastalloy X[12,22,38,47] and similar materials are generally used for the main burner liner with a useful upper-limit metal temperature of 1800°F. If film cooling is considered with $T_g = 2400$°F, $T_c = 1200$°F, and $T_m = 1800$°F, then Φ must be at least 0.5, which requires a coolant flow of at least 17% of the combustor flow. Transpiration cooling, using advanced liner construction (e.g., Lamilloy, Ref. 75), can obtain a cooling effectiveness of about 0.8 with 17% cooling air, which can be used to obtain lower average metal temperatures (longer life) or higher gas temperatures (improved performance). As future combustor exit temperature requirements increase, the percentage of combustor air available for cooling decreases and increased cooling effectiveness will be required.

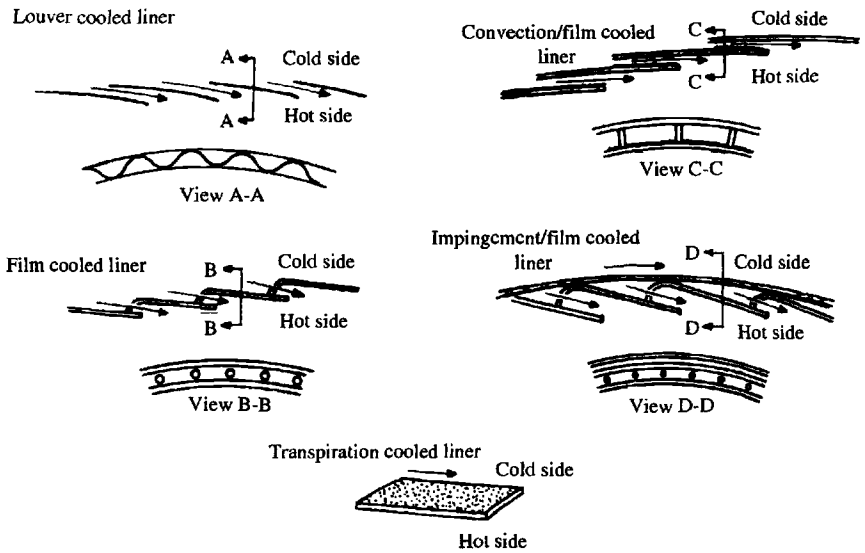

Fig. 10.78 Liner cooling techniques (Ref. 67).

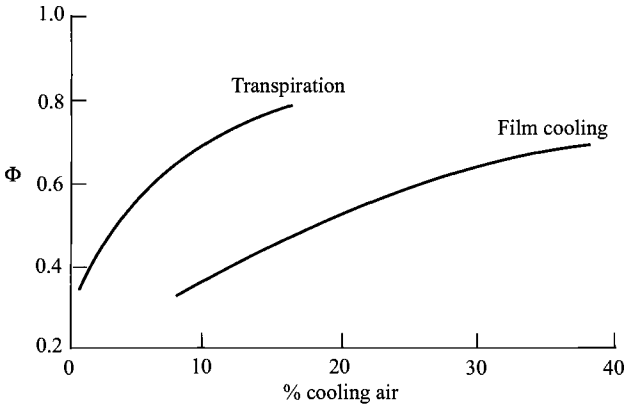

Fig. 10.79 Linear cooling effectiveness (Refs. 75–77).

10.7.4 Performance Parameters

10.7.4.1 Combustion efficiency. Because propulsion system fuel consumption has a direct effect on aircraft system range, payload, and operating cost, it is imperative that design-point combustion efficiency be as close to 100% as possible. By design, combustion efficiency at the high power/fuel consumption conditions of takeoff and cruise is near 100% (usually greater than 99.5%). However, off-design efficiency, particularly at idle, can be in the low 90s. With the advent of chemical emission controls and limitations, this parameter has particular significance during low-power operation because inefficiency and pollution are inextricably linked. For example, combustion efficiency at off-design conditions, such as idle, must now exceed 98.5% to satisfy regulations on exhaust carbon monoxide and unburned hydrocarbons.

One empirical model of combustion efficiency η_b is based on the reaction rate parameter θ and is plotted in Fig. 10.80. The *reaction rate parameter* θ is defined[38,67] as

$$\theta = \frac{P_{t3}^{1.75} A_{\text{ref}} H \exp(T_{t3}/b)}{\dot{m}_3} \times 10^{-5} \tag{10.45}$$

where

P_{t3} = main burner inlet pressure, psi
A_{ref} = main burner, reference area, in.^{2}
H = height of main burner, in.
T_{t3} = main burner inlet temperature, °R
$\dot{m}_3$ = main burner inlet airflow, lbm/s
b = function of local equivalence ratio ϕ and b, given by Herbert[70] as

$$b = 382\left(\sqrt{2} \pm \ell n \frac{\phi}{1.03}\right) \tag{10.46}$$

where plus is used when $\phi < 1.03$ and minus when $\phi > 1.03$.

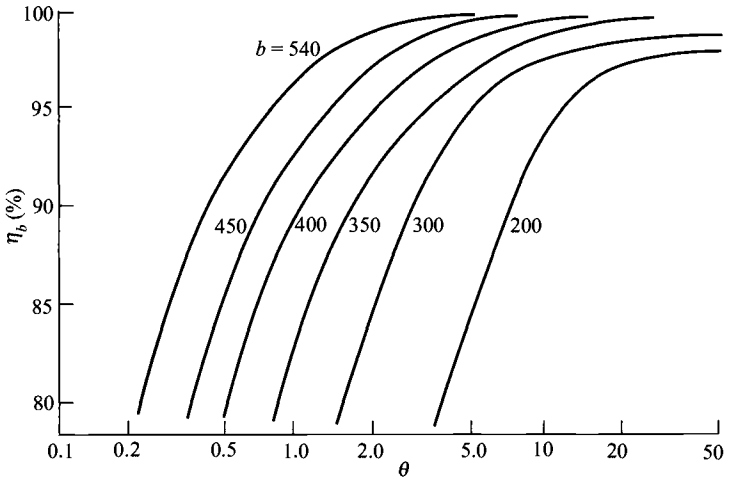

Fig. 10.80 Combustion efficiency vs reaction rate parameter (Ref. 67).

Example 10.9

Determine the combustion efficiency of a main burner with the following data:

$$P_{t3} = 300\,\text{psia}, \quad T_{t3} = 1500^\circ\text{R}, \quad \dot{m}_3 = 60\,\text{lbm/s}, \quad \phi = 0.8$$
$$A_{\text{ref}} = 1.0\,\text{ft}^2, \quad H = 2\,\text{in.}$$

Equation (10.46) gives $b = 444$, Eq. (10.45) gives $\theta = 30$, and Fig. 10.80 gives $\eta_b > 0.995$. For another example, consider the following main burner data:

$$P_{t3} = 2.4\,\text{MPa}, \quad T_{t3} = 800\,\text{K}, \quad \dot{m}_3 = 200\,\text{kg/s}, \quad \phi = 0.9$$
$$A_{\text{ref}} = 0.2\,\text{m}^2, \quad H = 6\,\text{cm}$$

Equation (10.46) gives $b = 488$, Eq. (10.45) gives $\theta = 43.2$, and Fig. 10.80 gives $\eta_b > 0.995$.

10.7.4.2 Overall total pressure loss. The overall total pressure loss of the main burner is the sum of inlet diffuser loss, burner dome and liner loss, and momentum loss resulting from main burner flow acceleration attendant with increased gas total temperature. It is normally expressed as a percentage of the compressor discharge pressure. Total pressure losses of 4–5% are typically encountered in current systems. Main burner system pressure loss is recognized as necessary to achieve certain design objectives (pattern factor, effective turbine cooling, etc.), and it can also provide a stabilizing effect of main burner aerodynamics. However, total pressure loss also impacts engine thrust and thrust

specific fuel consumption. Consequently, design goals for main burner total pressure loss represent a compromise among the preceding factors.

Equation (10.38) may be used to obtain a preliminary estimate of the main burner total pressure losses excluding the inlet diffuser and liner. Equation (10.42b), in combination with Fig. 10.73 and/or Eq. (10.43), may be used to obtain a preliminary estimate of the inlet diffuser total pressure ratio. Liner total pressure loss can be approximated as the dynamic pressure of the passage air.

10.7.4.3 Exit temperature profile. Two performance parameters are related to the temperature uniformity of the combustion gases as they enter the turbine. To ensure that the proper temperature profile has been established at the main burner exit, combustion gas temperatures are often measured by means of high-temperature thermocouples or via gas-sampling techniques employed at the main burner exit plane. A detailed description of the thermal field entering the turbine both radially and circumferentially can be determined from these data. A simplified expression called the *pattern factor* or *peak temperature factor* may be calculated from these exit temperature data. The *pattern factor* PF is defined as

$$\text{PF} \equiv \frac{T_{t\,\max\,\text{av}} - T_{t\,\text{av}}}{T_{t\,\text{av}} - T_{t\,\text{in}}} \tag{10.47}$$

where

$T_{t\,\max}$ = maximum measured exit temperature (local)
$T_{t\,\text{av}}$ = average of all temperatures at exit plane
$T_{t\,\text{in}}$ = average of all temperatures at inlet plane

Contemporary main burners exhibit pattern factors ranging from 0.25 to 0.45. Pattern factor goals are based primarily on the design requirements of the turbine first-stage stationary airfoils. Thus a pattern factor of 0.0 is not required. Durability considerations require the new high-temperature-rise main burners to have exit temperature profiles corresponding to pattern factors in the range of 0.15 to 0.25.

The *profile factor* P_f characterizes the main burner average exit temperature profile and is defined by

$$P_f \equiv \frac{T_{t\,\max\,\text{av}} - T_{t\,\text{in}}}{T_{t\,\text{av}} - T_{t\,\text{in}}} \tag{10.48}$$

where $T_{t\,\max\,\text{av}}$ is the maximum circumferential average temperature. Main burners exhibit profile factors ranging from 1.04 to 1.08, with 1.06 being the common design goal. Profile factor goals are based primarily on the design requirements of the turbine first-stage rotating airfoils, which are exposed to average gas temperature leaving the first-stage stationary airfoils.

Pattern factor and profile factor are important main burner design parameters. They describe the possible thermal impact on the turbine and are critical factors

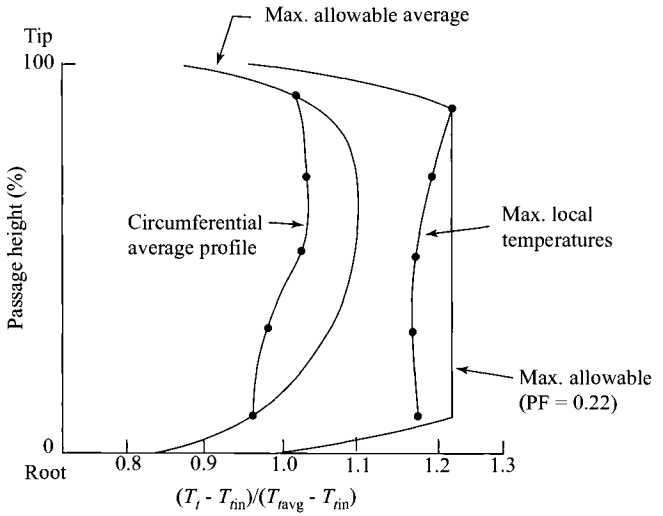

Fig. 10.81 Radial temperature profile at main burner exit (Ref. 67).

in matching the main burner and turbine components. Failure to achieve the required pattern factor and/or profile factor will normally result in shorter turbine life and may require redesign of the main burner and/or turbine.

Although the pattern factor and profile factor define the peak and average turbine airfoil gas temperatures, the shape of the burner exit temperature radial profile is the critical factor controlling turbine airfoil life. Figure 10.81 illustrates typical radial profile characteristics and their attendant relationship with the pattern factor. By proper control of dilution air, the burner exit temperature field is tailored to give the design pattern factor and radial profile consistent with turbine requirements.

10.7.4.4 Ignition. Reliable ignition in the main burner system is required during ground-level startup and for relighting during altitude windmilling. The broad range of main burner inlet temperature and pressure conditions encompassed by a typical ignition/relight envelope is illustrated in Fig. 10.82. It is well known that ignition performance is improved by increases in main burner pressure, temperature, fuel/air ratio, and ignition source energy. In general, ignition is impaired by increases in reference velocity, poor fuel atomization, and low fuel volatility.

Development work[78] in the application of the double-annular combustor design (Fig. 10.83) to main burners having a high temperature rise ($T_{t4} - T_{t3} =$ 1000–1400°C or 1800–2500°F) has shown very good low-throttle operation when the outer annulus is designed to operate as the pilot stage with lower airflows than the inner annulus. Only the pilot stage of this double-annular combustor is fueled at starting, altitude relight, and idle conditions. This pilot-stage design attains the desired low air velocities and rich fuel/air ratios at low-temperature-rise conditions of starting, altitude relight, and idle.

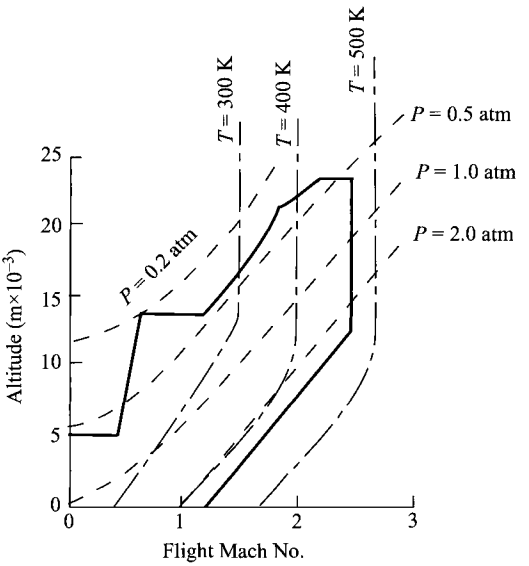

Fig. 10.82 Ignition/relight envelope (Ref. 67).

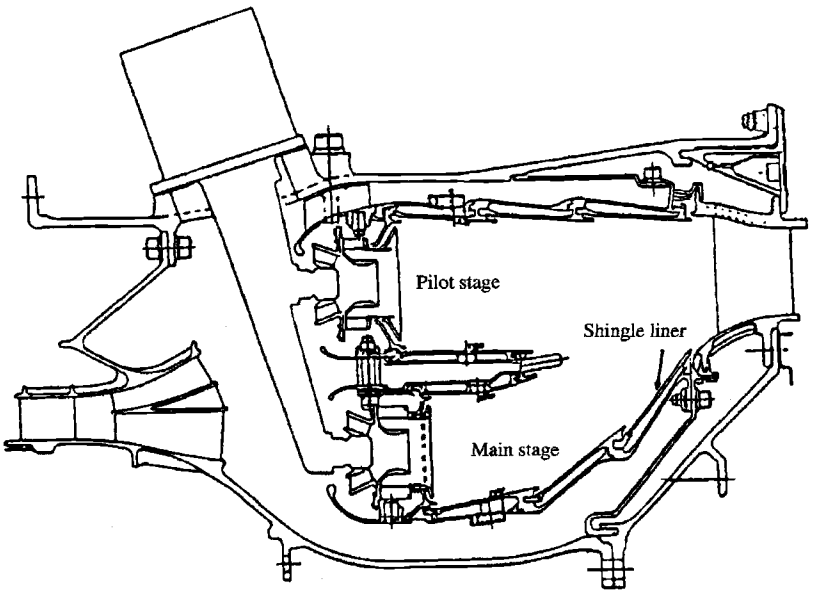

Fig. 10.83 Double-annular main burner (Ref. 78).

10.7.5 Main Burner Design Parameters

The design of main burner systems for aircraft gas turbine engines is a complex and difficult problem that is usually solved by reaching a reasonable compromise between the conflicting requirements. Design involves a broad range of technical disciplines including combustion chemistry, fluid dynamics, heat transfer, stress analysis, and metallurgy. Although there are many design parameters for a main burner, most experts would include the following in their list of most critical design parameters:

1) Equivalence ratio ϕ
2) Combustor loading parameter (CLP)
3) Space heat release rate (SR)
4) Reference velocity V_{ref}
5) Main burner dome height H_d
6) Main burner length/dome height ratio L_{mb}/H_d
7) Main burner dome velocity
8) Passage velocity V_{pass}
9) Number and spacing of fuel injectors
10) Pattern factor correlation parameters (PF)
11) Profile factor correlation parameters P_f

The *space heat release rate or space rate* (SR) is

$$\text{SR} \equiv \frac{f\dot{m}_3 h_{PR}(3600)}{P_{t3}(\text{volume})} \tag{10.49}$$

and generally is between 5×10^6 and 10×10^6 Btu/(h · ft^3 · atm) [0.5 and 1.0 W/(m^3 · Pa)]. The reference velocity is defined as

$$V_{\text{ref}} \equiv \frac{\dot{m}_3}{\rho_{t3} A_{\text{ref}}} \tag{10.50}$$

where A_{ref} is the cross-sectional area across the whole main burner at the primary combustion zone.

Taylor[79] gives the following typical values of design parameters: The reference velocity is typically from 60 to 100 ft/s (18–30 m/s); the ratio of main burner length to dome height L_{mb}/H_d is 2.73–3.5; velocities in the main burner dome are generally around 30 ft/s (9 m/s) and in the passages 120–200 ft/s (36–60 m/s); fuel injectors are typically spaced about one dome height apart in the circumferential direction; and fuel injectors require at least 25% of their design fuel rate to obtain good fuel atomization.

The use of selective fuel injection is a method of modulating primary zone equivalence ratio at very low engine throttle settings. Tests were reported in Ref. 78 on the minimum fuel/air ratio f for the CF6-50 main burner with selective fuel injection patterns, and these results are presented in Fig. 10.84. In addition to low engine throttle operation, use of a selective fuel injection pattern can improve engine starting and relight.

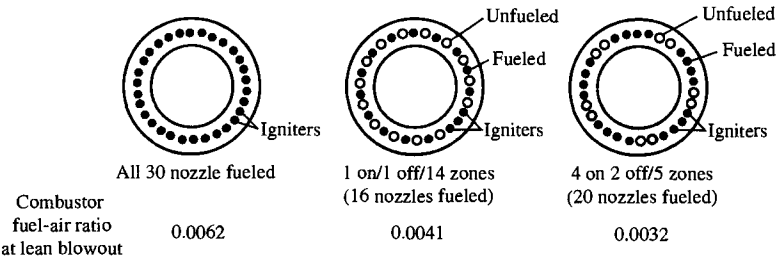

Fig. 10.84 Lean blowout characteristics of CF6-50 main burner with selective fuel injection patterns (Ref. 78).

10.8 Afterburners

Afterburning or reheating is one method of augmenting (increasing) the basic thrust of the turbojet engine or the turbofan engine, when required, without having to use a larger engine with its concurrent penalties of increased frontal area and weight. The afterburner increases thrust by adding thermal energy to the entering gas stream. For a turbojet engine, this gas stream corresponds to the exhaust gases of the turbine. However, for the augmented turbofan engine, this gas stream may be a mixture of the bypass air and the turbine exhaust gases. At the afterburner inlet, there is still much uncombined oxygen in the gas stream. The higher inlet temperatures and near-stoichiometric fuel/air ratio of the afterburners enable them to operate with a simpler configuration (see Figs. 10.85a and 10.85b) than the main burner can. The resultant increase in temperature raises the exhaust velocity of the exiting gases and, therefore, boosts engine thrust. Most afterburners will produce an approximate 50% thrust increase, but with a corresponding threefold increase in fuel flow.

Because the specific and actual fuel consumptions are considerably higher during the time the engine is in the afterburning or *hot* (also called *wet*) operation, as compared to the nonafterburning or *cold* (also called *dry*) mode of operation, afterburning is used typically for the time-limited operation of takeoff, climb, and maximum bursts of speed.

For a turbofan engine, augmentation can be used in both fan and core streams. Afterburning in a separate fan stream is normally referred to as *duct burning*, and this alone or in combination with afterburning in the core stream may be advantageous for certain flight conditions.

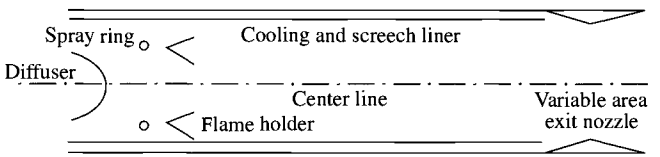

Fig. 10.85a Typical afterburner components.

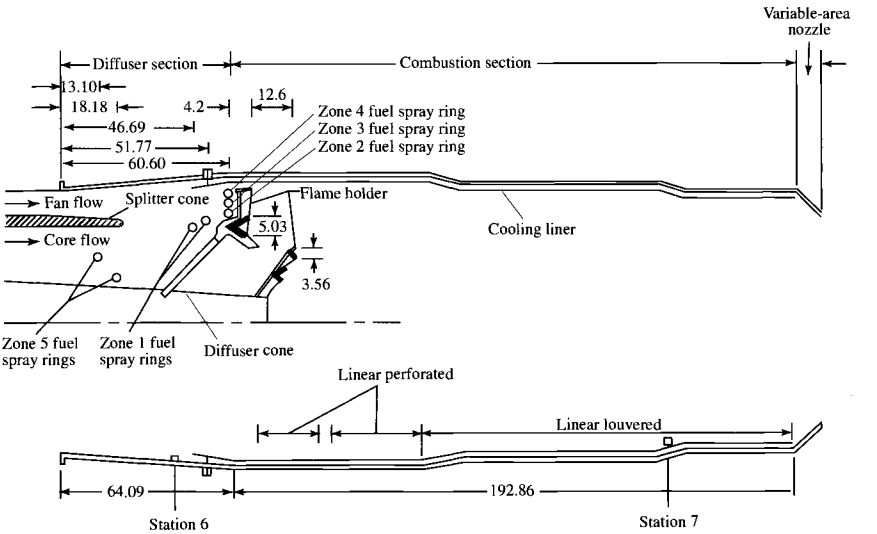

Fig. 10.85b Afterburner for TF30-P-3 augmented turbofan engine (all dimensions are in centimeters) (from Ref. 80).

The major components of an afterburner are shown in Figs. 10.85a and 10.85b. Gas leaving the turbine is deswirled and diffused, fuel is added by fuel spray bars (tubes) or rings, the combustion process is initiated by igniter or pilot burner in the wake of a number of flame-stabilizing devices (flame holders), and the thermal energy of combustion is mixed along flame surfaces spreading downstream from the stabilizing devices. Also, a liner is used in afterburners as both a cooling liner and a screech or antihowl liner (*screech* and *howl* are acoustic combustion instabilities). This liner can also serve as a passage for the cooling air required by the exhaust nozzle. All engines incorporating an afterburner must also be equipped with a variable-area throat exhaust nozzle to provide for proper operation under afterburning and nonafterburning conditions. In addition to these components, an afterburner will require the following components:

1) Afterburner fuel pump
2) Afterburner fuel control
3) Pressurizing valve, if multistage operation is required
4) Connections (mechanical and pressure) from the main fuel control, throttle, and engine

Specific design requirements for an afterburner are as follows:

1) Large temperature rise. The afterburner does not have to provide for the physical and temperature limits of the turbine. The temperature rise is limited mainly by the amount of oxygen that is available for combustion and the liner and nozzle cooling air requirements.

2) Low dry loss. The engine suffers a very slight penalty in thrust during cold operation due principally to the drag caused by the flame holders, fuel spray bars, and walls of the afterburner.

3) Wide temperature modulation. This is necessary to obtain *degrees* (also called *zones* or *stages*) of afterburning for better control of thrust.
4) High combustion efficiency.
5) Short length; light weight.
6) Altitude light-off capability.
7) No acoustic combustion instabilities.
8) Long life, low cost, easy repair.

10.8.1 Afterburner Components

This section covers the major afterburner components associated with the flow passage and combustion process. Although it is brief, the major features affecting preliminary engine design are addressed. The open literature contains a wealth of information on each individual component, and the interested reader may want to research a particular component further.

10.8.2 Diffuser

The flow entering the afterburner is first slowed to a Mach number that provides a balance between the total pressure loss and the afterburner cross-sectional area. The minimum Mach number entering the combustion zone of the afterburner is usually fixed by a requirement that the diameter of the afterburner section not exceed that of the engine components located upstream. A short diffuser length is desired without producing flow separation to reduce engine weight and length. In augmented turbofan engines, the diffuser may be combined with a mixer so that a mixed stream enters the combustion section.

10.8.3 Fuel Injection, Atomization, and Vaporization

This subject area is best summarized by Zukoski[67,70] and is quoted here:

> The goal of the fuel injection stream is to produce a specified distribution of fuel vapor in the gas stream entering the afterburner. In most engines, fuel is introduced in a staged manner so that heat addition rate can be increased gradually from zero to the desired value. Because ignition, flame stabilization, and flame spreading are easiest to achieve when the fuel/air ratio is close to the stoichiometric value, staging is usually produced by adding fuel to successive annular stream tubes so that the mixture ratio in each tube is nearly stoichiometric. Each stream tube has its own set of fuel injectors and control system which can be activated independently. For example, see the two sets of injectors used in the F100 engine shown as items 6 and 7 in [Fig. 10.86].
>
> The most remarkable fact concerning the fuel system for afterburners is their simplicity. In many engine systems, fuel is supplied to a circular tube which lies with its axis perpendicular to the gas stream. Fuel is injected into the gas through small diameter holes located in the sides of the tubes such that the liquid jet enters the gas stream in a direction perpendicular to the undisturbed flow direction. The liquid jet penetrates some distance into the gas stream before its momentum is dissipated. During this penetration process, the air stream tears the jet apart and produces droplets with diameters of micron size. Heat transfers from the hot gas stream then vaporizes the droplets.
>
> Given the wide range of values of mass flow of fuel required, it is remarkable that reasonably thorough mixing of the fuel with the air can be achieved with this simple

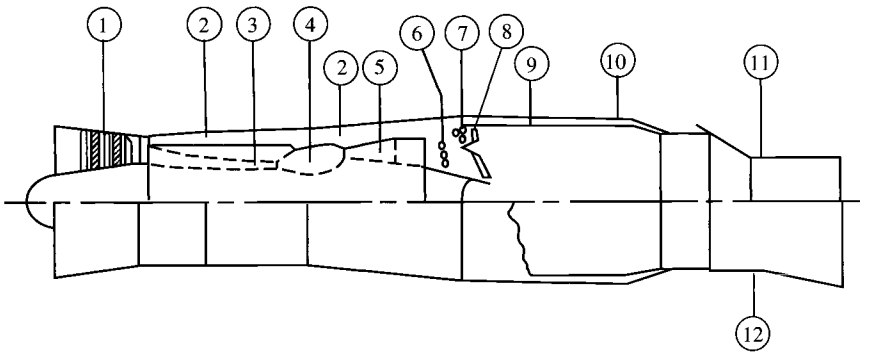

Fig. 10.86 Pratt & Whitney F100-PW-100 augmented turbofan engine (Ref. 67): 1) three-stage fan; 2) bypass duct; 3) core engine compressor; 4) main burner; 5) turbine; 6) fuel injectors for core engine gas stream; 7) fuel injections for bypass airsteam; 8) flame stabilizer for afterburner; 9) perforated afterburner linear; 10) afterburner case; 11) nozzle closed to minimum area; and 12) nozzle opened to maximum area.

injection system. In some recent engines, efforts are being made to use simple variable area injector ports which may possibly give better preparation of the fuel/air mixture.

The whole area of fuel penetration, atomization, and vaporization is not well understood from first principles and one of the time-consuming parts of an afterburner development program is to determine the optimum distribution of locations for injector tubes, injector parts, and port diameters.

10.8.4 Ignition

Ignition of the fuel/air mixture in the afterburner is usually accomplished by using a spark or arc igniter or a pilot burner. Once initiated in the primary stream tube, combustion continues in the wake of a flame stabilizer (a bluff body) and the process will spread to the rest of the flame stabilizers if the wakes of the stabilizers overlap.

The spark or arc igniter uses a high-energy electric arc to initiate combustion of the primary stream tube. The igniter is usually placed in the wake of a sheltered flame stabilizer having its own fuel supply. A stable flame results, and combustion is initiated behind other flame stabilizers by the mechanism mentioned previously.

As described earlier, ignition in an afterburner system will be easiest to achieve in gas having a local equivalence ratio near unity, in a region of the stabilization system where the residence times are longest, and where the pressures and temperatures are highest. When such a region is not available, a pilot burner can be used to locally create this region.

The pilot burner consists of a pilot zone where a small portion of the inlet air (usually 10% or less) is burned to stoichiometric temperatures in an enclosed protected region. The hot gases generated by the pilot burner are used as an ignition and stabilizing source for the main fuel injection system.

Afterburning for turbofan engines such as the Pratt & Whitney F100 is accomplished by adding fuel first to the core flow near the interface between the core and fan streams, then to the fan stream, and finally to the rest of the core flow. Afterburning in the fan stream produces the largest performance gain because of the low temperature of this stream. However, the fan stream's low temperature makes the fuel vaporization and afterburning very difficult. By adding fuel first to the core flow near its interface with the fan stream, the resulting afterburning stream can act as a pilot for the combustion process in the fan stream.

10.8.5 Flame Stabilization

Two general types of flame-stabilizing devices that have been used in afterburners are shown in Fig. 10.87: bluff-body vee-gutter flame holders and piloted burners where a small piloting heat source is used to ignite the main fuel flow. The bluff-body vee-gutter flame holders have the advantage of low flow blockage and low total pressure loss. They are simple and lightweight and have a good development history.

The wake of a flame holder, shown in Fig. 10.88, is divided into two regions: a recirculation zone and mixing zones. The recirculation zone is characterized by a strong circulating flow, very low reaction rates, and a temperature that is nearly equal to the adiabatic flame temperature corresponding to the fuel/air mixture ratio of the approaching stream. The mixing zones are characterized as turbulent regions of very strong shear, steep temperature gradients, and vigorous chemical reaction.

A stable flame is established in the mixing zones by a balance of the continuing entrainment of cool unburned gas and the heat and species transfer from the hot burned gases. The residence time of the gas in the mixing zone establishes whether a stable flame is established or the flame is blown off. Flame stabilization is characterized by the values of the velocity at the edge of the mixing zones V_2, the length of the recirculation zone L, and the characteristic ignition time t_c. This

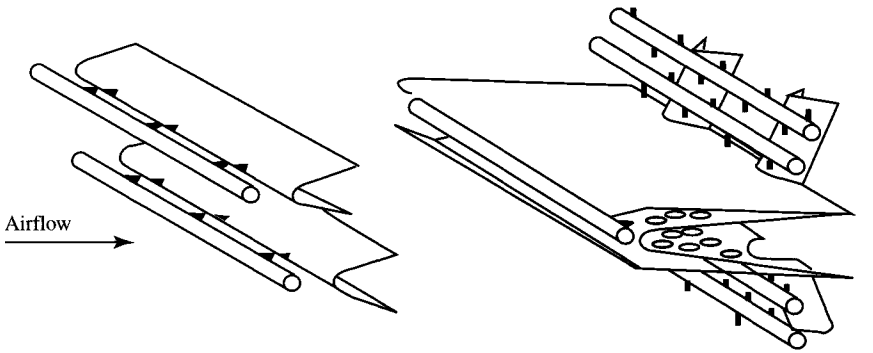

a) Vee-gutter flame holders **b) Piloted burner**

Fig. 10.87 Common afterburner flame holders (Ref. 81).

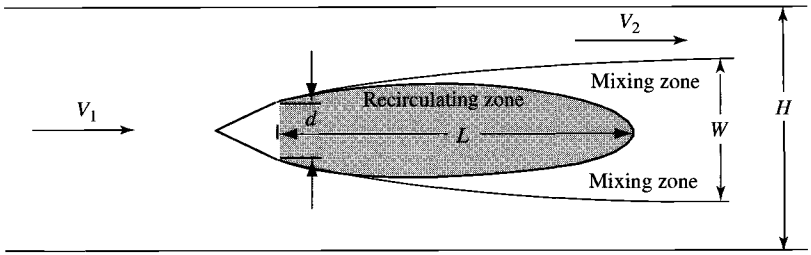

Fig. 10.88 Typical flame holder used in analysis of stabilization: V_1 = velocity of approaching steam, V_2 = velocity of flow at edge of mixing zone, d = width of flame holder, L = length of recirculation zone, W = width of wake, and H = height of the duct.

ignition time is determined experimentally at conditions that result in flame extinction or blowoff and the definition

$$t_c \equiv \frac{L}{V_{2c}} \tag{10.51}$$

where the subscript c denotes values corresponding to flame extinction or blowoff. Thus the flame extinction or blowoff criteria can be expressed as

$$\left(\frac{V_{2c}t_c}{L}\right)_{\text{blowoff}} = 1 \tag{10.52}$$

Numerous experiments with a wide range of flame holder and duct configurations have shown that the ignition time is essentially independent of the geometry and velocity as long as the flow is turbulent. The ignition time depends on a number of chemical parameters such as fuel type, fuel/air ratio, gas temperatures and pressures, and degree of vitiation.

The variation of the characteristic ignition time t_c with equivalence ratio ϕ is shown in Fig. 10.89 for a hydrocarbon fuel with a molecular weight of about 100. Note that t_c increases very rapidly for both high and low values of ϕ. In general, t_c decreases rapidly as the static temperature of the approach stream increases and varies inversely with static pressure for hydrocarbon fuels like JP-8. This variation with temperature and pressure can be approximated by

$$t_c \propto \frac{1}{PT^{2.5}} \tag{10.53}$$

Flame holder stability calculations using Eq. (10.52) required values of t_c,, V_2, and L. The characteristic ignition time can be obtained from Fig. 10.89. However, V_2 and L are not simply related to the size of the flame holder d and the velocity of the approach stream V_1. Rewriting Eq. (10.52) in a more

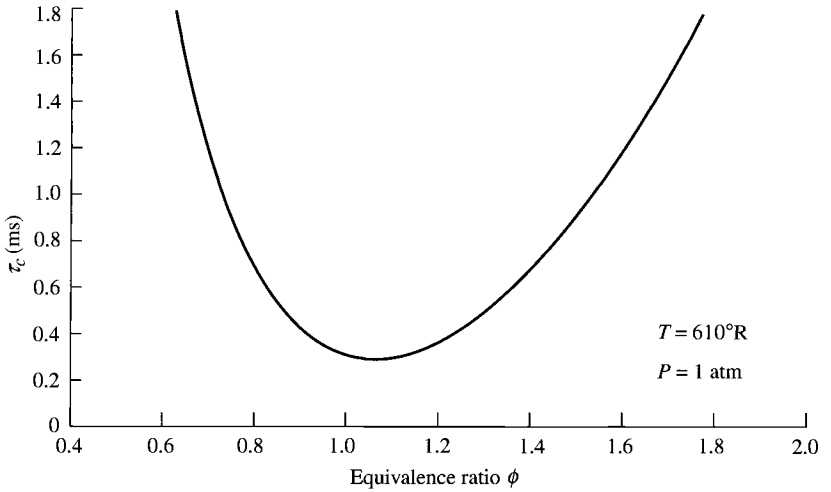

Fig. 10.89 Variation of characteristic ignition time with equivalence ratio (Ref. 67).

convenient form gives

$$\left(\frac{V_{1c}t_c}{H}\right)_{\text{blowoff}} = \frac{V_1}{V_2}\frac{L}{W}\frac{W}{H} \tag{10.54}$$

To apply this criterion, values of V_1/V_2, L/W, and W/H are needed as functions of flame holder geometry, fluid dynamic parameters, and the blockage ratio B, where

$$B \equiv \frac{d}{H} \tag{10.55}$$

Calculations by Cornell[82] yielded relationships between the blockage ratio B and values of V_2/V_1 and W/d for wedge half-angles of 15–90 deg (a flat plate) and are presented in Table 10.7. Tests of a variety of bluff-bodies show that the length/width ratio of the recirculation zone L/W depends only on the geometry of the bluff-body, and the majority of the data lie in the range of 3.6 to 4.0. For the preliminary design, this ratio can be approximated[67] by

$$\frac{L}{W} \approx 4 \tag{10.56}$$

Now, all of the parameters of Eq. (10.54) can be determined for a given flame holder shape and blockage ratio.

Example 10.10

Consider a flame holder stability calculation.

Given:

$$T = 1000°\text{R}, P = 0.2 \text{ atm}, M_1 = 0.25, \gamma = 1.3$$

$$\phi = 0.8, H = 1 \text{ ft}, B = 0.2$$

and a 15-deg half-angle flame holder. Table 10.7 gives $W/d = 1.5$ and $V_2/V_1 = 1.42$. Then $W/H = (W/d)(d/H) = (1.5)(0.2) = 0.3$. Thus, with $L/W = 4$, Eq. (10.54) gives

$$\left(\frac{V_{1c}t_c}{H}\right)_{\text{blowoff}} = \left(\frac{1}{1.42}\right)(4)(0.3) = 0.845$$

Figure 10.89 gives $t_c = 0.7$ ms at 610°R, $\phi = 0.8$, and 1 atm. Thus, at 1000°R, $\phi = 0.8$, and 0.2 atm, Eq. (10.53) gives $t_c = 1.017$ ms. Using this value of t_c and $H = 1$ ft, we get $V_{1c} = H/t_c = 983.3$ ft/s. For $T = 1000°\text{R}$, $M_1 = 0.25$, and $\gamma = 1.3$, then $V_1 = 373$ ft/s and $V_2 = 530$ ft/s. Since $V_1 < V_{1c}$, flame stabilization will occur at the given conditions.

10.8.6 Multiple-Flame-Holder Arrays

The material just presented on flame holder stabilization was restricted to a single flame holder located on the centerline of a constant-area duct. When multiple flame holders are positioned in a single plane perpendicular to the approaching flow and spaced so that each lies on the centerline of equivalent ducts of equal height, then the preceding analysis can be used directly to estimate the stability characteristics. When flame holders are spaced irregularly, the analysis just presented does not directly apply. However, this analysis is useful in a qualitative manner.

10.8.7 Flame Spread

To achieve maximum combustion efficiency, the afterburner length needs to be longer than the burning length. The complex flame holder shape and

Table 10.7 Dependence of wake width W and edge velocity V_2 on blockage ratio B and wedge half-angle α[a]

	$\alpha = 15$ deg		$\alpha = 90$ deg	
$B = d/H$	W/d	V_2/V_1	W/d	V_2/V_1
0.05	2.6	1.15	4.0	1.25
0.10	1.9	1.23	3.0	1.43
0.20	1.5	1.42	2.2	1.75
0.30	1.3	1.62	1.7	2.09
0.40	1.2	1.90	1.6	2.50
0.50	1.2	2.30	1.4	3.16

[a]Source: Ref. 12.

interactions do not permit determination of afterburner length from the burning length measurements of basic flame holder experiments. However, most modern afterburners use 17 deg total angle for estimating spread.

10.8.8 Afterburner Liner

The afterburner liner is used as a cooling liner and to improve combustion stability. As a cooling liner, it isolates the very high temperatures from the outer casing (similar to the liner of the main burner). A film of cooler air is distributed along the length of the cooling liner, which reduces the metal temperature of this liner and subjects the outer casing of the afterburner to the afterburner pressure and temperature of the cooling flow.

The liner is also used as a screech or antihowl liner to prevent extreme high frequency and amplitude pressure fluctuations resulting from combustion instability or the unsteady state of thermal energy. This function is accomplished by use of multiple holes along the initial length of the liner. Selective frequencies can be dampened by the selection of the proper size hole.

10.8.9 Total Pressure Loss

The total pressure loss of the afterburner is mainly composed of that due to the diffuser, to the drag of the flame holders, and to the combustion process. The total pressure ratio of the diffuser can be estimated by the methods presented earlier. The total pressure ratio due to the friction of the flame holders and combustion process can be estimated, by using Eqs. (10.35–10.38), provided that C_D of the flame holders, based on the duct area and upstream velocity V_1, is known. The drag coefficient of a bluff-body is about 1.0 (Ref. 83) based on the frontal area and the edge velocity (V_2 of Fig. 10.88). This drag coefficient can be expressed in terms of a C_D based on the duct area and upstream velocity V_1 by

$$C_D \approx B\left(\frac{V_2}{V_1}\right)^2 \tag{10.57}$$

where B is the blockage ratio [see Eq. (10.55)].

10.8.10 Afterburner Design Parameters

The design of the afterburner system for aircraft gas turbine engines is a difficult problem and involves compromise similar to the complexity of the main burner system. The major design parameters for the afterburner include: 1) equivalence ratio ϕ, 2) reference Mach number M_{ref}, 3) flame holder blockage B, 4) flame holder width d, 5) flame holder edge Mach number, 6) afterburner burning length, 7) spray bar spacing, and 8) space heat release rate (SR).

The reference Mach number is at the entrance to the afterburner and ranges from 0.20 to 0.25. Flame holder blockage is normally 30–40% with an edge Mach number of about 0.30. The burning length is 35–50 in. (0.9–1.3 m), and the spray bar spacing is about 3 in. (8 cm) at the outer flame holder position.[79]

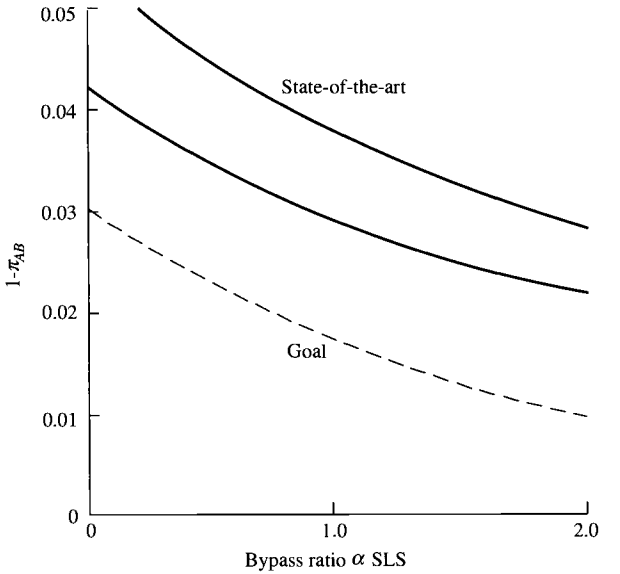

Fig. 10.90 Afterburner total pressure loss (Ref. 84).

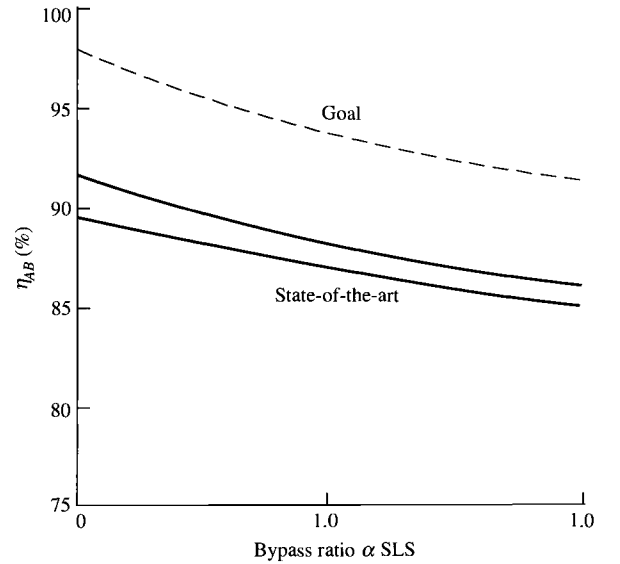

Fig. 10.91 Afterburner combustion efficiency (Ref. 84).

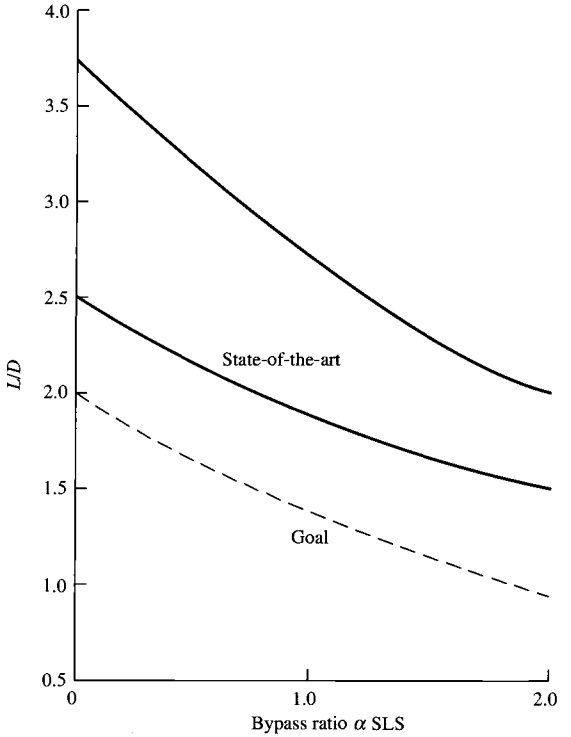

Fig. 10.92 Afterburner size (Ref. 84).

A space heat release rate [Eq. (10.49)] near 8×10^6 Btu/(h · ft^3 · atm) [0.8 W/(m^3 · Pa)] is desired.[81]

The performance and size of the afterburner of an augmented turbofan engine depend on the bypass ratio,[84] as shown in Figs. 10.90, 10.91, and 10.92. Both the current state-of-the-art and the goal of future afterburner development are shown.

Problems

10.1 Develop Eq. (10.1) in SI units.

10.2 Determine the throat diameter of an inlet for the turbojet engine of Example 8.4 for subsonic operation ($M_0 < 0.8$).

10.3 Determine the throat diameter of an inlet for the turbofan engine of Example 8.9 for subsonic operation ($M_0 < 0.8$).

10.4 Determine the throat diameter of an inlet for the turboprop engine of Example 8.11 for subsonic operation ($M_0 < 0.8$).

10.5 A fixed-area internal compression inlet has a capture/throat area ratio A_c/A_t of 1.2. Determine the following:
(a) The Mach number at which the inlet will start.
(b) The Mach number at the throat after starting.
(c) The π_d of the inlet after starting with the shock at the throat.
(d) The Mach number at which the inlet will unstart.

10.6 A ramjet is to fly at 9-km altitude and Mach 2.3. Determine the following:
(a) The inlet contraction ratio A_c/A_t of a fixed-area internal compression inlet for this ramjet and its maximum pressure recovery when operated at the preceding conditions.
(b) Maximum pressure recovery of the inlet of part a when operated at Mach 2.7.

10.7 A ramjet is to fly at 30-kft altitude and a speed of 2388 ft/s. Determine the following:
(a) The inlet contraction ratio A_c/A_t of a fixed-area internal compression inlet for this ramjet and its maximum pressure recovery when operated at the preceding conditions.
(b) Maximum pressure recovery of the inlet of part a when operated at a flight velocity of 2786 ft/s.

10.8 A ramjet that is to cruise at 20-km altitude and 767.2 m/s has the ability to overspeed to 914.7 m/s prior to attaining its final cruise condition. Determine the best inlet contraction ratio A_c/A_t of a fixed-area internal compression inlet for this ramjet and its maximum pressure recovery when operated at cruise conditions.

10.9 A ramjet that is to cruise at 60-kft altitude and Mach 2.5 has the ability to overspeed to Mach 3.0 prior to attaining its final cruise condition. Determine the best inlet contraction ratio A_c/A_t of a fixed-area internal compression inlet for this ramjet and its maximum pressure recovery when operated at cruise conditions.

10.10 You are required to design an internal compression inlet with a fixed capture area A_c of 14 ft^2 (1.3 m^2) that will operate for a cruise Mach number M_0 of 2.5 with an inlet throat Mach number M_t of 1.2.
(a) Determine A_t and A_c/A_t for cruise.
(b) If the throat area is held constant, can this inlet be started for M_0 of 4.0 or less?
(c) If it is desired to start the inlet at $M_0 = 2.0$, find the required values of A_c/A_t and A_t.

10.11 An aircraft with a turbojet engine uses a fixed contraction ratio, internal compression inlet designed for $M_0 = 3.0$. The aircraft is flying at $M_0 = 2.0$ with the inlet started, and the shock is optimally positioned when the inlet suddenly unstarts, popping the shock.
(a) Find the maximum pressure recovery for the started and unstarted conditions.

(b) Find the ratio of the unstarted inlet mass flow rate to the started inlet mass flow rate.

10.12 For supersonic flight conditions, a conservative estimate of the inlet drag is the momentum loss of the bleed and bypass air. Variable A_1 is the capture area of an inlet, and A_0 is the freestream area for the engine mass flow rate (see Fig. 10.36).

(a) Show that the inlet drag coefficient can be written as

$$\phi_{\text{inlet}} = \frac{\rho_0 V_0 (A_1 - A_0)(V_0 - V_e)}{F g_c}$$

where V_e is the axial velocity with which the bypass and bleed flows leave the inlet.

(b) For adiabatic flow with $M_e = 1$, show that the preceding equation becomes

$$\phi_{\text{inlet}} = \frac{(A_1/A_0 - 1)\{M_0 - \sqrt{2/(\gamma+1) + [(\gamma-1)/(\gamma+1)]M_0^2}\}}{F g_c/(\dot{m}_0 a_0)}$$

(c) Using the A_{0i}/A_1, results of Fig. 10.46, calculate and plot ϕ_{inlet} for $F g_c/(\dot{m}_0 a_0) = 3.0$.

10.13 Determine the total pressure recovery η_r and area ratio A_{0i}/A_s of a pitot inlet with a normal shock over the range of Mach numbers from 1 to 2. Compare this inlet's performance to that of Examples 10.3 and 10.4.

10.14 Determine the total pressure recovery η_r and area ratio A_{0i}/A_s of an external compression inlet with a single 10-deg ramp over the range of Mach numbers from 1 to 2. Compare this inlet's performance to that of Examples 10.3 and 10.4.

10.15 Determine the total pressure recovery η_r and area ratio A_{0i}/A_s of an external compression inlet with a single 8-deg ramp over the range of Mach numbers from 1 to 2. Compare this inlet's performance to that of Examples 10.3 and 10.4.

10.16 Calculate the dimensions and values of C_{fg}, F_g, and C_V, for an axisymmetric exhaust nozzle with a mass flow rate of 150 lbm/s and the following data:

$$P_{t8} = 25\,\text{psia}, \quad T_{t8} = 3600°\text{R}, \quad A_9/A_8 = 1.8, \quad \gamma = 1.3$$

$$R = 53.4\,\text{ft}\cdot\text{lbf}/(\text{lbm}\cdot°\text{R}), \quad P_{t9}/P_{t8} = 0.98, \quad C_D = 0.98, \quad P_0 = 3\,\text{psia}$$

10.17 Calculate the dimensions and values of C_{fg}, F_g, and C_V for an axisymmetric exhaust nozzle with a mass flow rate of 75 kg/s and the

following data:

$$P_{t8} = 350\,\text{kPa}, \quad T_{t8} = 1600\ \text{K}, \quad A_9/A_8 = 1.8, \quad \gamma = 1.33$$
$$R = 0.287\,\text{kJ(kg}\cdot\text{K)}, \quad P_{t9}/P_{t8} = 0.98, \quad C_D = 0.98, \quad P_0 = 40\,\text{kPa}$$

10.18 Determine the fuel/air ratios of the main burners listed in Table 10.5.

10.19 Estimate the length of a main burner similar to the JT9D but with $P_{t3} =$ 2.5 MPa at sea level and $T_{t4} = 1500$ K.

10.20 Estimate the length of a main burner similar to the F100 but with $P_{t3} = 300$ psia at sea level and $T_{t4} = 3200°$R.

10.21 Estimate the total pressure ratio P_{te}/P_{ti} and exit Mach number M_e of a main burner with $T_{te}/T_{ti} = 3$, $M_i = 0.05$, $C_D = 2$, $\gamma_i = 1.38$, and $\gamma_e = 1.3$.

10.22 Estimate the total pressure ratio P_{te}/P_{ti} and exit Mach number M_e of an afterburner with $T_{te}/T_{ti} = 2$, $M_i = 0.3$, $C_D = 1.5$, $\gamma_i = 1.33$, and $\gamma_e = 1.3$.

10.23 Estimate the total pressure ratio P_{te}/P_{ti} and exit Mach number M_e of a straight wall diffuser with an area ratio $A_e/A_i = 4$ and $L/H = 10$ for a gas with $\gamma = 1.38$ at $M_i = 0.1$.

10.24 Estimate the total pressure ratio P_{te}/P_{ti} and exit Mach number M_e of a dump diffuser with an area ratio $A_e/A_i = 4$ for a gas with $\gamma = 1.38$ at $M_i = 0.1$, 0.2, and 0.3.

10.25 Find the shortest L/H of a straight wall diffuser that gives a total pressure ratio P_{te}/P_{ti} of 0.999 with an area ratio $A_e/A_i = 4$ for a gas with $\gamma = 1.38$ at $M_i = 0.1$.

10.26 Determine the combustion efficiency of a main burner with the following data:

$$P_{t3} = 200\ \text{psia}, \quad T_{t3} = 1000°\text{R}, \quad \dot{m}_3 = 100\ \text{lbm/s}$$
$$\phi = 0.6, \quad A_{\text{ref}} = 1.5\,\text{ft}^2, \quad H = 2\,\text{in.}$$

10.27 Determine the combustion efficiency of a main burner with the following data:

$$P_{t3} = 1.8\,\text{MPa}, \quad T_{t3} = 600\,\text{K}, \quad \dot{m}_3 = 100\,\text{kg/s}$$
$$\phi = 1.3, \quad A_{\text{ref}} = 0.1\ \text{m}^2, \quad H = 6\,\text{cm}$$

10.28 Estimate the volume of the F100 main burner (see data in Table 10.5) if its space rate SR is in the range 5×10^6 to 10×10^6 Btu/(h · ft^3 · atm).

10.29 Determine the characteristic ignition time t_c, the blowoff velocity V_{1c}, and the flame holder stability for the following data: $T = 800°$R, $M_1 = 0.5$, $\gamma = 1.33$, $\phi = 1.4$, $H = 10$ in., $B = 0.3$, a 15-deg half-angle flame holder, and pressures P of 0.4 and 0.1 atm.

Appendices

Page is intentionally blank

Appendix A
Altitude Tables

A.1 Units

Table A.1 British Engineering (BE) units[a]

h, kft	δ, P/P_{std}	Standard day θ, T/T_{std}	Cold day θ, T/T_{std}	Hot day θ, T/T_{std}	Tropical day θ, T/T_{std}	h, kft
0	1.0000	1.0000	0.7708	1.0849	1.0594	0
1	0.9644	0.9931	0.7972	1.0774	1.0520	1
2	0.9298	0.9863	0.8237	1.0700	1.0446	2
3	0.8963	0.9794	0.8501	1.0626	1.0372	3
4	0.8637	0.9725	0.8575	1.0552	1.0298	4
5	0.8321	0.9656	0.8575	1.0478	1.0224	5
6	0.8014	0.9588	0.8575	1.0404	1.0150	6
7	0.7717	0.9519	0.8575	1.0330	1.0076	7
8	0.7429	0.9450	0.8575	1.0256	1.0002	8
9	0.7149	0.9381	0.8575	1.0182	0.9928	9
10	0.6878	0.9313	0.8565	1.0108	0.9854	10
11	0.6616	0.9244	0.8502	1.0034	0.9780	11
12	0.6362	0.9175	0.8438	0.9960	0.9706	12
13	0.6115	0.9107	0.8375	0.9886	0.9632	13
14	0.5877	0.9038	0.8312	0.9812	0.9558	14
15	0.5646	0.8969	0.8248	0.9738	0.9484	15
16	0.5422	0.8901	0.8185	0.9664	0.9410	16
17	0.5206	0.8832	0.8121	0.9590	0.9336	17
18	0.4997	0.8763	0.8058	0.9516	0.9262	18
19	0.4795	0.8695	0.7994	0.9442	0.9188	19
20	0.4599	0.8626	0.7931	0.9368	0.9114	20
21	0.4410	0.8558	0.7867	0.9294	0.9040	21
22	0.4227	0.8489	0.7804	0.9220	0.8965	22
23	0.4051	0.8420	0.7740	0.9145	0.8891	23
24	0.3880	0.8352	0.7677	0.9071	0.8817	24
25	0.3716	0.8283	0.7613	0.8997	0.8743	25

(continued)

The material in this appendix is reprinted from Mattingly et al. (pp. 511–517)[12] with permission of AIAA.

Table A.1 British Engineering (BE) units[a] (continued)

h, kft	δ, P/P_{std}	Standard day θ, T/T_{std}	Cold day θ, T/T_{std}	Hot day θ, T/T_{std}	Tropical day θ, T/T_{std}	h, kft
30	0.2975	0.7940	0.7296	0.8627	0.8373	30
31	0.2843	0.7872	0.7233	0.8553	0.8299	31
32	0.2715	0.7803	0.7222	0.8479	0.8225	32
33	0.2592	0.7735	0.7222	0.8405	0.8151	33
34	0.2474	0.7666	0.7222	0.8331	0.8077	34
35	0.2360	0.7598	0.7222	0.8257	0.8003	35
36	0.2250	0.7529	0.7222	0.8183	0.7929	36
37	0.2145	0.7519	0.7222	0.8109	0.7855	37
38	0.2044	0.7519	0.7222	0.8035	0.7781	38
39	0.1949	0.7519	0.7222	0.7961	0.7707	39
40	0.1858	0.7519	0.7222	0.7939	0.7633	40
42	0.1688	0.7519	0.7222	0.7956	0.7485	42
44	0.1534	0.7519	0.7095	0.7973	0.7337	44
46	0.1394	0.7519	0.6907	0.7989	0.7188	46
48	0.1267	0.7519	0.6719	0.8006	0.7040	48
50	0.1151	0.7519	0.6532	0.8023	0.6892	50
52	0.1046	0.7519	0.6452	0.8040	0.6744	52
54	0.09507	0.7519	0.6452	0.8057	0.6768	54
56	0.08640	0.7519	0.6452	0.8074	0.6849	56
58	0.07852	0.7519	0.6452	0.8091	0.6929	58
60	0.07137	0.7519	0.6452	0.8108	0.7009	60
62	0.06486	0.7519	0.6514	0.8125	0.7090	62
64	0.05895	0.7519	0.6609	0.8142	0.7170	64
66	0.05358	0.7521	0.6704	0.8159	0.7251	66
68	0.04871	0.7542	0.6799	0.8166	0.7331	68
70	0.04429	0.7563	0.6894	0.8196	0.7396	70
72	0.04028	0.7584	0.6990	0.8226	0.7448	72
74	0.03665	0.7605	0.7075	0.8255	0.7501	74
76	0.03336	0.7626	0.7058	0.8285	0.7553	76
78	0.03036	0.7647	0.7042	0.8315	0.7606	78
80	0.02765	0.7668	0.7026	0.8344	0.7658	80
82	0.02518	0.7689	0.7009	0.8374	0.7711	82
84	0.02294	0.7710	0.6993	0.8403	0.7763	84
86	0.02091	0.7731	0.6976	0.8433	0.7816	86
88	0.01906	0.7752	0.6960	0.8463	0.7868	88
90	0.01738	0.7772	0.6944	0.8492	0.7921	90
92	0.01585	0.7793	0.6927	0.8522	0.7973	92
94	0.01446	0.7814	0.6911	0.8552	0.8026	94
96	0.01320	0.7835	0.6894	0.8581	0.8078	96
98	0.01204	0.7856	0.6878	0.8611	0.8130	98
100	0.01100	0.7877	0.6862	0.8640	0.8183	100

[a]Density: $\rho = \rho_{std}\ \sigma = \rho_{std}(\delta/\theta)$. Speed of sound: $a = a_{std}\sqrt{\theta}$.
Reference values: $P_{std} = 2116.2$ lbf/ft^2; $T_{std} = 518.69°$R; $\rho_{std} = 0.07647$ lbm/ft^3; $a_{std} = 1116$ ft/s.

Table A.2 Système International (SI) units[a]

h, km	δ, P/P_{std}	Standard day θ, T/T_{std}	Cold day θ, T/T_{std}	Hot day θ, T/T_{std}	Tropical day θ, T/T_{std}	h, km
0	1.0000	1.0000	0.7708	1.0849	1.0594	0
0.25	0.9707	0.9944	0.7925	1.0788	1.0534	0.25
0.50	0.9421	0.9887	0.8142	1.0727	1.0473	0.50
0.75	0.9142	0.9831	0.8358	1.0666	1.0412	0.75
1.00	0.8870	0.9774	0.8575	1.0606	1.0352	1.00
1.25	0.8604	0.9718	0.8575	1.0545	1.0291	1.25
1.50	0.8345	0.9662	0.8575	1.0484	1.0230	1.50
1.75	0.8093	0.9605	0.8575	1.0423	1.0169	1.75
2.00	0.7846	0.9549	0.8575	1.0363	1.0109	2.00
2.25	0.7606	0.9493	0.8575	1.0302	1.0048	2.25
2.50	0.7372	0.9436	0.8575	1.0241	0.9987	2.50
2.75	0.7143	0.9380	0.8575	1.0180	0.9926	2.75
3.00	0.6920	0.9324	0.8575	1.0120	0.9866	3.00
3.25	0.6703	0.9267	0.8523	1.0059	0.9805	3.25
3.50	0.6492	0.9211	0.8471	0.9998	0.9744	3.50
3.75	0.6286	0.9155	0.8419	0.9938	0.9683	3.75
4.00	0.6085	0.9098	0.8367	0.9877	0.9623	4.00
4.25	0.5890	0.9042	0.8315	0.9816	0.9562	4.25
4.50	0.5700	0.8986	0.8263	0.9755	0.9501	4.50
4.75	0.5514	0.8929	0.8211	0.9695	0.9441	4.75
5.00	0.5334	0.8873	0.8159	0.9634	0.9380	5.00
5.25	0.5159	0.8817	0.8107	0.9573	0.9319	5.25
5.50	0.4988	0.8760	0.8055	0.9512	0.9258	5.50
5.75	0.4822	0.8704	0.8003	0.9452	0.9198	5.75
6.00	0.4660	0.8648	0.7951	0.9391	0.9137	6.00
6.25	0.4503	0.8592	0.7899	0.9330	0.9076	6.25
6.50	0.4350	0.8535	0.7847	0.9269	0.9015	6.50
6.75	0.4201	0.8479	0.7795	0.9209	0.8955	6.75
7.00	0.4057	0.8423	0.7742	0.9148	0.8894	7.00
7.25	0.3916	0.8366	0.7690	0.9087	0.8833	7.25
7.50	0.3780	0.8310	0.7638	0.9027	0.8773	7.50
7.75	0.3647	0.8254	0.7586	0.8966	0.8712	7.75
8.00	0.3519	0.8198	0.7534	0.8905	0.8651	8.00
8.25	0.3393	0.8141	0.7482	0.8844	0.8590	8.25
8.50	0.3272	0.8085	0.7430	0.8784	0.8530	8.50
8.75	0.3154	0.8029	0.7378	0.8723	0.8469	8.75
9.00	0.3040	0.7973	0.7326	0.8662	0.8408	9.00
9.25	0.2929	0.7916	0.7274	0.8601	0.8347	9.25
9.50	0.2821	0.7860	0.7222	0.8541	0.8287	9.50
9.75	0.2717	0.7804	0.7222	0.8480	0.8226	9.75
10.00	0.2615	0.7748	0.7222	0.8419	0.8165	10.00
10.25	0.2517	0.7692	0.7222	0.8358	0.8104	10.25
10.50	0.2422	0.7635	0.7222	0.8298	0.8044	10.50
10.75	0.2330	0.7579	0.7222	0.8237	0.7983	10.75
11.00	0.2240	0.7523	0.7222	0.8176	0.7922	11.00

(continued)

Table A.2 Système International (SI) units[a] (continued)

h, km	δ, P/P_{std}	Standard day θ, T/T_{std}	Cold day θ, T/T_{std}	Hot day θ, T/T_{std}	Tropical day θ, T/T_{std}	h, km
11.25	0.2154	0.7519	0.7222	0.8116	0.7862	11.25
11.50	0.2071	0.7519	0.7222	0.8055	0.7801	11.50
11.75	0.1991	0.7519	0.7222	0.7994	0.7740	11.75
12.00	0.1915	0.7519	0.7222	0.7933	0.7679	12.00
12.25	0.1841	0.7519	0.7222	0.7940	0.7619	12.25
12.50	0.1770	0.7519	0.7222	0.7947	0.7558	12.50
12.75	0.1702	0.7519	0.7222	0.7954	0.7497	12.75
13.00	0.1636	0.7519	0.7222	0.7961	0.7436	13.00
13.25	0.1573	0.7519	0.7145	0.7968	0.7376	13.25
13.50	0.1513	0.7519	0.7068	0.7975	0.7315	13.50
13.75	0.1454	0.7519	0.6991	0.7982	0.7254	13.75
14.00	0.1399	0.7519	0.6914	0.7989	0.7193	14.00
14.25	0.1345	0.7519	0.6837	0.7996	0.7133	14.25
14.50	0.1293	0.7519	0.6760	0.8003	0.7072	14.50
14.75	0.1243	0.7519	0.6683	0.8010	0.7011	14.75
15.00	0.1195	0.7519	0.6606	0.8017	0.6951	15.00
15.25	0.1149	0.7519	0.6529	0.8024	0.6890	15.25
15.50	0.1105	0.7519	0.6452	0.8031	0.6829	15.50
15.75	0.1063	0.7519	0.6452	0.8037	0.6768	15.75
16.0	0.1022	0.7519	0.6452	0.8044	0.6708	16.0
16.5	0.09447	0.7519	0.6452	0.8058	0.6774	16.5
17.0	0.08734	0.7519	0.6452	0.8072	0.6839	17.0
17.5	0.08075	0.7519	0.6452	0.8086	0.6905	17.5
18.0	0.07466	0.7519	0.6452	0.8100	0.6971	18.0
18.5	0.06903	0.7519	0.6452	0.8114	0.7037	18.5
19.0	0.06383	0.7519	0.6531	0.8128	0.7103	19.0
19.5	0.05902	0.7519	0.6611	0.8142	0.7169	19.5
20.0	0.05457	0.7519	0.6691	0.8155	0.7235	20.0
20.5	0.05046	0.7534	0.6771	0.8169	0.7301	20.5
21.0	0.04667	0.7551	0.6851	0.8180	0.7367	21.0
21.5	0.04317	0.7568	0.6930	0.8204	0.7410	21.5
22.0	0.03995	0.7585	0.7010	0.8228	0.7453	22.0
23	0.03422	0.7620	0.7063	0.8277	0.7539	23
24	0.02933	0.7654	0.7036	0.8326	0.7625	24
25	0.02516	0.7689	0.7009	0.8374	0.7711	25
26	0.02160	0.7723	0.6982	0.8423	0.7797	26
27	0.01855	0.7758	0.6955	0.8471	0.7883	27
28	0.01595	0.7792	0.6928	0.8520	0.7969	28
29	0.01372	0.7826	0.6901	0.8568	0.8056	29
30	0.01181	0.7861	0.6874	0.8617	0.8142	30

[a]Density: $\rho = \rho_{std}\ \sigma = \rho_{std}(\delta/\theta)$. Speed of sound: $a = a_{std}\sqrt{\theta}$.
Reference values: $P_{std} = 101{,}325\ N/m^2$; $T_{std} = 288.15\ K$; $\rho_{std} = 1.225\ kg/m^3$; $a_{std} = 340.3\ m/s$.

A.2 U.S. Bureau of Standards, Standard Atmosphere 1976

A computer model (e.g., ATMOS program) of the standard day atmosphere can be written from the following material extracted from Ref. 2. All of the following is limited to geometric altitudes below 86 km—the original tables go higher, up to 1000 km. In addition, the correction for variation in mean molecular weight with altitude is very small, below 86 km, and so it is neglected.

The geometric or actual altitude h is related to the geo-potential altitude z, only used for internal calculations (a correction for variation of acceleration of gravity, used only for pressure and density calculations), by

$$z = r_0 h/(r_0 + h)$$

where $r_0 =$ 6,356.577 km is the Earth's radius.

The variation of temperature T with geo-potential altitude is represented by a continuous, piecewise linear relation,

$$T = T_i + L_i(z - z_i), \quad i = 0 \text{ through } 7$$

with fit coefficients as shown in Table A.3.

With $T_0 = 288.15$ K given, the corresponding values of temperature T_i can be readily generated from the given piecewise linear curve-fit. Note that z_7 corresponds exactly to $h = 86$ km.

The corresponding pressure P, also a piecewise continuous function, is given by

$$P = P_i\left(\frac{T_i}{T}\right)^{\left(\frac{g_0 W_0}{R^* L_i}\right)}, \quad L_i \neq 0, \quad \text{or} \quad P = P_i \exp\left(\frac{-g_0 W_0 (z - z_i)}{R^* T_i}\right), \quad L_i = 0$$

where $g_0 = 9.80665\ \text{m/s}^2$, $R^* = 8{,}314.32$ J/kmol-K, $W_0 = 28.9644$ kg/kmol, and the pressure calculations start from $P_0 = 101{,}325.0\ \text{N/m}^2$.

Table A.3 Standard day temperature model

i	z_i, km	L_i, K/km
0	0	−6.5
1	11	0.0
2	20	+1.0
3	32	+2.8
4	47	0.0
5	51	−2.8
6	71	−2.0
7	84.852	——

Table A.4 Nonstandard day temperature models

	Cold day		Hot day		Tropical day	
i	h_i, km	L_i, K/km	h_i, km	L_i, K/km	h_i, km	L_i, K/km
0	0	+25	0	−7.0	0	−7.0
1	1	0	12	+0.8	16	+3.8
2	3	−6.0	20.5	+1.4	21	+2.48
3	9.5	0				
4	13	−8.88				
5	15.5	0				
6	18.5	+4.6				
7	22.5	−0.775				

The density ρ is given simply by the ideal gas law,

$$\rho = \frac{PW_0}{R^* T}$$

A.3 Cold, Hot, and Tropical Day Temperature Profiles

A computer model (e.g., ATMOS program) of the temperature profiles for cold, hot, and tropical days can be written from the following material extracted from linear curve-fits of the data in Refs. 85 and 86. The following is limited to pressure altitudes below 30.5 km. The variation of temperature T with pressure altitude is represented by a continuous, piecewise linear relation,

$$T = T_i + L_i(h - h_i), \qquad i = 0 \text{ through } 7$$

with fit coefficients as shown in Table A.4.

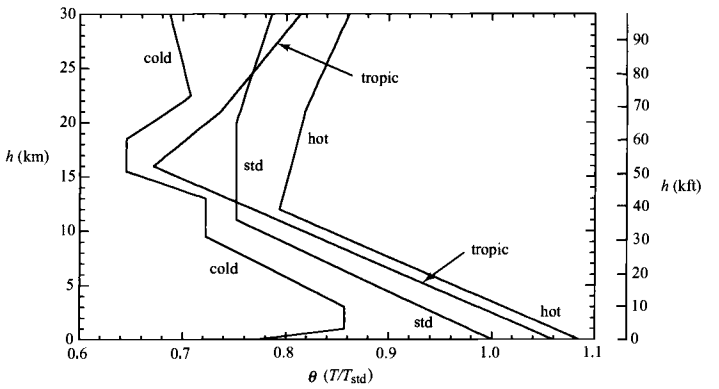

Fig. A.1 Four atmospheric temperature profiles vs pressure altitude h.

Table A.5 Sea-level base temperature

Day	Cold	Hot	Tropical
T_0, K	222.10	312.60	305.27

With T_0 given in Table A.5 for the respective temperature profile, the corresponding values of temperature T_i can be readily generated from the given piecewise linear curve-fit.

The pressure at the pressure altitude comes directly from the standard atmosphere calculation for the geometric or actual altitude h equal to that pressure altitude. Figure A.1 shows the three nonstandard day temperature profiles vs pressure altitude along with that of a standard day.

Page is intentionally blank

Appendix B
Gas Turbine Engine Data

Table B.1 Data for some military gas turbine engines

Model no.	Type	Max. thrust or power @ SLS	SFC[a] at max.	Airflow, lbm/s	OPR[b] (stages)[c]	Maximum *D*, in.	Maximum *L*, in.	Weight, lbf	TIT[d], °F	Application
J57-P-23	TJ[e]	16,000 lbf	2.10	165	11.5 (16)	40	246	5,169	1,600	AB, F-102A, F-100D
J57-P-43WB	TJ	11,200 lbf	0.775	180	12 (16)	39	167.3	3,870	1,600	Water-injected, KC-135
J58-P[f]	TJ	32,500 lbf	——	450	6 (9)	——	——	——	——	AB, YF-12A, SR-71
J60-P-3	TJ	3,000 lbf	0.96	50	7 (9)	23.4	79.5	460	1,600	T-39A, C-140A
J69-T-25	TJ	1,025 lbf	1.14	20.5	3.9 (0,1)	22.3	43.3	364	1,525	T-37B
J75-P-17	TJ	24,500 lbf	2.15	252	12.0 (15)	43	237.6	5,875	1,610	AB, F-106A/B
J79-GE-17	TJ	17,820 lbf	1.965	170	13.5 (17)	39.1	208.7	3,855	1,210	AB, F-4E/G
J85-GE-5H	TJ	3,850 lbf	2.20	44	7 (8)	20.4	109.1	584	1,640	AB, T-38A/B
J85-GE-17	TJ	2,850 lbf	0.99	44	7 (8)	17.7	40.4	395	1,640	A-37B
J85-GE-21	TJ	5,000 lbf	2.13	51.9	8 (8)	20	116	667	1,790	AB, F-5E/F
PT6A-42	TP[g]	850 eshp	0.601	8.0	8 (3,1)	19	67	391	——	C-12E
PT6A-45R	TP	1,197 eshp	0.553	8.6	8.7 (3,1)	19	72	434	——	C-23A
T400-CP-400	TS[h]	1,800 shp	0.606	6.51	7 (3,1)	43.5	66.3	716	1,920	Bell UH-1N

(continued)

The material in this appendix is reprinted from Mattingly et al. (pp. 519–522)[12] with permission of AIAA.

Table B.1 Data for some military gas turbine engines (continued)

Model no.	Type	Max. thrust or power @ SLS	SFC[a] at max.	Airflow, lbm/s	OPR[b] (stages)[c]	Maximum *D*, in.	Maximum *L*, in.	Weight, lbf	TIT[d], °F	Application
T406-AD-400	TS	6,150 shp	0.424	——	(14)	24.5	77.9	975	1,422	CV-22
T53-L-13	TS	1,400 shp	0.58	12.2	7 (5,1)	23	47.6	549	1,720	Bell UH-lH, AH-1G
T55-L-11	TS	3,750 shp	0.52	——	8 (6,1)	24.3	44	670	——	Boeing CH-47C
T56-A-7	TP	3,775 eshp	0.528	32.5	9.45 (14)	40.9	146	1,833	1,780	C-130B/E/F
T56-A-15	TP	4,591 eshp	0.54	32.5	9.55 (14)	44.6	146.3	1,848	1,970	C-130H/N/P
T58-GE-100	TS	1,500 shp	0.606	14	8.4 (10)	21.5	58.6	335	1,372	Sikorsky CH-3E, HH-3E, F
T64-GE-100	TS	4,330 shp	0.487	29.3	14 (14)	20.2	77.1	720	1,520	MH-53T
T700-GE-700	TS	1,622 shp	0.46	——	15 (5,1)	25	47	423	1,563	UH-60A
T76-G-10	TS	715 shp	0.60	6.16	8.6 (2)	27.1	44.5	348	1,818	OV-1OA

[a]SFC = specific fuel consumption. [b]OPR = overall pressure ratio. [c](stages) = (axial, centrifugal) compressor stages. [d]TIT = turbine inlet temperature. [e]TJ = turbojet. [f]J-58 Reference: Lockheed SR-71 by Jay Miller, Aerofax Minigraph 1, Aerofax, Inc., Arlington, TX, 1985. [g]TP = turboprop. [h]TS = turboshaft. (Sources: Manufacturers' literature).

Table B.2 Data for some military turbofan engines

Model no.	Thrust, lbf	TSFC[a], 1/h	Airflow, lbm/s	OPR[b]	Maximum *D*, in.	Maximum *L*, in.	Weight, lbf	TIT[c], °F	FPR[d]	BR[e]	Application
F100-PW-229	29,000 17,800	2.05 0.74	248	23.0	47	191	3,036	2,700	3.8	0.4	F-15, F16
F101-GE-102	30,780 17,390	2.460 0.562	356	26.8	55.2	180.7	4,448	2,550	2.31	1.91	B-1B
F103-GE-101	51,711	0.399	1,476	30.2	86.4	173	8,768	2,490	—	4.31	KC-10A
F107-WR-101	635	0.685	13.6	13.8	12	48.5	141	—	2.1	1.0	Air Launch Cruise Missile
F108-CF-100	21,634	0.363	785	23.7	72	115.4	4,610	2,228	1.5	6.0	KC-135R
F110-GE-100	28,620 18,330	2.08 1.47	254	30.4	46.5	182	3,895	—	2.98	0.80	F-16
F117-PW-100	41,700	0.33	—	31.8	84.5	146.8	7,100	—	—	5.8	(PW2040) C-17A
F118-GE-100	19,000	0.67	—	35.1	46.5	100.5	3,200	—	—	—	B-2
F119-PW-100	35,000	—	—	—	—	—	—	—	—	—	F-22 Rapton
F135-PW	40,000	—	—	—	—	—	—	—	—	—	F-35 JSF
F404-GE-FID	10,000	0.79	—	24	35	83	1,730	—	—	—	F-117A

(continued)

Table B.2 Data for some military gas turbine engines (continued)

Model no.	Thrust, lbf	TSFC[a], 1/h	Airflow, lbm/s	OPR[b]	Maximum *D*, in.	Maximum *L*, in.	Weight, lbf	TIT[c], °F	FPR[d]	BR[e]	Application
F404-GE-400	16,000	1.85	142	26	35	154	——	——	——	0.34	F-18, F-5G
F414-GE-400	22,000	——	——	30	35	154	——	——	——	——	F/A-18E/F
JT3D-3B	18,000	0.535	458	13.6	53	136.4	4,300	1,600	1.74	1.37	(TF33-102) EC/RC-135
JT8D-7B	14,500	0.585	318	16.9	45	123.7	3.252	1,076		1.03	C-22, C-9, T-43A
TF30-P-111	25,100	2.450	260	21.8	49	241.7	3,999	2,055	2.43	0.73	F-111F
	14,560	0.686									
TF33-P-3	17,000	0.52	450	13.0	53	136	3,900	1,600	1.7	1.55	B-52H
TF33-P-7	21,000	0.56	498	16.0	54	142	4,650	1,750	1.9	1.21	C-141
TF34-GE-100	9.065	0.37	333	20.0	50	100	1,421	2,234	1.5	6.42	A-10
TF39-GE-1	40,805	0.315	1,549	26.0	100	203	7,186	2,350	1.56	8.0	C-5A
TF41-A-1B	14,500	0.647	260	20.0	40	114.5	3,511	2,165	2.45	0.76	A-7D, K
TFE731-2	3,500	0.504	113	17.7	40	50	625	——	1.54	2.67	C-21A

[a]TSFC = thrust specific fuel consumption. [b]OPR = overall pressure ratio. [c]TIT = turbine inlet temperature. [d]FPR = fan pressure ratio. [e]BR = bypass ratio.
(Sources: Manufacturers' literature).

Table B.3 Data for some civil gas turbine engines

		Takeoff				Cruise				
Model no.	Manufacturer	Thrust, lbf	BR[a]	OPR[b]	Airflow, lbm/s	Alt, kft	Mach	Thrust, lbf	TSFC[c]	Application
CF 34-8	General Electric	14,500	5	28	—	—	—	—	0.68	Bombardier CRJ700 Embraer 170/175
CF6-50-C2	General Electric	52,500	4.31	30.4	1,476	35	0.80	11,555	0.630	DC10-10, A300B, 747-200
CF6-80-C2	General Electric	52,500	5.31	27.4	1,650	35	0.80	12,000	0.576	767-200, -300, -200ER
GE90-B4	General Electric	87,400	8.40	39.3	3,037	35	0.80	17,500	—	777
GEnx	General Electric	53,000–75,000	10	42	—	—	0.85	—	—	787, 747-8
JT8D-15A	Pratt & Whitney	15,500	1.04	16.6	327	30	0.80	4,920	0.779	727, 737, DC9
JT9D-59A	Pratt & Whitney	53,000	4.90	24.5	1,639	35	0.85	11,950	0.646	DC1O-40, A300B, 747-200
PW2037	Pratt & Whitney	38,250	6.00	27.6	1,210	35	0.85	6,500	0.582	757-200
PW4052	Pratt & Whitney	52,000	5.00	27.5	1,700	—	—	—	—	767, A310-300
PW4084	Pratt & Whitney	87,900	6.41	34.4	2,550	35	0.83	—	—	777
CFM56-3C	CFM International	23,500	6.00	22.6	655	35	0.80	5,540	0.648	737-300, -400, -500
CFM56-5C	CFM International	31,200	6.60	31.5	1,027	35	0.80	6,600	0.545	A340

(continued)

Table B.3 Data for some military gas turbine engines (continued)

		Takeoff				Cruise				
Model no.	Manufacturer	Thrust, lbf	BR[a]	OPR[b]	Airflow, lbm/s	Alt, kft	Mach	Thrust, lbf	TSFC[c]	Application
AE 3007	Rolls-Royce	8,600	4.8	20	—	—	—	—	—	Embraer 37, Global Hawk UAV
RB211-524B	Rolls-Royce	50,000	4.50	28.4	1,513	35	0.85	11,000	0.643	L1011-200, 747-200
RB211-535E	Rolls-Royce	40,100	4.30	25.8	1,151	35	0.80	8,495	0.607	757-200
RB211-882	Rolls-Royce	84,700	6.01	39.0	2,640	35	0.83	16,200	0.557	777
Trent 900	Rolls-Royce	70,000–76,500	8.7–8.5	—	2,655–2,745	—	—	—	—	A380
Trent 1000	Rolls-Royce	53,000–75,000	10–11	—	2,400–2,670	—	—	—	—	787
V2528-D5	International Aero Engines	28,000	4.70	30.5	825	35	0.80	5,773	0.574	MD-90
ALF502R-5	Honeywell	6,970	5.70	12.2	—	25	0.70	2,250	0.720	BAe 146-200, –200
TFE731-5	Honeywell	4,500	3.34	14.4	140	40	0.80	986	0.771	BAe 125-800
PW300	Pratt & Whitney Canada	4,750	4.50	23.0	180	40	0.80	1,113	0.675	BAe 1000
FJ44	Williams Rolls	1,900	3.28	12.8	63.3	30	0.70	600	0.750	—
Olympus 593	Rolls-Royce/SNECMA	38,000	0	11.3[d]	410	53	2.00	10,030	1.190	Concorde
GP7270	Engine Alliance	70,000	8.7[d]	45.6[e]	—	35	0.85	12,633	—	A380

[a]BR = bypass ratio. [b]OPR = overall pressure ratio. [c]TSFC = thrust specific fuel consumption. [d]At cruise. [e]max climb.
(Sources: Manufacturers' literature).

Table B.4 Temperature/pressure data for some engines

Temperature and pressure	Pegasus turbofan, separate exhaust	J57 turbojet w/AB exhaust	JT3D turbofan, separate exhaust	JT8D turbofan, mixed exhaust	JT9D turbofan, separate exhaust	F100-PW-100 turbofan, mixed w/AB exhaust
P_{t2}, psia	14.7	14.7	14.7	14.7	14.7	13.1
T_{t2}, °F	59	59	59	59	59	59
$P_{t2.5}$, psia	36.1	54	63	60	32.1	39.3
$T_{t2.5}$, °F	242	330	360	355	210	297
P_{t13}, psia	36.5	—	26	28	22.6	39.3
T_{t13}, °F	257	—	170	190	130	297
P_{t3}, psia	216.9	167	200	233	316	316
T_{t3}, °F	708	660	715	800	880	1,014
P_{t4}, psia	—	158	190	220	302	304
T_{t4}, °F	1,028	1,570	1,600	1,720	1,970	2,566
P_{t5} or P_{t6}, psia	29.3	36	—	2	20.9	38.0
T_{t5} or T_{t6}, °F	510	1,013	—	—	850	1,368
P_{t16}, psia	—	—	—	—	—	36.8
T_{t16}, °F	—	—	—	—	—	303
P_{t6A}, psia	—	—	—	29	—	37.5
T_{t6A}, °F	—	—	—	890	—	960
P_{t7}, psia	—	31.9	28	29	20.9	33.8
T_{t7}, °F	—	2,540	890	890	850	3,204
P_{t17}, psia	36.5	—	26	—	22.4	—
T_{t17}, °F	257	—	170	—	130	—
Bypass ratio α	1.4	0	1.36	1.1	5.0	0.69
Thrust, lbf	21,500	16,000	18,000	14,000	43,500	23,700
Airflow, lbm/s	444	167	460	315	1,495	224

Page is intentionally blank

Appendix C
Data for Some Liquid-Propellant Rocket Engines

Table C.1 Data for some liquid-propellant rocket engines

Engine[a]	Thrust (lbf) in vacuum	Expansion ratio ($\varepsilon = A_e/A_t$)	Design alt. (ft) ($P_e = P_a$)	I_{sp} (s)		Application
				Vacuum	SL	
LR-87-BC-13	16,000	45:1	60,000	293	—	Agena
LR-87-AJ-9	474,000	8:1	20,000	283	257	Titan 2—1st stage Titan 3—2d stage Titan Gemini—1st stage
LR-87-AJ-11	548,000	15:1	—	301		Titan 4—1st stage
LR-91-AJ-7	100,570	49:1	100,000	309	—	Titan 2—2d stage Titan 3A-Gemini Titan 3C—3d stage
LR-91-AJ-11	105,000	49.2:1	—	316	—	Titan 4—2d stage
LR-105*	83,700	24.9:1	100,000	304	212	Std. launch vehicle
F-1*	1,726,000	24.9:1	80,000	305	265	Saturn V—1st stage
H-1*	219,000	8:1	80,000	287	255	Saturn 1B
J-2*	200,000	25.5:1	100,000	426	380	Saturn V—2nd and 3d stages
RS-27*	231,700	8:1	—	—	263	Delta launch vehicle

(continued)

Table C.1 Data for some liquid-propellant rocket engines (continued)

Engine[a]	Thrust (lbf) in vacuum	Expansion ratio ($\varepsilon = A_e/A_t$)	Design alt. (ft) ($P_e = P_a$)	I_{sp} (s)		Application
				Vacuum	SL	
SSME*	470,000	77:1	44,600	455	364	Space shuttle main engine
STME*	650,000	45:1	—	428	364	Space transportation main engine
RL10A-4†	20,800	—	—	449	—	Atlas IIA upper stage
HM78†	14,300	83:1	—	446	—	Ariane 5 upper stage
RD-0110‡	30,400	82:1	—	326	—	Soyuz stage 2
RD-180¶	860,200(SL)	36:1	—	338	311	Atlas V
Vulcain 2	286,000	59:1	—	431	—	Ariane 5

[a]Manufacturers: BC = Bell Aerosystems Co.; AJ = Aerojet. * = Rocketdyne. ¶ = Pratt & Whitney. † = Snecma. ‡ = Russia.

Appendix D
Air and $(CH_2)_n$ Properties at Low Pressure

Table D.1 Système International (SI) units

T		$f = 0$		$f = 0.0169$		$f = 0.0338$		$f = 0.0507$		$f = 0.0676$	
K	°C	h, kJ/kg	P_r	h, kJ/kg	P_r	h, kJ/kg	P_r	h, kJ/kg	P_r	h, kJ/kg	P_r
170	−103	169.80	0.1903	170.82	0.1870	171.81	0.1840	172.76	0.1810	173.69	0.1783
180	−93	179.85	0.2324	180.95	0.2288	182.01	0.2254	183.04	0.2221	184.03	0.2190
190	−83	189.90	0.2809	191.08	0.2769	192.22	0.2731	193.33	0.2695	194.40	0.2661
200	−73	199.93	0.3361	201.21	0.3318	202.44	0.3278	203.63	0.3239	204.79	0.3202
210	−63	209.96	0.3985	211.34	0.3941	212.66	0.3899	213.95	0.3859	215.19	0.3821
220	−53	219.99	0.4688	221.47	0.4644	222.89	0.4602	224.28	0.4561	225.62	0.4522
230	−43	230.01	0.5475	231.60	0.5433	233.13	0.5392	234.62	0.5352	236.06	0.5315
240	−33	240.02	0.6352	241.73	0.6313	243.38	0.6276	244.98	0.6240	246.53	0.6205
250	−23	250.04	0.7325	251.87	0.7292	253.64	0.7260	255.36	0.7230	257.02	0.7201
260	−13	260.05	0.8399	262.01	0.8376	263.91	0.8353	265.75	0.8331	267.53	0.8310
270	−3	270.07	0.9581	272.17	0.9571	274.19	0.9561	276.16	0.9551	278.06	0.9542
280	7	280.08	1.0878	282.32	1.0885	284.49	1.0891	286.58	1.0898	288.61	1.0904
290	17	290.10	1.2296	292.49	1.2325	294.79	1.2352	297.03	1.2379	299.19	1.2406
300	27	300.13	1.3841	302.66	1.3897	305.11	1.3952	307.49	1.4005	309.79	1.4056
310	37	310.15	1.5521	312.85	1.5611	315.45	1.5699	317.97	1.5783	320.41	1.5865

(continued)

Table D.1 Système International (SI) units (continued)

T		$f = 0$		$f = 0.0169$		$f = 0.0338$		$f = 0.0507$		$f = 0.0676$	
K	°C	h, kJ/kg	P_r	h, kJ/kg	P_r	h, kJ/kg	P_r	h, kJ/kg	P_r	h, kJ/kg	P_r
320	47	320.19	1.7344	323.04	1.7474	325.80	1.7601	328.47	1.7724	331.05	1.7844
330	57	330.23	1.9315	333.25	1.9494	336.16	1.9667	338.99	1.9836	341.72	2.00
340	67	340.28	2.14	343.47	2.17	346.55	2.19	349.53	2.21	352.42	2.23
350	77	350.34	2.37	353.70	2.40	356.95	2.43	360.09	2.46	363.13	2.49
360	87	360.41	2.62	363.94	2.66	367.36	2.69	370.67	2.73	373.88	2.77
370	97	370.49	2.88	374.20	2.93	377.80	2.98	381.27	3.02	384.64	3.06
380	107	380.58	3.17	384.48	3.22	388.25	3.28	391.90	3.33	395.44	3.39
390	117	390.68	3.47	394.77	3.54	398.72	3.61	402.55	3.67	406.26	3.74
400	127	400.80	3.80	405.08	3.88	409.22	3.95	413.22	4.03	417.10	4.11
410	137	410.93	4.14	415.40	4.24	419.73	4.33	423.92	4.42	427.98	4.51
420	147	421.07	4.51	425.74	4.62	430.26	4.73	434.64	4.84	438.88	4.94
430	157	431.23	4.90	436.10	5.03	440.82	5.16	445.38	5.28	449.80	5.40
440	167	441.41	5.32	446.49	5.47	451.40	5.61	456.15	5.76	460.76	5.90
450	177	451.60	5.76	456.89	5.93	462.00	6.10	466.95	6.26	471.74	6.43
460	187	461.81	6.23	467.31	6.42	472.62	6.61	477.77	6.80	482.75	6.99
470	197	472.04	6.72	477.75	6.94	483.27	7.16	488.62	7.38	493.79	7.59
480	207	482.28	7.25	488.21	7.50	493.94	7.74	499.49	7.99	504.86	8.23
490	217	492.55	7.80	498.69	8.08	504.63	8.36	510.39	8.64	515.96	8.92
500	227	502.83	8.39	509.20	8.70	515.35	9.02	521.31	9.33	527.09	9.64
510	237	513.13	9.01	519.72	9.36	526.10	9.71	532.27	10.06	538.24	10.41
520	247	523.46	9.66	530.27	10.05	536.87	10.44	543.25	10.83	549.43	11.23
530	257	533.80	10.35	540.85	10.78	547.66	11.22	554.26	11.65	560.65	12.09
540	267	544.17	11.07	551.44	11.55	558.48	12.03	565.30	12.52	571.89	13.01
550	277	554.55	11.83	562.06	12.36	569.33	12.90	576.36	13.44	583.17	13.98

560	287	564.96	12.63	572.71	13.21	580.20	13.81	587.46	14.41	594.48	15.01
570	297	575.39	13.47	583.38	14.11	591.10	14.77	598.58	15.43	605.82	16.09
580	307	585.84	14.35	594.07	15.06	602.03	15.78	609.73	16.50	617.19	17.24
590	317	596.32	15.27	604.79	16.05	612.98	16.84	620.91	17.64	628.59	18.45
600	327	606.81	16.24	615.53	17.09	623.96	17.96	632.12	18.83	640.02	19.72
600	327	606.81	16.24	615.53	17.09	623.96	17.96	632.12	18.83	640.02	19.72
610	337	617.33	17.25	626.30	18.18	634.97	19.13	643.36	20.09	651.49	21.06
620	347	627.88	18.32	637.09	19.33	646.00	20.36	654.63	21.41	662.98	22.48
630	357	638.44	19.43	647.91	20.53	657.07	21.66	665.93	22.80	674.51	23.97
640	367	649.03	20.59	658.75	21.79	668.16	23.01	677.25	24.26	686.07	25.53
650	377	659.65	21.80	669.62	23.11	679.27	24.44	688.61	25.79	697.65	27.18
660	387	670.29	23.07	680.52	24.48	690.42	25.93	700.00	27.40	709.28	28.91
670	397	680.95	24.40	691.44	25.93	701.59	27.49	711.42	29.09	720.93	30.72
680	407	691.63	25.78	702.39	27.43	712.79	29.12	722.86	30.86	732.61	32.63
690	417	702.34	27.23	713.36	29.01	724.02	30.83	734.34	32.71	744.33	34.63
700	427	713.07	28.73	724.36	30.65	735.28	32.62	745.84	34.65	756.08	36.72
710	437	723.83	30.30	735.38	32.36	746.56	34.49	757.38	36.68	767.85	38.92
720	447	734.61	31.93	746.43	34.15	757.87	36.44	768.94	38.80	779.67	41.22
730	457	745.41	33.64	757.51	36.02	769.21	38.48	780.54	41.02	791.51	43.63
740	467	756.24	35.41	768.61	37.97	780.58	40.61	792.16	43.34	803.38	46.15
750	477	767.09	37.25	779.74	39.99	791.98	42.83	803.82	45.76	815.29	48.79
760	487	777.97	39.17	790.90	42.10	803.40	45.15	815.50	48.29	827.22	51.54
770	497	788.87	41.16	802.08	44.30	814.85	47.56	827.22	50.94	839.19	54.42
780	507	799.79	43.23	813.28	46.59	826.33	50.08	838.96	53.69	851.19	57.43
790	517	810.74	45.39	824.51	48.97	837.83	52.70	850.73	56.57	863.21	60.58
800	527	821.71	47.62	835.77	51.45	849.37	55.43	862.53	59.57	875.27	63.86
810	537	832.70	49.94	847.05	54.02	860.93	58.27	874.36	62.69	887.36	67.28

(continued)

Table D.1 Système International (SI) units (continued)

T		$f = 0$		$f = 0.0169$		$f = 0.0338$		$f = 0.0507$		$f = 0.0676$	
K	°C	h, kJ/kg	P_r	h, kJ/kg	P_r	h, kJ/kg	P_r	h, kJ/kg	P_r	h, kJ/kg	P_r
820	547	843.72	52.35	858.35	56.69	872.51	61.22	886.22	65.94	899.48	70.85
830	557	854.76	54.85	869.69	59.47	884.13	64.30	898.10	69.33	911.64	74.57
840	567	865.82	57.44	881.04	62.36	895.77	67.50	910.02	72.86	923.82	78.45
850	577	876.90	60.13	892.42	65.35	907.43	70.82	921.96	76.53	936.03	82.49
860	587	888.01	62.91	903.83	68.46	919.12	74.27	933.93	80.35	948.27	86.70
870	597	899.14	65.80	915.26	71.68	930.84	77.86	945.93	84.33	960.54	91.09
880	607	910.29	68.79	926.71	75.02	942.59	81.58	957.96	88.46	972.84	95.65
890	617	921.47	71.88	938.19	78.49	954.36	85.44	970.01	92.75	985.17	100.40
900	627	932.66	75.08	949.69	82.08	966.15	89.46	982.09	97.21	997.52	105.33
910	637	943.88	78.40	961.21	85.80	977.97	93.62	994.20	101.84	1009.91	110.46
920	647	955.12	81.82	972.76	89.66	989.82	97.93	1006.33	106.64	1022.32	115.80
930	657	966.38	85.37	984.33	93.65	1001.69	102.40	1018.49	111.64	1034.77	121.34
940	667	977.66	89.03	995.92	97.78	1013.58	107.04	1030.68	116.81	1047.24	127.10
950	677	988.96	92.82	1007.54	102.06	1025.50	111.84	1042.89	122.19	1059.73	133.09
960	687	1000.28	96.74	1019.17	106.48	1037.45	116.82	1055.13	127.76	1072.26	139.29
970	697	1011.62	100.78	1030.83	111.06	1049.41	121.97	1067.40	133.53	1084.81	145.74
980	707	1022.99	104.96	1042.51	115.79	1061.41	127.31	1079.69	139.52	1097.39	152.43
990	717	1034.37	109.27	1054.22	120.68	1073.42	132.83	1092.00	145.72	1110.00	159.36
1000	727	1045.77	113.72	1065.94	125.74	1085.46	138.54	1104.34	152.14	1122.63	166.55
1000	727	1045.77	113.72	1065.94	125.74	1085.46	138.54	1104.34	152.14	1122.63	166.55
1010	737	1057.19	118.31	1077.69	130.96	1097.52	144.45	1116.71	158.79	1135.29	174.01
1020	747	1068.63	123.05	1089.45	136.36	1109.60	150.56	1129.09	165.68	1147.97	181.74
1030	757	1080.09	127.94	1101.24	141.93	1121.70	156.88	1141.51	172.81	1160.68	189.74
1040	767	1091.56	132.98	1113.05	147.68	1133.83	163.41	1153.94	180.19	1173.42	198.03

1050	777	1103.06	138.18	1124.87	153.62	1145.98	170.15	1166.40	187.82	1186.18	206.6
1060	787	1114.57	143.53	1136.72	159.74	1158.15	177.13	1178.89	195.71	1198.97	215.5
1070	797	1126.10	149.05	1148.59	166.06	1170.34	184.32	1191.39	203.9	1211.78	224.7
1080	807	1137.65	154.73	1160.47	172.58	1182.55	191.76	1203.92	212.3	1224.61	234.2
1090	817	1149.22	160.59	1172.38	179.30	1194.78	199.43	1216.47	221.0	1237.47	244.1
1100	827	1160.80	166.62	1184.30	186.23	1207.04	207.4	1229.04	230.0	1250.35	254.3
1110	837	1172.40	172.83	1196.24	193.38	1219.31	215.5	1241.64	239.3	1263.26	264.8
1120	847	1184.01	179.22	1208.21	200.7	1231.61	224.0	1254.25	248.9	1276.18	275.7
1130	857	1195.65	185.79	1220.18	208.3	1243.92	232.7	1266.89	258.9	1289.13	287.0
1140	867	1207.29	192.55	1232.18	216.1	1256.25	241.6	1279.55	269.1	1302.11	298.6
1150	877	1218.96	199.51	1244.19	224.2	1268.60	250.9	1292.23	279.7	1315.10	310.6
1160	887	1230.64	206.7	1256.22	232.4	1280.97	260.4	1304.93	290.6	1328.12	323.0
1170	897	1242.33	214.0	1268.27	241.0	1293.36	270.2	1317.65	301.8	1341.16	335.9
1180	907	1254.05	221.6	1280.34	249.8	1305.77	280.3	1330.39	313.4	1354.22	349.1
1190	917	1265.77	229.4	1292.42	258.8	1318.20	290.8	1343.15	325.4	1367.30	362.8
1200	927	1277.51	237.4	1304.52	268.1	1330.64	301.5	1355.92	337.7	1380.41	376.8
1210	937	1289.27	245.6	1316.63	277.6	1343.10	312.5	1368.72	350.4	1393.53	391.4
1220	947	1301.03	254.0	1328.76	287.4	1355.58	323.9	1381.54	363.5	1406.68	406.4
1230	957	1312.82	262.6	1340.91	297.5	1368.08	335.6	1394.38	377.0	1419.84	421.9
1240	967	1324.61	271.5	1353.07	307.9	1380.59	347.7	1407.23	390.9	1433.02	437.8
1250	977	1336.43	280.6	1365.24	318.6	1393.12	360.1	1420.10	405.2	1446.23	454.3
1260	987	1348.25	290.0	1377.44	329.6	1405.67	372.8	1432.99	420.0	1459.45	471.2
1270	997	1360.09	299.6	1389.64	340.8	1418.23	385.9	1445.90	435.2	1472.69	488.7
1280	1007	1371.94	309.5	1401.86	352.4	1430.81	399.4	1458.83	450.8	1485.96	506.7
1290	1017	1383.80	319.6	1414.10	364.3	1443.41	413.3	1471.77	466.8	1499.24	525.2
1300	1027	1395.68	330.0	1426.35	376.5	1456.02	427.5	1484.73	483.4	1512.54	544.3
1310	1037	1407.57	340.6	1438.61	389.0	1468.64	442.2	1497.71	500.4	1525.85	564.0

(continued)

Table D.1 Système International (SI) units (continued)

T		$f = 0$		$f = 0.0169$		$f = 0.0338$		$f = 0.0507$		$f = 0.0676$	
K	°C	h, kJ/kg	P_r	h, kJ/kg	P_r	h, kJ/kg	P_r	h, kJ/kg	P_r	h, kJ/kg	P_r
1320	1047	1419.47	351.6	1450.89	401.8	1481.29	457.2	1510.70	517.9	1539.19	584.2
1330	1057	1431.38	362.7	1463.18	415.0	1493.94	472.6	1523.71	535.9	1552.54	605.0
1340	1067	1443.31	374.2	1475.49	428.6	1506.61	488.5	1536.74	554.4	1565.91	626.5
1350	1077	1455.25	386.0	1487.81	442.5	1519.30	504.8	1549.78	573.4	1579.30	648.5
1360	1087	1467.20	398.0	1500.14	456.7	1532.00	521.6	1562.84	593.0	1592.70	671.2
1370	1097	1479.16	410.3	1512.48	471.3	1544.72	538.8	1575.92	613.1	1606.13	694.6
1380	1107	1491.13	423.0	1524.84	486.3	1557.45	556.4	1589.01	633.7	1619.57	718.6
1390	1117	1503.11	435.9	1537.21	501.7	1570.19	574.5	1602.11	654.9	1633.02	743.3
1400	1127	1515.11	449.2	1549.59	517.4	1582.95	593.1	1615.23	676.7	1646.49	768.6
1400	1127	1515.11	449.2	1549.59	517.4	1582.95	593.1	1615.23	676.7	1646.49	768.6
1410	1137	1527.11	462.8	1561.99	533.6	1595.72	612.2	1628.37	699.1	1659.98	794.7
1420	1147	1539.13	476.7	1574.39	550.1	1608.51	631.7	1641.52	722.0	1673.49	821.5
1430	1157	1551.16	490.9	1586.81	567.1	1621.30	651.8	1654.68	745.6	1687.01	849.1
1440	1167	1563.20	505.4	1599.25	584.4	1634.12	672.4	1667.86	769.8	1700.54	877.4
1450	1177	1575.25	520.4	1611.69	602.2	1646.94	693.4	1681.06	794.6	1714.09	906.5
1460	1187	1587.31	535.6	1624.14	620.4	1659.78	715.1	1694.27	820.2	1727.66	936.4
1470	1197	1599.38	551.2	1636.61	639.1	1672.63	737.2	1707.49	846.3	1741.24	967.0
1480	1207	1611.46	567.2	1649.09	658.2	1685.49	760.0	1720.72	873.1	1754.84	998.5
1490	1217	1623.55	583.5	1661.58	677.8	1698.37	783.2	1733.97	900.7	1768.45	1030.8
1500	1227	1635.65	600.2	1674.08	697.8	1711.26	807.1	1747.24	928.9	1782.08	1064.0
1510	1237	1647.76	617.2	1686.59	718.3	1724.16	831.5	1760.51	957.8	1795.72	1098.1
1520	1247	1659.88	634.7	1699.11	739.3	1737.07	856.6	1773.80	987.5	1809.38	1133.1
1530	1257	1672.01	652.5	1711.65	760.7	1749.99	882.2	1787.11	1018.0	1823.05	1168.9
1540	1267	1684.15	670.7	1724.19	782.7	1762.93	908.5	1800.42	1049.1	1836.73	1205.7

1550	1277	1696.29	689.4	1736.75	805.2	1775.88	935.4	1813.75	1081.1	1850.43	1243.5
1560	1287	1708.45	708.4	1749.31	828.2	1788.84	962.9	1827.10	1113.9	1864.14	1282.2
1570	1297	1720.62	727.9	1761.89	851.6	1801.81	991.1	1840.45	1147.4	1877.86	1321.9
1580	1307	1732.80	747.7	1774.48	875.7	1814.80	1019.9	1853.82	1181.8	1891.60	1362.6
1590	1317	1744.98	768.0	1787.08	900.3	1827.79	1049.5	1867.20	1217.0	1905.36	1404.3
1600	1327	1757.18	788.8	1799.68	925.4	1840.80	1079.7	1880.59	1253.1	1919.12	1447.1
1610	1337	1769.38	810.0	1812.30	951.1	1853.81	1110.6	1893.99	1290.0	1932.90	1490.9
1620	1347	1781.59	831.6	1824.93	977.3	1866.84	1142.2	1907.41	1327.8	1946.69	1535.9
1630	1357	1793.82	853.7	1837.56	1004.2	1879.88	1174.6	1920.84	1366.6	1960.50	1581.9
1640	1367	1806.05	876.2	1850.21	1031.6	1892.93	1207.6	1934.28	1406.2	1974.31	1629.1
1650	1377	1818.29	899.2	1862.87	1059.6	1905.99	1241.5	1947.73	1446.8	1988.15	1677.4
1660	1387	1830.54	922.7	1875.54	1088.2	1919.06	1276.1	1961.19	1488.3	2001.99	1726.9
1670	1397	1842.79	946.7	1888.21	1117.4	1932.15	1311.5	1974.67	1530.8	2015.84	1777.6
1680	1407	1855.06	971.2	1900.90	1147.3	1945.24	1347.6	1988.15	1574.3	2029.71	1829.5
1690	1417	1867.33	996.1	1913.59	1177.8	1958.34	1384.6	2001.65	1618.8	2043.59	1882.6
1700	1427	1879.61	1021.6	1926.30	1209.0	1971.45	1422.4	2015.16	1664.3	2057.48	1937.0
1710	1437	1891.90	1047.6	1939.01	1240.8	1984.58	1461.0	2028.68	1710.8	2071.38	1992.8
1720	1447	1904.20	1074.1	1951.73	1273.2	1997.71	1500.5	2042.21	1758.4	2085.30	2049.8
1730	1457	1916.51	1101.1	1964.46	1306.4	2010.85	1540.8	2055.75	1807.1	2099.23	2108.1
1740	1467	1928.82	1128.7	1977.20	1340.2	2024.01	1582.0	2069.30	1856.9	2113.16	2167.8
1750	1477	1941.14	1156.8	1989.95	1374.8	2037.17	1624.1	2082.86	1907.8	2127.11	2229
1760	1487	1953.47	1185.5	2002.71	1410.0	2050.34	1667.1	2096.44	1959.8	2141.07	2291
1770	1497	1965.81	1214.7	2015.48	1446.0	2063.52	1711.0	2110.02	2013.0	2155.05	2355
1780	1507	1978.16	1244.5	2028.25	1482.7	2076.71	1755.8	2123.61	2067.3	2169.03	2421
1790	1517	1990.51	1274.9	2041.04	1520.1	2089.91	1801.6	2137.22	2122.8	2183.02	2488
1800	1527	2002.87	1305.8	2053.83	1558.3	2103.12	1848.3	2150.83	2179.6	2197.03	2556
1810	1537	2015.24	1337.4	2066.63	1597.3	2116.34	1896.0	2164.45	2238	2211.04	2626

(continued)

Table D.1 Système International (SI) units (continued)

T		$f = 0$		$f = 0.0169$		$f = 0.0338$		$f = 0.0507$		$f = 0.0676$	
K	°C	h, kJ/kg	P_r	h, kJ/kg	P_r	h, kJ/kg	P_r	h, kJ/kg	P_r	h, kJ/kg	P_r
1820	1547	2027.61	1369.5	2079.44	1637.0	2129.57	1944.8	2178.08	2297	2225.07	2697
1830	1557	2040.00	1402.3	2092.25	1677.6	2142.80	1994.5	2191.73	2357	2239.10	2771
1840	1567	2052.39	1435.7	2105.08	1718.9	2156.05	2045.2	2205.38	2419	2253.15	2845
1850	1577	2064.78	1469.7	2117.91	1761.0	2169.30	2097	2219.04	2482	2267.20	2922
1860	1587	2077.19	1504.3	2130.75	1804.0	2182.56	2150	2232.71	2547	2281.27	3000
1870	1597	2089.60	1539.6	2143.60	1847.8	2195.83	2204	2246.39	2613	2295.34	3080
1880	1607	2102.02	1575.6	2156.45	1892.4	2209.11	2259	2260.08	2680	2309.43	3161
1890	1617	2114.44	1612.2	2169.32	1938.0	2222.40	2315	2273.77	2748	2323.52	3244
1900	1627	2126.87	1649.4	2182.19	1984.3	2235.69	2372	2287.48	2818	2337.63	3329
1910	1637	2139.31	1687.4	2195.06	2031.6	2249.00	2430	2301.19	2890	2351.74	3416
1920	1647	2151.75	1726.0	2207.95	2079.8	2262.31	2490	2314.92	2963	2365.86	3505
1930	1657	2164.20	1765.4	2220.84	2128.8	2275.62	2551	2328.65	3037	2379.99	3595
1940	1667	2176.66	1805.4	2233.74	2178.8	2288.95	2612	2342.39	3113	2394.13	3688
1950	1677	2189.12	1846.2	2246.64	2230	2302.28	2676	2356.13	3191	2408.28	3782
1960	1687	2201.59	1887.7	2259.55	2282	2315.62	2740	2369.89	3270	2422.43	3879
1970	1697	2214.06	1929.9	2272.47	2334	2328.97	2805	2383.65	3350	2436.60	3977
1980	1707	2226.54	1972.8	2285.40	2388	2342.32	2872	2397.42	3433	2450.77	4078
1990	1717	2239.03	2016.6	2298.33	2443	2355.68	2940	2411.20	3516	2464.95	4180
2000	1727	2251.52	2061	2311.26	2499	2369.05	3010	2424.98	3602	2479.14	4285
2010	1737	2264.02	2106	2324.21	2556	2382.43	3080	2438.77	3689	2493.34	4392
2020	1747	2276.52	2152	2337.16	2614	2395.81	3152	2452.57	3778	2507.54	4501
2030	1757	2289.03	2199	2350.11	2672	2409.20	3226	2466.38	3869	2521.75	4612
2040	1767	2301.55	2247	2363.07	2732	2422.59	3301	2480.19	3961	2535.97	4725
2050	1777	2314.07	2295	2376.04	2793	2435.99	3377	2494.01	4055	2550.20	4841

2060	1787	2326.59	2345	2389.01	2855	2449.40	3454	2507.84	4152	2564.43	4959
2070	1797	2339.12	2395	2401.99	2919	2462.81	3533	2521.67	4249	2578.67	5079
2080	1807	2351.65	2446	2414.98	2983	2476.23	3614	2535.52	4349	2592.92	5202
2090	1817	2364.19	2497	2427.97	3048	2489.66	3696	2549.36	4451	2607.18	5327
2100	1827	2376.74	2550	2440.96	3115	2503.09	3779	2563.22	4554	2621.44	5455
2110	1837	2389.29	2604	2453.97	3183	2516.53	3864	2577.07	4660	2635.71	5585
2120	1847	2401.85	2658	2466.97	3252	2529.97	3950	2590.94	4767	2649.98	5717
2130	1857	2414.41	2713	2479.98	3322	2543.42	4038	2604.81	4877	2664.26	5853
2140	1867	2426.97	2769	2493.00	3393	2556.88	4128	2618.69	4988	2678.55	5990
2150	1877	2439.54	2827	2506.03	3465	2570.34	4219	2632.58	5102	2692.85	6131
2160	1887	2452.12	2885	2519.06	3539	2583.80	4312	2646.47	5218	2707.15	6274
2170	1897	2464.70	2944	2532.09	3614	2597.28	4406	2660.37	5336	2721.46	6420
2180	1907	2477.29	3004	2545.13	3690	2610.76	4502	2674.27	5456	2735.77	6568
2190	1917	2489.88	3065	2558.18	3768	2624.24	4600	2688.18	5578	2750.10	6720
2200	1927	2502.48	3126	2571.23	3847	2637.73	4699	2702.10	5702	2764.43	6874
2210	1937	2515.08	3189	2584.29	3927	2651.23	4801	2716.02	5829	2778.76	7031
2220	1947	2527.69	3253	2597.35	4008	2664.74	4904	2729.95	5958	2793.11	7191

Table D.2 British Engineering (BE) units

T		$f = 0$		$f = 0.0169$		$f = 0.0338$		$f = 0.0507$		$f = 0.0676$	
°R	°F	h, Btu/lbm	P_r	h, Btu/lbm	P_r	h, Btu/lbm	P_r	h, Btu/lbm	P_r	h, Btu/lbm	P_r
300	−160	71.55	0.1775	71.98	0.1744	72.40	0.1715	72.80	0.1687	73.19	0.1660
320	−140	76.36	0.2225	76.82	0.2190	77.27	0.2156	77.71	0.2124	78.13	0.2094
340	−120	81.16	0.2752	81.66	0.2712	82.15	0.2675	82.62	0.2639	83.08	0.2605
360	−100	85.95	0.3361	86.50	0.3318	87.03	0.3278	87.54	0.3239	88.04	0.3202
380	−80	90.74	0.4059	91.34	0.4015	91.91	0.3973	92.47	0.3933	93.01	0.3894
400	−60	95.53	0.4856	96.18	0.4812	96.80	0.4769	97.40	0.4729	97.99	0.4690
420	−40	100.32	0.5757	101.02	0.5716	101.69	0.5675	102.35	0.5637	102.98	0.5600
440	−20	105.10	0.6772	105.86	0.6736	106.59	0.6700	107.30	0.6667	107.99	0.6634
460	0	109.88	0.7909	110.70	0.7881	111.49	0.7854	112.26	0.7828	113.00	0.7803
480	20	114.67	0.9175	115.55	0.9160	116.40	0.9145	117.23	0.9131	118.03	0.9117
500	40	119.45	1.0580	120.40	1.0582	121.32	1.0585	122.21	1.0587	123.07	1.0589
520	60	124.24	1.213	125.25	1.216	126.24	1.218	127.19	1.221	128.12	1.223
540	80	129.02	1.384	130.11	1.390	131.17	1.395	132.19	1.400	133.18	1.406
560	100	133.81	1.572	134.98	1.581	136.11	1.590	137.20	1.599	138.25	1.608
580	120	138.61	1.777	139.85	1.791	141.05	1.805	142.21	1.818	143.34	1.831
600	140	143.41	2.00	144.73	2.02	146.00	2.04	147.24	2.06	148.44	2.08
620	160	148.21	2.24	149.61	2.27	150.97	2.30	152.28	2.32	153.55	2.35
640	180	153.01	2.51	154.50	2.54	155.94	2.58	159.33	2.61	158.68	2.64
660	200	157.83	2.79	159.40	2.84	160.92	2.88	162.39	2.92	163.81	2.96
680	220	162.65	3.10	164.30	3.16	165.91	3.21	167.46	3.26	168.97	3.31
700	240	167.47	3.44	169.22	3.50	170.91	3.57	172.55	3.63	174.13	3.70
720	260	172.30	3.80	174.14	3.88	175.92	3.95	177.64	4.03	179.31	4.11
740	280	177.14	4.18	179.07	4.28	180.94	4.37	182.75	4.47	184.51	4.56
760	300	181.99	4.59	184.02	4.71	185.98	4.82	187.88	4.93	189.72	5.04

780	320	186.84	5.04	188.97	5.17	191.02	5.30	193.01	5.44	194.94	5.57
800	340	191.71	5.51	193.93	5.67	196.08	5.82	198.16	5.98	200.18	6.13
820	360	196.58	6.02	198.90	6.20	201.15	6.38	203.32	6.56	205.43	6.74
840	380	201.46	6.56	203.89	6.77	206.23	6.97	208.50	7.18	210.70	7.39
860	400	206.35	7.13	208.88	7.37	211.32	7.61	213.69	7.85	215.98	8.09
880	420	211.25	7.74	213.89	8.02	216.43	8.29	218.89	8.57	221.28	8.84
900	440	216.17	8.39	218.90	8.70	221.55	9.02	224.11	9.33	226.59	9.64
920	460	221.09	9.08	223.93	9.43	226.68	9.79	229.35	10.14	231.92	10.50
940	480	226.02	9.81	228.97	10.21	231.83	10.61	234.59	11.01	237.27	11.42
960	500	230.96	10.58	234.03	11.03	236.99	11.48	239.86	11.94	242.63	12.39
980	520	235.92	11.40	239.09	11.91	242.16	12.41	245.13	12.92	248.01	13.44
1000	540	240.89	12.27	244.17	12.83	247.35	13.40	250.43	13.97	253.40	14.54
1020	560	245.86	13.18	249.26	13.81	252.55	14.44	255.73	15.08	258.82	15.72
1040	580	250.85	14.15	254.37	14.84	257.77	15.55	261.06	16.26	264.24	16.98
1060	600	255.86	15.17	259.49	15.94	263.00	16.72	266.39	17.51	269.69	18.31
1080	620	260.87	16.24	264.62	17.09	268.24	17.96	271.75	18.83	275.15	19.72
1100	640	265.89	17.37	269.76	18.31	273.50	19.26	277.12	20.23	280.62	21.22
1100	640	265.89	17.37	269.76	18.31	273.50	19.26	277.12	20.23	280.62	21.22
1120	660	270.93	18.56	274.92	19.59	278.77	20.64	282.50	21.72	286.12	22.80
1140	680	275.98	19.81	280.09	20.94	284.06	22.10	287.90	23.28	291.63	24.48
1160	700	281.05	21.12	285.27	22.37	289.36	23.64	293.32	24.93	297.15	26.25
1180	720	286.12	22.50	290.47	23.86	294.68	25.26	298.75	26.68	302.70	28.13
1200	740	291.21	23.95	295.68	25.44	300.01	26.96	304.20	28.52	308.26	30.11
1220	760	296.31	25.47	300.91	27.09	305.36	28.75	309.66	30.46	313.83	32.20
1240	780	301.42	27.06	306.15	28.83	310.72	30.64	315.14	32.50	319.43	34.40
1260	800	306.55	28.73	311.40	30.65	316.10	32.62	320.64	34.65	325.04	36.72
1280	820	311.69	30.48	316.67	32.56	321.49	34.70	326.15	36.91	330.66	39.17

(continued)

Table D.2 British Engineering (BE) units (continued)

T		$f = 0$		$f = 0.0169$		$f = 0.0338$		$f = 0.0507$		$f = 0.0676$	
°R	°F	h, Btu/lbm	P_r	h, Btu/lbm	P_r	h, Btu/lbm	P_r	h, Btu/lbm	P_r	h, Btu/lbm	P_r
1300	840	316.84	32.31	321.95	34.56	326.89	36.89	331.68	39.28	336.31	41.75
1320	860	322.00	34.22	327.24	36.66	332.31	39.18	337.22	41.78	341.97	44.46
1340	880	327.18	36.22	332.55	38.86	337.75	41.59	342.78	44.40	347.65	47.31
1360	900	332.37	38.28	337.87	41.16	343.20	44.11	348.35	47.16	353.34	50.30
1380	920	337.57	40.49	343.21	43.64	348.66	46.95	353.94	50.39	359.05	53.95
1400	940	342.79	42.77	348.56	46.07	354.14	49.51	359.54	53.07	364.78	56.75
1420	960	348.01	45.14	353.92	48.70	359.63	52.40	365.17	56.24	370.52	60.22
1440	980	353.25	47.62	359.30	51.45	365.14	55.43	370.80	59.57	376.28	63.86
1460	1000	358.50	50.21	364.69	54.31	370.67	58.59	376.45	63.04	382.06	67.67
1480	1020	363.77	52.90	370.09	57.30	376.20	61.90	382.12	66.69	387.85	71.66
1500	1040	369.04	55.70	375.50	60.42	381.75	65.35	387.80	70.49	393.66	75.85
1520	1060	374.33	58.62	380.93	63.67	387.32	68.96	393.50	74.48	399.48	80.23
1540	1080	379.63	61.66	386.37	67.06	392.90	72.72	399.21	78.64	405.32	84.81
1560	1100	384.95	64.83	391.83	70.59	398.49	76.65	404.93	82.98	411.18	89.61
1580	1120	390.27	68.11	397.30	74.27	404.10	80.74	410.68	87.52	417.05	94.62
1600	1140	395.60	71.53	402.78	78.10	409.72	85.01	416.43	92.26	422.93	99.86
1620	1160	400.95	75.08	408.27	82.08	415.35	89.46	422.20	97.21	428.83	105.33
1640	1180	406.31	78.77	413.78	86.22	421.00	94.09	427.98	102.36	434.75	111.05
1660	1200	411.68	82.60	419.29	90.53	426.66	98.91	433.78	107.74	440.68	117.01
1680	1220	417.06	86.58	424.82	95.01	432.33	103.93	439.60	113.34	446.63	123.24
1700	1240	422.45	90.70	430.36	99.66	438.02	109.15	445.42	119.18	452.59	129.73
1720	1260	427.86	94.98	435.92	104.50	443.72	114.59	451.26	125.26	458.57	136.51
1740	1280	433.27	99.42	441.48	109.52	449.43	120.23	457.12	131.58	464.56	143.56
1760	1300	438.70	104.02	447.06	114.73	455.15	126.11	462.98	138.17	470.57	150.92

1780	1320	444.13	108.78	452.65	120.13	460.89	132.21	468.86	145.02	476.59	158.58
1800	1340	449.58	113.72	458.25	125.74	466.64	138.54	474.76	152.14	482.62	166.55
1820	1360	455.03	118.83	463.86	131.55	472.40	145.12	480.66	159.55	488.67	174.85
1840	1380	460.50	124.13	469.48	137.58	478.17	151.95	486.58	167.24	494.73	183.49
1860	1400	465.97	129.60	475.11	143.82	483.96	159.03	492.51	175.24	500.80	192.47
1880	1420	471.46	135.27	480.76	150.29	489.75	166.38	498.46	183.55	506.89	201.8
1900	1440	476.95	141.13	486.41	157.00	495.56	174.00	504.42	192.17	512.99	211.5
1900	1440	476.95	141.13	486.41	157.00	495.56	174.00	504.42	192.17	512.99	211.5
1920	1460	482.46	147.19	492.08	163.93	501.38	181.90	510.39	201.1	519.11	221.6
1940	1480	487.97	153.46	497.75	171.11	507.21	191.09	516.37	210.4	525.23	232.1
1960	1500	493.50	159.93	503.44	178.55	513.05	198.57	522.36	220.0	531.37	243.0
1980	1520	499.03	166.62	509.13	186.23	518.91	207.4	528.37	230.0	537.53	254.3
2000	1540	504.57	173.53	514.84	194.2	524.77	216.4	534.38	240.4	543.69	266.0
2020	1560	510.12	180.66	520.55	202.4	530.64	225.9	540.41	251.1	549.87	278.2
2040	1580	515.68	188.02	526.28	210.9	536.53	235.6	546.45	262.2	556.06	290.8
2060	1600	521.24	195.62	532.01	219.7	542.42	245.7	552.50	273.8	562.26	303.9
2080	1620	526.82	203.5	537.75	228.7	548.33	256.1	558.56	285.7	568.47	317.5
2100	1640	532.40	211.6	543.50	238.1	554.24	266.9	564.63	298.0	574.70	331.5
2120	1660	537.99	219.9	549.26	247.8	560.16	278.1	570.72	310.8	580.93	346.1
2140	1680	543.59	228.5	555.03	257.8	566.10	289.6	576.81	324.0	587.18	361.2
2160	1700	549.20	237.4	560.81	268.1	572.04	301.5	582.91	337.7	593.44	376.8
2180	1720	554.82	246.5	566.60	278.7	578.00	313.8	589.03	351.9	599.71	393.0
2200	1740	560.44	255.9	572.39	289.7	583.96	326.5	595.15	366.5	605.99	409.8
2220	1760	566.07	265.6	578.20	301.0	589.93	339.6	601.28	381.6	612.28	427.1
2240	1780	571.71	275.6	584.01	312.6	595.91	353.1	607.43	397.2	618.58	445.1
2260	1800	577.35	285.8	589.83	324.6	601.90	367.1	613.58	413.4	624.89	463.6
2280	1820	583.00	296.4	595.66	337.0	607.90	381.5	619.74	430.0	631.21	482.8

(continued)

Table D.2 British Engineering (BE) units (continued)

T		$f = 0$		$f = 0.0169$		$f = 0.0338$		$f = 0.0507$		$f = 0.0676$	
°R	°F	h, Btu/lbm	P_r	h, Btu/lbm	P_r	h, Btu/lbm	P_r	h, Btu/lbm	P_r	h, Btu/lbm	P_r
2300	1840	588.66	307.3	601.49	349.8	613.90	396.4	625.91	447.3	637.54	502.6
2320	1860	594.33	318.5	607.34	362.9	619.92	411.7	632.10	465.0	643.89	523.1
2340	1880	600.00	330.0	613.19	376.5	625.94	427.5	638.29	483.4	650.24	544.3
2360	1900	605.68	341.8	619.05	390.4	631.97	443.8	644.49	502.3	656.60	566.2
2380	1920	611.37	354.0	624.91	404.7	638.01	460.6	650.69	521.8	662.97	588.8
2400	1940	617.06	366.5	630.78	419.5	644.06	477.9	656.91	542.0	669.35	612.1
2420	1960	622.76	379.4	636.66	434.7	650.12	495.7	663.14	562.8	675.74	636.2
2440	1980	628.46	392.6	642.55	450.3	656.18	514.1	669.37	584.2	682.14	661.1
2460	2000	634.17	406.2	648.45	466.4	662.25	533.0	675.61	606.3	688.55	686.7
2480	2020	639.89	420.2	654.35	482.9	668.33	552.4	681.86	629.1	694.97	713.2
2500	2040	645.62	434.5	660.26	499.9	674.42	572.5	688.12	652.5	701.39	740.5
2520	2060	651.34	449.2	666.17	517.4	680.51	593.1	694.39	676.7	707.83	768.6
2540	2080	657.08	464.3	672.09	535.4	686.61	614.3	700.66	711.6	714.27	797.7
2560	2100	662.82	479.8	678.02	553.8	692.72	636.1	706.95	727.2	720.72	827.6
2580	2120	668.57	495.7	683.95	572.8	698.83	658.6	713.24	753.6	727.18	858.4
2600	2140	674.32	512.0	689.89	592.3	704.96	681.7	719.53	780.8	733.65	890.2
2620	2160	680.08	528.8	695.84	612.3	711.09	705.4	725.84	808.7	740.13	923.0
2640	2180	685.84	546.0	701.79	632.8	717.22	729.8	732.15	837.5	746.61	956.7
2660	2200	691.61	563.6	707.75	653.9	723.36	754.9	738.47	867.1	753.11	991.4
2680	2220	697.38	581.6	713.72	675.6	729.51	780.6	744.80	897.6	759.61	1027.2
2700	2240	703.16	600.2	719.69	697.8	735.67	807.1	751.14	928.9	766.12	1064.0
2700	2240	703.16	600.2	719.69	697.8	735.67	807.1	751.14	928.9	766.12	1064.0
2720	2260	708.95	619.2	725.66	720.6	741.83	834.3	757.48	961.1	772.63	1101.9
2740	2280	714.74	638.6	731.65	744.0	748.00	862.2	763.83	994.2	779.16	1141.0

2760	2300	720.53	658.6	737.63	768.0	754.18	890.9	770.19	1028.3	785.69	1181.1
2780	2320	726.33	679.0	743.63	792.6	760.36	920.4	776.55	1063.3	792.23	1222.4
2800	2340	732.14	699.9	749.63	817.9	766.55	950.6	782.92	1099.2	798.77	1264.9
2820	2360	737.95	721.3	755.63	843.8	772.74	981.6	789.30	1136.1	805.33	1308.5
2840	2380	743.77	743.3	761.65	870.3	778.94	1013.5	795.68	1174.1	811.89	1353.4
2860	2400	749.59	765.8	767.66	897.5	785.15	1046.2	802.07	1213.1	818.46	1399.6
2880	2420	755.41	788.8	773.68	925.4	791.36	1079.7	808.47	1253.1	825.03	1447.1
2900	2440	761.24	812.3	779.71	954.0	797.58	1114.1	814.87	1294.2	831.61	1495.9
2920	2460	767.08	836.4	785.74	983.2	803.80	1149.3	821.28	1336.4	838.20	1546.0
2940	2480	772.91	861.1	791.78	1013.2	810.03	1185.5	827.69	1379.7	844.80	1597.5
2960	2500	778.76	886.4	797.82	1044.0	816.27	1222.6	834.12	1424.1	851.40	1650.4
2980	2520	784.61	912.2	803.87	1075.4	822.51	1260.6	840.54	1469.7	858.01	1704.7
3000	2540	790.46	938.6	809.93	1107.6	828.75	1299.6	846.98	1516.5	864.63	1760.5
3020	2560	796.32	965.7	815.98	1140.6	835.01	1339.5	853.42	1564.5	871.25	1817.9
3040	2580	802.18	993.3	822.05	1174.4	841.27	1380.5	859.87	1613.8	877.88	1876.7
3060	2600	808.05	1021.6	828.12	1209.0	847.53	1422.4	866.32	1664.3	884.51	1937.0
3080	2620	813.92	1050.5	834.19	1244.3	853.80	1465.4	872.78	1716.1	891.15	1999.0
3100	2640	819.79	1080.0	840.27	1280.6	860.07	1509.4	879.24	1769.2	897.80	2063
3120	2660	825.67	1110.2	846.35	1317.6	866.35	1554.4	885.71	1823.6	904.45	2128
3140	2680	831.55	1141.1	852.44	1355.5	872.63	1600.6	892.18	1879.4	911.11	2195
3160	2700	837.44	1172.6	858.53	1394.3	878.92	1647.8	898.66	1936.5	917.78	2263
3180	2720	843.33	1204.9	864.62	1433.9	885.22	1696.2	905.15	1995.1	924.45	2334
3200	2740	849.23	1237.8	870.73	1474.5	891.52	1745.8	911.64	2055	931.13	2406
3220	2760	855.13	1271.5	876.83	1515.9	897.82	1796.4	918.14	2117	937.81	2480
3240	2780	861.03	1305.8	882.94	1558.3	904.13	1848.3	924.64	2180	944.50	2556
3260	2800	866.94	1340.9	889.06	1601.7	910.45	1901.4	931.15	2244	951.20	2634
3280	2820	872.85	1376.8	895.17	1646.0	916.77	1955.7	937.66	2310	957.90	2714

(continued)

Table D.2 British Engineering (BE) units (continued)

T		$f = 0$		$f = 0.0169$		$f = 0.0338$		$f = 0.0507$		$f = 0.0676$	
°R	°F	h, Btu/lbm	P_r	h, Btu/lbm	P_r	h, Btu/lbm	P_r	h, Btu/lbm	P_r	h, Btu/lbm	P_r
3300	2840	878.77	1413.4	901.30	1691.2	923.09	2011	944.18	2378	964.60	2795
3320	2860	884.69	1450.7	907.43	1737.5	929.42	2068	950.70	2447	971.31	2879
3340	2880	890.61	1488.8	913.56	1784.8	935.75	2126	957.23	2518	978.03	2965
3360	2900	896.54	1527.8	919.69	1833.1	942.09	2186	963.76	2590	984.75	3053
3380	2920	902.47	1567.5	925.83	1882.4	948.43	2246	970.30	2665	991.48	3143
3400	2940	908.40	1608.1	931.98	1932.8	954.78	2309	976.84	2741	998.21	3235
3420	2960	914.34	1649.4	938.12	1984.3	961.13	2372	983.39	2818	1004.95	3329
3440	2980	920.28	1691.6	944.27	2037	967.48	2437	989.94	2898	1011.69	3426
3460	3000	926.23	1734.7	950.43	2091	973.84	2503	996.49	2979	1018.43	3524
3480	3020	932.18	1778.6	956.59	2145	980.20	2571	1003.05	3062	1025.18	3626
3500	3040	938.13	1823.4	962.75	2201	986.57	2640	1009.62	3147	1031.94	3730
3500	3040	938.13	1823.4	962.75	2201	986.57	2640	1009.62	3147	1031.94	3730
3520	3060	944.08	1869.1	968.92	2258	992.94	2711	1016.19	3234	1038.70	3836
3540	3080	950.04	1915.7	975.08	2317	999.31	2783	1022.76	3323	1045.46	3944
3560	3100	956.00	1963.2	981.26	2376	1005.69	2857	1029.34	3414	1052.23	4055
3580	3120	961.96	2012	987.43	2437	1012.07	2933	1035.92	3507	1059.01	4169
3600	3140	967.93	2062	993.61	2499	1018.46	3010	1042.50	3602	1065.78	4285
3620	3160	973.90	2111	999.80	2562	1024.85	3088	1049.09	3699	1072.57	4404
3640	3180	979.87	2163	1005.98	2627	1031.24	3169	1055.68	3798	1079.35	4525
3660	3200	985.85	2215	1012.17	2692	1037.63	3251	1062.28	3899	1086.14	4649
3680	3220	991.83	2268	1018.36	2759	1044.03	3334	1068.88	4003	1092.93	4776
3700	3240	997.81	2322	1024.56	2828	1050.44	3420	1075.48	4109	1099.73	4906
3720	3260	1003.79	2378	1030.76	2897	1056.84	3507	1082.09	4217	1106.53	5039
3740	3280	1009.78	2434	1036.96	2969	1063.25	3596	1088.70	4327	1113.34	5174

3760	3300	1015.77	2492	1043.16	3041	1069.66	3686	1095.31	4439	1120.15	5313
3780	3320	1021.76	2550	1049.37	3115	1076.08	3779	1101.93	4554	1126.96	5455
3800	3340	1027.76	2610	1055.58	3190	1082.50	3873	1108.55	4672	1133.77	5599
3820	3360	1033.75	2670	1061.80	3267	1088.92	3970	1115.17	4792	1140.59	5747
3840	3380	1039.75	2732	1068.01	3345	1095.34	4068	1121.80	4914	1147.41	5898
3860	3400	1045.76	2795	1074.23	3425	1101.77	4168	1128.43	5039	1154.24	6052
3880	3420	1051.76	2859	1080.45	3506	1108.21	4270	1135.06	5166	1161.07	6210
3900	3440	1057.77	2924	1086.68	3589	1114.64	4374	1141.70	5296	1167.91	6371
3920	3460	1063.78	2990	1092.91	3673	1121.08	4481	1148.34	5429	1174.74	6535
3940	3480	1069.80	3058	1099.14	3759	1127.52	4589	1154.99	5564	1181.58	6703
3960	3500	1075.81	3126	1105.37	3847	1133.96	4699	1161.63	5702	1188.43	6874
3980	3520	1081.83	3196	1111.61	3936	1140.41	4812	1168.29	5843	1195.28	7049
4000	3540	1087.86	3268	1117.85	4027	1146.86	4927	1174.94	5987	1202.13	7227

Page is intentionally blank

Appendix E
Turbomachinery Stresses and Materials

E.1 Introduction

Even though the focus of this textbook is the aerothermodynamics of the gas turbine engine, the importance of the engine structure is also very significant. Because of its importance, this appendix addresses the major stresses of the rotating components and the properties of materials used in these components. The rotating components of the compressor and turbine have very high momentum, and failure of one part can be catastrophic, with a resulting destruction of the engine and, in the extreme, the aircraft. This is especially true of the "critical" parts of the turbomachinery such as the long first-stage fan blades and the heavy airfoils and disks of the cooled high-pressure turbine.

Over their lives, the rotating parts must endure in a very harsh environment where the loads are very dependent on the engine use. For example, an engine developed for a commercial aircraft will not be subjected to as many throttle excursions as one developed for a fighter aircraft. As a result, the "hot section" [combustor and turbine(s)] of the fighter engine will be subjected to many more thermal cycles per hour of operation than that of the commercial aircraft.

The main focus of the analytical tools developed in this appendix is on the fundamental source of stresses in rotating components—the centrifugal force. To get some idea of the brutal climate in which these components must live, the centrifugal force experienced by an element of material rotating at 10,000 rpm with a radius of 1 ft (0.3 m) is equivalent to more than 34,000 g. Yet, there are many other forces at work that can consume the life of (or destroy) rotating parts, all of which must be considered in the design process. Some of the most important include:

1) Stresses due to bending moments like those due to the lift on the airfoils or pressure differences across disks.

2) Buffeting or vibratory stresses that occur as the airfoils pass through nonuniform incident flows such as the wakes of upstream blades. This can be most devastating when the *blade passing* frequency coincides with one of the lower natural frequencies of the airfoils.

3) Airfoil or disk flutter, an aeroelastic phenomenon in which a natural frequency is spontaneously excited, the driving energy being extracted from the flowing gas. This is most often found in fan and compressor rows, and once it has begun, the life of the engine is measured in minutes.

4) Torsional stresses that result from the transfer of power from the turbine to the compressor.

5) Temperature gradients that can give rise to very high stresses. These can be very extreme during throttle transients when the engine is moving from one power setting to another. These cyclic thermal stresses extract life from components, especially in the hot section of fighter engines. This is commonly called *thermal* or *low-cycle* fatigue.

6) Local stress concentrations that result from holes, slots, corners, and cracks—the most feared of all.

7) Foreign object damage (FOD) and domestic object damage (DOD) that result from external and internal objects, respectively. The need to withstand FOD or DOD can dramatically impact the design. The use of lightweight, nonmetallic materials for large fan blades has been prevented for several decades due to requirement that they withstand bird strikes.

Each of these areas and many others are included in the design of engine components and material selection. After these are accounted for, an *allowable working stress* is developed and commonly used for the principal tensile stresses alone.

The next section analyzes dominant stresses in the rotating components. Figure E.1 depicts a turbine rotor with its airfoils, rim, and disk. A compressor or fan rotor is constructed similarly. However, the portion of the airfoil stresses carried by the compressor or fan's rim is much greater than that of a turbine rotor; hence, its disk is either much smaller or nonexistent. We consider the principal stresses of each part, starting with the airfoils.

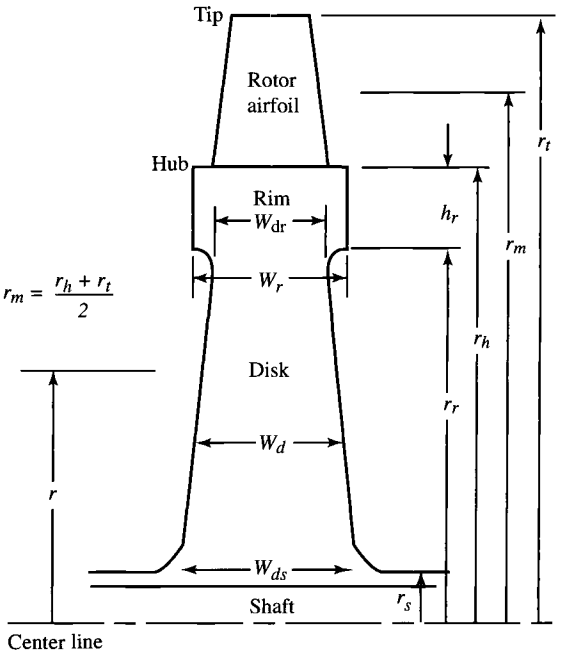

Fig. E.1 Turbomachinery rotor nomenclature.

E.2 Turbomachinery Stresses

E.2.1 Rotor Airfoil Centrifugal Stress σ_c

We start by considering the force in an airfoil at a cross section (see Fig. E.2). At any radius r, the force must restrain the centrifugal force on all the material beyond it. Thus the hub or base of the airfoil must experience the greatest force. The total centrifugal force acting on A_h is

$$F_c = \int_{r_h}^{r_t} \rho\omega^2 A_b r \, dr \tag{E.1}$$

so that the principal tensile stress is

$$\sigma_c = \frac{F_c}{A_h} = \rho\omega^2 \int_{r_h}^{r_t} \frac{A_b}{A_h} r \, dr \tag{E.2}$$

The airfoil cross-sectional area usually tapers down or reduces with, increasing radius, which, according to Eq. (E.2), has the effect of reducing σ_c. If the taper is *linear*, we can write

$$\frac{A_b}{A_h} = 1 - \left(1 - \frac{A_t}{A_h}\right)\left(\frac{r - r_h}{r_t - r_h}\right) \tag{E.3}$$

and Eq. (E.2) becomes

$$\sigma_c = \rho\omega^2 \left[\frac{A}{2\pi} - \left(1 - \frac{A_t}{A_h}\right) \int_{r_h}^{r_t} \left(\frac{r - r_h}{r_t - r_h}\right) r \, dr\right] \tag{E.4}$$

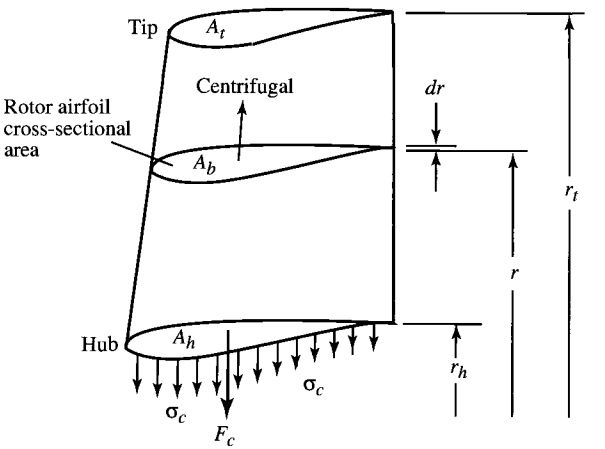

Fig. E.2 Rotor airflow centrifugal stress nomenclature.

where A is the flow path annulus area $\pi(r_t^2 - r_h^2)$. Integration of Eq. (E.4) gives

$$\sigma_c = \frac{\rho\omega^2 A}{4\pi}\left[2 - \frac{2}{3}\left(1 - \frac{A_t}{A_h}\right)\left(1 + \frac{1}{1 + r_h/r_t}\right)\right] \tag{E.5}$$

Equation (E.5) has an upper limit (corresponding to $r_h/r_t = 1$) of

$$\sigma_c = \frac{\rho\omega^2 A}{4\pi}\left(1 + \frac{A_t}{A_h}\right) \tag{E.6}$$

This equation reveals the basic characteristic that σ_c is proportional to $\rho\omega^2 A$. It also shows that tapering can, at most, reduce the stress of a *straight* airfoil (i.e., $A_t = A_h$) by half (i.e., $A_t = 0$).

Common practice in the industry is to refer to $\omega^2 A$ as the term AN^2 because it is easy to calculate and use. The COMPR computer program calculates and outputs AN^2 for each stage for proper material selection. For the TURBN computer program, the value of AN^2 is calculated and output for each stage.

We note that

$$AN^2 = A\omega^2\left(\frac{30}{\pi}\right)^2 \tag{E.7}$$

By using Eq. (E.7), we obtain for Eq. (E.6)

$$\frac{\sigma_c}{\rho} = AN^2\frac{\pi}{3600}\left(1 + \frac{A_t}{A_h}\right) \tag{E.8}$$

For a fixed value of AN^2, Eq. (E.8) shows the obvious reduction in centrifugal stress by using more lightweight materials [e.g., titanium with a density of about 9 slug/ft^3 (about 4600 kg/m^3)] rather than the heavier materials [densities of about 16 slug/ft^3 (about 8200 kg/m^3)]. This equation is given in graphical form in Fig. E.3 for several different airfoil taper ratios A_t/A_h for AN^2 values from 0 to 6×10^{10} in.$^2 \cdot$rpm^2 (3.87×10^7 m$^2 \cdot$rpm^2).

Example E.1

In this example, we determine the centrifugal stresses at 10,000 rpm in typical airfoil materials of a compressor ($\rho = 9.0$ slug/ft^3) and turbine ($\rho = 15.0$ slug/ft^3) with flow annulus areas of 2.0 and 1.0 ft^2, respectively. Table E.1 summarizes the results, using Eq. (E.8) for an airfoil taper A_t/A_h of 0.8. For the compressor, $\sigma_c = (\pi/3.6)(9/1.44^2)(2.88)(1.8) = 19.63$ ksi. Even though the compressor centrifugal stress is higher than that in the turbine airfoil, the turbine airfoils are subjected to higher temperatures and will, most likely, have a lower *allowable working stress.*

E.2.2 Rim Web Thickness W_{dr}

The rotating airfoils are inserted into slots in an otherwise solid annulus of material known as the *rim* (see Fig. E.1), which maintains their circular motion. The airfoil hub tensile stress σ_c is treated as though "smeared out"

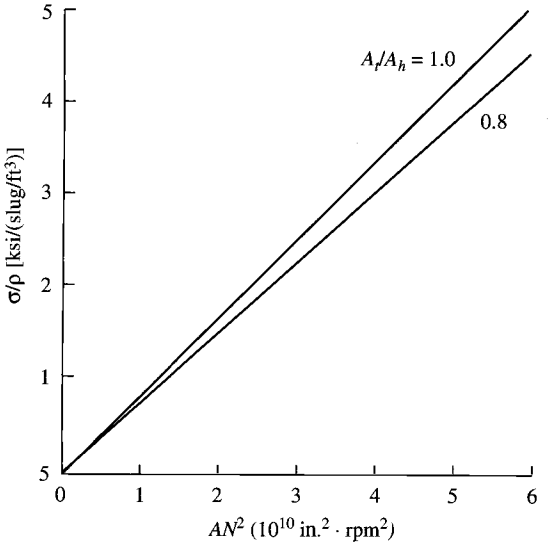

Fig. E.3 Variation of centrifugal stress-to-density ratio with AN^2.

over the outer rim surface, so that

$$\bar{\sigma}_{\text{blades}} = \frac{\sigma_c n_b A_h}{2\pi r_h W_r} \tag{E.9}$$

where n_b is the number of blades on the *wheel*.

Assuming uniform stress within the rim σ_r, we can use the force diagram of Fig. E.4 to determine the dimension W_{dr} (see Fig. E.1) necessary to balance

Table E.1 Centrifugal stress results for Example E.1

Variable	Compressor	Turbine
ρ slug/ft^3	9.0	15.0
(kg/m^3)	4611	7686
N rpm	10,000	10,000
A ft^2	2.0	1.0
(m^2)	0.186	0.0929
AN^2 in.^{2}·rpm^2	2.88×10^{10}	1.44×10^{10}
(m^2·rpm^2)	1.86×10^7	9.29×10^6
A_t/A_h	0.8	0.8
σ_c psi	19,630	16,360
(MPa)	135.3	112.8

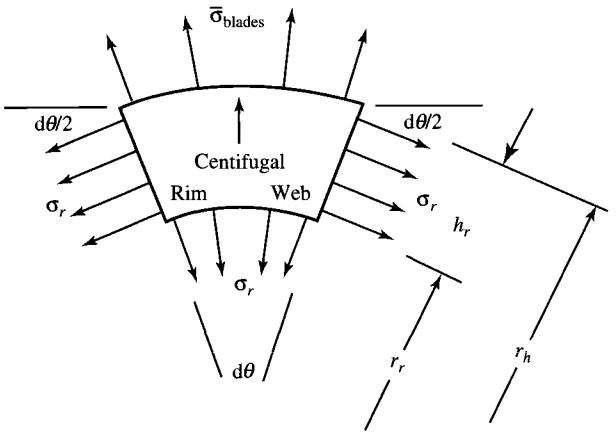

Fig. E.4 Rim segment radial equilibrium nomenclature.

the blade and rim centrifugal forces. Please note that W_r and h_r are simply sensible initial choices, where W_r approximates the axial chord of the airfoil and h_r is similar in magnitude to W_r. It is important to realize that it will always be possible to design a rim large enough to "carry" the airfoils. The real question is whether the size of the rim is practical from the standpoint of space required, weight, and manufacturing cost. Thus, there is no absolute solution, and the final choice must be based on experience and a sense of proportion.

A radial force balance of the differential rim element shown in Fig. E.4 gives

$$\bar{\sigma}_{\text{blades}} r_h W_r \, d\theta + \rho\omega^2 h_r W_r (r_r + h_r/2)^2 \, d\theta = \sigma_r r_r W_{\text{dr}} \, d\theta + 2\left(\sigma_r h_r W_r \frac{d\theta}{2}\right)$$

which, for any infinitesimal $d\theta$, becomes

$$\frac{W_{\text{dr}}}{W_r} = \left[\frac{\bar{\sigma}_{\text{blades}}}{\sigma_r}\left(1 + \frac{r_r}{h_r}\right) + \frac{\rho(\omega r_r)^2}{\sigma_r}\left(1 + \frac{h_r}{2r_r}\right)^2 - 1\right]\frac{h_r}{r_r} \tag{E.10}$$

If σ_r is sufficiently large, this equation clearly shows that W_{dr} can be zero or less, which means that the rim is *self-supporting*. Nevertheless, a token disk may still be required to transfer torque to the shaft and, of course, to keep the rim and airfoils in the right axial and radial position.

Example E.2

Using typical values of the terms in Eq. (E.10) for the compressor and turbine based on disk materials given in Table E.2, Eq. (E.10) yields $W_{\text{dr}}/W_r = 0.37$ for the compressor and $W_{\text{dr}}/W_r = 0.56$ for the turbine.

Table E.2 Typical data for Example E.2

Variable	Compressor	Turbine
$\bar{\sigma}_{\text{blades}}/\sigma_r$	0.10	0.20
h_r/r_r	0.05	0.10
$\rho(\omega r_r)^2/\sigma_r$	6.0	4.0

E.2.3 Disk of Uniform Stress

The disk supports and positions the rim while connecting it to the shaft. Its thickness begins with a value of W_{dr} at the inside edge of the rim and must grow as the radius decreases because of the accumulating centrifugal force that must be resisted. Just as was found for the rim, a disk can always be found that will perform the required job, but the size, weight, and/or cost may be excessive. Thus the final choice usually involves trial and error and judgment.

It is impossible to overemphasize the importance of ensuring the structural integrity of the disks, particularly the large ones found in cooled high-pressure turbines. Because they are very difficult to inspect and because massive fragments that fly loose when they disintegrate cannot be contained, they must not be allowed to fail.

The most efficient way to use available disk materials is to design the disk for constant radial and circumferential stress. Because the rim and disk are one continuous piece of material, the design stress would be the same throughout ($\sigma_r = \sigma_d$).

Applying locally radial equilibrium to the infinitesimal element of the disk of Fig. E.5 leads to the equation

$$\rho(\omega r_r)^2 W_d \, dr \, d\theta = \sigma_d \left[\left(r - \frac{dr}{2} \right) \left(W_d - \frac{dW_d}{2} \right) d\theta - \left(r + \frac{dr}{2} \right) \left(W_d + \frac{dW_d}{2} \right) d\theta + 2 \left(W_d \, dr \frac{d\theta}{2} \right) \right]$$

which becomes in the limit

$$\frac{dW_d}{W_d} + \frac{\rho\omega^2}{\sigma_d} d\left(\frac{r^2}{2}\right) = 0$$

This equation may be integrated, by starting from $r = r_r$ and $W_d = W_{\text{dr}}$, to yield the desired result:

$$\frac{W_d}{W_{\text{dr}}} = \exp\left\{ \frac{\rho(\omega r_r)^2}{2\sigma_d} \left[1 - \left(\frac{r}{r_r} \right)^2 \right] \right\} \tag{E.11}$$

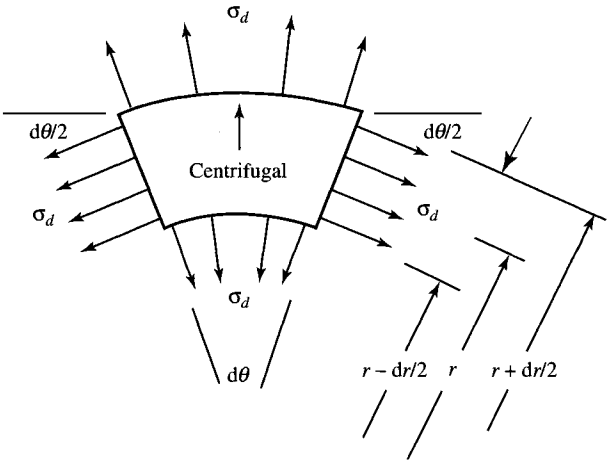

Fig. E.5 Disk element radial equilibrium nomenclature.

The fundamental feature of Eq. (E.11) is that the disk thickness W_d grows exponentially in proportion to $(\omega r_r)^2$, which is the square of the maximum or rim velocity of the disk. Because this parameter has such a great influence on disk design, it is normal to hear structural engineers talk in terms of *allowable wheel speed.*

Figure E.6 shows the thickness distribution for typical values of the *disk shape factor* (DSF) $\rho(\omega r_r)^2/(2\sigma_d)$ by using Eq. (E.11). Judging by the looks of these thickness distributions, the maximum allowable value of the disk shape factor

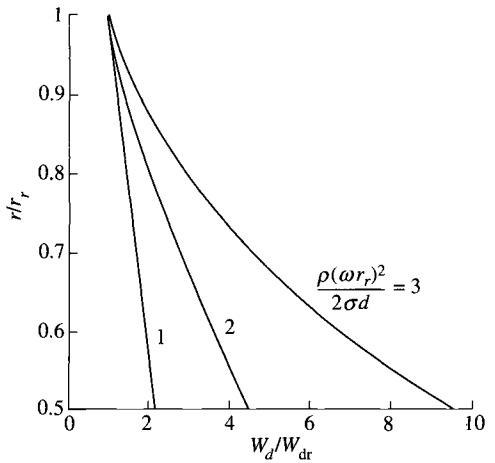

Fig. E.6 Disk thickness distributions.

is not much more than 2, so that

$$\omega r_r \approx \sqrt{\frac{4\sigma_d}{\rho}} \tag{E.12}$$

Note: At this point it should be apparent that, on the low-pressure spool where the annulus flow area A is largest, the rotational speed (ω or N) is most likely to be limited by the allowable blade centrifugal stress [Eq. (E.6) or Eq. (E.8)]. Conversely, on the high-pressure spool, where the annulus flow area is considerably less, the rotational speed will probably be limited by the allowable wheel speed [Eq. (E.12)].

Example E.3

Determine the allowable wheel speed for the typical compressor and turbine materials. The compressor material has $\sigma_d = 30$ ksi, $\rho = 9.0$ slug/ft^3, and thus $\sigma_d/\rho = 4.8 \times 10^5$ ft^2/s^2 (4.46×10^4 m^2/s^2). The turbine material has $\sigma_d = 20$ ksi, $\rho = 16.0$ slug/ft^3, and thus $\sigma_d/\rho = 1.8 \times 10^5$ ft^2/s^2 (1.67×10^4 m^2/s^2). Using Eq. (E.12), we see that the allowable wheel speed for the compressor is about 1400 ft/s (420 m/s) and that for the turbine is about 850 ft/s (260 m/s). This indicates that the allowable wheel speed is more likely to limit the design of a turbine than the design of a compressor.

E.2.4 Disk Torsional Stress τ_d

The tangential disk shear stress required to transfer the shaft horsepower to the airfoils is easily calculated, since

$$\text{HP} = \text{shear stress} \times \text{area} \times \text{velocity}$$

Thus

$$\tau_d = \frac{\text{HP}}{2\pi r^2 W_d \omega} \tag{E.13}$$

Example E.4

Determine the disk torsional stress for the following typical values:

$$\text{HP} = 10{,}000 \text{ hp } (7457 \text{ kW})$$
$$r = 0.30 \text{ ft } (0.0914 \text{ m})$$
$$W_d = 0.10 \text{ ft } (0.0305 \text{ m})$$
$$\omega = 1000 \text{ rad/s}$$

Equation (E.13) gives $\tau_d = 675$ psi (4.65 MPa), which makes a relatively small contribution to the overall stress.

E.2.5 Disk Thermal Stress σ_{tr} and $\sigma_{t\theta}$

For a disk of constant thickness with no center hole and a temperature distribution that depends only on radius [$T = T(r)$], it can be shown (Ref. 44) that the radial tensile stress is

$$\sigma_{tr} = \alpha E\left[\frac{1}{r_h^2}\int_0^{r_h} T(r)\mathrm{d}r - \frac{1}{r^2}\int_0^{r} T(t)\,\mathrm{d}r\right] \tag{E.14}$$

where α is the coefficient of linear thermal expansion and E is the modulus of elasticity, and the tangential tensile stress is

$$\sigma_{t\theta} = \alpha E\left[\frac{1}{r_h^2}\int_0^{r_h} T(r)\,\mathrm{d}r + \frac{1}{r^2}\int_0^{r} T(r)\,\mathrm{d}r - T\right] \tag{E.15}$$

both of which are zero if the temperature is constant. An interesting illustrative case is that of the linear temperature distribution $T = T_0 + \Delta T\ (r/r_h)$, for which Eq. (E.14) becomes

$$\sigma_{tr} = \frac{\alpha E\,\Delta T}{3}\left(1 - \frac{r}{r_h}\right) \tag{E.16}$$

and Eq. (E.15) becomes

$$\sigma_{t\theta} = \frac{\alpha E\,\Delta T}{3}\left(1 - 2\frac{r}{r_h}\right) \tag{E.17}$$

both of which have a maximum magnitude of $\alpha E\ \Delta T/3$ at $r = 0$.

Example E.5

For typical values of $\alpha = 1 \times 10^{-5}(°\mathrm{F})$ $[1.8 \times 10^{-5}\ 1(°\mathrm{C})^{-1}]$, $E = 10 \times 10^6$ psi (6.9×10^4 MPa), and $\Delta T = 100°\mathrm{F}$ (55.6°C), the maximum magnitude of σ_{tr} and $\sigma_{t\theta}$ is 6700 psi (46 MPa)! This simple case demonstrates forcefully that thermal stresses can be very large and, therefore, must be carefully accounted for and reduced as much as possible. This is especially true during transient operation.

With this perspective, it is possible to imagine that truly enormous stresses could be generated in the thin outer wall of the cooled turbine airfoils, if they are not very carefully designed. Because such stresses will be proportional to the temperature difference between the mainstream and the cooling air, there is also a limit to how cold a coolant may be used before it no longer truly *protects* the material.

Table E.3 Material types

Material no.	Type	Density slug/ft^3	Density kg/m^3
1	Aluminum alloy	5.3	2716
2	Titanium alloy	9.1	4663
3	Wrought nickel alloy	16.0	8200
4	High-strength nickel alloy	17.0	8710
5	Single-crystal superalloy	17.0	8710

E.3 Engine Materials

The harsh environment of the gas turbine engine requires special materials. Many of these materials are developed exclusively for this application by material experts—most of these experts work for either an engine company or a materials company. Therefore, the properties of many materials used for critical components in gas turbine engines are corporate secrets, and published data are limited. However, some materials have been and continue to be developed in the public sector, and their properties can be found in references such as the *Aerospace Structural Metals Handbook* (Ref. 87) and *The Superalloys* (Ref. 88), textbooks (Refs. 89 and 90), and journals (Ref. 91).

To provide examples and general guidance, the data for several materials commonly found in critical parts of gas turbine engines are given in Table E.3 and

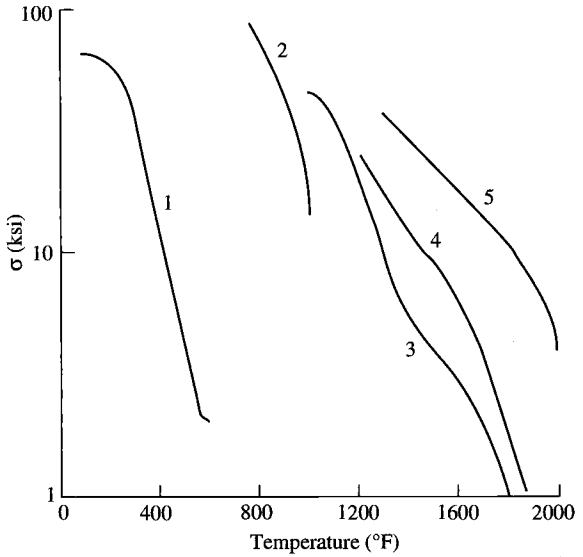

Fig. E.7 Strength at 1% creep for 1000 h.

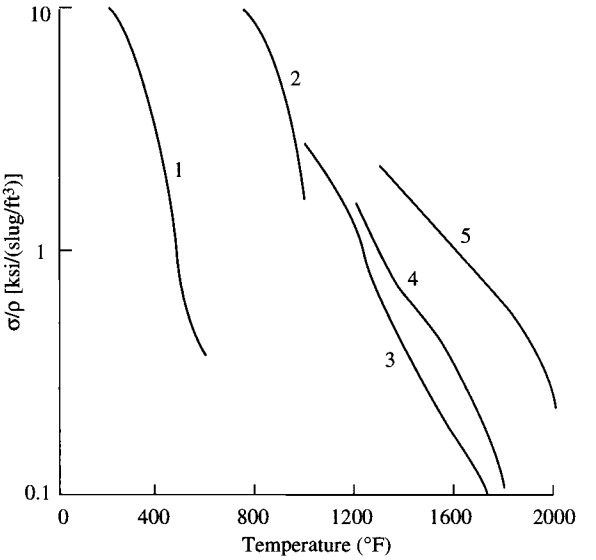

Fig. E.8 Strength-to-weight ratio at 1% creep for 1000 h.

Figs. E.7 and E.8. Figure E.7 gives the 1% creep curves of typical materials for 1000 h at temperatures between 0 and 2000°F. Dividing the material's creep strength by its density gives the material's strength/weight ratio. The variations of strength/weight ratio with temperature are given in Fig. E.8.

E.3.1 Compressor and Fan Materials

Normal practice for compressor and fan blades is to base designs on creep and creep-rupture data. Common practice is to allow less than 1% creep during the life of the part. A reasonable estimate of the *allowable working stress* is 30–50% of the value obtained from Fig. E.7 for 1000 h. For example, Fig. E.7 gives a 1% creep stress for material 1 of about 32 ksi at 300°F (220 MPa at 150°C) and 1000 h. Thus the *allowable working stress* for this material at these conditions would be from 10 to 16 ksi (70–110 MPa).

During its life, a fan or compressor blade is subjected to billions of *high-cycle fatigue* cycles due to vibrations. Thus it is important that the *run-out* stress, which the material can apparently withstand forever, not be exceeded. Aluminum 2124 alloy has a low run-out stress of about 12 ksi at room temperature while titanium 6246 alloy has a high run-out stress of about 140 ksi (about 1 MPa) at room temperature.[87] Because of the poor fatigue characteristics of aluminum alloys, titanium alloys are typically used for fan and low-pressure compressor blades and disks.

Titanium's strength/weight ratio is severely reduced at temperatures above 900°F (480°C). Hence nickel-base alloys are commonly used for the critical components of high-pressure compressors.

E.3.2 Turbine Materials

The critical components of the turbine are exposed to very high temperatures. Many of these parts require super materials, commonly called *superalloys*, and compressor air for cooling. Certain materials and environments also require protective coatings. Typical examples of these materials are Mar-M 509, a high-chromium, carbide-strengthened, cobalt-base superalloy, and René 80, a cast, precipitation-hardenable, nickel-base superalloy.[87] Many of the newer superalloys for turbine rotor blades are cast and solidified in such a manner as to align the crystals in the radial direction, called *directional solidification*, or to produce a single crystal. The resulting turbine blades are capable of operating at temperatures 100–200°F (55–110°C) above those of conventionally cast blades.

In high-pressure turbines, the blades are typically made of superalloys while high-strength, nickel-base alloys are used for the disks and rims. Because the temperatures are much lower in the low-pressure turbine, the critical components are not cooled and are frequently made from high-strength, nickel-base alloys.

Page is intentionally blank

Appendix F
About the Software

A comprehensive set of software is included to assist you in learning the text material, solving some of the problems in the text, and completing your design problems. The software programs use pull-down menus and edit fields that support a mouse to make them very user-friendly.

The AFPROP program defines the properties of air with hydrocarbon fuels and is provided in both executable and BASIC source code. The ATMOS program gives the properties of the atmosphere at any altitude for the user-selected temperature profile (standard, cold day, hot day, or tropic). The EQL program performs chemical equilibrium analysis for reactive mixtures of perfect gases. The GASTAB program gives complete one-dimensional gas dynamics tables for the user-selected ratio of specific heats.

PARA and PERF are a set of user-friendly computer programs written for the preliminary analyses of common airbreathing aircraft engine cycles. COMPR and TURBN are a set of computer programs that perform the preliminary analyses of axial-flow compressors and turbines, respectively. These programs allow you to solve a single problem, a number of "what if" solutions, or a design problem.

The current version of PARA, PERF, COMPR, and TURBN are written in Microsoft Visual Basic 6 with plotting procedures from APEX's Olectra Chart. Comprehensive user guides provided with the software will help answer most of your questions about the software.

F.1 Getting Started

To get started, you need a PC-compatible system with Microsoft Windows operation system (98 or later). The software is downloaded from the AIAA web site at *www.aiaa.org/publications/supportmaterials*. Follow the instructions provided and enter the following password: **GTandR2**.

Save the downloaded file and unpack into the files necessary for installation. Run the **Setup** program within the **EOP Software** folder and the opening installation window is displayed as shown in Fig. F.1

Select the OK button and the software destination window is displayed as shown in Fig. F.2.

Select the highlighted button in the upper left to install the programs in the default location (C:\Programs\EOP). The program group window is displayed as shown in Fig. F.3. It is recommended that the user uses the **EOP Software**

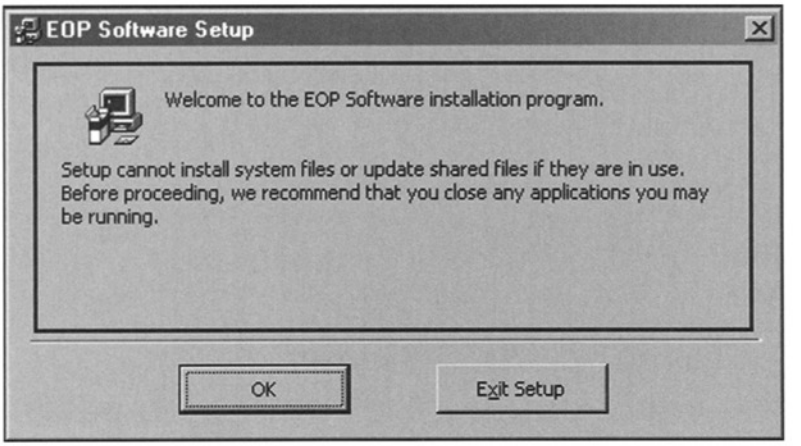

Fig. F.1 Opening installation window.

program group and presses the **Continue** button. Software installation will then proceed.

F.2 The Software

F.2.1 AFPROP.EXE (and AFPROP.BAS)

This program calculates the thermodynamic properties of air and fuel as a function of temperature and fuel/air ratio by using the equations in Chapter 2. Written in Microsoft Visual Basic 6, this program is supplied in both executable form (AFPROP.EXE) and source code (AFPROP.BAS). The source code can be used to write your own analysis programs with variable specific heats as discussed in Supporting Materials for Chapters 7 and 8.

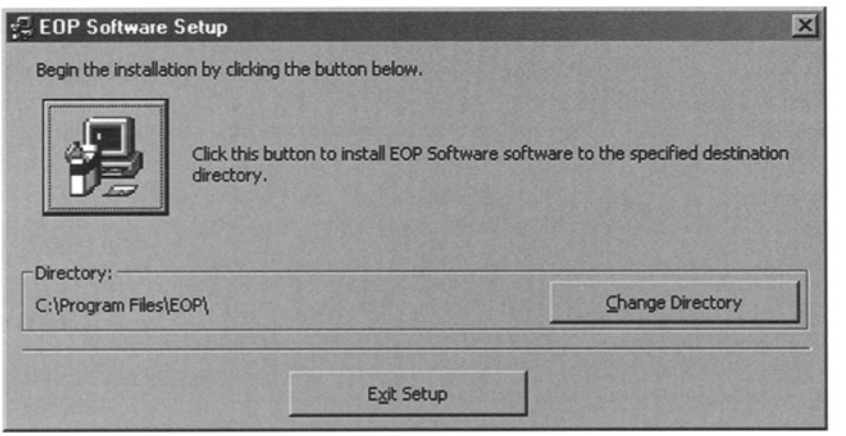

Fig. F.2 Installation destination window.

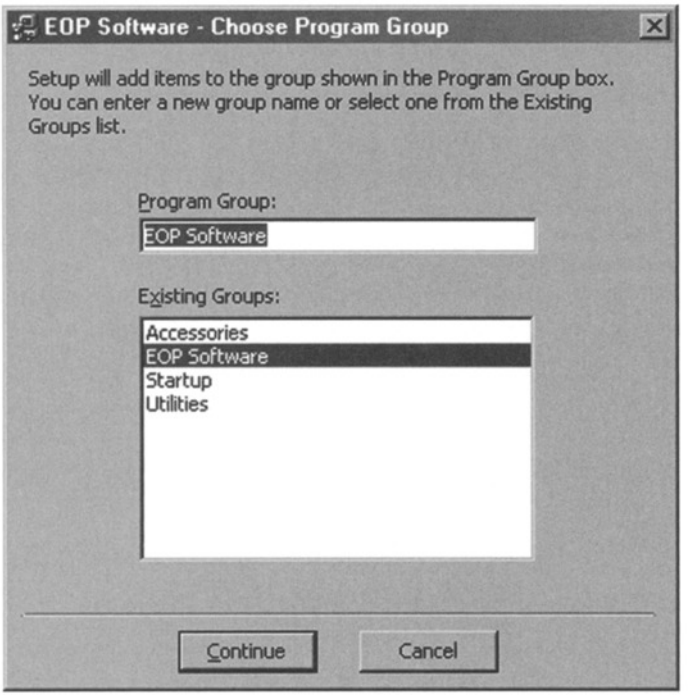

Fig. F.3 Program group window.

After selecting the unit system (English or SI), the user enters the fuel/air ratio and the temperature, or the enthalpy, or the reduced pressure. Input temperatures are limited to the range of 300°R (167 K) to 4000°R (2222 K), and the fuel/air ratio has a maximum value of 0.0676. The program will calculate the other properties in addition to the gas constant, specific heat at constant pressure, ratio of specified heats, and speed of sound.

F.2.2 ATMOS Program

This program calculates properties of the atmosphere for standard, cold, hot, and tropical days in either SI or English units.

F.2.3 EQL Program

The EQL program calculates equilibrium properties and process end states for reactive mixtures of perfect gases, for different problems involving hydrocarbon fuels. It supports the thermochemical analysis and problem in Chapters 2 and 3.

F.2.4 GASTAB.EXE

This program is equivalent to extensive, traditional, compressible flow appendices for the simple flows of calorically (constant specific heats) perfect gases.

It includes isentropic flow; adiabatic, constant area frictional flow (Fanno flow); frictionless, constant area heating and cooling (Rayleigh flow); normal shock waves; oblique shock waves; multiple oblique shock waves; and Prandtl-Meyer flow. The user inputs the ratio of specific heats γ, the mean molecular weight $\mathscr{M}$, and the known property. Then one clicks the check box beside this property and all other properties are calculated and displayed for that flow. The user can select the unit system (SI or English).

F.2.5 PARA.EXE

The PARA computer program determines the variation in gas turbine engine performance with cycle design variables such as the compressor pressure ratio. The program is based on the engine models contained in Chapters 5–7 of this book and is intended to be used with this textbook. The user can select the unit system (SI or English), the type of analysis model (ideal or real), the engine cycle (one of the eight engine cycles listed next), and the iteration variable (one of the five variables listed next or single-point calculation) along with its applicable range and increment. Data are entered and/or changed on data screens through edit fields. Results can be plotted on the screen by using defined ranges of plot data. In addition, the temperature vs entropy of the defined ideal engine cycle data can be plotted on the screen. The engine cycles and iteration variables are the following:

Engine cycles	**Variables**
Turbojet—single spool	Single point calculation
Turbojet—dual spool	Mach number
Turbojet with afterburner	Combustor exit temperature
Turbofan with two exhausts	Compressor pressure ratio
Turbofan with mixed exhaust	Fan pressure ratio
Turbofan with afterburning	Bypass ratio
Turboprop	
Ramjet	

This program is very useful for examining the trends of a selected engine cycle's specific performance (specific thrust and thrust specific fuel consumption) with changes in applicable design variables. Up to 21 sets of results can be plotted at a time. When one variable is used for calculations, results can be plotted vs the iteration variable. If more than one variable is used for calculations, only the specific performance (thrust specific fuel consumption vs specific thrust) of the cycle can be plotted.

The PARA program must have the default data file (PARA.PCA) in the same directory as the program. If the file is not in the current directory, the program will prompt you for the name of a Parametric Cycle Analysis file (*.PCA) as input.

F.2.6 PERF.EXE

The PERF computer program determines the performance of a specific engine and its variation with flight condition and throttle. The program is based on the engine models contained in Chapter 8 of this book and is intended to be used

with this textbook. Through pull-down menus, the user can select the specific engine cycle (one of the eight engine cycles listed next) and its design, the iteration variable (one of the eight variables listed next) along with its applicable range and increment, the control system limits (e.g., temperature leaving compressor), the unit system (SI or English), and the output device(s). Data are entered and/or changed on a data screen through edit fields. Results can be plotted on the screen by using defined ranges of plot data. The engine cycles and iteration variables are the following:

Engine cycles	**Variables**
Turbojet—single spool	Single point @% thrust
Turbojet—dual spool	Mach number
Turbojet with afterburner	Altitude
Turbofan with separate exhausts	Ambient temperature
Turbofan with mixed exhaust	Ambient pressure
Turbofan with afterburning	T_{14}—total temperature leaving combustor
Turboprop	T_{17}—total temperature leaving afterburner
Ramjet	Exit nozzle pressure ratio (P_0/P_9)

PERF is very useful for examining the variation of an engine's performance with changes in flight condition, throttle, and control system limits. Up to 21 sets of results can be plotted at a time. When one variable is used for calculations, results can be plotted vs the iteration variable. If more than one variable is used for calculations, only the thrust specific fuel consumption vs thrust of the engine can be plotted.

The PERF program must have the default data file (PERF.EPA) in the same directory as the program. If the file is not in the current directory, the program will prompt you for the name of an Engine Performance Analysis file (*.EPA) as input.

F.2.7 COMPR.EXE

The COMPR program calculates the change in properties along the mean line of a multistage, axial-flow compressor based on user input data. The program is based on the methods contained in Chapter 9 of this book and is intended to be used with this textbook. The user can select the type of design (one of the five types of design listed next), type of swirl distribution (one of the three swirl distributions listed next), and unit system (SI or English). Data are entered and/or changed on a data screen through edit fields. The results are given for the hub, mean, and tip radius for both rotor and stator blades of each stage and include flow angles, diffusion factors, degree of reactions, pressures, Mach numbers, temperatures, velocities, number of blades, and blade centrifugal stress. The types of design and swirl distributions are the following:

Type of design	**Swirl distribution**
Constant tip radius	Free vortex
Constant mean radius	Exponential
Constant hub radius	First power
User-specified tip radius	
Repeating row/stage	

After stage calculations are completed, the user can have the computer sketch a cross-sectional drawing on the graphics screen (e.g., see Figs. 9.33, 9.36a, and 9.36b). The user can also have the computer sketch the relative position and angle of rotor and stator blades, using the NACA 65A010 profile for a specified stage and number of blades. One can also look at the change in spacing and blade angles with changes in radius (e.g., see Figs. 9.30 and 9.31).

The COMPR program must have the default data file (COMPR.CMP) in the same directory as the program. If the file is not in the current directory, the program will prompt you for the name of a COMPR file (*.CMP) as input.

F.2.8 TURBN.EXE

The TURBN program calculates the change in properties along the mean line of a multistage, axial-flow turbine based on user input data. The program is based on the methods contained in Chapter 9 of this book and is intended to be used with this textbook. The user can select the unknown (one of the five cases listed next), the loss model (one of the two listed next), and the unit system (SI or English). Data are entered and/or changed on a data screen through edit fields. The results are given for the hub, mean, and tip radius for both stator and rotor blades of each stage and include flow angles, degree of reactions, pressures, Mach numbers, temperatures, velocities, number of blades, and solidities. The unknowns and loss models are the following:

Unknown	**Loss model**
Flow angle entering rotor	Polytropic efficiency
Flow angle leaving rotor—Case I	Loss coefficient
Flow angle leaving rotor—Case II	
Mach number entering rotor	
Total temperature leaving rotor	

After stage calculations are completed, the user can have the computer sketch a cross-sectional drawing of the turbine on the graphics screen (e.g., see Figs. 9.72, 9.76, and 9.78). The user can also have the computer sketch the relative position and angle of rotor and stator blades, using the British C4 or T6 profile for a specified stage and number of blades. One can also look at the change in spacing and blade angles with changes in radius (e.g., see Figs. 9.77, 9.79, and 9.80).

The TURBN program must have the default data file (TURBN.TBN) in the same directory as the program. If the file is not in the current directory, the program will prompt you for the name of a TURBN file (*.TBN) as input.

Appendix G
Answers to Selected Problems

1.1 50 kN
1.4 1973 ft/s
1.8 194,080 N, 33%, 10.23 (mg/s)/N
1.10 193.4 ft/s
1.11 78.5 m/s
1.14 (a) 7.906, 0.3162, 0.04; (b) 39.8 kft, 5,690 lbf; (c) 45 kft, 4,430 lbf; (d) 1,140 nm
1.15 (a) 5.774, 0.3464, 0.06; (b) 6.65 km, 19,050 N; (c) 12.07 km, 19,050 N
1.16 (a) 1,257 nm; (b) 1,127 nm
1.19 (a) 10.2, 0.2449, 0.024, 0.7946; (c) 0.80; (d) 0.76
1.20 9,970 s
1.22 5 kN, 91.84 s
1.23 (a) 14,700 m/s; (b) 568 kg/s

2.1 2,970 lbf
2.6 28,950 lbf
2.8 53,800 N
2.9 135,900 lbf
2.12 772.9 K, 0.22 m^2, 0.19 m^2
2.14 18.34 MW (24,590 hp)
2.16 (a) 98.6 lbm/s; (b) 904°R, 66.5 psia; (c) 1.69 ft^2
2.19 (a) 81.3 kg/s; (b) 1009.4 K, 1.601; (c) 0.307 m^2, −48,660 N
2.21 20.43 MW, 0.0988 m^3/kg, 17.61 J/(kg-K)
2.22 2880.7°R, 29.30 MW, 0.0077 Btu/(lbm-°R)
2.30 315.7°R, 1.7085, 1488 ft/s, 0.3929 ft^2
2.32 86.01 MW (115,340 hp)
2.34 6.87 kg/s, 0.263, 295.9 K, 90.53 m/s
2.39 311.1°R, 12.78 psia, 1729 ft/s; 560°R, 72.09 psia, 5525°R, 7.51 psia, 648.5 ft/s
2.41 (a) 0.2117 m^2; (b) 0.03811 MPa, 125 K; (c) 0.4752, 0.4597 MPa, 0.3938 MPa, 350 K, 334.9 K; (d) 0.1797, 0.4495 MPa, 347.8 K
2.44 27.38 deg, 96.3 psia, 500°R, 5.59 psia, 221.7°R

3.2 5,660 lbm/s
3.4 10.465

3.5 126,900 kg
3.8 6185 ft/s
3.11 227,980 N
3.13 1.820
3.16 (a) 250 lbm/s; (c) 758.9 psia; (e) 1.830; (g) 54 kft; (h) 78,830 lbf
3.21 (a) 2.529; (d) 4.323 lbm/s; (f) 1.405; (h) 180.4 s

4.1 108.9 kM, 1.64 kN
4.3 4,400 lbf
4.5 7.7 kN
4.6 0.045, 0.060
4.9 267.6 N

5.7 3.916, 7123 N/(kg/s), 35.8 (mg/s)/N
5.18 2.686
5.19 0.9425

6.4 (a) 0.8623, 0.8849, 0.8923, 0.9074; (b) 0.8932, 0.8739; (c) 0.9461, 1.8125, 0.8861, 2.037
6.5 0.979
6.6 0.670
6.7 (a) 0.9561, 0.9585; (b) 0.8594, 0.8737, 0.8996, 0.925; (c) 0.9225, 0.8924; (d) 30,035 hp (22.4 MW), 12,776 hp (9.53 MW), 57,702 hp (43.03 MW); (e) 105,160 hp (78.42 MW)

7.8 390 kPa, 540.6 K, 188.5 kPa, 1550.1 K, 1.724
7.9 (a) 5.502 ft^2; (b) 3.548 ft^2; (c) 8.165 lbm/s, 5.405 ft^2
7.11 Compressor pressure ratio range from 17.8 to 53
7.15 15.45 lbf/(lbm/s), 0.6075 (lbm/h)/lbf
SM7.1 111.9 lbf/(lbm/s), 1.852 (lbm/h)/lbf
SM7.3 Compressor pressure ratio range from 14.84 to 19.9 with a corresponding fan pressure ratio range of 2.860 to 2.847
SM7.8 $M_9 = 0.7657$, 1242 N/(kg/s), 16.05 (mg/s)/N
SM7.9 Compressor pressure ratio range from 10.83 to 17.71 with a corresponding turbine temperature ratio range of 0.5996 to 0.5400

8.2 (a) 0.0004508, 132.58; (b) 4.055, 16.28 kg/s; (c) 1620 K, 8, 25 kg/s, 1800 K, 6.92, 22.67 kg/s
8.6 (c) $M_9 = 2.715$, 605 N/(kg/s), 57.74 (mg/s)/N
8.7 2.2657, 14.316, 0.7750
8.8 $M_9 = 1.6276$, 18.622 kg/s, 10,590 N
8.9 (a) 97.0 lbm/s, 3.5124, 5.5672, 3223.6 ft/s, 10,129 lbf, 1.4445 (lbm/h)/lbf; (b) 4.7109, 86.01 lbm/s, 2.7578, 4.6393, 0.9129; (c) 5.3276, 92.74 lbm/s, 3.1188, 5.1032, 0.9574
8.14 525.8 lbm, 7,111 lbf, 0.6263 (lbm/h)/lbf
8.15 1918 lbm/s, 68,330 lbf, 0.3772 (lbm/h)/lbf

9.2 20.86 m/s, 41.72 m/s
9.3 120 m/s, 1.328
9.6 (a) 646.9 ft/s, 495.6 ft/s, 415.8 ft/s; (b) 495.6 ft/s, 783.0 ft/s, 926.7 ft/s; (c) 73.36°R, 1.1414; (d) 1.5168, 22.29 psia
9.11 Betal = 56.468, Stage pressure ratio = 1.3444
9.18 3.129×10^{10} in.^{2}-rpm^2
9.19 2133.5 rad/s, 163.2 K, 82.0%, 327.7 kW
9.21 (a) 827.82 m/s, 585.36 m/s, 585.36 m/s; (b) 585.36 m/s, 51.21 m/s, 587.6 m/s; (c) −184.26 K, 0.89763; (d) 0.59106, 591.06 kPa
9.28 5.282×10^6m^2-rpm^2
9.30 (a) 0.1569 m^2; (b) 5561 rpm; (c) 0.64027 m, 0.62014 m, 200.9 K
9.33 (a) 1440.5 ft/s, 2160.7 rad/s; (b) 0.850; (c) 96.3 psia; (d) 0.8614
9.34 (a) 155.46 m/s, 309.86 K; (b) 145.32 m/s, 1.128 atm; (c) 881.75 K; (d) 0.0742 m, 0.0694 m

10.2 1.636 ft
10.3 2.039 m
10.4 0.282 m
10.5 (a) 1.9228; (b) 1.697; (c) 0.7544; (d) 1.534
10.6 (a) 1.27924, 0.71204; (b) 0.52442
10.9 1.39, 0.6572
10.11 (a) 0.9122, 0.7209; (b) Fraction spilled = 12.7%
10.17 $C_V = 0.9937$, $C_{fg} = 0.9764$, $F_{g\ \text{actual}} = 92{,}583$ N
10.19 0.4103 m
10.21 0.9930, 0.0909
10.23 0.99884, 0.0249
10.25 10
10.27 98.5%
10.28 0.782 to 1.564 ft^3

References

[1]*The Random House College Dictionary*, Rev. ed., Random House, New York, 1975.

[2]NOAA, NASA, and USAF, "U.S. Standard Atmosphere, 1976," U.S. Government Printing Office, Washington, DC, Oct. 1976.

[3]"1989 AIAA/General Dynamics Corporation, Team Aircraft Design Competition, Engine Data Package," Director of Student Programs, AIAA, Washington, DC, 1988.

[4]Oates, G. C. (ed.), *Aerothermodynamics of Gas Turbine and Rocket Propulsion*, third ed., AIAA Education Series, AIAA, Reston, VA, 1997.

[5]"2000 Is (Nearly) Now," *Air Force Magazine*, Feb. 1987, pp. 52–63.

[6]"Squeezing More Power from Turbine Engines," *Machine Design*, 10 March, 1988, pp. 44–60.

[7]Mattingly, J. D., "Improved Methodology for Teaching Aircraft Gas Turbine Engine Analysis and Performance," 1992 *ASEE Annual Conference Proceedings*, Vol. 1, ASEE, Washington, DC, 1992, pp. 240–247.

[8]Nicolai, L. M., *Fundamentals of Aircraft Designs*, METS, San Jose, CA, 1975.

[9]Raymer, D. P., *Aircraft Design: A Conceptual Approach*, fourth ed., AIAA Education Series, AIAA, Reston, VA, 2006.

[10]Hale, F. J., *Introduction to Aircraft Performance, Selection and Design*, Wiley, New York, 1984.

[11]Anderson, J. D., *Introduction to Flight*, 3rd ed., McGraw-Hill, New York, 1989.

[12]Mattingly, J. D., Heiser, W. H., and Pratt, D. T., *Aircraft Engine Design*, second ed., AIAA Education Series, AIAA, Reston, VA, 2002.

[13]Heiser, W. H., and Pratt, D. T., *Hypersonic Airbreathing Propulsion*, AIAA Education Series, AIAA, Washington, DC, 1994.

[14]Penner, S. S., *Chemistry Problems in Jet Propulsion*, Pergamon Press, London, 1957.

[15]Keenan, J. H., and Kaye, J., *Gas Tables*, Wiley, New York, 1948.

[16]McKinney, J. S., "Simulation of Turbofan Engine (SMOTE)," AFAPL-TR-67-125, Air Force Aero Propulsion Laboratory, Wright-Patterson AFB, OH, Nov. 1967.

[17]Pratt, D. T. and Heiser, W. H., "Isolator–Combustor Interaction in a Dual-mode Scramjet Engine," AIAA Paper 93-0358, 1993.

[18]Gordon, S., and McBride, B., "Computer Program for Calculation of Complex Chemical Equilibrium Compositions," NASA SP-273, 1971.

[19]Sutton, G. P., *Rocket Propulsion Elements*, 6th ed., Wiley, New York, 1992.

[20]Summerfield, M., Foster, C. R., and Swan, W. C., "Flow Separation in Overexpanded Supersonic Exhaust Nozzles," *Jet Propulsion*, Vol. 24, Sept.–Oct. 1954, pp. 319–321.

[21]Kubota, N. "Survey of Rocket Propellant and their Combustion Characteristics," *Fundamentals of Solid-Propellant Combustion*, Vol. 90, Progress in Astronautics and Aeronautics, AIAA, New York, 1984.

[22]Hill, P. G., and Peterson, C. R., *Mechanics and Thermodynamics of Propulsion*, 2nd ed., Addison-Wesley, Reading, MA, 1992.

[23]Haven, B. A., and Wood, C. W., "The Rocket Laboratory in the USAF Aero-Propulsion Curriculum," AIAA Paper 93-2054, 1993.

[24]Ferri, A., and Naucci, L. M., "Preliminary Investigation of a New Type of Supersonic Inlet," NACA Rept. 1104, 1953.

[25]Wyatt, D. D., "Aerodynamic Forces Associated with Inlets of Turbojet Installations," *Aero Engr. Review.*, Oct. 1951.

[26]Sibulkin, M., "Theoretical and Experimental Investigation of Additive Drag," NACA Rept. 1187, 1954.

[27]"Definition of the Thrust of a Jet Engine and Internal Drag...," *Journal of the Royal Society*, Aug. 1955, pp. 517–526.

[28]Kerrebrock, J. L., *Aircraft Engines and Gas Turbines*, second ed., MIT Press, Cambridge, MA, 1992.

[29]Cohen, H., Rogers, G. F. C., and Saravanamuttoo, H. I. H., *Gas Turbine Theory*, Wiley, New York, 1972.

[30]"Gas Turbine Engine Performance Station Identification and Nomenclature," Aerospace Recommended Practice (ARP) 755A, Society of Automotive Engineers, Warrendale, PA, 1974.

[31]Heiser, W. H., and Pratt, D. T., "Thermodynamic Cycle Analysis of Pulse Detonation Engines," *Journal of Propulsion and Power*, Vol. 18, No. 1, Jan.–Feb. 2002.

[32]Kailasanath, K., "Applications of Detonations to Propulsion: A Review," AIAA Paper 99-1067, 1999.

[33]Strehlow, R. A., *Combustion Fundamentals*, McGraw-Hill, New York, 1984.

[34]Shapiro, A. H., *The Dynamics and Thermodynamics of Compressible Fluid Flow*, Vol. 1, Ronald, New York, 1953.

[35]Pratt, D. T., Humphrey, J. W., and Glenn, D. E., "Morphology of Standing Oblique Detonation Waves," *Journal of Propulsion and Power*, Vol. 7, No. 5, 1991.

[36]*Model Specification for Engines, Aircraft, Turbojet*, MIL-SPEC MIL-E-5008B, U.S. Dept. of Defense, Jan. 1959.

[37]Dixon, S. L., *Thermodynamics of Turbomachinery*, 3rd ed., Pergamon Press, Elmsford, NY, 1978.

[38]Oates, G. C. (ed.), *Aerothermodynamics of Aircraft Engine Components*, AIAA Education Series, AIAA, Washington, DC, 1985.

[39]Horlock, J. H., *Axial Flow Compressors*, Krieger, Melbourne, FL, 1973.

[40]Horlock, J. H., *Axial Flow Turbines*, Krieger, Melbourne, FL, 1973.

[41]Johnsen, I. A., and Bullock, R. O. (eds.), *Aerodynamic Design of Axial-Flow Compressors*, NASA SP-36, 1965.

[42]Glassman, A. J. (ed.), *Turbine Design and Application*, Vols. 1–3, NASA SP-290, 1972.

[43]Wilson, D. G., *The Design of High-Efficiency Turbomachinery and Gas Turbines*, MIT Press, Cambridge, MA, 1984.

[44]Sorensen, H. A., *Gas Turbines*, Ronald, New York, 1951.

[45]Hess, W. J., and Mumford, N. V., *Jet Propulsion for Aerospace Applications*, 2nd ed., Pitman, New York, 1964.

[46]Bathie, W. W., *Fundamentals of Gas Turbines*, Wiley, New York, 1972.

[47]Treager, I. E., *Aircraft Gas Turbine Engine Technology*, 2nd ed., McGraw-Hill, New York, 1979.

[48]Glauert, H., *The Elements of Aerofoil and Airscrew Theory*, 3rd ed., Cambridge Univ. Press, Cambridge, UK, 1959.

[49]Theodorsen, T., *Theory of Propellers*, McGraw-Hill, New York, 1948.

[50]Theodorsen, T., "Theory of Static Propellers and Helicopter Rotors," Paper 326, 25th Annual Forum, American Helicopter Society, Alexandria, VA, May 1969.

[51]Abbott, I. H., and Von Doenhoff, A. E., *Theory of Wing Sections*, Dover, New York, 1959.

[52]Nikkanen, J. P., and Brooky, J. D., "Single Stage Evaluation of Highly Loaded High Mach Number Compressor Stages V," NASA CR 120887 (PWA-4312), March 1972.

[53]Zweifel, O., "The Spacing of Turbomachinery Blading, Especially with Large Angular Deflection," *Brown Boveri Review*, Vol. 32, 1945, p. 12.

[54]Seddon, J., and Goldsmith, E. L., *Intake Aerodynamics*, second ed., AIAA Education Series, AIAA, New York, 1999.

[55]Goldsmith, E. L., and Seddon, J., Practical Intake Aerodynamic Design, AIAA Education Series, AIAA, 1993.

[56]Younghans, J., "*Engine Inlet Systems and Integration with Airframe,*" lecture notes for aero propulsion short course, Univ. of Tennessee Space Institute, Tullahoma, TN, 1980.

[57]McCloy, R. W., *The Fundamentals of Supersonic Propulsion*, Publ. D6A-10380-1, Supersonic Propulsion Test Group, Boeing, Seattle, WA, May 1968.

[58]Kline, S. J., "On the Nature of Stall," *Journal of Basic Engineering*, Vol. 81, Series D, No. 3, Sept. 1959, pp. 305–320.

[59]Taylor, H. D., "Application of Vortex Generator Mixing Principle to Diffusers, Concluding Report," Air Force Contract W33-038 AC-21825, United Aircraft Corp. Rept. R-15064-5, United Aircraft Corp. Research Dept., East Hartford, CT, Dec. 31, 1948.

[60]"Stealth Engine Advances Revealed in JSF Designs," *Aviation Week and Space Technology*, 19 March 2001.

[61]Fabri, J. (ed.), *Air Intake Problems in Supersonic Propulsion*, Pergamon Press, Elmsford, NY, 1958.

[62]Sedlock, D., and Bowers, D., "Inlet/Nozzle Airframe Integration," lecture notes for aircraft design and propulsion design courses, U.S. Air Force Academy, Colorado Springs, CO, 1984.

[63]Swan, W., "Performance Problems Related to Installation of Future Engines in Both Subsonic and Supersonic Transport Aircraft," 2nd International Symposium on Air-Breathing Engines, Sheffield, UK, March 1974.

[64]Surber, L., "Trends in Airframe/Propulsion Integration," lecture notes for aircraft design and propulsion design courses, Dept. of Aeronautics, U.S. Air Force Academy, Colorado Springs, CO, 1984.

[65]Hunter, L., and Cawthon, J., "Improved Supersonic Performance Design for the F-16 Inlet Modified for the J-79 Engine," AIAA Paper 84-1271, 1984.

[66]Stevens, C., Spong, E., and Oliphant, R., "Evaluation of a Statistical Method for Determining Peak Inlet Flow Distortion Using F-15 and F-18 Data," AIAA Paper 80-1109, 1980.

[67]Oates, G. C. (ed.), *The Aerothermodynamics of Aircraft Gas Turbine Engines*, AFAPL-TR-7852, Air Force Aero Propulsion Laboratory, Wright-Patterson AFB, OH, July 1978. (Note: This extensive reference is no longer available. However, the contents have been updated and are published in three textbooks; see Refs. 4, 38, and 70.

[68]Aronstein, D., and Piccirillo, A., *Have Blue and the F-117A: Evolution of the "Stealth Fighter," AIAA, Reston, VA, 1997.*

[69]Lefebvre, A. H., *Gas Turbine Combustion*, Hemisphere, New York, 1983.

[70]Oates, G. C. (ed.), *Aircraft Propulsion Systems Technology and Design*, AIAA Education Series, AIAA, Washington, DC, 1989.

[71]Williams, F. A., *Combustion Theory*, Addison-Wesley, Reading, MA, 1965.

[72]Spalding, D. B., *Combustion and Mass Transfer*, Pergamon Press, Elmsford, NY, 1979.

[73]Grobman, J., Jones, R. E., and Marek, C. J., "Combustion," *Aircraft Propulsion*, NASA SP-259, 1970.

[74]Barclay, L. P., "Pressure Losses in Dump Combustors," AFAPL-TR-72-57, Air Force Aero Propulsion Laboratory, Wright-Patterson AFB, OH, 1972.

[75]Nealy, D. A., and Reider, S. B., "Evaluation of Laminated Porous Wall Materials for Combustor Liner Cooling," American Society of Mechanical Engineers, Paper 79-GT-100, March 1979.

[76]Hopkins, K. N., "Turbopropulsion Combustion—Trends and Challenges," AIAA Paper 80-1199, 1980.

[77]Norgren, C. T., and Riddlebaugh, S. M., "Advanced Liner-Cooling Techniques for Gas Turbine Combustors," AIAA, Paper 85-1290, 1985.

[78]Bahr, D. W., "Technology for the Design of High Temperature Rise Combustors," AIAA Paper 85-1292, 1985.

[79]Taylor, J. R., "Combustion System Design," lecture notes for aero propulsion short course, Univ. of Tennessee Space Institute, Tullahoma, TN, 1978.

[80]McAuley, J. E., and Abdelwahab, M., "Experimental Evaluation of a TF30-P-3 Turbofan Engine in an Altitute Facility: Afterburner Performance and Engine-Afterburner Operating Limits," NASA TN D-6839, July 1972.

[81]Marshall, R. L., Canuel, G. E., and Sullivan, D. J., "Augmentation Systems for Turbofan Engines," *Combustion in Advanced Gas Turbine Systems*, Cranfield International Symposium Series, Vol. 10, Pergamon Press, Elmsford, NY, 1967.

[82]Cornell, W. G., "The Flow in a Vee-Gutter Cascade," *Transactions of the American Society of Mechanical Engineers*, Vol. 78, 1956, p. 573.

Index

[83]VonMises, R., *Theory of Flight*, Dover, New York, 1958.

[84]Cifone, A. J., and Krueger, E. L., "Combustion Technology: A Navy Perspective," AIAA Paper 85-1400, 1985.

[85]*Climatic Information to Determine Design and Test Requirements for Military Equipment*, MIL-SPEC MIL-STD-210C, Rev. C, U.S. Dept. of Defense, Jan. 1997.

[86]*Climatic Information to Determine Design and Test Requirements for Military Equipment*, MIL-SPEC MIL-STD-210A, U.S. Dept. of Defense, Nov. 1958.

[87]*Aerospace Structural Metals Handbook*, Batelle, Columbus Laboratories, Columbus, OH, 1984.

[88]Sims, C. T., and Hagel, W. C., *The Superalloys*, Wiley, New York, 1972.

[89]Smith, W. F., *Structure and Properties of Engineering Alloys*, 2nd ed., McGraw-Hill, New York, 1993.

[90]Brick, R. M., Pense, A. W., and Gordon, R. B., *Structure and Properties of Engineering Materials*, 4th ed., McGraw-Hill, New York, 1977.

[91]Imarigeon, J. P., "The Super Alloys: Materials for Gas Turbine Hot Section Components," *Canadian Aeronautics and Space Institute Journal*, Vol. 27, 1981.